

ISSN 1738-1142

Volume 16[2] 2018

KOREAN RADIOACTIVE WASTE SOCIETY

2018 추계학술논문요약집

| 일시 |

2018. 10. 31(수) ~ 11. 2(금)

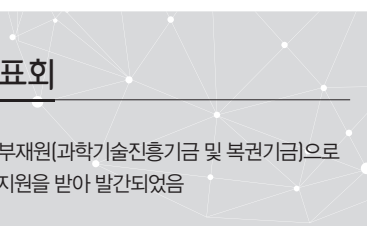
| 장소 |

제주오리엔탈호텔

Abstracts of Proceedings of the
Korean Radioactive Waste Society
AUTUMN 2018



사단 한국방사성폐기물학회
법인 Korean Radioactive Waste Society



2018 추계학술발표회

이 발표논문집은 2018년도 정부재원(과학기술진흥기금 및 복권기금)으로
한국과학기술단체총연합회의 지원을 받아 발간되었음

KOREAN RADIOACTIVE WASTE SOCIETY

2018 추계학술논문요약집

| 일시 |

2018. 10. 31(수) ~ 11. 2(금)

| 장소 |

제주오리엔탈호텔

Abstracts of Proceedings of the
Korean Radioactive Waste Society
AUTUMN 2018



사단 한국방사성폐기물학회
법인 Korean Radioactive Waste Society

Contents

KOREAN
RADIOACTIVE WASTE
SOCIETY

1분과 핵주기정책 및 핵비확산 (Oral)

- 09:00~09:20 Review of the US Cyber Security Self-assessment Method From the Regulatory Perspective 27
Chaechang Lee[KINAC]
- 09:20~09:40 Algorithm Development for Detecting a Crane on Surveillance Camera in Pyroprocessing Based on Machine Learning Technique 29
Byung Hee Won, Se Hwan Park, Hee-Sung Shin, and Seong-Kyu Ahn[KAERI]
- 09:40~10:00 Main Outcomes From Participation to the 6th Review Meeting of Joint Convention on the Safety Spent Fuel Management and on the Safety of Radioactive Waste Management 31
Je-Keun CHON, Gyeong-Uk KANG, and Sangmyeon Ahn[KINS],
Sung-Soo HUH and Ho-Seong CHU[NSSC]
- 10:00~10:20 Current Status of Management of Human Resource for Enhancement of Radiation Safety 33
Donghyun Lee, Manki Lee, Hee Reyoung Kim, and Byung Joo Min[UNIST]
- 11:20~11:40 Identification of Sr Compound in Radiological Terror Scene by Laser-induced Breakdown Spectroscopy at Long Distance 35
Yunu Lee and Sungyeol Choi[KAIST]
- 11:40~12:00 Development of Safeguards Approach of Intermediate-Sized Pyroprocessing Facility 37
Se-Hwan Park, Ho-Dong Kim, Chae Hoon Lee, Dae-Yong Song, Byung-Hee Won, and Seong-Kyu Ahn[KAERI], Hee Seo[Chonbuk Natl. Univ.]
- 12:00~12:20 A Study on the Safeguards of Nuclear Facility During Whole-life 39
Sung Ho Lee, In Chul Kim, Byung Doo Lee, Hyun Jo Kim, Hyun Sook Kim, and Ju Ang Jung[KAERI]
- 12:20~12:40 Research on the Applications of Computer Security Zone for Vital Digital Assets 41
Yeeun Byun, Inkyung Kim, and Kookhei Kwon[KINAC]

1분과 핵주기정책 및 핵비확산 (Poster)

- P0101 A Conceptual Design of the Information Analysis System for Searching Nuclear Fuel Cycle Related R&D Projects 45
Sung-ho Yoon and Dong-hoon Shin[KINAC]

P0102	Legal Case Study About the Lawsuit to the Korea Government's 8th Basic Plan for Electricity Supply and Demand47 Daesung Lee and Jaeyoung Bang[KAERI]
P0103	The Education and Training Activities and Future Challenges of INSA in ROK49 Jin Young Lee[KINAC]
P0104	Analysis of Regulatory Technology Support Status Using Milestone Approach for Supporting Establishment of National Safeguards Systems in the Middle East Region51 Jin Young Lee[KINAC]
P0105	A Study on the Nuclear Nonproliferation Obligations of Nuclear Fuel Cycle Research Activities Funded by the Government53 Seunghyo Yang, Sangjun Lee, and Donghoon Shin[KINAC]
P0106	The Present Status and Future Challenges of Nuclear Forensics in ROK ..54 Seung Ho Jeong, Na Young Lee, Jin Young Lee, Ho Jung Do, and Hana Seo[KINAC]
P0107	System Understanding of Long-term Safeguards for a Closed Repository ...57 Heejae Ju and Sungyeol Choi[KAIST], Il Soon Hwang[Seoul Natl. Univ.]
P0108	The Current Status and Prospects of GIF PR&PP and KAERI's Research Activities for Applying PRPEM59 Ji-Song Jeong, Ho-Dong Kim, and Seong-Kyu Ahn[KAERI]
P0109	Application of PROMETHEE-GAIA Method for Future Nuclear Energy System Selection61 Ruxing Gao, Hyo On Nam, and Hong Jang[KAERI]
P0110	A Study on the Development and Operation of the System for the IAEA Additional Protocol Declaration in KAERI63 Juang Jung, Sung Ho Lee, Byung-Doo Lee, In-Chul Kim, Hyun-Sook Kim, Hyun-Jo Kim, and Seongmi Han[KAERI]
P0111	A Study on the Public Perception of Radiation After the De-nuclearization65 Seungkook Roh, Young joon Lee, and Junghyun Suh[KAERI], YongJun Kim, Hyungsu Chung, and Kibo Shim[KEIA], Jee eun Yoon[Hanyang Univ.]
P0112	Status of Management of the Items Subject to Nuclear Cooperation Agreement at KAERI67 Hyun-Jo Kim, In-Chul Kim, Byung-Doo Lee, Sung-Ho Lee, Hyun-Sook Kim, and Juang Jung[KAERI]

2분과

사용후핵연료 처분전관리 (Oral)

초청발표

09:00~09:20	U.S. Doe Spent Nuclear Fuel Storage & Transportation R&D Activities Sylvia Saltzstein[Sandia Natl. Laboratories, US]
-------------	---

09:20~09:40	Characterization of U–Zr System Fuel Melt Residue for Recycle of Metallic Fuel Scrap	71
	Ki–Hwan Kim, Seong–Jun Ha, Seung–Uk Mun, Jong–Hwan Kim, Young–Mo Ko, and Jeong–Yong Park[KAERI]	
09:40~10:00	Effect of Electrode Materials on the Exchange Current Density Using Tafel Measurement	73
	K. H. Lim and J. I. Yun[KAIST]	
10:00~10:20	Evaluation of Acceptance Criterion for Dryness of Canister and Spent Nuclear Fuel for Dry Storage	75
	Suk–Nam Lim, Gyung–Wook Shin, Gyung–Sun Chae, and Jae–Seok Park[SAE–AN ENGINEERING Co.]	
11:20~11:40	Effects of Hydride Re–orientation and Hydride Rim on Fracture Energy of Zircaloy–4 Cladding	77
	Ho–a Kim and Yong–soo Kim[Hanyang Univ.], Jae–soo Noh[ACT Co. Ltd], Ju–seong Kim[KAERI]	
11:40~12:00	Manufacturing Technology of Dry Storage Cask	79
	Yeon–oh Lee, Sung–kug Hwang, Jong–sul Park, and Jae–min Lee[SeAH Besteel Corp.]	
12:00~12:20	Numerical Analysis on Natural Convection of Backfill Gases in a Dry Storage System for Spent Nuclear Fuels	81
	Hak Min Lee and Jae–Sung Kwon[Incheon Natl. Univ.]	
12:20~12:40	Neutron Tomography as a Spent Fuel Cask Verification Technique	83
	Myungsoo Kim, Juyoung Jeon, Seokryung Yoon, In–Jung Chang, Jinha Choi, and Heejun Chung[KINAC]	

2분과

사용후핵연료 처분전관리 (Poster)

P0201	Thermal Test of KORAD–21 Cask	87
	K.S. Bang, S.H. Yu, J.C. Lee, K.S. Seo, and W.S. Choi[KAERI]	
P0202	Criticality Analysis for Loading Curve Generation for OASIS–32D Cask With PLUS7 Fuel	89
	Keon Young Bae, Young Tae Han, Yong Il Kim, Joon Gi Ahn, In Ho Song, and Gyu Cheon Lee[KEPCO E&C]	
P0203	Comparison Analysis of the Uncertainty Due to Fuel Depletion in the Criticality Analysis for OASIS–32D	91
	Young Tae Han, Yong Il Kim, Joon Gi Ahn, In Ho Song, and Gyu Cheon Lee[KEPCO E&C]	
P0204	Shielding Effects of Reinforcement Structure and Heat Transfer Fin in the OASIS–32D Cask	93
	Yong Il Kim, Young Tae Han, Joon Gi Ahn, In Ho Song, and Gyu Cheon Lee[KEPCO E&C]	

P0205	Scaling Analysis of Spent Fuel Storage Cask for Thermal Test Using a Scaled Down Model	95
	Ju-Chan Lee, Kyung-Sik Bang, Seung-Hwan Yu, and Woo-Seok Choi[KAERI], Sungho Ko[Chungnam Natl. Univ.]	
P0206	Analysis of Electrolytic Reduction Behavior by Oxide Fuel Characteristics ..	97
	Eun-Young Choi and Jeong Lee[KAERI]	
P0207	Simplified Beam Model of Spent Nuclear Fuel Rod	99
	Sanghoon Lee and Seyeon Kim[Keimyung Univ.]	
P0208	Canceled Best Practice Guidelines for the Use of CFD in Dry Cask Applications of US NRC Gyeong-Uk KANG, Dae-Sik YOOK, and Jung-Hoon CHA[KINS]	
P0209	Distillation of Cd- ZrO ₂ and Cd- Bi in Crucible With Splatter Shield ..	103
	S.W. Kwon, Y.W. Kwon, J.H. Jung, S.H. Kim, and S.J. Lee[KAERI]	
P0210	Decay Heat Evaluation of Spent Fuel Assemblies in SFP of Kori Unit-1 ..	104
	Kiyong Kim, Yongdeog Kim, and Sunghwan Chung[KHNP-CRI]	
P0211	Measures for the Failure Evaluation of SNF Cladding During the Transportation	105
	J. S. Noh and H.A. Kim[ACT Co. Ltd.], T.W. Kim[Hanyang Univ.]	
P0212	Methodologies and Properties of Safety Analyses for Pyroprocessing Facilities	107
	Gilsung You, Seokjun Seo, Woojin Jo, Siwan Noh, Hyojik Lee, Hohee Lee, Seungnam Yu, and Jeonghoe Ku[KAERI]	
P0213	PCR Evaluation of NIM Module Based Compton Suppression Gama Spectroscopy System by Source-to-Detector Distance	109
	HaJin Song, ChaeHun Lee, SeongKyu Ahn, and YoungGun Ko[KAERI]	
P0214	The Evaluation of the Fire Protection in Hot Cell Facilities	111
	Woo Jin Jo, Seok-Jun Seo, Siwan Noh, Hyo Jik Lee, and Seung Nam Yu[KAERI]	
P0215	Preliminary Critical Analysis for Review of Multipurpose Utilization of PWR Spent Nuclear Fuel Disposal Canister	113
	Taeman Kim, Ho-Seog Dho, and Sang-Jin Lee[KORAD]	
P0216	PWR SF Transportation Optimization: the Effect of Constraint Variation on the Interim Storage Plan	115
	Hong Jang and Hyo On Nam[KAERI]	
P0217	Simplified Geometric Model Development to Evaluate Spent Fuel Integrity of Representative in Long-term Dry Storage	117
	Jaeyong Kim, Sunguk Lee, and Donghak Kook[KAERI]	
P0218	A Free Drop Analyses of Spent Nuclear Fuel Metal Cask for Various Positions	119
	Hye Jin Lim, Jung Gyu Kim, and Hyun Min Kim[KEPCO E&C]	

P0219	Effect of Cooling Rate on the Hydride Reorientation of Non-irradiated Zircaloy-4 Cladding Tube : 0.5°C/min vs. 0.5°C/hr 121 DaeHo Kim, JongDae Hong, Jegeon Bang, Iksung Lim, EuiJung Kim, and DongHak Kook[KAERI]
P0220	Effect of Hoop Stress on the Hydride Reorientation of Non-irradiated Zircaloy-4 Cladding Tube : 90 MPa, 120 MPa & 150 MPa 123 DaeHo Kim, JongDae Hong, Jegeon Bang, Iksung Lim, EuiJung Kim, and DongHak Kook[KAERI]
P0221	Effect of Thermal Cycling on the Hydride Reorientation of Non-irradiated Zircaloy-4 Cladding Tube : 1 Cy, 3 Cy & 10 Cy 125 DaeHo Kim, JongDae Hong, Jegeon Bang, Iksung Lim, EuiJung Kim, and DongHak Kook[KAERI]
P0222	Preliminary Study on Load and Stress Characteristic Evaluation for Handling Reinforcement Device of Spent Nuclear Fuel 127 Jaejun Lee, Hyeongkoo Kim, Manseok Do, Seongki Lee, and Jongsung Yoo[KEPCO NF]
P0223	Predicting Amount of Radial Hydrides in Spent Fuel during Dry Storage 129 Donghyo Lee, Seongki Lee, and Jongsung Yoo[KEPCO NF]
P0224	Development of Fabrication Technology of Annular Fuel by Hot Extrusion Method 131 Sang-Gyu Park and Kiho Kim[KAERI]
P0225	Design Concept of Package Stowage and Retention Systems During the Road and Sea Transport 133 Chang-Yeal Baeg and Sang-Jin Lee[KORAD]
P0226	Peak Cladding Temperature Analysis of a Spent Fuel Assembly According to Heat Transfer Modes 135 Hyungjin Kim and Hyung-rak Kim[KORAD]
P0227	Modal Analysis of Alternative Spent Nuclear Fuel Transportation Cask for Normal Conditions of Transport Test 137 JaeHoon Lim, Sang Soon Cho, Kiseog Seo, and Woo-seok Choi[KAERI]
P0228	Comparative Study of Servo-type Telemanipulator Systems for Nuclear Facilities 139 Seungnam Yu, Jongkwang Lee, and Byungsuk Park[KAERI]
P0229	Investigation of Thermodynamic Behaviors of SrO in LiCl Molten Salt at 923 K 141 Dokyuu Kang and Sungyeol Choi[KAIST], Byung Heung Park[Korea Natl. Univ. of Transportation]
P0230	A Study on Innovative Metallic Fuel Shapes and Their Manufacturing Requirements 143 Young-Ho Lee, Sang-Gyu Park, ByoungOon Lee, KiHo Kim, and Jeong-Yong Park[KAERI]

P0231	Development of Spent Fuel Cladding Degradation Model in Integrated Platform	145
	Jong-Dae Hong, Yong-Sik Yang, Changhwan Shin, and Dong-Hak Kook[KAERI]	
P0232	A Study on the Impact Analysis for the Spacer Grid by Peripheral Temperature	147
	Sung-Uk Lee, Jae-Yong Kim, Hong-Ryoul Oh, Kyung-Ho Yoon, Hyo-Chan Kim, and Dong-Hak Kook[KAERI]	
P0233	Improvement of Maintenance Method for the Three Piece MSM	149
	SungHyun Kim, SunSuck Hong, and EunYoung Choi[KAERI]	
P0234	Single Fuel Assembly Temperature Experimental Facility (STEP)	151
	Dong-seok Oh, Sun-joon Byun, Chang-hwan Shin, and Dong-hak Kook[KAERI]	
P0235	Comparison of CFD Analysis Methodology for SFP Cooling Performance Evaluation	153
	Taehyeon Kim[KHNP-CRI]	
P0236	Study on the Methodology of Fast Neutron Detection Based on Plastic Scintillators for Safeguards Research	155
	Seonkwang Yoon, Chaehun Lee, Seong-Kyu Ahn, Jong-Myeong Oh, and Ho-Dong Kim[KAERI], Hee Seo[Chonbuk Natl. Univ.]	
P0237	Development and Application of Customized Shielded Cask Transport System	157
	Jong Kwang Lee, Min Ku Jeon, Yunmock Jung, Wooshin Park, Sun Seok Hong, and Eun-Young Choi[KAERI]	
P0238	Link Mechanism of ACPF Argon Cell Gastight Emergency Door	159
	ByungSuk Park, Jongkwang Lee, and Eunyoung Choi[KAERI]	
P0239	Shielding Evaluations of Fuel Failure Scenarios Using MAVRIC	161
	Kyoong-Ho CHA, Minchul KIM, and Taehyeon KIM[KHNP-CRI]	
P0240	Analysis of Uranium Concentration in LiCl-KCl Salt of Electrowinning Process Using LIBS	163
	Seul-Ki Han, Se-Hwan Park, Bo-Young Han, and Seong-Kyu Ahn[KAERI]	
P0241	The Study of Spent Nuclear Fuel Storage Facility to Consider Beyond Design Basis Accident	165
	Dong-bin Shon[KEPCO E&C]	
P0242	Input Accountancy of Pyroprocessing With Different Head-end Process Options	167
	Chaehun Lee, Byung-Hee Won, Se-Hwan Park, Seonkwang Yoon, Ho-Dong Kim, and Seong-Kyu Ahn[KAERI]	
P0243	Current Status of Spent Nuclear Fuel Integrity Evaluation R&D in the Major Countries	169
	Donghak Kook, Jaeho Yang, and Yanghyun Koo[KAERI]	

P0244	Analytic Approach to Simulate Vacuum Drying for Canister	171
	Seung-hwan Yu, Ju-chan Lee, Kyung-sik Bang, and Woo Seok Choi[KAERI]	
P0245	Design of Integrated Analysis Tool for Degradation Evaluation of Spent Nuclear Fuel in Dry Storage System	173
	ChangHwan Shin, Kyong-Won Seo, Yong-Sik Yang, Jong-Dae Hong, Seoung Uk Lee, and Dong-Hak Kook[KAERI]	
P0246	Evaluation of Preliminary Criticality Safety for Metal Storage Cask	175
	Yun-sik KIM and Dong-gyu LEE[KONES Corp.]	
P0247	Evaluation of Cesium Trapping Characteristic With SA Filter	177
	Seok-Min Hong, Jae Hwan Yang, Do-Youn Lee, and Yung-Zun Cho[KAERI]	
P0248	A Study on Electrochemical Characteristics Aluminum Multi Matrix Compound (Al-MMC) of Neutron Absorber Material	179
	Jung Hwan Lee, Yunju Lee, Seung Chang Yoo, Seunghyun Kim, and Ji Hyun Kim[UNIST]	
P0249	Electrochemical Formation of Bi-Hf Alloy in LiCl-KCl for Actinides Separation Process by Density Distribution	181
	Sungjune Sohn and Jaeyeong Park[UNIST], Il Soon Hwang, Jungho Hur, and Seongjin Jeong[Seoul Natl. Univ.]	
P0250	CFD Simulation of Molten-Salt Suction Drain From a Pyrochemical Reactor	183
	Kwang-Rag Kim, Sung-Ki Kim, and Hyo-On Nam[KAERI]	
P0251	Automation System for the Pyroprocessing Automation Verifying Mockup ..	185
	Dongseok Ryu, Jongkwang Lee, Jonghui Han, and Seungnam Yu[KAERI]	
P0252	Development of Standard Reference Data of Nuclear Fuels and Materials ..	187
	Kweon Ho Kang, Seok Min Hong, Jae Hwan Yang, and Yong Jun Cho[KAERI]	
P0253	Effect of Hydrogen on Mechanical Behavior of Zr-based Alloy Fuel Cladding at High Temperature	189
	Dong Jun Park, Yang Il Jung, Jung Hwan Park, Byoung Kwon Choi, Young Ho Lee, and Hyun Gil Kim[KAERI]	
P0254	Optimum Angle of Cutting Roller of 2-Row Blades Slitter for Rod-cuts ...	191
	Younghwan Kim, Yungzon Cho, and Youngsoon Lee[KAERI]	
P0255	Characteristic of Zircaloy-fuel Mechanical Interaction in Failed Spent PWR Fuel	193
	Y. H. Jung, S.J. Baik, and S.B. Ahn[KAERI]	

3분과

고준위폐기물처분 (Oral)

09:00~09:20	Vitrification of the Spent Nuclear Fuel Using Iron Phosphate Glasses ...	197
	Cheong Won Lee, Sung Gyun Shin, Yong Uk Kye, and Jong Heo[POSTECH]	

09:20~09:40	Sorption Characteristics of Iodide on Container Corrosion Products Under the Disposal Conditions: Case Study for Chalcocite and Mackinawite in Alkaline Conditions	199
	Chung-Kyun PARK, Tae-Jin PARK, Seung-Yup LEE, and Jae-Kwang LEE[KAERI]	
09:40~10:00	Preliminary Thermal Analysis for an Alternative Disposal System	201
	Jong-Pil Park, Jong-Youl Lee, Heui-Joo Choi, and Dong-Keun Cho[KAERI]	
10:00~10:20	Buffer Retardation Experiment for Radionuclides Under the Elevated Temperature Conditions: Strategy and Methodology Development for the Korean Bentonite	203
	Tae-Jin Park, Ji-Hun Ryu, Young-Chul Choi, Wan Hyoung Cho, and Jae-Kwang Lee[KAERI]	
11:20~11:40	Procedure Consideration of Site Evaluation of Geological Disposal for HLW	205
	Jeong-Hwan Lee, Sang-Jin Lee, Hyungjin Kim, Taeman Kim, Ho-Seok Dho, Min-Seok Kim and Seoung-Hyun Kim[KORAD]	
11:40~12:00	Microbial Effects of the Alteration of KJ-II Bentonite Containing a Corrosion Product (Fe_2O_3) Under Anaerobic Alkaline Conditions	207
	Hyo-Jin Seo, Seung Yeop Lee, and Jae-Kwang Lee[KAERI]	
12:00~12:20	Preliminary Analysis on Characteristics of the Wastes From the Pyro-processing of SFR SNFs Based on the Material Balance of SFR FSv5.1	209
	In-Young Kim and Dong-Keun Cho[KAERI]	
12:20~12:40	Development of EBS Modules for a Process-based Total System Performance Assessment of a Geological Disposal System	211
	Jung-Woo Kim, Jaewon Lee, Inyoung Kim, and Dong-Keun Cho[KAERI]	

3분과

고준위폐기물처분 (Poster)

P0301	A Bayesian Updating for an Earthquake Frequency Associated With an HLW Repository	215
	Youn-Myoung Lee and Dong-Keun Cho	
P0302	Update of Model Probability for Release Rates of Radionuclides Using Bayes' Theorem	217
	Jongtae Jeong, Dong-Keun Cho, and Youn-Myoung Lee[KAERI]	
P0303	Statistical Approach for the Distribution of Natural Uranium in the KURT Groundwater	219
	Jihye Jeong and Jae-Kwang Lee[KAERI]	
P0304	Preliminary Shielding Analysis for Review of Multipurpose Utilization of PWR Spent Nuclear Fuel Disposal Canister	221
	Ho-Seog Dho and Taeman Kim[KORAD]	

P0305	Fracture Stress Condition and Its Relationship With Hydraulic Conductivity in the KURT Site	223
	Yeonguk Jo, Kyung-Woo Park, and Sung-Hoon Ji[KAERI]	
P0306	Interpretation of Geological Deformation History Using Flat-cutting Surfaces of the Inner Wall of KURT	225
	Soolim Jung, Sung-Hoon Ji, and Kyung-Su Kim[KAERI]	
P0307	Preparation of Anoxic Corrosion Test of Canister Materials in a Deep Borehole	227
	Minsoo Lee, Kyung-Woo Park, Yeonguk Jo, Jihye Jeong, Jang-Soon Kwon, and Sung-Hoon Ji[KAERI]	
P0308	Synthetic Study Between Mechanical and Geological Characteristics in Crystalline Rock	229
	Kyung-Woo Park, Younguk Jo, Sung-Hoon Ji, and Kyung-Su Kim[KAERI]	
P0309	Mechanical Constitutive Models of Unsaturated Expansive Clays: A Review of BExM	231
	Jae Owan Lee, Seok Yoon, and Geon Young Kim[KAERI]	
P0310	A Conceptual Development of Coupled Thermo-Hydro-Mechanical Damage (THM _D) Model in a Nuclear Waste Repository	233
	Jin-Seop Kim and Geon-Young Kim [KAERI], Jun-Seo Jeon and Min-Seop Kim[KAIST]	
P0311	Alternative Concepts of Deep Geological Disposal for Spent Fuels	235
	Jong-youl LEE, Heui-joo CHOI, Hyun-a KIM, and Dong-keun CHO[KAERI]	
P0312	Characteristics of Water Retention Capacity for Korean Compacted Bentonite	237
	Seok Yoon, Changsoo Lee, Jae Owan Lee, Won-Jin Cho, and Geon-Young Kim[KAERI]	
P0313	Implementation of Non-isothermal Two-phase Flow Model into COMSOL Multiphysics	239
	Jaewon Lee, Jung-Woo Kim, and Dong-Keun Cho[KAERI]	
P0314	Numerical Analysis of In-situ Flow Tests for Locally Variable Hydraulic Property on a Borehole	241
	Nak-Youl Ko and Sung-Hoon Ji[KAERI]	

4분과

중저준위폐기물관리(Oral)

09:00~09:20	Necessity of Reasonable Consideration About Disposal Condition for VLLW (Very Low Level Radioactive Waste) of NPP Decommissioning ...	245
	Hyun-Tae Choi, Byeoung-Kug Lee, Hyun-Keun Shin, and Jun-Ki Yum[KHNP]	
09:20~09:40	Surface Complexation Modeling of Nickel Sorption Under Varying Geochemical Conditions at the Wolsong Repository Site	247
	Jongkul Park and Wooyong Um[POSTECH]	

09:40~10:00	Development of Radioactive Waste Drum Cutting System Using STD-11 Cutter	249
	Jin Ho Ha, Hyun Chae Song, and Myeong Ho Kim[Hana Nuclear Power Engineering Co., Ltd.]	
10:00~10:20	Preliminary Safety Assessment for the Disposal of Neutron Activated Concrete Waste	251
	Sol-Chan Han, Yongheum Jo, and Jong-Il Yun[KAIST], Tae-Hyeong Kim[KAERI], Chang Je Park[Sejong Univ.]	
11:20~11:40	Competitive Sorption and Desorption Modeling of Sr Under the Binary Exchange System	253
	Seeun Chang and Wooyong Um[POSTECH]	
11:40~12:00	Preliminary Studies on Lower Limits of Detection for Gaseous Radioactive Effluent Based Upon Risk-based Approach	255
	Na Yoon Choi and Jae Hak Cheong[Kyunghee Univ.]	
12:00~12:20	Effect of Permanent Shutdown on the Characteristics of Radioactive Effluent Discharges From European and Japanese Nuclear Power Plants	257
	Ji Su Kang, Na Yoon Choi, and Jae Hak Cheong[Kyunghee Univ.]	
12:20~12:40	Review on Characteristics of Decommissioning Waste Generation in Foreign Nuclear Power Plants and Potential Waste Characterization Issues	259
	Ki Nam Kwon, Sae Geun Lee, and Jae Hak Cheong[Kyunghee Univ.]	

4분과

중저준위폐기물관리 (Poster)

P0401	Development of Plasma Melter for Melting & Volume Reduction	263
	Mi-Hyun Lee, and Hyun-Je Cho[KHNP-CRI]	
P0402	A Preliminary Study of Hydraulic Performance Assessment of a Multi Barrier System in Near Surface Disposal Facility	265
	Se-Ho Choi, Mi-Jin Kwon, and Jae-Yeol Cheong[KORAD]	
P0403	The Economic Evaluation of Solid Radioactive Waste Treatment Units for Centralized Radioactive Waste Treatment Facility	267
	Jin-Kyu Choi, Young-Hwan Kim, and Eun-Young Kim[KEPCO E&C]	
P0404	Optimum Method for Accommodation of Fire-fighting Water in Control Building of 2 nd LILW Disposal Facility	269
	Mu-gap Shin, and Young-hwan Kim[KEPCO E&C]	
P0405	Treatment of Spent Uranium From Medical Radioisotope Production ..	271
	Seung-Kon Lee, Suseung Lee, Myunggoo Kang, Kyungsoek Woo, and Junsig Lee[KAERI]	
P0406	Analysis of Strengths of Korean Vitrification Technology Comparing to UK	273
	Kyungho Lee, Sewon Chung, Unjang Lee, and Dohyung Kim[ORION EnC Co., Ltd.]	

P0407	Waste Management of Dismantling North Korean Nuclear Facilities : Investigation of Facilities Subject to Vitrification for Decommissioning Waste	275
	Kyungho Lee, Sewon Chung, Unjang Lee, and Dohyung Kim[ORION EnC Co., Ltd.]	
P0408	Safety Considerations for Optimal Development of National LILW Repository Complex	277
	Chan Woo Jeong, Eun Jin Seo, Ayeong Kim, Jeheon Bang, Hyo Sook Jung, and Jinyong Park[KINS]	
P0409	A Safety Concept of Landfill Disposal for National LILW Repository Complex	279
	Chanwoo Jeong, Jinyong Park, Jungjin Kim, Yohan Kim, and Sang Myeon Ahn[KINS]	
P0410	Leaching Test for Polymer Waste Form of Spent Ion-exchange Resins ..	281
	Seongye Kwon, Won-Seok Kim, and Wooyong Um[POSTECH]	
P0411	Development of Low-contaminated Sludge Separation Technology	283
	Heedjin Ahn, MiHyun Lee, and KangOk Cho[KHNP-CRI]	
P0412	A Plan to Build a Total Radwaste Management, STAR (Storage and Treatment of All Radwastes in KAERI) Facility	285
	Jeong Guk KIM, Jongjin KIM, Won Hyuk JANG, Hongrae JEON, and Dae Seok HONG[KAERI]	
P0413	Selective C-14 Stripping Method From Waste Resin Generated From HWR via Microwave Treatment	287
	Ki Rak Lee, Geun-Il Park, Hwan-Seo Park, Hong-Joo Ahn, Jung-Hoon Choi, and Seung Youb Han[KAERI], Hyeon-Oh Park and Young Ku Choi[Sunkwang T&S Co., Ltd.]	
P0414	Corrosion Properties of Metal Waste Alloys for Long-lived Radionuclides Immobilization	289
	Seungyoub Han, Junghoon Choi, Kirak Lee, and Hwanseo Park[KAERI]	
P0415	Research and Development of High-dose Radioactive Material Transport Wagon Using Water Shielding	291
	Dong Hyun Park, Sang Tae Lee, Myeong Ho Kim, Joon Jeon, and Sung Jun Hong[HANA Nuclear Power Engineering Co., Ltd.]	
P0416	Characteristics of the Precipitate From Cs ⁺ Extraction Using Ionic Liquids	293
	Jungweon Choi, Hayeon Ryu, Wonzin Oh, and Sang-June Choi[Kyungpook Natl. Univ.]	
P0417	A Study on Characteristics for Manufacturing the Sintered Green Body of Moist Particulate and Sludge-type Radioactive Waste	295
	Hyoungmin Park, Byunggu Lee, Seonghun Yoon, and Jeongsu Kim[TAEKWANG Co., Ltd.], Yongho Hong, Minsu Kim, Heekyung Kim, Eunsuk Choi, Dongchul Kim, and Taekyu Lee[ACT Co., Ltd.]	
P0418	Development of a 200 Liter-disposal Container (Drum) Cutting Machine for Nuclear Facilities	297
	SeungGeon An, SeakJun Yoo, Seongil Cho, JungSik So, and DaeHwan Kim[Sunkwang T&S Co., Ltd.]	

P0419	Examination on Electrochemical Behaviors of Niobium Chloride in Molten LiCl-KCl by Cyclic Voltammetry	299
	Gwan Yoon Jeong and Jaeyeong Park[UNIST]	
P0420	Estimation and Measurement of Centerline Temperature of the Glass Waste Form	301
	Jung-Hoon Choi, Ki-Rak Lee, Seung-Youb Han, and Hwan-Seo Park[KAERI]	
P0421	Database Design for Development of Waste Management Program for Clearance Level Waste	303
	Gyo Hyeok Song, Ji Young Song, Bo Haeng Lee, and Kwang Pyo Kim[Kyunghee Univ.], Seung Cheol Oh[KINS]	
P0422	A Study on ¹⁴ C Desorption From Spent Activated Carbon of Air Cleaning Units in Domestic Nuclear Power Plants	305
	HangRae Cho and Cheon-Woo Kim[KHNP-CRI]	
P0423	The Guideline for Low and Intermediate Level of Radioactive Waste Management Life Cycle - A Reference for Waste Tracking System (WTS) and Waste Certification Program (WCP)	307
	Kwangyoung SOHN, ChangHwan CHO, and Sungjong KIM[MIRAE-EN Co., Ltd.]	
P0424	Radioactive Waste Tracking System (WTS) for the Decommissioning of Nuclear Power Plants	309
	Sungjong KIM, Kwangyoung SOHN, and Changhwan CHO[MIRAE-EN Co., Ltd.]	
P0425	Overview of Radioactive Waste Acceptance Criteria for Treatment and Management of Radioactive Waste	311
	Won-Seok Kim, Jaeeun Kang, and Wooyong Um[POSTECH]	
P0426	Introduction on Revised Technical Standard for LILW Incineration in Korea	313
	Jungjoon Lee, Kyungwoo Choi, and Sangmyeon Ahn[KINS]	
P0427	KO-CN Tritium Analysis Benchmark for HCCR and HCCB TBS	315
	Hyung Gon Jin, Dong Won Lee, Jae Sung Yoon, Suk Kwon Kim, Eo Hwak Lee, Seong Dae Park, and Chang Wook Shin[KAERI], Seungyon Cho[NFRI]	
P0428	Development of Cement Form an Enhancement for Leaching Resistance ..	317
	Gi Yong Kim, Won Hyuk Jang, Junhyuck Im, Dae Seok Hong, and Jong Sik Shon[KAERI]	
P0429	Application of Averaging Representative Sampling for a Various Surface Contaminated Wastes	319
	MaIGoBaIGaeBiNaLa Yoo, WonHyuk Jang, and JeongGuk Kim[KAERI]	
P0430	A Strategy of Soil Washing Water Purification Using Selective Media ..	321
	DamHyang Kim, Pil-yong Jeon, Woo-hyeon Rhee, Seung-il Kim, Deok-won Kang, and Joon-seok Lee[Elim-Global Co., Ltd.]	
P0431	An Experimental Study on the Melting Decontamination for Radioactive Metal Waste Treatment Using Nuclide Coated Specimens	323
	MinHwan Mo, YongHo Cho, NakJeom Kim, and SangHun Choi[KEPCO KPS]	

P0432	Manufacture of KJRR Cement Waste From for Enhancement of Cesium Leaching Resistance	325
	Won Hyuk Jang, Gi Yong Kim, Dae Seok Hong, Jeong Guk Kim, and Jong Sik Shon[KAERI]	
P0433	Design Factor Analysis of the Treatment Equipment for the Spent Resin Mixture From Pressurized Heavy Water Reactor	327
	Kyu-Tae Park, Jung-Min Yoo, Hyeon-Oh Park, Ki-Hyun Kown, and Young-Ku Choi[Sunkwang T&S Co., Ltd.]	
P0434	Analysis of International Standards and Guidelines for Optimal Management of Decommissioning Waste and Its Implication	329
	Ji Woo Lee, Wang Hyeon Lee, and Jae Hak Cheong[Kyunghee Univ.]	
P0435	Development of Radioactive Contaminated Waste Filter Disposal System in NPP	331
	YongHo Cho, NakJeom Kim, HeeCheol Yoon, MinHwan Mo, and SangHoon Choi[KEPCO KPS]	
P0436	Performance Evaluation of Ca-based Adsorbent for C-14 Trapping ...	333
	In-Hak Cho and Young-Seok Lee[Chungnam Natl. Univ.], Hwan-Seo Park, Ki Rak Lee, In-Tae Kim, and Geun-Il Park[KAERI]	
P0437	Radiological Impact Assessment for the New Radioactive Isotope Wastes Land Transportation Route Using RADTRAN	335
	Hyeon-Oh Park, Bong-Ki Ko, Kyu-Tae Park, Ki-Hyun Kown, and Young-Ku Choi[Sunkwang T&S Co., Ltd.] Myunghwan Seo and Jin Beak Park[KORAD]	
P0438	An Experiment on Pellet Manufacturing Using the High-Volume-Reduction Forming Device Based on the Roll Compaction System	337
	Jong Soon Song, Min Young Jung, and Sang Hyun Lim[Chosun Univ.]	
P0439	Structural Design and Stability Simulation of Polymer Sponge for TBP and Dodecane Separation In Liquid Waste	339
	Junhyuck Im and Jongjin Kim[KAERI], Hyungwoo Kim and Donghoon Seoung[Chonnam Natl. Univ.]	
P0440	A Preliminary Experiment on the Disposal Compatibility of the Polymer Solidification Incorporating Pellets	341
	Jong Soon Song, Sang Hyun Lim, and Min Young Jung[Chosun Univ.]	
P0441	Sampling Design for Defluorination of D-UF ₆	343
	Jongjin Kim, Jeongwook Moon, Yunjeong Hong, Jeong-guk Kim, and Dae-Seok Hong[KAERI]	
P0442	Measurements of Two Dimensional Gamma Ray Distributions of Low and Intermediate Level of Radioactive Wastes Using Fiber-optic Radiation Sensors	345
	Si Won Song, Sang Hun Shin, Hyun Young Shin, Hyungi Byun, and Bongsoo Lee[Chung-Ang Univ.], Cheol Ho Pyeon[Kyoto Univ.]	

P0443	Study on Solidification of Spent-ion Exchange Resin Using Epoxy347 Seong Gon Ryu, Kyoung Yong Noh, Misuk Jang, and Seoung Rae Kim[NESS]
P0444	Study on Modification of Solid Radioactive Waste Management System at KAERI 349 Dong-Ju Lee, Il-Sik Kang, and Dae-Seok Hong[KAERI]
P0445	Physicochemical Properties of Cation Exchange Resin and Binary Cation Exchange Selectivity 351 Hyun Kyoung Ahn, Yean Ju Lee, Jieun An, and In Hyoung Rhee[Soonchunhyang Univ.], Ki-Bang Sung[KHNP-CRI]
P0446	Investigation of Leakage Trend by Ion Exchange Column Experiment in Secondary System of Nuclear Power Plant 353 Hyun Kyoung Ahn, Yoon Soo Kim, Woo Chan Ahn, and In Hyoung Rhee[Soonchunhyang Univ.], Kyung Hee Lee[KHNP-CRI]
P0447	Treatment of Ethanolamine and Hydrazine in CPP Regeneration Wastewater Using Zero-valent Iron Nanoparticle and Hydrogen Peroxide 355 Jun Hee Lee, Jung Yeul Lee, and So Yeon Park[Michigan Technology Co., Ltd.], Ki-Bang Sung[KHNP-CRI], Byoung Ho Lee[Ulsan Univ.]

5분과

제염해체 (Oral)

09:00~09:20	Critical Factors for Creating Effective Relations With Stakeholders During Decommissioning of Nuclear Facilities 359 KwanSeong Jeong, SeungKook Park, DaeSeo Koo, InHye Hahm, SangBum Hong, and BumKyoung Seo[KAERI]
09:20~09:40	Design and Experimental Setup for In-situ Underwater Beta Monitoring System 361 UkJae Lee, Woo Nyun Choi, and Hee Reyoung Kim[UNIST]
09:40~10:00	Efficiency Analysis for In-situ Beta Measurement System in Groundwater 363 Woo Nyun Choi, UkJae Lee, and Hee Reyoung Kim[UNIST]
10:00~10:20	On-site Analytical Laboratory During Decommissioning: Mobile Lab .. 365 Hyuncheol Kim, Chang-Jong Kim, Mee Jang, Jin-Hyung Lee, and Jong-Myoung Lim[KAERI]
11:20~11:40	Fundamental Study on Underwater Laser Cutting for Dismantling Nuclear Facilities 367 Jae Sung Shin, Seong Yong Oh, Hyunmin Park, Taek-Soo Kim, Lim Lee, Chin-Man Chung, and Jonghwan Lee[KAERI]
11:40~12:00	Digital Mock-up Update Based on 3D Scanned Environmental Information for Nuclear Facility Decommission 369 Ikjune Kim, Dongjun Hyun, Jonghwan Lee, and Sungmoon Joo[KAERI]

12:00~12:20	Negative Impact on Radiation Safety of Workers in D&D by Nano-Scale Aerosols From Metal Cutting Process	371
	Sungyeol Choi, Min-Ho Lee, Wonseok Yang, and Nakkue Chae[KAIST]	

12:20~12:40	Ceramicrete Solidification of Concrete Wastes From Nuclear Power Plants Decommissioning	373
	Jae-Young Pyo and Jong Heo[POSTECH]	

5분과

제염해체 (Poster)

P0501	Resin Treatment Using Fenton Like Process With Cu Catalysis	377
	Wooyong Um and M.Aamir Hafeez[POSTECH]	
P0502	Three-dimensional MXene ($Ti_3C_2T_x$) Film for Radionuclide Removal From Aqueous Solution	379
	Jiseon Jang and Dae Sung Lee[Kyungpook Natl. Univ.]	
P0503	A Study on Decommissioning Strategy for Wolsong-1	380
	Byeong Ik Park, Eu Tteum Oh, Hyoung Woo Lee, Ji Han Jeon, and Chang Lak Kim[KINGS]	
P0504	Proposal of Decommissioning Planning for Kori Site	382
	KiHo Cho, YoungJu Son, EunHee Lee, JaeYeon Jung, and ChangLak Kim[KINGS]	
P0505	Cerium Effect on Decontamination of Stainless Steel 304 Metal Oxide ..	384
	Byung-Seon CHOI and Seon-Byeong Kim[KAERI]	
P0506	Case Study on the Soil Remediation Experience in the U.S.	386
	Hyoung-woo Lee, Jung-ha Kim, Ju-youl Kim, and Chang-lak Kim[KINGS]	
P0507	Thermodynamic Analysis of Dissolution Reaction Mechanism of Magnetite in HyBRID Chemical Decontamination	388
	Byung-Chul Lee, and Eun-Ju Lee[Hannam Univ.], Seon-Byeong Kim, Jei-Kwon Moon, and Hui-Jun Won[KAERI]	
P0508	Study on HyBRID Chemical Decontamination and Waste Water Treatment by Using Pilot Scale Equipment	390
	Ki-Chul Kim, Ju-Hyeon Park, Dong-Yeon Kim, and Jung-Hyun Lee[KEPCO KPS]	
P0509	Structural Change of Non-expandable Mineral Illite by Treatment With Organic Acid (Oxalic Acid) and Extraction of Cesium	392
	Sung Man Kim, Chan Woo Park, Il-Gook Kim, Hee-Man Yang, Kune-Woo Lee, and In-Ho Yoon[KAERI], So-Jin Park[Chungnam Natl. Univ.]	
P0510	Study on Dismantling Scenario for Large Components of Kori Unit 1 ..	394
	YoungHwan Hwang, Seok-Ju Hwang, and Cheon-Woo Kim[KHNP-CRI]	
P0511	Modeling of Dissolution Rate of Magnetite in HyBRID Chemical Decontamination	396
	Byung-Chul Lee and Eun-Ju Lee[Hannam Univ.], Seon-Byeong Kim, Jei-Kwon Moon, and Jeongsun Park[KAERI]	

P0512	Grouping of Radioactive Wastes During the Decommissioning of PWR NPPs	398
	Ji-Hoon Lee and Kang-Ok Cho[KHNP-CRI]	
P0513	γ -ray Irradiation Effects on the Polypropylene Yarns	400
	N.O. Chang, H.J. Won, S.Y. Park, S.B. Kim, and B.K. Seo[KAERI], Y.S. Kim[Hanyang Univ.]	
P0514	A Methodology of Selecting Potential Radionuclides for the Kori Unit 1 DCGL Calculation	402
	Hyung-Woo Seo and Dong-Hee Lee[KHNP-CRI]	
P0515	Studies on the Decomposition Behavior of Oxalate Organic Waste by UV-photo-Fenton AOP Using a Medium Pressure UV Lamp	404
	Yoon-Ji Park, Jin-Hee Kim, Sae-Binna Lee, and Sang-June Choi[Kyungpook Natl. Univ.], Hyun-kyu Lee and Wonzin Oh[RIAET]	
P0516	Review of Control Methods of Full System Decontamination Operation Temperature and Decontamination Facility Inlet Temperature	406
	Hak-Soo Kim and Cho-Rong Kim[KHNP-CRI]	
P0517	US-APR1400 Design Features to Facilitate Decommissioning	408
	Hye-Young Shin[KHNP-CRI]	
P0518	Decontamination of Concrete Waste Generated From Nuclear Power Plant Decommissioning With Different Organic Solvents	410
	Seok-ju Hong, Sangsoo Han, Seongsik Nam, Won-Seok Kim, and Wooyong Um[POSTECH]	
P0519	Radionuclides Removal Using Cancrinite and Chalcogel Sorbents	412
	Sangsu Park, Jaehyuk Kang, and Wooyong Um[POSTECH]	
P0520	Treatment of Radionuclide From CRUD Using Underwater Microwave Plasma	414
	Seongsik Nam and Wooyong Um[POSTECH]	
P0521	Review on the Liquid Radioactive Material Leakage Accidents in the U.S. ...	416
	Jung-ha Kim, Hyoung-woo Lee, Ju-young Kim, and Chang-lak Kim[KINGS]	
P0522	Application of a Logistical Simulation Model to Planning of Soil Washing Process	418
	Jihan Jeon, Jaeyeon Jung, Eutteum Oh, David S. Kessel, and Changlak Kim[KINGS]	
P0523	The Study for Method of Full System Decontamination to Remove the Inner CRUD Layer on the Primary Piping	420
	Dong-Kyun Ko, Eui-Dong Lee, Geon-Hwa Lee, and Sung-Jun Hong[Hana Nuclear Power Engineering Co., Ltd.], Chang-Sik Kong and Kwang-Soo Park[Doosan HI&C]	
P0524	A Study on the Reduction Behavior of the Ferric Ion From Phosphoric Electrolyte by Hydrazine	422
	Sae-Binna Lee, Hyun-Kyu Lee, June-Hyun Kim, Jin-Hee Kim, Yoon-Ji Park, Seung-Won Lee, Won-Zin Oh, and Sang-June Choi[Kyungpook Natl. Univ.]	

P0525	A Study on the Radioative Decomposition Characteristics of Oxalic Acid Using Metal Catalysts	424
	Dongwoo Kim, Kang Lee, Tak-hyun Kim, and Seungjoo Lim[KAERI]	
P0526	The Analysis for Corrosion Products in Primary Circuit Structures to Increase FSD (Full System Decontamination) Efficiency	426
	HeeDong Sohn, KwangSoo Park, HaeWoong Kim, and HanSol Im[Doosan HI&C], ChangJe Park[Sejong Univ.]	
P0527	Selective Adsorption of Aquatic Strontium Using Monosodium Titanate Species	428
	Gyuhyeon Kim and Jong Moon Park[POSTECH], Dae Sung Lee[Kyungpook Natl. Univ.]	
P0528	Mineralization of Oxalic Acid by Ni(II) With Gamma Radiation	430
	Kang Lee, Dongwoo Kim, TaeHun Kim, Tak-hyun kim, and Seungjoo Lim[KAERI]	
P0529	Decomposition of Oxalic Acid by Gamma-ray Irradiation	432
	Seung Joo Lim, Kang Lee, and Dong Woo Kim[KAERI]	
P0530	Development of Gamma Scanning System for Irradiated Materials	434
	Young-Jun Kim, Seung-Je Baik, and Ki-Soo Heo[KAERI]	
P0531	Purolite S957 Ion Exchange Resin for Uranium Removal From Effluents Generated During a Spent Catalyst Treatment Process: Real Waste Uptake and Elution Studies	436
	Richard I. Foster, Keun-Young Lee, and Kwang-Wook Kim[KAERI], James T. M. Amphlett[Manchester Univ.]	
P0532	Task Analysis of Decommissioning Activities in Nuclear Power Plants ...	438
	Hyun-Jae Yoo, Chang-su Nam, and Byung-Sik Lee[Dankook Univ.]	
P0533	Preliminary Study on the Heating and Grinding Method for Volume Reduction of Radioactive Concrete Waste From Decommissioning Process	440
	Maeng-Kyo Oh and Chang-Ha Lee[Yonsei Univ.], Keun-Young Lee and Richard I. Foster[KAERI]	
P0534	Weighting Factors of the Performance Shaping Factors for the Segmentation of Reactor Pressure Vessel Internals Using Fuzzy AHP	442
	Chang-Su Nam , Hyun-Jae Yoo, and Byung-Sik Lee[Dankook Univ.]	
P0535	Dismantling Process Development of the Containment Building of Nuclear Power Plant	444
	Myungduck Yang, Wanil Jung, and Junhee Lee[KEPCO E&C]	
P0536	An Approach to the Inventory Assessment for Decommissioning Design of Nuclear Facilities	446
	Su Jung Min, Kwan Seong Jeong, and Seung Kook Park[KAERI], San Chae and Kyung Min Kim[Hanyang Univ.]	
P0537	Effective Decontamination Treatment Process of Steam Generator	448
	Daeseo Koo, Sang Bum Hong, In Hye Hahm, Jea Hyun Ha, Seung-Kook Park, Kwan Seong Jeong, Bum Kyoung Seo, and Kook-Nam Park[KAERI]	

P0538	System for Measuring Characteristic of Aerosol From Metal Cutting ...450 Wonseok Yang, Nakkyu Chae, Minho Lee, and Sungyeol Choi[KAIST]
P0539	Gamma Spectroscopy System With Automatic Sample Feeder in Mobile Laboratory452 Mee Jang, Chang Jong Kim, Hyunchul Kim, Jinhyung Lee, and Jong Myoung Lim[KAERI]
P0540	Case Study of Soil Characterization Techniques at Decommissioning Nuclear Power Plants454 Donghee Lee, Wook Shon, Suk Bon Yoon, and Suhee Lee[KHNP-CRI]
P0541	Study on Metal Ions Treatment From Electro-Decontamination Wastes Using Pilot Scale Equipment456 Jung-Hyun Lee, Dong-Yeon Kim, and Ki-Chul Kim[KEPCO KPS]
P0542	Study on the Dissolution of Concrete for Volume Reduction of Radioactive Concrete Waste458 Iksoo Kim, Maengkyo Oh, and Keunyoung Lee[KAERI]
P0543	A Study on the Assessment of Internal Exposure Effect by Radioactive Aerosol Generated During Melting Facility of NPPs Using Internal Exposure Code460 Sun Il Kim, Hak Yun Lee, and Jong Soon Song[Chosun Univ.]
P0544	A Study on Sign Test Procedure in MARSSIM Used to Site Release of Haddam Neck Nuclear Power Plant462 Jong Hyun Kim, Ji Young Koo, and Yong Soo Kim[Hanyang Univ.]
P0545	Review of MARSSIM Methodology for Nuclear Decommissioning Site Restoration and Environmental Impact Assessment464 Young-hyun Lee, Hyun-jin Park, and Je-geun Jeon[Ujuenertech]
P0546	Regulatory Framework for Decommissioning of Nuclear Facilities in Japan ...466 Jungjoon Lee and Kyungwoo Choi[KINS]
P0547	Full System Decontamination by ASDOC_D-MOD Method468 HanSol Im, ChangSig Kong, HeeDong Sohn, and KyuHo Chang[Doosan HI&C], Laura Schneider[Siempelkamp NIS Ingenieurgesellschaft mbH]
P0548	Introduction to Decontamination Technology of Soil in Decommissioning NPP470 Seungil Kim, Dam-hyang Kim, Pil-yong Jeon, Woo-hyeon Rhee, Deok-won Kang, and Joon-seok Lee[Elim-Global Co., Ltd.]
P0549	Canceled Utilizing of Cognitive Work Analysis Across the System Life Cycle in the Phases of Nuclear Power Plant Kwang Hun Choi[Hanyang Univ.]
P0550	Analysis of Oxide Layer by Simulating NiFe ₂ O ₄ Film on Stainless Steel, Incoloy-600 and Carbon Steel474 Ayantika Banerjee, Yang-II Jung, Wangkyu Choi, Mansoo Choi, and Seonbyeong Kim[KAERI]

P0551	Assessment of Co and Cs Removal From Nuclear Power Plant Soil Using Acidithiobacillus Thiooxidans	476
	Young-Gwang Kim and Kyoung-Woong Kim[GIST], Myoung-Soo Ko[Kangwon Univ.]	
P0552	Technical Status of Remediation Technologies in Radionuclide-contaminated Groundwater of Nuclear Facilities	478
	In-Ho Yoon, Hee-Man Yang, Chan-Woo Park, Ilgook Kim, Sung-Man Kim, and Kune-Woo Lee[KAERI]	
P0553	Radiation Shielding Analysis for Conceptual Design of Reactor Coolant System Decontamination Equipment of Kori Unit 1	480
	Jonghoa Kim, Kyeongho Han, Homin Jeon, and Yongsik Kim[Sae-An Engineering Co., Ltd.]	
P0554	Removal of ⁶⁰ Co and ¹⁵² Eu in Wastewater From Volume Reduction Treatment of Activated Concrete Waste	482
	Woojung Shon[UST], Maeng-Kyo Oh, Richard I. Foster, Keun-Young Lee, and Kwang-Wook Kim[KAERI]	
P0555	A Study on the Post-Treatment Process of Decontamination Waste of Nuclear Power Plant System	484
	Seon-Byeong Kim, Jun-Young Jung, Hui-Chul Eun, Sang-Yoon Park, and Bum-Kyoung Seo[KAERI]	
P0556	Development of Automated System of Classification and Sampling on Radioactive Wastes	486
	Chang-Jong Kim, Jin-Hyung Lee, Mee Jang, Hyuncheol Kim, and Jong-Myoung Lim[KAERI]	
P0557	Behavior Diagram Analysis to Define Requirements on Site Clearance and Remediation	488
	Yunjeong Hong, Heeseoung Park, and Jeong-Guk Kim[KAERI]	
P0558	Removal of Corrosion Oxide Film Using Acidic and Reductive Decontamination Foams	490
	Wangkyu Choi, Seungeun Kim, and Seonbyeong Kim[KAERI]	
P0559	Comparison of Point Cloud Segmentation Methods for Calibration of 3D Environment Scanning System	492
	Sungmoon Joo, Jonghwan Lee, Ikjune Kim, and Dongjun Hyun[KAERI]	
P0560	Risk Assessment on Hazards for Safety of Nuclear Power Plant Decommissioning	494
	HaeWoong Kim, KyuHo Chang, KwangSoo Park, and HeeDong Sohn[Doosan HI&C], ChangJe Park[Sejong Univ.]	
P0561	Experimental Research on Decontamination of Co Containing Metal by Induction Melt	496
	Beom-Kyu Kim, Hwa-Jeong Han, Jun-Hyeok Lee, Jae-Hong Yim, and Byung-Gi Park[Soonchunhyang Univ.]	

P0562	Major Concerns of the Dismantling Project Schedule Development of Nuclear Power Plant	498
	Jun Hee Lee and Myung Duck Yang[KEPCO E&C]	
P0563	Radioactive Contaminated Soil Segregation System for Waste Volume Minimization	500
	Jae-Mun Han, Sang-Chul Lee, and Min-Jung Kim[HYUNDAI E&C]	
P0564	Dismantling Procedure on the Decommissioning Cost for the Research Reactor	502
	Hee-Seoung Park, Yun-Jeong Hong, and Jeong-Guk Kim[KAERI]	

6분과 방사선환경 및 안전 (Oral)

초청발표		
09:00~09:40	History of the Environmental Radioactivity Survey in Korea	507
	Ju-Yong Yun[KINS]	
09:40~10:00	Experiences With the Ground Based and Mobile Gamma-Ray Spectrometry in Contaminated Areas of the Fukushima Prefecture	509
	Young-Yong Ji, Mee Jang, Kun Ho Chung, Mun Ja Kang, and Wanno Lee[KAERI], Taehyung Lim[SI]	
10:00~10:20	Gaseous Tritium Measurement Using Plastic Scintillator	511
	Jun Woo Bae and Hee Reyoung Kim[UNIST]	
11:20~11:40	Review of Radiological Criteria for License Termination in Korea	513
	Jung Hwan Jang, Ki Hoon Kim, Sang Jin Kim, and Kwang Pyo Kim[Kyunghee Univ.], Cheol Kyu Choi[KINS]	
11:40~12:00	Geometric Effects of YAlO ₃ :Ce Scintillator to Autonomous Radiation Monitoring Performance in the Marine Environment	515
	Chanki Lee and Hee Reyoung Kim[UNIST]	
12:00~12:20	Experimental Characterization on Accuracy of Multi-Detector Boron Meter	517
	Si Hyeong Sung and Hee Reyoung Kim[UNIST], Jin Bok Cho[USERS]	
12:20~12:40	Environmental Radioactivity Evaluation of Water Samples Around Nuclear Power Plant Near Ulsan	519
	Ki Joon Kang, Chan Ki Lee, and Hee Reyoung Kim[UNIST]	

6분과 방사선환경 및 안전 (Poster)

P0601	Review of Emergency Alert System for Foreigner	523
	Bongseok Kim, Goanyup Lee, Jongsoo Kim, Hyun Ki Kim, Seungyeon Baek, Kanghyeon Lee, and Hae-Cho Lee[KAERI]	
P0602	Safety Evaluation of a NORM Site Restoration in Korea	525
	Z.H. Woo, Y.J. Kim, B.U. Chang, and J. H. Jang[KINS], N.M. Hassan[Zagazig Univ.]	

P0603	A Practical Measure to Deal With Linear Power Signal Saturation of a WRFC	527
	Sanghoon Bae, I.K. Hwang, W.M.Park, G.Y.Park, and C.H.Kim[KAERI]	
P0604	The Long-Term Simulation of ¹³⁷ Cs in the North Atlantic Ocean Using the Lagrangian Particle Model	529
	Byung-Il Min, Kihyun Park, Sora Kim, Byung-Mo Yang, Jiyeon Kim, and Kyung-Suk Suh[KAERI]	
P0605	Field Experiment for Evaluation of Long-term Behavior of Radiocesium Deposited on Land	531
	Byung-Il Min, Kihyun Park, Sora Kim, Byung-Mo Yang, Jiyeon Kim, and Kyung-Suk Suh[KAERI]	
P0606	The Quantitative Analysis of Uranium and Thorium in Soil Using HPGe Gamma-ray Spectrometry	533
	Kwang Heon Park and Hyoung Gyu Park[Kyunghee Univ.]	
P0607	Radiation Measurement by Compensation Method Using Optic Fiber Scintillator With Passive Fiber Cable	535
	Jongsoo Kim, Sung-Ho Lee, and Hae-Cho Lee[KAERI]	
P0608	A Consideration of Emergency Action Level Initiation Condition for Research Reactor HANARO	537
	Hae-Cho Lee, Jongsoo Kim, GY Lee, JS Kim, HK kim, BS Kim, GH Lee, and SY Baek[KAERI]	
P0609	Shielding Capability Simulation for Neutron and Gamma Rays Using Metal Hydride Materials	539
	Jeong-Kwon Kwak, Muth Boravy, Chang-Je Park, and Sun-Jae Kim[Sejong Univ.]	
P0610	Derivation of Preliminary Derived Concentration Guideline Level (DCGL) by Containment Building Reuse Scenario for Kori Unit 1 Using RESRAD-BUILD	541
	SangJune Park, Jihyang Byon, and Seokyoung Ahn[Pusan Natl. Univ.]	
P0611	Derivation of Surface Soil Area Factor for Kori-1 NPP by Using RESRAD-ONSITE	543
	Ji Hyang Byon, Sang June Park, and Seokyoung Ahn[Pusan Natl. Univ.]	
P0612	A Study on Calculation Program Verification Test Method to Reflect the Latest Standard of Sample Transfer Rate	545
	Ju-Young Yoon and Cheon-Woo Kim[KHNP-CRI]	
P0613	Analysis of Occupational Radiation Exposure in Nuclear Power Plant in Korea	547
	Gang Woo Ryu, Woo Jin Kim, and Kwang Pyo Kim[Kyunghee Univ.], Byeong Soo Kim[KINS]	
P0614	Evaluation of Ambient Dose Equivalent of Silicon Carbide by Neutron Irradiation	549
	Ki-Man Lee and Byong-Gun Park[KAERI]	

P0615	Development of a Concept of Dynamic Integrated Safety Analysis for Accident Predictions	551
	Seok-Jun Seo and Seung Nam Yu[KAERI], Jong Yol Park[RIA Institute Inc.]	
P0616	Improved Facility Exhaust Stability Using Drive Synch System	553
	Heeseok Kang, Seonho Noh, Youngkuk Jang, Wonkyoung Lee, Daeyong Song, and Ilje Cho[KAERI]	
P0617	Study of the ECCS Water's pH Agent (TSP) Neutralizing Ability Performance Test	555
	Ki-Bang Sung and Kyunghee Lee[KHNP-CRI]	
P0618	Estimation of X-ray Beam Qualities for Performance Test on Personal Dosimetry Systems	557
	Hyeongjin Kim, Yuho Won, Moonhyung Cho, and Jae-eun Lee[KHNP-CRI]	
P0619	Deduction of the Optimal Operation Mode of Purifier System	559
	Youngkuk Jang, Seonho Noh, Hui-Seok Kang, and Ilje Cho[KAERI]	
P0620	A Study of ^{222}Rn Concentration in Jeju Spring Water (Yongcheonsoo) ..	561
	Chung-Hun Han[Jeju Natl. Univ.], Seong-Pil Ryu[Jeju Special Self-Governing Provincial Council]	

7분과

방사화학 (Oral)

초청발표		
09:00~09:25	Research on High-level Waste at KIT-INE in the Context of Prolonged Interim Storage and the New Site-selection Process for a Deep Geological Repository in Germany	565
	Volker Metz and Horst Geckeis[KIT, Germany]	
09:25~09:50	Research on Radiochemistry and Geochemistry at KIT-INE, Germany, in Support of the Nuclear Waste Disposal Safety Case	567
	Marcus Altmair and Horst Geckeis[KIT, Germany]	
09:50~10:15	Institute of High Temperature Electrochemistry (IHTE), Ekaterinburg, Russia, Current Status of Pyrochemical Research in IHTE	569
	Alexei Potapov, Kirill Karimov, Alexey Shishkin, Vladimir Shishkin, Alexander Dedyukhin, and Yury Zaykov[IHTE, Russia]	
11:20~11:40	ATR-FTIR Spectroscopic Investigation on the Interaction of U(IV) Nanoparticles With Organic Molecules	571
	Hyejin Cho and Wansik Cha[KAERI]	
11:40~12:00	Synthesis of Functionalized Mesoporous Carbon for Uranium Sorption in Acidic Conditions	573
	Hyeseung Kim, Yongheum Jo, and Jong-Il Yun[KAIST]	
12:00~12:20	Electrochemical Properties of Uranium and UxBiy IMC in the LiCl-KCl Eutectic	575
	Beom-Kyu Kim and Byung-Gi Park[Soonchunhyang Univ.], Sang-Eun Bae and Tae-Hong Park[KAERI]	

12:20~12:40	Raman Spectroscopic Study of Eu(II) and Yb(II) in Molten LiCl–KCl Eutectic ...577
	Seung Park and Jong-Il Yun[KAIST]

7분과

방사화학 (Poster)

P0701	Electrolytic Reduction of Uranium and Rare Earth Oxides in LiCl–Li ₂ O Molten Salt581
	Alexei Shishkin, Vladimir Shishkin, Albert Mullabaev, Vadim Kovrov, Alexander Dedukhin, Anna Kholkina, Vladimir Tsvetov, and Yury Zaykov[IHTE], Sang-Eun Bae[KAERI]
P0702	Distillation of Lithium Chloride From the Metallization Products of Uranium Dioxide582
	Alexander Salyulev, Alexey Shishkin, Alexei Potapov, Vladimir Shishkin, and Yury Zaykov[IHTE]
P0703	Electrical Conductance of Molten (LiCl–KCl) _{eut} with Components of Spent Nuclear Fuel583
	Alexander Salyulev, Alexei Potapov, Vladimir Shishkin, and Yury Zaykov[IHTE]
P0704	Influence of Metal–doping on the Surface Structure and Electrochemical Reactivity of Uranium Dioxide584
	Jeongmook Lee, Jandee Kim, Young–Sang Youn, Seohyun Park, Jeong–mi Park, Jong–Yun Kim, and Sang Ho Lim[KAERI]
P0705	Formation of Calcium Uranyl Carbonate Species at Variable Temperatures ..586
	Yongheum Jo and Jong-Il Yun[KAIST], Hee-Kyung Kim[KAERI]
P0706	The Comparison of Selective Zirconium Removal Between TBP Extraction and POM Complexation588
	Kyungwon Suh, Jaeseok Lee, and Jong–Yun Kim[KAERI]
P0707	Laser–Based Spectroscopic Studies of Actinide Complexes: Uranium ..590
	Euo Chang Jung, Hye–Ryun Cho, Hee–Kyung Kim, Tae–Hyeong Kim, Hyejin Cho, and Wansik Cha[KAERI]
P0708	Laser–Based Spectroscopic Studies of Actinide Complexes: Plutonium ..592
	Hye–Ryun Cho, Euo Chang Jung, Hee–Kyung Kim, and Wansik Cha[KAERI]
P0709	Laser–Based Spectroscopic Studies of Actinide Complexes: Americium ..594
	Hee–Kyung Kim, Hye–Ryun Cho, Euo Chang Jung, and Wansik Cha[KAERI]
P0710	Study on Chemical Variation of Interface Between Gd–doped UO ₂ and Zr Through Annealing With Various Temperatures596
	Jeongmi Park, Young–Sang Youn, Jeongmook Lee, Jandee Kim, Seohyeon Park, and Sang Ho Lim[KAERI], Choong Kyun Rhee[Chungnam Natl. Univ.]
P0711	The Influence of Neodymium Doping and Non–stoichiometry on the Structural and Electrochemical Properties of Uranium Dioxide598
	Seohyeon Park, Jandee Kim, Jeongmook Lee, Jeong–mi Park, Young–Sang Youn, and Sang Ho Lim[KAERI], Choong Kyun Rhee[Chungnam Natl. Univ.]

P0712	First-principles Computational Study on Nucleation and Growth Mechanisms of U on Mo(110) Surface Solvated in an Eutectic LiCl-KCl Molten Salt	600
	Choah Kwon, Joonhee Kang, and Byungchan Han[Yonsei Univ.]	
P0713	Determination of Sr and Zr Using Microextraction Chromatography	602
	Jihye Kim, Jong-yun Kim, and Taehong Park[KAERI]	
P0714	Direct Formation of Lanthanide Trichloride From Lanthanide Oxide	604
	Sang-Eun Bae, Dong-Chul Choi, and Tae-Hong Park[KAERI]	
P0715	Microfluidic Fabrication of Macroporous Polymer Particles for the Separation of Uranium in Aqueous Solution	606
	Jai Il Park, Kwang-eun Lee, Sang Ho Lim, and Jong Yun Kim[KAERI]	
P0716	Determination of Uranium, Molybdenum and Aluminum of U-Mo Alloy by Isotope Dilution Mass Spectrometry and Inductively Coupled Plasma Atomic Emission Spectrometry	608
	Jung Suk Kim, Byungman Kang, Yang-Soon Park, Kyungwon Suh, and Yeong Keong Ha[KAERI]	
P0717	Characterization of Neutron Irradiated Materials Using ESR Spectroscopic Method	610
	Young Hwan Cho[KAERI]	
P0718	Preliminary Calculation of CRUD Source-term With Modified Corrosion Product Transport Model for PWR Primary Circuit	612
	Hwa Jeong Han, Beom Kyu Kim, and Byung Gi Park[Soonchunhyang Univ.]	
P0719	Improved Analytic Crackling Core Model for the Description of UO ₂ Sphere and Pellet Oxidation	614
	Ju Ho Lee, Jae-Won Lee, and Yung-Zun Cho[KAERI]	
P0720	Measurement of Dew Point Temperature of Pyroprocess Automation Mock-up for Basic Design of Emergency Gas Supply System	616
	Jonghui Han, Byungsuk Park, and Seungnam Yu[KAERI]	
P0721	Quality Assurance of Head-end Process of PYRO	618
	Kweon Ho Kang, Yung Jun Cho, Seok-Min Hong, Jae Won Lee, Young Hwan Kim, Ju Ho Lee, Do Youn Lee, Young Soon Lee, and Joo Young Yoon[KAERI]	

1분과

핵주기정책 및 핵비확산 (Oral)



Review of the US Cyber Security Self-assessment Method From the Regulatory Perspective

Chaechang Lee*

Korea Institute of Nuclear Nonproliferation and Control, 1534, Yuseong-daero, Yuseong-gu, Daejeon, Republic of Korea

*chiching@kinac.re.kr

1. Introduction

Nuclear Safety and Security Commission (NSSC) and Korea Institute of Nuclear Nonproliferation and Control (KINAC), regulators for the ROK's nuclear facilities, developed and distributed a regulatory standard for the licensees' Cyber Security Regulation. Nuclear licensees have been phasing in and implementing procedures for the regulation to comply with the standard, KINAC/RS-015 [1].

As one of the activities of the regulation, nuclear facilities licensee shall carry out the continuous assessment of the cyber security controls at least at every overhaul period to validate that the security controls developed according to the cyber security controls of KINAC Regulatory standard (RS-015) are actually applied on the site and properly working. In addition, nuclear facilities licensee shall also evaluate whether the previously established cyber security controls are effectively working in continuously changing cyber threat and environment.

This paper presents how the U.S. nuclear licensees perform cyber security self-assessment and regulator's perspective to introduce and apply the method to the ROK's nuclear facilities. However, it does not represent the official position of regulatory body.

2. U.S. Cyber Security Self-Assessment

U.S. Nuclear Power Plant (NPP) licensees should assess the cyber security risk of nuclear safety systems, physical security systems, and emergency

preparedness systems in accordance with Regulatory Guide (RG) 5.71 of Nuclear Regulatory Commission (NRC) [2]. NRC had contracted with the Pacific Northwest National Laboratory (PNNL) to develop a method to support this. Licensees can select their own practices and tools that are appropriate to them to collect information, estimate cyber security risk, and perform risk management activities.

NUREG/CR-6847 "Cyber Security Self-Assessment Method for U.S. Nuclear Power Plants" was originally a limited release document and withheld from public disclosure under 10 CFR 2.390. The USNRC released the document under FOIA/PA NO:2015-0209 [3]. Nuclear power reactor licensees can use the method to assess and manage cyber risk of any systems in their facilities.

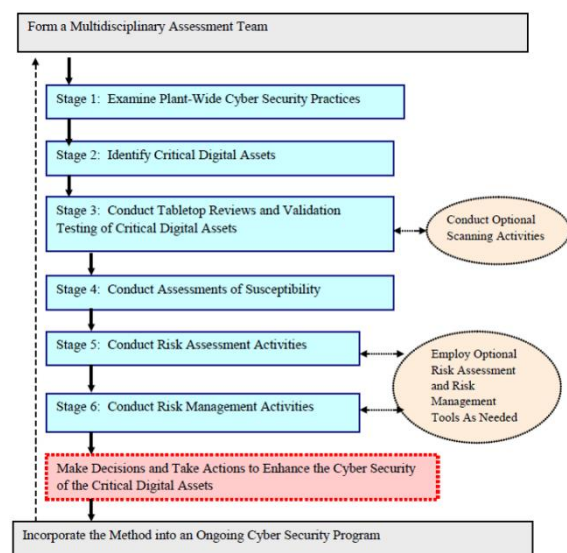


Fig. 1. Simple Flowchart for the Cyber Security Self-Assessment Method for U.S. NPP [3].

The method provides a systematic and phased approach that enables licensees to conduct a thorough self-assessment of cyber security at their respective facilities. And it allows the users a fair amount of latitude in selecting tools and techniques that work best for their specific needs. Figure 1 shows a six-stage process for the self-assessment approach.

3. Regulatory Point of View

This section describes from a regulator's perspective what the ROK's regulator and licensees should consider when introducing and applying the US cyber security self-assessment method.

First, all activities for self-assessment should be performed by the licensees, because it is the licensees that know best what systems affect the plant, how they are connected with each other, and what security constraints they have. Regulators can inspect that appropriate procedure is in place for the licensee to conduct self-assessment and that the composition of teams for self-assessment is appropriate and that the self-assessment process and results are reasonable.

Second, it is difficult for nuclear licensees to derive a high-risk score as an outcome through self-assessment. This could be evidence of a lack of their cyber security activities. Thus, rather than focusing on the results of the self-assessment itself, regulators should focus on whether the self-assessment has resulted on a reasonable basis through the appropriate process. This should ensure that the nuclear licensee's self-assessment is not to be a means to cover their cyber security vulnerabilities or exaggerate their cyber security activities in its facilities but to be a meaningful assessment.

Third, regulatory agencies should inspect that corrective action by the licensee against the results of the self-assessment is appropriate. The risk level derived from the results of the method should be

mitigated through corrective action. While nuclear licensees are reviewing the cost-effectiveness of corrective action to deal with the risk, regulators can check its effectiveness to verify if corrective actions can lower the level of risk from which it was derived.

Finally, it is impractical to perform a self-assessment for all CDAs at once. The available time period is an overhaul, and the number of people is limited to three to seven. Therefore, the selection of critical systems and CDAs to apply the self-assessment method should be appropriate. Critical systems and CDAs that span several areas of security level in defense-in-depth strategy and can seriously impact on NPP if compromised should be chosen first.

4. Conclusion

The cyber security self-assessment method was specifically designed for cyber security evaluations of nuclear facilities. The method can be used by licensees to determine their cyber security posture. The licensees also can make their own method that are appropriate to them to collect information, estimate cyber security risk, and perform risk management activities.

REFERENCES

- [1] KINAC, "Regulatory Standard – Security for Computer and Information System of Nuclear Facilities", Oct. 2014.
- [2] U.S. NRC, Regulatory Guide 5.71, "Cyber Security Programs for Nuclear Facilities", 2010.
- [3] C. S. Glantz et al., NUREG/CR-6847 PNNL-14766, "Cyber Security Self-Assessment Method for U.S. Nuclear Power Plants", Jul. 2004, Released under FOIA/PA NO:2015-0209.

Algorithm Development for Detecting a Crane on Surveillance Camera in Pyroprocessing Based on Machine Learning Technique

Byung Hee Won*, Se Hwan Park, Hee-Sung Shin, and Seong-Kyu Ahn

Korea Atomic Energy Research Institute, 111, Daedeok-daero 989beon-gil, Yuseong-gu, Daejeon, Republic of Korea

*wonbh@kaeri.re.kr

1. Introduction

Containment and Surveillance (C&S) system is one of the main safeguards measures to monitor major locations in a facility handling nuclear materials. Especially it is expected that the role of surveillance will become more important in pyroprocessing facilities having cell based structure. Surveillance under isolated and separated space of a pyroprocessing facility can achieve a significant level of performance and reliability. However, the introduction of many surveillance equipment has a disadvantage that it requires a lot of human resources to confirm normal and abnormal conditions. This issue about human resource is a burden not only for IAEA but also for facility operator. Therefore, it is necessary to develop algorithm that automatically detect normal and abnormal conditions in order to introduce many surveillance devices while minimizing manpower.

In this study, the algorithm development was performed by using the hypothetical surveillance camera in electro-refining cell, which is the main process cell of pyroprocessing. The key technology to check operation condition automatically is to detect any object to classify normal and abnormal conditions. The movement of a crane can be an important factor in monitoring within electro-refining cell. The algorithm to detect the crane, which indicates transportation of process materials in main processes, has been developed based on the hypothetical video data showing process condition in the electro-refining cell.

2. Method & Results

The hypothetical camera which monitors the main processes in a fixed position of electro-refining cell

has been utilized in this study. Fig. 1 shows a frame obtained by the hypothetical surveillance camera. As shown in the Fig., the camera was installed at the start of the processes and electro-refining process begins sequentially from near the camera to far away. The crane moves to transfer process materials according to process schedule.

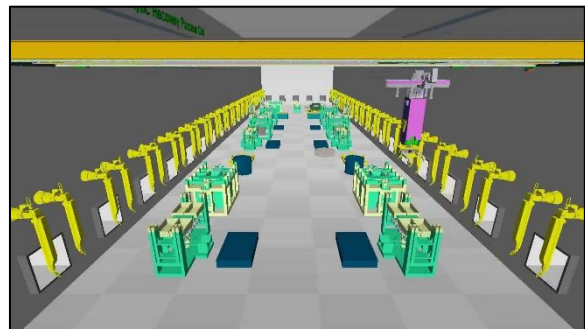
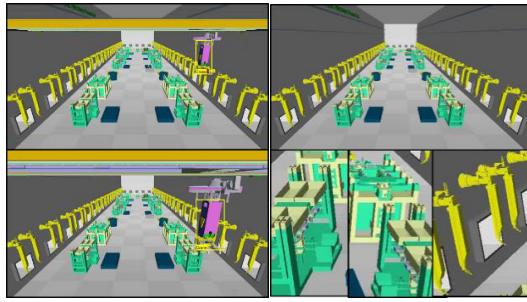


Fig. 1. Screen of Hypothetical Surveillance Camera.

The cascade classifier [1], which is a type of machine learning technique, has been applied to detect crane object in this study. The first step to utilize the cascade classifier is to generate training data set. Fig. 2 shows some training data generated as positive images and negative images. Positive images show the frames having crane and the region of crane marked as Region of Interest (ROI). These frames were obtained from the hypothetical video. Since there are various crane shapes and sizes depending on the distance and position between the camera and the crane, the positive images were considered to reflect the relevant information. Negative images show the scenes without a crane. These images without a crane help the cascade classifier distinguish crane from background. 1,316 positive images and 2,812 negative images were used to train the classifier in this study.



(a) Positive Images (b) Negative Images
Fig. 2. Training Data Set.

The cascade classifier has been trained based on the positive and negative images and then the trained classifier to detect a crane has been evaluated using the hypothetical video data. There are three cases in the algorithm that can indicate false detection results. In the first case, the classifier falsely detects crane on a screen having no crane. In the second case, the classifier dose not detect anything on a screen where a crane exists. In the last case, the classifier indicates two or more cranes on a screen having only one crane. There are total 13,223 frames in the video having 460 seconds length. All false cases have been analyzed for whole frames. Table 1 shows the evaluation result of false detection. As shown in the table, only 3 times of incorrect detection were occurred among 837 frames having no crane. It shows good performance when a crane is out of camera. However, about 20% and 14% among the frames having a crane were failed to correctly detect a crane by detecting wrong object or nothing. It particularly shows poor performance when a crane was located near to the camera or far to the camera.

Table 1. Evaluation Result of False Detection

Case	Number of Failures	Probability of Failures
Case 1: crane detection in the frame having no crane	3	0.36%
Case 2: crane detection failure in the frame having a crane	1721	13.89%
Case 3: two or more cranes detection in the frame having a crane	2511	20.27%

3. Conclusion

The study on detecting a crane in the hypothetical video obtained surveillance camera was performed. The machine learning technique, called as cascade classifier, was applied for crane detection. 1,316 positive images among total 13,223 frames were used for training the classifier. The trained classifier showed good performance when there was no crane on the surveillance screen. On the other hand, about 34% false detection was occurred when there was a crane on the screen. These false detection rate can be reduced by increasing training data set and optimizing some parameters of the classifier. It is expected that the algorithm for detecting important objects would be useful for building considerably efficient and reliable C&S system in pyroprocessing facility.

ACKNOWLEDGEMENT

This work was supported by a National Research Foundation of Korea (NRF) grant funded by the Korean government (MSIP) (No. NRF-2017M2A8A5015084).

REFERENCES

- [1] Viola, P., and M. J. Jones. "Rapid Object Detection using a Boosted Cascade of Simple Features." Proceedings of the 2001 IEEE Computer Society Conference. Volume 1, 15 April 2001, pp. I-511-I-518.

Main Outcomes From Participation to the 6th Review Meeting of Joint Convention on the Safety Spent Fuel Management and on the Safety of Radioactive Waste Management

Je-Keun CHON ^{a)*}, Gyeong-Uk KANG ^{a)}, Sung-Soo HUH ^{b)}, Ho-Seong CHU ^{b)}, and Sangmyeon Ahn ^{a)}

^{a)} Korea Institute of Nuclear Safety, 62, Gwahak-ro, Yuseong-gu, Daejeon, Republic of Korea

^{b)} Nuclear Safety and Security Commission, 178, Sejongdae-ro, Jongno-gu, Seoul, Republic of Korea

*k393cj@kins.re.kr

1. Introduction

The Joint Convention on the Safety of Spent Fuel Management and on the Safety of Radioactive Waste Management (hereinafter referred to as ‘Joint Convention’) is the only international legally binding instrument to address, on a global scale, the safety of spent fuel (SF) and radioactive waste management (RWM). Since the Joint Convention was entered into force in 2001, it has contributed significantly to the safety of SF and RWM.

The 6th Review Meeting of the Joint Convention was held from 21 May to 01 June 2018 at the Headquarters of the International Atomic Energy Agency (IAEA), which is the depositary and Secretariat for the Joint Convention.

Since joining the Joint Convention in 2002, Korea has faithfully fulfilled the Contracting Party’s obligations.

This paper summarizes the steps, efforts made in preparation of the 6th Review Meeting and main outcomes of the Review Meeting.

2. Implementation of National Obligations for 6th Review Meeting of Joint Convention

2.1 Status of Joint Convention

The Convention was adopted on 5 September 1997 at a diplomatic conference convened by the IAEA Headquarter in Vienna. The Joint Convention was opened for signature on 29 September 1997, at the 41st regular session of the IAEA’s General Conference. The Joint Convention was entered into force on 2001[1].

The Contracting Parties should demonstrate commitment to apply stringent safety measures, to prepare a National Report on the applied measures and to submit it for review by all other Contracting Parties, as well as to actively participate in the Review Meetings of the Contracting Parties. The Joint Convention is an ‘incentive’ convention

through a peer review process every three years.

As of July 2018, there are 79 Contracting Parties[2].

2.2 Main Milestones for Implementation of National Obligation for 6th Review Meeting

The peer review process of Joint Convention is implemented based on following steps; 1) Submission of National Reports, 2) Questions and answers on the National Reports, 3) Participation to the Review Meeting.

Fig. 1 illustrates the main milestones for the 6th Review Meeting.

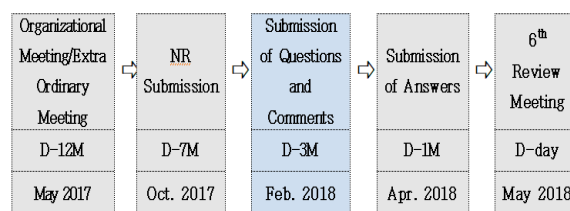


Fig. 1. Main milestones for the 6th Review Meeting.

2.3 Preparation of National Report

In order to fulfill the national obligations to the Joint Convention, a working level team composed of relevant organizations in nuclear industries including Nuclear Safety and Security Commission (NSSC), Korea Institute of Nuclear Safety (KINS), Korea Radioactive Waste Agency (KORAD), Korea Atomic Energy Research Institute (KAERI), Korea Hydro & Nuclear Power Co., Ltd (KHNP), Korea Electric Power Corporation Nuclear Fuel Co., Ltd (KEPCO NF) was organized to enhance the completeness of the implementation of the national obligations and to improve the efficiency of the implementation process by establishing a proper strategy before beginning each phase of obligatory matter.

In preparation of the 6th Review Meeting, the

National Report containing the implementation of national obligations and the good practices of the safe management of RW and SF in Korea was drafted in accordance with the “Guidelines Regarding the Form and Structure of National Reports (INFCIRC/604/Rev.3)” under the Joint Convention[3]. The National Report of Korea was submitted to the secretariat within the due date.

2.4 Question and Answer to the National Reports

The National Reports of 19 other Contracting Parties were reviewed to post the questions and comments, taking into account their significance on radioactive waste management facilities or program and the member of 8th Country Group(Lithuania, Canada, Georgia, Ghana, Morocco, Netherlands, and Uzbekistan). 158 questions and comments were submitted to the secretariat on timely fashion.

Afterward, Korea received a total number of 84 written questions/comments on the National Report of Korea from 18 Contracting Parties. The questions/comments on Korean report were focused on mainly following topics; LILW Predisposal, SF Public engagement and action plan, SF Management, HLW and LILW Disposal, Legislation and Regulatory Framework, etc. The answers to the questions/comments were submitted within the due date, on April 2018.

3. Participation to the 6th Review Meeting of Joint Convention and Main Outcomes

3.1 Presentation of National Report to 6th Review Meeting of JC

The National Report of Korea was presented at the 8th Country Group session on 23 May, 2018. The presentation of Korea highlighted the major changes since the 5th Review Meeting and safety improvement activities for RW and SF management, etc.

From the peer review process at 8th Country Group session, 1 Good Practice and 3 Area of Good Performances were identified for Korea as listed below, recognizing the efforts to enhance the safety of RWM;

- Good Practice: Establishment Nuclear Safety Consultative Council at each nuclear facility site
- Area of Good Performance; 1) Site selection

procedures and support for host community of HLW management facilities, 2) Establishment of safety requirements for HLW, and 3) Information disclosure and transparency activities.

At the 6th Review Meeting, the stricter application of the definition of “Good Practice” led to only 6 good practices being identified during the Country Group Sessions.

3.2 Main Outcomes from 6th Review Meeting of JC

The 6th Review Meeting identified that good progress is being made in many areas of SF and RW safety. Constructive discussions and sharing of knowledge took place in a frank and open manner and Contracting Parties recognized the importance of peer review process of the Joint Convention.

The Contracting Parties agreed to hold the 7th Review Meeting at IAEA Headquarters on 24 May to 4 June 2021.

4. Conclusion

Korea has committed to the objectives of Joint Convention and fully complied with the obligations and terms of the Joint Convention.

In preparation of the 6th Review Meeting, the national obligations were faithfully fulfilled by submitting the National Report and questions/answers within due date.

At the Country Group session of the Review Meeting, the efforts of Korea to enhance the safety of SF and RW management were recognized by other Contracting Parties.

Korea will continue to demonstrate its commitment to the Joint Convention through strengthening of national measures and international cooperation.

REFERENCES

- [1] www.IAEA.org, Joint Convention Brochure (2017).
- [2] www.IAEA.org, Latest Status of Signature and Ratification (2018).
- [3] INFCIRC/604/Rev.3, Guidelines Regarding the Form and Structure of National Reports (2014).

Current Status of Management of Human Resource for Enhancement of Radiation Safety

Donghyun Lee*, Manki Lee, Hee Reyoung Kim, and Byung Joo Min

Ulsan National Institute of Science and Technology, 50, UNIST-gil, Eonyang-eup, Ulju-gun, Ulsan, Republic of Korea

*calvinjl@unist.ac.kr

1. Introduction

According to the emerging change on national energy transition policy in the Republic of Korea, the interest on radiation safety of domestic nuclear field has been increased [1]. Not only change of the governmental energy policy consulted by foreign nuclear phase-out policy such as Germany and Belgium, but social impact from Fukushima Daiichi accident and, recent earthquake which occurred in Gyeongju and Pohang had led reinforcement of public opinion to radiation safety as the safety of nuclear power plants and related facilities. In response, it is crucial to identify the competence of human resource (HR) that could contribute to safety of radiation facility. Full scale enumeration on nuclear engineering related academic and research area had been pre-studied. However, despite of the importance, specific survey on radiation safety related field, which could identify the HR balance between supply and demand has not been initiated. The present survey analysis research is aimed to estimate expectation of human resource supply and demand on KAERI, KINS, KINAC and KHNP Central Research Institute so as to evaluate its balance status for long term stable HR management for ensuring and enhancing the radiation safety.

2. Methods

2.1 Research Scope

Detailed research objects are analyzing radiation safety, which covers the area from controlling reactor safety to manage related sites as regulated supply and demand of human resource and assessment of sustainable and practical method for continuous human resource. To analyze the enumerated human resource data, the field of academic nuclear engineering has been classified into seven parts in order to identify, which enables the identifying radiation safety related human resource.

2.2 Expert Supply Status in the Field of Radiation Safety

For specification of the supply of radiation safety management professional HR, the academic field of nuclear engineering had been classified into reactor physics, thermal hydraulics, radiation, nuclear material, instrumentation control chemistry control, and etc. [2]. As shown in Table 1, the database

constructed by survey in the 16 universities represented, total number of 844. In terms of academic background, radiation field was surveyed, the highest increasing with 111 followed by etc. as 90 people, which indicates interest of pre-professional human resources to rational safety are increasing.

In the field of research and industry, researchers positioned on radiation safety are 783, respectively as 30% out of total number of 2587 people that professional HR working for KAERI, KINS, KINAC and KHNP Central Research Institute as shown in Table 2.

Table 1. Change of human resources in domestic universities

Field	2018 year	2017 year	Change
Reactor Physics	115	83	32
Thermal Hydraulics	169	156	13
Radiation	150	39	111
Nuclear Material	103	89	14
Instrumentation and Control	70	26	44
Chemistry Control	39	35	4
Etc.	198	108	90
Total	844	536	308

Table 2. Status of human resources in the area of research and industry

Institute	No. of Researchers	Radiation Safety Area	No. of Researchers
KAERI	1452	Radiation Safety Researcher	56
KINAC	96	All	96
KINS	524	All	524
KHNP Central Research Institute	515	Safety Assessment	25
		System Safety	30
		Safety Technology	52
Total	2587	N/A	783

2.3 Expert Demand Status in the Field of Radiation Safety

Research and management of radiation safety is being carried out mainly in KAERI and KINS. Expected demand for the human resource was cited from pre-initiated research [1, 3, 4], which was initiated based on 4th and 8th basic plan for long-term electricity supply and demand and the data was

evaluated with human resource from 2018 on the related organizations. In addition, HR supply analysis based on the 8th basic plan for long-term electricity supply and demand, which is the most recent program, was also initiated with top-down method. The reliability evaluation of the KAERI and KINS radiation safety management experts demand data was done by comparing with current human resource full scale enumeration result [1].

3. Results

KAERI in 2018, total researchers showed 47 people less and 115 people larger compared with 4th and 8th basic plan for long-term electricity supply and demand respectively. In Fig. 1 and 2, the results were cited from previous research [1], which shows expected radiation safety personnel demand on each institution. Radiation safety management experts showed 15 people less and 25 people larger compared with 4th and 8th basic plan for long-term electricity supply and demand.

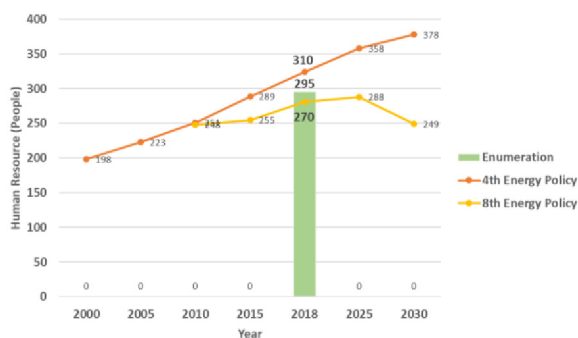


Fig. 1. KAERI Radiation Safety Management HR [1, 3, 4].

KINS in 2018, total researchers showed 137 people less and 39 people larger compared with 4th and 8th electricity plan. In Fig. 2, personnel in radiation safety management showed 3 people less and 38 people larger compared with 4th and 8th basic plan for long-term electricity supply and demand.

The analysis based on 8th demand supply program on energy was done focused on Personnel in radiation safety management on KAERI and KINS, and resulted major difference not larger than 25 and 38 experts, which is respectively, 1% and 7% error out of total 1452 and 524 researchers in KAERI and KINS.

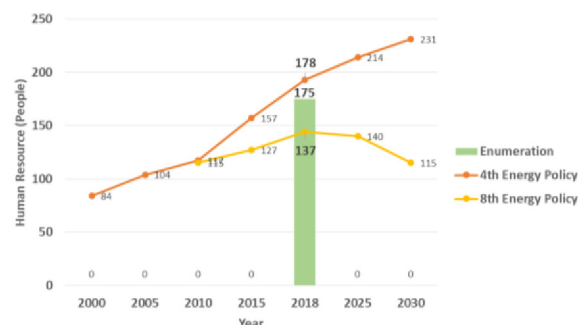


Fig. 2. KINS Radiation Safety Management HR [1, 3, 4].

4. Conclusion

The difference in nuclear power portion between the 4th and 8th basic plan for long-term electricity supply and demand makes difference to the HR supply. Which also leads to decreasing of HR demand from 2025 year both on KAERI and KINS. For keeping continuous balance on supply and demand of radiation safety management human resource which holds key on future radiation safety and public acceptance, it is crucial to make provision on safety of radiation expert demand and supply. Under sudden change on domestic and foreign nuclear industry atmosphere, it is inevitable to experience imbalance on human resource. However, the importance of competitive human resource development on radiation safety to enhance the safety of radiation facility has increased for ensuring public acceptance.

ACKNOWLEDGEMENT

This work was supported by the National Research Foundation of Korea (NRF) grant funded by the Korean government (MSIP: Ministry of Science, ICT) NRF- 2017M2B2A8A09094071

REFERENCES

- [1] B.J.,Min, "A study on the Competence and HRD of Nuclear Safety Experts to Enhance the Safety of Nuclear Facility", UNIST-2017M2B2A8A09094071-01.
- [2] IAEA. "Decommissioning of Nuclear Facilities: Training and Human Resource Considerations", NG-T-2.3, 2008.
- [3] B.J.,Min, "Formulating Human Resources Development Strategies for Nuclear R&D, Safety and Security", KAERI/ RR-3162/ 2010.
- [4] Seongyeol Choi, "Human Resources Development and Demand of Sustainable National Nuclear Power Programs", KAIST/ Research Report, 2017.
- [5] B.J., Min "Nuclear human resource projection up to 2030 in Korea"/NET/ Vol.43 No.4, pp375-382/ 2011.

Identification of Sr Compound in Radiological Terror Scene by Laser-induced Breakdown Spectroscopy at Long Distance

Yunu Lee and Sungyeol Choi*

Korea Advanced Institute of Science and Technology, 291, Daehak-ro, Yuseong-gu, Daejeon, Republic of Korea

*sungyeolchoi@kaist.ac.kr

1. Introduction

The nuclear incidents is increasing by militant groups such as ISIS and Al-Qaeda. They are eager to obtain hazardous materials. In addition, a lot of terrorism were carried out by these groups like an accidents arise at a concert box in Manchester (May 2017). One of the most common nuclear materials stolen is Sr in radioisotope thermoelectric generators (RTG) [1].

Sr is the only one isotope that emit purely beta in nine suggested potential radiological terror source by Argonne National Laboratory [2]. Such a beta emitter can be hard to detect with conventional instrument such as Guiger-Muller counter. Therefore, the research aim of the present paper was to perform assessment of feasibility for identifying Sr by Laser-Induced Breakdown Spectroscopy (LIBS) at long distance with protecting inspectors.

2. Experimental and results

2.1 Experimental setup

Fig. 1 describes the setup of remote-LIBS detection system. To ablate targets, a compact Q-switched Nd:YAG laser (532 nm, 220 mJ, 5 ns, 20Hz) was used. For measuring spectra of targets, an Echelle spectrograph (f/7, 200 – 975 nm of operating range, 195 mm focal length) combined with intensified-CCD (13 x 13 μm^2 pixel size) was established. To collect the light of plasma which has information of atomic spectra, a small Maksutov-Cassegrain Optical telescope (90 mm of aperture, f/14, 1200 mm of focal length) was employed. The distance between this telescope and samples is about 3 m away. The laser lights were transmitted to targets through plane mirrors and plano-convex lens with focal length of 125 mm. The obtained spectra was used with delay time of 500 ns, integration time of 1 ms, and laser power of ca. 22.5 mJ.

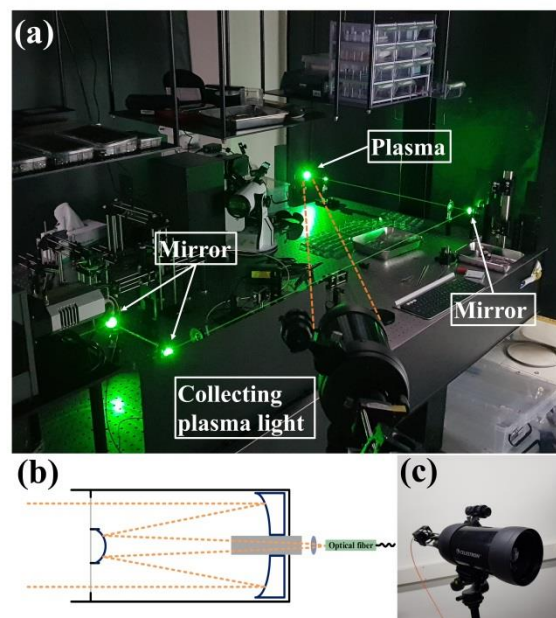


Fig. 1. Photo and schematic view of experimental setup. (a): Photo of measuring the plasma light at long distance, (b): Schematic view of light path in telescope to optical fiber, (c): Photo of cassegrain telescope.

2.2 Samples

The samples are comprised of SrCO_3 onto Al, SUS304, mortar and polyester. In fabricating of RTGs, SrCO_3 is generated as intermediate products during the process of solvent extraction [3]. These fabrication plant is relatively accessible than reprocessing or interim storage facility for used nuclear fuel. This study proposes the method to identify Sr in radiological terror scene. The proposed method attempts to consider the terror is arise in huge city by using Al, SUS304, mortar and polyester. It is because Al, SUS304, mortar and polyester can be component of radiological dispersal devices outer container, bridge or pipe, pavement or building, and clothes respectively. Finally, SrCO_3 was dissolved into highly purified water and sprayed on the surface of matrices homogeneously.

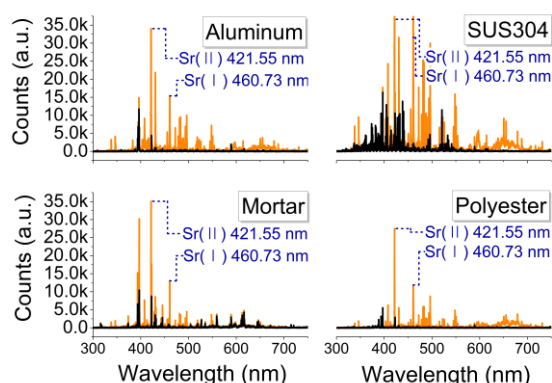


Fig. 2. LIBS spectra at long distance of SrCO_3 including Al, SUS304, mortar, and polyester. Orange line: matrix with SrCO_3 , Black line: only matrix.

Fig. 2 summarizes the spectra of SrCO_3 on various matrices. All of the peaks were analyzed using National Institute of Standards and Technology (NIST) spectroscopy database [4]. Two wavelength of 421.55 and 460.73 nm were employed to identifying Sr from the samples. It is because these peaks are most powerful intensity. Especially 460.73 nm is a persistent spectrum of Sr. For comparison, the spectra of close contact experiments also summarized as shown in Fig. 3. In case of close contact experiment, the same condition such as delay time, integration time and laser power, but only difference is distance between gathering devices and plasma lights. While searching Sr for ensuring an evidence of radiological terrorism at a long distance to minimize exposure for inspectors, there are not such difference between the spectra at long distant and close contact in terms of identifying Sr from the various matrices. The whole intensity, however, are reduce where detect in a far away.

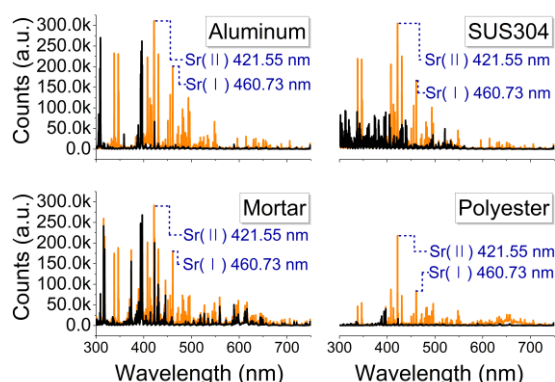


Fig. 3. LIBS spectra at close contact of SrCO_3 including Al, SUS304, mortar, and polyester. Orange line: matrix with SrCO_3 , Black line: only matrix.

3. Conclusion

The present study may suggest that LIBS at long distant can be used to find evidence of Sr radiological terror. For each matrix (Al, SUS304, mortar, polyester) with SrCO_3 , the feasibility that can be detect radioactive materials in Sr radiological terror scene was demonstrated easily. The advantages of remote detection are identification of targets with minimized exposure rate for inspectors, and rapid collection of information by enhanced area of detection systems covered in one place.

ACKNOWLEDGEMENT

This work was supported by the Korea Institute of Nuclear nonproliferation And Control (KINAC) granted financial resource from the Nuclear Safety and Security Commission (NSSC), Republic of Korea (No. 1803026).

REFERENCES

- [1] R. Alimov, Radioisotope Thermoelectric Generators, in: Nuclear issues in ex-soviet republics, Radioactive waste and spent nuclear fuel, Bellona working paper, 2005. Reference to a website: <http://bellona.org/news/nuclear-issues/radioactive-waste-and-spent-nuclear-fuel/2005-04-radioisotope-thermoelectric-generators-2> (accessed 12 August 2018).
- [2] J.M. Peterson, M. Mac Donell, L. Haroun, F. Monette, R.D. Hildebrand, A. Taboas, Radiological and Chemical Fact Sheets to Support Health Risk Analyses for Contaminated Areas, Argonne National Laboratory Environmental Science Division in collaboration with U.S. Department of Energy, 2007.
- [3] W.R. Corliss, R.L. Mead, Power from Radioisotopes, U. S. ATOMIC ENERGY COMMISSION, Division of Technical Information, 1966.
- [4] J.E. Sansonetti, W.C. Martin, S.L. Young (2005), Handbook of Basic Atomic Spectroscopic Data (version 1.1.3), National Institute of Standards and Technology, [Online] Available: <https://dx.doi.org/10.18434/T4FW23> (Accessed 22 August 2018).

Development of Safeguards Approach of Intermediate-Sized Pyroprocessing Facility

Se-Hwan Park^{a)*}, Ho-Dong Kim^{a)}, Chae-Hoon Lee^{a)}, Hee Seo^{b)}, Dae-Yong Song^{a)}, Byung-Hee Won^{a)}, and Seong-Kyu Ahn^{a)}

^{a)} Korea Atomic Energy Research Institute, 111, Daedeok-daero 989beon-gil, Yuseong-gu, Daejeon, Republic of Korea

^{b)} Chonbuk National University, 567, Baekjedae-ro, Deokjin-gu, Jeonju-si, Jeollabuk-do, Republic of Korea

*ex-spark@kaeri.re.kr-mail

1. Introduction

Safeguards approach is a set of safeguards measures to allow the IAEA to meet the applicable safeguards objectives [1]. Safeguards approaches of the existing nuclear material handling facilities were already developed, and a safeguards approach of a pyroprocessing facility is required for the effective and efficient safeguards implementation in the pyroprocessing facility.

Korea Atomic Energy Research Institute (KAERI) developed the safeguards approach of a reference facility named Reference Engineering-scale Pyroprocessing Facility (REPF) in collaboration with Korea Institute of Nuclear Nonproliferation and Control (KINAC) from 2008 to 2011 as an IAEA Member State Support Program (MSSP). The annual throughput of the REPF was 10 MtHM. At present, KAERI is developing a safeguards approach of an intermediate-sized facility named Reference Engineering-scale Pyroprocessing Facility plus (REPF+) also as a task of a MSSP. This presentation provides the overview of the REPF+ safeguards approach, which is under development.

2. Methods and Results

The REPF+ is a conceptually designed pyroprocessing facility. SFR fuel fabrication process as well as pyroprocessing process is included to the

REPF+. The input material of the REPF+ is PWR spent fuel, and the output materials are SFR fuel assembly, and U ingot. The annual throughput is 30 MTH and the total operation days are roughly 200 days.

The facility is divided into four Material Balance Areas (MBAs). Inventory Key Measurement Points (IKMPs) are identified mainly based on the material type. Flow Key Measurement Points (FKMPs) are also identified to verify the nuclear material streams across the MBA boundaries. Other Strategic Points (OSPs) are defined for the verification of nuclear material flow within MBA.

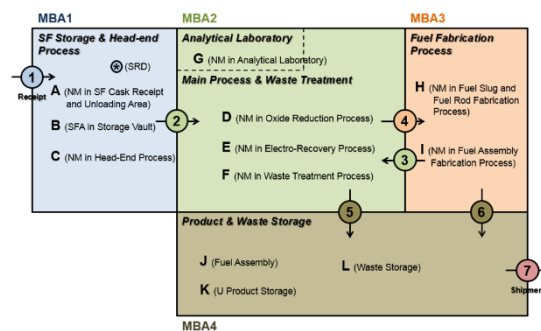


Fig. 1. Draft MBA and KMP structure of the REPF+.

MBA1 consists of a spent fuel receipt and storage area and an air-filled hot cell named Head End Process (HE) cell. The spent fuel assembly is converted into feed material of an oxide reduction process such as fragment and porous pellet. The Shipper Receiver Difference (SRD) is evaluated in the MBA1. The containment/surveillance plays

important role before determining the receiver value in the MBA1. Near Real Time Accountancy (NRTA) is not applied to the MBA1.

MBA2 consists of an Oxide Reduction process (OR) cell, an Electro Recovery (ER) cell, a Waste Treatment (WT) cell, and Analytical Laboratory (AL). Most of the material form in the MBA2 is bulk. The NRTA is applied to the OR cell, the ER cell, and WT cell, but the NRTA is not applied to the AL.

The MBA3 consists of a Fuel Slug Fabrication/Fuel rod Welding Process (FF) cell and Fuel Assembly Fabrication (FA) cell. The input material of the MBA3 are the U/TRU product, and the U product, and the output material of the MBBA3 are the fuel assembly. Process materials in the FF cell are contained in a container, on which an ID is attached. The NRTA is only applied to the FF cell, and the NRTA is not applied to the FA cell.

MBA4 consists of a fuel assembly storage, and a U product & waste storage. The input material of the MBA4 is fuel assembly, U product and waste form. They can be shipped to outside facility. The material form in the MBA4 is item, and the MUF is not evaluated in the MBA4. The NRTA is not applied to the MBA4.

Physical Inventory Verification (PIV) is carried out once per year. Facility operators should arrange the process plan to complete the last campaign prior to the PIT. The Interim Inventory Verification (IIV) is carried out once a month or every three months, and Short Notice Random Inspection (SNRI) and unannounced inspection can be included. Inventory change verification methods at each FKMP are specified.

Joint use of the operator's DA/NDA system and automatic sampling system are included to the verification methods in the REPF+ safeguards approach.

3. Summary

A safeguards approach of the intermediate-sized pyroprocessing facility is being developed. The safeguards measures in the safeguards approach are based on the current IAEA equipment and the safeguards technology under development. The NRTA is applied to the specified area of the REPF+. The operator's DA/NDA system is jointly used for the verification. The process monitoring and the C/S on the material and equipment transfer door are included to increase the effectiveness.

Our effort will help the effective and efficient safeguards implementation in future pyroprocessing facility.

ACKNOWLEDGEMENT

This work was supported by a National Research Foundation of Korea (NRF) grant funded by the Korean government's Ministry of Science and ICT (MSIT) (No. NRF-2017M2A8A5015084).

REFERENCES

- [1] IAEA Safeguards Glossary 2001 Edition.

A Study on the Safeguards of Nuclear Facility During Whole-life

Sung Ho Lee*, In Chul Kim, Byung Doo Lee, Hyun Jo Kim, Hyun Sook Kim, and Juang Jung

Korea Atomic Energy Research Institute, 111, Daedeok-daero 989beon-gil, Yuseong-gu, Daejeon, Republic of Korea

shlee10@kaeri.re.kr

1. Introduction

Generally, a nuclear facility is built and operated through plan stage, construction stage, operation stage, and dismantling stage. Safeguards activities should be carried out from plan stage to dismantling stage. After dismantling stage, IAEA informs that the dismantled facility will be excluded from safeguards.

In the safeguards aspect, the status of facility function and nuclear material is the most important components. Recent issues in domestic nuclear fields are related to the decommissioning and dismantling of nuclear facilities. But safeguards activities during dismantling stage are only a part of safeguards during whole-life of facility.

In this paper, safeguards implementation activities under legal basis are investigated during the whole-life of nuclear facility including the decommissioning and dismantling stage.

2. Legal aspects of Safeguards

Originally safeguards concept was initiated from NPT and established from IAEA, hence safeguards should be implemented to meet the requirements of IAEA safeguards.

In the international legal aspects, ROK(Republic of Korea) should implement safeguards under the Agreement between ROK and IAEA for the Application of Safeguards and Additional Protocol.

In the domestic legal aspects, safeguards

obligations are regulated on the law of nuclear safety and security. Basically most of safeguards in the law is to support the implementation of IAEA safeguards practically. Therefore, the main stream related to the decommissioning and dismantling is almost the same to IAEA safeguards.

3. Whole-life Safeguards

3.1 Planed Stage

According to the need on nuclear facility, government/organization makes a plan to construct a nuclear facility including cost, location, and others. From the planed stage, safeguards obligations occur as follows;

First, Preliminary Design Information should be provided to IAEA based on the authorization /decision of construction.

Second, Further Design Information should be provided to IAEA based on the developed design.

Third, completed DIQ should be provided to IAEA based on the preliminary construction plans.

Fourth, completed DIQ should be provided to IAEA based on "as built" design.

Because of no nuclear material during the planed stage in facility, actual nuclear material accounting is not necessary.

3.2 Operation Stage

Main content of the Agreement between ROK and IAEA is to confirm that there is no undeclared nuclear material as well as nuclear activity. For this, safeguards activities should be implemented as follows;

First, DIQ(Design Information Questionnaire) including information on nuclear material and facility should be updated and provided to IAEA.

Second, NMCR(Nuclear Material Accounting Reports such as ICR, PIL and MBR) should be provided to IAEA monthly.

Third, based on the DIQ and NNCR, IAEA inspection is carried out for the confirmation of facility declaration that facility activity is described in the DIQ and nuclear materials are kept in the declared location.

Fourth, except for the illegal activity and nuclear material, unexpected cases happening during the operation of facility should be solved based on the discussion with IAEA.

3.3 Decommissioning & dismantling Stage

There is normal procedure for the decommissioning and dismantling as follows;

First, nuclear material kept in the MBA should be removed. For example, spent fuel should be moved to other MBAs.

Second, DIQ for decommissioning and dismantling should be provided to IAEA step by step. Normally DIQ includes the decommissioning and dismantling schedule.

3.4 Termination from Safeguards

Based on the DIQ for the decommissioning and dismantling from facility, IAEA decides to terminate the nuclear facility from safeguards after the review

on remained nuclear material in the MBA, possibility on the reoperation, facility declared information, and others. Especially, facility side should be careful not to find nuclear material later.

4. Results

Overall safeguards activities were reviewed to be carried out during whole-life of nuclear facility. This study is applicable to most of nuclear facilities such as reactors, fuel fabrication plant, and others. Though some kind of facilities can be discussed with IAEA additionally, the above explained safeguards activities should be carried out in the legal basis.

Above all, before the safeguards termination of the facility, it is the most important to make no nuclear material state in the facility.

REFERENCES

- [1] “Agreement between ROK and IAEA for the Application of Safeguards in connection with the treaty on the non-proliferation of nuclear weapons, Oct. 31, 1975.
- [2] “The Law of Nuclear Safety and Security”, Jun. 20, 2018.

Research on the Applications of Computer Security Zone for Vital Digital Assets

Yeeun Byun*, Inkyung Kim, and Kookhei Kwon

Korea Institute of Nuclear Nonproliferation and Control, 1534, Yuseongdae-ro, Yuseong-gu, Daejeon, Republic of Korea

*hibye@kinac.re.kr

1. Introduction

As cyber threats to nuclear facilities are increasing, cyber security for nuclear facilities are getting strengthened at home and abroad. In R.O.K, Korea Institute of Nuclear Nonproliferation and Control (KINAC) regulate nuclear facilities to strengthen cyber security. In this paper, after introducing concepts of critical digital assets (CDA) which are current object of regulation, vital digital assets (VDA) and zone, we discuss how the concept of zone could be applied when prepare a scheme for regulating VDA.

2. Concepts of Vital Digital Assets

2.1 Critical Digital Assets

According to Regulatory Standard “Security for Computer and Information System of Nuclear Facilities(KINAC/RS-015)”[1], licensees should identify CDA which performs or are relied upon for SSEP functions (Safety-related and Important-to-Safety, Security, Emergency Preparedness)

2.2 Vital Digital Assets

This concept is defined in the research and development and this covers digital assets that could cause nuclear accidents through failure to mitigate after initiating event.

3. Applications of Zone for preparing a scheme for regulating VDA

In this section, we will show the concepts of computer security zone stated in technical guidance of IAEA and how this could be applied for this research and developments.

3.1 Concept of Computer Security Zone

According to Technical Guidance “Computer Security of Instrumentation and Control Systems at Nuclear Facilities”[2], the security zone concept covers the logical and/or physical grouping of computer based systems that share common security requirements.

In the Draft Technical Guidance “Computer Security Techniques for Nuclear Facilities”[3], the application examples are introduced as below, and this application model could be applied differently depending on the situation of nuclear facilities.

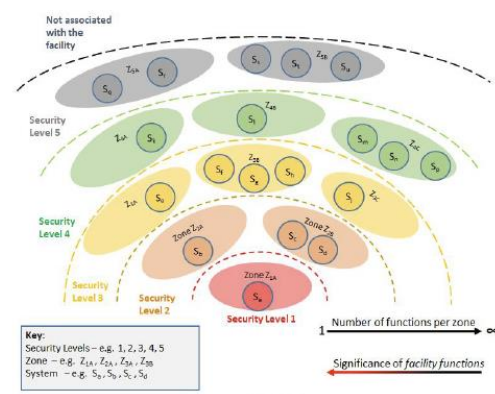


Fig. 1. Application Model of Computer Security Zone.

3.2 Applications of Computer Security Zone for VDA

Currently, the concept of computer security zone is not applied to the domestic regulation system and for the defense-in-depth the concept of computer security level is applied. In order to prepare a scheme for regulating VDA, a model applying the concept of computer security zone was developed.

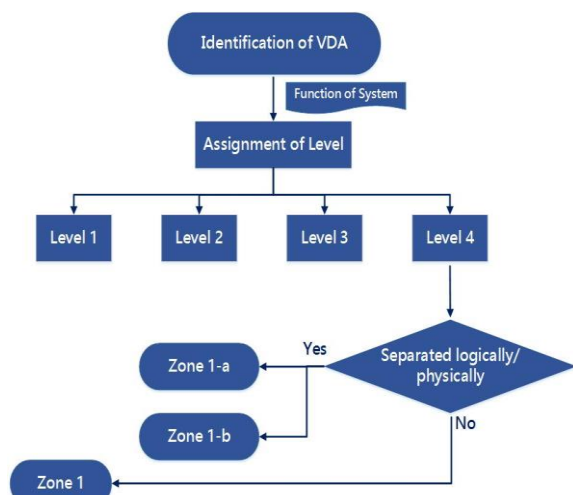


Fig. 2. Model for prepare a scheme for regulating VDA.

After identifying VDA, computer security levels could be assigned as function of each systems and suppose some system is assigned level 4 (more important than level 1). Then whether it is separated logically/physically could assign computer security zone. If it is separated, the zone would be separated even they have same level, and if not, they would be assigned same zone.

4. Conclusion

There are many things to consider when develop a model to apply the concept of computer security zone, such as boundary of zone or internal communication. Now that we have identified VDA, we have only considered what model could be applied to prepare a scheme for regulating VDA. In addition, there may

be other ways to develop a scheme, and further research will be needed. Through such research, it can be said that it will be effective in the regulation of CDA.

ACKNOWLEDGEMENT

This work was supported by the Nuclear Safety Research Program through the Korea Foundation Of Nuclear Safety (KoFONS), using the financial granted by the Nuclear Safety and Security Commission (NSSC), Republic of Korea. (No. 1605007)

REFERENCES

- [1] KINAC, "Regulatory Standard – Security for Computer and Information System of Nuclear Facilities", 2015.
- [2] IAEA, "Computer Security of Instrumentation and Control Systems at Nuclear Facilities-Technical Guidance", IAEA Nuclear Security Series No. 33-T, 2018.
- [3] IAEA, "Computer Security Techniques for Nuclear Facilities-Draft Technical Guidance", IAEA Nuclear Security Series, 2017.

1분과

핵주기정책 및 핵비확산 (Poster)



A Conceptual Design of the Information Analysis System for Searching Nuclear Fuel Cycle Related R&D Projects

Sung-ho Yoon and Dong-hoon Shin*

Korea Institute of Nuclear Nonproliferation and Control, 1534, Yuseong-daero, Yuseong-gu, Daejeon, Republic of Korea

*nucleo@kinac.re.kr

1. Introduction

Korea has concluded an additional protocol with the IAEA in 2004. In a part of additional protocol, information of nuclear fuel cycle related R&D projects supported by governmental funding should be reported to the IAEA. However, reports for some projects have been missed and IAEA occasionally found those missing by their information analysis system. This situation can cause distrust of the national transparency for nuclear nonproliferation. Therefore, we developed the system construction plan which can reduce some problems such as the report missing. This paper presents the result of the concept design as the first step of System development such as overall system structure, data collection and classification direction, post processing, and so on.

2. Related researches

There are lots of document categorization systems using computing based algorithm including machine learning. In the past, the majority of systems use the term-based classification method due to simple and powerful performance. But in recent, increasing computing power and processed big-data allow to develop real-time based adaptive method [1]. Our conceptual design is composed of previous methods and some of specialized functions to nuclear part.

3. Conceptual design

3.1 Overall system structure

The proposed system consists of four steps as

shown in Fig. 1 including data collection, pre-processing, classification, and post-processing.

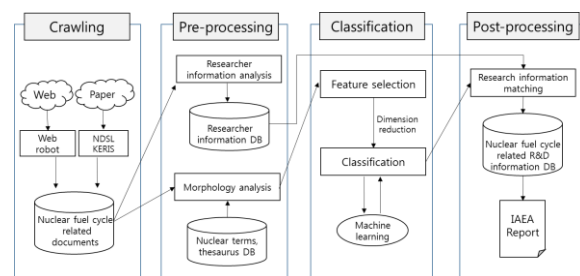


Fig. 1. Overall system diagram.

3.2 Data collection

At this stage, public research data (papers, project reports, technical reports, etc.) are collected from the open source such as website. In order to selectively collect data for nuclear fuel cycle, we use web-robot provided by search engines such as Naver or Google based on a pre-configured URL and a set of search keywords to automatically collect public information. For most papers that are not provided or published on the web, we will develop meta-search engine indirectly connected to the NDSL, DBPia, and so on.

3.3 Pre-processing

Most of the collected information will be in the form of a paper. Since the paper has a standardized format, at this stage, meaningful information such as title, author information (name, affiliation, e-mail address, etc.) and journal name can be acquired. In addition, only the title or abstract part containing the main contents of the paper can be set to the domain.

In the following, tags and abbreviations are removed and nouns necessary for feature selection

are extracted through morphological analysis.

3.4 Classification

Automatic document classification is roughly divided into two processes. The first is a feature selection process for converting initial data composed of a set of words to input data for machine learning. The second is a process for adjusting document classifier to target document group by conducting machine learning. Therefore, feature selection and machine learning algorithms are important for improving system performance.

3.4.1 Feature selection. If all the words are used as feature, it is difficult to conduct machine learning due to limited computing resource. Therefore, it is important to select the appropriate words that can reflect the characteristics of the document. There are several commonly used feature selection method such as Boolean weighting, TF/IDF, Information gain, Mutual information, etc.

3.4.2 Machine learning algorithm. There are several machine learning algorithms such as decision tree, artificial neural network, Bayesian network, genetic algorithm, etc. For this system, it is important to determine whether it is object or not. SVM (Support Vector Machines) [2] is an algorithm to select the most optimal hyperplane in the two-dimensional data classification problem as the decision boundary, therefore it seems that SVM meets the system purpose to distinguish between documents related to nuclear fuel cycle research and those that are not.

3.5 Post-processing

At this stage, the documents related to the classified nuclear fuel cycle are matched with the information of the researchers acquired in the pre-processing step and are automatically generated as a database and IAEA report.

4. Conclusion

In this study, a conceptual design was developed to construct a system that automatically classifies documents with a specific topic, nuclear fuel cycle research, from unspecific public document data.

There are several things to consider when constructing an actual system. First, the limitation of web robots for crawling public data. Recently, web robots are often blocked on internet search sites. Second, the difficulty of collecting and analyzing unstructured documents on the web. Because web documents are not formatted, character recognition and domain setting are difficult. Third, the optimization of machine learning algorithm. To customize algorithm to system a lot of training set are needed.

ACKNOWLEDGEMENT

This work was supported by the Nuclear Safety Research Program through the Korea Foundation Of Nuclear Safety(KoFONS) using the financial resource granted by the Nuclear Safety and Security Commission(NSSC) of the Republic of Korea. (No. 1803021)

REFERENCES

- [1] W.H. Lee, S.J. Chung, and D.U. An, "Harmful Document Classification Using the Harmful Word Filtering and SVM", Journal of Korea Information Processing Society, 1(16), 85-92 (2009).
- [2] T. Joachims, "Text categorization with support vector machines: learning with many relevant features", Proceedings of ECML-98, 10th European Conference on Machine Learning, 137-142 (1998).

Legal Case Study About the Lawsuit to the Korea government's 8th Basic Plan for Electricity Supply and Demand

Daesung Lee* and Jaeyoung Bang

Korea Atomic Energy Research Institute, 111, Daedeok-daero 989beon-gil, Yuseong-gu, Daejeon, Republic of Korea

*dslee@kaeri.re.kr

1. Introduction

Since the 2011 Fukushima nuclear accident and the 2016 Kyongju earthquake, domestic concern for nuclear power has grown rapidly and demands for nuclear safety have come to the fore. As a result, the current government has announced the eighth basic plan for power supply in 2017, which has a lot of radical changes. This has led to disagreements among related stakeholders, leading to legal disputes.

In this study, we will review the basic outline of the Eighth Basic Plan for Electricity Supply and Demand, and analyze main legal issues of administrative revocation lawsuit against the Korea government for cancelling the Plan.

2. Eighth Basic Plan and Administrative Lawsuit

2.1 Eighth Basic Plan for Electricity Supply and Demand

In December 2017, the Ministry of Commerce, Industry and Energy has announced the eighth basic plan for power supply and demand. Reflecting the energy conversion road map, which is the basic direction of the current government energy policy, to reduce the number of nuclear power plants gradually and to expand renewable energy to 20% of the generation capacity by 2030, the project will focus on the early abolition of coal power generation and LNG conversion. Among them, the main issues that the plaintiffs of the lawsuit are having trouble with are related to nuclear power plants plans: first, the cancellation of six new nuclear power plants construction; second, the suspension of life extension of 10 old nuclear power plants; third, the early closure of Wolsong 1, which takes into account power supply and demand. As of 2017, the government plans to reduce the total number of

nuclear power plants from 24, 22.5 GW by 2030 to 18, 20.4 GW.

2.2 Revocation lawsuit of the Eighth Basic Plan for Electricity Supply and Demand

In January 2018, the plaintiffs, comprised of 216 persons, including civilian and environmental group representatives from nuclear-related regions, nuclear-related labor unions such as nuclear suppliers, nuclear equipment manufacturers, and nuclear radiation safety management service companies has filed a lawsuit against the Korea government for cancelling the Eighth Basic Plan for Electricity Supply and Demand. Plaintiffs argued that the Plan had a direct and detrimental effect on the rights of the plaintiffs in the lawsuit.

2.2.1 Issue1. Disposability of Basic Plan for Electricity Supply and Demand. The first major issue is whether the Plan has an administrative disposition power or not. The ultimate purpose of administrative litigation lies in the relief of the people's rights from administrative acts. In the case of an administrative litigation, the revocation lawsuit, is subject to "disposition, etc.", and "disposition" means the act or exercise of public power as a law enforcement on concrete facts performed by the administrative office, it means reconciliation. Therefore, it should be recognized that the Plan has a "nature as an administrative disposition" in order to be relieved through a lawsuit of revocation.

From that point, the plaintiffs claim that the plan has an administrative disposition power because the plan will dominate government's nuclear power plant project and damage to the plaintiffs' interest. So the Plan shall be the object of this lawsuit. By the way, the government is in the position that the plan is only a sketch of future energy mix. It does not have a disposability power. This lawsuit should be dismissed.

2.2.2 Issue2. Plaintiffs' Legal Eligibility (Status).

The second major issue is the eligibility (status) of plaintiffs. Plaintiff eligibility means that only a person who is violated or damaged by law by the administrative act seeks the profit or cancelling the government's action under administrative lawsuit. If a Plaintiff is only a bystander or has an indirect relationship with the government's action, the Plaintiff shall not be considered as an eligible plaintiff of lawsuit and the lawsuit shall be dismissed.

The plaintiffs claim that this plan will undermine the concrete and direct economic benefits of the plaintiffs. Defendant, the Korea government, counter argues that the claims is about collateral and superficial damages, not the direct and specific victims' damage. Thus this lawsuit should be dismissed.

2.2.3 Issue3. Consistency with Energy Basic Plan. The third major issue is a consistency with the Energy Basic Plan. In January 2014, the Ministry of Commerce, Industry and Energy announced the Second Energy Basic Plan. The plaintiffs believe that this is the highest plan of the energy sector and that all fields of the energy sector are systematically linked to and coordinated with other energy-related schemes, so that the philosophy and basic principles of Energy Basic Plan shall govern the 8th basic plan as highest and earlier plan. In detail, the Energy Basic Plan covers the expansion of the proportion of nuclear power by 2935 to 43 GW by 2035, while the 8th basic plan for power supply is from 20.5 GW to 20.4 GW by 2030. There is an undue discrepancy between the two plans.

Thus, the plaintiffs argue that this supply and demand plan is very different from the basic energy plan, so that even basic rationality is not available and should be cancelled. Government's counter argue is that plan is just a plan for future, so government has a very large autonomous authority for administrative planning.

2.2.4 Issue4. Abuse of Discretionary Authority. The last major issue is an abuse of Discretionary Authority. The plaintiffs argue that current government planning process is only based on the president's pledge. There is no clear and firm process for hearing people's opinion before proceeding the

Plan. This is an act of defection beyond a government discretion. In the case of Switzerland, the national opinion was collected through a referendum five times prior to the nuclear power plant, and in Germany, after 20 years of discussions, the legislative process was applied for nuclear power plants. However, it is said that the sudden change comparing with the 7th power supply and demand plan to rapidly reduce the size of nuclear power in the 8th plan is that government abuse its' the discretion.

Thus the plaintiffs asserted that the plan is an outcome of the administrative act of abandonment of discretionary rights, so it should be canceled as a defective administrative act, although the government insist that it has a very diverse discretionary scope in the administrative plan and the plan is under a legitimate procedure and law.

3. Conclusion

In the future, the court will closely examine whether the plan has the disposition power to be the object of the administrative litigation and whether the plaintiffs are qualified as specific and direct victims of the plan. This lawsuit shall be a very meaningful legal case in the fields of legal academy and nuclear industry.

REFERENCES

- [1] Park Kyunsung, "Public Administrative Law", Parkyoung-sa, 2014.
- [2] Korea Electricity Paper webpage, <http://www.electimes.com/article.php?aid=1527642514158450003>, searched on September 1, 2018.

The Education and Training Activities and Future Challenges of INSA in ROK

Jin Young Lee*

Korea Institute of Nuclear Non-Proliferation and Control, 1534, Yuseong-daero, Yuseong-gu, Daejeon, Republic of Korea

*jylee86@kinac.re.kr

1. Introduction

Domestic safeguards implementation activities of ROK are implemented based on the Nuclear Safety Act. It emphasize the importance of education and training with respect to nuclear non-proliferation. ROK has used education and training activities as an important means to strengthen international nuclear non-proliferation regime and cooperate with the international community and implement domestic safeguards activities effectively. With the establishment of International Nuclear Non-proliferation and Security Academy (INSA), ROK started an international and domestic education and training regarding nuclear non-proliferation in earnest.

2. ESTABLISHMENT OF INSA, AND ITS MISSION

On the occasion of the first Nuclear Security Summit (NSS) in 2010, ROK pledged to contribute to the international community through the establishment of "Center of Excellence (COE)", which was established in 2014 under KINAC, named INSA.

INSA has strength in its capabilities of conducting education and training activities due to being capable of utilizing experienced national safeguards inspector as instructor.

INSA organized an education and training

program to support the establishment and reinforcement of safeguards system in newcomer countries and strengthening of domestic safeguards system in Korea. In particular, it is based on systemic approach to training (SAT) which is composed of five elements such as analysis, design, development, implementation, and evaluation (ADDIE) [1,2].

3. INTERNATIONAL AND DOMESTIC TRAINING COURSE OF INSA

INSA has international and domestic education and training program regarding nuclear non-proliferation.

Firstly, INSA has two kinds of program; INSA-initiated course and INSA-IAEA International/Regional Training Course (ITC/RTC).

INSA-initiated course have been developed in cooperation with Department of Energy (DOE) / National Nuclear Security Administration (NNSA) of U.S.A. and IAEA; Fundamentals of Nuclear Safeguards (Introductory, 5 days); Provision of Safeguards Information to the IAEA (Specialized, 5 days); Strengthening State Safeguards Regulatory Authority (Specialized, 5 days).

With close cooperation between ROK and IAEA, the first INSA-IAEA RTC was held from 6-17 October in 2014 which was titled "Regional Training Course on State System of Accounting for and Control of Nuclear Material (SSAC)". It is mainly targeted to Small Quantities Protocols (SQP)

countries and not only IAEA experts but also KINAC and other domestic experts were participated in the lectures. It became significant corner stone for close and strong cooperation between INSA and IAEA in order to enhance international nuclear non-proliferation regime especially for the countries which wish to start nuclear energy program.

Secondly, INSA has domestic course such as nuclear non-proliferation course for facility operators and project managers on nuclear fuel cycle research, nuclear safeguards inspector course, and awareness program. Nuclear non-proliferation course for facility operators and project managers on nuclear fuel cycle research and nuclear safeguards inspector course are legally mandated, which are based on Nuclear Safety Act.

Regarding awareness program which is not legally mandated, INSA tried to expand it for the strengthening of a nuclear non-proliferation culture of the public [3].

4. Conclusion

Recently, INSA has developed Substitutional Reality (SR) based Field Training Exercise (FTX) for physical protection training programs by using virtual reality (VR) technology. It might be modified and could help to provide very realistic situation-based safeguards training exercise as if trainee visited real site. This will help overcome constraints for education and training such as safety and cost, and maximize trainee's immersion in the training [4].

INSA also need to consider preparing tailored program with IAEA for full nuclear fuel cycle of next generation reactor such as sodium-cooled fast reactor (SFR), high temperature gas reactor (HTGR).

For strengthening INSA's HRD capacities, even though INSA has experienced experts as instructor who are in charge of safeguards implementation on

site, still INSA is required to have more excellent faculty in terms of having good foreign language ability and availability. Recently INSA has supplemented four full-time professors.

Finally, INSA will keep accomplishing its original mission to strengthen international nuclear non-proliferation regime by providing international and domestic education and training with active utilization of new technology. INSA will keep its sustainability by means of two measures; development tailored education and training program for newcomer countries; enhancing INSA's outreach program, which result in not only strengthen international nuclear non-proliferation regime but also continuously contribute to international society.

REFERENCES

- [1] INTERNATIONAL ATOMIC ENERGY AGENCY, "Experience in the Use of Systematic Approach to Training (SAT) for Nuclear Power Plant Personnel", IAEA-TECDOC-1057, IAEA, Vienna (1999).
- [2] INTERNATIONAL ATOMIC ENERGY AGENCY, "Establishing a National Nuclear Security Support Centre", IAEA-TECDOC-1734, IAEA, Vienna (2014).
- [3] Choe, Kwan Kyoo, "International Relations and HRD Activities of the International Nuclear Nonproliferation and Security Academy of the ROK," International Journal of Nuclear Security: Vol. 1: No. 1, Article 9, (2015).
- [4] Kim, Jongsook; Lee, Hyung-kyung; and Lee, Jin-young, "Challenges and Responses for Ensuring Sustainability of INSA Training Programs," International Journal of Nuclear Security: Vol. 2: No. 1, Article 16, (2016).

Analysis of Regulatory Technology Support Status Using Milestone Approach for Supporting Establishment of National Safeguards Systems in the Middle East Region

Jin Young Lee*

Korea Institute of Nuclear Non-Proliferation and Control, 1534, Yuseong-daero, Yuseong-gu, Daejeon, Republic of Korea

*jylee86@kinac.re.kr

1. Introduction

Recently, Saudi Arabia addressed their willingness to develop nuclear weapons under certain condition, which have been heightened tensions regarding nuclear proliferation over the of the Middle East region. As a result, bilateral cooperation for establishing national safeguards system of the states which are willing to build nuclear power plants has become significantly important ever before in terms of setting preventing mechanism of nuclear proliferation in the Middle East. This paper will describe the results of analysis of regulatory technology support status using milestone approach for supporting establishment of national safeguards systems in the Middle East Region.

2. The Detailed Analysis of Safeguards-Related Needs through a Milestone Approach to Establishment of National Safeguards System

From early November 2010 to November 2017, the regulatory technology support activities, largely within the framework of the Technical Meeting and the Annual Meeting, to the UAE for establishing national nuclear safeguards system were conducted by ROK as follows.

Table 1. Specific Items of Regulatory technology support [3]

No	Items
1	Establishing process of SSAC
2	National inspection
3	Education and Training
	Safeguards Implementation of ROK
	- Legal framework
	- Cooperation system with IAEA
	- Experience on reporting to IAEA
4	- Experience on reporting to IAEA by mailbox
	- Experience on unannounced inspection (UI)
	- ROK National LOF Web Management System
	- Experience on reviewing documents and inspection

For providing more systematic support to the beneficiary countries, the analysis was conducted by using the tool named milestone approach [1, 2]. The results of mapping the existing infrastructure milestones in the areas of safeguards regulatory technology with the existing demand from the Middle East countries are as follows:

In the early stages (Milestone 1) of the UAE, Saudi Arabia, and Jordan, three countries also asked for regulatory technology in connection with the establishment of legal framework and regulatory body. In most cases, regulatory technology support will be tailored to identify the needs of the beneficiary countries. In the case of Saudi Arabia, they already prepared legislation proposal to the government in assistance with technical cooperation with other agencies such as STUK in Finland. In this case, ROK would rather provide technical support

regarding making regulatory implementation guides for safeguards inspection.

In addition, in early cooperation, it is the most important issue to let beneficiary countries recognize the necessity of the obligation demanded by international community. For example, if beneficiary countries signed CSA with IAEA under the NPT, the country is obliged to establish SSAC.

Analysis of existing regulatory technology support cases indicates that the beneficiary countries mainly focused on establishing their legal system, regulatory framework and sharing implementation status and procedure. In this regard, beneficiary countries will be more satisfied if the right regulatory technology is provided by following milestone and conducting needs survey to the beneficiary countries.

The UAE completed an agreement for commercial reactor in 2009, for Jordan signed agreement for research reactor in 2009, for commercial reactor in 2013.

In the case of UAE, the operation of the first BARAKAH nuclear plant is imminent, while in Saudi Arabia, the site selection process for smart nuclear power plants is still underway. Jordan also has a plan to operate the first nuclear power plant around 2021. Therefore, this three-stage milestone will need to be applied to the UAE.

In 2017, the international transportation of nuclear fresh fuel for Barakah NPP was carried out, and the recent agenda of the Technical Meeting and Annual Meeting with UAE/FANR, regulatory infrastructure such as the establishment of the legal framework and SSAC has been remarkably improved.

In addition, the UAE is eager to share their experience and support regulatory technology to its neighbor countries in the Middle East. It is a very desirable model in terms of not only strengthening international nuclear non-proliferation regime but also UAE provide their own experience to other

countries, especially neighbor countries in the Middle East, which will solidify nuclear non-proliferation regime in the region.

3. Conclusion

ROK should continue to play an important role in strengthening international nuclear non-proliferation regime with interest in countries that want to introduce nuclear power programs such as Saudi Arabia in the Middle East region. Starting with Belarus, Turkey, Lithuania, Bangladesh, Jordan, Poland, Egypt, Bahrain and Yemen are actively considering introducing nuclear power program, which could be biggest threat and challenge to international society. The milestone approach will be used as very useful tool for analyzing national status of readiness and delivering regulatory technology to these countries for establishing national safeguards system, which result in facilitating peaceful use of nuclear energy.

REFERENCES

- [1] JIN YOUNG LEE, "Support Strategy of Nuclear Regulation Technology for Newcomer Countries", KINAC, (2017).
- [2] INTERNATIONAL ATOMIC ENERGY AGENCY, "Milestones in the Development of a National Infrastructure for Nuclear Power", IAEA Nuclear Energy Series No. NG-G-3.1 (Rev. 1), IAEA, Vienna (2015).
- [3] CHAN-SUH LEE, "A Study on a Direction of Development of Export Control in ROK through analyzing export of UAE BNPP and cooperation between ROK-UAE", KINAC, (2014).

A Study on the Nuclear Nonproliferation Obligations of Nuclear Fuel Cycle Research Activities Funded by the Government

Seunghyo Yang, Sangjun Lee, and Donghoon Shin*

Korea Institute of Nuclear Nonproliferation and Control, 1534, Yuseong-daero, Yuseong-gu, Daejeon, Republic of Korea

*nucleo@kinac.re.kr

1. Introduction

Recently, international community pays close attention to the nuclear fuel cycle research activities and IAEA also observes carefully those unreported activities of the respective member countries.

Korea has signed the full safeguards agreement and additional protocols to comply with the international nuclear nonproliferation regime. However, the difficulty lies for researchers in obeying international nuclear nonproliferation obligation due to current domestic legal system.

In this paper, nuclear nonproliferation obligations reflected to domestic laws will be reviewed and troubles and improvements for researchers to implement those duties when they conduct national R&D projects associated nuclear fuel cycle will be discussed.

2. Analysis of domestic laws

2.1 Nuclear Safety Act

Article 98 of the Nuclear Safety Act [1] stipulates the duty to report information for nuclear fuel cycle research activities funded by the government. It includes the specific report subject, the content of the research, procedures, outputs, the deadline and etc.

However, there is high probability for researchers to violate reporting obligations because there is no separate procedures to ensure that their national R&D projects are related to the nuclear fuel cycle. Therefore, they must determine the need for reporting by themselves. Furthermore, if researchers

use special nuclear materials, State Systems of Accounting for and Control of Nuclear Materials (SSAC) substitutes for the obligation to report research activities. Researchers should be well aware of these legal systems to fulfill their reporting duties.

In order to include researchers studying nuclear fuel cycle in the international nuclear nonproliferation regime, it is necessary to extensively inform the nuclear nonproliferation obligations by active outreach activities such as holding briefing session and distributing brochures containing related subjects.

2.2 Foreign Trade Act

Korea has implemented strategic export control under NSG Export Control Guidelines and Foreign Trade Act [2] since Korea joined NSG in 1995. In order to export nuclear-related materials, equipment and facilities corresponding to strategic items, it is necessary to obtain the export license from the Nuclear Safety and Security Commission.

The revised Foreign Trade Act in 2015 put the intangible transfer of technology under strategic export control regime and it is required to acquire an export permit to provide education and training program for foreigners in Korea.

In case of participation of foreigners in national R&D projects associated with strategic technologies, it is highly possible to occur intangible transfer of technology. Hence, foreign students and researchers conducting national R&D projects related to strategic technologies should obtain export permits in advance

not to violate the Foreign Trade Act.

The Foreign Trade Act prescribes to obtain an export permit if research results are corresponding to strategic items and they are transferred to out of a country. Research results would be various form like equipment, technical data, design drawings, patents, and so on. Although the criteria for strategic items are stipulated at Table 2 in the Strategic Items Import and Export Notice, there is difficulty for researchers to determine whether their research result are relevant with strategic items.

Hence, it is strongly recommended for researchers to request classification service for their research outputs to specialized government organization, Korea Institute of Nuclear Nonproliferation and Control(KINAC), to ensure whether they need to get an export permit. Consequently, they can reduce the possibility of illegal export.

2.3 Framework Act on Science and Technology

In accordance with the Framework Act on Science and Technology [3], if National R&D projects handle manufacture, development, or use of strategic items, those projects should be designated as security projects. Security projects are required to prepare security measures that prevent to divulge research outcomes outside.

However, the procedure to designate security projects are arbitrary in current legal system because selection reviews of security projects follow non-mandatory provision. According to the Foreign Trade Act and Nuclear Safety Act, national R&D projects can be reviewed for relevance to security projects by Korea Strategic Trade Institute or KINAC only at researchers' request.

Therefore, some national R&D projects related with strategic items are highly likely to be classified as non-security projects, which do not need to prepare security measures, without any review

process. This arbitrary procedure can lead violation of both export permits under Foreign Trade Act and reporting obligations under the Nuclear Safety Act.

In order to remove loopholes in selection of security projects, it is necessary to make the abovementioned procedure to be mandatory obligations.

3. Conclusion

We have discussed nuclear nonproliferation obligations reflected to domestic laws for nuclear fuel cycle research activities funded by government.

It is analyzed that the duties of nuclear nonproliferation are divided into several laws and implementation procedures are not systematic.

In order to enhance the export control regime for nuclear fuel cycle research activities in current legal system, it is essential to strengthen outreach activities and control of intangible transfer of technology. In addition, mandatory procedures for selecting security projects should be established.

ACKNOWLEDGEMENT

This work was supported by the Nuclear Safety Research Program through the Korea Foundation Of Nuclear Safety (KoFONS), granted financial resource from the Nuclear Safety and Security Commission (NSSC), Republic of Korea. (No. 1803021)

REFERENCES

- [1] The National Assembly of the Republic of Korea, "Nuclear Safety Act", Act No. 15281, June.20, 2018.
- [2] The National Assembly of the Republic of Korea, "Foreign Trade Act", Act No. 13838, Jan.27, 2016.
- [3] The National Assembly of the Republic of Korea, "Framework Act on Science and Technology", Act No. 15556, July.18, 2018.

The Present Status and Future Challenges of Nuclear Forensics in ROK

Seung Ho Jeong*, Na Young Lee, Jin Young Lee, Ho Jung Do, and Hana Seo

Korea Institute of Nuclear Nonproliferation and Control, 1534, Yuseong-daero, Yuseong-gu, Daejeon, Korea

*shjeong@kinac.re.kr

1. Introduction

During the nuclear security summit process, we observed the emergence of various new nuclear security areas. Nuclear forensics is one of them. Nuclear forensics is the investigation of nuclear materials to identify the origin and history of radioactive materials out of the regulatory control (MORC). Therefore, it has a strong deterrence effect against illicit trafficking. Many states realized its necessity and joined efforts in international collaboration and research programs.

Analysis of nuclear materials is an important measure in the field of nuclear safeguards and has been developed so far. In the case of the ROK, we established nuclear materials analysis systems which can be adopted in nuclear forensics field. So far, we focused more on the technical aspect of nuclear forensics such as analytical techniques and establishment of the national nuclear forensic library (NNFL). For an effective implementation of the nuclear forensics, however, it needs to be bridged with the national response system.

In this paper, we will review what have been done and what needs to be done in view of the NNFL developer in ROK.

2. Evolution of nuclear forensics

In December 1991, the Soviet Union collapsed and was divided into several independent states while nuclear weapons and facilities were located outside

of the Russian Federation. At the time, illegal nuclear materials were found in the European countries. Even though the nuclear materials were recovered, it was difficult to identify whether it was weapon grade or where it was from and so on. Therefore, these materials were sent to the Institute for Transuranium Elements (ITU) in Germany, which was the only laboratory that could do the job at the time of the seizures [1]. That became the first nuclear forensics activity. Then, nuclear forensics arose in response to various seizures of HEU and plutonium cases.

3. Nuclear forensic system in ROK

The NNFL in ROK was developed by KINAC, and KINAC classified the nuclear forensics into 4-tier system [2]. 4-tier system consists of 1) Legal basis, 2) radiological crime scene management, 3) nuclear forensics library and 4) analysis. Legal system means law enforcement against nuclear terrorism. Response has two complementary tiers. Radiological crime scene management includes the sampling of radiological nuclear materials as well as collection of other traditional forensic evidence. The NNFL is a database containing broad categories of information to identify and verify analysis results. Analysis is the base tier supported by technical capability and is essential in finding signatures. In the paper, it listed action items for each tier and evaluated the current nuclear forensics development and implementation status. Legal framework was established before the 3rd nuclear security summit.

Articles of International Convention on Suppression of the Act of Nuclear Terrorism(ICSANT) and amendment to the Convention on the Physical Protection of the Nuclear Material(CPPNM) were reflected in the domestic law.

Regarding the radiological crime scene management, we had already set up the procedure for collecting evidence and developed equipment.

Analysis parts and establishment of NNFL also showed rapid progress thanks to the nuclear security summit process.

Most of these efforts have been done in piecewise. Now we need more effort in putting the puzzle together. It means that we need interfaces between relevant tiers. According to the ICSANT, we already established the national law to set penalty for criminal offences, however, in case of such event, response procedure includes responsible organization and role. We need to include nuclear forensics in the national response plan to support investigations. Even though we have analytical capabilities, if the investigation team does not react or contact to the technical counterpart, technical capability cannot be used in timely manner. It needs to be simulated through exercise.

The US, a strong supporter in the field of nuclear forensics, actively encourages and supports the programs to boost the ROK's nuclear forensics capabilities. It includes exercises of incident responses where all the relevant personnel in various fields participate. This is partly because of the geopolitical circumstances we face now. We need to take full advantage of these environments to establish national response system and implementation plan.

In case of NNFL, we have a database of representative samples from nuclear fuel manufacturer. It is essential to establish nuclear forensic database through data compilation to support nuclear forensic interpretation. But, we have not yet specified in law on the responsibility to submit

nuclear materials data for the NNFL. Therefore, our NNFL is insufficient.

We have the ability to analyze the signatures of the nuclear materials which is essential to the nuclear forensics, but we still need traditional forensic evidence. So, we should refine the procedure in the scene and establish cooperation system to analyze the combined evidence both from nuclear and traditional forensics. Regarding the analysis capability, we can do better once we set up the proper and timely procedures.

4. Conclusion

The newly issued Coordinated Research Project proposed by the IAEA lists technologies that can be used in the scene. To further develop the analysis capability, IAEA suggested using Gamma ray spectrometry to increase speed, accuracy and precision. It also emphasized the necessity to further research to identify signatures. To improve the on-scene response, various sampling and packaging ideas will be reviewed. NNFL needs to be an integrated information system combined with computerized algorithm with strengthened traditional evidence.

The efforts to refine the nuclear forensics system continues through the participation of leading countries. Likewise, we need to continue the efforts which would be the strong deterrence measure of the nuclear security.

REFERENCES

- [1] S. Niemeyer, L.Koch, "The historical evolution of nuclear forensics: A technical viewpoint" International conference on Advances in nuclear forensics, 2014.
- [2] Yujeong Choi et al., "The development of national nuclear forensics capability of ROK", WM, 2018.

System Understanding of Long-term Safeguards for a Closed Repository

Heejae Ju¹⁾, Il Soon Hwang²⁾, and Sungyeol Choi¹⁾*

¹⁾ Korea Advanced Institute of Science and Technology, 291, Daehak-ro, Yuseong-gu, Daejeon, Republic of Korea

²⁾ Seoul National University, 1, Gwanak-ro, Gwanak-gu, Seoul, Republic of Korea

*hiheejae@kaist.ac.kr

1. Introduction

Spent nuclear fuel is a common global challenge. It contains Pu having potential to be misused for nuclear weapons. Unfortunately, the weapon-usable potential of the Pu is enhanced with time because the half-life of fissionable Pu-239 is much longer than that of non-fissionable Pu-238. Also, the self-protection of spent nuclear fuel due to strong gamma radiation disappears rapidly. This fact causes a heated discussion within international domains for long-term safeguards on final disposal, which eventually increases the total costs of nuclear energy.

2. Long-term safeguards requirements

2.1 Utility of SNF as explosives

The quality of Pu in SNF improves over time as the concentration of Pu-239 increases due to its long half-life. In addition, the decay heat and radioactivity of reactor-grade Pu reduces over time so that handling becomes easier. Accordingly, the utility of Pu grows [1]. Mark et. al. concluded that [2]:

- (1) “Reactor-grade plutonium with any level of irradiation is a potentially explosive material”;
- (2) “The need for safeguards to protect against the diversion and misuse of separated plutonium applies essentially equally to all grades of plutonium”.

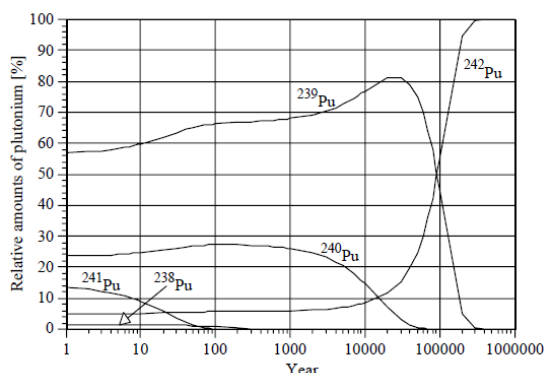


Fig. 1. Isotopic composition of reactor-grade Pu over cooling time [1].

2.2 IAEA safeguards

The safeguards agreement, INFCIRC/153, requires the conditions for the termination time of safeguards in paragraph 11 as follow [3]:

“The Agreement should provide that safeguards shall terminate on nuclear material subject to safeguards thereunder upon determination by the Agency that it has been consumed, or has been diluted in such a way that it is no longer usable for any nuclear activity relevant from the point of view of safeguards, or has become practicably irrecoverable.”

Detailed explanation of the conditions above is stated in the paragraph 35 in the same document:

‘The Agreement should provide that safeguards shall terminate on nuclear material subjective to safeguards thereunder under the conditions set forth in paragraph 11 above. Where the conditions of that paragraph are not met, but the State considers that the recovery of safeguarded nuclear material from residues is not for the time being practicable or desirable, the Agency and the State shall consult on the appropriate safeguards measures to be applied.’

A clear definition of the term ‘practicably irrecoverable’ is absent yet. Nevertheless, the IAEA considers that SNF in a closed repository is the subject to safeguards [4]. Hence, no clear guideline to prove that a recovery of Pu from a closed repository exist.

3. System thinking on the long-term safeguards of a closed repository

3.1 System analysis

Reinforced safeguards system increases detection probability of clandestine human intrusion. Therefore, safeguards efforts have negative effect on intruder’s motivation because reinforced safeguards would increase the cost of intrusion. Because the motivation and intrusion attempt have positive relationship,

negative feedback loop is formed. Accordingly, the diversion risk can be minimized with the low fixed safeguards cost. However, the external constraint, benefit of intruder, shall undermine the negative effect of the feedback loop. The benefit to intruder is expected economic gain to intruder in case of successful intrusion. If the benefit is higher than the intrusion cost increased by reinforced safeguards, the negative effect of safeguards on the motivation would be invalid. Consequently, safeguards cost burden on society would increase.

3.2 Game theory of Pu mine

A problem of clandestine human intrusion can be thought as plutonium mine game. The players participating in plutonium mine game represent two groups including the group of malicious actors who try to procure plutonium and society who try to defend a repository from malicious actor group. For convenience, the group of malicious actors is designated by intruder; and society is designated by safeguards agent. Each player has two strategies. Safeguards agent chooses one of two strategies, either safeguards or no safeguards; and simultaneously intruder chooses one of strategies described in columns, intrude or not intrude.

The preference of decision of each player is determined by the decision of another player. The intruder has incentive to intrude a repository owing to significant value of plutonium. The safeguards agent would like to assure so that intrusion attempt does not exist, but doing so requires cost for safeguards system. If intruder does not try to intrude, the safeguards agent would prefer no safeguards strategy.

4. Results

Simple example model is developed using current available data. The estimated players' strategic decision map is depicted in Fig. 2.

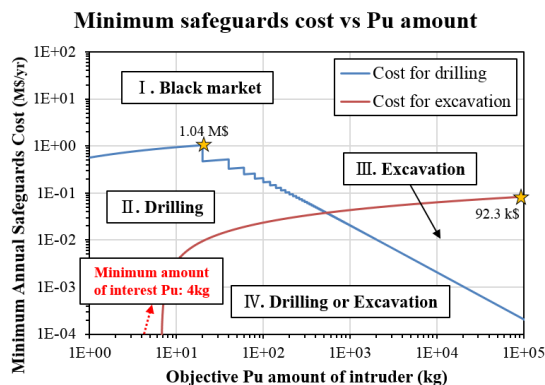


Fig. 2. Minimum safeguards cost by Pu recovery.

5. Conclusion

This paper analyses the costs and benefits of long-term safeguards on final disposal by combining a game theory with a system thinking model. The existing studies only focuses on why safeguards need rather than how to implement. Proliferation scenarios of a closed repository were identified by considering technological innovation in the field of underground mining. Then, strategic interactions between a proliferator and a safeguards agent was defined. A case model showed that the suggested approach can support political decision making of spent nuclear fuel management.

ACKNOWLEDGEMENT

This work was supported by the Nuclear Safety Research Program through the Korea Foundation of Nuclear Safety (KOFONS), granted financial resource from the Nuclear Safety and Security Commission (NSSC), Republic of Korea (Grant No. 1703008).

REFERENCES

- [1] Swahn, J. (1992), "The Long-term Nuclear Explosives Predicament: The Final Disposal of Militarily Usable Fissile Material in Nuclear Waste from Nuclear Power and from the Elimination of Nuclear Weapon", Technical Peace Research Group.
- [2] Mark, J.C., Hippel, F., Lyman, E., "Explosive Properties of Reactor-Grade Plutonium". Science and Global Security, 4, 111-128 (1993).
- [3] IAEA (1972). "The Structure and Contents of Agreements Between the Agency and States Required in Connection with the Treaty on the Non-Proliferation of Nuclear Weapons", INFCIRC/153. IAEA, Vienna.
- [4] IAEA (2010), "Technological Implications of International Safeguards for Geological Disposal of Spent Fuel and Radioactive Waste". IAEA, Vienna.

The Current Status and Prospects of GIF PR&PP and KAERI's Research Activities for Applying PRPPEM

Ji-Song Jeong ^{a),b)}, Ho-Dong Kim ^{a)*}, and Seong-Kyu Ahn ^{a)}

^{a)} Korea Atomic Energy Research Institute, 111, Daedeok-daero 989beon-gil, Yuseong-gu, Daejeon, Republic of Korea

^{b)} University of Science & Technology, 217, Gajeong-ro, Yuseong-gu, Daejeon, Republic of Korea

*khd@kaeri.re.kr

1. Introduction

The Generation IV International Forum (GIF) emphasizes proliferation resistance and physical protection (PR&PP) as one of the main aspects to be considered regarding future nuclear energy systems (NESs). Also, the PRPP Working Group developed an Evaluation Methodology (PRPPEM) which can assess PR&PP characteristics of NESs. It was refined over the years through several case studies. This paper presents the current status of PRPPEM, researches that KAERI has done, and future WG's activities to update them.

2. Current Status of GIF PRPP Evaluation

Methodology

2.1 The Beginning of GIF PRPPWG

Starting in 2002, the Proliferation Resistance and Physical Protection Working Group (PRPPWG) which aims to develop measures for expressing safeguardability of NESs was established by GIF. The group developed a PR&PP Evaluation Methodology (PRPPEM) that was refined over the years through several case studies, such as a hypothetical 'Example Sodium Fast Reactor'. According to the 2002 GIF Roadmap, nine PR&PP R&D areas were identified, including R&D on potential vulnerabilities, safeguards approaches,

protective barriers, material deployed, potential misuse, material protection, accounting and control for each fuel cycle step.

2.2 The current Status of GIF PRPPWG and Interactions with System Steering Committees (SSCs)

In 2007, the PRPPWG and SSCs/pSSCs (provisional SSCs) for each of the six GIF reactor technologies held workshops to discuss about the PRPP characteristics of some system designs and update the PRPP concepts. As a result, a series of internal reports, "White Papers" are published. It reports the six GIF reactor technologies, the main system design options with a mention of the analysts and definition about PR measures. The 2014 GIF Technology Roadmap Update motivated the PRPPWG to assess the progress since the 2011 white paper. By conducting survey with SSCs, in April 2017, the PRPPWG organized a joint workshop in Paris with the participation of representatives of all six SSCs, GIF Senior Industry Advisory Group Panel (SIAP) and IAEA. It gave the opportunity to address some of the comments provided by the SSCs in their reply to the questionnaire, refresh the main aspects of the PRPPEM and of "PR&PP by Design" concept, update the PRPPWG on the evolutions and current status of the six GIF reactor technologies. The update activities are still ongoing and expected to complete the activity in next year.

KAERI has contributed to the development of the proliferation resistance evaluation methodology by taking a leading role in GIF PRPPWG. The PRPP Methodology was applied to evaluate a proliferation resistance for a pyroprocessing facility design. The study identified new metrics and a pathway analysis algorithm based on the GIF PRPP measures and analysis approach. KAERI recognized that the process of safeguards or a PR evaluation should be managed in an iterative manner. The ROK is actively participating in GIF PRPPWG and planning to increase the effectiveness of the research by sharing the results of nuclear nonproliferation studies with the GIF PRPPWG in the nuclear fuel cycle. Also, KAERI recently translated “Evaluation Methodology for Proliferation Resistance and Physical Protection of Gen.IV Nuclear Energy Systems – Revision 6”, which is a technical report by GIF PRPPWG in 2011, into Korean.

3. The Prospects and Outlook

With the 2018 GIF R&D Outlook document, the PRPPWG will concentrate its future R&D activities on specific goals with an indication of possible aspects that might have to be investigated. Currently, the PRPPWG and the six SSCs/pSSCs are collaborating to update the document in view of the design evolutions and changes that have occurred in recent years.

KAERI is continuing its nonproliferation research such as the development of safeguard systems and proliferation resistance for the innovative nuclear fuel cycles including spent fuel treatment, which can contribute to enhancing international efforts to secure nuclear nonproliferation.

4. Conclusion

The experience in the process of developing and testing the PRPEM formed the basis for a close interaction with the GIF SSCs/pSSCs in 2011 and gave light to a joint document which is emphasizing the PR&PP characteristics of the six GIF reactor technologies. This activity will not only shed light on PR&PP advancements of the current system designs, but also inform the PRPPWG future activities. As one of PRPPWG, KAERI will actively take part in further studies.

REFERENCES

- [1] Generation IV International Forum (GIF), “A Technology Roadmap for Generation IV Nuclear Energy Systems” Tech. Rep, (2002).
- [2] Generation IV International Forum (GIF) PRPP Working Group and System Steering Committees, “Proliferation Resistance and Physical Protection of the Six Generation IV Nuclear Energy Systems” Tech. Rep, (2011).
- [3] S.K. Ahn et al., “A Proliferation Resistance Evaluation for a Pyroprocessing Facility Design”, INMM 55th Annual Meeting (2014).
- [4] H.D. Kim, S.K. Ahn, J.H. Ku, J.M. Park, and K.S. Lee, “The History and Status of KAERI’s Research Activities to Strengthen Non-proliferation for Nuclear Fuel Cycle”, INMM 59th Annual Meeting (2018).
- [5] H.D. Kim, S.K. Ahn, and J.S. Jeong, “Evaluation Methodology for Proliferation Resistance and Protection of Generation IV Nuclear Energy Systems”, KAERI/TS-333/2018, (2018).

Application of PROMETHEE-GAIA Method for Future Nuclear Energy System Selection

Ruxing Gao*, Hyo On Nam, and Hong Jang

Korea Atomic Energy Research Institute, 111, Daedeok-daero 989beon-gil, Yuseong-gu, Daejeon, Republic of Korea

*grxing@kaeri.re.kr

1. Introduction

China is playing a growing role in the world economy, with its soaring energy demand and air pollution problems. In the race to replace its part of coal-fire power generation with low-carbon energy sources, Chinese government selected nuclear power as the most promising solution. Under the National 13th Five-Year Plan (2016-2020), China's nuclear power capacity will increase to 58 GWe in 2020 with an additional 30 GWe under construction [1]. The large expansion of nuclear power accompanied with the existing Once-Through (OT) fuel cycle, which inevitably bring the tough problem of rapid accumulation of radioactive nuclear wastes. However, China's current spent fuel reprocessing technologies are still far from maturation in the industrial scale.

The aim of this paper was to conduct a Multi-Criteria Decision Making (MCDM) case study analysis for a national-scale sustainability assessment of future nuclear energy systems and to further improve the weighting system for robustness enhancement in decision-making process.

2. Methodology

2.1 MCDM Framework of China's Nuclear Fuel Cycle (NFC)

In our past studies [2-3], we developed an MCDM framework to evaluate the nuclear sustainability in China based on dynamic modeling of NFC transition from the existing to advanced nuclear energy systems through 2100. Four nuclear energy system options for future NFC transition are selected: OT cycle, PWR(MOX) cycle, PWR(MOX)-FR(MOX) cycle,

and PWR-FR(MOX)) cycle. Also to evaluate the sustainability of these NFC options, six major criteria (resource utilization, nuclear waste management, economic competitiveness, proliferation risk, environmental impact, and technological readiness) associated with total 12 detailed sub-criteria are defined, as shown in Fig. 1.

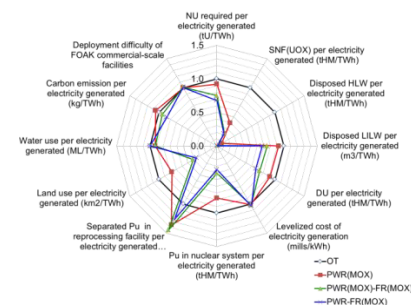


Fig. 1. Overall system performance comparison of the 12 sub-criteria in the Options 2-4 against OT.

2.2 PROMETHEE-GAIA

In some circumstances of MCDM applications, there are always many difficulties to select and determine the evaluation criteria, weight assignment, and decision-making methods due to challenging trade-offs and input data uncertainties. This paper applies an integrated Preference Ranking Organization Method for Enrichment Evaluation (PROMETHEE) and Geometrical Analysis for Interactive Aid (GAIA) method to help the decision makers in selecting an optimal transitional path of future nuclear energy system from a sustainability perspective.

To stress on the uncertainties of weight assignment cause by the inherent weakness of any single Fuzzy Analytic Hierarchy Process (AHP) methodology, three different Fuzzy AHP approaches including

Interval Arithmetic (IA), Synthetic Extend Analysis (SEA), and Fuzzy Preference Programming (FPP) are selected in terms of different aggregation methods to derive fuzzy priorities and final weights for the overall criteria, and are tested to China's MCDM case study of NFC. All the original pair-wise comparison matrices for weighting the 12 sub-criteria were derived through a Matlab random sampling model [2]. Finally, by adopting the above three Fuzzy AHP approaches, the resultant weights for the 12 sub-criteria were simply aggregated to the final weights through the geometric mean, as shown in Fig. 2.

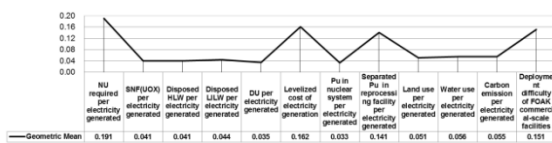


Fig. 2. Final weights for the 12 sub-criteria by using three Fuzzy AHP approaches.

3. Results and Discussions

The final weights for the 12 sub-criteria were applied in the MCDM analysis. The PROMETHEE rankings of four NFC options with the corresponding values of net flow score are displayed in Fig. 3.

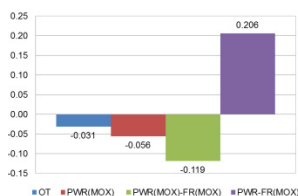


Fig. 3. The net flow scores of the four NFC options by using PROMETHEE.

PWR-FR(MOX) cycle got the top score among four candidate options, followed by OT cycle. PWR(MOX)-FR(MOX) cycle is the lowest-ranked option. Fig. 4 shows the GAIA plane for the case study in a standard 2D (U,V) view with a quite high information quality of 97.2%. In this plane, the 12 sub-criteria are represented by axes and the four options are shown as points. A long and thick decision axis in red indicates a strong decision power to compromise the confliction among the criteria and

candidate options. Here, the decision axis clearly points towards PWR-FR(MOX) cycle, which indicates its best performance based on the given criteria weights. Additionally, the orientation of the decision axis indicates the proliferation risk criterion is in highest agreement with the PROMETHEE rankings compared to the other criteria.



Fig. 4. GAIA plan for China's MCDM case study.

4. Conclusions

From the above MCDM analysis results of four nuclear energy system options by applying PROMETHEE-GAIA method, the PWR-FR(MOX) cycle is proven to be a sustainable NFC transitional candidate. In the future, more integrated evaluation metrics and more reliable weighting system for assessing China's future NFC transitional path should be continuously developed.

REFERENCES

- [1] World Nuclear Association, China nuclear power (2018.08).
- [2] Gao, R., et al. "National Options for a Sustainable Nuclear Energy System: MCDM Evaluation Using an Improved Integrated Weighting Approach." *Energies* 10.12 (2017).
- [3] Gao, R., et al. "Integrated system evaluation of nuclear fuel cycle options in China combined with an analytical MCDM framework." *Energy Policy* 114 (2018): 221-233.

A Study on the Development and Operation of the System for the IAEA Additional Protocol Declaration in KAERI

Juang Jung*, Sung-Ho Lee, Byung-Doo Lee, In Chul Kim, Hyun Sook Kim, Hyun Jo Kim, and Seongmi Han
Korea Atomic Energy Research Institute, 111, Daedeok-daero 989beon-gil, Yuseong-gu, Daejeon, Republic of Korea
*jajung@kaeri.re.kr

1. Introduction

The AP (additional protocol) is a legal document granting the IAEA (International Atomic Energy Agency) complementary inspection authority to assure the absence of undeclared nuclear material and activities. The ROK (Republic Of Korea) signed the additional protocol in June 1999 and it entered into force in Feb. 2004 when the ROK national assembly was ratified. Under the AP, KAERI has submitted the annual report on the expanded declaration to the IAEA, and the IAEA has carried out the CA (Complementary Access) of the KAERI site since 2004. As you know, our institute has so many facilities and projects that it is very difficult and complicated to report. So, we are building a system for expanded declarations inside the institute. This paper describes the establishment of AP system at KAERI.

2. The Additional Protocol at KAERI

Under the AP, the KAERI has annually submitted a report on expanded declaration to the IAEA, and the IAEA has carried out the CA of the KAERI site to assure the absence of undeclared nuclear material and activities since 2004.

2.1 Expanded Declaration

In the ROK, a report on the expanded declaration under the AP should be submitted to KINAC by 31 March of each year. The KINAC coordinates the ROK AP information and submits it to the IAEA by 15 May. KAERI has submitted the reports on expanded declaration to the KINAC in a timely manner since 2004. The information of the declaration under the AP is as follows:

(1) A general description of and information specifying the location of nuclear fuel cycle-related research and development activities not involving nuclear material carried out anywhere that are funded, specifically authorized or controlled by, or carried out on behalf of the government (Article 2.a.(i) of the AP)

(2) A general description of each building on each site including a map (Article 2.a.(iii) of the AP)

(3) A description of the scale of operations for each location engaged in the activities specified in Annex I to the AP [1] (Article 2.a.(iv) of the AP)

(4) General plans for the succeeding ten-year period relevant to the development of the nuclear fuel cycle (including planned nuclear fuel cycle-related research and development activities) when approved by the appropriated authorities in the government (Article 2.a.(x) of the AP). Nuclear fuel cycle-related research and development activities are those activities that are specifically related to any process or system development aspect of any of the following:

- Conversion of nuclear material,
- Enrichment of nuclear material,
- Nuclear fuel fabrication,
- Reactors,
- Critical facilities,
- Reprocessing of nuclear fuel,
- Processing (not including repacking or

conditioning not involving the separation of elements, for storage or disposal) of intermediate or high-level waste containing plutonium, high enriched uranium or uranium-233,

But these do not include activities related to theoretical or basic scientific research or to research and development on industrial radioisotope applications, medical, hydrological and agricultural applications, health and environmental effects and improved maintenance.

2.2 Complementary Access at KAERI

Table 1 shows the status of the CA at KAERI. The IAEA has conducted 45 CAs on the KAERI site since 2004. The CA is for IAEA inspectors to assure the absence of undeclared nuclear material or to resolve questions or inconsistencies in the information a State has provided about its nuclear activities. The IAEA gives an advanced notice of the CA of at least 24 hours to KAERI. The advanced notice is shorter- at least two hours- for access to any place on the KAERI site that is sought in conjunction with the DIV (Design Information Verification) or ad hoc or routine inspections.

IAEA activities such as an examination of records, visual observations, environmental sampling, utilization of radiation detection and measurement devices are conducted during the CA.

Table 1. The status of the CA at KAERI (as of Sep 2018)

	2012	2013	2014	2015	2016	2017	2018
The number of the CA	1	3	1	3	3	1	2

3. The Implementation System of AP at KAERI

As you know, our institute has so many facilities and projects that it is very difficult and complicated to report. Since KAERI AP implementation system was designed not only to prepare the expanded declaration efficiently at KAERI but also to meet the requirements established by the IAEA under the AP. All AP information such as the building information at the KAERI site, R&D project information, and the status of the annual expanded declaration can be managed in this system.

KAERI has upgrading it for the sake of user convenience. The experience obtained from the development of the AP implementation system may be helpful in the implementation of the AP at KAERI.

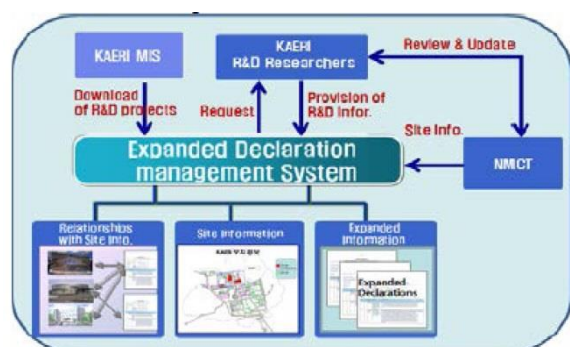


Fig. 1. Schematic Diagram of Expanded Declaration.

3.1 2.a.(i) Research Project

The list of KAERI R&D projects downloaded from the KAERI MIS (Management Information System) is managed in this system. This system notifies all R&D project managers automatically that the project information should be submitted if it needs to be reported under article 2.a.(i), (iv) or (x) of the AP. On the basis on the information the project manager provides, In general, more than 600 projects are reported as projects to report and not to report. When the project name is changed or the research contents change to the contents to be reported, it is added to the system according to the judgment of the project manager. It is linked to the report of 2.a. (iii), depending on which buildings the projects are undertaken.

3.2 2.a.(iii) Building Information

With regard to building information, this is obtained in two ways. One gets information from walking around the institute, and secondly from the relevant departments. Then enter the information into the system and it will automatically link with 2.a.(i) related projects. You will know which projects perform in which building. We've just started this system and checking the system for errors and missing parts in parallel with the manual operation.

3.3 Pros and Cons

The advantage of the system is that the system processes it, which reduces human errors and missing parts. In fact, we have been helped by the system from human errors. The only disadvantage is the project managers should make their own decisions as to whether or not their project is an AP declaration. However, if a PM is not fully aware of the AP declaration, it is considered necessary to have a system that can automatically validate projects.

4. Conclusion

The AP implementation system developed by KAERI was designed not only to prepare the expanded declaration efficiently at KAERI but also to meet the requirements established by the IAEA under the AP. The system is currently being updated, and if there is still difficulty, but the system can be trusted even if it is developed to a good level, it will be possible to shorten the time to write the report and increase the reliability. The experience obtained from the development of the AP information management system may be helpful in the efficient implementation of the AP at KAERI.

KAERI will make continuous efforts to implement the AP efficiently, as well as meet the requirements established by the IAEA under the AP.

REFERENCES

- [1] Model protocol additional to the agreement(s) between state(s) and the international atomic energy agency for the application of safeguards, Annex I.
- [2] Model protocol additional to the agreement(s) between state(s) and the international atomic energy agency for the application of safeguards, p14.

A Study on the Public Perception of Radiation After the De-nuclearization

Seungkook Roh^{a)*}, Youngjoon Lee^{a)}, Junghyun Suh^{a)}, Yongjun Kim^{b)}, Hyungsu Chung^{b)}, Kibo Shim^{b)}, and Jee Eun Yoon^{c)}

^{a)} Korea Atomic Energy Research Institute, 111, Daedeok-daero 989beon-gil, Yuseong-gu, Daejeon, Republic of Korea

^{b)} Korea Energy Information Culture Agency, 1418, Nambusunhwan-ro, Geumcheon-gu, Seoul, Republic of Korea

^{c)} Hanyang University, 222, Wangsimni-ro, Seongdong-gu, Seoul, Republic of Korea

*skroh@kaeri.re.kr

1. Introduction

In June 2017, the new government declared its policy of de-nuclearization. This declaration was made in accordance with the Presidential Commitment. After these results, the nuclear power sector in the field of nuclear power was significantly affected. This is because the public perception of nuclear power plants has been steadily deteriorating. However, the field of radiation had a considerable distance from the enucleation movement. Therefore, we need to study how the public's perception of radiation has changed since the government's declaration. On the other hand, the explosion of Internet users has increased the influence of cyberspace[1]. Modern people are using Cyberspace to present their opinions because of time and space constraints. In addition, many organizations, such as government and companies, are constantly confirming public opinion in cyberspace[2]. Therefore, this paper investigated the public perception and change of radiation in cyberspace after the declaration of the government.

2. Data and methodology

2.1 data

The data used in this study are news and comments about radiation from May 2017 to June 2018. In addition, 'nuclear' and 'renewable energy' data were collected together for radiological comparison. The word 'nuclear energy' and 'renewable energy' are social issues due to the government's policy of nuclear power.

2.2 methodology

This study performed time series analysis, association analysis and frequency analysis for data analysis. Through time series analysis, we can compare how much radiation, nuclear energy, and renewable energy are concerned in our society. Associative analysis provides information on what

words people think about 'radiation'. Finally, frequency analysis provides quantitative information on all words exposed with radiation.

3. Result

3.1. Time series analysis result

As shown in Figure 1, the news volume for nuclear power was the highest from May 2017 to June 2018. In particular, about 4500 nuclear news stories were generated in October 2017. This figure is 9 times more than the amount of news about radiation during the same period. News volume on renewable energy was 3-4 times more than news volume on radiation. The amount of news about radiation was steady at 500 cases per month without any major change. Meanwhile, the news about radiation was more than twice as high as usual in May 2018 due to the problem of radon bed.

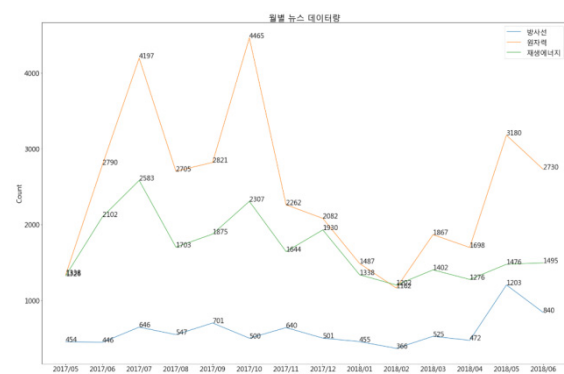


Fig. 1. comparison among Radiation, nuclear power, and renewable energy news volume.

News is information provided to the public in the media. The comments show the opinion of the public and the actual public opinion.

Figure 2 shows that public interest in nuclear energy is 16 to 4 times higher than radiation. Radiation has not been able to produce big issues and has received no public attention.

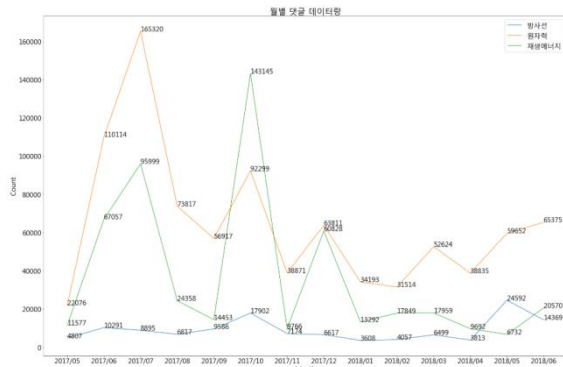


Fig. 2. Comparison among Radiation, Nuclear, Renewable Energy News reply.

3.2 Association analysis result

Associated analysis indicated that radiation was associated with radiation dose, radiation control method, and annual radiation dose[3]. When people think about radiation, they can think of these words as thinking at the same time.

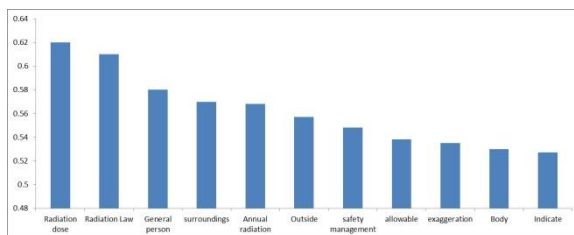


Fig. 3. Radiation-related analysis results.

3.3 Frequency analysis result

Radiation related frequency analysis revealed many words such as treatment, patient, hospital, examination, and surgery. This result can be interpreted as a result of the mass use of radiation for medical purposes.



Fig. 4. Wordcloud[4] results about radiation.

4. Conclusion

Radiation is a field of nuclear power. However, the public does not consider nuclear power the same field. The public thinks nuclear power is dangerous because of radiation, but does not pay much attention to actual radiation and is considered medical. In other words, the nuclear energy sector must actively respond to the nature of the risks in order to overcome the government's policy of de-nuclearization.

ACKNOWLEDGEMENT

This research was carried out by the research fund of the Korea Energy Information Culture Agency.

REFERENCES

- [1] Slouka M. War of the worlds: Cyberspace and the high-tech assault on reality: HarperCollins Publishers, 1996.
- [2] Parks MR, Floyd K. Making friends in cyberspace. Journal of computer-mediated communication. 1996;1(4):JCMC144.
- [3] Saxena R, Voight BF, Lyssenko V, Burt NP, de Bakker PI, Chen H, et al. Genome-wide association analysis identifies loci for type 2 diabetes and triglyceride levels. Science. 2007;316(5829):1331-6.
- [4] Cui W, Wu Y, Liu S, Wei F, Zhou MX, Qu H. Context preserving dynamic word cloud visualization. Conference Context preserving dynamic word cloud visualization. IEEE, p. 121-8.

Status of Management of the Items subject to Nuclear Cooperation Agreement at KAERI

Hyun-Jo Kim*, In-Chul Kim, Byung-Doo Lee, Sung-Ho Lee, Hyun-Sook Kim, and Juang Jung
Korea Atomic Energy Research Institute, 111, Daedeok-daero 989beon-gil, Yuseong-gu, Daejeon, Republic of Korea
*keiki@kaeri.re.kr

1. Introduction

ROK has nuclear cooperation agreements with several countries for the peaceful use of nuclear power. The agreements and administrative arrangements for implementing these agreements with some countries include the management of the items subject to the agreement and providing of annual report on inventory and inventory changes of the items. Generally, the items subject to the agreement refer to nuclear material, material, equipment and information, and some countries include the items derived from the transferred items.

KAERI has been providing the annual reports on the inventory and inventory changes of the items subject to the agreement to Canada and Australia since 1980s and Japan since 2013. The annual report on US items was added after the nuclear cooperation agreement between ROK and US was revised in 2015 and an administrative arrangement was signed in 2016. ROK had managed the origin of nuclear material, but since the revision of the agreement with the US, it has replaced by the obligation instead of the origin.

This paper describes the status on the management of the items subject to the bilateral agreement at KAERI.

2. Management of items subject to the agreements

2.1 Status of annual report on the items subject to the agreements

ROK has obligation to provide the annual report to Canada, Australia, Japan and the US. The items in the annual report may differ slightly by the country of agreement.

(1) Australia

ROK should provide an annual report on all nuclear materials transferred between ROK and Australia every January. KAERI has been providing the annual report on nuclear materials including yellow cake transferred from Australia since 1987.

(2) Canada

ROK should provide the annual report on all nuclear materials, material, equipment and information subject to the agreement every March. In addition, the items, which are used, produced, developed, processed, reprocessed, enriched, fabricated or converted from, by, in or with the items supplied pursuant to the agreement, should be included. Thus, KAERI manages the nuclear materials irradiated at HANARO research reactor that includes Canadian equipment and information as non-canadian origin. KAERI has been providing the annual report on Canadian nuclear materials, non-canadian nuclear materials, material and some equipment and information related to HANARO research reactor since 1983.

(3) Japan

The items that should be provided in the annual report to Japan are nuclear materials, material, equipment and technology. KAERI has been providing Japan with the annual report on technology

of plant specification since 2013.

(4) United States

The items and forms included in the annual report were finalized after an administrative arrangement was signed. ROK should provide the annual report on nuclear materials, moderator material, equipment and components subject to the agreement every June. In addition, special fissionable material that was produced through the use of equipment or device that were transferred pursuant to the 1972 agreement includes US obligated nuclear materials. Therefore, KAERI also manages the plutonium produced from non-US nuclear material which was irradiated in US supplied reactor as US obligation. KAERI has been providing the US with the annual report on nuclear materials since 2017.

2.2 Procedures for preparation of annual report

NM control department manages and provides the annual report under the bilateral agreements at KAERI. The procedures for preparation of an annual report are as follows.

- (1) In case of the items except nuclear materials, NM control department requests to all departments at KAERI to confirm if they have the items pursuant to the agreement before submitting the annual report.
- (2) For nuclear materials, NM control department manages the inventory and inventory changes of the nuclear materials by origin management system. KAERI developed the origin management system in 2015 to efficiently manage the origin information. The system is connected with the KASIS (KAeri Safeguards Information treatment System) which has the function of a near real-time accounting. When the operator input the data on inventory

changes in KASIS, it is automatically reflected in the origin management system. Then, NM control department fixes the origin information after the review of invoice and nuclear material transaction report.

- (3) Finally, NM control department review the import and export information and the documents received from other department and prepare the annual report.

3. Conclusion

This paper reviewed the management status of the items subject to the bilateral nuclear cooperation agreement at KAERI. In particular, nuclear materials are managed using the origin management system because they have many inventory changes and are more complicated than other items. However, it is difficult to manage US obligated nuclear material since the origin management system was developed before an administrative arrangement between ROK and US took effect. Therefore, it is necessary to revise the system to manage the obligated nuclear material rather than the origin of nuclear material.

REFERENCES

- [1] H.J.Kim et al, "Approach on origin management of nuclear material at KAERI", Transactions of the KNS Spring Meeting, May 18-19, 2017, Jeju.
- [2] Bilateral nuclear cooperation agreement with Australia, Canada, Japan and the United States, <http://www.mofa.go.kr>.

2분과

사용후핵연료 처분전관리 (Oral)

Characterization of U-Zr System Fuel Melt Residue for Recycle of Metallic Fuel Scrap

Ki-Hwan Kim^{1)*}, Seong-Jun Ha^{1,2)}, Seung-Uk Mun^{1,3)}, Jong-Hwan Kim¹⁾, Young-Mo Ko¹⁾, and Jeong-Yong Park¹⁾

¹⁾ Korea Atomic Energy Research Institute, 111, Daedeok-daero 989beon-gil, Yuseong-gu, Daejeon, Republic of Korea

²⁾ Yonsei University, 50, Yonsei-ro, Seodaemun-gu, Seoul, Republic of Korea

³⁾ Chungnam National University, 99, Daehak-ro, Yuseong-gu, Daejeon, Republic of Korea

*khkim2@kaeri.re.kr

1. Introduction

Sodium-cooled Fast Reactor (SFR) is a promising reactor among Gen-IV reactors for future. Metallic fuel slugs for SFR have conventionally been fabricated by injection casting method since 1950s. The injection casting method has the advantages of high productivity and excellent remote control, but the drawback of low yield of about 50%.

In this study, the characteristics of the residue scraps of U-Zr alloy system fuel in as-cast state and after surface treatment such as mechanical and chemical treatment have been examined to evaluate the feasibility the recycle of the fuel scraps, in order to improve the yield during the fuel fabrication process. In further, metallic fuel slugs were re-fabricated using recycled metallic fuel scraps by injection casting method.

2. Methods and Results

2.1 Experimental Methods

U-10wt.%Zr and U-10wt.%Zr-5wt.%RE fuel slugs have been fabricated using pure depleted uranium and zirconium metal, and RE mother alloy with injection casting method. RE is a rare-earth alloy consisting of 53wt%Nd, 25wt%Ce, 16wt%Pr, and 6wt%La. After injection casting, the melt residue scraps have been obtained and treated on the impurity layer of the

surface by either chemical or mechanical method. The metallic fuel slugs were also fabricated using recycled metallic fuel scraps by injection casting method. The microstructure and the composition of the melt residue scraps and metallic fuel slugs were analyzed using inductively coupled plasma atomic emission spectroscopy (ICP), elemental analysis (EA), scanning electron microscopy (SEM) and energy-dispersive spectroscopy (EDS).

2.2 Experimental Results

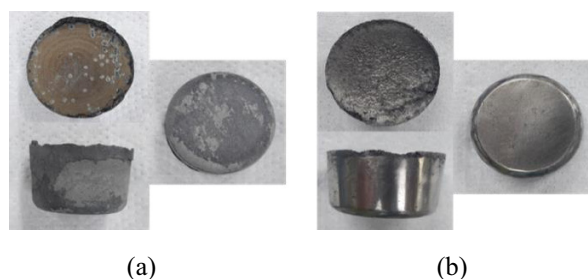
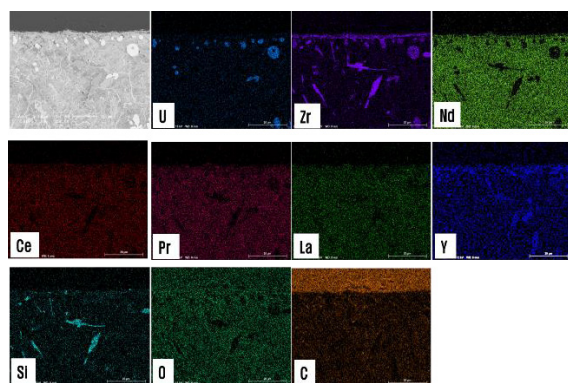


Fig. 1. The surface states of U-10Zr-5RE melt residue in as-cast state (a) and after (b) mechanical treatment.

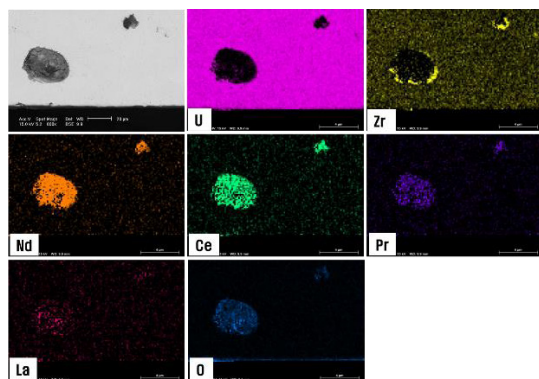
The surface states of U-10Zr-5RE melt residue before (a) and after (b) mechanical treatment are shown in Fig. 1. The U-10Zr-5RE melt residue in the top surface with as-cast state showed RE-compounds ranging from 5 to 30 μm in thickness as the first impurity layer on the top surface and RE-rich layer ranging from 1 to 2 mm in thickness as the second impurity layer, according to the integrated results of SEM, EDS and XRD analyses. The U-10Zr-5RE melt residue in the bottom surface showed Y_2O_3

plasma-spray coating layer of about 20 μm in thickness as the first impurity layer on the bottom surface and RE-rich layer of about 40 μm in thickness as the second impurity layer.

RE-compound layer as the first impurity layer on the top surface in the U-10Zr-5RE melt residue have been removed on the whole in the top surface after mechanical treatment. Y_2O_3 plasma-spray coating layer as the first impurity layer on the bottom surface and RE-rich layer as the second impurity layer have



(a)



(b)

Fig. 2. Scanning electron micrograph and energy-dispersive X-ray spectroscopic mapping showing the surface layer of U-10Zr-5RE melt residue after mechanical treatment; (a) top, (b) bottom.

been generally cleaned in the top surface after mechanical treatment. U-10Zr-5RE fuel slugs with a diameter of about 5.5 mm and a length of about 300 mm were fabricated soundly without cracks or thin sections, recycling metallic fuel scrap of melt residue.

3. Conclusion

The characteristics of the melt residue scraps of U-Zr alloy system fuel in as-cast state and after surface treatment have been examined to evaluate the feasibility the recycle of the fuel scraps. Surface impurity layers on the surface have been removed on the whole after mechanical treatment. Metallic fuel slugs were also re-fabricated soundly with mold length of 300 mm. The feasibility of the recycling of the fuel slug scraps has been demonstrated by the re-fabrication of the metallic fuel slugs.

ACKNOWLEDGEMENT

This work has been carried out under the Nuclear Research and Development Program supported by the Ministry of Science and Technology in the Republic of Korea.

REFERENCES

- [1] L. C. Walters, B. R. Seidel, J.H. Kittel, "Performance of Metallic Fuels and Blankets in Liquid-Metal Fast Breeder Reactors. Nuclear Technology", 65, 179-231 (1984).
- [2] G. L. Hofman, L. C. Walters, T. H. Bauer, "Metallic Fast Reactor fuels". Progress in Nuclear Energy, 31, 83-110 (1997).
- [3] Crawford DC, Porter DL, Hayes SL. "Fuels for Sodium-cooled Fast Reactors: US Perspective", Journal of Nuclear Materials, 371, 202-231 (2007).

Effect of Electrode Materials on the Exchange Current Density Using Tafel Measurement

K. H. Lim and J. I. Yun*

Korea Advanced Institute of Science and Technology, 291, Daeheok-ro, Yuseong-gu, Daejeon, Republic of Korea

*jiyun@kaist.ac.kr

1. Introduction

For the optimization of pyroprocessing, the electrochemical data, especially the exchange current density of lanthanides and actinides are of importance. However, the knowledge of the exchange current density in high temperature eutectic is rare, and there are controversial opinions and estimates about the effect of various electrode materials on the exchange current density [1]. In this study, the effect of different electrode materials such as tungsten, glassy carbon, nickel, and platinum on the exchange current density was investigated using Tafel measurement.

2. Experimentals

2.1 Chemicals

For the Tafel measurements, CeCl_3 and SmCl_3 were melted in anhydrous LiCl-KCl eutectic salt at 500°C . The concentration of CeCl_3 varied in the range of 1.0wt%, and the concentration of SmCl_3 was prepared to be 5.0wt%. For each electrode, three samples were prepared to examine the reproducibility of exchange current densities.

2.2 Apparatus

CeCl_3 and SmCl_3 were contained in the LiCl-KCl eutectic salt in a 40 mm diameter quartz cell. A cap with 6 holes was closed at the top of cell for stable positioning of electrodes.

Tungsten rod (Nilaco, 1.0 mm in diameter, 99.95%

purity) was used as a counter electrode and an Ag/AgCl electrode (Alfa Aesar 99.99%, 1.0 mm diameter Ag wire in 1wt% AgCl-LiCl-KCl) was used as a reference electrode encased in a thin-end pyrex glass tube. For the measurements of exchange current densities using different electrode materials, tungsten ($\varnothing = 1.0$ mm), glassy carbon ($\varnothing = 2.0$ mm), nickel ($\varnothing = 1.0$ mm), and platinum ($\varnothing = 1.0$ mm, molded onto the tungsten rod) were used as the target working electrodes.

Experiments were performed in a glove box under high-purity argon gas condition (99.999% Ar, H_2O and $\text{O}_2 < 10$ ppm). The temperature was maintained at $500 \pm 10^\circ\text{C}$ in the furnace placed at the bottom of glove box.

3. Results and Discussion

3.1 Tafel measurement

The exchange current density of CeCl_3 was determined using Tafel equation (Eq. 1), a simplified Butler-Volmer equation. Fig. 1 shows the Tafel plot of CeCl_3 in LiCl-KCl molten salt at 500°C measured in the potential range of -2.10 V to -1.95 V, including the equilibrium potential of -2.00 V. The Tafel measurement was first initiated after the deposition of Ce metals on the electrode by applying the overpotential of -0.15 V for 5 sec with a scan rate of 20 mV/s. By fitting the linear Tafel slope to the zero-overpotential, as presented in Fig. 1, the exchange current densities were obtained.

$$\ln(-j) = \ln(j_0) - \frac{\alpha_c n F \eta}{RT} \quad (1)$$

where j is the exchange current, j_0 is the exchange current density, α_c is the cathodic charge transfer coefficient, η is the overpotential, F is the Faraday constant, R is the gas constant, and T is the absolute temperature.

Using the tungsten working electrode, the exchange current density of Ce was determined to be $17.61 \pm 0.20 \text{ mA/cm}^2$, which is in good agreement with other literature data studied by K.C. Marsden and B. Pesic [2] by considering the concentration dependency of the exchange current density.

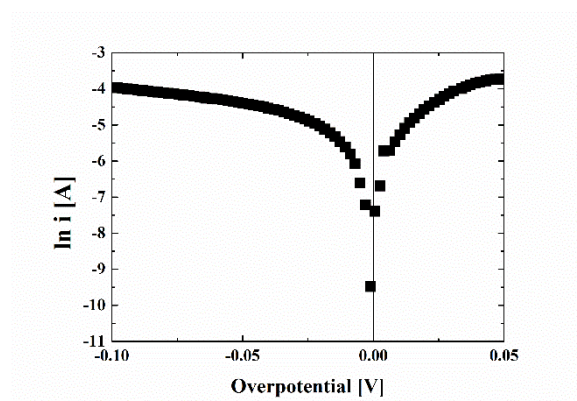


Fig. 1. Tafel plot of CeCl_3 with tungsten electrode in LiCl-KCl eutectic salt at 500°C .

3.2 Effect of different working electrodes on the exchange current density

As shown in Fig. 2, the exchange current densities of Ce(III)/Ce(0) and Sm(III)/Sm(II) were obtained with different electrode materials of tungsten, glassy carbon, nickel, and platinum. The difference in the exchange current density of CeCl_3 was marginal within the uncertainty level, whereas SmCl_3 showed a remarkable difference in the exchange current density, depending on the electrode materials. The possible reason was that the working electrode is coated by deposition on its surface with Ce metals. Therefore, it was concluded that there are only interactions between the Ce(0) coated working electrode (W, GC, Ni, and Pt) and the Ce(III) ions. This was confirmed by the soluble/soluble reaction of Sm(III)/Sm(II) , which is not subject to the deposition process.

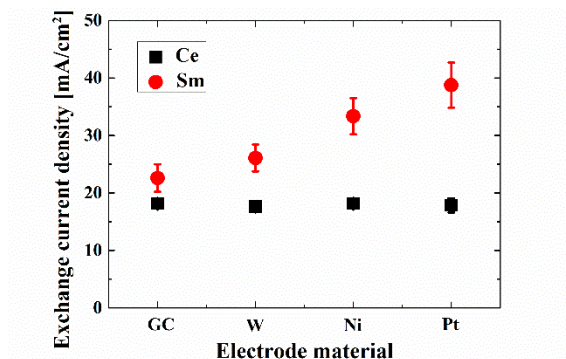


Fig. 2. The exchange current density of CeCl_3 and SmCl_3 with various electrode materials.

4. Conclusion

We investigated the effect of different electrode materials on the exchange current density by the soluble/insoluble reaction of Ce(III)/Ce(0) and the soluble/soluble reaction of Sm(III)/Sm(II) . The former is probably associated with the deposition of target elements on the electrode surface by applying negative overpotential before the Tafel measurement for the Ln(III)/Ln(0) reactions.

REFERENCES

- [1] I. Choi, B.E. Serrano, S.X. Li, S. Herrmann, S. Phongikaroon, "Determination of exchange current density of U^{3+}/U couple in LiCl-KCl eutectic mixture", Proceedings of Global 2009, Paris, France (2009).
- [2] K.C. Marsden, B. Pesic, "Evaluation of the electrochemical behavior of CeCl_3 in molten LiCl-KCl eutectic utilizing metallic Ce as an anode", J. Electrochem. Soc. 158, F111 (2011).

Evaluation of Acceptance Criterion for Dryness of Canister and Spent Nuclear Fuel for Dry Storage

Suk-Nam Lim*, Gyung-Wook Shin, Gyung-Sun Chae, and Jae-Seok Park

SAE-AN ENGINEERING Co., 184, Gasandigital2-ro, Geumcheon-gu, Seoul, Republic of Korea

*limsn@sae-an.co.kr

1. Introduction

As the transition to storing the spent nuclear fuel (SNF) from spent fuel pool in dry storage facilities for extended period, NPPs must be prepared to dry SNFs. The Forced Helium Dehydration (FHD) technology has been developing to preserve the integrity of SNFs and fuel storage system as a R&D project of KETEP. FHD drying is specified for a canister that contains high-burn up fuel assembly.

For commercial SNF, the typical acceptance criterion is maintaining a 3.0 torr pressure for 30 minutes. Other measurement techniques may be used to show drying adequacy. Application of those techniques and the metrics for dryness would need concurrence from the regulatory agency. Adequacy of water removal should be evaluated by pressure rebounding measurement or monitoring the moisture content in process gas removed from the dried container.

Monitoring the moisture content in process gas method can be used for FHD drying. There are several practical methods for moisture content such as relative humidity (RH), temperature measurement of process gas and dew-point (DP) measurement of process gas in the canister corresponding to the partial pressure of water vapor at 3 torr. It is necessary to select a reasonable measurement method and measurement guide as a regulation.

2. Moisture Measurement Technology

2.1 FHD Drying Concept

The fuel drying by FHD process is effectuated by

circulating the heated process gas such as Helium and removing the moisture through condenser and freezer.

Adequate dryness for FHD can be confirmed by DP of canister exit process gas, the temperature of the process gas exiting the freezer and, or humidity.

2.2 Selection of measuring technology for dryness confirmations

The adequate moisture removal verification should be verified by proper method to applied system. There are two methods as a industrial applicable methods; one is capacitive sensor, other optical (chilled mirror) hygrometer.

Capacitive sensors (CS) respond to small changes in water vapor pressure feature. The sensor measures the capacitive or resistive output of a sensing element. Capacitive sensor measures relative humidity and others can provide by calculating and converting between humidity values in terms of DP, vapor pressure.

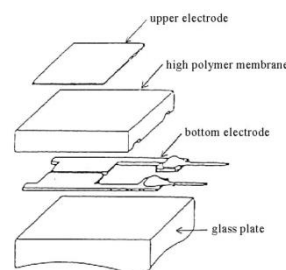


Fig. 1. Structure of CS with polymer membrane.

DP is defined as the temperature that moisture just begins to condense on a surface. The chilled mirror DP sensor measures this parameter directly. Since the mirror surface is always at the dew point, measuring the mirror temperature provides actual DP.

The chilled Mirror is more precise than capacitive technology offering accuracy to $\pm 0.1^{\circ}\text{C}$ to versus $\pm 2.0^{\circ}\text{C}$ for capacitive.

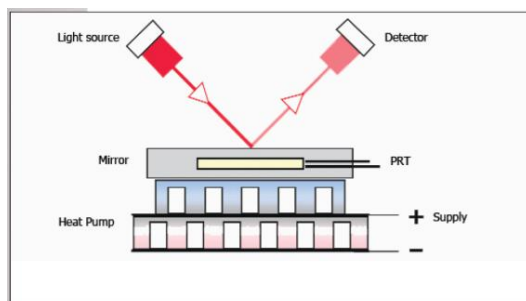


Fig. 2. Structure of Chilled mirror Detector.

Measurement techniques include direct insertion in the gas and sample by pass methods. Sample bypass system diverts a sample of the gas to the sensor. Sampling systems are critical to insure accurate and reliable moisture measurements. Materials of construction, length of flow path, diameter of tubing and myriad other factors are critical in the design of a properly functioning system.

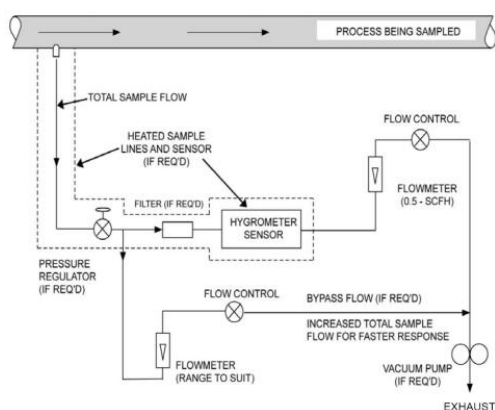


Fig. 3. Typical sampling system.

3. Summary

Canister is considered to be dry when the temperature of the gas exiting the freezer or canister exit gas is below the preset temperature or DP for 30 minutes which correspond to the partial pressure of the water vapor in the canister of less than 3 torr.

The chilled Mirror is more precise and proper method for FHD drying confirmation than capacitive technology.

Regulatory guide for measuring technology for dryness identification must be prepared by regulatory body.

REFERENCES

- [1] Standard Guide for Drying Behavior of SNF (ASTM C-1553-16).
- [2] Standard Review Plan for SFDSS at a GENERAL license Facility (NUGER-1536 Revision 1).

Effects of Hydride Re-orientation and Hydride Rim on Fracture Energy of Zircaloy-4 Cladding

Ho-a Kim^{a),b),*}, Jae-soo Noh^{b)}, Ju-seong Kim^{c)}, and Yong-soo Kim^{a)}

^{a)} Hanyang University, 222, Wangsimni-ro, Seongdong-gu, Seoul, Republic of Korea

^{b)} Atomic Creative Technology Co., Ltd., 35, Techno 9-ro, Yuseong-gu, Daejeon, Republic of Korea

^{c)} Korea Atomic Energy Research Institute, 111, Daedeok-daero 989beon-gil, Yuseong-gu, Daejeon, Republic of Korea

*pissan@hanyang.ac.kr

1. Introduction

Spent nuclear fuel (SNF) is subjected to a vacuum drying process at up to 400 °C and cooled down during dry storage. In this process, hydrides are re-precipitated in the zirconium matrix and these re-precipitated hydrides reduce the ductility of the fuel claddings. Then the claddings can be easily damaged by external impacts such as pinch-type loading that can happen during SNF transportation. Many studies have been carried out on the integrity degradation of the claddings, but most of which have uniform hydride morphology. Some phenomena, such as hydride rim and hydride re-orientation, can occur in SNF claddings and they can worsen the integrity of the claddings more than uniformly precipitated hydrides. In this study, hydrogen charging and hydride re-orientation treatment were implemented to simulate SNF claddings and ring compression tests were adopted as a test method to evaluate the fracture energy of claddings which shall be subjected to shock loads during transportation. Then, effects of hydride re-orientation and hydride rim on fracture energy were analyzed based on the RCT results.

2. Experimental

2.1 Specimen preparation

In this work, cold worked stress relieved (CWSR) Zircaloy-4 cladding tube with outer diameter of 9.5 mm and wall thickness of 0.57 mm was used. Two types of specimens were prepared to evaluate an effect of hydride rim: uniform hydride specimens (U1-U4) and hydride rim specimens (R1-R4). To form hydride rim, outer surface of cladding tube was plated with Ni, which has good hydrogen affinity before hydrogen charging [1]. Then, specimens were charged with hydrogen using a Sievert type apparatus. After hydrogen charging, to form hydride re-orientation specimens were pressurized by argon gas at initial hoop stresses of 90-150 MPa at 400 °C. Hydrogen contents of the specimen were determined using a hydrogen analyzer (ELTRA ONH-2000).

Table 1. Conditions of specimen used in this study

specimen	Hydrogen concentration (wppm)	Initial hoop stress at 400 °C (MPa)	Peak Temperature (°C)
Uniform hydride specimen	U1	272	150
	U2	272	140
	U3	262	110
	U4	191	90
Hydride rim specimen	R1	1246	150
	R2	1281	140
	R3	1148	110
	R4	931	90

2.2 Ring compression test

Ring compression test (RCT) was conducted at a temperature range of room temperature (RT) to 300 °C using a universal testing machine (INSTRON model 5582) with a displacement rate of 1 mm/min.

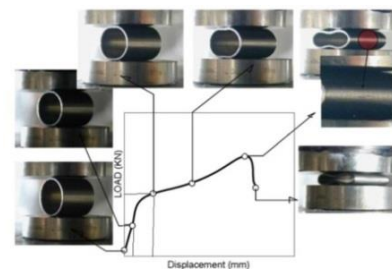


Fig. 1. Ring compression test and load-displacement curve.

3. Results and discussions

Based on the RCT results, fracture energy of SNF claddings was evaluated on two parameters: (1) degree of hydride re-orientation, and (2) ductile to brittle transition temperature (DBTT).

3.1 Fracture energy/area by degree of hydride re-orientation

In RCT, cladding ductility can be evaluated by fracture energy/area similar to strain energy density (SED) concept [2]. Radial hydride continuity factor (RHCF) is one of methods that indicate degree of hydride re-orientation [3]. Fig. 3 shows fracture energy/area by RHCF with hydride rim specimens

(R1-R3 and U1-U3) at a temperature ranges from RT to 150 °C. The fracture energy/area at RT, 100 °C and 150 °C decreases with an increase in the RHCF. It means that radial hydride can be an important factor to evaluate fracture energy of claddings.

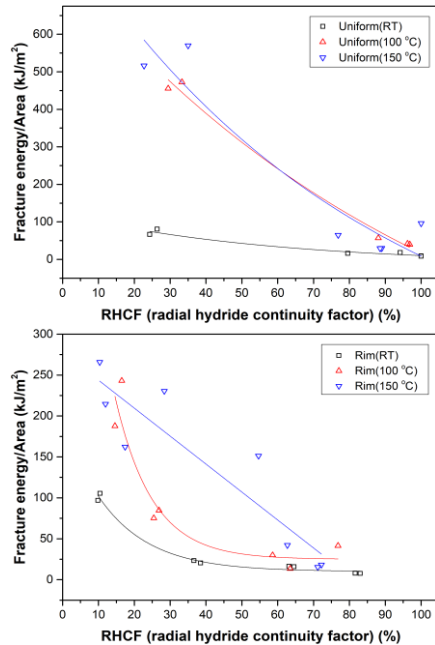


Fig. 2. Fracture energy/area by radial hydride continuity factor.

3.2 Ductile to brittle transition temperature (DBTT)

Ductile to brittle transition temperature (DBTT) is important as claddings slowly cooled down after vacuum drying process. If claddings become brittle as temperature goes down, cladding rupture can happen by external impact during transportation. Fig. 3 is fracture energy/area by the temperature of uniform hydride specimens (U1-U4) and hydride rim specimens (R1-R4). DBTT of claddings increases as cladding hoop stress increases. It is considered that radial hydrides can be more easily generated as hoop stress goes up and they make claddings brittle. With high hoop stress (e.g. U1, U2, R1, and R2), claddings can be brittle even in 150-200 °C. Claddings with hydride rim can be ruptured by low external energy although cladding hoop stress is low.

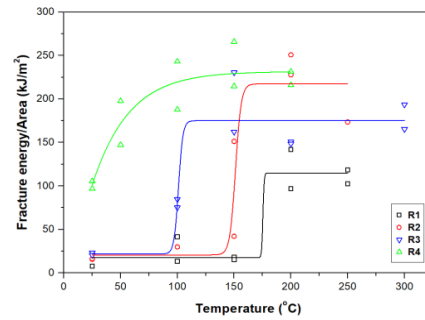
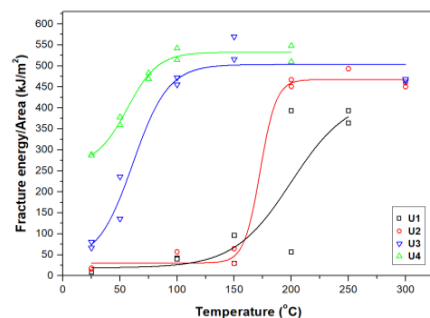


Fig. 3. Fracture energy/area by the temperature of uniform hydride (U1-U4) and hydride rim specimens (R1-R4).

4. Conclusions

RCTs were conducted using uniform hydride specimens and hydride rim specimens treated hydride re-orientation in 90-150 MPa at a temperature ranges from RT to 200 °C. Mechanical properties of SNF claddings were evaluated on two parameters, and results are as follows:

(1) The fracture energy/area at RT, 100 °C and 150 °C decreases with an increase in the RHCF. Radial hydride can be an important factor to evaluate fracture energy of claddings.

(2) With high hoop stress (e.g. U1, U2, R1, and R2), claddings can be brittle even in 150-200 °C. Claddings with hydride rim can be ruptured by low external energy although cladding hoop stress is low.

ACKNOWLEDGEMENT

This research was supported by the Radioactive Waste Management Technology Program of the Korea Institute of Energy Technology Evaluation and Planning (KETEP), funded by the Ministry of Trade, Industry & Energy (MOTIE), Republic of Korea (No. 20181710201770)

REFERENCES

- [1] T. Kido, M. Sugano, Trans. Of Atomic Energy Society of Japan, 1 (2002) 469-471.
- [2] M. Elices, J. Planas, Mater models, in: L. Elfgren (Ed.), Fracture Mechanics of Concrete Structures, Chapman and Hall, London (1989) 16-66.
- [3] M. C. Bilone, T. A. Burtseva, and R. E. Einziger, J. Nucl. Mater. 433 (2013) 431-448.
- [4] J. S. Kim, T. H. Kim, D. H. Kook, Y. S. Kim, J. Nucl. Mater. 456 (2015) 235-245.

Manufacturing Technology of Dry Storage Cask

Yeon-oh Lee, Sung-kug Hwang, Jong-sul Park, and Jae-min Lee*,
SeAH Besteel Corp., 522, Oehang-ro, Gunsan-si, Jeollabuk-do, Republic of Korea

*sb205sk@seah.co.kr

1. Introduction

Most of spent fuels have been storing in the pool of domestic plant, the current capacity of spent fuel pools is not enough for the increasing generation of spent fuels. Unit 1 of Kori nuclear power plant was permanently shut-downed, spent fuels of the domestic plant will be offload to a storage cask. With premature reactor shutdowns by a government policy, the number of Casks required in the near term will increase as the full pool, including reactor core in the world. but there are a lack of experiences & technology for the manufacturing storage cask, just having a fabrication & operation experience of transport cask in Korea. Based on this, studies on finding improved material and manufacturing process for storage casks are needed

2. Storage Cask

2.1 General Information

Dual purpose cask (storage & transportation) has been successfully adopted worldwide and metal cask system is unique in dry storage. metallic cask generally are made from cask steel with one or two lid that are bolted or welded at the cask body. The steel cask provides a leak-tight containment of the spent fuel and provides shielding against gamma radiation. Inside the cask, there is a special resin (e.g., polyethylene) that shields neutrons. The external surface of the cask has trunnions which allow the cask to be lifted and displaced. The basket structure

consists of an assembly of stainless steel cells with borated aluminum or aluminum metal matrix composite plates for the necessary criticality control and to provide the heat conduction paths from the fuel assembly to the cask cavity wall. A general schematic structure of dry storage cask is given in Fig. 1.

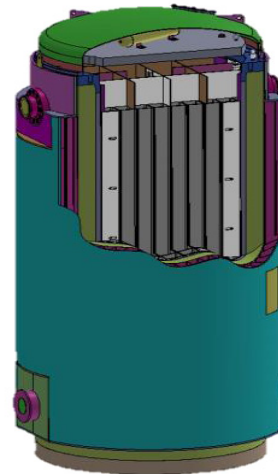


Fig. 1. Dry Storage Cask.

2.2 Applicable Code and Standard

Metal cask will be fabricated in accordance with Code and standard as follows

- ASME Boiler & Pressure Vessel Code
- American National Standard Institute (ANSI)
- American Society for Non-Destructive Testing
- Regulations

Code of Federal Regulations, Title 10, Part 21 / 50
/ 71 / 72

- Regulatory Guides
- US NRC Regulatory Guide 1.38

- KOREA NSSC Notification No.2014-50
- IAEA Safety Series No. TS-R-1 & 116

2.3 Metallic Cask

During manufacturing of cask, the material and assembly of cask shall be especially controlled and managed as below

2.3.1. Material of Cask Body. Cask body for KN-18 Spent Fuel Transport Cask shall be designed by Metal Design Minimum Temperature(MDMT) -40°C , Drop Weight Test shall be performed at -74°C according to the requirement of Code and the result of Drop Weight Test is satisfied.

2.3.2 Shrink Fitting. In case of metal cask such as Fig. 1, Shield shell will be shrink fit onto the inner shell which is a pressure part & containment boundary as below.

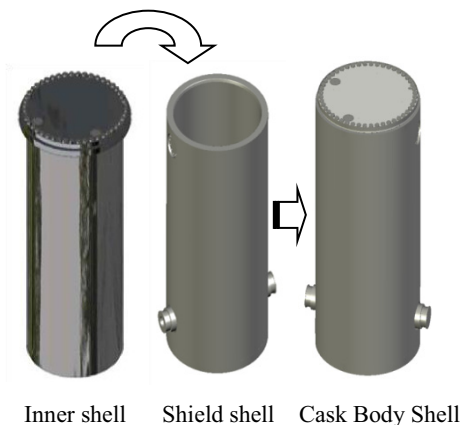


Fig. 2. Shrink Fitting Flow.

2.3.3 Neutron Shielding Material (RESIN). Radial neutron shield boxes filled in resin are arrayed around shield shell and outer shell will be assembled to the outside of cask as per Fig. 1.

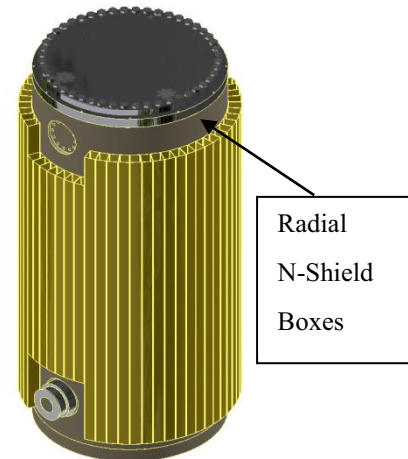


Fig. 3. Neutron Shield Box Assembly.

2.3.4 Sealing Surface between cask body and lid. Mock-Up Test performed to verify welding overlay process of Stainless Steel and leakage. The result is satisfied for such as below ;

- Surface Roughness
- Liquid Penetrant
- Helium leak test

3. Conclusions

According to the international standard and domestic standard, A full scale Prototype has being manufactured, that manufacturing techniques have also developed to meet the requirements. And the tests and inspections have been performed.

REFERENCE

- [1] Development of SNF Transportation and Storage Cask in Korea, Cho chun-hyung Ph.d (2016).
- [2] Dry Cask Storage, Hoi Ng (2014).
- [3] Advantages of Dry Hardened Cask storage over wet storage for spent nuclear fuel, Luiz Sergio Romanto (2011).

Numerical Analysis on Natural Convection of Backfill Gases in a Dry Storage System for Spent Nuclear Fuels

Hak Min Lee and Jae-Sung Kwon*

Incheon National University, Republic of Korea, 119, Academy-ro, Yeonsu-gu, Incheon, Republic of Korea

*jsungkwon@inu.ac.kr

1. Introduction

Dry storage systems cool down spent nuclear fuels passively, depending on the natural convection of backfill gases filled in the storage cask. As the representative backfill gases, there are helium, air nitrogen, and argon. This study was devised to investigate the characteristics of natural convection of the backfill gases and compare their cooling capability for spent nuclear fuels.

2. Numerical Analysis

The numerical modeling of the dry storage system was performed with Ansys Fluent software 14.0. For the modeling, some assumptions were taken into account. First, the system height was downscaled by a ratio of 1/2. Second, the assembly containing 8×8 spent nuclear fuel rods was considered in the system, instead of the full-scaled assembly of 16×16 fuel rods.

Figure 1 shows the side-view and top-view of inner structure of the dry storage system. Region 1 and 2 indicate the heated and plenum region of the fuel rods respectively. Region 3 represents the fluid region where a natural convective flow of backfill gases occurs. Each of region 4 and 5 indicates the canister and free air space. Stainless steel grade 304 (SS304) was used as a canister material. The FD 1, 2, and 3, and FR 1, 2, and 3 present the locations to extract data set in the fluid region. Heated region of the fuel rods was applied with a constant heat flux of 53.83 W/m^2 .

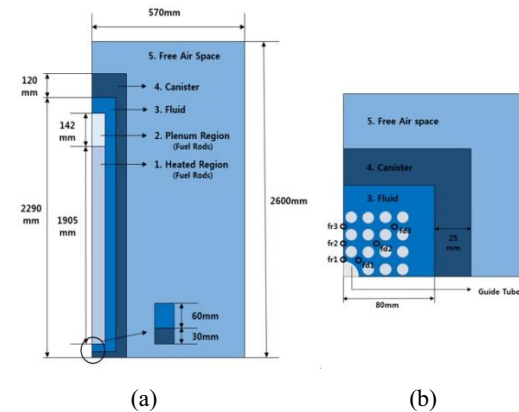


Fig. 1. (a) side view, (b) top view of modeled geometry.

3. Results

3.1 Peak Cladding Temperature (PCT)

Cladding surface temperature is an important parameter to estimate the effectiveness of passive heat removal by natural convection of the backfill gases and the integrity of fuel claddings. According to the Table 1 obtained from this study, the PCT increased in the order of nitrogen, air, helium and argon. While the PCT of nitrogen gas is about 433 K, argon is close to 456 K. It implies that the nitrogen shows the best heat dissipation among the four backfill gases.

Table 1. PCT value for each of back-fill gases

Fluid	Helium	Air	Nitrogen	Argon
PCT(K)	447.35	444.46	433.41	455.91

3.2 Axial Direction Reynolds Number Distribution

Figure 2 shows the axial distribution of Reynolds number (Re) in the sub-channels of the fuel rods

when using air. Except vicinity of the plenum region of the fuel rods, the Re values increase in the axial direction. The inertia of the natural convection flow is strongest at $z=1.0$ for all the sub-channels. Compared to the air, helium showed a very weak axial flow (data not shown). The Re of the flows range from 2 to 11. While argon showed a highest Re range, nitrogen showed a similar behavior with air but a slightly higher Re range.

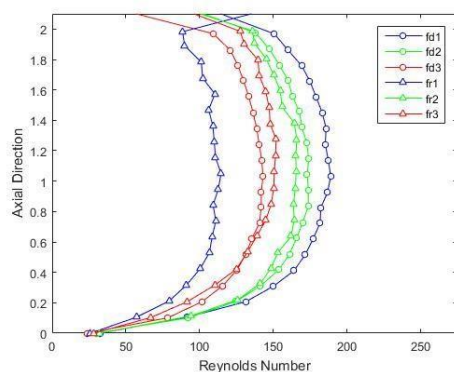


Fig. 2. Axial Reynolds Number distribution along the sub-channels for air.

3.3 Comparison of correlations between the Rayleigh and Nusselt Number

The overall empirical equation between Nu and Ra was compared with that defined by the Chu & Churchill's vertical wall correlation based on diameter of the canister.

The result with helium (data not shown) does not match very well as the average error was estimated about 67.02%. Argon shows average error of 16.10%, which is much less than helium. But natural convection of the gas was not observed in the subchannels. Air and nitrogen are in good agreement with the correlation with average error of 9.96% and 4.73%, respectively. These results give the conclusion that natural convection flows of air and nitrogen provide a better cooling capacity than helium and argon for spent nuclear fuels.

4. Conclusion

This study investigated the cooling capability of backfill gases in a dry storage system for spent nuclear fuels. The chosen gases are as follows: helium, air, nitrogen, and argon. Among the gases, nitrogen showed largest amount of heat dissipation.

ACKNOWLEDGEMENT

This research was supported by the National Research Foundation of Korea (NRF) grant funded by the Korean government (MSIP: Ministry of Science, ICT and Future Planning) (No. NRF-2018M2B2A9065822).

REFERENCES

- [1] Keyhani, M., Kulacki, F. A., and Christensen, R. N., 1985, "Experimental Investigation of Free Convection in a Vertical Rod Bundle-A General Correlation for Nusselt Numbers," *Journal of Heat Transfer*, Vol. 107, No. 3, pp. 611 ~ 623.
- [2] In, W. K., Kwack, Y. K., Kook, D. H., and Koo, Y. H., 2014, "CFD Simulation of Heat and Fluid Flow for Spent Fuel in a Dry Storage," *Transactions of Korean Nuclear Society Spring Meeting*, Jeju, Korea.
- [3] Churchill, S. W. and Chu, H. H. S., 1975, "Correlating equations for laminar and turbulent free convection from a vertical plate," *International Journal of Heat and Mass Transfer*, Vol. 18, No. 11, pp. 1323 ~ 1329.

Neutron Tomography as a Spent Fuel Cask Verification Technique

Myungsoo Kim, Juyoung Jeon, Seokryung Yoon, In-Jung Chang, Jinha Choi, and Heejun Chung*

Korea Institute of Nuclear Nonproliferation and Control, 1534, Yuseong-daero, Yuseong-gu, Daejeon, Republic of Korea

*hjchung2@kinac.re.kr

1. Introduction

Dry storage facilities with storage casks necessitate a reliable safeguarding technology that can detect diversions of spent fuel assemblies held in the casks. Recent studies performed by KINAC have shown that fast neutron counting can identify a cask having missing spent fuel assemblies. The demonstrated technique, however, has a limitation that the location of missing fuel assemblies cannot be specified.

As an alternative, we paid attention to neutron tomography, which is a technique that produces internal cross-sectional images by reconstructing multiple image profiles. Dry casks bearing spent fuel inevitably incorporate the emission of neutrons despite heavy neutron shielding. Hence neutron tomography can be a promising method to acquire cross-sectional images of the cask so that locations of missing assemblies can be pinpointed.

In this study, we designed a tomography system comprising detectors that simultaneously measure both fast and thermal neutrons. Two system configurations were taken into account to devise a system that can produce images with a better spatial resolution. Monte Carlo N-Particle transport code (MCNP) 6.2 was utilized to evaluate performances of systems.

2. Methods

We used Arktis S670e, combined fast and thermal neutron detector, that allows simultaneous detections of fast and thermal neutrons. The detector has a cylindrical shape with a diameter of 52 mm and active length of 600 mm. The detector inner wall is lined with Li-6 for thermal neutron detection. The cylindrical body is filled with He-4 gas with an approximate pressure of 180 bar and a gas density of 32.2 mg/cm^3 for fast neutron detection. Either fast or thermal neutrons produces an analog pulse signal as output. The control unit distinguishes whether the signal is produced from fast or thermal neutrons by applying Time Over Threshold (TOT) based on Pulse Shape Discrimination (PSD) method [1]. Using this detector model, tomography systems were constructed.

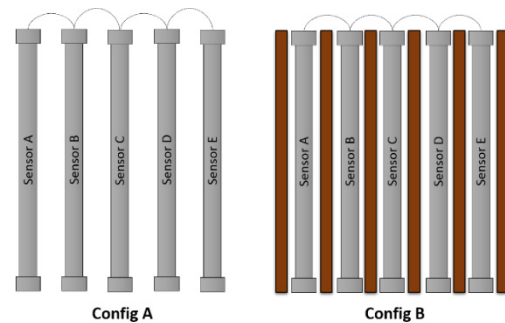


Fig. 1. System configurations; system without collimators (Config A) and system with collimators (Config B).

Figure 1 illustrates system configurations (Configs) evaluated in this study. Both Configs are designed in a 1-by-5 detector array. Config A plainly includes five detectors with 68 mm even spacing. Config B is constructed with plastic wall-shape collimators. The collimators placed between the detectors extend towards the cask as shown in Figure 2. The system intends to be installed vertically on the ground.

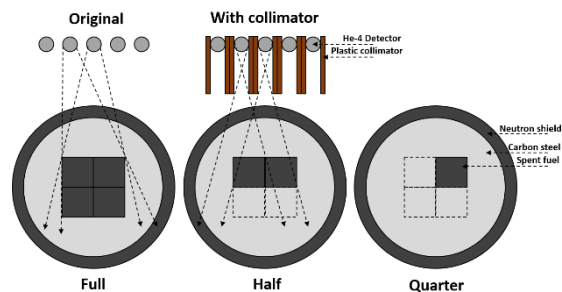


Fig. 2. Schematic diagrams of dry storage casks holding no (full), two (half), and three (quarter) missing assemblies.

Figure 2 demonstrates modelled 1/4-size casks and systems located at zero-degree position. The cask is designed to hold maximum four assemblies with carbon steel and Holtite neutron shielding. System performances were investigated with two diversion scenarios that involve two and three missing fuel assemblies as given in Figure 2. Multiple image profile around the cask was simulated by changing the measurement position along the perimeter in increments of 20 degrees. The simulations were run until simulated fluxes at He-4 gas were calculated to within a 10% error. Inverse radon transform method [2] was used to reconstruct images from the profiles.

3. Results and discussions

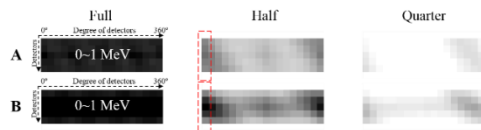


Fig. 3. Sinogram from Configs A (above) and B (below).

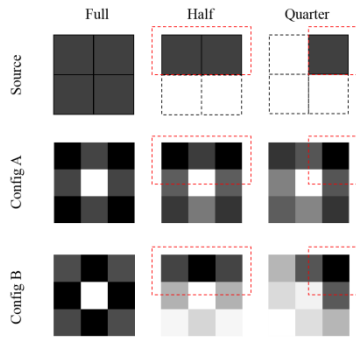


Fig. 4. Reconstruction image from Configs A and B.

Tallied neutron fluxes in the energy of 0~1 MeV were used to generate sinograms shown in Figure 3. Darker pixels represent higher counts recorded, and vice versa. A sinogram contains a 5-by-18 pixel array. Five pixels in a column (highlighted in red-dotted-line) describe tallied flux from five individual detectors. Each column indicates a single measurement position. Figure 4 contains their reconstruction images with fuel assembly positions highlighted in red-dotted-line. The minimum and maximum value of each images were used as white and black of each images, respectively.

Figure 4 proves that empty assembly positions are identified as brighter pixels in the image. Both images from Configs A and B demonstrate that missing assemblies contribute to less neutron counts, which in turn gives rise to brighter pixels. The figure also shows that Config B including the collimators allows the clearer recognition of the positions. Since Config A suffers from the neutron scattering, the system is prone to having the deteriorated spatial resolution.

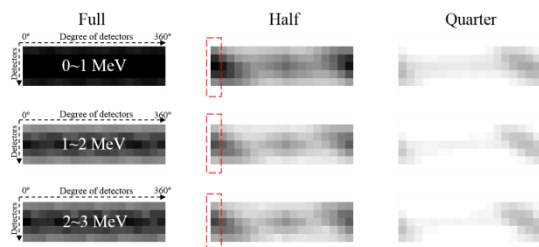


Fig. 5. Sinogram from Config B in different energy ranges.

Results from Config B were further studied. Figure 5 includes additional sinograms generated with two more energy ranges, 1~2 MeV and 2~3 MeV. We then performed the image reconstruction as illustrated in Figure 6. All the images has the same display range.

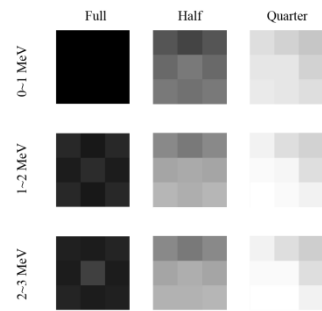


Fig. 6. Reconstruction image from Config B using different energy ranges.

In Figure 6, it is noteworthy that better radiometric resolution can be attained in 0~1 MeV range, whereas better special resolution can be achieved in 2~3 MeV range. It implies that combining images reconstructed using different energy ranges can improve the quality.

4. Conclusions

In this study, we investigated the feasibility of neutron tomography to locate positions of missing spent fuel assemblies accommodated in dry storage cask. Utilizing combined thermal and fast neutron detectors, tomography systems were devised and demonstrated in Monte Carlo space.

The simulation study proved that the modelled tomography system was able to provide location information on the missing fuel assemblies. Taking advantage of the reduced scattering effect, the system with collimators led to the better special resolution. We also found that there is room for improvement in the image quality by consolidating information that can be obtained from different energy ranges. Future works include the development of an optimized algorithm that can allows the effective identification of missing fuel assemblies.

ACKNOWLEDGEMENT

This work was supported by the Nuclear Safety Research Program through the Korea Foundation Of Nuclear Safety (KoFONS) using the financial resource granted by the Nuclear Safety and Security Commission (NSSC) of the Republic of Korea. (No.1803025)

REFERENCES

- [1] Zhu, Ting, et al. "Improved fission neutron energy discrimination with ^4He detectors through pulse filtering." Nuclear Instruments and Methods in Physics Research Section A: Accelerators, Spectrometers, Detectors and Associated Equipment 848 (2017): 137-143.
- [2] Avinash C. Kak, and Malcolm Slaney. Principles of computerized tomographic imaging. New York: IEEE press, 1988.

2분과

사용후핵연료 처분전관리 (Poster)



Thermal Test of KORAD-21 Cask

K.S. Bang*, S.H. Yu, J.C. Lee, K.S. Seo, and W.S. Choi

Korea Atomic Energy Research Institute, 111, Daedeok-daero 989beon-gil, Yuseong-gu, Daejeon, Republic of Korea

*nksbang@kaeri.re.kr

1. Introduction

A KORAD-21 cask containing 21 spent fuel assemblies is under development by the Korea RADioactive waste agency (KORAD) in Korea.

Since the KORAD-21 cask is used for not only storage but also transport of the spent fuel assemblies, it should satisfy the requirements that are prescribed in the Korea NSSC Act 2017-56, IAEA Safety Standard Series No. TS-R-1 and US 10 CFR Part 71 [1~3]. These regulatory guidelines classify the KORAD-21 cask as a Type B package, and state that a Type B package for transportation of radioactive materials should be able to withstand a period of 30 minutes under a thermal condition of 800°C. Accordingly, a thermal test using a 1/6 sliced model of a real cask have been performed to estimate the thermal integrity of the KORAD-21 cask under a thermal condition of 800°C.

2. Thermal Test

2.1 Description of the KORAD-21Cask

The KORAD-21 cask was designed as a shipping cask to accommodate 21 pressurized water reactor (PWR) spent fuel assemblies with a burn-up of 45,000 MWD/MTU and a cooling time of 10 years. The decay heat from the 21 PWR spent fuel assemblies is 16.8 kW. Its outer diameter is 2,126 mm and its overall height is 5,285 mm. It weighs approximately 125 t. It consists of a thick-walled cylindrical cask body, a neutron shielding, a dry shielded canister (DSC), a lid, baskets to hold the spent nuclear fuel, and impact limiters (Fig. 1). The cask body is made of carbon steel. The outer-shell is made of stainless steel. The baskets containing the spent fuel assemblies are made of stainless steel. The inner cavity between the outer-shell and the cask body is filled with NS-4-FR, which acts as a neutron shielding. NS-4-FR has a low thermal conductivity. Therefore, heat transfer fins are embedded to enhance heat transfer from the cask body to the outer-shell.

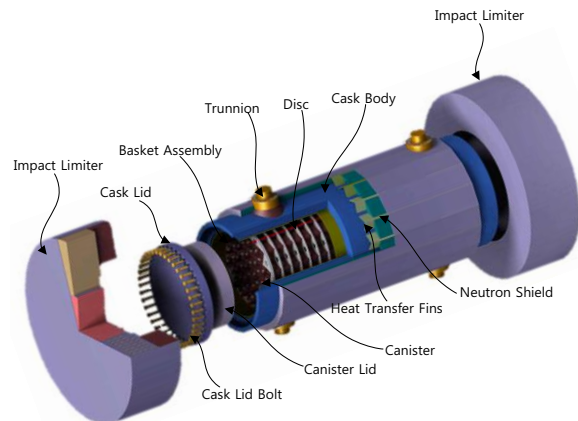


Fig. 1. Configuration of KORAD-21 Cask.

2.2 Open Pool Fire Test

As shown in Fig. 2, the thermal test was carried out in a fire test facility with the dimensions of 3.5 m x 4.0 m x 3.0 m.

The thermal test was performed as follows:

- The supporter to set the test model within the fire test facility was installed.
- The test model was set onto the supporter.
- 21 thermocouples for measuring the flame temperature inside the fire test facility were installed.
- The water was filled with a height of 5 cm in the pit, and the kerosene was filled with a height of 10 cm from the surface of the water.
- The test model was allowed to stand for a period of at least 30 minutes under a fully engulfed thermal environment with an average flame temperature of at least 800°C.



Fig. 2. Test model in the fire test facility.

In the fire test, the environmental temperature in the fire test facility was maintained at approximately 25°C before the ignition of the fire. The fire was applied for approximately 35 minutes. Fig. 3 shows a photograph of the test model fully engulfed in flames. Fig. 4 shows the change in the flame temperature during the fire test. The average flame temperature during the fire test was 438°C in the growth period, 851°C in the steady-state period, and 462°C in the decay period. Therefore, the thermal conditions prescribed in the regulatory guidelines were satisfied.

The maximum temperatures measured in the test model during the fire test are listed in Table 1. The maximum surface temperature was 957°C after 24 min in the middle part. The surface temperature was very high because the flame temperature was at the maximum of 1000°C during this time, and the conductive heat transfer coefficient of the neutron shielding was not good, leading to the accumulation of thermal energy at the model surface. However, the temperature of the surface where the heat transfer fin was installed was 624°C. From these results, we can determine that the surface temperatures were lower in the presence of the heat transfer fins because the high heat generated by the flame was transferred to the body of the test model through the heat transfer fin.

The maximum temperature of the neutron shield was measured to be 151°C after 75 min.

The initial temperature of the basket before the pool fire test was 23°C. The maximum temperature was 58°C after the fire was extinguished and when 19.8 h had passed. Accordingly, the temperature rise in the basket during the fire test was 35°C. Therefore, the temperature rise of the spent nuclear fuel rod can be anticipated to be within this range.



Fig. 3. Test model engulfed in flames.

From the results of the pool fire test, the thermal integrity of the dual purpose cask can be maintained at a temperature of 800°C for a period of 30 min.

3. Conclusion

As a part of the safety tests, the thermal test was carried out to evaluate the thermal integrity of the KORAD-21 cask. The main results were as follows:

- i) The temperature rise of the basket during the fire test was 35°C. Therefore, the temperature rise of the spent nuclear fuel rod can be anticipated to be within this range. Accordingly, the integrity of a spent nuclear fuel is estimated to be maintained.
- ii) The surface temperature was lower when a heat transfer fin was installed because the high heat generated by the flame was transferred to the body of the test model through the heat transfer fin. The neutron shielding was therefore adequately protected by the heat transfer fin.

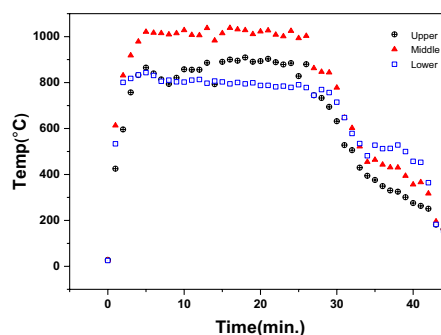


Fig. 4. Flame temperature during the thermal test.

Table 1. Summary of the thermal test results

Location	Temp(°C)	Steady State	Transient	Elapsed Time(h)
Basket		23	58	19.8
Canister Surface		24	64	10.9
Body Surface		26	141	0.3
Neutron Shield		32	151	1.25
Cask Surface		43	957	0.4
Ambient(Average)		25	851	

REFERENCES

- [1] KOREA NSSC Act. 2017-56, "Regulations for the Safe Transport of Radioactive Material", 2017.
- [2] IAEA Safety standard Series No. SSR-6, "Regulations for Packaging and Transportation of Radioactive Material", 2012 Ed.
- [3] U.S. Code of Federal Regulations, Title 10, Part 71, "Packaging and Transportation of Radioactive Material", 2005 Ed.

Criticality Analysis for Loading Curve Generation for OASIS-32D Cask With PLUS7 Fuel

Keon Young Bae*, Young Tae Han, Yong Il Kim, Joon Gi Ahn, In Ho Song, and Gyu Cheon Lee
Korea Electric Power Corporation E&C, 111, Daedeok-daero 989beon-gil, Yuseong-gu, Daejeon, Republic of Korea
*kybae@kepco-enc.com

1. Introduction

The OASIS-32D is a dual purpose (storage and transportation) metal cask under development by KEPCO E&C. It is designed to store 32 spent nuclear fuels (SNF). In this study, the depletion and criticality calculations are performed to evaluate criticality safety of the OASIS-32D. The cask is modeled as loaded with 10-year cooled PLUS7 fuel as shown in Figure 1.

The NUREG-1536 [1] subsection 7.4 is applied as the criticality safety design criteria. The acceptance criterion is such that k_{eff} including all biases and uncertainties at 95 percent confidence level should not exceed 0.95 under all credible normal, off-normal, and accident-level conditions.

The loading curves are generated for a target k_{eff} value of 0.95. The biases and uncertainties associated with the calculation methods as well as variations of design parameters are included in k_{eff} calculations.

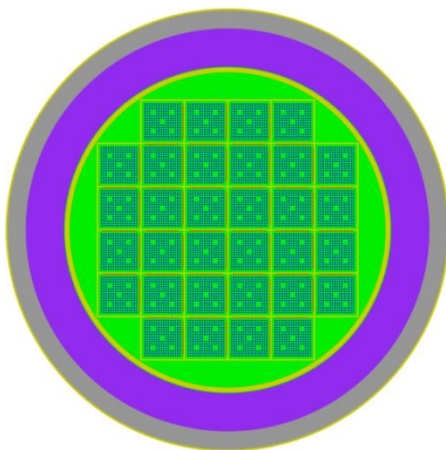


Fig. 1. X-Y cross-section View of OASIS-32D with PLUS7 Fuel.

2. Methods and Results

The SCALE 6.0 code package [2] is used for depletion and criticality calculations. The depletion calculations are performed using the ORIGEN-ARP with cross section libraries which are pre-generated by the TRITON-NEWT for the PLUS fuel depletion. The criticality calculations are performed using the CSAS5/KENO-V.a with the ENDF/B-VII 238-neutron energy-group library.

In order to determine the loading curve, criticality analyses are performed to find the minimum burnup which produces k_{eff} less than 0.95 at each initial enrichment of fuel assemblies.

The biases and uncertainties associated with the calculation methods, variations of design parameters and the depletion calculation are estimated from the following items:

- Biases and bias uncertainties of the criticality calculation method,
- Statistical uncertainty of the Monte Carlo calculation,
- Uncertainty due to tolerances or variations in the design parameters,
- Uncertainty due to eccentric fuel assembly positioning,
- Bias due to axial burnup distribution (end effect),
- Bias due to the fuel temperature in depletion calculation,
- Bias due to minor actinides and fission products,

- Uncertainty due to reactor burnup record, and
- Uncertainty due to the depletion calculation.

All biases are directly added to determine the total bias. Therefore, the total bias is the sum of all the biases due to the methodology, the minor actinides and fission products, the axial power distribution, and the fuel temperature in depletion calculation. etc.

All uncertainty values are statistically combined (the square root of the sum of the squares) to determine the total uncertainty. The uncertainties are due to the methodology, the Monte Carlo calculation, the mechanical tolerance, the reactor burnup record, and the depletion.

The calculated k_{eff} values considering the total bias and uncertainty are summarized in Table 1.

Table 1. k_{eff} with Bias and Uncertainty

Burnup (gwd/mtu)	Final k_{eff} + bias and uncertainty			
	2.0wt%	3.0wt%	4.0wt%	5.0wt%
2.25	0.91294			
6.75	0.89005	0.97341		
11.25		0.93488		
13.50		0.91901		
18.00			0.96666	
20.25			0.95448	
24.75			0.93416	
27.00				0.98024
31.50				0.96248
36.00				0.94543

The loading curve is the minimum burnup which satisfies the target k_{eff} for each initial enrichment. The curve is produced by targeting the k_{eff} less than 0.95 with considering all the biases and uncertainties in this analysis.

The calculated loading curve for OASIS-32D bounds 98.9% of the discharged fuel population as indicated in Figure 2. Discharged fuel population data are from the 2013 Energy Information Administration (EIA) GC-859 Nuclear Fuel Data Survey [3] which is a reliable and relatively recent estimate of the discharged fuel population.

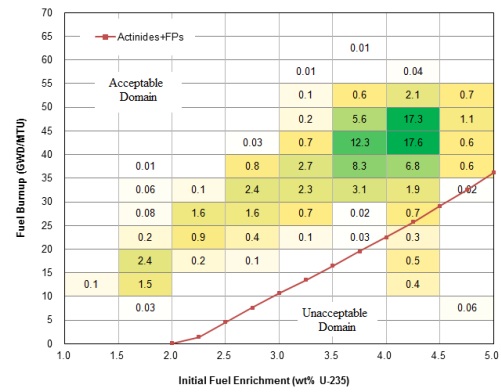


Fig. 2. Loading Curves for the OASIS-32D Superimposed over the GC-859 Data (%).

3. Conclusion

The k_{eff} s for various cases of initial enrichments and burnups of SNF loaded in the OASIS-32D cask are calculated to obtain loading curve in this study. The biases and uncertainties are properly applied for a conservatism in the loading curve. The loading curve for the OASIS-32D cask with PLUS7 fuel has been successfully generated. The loading curve bounds 98.9% the discharged fuel population [3]. Therefore, it is concluded that most of the discharged fuel can be stored in the OASIS-32D cask.

REFERENCES

- [1] NUREG-1536, Rev.1, "Standard Review Plan for Spent Fuel Dry Storage Systems at a General License Facility," U.S. Nuclear Regulatory Commission, July 2010.
- [2] "SCALE: A Modular Code System for Performing Standardized Computer Analyses for Licensing Evaluations," ORNL/TM-2005/39, Version 6, Vols. I-III, Oak Ridge National Laboratory, Jan. 2009.
- [3] GC-859 Nuclear Fuel Data Survey 1968 through June 30, 2013, Energy Information Administration, Washington, D.C.

Comparison Analysis of the Uncertainty Due to Fuel Depletion in the Criticality Analysis for OASIS-32D

Young Tae Han*, Yong Il Kim, Joon Gi Ahn, In Ho Song, and Gyu Cheon Lee

Korea Electric Power Corporation E&C, 111, Daedeok-daero 989beon-gil, Yuseong-gu, Daejeon, Republic of Korea

*ythan@kepco-enc.com

1. Introduction

The burnup credited criticality safety analysis shall consider the uncertainty due to fuel depletion. Historically the uncertainty has been based on a rough engineering judgment such as 5% of the reactivity decrement to the burnup according to Kopp's memo [1]. However, more definite validation analysis of the uncertainty due to fuel depletion has been performed and published as NUREG/CR-7108 [2].

In this study, a comparison analysis of the criticality uncertainty due to fuel depletion based on Kopp's memo and NUREG/CR-7108 is performed for the KEPKO E&C's OASIS-32D dual purpose metal cask model.

2. Uncertainty Analysis and Results

2.1 Uncertainty Calculation based on Kopp's memo

Suggested by Kopp's memo, the reactivity uncertainty due to uncertainty in the fuel depletion calculations is assumed as 5% of the reactivity decrement to the burnup, which means that 5% of the calculated reactivity difference between fresh fuel and burned fuel models is the uncertainty involved.

The effective multiplication factors (k_{eff}) are calculated for the OASIS-32D cask model (Figure 1) with ACE7 fuel having various burnup-enrichment combinations using the SCALE6.0/CSAS5. The computer program and cross section library used for the fuel depletion calculation are SCALE6.0/ TRITON and ENDF/B-VII. The calculated reactivity decrement

by fuel depletion is summarized in Table 1.

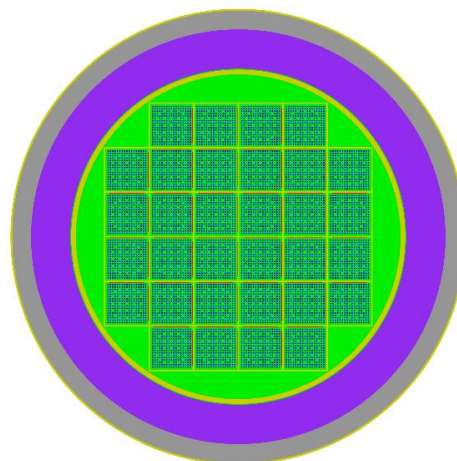


Fig. 1. Cross Section View of the OASIS-32D Cask.

Table 1. Uncertainty Calculated based on Kopp's memo

Burnup (gwd/mtu)	The uncertainty (Δk) due to depletion			
	2.0wt%	3.0wt%	4.0wt%	5.0wt%
2.25	0.00100	0.00137		
9.00		0.00471		
15.75			0.00743	
24.75			0.01130	0.01038
33.75				0.01399

The uncertainty due to fuel depletion based on Kopp's memo increases with burnup. The reason of this trend is clear because the reactivity difference is increasing as burnup increases.

2.2 Uncertainty Provided in NUREG/CR-7108

NUREG/CR-7108 addresses the validation of depletion calculations which is performed by comparing calculated nuclide concentrations to available measurements of nuclide concentrations, and provides reference k_{eff} bias and bias uncertainty results as shown in Table 2. The uncertainty in Table

2 was evaluated for the representative PWR cask model, GBC-32, using SCALE6.1/TRITON and ENDF/B-VII.

Table 2. Uncertainty Provided in NUREG/CR-7108

Burnup (gwd/mtu)	The uncertainty (Δk) due to depletion			
	2.0wt%	3.0wt%	4.0wt%	5.0wt%
2.25	0.01500	0.01500		
9.00		0.01480		
15.75			0.01570	
24.75			0.01540	0.01540
33.75				0.01630

As shown in this table, the uncertainties due to fuel depletion in NUREG/CR-7108 are almost same for all combinations of burnup-enrichment. The reason described in NUREG/CR-7108 is that the uncertainties in the calculated U-235 & Pu-239 concentrations contribute about 90% of the k_{eff} bias uncertainty, while the uncertainty in the calculated fission product concentrations is small (<3% of the k_{eff} bias uncertainty).

2.3 Comparison of Results

The computer program and cross section library used for the fuel depletion calculation in the *subsection 2.1* (SCALE6.0/TRITON, ENDF/B-VII) are same as those used in *subsection 2.2* (SCALE6.1/TRITON, ENDF/B-VII) because the difference between SCALE6.0 and SCALE6.1 is negligible. The OASIS-32D cask model for *subsection 2.1* is similar to the GBC-32 cask model for *subsection 2.2* because both of them can accommodate 32 PWR assemblies, and use Boral panels containing B-10 as a fixed neutron poison. Also, the burnup credit in *subsection 2.1* is limited to the specific 28 actinide and fission product nuclides listed in NUREG/CR-7108. Therefore, the two sets of uncertainties are comparable.

Table 3 shows the comparison of the uncertainty due to fuel depletion according to Kopp's memo and NUREG/CR-7108

Table 3. Comparison of Uncertainties

Burnup (gwd/mtu)	(Kopp's memo) / (NUREG/CR-7108)			
	2.0wt%	3.0wt%	4.0wt%	5.0wt%
2.25	7%	9%		
9.00		32%		
15.75			47%	
24.75			73%	67%
33.75				86%

As shown in this table, the uncertainty due to depletion provided in NUREG/CR-7108 is higher than that calculated according to Kopp's memo.

3. Conclusion

The results showed that the uncertainty due to depletion provided in NUREG/CR-7108 is higher than that calculated according to Kopp's memo over the whole evaluated burnup range for OASIS-32D.

The uniform uncertainty regardless of burnup provided in NUREG/CR-7108 shows that the uncertainty contribution from the fission products takes small portion while the contribution from the other nuclides takes great portion.

So, the uncertainty of NUREG/CR-7108 is applied to the criticality analysis of OASIS-32D.

REFERENCES

- [1] Memorandum from L. Kopp to T. Collins, "Guidance on the Regulatory Requirements for Criticality Analysis of Fuel Storage at Light-Water Reactor Power Plants," U.S. NRC, August 19, 1998.
- [2] G. Radulescu, I. C. Gauld, "An Approach for Validating Actinide and Fission Product Burnup Credit Criticality Safety Analyses – Isotopic Composition Predictions," NUREG/CR-7108 (ORNL/TM-2011/509), U.S. NRC, Oak Ridge National Laboratory, April 2012.

Shielding Effects of Reinforcement Structure and Heat Transfer Fin in the OASIS-32D Cask

Yong IL Kim*, Young Tae Han, Joon Gi Ahn, In Ho Song, and Gyu Cheon Lee

Korea Electric Power Corporation E&C, 111, Daedeokdae-ro 989beon-gil, Yuseong-gu, Daejeon, Republic of Korea

*yongil@kepco-enc.com

1. Introduction

The shielding effects of Reinforcement Structure (RS) and Heat Transfer Fin (HTF) in the OASIS-32D cask have been examined. The OASIS-32D is a dual purpose metal cask for spent nuclear fuel transport and storage developed by KEPSCO E&C. It is designed to store 32 PWR spent fuel assemblies (FA) that have been cooled for 10 years. The RS is a component lying between basket and canister for fixing the basket. The HTF is a component embedded in the neutron shield outside of cask shell for heat removal from inside to cask surface. Both components have discontinuity in shielding point of view, axial in RS and azimuthal in HTF. The shielding effects of RS and HTF have been examined in this paper by using MAVRIC module of SCALE 6.1 code [1]. MAVRIC is a 3-dimensional Monte Carlo particle transport code with automated variance reduction using importance calculations by deterministic method to enhance calculation efficiency.

2. Methods and Results

2.1 Source term calculation

The radiation sources for the shielding analysis are neutrons and gammas from ACE7 spent nuclear fuel with 10 years of cooling time obtained from the depletion calculation using ORIGEN-ARP module of SCALE 6.1 code. In the depletion calculation, the

ACE7 fuels with an initial enrichment of 3.5wt% are assumed to be burned for three cycles at a power level of 40 MWt/MTU in the reactor core and have total discharge burnup of 45 GWD/MTU.

2.2 Shielding analysis

To examine the shielding effects of the RS and HTF, transport calculations have been performed and compared for various combination of cases with and without the corresponding structures. The calculation cases were setup as shown in Table 1 to compare the shielding effects of the RS and HTF.

Table 1. Calculation models

Case	Component Combination	Note
1	RS, HTF (bent shape)	All components included, Reference case
2	No RS, HTF (bent shape)	RS removed
3	RS, No HTF	HTF removed and replaced by neutron shield material
4	RS, HTF (straight shape)	All components included, straight shape HTF used

The partial view of OASIS-32D cask is shown in Figure 1. The basic model of HTF has a shape with a bent at 60 degrees as shown in Figure 1-a and made of aluminum. In addition to the basic HTF model, the shielding effect of the HTF shape was also evaluated by replacing with a straight shape HTF as shown in Figure 1-b. The neutron shield material, resin, is not shown in Figure 1 to represent the HTF structure clearly.

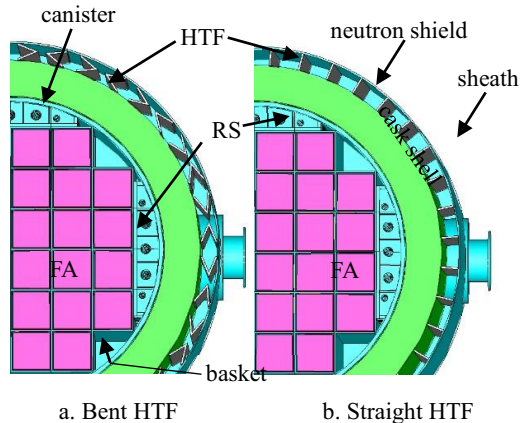


Fig. 1. Partial view of OASIS-32D cask.

2.3 Results

The calculated dose rate distributions for analyzed cases are shown in Figure 2.

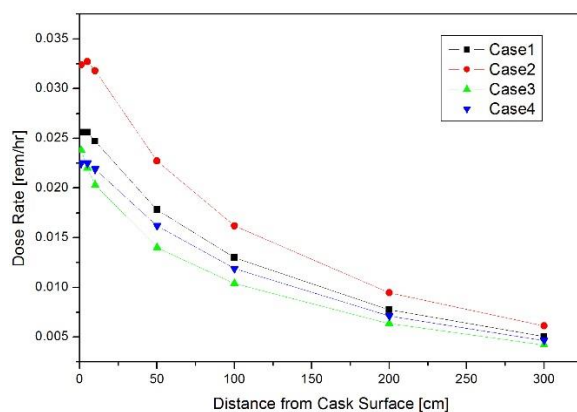


Fig. 2. Dose rate distributions.

Previous OASIS-32D cask shielding analysis experience [2] has shown that the most demanding dose requirements required by the relevant regulations [3] is the dose condition at a distance of 2m from the side of the cask surface. Therefore, the shielding effects of RS and HTF based on the 2m dose rate are summarized as follows:

1. No RS (Case 2): 22% increase
2. No HTF (Case 3): 18% decrease
3. Straight shape HTF (Case 4): 8% decrease

The results show that the RS has shielding effect of 22% compared to No RS model and the shielding

effect is higher when the HTF is not used unlike the RS. The negative shielding effect of HTF is due to the fact that the amount of shielding material, resin, is reduced by the inclusion of HTFs in the neutron shield that is effective in neutron shielding. The shielding effect of the HTF shape can be interpreted in the same context because the amount of shielding resin is smaller in the basic model, the bent shape, than that in the straight shape model. It should be noted that the specific figures of the shielding effects are only valid for OASIS-32D cask model and they depend on the specific geometry and materials.

3. Conclusions

The analyses performed on shielding effects of RS and HTF showed that the straight HTF is more effective on the shielding point of view than the bent HTF. Also, the straight shape HTF is known as more efficient on heat transfer point of view than the bent shape. Therefore, it is recommended that the HTF of the OASIS-32D cask be designed in a straight shape.

REFERENCES

- [1] "SCALE: A Comprehensive Modeling and Simulation Suite for Nuclear Safety Analysis and Design," ORNL/TM-2005/39, Version 6.1, Oak Ridge National Laboratory, June 2011.
- [2] "Shielding Design for the Development of Spent Fuel CASK for Transportation and Storage," Proc. KRS Autumn 2015, Busan, Sec. I, p. 33, Korean Radioactive Waste Society, October 14-16, 2015.
- [3] 10CFR71, "Packaging and Transportation of Radioactive Material," 1996.

Scaling Analysis of Spent Fuel Storage Cask for Thermal Test Using a Scaled Down Model

Ju-Chan Lee^{1)*}, Kyung-Sik Bang¹⁾, Seung-Hwan Yu¹⁾, Woo-Seok Choi¹⁾, and Sungho Ko²⁾

¹⁾ Korea Atomic Energy Research Institute, 111, Daedeok-daero 989beon-gil, Yuseong-gu, Daejeon, Republic of Korea

²⁾ Chungnam National University, 99, Daehak-ro, Yuseong-gu, Daejeon, Korea

*sjclee@kaeri.re.kr

1. Introduction

Concrete storage cask loaded with 21 spent PWR fuel assemblies is more than 100 tons in weight. Thermal test using a full scale model requires a lot of cost and time. Therefore, a scale down model is generally used for efficient thermal test. The purpose of this study is to derive the scaling factors for simulating the thermal flow phenomenon using a scale down model, and to evaluate the similarity between the full scale and scale down models.

2. Scaling analysis of concrete storage cask

Concrete cask has four air inlet & outlet ducts, and air flow path between the cask body and canister for a natural cooling system. Decay heat generated from the spent fuel is transferred to the outside through the air circulation from the air path, conduction from the cask body, and convection & radiation from the cask surface. Scale ratios were derived based on the theoretical approach for the heat transfer through the air path and the cask body.

2.1 Heat transfer mode through air flow path

Scale ratios for the conditions that all heat is removed through the air path and the temperature at the air outlet is conserved between the full scale and scale down models are derived as follows[1].

- Heat flux and heat generation rate:

$$q'' = \frac{q}{\pi DH}, \quad \dot{q} = \frac{q}{A_{canH}} \quad (1)$$

$$[q'']_{ratio} = [\dot{q} \times L_c]_{ratio}, \quad [\dot{q}]_{ratio} = \left[\frac{q''}{L_c} \right]_{ratio} \quad (2)$$

- Heat transfer rate through air outlet:

$$q = \dot{m} C_p (\Delta T) = \rho u A_{duct} \times C_p (\Delta T) \quad (3)$$

- Conservation of temperature difference:

$$[q]_{ratio} = [\dot{m}]_{ratio} \quad (4)$$

- Temperature increase at the air outlet:

$$\Delta T = \frac{q}{\dot{m} C_p} = \frac{\dot{q} \times A_{can} \times H}{\rho u A_{outlet} \times C_p} \quad (5)$$

$$[\dot{q}]_{ratio} = \left[\frac{u}{H} \right]_{ratio} = \left[\frac{u}{L_c} \right]_{ratio} \quad (6)$$

- Buoyancy and pressure drop from the air outlet:

$$(\Delta \rho) g H_p = \rho \beta \Delta T \times g H_p = \frac{1}{2} \rho u^2 \times f \quad (7)$$

$$\rho \beta \frac{\dot{q} A_{can} H}{\rho u A_{flow} C_p} g H_p = \frac{1}{2} \rho u^2 f \quad (8)$$

$$u^3 = 2 g \beta \frac{\dot{q} H A_{can}}{\rho C_p A_{flow}} H_p \times \frac{1}{f} \quad (9)$$

- Scale ratio for velocity of air:

$$[u]_{ratio} = \frac{u_m}{u_p} = \left[\left(2 g \beta \frac{\dot{q} H A_{can}}{\rho C_p A_{flow}} H_p \times \frac{1}{f} \right)^{\frac{1}{3}} \right]_r \quad (10)$$

$$[u]_{ratio} = \left[(\dot{q} H H_p)^{\frac{1}{3}} \right]_r = \left[(\dot{q} L_c^2)^{\frac{1}{3}} \right]_{ratio} \quad (11)$$

$$[u]_{ratio} = \left[\left(\frac{u}{L_c} L_c^2 \right)^{\frac{1}{3}} \right]_{ratio} = [L_c^{\frac{1}{2}}]_{ratio} \quad (12)$$

- Scale ratio for heat generation rate:

$$[\dot{q}]_{ratio} = \left[\frac{u}{L_c} \right]_{ratio} = \left[\frac{L_c^{\frac{1}{2}}}{L_c} \right]_{ratio} = \left[\frac{1}{L_c^{\frac{1}{2}}} \right]_r \quad (13)$$

$$[q'']_{ratio} = [\dot{q} L_c]_{ratio} = [L_c^{\frac{1}{2}}]_{ratio} \quad (14)$$

$$[q]_{ratio} = [\dot{q} A_{can} H]_{ratio} = [L_c^{\frac{5}{2}}]_{ratio} \quad (15)$$

- Scale ratio for mass flow rate:

$$[\dot{m}]_{ratio} = [q]_{ratio} = [L_c^{\frac{5}{2}}]_{ratio} \quad (16)$$

2.2 Heat transfer through air path and cask body

In the real cask, the decay heat from the spent fuel is removed through the air path and the cask body. In the full scale prototype cask, it was analyzed that about 77% of the heat was removed through the air path, and the remaining 23% was removed through the cask body. In the half scale model, about 64% of the heat was removed through the air path. Therefore, it is necessary to derive the scale ratios considering the heat loss through the cask body. A correction factor is introduced in order to derive the scale ratios considering the heat loss of the cask body.

$$\alpha q = \dot{m} C_p (\Delta T) = \rho u A_{duct} \times C_p (\Delta T) \quad (17)$$

In the equation (17), α is the correction factor of

the heat source. The correction factor is expressed as the ratio of the heat transfer rate through the air path in the full scale and half scale models.

$$\alpha = \frac{q_p}{q_m} + \frac{0.767}{0.637} = 1.204 \quad (18)$$

From the equation (13) ~ (15), the scale ratios for the heat generation rates considering the heat loss from the cask body are calculated by multiplying the correction factor. Table 1 summarizes the scale ratios of the half scale model for the heat transfer modes through the air path and the cask body.

$$[\dot{q}]_{ratio} = \left[\frac{1}{L_c^{1/2}} \right]_{ratio} \alpha = \sqrt{2} \alpha = 1.702 \quad (19)$$

$$[q'']_{ratio} = \left[L_c^{1/2} \right]_{ratio} \alpha = \frac{1}{\sqrt{2}} \alpha = 0.851 \quad (20)$$

$$[q]_{ratio} = \left[L_c^{5/2} \right]_{ratio} \alpha = \frac{1}{\sqrt{2^5}} \alpha = 0.213 \quad (21)$$

Table 1. Scale ratios for a half scale model of storage cask

Scale ratios		
	air path	air path & cask body
$[\dot{q}]_{ratio}$	$\sqrt{2} = 1.414$	$\sqrt{2} \alpha = 1.702$
$[q'']_{ratio}$	$\frac{1}{\sqrt{2}} = 0.707$	$\frac{1}{\sqrt{2}} \alpha = 0.851$
$[q]_{ratio}$	$\frac{1}{\sqrt{2^5}} = 0.177$	$\frac{1}{\sqrt{2^5}} \alpha = 0.213$
$[u]_{ratio}$	$\frac{1}{\sqrt{2}} = 0.707$	$\frac{1}{\sqrt{2}} = 0.707$
$[\dot{m}]_{ratio}$	$\frac{1}{\sqrt{2^5}} = 0.177$	$\frac{1}{\sqrt{2^5}} = 0.177$

3. Similarity analysis between full scale and scale models using a scale ratio

3.1 Heat transfer mode through air flow path

The CFD analysis was performed for a half scale model using the scale ratio obtained in the heat transfer mode through the air flow path. The air outlet temperatures were similar between the full scale and half scale models. The ratios for air velocity and mass flow rate of the air outlet in the half scale model were similar to the theoretical scale ratios. Therefore, the reliability of the scale ratios has been proven.

3.2 Heat transfer through air path and cask body

The CFD analysis was performed for the heat transfer modes through the air path and cask body. Table 2 summarizes the analysis results between the full scale and half scale models. In the full scale model, 76.7% of decay heat was removed through the air path. In the half scale model, the convection effect was reduced, and 63.7% of the decay heat was removed through the air path. The temperatures of the air outlet were calculated as 63.9°C and 62.8°C in

the full scale and half scale models, respectively. The mean velocity of the air outlet is 0.520 m/s in the half scale model, which is 0.701 times compared to the full scale model.

Velocity ratio is similar to the theoretical scale ratio of 0.707. The mass flow rates at the air outlet were calculated as 0.2923 kg/s and 0.0509 kg/s in the full scale and half scale models, which is similar to the scale ratio of 0.177. Therefore, the reliability of the scale ratios has been proven. In the half scale model using the scale ratio with the correction factor, the temperature distributions were similar to those of the full scale model except for the cask surface temperature.

Table 2. CFD analysis results using scale ratios for heat transfer mode through the air path and cask body

	Full scale ($q''=1.0$)	Half scale ($q''=0.851$)	Ratio
Heat source	16.8 kW	3.574 kW	0.213
Heat flux from canister	553 W/m ²	471 W/m ²	0.851
Heat transfer rate through air path	12.886 kW (76.7%)	2.278 kW (63.7%)	.177(~.177)
Temp. of air outlet	63.87°C	62.82°C	0.984(~1.0)
ΔT (air inlet ~ outlet)	43.87°C	42.82°C	0.976(~1.0)
Velocity of air outlet	0.741 m/s	0.520 m/s	0.701(.707)
Mass flow rate	0.292 kg/s	0.051 kg/s	0.174(.177)
Cask's mean temp.	36.5	38.1	1.044
Canister temp.	96.0	93.2	0.971
Cask inside temp.	44.4	43.1	0.971
Cask outside temp	29.7	32.7	1.101

4. Conclusion

Scale ratios between the full scale and scale down models were derived through the scaling analysis. As a result of the thermal analysis using the scale ratio, similar temperature distributions were obtained between the full scale and half scale models. Therefore, the similarity to the temperature was verified. Especially, it is possible to predict the overall temperature distributions of the full scale prototype cask by using the half scale model. The results of this study can be used as the basic data for the scale model thermal test of concrete cask.

REFERENCES

- [1] H.M. Kim et al., "Development of scaling laws of heat removal and CFD assessment in concrete cask air path", Nuclear Engineering and Design, 278 (2014).

Analysis of Electrolytic Reduction Behavior by Oxide Fuel Characteristics

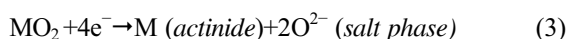
Eun-Young Choi* and Jeong Lee

Korea Atomic Energy Research Institute, 111, Daedeok-daero 989beon-gil, Yuseong-gu, Daejeon, Republic of Korea

*eychoi@kaeri.re.kr

Accumulation of spent nuclear fuel from nuclear power plants is a core challenge in nuclear energy technology. Pyroprocessing technology has been developed for recycling of the spent fuel into metal fuel for fast nuclear reactors by converting the spent oxide fuel into U/TRU(uranium/transuranium) metal ingots via electrochemical processes utilizing high-temperature molten salt. These electrochemical processes employ electrolytic reduction (also referred to as oxide reduction, OR) for the reduction of spent oxide fuel to metal, and electrorefining for the recovery of U/TRU [1–9].

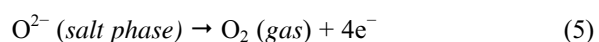
Generally, molten LiCl containing Li₂O at 650°C is used as the electrolyte in the OR process. The spent oxide fuels, loaded in a permeable basket, and platinum (Pt) are used as the cathode and anode, respectively. The cathode reactions (1–3) can be summarized as follows:



Li₂O produced by reaction (2) in molten LiCl dissociates into Li⁺ and O²⁻:



The anode reaction can be described as follows:



When an electrical potential is applied, the actinide metal oxide is reduced to metal and remains at the cathode. The oxygen ions (O²⁻) produced at the

cathode are transported through the salt and discharge at the anode to form O₂ gas [10–16]. Hence, the diffusion of O²⁻ ions from the inside of the oxide fuel to the bulk salt affects significantly the reduction rate and current efficiency during the OR process [17]. In this presentation, two previous reports [18,19] on analysis of electrolytic reduction behavior by oxide fuel characteristics will be summarized.

In the first study [18], we investigated complete OR of high-density UO₂ to metallic U without any remaining UO₂. The size and density of the used UO₂ pellets were ϕ 8.3 mm \times 9.9 mm (H) and 10.67 g/cm³, respectively, i.e., values that are similar to those of spent fuel pellets from pressurized water reactor. In the second study [19], We show that the reduction of REOs to rare earth metals in Li₂O–LiCl salt can be enhanced significantly by using lithium metal. Specifically, REOs in the fuel are reduced to a high extent in the electrolytic reduction of simulated oxide fuel in 1.0-wt% Li₂O–LiCl salt following the application of electrical charge in order to induce the production of Li metal.

ACKNOWLEDGEMENT

This study was supported by the National Research Foundation of Korea (NRF) of the Korean Government (MISP) (Grant No. 2017M2A8A5015077).

REFERENCES

- [1] J.J. Laidler, J.E. Battles, W.E. Miller, J.P. Ackerman, E.L. Carls, Development of

- pyroprocessing technology, *Prog. Nucl. Energ.* 31 (1997) 131–140.
- [2] R.W. Benedict, H.F. McFarlane, *Radwaste Magazine*, 5 (1998) 23.
- [3] K.M. Goff, J.C. Wass, K.C. Marsden, G.M. Teske, Electrochemical processing of used nuclear fuel, *Nucl. Eng. Technol.* 43 (2011) 335–342.
- [4] K. Nagarajan, B.P. Reddy, S. Ghosh, G. Ravisankar, K.S. Mohandas, U.K. Mudali, K.V.G. Kutty, K.V.K. Viswanathan, C.A. Babu, P. Kalyanasundaram, P.R.V. Rao, B. Raj, Development of pyrochemical reprocessing for spent metal fuels, *Energy Procedia* 7 (2011) 431–436.
- [5] T. Koyama, Y. Sakamura, M. Iizuka, T. Kato, T. Murakami, J.-P. Glatz, Development of pyroprocessing fuel cycle technology for closing actinide cycle, *Procedia Chem.* 7 (2012) 772–778.
- [6] H. Lee, G.I. Park, J.W. Lee, K.H. Kang, J.M. Hur, J.G. Kim, S. Paek, I.T. Kim, I.J. Cho, Current status of pyroprocessing development at KAERI, *Sci. Technol. Nucl. Install.* 2013 (2013) 343492.
- [7] K.C. Song, H. Lee, J.M. Hur, J.G. Kim, D.H. Ahn, Y.Z. Cho, Status of pyroprocessing technology development in Korea, *Nucl. Eng. Technol.* 42 (2010) 131–144.
- [8] H. Lee, J.M. Hur, J.G. Kim, D.H. Ahn, Y.Z. Cho, S.W. Paek, Korean pyrochemical process R&D activities, *Energy Procedia* 7 (2011) 391–395.
- [9] E.-Y. Choi, S. M. Jeong, Electrochemical processing of spent nuclear fuels: An overview of oxide reduction in pyroprocessing technology, *Prog. Nat. Sci: Mater. Int.* 25 (2015) 572–582.
- [10] L.I. Redey, K.V. Gourishankar, US Patent 6, 540, 902 B1.
- [11] K.V. Gourishankar, L. Redey, M. Williamson, *Light Metals*, W.A. Schneider (Ed.), The Minerals, Metals, and Materials Society, Warrendale, PA, (2002) 1075.
- [12] M. Kurata, T. Inoue, J. Serp, M. Ougier, J.-P. Glatz, Electro-chemical reduction of MOX in LiCl, *J. Nucl. Mater.* 328 (2004) 97–102.
- [13] Y. Sakamura, M. Kurata, T. Inoue, Electrochemical reduction of UO_2 in molten CaCl_2 or LiCl, *J. Electrochem. Soc.* 153 (2006) D31–D39.
- [14] Y. Sakamura, T. Omori, T. Inoue, Application of electrochemical reduction to produce metal fuel material from actinide oxide, *Nucl. Technol.* 162 (2008) 169–178.
- [15] S.M. Jeong, H.S. Shin, S.H. Cho, J.M. Hur, H.S. Lee, Electrochemical behavior of a platinum anode for reduction of uranium oxide in a LiCl molten salt, *Electrochim. Acta* 54 (2009) 6335–6340.
- [16] J.H. Hur, S.M. Jeong, H. Lee, Underpotential deposition of Li in a molten $\text{LiCl-Li}_2\text{O}$ electrolyte for the electrochemical reduction of U from uranium oxides, *Electrochem. Commun.* 12 (2010) 706–709.
- [17] E.Y. Choi, J.K. Kim, H.S. Im, I.K. Choi, S.H. Na, J.W. Lee, S.M. Jeong, J.M. Hur, Effect of the UO_2 form on the electrochemical reduction rate in a $\text{LiCl-Li}_2\text{O}$ molten salt, *J. Nucl. Mater.* 437 (2013) 178–187.
- [18] Eun-Young Choi, Jeong Lee, Complete reduction of high-density UO_2 to metallic U in molten $\text{Li}_2\text{O-LiCl}$, *Journal of Nuclear Materials*, 494 (2017) 439.
- [19] Eun-Young Choi, Jeong Lee, *Journal of Nuclear Materials*, <https://doi.org/10.1016/j.jnucmat.2018.09.017>.

Simplified Beam Model of Spent Nuclear Fuel Rod

Sanghoon Lee and Seyeon Kim

Keimyung University, 1095, Dalgubeol-daero, Dalseo-gu, Daegu, Republic of Korea

*shlee1222@kmu.ac.kr (s)

1. Introduction

Structural integrity of spent nuclear fuel assembly should be carefully examined under storage and normal condition of transportation. Due to the complicated shape and uncertainties in the mechanical properties, the structural evaluation of spent fuel assembly is a challenging task. During analyses for storage and transportation, the spent fuel assemblies are often simplified to reduce the computational burdens. In the simplified model, the spent fuel rods are replaced by beam elements with effective material properties calculated from the properties of cladding and fuel pellets. However, a well agreed procedure for the model degeneration has not been developed yet and the validity of the effective material properties have not been discussed in depth. In some approach, the stiffness of the pellets is ignored while their masses are lumped into cladding. In others, the average values of Young's modulus are used while no considerations are made on the plastic properties of cladding. In this work, a procedure for material property calibration for spent nuclear fuel rods is proposed based on the static analyses and optimization and the validity of the properties are checked using the dynamic impact simulations.

2. Material Properties

2.1 Storage condition and material properties

The material properties of spent fuel rods with Zircaloy cladding can be calculated from a sophisticated models proposed in [1]. They are given as functions of neutron fluence, temperature, cold work ratio, strain rate, hydrogen concentration, and oxide thickness.

2.2 Storage conditions

During the storage pool stage, the temperatures are roughly maintained at 30°C, while the initial temperature at the vacuum drying stage is around 400°C (the maximum fuel cladding temperature) which decreases gradually during the dry storage period. The temperature typically drops from 400°C to 250°C in the first ten years. The neutron fluence of HBF (45–60 GWd/MTU) in a light-water reactor roughly ranges from 7×10^{25} n/m² to 12×10^{25} n/m². For discharge burnup in the range of 45–60 GWd/MTU, the average hydrogen concentration ranges between 200–600 ppm. These variables are considered in the material properties calculation for cladding and fuels.

3. Simplified Beam Model

3.1 Overall procedure

A segment of fuel rod is considered in this work. A detailed model of the segment is constructed with enough details of cladding and pellets. Two separate

models are built based on the interfacial conditions between the pellets and cladding. Then, static analyses are performed to capture important mechanical response of the model to external load, namely the maximum equivalent plastic stain which can be a measure for determining the fracture of cladding, the compliance of fuel rod which is important in determining the load exerted on the rod due to the interaction with other fuel rods and structural component within a cask. Then, a beam model with the same diameter of fuel rod is considered and its material properties are calibrated which generate the same equivalent plastic strain and displacement under the given load. The whole procedure is implemented using the optimization platform i-Sight integrating ABAQUS and MATLAB. The design variable of the calibration procedure is the Young's modulus, strength coefficient, and the hardening coefficient.

3.2 Results of material calibration

For two cases, the effective material propeties of beams which produces the same plastic strain and displacement at critical load is identified. The results are illustrated in the following figures.

Table 1. Effective material properties of beam

Cases	E	n	K
Bonded	235697	0.15	1682
De-bonded	83042	0.15	781

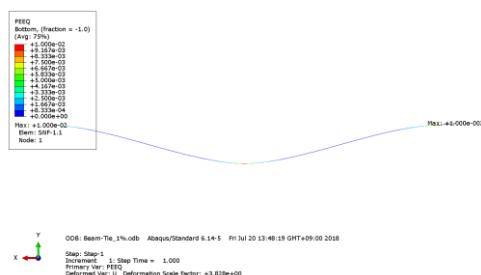


Fig. 1. Fully bonded case.

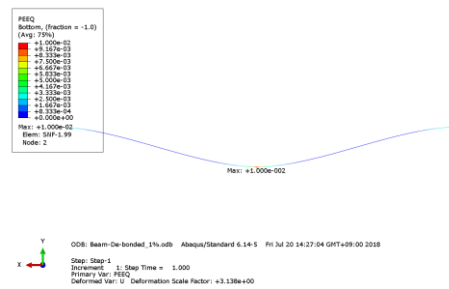


Fig. 2. Fully de-bonded case.

4. Conclusions

Using a sophisticated calibration procedure, the effective material properties of simplified beam model of spent fuel rods can be successfully determined. These material properties produce exactly same plastic strain and displacement at critical load. However, the validity of thus found properties should be carefully examined in dynamic simulations before using them in structural integrity assessment of spent nuclear fuel.

REFERENCES

- [1] Adkins, H. et al. Used Nuclear Fuel Loading and Structural Performance under Normal Conditions of Transport— Demonstration of Approach and Results on Used Fuel Performance Characterization, US DOE, 2013.

Distillation of Cd- ZrO₂ and Cd- Bi in Crucible With Splatter Shield

S.W. Kwon*, Y.W. Kwon, J.H. Jung, S.H. Kim, and S.J. Lee

Korea Atomic Energy Research Institute, 111, Daedeok-daero 989beon-gil, Yuseong-gu, Daejeon, Republic of Korea

*swkwon@kaeri.re.kr

Abstract

The liquid cathode processing is necessary to separate cadmium from the actinide elements in the pyroprocessing since the actinide deposits are dissolved or precipitated in a liquid cathode. Distillation process was employed for the cathode processing owing to the compactness. It is very important to avoid a splattering of cadmium during evaporation due to the high vapor pressure. Several methods have been proposed to lower the splattering of cadmium during distillation. A multi-layer porous round cover was proposed to avoid a cadmium splattering in our previous study. In this study, distillation behavior of Cd - ZrO₂ and Cd - Bi systems were investigated to examine a multi-layer porous round cover for the development of the cadmium splatter shield of distillation crucible. It was designed that the cadmium vapor can be released through the holes of the shield, whereas liquid drops can be collected in the multiple hemisphere. The cover was made with three stainless steel round plates with a diameter of 33.50 mm. The distance between the hemispheres and the diameter of the holes are 10 and 1 mm, respectively. Bismuth or zirconium oxide powder was used as a surrogate for the actinide elements. About 40 grams of Cd was distilled at a reduced pressure for two hours at various temperatures. The mixture of the cadmium and the surrogate was distilled at 470, 570 and 620°C in the crucible with the cover. Most of the bismuth or zirconia remained in the crucible after distillation at 470 and 570°C for two hours. It was considered that the crucible cover hindered the splattering of the liquid cadmium from the distillation crucible. A considerable amount of the surrogate material reduced after distillation at 620°C due to the splattering of the liquid cadmium. The low temperature is favorable to avoid a liquid cadmium splattering during distillation. However, the optimum temperature for the cadmium distillation should be decided further, since the evaporation rate decreases with a decreasing temperature.

ACKNOWLEDGEMENT

This work was supported by a National Research Foundation of Korea (NRF) grant funded by the Korean Government (MSIP) (No. 2017M2A8A5015079)

Decay Heat Evaluation of Spent Fuel Assemblies in SFP of Kori Unit-1

Kiyoung Kim*, Yongdeog Kim, and Sunghwan Chung

Korea Hydro & Nuclear Power Co., Ltd. Central Research Institute, 1655, Bulguk-ro, Yangbuk-myeon,
Gyeongju-si, Gyeongsanbuk-do, Republic of Korea

*kiyoungkim@khnp.co.kr

Abstract

Kori Unit 1 is the first permanent shutdown nuclear power plant in Korea and it is on June 18th, 2017. Spent fuel assemblies began to be discharged from the reactor core to the spent fuel pool(SFP) within one week after shutdown of Kori unit 1 and the campaign was completed on June 27th, 2017. The total number of spent nuclear fuel assemblies in SFP of Kori Unit-1 is 485 and their discharging date is different respectively. So, decay heat was evaluated considering the actual enrichment, operation history and cooling time of the spent fuel assemblies stored in SFP of the Kori Unit-1. The code used in the evaluation is the ORIGEN-based CAREPOOL system developed by KHNP. Decay heat calculation of PWR fuel is based on ANSI/ANS 5.1-2005, "Decay heat power in light water reactors" and ISO-10645, "Nuclear energy - Light water reactors - Calculation of the decay heat power in nuclear fuels. Also, we considered the contribution of fission products, actinide nuclides, neutron capture and radioactive material in decay heat calculation. CAREPOOL system calculates the individual and total decay heat of all of the spent fuel assemblies in SFP of Kori Unit-1. As a result, the total decay heat generated in SFP on June 28th, 2017 when the spent fuel assemblies were discharged from the reactor core, is estimated to be about 4,185.8 kw and to be about 609.5 kw on September 1st, 2018. It was also estimated that 119.6 kw is generated in 2050 when it is 32 years after the permanent shutdown. Figure 1 shows the trend of total decay heat in SFP of Kori Unit-1.

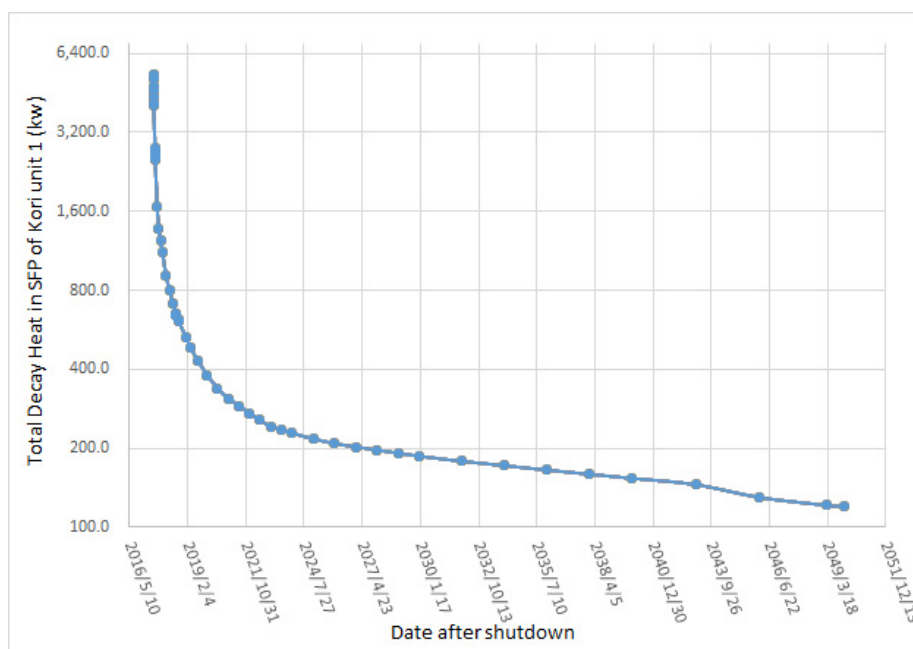


Fig. 1. Total Decay Heat in SFP of Kori Unit 1 according to the Storage Time.

Measures for the Failure Evaluation of SNF Cladding During the Transportation

J. S. Noh^{1)*}, H.A. Kim¹⁾, and T.W. Kim²⁾

¹⁾ ACT Co., Ltd., 35, Techno9-ro, Yuseong-Gu, Daejeon, Republic of Korea

²⁾ Hanyang University, 222, Wangsimni-ro, Seongdong-gu, Seoul, Republic of Korea
*jsnoh@actbest.com

1. Introduction

In order to evaluate the SNF cladding integrity during the transportation, knowing the loads at first, then the responses from the fuel itself is essential. First of all, it would be the priority to know whether the cladding fails or not, which requires the failure criteria to which the loads and the responses need to be referred. This paper presents a few of failure measures used to determine the possibility of cladding failure during the transportation. Also proposition for appropriate failure measures which would be used as failure criteria for the SNF cladding during the transportation with quantification is presented.

2. Examples of failure measures applied to cladding integrity evaluation

2.1 Strain and K_{IC} for the failure determination of cladding due to impact [1]

The release of rod contents under normal transport or regulatory accident conditions is postulated for two types of failure: material rupture as a result of strains exceeding the ductility limit, and fracture as a result of excessive stress on an existing crack in the material. Three modes of failure are described by these two failure mechanisms: (1) transverse tearing initiated by material rupture, (2) rod breakage caused by crack propagation, and (3) longitudinal tearing initiated by material fracture in Fig. 1. The failure criteria used to determine these failure modes are the strain, ϵ_f (material rupture) and fracture toughness, K_{IC} (material fracture) failure mechanisms.

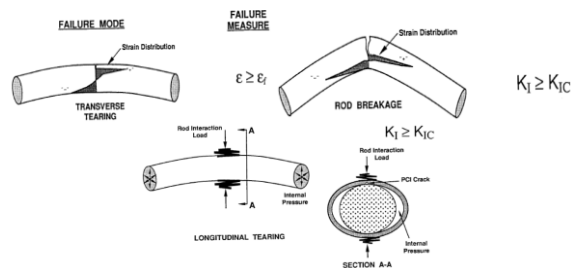


Fig. 1. Fuel rod failure mode [1].

2.2 Uniform Elongation and Fatigue Strength under NCT(Normal Conditions of Transportation) [2]

The potential failure modes under NCT where criteria could be established are classified as follows:

- Classic failure due to excessive stress or strain: This type of failure could be caused by a large shock load on the fuel rods due to a normal event such as

road bump and rail car coupling. For this activity, the uniform elongation (plastic strain at maximum load) was used to assess damage fraction as well as failure rate under those events.

- Fatigue failure: Failure of the rods due to excessive strain cycling at low amplitude. The mechanism causing this strain cycling would be vibrations normal to the axial direction of the fuel rods as they are transported by rail or road. This is the most likely failure mechanism for UNF under NCT. The fatigue-design curve for the cladding was used to assess failure under vibrational loading.

2.3 CSED(Critical Strain Energy Density) in terms of Total Elongation and Uniform Elongation

These were developed first as a Hydrogen-Enhanced PCMI Cladding Failure Criteria during Reactivity-Initiated Accident (RIA) and then applied to the cladding of SNF. The clad ductility is measured in terms of strain energy density (SED). Clad failure is assumed to occur when the strain energy density in the material reaches and exceeds a critical strain energy density (CSED), which is determined from mechanical property tests.

The PCMI cladding failure thresholds proposed in the EPRI report are based on total elongation data (i.e., CSED (TE)). However, in response to staff concerns, the EPRI report also includes CSEDs based on uniform elongation data, which showed a significant reduction in CSED as expected. Cladding hydrogen content and hydride distribution and orientation are also likely to influence this relationship.

2.4 Hoop plastic strain

A strain-based criterion for clad tube failure under RIAs is proposed by Sweden researchers.[3] The criterion is intended for prediction of clad tube failures caused by pellet-clad mechanical interaction during the early heat-up phase of RIAs.

The mechanisms responsible for fuel rod failure under RIAs was delineated first, based on an evaluation of RIA simulation tests performed on pre-irradiated fuel rods in pulse reactors. The ability of the clad tube to expand radially by plastic deformation is found to be crucial for fuel rod survival under RIAs. From an experimental database of more than 200 out-of-pile mechanical property tests, a correlation for clad hoop plastic strain at failure with respect to clad temperature, irradiation damage, strain rate and hydrogen content was formulated. Cladding tube failure is assumed to take place when the clad hoop plastic strain exceeds the ductility limit defined by this correlation.

2.5 Yield Stress

The failure criteria assumed for the determination of the structural integrity of irradiated fuel rod cladding under axial loads from hypothetical transportation accident was that axial stresses in the cladding reach the yielding stress of the irradiated. Due to the inertial load on end drop, fuel rod buckles and, then, failure criterion (yielding) could be reached.

3. Discussions of failure measures

There could not be one generic failure criterion which can cover the all kinds of failure modes in claddings. Each has its own pros and cons. Different loads are subjected to cladding during transportation should be examined accordingly to their orientations and cladding microstructures.

Stress based failure criteria do not appear to be suitable for the evaluation of materials which would experience elastic-plastic strain, because of far more incremental strain with less increase of stress, and especially for the anisotropic materials. Strain could be one of candidate criteria for its simple measurability.

Strain based failure criteria for the cladding subjected to shock loads appears to be a simple measure to determine the cladding integrity during NCT. However, applying the test sample data to actual cladding in complicated stress environments needs a lot of experiments to be justified, especially a series of criteria for the various types of cladding alloy, burnup history, and hydride morphology, etc. are needed. A failure criterion based on strain alone could not cover the whole failure modes, of course, especially for the accident conditions.

The energy based criteria, i.e. K_{IC} /CSED would be appropriate better for the impact loads encountered during accident conditions than the other measures.

CSED was first proposed to evaluate the cladding integrity for the RIA events as a failure measure. And then, EPRI applied it to the evaluation of high burnup SNF cladding during hypothesized accident condition of transportation, which requires the assessments of the shock and impact loads for the cladding, while strain and K_{IC} were used as failure measures to evaluate the impact loads for cladding in SAND90-2406. However, it is not easy to deduce the K_{IC} without knowing the crack size in material. Furthermore, the SAND90-2406 methodology is of general applicability independently of burnup level, its quantitative results are not directly transferable to high-burnup fuel because of significant changes in mechanical and failure properties with burnup and the potential effects of dry storage on modifying the cladding hydride morphology. One of the critical areas in which the SAND90-2406 methodology needs to be updated is in the choice of failure criteria to replace the low burnup criteria, which were based on the cladding rupture strain and fracture toughness. To this end, the CSED, which combines the states of stresses and strains, has been proposed as a failure measure most suited for cladding with hydride-

morphology-dependent failure mechanisms as can potentially exist in high-burnup spent fuel subjected to several decades of dry storage. Because the direction dependence of fracture toughness is more pronounced at high hydride concentrations, this limitation on K_{IC} data has a larger impact on high-burnup cladding. Further, radial hydrides have virtually no effect on Mode-I and -II failures, because the dominant stress acts in a direction parallel to the hydrides, unlike Mode-III failure where the highest stress is normal to the plane of the hydrides. That is, another important factor in the choice of CSED as a cladding failure measure is its ability to capture the behavior of radial hydrides.

For the vibration loads, the **fatigue-design curve** for cladding would be used to assess failure due to excessive strain cycling at low amplitude under vibrational loading.

Anyhow, it is important to determine an appropriate failure criterion for a certain failure mode selectively because no one measure can cover the whole set of failure modes fully. A lot of experiment with various types of cladding conditions, especially hydride morphologies, should be implemented to evaluate the appropriateness of a certain failure criterion for a specific failure mode.

4. Summary

It is important to set up a reasonable failure criterion for cladding, because being able to determine the cladding integrity during transportation is essential for the evaluation of SNF transportation system.

There are a few of measures which can be used as a failure criterion for cladding subjected to its specific failure mode. Therefore, to select and to use appropriate failure criterion measures, i.e. strain(UE), K_{IC} , and CSED would be a key in evaluating the cladding integrity during transportation with every aspects. In order to justify and quantify that criterion properly, various experiments for the mechanical properties of the claddings with different conditions shall be implemented, which data will enable to justify the failure criteria proposed.

ACKNOWLEDGEMENT

This work was supported by the KETEP granted financial resource from the Ministry of Trade, Industry and Energy, Republic of Korea (No. 20181710201770)

REFERENCES

- [1] Sandia Report SAND90-2406, 'A Method for Determining the Spent-Fuel Contribution to Transport Cask Containment Requirements'.
- [2] Used Nuclear Fuel Loading and Structural Performance Under NCT, FCRD-UFD-2013-000325.
- [3] A strain-based clad failure criterion for RIA in light water reactors, Sweden TR 03-008, 2004.

Methodologies and Properties of Safety Analyses for Pyroprocessing Facilities

Gilsung You*, Seokjun Seo, Woojin Jo, Siwan Noh, Hyojik Lee, Hohee Lee, Seungnam Yu, and Jeonghoe Ku
Korea Atomic Energy Research Institute, 111, Daedeok-daero 989beon-gil, Yuseong-gu, Daejeon, Republic of Korea
*yougil@kaeri.re.kr

1. Introduction

KAERI is being developed pyroprocessing technology for a safe and an effective disposal of spent fuel. For the study and verification of this technology, it is necessary to develop the experimental facility with hot cells and auxiliary systems in the future [1]. In this paper, several safety analysis methodologies of Korea and the United States for the development of fuel cycle facilities are introduced, and the properties of the experimental pyroprocessing facility are practically analyzed using the associated safety analysis approaches.

2. Safety Analysis Methodologies

Safety analysis methodologies for a fuel cycle facility (including a pyroprocessing facility) are a traditional deterministic method (the Korean Nuclear Safety Act), an ISA method (the US NRC), a hybrid ISA-PSA method (developing by the US NRC) and a PSA method.

2.1 Korean Nuclear Safety Act (KNSA)

The Paragraph (3) of Korean Nuclear Safety Act article 35 requires that a person, who intends to carry on the spent fuel processing business, shall submit to the competent minister an application for the permit or the designation together with radiation environmental report, safety control regulations, explanatory statement of design and work methods, quality assurance program for the operation of the business and other documents as prescribed by the Ordinance of the Prime Minister. The Korean Nuclear Safety Act requires applicants to conduct a standard safety analysis methodology similar to that of nuclear power reactor, such as deterministic and defense-in-depth safety methodologies [2].

2.2 U.S. 10CFR70 (NUREG-1520, ISA)

NUREG-1520 provides U.S. NRC guidance for reviewing and evaluating the health, safety, and environmental protection aspects of applications for licenses to possess and use special nuclear material to produce nuclear reactor fuel. This guidance addresses the longstanding health, safety, and environmental-protection requirements of 10 CFR Part 20 and 10 CFR Part 70, as well as the accident safety requirements reflected in Subpart H, “Additional requirements for certain licensees authorized to possess a critical mass of special nuclear material,” of 10 CFR Part 70. Subpart H of 10 CFR Part 70 identifies risk-informed performance requirements and requires applicants and existing licensees to conduct an Integrated Safety Analysis (ISA) [3].

2.3 U.S. NRC SECY-0136 (an Enforced Risk Analysis and Hybrid ISA-PSA)

The NRC considers an ISA method required by 10 CFR Part 70 to be appropriate to address the types of hazards and accident sequences associated with existing fuel cycle facilities. However, the presence and processing of large quantities of fission products and TRU isotopes at reprocessing facilities have the potential to greatly increase consequences far above the 10 CFR Part 70 high-consequence thresholds for some accident sequences (e.g., fires, explosions), and, therefore, 10 CFR Part 70 is not appropriate for reprocessing facilities. The NRC concludes approaches that incorporate more quantitative risk assessment, including PRA, are needed to adequately address safety and risk at reprocessing facilities. The NRC is considering two basic approaches—a hybrid ISA-PRA approach and a PRA approach. The NRC considers the hybrid approach is a reasonable starting point at this preliminary stage of the NRC’s efforts in support of potential future rulemaking activities [4-6].

2.4 PSA

Recently NUREG/CR-7168 studied the possibility of using a PSA method for reprocessing facilities. This guidance concludes that the ISA approaches may identify potential weaknesses in a facility's design or operation for relatively simple nuclear fuel-cycle systems. However, since the approaches do not incorporate inter-system dependencies, nor provide an integrated assessment of risk, they could miss some essential risk outliers in more complex facilities. Varying degrees of PRAs for reprocessing facilities already have been carried out in several countries. Notwithstanding the limited data available for PRAs of this type of facilities compared to that for power reactors, the safety analyses of these facilities can benefit from the potential understanding gained by uncovering potential weaknesses in design and identifying dominant contributors to the risk of a plant or facility, such as human errors and dependencies [7].

3. Properties of Safety Analyses for Pyroprocessing Facilities

In Korea SF handling facilities are regulated as one of fuel cycle facilities under the Korean Nuclear Safety Act [2]. The act describes the safety requirements for the license and operation of fuel cycle facilities. Although the safety requirements for fuel cycle facilities show small differences compared to those of nuclear power plants, but a large parts of the requirements use the same technical criteria with nuclear power plants. The U.S. NRC is using an ISA safety analysis approaches and recently studied about an adaptability of a hybrid ISA-PSA [5,6] and a PSA to reprocessing facilities [7].

Table 1. Properties and ratings for each safety analysis methodology

Methodology Property	KNSA	ISA (NUREG-1520)	Hybrid ISA-PSA (SECY-0136)	PSA (NUREG/CR-7168)
Simplicity	G	M	B	B
Safety Effectiveness to Pyro	M	G	G	G
Adaptability to Pyro	G	G	M	B
Event Analysis	B	M	M	G
Risk-Informed Performance	B	B	M	G

Necessity of Data (Fault & Likelihood) for Pyro	B	M	M	G
Human errors and dependencies Analysis	B	M	M	G

G: Good, M: Medium good, B: Bad

For developing safer pyroprocessing facilities it is necessary to analyze the basic properties of these safety analysis methodologies. The table 1 shows some basic properties and ratings evaluated by authors for each safety analysis methodology.

REFERENCES

- [1] Gil-Sung You, et al., "Concept and Safety Studies of an Integrated Pyroprocess Facility, Nuclear Engineering Design", No. 241, pp. 415 ~ 424 (2011).
- [2] Korean Nuclear Safety Act (2018).
- [3] NUREG-1520 rev.2, "Standard Review Plan for Fuel Cycle Facilities License Applications", (2015).
- [4] US NRC SECY-0136, "Draft Regulatory Basis for Licensing and Regulating Reprocessing Facilities", (2011).
- [5] Gilsung You, et al., "Adaptability Study of Hybrid ISA-PSA Method on Safety of Pyroprocess Facilities", Proc. of the KRS 2017 Spring Conference, 15(1), May 24-26, 2017, BuSan.
- [6] Gilsung You, et al., "Enforced Risk Criteria for SF Recycling Facilities in US and Its Availability in Korea", Proc. of the KRS 2017 Fall Conference, 15(2), Oct 18-20, 2017, ChangWon.
- [7] NUREG/CR-7168, "Regulatory Approaches for Addressing Reprocessing Facility Risks: an Assessment", (2015).

PCR Evaluation of NIM Module Based Compton Suppression Gama Spectroscopy System by Source-to-Detector Distance

HaJin Song*, ChaeHun Lee, SeongKyu Ahn, and YoungGun Ko

Korea Atomic Energy Research Institute, 111, Daedeok-daero 989beon-gil, Yuseong-gu, Daejeon, Republic of Korea

*hjsong@kaeri.re.kr

1. Introduction

Compton scattering produces Compton continuum over a large area in the gamma-ray spectrum. Compton scattering makes it difficult to precisely measure the low X-ray energy peaks of the Compton continuum area. This problem occurs in the measurement of spent fuel containing various fission product to emit high energy gamma. Compton continuum is mainly generated by gamma rays of 662 keV from ^{137}Cs in the spent fuel. This makes it difficult to perform low energy area peak analysis from 100 to 400 keV [1]. The Compton continuum area can be suppressed using a Compton suppression system. The greatest advantage of Compton suppression system is to significantly reduce the Compton continuum and improve the detection limit [2]. In this study, the performance of the developed Compton suppression system with various source positions was evaluated.

2. Methods and Results

NIM Module using a traditional analog signal was used to implement the Anti-Coincidence. The main detector is a HPGe(P-type Coaxial HPGe). BGO(Well-type BGO) and NaI(Well-type NaI) detector were used as guard detectors to measure scattered gamma rays. A Cs-137 source was placed in several distances from the surface of HPGe detector. The configuration of each NIM Module is shown in the Fig. 1.

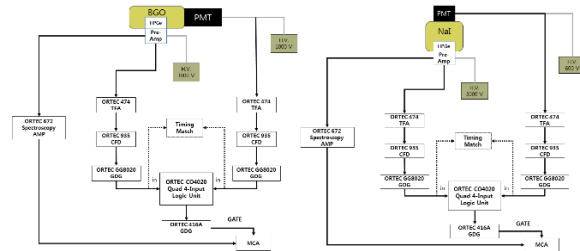


Fig. 1. NIM Module schematic diagram.

2.1 HPGe and BGO Compton suppression result

As shown in Table 1, the Compton continuum of measured spectra of the Compton suppression system are clearly different from the unsuppressed spectra. As the distance increases, the measured counts are lower, but the Peak to Compton ratio (PCR) increases. The PCR factor of the Compton suppression system is about three times better compared to the unsuppressed system.

2.2 HPGe and NaI Compton suppression result

As shown in Table 2, the measurement results of Compton continuum are clearly different when the Compton suppression system is used or not. As the distance increases, the counts are measured lower but the Peak to Compton ratio increases. We can see that the Compton suppression system is PCR factor over three times when using it.

Table 1. HPGe and BGO Cs-137 Peak to Compton ratio

Distance	State	358~385 keV	662keV	Peak to Cpmpton ratio	PCR factor
20 cm	w/o suppression	91184	88590	96.2	2.5
	w/ suppression	35088	84096	237.3	
30 cm	w/o suppression	38364	38528	99.4	2.6
	w/ suppression	14315	38048	263.1	
40 cm	w/o suppression	21913	23396	105.7	2.8
	w/ suppression	7699	23342	300.2	

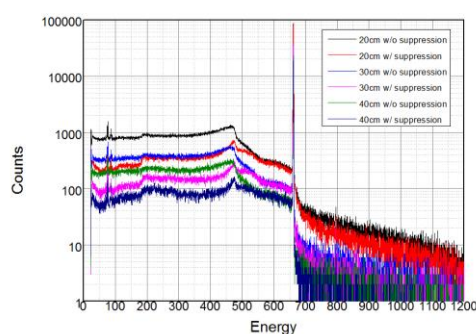


Fig. 2. Cs-137 Spectrum Using HPGe and BGO.

Table 2. HPGe and NaI Cs-137 Peak to Compton ratio

Distance	State	358~385 keV	662keV	Peak to Cpmpton ratio	PCR factor
20 cm	w/o suppression	119895	80208	66.2	2.3
	w/ suppression	51486	78050	150.1	
30 cm	w/o suppression	61324	39967	64.5	3.7
	w/ suppression	16542	40116	240.1	
40 cm	w/o suppression	35276	24926	69.9	3.7
	w/ suppression	9370	24734	261.3	

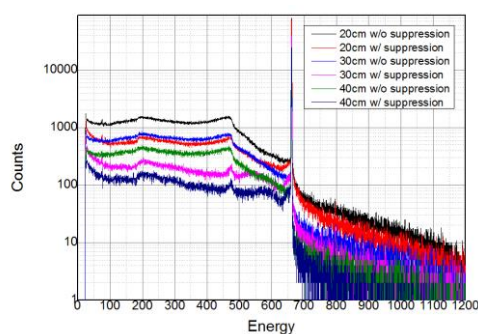


Fig. 3. Cs-137 Spectrum Using HPGe and NaI.

3. Conclusion

Comparisons using two different guard detectors confirm that the most ideal position for measuring the 662 keV gamma ray from ^{137}Cs is 40 cm. The two methods are no measured under the same conditions, so there are difficult to compare. As a result of comparison, Peak to Compton ratio is clearly high for BGO. The low 100 keV area means that the high density BGO absorbed the high gamma energy of 500 keV. However, the PCR factor shows that Compton suppression is higher in NaI. The reason is that NaI absorbs energy well below 100 keV at the Compton edge, and the light intensity is high enough to keep the low threshold. Therefore, the two BGO is additionally installed behind NaI, so that it is designed to catch X-ray of low energy area. We will continue to measure the Compton suppression system.

ACKNOWLEDGEMENT

This work supported by the National Research Foundation of Korea (NRF, NRF-2017M2A8A5015084) and the Korea Foundation Of Nuclear Safety (KoFONS, No. 1705007) grants funded by MSIP and Nuclear Safety and Security Commission (NSSC) of the Republic of Korea.

REFERENCES

- [1] Seung-Kyu Lee et al, "Performance Evaluation of Compton Suppression System in the Low Energy Area of Spent Nuclear Fuel Measurement Using XRF.", K RS, Vol.2015, No.5, pp. 41-42, 2015.
- [2] W.Zhang, "A digital Compton suppression spectroscopy without Gamma-ray coincidence-summing loss using list-mode multispectral data acquisition.", JRNC, Vol.292, No.3, pp. 1265-1272, 2012.

The Evaluation of the Fire Protection in Hot Cell Facilities

Woo Jin Jo^{*}, Seok-Jun Seo, Siwan Noh, Hyo Jik Lee, and Seung Nam Yu

Korea Atomic Energy Research Institute, 111, Daedeok-daero, 989beon-gil, Yuseong-gu, Daejeon, Republic of Korea

^{*}wjjo@kaeri.re.kr

1. Introduction

The Korea Atomic Energy Research Institute (KAERI) has been developing a pyroprocess technology to reduce the waste volume and recycle some of the elements in spent nuclear fuel. KAERI conducted the preliminary concept design of the Korea Advanced Pyroprocessing Facility (KAPF) based on the design requirements and criteria.

Hot cell facilities shall be designed in such a way that the possibilities of fire and its effects are minimized, since it involves the release of radioactive material during a fire. In addition, the facilities should prevent fire and need a rapid fire detection and extinguish. Structures, Systems, and Components of the facilities should be designed to protect the safety functions of the facilities even if they are not quickly extinguished by fire-fighting system.

In this paper, the design criteria and Codes&Standards as well as domestic and foreign regulations related to the fire protection were analyzed. In addition, anticipated fire accidents in the hot cell facilities were derived and the fire load was calculated.

2. Fire Protection for the Hot Cell Facilities

2.1 Act, Standards, Guides, Regulations, and Codes&Standards

In Korea, article 110 of the enforcement decree of the Nuclear Safety Act requires the necessary measures for the nuclear when a fire accidents occurs with leakage of radioactive materials. In addition, documents related to Codes&Standards, planning, and safety analysis of fire protection are provided in the public notice and enforcement rule on Nuclear Safety Commission.

Unlike Korea, the United States has many experiences in facility operation, so Act and regulatory authority can provide more details.

Domestic and foreign regulations related to the fire protection are listed in the table blow.

Table 1. Applicable regulations and guides on fire protection for nuclear fuel cycle facilities

Applicable regulation, guides and Codes&Standards	
Regulations	ROK <ul style="list-style-type: none">• Enforcement regulations of Nuclear Safety Act• Enforcement rule of the Radiation Safety Criteria• Act on Fire Prevention and Installation, Maintenance, and Safety Control of Fire-fighting Systems• Enforcement Act on Fire Prevention and Installation, Maintenance, and Safety Control of Fire-fighting Systems
	USA <ul style="list-style-type: none">• 10CFR Part 50 appx. A Criterion 3• 10CFR Part 70 subpart H
Guides	ROK <ul style="list-style-type: none">• Public Notice on the establishment and implementation of fire protection plan• Public Notice on the fire risk analysis
	USA <ul style="list-style-type: none">• NUREG-0800• DOE-STD-1066• NFPA 80, 780, 801• NCR BTP CMEB 9.5-1• UL 555
Codes&Standards	NFPA 801, 12, 13, 2001 NFFSC 101, 102, 106, 107A, 109 ASTM Material standards UL 555 KEPIC FPN-801, FPC-11, 12, 13, 14, 20, 24, 2001

3. Evaluation of the Fire Protection

3.1 Flow of the Evaluation of the Fire Protection

For the evaluation of the fire severity and required fire resistance rating, the fire load should be calculated. In order to calculate the fire load, the evaluation area must be set up first. Then the calculated fire load can be used for evaluation of fire severity and the fire resistance rating. The procedure of the fire protection evaluation for hot cell facilities is performed in the flow chart as shown in Fig. 1.

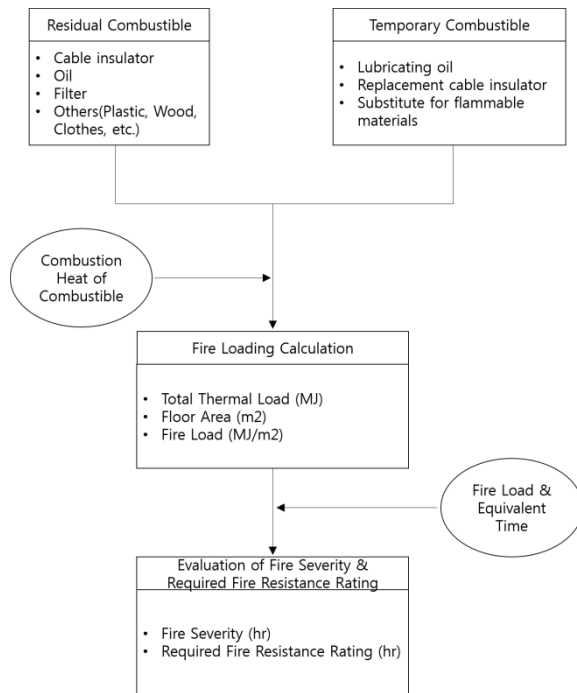


Fig. 1. Flow chart for the evaluation of fire severity and required fire resistance rating.

3.2 Evaluation of the Fire Protection

For the evaluation of fire severity and required resistance rating, it is necessary to determine the place where fire is expected from the entire facility area. Then fire hazards, that is, of the amount of combustible materials in the area of interest were identified. Using the identified the amount of combustible materials, which means the fire hazards in the area of interest, fire loads can be calculated by following equation.

$$Q = \sum m_i h_{ci} \quad (1)$$

$$Q'' = Q/A \quad (2)$$

where, Q is the total fire load (MJ), m_i is the mass of the combustible material i (kg), h_{ci} is the calorific value of the combustible materials i (MJ/kg), A is the floor area of the place of interest (m^2), and Q'' is the fire load in the area of interest (MJ/m^2).

The equivalent fire severity can be obtained by dividing the fire load per area of interest by the calorific value of the general combustible materials, W (kg/m^2), given as:

$$W = Q''/18.608 \quad (3)$$

In this paper, a part of the headend process cell derived from the KAPF preliminary concept design were analyzed. Because of the lack of design information, it is assumed that the combustible materials in the headend process cell is only cables. The calorific value of the cable and general combustible materials were assumed as 28.3 and 18.608 MJ/kg, respectively. The calculated fire load and fire severity were $11.9 MJ/m^2$ and 30 mins respectively.

Headend process cell is equipped with a fire detector, a gas type extinguish system and an alarm system, and the hot cell structure it self is set to fire rating 3 hours (highest grade), so that it functions as a fire barrier. In addition, the damper installed at the confinement boundary can prevent the leakage of the radioactive material that generated by the fire. Therefore, safety can be secured even in case of the fire accident at the headend process cell.

4. Conclusion

In this paper, the regulations, standards, and guides related to the fire protection for the hot cell facilities are summarized. Based on the previous KAPF preliminary concept design, the fire protection capability of the headend process cell as evaluated using the fire load and the fire severity.

It is also important to establish the fire protection system in compliance with the laws and standards, but it is important to establish a reasonable and optimized the fire protection plan through performance-based fire protection evaluation as previously described.

ACKNOWLEDGEMENT

This work was supported by Nuclear Research & Development Program of National Research Foundation of Korea (NRF) funded by Minister of Science, ICT and Future Planning (MSIP).

Preliminary Critical Analysis for Review of Multipurpose Utilization of PWR Spent Nuclear Fuel Disposal Canister

Taeman Kim*, Ho-Seong Dho, and Sang-Jin Lee

Korea Radioactive Waste Agency, 174, Gajeong-ro, Yuseong-gu, Daejeon, Republic of Korea

*tmkim@korad.or.kr

1. Introduction

Most of countries are developing and using a variety types of cask for efficient and safe management of Spent Nuclear Fuel (SNF). In particular, the Disposal Cask used in the final management phase provides a primary barrier to isolate spent fuel and maintains airtightness in deep environments during its design lifetime to prevent leakage of internal radionuclides.

The disposal casks or system should make sure that nuclear criticality accidents never occur at any circumstances and transportation or storage should be designed to prevent nuclear criticality from both normal and abnormal accidents [1][2][3].

In this study, the spacing and vessel diameter of the fuel assemblies satisfying the criterion of effective multiplication factor which is less than 0.95 in transportation, storage and disposal are established. Furthermore, the basic data of the multi-purpose canister is used for safety analysis.

2. Method and Assumption

2.1 General Information of Disposal Cask

The inserting channel of SNF was designed with a width of 23.5 cm and a height of 454.8 cm, which can facilitate APR-1400, WH fuel, and standard type with a width of 20.7 cm and a height of 453 cm (Fig.1). The loading capacity of SNF is 4 bundles made of corrosion resistant copper outside and cast nodular iron inside [4].

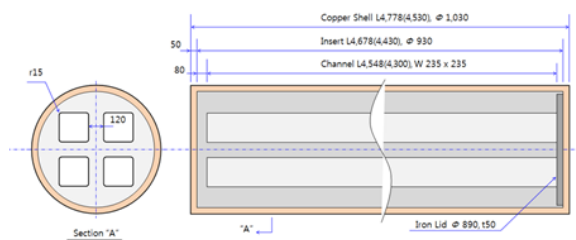


Fig. 1. Disposal Canister for KORAD EBS.

2.2 General Assumption

Based on the study by the KORAD (Korea Radioactive Waste Management Corporation), the Basis Fuel for the nuclear criticality analysis is selected as CE type PLUS7 with the initial concentration of 4.0%, the emission combustion of 45 GWD/ MTU and the cooling period of 40 years. Only the major actinide nuclear species was considered as a composition of SNF in order to assume the combustion state and Burnable Rod and Control Rod were excluded to secure maintenance.

The analytical conditions are as follows: both normal condition (dry internal cask and rock maintaining the integrity of the disposal system) and accident(flooding)condition (rock, bentonite, and the submerged interior making the optimal deceleration condition by groundwater).

2.3 Special Assumption

In this study, the IRON INSERT of the disposal cask in the previous research is named 'internal canister'. Furthermore, in order to utilize it for transportation or storage, some assumptions are established with its inside structural change as shown in Fig. 2.

- For simulating the weight reduction and immersion conditions in transport and storage use, to change the inside of the canister to empty space, change the fuel loaded tube to the basket

- To alter material of the changed inner canister to stainless steel, and to maintain the thickness of the outer wall with the upper thickness of 5 cm of the original canister and the lower thickness of 8 cm.

- Considering the uncertainty about long-term material quality, neutron absorbers used in canisters for transportation and storage are not applied.

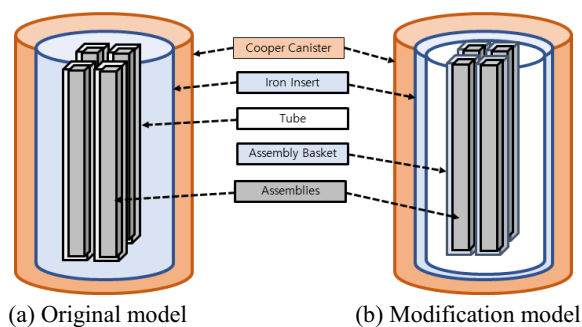


Fig. 2. Design modify of Disposal Cask and Canister.

3. Result

The pitch and canister diameter of the fuel assemblies that can be used for transportation and storage of the IRON INSERT of the disposal cask which cannot guarantee the long-term storage due to not applying neutron absorber were calculated (Table 1).

Table 1. Criticality of Modification model

(Unit: k_{eff})			
Gap	Conditions / Fuel irradiation	Criticality	Satisfaction
3cm	Normal Spent	0.21476	○
	Normal Fresh	0.27652	○
	Accident Spent	0.74676	○
	Accident Fresh	1.06053	×
6cm	Normal Spent	-	○
	Normal Fresh	-	○
	Accident Spent	-	○
	Accident Fresh	0.94889	×
7cm	Normal Spent	-	○
	Normal Fresh	-	○
	Accident Spent	0.65556	○
	Accident Fresh	0.92590	○
12cm	Normal Spent	0.18870	○
	Normal Fresh	0.24940	○
	Accident Spent	0.61455	○
	Accident Fresh	0.86455	○

First, in the case of the changed model with a 12 cm fuel gap, both the combustion fuel and the new fuel meet the nuclear critical criteria for transportation, storage and disposal, even under normal and accident conditions. According to the results, the empty changed canister- type vessel(inner diameter 71 cm) with the 3 cm fuel gap satisfied the assumptions under the dried condition, but in the case of the new fuel by the accident (flooding) exceeded effective multiplication factor. The changed canister- type vessel with the 6 cm fuel gap(inner diameter 77 cm) was evaluated as 0.94889 by the accident (flooding) and the dry condition was all

possible and but when applying the nuclear critical uncertainty of 0.0085 calculated in the KORAD21, transportation cask exceeded effective multiplication factor. Lastly, The changed canister- type vessel with the 7 cm fuel gap(inner diameter 78 cm) met the criticality criteria for both combustion and new fuel under normal and accident conditions.

4. Conclusion

The preliminary nuclear criticality safety analysis was carried out to examine the multipurpose utilization by changing the internal structure of the four-assembly disposal cask developed by the existing research. When the internal diameter was 78 cm and the fuel gap was 7 cm, both the combustion fuel and the new fuel did not exceed the nuclear critical standard value (0.95) under the normal - accident condition.

With the nuclear criticality analysis method, it is possible to derive the basic specifications of the canister meeting all the transportation, storage and disposal standards. Also, it is considered that the optimum multi-purpose canister can be developed by analyzing the shielding, heat and structure.

ACKNOWLEDGEMENT

This work was supported by the Korea Institute of Energy Technology Evaluation and Planning (KETEP Project No. 20171720201000) and the Ministry of Trade, Industry & Energy (MOTIE) of the Republic of Korea.

REFERENCES

- [1] U.S. NRC, 10CFR60 Disposal of High Level Radioactive Waste in Geologic Repositories, (2012).
- [2] U.S. NRC, 10CFR71 Packaging and Transportation of Radioactive Material, (2012).
- [3] U.S. NRC, 10CFR72 Licensing Requirements for the Independent Storage of Spent Nuclear Fuel, High-level radioactive Waste, and Reactor Related Greater than Class C Waste, (2012).
- [4] Korea Radioactive Waste Agency, Development of Engineering Barrier System for Disposal of Spent Nuclear Fuel, KORAD/EBS-TR/2014-06, (2014).

PWR SF Transportation Optimization: the Effect of Constraint Variation on the Interim Storage Plan

Hong Jang* and Hyo On Nam

Korea Atomic Energy Research Institute, 111, Daedeok-daero 989beon-gil, Yuseong-gu, Daejeon, Republic of Korea

*janghong@kaeri.re.kr

1. Introduction

A short-term solution to the wet storage saturation problem of older nuclear power plants (NPPs) is to construct additional on-site dry storages or off-site interim storages [1]. Assumed a single on-site dry storage with the same capacity for each NPP site in Korea, this work studies the effect of the limited on-site storage capacity and PWR SF movement on the off-site interim storage plan by solving a dynamic optimization problem for the PWR SF transportation with the constraint variation

2. Korean Phase-out Scenario

Based on the present governmental policy on the nuclear energy, total 29 NPPs (25 PWRs and 4 PHWRs) are expected to be operated until their lifetime without life extension or addition of new fleets (Fig. 1) [2]. According to this, the accumulated SFs generated from PWRs are expected to reach about 27,000 tHM.

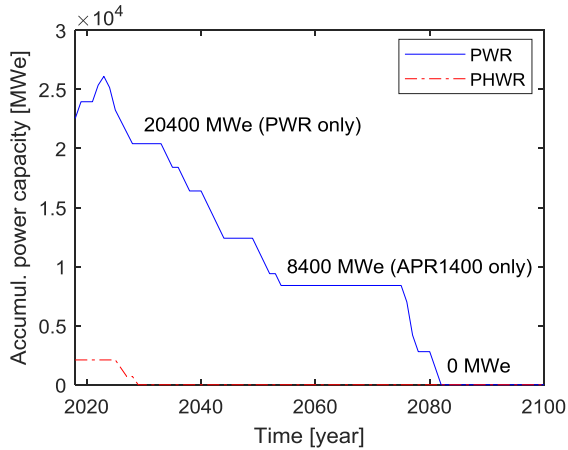


Fig. 1. Accumulated power capacity in the phase-out scenario.

In the Basic Plan on HLW Management (draft) [3], the expected time of wet storage saturation for each NPP site and the construction plan for the off-site interim storage is specified. But since the interim storage plan is based on the time required for siting the storage facility, it is necessary to validate the plan with the future predictions for the PWR SF generations and transportations between hypothetical storages under the nuclear phase-out scenario. In addition, the limitations of the on-site storage capacity and PWR SF movement should be considered in validating the interim storage plan.

3. Dynamic Optimization

Assumed a single dry storage per each NPP site, the required construction times for the on-site dry storages and off-site interim storage are obtained by

solving a dynamic optimization problem for the PWR SF transportation. It is assumed that there is no additional installation of the compact rack for existing wet storages. And the on-site PWR SF transportation between wet storages is simplified by aggregating NPPs as a single fleet.

The first optimization problem is to maximize the delay of PWR SF transportation to a new on-site dry storage from the wet storage in each j th site, which can be formulated as follows,

$$\min_{m_{ds}(j,k), \forall k=t_0, \dots, T} \sum_{k=t_0}^T |x_{ds}(j,k)| \quad (1)$$

subject to,

$$0 \leq x_{ws}(j,k) \leq x_{ws}^u(j,k) \quad (2)$$

$$0 \leq m_{ds}(j,k) \leq m_{ds}^u(j,k) \quad (3)$$

$$x_{ws}(j,k) = x_{ws}(j,k-1) - m_{ds}(j,k) + g(j,k) \quad (4)$$

$$g(j,k) = \frac{p(j,k) \times CF \times 365}{\varepsilon \times BU} \quad (5)$$

$$x_{ds}(j,k) = x_{ds}(j,k-1) + m_{ds}(j,k) \quad (6)$$

where $x_{ds}(j,k)$ is the accumulated SFs at time k in the j th site dry storage, $x_{ws}(j,k)$ is the accumulated SFs at time k in the j th site wet storage, $x_{ws}^u(j,k)$ is the upper boundary of $x_{ws}(j,k)$, $m_{ds}(j,k)$ is the amount of PWR SFs transported to the dry storage at time k in the j th site, $m_{ds}^u(j,k)$ is the upper boundary of $m_{ds}(j,k)$, $g(j,k)$ is the amount of PWR SFs generated at time k in the j th site, $p(j,k)$ is accumulated power capacity at time k in the j th site, CF is the capacity factor, ε is the efficiency, BU is the burn-up, t_0 is the current time, and T is the final time.

The second optimization problem is to maximize the delay of PWR SF transportation to a new off-site interim storage from the on-site storages, which can be formulated as follows,

$$\min_{m_{is}(j,k), \forall j=1, \dots, N_s, \forall k=t_0, \dots, T} \sum_{k=t_0}^T |x_{is}(k)| \quad (7)$$

subject to,

$$0 \leq x_{ds}(j,k) \leq x_{ds}^u(j,k), \forall j = 1, \dots, N_s \quad (8)$$

$$0 \leq \sum_{j=1}^{N_s} m_{is}(j,k) \leq m_{is}^u(k) \quad (9)$$

$$x_{ds}(j,k) = x_{ds}(j,k-1) + m_{ds}(j,k) - m_{is}(j,k),$$

$$\forall j = 1, \dots, N_s \quad (10)$$

$$x_{is}(k) = x_{is}(k-1) + \sum_{j=1}^{N_s} m_{is}(j,k) \quad (11)$$

where $x_{is}(k)$ is the accumulated SFs at time k in the interim storage, $x_{ds}^u(j,k)$ is the upper boundary

of $x_{ds}(j, k)$, $m_{is}(j, k)$ is the amount of PWR SFs transported to the interim storage at time k from the j th site, $m_{is}^u(k)$ is the upper boundary of the sum of $m_{is}(j, k)$ for all sites N_s .

To see the effect of the constraint variations for the on-site dry storage capacity and PWR SF movement on the optimization result, we change $x_{ds}^u(j, k)$ in a range from 2000 tHM to 3000 tHM and $m_{ds}^u(j, k)$ in a range from 200 tHM/y to 1000 tHM/y. $m_{is}^u(k)$ is fixed with 1000 tHM/y because it doesn't affect the interim storage plan. Fig. 2 and Table 1 show representative results.

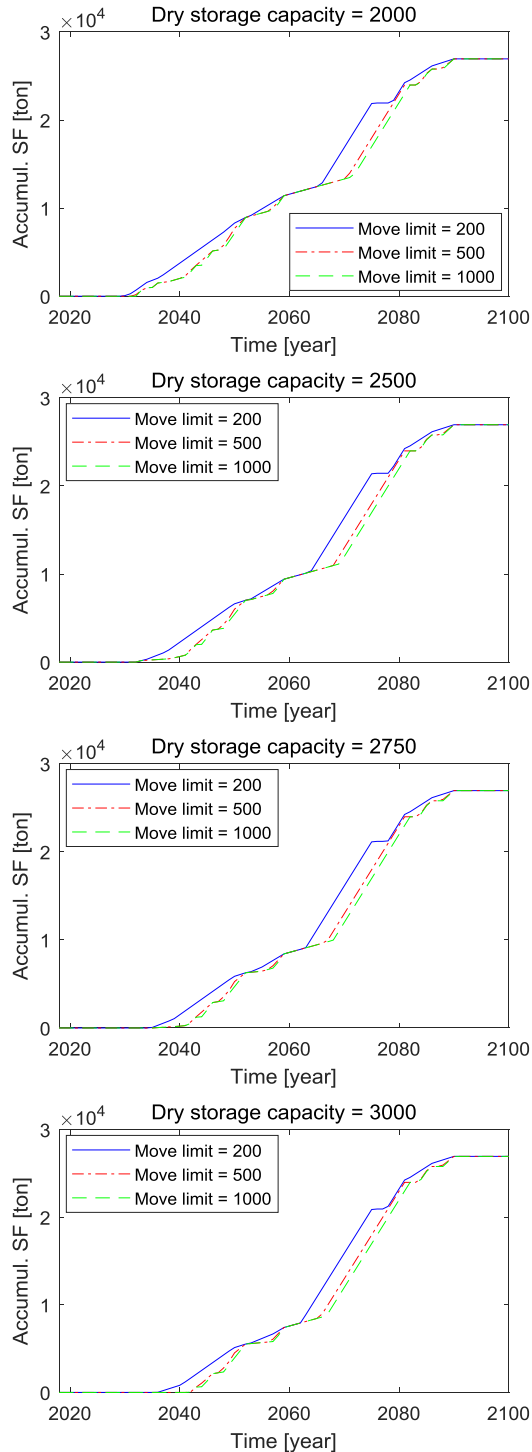


Fig. 2. Accumulated SF after the interim storage.

Table 1. Required construction time of the interim storage for different constraints for the on-site dry storage capacity $x_{ds}^u(j, k)$ and PWR SF movement $m_{ds}^u(j, k)$

$x_{ds}^u(j, k)$ [tHM]	$m_{ds}^u(j, k)$ [tHM/y]	Required time
2000	200	2030
	500	2032
	1000	2033
2500	200	2033
	500	2033
	1000	2033
2700	200	2034
	500	2034
	1000	2034
2750	200	2035
	500	2035
	1000	2035
2800	200	2035
	500	2037
	1000	2037
2900	200	2036
	500	2039
	1000	2039
3000	200	2036
	500	2042
	1000	2042

As shown in Fig. 2 and Table 1, the constraint variations for both on-site dry storage capacity and PWR SF movement affect the interim storage plan significantly. In particular, the constraint for the on-site dry storage capacity determines the latest construction time for the interim storage. And the impact of the constraint variation for the PWR SF movement higher than 500 tHM/y is negligible.

As a result, regardless of the PWR SF movement higher than 200 tHM/y, the on-site dry storage capacity should be more than 2750 tHM to follow the governmental interim storage plan (until 2035 [3]).

4. Conclusion

Under the Korean nuclear phase-out policy, the effect of the limitations of the on-site storage capacity and PWR SF movement on the interim storage plan was explored by solving a dynamic optimization problem of PWR SF transportation with the constraint variation. As a result, the constraint variation for the on-site storage capacity gave a significant impact on the interim storage plan. As a next step, the effect of the limitations of the interim storage capacity and PWR SF movement on the disposal plan will be studied.

REFERENCES

- [1] MIT Nuclear Fuel Cycle Study Advisory Committee, The Future of the Nuclear Fuel Cycle: An Interdisciplinary Study, MIT, Boston, MA, US, 2011.
- [2] MOTIE, The 8th Basic Plan on Electricity Demand and Supply (2017~2031), MOTIE, Seoul, Korea, 2017
- [3] MOTIE, Basic Plan on High-level Radioactive Waste Management (Draft), MOTIE, Seoul, Korea, 2016.

Simplified Geometric Model Development to Evaluate Spent Fuel Integrity of Representative in Long-Term Dry Storage

Jaeyong Kim*, Sunguk Lee, and Donghak Kook

Korea Atomic Energy Research Institute, 111, Daedeok-daero 989beon-gil, Yuseong-gu, Daejeon, Republic of Korea

*kjdkj@kaeri.re.kr

1. Introduction

The research about dry storage for interim storage of low burn-up Spent Nuclear Fuels (SNFs) is still a work in progress because PWR spent fuel pools will be saturated with SNF in 2024 [1]. The Korea Atomic Energy Research Institute (KAERI) has conducted various kinds of tests and analyses to obtain useful data for predicting the integrity and retrievability of SNFs after transportation and long-term dry storage. Among several fuel assembly (FA) components, spacer grids (SGs) protect the fuel rods from external impact loads issued by transportation, earthquake and abnormal events during handling. Before buckling of SGs, they sustains the external impact load. The dynamic buckling strength of a SG is important characteristics to determine whether it is possible to handle SNFs experienced external loads or not. FE model of a kind of SGs, 14 KNF-OFA, has been developed to predict dynamic buckling strength. But its shape is so complicated that it takes a lot of time and efforts to generate a geometric model. In this paper, a simplified geometric model, KAERI model, to replace a SNF representative SG, a 14 KNF-OFA SG, is suggested and validated by comparing predicted reaction forces versus time with those of a detail geometric model.

2. KAERI Model

2.1 KAERI model development

PNNL suggested simplified finite element model

[2]. They used a plate shape model with suitable shell thickness which was decided by the equivalent slot study to produce similar lateral response to a finely-meshed grid slot that included the springs and dimples. But KAERI model is decided by using same cross-sectional area and volume as a detail geometric model shown in Fig. 1.

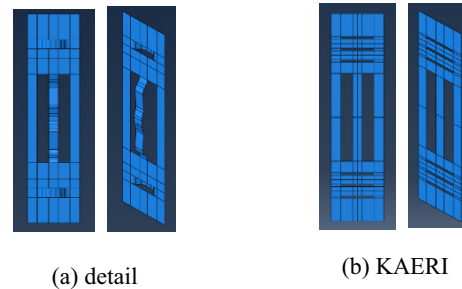


Fig. 1. Geometric models of 14 KNF-OFA.

2.2 Spring and dimple stiffness

Because the KAERI model has flat springs and dimples, we apply a connector element [3] having the characteristics of an axial spring to replace curved springs and dimples in a detail model. To input spring and dimple stiffness, spring characteristic analyses of a spring and a dimple in a detail model are performed.

3. Validation of KAERI model

3.1 Load and boundary conditions

Since the development objective of the FE model

is to predict the dynamic buckling strength, dynamic impact analyses were performed to validate KAERI model. The rotational degree of freedom of the cladding tube was constrained. The degree of freedom in all directions of the center point on the upper surface was constrained. Reaction forces in y-direction (RF2) were calculated on this point. The mass of a hammer was 48.85 kg and it collided with a 1x1 spacer grid in upper direction at a speed of 256.322 mm/s. The speed for a 3x3 spacer grid was 443.963 mm/s [4].

3.2 Analyses results

Three kinds of geometric models were used such as a detail, PNNL and KAERI. Same mesh size, load, constraints and boundary conditions were applied. To confirm the size effect, several arrays of SGs were analyzed. Fig. 2 shows that RF2 obtained by the KAERI model is similar to the result of the detail model in the case of 1x1 and 3x3 SGs. It means that the KAERI model is useful.

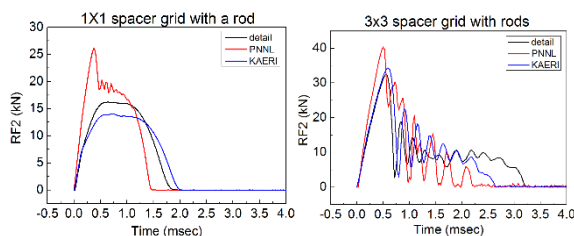


Fig. 2. Analyses results in the case of 1×1 and 3×3 SGs.

4. Conclusions

KAERI suggested a simplified geometric model with the same cross-sectional area and volume as a detail model. A connector element was used to simulate the spring and dimple of the detailed model. In order to confirm the validity of the KAERI model, dynamic impact analyses were performed on the detail, PNNL and KAERI model and the results were compared. Through the analyses results, it is

confirmed that the KAERI model are valid. It could reduce the time to generate a geometric model. The KAERI model will be used for a full-size 14 KNF-OFA SG dynamic impact analyses and for a 14 KNF-OFA fuel assembly to evaluate the mechanical integrity during transportation.

ACKNOWLEDGEMENT

This work was supported by the Korea Institute of Energy Technology Evaluation and Planning (KETEP) and the Ministry of Trade, Industry & Energy (MOTIE) of the Republic of Korea (No. 2014171020166A).

REFERENCES

- [1] Ministry of Trade, Industry and Energy, “Roadmap for High-Level Radioactive Waste Management (final version)”, (2016).
- [2] Harold Adkins et al., “Used Nuclear Fuel Loading and Structural Performance under Normal Conditions of Transport – Demonstration of Approach and Results on Used Fuel Performance Characterization”, FCRD-UFD-2013-000325, (2013).
- [3] Dassault Systemes, Abaqus 6.14 Online Documentation, (2014).
- [4] J.Y. Kim et al., “Pendulum Impact Tester for Thin Plates Structure”, No. KAERI/TR-6942/2017, (2017)

A Free Drop Analyses of Spent Nuclear Fuel Metal Cask for Various Positions

Hye Jin Lim*, Jung Gyu Kim, and Hyun Min Kim

Korea Electric Power Corporation E&C, 269, Hyeoksins-ro, Gimcheon-si, Gyeongsangbuk-do, Republic of Korea

*jin@kepc-eenc.com

1. Introduction

OASIS-32D, the spent nuclear fuel metal cask developed by KEPCO E&C, needs to go through a free drop test through a distance of 9m in accordance with 10 CFR 71[1]. This study is to find a drop position for which maximum damage is expected, and to confirm the structural integrity of OASIS-32D. For the purpose of the study, various drop positions - 0°, 30°, 45°, 60°, 90° and 180° off-angle drops as described in Table 1 and Fig. 2 are taken into considerations. The analyses are performed using ANSYS LS-DYNA. As a result of analyses, the structural integrity of OASIS-32D is maintained.

2. 9m free drop analyses

2.1 Analysis model and method

OASIS-32D finite element model consisting of the cask, canister and fuel assemblies was developed using the solid, shell and mass elements in ANSYS as shown in Fig. 1.

The velocity of 13.3 m/s corresponding to 9m free drop under 1g (gravitational acceleration) is applied on the cask, canister and fuel assemblies as the initial condition for the analyses. The contact condition between bumper and the rigid target surface is the node to surface contact used in impact analysis.

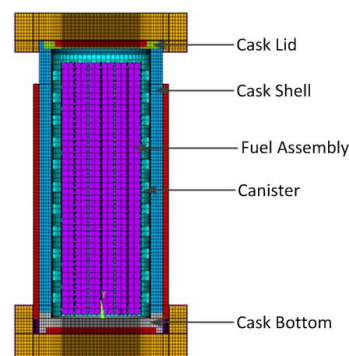


Fig. 1. FE model of OASIS-32D.

2.2 Positions of cask

The 6 cases of 0, 30, 45, 60, 90 and 180 degrees cask positions shown in Table 1 were used in the free drop analyses. The cask positions of cases 1, 3 and 5 are shown in Fig. 2, from the left side.

Table 1. Drop analysis cases

Case	Degree of Cask	Description
1	0	Bottom-Vertical Drop
2	30	Corner Drop
3	45	
4	60	
5	90	Horizontal Drop
6	180	Top-Vertical Drop

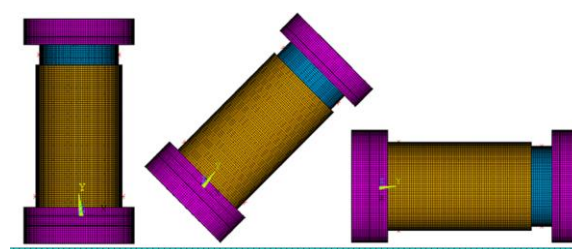


Fig. 2. Positions of cask drop (Cases 1, 3 and 5).

Table 2. Ratio of analysis results to allowable stresses

Comp.	Stress	Case 1	Case 2	Case 3
Cask Lid	Pm	0.74	0.69	0.31
	Pm + Pb	0.52	0.50	0.22
Cask Shell	Pm	0.13	0.19	0.02
	Pm + Pb	0.10	0.21	0.02
Cask Bottom	Pm	0.44	0.25	0.17
	Pm + Pb	0.44	0.22	0.12

Comp.	Stress	Case 4	Case 5	Case 6
Cask Lid	Pm	0.08	0.15	0.49
	Pm + Pb	0.11	0.15	0.36
Cask Shell	Pm	0.15	0.37	0.31
	Pm + Pb	0.12	0.26	0.37
Cask Bottom	Pm	0.27	0.42	0.26
	Pm + Pb	0.19	0.41	0.17

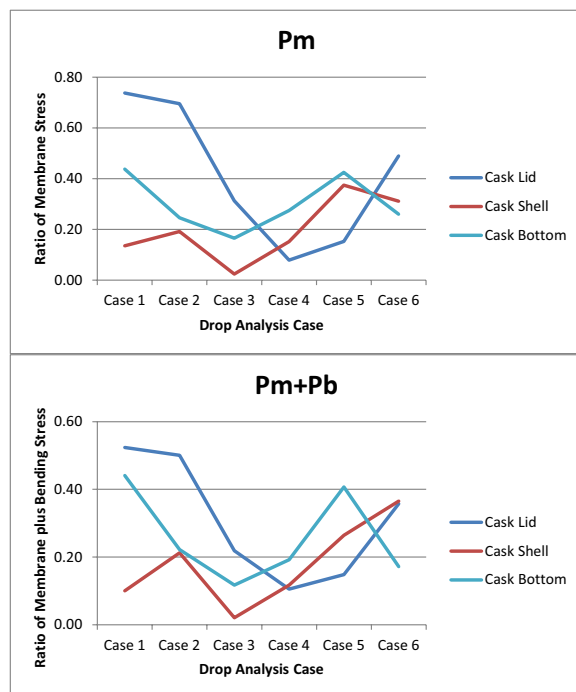


Fig. 3. Variation of ratio for each case.

2.3 Results

Since the purpose of these analyses is to check the structural integrity of the cask, the stresses of cask components are described in Table 2 and Fig. 3. The ratio of the result stresses to the allowable stresses, i.e., membrane stress and membrane plus bending stress to the allowable stresses are tabulated in Table 2. As shown in Table 2, each component of OASIS-

32D has a lot of margins. Fig. 3 shows that the maximum stresses of each component vary along with the positions of the cask. According to the Table 2 and Fig. 3, the position that causes the maximum damage is the bottom-vertical drop position (Case 1).

3. Conclusion

To find a position for which maximum damage is expected, the 9m free drop analyses for various cask positions are carried out. The maximum stress for cask lid is occurred in Case 1, bottom-vertical cask drop. All of the stresses are within the allowable stresses, and have margins bigger than 25%. Therefore, the integrity of OASIS-32D is maintained under the 9m free drop condition.

REFERENCES

- [1] 10 CFR 71, "Packaging and Transportation of Radioactive Material", Jan. 2017.

Effect of Cooling Rate on the Hydride Reorientation of Non-irradiated Zircaloy-4 Cladding Tube : 0.5°C/min vs. 0.5°C/hr

DaeHo Kim*, JongDae Hong, Jegeon Bang, Iksung Lim, EuiJung Kim, and DongHak Kook
Korea Atomic Energy Research Institute, 111, Daedeok-daero 989beon-gil, Yuseong-gu, Daejeon, Republic of Korea
*kdh@kaeri.re.kr

1. Introduction

In a dry storage environment, the spent fuel will have a long period of cooling time at high temperatures. At this time, the dissolved circumferential hydride is slowly precipitated from the radial hydride, which makes it more brittle and thus degrading the integrity of the cladding tube. The hydride reorientation occurs by internal rod pressure of the fission gas in cladding tube, and the hoop stress is applied to the outer diameter of the cladding, causing hydrogen to flow in a radial direction.[1]

The effects of cooling rate of hydride reorientation, which could occur during long-term dry storage process in the spent fuel cladding, were evaluated.

2. Experiment

2.1 Hydride Reorientation Test Method

Using a 400 ppm and 600 ppm of the non-irradiated Zircaloy-4 cladding tube, the hydride reorientation test(HRT) from 400°C of maximum temperature to 100°C on decreasing 0.5°C/min and 0.5°C/hr were performed at hoop stress 90 MPa respectively. Table 1 and 2 is HRT temperature program of 0.5°C/min and 0.5°C/hr. And the Fig. 1 is test profiles of temperature and hoop stress.

Table 1. HRT temperature program of short-term [2]
0.5°C/min Cooling Rate HRT Program

Segment	Target Temperature	Heating(Cooling) Rate	Step Time
1	420 °C	+ 5 °C/min	1.20 hr.min
2	420 °C	Holding	1.00 hr.min
3	100 °C	- 0.5 °C/min	10.40 hr.min
4	RT	-	End

Table 2. HRT temperature program of long-term [3]
0.5°C/hr Cooling Rate HRT Program

Segment	Target Temperature	Heating(Cooling) Rate	Step Time
1	418 °C	+ 2 °C/min	3.29 hr.min
2	418 °C	Holding	1.00 hr.min
3	100 °C	- 0.5 °C/hr	636.00 hr.min
4	RT	-	End

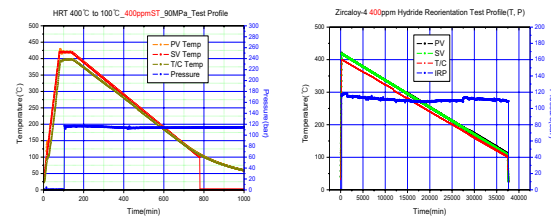


Fig. 1. HRT profiles of temperature and hoop stress.

2.2 Specimens and Test Condition

The test specimen of non-irradiated Zircaloy-4(cold-worked, stress-relief annealed, CWSRA) cladding were 400 ppm and 600 ppm of the treated homogenization hydrogen respectively, using the injection chamber of the volume of a mass system. And each specimen length is 150 mm used fitting at top and bottom. Table 3 lists the specimen and test conditions.

Table 3. Specimen and Test Condition

Material	Specimen		Condition		
	Length (mm)	Hydrogen Concentration (ppm)	Diameter (mm)	Hoop Stress (MPa)	IRP (MPa)
Zry-4	150	400	9.5	90	11.536
		600			

3. Test Results

After hydride reorientation test of non-irradiated Zircaloy-4 cladding tube, the offset strain was assessed from ring compression test at room temperature, 100°C and 300°C respectively. And the specimens were reviewed micro-structure of hydride morphology.

3.1 Morphology after HRT

Fig. 2 is a micro-structure of 400ppm and 600ppm specimen after HRT. Through the visualized review, it is difficult to observe the change in radial hydride.

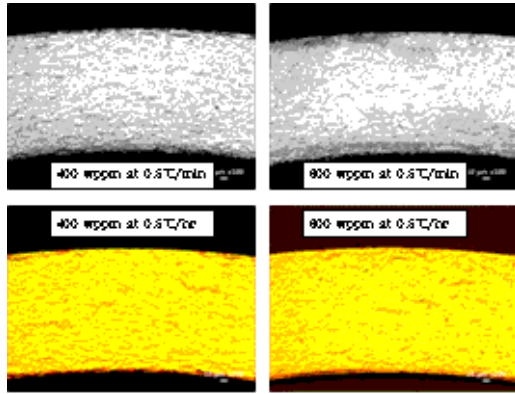


Fig. 2. Morphology after HRT.

3.2 RCT Results at RT

Table 4 and Fig. 3&4 are ring compression test results at room temperature. At result of offset strain, the 600wppm specimen of long-term cooling speed was assessed the brittle by radial hydride.

Table 4. Results of RCT and Offset Strain

RCT at RT	Hydrogen Concentration (ppm)	Diameter (mm)	Length (mm)	Max. Load (N)	Offset Dis (mm)	Offset Strain (%)
Non-HRT	400	9.50	10.01	907.9	2.53	26.65
	600	9.50	10.00	867.2	2.025	21.32
Short-term	400	9.51	10.01	925.4	2.51	26.40
	600	9.50	10.01	694.4	0.50	5.26
Long-term	400	9.51	9.18	744.9	1.70	17.88
	600	9.50	10.01	655.8	0.23	2.42

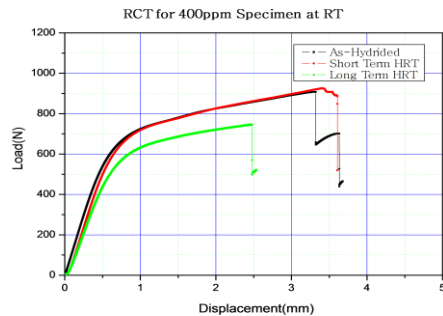


Fig. 3. Results of 400 ppm RCT at RT.

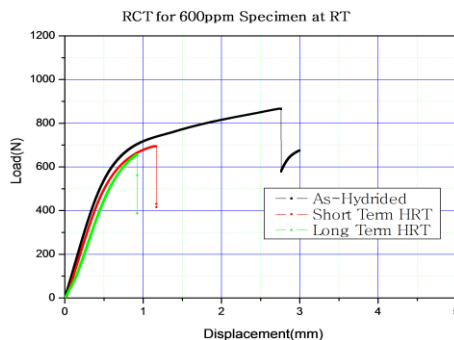


Fig. 4. Results of 600 ppm RCT at RT.

4. Conclusion

Using a 400 ppm and 600 ppm non-irradiated Zircaloy-4 cladding tube, the hydride reorientation test (HRT) from 400 °C of maximum temperature to 100 °C on decreasing 0.5 °C/min and 0.5 °C/hr respectively were performed at hoop stress 90 MPa. The test results of offset strain of the 400 ppm specimen at the short-term cooling rate of 0.5 °C/min were 26.65%, 26.4% and 17.88% respectively. And the results of offset strain of the 600 ppm specimen at the long-term cooling speed of 0.5 °C/hr were 21.32%, 5.264% and 2.42% respectively. In order to assess the effect of the cooling speed on the hydride reorientation, a repetition test is required in various conditions.

ACKNOWLEDGEMENT

This work was supported by the Korea Institute of Energy Technology Evaluation and Planning (KETEP) granted financial resource from the Ministry of Trade, Industry and Energy, Republic of Korea (No. 2014171020166A).

REFERENCES

- [1] Y.J. Kim, "Evaluation of hoop stress on the hydride reorientation and mechanical properties", Proc. of the KRS 2014 Spring Conference, May 8, 2014, Pyung Chang.
- [2] Billone. M.C., "Used Fuel Disposition Campaign, Phase I, Ring Compression Testing of High-Burnup Cladding", ANL-13/05, FCRD-USED02012-000039, 2011.
- [3] Aomi. M, etc. , "Evaluation of Hydride Reorientation Behavior and Mechanical Properties for High-Burnup Fuel-Cladding Tubes in Interim Dry Storage", Journal of ASTM International, Vol. 5, No. 9 2008.

Effect of Hoop Stress on the Hydride Reorientation of Non-irradiated Zircaloy-4 Cladding Tube : 90 MPa, 120 MPa & 150 MPa

DaeHo Kim*, JongDae Hong, Jegeon Bang, Iksung Lim, EuiJung Kim, and DongHak Kook
Korea Atomic Energy Research Institute, 111, Daedeok-daero 989beon-gil, Yuseong-gu, Daejeon, Republic of Korea
*kdh@kaeri.re.kr

1. Introduction

When nuclear fuel is burning, internal rod pressure acts on the inside of the cladding, and the hydride is injected into the radius of the cladding, resulting in a hydride reorientation by hoop stress. At this time, the dissolved circumferential hydride is slowly precipitated from the radial hydride, which makes it more brittle and thus degrading the integrity of the cladding tube. The hydride reorientation occurs by internal rod pressure of the fission gas in cladding tube, and the hoop stress is applied to the outer diameter of the cladding, causing hydrogen to flow in a radial direction [1,2,3].

The effects of hydride reorientation, which may be caused by hoop stress, were evaluated during long-term dry storage of spent fuel cladding.

2. Experiment

2.1 Hydride Reorientation Test Method

Using a 100 ppm of the non-irradiated Zircaloy-4 cladding tube, the hydride reorientation test(HRT) from 400°C of maximum temperature to 100°C on decreasing 0.5°C/min was performed at the hoop stress 90 MPa, 120 MPa and 150 MPa respectively. At this time, the hoop stress is not constants. Table 1 is HRT temperature program of 0.5°C/min cooling rate. And the Fig. 1 is test profiles of temperature and hoop stress.

Table 1. HRT temperature program

Segment	Target Temperature	Heating(Cooling) Rate	Step Time
1	420°C	+ 5 °C/min	1.20 hr.min
2	420°C	Holding	1.00 hr.min
3	100°C	- 0.5 °C/min	10.40 hr.min
4	RT	-	End

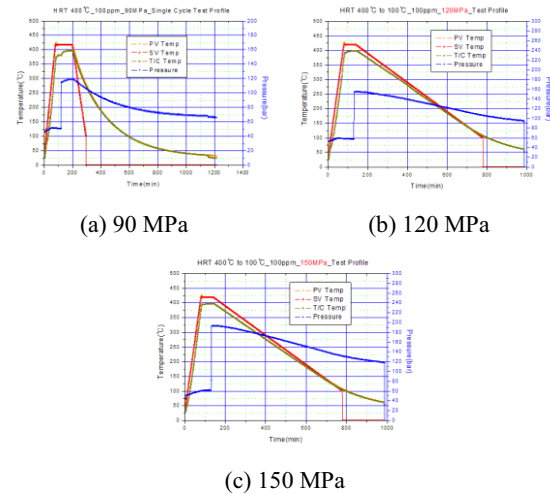


Fig. 1. HRT profiles of temperature and hoop stress.

2.2 Specimens and Test Condition

The test specimen of non-irradiated Zircaloy-4(cold-worked, stress-relief annealed, CWSRA) cladding was a 100 wppm of the treated homogenization hydrogen, using the vacuum chamber of the volume of a mass system. And each specimen length is 150 mm used fitting at top and bottom. Table 2 lists the specimen and test conditions.

Table 2. Specimen and Test Condition

Material	Specimen			Condition	
	Length (mm)	Hydrogen Concentration (ppm)	Diameter (mm)	Hoop Stress (MPa)	IRP (MPa)
Zry-4	150	100	9.5	90	11.54
				120	15.38
				150	19.22

3. Test Results

After hydride reorientation test of non-irradiated Zircaloy-4 cladding tube, the offset strain was assessed from ring compression test at room temperature, 100°C and 300°C respectively. And the specimens were reviewed micro-structure of hydride

morphology.

3.1 Morphology and RHCF after HRT

Fig. 2 is a micro-structure of 100 ppm specimen after HRT. It is difficult to observe changes in radial hydrides at 90 MPa hoop stresses through visualized studies. However, radial hydrides were observed at 120 MPa and 150 MPa specimens. Result of RHCF analysis showed 8.21%, 28.77% and 54.79% at 90 MPa, 120 MPa and 150 MPa hoop stress, respectively.

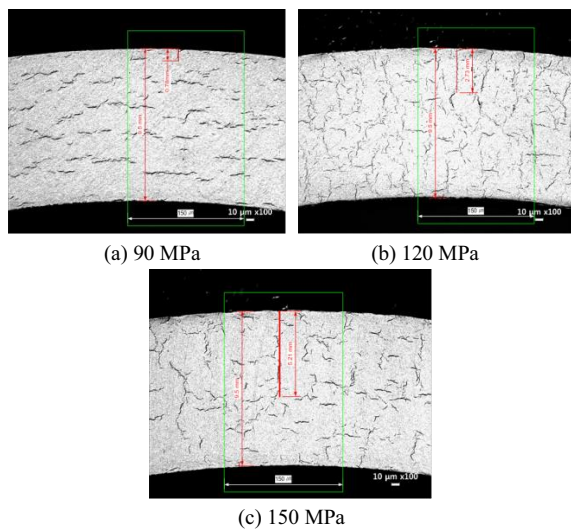


Fig. 2. Morphology and RHCF after HRT.

3.2 RCT Results at RT

Table 3 and Fig. 3 are ring compression test results at room temperature. The 100 ppm specimens were assessed the brittle by radial hydride. At result of offset strain evaluated 29.82%, 2.84% and 0.63% at 90 MPa, 120 MPa and 150 MPa hoop stress respectively. The 150 MPa specimen is very brittle and rated at creep limits of less than 2%.

Table 3. Results of RCT and Offset Strain at RT

Hoop Stress (σ_h)	Hydrogen Concentration (ppm)	Diameter (mm)	Length (mm)	Max. Load (N)	Offset Dis (mm)	Offset Strain (%)
Non- σ_h	100	9.50	10.05	1098	4.114	43.31
90 MPa	93.8	9.49	10.06	933	2.83	29.82
120 MPa	99.5	9.51	10.06	677	0.27	2.84
150 MPa	110.5	9.49	10.02	481	0.06	0.63

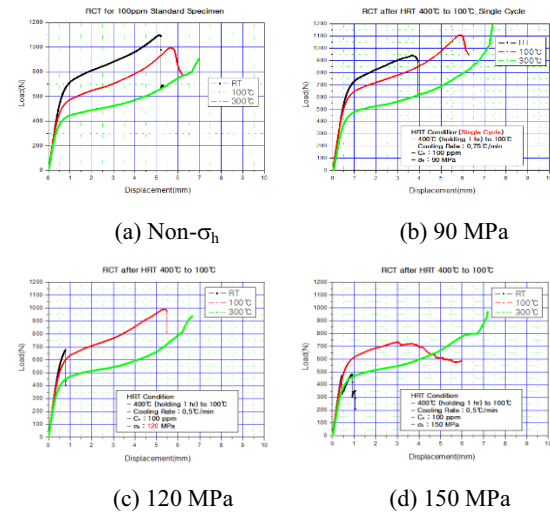


Fig. 3. Results of 100 ppm RCT.

4. Conclusion

Using a 100 ppm non-irradiated Zircaloy-4 cladding tube, the hydride reorientation test (HRT) from 400 °C of maximum temperature to 100 °C on decreasing 0.5 °C/min were performed at each other hoop stresses. Using the morphology, result of RHCF analysis showed 8.21%, 28.77% and 54.79% at 90 MPa, 120 MPa and 150 MPa hoop stress, respectively. The test results of offset strain at 90 MPa, 120 MPa and 150 MPa of the 100 ppm specimens were 29.82%, 2.84% and 0.63% respectively. The 150 MPa specimen is very brittle and rated at creep limits of less than 2%.

ACKNOWLEDGEMENT

This work was supported by the Korea Institute of Energy Technology Evaluation and Planning (KETEP) granted financial resource from the Ministry of Trade, Industry and Energy, Republic of Korea (No. 2014171020166A).

REFERENCES

- [1] Oohama, T., M. Okunishi, Y. Senda, K. Murakami, M. Sugano, Nuclear reactor thermal hydraulics, operations and safety 2004 N6P117 (2004).
- [2] Bai, J.B., C. Prioul, and D. Francois, Metall. Trans. A 25A, 1199-1208 (1994).
- [3] Daum, R.S., Saurin Majumdar, Yung Liu, and Michael Billone, "Radial-hydride Embrittlement of High-burnup Zircaloy-4 Fuel Cladding, Journal of Nuclear Science and Technology, 43(9), 1054-1067 (2006).

Effect of Thermal Cycling on the Hydride Reorientation of Non-irradiated Zircaloy-4 Cladding Tube : 1 Cy, 3 Cy & 10 Cy

DaeHo Kim*, JongDae Hong, Jegeon Bang, Iksung Lim, EuiJung Kim, and DongHak Kook

Korea Atomic Energy Research Institute, 111, Daedeok-daero 989beon-gil, Yuseong-gu, Daejeon, Republic of Korea

*kdh@kaeri.re.kr

1. Introduction

During long-term dry storage, spent fuel undergoes several thermal cycles. In particular, after charging into spent fuel storage casks, vacuum drying is performed to remove water, and this vacuum drying process undergoes several heat cycles. This heat cycle can affect the hydride reorientation in the fuel cladding. [1]. The United States NRC is an ISG-11, Rev. 3 (2003), it is necessary to confirm the radial hydride reorientation in the conditions related to the dry transfer operation and storage. It is recommended that the heating/cooling cycle be allowed up to 10 times during loading of the fuel in the dry storage cask and the temperature variation width should be less than 65°C (included vacuum drying).[2,3]

The effects of thermal cycling on the hydride reorientation, which could occur during vacuum drying process of the spent fuel cladding in dry storage cask, were evaluated.

2. Experiment

2.1 Hydride Reorientation Test Method

Using a 100 ppm and 300 ppm of the non-irradiated Zircaloy-4 cladding tube, the hydride reorientation test(HRT) from 400°C of maximum temperature to 100°C on decreasing 0.5°C/min was performed at the single cycle, 3 cycles and 10 cycles respectively. At this time, the hoop stress is not constants. Table 1 is HRT temperature program of 0.5°C/min cooling rate. And the Fig. 1 is test profiles of temperature and hoop stress.

Table 1. HRT temperature program

Thermal Cycling HRT Temperature Program				
Segment	Target Temp.	Heating Rate	Step Time	Remarks
1	420°C	+ 5°C/min	1.20 hr.min	
2	420°C	Holding	1.00 hr.min	
3	335°C	- 0.5°C/min	2.50 hr.min	
4	335°C	Holding	0.30 hr.min	

5	420°C	+ 5°C/min	0.17 hr.min	
Repeat 2~5 segments 10 times				
6	420°C	+ 5°C/min	0.17 hr.min	
7	420°C	Holding	1.00 hr.min	
8	100°C	- 0.5°C/min	10.40 hr.min	
9	RT	-	-	End

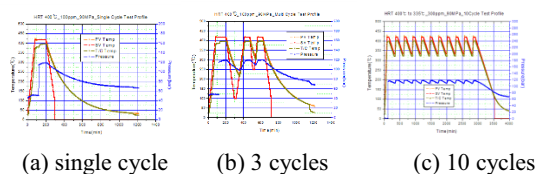


Fig. 1. HRT profiles of temperature and hoop stress.

2.2 Specimens and Test Condition

The test specimen of non-irradiated Zircaloy-4(cold-worked, stress-relief annealed, CWSRA) cladding were a 100ppm and 300ppm of the treated homogenization hydrogen, using the vacuum chamber of the volume of a mass system. And each specimen length is 150 mm used fitting at top and bottom. Table 2 lists the specimen and test conditions.

Table 2. Specimen and Test Condition

Specimen			Condition			
Hydrogen Concentration (ppm)	Length (mm)	Dia. (mm)	Hoop Stress (MPa)	IRP (MPa)	ΔT ($^{\circ}C$)	Cycle
100	150	9.5	90	11.5	300	1
				11.5	180/100	3
300	150	9.5	90	11.5	80	10
			120	15.3	80	10

3. Test Results

After hydride reorientation test of non-irradiated Zircaloy-4 cladding tube, the offset strain was assessed from ring compression test at room temperature, 100°C and 300°C respectively. And the specimens were reviewed micro-structure of hydride morphology.

3.1 Morphology after HRT

Fig. 2 is a micro-structure of specimen after HRT of thermal cycle conditions. It is difficult to observe changes in radial hydrides at 90 MPa hoop stresses through visualized studies. However, radial hydrides were observed in some of the 120 MPa hoop stress specimen in 10 cycles.

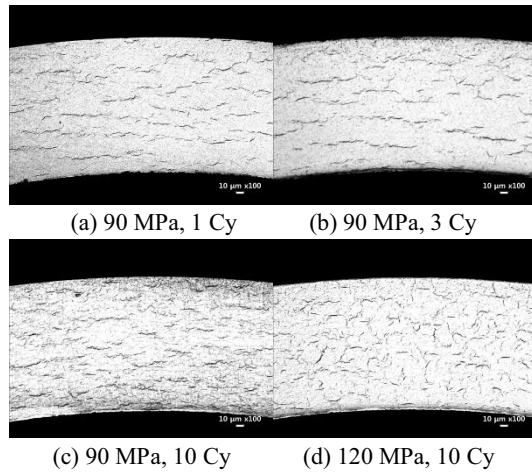


Fig. 2. Morphology after HRT.

3.2 RCT Results at RT

Table 3 and Fig. 3 are ring compression test results at room temperature. In this hydride reorientation test, the offset strain results of 1-cycle, 3-cycle and 10-cycle of 90 MPa hoop stress specimens were assessed 29.82%, 27.05% and 24.65% respectively. The 120 MPa hoop stress specimen was evaluated as susceptible to fracture by radial hydrides. However, it was evaluated as not exceeding the creep limit of less than 2%.

Table 3. Results of RCT and Offset Strain at RT

Specimen	Hydrogen Concentration (ppm)	Diameter (mm)	Length (mm)	Max. Load (N)	Offset Dis (mm)	Offset Strain (%)
90 MPa, 1 Cy	93.8	9.49	10.06	933	2.83	29.82
90 MPa, 3 Cy	135.3	9.50	10.23	916	2.57	27.05
90 MPa, 10 Cy	366.0	9.50	10.01	915	2.34	24.65
120 MPa, 10 Cy	375.6	9.50	9.98	764	0.75	7.86

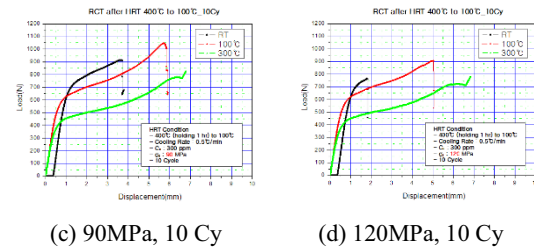
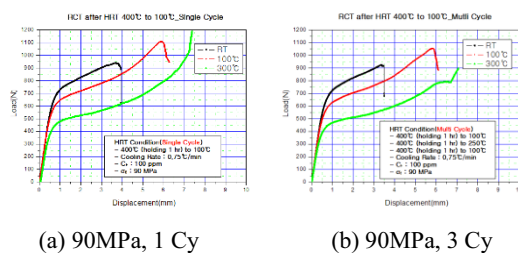


Fig. 3. Results of RCT.

4. Conclusion

This hydride reorientation test was performed at the various thermal cycling conditions for integrity of cladding. In this hydride reorientation test, the offset strain results of 1-cycle, 3-cycle and 10-cycle of 90MPa hoop stress specimens were assessed 29.82%, 27.05% and 24.65% respectively. The 120 MPa hoop stress specimen was evaluated as susceptible to fracture by radial hydrides. However, it was evaluated as not exceeding the creep limit of less than 2%.

This results of offset strain at the 10-cycle was similar to other hydride reorientation test cases. It is difficult to assess that a thermal cycle effect is affecting the hydride reorientation. However it has a significant impact on the thermal degradation of the spent fuel cladding.

ACKNOWLEDGEMENT

This work was supported by the Korea Institute of Energy Technology Evaluation and Planning (KETEP) granted financial resource from the Ministry of Trade, Industry and Energy, Republic of Korea (No. 2014171020166A)

REFERENCES

- [1] Billone MC, TA Burtseva, and RE Einziger. 2013. "Ductile-to-brittle transition temperatures for high-burnup cladding alloys exposed to simulated drying-storage conditions." Journal of Nuclear Materials 433:431-448.
- [2] Nuclear Regulatory Commission, Interim Staff Guidance (ISG)- 11, Revision 3, "Cladding Considerations for the Transportation and Storage of Spent Fuel," November 2003.
- [3] ASTM C1553, Standard Guide for Drying Behavior of Spent Nuclear Fuel, ASTM Designation: C1553 – 08, 2008. 1.

Preliminary Study on Load and Stress Characteristic Evaluation for Handling Reinforcement Device of Spent Nuclear Fuel

Jaejun Lee*, Hyeonkoo Kim, Manseok Do, Seongki Lee, and Jongsung Yoo

Korea Electric Power Company Corporation Nuclear Fuel, 242, Daedeok-daero 989beon-gil, Yuseong-gu, Daejeon, Republic of Korea

*jaejunlee@knfc.co.kr

1. Introduction

Spent Nuclear Fuels (SNFs) have been stored in spent fuel pools of the nuclear power plants since the plants started commercial operation. In some case, it is necessary to enhance handling safety for imported nuclear fuel types with Inter-Granular Stress Corrosion Cracking (IGSCC) [1]. To do this end, global nuclear vendors developed reinforcement devices. In recent years, the inventive reinforcement devices have been developing in Korea.

The developing device will be installed in Guide Tube (GT) of SNF, and various working mechanisms of the device have been considering. In this study, the load and stress characteristics are evaluated for the device with the friction coupling working mechanism. For the evaluation, a Finite Element (FE) model has been developed and FE analyses are performed. Also, the correlations for FE analysis results are evaluated using regression analysis. The FE model is generated based on the Westinghouse 17×17 type Fuel Assembly (FA), which is the heaviest among the FAs with the IGSCC concern.

2. FE Analysis for Characteristic Evaluation

2.1 Finite Element Model

The FE model is developed based on the sensitive parts under the handling condition of SNF. The developed FE model is a quarter model, and symmetric boundary conditions are used for each

symmetry plane. The schematic of device and the FE model are illustrated in Fig. 1 and 2.

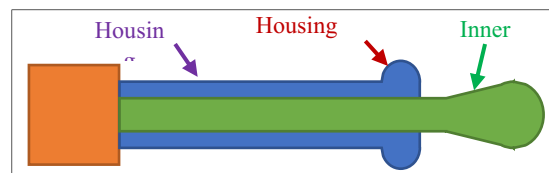


Fig. 1. Schematic of reinforcement device (Sectional view).

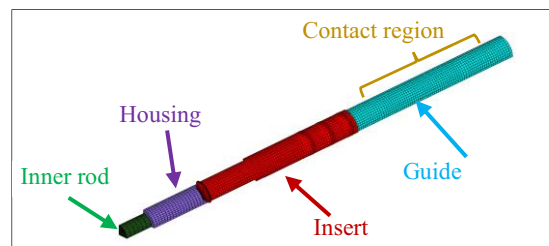


Fig. 2. FE model.

2.2 FE Analysis

The FE analysis is sequentially performed friction coupling analysis and handling analysis. The friction coupling analysis is carried out to simulate fastening between GT and device, and the handling analysis is performed to simulate handling operation of SNF with the device.

Boundary and loading conditions of friction coupling analysis are that one ends of GT and housing are fixed and inner rod is moved. Those of handling analysis are that end of GT is fixed and both inner rod and housing are moved.

2.3 FE Analysis Results

The load and stress characteristics for SNF with the device are evaluated from graphs using responses from each analysis. The graphs between each response are illustrated in Fig. 3, 4 and 5. The stress response is calculated from stress of GT, and the load response is calculated from reaction force of GT. Each regression curve is generated to describe correlation between each response, and R^2 value is calculated to verify the statistical significance of regression curve [2].

All data in these figures are non-dimensional values. Non-dimensional stresses are calculated based on the yield strength of GT material, and non-dimensional loads are calculated based on the handling load of SNF with 4 devices.

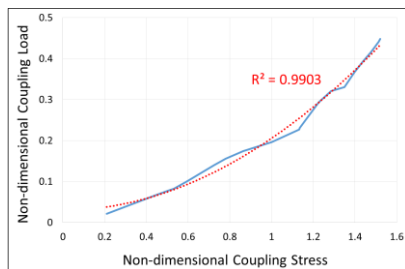


Fig. 3. Coupling stress vs. coupling load.

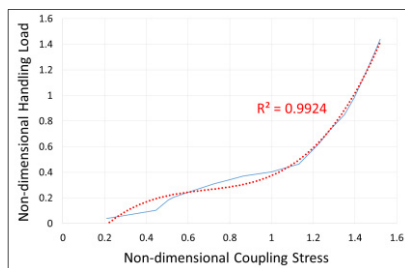


Fig. 4. Coupling stress vs. handling load.

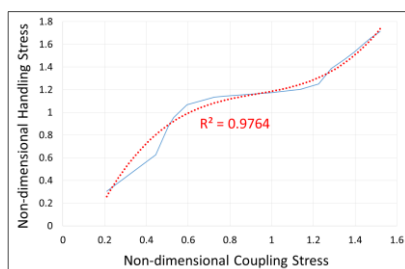


Fig. 5. Coupling stress vs. handling stress.

From these curves, it can be concluded that

relationships between coupling stress and other responses are increasing functions although trends of functions are different. When coupling stress is over than yield stress, the gradients of handling load and stress are rapidly increased. If the high handling load is necessary, the plastic deformation of GT should occur due to high friction coupling load.

3. Conclusion

The FE analyses are performed to evaluate load and stress characteristics for reinforcement device. The correlations are verified using statistical analyses among each response. To obtain high performance of the device, coupling stress is larger than yield stress. In the future, coupling load will be optimized to increase handling load using stress limit constraints.

ACKNOWLEDGMENTS

This work was supported by the Korea Institute of Energy Technology Evaluation and Planning (KETEP) and the Ministry of Trade, Industry & Energy (MOTIE) of the Republic of Korea (No. 2014171020166C).

REFERENCES

- [1] IAEA, "Spent Fuel Performance Assessment and Research", IAEA-TECDOC-1343, IAEA, Vienna, Austria (2003).
- [2] W. C. Kim, J. J. Kim, B. W. Park, S. H. Park, M. S. Song, S. Y. Lee, Y. J. Lee, J. W. Jeon and S. S. Cho, "General Statics", Yongchi Publishers, Seoul, Korea (2007).

Predicting Amount of Radial Hydrides in Spent Fuel During Dry Storage

Donghyo Lee*, Seongki Lee, and Jongsung Yoo

Korea Electric Power Company Nuclear Fuel, 242, Daedeok-daero 989beon-gil, Yuseong-gu, Daejeon, Republic of Korea

*donghyo@knfc.co.kr

1. Introduction

When spent fuels are placed in dry storage, hydrides from corrosion are dissolved and reprecipitated radially. Such radial hydrides can have a severe effect on mechanical properties of spent fuel at drop accident during transportation. In this report, we reviewed and analyzed the process of the predicting amount of radial hydrides [1].

2. Hydride Precipitation Model

2.1 Radial Hydride Fraction

A hysteresis effect between the hydride dissolution solvus and the precipitation solvus is observed in Fig. 1 [2].

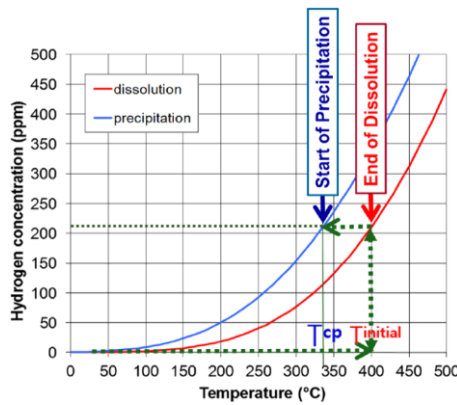


Fig. 1. Dissolution and precipitation curves of hydrides.

A red curve is stress-free hydride dissolution solvus during heating, namely,

$$C_{eq} = C_1 e^{-C_2/RT} \quad (1)$$

A blue curve is stress-free hydrogen precipitation solvus during cooling, namely,

$$C_p = C_3 e^{-C_4/RT} \quad (2)$$

Constants are given by:

T: Absolute temperature

R = 1.986 cal/mole·K

C₁ = 6.6E4 ppm

C₂ = 7.69E3 cal/mol

C₃ = 3.1E4 ppm

C₄ = 6.038E3 cal/mol

When the hydrogen atoms in the matrix are cooled under constant stress σ , some portion of them are reprecipitated radially. The following mathematical expression is derived for the radial hydride fraction [3].

$$F_\sigma(T^{\text{initial}}, T^0, \sigma) = \left[1 + \left(\frac{1-F_0}{F_0} \right) \exp \left\{ -\frac{579.7\delta_\varepsilon}{T^{\text{initial}}} (\sigma - \sigma_r) \right\} \right]^{-1} \quad (3)$$

Where F_0 is the volume fraction of radial hydrides relative to the hydrogen concentration in solid solution in the Zirconium alloy. The model parameters are follows:

F_0 : Initial value of F_0

δ_ε : "Misfit" strain, due to hydride formation (m/m)

T^{initial} : Initial temperature (K)

T^0 : Observation temperature (K)

σ : Applied stress (MPa)

σ_r : Internal stress due to hydrides volume expansion (MPa)

2.2 Evolution of Radial Hydrides over Time

Eq. (3) does not provide information for intermediate observation temperatures. To apply to continuous cooling, a general expression for the radial hydrides concentration at any intermediate temperature T under any temperature and stress history is given below,

$$C_R(T) - C_R(T^{cp}) = - \int_{T^{cp}}^T \frac{d}{dT} \{ F_\sigma(T^{cp}, T, \sigma) C_p(T) \} dT \quad (4)$$

$$C_R(T) - C_R(T^{cp}) = - \int_{T^{cp}}^T F_\sigma(T^{cp}, T, \sigma) \frac{dC_p(T)}{dT} + C_p(T) \frac{d}{d\sigma} F_\sigma(T^{cp}, T, \sigma) \frac{d\sigma}{dT} dT \quad (5)$$

If the eq. (5) is carried out under constant stress, over the temperature T^{cp} to the temperature T , the second term in the integrand drops out, and the model results can be compared to experimental data [4] usually generated under constant stress.

3. Results and Discussion

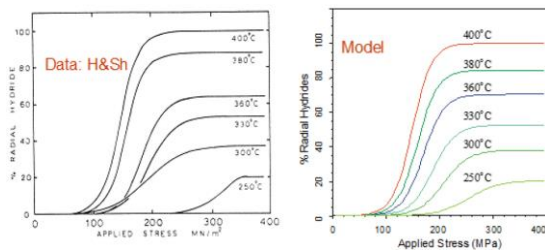


Fig. 2. Model and experimental results of radial hydrides.

The model has been validated by experimental data [4] in Fig. 2, left curves are radial hydrides fraction data from Hardie and Shanahan and right curves are model results simulated by FORTRAN.

4. Conclusion

Only a small fraction of the hydrides reprecipitated radially in dry storage. As depicted in Fig. 3, less than 15 ppm of radial hydrides is expected after 40 years of dry storage. These model results will be used in integrity evaluation process to predict the mechanical properties of spent fuel rods.

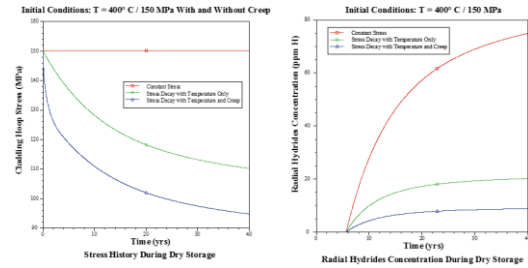


Fig. 3. Evolution of radial hydrides under stress histories.

ACKNOWLEDGEMENT

This work was supported by the Korea Institute of Energy Technology Evaluation and Planning (KETEP) and the Ministry of Trade, Industry & Energy(MOTIE) of the Republic of Korea (No. 2014171020166C)

REFERENCES

- [1] J. Rashid, A. Machiels, "Hydride Precipitation in Spent Fuel Cladding during Storage", ICEM05, Sept 4-8, 2005, Glasgow.
- [2] Kammenzind, Bruce F., et al., "Hydrogen Pickup and Redistribution in Alpha-Annealed Zircaloy-4," Zirconium in the Nuclear Industry", ASTM STP 1295.
- [3] Puls, M., in: Solute-Defect Interaction: Theory and Experiment, eds. S. Saimoto, G.R. Purdy and G.V. Kidson (Pergamon, Toronto, 1986) p.426.
- [4] Hardie, D., Shanahan, M.W., "Stress Reorientation of Hydrides in Zirconium-2.5% Nb", J. Nucl. Mater. 55, (1975), pp.1-13.

Development of Fabrication Technology of Annular Fuel by Hot Extrusion Method

Sang-Gyu Park* and Kiho Kim

Korea Atomic Energy Research Institute, 111, Daedeok-daero 989beon-gil, Yuseong-gu, Daejeon, Republic of Korea

*sgpark82@kaeri.re.kr

1. Introduction

The motivation for innovative fuel development is the development of the advanced ultra-high burnup sodium-cooled fast reactor metallic fuel concepts. The fabrication experiment in INL seeks to investigate advanced fuel designs with the following features: decreased fuel smeared density (SD), venting of the fission gas to the sodium coolant, a uranium-molybdenum (U-Mo) based alloy fuel system, coating or liner on the cladding inner surface, and/or targeted fuel alloy additions to reduce FCCI, and an advanced fabrication method that includes consideration of annular fuel and co-extruded fuel and cladding [1]. From the experiment result in INL, annular fuel shows the possibility of the reduction of swelling effect and then prevention of the FCMI (Fuel Cladding Mechanical Interaction). However, the fabrication technology of the annular fuel has not been developed yet. Therefore, KAERI has started to study the annular fuel fabrication method by using hot extrusion method. In this study, the prototype of annular fuel has been fabricated by using Cu billet. The design of billet and annular fuel has been determined, and then design and material for the mold has been determined by using Deform 3D program. After the mold fabrication, the prototype annular fuel has been fabricated and its texture were examined by us EBSD (Electron Back Scatter Diffraction).

2. Result & Discussion

2.1 Design of billet & annular fuel

The size of the billet and the fuel core specimens for the production of the annular simulated fuel shims were determined. In the case of the fuel padding, the annular shape having a diameter of 5 mm and a smear density of 75% was selected as a ring 10 mm in diameter. In the case of a billet, a diameter of 40 mm was selected by extrusion. The inside of the billet was designed to be easily manufactured into an annular shape by extruding holes of the same size as the annular fuel slug.

2.2 Design and manufacture of extrusion mold

A mold for extruding annular metal fuel shims was designed using Deform 3D analysis program. In this study, Cu which is similar to the dissolution condition of uranium was selected as the material for making the simulated annular metal fuel shims, Deform 3D was used to select the jig design suitable for extruding Cu and stress and temperature conditions. Fig. 1 is an analysis of the stresses at each part generated during extrusion using Deform 3D. As a result of the analysis, it was confirmed that a stress of about 900 MPa was generated at the center portion, and a stress of about 1800 MPa was expected to occur when the actual extrusion was performed.

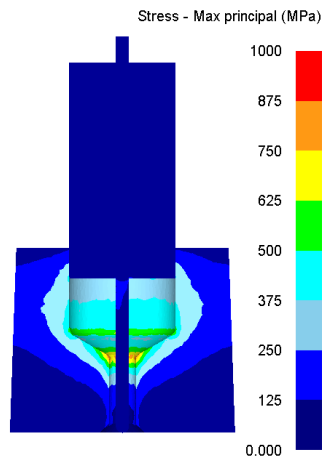


Fig. 1. Stress analysis of the extrusion mold.

Fig. 2 shows the result of analyzing the temperature at each part during actual extrusion. The extrusion conditions were selected based on the extrusion of the annular simulated fuel core with Cu at a maximum temperature of 726 °C.

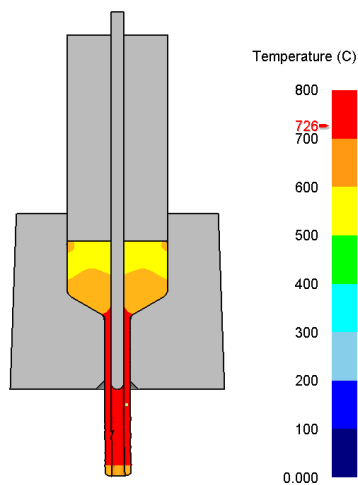


Fig. 2. Temperature analysis result of extrusion mold.

2.3 Production of annular simulated fuel shims

Based on the analysis results, the jig design was designed as shown in Fig. 2, and the mold was manufactured based on the design. In the simulated fuel core extrusion, a press machine capable of extruding a maximum of 200 tons was used, and the extrusion was performed by inserting the billet before extrusion into a mold set at 450°C after

heating at 600°C. As a result of the extrusion, it was possible to successfully produce the annular simulated fuel slug, and the characteristics evaluation will be conducted and discussed.



Fig. 3. Sample Figure.

3. Conclusion

In this study, the prototype of annular fuel has been fabricated by using hot extrusion method. The mold for annular fuel was designed using Deform 3D, and the fabrication was successfully done by press extrusion method.

ACKNOWLEDGEMENT

This work was supported by the National Research Foundation of Korea funded by the Ministry of Science and ICT (2017M2A8A5014888).

REFERENCES

- [1] A. name, B. name, and C. name, "Article Title", Journal of Nuclear Fuel Cycle and Waste Technology, 1(1), 1-10 (2003).

Design Concept of Package Stowage and Retention Systems During the Road and Sea Transport

Chang-Yeal Baeg* and Sang-Jin Lee

Korea Radioactive Waste Agency, 174, Gajeong-ro, Yuseong-gu, Daejeon, Republic of Korea

*baegcy@korad.or.kr

1. Introduction

This paper describes the design concept of package stowage and retention systems, such packages should be restrained from movement within or on the conveyance during the transport operation, as required by the transport mode and regulations. The components of the package, its contents and their respective retention systems shall be designed so that the package integrity will not be affected under routine conditions of transport.

2. Design Concept and Requirements of Package Stowage and Retention systems

The integrity of the package shall not be impaired by the stresses imposed on the package or its attachment points by the tie-downs or other retention systems under either normal or accident conditions of transport accordance with the competent authority and regulations (Fig. 1. Package retention systems) [1].

In particular, the accelerations derived from routine conditions of transport should not cause any component of the package or its retention system to yield. Table 1 gives an indication of the magnitude of the acceleration factors which might be used for the design of the package and its retention system for routine conditions of transport. The values given for each mode would be in accordance with most

national and international regulations. Table 2 details a limited number of such packages and other examples. And the specific systems, such as tie-down and lifting device that are structural parts of a package must consider its acceleration factors as follows [2, 3];

- Tie down : Longitudinal(10g), Lateral(5g)
Vertical(2g)
- Lifting device : Vertical(3g)

Table 1. Acceleration factors for package retention system design [1]

Mode	Acceleration factors		
	Longitudinal	Lateral	Vertical
Road	2 g	1 g	2 g up, 3 g down
Rail	5 g	2 g	2 g up, 2 g down
Sea/ water	2 g	2 g	2 g up, 2 g down

3. Conclusion

This paper describes the design requirement of package stowage and retention systems. Also the package designers and users to ensure that the package systems were designed in compliance with those values specified by the relevant competent authorities and organizations. We are now

performing the research project, “development evaluation technology for vibration and shock load characteristics and PWR spent nuclear fuel integrity under normal conditions of load and sea transport” during 2018 to 2023. On the basis of survey and analysis above, development of the road and sea transport systems and related technologies that can be used optimally will be available.

Table 2. Acceleration factors for package retention system design for specific packages [1]

Type of package	Acceleration factors		
	Longitudinal	Lateral	Vertical
Certified fissile and Type B(U) or Type B(M) packages in the USA	10g	5g	2g
Radioactive material packages in Europe by rail	4g(1g)	0.5g	1g±0.3g
Carriage of irradiated nuclear fuel, plutonium and high level radioactive waste on vessels	1.5g	1.5g	1g up 2g down
Domestic barge transport of radioactive material packages by Sea/water	1.5g	1.6g	2g



Fig. 1. Package stowage and retention systems
(Examples, AREVA TN).

ACKNOWLEDGEMENT

This work was supported by the Korea Institute of Energy Technology Evaluation and Planning (KETEP) granted financial resource from the

Minister of Trade, Industry and Energy, Republic of Korea.

REFERENCES

- [1] IAEA SSG 26, “Advisory Material for the IAEA Regulations for the Safe Transport of Radioactive Material” (2012).
- [2] Korea NSSC Notice No. 2017-56, “Regulations for the Packaging and Transportation of Radioactive Materials” (2017).
- [3] US NRC 10CFR Part 71, “Packaging and Transport of Radioactive Material” (2012).

Peak Cladding Temperature Analysis of a Spent Fuel Assembly According to Heat Transfer Modes

Hyungjin Kim* and Hyungrak Kim

Korea Radioactive Waste Agency, 174, Gajeong-ro, Yuseong-gu, Daejeon, Republic of Korea

*hjkim@korad.or.kr

1. Introduction

Thermal evaluation of a cask using three-dimensional models is especially difficult if the spent fuel assemblies are modeled explicitly and included in the analysis. The method, which explicitly models spent fuel assemblies, is costly in time of setup and computational time and does not lend itself to parametric evaluation of cask design. Therefore, these assembly elements are modeled as solids with homogenous “smeared” or “effective properties”. This solid method can predict the peak cladding temperatures of casks with reasonable accuracy [1, 2]. One of the solid methods is CFD simulation on transverse cross-section of a spent fuel assembly [3]. The CFD simulation has used the convection and radiation for heat transfer.

In this work, the temperatures of a spent fuel assembly were calculated by using the conduction, convection and radiation in heat transfer. 3D CFD simulation is used for this calculation.

2. Modeling and method

2.1 Modeling for peak cladding temperature

14x14 PWR spent fuel type is selected to calculate the peak cladding temperature. The assembly heat load is 796.2W. Fig. 1 shows the three-dimensional CFD mesh model of the assembly which includes the gap between fuel rods and cladding. The result of mesh work has over 2 million elements.

Thermal properties of helium, claddings, guide tubes, fuel rods are used with a temperature-dependent value [4]. The emissivity is 0.8 for zircaloy and 0.36 for stainless steel (basket wall).

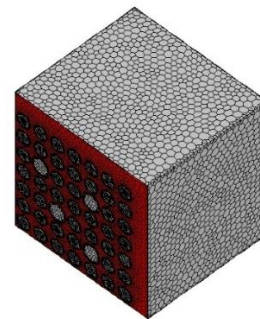


Fig. 1. CFD model for 14x14 assembly.

2.2 Physics model and solution method

The discrete ordinates (DO) radiation model was selected to solve the radiation of spent fuel assembly. The DO radiation model solves the radiative transfer equation (RTE) for a finite number of discrete solid angles, each associated with a vector direction fixed in the global Cartesian system. The value of angular discretization and pixelation available in the discrete ordinates radiation model significantly affects the behavior of temperature. The constants were determined to solve the spent fuel assembly: 3x3 for pixelation, 5x5 for discretization.

The convergence of a natural convection problem is not good with the normal steady-state calculation. So, the pseudo-time progression method has been used to obtain a converged solution. This method works by using a steady calculation and introducing a

pseudo-time term to relax the equation. The settings for this method were: PRESTO! spatial discretization for pressure, second order space discretization for momentum and energy, 0.5 relaxation coefficients for momentum and pressure, 10 for timescale factor, 1 for verbosity. For turbulent flow, the first cell height around wall is calculated from $y^+ (<10)$.

3. Results and discussion

Fig. 2 shows the Pseudo transient method converged. In Fig. 3, temperature distribution of a 14x14 assembly is shown for 300K of basket wall temperature. The maximum temperature is 317K. The temperature difference between 2D and 3D simulation is above 30K [3]. The lower temperature would result from convection in heat transfer mode. Effective thermal conductivity of solid method will increase in comparison with the 2D simulation.

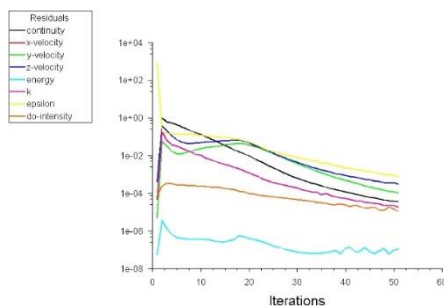


Fig. 2. Residuals graph for pseudo transient coupled solver.

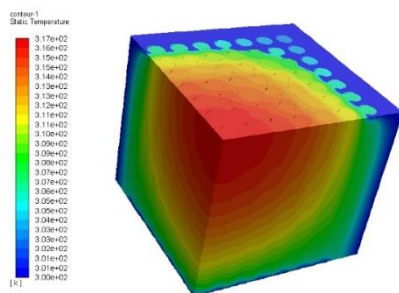


Fig. 3. Temperature distribution of 14x14 fuel assembly.

4. Conclusions

3D CFD simulation was performed to predict the peak cladding temperature of a spent fuel assembly. The maximum temperature of 3D simulation is lower than that of 2D. This result would come from the difference of heat transfer modes used for simulation.

The axial length of the assembly modeling would be not enough to study the trend of the temperature. But, one knows that the temperature change requires engineers to perform 3D simulation on spent fuel assemblies. This work will be expanded with larger domain and other fuel types.

ACKNOWLEDGEMENT

This work was supported by the National Institute of Supercomputing and Network/Korea Institute of Science and Technology Information with supercomputing resources including technical support (KSC-2016-S1-0028)

REFERENCES

- [1] EnergySolutions, FuelSolutions™ storage system final safety analysis report, WSNF-220, (2007).
- [2] Babcock & Wilcox Fuel Company, BR-100 100-ton rail/barge spent fuel shipping cask, No. 51-1203400-01, (1991).
- [3] H. Kim, O. J. Kwon, G. U. Kang and D. G. Lee, "Comparisons of prediction methods for peak cladding temperature and effective thermal conductivity in spent fuel assemblies of transportation/storage casks," Annals of Nuclear Energy, Vol. 71, (2014).
- [4] Korea Radioactive Waste Agency (KORAD), Safety analysis report of KORAD21 spent fuel transportation cask, (2016).

Modal Analysis of Alternative Spent Nuclear Fuel Transportation Cask for Normal Conditions of Transport Test

JaeHoon Lim*, SangSoon Cho, Kiseog Seo, and Woo-seok Choi

Korea Atomic Energy Research Institute, 111, Daedeok-daero 989beon-gil, Yuseong-gu, Daejeon, Republic of Korea

*jhl85@kaeri.re.kr

1. Introduction

During the past 40 years since 1978, when commercial nuclear power generation started in Republic of Korea, various types of spent nuclear fuel have been generated and temporarily stored in wet spent fuel storage pools in a nuclear power plants. However, the capacity of such temporary storage is expected to be full in the near future. Currently, construction of interim dry storage facility inside or outside of the nuclear power plant is being discussed to solve this problem. Therefore, it is expected that transport of the spent nuclear fuel in the wet storage pools will be conducted within a short time and thus, the safe transport of spent nuclear fuel should be secured.

Therefore, it is necessary to perform the normal transport test on the road and sea transport conditions to measure the applied loads to the transportation platform, cask, and fuel assemblies and to check whether the spent nuclear fuels can maintain its integrity under the measured loads.

To verify this, normal transport test is being planned to measure shock and vibration loads and strain of fuel rods under normal transport conditions. It is best to perform the normal transport test with a cask which will be used for spent nuclear fuel transport. However, it has not determined yet which cask will be used for spent nuclear fuel transport. Therefore, it is planned that the test will be conducted by using the currently available cask as an alternative.

In this study, modal analysis of the available cask is performed and important modes related to the

normal conditions of transport were investigated.

2. Modal Analysis

The KORAD-21 cask was designed for the transport of low burn-up PWR spent nuclear fuel. The 1/3 scale model of KORAD-21 was manufactured and related safety examinations including drop test, water immersion test, high temperature test and thermal test were carried out, but it is difficult to use it to this normal transport test because real scale model was not manufactured [1]. As an alternative way, OCL cask owned by Doosan Heavy Industries & Construction will be used for the present transport test. However, it is required to be investigated whether its dynamic characteristics is similar with KORAD-21 which is expected to be used for spent nuclear fuel transport in Republic of Korea.

If the dynamic characteristics between the two different casks are similar, the test results will be applicable for KORAD-21 cask. Therefore, the modal analysis of OCL cask and KORAD-21 cask was performed and the results were compared.

The modal analysis is performed by applying a frictionless boundary condition to the trunion as shown in the Figure 1. The results of modal analysis are shown in Table 1. As a result of the modal analysis, it was observed that the major lower order modes are not related to the cask bending or torsional modes but it is related to the bending or torsional modes of trunion itself.

Table 1 also shows the results of comparing the frequency of each mode frequency of the OCL cask

with those of the KORAD21.

It is believed that vertical translation and pitching modes are the most important for the normal conditions of transport because the vertical shock and vibration loads will be dominant during transport by truck or ship.

As shown in the table, the pitching frequency of OCL cask is well matched with that of KORAD-21 cask. However, the vertical translation frequency of OCL cask is quite different compared with that of KORAD-21.

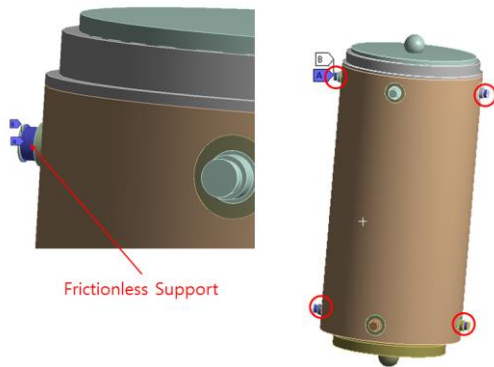
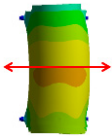

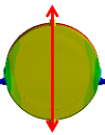
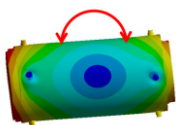

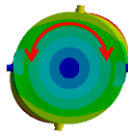


Fig. 1. Boundary condition of the present modal analysis.

Table 1. Mode shapes for OCL cask

Mode no.	OCL	Frequency (compared with that of KORAD21)
Translation-horizontal (1)		
1		-29.5%
Translation-horizontal (2)		
2		-27.8%
Translation-vertical		
3		-25.8%
Rotation-pitching		
4		-3%

Rotation-yawing		
5		-7.3%
Rotation-rolling		
6		-30.3%

It is expected that the frequency difference on vertical translation mode can be minimized by adjusting the boundary condition of the trunion and adjusting the weight and center of gravity of the impact limiter.

3. Conclusion

Modal analysis of the transportation cask for the normal transport test was carried out. Modal analysis of OCL cask and KORAD21 was conducted and discussed. As a result of the modal analysis, it was observed that the major lower order modes were not related to the cask bending or torsional modes but it was related to the bending of torsional deformation of trunion itself. It was expected that the frequency difference on vertical translation mode can be minimized by adjusting the boundary condition of the trunion and adjusting the weight and center of gravity of the impact limiter.

REFERENCES

- [1] Cho, S. S., et al, Safety Test Report of KORAD-21 Transportation Cask, KAERI-CR-685.2018.

Comparative Study of Servo-type Telemanipulator Systems for Nuclear Facilities

Seungnam Yu*, Jongkwang Lee, and Byungsuk Park

Korea Atomic Energy Research Institute, 111, Daedeok-daero 989beon-gil, Yuseong-gu, Daejeon, Republic of Korea

*snyu@kaeri.re.kr

1. Introduction

Practically, various control schemes have been established to the servo manipulator for teleoperation. The level of control algorithm and operational reliability of such systems are now highly improved, and these have been proven during the long-term evaluation of operation and maintenance programs. This study tries to classify the existing development cases of servo-type telemanipulator systems in a nuclear area, and introduce the specification of the BDSM developed by KAERI for the performance comparison [1-3].

2. Comparison of existing telemanipulator systems

Table 1 shows the typical classification of telemanipulator system according to the components, operation type and payload. Table 2 shows the characteristics of servo-type telemanipulators for their specifications, and several development cases are introduced as follows. First, the remote handling

system for ORNL SNS hot-cell had developed for the facility maintenance. This system is a servo-type EMSM-2B (TelerobTM) with 24 kgf payload and integrated with bridge transporter developed by PaR Systems. The target operation had started in April 28, 2006 and the 1st module replacement had performed in Aug. 2009. Second, the remote handling system for fusion had developed for remote maintenance in the nuclear fusion research facility by Joint European Torus (JET). The system has long reach with the articulated boom, and the servo-manipulator is based on the MASCOT-IV system with 20 kgf payload. This system extensively performed various remote tasks such as a welding, cutting, bolting, and inspection. Third, the equipment handling system operated in INL has around 5 Ton (4,540 kg) of maximum capacity with 3.91 m of maximum lifting height. A repair hoist (for maintenance only) and crane operated in INL has 6 ton and 5 ton capacity respectively. Table 3 shows the specification of BDSM system which has dual arm servo manipulator and telescopic tube mechanism for teleoperations in the confined argon cell of KAERI [4].

Table 1. Types of telemanipulator systems





Types	Components	Operation	Payload	
MSM (~45 kg) Mechanical force reflection	1. Dual arm master manipulator 2. Dual arm slave manipulator 3. Hot cell trough-tube	Through the working window, operate the slave system with master (Force reflection)	Middle and low payload (Material handling)	
EMSM (~25 kg) Electrical force reflection	1. Dual arm master manipulator 2. Dual arm slave manipulator 3. Bridge-transported system 4. Control panel (Camera, Monitor, Electric/Computing system)	Through the monitor, operate the slave with master (Force reflection)	Similar to MSM (Spatial transportation of low weight materials)	
PM (100 kg~)	1. Joystick (Master) 2. Slave manipulator (Single arm) 3. Bridge-transported (Slave attached) 4. Control panel (Camera, Monitor, Electric/Computing system)	Through the monitor, operate the slave with joystick (Force reflection is not applied)	Handling of high and middle weight materials	
Robot (~100 kg)	1. Joystick 2. Various kinds of robot system 3. Control panel (Camera, Monitor, Electric/Computing system)	Running the program and use the joystick for system operation	Repetitive works and Decommissioning	

Table 2. Comparison of the teleoperated servo manipulator systems

Model	Manufacturer	DOF (Master, Slave)	Type of DOF**	Lift Capacity (kg)***	Reach (m)	Tip Speed (m/s)	Force- Reflecting Ratios	System Launching (Year)
SM-229	Teleoperation Systems, USA	6, 6	PRPRPR	10	1.23	~ 1	1:1	1981
M2	CRL/ORNL, USA	6, 6	PRPRPR	23	1.26	0.15 (1.5)	1,2,4,8:1	1978-1983
ASM	ORNL, USA	6, 6	PRPPYR	23	1.40	~ 1	1:1 o 16:1	1983-1989
BSM	JAEA, JPN	6, 6	PRPPYR	23	1.40	~ 1	1:1 o 16:1	1982-1989
LTM	ORNL, USA	7, 7	PYPYPYR	20	1.40	>1	1,2,8,16:1	1987-1989
CESARm	ORNL, USA	7, 6	YPRPPYR	13	1.52	3.0	1:1 to 8:1	1990
Telemate	TeleRobotics, USA	6, 6	PRPYPR	12	1.1	>1	0.5 kgf ****	1992
EMSM-2C	Telerob, GER	6, 6	PRPYPR	10;	0.85	>1	1:1 to 4:1	1997
EMSM-2B	Telerob, GER	6, 6	PRPYPR	24;	1.6	>1	2,6,20:1	-
MA-23	CEA, FRA	6,6	PRPYPR	25		0.5~1.5	1:4	1979
MASCOT IV	Oxford Tech., GBR	6, 6	PRPYPR	12	1.43	0.79	1:1,5,3,6	-
BTSM	KAERI, KOR	5, 5	PPYPR	15	0.82	>1	1,2,4,6:1	2006
FSM	BARC*, IND	6, 6	PRPYPR	25	1.2	-	< 8 kgf	2009
BDSM	KAERI, KOR	6, 6	PRPYPR	25	1.52	>1	1,2,4,6:1	2012

*BARC: Bhabha Atomic Research Centre, ** P: Pitch, R: Roll, Y: Yaw, *** Continuous Peak, **** Force-Reflection Sensitivity,

Table 3. Specification of BDSM

Mechanical specifications (Replica type)	
Degree of freedom	6 + gripper/handle
Load capacity (Slave)	250 N (Continuous)
Force feedback capacity (Master)	50 N (Continuous)
Upper arm	Incline (axis 1) $\pm 45^\circ$
	Rotation (axis 2) $\pm 45^\circ$
	Length (mm) 600 (Slave), 375 (Master)
Forearm	Incline (axis 3) $\pm 45^\circ$
	Rotation (axis 4) $\pm 110^\circ$
	Length (mm) 800 (Slave), 500 (Master)
Wrist	Incline (axis 5) $+37 \sim -143^\circ$
	Rotation (axis 6) $\pm 170^\circ$
Grip opening width (mm)	0 ~ 100
Reach (Master/Slave)	0.95 m / 1.56 m
Total weight (Master/Slave)	45 / 165 kg
Power transmission	Gear/belt (#1), Motion-decoupled wire cable (#2~#7)
Contamination protection	Boots, cover
Electrical/Control specifications	
Motor type	BLDC with resolver
Motion control hardware	DSP controller
Motion control software	GUI (PC) Firmware (DSP)
Control algorithm	PD, PID, TDC, etc.
Camera	2 EA, attached to gripper

3. Conclusions

This paper covers a comparison of telemanipulators which have different specifications of in their geometry, actuation type and control strategy as well as the comparison of their performances and specifications with the ones of BDSM system originally developed in KAERI. As a future work, it is required to standardize the effective handling capacity with the corresponding static and

dynamic safety factors. It is important, especially in nuclear facility when various kinds of customized telemanipulator systems have to be compared each other technically. Also, up-to-date telemanipulator systems and their innovative applications will be surveyed even the teleoperation systems in a nuclear area have a tendency to stick to the traditional approaches for safety and reliability.

REFERENCES

- [1] S.N. Yu, et al., "Technical Review of Force-Reflecting Telemanipulator System", Korean Radioactive Waste Society, Spring Annual Conference, 2018.
- [2] A.C. Rolfe, P. Brown, P. Carter, R. Cusak, A. Gaberscik, L. Galbiati, B. Haist, R. Horn, M. Irving, D. Locke, A. Loving, P. Martin, S. Mills, R. Minchin, J. Palmer, S. Sanders, S. G. Sanders, R. Stokes, "A report on the first remote handling operations at JET", Fusion Engineering and Design, Vol. 46, No. 2-4, pp. 299-306, 1999.
- [3] A.C. Rolfe, "A perspective on Remote Handling Techniques", Fusion Engineering and Design, Vol. 82, No. 15-24, pp. 1917-1923, 2007.
- [4] J.K. Lee, et al., "Bridge-transported bilateral master-slave servo manipulator system for remote manipulation in spent nuclear fuel processing plant." Journal of Field Robotics, Vol. 29, No. 1, pp. 138-160, 2012.

Investigation of Thermodynamic Behaviors of SrO in LiCl Molten Salt at 923 K

Dokyu Kang^a, Byung Heung Park^b, and Sungyeol Choi^{a,*}

^aKorea Advanced Institute of Science and Technology, 291, Daehak-ro, Yuseong-gu, Daejeon, Republic of Korea

^bKorea National University of Transportation, 50, Daehak-ro, Daesowon-myeon, Chungju-si, Chungcheongbuk-do, Republic of Korea

* sungyeolchoi@kaist.ac.kr

1. Introduction

After burning U fuel in the nuclear power plant, wide range of fission products are produced from light alkali, alkaline earth elements to heavy transuranic metals. Among them, Sr and Cs emit high radiation and heat and threaten safety of researchers and workers dealing with spent nuclear fuels. Therefore, it is important to understand the behaviors of the fission products during the reprocessing process [1].

Especially in South Korea, pyroprocessing have been developed and the highly radioactive fission products are separated by reacting with LiCl molten salt during electrolytic reduction process which is a subprocess of pyroprocessing. However, the behavior of Sr is still not clearly identified, because of its little positive Gibbs reaction free energy with LiCl molten salt [2].

Therefore, experimental methods to investigate thermodynamic behaviors of SrO in LiCl molten salt at 923 K were designed in this paper.

2. Method

2.1 Experimental setup

All experiment will be conducted in an electrochemical system which consists of a glovebox, a furnace, a potentiostat as shown in Fig. 1. The glovebox maintains oxygen and moisture concentration below 1 ppm. The furnace consists of kanthal heating elements, heat controller, and heat insulator, which controls temperature from 25 °C to 900 °C. The electrochemical techniques will be conducted with PARSTAT 4000 A which is a high performance potentiostat. It can apply current and potential in a wide range (± 4 A, ± 10 V).

Fig. 2. shows the experimental cell configuration and experimental configuration of the experiment. The experimental cell consist of quartz cell containing 5 g of LiCl molten salt and various concentration of SrO, tungsten working electrode and counter electrode, and an Ag/Ag⁺ reference electrode with mullite membrane.



Fig. 1. Electrochemical system.

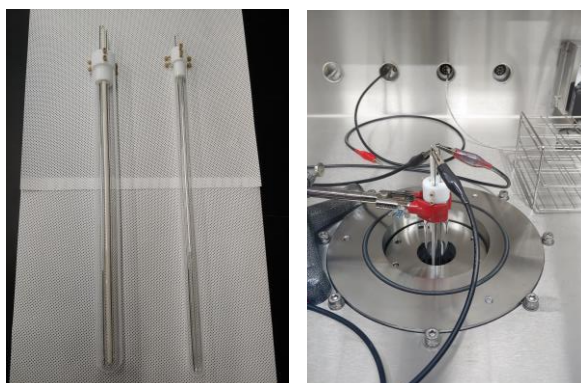


Fig. 2. (a) Cell configuration, (b) Experimental configuration.

2.2 Experimental procedures

The series of experimental procedures are described in Fig. 3. Initially, 5 g of LiCl powder and various concentration of SrO powder are added into the quartz cell and the quartz cell is heated up to 923 K in the furnace. The quartz cell is maintained for 2 hours until the composition of molten salt reaches the thermodynamic equilibrium.

After equilibrium, potentiometric titration is conducted. The potentiometric titration is a method to measure the O²⁻ concentration as the amount of metal oxide increases [3]. At point where the measured potential reaches to a plateau, the solubility limit of metal oxide can be determined as shown in Fig. 4.

Next, the surface of the molten salt is sampled by

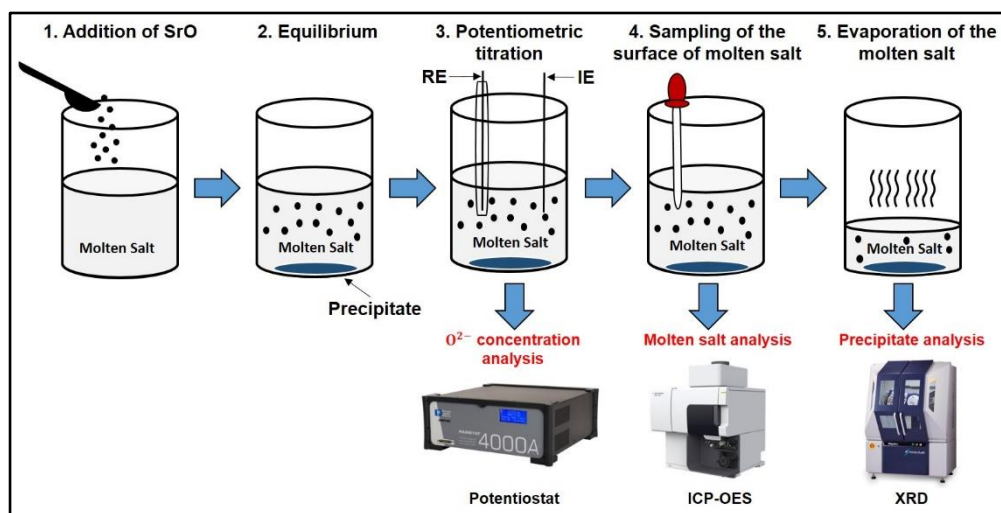


Fig. 3. Schematic of experimental procedures.

an aspirator with glass fiber filter to prevent absorption of precipitates. The sample is dissolved into water and the composition of molten salt is analyzed by inductively coupled plasma optical emission spectrometry (ICP-OES).

This work was supported by the National Research Foundation of Korea (NRF) funded by the Ministry of Science and ICT (The grant number: NRF-2016M2B2B1945249).

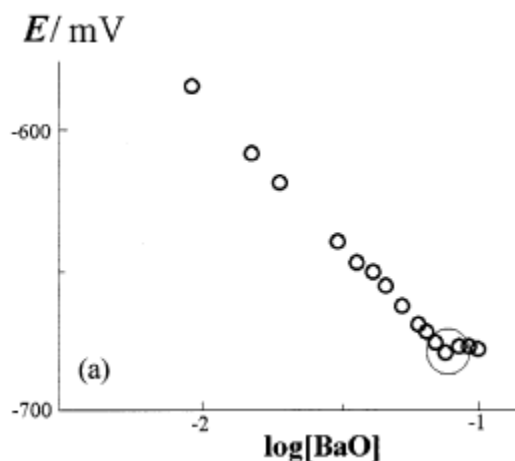


Fig. 4. (a) Plots of E Vs. initial oxide molality in KCl-NaCl-BaO systems at 727°C [3].

Finally, the molten salt is vaporized by vacuum distillation method [4] and the remaining precipitates are analyzed by X-ray diffraction (XRD).

The above procedures are repeated with increasing concentration of SrO from $10^{-4}\text{wt.}\%$ to $10^{-1}\text{wt.}\%$ in LiCl molten salt to determine the solubility limit and their thermodynamic behavior of SrO in LiCl molten salt.

3. Conclusion

In this paper, a method to investigate thermodynamic behaviors of SrO in LiCl molten salt at 923 K is designed with potentiometric titration method, ICP-OES, and XRD analysis.

ACKNOWLEDGEMENT

REFERENCES

- [1] E.-Y. Choi, S.M. Jeong, Electrochemical processing of spent nuclear fuels: An overview of oxide reduction in pyroprocessing technology, *Progress in Natural Science: Materials International*, 25 (2015) 572-582.
- [2] B.H. Park, Residual Liquid Behavior Calculation for Vacuum Distillation of Multi-component Chloride System, *Journal of the Korean Radioactive Waste Society*, 12 (2014) 179-189.
- [3] V.L. Cherginets, T.G. Deineka, O.V. Demirskaya, T.P. Rebrova, Potentiometric investigation of oxide solubilities in molten KCl-NaCl eutectic.: The effect of surface area of solid particles on the solubilities, *Journal of Electroanalytical Chemistry*, 531 (2002) 171-178.
- [4] I. Kim, D. Y. Chung, M. S. Park, J.-M. Hur, J.-K. Moon, Evaporation of CsCl, BaCl₂, and SrCl₂ from the LiCl-Li₂O molten salt of the electrolytic reduction process, 2014.

A Study on Innovative Metallic Fuel Shapes and Their Manufacturing Requirements

YoungHo Lee*, SangGyu Park, ByoungOon Lee, KiHo Kim, and JeongYong Park

Korea Atomic Energy Research Institute, 111, Daedeok-daero 989beon-gil, Yuseong-gu, Daejeon, Republic of Korea

*leeyh@kaeri.re.kr

1. Introduction

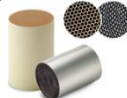


Improving economy and enhancing safety of sodium fast reactors require nuclear fuel with high power density and low pressure drop. Therefore, it has been proposed that an annular and bottle-shaped fuel by [1], which can maintain outstanding heat transfer performances and lower fuel temperature compared to conventional solid metallic fuels. In the case of annular nuclear fuel system including UO_2 annular pellet, enlarged Zr-based cladding, supporting structures, etc., systematic studies have been carried out for replacing conventional solid fuel with annular oxide fuel in operating PWRs in Korea [2-4]. The concepts of annular and bottle-shaped fuel for SFR show an increase of the power density by 20% in low-conversion ratio (burner) cores with metal fuels. Especially, annular metal fuel can survive a complete flow blockage of the hottest inner channel [1]. In this study, three types of metallic fuels which were not studied due to the difficulties of the manufacturability were proposed to evaluate their manufacturing requirements. The basic performance and their manufacturing requirements with complicated shapes have been examined. In particular, the recent development of additive manufacturing technology based on the 4th industry has reduced the production limits of complicated fuel shapes.

2. Reference Fuel Shapes

In this study, shapes for honeycomb, multi-hole and bamboo-wife structures were derived, and the

expected performances are summarized in Table 1.

Table 1. Proposed concept of metallic fuel

Type	Honeycomb	Multi-hole	Bamboo-wife
Concept			

First, it is expected that all three shapes show excellent thermal conductivity and melting allowance, which is expected to have outstanding fuel performance when the gap conductance was used as simple conduction through the sodium bond. However, it is necessary to evaluate FCMI (Fuel Cladding Mechanical Interaction) and FCCI (Fuel Cladding Chemical Interaction) for application of barrier cladding. In order to prevent swelling, the smear density should be maintained below 75% and element redistribution should be verified.

3. Manufacturing Requirements

For manufacturing above complicated metallic fuel shapes, it is difficult to apply the conventional manufacturing process such as casting. Recently, the breakthrough of additive manufacturing technology enables to manufacture complicated fuel shapes that were almost impossible with conventional methods. Among various methods, two kinds of additive manufacturing (i.e., selective layer sintering (SLS) and direct energy deposition (DED)) can be applied to innovative metallic fuel as shown in Fig. 1 and their specifications can be referred in previous literature [5]. Table 2 summarized effective

manufacturing methods of each fuel shape with the consideration of manufacturing requirements.

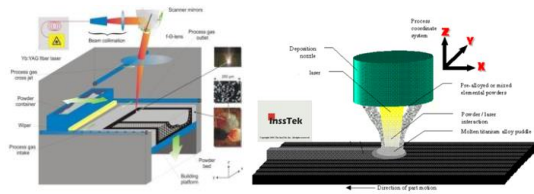


Fig. 1. Typical additive manufacturing methods; (left) SLS, (right) DED.

Table 2. Summary of manufacturing requirement

Type	Honeycomb	Multi-hole	Bamboo-wife
Methods	SLS, DED	Conventional casting or extrusion	SLS, DED
Manufacturability	High	Low	High
Raw material	Powder	Any	Powder
Loss during manufacturing	Low(SLS) High (DED)	Low	Low(SLS) High (DED)

Consequently, it is difficult to manufacture complicated fuel shapes using U or TRU powder by any additive manufacturing method. This is because one of the key factors determining the application of additive manufacturing to complicated metallic fuel shapes is to handle and manufacture TRU, U and Zr powders for supplying powder bed in SLS process and nozzle in DED process. Therefore, the additive manufacturing should be an auxiliary methods for making complicated metallic fuel.

4. Summary

In order to develop innovative metallic fuels with improved economy and enhanced safety of SFR, it is necessary to develop powder manufacturing technology for applying additive manufacturing technology.

ACKNOWLEDGEMENT

This work was supported by the National Research Foundation of Korea funded by the Ministry of

Science and ICT (2017M2A8A5014888).

REFERENCES

- [1] M. Memmott, J. Buongiorno, and P. Hejzlar, "An Evaluation of the Annular Fuel and Bottle-shaped Fuel Concepts for Sodium Fast Reactors", *Nuclear Technology*, 173(2), 162-175 (2011).
- [2] T. Chun, C. Shin, W. In, K. Lee, S. Park, H. Kim, K. Bae, K. Song, "A potential of dual-cooled annular fuel for OPR 1000 power uprate", *Proceedings of TopFuel 2009*, Paris, France September 6–10, 2009, Paper no.2185.
- [3] H. Kim, J. Kim, K. Yoon, "Mechanical design issues and resolutions of a dual cooled fuel for the OPR-1000", *Nuclear Engineering and Design*, 241, 2119 (2011).
- [4] Y. Yuan, "The Design of High Power Density Annular Fuel for LWRs", 2004 MIT PhD Thesis.
- [5] N. Shamsaei, A. Yadollahi, L. Bian, S. Thompson, "An overview of direct laser deposition for additive manufacturing; Part II: Mechanical behavior, process parameter optimization and control", *Additive Manufacturing*, 8, 12-35 (2015).

Development of Spent Fuel Cladding Degradation Model in Integrated Platform

Jong-Dae Hong*, Yong-Sik Yang, Changhwan Shin, and Dong-Hak Kook

Korea Atomic Energy Research Institute, 111, Daedeok-daero 989beon-gil, Yuseong-gu, Daejeon, Republic of Korea

*jongd@kaeri.re.kr

1. Introduction

During dry storage, the spent fuel claddings could degrade through degradation mechanisms such as creep, hydride reorientation, and delayed hydride cracking (DHC). Thermal analysis is crucial for a reliable degradation analysis, because the cladding temperature is a major factor of these degradation mechanisms. In this regards, the new analysis platform has been developed to evaluate the integrity of domestic spent fuel during dry storage. For the analysis, cladding degradation models such as creep and DHC were developed and implemented to this platform. Each model are developed based on well-developed existing model and updated based on our own experimental data. This data was mainly produced under QA (quality assurance) program. In this paper, the developed creep and DHC models are introduced.

2. Integrated Platform

The schematic diagram of integrated platform for spent fuel cladding integrity evaluation during dry storage is described in Fig. 1. According to fuel/rod design and power history, decay heat is calculated by decay code such a SCALE code and fuel initial condition before storage is calculated by FRAPCON code. FRAPCON gives information such as fuel rod outer diameter, rod internal pressure and material status (hydrogen content, oxide thickness, etc). Input for COBRA-SFS is generated from this information and used for temperature distribution analysis. When the cladding temperature distribution is calculated, updated fuel outer diameter and rod internal pressure are calculated by developed creep model and re-used for thermal analysis of next time-step. In addition, at each time-step, DHC occurrence is judged using

calculated temperature, geometry and rod internal pressure. And these procedures are iterated as storage time goes by.

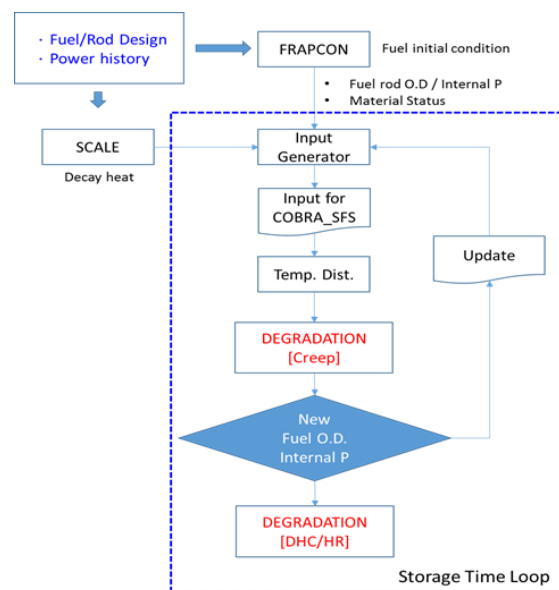


Fig. 1. Schematic diagram of the integrated platform for spent fuel cladding integrity evaluation [1].

More details of each degradation model, marked in red on Fig. 1, are described in the following section.

3. Cladding degradation model

3.1 Creep

To evaluate the behaviors of post-irradiation creep for PWR spent fuel cladding, the EPRI model which is modified for annealing and hydrogen effect based on EDF-CEA model-3 was used [2]. This model can apply to the stress and temperature range of interest in dry storage and easily modify reflecting the effect of each parameter using our experimental data. So, we improved with a model constant change based on our data produced using temperature, stress, and hydrogen content as a variable (Fig. 2). In addition,

the irradiation hardening effect will be reflected as soon as hot-cell test results.

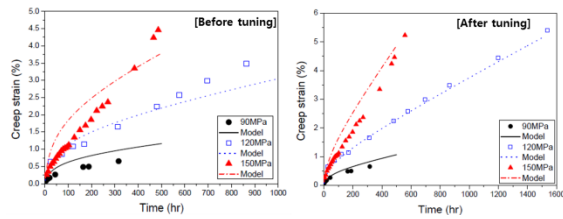


Fig. 2. Improvement with a model constant change based on unirradiated Zircaloy-4 creep experimental data.

3.2 Delayed hydride cracking (DHC)

The overall flow of developed DHC assessment model is shown in Fig. 3. For the assessment, the K_{IH} (threshold stress intensity factor) of Zircaloy-4 fuel cladding is key parameter and many tests and analysis had been performed to evaluate that. Among the prediction models, the Shi & Puls model [3] correspond with the behavior of existing experimental results. So, Shi & Puls model with modified relevant parameter values was used for K_{IH} prediction and would be improved by our experimental data under QA program.

A comparison with K_I (applied stress intensity factor) and K_{IH} was applied to determine whether the crack on the cladding grows. In the case where the K_I is larger than the K_{IH} , the initial crack grows at the rates calculated in the crack growth module. More details of DHC model was described in another papers [4,5].

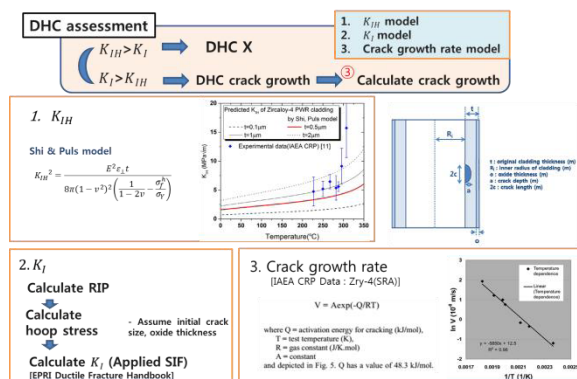


Fig. 3. Methodology of DHC assessment of spent fuel cladding. [3]

4. Conclusion

The platform integrated thermal analysis and cladding degradation model was developed to evaluate the integrity of domestic low burnup PWR spent fuel. For the analysis, cladding degradation models (creep and DHC) were developed and adopted to this platform. Each model are developed based on well-developed existing model and updated based on our own experimental data.

ACKNOWLEDGMENT

This work was supported by the Radioactive Waste Management Technology Program of the Korea Institute of Energy Technology Evaluation and Planning (KETEP), granted financial resource from the Ministry of Trade, Industry & Energy, Republic of Korea. (No. 2014171020166A)

REFERENCES

- [1] C.-H. Shin et al, "Design of Integrated Analysis Tool for Degradation Evaluation of Spent Nuclear Fuel in Dry Storage System", Proc. of the KRS 2018 Autumn Conference, Oct 31-Nov 2, 2018, Jeju.
- [2] Y. Rashid, R. Dunham, "Creep Modeling and Analysis Methodology for Spent Fuel in Dry Storage", 1003135, Electric Power Research Institute (2001).
- [3] S.-Q. Shi, M.P. Puls, "Criteria for fracture initiation at hydrides in zirconium alloys I. Sharp crack tip", J. Nucl. Mater. 208 (1994) 232-242.
- [4] J.-D. Hong, E. Kim, Y.-S. Yang, D.-H. Kook, "Methodology of Delayed Hydride Cracking Assessment of Spent Fuel Cladding", Proc. of the KRS 2017 Spring Conference, May 24-26, 2017, Busan.
- [5] J.-D. Hong et al., "Delayed hydride cracking assessment of PWR spent fuel during dry storage", Nucl. Eng. Des. 322 (2017) 324-330.

A Study on the Impact Analysis for the Spacer Grid by Peripheral Temperature

Sung-Uk Lee*, Jae-Yong Kim, Hong-Ryoul Oh, Kyung-Ho Yoon, Hyo-Chan Kim, and Dong-Hak Kook
Korea Atomic Energy Research Institute, 111, Daedeok-daero 989beon-gil, Yuseong-gu, Daejeon, Republic of Korea
*leesunguk@kaeri.re.kr

1. Introduction

As the amount of Spent Nuclear Fuel (SNF) in KOREA domestic spent fuel pool increases dramatically, the storage capability of the PWR SNF is expected to saturate in 2024 [1]. The SNFs in the pool must be transferred to the designated wet or dry spent fuel storage facility. In the issues of the SNF treatment, handling and transport of the SNF have been considered as an important factors. The integrity of SNF during dry storage should be assessed.

The spacer grid (SG) is the main structure for securing the fuel rods from an external impact. A typical test method for evaluating the soundness of SG is a pendulum type impact test. In this study, we analyzed the uncertainty factors that may occur in the impact test and try to simulate by reflecting the factors. We investigated the impact behavior of the SG according to various temperature.

2. Property of Zry according to Temperature

In order to carry out the impact analysis of the spacer grid under dry storage condition, the temperature-dependent property of the zircaloy(Zry) which is the spacer grid material is required. The zircaloy properties were determined by the MATPRO.[2] As the temperature increases, the stress of the Zry decreases, and as the strain rate increases, the stress of the Zry increases as with ordinary metal materials.

3. Uncertainty Analysis in Impact Analysis

As shown in Fig. 1, the pendulum impact tester is divided into two parts. One is equipment to impact the SG by the kinematic energy of the pendulum and the other is a furnace to heat the SG itself. The furnace is designed to have temperature deviation per

position within ± 10 K. Under the assumption that all kinematic energy of the pendulum is transferred to the SG itself, the uncertainty that could occur in the impact test is defined as three factors: misalignment angle (θ , ϕ) and coefficient of friction (COF)). In order to analyze the impact analysis with the uncertainly factors, each factor is represented by three levels as shown in Table 1.

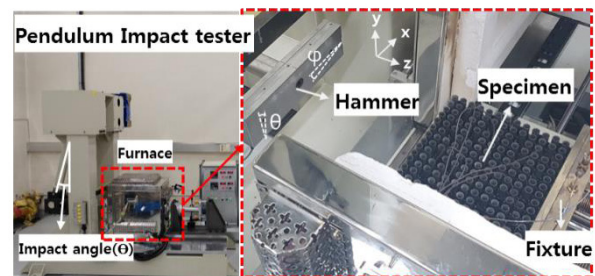


Fig. 1. Pendulum impact tester.

Table 1. DOE of impact simulation

Case	θ (A)	ϕ (B)	COF (C)
1	0°	0°	0.1
2	0°	1°	0.2
3	0°	2°	0.3
4	1°	0°	0.2
5	1°	1°	0.3
6	1°	2°	0.1
7	2°	0°	0.3
8	2°	1°	0.1
9	2°	2°	0.2

4. Impact Analysis for Spacer Grid

In evaluating the mechanical integrity, the strength of SG is determined by the impact load after buckling under successive impacts of increasing kinetic energy. In order to simulate the impact of SG, the commercial FE code, ABAQUS 6.14/explicit is used. The analysis was carried out under the same conditions as the impact test, which was performed by increasing the pendulum angle from 27° to 32°.

The temperature of dry storage system of a SNF decrease at a very slow rate over its lifetime. [3] There are various atmospheric temperature (673 K ~ 298 K) during dry storage. The impact tests and analysis are carried out at room temperature up to 673 K. Figure 2 compares the results of the impact test specimens and analysis result by temperature. It could be seen that the deformed shaped are similar except for 573 K.

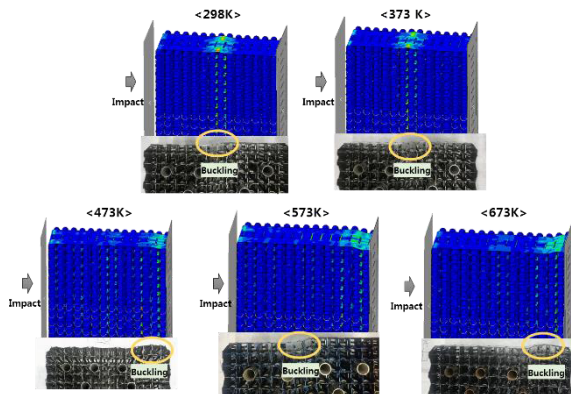


Fig. 2. Comparison of numerical and experimental deformation shape of spacer grid at various temperature conditions.

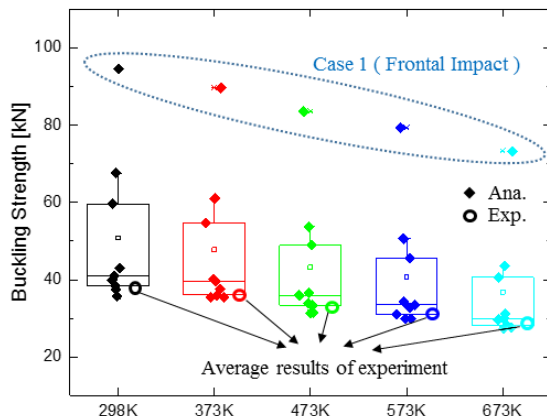


Fig. 3. Comparison of numerical and experimental buckling strength of spacer grid at various temperature conditions.

Figure 3 shows the buckling strength of the SG at various temperature conditions. As expected, the buckling strength decreases as the temperature increases, due to softening of the SG material (Zry). When impact is applied ideally, it shows the highest buckling strength. It could be seen that the results of the impact test are included in the range of the results

for analysis in considering the uncertainty.

5. Conclusions

Impact analysis was performed to evaluate the mechanical integrity of the SG under dry storage condition. In order to reflect the change of the properties for the SG material according to the ambient temperature, the property of Zry from MATPRO was applied to the analysis. In addition, the main uncertainty factor was defined, and the experiment of design for impact analysis was established to consider the uncertainty of the test. The impact test results are located within the range of the impact analysis results taking into account the uncertainty of the test. However, the range of impact analysis results was wide and the test results were in the lower range of the analysis results. In order to better analyze the test results, we plan to analyze the influence of welds on the SG itself and the dissipated energy in the test.

ACKNOWLEDGEMENT

This work was supported by the Korea Institute of Energy Technology Evaluation and Planning (KETEP) and the Ministry of Trade, Industry & Energy(MOTIE) of the Republic of Korea (No. 2014171020166A).

REFERENCES

- [1] Ministry of Trade, Industry and Energy, "Roadmap for High-Level Radioactive Waste Management (final version)", (2016).
- [2] SCDAP/RELAP5/MOD3.1 code manual volume IV : MATPRO, NUREG/CR-6150, INL (1993).
- [3] D.H Kook et al., "Review of spent fuel integrity evaluation for dry storage", NET Vol. 45(1), pp. 115-124 (2013).

Improvement of Maintenance Method for the Three Piece MSM

SungHyun Kim*, SunSuck Hong, and EunYoung Choi

Korea Atomic Energy Research Institute, 111, Daedeok-daero 989beon-gil, Yuseong-gu, Daejeon, Republic of Korea

*hyun@kaeri.re.kr

1. Introduction

Korea Atomic Energy Research Institute (KAERI) has built a pyroprocess test facility as a mock-up to develop pyroprocess technology. PRIDE uses a remote handling device to operate the process equipment installed in the work cell. The remote handling device is equipped with a BDSM (Bridge transported Dual-arm Servo Manipulator), a crane and master-slave manipulator (MSM). This paper describes the procedures for removing and repairing a manipulator when a master-slave manipulator failure. I will describe the development of a repair tool that improves the procedure and time to repair a specific fault in the manipulator.

2. Outline of PRIDE facility

2.1 Composition of PRIDE facility

Pride facility is a cell filled with an argon. The argon cell should be able to operate the process unit in an argon atmosphere and should not leak out. 34 master slave manipulators are installed on the front of the cell. Inside the cell, devices for electrolytic reduction, electrolytic recovery, and waste treatment are installed. All operations are subject to process operation and maintenance using remote handling devices and tools. There are LTL (Large equipment Transfer Lock system) and STL (Small equipment Transfer Lock system) devices for material import and export.

2.2 Configuration of Master Slave Manipulator

The mechanical MSM installed in the mockup consists of three parts: a slave arm, a through tube, and a master arm as shown figure 1. The MSM unit has the function of sealing the inside and the outside of the cell through a through tube installed on the wall of the argon cell. The slave arm of the MSM installed in the mockup is installed inside the cell. The through tube is installed on the wall of the mockup. A master arm is installed outside the cell. The MSM installed in the hot cell has a one-piece type and a three-piece type. The one-piece manipulator can't be separated into one body. The three-piece manipulator can be separated three bodies.

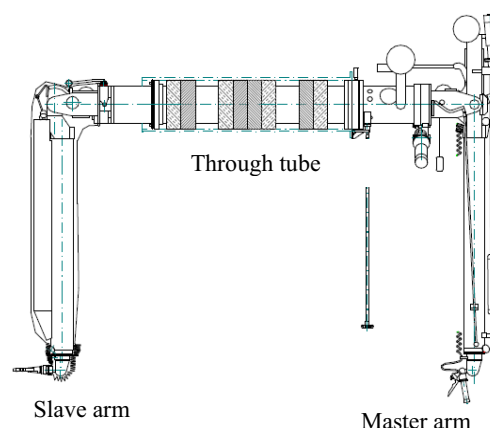


Fig. 1. Configuration of master-slave manipulator.

3. Repair of master-slave manipulator

3.1 Repair procedure of master-slave manipulator

The 3-piece manipulator can be separated into the three parts. If the slave arm of the 3-piece manipulator fails, the slave arm is detached from the through tube. The separated slave arm is taken out of

the cell. The surface of the arm and booting is decontaminated. Repair technician repairs the faulty part of the slave arm. The repaired slave arm is carried into the cell. The worker connects the slave arm to the through tube.

If the master arm fails, the worker separates the master arm and the slave arm or only the master arm from the through tube according to the fault location. The slave arm is separated and taken out of the cell and decontaminated. Repair technician repairs the faulty part of the master arm. The coupling position of the slave arm is adjusted to the position so that it can engage with the master arm and is carried into the cell. After connecting the master arm to the through tube, the worker connects the slave arm to the through tube.

3.2 Configuration of positioning tool to improve process procedures

The combination of the master arm and the slave arm has a constant home position. If the master arm of the MSM is removed from the through tube for repair, depending on the failure location, the master arm is disengaged away from the home position. Therefore, the home position of the slave is changed. To adjust this, the slave arm is taken out of the cell and decontaminated. The worker adjusts the coupling of the slave arm and brings it into the cell. After connecting the master arm, the worker connect the slave arm to the through tube. In this paper, we developed a positioning tool that can modify the coupling of the slave arm without taking the slave arm out of the cell as shown in the following figure 2. The positioning tool is replaced with a master arm, and is composed of 7 axes. When the slave arm is connected to the through tube, the three axes of the slave arm are shifted in position. The positioning tool has a lock function for 3 axes and a coupling adjustment function for 7 axes.

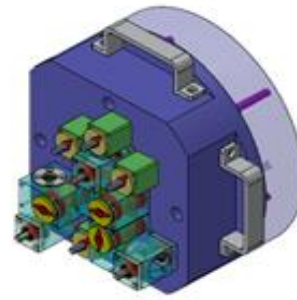


Fig. 2. Positioning tool.

3.3 Result of improvement procedure

The results of using the positioning tool are as follows. The slave arm did not move the outside and inside of the cell and did not have to change the position of the coupling and decontaminate outside the cell. This has resulted in shortening of the working time and simplification of the procedure.

4. Conclusion

This paper describes the development of a positioning tool that can save repair procedures, time and effort in master arm maintenance procedures. The failed master arm was repaired and the slave arm was taken out of the cell due to the mismatch of the coupling position of the master arm and the slave arm. Using the positioning tool working time saved at least 5 hours.

REFERENCES

- [1] Walishmiller Engineering GMBH, "Operating Manual", 2009.

Single Fuel Assembly Temperature Experimental Facility (STEP)

Dong-seok Oh*, Sun-joon Byun, Chang-hwan Shin, and Dong-hak Kook

Korea Atomic Energy Research Institute, 111, Daedeok-daero 989beon-gil, Yuseong-gu, Daejeon, Republic of Korea

*dsoh1@kaeri.re.kr

1. Introduction

The government has proposed a high-level radioactive waste management plan to store temporarily high-level radioactive wastes at plant sites in a dry storage method until an interim storage facility or a permanent disposal facility is in operation [1].

One of the most important results of the dry storage system thermal evaluation is confirmation that the fuel cladding temperature will remain below a specified limit to prevent unacceptable degradation during storage [2].

COBRA-SFS(Spent Fuel Storage) code for thermal-hydraulic analysis of multi-assembly spent fuel storage has been developed to analysis of spent fuel storage [3]. Recently, The KAERI has performed the sensitivity analysis by using the COBRA-SFS to determine the priority of the model development and experiment variables [4] and also figured out and constructed a temperature experimental facility with a model PWR spent fuel assembly named STEP.

This paper discusses the experimental setup, experiment carried out and initial test results of STEP.

2. Hardware Description

The equipment can be categorized in three general groups; mechanical, electrical, and instrument/data acquisition system.

2.1 Mechanical system

STEP consists of the assembly storage cask, the 14x14 electrically heated model fuel assembly, the transition piece, fuel tube, the cask lid, and chamber as shown in Fig.1. The cask comprises the containment and pressure boundary for the STEP equipment. The cask is fabricated from pipe with a 5 mm thick, 545.8 mm diameter inner wall, and 4,400 mm long of stainless steel. Top of the cask has a

bolted cask lid, which the bulk of various internally mounted thermocouple leads are passed through. An insulating blanket of 50 mm thick of ceramic wool covered the cask to minimize the heat loss.

The model fuel assembly is designed and built to be structurally and thermally characteristic of a typical 14x14 commercial PWR spent fuel assembly. With a total power range of 0~1 kW, the assembly consists of 179, 9.5 mm diameter, independently powered, resistance element tubular heater units. The heater pin has a 3,800 mm heated length. Also 17 unheated 12.7 mm pins are simulating control rod guide tubes. The transition piece and fuel tube assembly serves the functions of supporting the model fuel bundle assembly within the cask. The fuel tube is a rectangular 220 mm I.D., 5 mm thick, and 3,870 mm length with stainless steel. The chamber supports the load of a fuel tube and an assembly as well as provides paths for electric power lines and for gas backfill system.

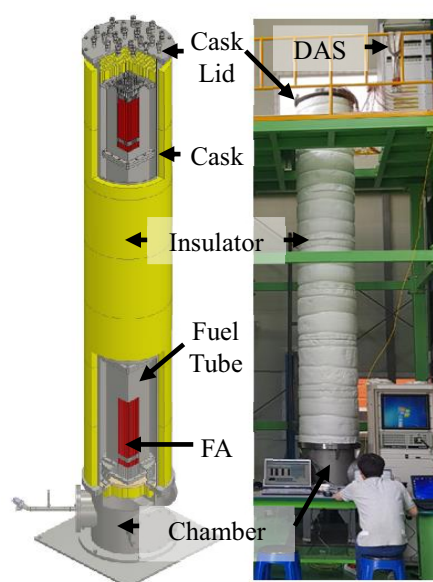


Fig. 1. Single Fuel Assembly Temperature Experimental Facility (STEP).

2.2 Electrical system

The model fuel assembly power is fed from a 220 V AC. 5 separate electrical power supply and control systems are needed for STEP to simulate the 5 radial power distributions. Power is manually controlled by controller which allowed the total assembly power to be set to the appropriate level of 0.5 ~ 3 kW. Each heater rods in the assembly has their respective electrical leads terminated at a connector in power distribution box in the chamber.

2.3 Instrumentation/Data Acquisition System.

A total of 190 separate thermocouples are mounted on the STEP. 1 through 104 are attached on assembly at eight different axial levels. 105 through 128 are positioned on outer surface of fuel tube. 129 through 152 and 153 through 160 are attached on inner and outer surface of cask, respectively. 161 through 190 are located in the center of subchannels by supporting device. Electric transducers are installed in the each power supply system. The electric transducers has specification with 50 A and 300 Volt input as well as 1~5 Volts analog output signal. Reading from the thermocouples and power supply system are stored in data acquisition system. DAS is equipped with 4 Keysight 34972a data loggers and a laptop with Agilent VEE Pro. 9.0 Program.

3. Test Operation

We measured the surface temperature of fuel rods, a fuel tube, and a cask as well as the temperature in exit subchannels at the steady state condition under the 1kW power supply with uniform and non-uniform radial power distribution at an initial operation. The powers of 5 rod group are 205 kW, 202 kW, 202 kW, 205 kW, and 206 kW as well as 0 kW, 0 kW, 333 kW, 333 kW, and 333 kW for uniform and non-uniform power distribution, respectively. The Fig. 2 shows the axial temperature distribution of a hottest rod as radial power distribution change. The maximum temperature is 272°C and 295°C on uniform and non-uniform radial power distribution, respectively. The temperature increase factor, at which is ratio of temperature percent increase to power percent increase, is 0.135. We obtained a heat transfer coefficient from the measured data of temperature difference between on the surface of rods and in the middle of a subchannel. The heat

transfer coefficient for a hottest fuel rod is $3.48 \text{ W/m}^2 \cdot ^\circ\text{C}$ and is close to the recommended user input value of 3.66 in the COBRA-SFS code.

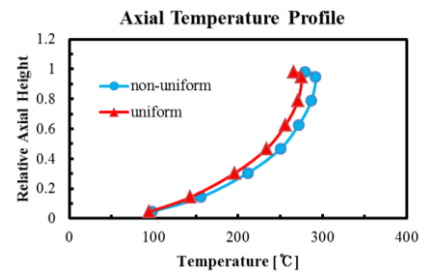


Fig. 2. Axial Temperature Profile on a Hottest Rod.

4. Conclusions

The STEP is designed and constructed to investigate the heat transfer characteristics of a spent fuel under simulated dry storage conditions. We have confirmed the performance of the STEP through an initial operation. The fuel cladding temperatures will be measured as functions of cask backfill gases. The test data are intended to be used in evaluating predictions of a thermal analysis computer code used to model spent fuel dry storage systems.

ACKNOWLEDGEMENT

This work was supported by the Korea Institute of Energy Technology Evaluation and Planning (KETEP) granted financial resource from the Ministry of Trade, Industry and Energy, Republic of Korea (No. 2014171020166A)

REFERENCES

- [1] Ministry of Trade, Industry and Energy, "Roadmap for Disposal of High-level Radioactive Wastes," (2016).
- [2] NRC, "Standard Review Plan for Spent Fuel Dry Storage Systems at a General License Facility," NUREG-1536 Rev. 1, (2010).
- [3] T. Micherner, et al., "COBRA-SFS, A Thermal-Hydraulic Analysis Code for Spent Fuel Storage and Transportation Casks, Cycle 4," PNNL-24841, (2015).
- [4] C. H. Shin, K. W. Seo, D. H. Kook, "Sensitivity Analysis of COBRA-SFS for Dry Storage of Spent Fuel." Proc. of the KRS 2017 Spring Conference, 15(1), May 24-26, 2017, Busan.

Comparison of CFD Analysis Methodology for SFP Cooling Performance Evaluation

Taehyeon Kim*

Korea Hydro & Nuclear Power Co., Ltd Central Research Institute, 70, Yuseong-daero 1312beon-gil,

Yuseong-gu, Daejeon, Republic of Korea

*taehyeon.kim@khnp.co.kr

1. Introduction

The cooling performance evaluation of spent fuel pool(SFP) is necessary to verify for spent fuel safety with racks configuration. The adequacy of external cooling by SFP cooling system and of internal pool water circulation by natural convection are analyzed with SFP filled to full storage capacity about 20 years storage. In order to take into account the interaction between the racks, which is not considered in convectional Computational Fluid Dynamics(CFD) methods, which enables to analyze the global behavior of the cooling pool including particularities of all racks. Thus, it is possible to determine mass flow rates flowing through each of the racks, and therefore the temperature distribution. CFD results should show that maximum local water temperature and cladding temperatures lower than the saturation temperature, thus, localized boiling will not occur. In CFD calculation, it is very important to determine the analysis methodology. Therefore, I compared the SFP licensing report of Hanul 2 with realistic CFD analysis models and assessed the impact of model difference.

2. CFD Model for Licensing

The analysis criteria is that each of the redundant spent fuel pit cooling system trains, during normal operation, is designed to remove the heat loads of normal storage of 1,062 assemblies with a burnup of 60,000 MWD/MTU and stored for 17 months up to 22.6 years. At that case, the maximum normal

temperature is 66°C. The pool size of south-north, east-west and pool water depth are 12.6 m, 8.0 m and 12.06 m, respectively. The active length of fuel assembly is 3.658 m and cell pitch of racks are 0.2848 m.

The pool and pipes are modeled according to their geometrical characteristics. In order to avoid a detailed CFD model of each fuel assembly, what is impossible from the computational point of view, equivalent racks have been used in the CFD model. These equivalent racks are based on the porous domain approach. A porous domain is a fluid volume region where specific parameters can be defined in order to obtain the same physical behavior of the region, not been necessary a real detailed model of the racks. The CFD code solves the whole fluid domain, thus temperature distribution is obtained for any point of the SFP. Figure 1 shows the CFD model using in thermal-hydraulic licensing reports. Decay heat from freshly discharged fuels modeled as a two zone heat source in the center of the racks, conservatively. Decay heat from previously discharged fuel assemblies is applied to the balance of the fuel racks region. Temperature contour in a vertical cross-section of the hot fuel region is shown in Figure 2. The plots confirm that hot fuel is safely and reliably cooled by thermosiphon action. Cold water is rising up in the hot fuel rack cells from the bottom and hot water issuing out of the top of the rack cells. Local hot spots induced by water circulation in the racks is rapidly dissipated in the pool water resulting in a nearly uniform temperature distribution away from the hot racks. Maximum local water temperature and cladding temperature for the evaluated case are 63.9°C

and 87°C, respectively. The saturation temperature for water at this local pressure is given as 115°C, it is concluded that local water and cladding temperature remains below saturation.

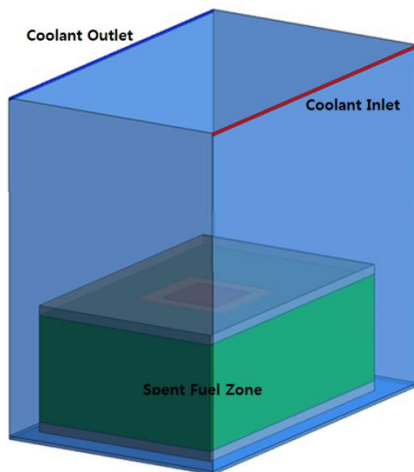


Fig. 1. The CFD model for licensing.

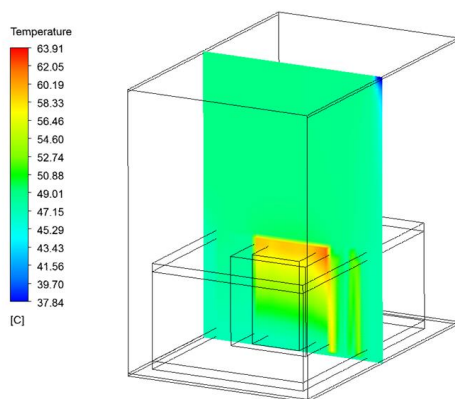


Fig. 2. Temperature contour of licensing model.

3. Realistic CFD analysis model

The realistic CFD model is similar to licensing model except for the region 1 and 2 racks layout. A schematic of the realistic model is shown in Figure 3. At the center of the pool where racks are fully surrounded by other racks. The Surrounding racks are demanding coolant from the closets regions. Since the inter rack space is not modeled, the central rack (with higher decay heat) can be only feeded by the rack to pool bottom space dealing with the

surrounding racks, what makes a conservative isolation effect. Maximum local water temperature and cladding temperature for the evaluated case are 62°C and 85°C, respectively. It is also concluded that local water and cladding temperature remains below saturation.

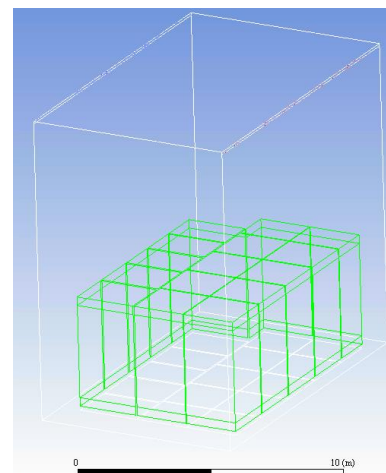


Fig. 3. The realistic CFD model.

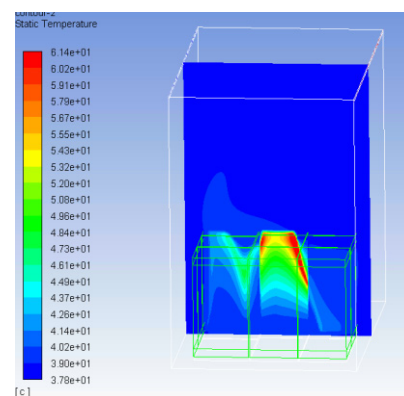


Fig. 4. Temperature contour of realistic model.

4. Discussion

CFD results of the SFP licensing report in Hanul 2 are compared with the realistic CFD analysis models. Maximum local water temperature of licensing model was evaluated to be higher than the maximum temperature of realistic model. Therefore, licensing model is more conservative than realistic model. If using a realistic model in the thermal evaluation of SFPs, we can achieve more heat margin.

Study on the Methodology of Fast Neutron Detection Based on Plastic Scintillators for Safeguards Research

Seonkwang Yoon^{a),b)}, Hee Seo^{c)}, Chaehun Lee^{a)}, Seong-Kyu Ahn^{a)}, Jong-Myeong Oh^{a)}, and Ho-Dong Kim^{a),*}

^{a)} Korea Atomic Energy Research Institute, 111, Daedeokdae-ro 989beon-gil, Yuseong-Gu, Daejeon, Republic of Korea

^{b)} University of Science & Technology, 217, Gajeong-ro, Yuseong-Gu, Daejeon, Republic of Korea

^{c)} Chonbuk National University, 567, Baekjedae-ro, Deokjin-gu, Jeonju-si, Jeollabuk-do, Republic of Korea

*khd@kaeri.re.kr

1. Introduction

Safeguards is a fundamental approach to verify the diversion of special nuclear materials (SNM), e.g., ^{235}U or plutonium. Traditionally He-3 based thermal neutron detectors has been used for nuclear material accountancy (NMA) because of its high detection efficiency. However the He-3 gas became an uneconomical measure as demand increased, so fast neutron detection was focused as a substitutive technique. This is because fast neutron detection has potential advantages compared to the thermal system. Therefore we have tried to design and optimize an advanced nuclear material accounting system.

2. Comparison to the conventional system

2.1 Properties of the Conventional Thermal System

Over 50-years, He-3 based thermal neutron detection has been considered as standard for NMA. This is because it has high neutron detection efficiency ($\approx 50\%$), very low gamma sensitivity, high reproducibility of results ($\pm 0.15\%$), and simple operation (≈ 10 mins). However information of prompt neutrons with respect to fission event is not available because of moderation process. This also make measurement system to take longer time for each single event. Also thermalized neutrons are relatively slower than prompt neutron, so longer gate time ($\approx 50 \mu\text{s}$) for coincidence accounting is required. This point can be

a source of measurement uncertainty as a result of counting neutrons uncorrelated with fission events; such as scattered neutrons. Therefore the thermal system could not be appropriate for larger samples.

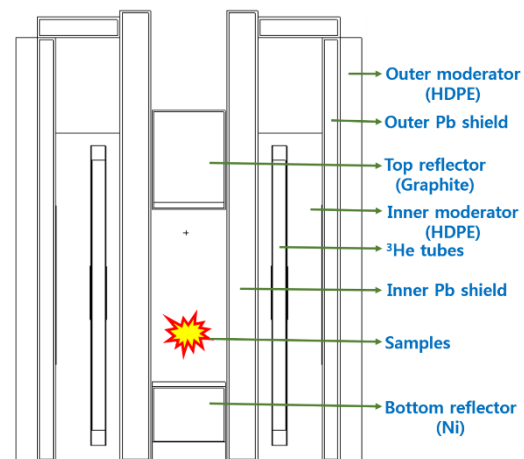


Fig. 1. Well-type He-3 proportional counter modelling.

2.2 Properties of fast neutron detection

The fast neutron detection is possible to deduce fission informative data from prompt neutrons because no moderation process is needed^[1]. Also lower random uncertainty could be achieved^[2] because of much shorter gate time (≈ 50 ns). Therefore, fast system might show higher precision for large samples even with shorter measurement time. Nevertheless one fatal limitation is very high gamma sensitivity which distorts neutron induced signals to be indistinguishable from gamma induced signals. However this can be mitigated through pulse analysis

algorithms called pulse shape discrimination (PSD).

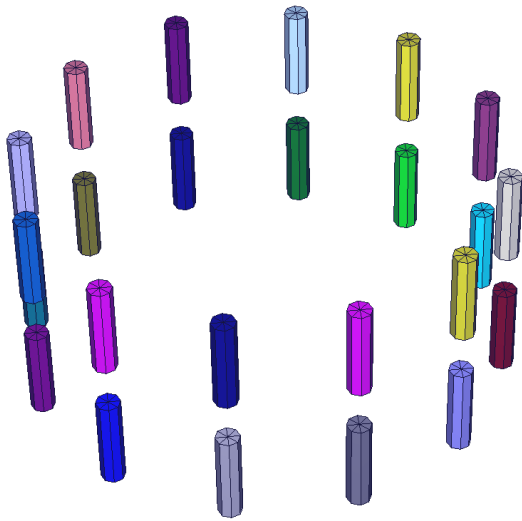


Fig. 2. Well-type plastics detectors modelling using MCNP.

Table 1. Properties of EJ-299-33 Plastic Scintillator

Properties	EJ-299-33 Plastics
Light Output (% Anthracene)	56
Scintillation Efficiency (Photons/1 MeV e ⁻)	8600
Wavelength of Maximum Emission (nm)	425
H : C Ratio	0.927
PSD	Capable

3. Methodology

We are planning to conduct both experimental and computational approaches for this research. For the experiment, EJ-299-33 plastic scintillation detector was selected, and the critical reason is its PSD capability. In addition, plastics have geometrical flexibility with relatively stable chemical, mechanical properties. The optimization process will be achieved via Monte Carlo Neutron Particle code (MCNP 6.2 version). We considered Geant4.10.2 with a specific data card, FREYA (Fission Reaction Event Yield Algorithm) which is a fission event generator to model complete fission events^[3].

4. Conclusion

We studied methodology for the future research with plastics based fast neutron measurement for the purpose of safeguards. We have designed our own fast neutron detection system with using Monte Carlo code, and optimization procedure is needed. Considerable further tasks should be analytic comparison to other fast systems, and categorization of diverse PSD techniques with analysis of their performance dependent of other options consisting measurement system. There is indeed no commercial applications of fast neutron detection for safeguards, so there are a lot of future works. Finally this research will be highly contributive for IAEA safeguards impregnability.

ACKNOWLEDGEMENT

This work was supported by a National Research Foundation of Korea (NRF) grant funded by the Korean government (MSIP) (No. NRF-2017M2A8A5015084).

REFERENCES

- [1] R. K. Weinmann-Smith, M. T. Swinhoe, A. Trahan et al., "A comparison of Monte Carlo fission models for safeguards neutron coincidence counters", Nuclear Inst. And Methods in Physics Research, A(903), 99-108, (2018).
- [2] L. F Nakae, G. F. Chapline, A. M. Glenn et al., "The use of fast neutron detection for materials accountability", The 2013 International Conference on Applications of Nuclear Techniques, June 22-29, 2013, Greece.
- [3] J. M. Verbeke, J. Randrup, R. Vogt, "Fission Reaction Event Yield Algorithm FREYA 2.0.2", Computer Physics Communications, Vol. 222, 263-266, (2018).

Development and Application of Customized Shielded Cask Transport System

Jong Kwang Lee*, Min Ku Jeon, Yunmock Jung, Wooshin Park, Sun Seok Hong, and Eun-Young Choi

Korea Atomic Energy Research Institute, 111, Daedeok-daero 989beon-gil, Yuseong-gu, Daejeon, Republic of Korea

*leejk@kaeri.re.kr

1. Introduction

The PADIRAC™ is a lead shielded container with a sliding shielded door, designed to move equipment, materials or waste into or out of any Alpha, Beta or Gamma containment while maintaining confinement and with full protection against irradiation [1]. A PADIRAC cask, RD 15, manufactured by La Calhène, is used in the ACPF hot-cell of KAERI. For the proper use and successful operation of the cask, a crane system is indispensable because it provides means to accurately adjust the position and orientation of the cask when connecting it to hot-cell door system. In this work, we propose a customized PADIRAC cask transport system used where no crane service is available near the docking position like ACPF hot-cell.

2. Design of Customized Transport System

2.1 Design Requirements

The ACPF hot-cell is located in a basement of the Irradiated Material Examination Facility of KAERI. Because crane service is not available for operating the cask, a crane system installed on the ceiling of the upper floor is used to lower the cask down through a hatch opening and place it on the transport system. Therefore, the transport system needs to move the cask to the hot-cell door and provide a proper means to adjust the position and orientation of the cask. More specific design requirements are as follows:

- Accurate adjustment of the position and orientation of the cask without the use of a crane
- Sufficient structural safety

2.2 Rail-guided Travelling Unit

The rail-guided travelling unit is driven by chain mechanism with simple structure, high reliability and low cost. In addition, a clutch is adopted to prevent slipping of the transport system after docking on the hot-cell. Two (low and high) speed modes are implemented for cautious docking after relatively rapid travelling. The motor base is designed for easy adjustment of the chain tension and maintenance.

2.3 Screw Elevator

As shown in Fig. 1, a double screw elevator lifts up and down the two sliding doors, coupled with keys, of an approximated mass of 750 kg. Each of the screw is provided with a nut so that the position of the door supported by the nut changes as the chain drive rotates the vertical screws. The chain tension can be adjusted by shifting the motor using the slotted mounting holes.

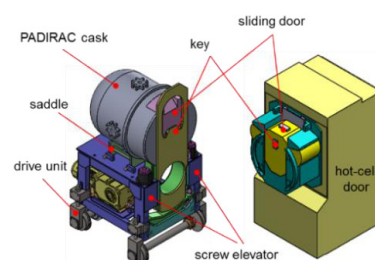


Fig. 1. PADIRAC transfer system and hot-cell door.

- Rail guided traveling unit

2.4 Adjustment of Cask Position and Orientation

Figure 2 shows adjustment mechanism for both a horizontal and vertical position of the PADIRAC cask. The vertical position and inclination of the support table can be adjusted by using a stud bolt and nut installed on the leg module. Hydraulic jacks are used to facilitate the adjustment by applying relatively small force. On the top plate of the transfer table, a saddle for placing the shielded cask is mounted and its orientation can be adjusted by using four bolts. In this way, the position and orientation of the cask can be adjusted without the use of a crane system.

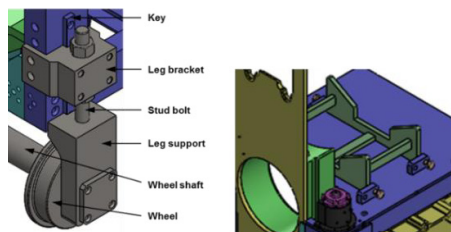


Fig. 2. Position and orientation adjustment mechanism.

2.5 Structural Analysis

To verify the structural safety of and find a proper shape for the transport system, structural analysis of a complete model of the transport system was conducted. A maximum stress of 48 MPa was observed in a nut housing, which was approximately 20% of the yielding stress of the material, as shown in Fig. 3. Moreover, the maximum deflection was approximately 0.25 mm.

3. Hot-cell Operation

Figure 4 shows the shielded cask transport system operated in the ACPF hot-cell. After introducing the transport system to the hot-cell, several mechanical and electrical tests were performed to check whether

the transport system performed at a desired level. Several operation tests of the transport system showed that all design goals were achieved in general, especially accurate docking capability.

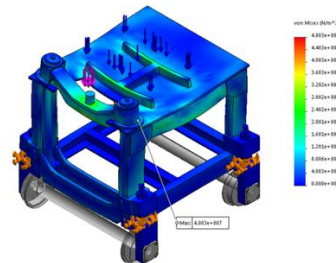


Fig. 3. Results of the stress analysis.

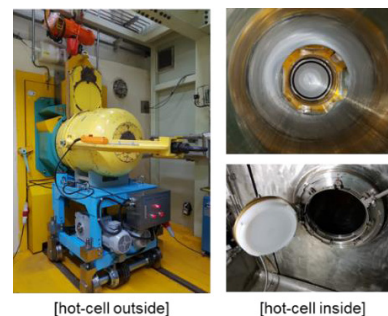


Fig. 4. The operation of shielded cask transport system.

4. Summary

In this work, we developed a customized shielded cask transport system which is equipped with a rail-guided travelling unit and a position adjustment unit for the cask without any crane service. The designed solid model was verified to have sufficient safety margin by using structural analysis. The developed system was introduced to a hot-cell and successfully tested and verified to have required target performance.

REFERENCES

- [1] PADIRAC™ a robust, safe transfer and transport solution, Getinge La Calhène.

Link Mechanism of ACPF Argon Cell Gastight Emergency Door

Byungsuk Park*, Jongkwang Lee, and Eunyoung Choi

Korea Atomic Energy Research Institute, 111, Daedeok-daero 989beon-gil, Yuseong-gu, Daejeon, Republic of Korea

*nbspark@kaeri.re.kr

1. Introduction

The advanced spent fuel conditioning process facility (ACPF), which was constructed with air cell, was modified to consist of an air cell and an argon cell. The argon cell was constructed by isolating a part of the air cell, and argon gas is circulated. This paper describes a gastight door installed in preparation for situations such as installation of equipment and utilities during argon cell construction and emergency operation.

2. Overview of Argon Cell

The argon cell system consists of an argon cell (AC), purifier, cooler, HEPA filter, temperature/pressure sensor, controller and remote handling system. The Argon cell was designed to minimize leakage and was constructed by isolating the first window area with the boundary between the first window and the second window to the right side of the existing ACPF Air Cell (AC). The internal dimensions of the argon cell are 1,728 (L) x 1,990 (D) x 2,740 (H) mm (480 mm in working table height). Figure 1 (a) shows the front view of the argon cell seen in the operating area (OA), and Figure 1 (b) shows the side view of the argon cell seen inside the AC. An electrolytic reduction device was placed on the work table. A pair of master-slave manipulators (MSM) was installed on the left and right sides of the the shield window, respectively, and a 150 kgf capacity crane was installed in the ceiling inside the argon cell.

A material transfer system with internal

dimensions of 600 (L) x 600 (D) x 600 (H) mm was installed between the cells as a means of transferring material between the air cell and the argon cell. In addition, a gastight emergency door with an internal size of 600 (L) x 1,000 (H) mm was installed for situations during the construction and emergency operation of the argon cell.



(a) View from OA (b) View from AC

Fig. 1. Constructed Argon Cell.

3. Emergency Door

3.1 Design and kinematics of door

The emergency door should be kept gastight as a door between the argon cell and the air. This is not used during the operation of the argon cell except during an emergency, and it is used for installing the equipment and utilities or an operator entry during the construction of the argon cell. Thus, unlike a material transfer system that transfers process materials during the operation of the argon cell, it is opened only in the air cell by the master-slave manipulator in an emergency situation. The interior width of the door frame is 600 mm, the height is

1,000 mm, and the door is composed of three link mechanisms. To maintain the gas tightness of the door, a gasket with an air layer, which is often used in windows, was selected. Its three-dimensional schematic is shown in Figure 2.

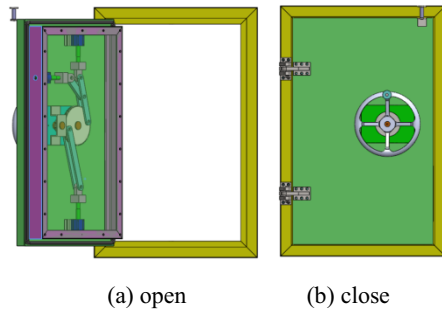


Fig. 2. Three-dimensional model of emergency door.

Figure 3 shows the position of the link when the door is opened and closed. When the drive shaft is rotated by the handle, the small gear rotates the large gear to move the three pins simultaneously with a small force.

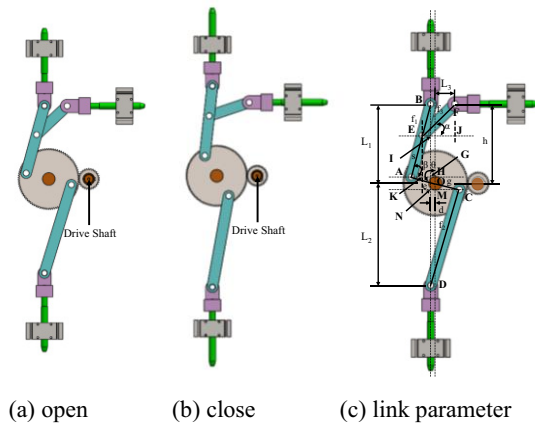


Fig. 3. Drive link of door.

Figure 3 (c) shows the schematic diagram for deriving the kinematics of the link mechanism. The calculation formula for the movement of the three pins when the door is opened and closed is shown below.

$$d = offset \quad (1)$$

$$L1 = e \cos \theta + \sqrt{f_1^2 - (e \sin \theta - d)^2} \quad (2)$$

$$L_2 = g \cos \theta + \sqrt{f_2^2 - (g \sin \theta + d^2)} \quad (3)$$

$$L_3 = f_3 \cos (\sin^{-1}((h - e \cos \theta - s \sin (\cos^{-1}((e \sin \theta - d)/f_1)))/f_3)) - e \sin \theta + s \cos (\cos^{-1}((e \sin \theta - d)/f_1)) \quad (4)$$

3.2 Installation of emergency door

Figure 4 (a) shows the installation of the emergency door. Figure 4 (b) and (c) show the locking mechanism when the door is closed and opened, respectively.



Fig. 4. Emergency door operated by MSM.

4. Conclusion

The emergency door is designed with three link mechanism, so it can tightly push three surfaces. Also, it can be remotely operated with small force using the MSM.

ACKNOWLEDGEMENT

This work was supported by the Nuclear Research and Development Program of the National Research Foundation of Korea (NRF) funded by the Ministry of Science and ICT.

REFERENCES

- [1] B.S. Park, "Construction of ACPF Argon Cell using Reverse Engineering Technique", KRS 2016 Spring Conference, 14(1), 99-100, 2016.

Shielding Evaluations of Fuel Failure Scenarios Using MAVRIC

Kyoon-Ho CHA*, Minchul KIM, and Taehyeon KIM

Korea Hydro & Nuclear Power Co., Ltd Central Research Institute, 70, Yuseong-daero 1312beon-gil,
Yuseong-gu, Daejeon, Republic of Korea

* khcha.cri@khnp.co.kr

1. Introduction

A spent nuclear fuel transport cask should be demonstrated by performing critical, shielding, thermal, and structural analyzes to ensure safe transport of nuclear fuel. However, Spent fuels with high burnup values of 60 to 80 GWd/MTU increase the potential to fail due to the degradation of fuel and cladding materials [1].

The purpose of this study is to investigate the results of potential fuel failures on the external radiation dose rates for a transport cask. The dose rates may be changed by fuel failures which are considered very improbable.

Shielding evaluations for fuel failure scenarios in which the geometric structure or conditions of spent fuel assemblies and fuel rods are changed due to beyond design basis accidents are evaluated for KN-18 transport cask. MAVRIC was used to evaluate the dose rates for the conditions of the cask [2].

2. Shielding Evaluations

KN-18 is a transport cask for 16×16 CE type fuels. In this study, Plus7 fuel assemblies with 5wt% concentration were selected and KN-18 cask body, neutron absorber and fuel baskets were used as described in its safety analysis report. The criteria for the shielding evaluation are different from the dose rate limits described in table 5-1 of NUREG-1617. [3]

The source term evaluation was carried out by ORIGEN-ARP to evaluate the neutron and gamma source of the cask. The total neutron and gamma ray intensity per cask is calculated as 3.17e+09 n/s and 7.64e+16 p/s.

For the calculations of the dose rate, ANSI standard (1977) incorporated in MAVRIC was used for flux-to-dose-rate factors [4] and the latest ENDF/B-VII.0 'v7-200n47g' was used for the cross section library.

2.1 Evaluations for normal condition

The MAVRIC modeling of the cask which

includes the fuel assemblies is shown in Fig. 1. Shielding for the K-18 is provided by the thick-walled cask body and the lid. For neutron shielding, resin material surrounds the vessel wall and resin material is placed below the cask bottom and above the cask lid. Additional shielding is provided by the basket structure and support disks [5]. Table 1 summarizes the surface dose rates of the cask. 100 batches and 100,000 particles per batch were used for both neutron and gamma dose calculations.

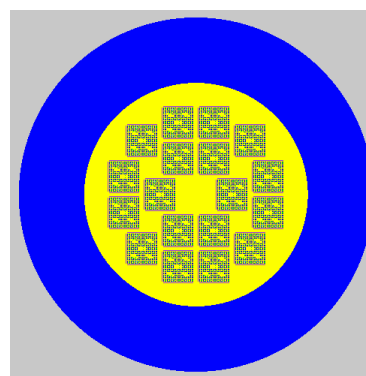


Fig. 1. MAVRIC Modeling of KN-18 Cask.

Table 1. Surface Dose Rates of KN-18 Cask

helium	Neutron (mSv/h)	Gamma (mSv/h)
Side	1.14674E-02	9.09986E-04
Bottom	3.81165E-01	2.75457E-02
Top	1.46653E-05	1.09467E-03

2.2 Evaluations for fuel failure scenarios

It has been grown particular concerns when high burnup spent fuels had been analyzed under hypothetical accident conditions. For shielding evaluations under those circumstances, several assumptions were made as internal and external structures within the cask, the basket structures with neutron absorbers, especially nuclear fuel assemblies, are maintained as their original states. In addition, fuel failure scenarios are assumed to be within the scope of severe accidents.

The axial burnup distribution is assumed to be uniform. In general, the uniform axial distribution is

more conservative in the shielding evaluation. The shape change due to the fuel damage plays a very important role in the shielding evaluation, and thus a large change in the uncertainty is expected.

For the fuel failure scenarios, the following two cases which are unlikely to occur are considered as shown in Fig. 2.

- Loss of multiple fuel rods (5%, 10%, 20%)
- Loss of rod cladding

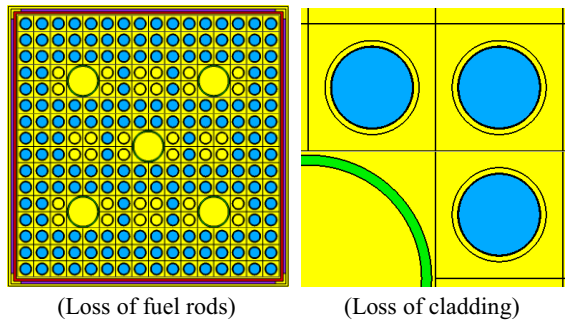


Fig. 2. MAVRIC modeling of fuel failures.

These scenarios investigate the effect of loss of rods and claddings by considering the reduction in source terms and fuel region density as well which would tend to reduce or increase dose rates. To model these scenarios, various numbers of rods and claddings were simply assumed to be absent from the fuel assembly model.

Table 2 and 3 summarize the dose rates according to the conditions of the loss of fuel rods and rod claddings. For every case, the results of the dose rate evaluations at 1m from the accessible surface of the cask were also added.

Table 2. Surface Dose Rates for Loss of Rods

		Neutron(mSv/h)	Gamma(mSv/h)
5% loss	Side	1.15541E-02	1.22902E-02
	Bottom	3.64869E-01	2.81504E-02
	Top	1.47807E-05	1.95238E-03
	Side(1m)	3.87871E-03	2.12198E-04
	Side	1.16270E-02	1.31744E-03
10% loss	Bottom	3.33898E-01	3.17590E-02
	Top	1.36663E-05	2.89536E-03
	Side(1m)	3.96452E-03	4.80720E-04
	Side	1.21776E-02	1.28801E-02
20% loss	Bottom	3.31592E-01	2.89582E-02
	Top	1.37205E-05	3.69868E-03
	Side (1m)	1.45155E-03	2.28862E-04
	Side	1.21776E-02	1.28801E-02

Table 3. Surface Dose Rates for Loss of Cladding

	Neutron (mSv/h)	Gamma (mSv/h)
Side	1.14616E-02	1.33337E-02
Bottom	3.60088E-01	3.84408E-02
Top	1.42856E-05	2.21159E-03
Side(1m)	3.69469E-03	2.56909E-04

The absent of fuel rods and claddings reduces the external dose rates. The total dose rates are the sum of neutron and gamma dose rates. The results show that most calculated dose rates meet the criteria; 2mSv/hr for cask surface of normal condition and 10mSv/hr for 1m from the surface of accident condition. This means that the fuel failures like the loss of rods and rod cladding would not affect the shielding criteria of the SAR.

3. Conclusion

In this study, the shielding evaluations of KN-18 cask for spent fuel transportation were carried out for normal conditions and various fuel failure scenarios. It is expected that the shielding evaluations using MAVRIC for normal and these fuel failure scenarios can be used for the development of a new cask for future transportation or storage purposes. Moreover it is necessary to consider the detailed specifications of the transport cask to evaluate sufficiently reliable results.

REFERENCES

- [1] K.R. Elam, J.C. Wagner, C.V. Parks, "Effects of Fuel Failure on Criticality Safety and Radiation Dose for Spent Fuel Casks," NUREG/CR-6835, ORNL, September 2003.
- [2] D.E. Peplow and C. Celik, "MAVRIC: MONACO with Automated Variance Reduction using Importance Calculations in SCALE6.2," 2016.
- [3] NUREG-1617, "Standard Review Plan for Transportation Packages for Spent Nuclear Fuel," U.S. Nuclear Regulatory Commission, March 2000.
- [4] ANSI/ANS 6.1.1-1977, "American National Standard for Neutron and Gamma-ray Flux-to-Dose-Rate Factors," March 1977.
- [5] "KN-18 Spent Nuclear Fuel Transport Cask Safety Analysis Report (Rev.01)," KHNP, November 2013.

Analysis of Uranium Concentration in LiCl-KCl Salt of Electrefining Process Using LIBS

Seul-Ki Han, Se-Hwan Park*, Bo-Young Han, and Seong-Kyu Ahn

Korea Atomic Energy Research Institute, 111, Daedeok-daero 989beon-gil, Yuseong-gu, Daejeon, Republic of Korea

*ex-spark@kaeri.re.kr-mail

1. Introduction

Laser Induced Breakdown Spectroscopy (LIBS) has been developed for the effective and efficient safeguards of pyroprocessing at Korea Atomic Energy Research Institute (KAERI) [1]. LIBS analyzes based on the optical analysis of the radiation emitted by the plasma generated by concentrating a strong laser beam on the surface of the sample. LIBS has characteristic such as real-time analysis, no sample preparation before the analysis, and possible in situ implementation. In this study, U and lanthanide element in LiCl - KCl salt are measured as electrefining process material of pyroprocessing via LIBS and the possibility of measurement of actinide (Pu, Cm) element is analyzed in the future try to. In fact, in the refining process delivered in the pyroprocessing, there are substances in the state of molten salt at 500°C. In this study, LiCl - KCl based salts LaCl_3 , CeCl_3 , BaCl_2 , PrCl_3 , NdCl_3 , YCl_3 , SmCl_3 and UCl_3 were added and melted and then sampled the salt in the solid state was measured in order to reduce the measurement error.

2. Methods and Results

At first, five LiCl-KCl samples containing UCl_3 were fabricated to obtain the preliminary calibration curve. Sample contained from 1wt% to 10wt% UCl_3 .

Composition materials of the samples were placed in the glassy carbon crucible, and they were heated up to 650°C to melt. The molten salt samples were slowly cooled to solid form in the furnace.

Experiments were conducted in a glove box with an atmosphere of Ar gas with moisture and oxygen content of 100 ppm or less for samples with high deliquescence. A laser beam was injected through the port of the glove box and the optical fiber cable was inserted I received it. The sample surface was somewhat irregular and the distance between the sample and the focusing lens was corrected each time the sample surface was changed by interlocking the XYZ moving sample table with a high precision distance meter to match the same focal length. A beam of Q-switched Nd: YAG pulse laser (Brilliant B, Quantel) with a wavelength of 532 nm is focused on the sample surface to generate plasma and Echelle spectroscopy with $20,000(\lambda/\Delta\lambda)$ resolution to detect plasma emission line and ICCD camera was used. The emission lines of U and other emission line were selected in the wavelength region of 200 to 400 nm where spectroscopy is permitted. The number of laser pulses in the measurement was 100. After collecting of LIBS spectrum at a position, the sample was moved horizontally to obtain the scan data of the sample surface. As shown figure 1, the measured U spectrum in the wavelength 290.825 nm were analyzed. And then As shown figure 2, The relative standard deviation of K peak are ~ 10%, However, the

amount shown on the X-axis in the figure 2 is nominal amount before chemical analysis. For better analysis of the performances, multivariate calibration using a partial least squares regression [2] was employed to take into account the intensity correlations between the analyte lines and reference signal. The quality of the calibration could be improved through a multivariate analysis.

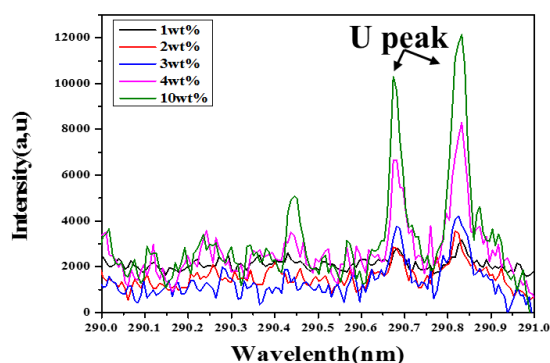


Fig. 1. U spectrum in a sample containing from 1.0wt% to 10.0wt% U in LiCl-KCl.

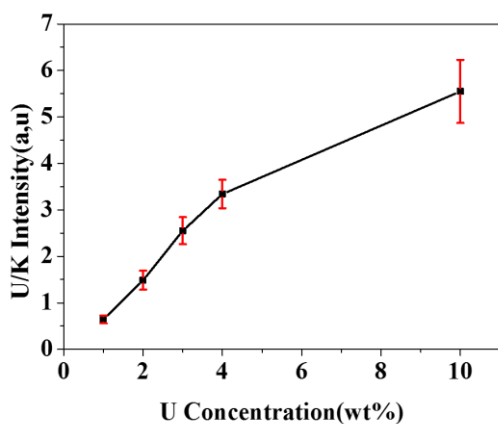


Fig. 2. The count ratio of U/K with increasing U concentration.

3. Summary

LIBS is a promising technology as the process monitoring technology applicable to the pyroprocessing safeguards. The uranium concentration in LiCl-KCl salt were measured using LIBS system, and the quantitative analysis

performance of LIBS such as repeatability and Limit of Detection (LOD) are analyzed. These effort will help to assess the applicability of LIBS to the off-normal process in the electrorefining process.

ACKNOWLEDGEMENT

This work was supported by a National Research Foundation of Korea (NRF) grant funded by the Korean government's Ministry of Science and ICT (MSIT) (No. NRF-2017M2A8A5015084).

REFERENCES

- [1] B.Y. Han et al., Analysis of the applicability of LIBS to address safeguards needs with respect to pyroprocessing, KAERI/TR-6607/2016 (2016).
- [2] S. Wold, M. Sjöström, L. Eriksson, Chemometrics and Intelligent Laboratory System 58 (2001) 109-130.

The Study of Spent Nuclear Fuel Storage Facility to Consider Beyond Design Basis Accident

Dong-bin Shon

Korea Electric Power Corporation E&C, 269, Hyeoksin-ro, Gimcheon-si, Gyeongsangbuk-do, Republic of Korea

*linusvan@kepc-eenc.com

1. Introduction

The government has established a spent nuclear fuel storage plan to be applied to storage facilities before disposal through the Atomic Energy Promotion Council in 2016.

Spent nuclear fuel storage facilities provide for safe, stable and secure storage of spent nuclear fuel before it is disposed of as radioactive waste.

To achieve these objectives, the design of spent nuclear fuel storage facilities shall incorporate features to maintain subcritical spent nuclear fuel and to maintain containment over the anticipated lifetime of the storage facilities.

Therefore, after the 9.11 accidents, we will analyze the latest technologies from abroad in terms of designing to consider Beyond Design Basis Accident that have emerged as a major design issue in the design of spent nuclear fuel storage facilities.

2. Status of Beyond Design Basis Accident

2.1 Domestic Background and Status

The wet storage of NPPs that store spent nuclear fuel is expected to be saturated from 2024 in this order, so it is necessary to design the spent nuclear fuel storage facility as a top priority.

However, Design to consider Beyond Design Basis Accident was carried out within the framework

of probabilistic safety evaluation because it is an extremely low incidence.

Especially, aircraft impact assessment of Beyond Design Basis Accident was typical example.

For example, if the probability of occurrence of radioactive disaster due to aircraft impact is less than $10^{-7}/\text{yr}$, it does not take into consideration the risk of impact.

2.2 Situation change and overseas situation

In addition to the accident conditions that occurred during the flight of the aircraft after the 9.11, there was a need for safety assessment and design standards in preparation for the impact caused by the abduction of aircraft by terrorism.

In the United States, the NRC has created an "AIA" since September 11, 2009 to allow nuclear licensees and licensee applicants to carry out a design to consider Aircraft Impact Assessment. The evaluation criteria are to maintain the reactor core cooled or the containment remains intact and to maintain spent nuclear fuel pool integrity of the nuclear power plant.

Also, the general characteristics such as fuel injection amount, crash speed and angle, ability of both experienced and inexperienced pilots to control large, commercial aircraft were considered.

For the same reason as nuclear power plants, there is a need to evaluate aircraft impact in the spent

nuclear fuel transportation and storage system. Further, there is a need for further strengthened requirements such as impact evaluation for large commercial aircraft (Boeing 767 etc.) as well as small fighter crashes.

In Germany, there are two types of spent nuclear fuel storage facilities in the form of "WTI" and "STEAG" according to the designers.

After the 9.11, the evaluation of aircraft crashes of existing facilities was performed by a licensing organization. In the case of small aircraft impact evaluation, it was carried out before 9.11. But in this case, the impact evaluation of large commercial aircraft was taken into account and the safety of the structure was confirmed.

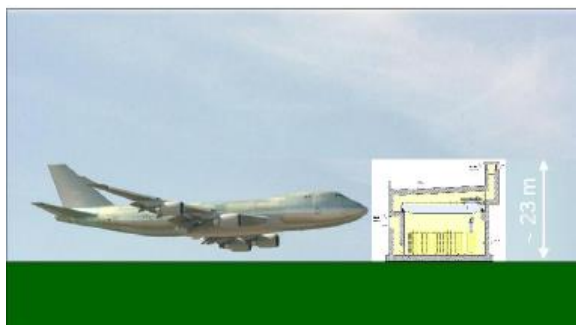


Fig. 1. STEAG-Building, Boeing 747, True Ratio of Size.

In the case of Japan, the Ministry of Economy, Trade and Industry (METI) issued a report (2008) containing the contents of the regulation on the safety evaluation of spent nuclear fuel intermediate storage facilities using metal dry cask.

3. Conclusion

Design to consider Beyond Design Basis Accident was carried out within the framework of probabilistic safety evaluation because it is an extremely low incidence.

But, after the 9.11, there was a need for safety

assessment and design standards in preparation for the impact caused by the abduction of aircraft by terrorism.

Whether to apply the design considering the aircraft impact assessment to the storage facility will be decided according to the regulatory requirements, but it is necessary to build a storage system suitable for the situation in Korea through overseas cases.

REFERENCES

- [1] U.S.NRC, "50.150 Aircraft impact assessment" (2009).
- [2] Federal Office for Radiation Protection, "Interim storage of spent nuclear fuel in Germany" (2002).
- [3] CRIEPI, "Spent fuel storage in japan" (2015).

Input Accountancy of Pyroprocessing With Different Head-end Process Options

Chaehun Lee *, Byung-Hee Won, Se-Hwan Park, Seonkwang Yoon, Ho-Dong Kim, and Seong-Kyu Ahn
Korea Atomic Energy Research Institute, 111, Daedeok-daero 989beon-gil, Yuseong-gu, Daejeon, Republic of Korea
*chlee80@kaeri.re.kr

1. Introduction

In the prospective of spent nuclear fuel management, pyroprocessing is one of the options to reduce the volume and toxicity of spent nuclear fuel waste [1]. To secure proliferation resistance in spent nuclear fuel recycling, safeguards approaches should be developed. Among material accountancy, input material in the head-end process of pyroprocessing, which is the Material Balance Area (MBA) to declare Shipper-Receiver Difference (SRD), is an issue because materials exist in the solid form such as small and large fragment, powder, and/or porous pellet which can increase the sampling uncertainty when taking Destructive Analysis (DA) samples. Material forms and size largely depend on the head-end process. Regardless of the head-end process, input material accounting methods should be established. In this study, two input accounting methods according to the head-end process options such as decladding methods, spent nuclear fuel particle size, and process equipment were proposed and evaluated.

2. Double Stage Homogenization

In the previous work [2], double stage homogenization was proposed in case that the material form is powder and the performance of homogenization mixers with metal oxide powder as surrogate material was evaluated in terms of heterogeneity, sampling uncertainty, and accounting uncertainty. The tumbler mixer known as a diffusive-type mixer may have poor heterogeneity in case of mixing powder with different sizes and/or different density. In this study, to check the segregation effect, the tumbler mixer of 50 kg capacity was tested with depleted uranium powder and metal oxide powder of various particle sizes as shown in figure 1. DA samples were taken in 10 different positions of the tumbler mixer container at each mixing time, and

analyzed by a titration method to measure the mass of total uranium in the samples. The analyzed heterogeneity was less than 0.5% which was similar to the previous test in which the metal oxide powder of the same particle size was mixed. It means that the heterogeneity of the diffusive mixer such as tumbler mixers is barely affected by segregation with powder of 10 to 75 μm particle size.

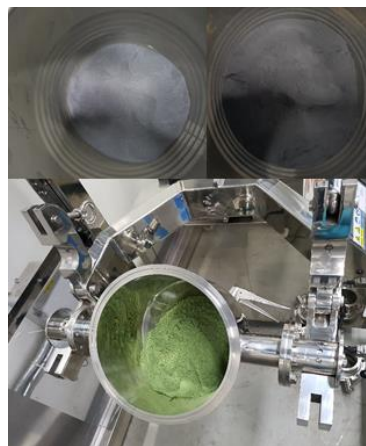


Fig. 1. Depleted uranium powder of 10 μm & 40 μm tumbler mixer.

3. Representative sampling & Homogenization

In input accountancy with the double homogenization process, it was assumed that the oxidative decladding is used and whole spent nuclear fuel is pulverized by the voloxidation process. Thus, the sampling uncertainty can be reduced by homogenization mixing of spent nuclear fuel powder. On the other hand, in case of using the mechanical decladding instead of the oxidative decladding, the decladded spent nuclear fuel exists as small and large fragments which cannot be homogenized by mixing. Thus, combination of representative sampling and homogenization was proposed for input accountancy. The description of the head-end process is shown in figure 2. Spent nuclear fuel fragment were sieved to separate small and big fragments, and a sample up to

30 kg from big fragments is taken. Then, the sample is pulverized by the voloxidation process, then final samples of 1 g are taken for DA analysis after homogenization mixing. Small fragments and spent nuclear fuel remained in hulls go into the voloxidation process followed by the homogenization process, and DA samples taken same as sampling of big fragment.

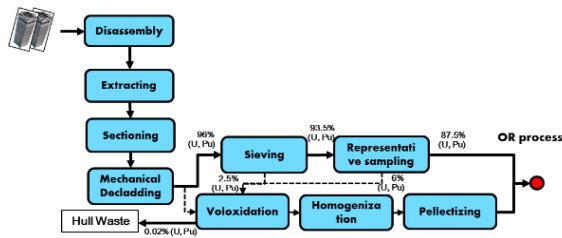


Fig. 2. Diagram of the head-end process.

In addition to the uncertainty arising from the homogenization process such as the heterogeneity, DA uncertainty, and the distribution of Pu concentration in spent nuclear fuel, a combination of the representative sampling and homogenization causes the sampling uncertainty which largely depends on the particle size, the sampling mass, and the performance of the sampling device. The performance of the sampling device, called the sample divider, was evaluated in previous work [3]. The sampling uncertainty was similar to the theoretical value (binomial distribution) which is a function of particle size/density, and the number of samples to be divided, as the below equation [4, 5]. M is the sample mass, f_i is the overall mass fraction of component i , ω_i is the mass of a single particle of the component, and $\bar{\omega}$ is the overall mean particle mass in the equation.

$$(\sigma_m^2)_i = \frac{f_i(1-f_i)\omega_i + f_i^2(\bar{\omega} - \omega_i)}{M} \quad (1)$$

By the mechanical decldding of PWR spent nuclear fuel, the particle size is roughly smaller than 2 mm, thus the sample mass should be at least 34 kg to achieve the sampling uncertainty of 1 % with 99.7 % confidence. The sampling uncertainty with respect to the particle size will be more discussed in detailed in the conference after the statistical model calculation.

4. Discussion

Double stage homogenization and a combination of homogenization and representative sampling were proposed as Input accounting methods, depending on the head-end process options. The candidate mixer has no meaningful segregation effect to degrade the heterogeneity. Thus, The Pu accounting uncertainty of 1% (1σ) with the double stage homogenization can be achievable as estimated in the previous work [4]. And in case of taking enough sample mass from the fragment with the representative sampling device, the representative sampling can achieve a low sampling uncertainty which depends on the sampling mass, and particle size. Regardless of the head-end process, it is expected that nuclear material accounting in the head-end process with a low uncertainty is possible with the proposed methods.

ACKNOWLEDGEMENT

This work was partly supported by a National Research Foundation of Korea (NRF) grant funded by the Korean government (MSIP). (NRF-2017M2A8A5015084).

REFERENCES

- [1] Seong-Kyu Ahn, et al., "Development of safeguards system requirements for the pre-concept design of a pyroprocessing facility", Proc. Of KRS Spring, May 19-20, 2015, Incheon.
- [2] Chaehun Lee, et al., "Input Material Accounting Method with Homogenization mixers for an Engineering Scale Pyroprocessing Facility", Proc. Of the KRS 2017 Spring Conference, May 24-27, 2017, Busan.
- [3] Chaehun Lee, et al., "Input material accountancy approach of pyroprocessing", Proc. Of the KRS 2015 Fall Conference, October 14-16, Busan.
- [4] Chaehun Lee, et al., "Input Material Accounting Method for an Engineering Scale Pyroprocessing Facility", KAERI/TR-6622, 2016.
- [5] R. Hogg, "Characterization of relative homogeneity in particulate mixtures", Int. J. Miner. Process. 72, 477-487 (2003).

Current Status of Spent Nuclear Fuel Integrity Evaluation R&D in the Major Countries

Donghak Kook*, Jaeho Yang, and Yanghyun Koo

Korea Atomic Energy Research Institute, 111, Daedeok-daero 989beon-gil, Yuseong-gu, Daejeon, Republic of Korea

*syskook@kaeri.re.kr

1. Introduction

Interim SNF (Spent Nuclear Fuel) Dry Storage could be defined as to be located inside nuclear power plant site and has been managed by the utility (not the government). The definition of 'interim' is getting longer than the initial expectation because of huge delay of disposal facility opening and no more fascinating processing option. The cask or canister has been concerned for containment safety in the last decades, but these systems have developed very robustly by the commercial cask vendors. By the way, SNF itself faces another challenges of integrity evaluation for the extended storage time beyond its initial licensed period. This article is willing to briefly introduce what is current situation in the major SNF dry storage countries for this and where should our country take a step towards.

2. Status of Europe

2.1 Overall Status

European Union is now planning a joint program on radioactive waste management and disposal which includes SNF integrity R&D work for 10 years in two steps. Following each national topics belong to this joint program.

2.2 Germany

SNF R&D Project title of the joint program is 'Development of a fracture mechanics approach to describe brittle failure of fuel cladding during long term interim storage (BRUZL)' . BAM, Germany R&D licensing organization takes a header role by leading Spanish university for thermo-mechanical-chemical properties, Spanish research organization for pellet behavior and Germany university for pellet-cladding interactions in dry storage & transportation situation. Figure 1 shows the basic testing and modeling plan of BRUZL project.

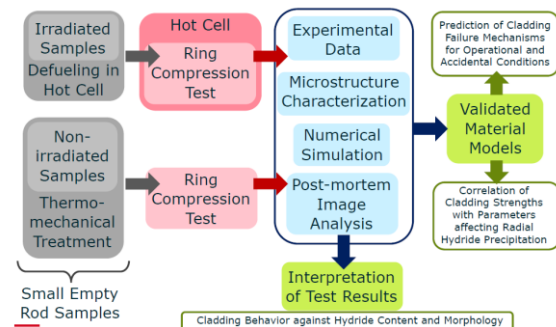


Fig. 1. Testing Plan of Cladding in BRUZL.

2.3 Swiss

NAGRA [1], the Swiss radioactive waste management organization, has started SNF integrity R&D like Figure 2 even though their fundamental mission is deeply dispose SNF underground. The reason of their research is to keep SNF handling facility and space clean while they do repackaging.

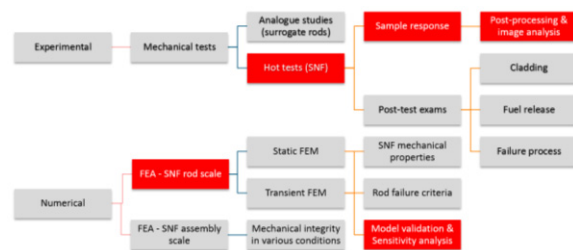


Fig. 2. SNF Integrity R&D in NAGRA.

2.4 Spain

ENUSA, the Spanish nuclear fuel supply company, is doing SNF integrity R&D which is dedicated to handling problem. This R&D has three step: first, they lowered the initially 100% concerned SNF to 75% by analyzing already existing available information. Secondly, they eliminate 28% possible concerns by performing visual inspection. Finally, they narrow down the concerning target from 47% to 11% by testing fuel assembly condition. This approach is very reasonable and acceptable to plan the fuel testing matrix.

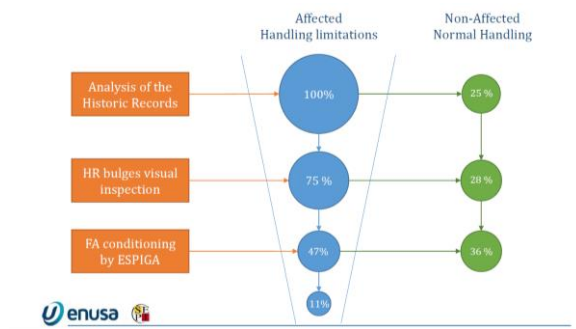


Fig. 3. SNF Assembly based Integrity R&D in Spain.

3. Status of USA

3.1 High Burnup DEMO Sister Rod Testing

High Burnup DEMO program has started its 10 years operation from November 2017. One of the main goal of this demo is to clarify SNF degradation while dry storage operation. For the 'before DEMO condition (t=0)', 25 sister rods are under examination in ORNL, PNNL and ANL for various single effect testing. These initial testing results could contribute to produce high burnup (~55 GWd/t) characterization material data.

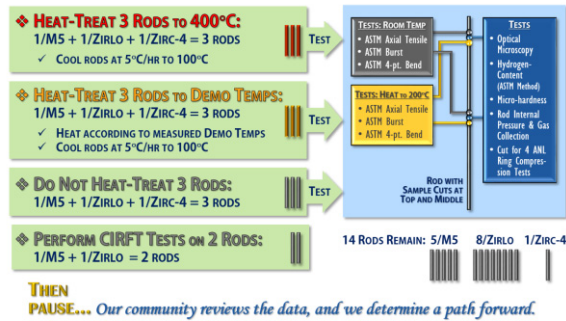


Fig. 4. High Burnup DEMO Sister Rod Testing Plan.

4. Status of Korea

4.1 Where are we standing?

Majority(over 70%) of SNF already discharged from reactor is less than 45 GWd/t level and therefore current Korean R&D is focusing on this burnup range. The distinguished meaning of this step is to develop testing device, establish quality assurance procedure for the testing, arrange testing matrix, integrate anticipation coding, and broaden expertise network. Expected main results of this step is shown in Figure 5 which includes SNF testing data, material property anticipating code, and small-scale

demonstration exam.

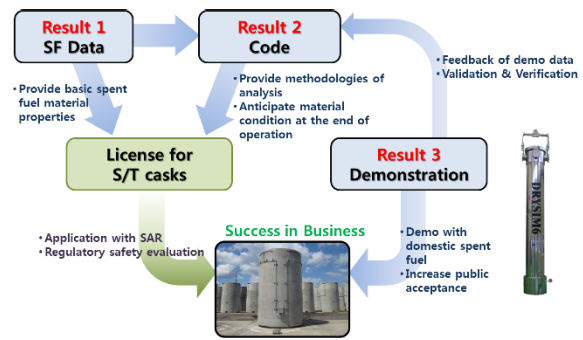


Fig. 5. Expected Korean SNF R&D results.

4.2 What is our next step?

Based on the current R&D results, next step have to expand work level up to fuel assembly-wise integrity severely because the fuel retrievability which is the mandatory mission of dry storage management is the most important goal in the SNF handling with burnup level increasing.

5. Conclusion

As SNF Dry Storage is getting longer than the initial 'interim' purpose, the importance of SNF integrity evaluation work is getting higher, especially for the extended storage era. Current status of the major countries on this shows us the near future SNF R&D direction.

ACKNOWLEDGEMENT

This work was supported by the Korea Institute of Energy Technology Evaluation and Planning (KETEP) granted financial resource from the Ministry of Trade, Industry and Energy, Republic of Korea (No. 2014171020166A).

REFERENCES

- [1] NAGRA, "Overview of European Joint Project activities on WP proposal-Spent Fuel Characterization & Evolution Until Disposal, 2nd GRS Workshop on Safety of Extended Dry Storage of Spent Nuclear Fuel, 2018.

Analytic Approach to Simulate Vacuum Drying for Canister

Seung-hwan Yu*, Ju-chan Lee, Kyung-sik Bang, and Woo-seok Choi

Korea Atomic Energy Research Institute, 111, Daedeok-daero 989beon-gil, Yuseong-gu, Daejeon, Republic of Korea

*shyu80@kaeri.re.kr

1. Introduction

Drying process of spent nuclear fuel must be required when spent nuclear fuel is transferred from wet storage to dry storage because oxidation composition could be bad effect of fuel cladding and long-term integrity of fuel cladding could not be guaranteed. Vacuum drying method is widely used in nuclear industry. In vacuum drying process, dryness criteria is that internal pressure is less than 3 Torr for 30 min without vacuum pump operation.

Analytic approach to simulate vacuum drying was suggested. Simple vacuum drying process and repeated vacuum drying process were analyzed.

2. Concept of analytic calculation

2.1 Simple drying process

In simple drying process, only pressure change from 760 Torr to 3 Torr is focused. Dryness criteria is not considered. The purpose of simple drying process is to check possibility of vacuum drying simulation. Vacuum drying is based on pressure change in canister due to vacuum pump and water evaporation. The modeling of vacuum drying process is consisted of 2 parts. One is pressure evacuation by vacuum pump and the other is pressure increase by water evaporation.

2.2 Repeated drying process

In repeated drying process, dryness criteria was considered. To meet dryness criteria, vacuum pumps operated until pressure went down under 3 Torr. Even if pressure was less than 3 Torr, pressure could rebound more than 3 Torr because very few residual water could evaporate and it led to increase pressure. This phenomenon is called as pressure rebound. To avoid pressure rebound, drying process should be performed several times.

3. Results and discussion

Assumptions of calculation are below as

- Temperature inside canister was constant.
- Residual water only naturally evaporated.
- Initial pressure is 101.325 kPa.
- Initial residual water at bottom was 50 g.

3.1 Simple drying process

To check the effect of residual water, case with residual water and case without water were compared. Required time until pressure was less than 0.4 kPa (3 Torr) is 111 s for result without water and is 35907 s for result with water. It took much longer time for vacuum drying of case with residual water.

3.2 Repeated drying process

Fig. 3. is calculation result of repeated drying

process. To meet dryness criteria, vacuum drying process was repeated 24 times and it took 26.5 hour. Pressure rebound could be found at each drying stage.

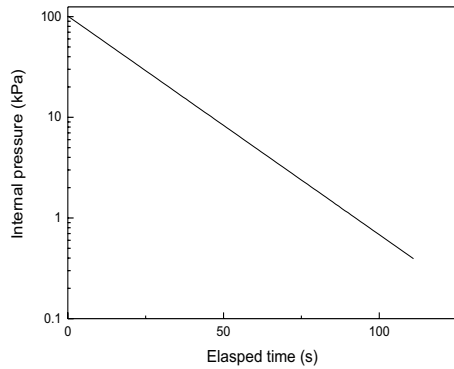


Fig. 1. Result of pressure change without residual water.

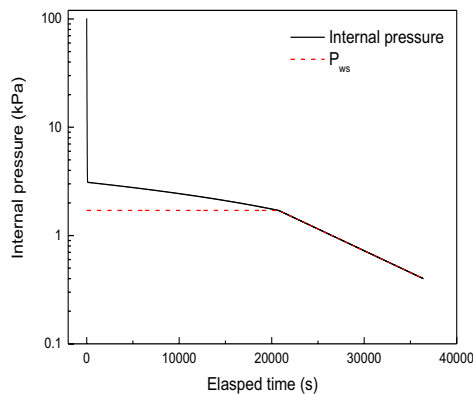


Fig. 2. Result of pressure change with residual water.

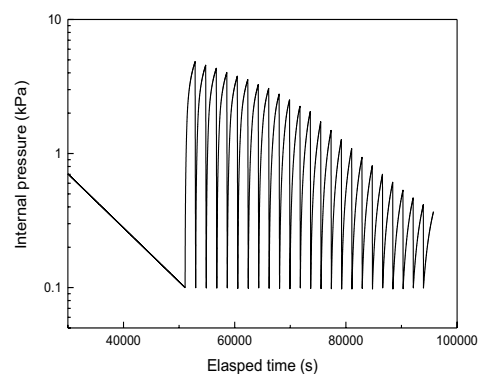


Fig. 3. Result of repeated drying process.

4. Conclusion

The calculation program of vacuum drying was developed to analyze analytically vacuum drying

process. The effect of residual water and temperature on vacuum drying was compared. As the temperature increased, required time for vacuum drying decreased due to faster evaporation of residual water. To meet vacuum dryness criteria, vacuum drying process should be repeated

ACKNOWLEDGEMENT

This work was supported by the Korean Ministry of Trade, Industry, and Energy (MOTIE) as a part of the Radioactive Waste Management Technology Development Project (20181720201020).

REFERENCES

- [1] USNRC, 2010, Standard Review Plan for Spent Fuel Dry Storage Systems at a General License Facility, NUREG-1536.

Design of Integrated Analysis Tool for Degradation Evaluation of Spent Nuclear Fuel in Dry Storage System

ChangHwan Shin*, Kyong-Won Seo, Yong-Sik Yang, Jong-Dae Hong, SeounGuk Lee, and Dong-Hak Kook
Korea Atomic Energy Research Institute, 111, Daedeok-daero 989beon-gil, Yuseong-gu, Daejeon, Republic of Korea
*shinch@kaeri.re.kr

1. Introduction

The spent nuclear fuel must be safely managed until appropriately disposed. At present, the spent fuel used in the pressurized water reactor in Korea is safely stored in wet storage pool of the reactor. The dry storage of spent nuclear fuel is a practical alternative until it is appropriately disposed. During storage, spent nuclear fuel undergo material property changes, so called degradation, as a function of time. The degradation of the spent fuel during the dry storage depends on the temperature. Thus the detailed temperature profile is suggested as the first item on the gap analysis report [1]. The UNF-ST&DARDS in the USA is being developed to streamline computational analysis capabilities for characterizing input for the overall waste management system [2]. This study is focused on a platform design for integrated evaluation of temperature change and degradation characteristics of the spent nuclear fuel.

2. Design of Integrated Analysis

In order to evaluate the integrity of the spent fuel in dry storage cask, the temperature distribution of the fuel and the degradation of the cladding should be evaluated accordingly. The degradation of the cladding depends on the temperature, and the temperature changed depending on the fuel geometry. The creep, which is one of the key degradation mechanism of the cladding, can cause a diameter change of the fuel cladding and the rod internal pressure. Therefore, an integrated analysis platform was designed to evaluate the two closely related phenomena.

2.1 Thermal hydraulics

Based on the COBRA-SFS [3] developed for thermal hydraulics analysis of dry storage system, an integrated analysis platform has been modified. The flow chart and the modified structures of COBRA-

SFS are illustrated in the Fig. 1.

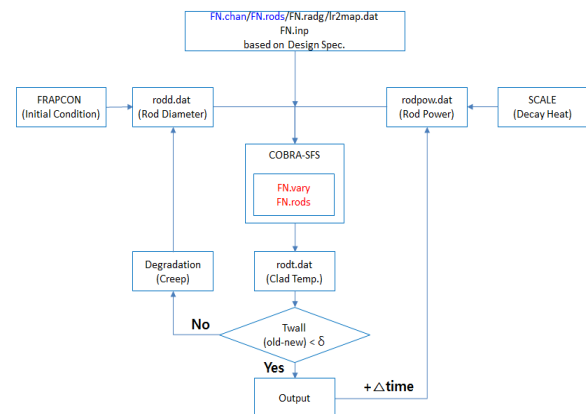


Fig. 1. The flow chart of thermal hydraulics for integrated analysis.

In COBRA-SFS, the inputs related to the fuel geometry are prepared for the initial design of the fresh fuel. The spent fuel geometries for initial conditions of dry storage are produced by the fuel performance code, and these results are read during COBRA-SFS calculation process. At a certain time step, the temperature and geometry changes are iterated until the convergence condition is reached.

2.2 Degradation

In the current version, the integrated platform allowed to evaluate the degradation of creep and DHC (Delayed hydride cracking). For the creep evaluation, the modified EPRI model was modularized. The threshold stress intensity factor, KIH is calculated by Shi & Puls Model and the applied stress intensity factor, KI is calculated by ductile fracture handbook of EPRI [4].

3. Integrated Analysis

The initial conditions of spent fuel at the dry storage beginning are produced with fuel performance code, such as FRAPCON, to reflect power history during irradiation. The decay heat, which is the heat source of spent fuel, is designed to

be calculated from a specific code such as SCALE. Variables delivered from FRAPCON are cladding diameter, rod internal pressure, nodal burnup, hydrogen content, total/plastic strain, stress and fast fluence. The calculation flow diagram of the integrated analysis is shown in Fig. 2 and the calculation process can be summarized as follows.

- (1) Calculation of initial condition with FRAPCON.
- (2) Calculation of decay heat with SCALE.
- (3) Generation of input file for storage cask, boundary conditions, calculation conditions.
- (4) Generation of geometry input files for COBRA-SFS based on design specification.
- (5) Run the integral analysis tool
- (6) Update changed geometry
- (7) Calculation of temperature distribution.
- (8) Calculation of geometry change and rod internal pressure by degradation.
- (9) Iteration from (6) to (8)
- (10) Estimation of DHC
- (11) Go to next time step

The cumulative strain rate obtained from the preliminary calculation is shown in Fig. 3.

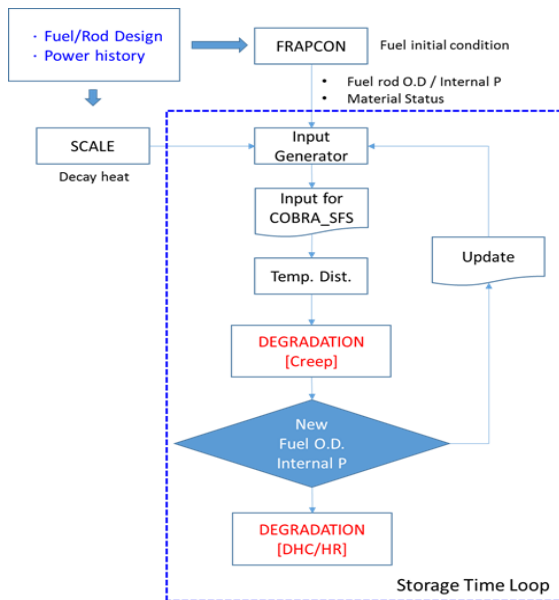


Fig. 2. Flow diagram of the integrated platform.

4. Conclusions

The integrated analysis tool for evaluation of spent fuel cladding integrity during dry storage is designed. This integrated analysis platform has been developed

to evaluate the detailed fuel temperature and fuel degradation, simultaneously. The input structure of COBRA-SFS has been modified in order to conveniently apply the geometry change of spent fuel due to creep deformation. The developed degradation models within the integrated analysis tool have been verified.

As a future work, the module to calculate the decay heat for each rod and the database system to manage the fuel information and the analysis results should be linked or integrated.

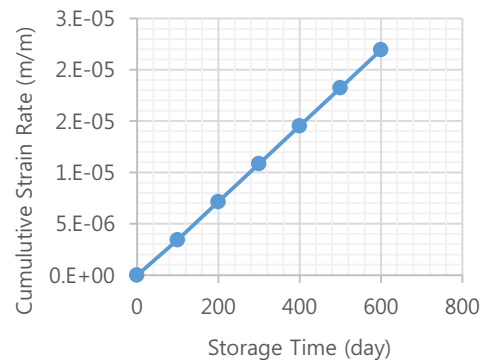


Fig. 3. Cumulative strain rate of integrated analysis tool.

ACKNOWLEDGEMENT

This work was supported by the Korea Institute of Energy Technology Evaluation and Planning (KETEP) granted financial resource from the Ministry of Trade, Industry and Energy, Republic of Korea (No. 2014171020166A).

REFERENCES

- [1] B. Hanson, et al., "Gap Analysis to Support Extended Storage of Used Nuclear Fuel, Rev. 0," PNNL-20509, (2012).
- [2] R.A. Lefebvre, et al., "Development of Streamlined Nuclear Safety Analysis Tool for Spent Nuclear Fuel Applications," Nuclear Technology, Vol. 199, 227-244, (2017).
- [3] T. Michener, et al., "COBRA-SFS, A Thermal-Hydraulic Analysis Code for Spent Fuel Storage and Transportation Casks, Cycle 4," PNNL-24841, (2015).
- [4] Y.S. Yang, et al., "Study on Spent Fuel Degradation : Development of Degradation model and Verification Test Apparatus," KAERI/TR-6459/2016, (2016).

Evaluation of Preliminary Criticality Safety for Metal Storage Cask

Yun-sik KIM* and Dong-gyu LEE

Kones Nuclear Engineering & Service Corp., 798-1, Yuseong-daero, Yuseong-gu, Daejeon, Republic of Korea

*yunsik@kones21.com

1. Introduction

The purpose of this analysis is to identify the criticality margin for the metal storage cask. The metal storage cask assumed that 32 spent fuel assemblies could be stored and considered the worst conditions. The criticality evaluation was carried out applying burnup credit effect according to SFST-ISG-8(Re.3). And the reduction of the reactivity according to the cooling period was also considered.[1]

2. Modeling Approach and Assumptions

2.1 Spent Nuclear Fuel

The spent fuel data applied to the analysis are as follows.

- Fuel Type : 17x17 WH V5H
- Enrichment : 2.0 ~ 4.5wt%
- Burnup : 0 ~ 45,000MWd/MTU
- Cooling : 5 year
- Axial Burnup : NUREG/CR-6801 Profiles[2]

2.2 Storage Cask

Specifications of the storage cask used to the analysis are as follows and modeled as Figure 1.

- Number of Stored Fuels : 32 assemblies

- Canister ID/OD : 163.6/168.6 cm
- Cask ID/OD : 169.6/212.6 cm
- Neutron Absorber
 - Thickness : 0.3 cm
 - B-10 Areal Density : 0.0317732 g/cm²

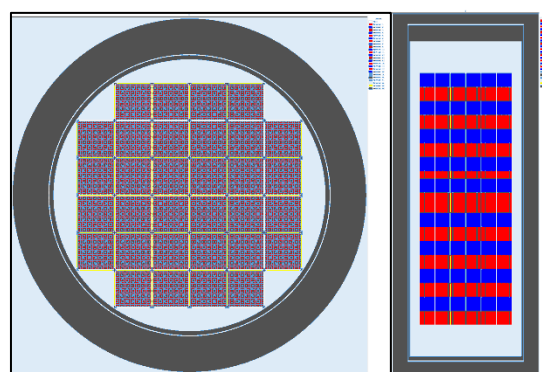


Fig. 1. Analysis model.

2.3 Computer Codes, Cross Section Library

For this analysis, SCALE 6.1 and the 238-group ENDF/B-VII cross section library was used. SCALE 6.1 is the most recent release of the SCALE code system which has been heavily used throughout the world for criticality analysis. The SCALE code system is a series of modules run by sequence drivers. For this work, TRITON sequence was used for depletion and CSAS5 sequence was used for calculation of k_{eff} . [3]

2.4 Applied Set of Nuclides

28 nuclides set was applied for burnup credit as Table 1.

Table 1. Applied set of nuclides for burnup credit

Nuclides			
²³⁴ U	²³⁵ U	²³⁸ U	²³⁸ Pu
²³⁹ Pu	²⁴⁰ Pu	²⁴¹ Pu	²⁴² Pu
²⁴¹ Am	⁹⁵ Mo	⁹⁹ Tc	¹⁰¹ Ru
¹⁰³ Rh	¹⁰⁹ Ag	¹³³ Cs	¹⁴⁷ Sm
¹⁴⁹ Sm	¹⁵⁰ Sm	¹⁵¹ Sm	¹⁵² Sm
¹⁴³ Nd	¹⁴⁵ Nd	¹⁵¹ Eu	¹⁵³ Eu
¹⁵⁵ Gd	²³⁶ U	²⁴³ Am	²³⁷ Np

2.5 Code Validation – Isotopic Depletion

The depletion bias uncertainty was applied as a function of assembly average burnup (Table 2) according to SFST-ISG-8(Re.3).

Table 2. Isotopic uncertainty for burnup range

Burnup Range (GWd/MTU)	Isotopic uncertainty
0-5	0.0150
5-10	0.0148
10-18	0.0157
18-25	0.0154
25-30	0.0161
30-40	0.0163
40-45	0.0205
45-50	0.0219
50-60	0.0300

2.6 Code Validation – K_{eff} Determination

According to SFST-ISG-8(Re.3), if 28 nuclides set was applied for burnup credit as Table 1, 1.5% of the worth of the minor actinides and fission products conservatively covers the bias.

3. Analysis Result

The result of preliminary criticality safety analysis shows that initial enrichment less than 2.0wt% fuel can be stored without burn. 4.5wt% fuel can be stored burnup more than 36,000MWd/MTU. The loading curve is shown in Figure 2.

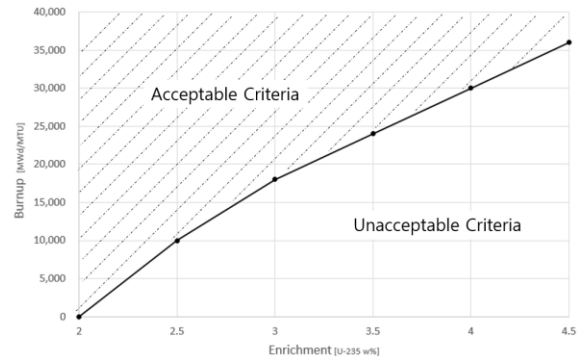


Fig. 2. The loading curve.

4. Conclusion

Evaluation was performed to identify critical margins for the metal storage cask. The cask assumed the worst conditions and the critical evaluation was based on the burnup credit. The result of preliminary criticality safety analysis shows that the critical margin was larger than expected.

REFERENCES

- [1] Division of Spent Fuel Storage and Transportation Interim Staff Guidance - 8, Revision 3 - Burnup Credit in the Criticality Safety Analyses of PWR Spent Fuel in Transportation and Storage Casks, 2012.
- [2] J.C. Wagner, M. D. DeHart, and, C. V. Parks, Recommendations for Addressing Axial Burnup in PWR Burnup Credit Analyses, US NRC, NUREG/CR-6801, Oak Ridge National Laboratory, 2003.
- [3] Scale. A Comprehensive Modeling and Simulation Suite for Nuclear Safety Analysis and Design, Version 6.1, 2011.

Evaluation of Cesium Trapping Characteristic With SA Filter

Seok-Min Hong*, Jae-Hwan Yang, Do-Youn Lee, and Yung-Zun Cho

Korea Atomic Energy Research Institute, 111, Daedeok-daero 989beon-gil, Yuseong-gu, Daejeon, Republic of Korea

*seokminhong@kaeri.re.kr

1. Introduction

An accumulation of spent fuel has brought a considerable interest due to its energy and environmental issue. Pyroprocessing has been investigated in Korea Atomic Energy Research Institute (KAERI) which reduces the accumulated spent fuel and increases the efficiency of fuel cycle. In head-end process of pyroprocessing, UO_2 pellets are produced from a fuel bundle and various radioactive gases from a spent fuel are released during thermal treatment. Within these gases, Cs-137 is a semi-volatile gas which had very high radioactivity, and therefore it is important to trap Cs.

It is well known that Cs highly reacts with aluminosilicate to form $\text{CsAlSi}_2\text{O}_6$ or CsAlSiO_4 , and these structures are very stable in storing for long period. KAERI had developed a silica-alumina (SA) filters from kaolinite and had confirmed that it is effective in trapping Cs [1]. It is advantageous to fabricate SA filters because the size, shape, and porosity can be easily controlled by using suitable support material. In this study, SA filters were fabricated and the capture characteristic was investigated by using highly developed trapping system with SA filters.

2. Experimental Section

The silica-alumina (SA) based filters were prepared from kaolinite. Kaolinite ($\text{Al}_2\text{Si}_2\text{O}_5(\text{OH})_4$)

solution was mixed with 2wt% PVA solution and sprayed to polyurethane sponge and for several times and then calcined at 1200°C for overnight in air. The fabricated SA filters were placed in horizontal alumina tube and reduced at 1000°C for overnight using 4%- H_2 based Ar gas.

The Cs trapping system was consisted of two high temperature regions; vaporization and adsorption zones.

Cs_2CO_3 was placed in the alumina boat in the center of the vaporization zone and temperature fixed to 1100°C . In the adsorption zone, a horizontal Inconel cartridge was filled with cylindrical SA filters as shown in Fig. 1. The temperature of adsorption zone is operated at 1000°C for Cs to react SA filters. For the untrapped gas, Cs particles might be condensed on the condensation zone at low temperature, and the water scrubbers were installed at the end of the system for aqueous absorption. The trapping atmosphere was ~ 1.5 bar in alumina tube caused by four water scrubbers and the flow rate was 1 L min^{-1} .

3. Cs Trapping Characteristic

Cs trapping efficiency was calculated based on the mass increased on the SA filters after Cs_2CO_3 vaporization. In addition, Cs concentration of water in scrubbers can be used chemically analyzed to evaluate the trapping characteristic.

4. Conclusion

Trapping process was designed for Cs capture using trapping system with SA filters. Cs trapping performance was investigated and it was confirmed that most of Cs vaporized were effectively captured in the trapping system using SA filters.



Fig. 1. SA filters and SA filter cartridge.

REFERENCES

- [1] Jae Hwan Yang et al., “A kaolinite-based filter to capture gaseous cesium compounds in off-gas released during the pyroprocessing head-end process”, *Annals of Nuclear Energy* (2017), Volume 103, page 29–35.

A Study on Electrochemical Characteristics Aluminum Multi Matrix Compound (Al-MMC) of Neutron Absorber Material

Jung Hwan Lee, Yunju Lee, Seung Chang Yoo, Seunghyun Kim, and Ji Hyun Kim*

Ulsan National Institute of Science and Technology, 50, UNIST-gil, Eonyang-eup, Ulju-gun, Ulsan, Republic of Korea

*kimjh@unist.ac.kr

1. Introduction

In a Spent Nuclear Fuel (SNF) pool, a neutron absorber has been used to inhibit neutronic coupling between fuel assemblies and to maintain fuels in a subcritical condition. Among them, a composite of aluminum-boron carbide is used because it's the compatibility in radiation and elevated temperature environment. [1] However, it has been reported that neutron absorber materials suffer from pitting corrosion and galvanic corrosion in SNF pool, 2500 ppm boron, as boric acid environment, which is like that of SNF pool [2]. Therefore, to investigate the degradation behavior of Al/B₄C corrosion behavior of the composite is investigated by exploiting electrochemical techniques. And its microstructure and chemistry are analyzed by electron microscopy.

2. Experimental

2.1 Materials Preparation

To geometry of specimen is presented in the Fig 1., and the dimension of specimen was 2.54 cm * 5.1 cm * 0.7 cm. It consists of Al 5052 outer clad tightly bound to an inner core of Al 1070 with boron carbide. For the electrochemical tests, the cross section of specimen is prepared to investigate the galvanic corrosion between the outer clad and the inner core. The cross section of the composite was polished with 320, 400, 600, and 800 grit Si-C papers and 0.25 μm diamond suspension.

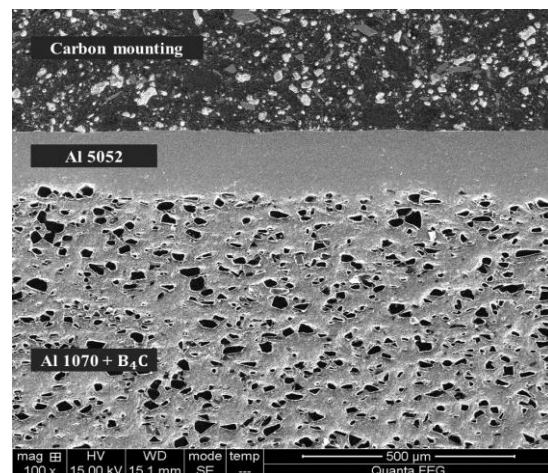


Fig. 1. Cross section results about Al – MMC.

2.2 Electrochemical Test

In electrochemical test, combined measurement of potential and current relationships for an operating corrosion cell over a wide range of oxidizing conditions results in polarization curves that describe the electrochemical reactions. The specimens for electrochemical test were positioned into an electrochemical cell with 1.0 cm^2 surface immersed in air saturated and 3.5wt. % NaCl solution for 3600 seconds to measure open circuit potential (OCP).

Potentiodynamic Electropolarization (PE) was conducted by the potential at open-circuit with a scan rate of 0.1667 mV s^{-1} from -0.5 V to 1.5 V (vs SCE). The potentiodynamic curves were plotted with potential vs current density. The electrochemical tests (OCP, PE) were performed in Al - MMC's cross section and surface respectively.

3. Results and Discussion

3.1 OCP and PE results of Al – MMC

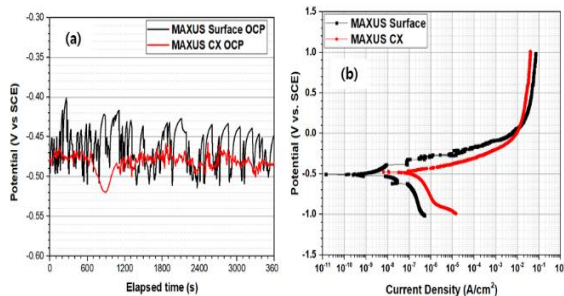


Fig. 2. OCP and PE result of Al – MMC.

Experiments were performed at 3.5wt.% NaCl solution. Unstable OCP curve appears to be related to pit formation and galvanic corrosion. [3] Some passive regions appear to be short. Passivity is lost due to the pitting corrosion of the surface Al cladding.

3.2 Cross section of Al - MMC after electrochemical test

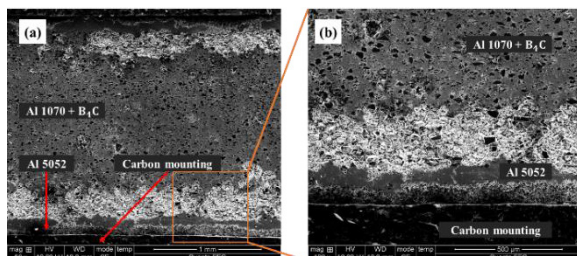


Fig. 3. After electrochemical test cross section (a) and bottom (b).

In Fig 3., Al/B₄C corrosion has been actively occurred near Al cladding. Mainly Al was oxidized, B₄C was not oxidized. It can be seemed occurrence galvanic corrosion between Al 1070 and Al 5052.

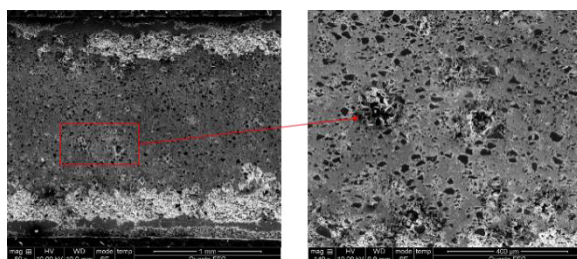


Fig. 4. Possible pitting corrosion on material's edge.

In Fig 4., the SEM image shows a site that is believed to have caused pitting corrosion. [4] The diameter of the corrosion estimated by pitting corrosion is 50 μm .

4. Summary

Al - MMC, used as a neutron absorber, shows pitting corrosion and/or galvanic corrosion in 3.5wt.% NaCl solution. If pitting corrosion penetrates the core, neutron absorption performance could be affected. Galvanic corrosion was observed between Al 5052 and Al 1070, and pitting corrosion was observed around B₄C.

ACKNOWLEDGEMENT

This work was supported by KOREA HYDRO & NUCLEAR POWER CO., LTD (No. 2017-RFP-2018-Tech-18-1) and by the Human Resources Development of the Korea Institute of Energy Technology Evaluation and Planning (KETEP) grant funded by the Korea Government Ministry of Trade Industry and Energy (MOTIE) (No. 20174030201430).

REFERENCES

- [1] W. Emma, (2009) Degradation of Neutron Absorbing Materials in Spent Fuel Pool, Nuclear Regulatory Commission, NRC, 2009-2026.
- [2] Description, E., & Amendment, P. L. (2015). Material Qualification Report of MAXUS® for Spent Fuel Storage.
- [3] Sori Won, et al (2018), Corrosion behaviors of friction welded dissimilar aluminum alloys, *Materials Characterization*, 144, 652-660.
- [4] F. LOCKWOOD, et al (1985), PITTING CORROSION OF 5052 ALUMINUM ALLOY. *Application of Surface Science*, 20, 339-346.

Electrochemical Formation of Bi-Hf Alloy in LiCl-KCl for Actinides Separation Process by Density Distribution

Sungjune Sohn^{a),*}, Jungho Hur^{b)}, Seongjin Jeong^{b)}, Jaeyeong Park^{a)} and Il Soon Hwang^{b)}

^{a)} Ulsan National Institute of Science and Technology, 50, UNIST-gil, Eonyang-eup, Ulju-gun, Ulsan, Republic of Korea

^{b)} Seoul National University, 1, Gwanak-ro, Gwanak-gu, Seoul, Republic of Korea

*sungjunes89@gmail.com

1. Introduction

The pyrochemical processing technology for recycling spent nuclear fuel has been developed to recover useful resources and to reduce the longevity of final wastes with the enhanced proliferation-resistance and accident-tolerance. Liquid metal cathodes are effectively used in the pyroprocessing [1, 2]. It is desirable for the proliferation resistance that solubility of actinides in liquid metal are low enough to co-electrodeposit TRU elements as intermetallic particles. It is reported that liquid bismuth is better than liquid cadmium in terms of the greater lanthanide to actinide separation factor [3]. Also the density of Bi is located between lanthanides and actinides, therefore, separation performance can be enhanced. In this study, we investigated electrochemical behavior for Hf element on liquid Bi cathode and potentiostatic electrolysis was carried out. Hf was chosen as an actinides surrogate since Hf has similar redox potential on Bi cathode and intermetallic density with Bi compared with actinides.

2. Experimental

2.1 Apparatus and materials

Experiments were carried out in a glove box filled

of argon gas with 99.999% purity. The oxygen and moisture concentrations were maintained below 0.1 ppm. The temperature of molten salts was maintained at 500°C to a stability within $\pm 2^\circ\text{C}$. Three electrodes system was applied to electrochemical experiments. Liquid Bi and graphite rod were utilized for working electrode and counter electrode, respectively. Reference electrode was Ag/AgCl (1wt. %). Eutectic LiCl-KCl (Sigma Aldrich, 99.99%) and HfCl₄ (Alfa Aesar, 99.9%) was used as an electrolyte.

2.2 Experiments

CV technique was employed to investigate the redox behavior on the liquid Bi film electrode and to identify electrochemical intermetallics formation of Bi and Hf. To produce Bi film electrode, BiCl₃ was loaded into the molten salt at 500°C. When the potential scan is started from Bi reduction potential toward to negatively, Bi³⁺ is reduced to the tungsten and then Hf can be reduced to the Bi filmed electrode. Potentiostatic electrolysis was carried out to form Bi-Hf alloy. After electrolysis, liquid Bi cell was solidified to reveal the vertical distributions. The ingot cross section was microscopically and crystallographically analyzed to investigate the stoichiometry of intermetallic phase and the vertical location of intermetallic particles in Bi.

3. Results and Discussions

3.1 Cyclic voltammetry

Figure 1 presents cyclic voltammogram of HfCl_4 (1.20wt.%) on liquid Bi electrode at 500°C. As the scan was made from positive to negative potential, Bi^{3+} is reduced to Bi metal and the Bi metal is filmed at the W electrode surface at around +0.2 V. The second reduction peak and the second oxidation peak are attributed to redox couple of Hf^{4+} on the Bi film electrode. As the redox peak seems to be irreversible, exchange current density was explored prior to derive apparent standard potential. Tafel plot was built and exchange current density is calculated to be $3.13\text{E-}2 \text{ A/cm}^2$. Apparent standard potential is derived to be -1.047 V.

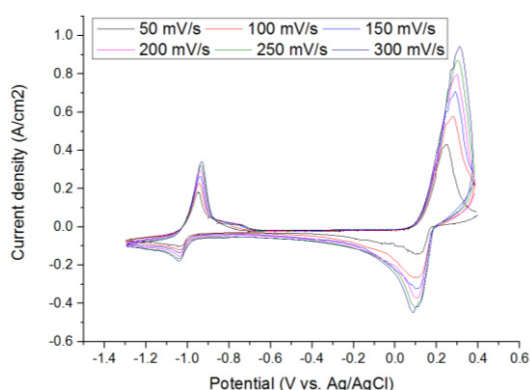


Fig. 1. Cyclic voltammogram of LiCl-KCl-HfCl_4 (1.20wt.%) on liquid Bi film working electrode at 500°C.

3.2 Potentiostatic electrolysis

Potentiostatic electrolysis were carried out to produce Bi-Hf alloy at 500°C. Constant cathodic potential of -1.1 V was applied that the potential was determined from the apparent standard potential derived by CV. The top phase is equivalent to the liquid Bi cathode surface. Almost all intermetallics was shown to locate at the bottom of Bi. The

boundary layer seems to be clarified between Bi bulk and Bi-Hf intermetallic riched phase. Hf was not found from the stoichiometric analysis by EDS for the Bi bulk. Regarding the detection limit of on the EDS apparatus is within the range of 1 at. %, Hf can be attributed to exist as much as its solubility in Bi. For the bottom phase, the atomic ratio of Hf to Bi is close to 1 for the intermetallics particles by EDS and that can be explained to HfBi . Since the density of liquid Bi and HfBi is 9.75 g/cm^3 and 12.6 g/cm^3 , respectively, the results of spatial distribution of HfBi is reasonable. Also, Hf is shown to be separated in liquid Bi media.

4. Conclusions

In order to investigate actinides behavior in liquid Bi electrode, Hf was selected as a surrogate and CV and electrolysis was carried out. Electrochemical redox behavior was observed from the CV. As the results of electrolysis, HfBi intermetallics were analyzed at the bottom of the Bi alloy and it is well agreed with the density information. Therefore, the feasibility of actinides separation could be shown in Bi.

REFERENCES

- [1] Chemical Technology Division, Annual technical report, ANL, 1994.
- [2] T. Koyama et al., Journal of Nuclear Materials 247: 227-231, 1997.
- [3] K. Kinoshita et al., Journal of Nuclear Science and Technology 36(2): 189-197, 1999.

CFD Simulation of Molten-Salt Suction Drain from a Pyrochemical Reactor

Kwang-Rag Kim*, Sung-Ki Kim, and Hyo-On Nam

Korea Atomic Energy Research Institute, 111, Daedeok-daero 989beon-gil, Yuseong-gu, Daejeon, Republic of Korea

*krkim1@kaeri.re.kr

1. Introduction

Pyrochemical processing based on molten-salt electrolysis is preferred over the conventional wet process for treating spent nuclear fuels in view of several advantages such as its simplicity and less secondary wastes, etc. [1]. This process typically involves the dissolution of spent fuel into a molten-salt media.

The transfer of molten-salt to a next unit process is one of the most common and important operations in the molten-salt based integrated pyroprocessing technology. During the handling radioactive molten-salt fluids, the important issues are maintaining containment and preventing dose exposure for operators.

A transport application of the mechanical pumps has significant disadvantages in this area of the high-temperature molten salt system because of the leakage problems and maintenance of moving parts.

Recently, no-moving-parts pumping technologies have been tested in the molten salt applications such as gravity transfer or suction pumps [2].

In this study, a CFD (Computational Fluid Dynamics) modeling approach was proposed and simulated to illustrate the suction behaviors in the molten-salt tank draining system.

2. Theory

2.1 Free surface model

Free surface with a immiscible fluid flow is encountered in the multiphase system of salt-argon.

The numerical model directly solves the equations governing an incompressible isothermal multi-fluid flow within a CFD platform. The dynamics of two (or more) immiscible fluids are governed by the Navier-Stokes and continuity equations [3]:

$$\nabla \cdot U = 0 \quad (1)$$

$$\frac{\partial U}{\partial t} + \nabla \cdot UU = -\frac{1}{\rho} \nabla P + \frac{1}{\rho} \nabla \cdot \tau + g + \frac{1}{\rho} S \quad (2)$$

where t , U , P , g , S , ρ , and μ represent the temperature, velocity, pressure, stress tensor, acceleration due to gravity, surface force due to surface tension, density and viscosity of the fluid.

2.2 VOF model

In addition, the modeling of the free surface flow (or multiphase flow) requires a further coupled volume tracking approach. A recognized method is the so-called VOF (volume of fluid) models, which incorporate a moving free boundary [4]. This is done by defining a volume fraction F (or degree of filling) in each computational cell, which can take the following values:

$$F = \begin{cases} 1 & \text{in cells full of a particular fluid} \\ 0 & \text{in cells devoid of that particular fluid} \\ 0 < F < 1 & \text{cell contains free interface} \end{cases} \quad (3)$$

The location of the interface is not explicitly tracked, but is instead captured by the distribution of F , since F takes the values $0 \leq F \leq 1$ in interface cells. In order to track the location of the interface, a continuity equation for F is established in the following form:

$$\frac{\partial F}{\partial t} + \nabla \cdot (UF) = 0 \quad (4)$$

The equations presented above can be solved numerically using the commercial CFD code, in which the control volume method is used to discretize the transport equations.

3. Results and discussion

Tank draining of high temperature molten-salt system was simulated using the volume of fraction model in a CFD platform. This approach is a volume tracking technique applied to a fixed Eulerian mesh.

Representative simulation results are presented to illustrate the capabilities of this method for a molten-salt/argon system. Simulation is transient and solved as a two immiscible multiphase fluid. The salt level is decreased during that salt flows out the transport pipe generated from a suction effect which effectively empties the tank (Fig. 1). The salt level fluctuation was slightly observed in the CFD demonstration.

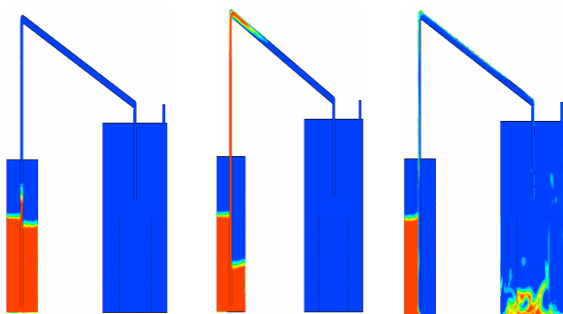


Fig. 1. CFD Simulation of Molten-Salt Suction Drain.

4. Conclusion

A CFD model has been demonstrated to simulate the draining out of a molten-salt tank using a suction dip system. It was found that this approach was capable of tracking a technology of salt transport system.

REFERENCES

- [1] OECD NEA, "Spent Nuclear Fuel Reprocessing Flowsheet," NEA/NSC/WPFC /DOC, Paris, 15 (2012).
- [2] E. Mullen et al., "Transfer Characteristics of a Lithium Chloride-Potassium Chloride Molten Salt," Nuclear Engineering and Technology, 49, 1727-1732 (2017).
- [3] V. G. Levich, Physicochemical Hydrodynamics, Chapter XI, Prentice Hall, Englewood Cliffs, New Jersey (1962).
- [4] C.W. Hirt and B. D. Nichols, "Volume of Fluid (VOF) Method for the Dynamics of Free Boundaries," Journal of Computational Physics, 39, 201-225 (1981).

Automation System for the Pyroprocessing Automation Verifying Mockup

Dongseok Ryu*, Jongkwang Lee, Jonghui Han, and Seungnam Yu

Korea Atomic Energy Research Institute, 111, Daedeok-daero 989beon-gil, Yuseong-Gu, Deajeon, Republic of Korea

*sayryu@kaeri.re.kr

1. Introduction

Various fuel cycles replacing the classical reprocessing method have been explored at KAERI. The Pyroprocessing was studied as one option of the fuel cycles. Several pieces of electrolytic equipment are essential for the Pyroprocessing, and those used molten salt. Various experiments with the equipment have been conducted in radiation area by using simulated fuel. After the experiments, the used material, tools, or devices in the radiation area are regarded as radiation waste. The more experiments were conducted, the more waste were stacked in the radiation area. The use of molten salt made worse to increase the radiation waste, because the molten salt is highly corrosive and damages equipment. Various parts of experimental equipment have been destroyed and disabled in the molten salt.

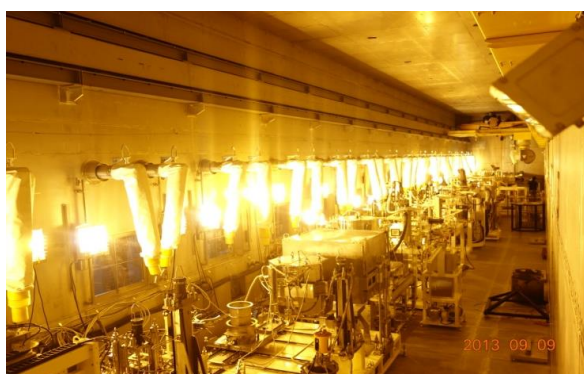


Fig. 1. conventional facilities for Pyroprocessing in radiation area.

The needs for the non-radiation experimental space were demanded only for molten salt test. The reliabilities of mechanical parts interacting with molten salt should be thoroughly examined in

advance to conduct a radiation experiment. When the humidity in air is regulated as low enough to mitigate chemical reactions, The reliability of equipment against molten salt can be tested the dry air environment. A dry room is planned for the purpose, and new concept for handling of basket to immerse into molten salt was proposed. Finally, the dry room installed the automated handling device, as named Pyroprocessing Automation verifying mockup (PAVM), was designed. The remainder of this paper explains the PAVM and the automation system.

2. Pyroprocessing Automation Verifying Mockup

Pyroprocessing Automation Verifying Mockup (PAVM) was designed for molten salt test of the developed equipment [1]. The PAVM is designed to strictly control the humidity, and the dew point inside is designed to be under -40 degree Celsius. The space of the PAVM is planned to locate two pieces of different engineering scale equipment, so that the basket handling can be examined in between neighboring equipment. An automation system to handle the basket was designed to be installed on ceil. The figure shows 3D design of the PVAM and the automation system.

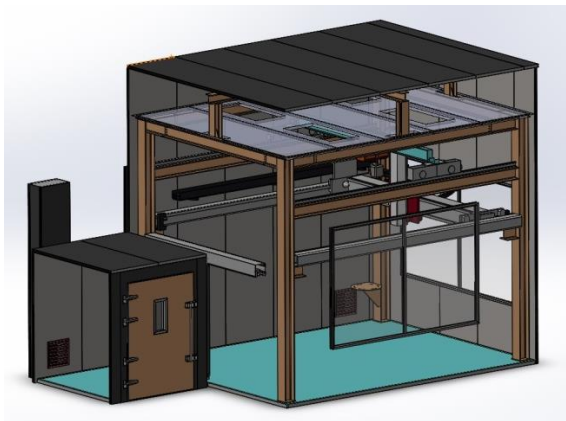


Fig. 2. 3D design of the PVAM.

3. Automation System in the PAVM

In the radioactive area, the experimental space is enclosed in a glove box or a processing cell, and human workers are not allowed to access into the space. Several remote systems, such as a conventional MSM (Master slave manipulator) and crane, are utilized to handle material or to control equipment.



Fig. 3. human worker controls the automation system in the PVAM.

The PAVM is different from the conventional radioactive space, and human workers can access into the experimental space, as shown in Fig 3. Therefore, MSM is not required anymore, but the crane is still useful to move heavy part or material.

The most frequent and difficult task was moving

the material basket from equipment to the other [2]. An automation system is designed to dedicate the basket handling. In advance to the experiment, human worker predefines several positions to make the path for transporting the material basket, such as, an installed position on equipment, a moved position on the other equipment, and a waiting location on station. After teaching several paths, human worker easily control the automation system out of the PVAM, looking inside how the basket moves. Finally, the basket handling in the PVAM is easily accomplished under the control of one human worker.

4. Conclusion

The PAVM, a new experimental space for non-radioactive experiment, was designed to examine the reliability of equipment against molten salt. An automation system is designed for the PVAM. The installation of the automation system is underway.

REFERENCES

- [1] Dongseok Ryu, et al. "Needs and Goals of the Pyroprocessing Automation Verifying Mockup," Proc. of KRWS 2017 Fall, pp. 53-4, (2017).
- [2] Dongseok Ryu, et al. "Example Operating Procedure for an Automation Concept of Electrochemical Process," Proc. of KRWS 2017 Spring, pp. 151-2, (2017).

Development of Standard Reference Data of Nuclear Fuels and Materials

Kweon Ho Kang*, Seok Min Hong, Jae Hwan Yang, and Yong Jun Cho

Korea Atomic Energy Research Institute, 111, Daedeok-daero 989beon-gil, Yuseong-gu, Daejeon, Republic of Korea

*nghkang@kaeri.re.kr

1. Introduction

Nuclear energy is categorized as the most economic and sustainable energy by IAEA. However, demand and needs for safety and reliability of nuclear industry are increasing after FUKUSHIMA. Especially, reliable data on the stability of nuclear fuel in a reactor and spent fuel is necessary for safety analysis of nuclear reactor and spent fuel.

In this study standard reference data were developed and uploaded to the database of national standard reference center.

2. Nuclear Fuel and Materials Data Center

NFDC (Nuclear Fuel and materials Data Center) is designated as a one of the data center of National Standard Reference Center from Ministry of Trade Industry and Energy at Dec. 30 2018. The fields of designation were nuclear fuel and energy materials. Target materials that we aim to produce standard reference data include the nuclear fuels such as uranium metal, uranium oxide, and spent fuel and the nuclear cladding materials, such as Zircaloy-4, Zirlo, and HANA. Specifically, we plan to generate the reference thermal properties such as thermal expansion, density, thermal conductivity, and specific heat to analysis the thermal stress of cladding materials, the temperature profile of nuclear fuel, and the heat transfer through the fuel and cladding materials. We also plan to produce the mechanical properties to analysis the PCMI (pellet cladding mechanical interaction). Finally, we plan to produce the chemical properties to analysis the PCCI

(pellet cladding chemical interaction). Table 1 shows the yearly-basis road map for incorporating standard reference to nuclear fuel and materials data center.

Table 1. Road map of nuclear fuel and materials data center

	2009	2010	2012	2013	2014	2018	2019	2020
Direct Measurement		UO ₂ Thermal expansion	Zircaloy Thermal expansion	Zirlo Thermal expansion	Zircaloy Thermal Diffusivity	Zircaloy Oxidation	Zircaloy strength	Zircaloy Creep
		UO ₂ Density	Zircaloy Density	Zirlo Density	Zirlo Thermal Diffusivity	Zirlo Oxidation	Zirlo strength	Zirlo Creep
		Simulated fuel thermal expansion	Zircaloy Specific heat	Zirlo Specific heat				
		Simulated fuel Density						
Indirect collection		UO ₂ Creep						
		U Creep						
		UO ₂ Specific heat						
		U Specific heat						

3. Produce Standard Reference Data

Data collection follows the data collection procedure [1] established by NFDC. There are two kinds of method in data collection. In direct method, the data is collected through the direct measurements, and in indirect method, the data is obtained from published papers, database, reports and books. Uncertainty of collected data should be evaluated following the guide to expression of uncertainty in measurements. [2] The result of measurement informs the magnitude of a quantity, obtained experimentally. The standard reference data present an estimate \pm uncertainty.

Table 2 shows the standard reference data, which were produced from nuclear fuel and materials data center.

Table 2. The standard reference data produced from nuclear fuel and materials data center

Standard Reference Data	Condition	Grade	Resistration	Year
UO ₂ Specific heat	293~3000 K	Certificated	56	2009
U Specific heat	293~900 K	Validated	14	2009
UO ₂ Creep	1473~2073 K	Validated	133	2009
U Creep	1473~2073 K	Validated	19	2009
UO ₂ Thermal expansion	300~3100 K	Certificated	57	2010
UO ₂ Density	300~3100 K	Certificated	57	2010
Simulated fuel thermal expansion	300~1500 K	Certificated	87	2010
Simulated fuel Density	300~1500 K	Certificated	87	2010
Zircaloy Thermal expansion	323~1473 K	Certificated	44	2012
Zircaloy Specific heat	298~673 K	Reference data	16	2012
Zirlo Thermal expansion	340~780 K	Certificated	12	2013
Zirlo Density	340~780 K	Certificated	12	2013
Zircaloy Thermal Diffusivity	400~800K	Validated	17	2014
Zirlo Thermal Diffusivity	400~775 K	Validated	16	2014
Total			627	

4. Uncertainty Evaluation

To ensure reliability of experimental data uncertainty should be estimated. There are two kinds of uncertainty: A-type uncertainty from tester and B-type uncertainty from experimental equipment. To reduce the former, the measurement should be repeated for sufficient amount of times, and to reduce the latter type uncertainty all equipment have to be calibrated.

Fig. 1 shows the procedure of uncertainty evaluation; establishing the measurement model, analysis factors affected to uncertainty, uncertainty evaluation of each factor using sensitivity coefficient, calculation of combined uncertainty, and calculation of expanded uncertainty using coverage factor.

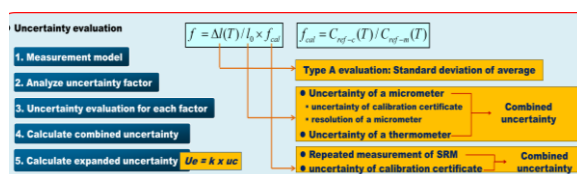


Fig. 1. Procedure of uncertainty evaluation.

5. Database of Nuclear Fuel and Materials Data Center

To supply and service the standard reference data produced from NFDC the database based on website were constructed. The address of URL is www.numat.re.kr. Graph and model as well as standard reference data are serviced in the database. Fig. 2 shows the website of NFDC, which contains the specification of materials, standard reference data, graph and model representing the data, and the reference.



Fig. 2. Website of NFDC.

6. Conclusion

The standard reference data produced in NFDC will be helpful for increasing reliability and stability evaluation of nuclear fuel and spent fuel.

ACKNOWLEDGEMENT

This work was supported by the Korea Institute of Energy Technology Evaluation and Planning (KETEP) granted financial resource from the Ministry of Trade, Industry and Energy.

REFERENCES

- [1] Korea Reference Standard Center, Nuclear Fuel and Material Data Center, "The Procedure of Collection/Production for Nuclear Fuels and Materials Properties" LOP-NFDC-CG-01, (2018).
- [2] Korea Research Institute of Standard Science, "KRISS Guide to the Expression of Uncertainty in Measurement, KRISS-98-096-SP (1998).

Effect of Hydrogen on Mechanical Behavior of Zr-based Alloy Fuel Cladding at High Temperature

Dong Jun Park*, Yang Il Jung, Jung Hwan Park, Byoung Kwon Choi, Young Ho Lee, and Hyun Gil Kim
Korea Atomic Energy Research Institute, 111, Daedeok-daero 989beon-gil, Yuseong-gu, Daejeon, Republic of Korea

*pdj@kaeri.re.kr

1. Introduction

The nuclear fuel cladding should maintain good performance without serious degradation under not only normal operating conditions, but also various accident condition. Therefore, it is very important to investigate the behavior or performance of fuel cladding under various range of temperature. At the present, however, most of research results have been obtained from non-pressurized claddings specimens. However, integrity of fuel cladding can be significantly affected by ballooning and rupture that caused by pressure difference between inner and outer cladding. Ballooning may cause the fuel relocation or fuel dispersal due to its rupture opening during accidents. In addition, wall thickness of cladding can be reduced and local regions near the rupture open would become heavily oxidized and hydrided [1]. Therefore, integral test that can simulate pressure difference should be carried out for comprehensive safety analysis. Although a number of researches have been conducted, most investigations of them were performed using as-received cladding specimens.

In this study, mechanical behavior of zirconium based alloys cladding was investigated by high temperature test and high burnup effects on the ballooning behavior of fuel cladding were also examined using H charged cladding sample..

2. Experimental Procedure

Figure 1 shows the schematic illustration of

integral LOCA test apparatus used in this study. For integral LOCA tests, 400 mm long cladding sample was used and filled with 10 mm-long alumina pellets to simulate the heat capacity of the fuel. The stack length of these pellets was about 360 mm long. The pressure was injected through stainless tube at the top and the cladding specimen was supported at the top to minimize specimen bowing. For comparison study, as-received and prehydrided (300 wppm) cladding sample were used. The Specimen temperature was measured by type-R thermocouple located near the sample center and the quartz tube provides an enclosed volume for steam flow and water quench, both of which are into the chamber, furnace heating started for a pre-test hold temperature of 300°C.

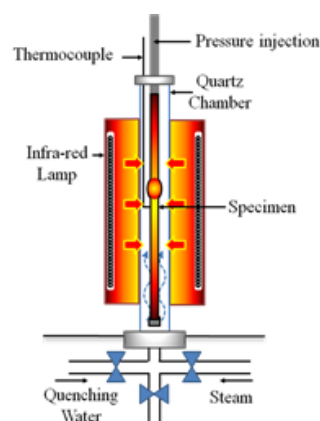


Fig. 1. Schematic illustration for the integral LOCA apparatus.

Steam flow and 300°C of sample temperature were stabilized within 180 s. Heating rate was 28°C/s from 300°C to 1200°C. After oxidation at 1200°C with hold time of 300s, the tube was cooled slowly and quenched at $\approx 800^\circ\text{C}$ by bottom flooding..

3. Results and discussion

Cross-sectional images of the test samples of Zr alloy cladding were obtained at burst midplane and shown in Fig. 2. Figs. 2 (a) and (b) show a burst behavior with heating rate of 28 C/s. As received and prehydrided (300 wppm) sample shows similar circumferential strain at burst midplane. On the other hand, Zr alloy claddings with heating rate of 1 C/s show a significant difference in circumferential strain. Prehydrided (300 wppm) sample shows a lower circumferential strain than that of as-received sample. Fig. 3 shows burst temperature and maximum circumferential strain of as-received and H charged samples after the test. H precharged cladding samples shows much lower burst temperature regardless of their heating rate [Fig. 3(a)].

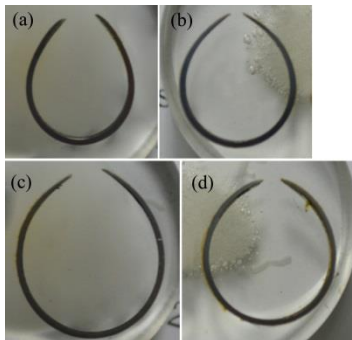


Fig. 2. Cross-sectional optical micrographic images at burst midplane for (a) as-received cladding with heating rate of 28 C/s, (b) prehydrided (300 wppm) cladding with heating rate of 28 C/s, (c) as-received cladding with heating rate of 1 C/s, and (d) prehydrided (300 wppm) cladding with heating rate of 1 C/s.

Burst strain at the location of rupture generally depends on temperature, internal pressure, and heating rate. Fig. 3 (b) shows burst strain as a function of heating rate. Internal pressure was fixed as 8 MPa. Difference in maximum circumferential strain of as-received and prehydrided cladding was increased with decreasing heating rate.

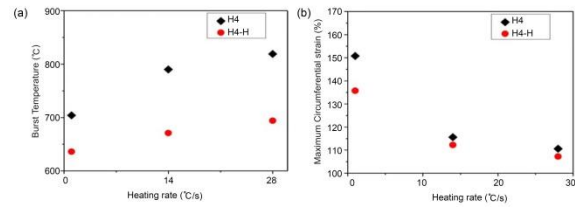


Fig. 3. (a) Burst temperature and (b) maximum circumferential strain as a function of heating rate for H4 and H4 cladding specimens.

4. Conclusion

To investigate the high burnup effects on rupture behavior of fuel cladding at high temperature, H charged claddings were examined. Prehydrided cladding shows the lower burst temperature and circumferential strain than that of as-received cladding. These results indicate that hydrogen uptake in high burnup fuel cladding may affect significantly on the burst behavior at high temperature.

ACKNOWLEDGEMENT

This work was supported by the National Research Foundation of Korea (NRF) grant funded by the Korea government (MSIP) (No. 2017M2A8A5015058).

REFERENCES

- [1] M. Billone, Y. Yan, T. Burtseva, and R. Daum, Cladding Embrittlement during Postulated Loss-of-Coolant Accidents, NUREG/CR-6967, 2008 (available online in NRC ADAMS as ML082130389 at <http://www.nrc.gov/NRC/reading-rm/adams.html>).

Optimum Angle of Cutting Roller of 2-Row Blades Slitter for Rod-cuts

Younghwan Kim*, Yungzon Cho, and Youngsoon Lee

Korea Atomic Energy Research Institute, 111, Daedeok-daero 989beon-gil, Yuseong-gu, Daejeon, Republic of Korea

*Yhkim3@kaeri.re.kr

1. Introduction

Mechanical head-end processing of SF disassembly, extraction of the rods, and the shearing of the extracted rods shall be performed in advance as the head-end process of the pyro electro-reduction process. Also, in the head-end process, for oxidation treatment of the spent fuel, a 2-row blades slitter for decladding the cut rods is necessary. Major requirements were based on KSFA type (16x16) rods. For the 2-row blades slitter performance evaluation, the simulated rods of zircaloy (Zry-4) were used to carry out the 2-row blades slitter performance test, and in the 2-row blades slitter method, the enhancement plan for horizontal device was derived. Also, for the slitting test, prototype 2-row blades slitter was made, the device is driven with hydraulic pressure, and it is composed of driving part, step input part, slitting part, and fuel supply part. As a result, the enhancements were derived. Also, the optimal angle of the cutter angle that can process multiple types of nuclear fuel rods was obtained, and the enhancements after the test were reflected for the enhanced design of the 2-row blades slitter.

2. Two-row blades slitter Test

2.1 Decision of the optimal angle of the roller

As in Fig. 1, to split multi type of PWR assembly rods, the optimal angle of the roller is obtained. If the contacting surface of the roller and the rods is a round shape, it can only handle 1 type of the rods. Therefore, we made the roller contact surface as a straight line to process various rods.

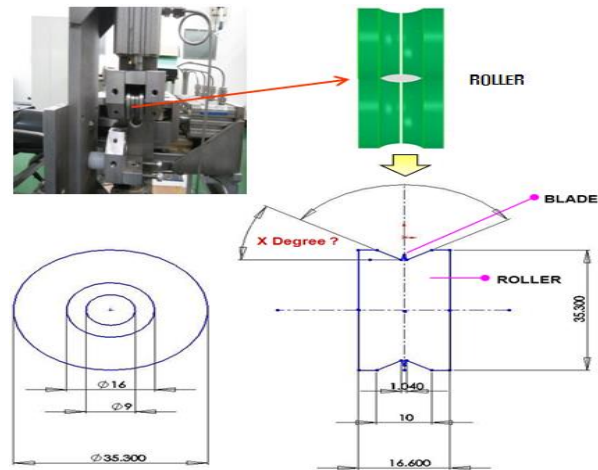


Fig. 1. Two-row blades slitter roller.

As in Fig. 2, to decide the optimal angle, the outer diameter and inner diameter averages of the domestic PWR assembly rods were obtained, and the optimal angle of 32.7° was assumed. Also, Solid works was used to match the cutter roller and each rod for the verification. As a result, each rod was within the cutting boundary.

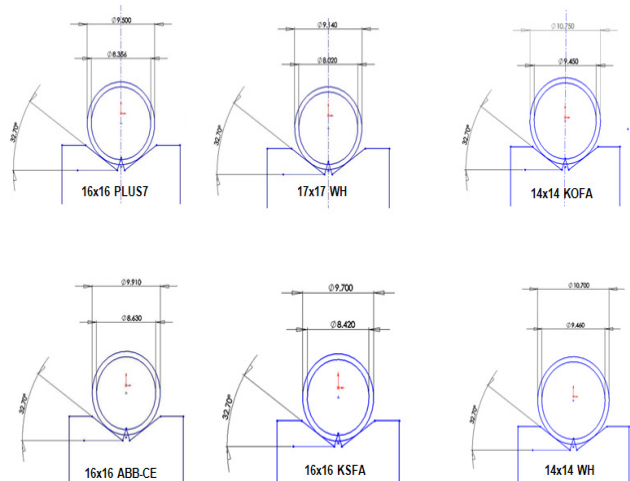


Fig. 2. Roller optimal angle for slitting (32.7°).

2.2 Two-row blades slitter enhancements

Zircaloy rods were used to carry out the 2-row blades slitter performance test (Fig. 3-(a)). As in Fig.

3-(b), rods were not split by the leveled force of step input part and slitting part with the hydraulic driving. Therefore, independent hydraulic system enhancement is required for each part. Also, the problem in the progress of the following rods and the remaining sheared rods processing problem shall be enhanced.

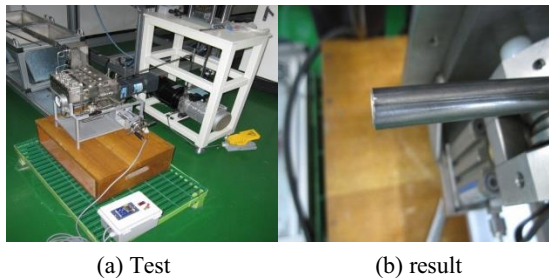


Fig. 3. Capacity test of horizontal 2-row blades splitter.

As in Fig. 4, the enhancements for 2-row blades splitter were derived by the horizontal device performance test. To reinforce the friction of the step input part roller, knurling was reflected in the roller guide surface, and in the double driven hydraulic system shall be changed to single driven type with elastic recovery power. Also, in the hydraulic driving system, it shall be driven with the driving part composed of 2 hydraulic utilities, the slitting part roller enhancement is required, and it was composed of 2 level structure roller slitting parts. The above enhancements were reflected in the enhanced design of the 2-row blades splitter. In the future, using the enhanced device, the performance comparison against the slant slitting device will be carried out through the simulated rods slitting test.

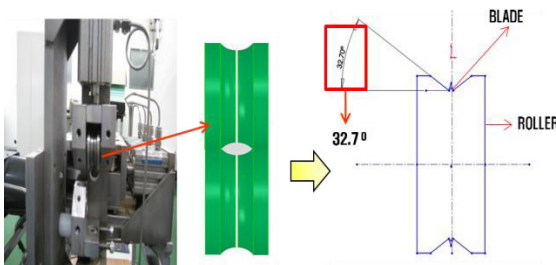


Fig. 4. Improvement item of 2-row blades splitter.

3. Conclusion

Simulated nuclear fuel rods were used to carry out

the 2-row blades splitter performance evaluation. Also, Solid works was used for modeling of multi types of the rods, and as a result of matching and verifying the cutter roller and various rods, the optimal angle of the cutter roller for multi types of PWR assembly rods slitting was derived as 32.7° , and as a result of using zircaloy rods for the 2-row blades splitter performance test, the 2-row blades splitter enhancements for hydraulic system, rods step input part, and cutter roller output part, etc. were derived and the design data were obtained.

ACKNOWLEDGEMENTS

This paper is the study carried out with the 2013 funding of the Ministry of Education, Science and Technology and the support from National Research Foundation of Korea (Nuclear Energy Technology Development Project, No. 2012M2A8A5025 696).

REFERENCES

- [1] B. D. Cul, R. H. Hunt, "Advanced head-end processing of spent fuel," 2004 ANS Winter Meeting, Washington DC, Nov. 16, 2004.
- [2] T. Nishimura, Y. Sakamura, T. Inoue, "Conceptual design study of pyroprocessing facilities for LWR MOX fuel using electroreduction and electrorefining techniques," Proceedings of GLOBAL 2005, Tsukuba, Japan, Oct. 9-13, 218, 2005.
- [3] W. Zhao, D. Mitchell, R. Oelrich, "Simulating pellet and clad mechanical interactions of nuclear fuel rod for pressure water reactors," 14th international LS-YNA users conference. 2016.

Characteristic of Zircaloy-fuel Mechanical Interaction in Failed Spent PWR Fuel

Y.H. Jung*, S.J. Baik, and S.B. Ahn

Korea Atomic Energy Research Institute, 111, Daedeok-daero 989beon-gil, Yuseong-gu, Daejeon, Republic of Korea

*nyhjung@kaeri.re.kr

1. Introduction

In typical PWR fuel rods, the end-of-life internal pressure can be significant because of the initial helium backfill pressure and the added pressure from the release of fission gases. Fuel-clad interaction and the formation of fuel-clad bonding layers with specified chemical, physical and mechanical properties are of importance with regard to the evolution of thermal conductivity as well as in the context of a Pellet-Clad Mechanical Interaction (PCMI). It is also important in the framework of the long-term storage of spent fuel where the phases formed at the fuel-clad boundary are considered to be the first to be leached in the case of a cladding failure [1]. The small volume of material analyzed and the easy of quantification made EPMA the ideal analytical tool with which to study the nuclear industry by providing fundamental information about the behavior of nuclear fuel under extreme irradiation conditions and about the performance of new fuel designed for the in-pile incineration of nuclear waste [2].

2. Sample preparation

A thin diamond wheel was used to cut off the samples from a PWR failed spent fuel rod with 53,000 MWd/tU and normal spent fuel rod with 62,000 MWd/tU, which were withdrawn from the nuclear power plant and cooled down for 2 and 4 years, respectively. The samples were embedded in an epoxy resin and polished with diamond grinding disks of successively finer grain size, finishing on cloth with diamond paste of 1 μm as the final stage. Before mounting the sample in the EPMA, the samples were coated with carbon to prevent charging. The carbon-coated specimen was mounted in a holder together with the X-ray standard. The EPMA was performed on a CAMECA SX-50R equipped with a two wavelength dispersive X spectrometer shielded with tungsten.

3. Results and discussions

Fig. 1-A shows an SEM image of failed spent fuel with 53,000 MWd / tU. In the figure, the fuel-clad gap has an empty space of about 10 μm . This is a normal shape observed in spent fuel. At the boundary of the cladding, the fuel portion was observed at a thickness of about 5 to 10 μm , and the thick oxide film was clearly observed in the region corresponding to the fuel portion. Of course, such an

oxide film was not observed over the entire region. Performed a quantitative analysis at a distance of 30 μm as indicated by the arrows on the part of the oxide film observed.

Figure 1-B shows the result of a 30 point quantitative analysis for the fission products. The horizontal axis of the figure is the point analyzed at 1 μm intervals, and the vertical axis is the quantitative analysis value. As shown in the figure, the concentration of the fission product from 1 to 17 points hardly appears, but it shows a rapid increase in the concentration until the oxide film thickness of 17 to 23 points is reached. In particular, the concentrations of Cs and Ce are as high as 0.5wt%. It is considered that the fission products in the fuel-clad gap penetrated into the oxide layer.

Figure 1-C shows the results of a quantitative analysis of O, Zr, and U at 53,000 MWd / tU with failed spent fuel. The zirconium concentration was 42wt% at 15 to 23 points, which is the oxide layer part, and the concentration of oxygen was 58wt%. It is represented through the formula of $\text{ZrO}_{1.8x}$. It was confirmed that the concentration of oxygen was more than twice that of the zirconium dioxide layer. This expansion of the oxide layer not only weakens the properties of the cladding but also has the possibility of breakage.

Figure 1-D shows the results of a quantitative analysis of O, Zr, and U with 62,000 MWd / tU of normal spent fuel. The oxygen concentration at 15 to 25 points is about 15 to 18wt%. At a high burn-up, the oxidation thickness and oxygen concentration in the fuel-clad gap of the spent fuel were much smaller than in Figure 1-C. The concentration distribution of Zr and U at the higher oxygen region is illustrating the general trend for the redistribution in the fuel-clad gap region.

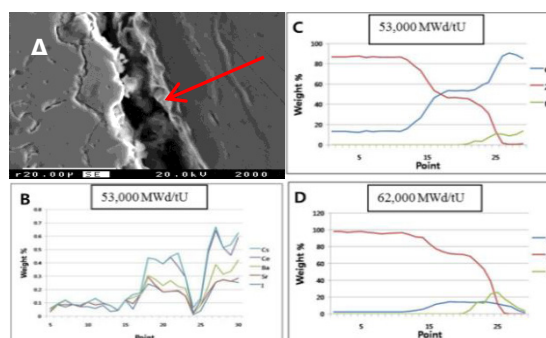


Fig. 1. SEM image of 53,000 MWd/tU and 62,000 MWd/tU fuel rods and quantitative analyses of O, Zr, U and, Cs, Ce, Ba, Sr and I on the marked point.

Fig. 2 illustrates the general trend for the release and cesium redistribution in the fuel-clad gap with 53,000 MWd. The distribution of O, Zr, and U in the figure clearly shows the state at the periphery of the fuel-clad gap. However, the distribution of fission products cannot observe a specific trend. The reason for this is that the concentration of fission product is extremely low, indicating only a general tendency. The distribution of fission products was tested under the same conditions in high burn-up spent nuclear fuel, but no particular trend was observed.

Halogen and iodine are two of the most volatile fission products, and their high release has been reported from early isochronal annealing experiments on irradiated UO₂ at various temperatures. The diffusion coefficient of the halogen in single and polycrystalline UO₂ during irradiation is two orders of magnitude higher than that of xenon.

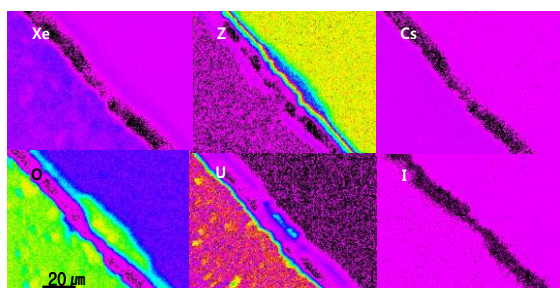


Fig. 2. Image mapping of Xe, Zr, O, U, Cs and I on fuel-clad gap with 53,000 MWd/tU.

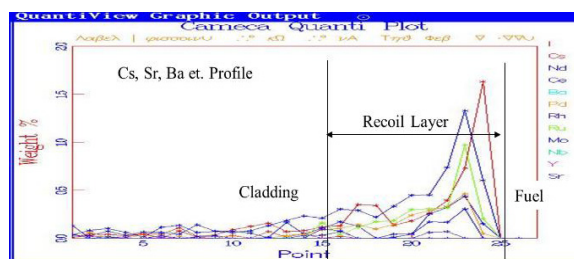


Fig. 3. Distributions of fission products in Recoil layer region with 53,000 MWd/tU.

Fig. 3 shows a qualitative concentration profile along the clad-fuel gap with 53,000 MWd / tU. Zircaloy cladding is known to have a strong affinity for oxygen. The in-reactor corrosion of the cladding typically produces a thin outer layer of oxide 8-40 μm in thickness. Under PWR operating conditions, the oxidation of Zircaloy is suppressed by the time presence of dissolved hydrogen in the primary coolant. However, oxidation rates in air at temperatures of 400 $^{\circ}\text{C}$ can be significantly higher. Thus, at a storage temperature of 400 $^{\circ}\text{C}$, the degradation of cladding due to oxidation is found to be for all of the zircaloy cladding, which will be oxidized. During reprocessing of spent fuel elements, the fuel rods are chopped into pieces a few cm in length and the spent fuel content is dissolved in an acid solution. The remaining hulls are

contaminated with actinides and fission products [3]. The characterization of the hulls is of interest not only for the safety of waste disposal but also for improving the processing process. The cladding materials remain after the processing of nuclear fuel, generally called hulls [4, 5].

4. Conclusion

A failed spent fuel rod with 53,000 MWd/tU and a normal spent fuel rod with 62,000 MWd/tU from a nuclear power plant were characterized to compare and observe the fission products in the fuel-clad gap region using the EPMA. The concentration of fission product shows a rapid increase in the concentration until the oxide film. In particular, the concentrations of Cs and Ce are as high as 0.5wt%. The zirconium concentration was 42wt% at the oxide layer part, and oxygen was 58wt% on 53,000 MWd/tU sample. It is represented through the formula of ZrO_{8x}. It was confirmed that the concentration of oxygen was more than twice that of the zirconium dioxide. The formation of such an oxide layer causes a fatal defect in the integrity of the cladding tube, which can be considered as a fear of damage in the past. On the other hand, it was confirmed that the oxygen concentration of the oxidized layer of normal high burn-up spent fuel was about 15-18wt%.

REFERENCE

- [1] S. Van den berghe, A. Leenaers..., Seminar NEA proceedings on the PCI in Water Reactor Fuels, Aix-en-provence, France, 266, 9-11 March (2004).
- [2] Clive Walker "Electron Probe Microanalysis of irradiated nuclear fuel: an overview" J. Analytical Atomic Spectrometry 1999, 14, 447-452 The MTI Mechanical tester for JEOL-7600: (Info from Jan-Fong on 4-18-2016).
- [3] R. Restani, E.T. Aerne et al. "Characterization of PWR Cladding Hulls from Commercial Reprocessing" Technical Report 92-13, NAGRA (1992).
- [4] In-Ha Jung, et al. "Investigation of PWR Hull with a View to Downgrade" J. Separation Science and Technology, 41(10), 2006.
- [5] Shin J. M. et al. "A state of the art report on the characterization of the spent PWR cladding hull" Technical report. KAERI/AR-630/2002.

3분과

고준위폐기물처분 (Oral)



Vitrification of the Spent Nuclear Fuel Using Iron Phosphate Glasses

Cheong Won Lee*, Sung Gyun Shin, Yong Uk Kye, and Jong Heo

Pohang University of Science and Technology, 77, Cheonam-ro, Nam-gu, Pohang-si, Gyeongsanbuk-do, Republic of Korea

*schwarz@postech.ac.kr

1. Introduction

Average amount of the spent nuclear fuel (SNF) being discharged from the nuclear power plants (NPP) in Korea reached 760 MTU per year. They have been stored in the spent fuel pool inside the NPP and the storages will be saturated by 2024 [1]. Direct disposal inside the deep geological repository has been considered for a safe disposal of SNF. We propose the direct vitrification using phosphate glass can reduce the amount of SNF that needs to be stored inside the repository.

2. Experimental procedure

2.1 Preparation of the glasses

The nominal compositions of the iron phosphate glasses are given in Table 1. Starting powders of $\text{NH}_4\text{H}_2\text{PO}_4$, Fe_2O_3 and Al_2O_3 were mixed and CeO_2 powders were used as a surrogate for UO_2 . Batch mixtures were calcined in alumina crucibles at 220°C for 1 hour and melted at 1300°C for 1 hour. Melts were then quenched by pouring and pressing between two brass molds in the air to form glasses black in color.

Table 1. Nominal and analyzed composition of the iron phosphate glass prepared

Elements	Nominal composition		Analyzed composition
	(mol%)	(wt.%)	(wt.%)
P_2O_5	60	57.30	55.45
Fe_2O_3	15	16.12	18.43
Al_2O_3	5	3.43	4.20
CeO_2 (UO_2)	20	23.16 (32.10)	21.92 (30.38)
Total	100.00	100.00	100.00

2.2 Properties analysis

X-ray fluorescence (XRF) spectroscopy was used to analyze the glass composition quantitatively. Density was measured at room temperature by the Archimedes method using deionized water as a medium. Glass transition temperature (T_g) and specific heat (C_p) were determined using a differential scanning calorimetry (DSC) at a heating rate of $10^\circ\text{C}/\text{min}$ and thermal conductivity (k) was measured using laser flash method (LFA).

Chemical durability of the glasses were evaluated using the product consistency test (PCT) [2]. Glasses were crushed and sieved to $75 \sim 150 \mu\text{m}$ in size. Glass powders were then washed with deionized water and ethanol and 1.5 g of powders were soaked in 15 mL of deionized water inside a Teflon vessel and kept at $90 \pm 2^\circ\text{C}$ for 7 days. The leachate was filtered using syringe with a $0.45 \mu\text{m}$ filter. Concentrations of elements in the leachate were analyzed using inductively coupled plasma mass spectrometer (ICP-MS).

Assessment of nuclear criticality safety and the stabilities of the glasses against the heat was performed using Monte Carlo N-particle 6 (MCNP 6) and computational fluid dynamics (CFD).

3. Results

3.1 General properties

Compositions of the glasses analyzed were similar to the nominal composition without any significant loss of individual components (Table 1). The glass contains 21.92wt.% of CeO_2 . If UO_2 were used, concentration should be 30.38wt.%. Normalized elemental release of Ce after PCT was $2.3 \times 10^{-4} \text{ g/m}^2$ and all other elements were $< 0.2 \text{ g/m}^2$ significantly below US regulation of 2 g/m^2 . The iron phosphate

glasses have $T_g = 540 \pm 2^\circ\text{C}$, $C_p = 320.0 \pm 15 \text{ J/kg } ^\circ\text{C}$ and $k = 0.33 \pm 0.015 \text{ W/m K}$ with a density of 3.15 g/cm^3

3.2 Evaluation of the vitrified SNF

Values of effective multiplication factor (k_{eff}) were 0.495 and 0.755 when the canisters were in the normal state and accident case, respectively. Both values were much lower than regulation of 0.95. It indicated that vitrified SNF has enough nuclear criticality safety for a disposal inside the repository.

Temperature of the buffer in repository for vitrified SNF reaches as high as 82.23°C when a spacing between canisters is 2m and distance between disposal tunnels is 10m. Area efficiency of the vitrified SNF disposal is almost 7 times higher than the case of the direct disposal [3]. In addition, the highest temperature expected at the center of the glass is 82.73°C and it is considerably below the glass transition temperature of the glass prepared (540°C).

4. Conclusion

Iron phosphate glasses containing CeO_2 , as a surrogate for UO_2 , were developed as a potential waste form for immobilization of SNF. The waste loading of CeO_2 (UO_2) in the glass was 21.92wt.% (30.38wt.%). Normalized elemental releases of all elements were $< 0.2 \text{ g/m}^2$, well below the US regulations. k_{eff} (0.495 and 0.755) were below the criticality safety regulations (0.95). Glass transition temperature (540°C) of the iron phosphate glass is much higher than the peak temperature of the vitrified SNF (82.73°C) inside the repository, thus providing the thermal stability of the waste forms.

ACKNOWLEDGEMENT

This research was supported by Basic Science Research Program through the National Research Foundation of Korea (NRF) funded by the Ministry of Science and ICT (NRF-2017R1A2B4006754)

REFERENCES

- [1] B.H. Park, "Assessment of spent nuclear fuel amounts to be managed based on disposal option in Republic of Korea", *Annals of Nuclear Energy*, 109, 199-207 (2017).
- [2] The Product Consistency Test (PCT), C 1285-02, ASTM International, West Conshohocken, PA, 2008 <www.astm.org>.
- [3] W. J. Cho, J. S. Kim, H. J. Choi, "Hydrothermal modeling for the efficient design of thermal loading in a nuclear waste repository", *Nuclear Engineering and Design*, 276, 241-248 (2014).

Sorption Characteristics of Iodide on Container Corrosion Products Under the Disposal Conditions: Case Study for Chalcocite and Mackinawite in Alkaline Conditions

Chung-Kyun Park*, Tae-Jin Park, Seung-Yup Lee, and Jae-Kwang Lee

Korea Atomic Energy Research Institute, 111, Daedeok-daero 989beon-gil, Yuseong-gu, Daejeon, Republic of Korea

*ckpark@kaeri.re.kr

1. Introduction

In terms of long-term safety for radioactive waste disposal, the anionic iodide (I-129) with a long half-life (1.6×10^6 yr) is of a critical importance because this radionuclide migrates in geological media without any interactions. Various studies have been performed to retard the iodide migration. Recently, some minerals that are likely generated from waste container corrosion, have been suggested to have a considerable chemical interaction with iodide. In this study, chalcocite (Cu_2S) and mackinawite (FeS) were selected for underground corrosion materials, and an iodide sorption experiment were carried out.

2. Sorption experiment

NaI was used as the iodide for the sorption. Chalcocite and mackinawite were used as sorption minerals. In the sorption test, 50 ml of the experimental solution was put into 1 g of the target mineral, and 0.01 M of sodium hydrosulfite ($\text{Na}_2\text{S}_2\text{O}_4$) was added to maintain the reducing conditions. The initial concentration of iodine is about 1 mM. In order to investigate the pH effect in the alkaline condition, the pH of the solution was divided into four different regions: 8.4, 10.3, 11.4 and 12.4. The NaOH was used to adjust the pH of the system. After the two weeks of the sorption reaction, the sample solution was centrifuged at 8600 rpm for 20 minutes

and then filtered through a 0.2 μm filter. The minerals that reacted with iodide were separately collected and the amount of iodine was determined using the sequential chemical extractions with 0.1 M CaCl_2 and KCl on the minerals collected [1].

3. Results and Discussion

3.1 Iodide sorption onto the iron-copper-sulfur minerals as corrosion products

In general, the surface of the minerals are electrically negative, so the sorption is not expected for anions such as iodide. However, the sorption occurred at a considerable level for the two minerals tested. We note that this suggests an important reaction that prevents the notorious anion migration in a deep underground environment in the field of disposal safety. In Fig.1, the K_d calculated for I^- sorption onto the chalcocite was larger than that for the mackinawite. This likely indicates that the I^- substitution with OH^- on the Cu-minerals is much easier than that on the Fe-minerals and this behavior can be explained by the hard-soft acid-base theory [2]. In the theory, the hard molecules or ions possess a high electronegativity, high charge density, low polarity and low oxidative potential, and reacts better with the hard ones, whereas the soft ones react better with the soft ones. Thus, the iodide or sulfide as the weaker base reacts better with the cation, such as Cu^+ , Hg^+ , and Ag^+ , as the weaker acid than the hydroxide,

which is the harder base. The Fe^{2+} ions are relatively neutral, and thus their reactivity with iodide is relatively low and exhibits a low sorption ability.

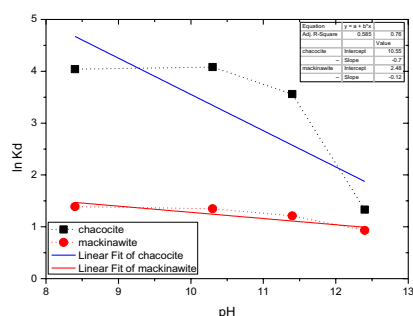


Fig. 1. Curve fittings of K_d for the iodide sorption onto chalcocite and mackinawite as a function of pH.

3.2 Competition between the iodide and chloride sorbed onto the minerals

Fig. 2 shows the amount of iodide extracted by chloride with respect to the pH and the iodide sorption ratios onto the minerals. For the chalcocite, about 80% of the iodide was desorbed under a pH of 11. This indicates that the chloride does not have an absolute advantage in the reaction with Cu over the iodide, because about 20% of the iodide is still bound to Cu, when the iodide is 100 times less than the chloride. On the other hand, about 70% of the iodide is still bound to Fe for the mackinawite. This indicates that the iodide sorbed onto the mackinawite surface forms even stronger bonds than the chalcocite, and it is harder to exchange the iodide with the chloride.

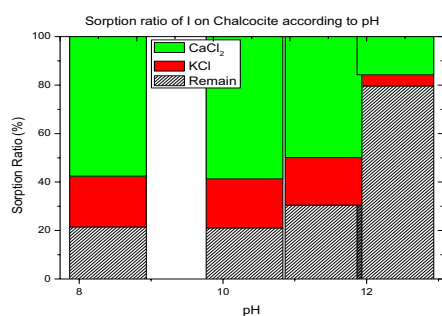


Fig. 2. Extracted iodide sorption ratios according to the pH.

4. Conclusion

Chalcocite exhibited better iodide sorption ability than mackinawite for most of the pH range, indicating that the softer iodide can react better with softer copper ions than with iron. When the pH was higher than 12, the iodide sorption ability decreased for both minerals, likely due to the competition with the hydroxides in the iodide sorption. Our results suggest that chalcocite and mackinawite, which can be the secondary minerals from corrosion, can retard the iodide migration under alkaline conditions with a pH value of less than 12.

ACKNOWLEDGEMENT

We acknowledge the Korean Government, Ministry of Science, ICT and Future Planning (MSIP), for support (No. 2017M2A8A5014859).

REFERENCES

- [1] C.K.PARK, M.H.BAIK, and Y.K.KOH, "Diffusion and sorption properties of some sorbing nuclides onto granodiorite", Nuclear Technology, 196, 121-129 (2016).
- [2] R. Pearson, "hard and soft acids and bases – the evolution of a chemical concept", Coordination chemistry reviews, 100, 403-425, (1990).

Preliminary Thermal Analysis for an Alternative Disposal System

Jong-Pil Park*, Jong-Youl Lee, Heui-Joo Choi, and Dong-Keun Cho

Korea Atomic Energy Research Institute, 111, Daedeok-daero 989beon-gil, Yuseong-gu, Daejeon, Republic of Korea

*pjp3381@kaeri.re.kr

1. Introduction

Yucca Mountain repository type [1], which is a geologic repository, is being considered as one of alternative disposal concepts in KAERI. This disposal system has two types of cooling mode to remove decay heat generated from PWR spent fuels in the waste packages. For the first cooling phase, the decay heat is cooled by forced convection during a certain period (pre-closure). Then, it will be cooled by natural convection (the second cooling phase, post-closure). In the present work, thermal analysis was carried out using a commercial CFD code, CFX, to establish cooling concept of the alternative disposal system.

2. Methods

2.1 Numerical Model

The half model of the alternative disposal system was used in the present simulation as shown Fig. 1. This computational model consists of a waste package, a storage drift (tunnel), and rock. The 2 million computational meshes were generated in the fluid (tunnel, air) and solid domain (rock) for 3-dimensional conjugated heat transfer analysis.

2.2 Numerical Method

The 3-dimensional flow field of air flowing through a tunnel was solved using the steady-state RANS equation with SST turbulence model. Major heat transfer modes of conduction, convection, and

thermal radiation were also considered in the present simulation.

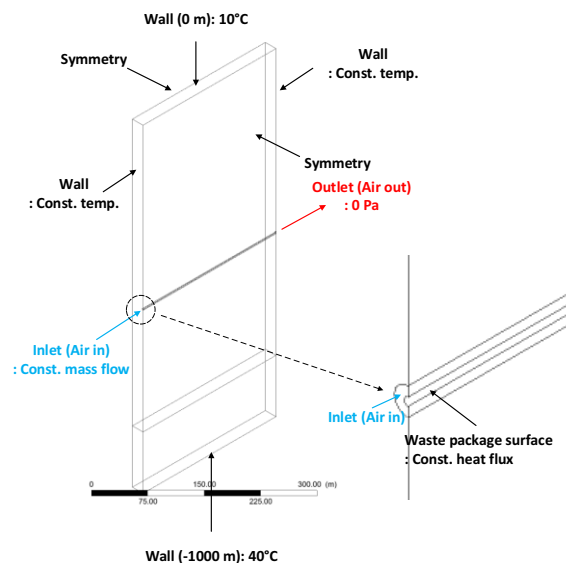


Fig. 1. Schematic of computational domain.

2.3 Initial and Boundary conditions

The inlet boundary condition was set constant mass flow rate ($15 \text{ m}^3/\text{s}$) at the entrance of tunnel and the outlet boundary condition was modeled as a relative pressure of 0 Pa at the end of tunnel. The symmetry boundary condition was applied on two vertical side planes of solid computational domain (rock) as shown in Fig. 1. The rest of wall boundary was set as the constant temperature wall. The uniform heat flux at waste package surface was taken into consideration as shown in Fig. 1.

3. Results

Fig. 2 shows the maximum temperature variation

during the forced convection cooling phase (0~100 years). The temperatures slightly decrease with decreasing decay heat. The maximum temperatures do not exceed temperature limits (waste package surface=300°C, tunnel wall=200°C, between tunnels=100°C) in the present simulation. Additional simulation was performed to assess the effect of air flow rate. Fig 3 shows the maximum temperatures after waste package placement (0 year) for various inlet conditions. If air flow rate is set to 5 m³/s or more, the maximum temperature between the tunnels does not reach the temperature limit (100°C). Based on the numerical simulation on forced convection phase (air flow rate=15 m³/s), the numerical simulation on natural convection cooling was performed to assess cooling capability for post-closure. Fig. 4 shows the maximum temperature variation for natural convection cooling phase (after 100 years). The temperature rapidly increases as the cooling mode change from the forced convection to the natural convection. The maximum temperature between the tunnels (106°C) slightly exceeds limit temperature (100°C) at this time.

4. Conclusion

The present study was carried out using CFD code to investigate thermal behavior of the preliminary conceptual design of the alternative disposal system. In present work, the predicted maximum temperature between tunnels exceeds temperature limit at the time of cooling mode conversion. Therefore, it is necessary to carry out further study on natural convection cooling of the alternative disposal system.

ACKNOWLEDGEMENT

This work was supported by the Ministry of Science and ICT within the framework of the national long-

term nuclear R&D program (NRF-2017M2A8A5014856).

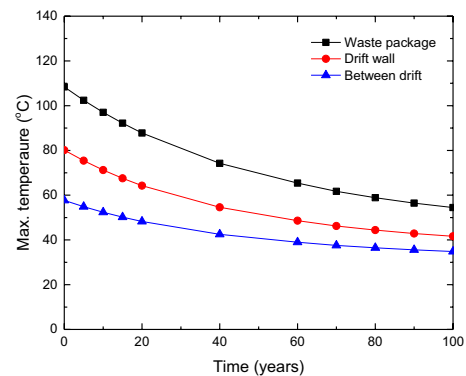


Fig. 2. Max. temperature variation during pre-closure (forced convection cooling phase).

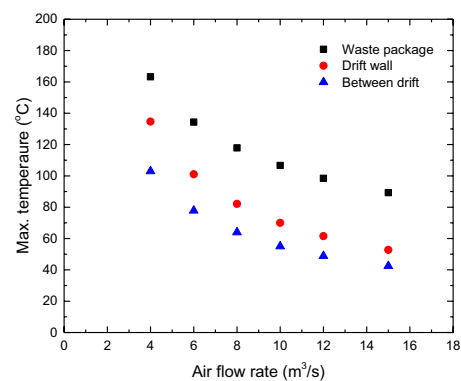


Fig. 3. Max. temperature in various air flow rates.

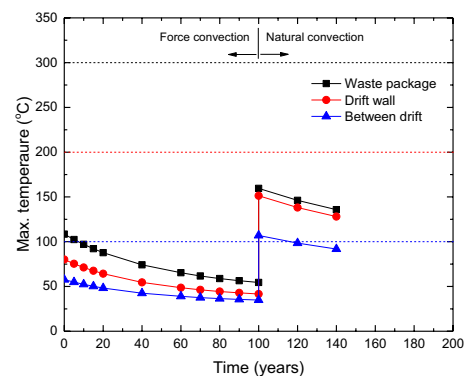


Fig. 4. Max. temperature variation during post-closure (natural convection cooling phase).

REFERENCES

- [1] G.S. Bodvarsson et al., "Overview of scientific investigations at Yucca Mountain" Journal of Contaminant Hydrology, 38, 3-24, (1999).

Buffer Retardation Experiment for Radionuclides Under the Elevated Temperature Conditions: Strategy and Methodology Development for the Korean Bentonite

Tae-Jin Park*, Ji-Hun Ryu, Young-Chul Choi, Wan-Hyoung Cho, and Jae-Kwang Lee

Korea Atomic Energy Research Institute, 111, Daedeok-daero 989beon-gil, Yuseong-gu, Daejeon, Republic of Korea

*etjpark@kaeri.re.kr

1. Introduction

To validate the performance of buffer materials for the high-level radioactive waste disposal in Korea, understanding the properties of domestic buffer materials is a prerequisite. Bentonites are to be used as buffer materials in a geological repository designed to host high-level radioactive wastes. Under the repository conditions, the long-term behavior of bentonites in the engineered barrier system is of crucial importance in the geological timescale safety assessment as well as safety cases. KAERI has been investigating the long-term behaviors of the bentonite under the Korean granite environments.

The spent nuclear fuels generate decay heats for a very long time. Thus, the thermal criteria for the hosting buffer materials must be set for the disposal repository. In most countries, it is set to below 100°C, due to the possible transformation of the smectite to illite which will result in the loss of their requested properties including the swelling capacity. Recently, some efforts (*e.g.*, Grimsel Test Site (GTS) HotBENT Project) have been started to reconsider the thermal criteria for the buffer, because if the maximum temperature allowed for the disposal repository increases, the disposal density decreases dramatically [1]. This will help certain nation with a high population density, especially from a viewpoint of the national economy, site availability, and public acceptance. However, the database for the buffer retardation at the elevated temperature conditions (*e.g.*, $T > 150^{\circ}\text{C}$) are still lacking.

Here, we have developed a strategy and methodology for the Korean bentonite retardation experiments to rationally address the issues related to the thermal criteria. First, we have illustrated a scienario for the Korean bentonite in the disposal repository with time. Second, the alteration of the Korean bentonite in the absence and/or presence of

the groundwater at the elevated temperatures must be investigated due to the buffer saturation period, which will likely take several-hundred years up to one thousand years. Lastly, we need to construct the database for the Korean bentonite retardation at the elevated temperature conditions for the radionuclides.

2. Conditions for the Korean buffer system with time

The condition for the Korean bentonite changes with time. In general, it is expected that the early stage of the SF disposal, the buffer system will be exposed to the elevated temperatures. Then, the system will be cooled down to the ‘normal’ temperatures. From the viewpoint of the wettability of the Korean bentonite, the bentonite will be dry at the early stage of the disposal, and then become wet. We have illustrated a condition for the Korean bentonite in the disposal repository with time (Fig. 1). This allows us to apply appropriate experimental methods to understand the phenomena related.

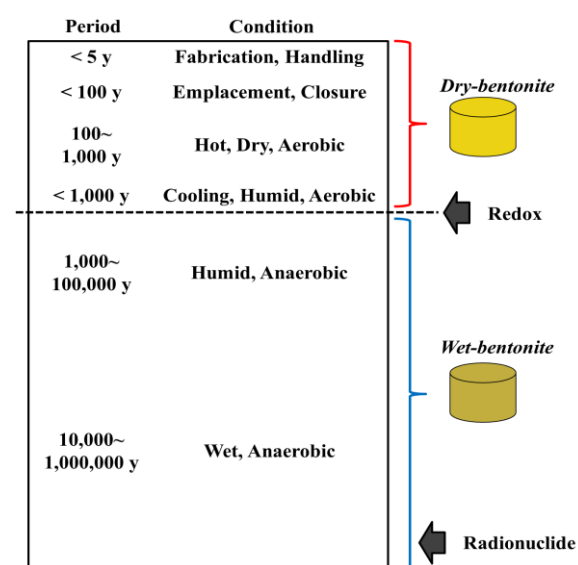


Fig. 1. Illustration of the conditions for the Korean buffer system with time (modified from Peter Keech's work).

3. Korean bentonite at the elevated temperatures

Prior to verify the retardation performances of the buffer for the radionuclides at the elevated temperature conditions, the performances associated with the buffer itself must be understood. Thus, the thermal properties, especially the thermal conductivity and specific heat, and related properties (e.g., density, etc.) for the Korean bentonite must be investigated at the elevated temperatures. In addition, the bentonite properties must be studied in the absence and/or presence of the groundwater at the elevated temperatures due to the buffer saturation periods, which will likely take several-hundred years up to one thousand years [2]. Furthermore, the most crucial factor for the bentonite alteration will be the mineral phase transformation, thus the mineralogical properties associated with the Korean bentonite scenario (Fig. 1) for the disposal is of crucial importance.

4. Database for the Korean bentonite retardation at the elevated temperature conditions

To verify the retardation performances of the buffer for the radionuclides, we need to construct the database for the Korean bentonite retardation at the elevated temperature conditions. We suggest two approaches on the methodologies related. One is to expose the bentonite to the target temperatures (e.g., 90, 120, 150°C, and higher), then followed by the radionuclides sorption experiments. The other is to see any phenomena related to the bentonite-radionuclides interactions at the elevated temperatures simultaneously. Furthermore, the properties from the bentonite blocks as well powders must be equally and importantly considered, because some conditions are almost impossible to realize in the laboratory. For example, once the bentonite blocks are fully saturated, they become difficult to deal with for further experiments.

For the bentonite powders, sorption experiments can be suggested using autoclaves and other similar containers to apply bentonite solid, groundwater, and

the heat (e.g., 90, 120, and 150°C). However, for the bentonite blocks, a sorption test equipment to saturate and obtain the distribution coefficient is developed and designed.

5. Conclusion

The strategy and methodology for the Korean bentonite retardation experiments for the radionuclides are developed and suggested to verify the performance of buffer materials at the elevated temperature conditions. A scenario for the Korean bentonite in the disposal repository with time is suggested. At the elevated temperatures, the thermal and mineralogical properties of the Korean bentonite, as a powder as well as a block, in the absence and/or presence of the groundwater need to be investigated. The database construction suggested for the Korean bentonite retardation at the elevated temperature conditions for the radionuclides will further pursue and help in providing useful information on the scientific and technological reasoning behind the decision making for the disposal repository.

ACKNOWLEDGEMENT

We acknowledge the Korean government, Ministry of Science, ICT and Future Planning (MSIP), for support (No. 2017M2A8A5014859).

REFERENCES

- [1] Cho, W.-J. and Kim, G. Y., "Reconsideration of thermal criteria for Korean spent fuel repository," *Annals Nucl. Ener.* 88, 73-82 (2016).
- [2] Leupin, O.X., Birgersson, M., Karnland, O., Korkeakoski, P., Sellin, P., Mader, U., Wersin, P., "Montmorillonite stability under near-field conditions," Technical Report 14-12, Nagra (2014).

Procedure Consideration of Site Evaluation of Geological Disposal for HLW

Jeong-Hwan Lee*, Sang-Jin Lee, Hyungjin Kim, Taeman Kim, Ho-Seok Dho, Min-Seok Kim, and Seoung-Hyun Kim
Korea Radioactive Waste Agency, 174, Gajeong-ro, Yuseong-gu, Daejeon, Republic of Korea

*oathway@korad.or.kr

1. Introduction

After presenting the concept of land disposal of US National Academy of Science (NAS), the current concept of geological disposal, methodology, and safety assessment method was established at the end of the 1970s [1].

Finland, Sweden, and France have successfully selected the site, and other sites are being selected including UK, Japan, Switzerland, and Canada. Most of these countries establish procedural legitimacy by stipulating clear legal framework for the site selection process prior to site selection.

In this paper, site evaluation procedure and evaluation methods are analyses based on overseas status and it consider the step-wise conceptual work related to implication derived from the result.

2. Procedure of siting process

2.1 Procedure of siting process of IAEA

The site selection process for securing high-level radioactive waste disposal facilities can be divided into the four stages [2].

During the concept and planning phase, identify potentially important site selection factors, potential sites and possible site selection areas, and define survey objectives and research programs. In the regional mapping step, a literature survey is conducted on the metropolitan area to identify one or two target areas for further investigation.

In the stage of site investigation, a site survey is conducted on the potential site, the safety of the in-depth disposal system to be considered is judged, and a detailed site survey is conducted based on this, and a preferred site for characterizing the detailed site is selected.

2.2 Procedure of siting process in Korea

The "Basic Plan for the Management of High Level Radioactive Waste Management" (hereinafter referred to as the "Basic Plan") announced in 2016 is scheduled to be reviewed in connection with developing a geological disposal system. The master plan outlines the site selection procedures for the three stages.

3. Procedure of site evaluation

The Sweden of many overseas countries is advanced nation related to site evaluation based on step-wise procedure of siting process. So we firstly focus on procedure of site evaluation for geological disposal in Sweden.

According to the siting requirement of Sweden, one is that suitable bedrock must exist on the selected site. The other is that acceptance and confidence must exist on a local level for both the siting work and an establishment of the final repository.

These requirements can be associated with performance and/or individual parameters. It defined unacceptable thresholds for sites. And the siting factor means the data, characteristics and conditions

that can be used in the siting to determine that the requirements are satisfied. Requirement driven siting factors are divided into the four main groups ‘Safety related site characteristics’, ‘Technology for execution’, ‘Societal’ and ‘Environment and land use’. Based on these siting factors, the work of siting of geological disposal is conducted to process in the three stages [4].

The general siting stage is presented regional general siting studies for all countries. The study focused on long-term safety and thereby on bedrock conditions but also included the general surveys of environmental and transport infrastructure.

The feasibility study stage was to determine whether premises existed for further siting studies for a geological disposal. Therefore geological studies were a principal component based on existing knowledge, but no drilling was done.

The site investigation stage has included investigation of the biosphere and geological conditions as well as geophysical survey on potential site. Most of the work during the site investigation stage has been done within four technical main activities: investigation, site modeling, design and safety assessment.

The site investigation phase was carried out in two main steps: initial site investigation (ISI) and complete site investigation (CSI). After the initial stage, a preliminary safety evaluation was made of the site in question, which included comparing the data collected on conditions on the site with pre-established criteria. An essential goal was to evaluate the assessment that had justified the choices of candidate sites, i.e. to ensure that these sites have good prospects of meeting the requirements for a final repository. Another goal was to give feedback to the continued investigations and the work with the repository layout and to identify geoscientific

questions that might require particular attention in the continued work.

4. Conclusion

For siting process, the site selection process should demonstrate evidence of natural containment and isolation characteristics prevailing over the types of radioactive waste under consideration. Based on basic plan, the preliminary investigation stage was conducted the feasibility study and preliminary site investigation for evaluating the identification of potential site. And then, detailed investigation stage is carried out in order to confirm the preliminary design and preliminary safety assessment based on detailed 3D site descriptive modeling.

ACKNOWLEDGEMENT

This work was supported by the Korea Institute of Energy Technology Evaluation and Planning (KETEP Project No. 2017720201000) and the Ministry of Trade, Industry & Energy (MOTIE) of the Republic of Korea.

REFERENCES

- [1] J. Haeryoung, K. Hyun-Joo, C. Jae-Yeol, L. Eun Youg and Y. Jeong Hyoun, “Analysis of siting criteria of overseas geological repository (Ⅱ): Hydrogeology, JNFCWT(Korean), 11(3), 253-257 (2013).
- [2] International Atomic Energy Agency (IAEA), “Siting of Geological Disposal Facilities”, Safety Series No. 111-G-4-1, Vienna (1994).
- [3] SKB, “Site selection - siting of the final repository for spent nuclear fuel”, R-11-07 (2011).

Microbial Effects of the Alteration of KJ-II Bentonite Containing a Corrosion Product (Fe_2O_3) Under Anaerobic Alkaline Conditions

Hyo-Jin Seo*, Seung-Yeop Lee, and Jae-Kwang Lee

Korea Atomic Energy Research Institute, 111, Daedeok-daero 989beon-gil, Yuseong-gu, Daejeon, Republic of Korea
*hjseo@kaeri.re.kr

1. Introduction

The underground disposal sites of high-level radioactive wastes are mostly an anaerobic environment. There are various native microbes involving sulfate-reducing bacteria (SRB) in deep underground environments, and they could cause oxidation-reduction changes of groundwater through biochemical metabolism. It has been reported that the activity of microbes can affect the corrosion of metal canisters that are used to protect high-level radioactive wastes. The metal corrosion products can be also altered by underground water and radiation for a long time. The alteration can make them release some metal ions, for example, copper (Cu) and iron (Fe), which are the main materials of the corrosion products. These metal ions can replace some cation ions that exist between clay layers of bentonite, which are the buffer material. This alternation of bentonite may affect the chemical behavior of radionuclides, diffusing from it.

In this study, we investigated the effect of microbial activity on the alternation of KJ-II (Gyeongju) bentonite with corrosion products under anaerobic alkaline environment, which is very similar to the actual disposal site.

2. Materials and methods

2.1 Materials

The bentonite used in this study was taken from Gyeongju. We named it as “KJ-II bentonite” (Clariant Chemicals Korea Ltd.). It is a Ca-type bentonite with its ratio of $\text{CaO} : \text{Na}_2\text{O}$ as 5.5:1, containing montmorillonite with > 65% in its total amount [1]. The KJ-II bentonite was mixed with hematite (Fe_2O_3) powder (10% w/w) that can be one of the corrosion products of the metal canister.

Distilled water sterilized was added to the KJ-II bentonite to make a solid-liquid ratio (S/L) to be 1 g/30 ml in a centrifuge tube of 50 ml. To remove some oxygen in the bentonite, it was saturated and shaken for 3 days (120 rpm, 30°C). Finally, the

supernatant was removed after centrifugation (10,000 rpm, 5 minutes).

In the clean bench, Cesium (Cs) solution of 1000 ppm (mg-Cs/L) was prepared to know its adsorption amount onto the bentonite. Distilled water and cesium solution were purged with N_2 gas for 40 minutes to remove oxygen in the solution.

2.2 Methods

An experiment was conducted under anaerobic conditions using the glove box filled with N_2 gas. The prepared distilled water was poured into centrifuge tube containing bentonite. The cesium solution was added into it to be 20 ppm-Cs by filtering 0.20 μm (ADVANTEC). NaOH solution was used to adjust the pH of the solution media as 9. The experiments were carried out for 3 months. After 3 months, the remaining solution was centrifuged (10,000 rpm, 5 minutes), and the precipitated solid samples were analyzed by XRD (X-ray diffraction) and SEM (scanning electron microscope) to detect some secondary products from the alteration of bentonite.

3. Results and discussion

3.1 Changes of chemical compositions

The supernatant of bentonite was extracted and analyzed to examine the concentrations of Ca and Cs by using ICP-MS (inductively coupled plasma mass spectrometer). The result shows that the concentration of Ca has increased under anaerobic condition (Fig. 1(a)). On the other hand, another sample did not show the increase of Ca under aerobic condition. During the experiment, the hematite in the bentonite was reduced under anaerobic condition, causing Fe^{3+} ions of the hematite to be Fe^{2+} ions. In addition, structural Fe^{3+} bioreduction to Fe^{2+} by SRB that are surviving in the bentonite may promote to release Fe ions from the bentonite. As a result, interlayer Ca^{2+} ions in the bentonite can be

exchanged with Fe^{2+} ions. These processes can affect the bentonite [2].

The alternation can also affect the adsorption of radionuclides. The adsorption of Cs ions was relatively faster under aerobic condition (Fig. 1(b)). The adsorption amount of Cs ions was about 4.2% higher under aerobic condition than under anaerobic condition. It demonstrated that the alternation of bentonite interferes with the adsorption of Cs onto bentonite under anaerobic condition.

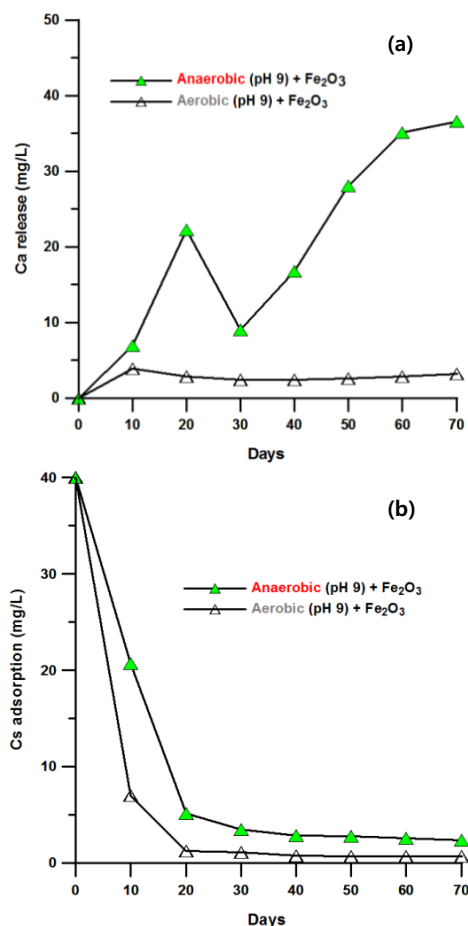


Fig. 1. (a) Concentrations of Ca ions released from bentonite and (b) Cs adsorption onto KJ-II bentonite with Fe_2O_3 under anaerobic or aerobic conditions.

3.2 Formation of secondary minerals

CaCO_3 (calcite), a secondary mineral, was formed under anaerobic conditions in Fig. 2. The generation of the secondary mineral was also found in the SEM analysis. It is assumed that the presence of the newly formed CaCO_3 materials on the bentonite surface interrupted the adsorption of Cs ions. In addition, the decrease of d-spacing was caused by the exchange of Fe ions (atomic radius: 140 pm) for Ca ions (atomic radius: 180 pm).

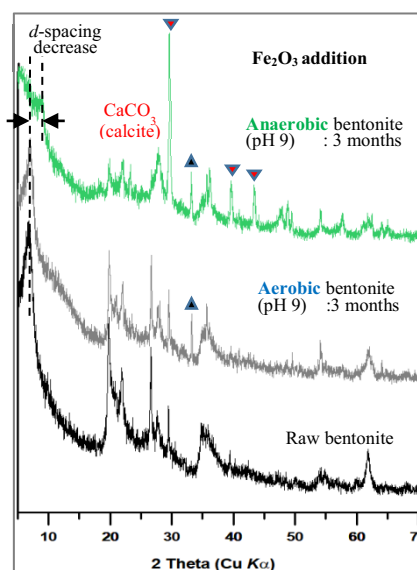


Fig. 2. X-ray diffraction patterns of bentonites with Fe_2O_3 under anaerobic and aerobic conditions.

4. Conclusion

The effect of microbial activity was investigated under anaerobic alkaline conditions. In this study, the calcite, a secondary mineral, was found in the KJ-II bentonite with Fe_2O_3 , which was altered during the experiment. It seems that the secondary mineral prevents Cs from adsorbing onto the bentonite. In the natural disposal site, therefore, the corrosion products of canister may affect the long-term behaviors of radionuclides in the altered bentonite with microbes.

ACKNOWLEDGEMENT

This research was supported by National Research Foundation of Korea (NRF) funded by the Ministry of Science, ICT and Future Planning (The nuclear research and development program No. 2017M2A8A5014859).

REFERENCES

- [1] Yoo, M., et al., "Measurement of Properties of Domestic Bentonite for a Buffer of an HLW Repository", JNFCWT, 14(2), 135-147 (2016).
- [2] Jing Zhang, et al., "Microbial reduction of Fe(III) in smectite minerals by thermophilic methanogen Methanothermobacter thermautotrophicus", Geochim. Cosmochim. Acta, 106, 203-215 (2013).

Preliminary Analysis on Characteristics of the Wastes From the Pyro-processing of SFR SNFs Based on the Material Balance of SFR FSv5.1

In-Young Kim* and Dong-Keun Cho

Korea Atomic Energy Research Institute, 111, Daedeok-daero 989beon-gil, Yuseong-gu, Daejeon, Republic of Korea

*iykim@kaeri.re.kr

1. Introduction

To reuse valuable materials in SNFs and reduce volume and toxicity of SNFs, the P&T technology based on the pyro-processing and the SFR has been under development in KAERI. SFR burners are necessary to transmute long-lived actinides and fission products and inevitable SNFs generation is accompanied. Thus, characteristics of SFR SNFs and wastes from the pyro-processing of SFR SNFs must be identified for accurate fuel cycle analyses. In this study, preliminary analysis on characteristics of wastes from the pyro-processing of SFR SNFs based on the material balance of SFR FS v5.1 is conducted.

2. Methods and Results

2.1 Assumptions and Methods

The reference reactor and fuel type described below are considered [1]. The characteristics of wastes from the pyro-processing of SFR SNFs had been evaluated using the Origen-arp in the SCALE6.1 and the problem dependent cross-section library for reference reactor [2] is used.

- Reference reactor: 400 MWe annular type burner
- Average discharge burnup: 133 GWd/tHM
- Fuel cycle length: 332 EFPD/cycle
- Driver fuel type: U-TRU-10Zr
- TRU inventory of BOEC/EOEC: 3.485/3.276 ton

The material balance of SFR FS v5.1 had been used to analyze characteristics of wastes from the pyro-processing of SFR SNFs. The brief information about wastes from the pyro-processing of 2.46 ton initial heavy metal of SFR SNFs based on SFR FSv5.1 is listed in Table 1.

Table 1. Wastes from the pyro-processing of SFR SNFs based on SFR FSv5.1 (basis: 2.46 tHM/SNF) [3]

	Nuclide+filter mass [kg]	Total mass [kg]	Major Nuclides
Metal Waste	1.36E+02	9.0E+03	Duct, Clad, Shield, U, NM, Tc
I-Filter Waste	4.60E+00	4.60E+00	I, Br
Te-Filter Waste	6.10E+00	1.22E+01	Tc, Te, Se, Sb
H-Filter Waste	1.60E+02	4.80E+02	H-3
Cs-Filter Waste	2.80E+02	4.20E+02	Cs, Rb, Cd, Ag
Sr Waste	3.66E+01	2.34E+02	Sr, Ba, RE, Se, Te
REE Waste	7.88E+01	9.34E+01	RE/TRU
Salt Waste	6.21E+01	7.65E+02	Sr, Cs, I, RE, LiCl-KCl salt

2.2 Results

Figure 1-3 show evaluated decay heat, radioactivity, and radiotoxicity of outputs from the pyro-processing of SFR SNFs based on SFR FSv5.1. Table 2 shows decay heat, radioactivity, radiotoxicity of wastes and products at the disposal time. Total cooling time before the disposal is 40 years. Most of decay heat, radioactivity, and radiotoxicity are generated from the U/TRU ingot. Therefore, heat load of repository can be reduced by complete reuse of the U/TRU ingot.

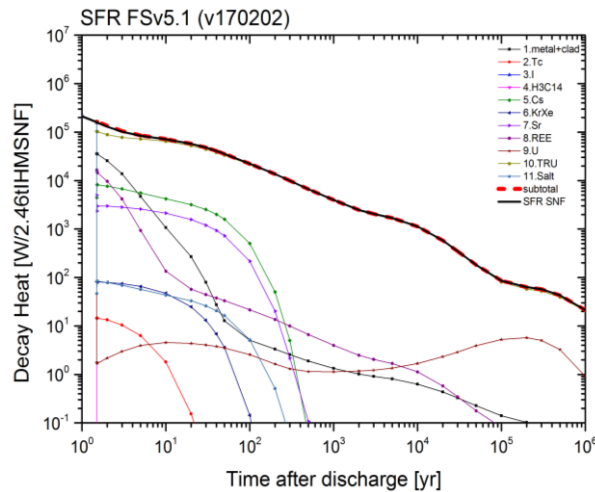


Fig. 1. Decay heat of wastes and products from the pyro-processing of SFR SNFS based on FSv5.1.

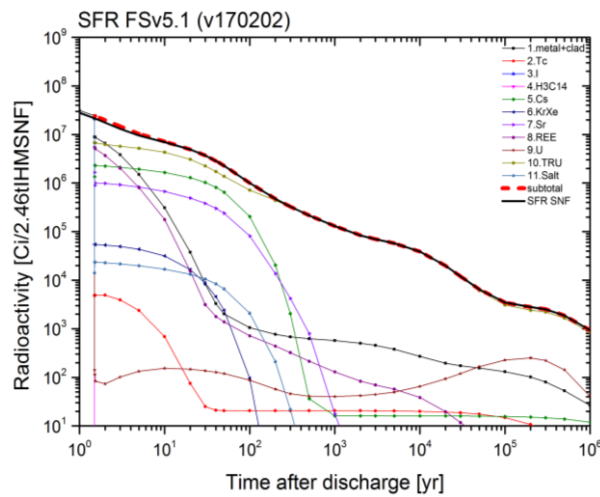


Fig. 2. Radioactivity of wastes and products from the pyro-processing of SFR SNFS based on FSv5.1.

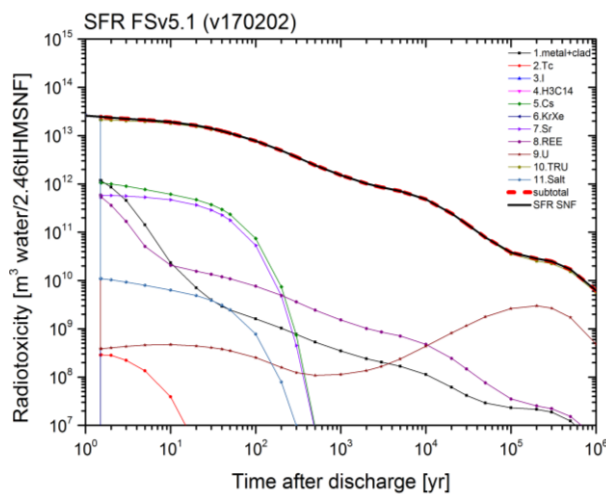


Fig. 3. Radiotoxicity of wastes and products from the pyro-processing of SFR SNFS based on FSv5.1.

Table 2. Decay heat, radioactivity, radiotoxicity of wastes and products at the disposal time (basis: 2.46 tHM/SNF)

Basis: 2.46 tHM	Decay heat		Radioactivity		Radiotoxicity	
	[W/basis]	[%]	[Ci/basis]	[%]	[m ³ water/basis]	[%]
Metal Waste	2.75E+01	0.07%	3.30E+03	0.12%	2.93E+09	0.02%
I -Filter Waste	1.57E-05	0.00%	3.59E-02	0.00%	2.14E+05	0.00%
Tc-Filter Waste	7.70E-03	0.00%	2.10E+01	0.00%	7.34E+05	0.00%
H-Filter Waste	8.60E-07	0.00%	2.55E-02	0.00%	5.79E+01	0.00%
Cs-Filter Waste	2.01E+03	4.92%	8.17E+05	28.54%	2.96E+11	2.37%
Sr Waste	9.30E+02	2.28%	3.02E+05	10.53%	2.26E+11	1.80%
REE Waste	3.79E+01	0.09%	1.79E+03	0.06%	1.20E+10	0.10%
Salt Waste	2.06E+01	0.05%	8.37E+03	0.29%	3.08E+09	0.02%
U ingot	3.77E+00	0.01%	1.28E+02	0.00%	3.79E+08	0.00%
U-TRU ingot	3.77E+00	92.59%	1.73E+06	60.37%	1.20E+03	95.68%
SNF	4.08E+04	100.00%	2.86E+06	100.00%	1.25E+03	100.00%

3. Conclusion

Characteristics of wastes and products from the pyro-processing of SFR SNFs based on material balance of SFR FSv5.1 are evaluated in this study. The large reduction in heat load of repository at the disposal time can be achieved by complete reuse of the U/TRU ingot because most of the decay heat, radioactivity, and radiotoxicity are generated from the U/TRU ingot. Characteristics of SFR pyro-wastes identified in this study will be used to design disposal system for comparison between direct disposal scenario and closed fuel cycle scenario.

REFERENCES

- [1] Myung Hyun Kim et. al., Conceptual Design of Future Commercial TRU Burner Cores, KAERI/CM-1880/2013, KAERI, 2013.
- [2] Dong-Keun Cho, Problem dependent library of the 400 MWe annular type SFR burner for the Origen-arp, KAERI, 2018.
- [3] Hun Suk Im, et. al., Flowsheet for Pyro-processing Facility with 2.46 tHM capacity for SFR SNFs (SFR FS v.5.1), KAERI, 2017.

Development of EBS Modules for a Process-based Total System Performance Assessment of a Geological Disposal System

Jung-Woo Kim*, Jaewon Lee, Inyoung Kim, and Dong-Keun Cho

Korea Atomic Energy Research Institute, 111, Daedeok-daero 989beon-gil, Yuseong-gu, Daejeon, Republic of Korea

*jw_kim@kaeri.re.kr

1. Introduction

Recently, KAERI has proposed developing a process-based total system performance assessment model for a geological disposal system (APro which stands for “**A**dvanced **P**rocess-based total system performance assessment framework for a geological disposal system”) to cope with the limitations of system-level model to reflect short- and long-term evolution of the disposal system and to realistically simulate thermal, hydraulic, mechanical, and chemical complex phenomena.

As the first step of development of the model, the modeling interface was designed in the previous study [1]. For further works, in this study, the EBS-related modules, such as radioactive decay heat and thermal transfer, canister corrosion, and radionuclide release, were developed and embedded into APro.

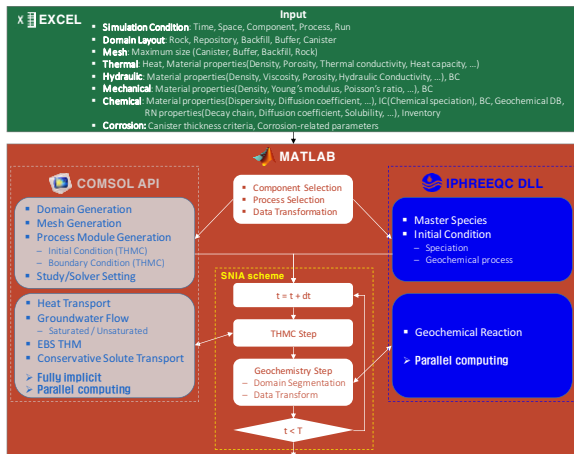


Fig. 1. Flowchart of APro.

2. APro

APro employs a bottom-up approach unlike a system-level model which uses top-down approach. APro was basically designed to be able to simulate all the processes that could occur in a geological disposal system including thermal, hydraulic, mechanical, and chemical (radiological) processes. The flowchart of APro is depicted in Fig. 1.

2.1 APro's Thermal Transfer Module

APro's *Default Process* with respect to the thermal transfer assumes that the EBS and NBS are fully saturated. The thermal transfer in fully-saturated porous media is governed by the following equation:

$$(\rho C_p)_{\text{eff}} \frac{\partial T}{\partial t} + \rho C_p \mathbf{u} \cdot \nabla T + \nabla \cdot \mathbf{q} = Q \quad (1)$$

$$(\rho C_p)_{\text{eff}} = (1 - \varepsilon_p) \rho_p C_{p,p} + \varepsilon_p \rho C_p \quad (2)$$

$$\mathbf{q} = -\{(1 - \varepsilon_p)k_p + \varepsilon_p k\} \nabla T \quad (3)$$

where, T is temperature, ρ is density of water, ρ_p is density of solid, C_p is heat capacity of water, $C_{p,p}$ is heat capacity of solid, ε_p is porosity, \mathbf{u} is Darcy velocity of water, k is thermal conductivity of water, k_p is thermal conductivity of solid, and Q is heat source.

As the heat source, decay heat of the reference spent fuel whose initial enrichment is 4.5wt% and burnup is 55 GWd/MtU was considered as the following regression equation [2].

$$Q = C_0 + C_1 e^{-\frac{t-t_0}{t_1}} + C_2 e^{-\frac{t-t_0}{t_2}} + C_3 e^{-\frac{t-t_0}{t_3}} \quad (4)$$

Table. 1. Coefficients of decay heat regression equation

t	1yr < t ≤ 100yr	100yr < t ≤ 1,000yr
C_0	297.9526	32.1858
t_0	0.7805	101.6499
t_1	2.9441	40.5612
t_2	1.0966	121.288
t_3	42.7499	622.1932
C_1	3,218.383	146.7649
C_2	10,394.94	110.4017
C_3	2,036.431	197.2185

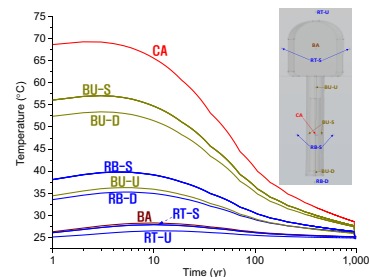


Fig. 2. Temporal distributions of temperature around EBS.

For the single borehole of the KRS, the temporal distributions of temperature around EBS are depicted in Fig. 2. From the result, the peak of temperature

was observed within 10 years, and the highest temperature was less than about 70°C.

2.2 APro's Canister Corrosion Module

APro's *Default Process* with respect to the canister corrosion assumes that every canister is failed after a certain life-time. Before the canister failure, the canister is considered as an impermeable barrier. Once the canisters are failed, the radionuclide release will commence.

Fig. 3 shows the change of Darcy velocity after canister failure.

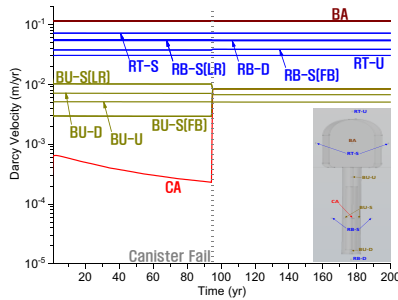
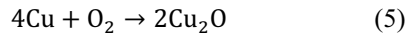


Fig. 3. Temporal distributions of Darcy velocity around EBS.

APro's *Alternative Process* with respect to the canister corrosion considers copper oxidation by dissolved oxygen in groundwater as follows.



From the reaction, the change of canister thickness can be computed by the following equation:

$$\frac{\partial \tau_{\text{Cu}}}{\partial t} = - \frac{R_{\text{Cu}|\text{O}_2} \cdot Q_{\text{O}_2} \cdot W_{\text{Cu}}}{\rho_{\text{Cu}}} \quad (6)$$

where, τ_{Cu} is canister thickness, $R_{\text{Cu}|\text{O}_2}$ is the reactant ratio, Q_{O_2} is influx of dissolved oxygen, W_{Cu} is atomic weight of Cu, and ρ_{Cu} is density of Cu. The concentration of dissolved oxygen at the canister surface is constant as 0 mol/m³ since it is assumed that all dissolved oxygen at the canister surface is consumed with copper oxidation.

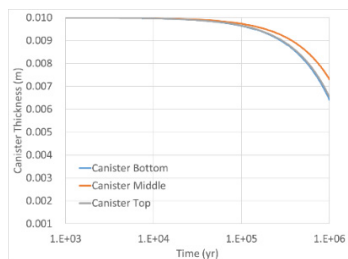


Fig. 4. Temporal distributions of canister thickness.

Fig. 4 shows the temporal distribution of canister thickness for a certain condition.

2.3 APro's Radionuclide Release Module

APro's *Default Process* with respect to the radionuclide release assumes the solubility-limited release for the radionuclides having finite solubility and the instant release for the radionuclides having infinite solubility. The solubility-limited release can be computed by the following equation:

$$Q_n = \min(C_{0,n}, S_n) \cdot q \quad (7)$$

where, Q_n is radionuclide release rate, $C_{0,n}$ is radionuclide inventory, S_n is radionuclide's solubility, and q is Darcy flux in the canister. And the radionuclide inventory will be changed as follows:

$$\frac{\partial C_{0,n}}{\partial t} = \Lambda C_{0,n} - Q_n \quad (8)$$

where, Λ is the matrix of radioactive decay chain.

3. Conclusion

In this study, the EBS-related modules, such as radioactive decay heat and thermal transfer, canister corrosion, and radionuclide release, were developed and embedded into APro. Through the development, it is expected that the coupling effects of EBS-related processes can be confirmed in the future. For further work, the EBS THM processes will be added into APro in the near future.

ACKNOWLEDGEMENT

This work was supported by the Nuclear Research and Development Program (No. 2017M2A8A5014856) of the National Research Foundation of Korea (NRF) funded by the Ministry of Science and ICT (MSIT).

REFERENCES

- [1] J.-W. Kim et al., "Development of Modeling Interface for a Process-Based Total System Performance Assessment of a Geological Disposal System", Proceeding of 2018 KRS Spring Meeting (2018).
- [2] I. Kim et al., "Evaluation on Thermal Performance and Thermal Dimensioning of Direct Deep Geological Disposal System for High Burn-up Spent Nuclear Fuel", KAERI/TR-5230/2013 (2013).

3분과

고준위폐기물처분 (Poster)



A Bayesian Updating for an Earthquake Frequency Associated With an HLW Repository

Youn-Myoung Lee* and Dong-Keun Cho

Korea Atomic Energy Research Institute, 111, Daedeok-daero 989beon-gil, Yuseong-gu, Daejeon, Republic of Korea

*ymlee@kaeri.re.kr

1. Introduction

Through this study, an imaginary disruptive event owing to earthquakes whose magnitude are over a certain limitation that could be set as required was considered. Earthquakes could result an increase of groundwater flow and a direct connection to MWCs of the repository providing the shortest nuclide release pathway, which has been revised and extended from the previous study [1] in Bayesian point of view.

We still used the assumption that two principal parameters, the magnitude of the earthquake and the distance between a repository and its epicenter are enough to characterize earthquakes, and that they follow statistical behaviors of the distributions; a log-uniform distribution for the magnitude, $\sim \text{uniform}[5.5, 8.0]$ and a triangular distribution, $\sim \text{triangular}[0, 5, 25]$ km for the distance, respectively, which do not have any evidence yet for the time being though. Earthquake events used to be assumed to occur based on a simple Poisson distribution at a random time interval, but this time these are differently modeled.

Magnitude-to-distance ratios (M/T) over 0.1 for a flow increase in the MWCs one time and/or direct MWC connection when $M > 7.5$ are postulated in view of the long-term safety that might be disruptive enough to reduce the performance of the repository.

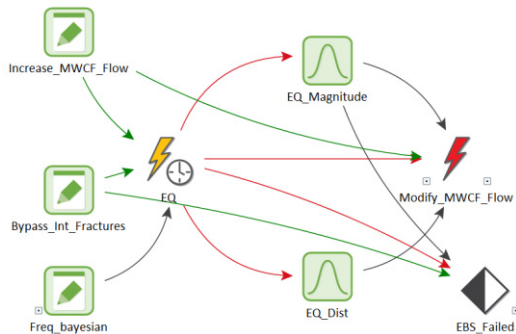


Fig. 1. GoldSim module for earthquake disruptive event with Bayesian updating routine.

In Fig. 1, a GoldSim model implemented for such an earthquake scenario is shown, in which the magnitudes and distances are generated by the distributions specified. The occurrence rates of earthquakes are modeled to be Bayesian updated sequentially in this study: In this model, the occurrence of earthquakes are assumed to follow a log-uniform distribution $\sim \text{log-uniform}[10^{-5}, 10^{-3}] \text{yr}^{-1}$ which seem rather appropriately chosen in view of historically recording, which has been Bayesian updated for three times sequentially with a likelihood which should and is assumed to be originated from recent measurements and expert elicitation, follows a Log-normal distribution, $\sim \text{Log-normal}[10^{-4}, 10^{-5}] \text{yr}^{-1}$.

2. Bayesian Updating

Although reliable estimation of the distributions expressed as probability density functions for input parameters needs large amount of measured data, in most cases, especially in the safety assessment of the repository which is typically associated with long time span, observed data are usually limited resulting conventional probabilistic calculations rather uncertain.

In such case avoiding relying on such limited data available and/or some historical prior knowledge, a posterior distribution that could result from those prior distribution multiplied by supplementary distribution based on experts' elicitation form their beliefs and judgment regarding the parameter as well as recent measurements, as represented in Eq.(1).

$$p(\vec{\theta}|H_i, I, D) = \frac{p(D|\vec{\theta}, H_i, I)}{p(D|H_i, I)} \cdot p(\vec{\theta}|H_i, I) \propto \mathcal{L}_{\theta}(H_i) \cdot p(\vec{\theta}|H_i, I) \quad (1)$$

which means the posterior is proportional to the likelihood times the prior showing the posterior has all the information from prior beliefs and data as an

evidence, where: $\vec{\theta}$ =parameter vector, H =hypothesis or Model, I =information, D =data. Prior probability, $p(\vec{\theta}|H_i, I)$ is based on the output from previous observations and general historical belief and the likelihood, $\mathcal{L}_{\theta}(H_i)$ that represents a probability of obtaining data, D , for a given prior information I and a parameter set, $\vec{\theta}$.

For Bayesian updating, despite of its advantage, practical application might be very limited due to difficulty to get a posterior distribution easily or analytically except e.g., conjugate prior distributions. That is the reason Markov Chain Monte Carlo (MCMC) sampling algorithm widely used is adapted to the study.

3. Results

Through this study, for illustrative purposes, nuclide releases, frequency of the earthquakes were investigated under an earthquake disruptive event scenario in the hypothetical HLW repository system as an extended work done previously.[1]

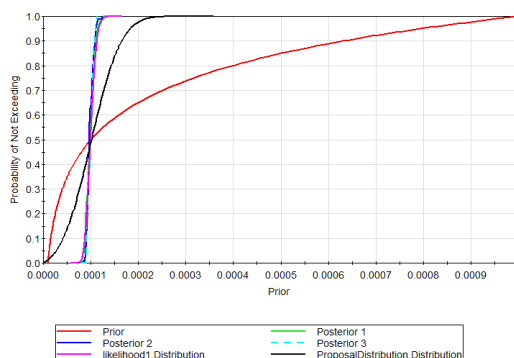


Fig. 2. Prior and posterior distributions compared to likelihood and proposal.

Assumed prior distribution and posterior distributions based on the very first prior probability and then sequentially used to substitute next two priors are shown in Fig. 2, in which a proposal distribution that is arbitrarily chosen and used for MCMC is also seen together.

With each posterior distribution probabilistic assessments for the dose exposure rates sequentially performed are also shown in Fig. 3, which represents probabilities for dose rates expressed in pdf and CDF, alternatively, by which broad distributions for the results become narrow down as Bayesian updated for

the parameter of earthquake frequency, which shows four each total exposure rate in accordance with the first prior and three posterior distributions. In Fig. 4, realizations of the earthquake frequency from each sequential Bayesian updated distribution are also shown, being compared among each other.

Total exposure dose rates seem to migrate in turn to lower, rather less conservative values as priors are consequently replaced with previous posteriors, as is seen in Fig. 5.

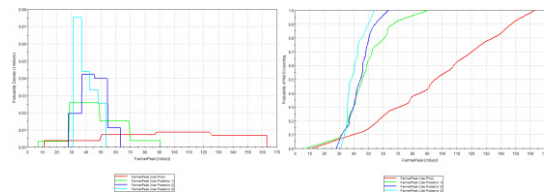


Fig. 3. Probabilistic calculation results in pdf/CDF for each Bayesian update.

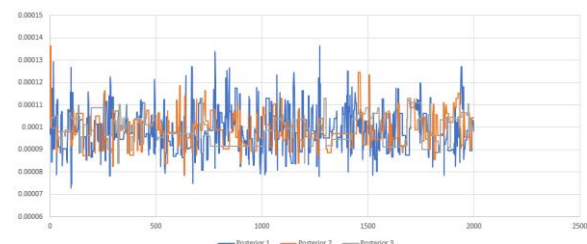


Fig. 4. Realizations of the earthquake frequency (yr^{-1}) from each sequential Bayesian updated distribution.

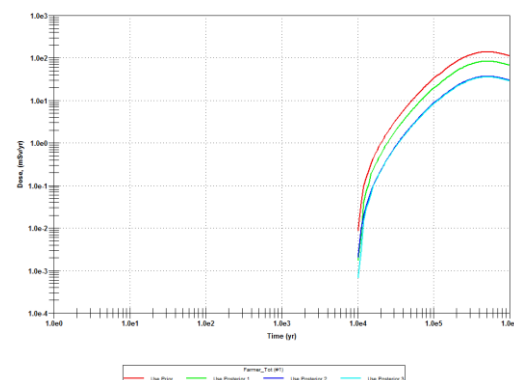


Fig. 5. Total exposure dose rates to farming exposure group for each Bayesian update for earthquake frequency distribution.

REFERENCES

- [1] Youn-Myoung Lee et al., "An evaluation of an earthquake scenario for a pyroprocessed waste repository," Progress in Nuclear Energy, 66, 133-145 (2013).

Update of Model Probability for Release Rates of Radionuclides Using Bayes' Theorem

Jongtae Jeong*, Dong-Keun Cho, and Youn-Myoung Lee

Korea Atomic Energy Research Institute, 111, Daedeok-daero 989beon-gil, Yuseong-gu, Daejeon, Republic of Korea

*jtjeong@kaeri.re.kr

1. Introduction

Simulation models for a system are usually generated by conceptualizing the system and representing it in computer code. Model uncertainties are unavoidable during these processes. The quantification of model uncertainty based on model probability can be an efficient methodology for obtaining the degree of belief of a model. In this paper, we adopted the Bayes' theorem for the quantification of model uncertainty and applied it to simulation models for release rates of radionuclides from the radioactive waste repository.

2. Quantification of model uncertainty using Bayes' theorem

2.1 Bayes' Theorem

The way to update prior probability of model M_k into posterior probability using Bayes' theorem for a set of models and experimental data D is given by the following equation [1]:

$$\Pr(M_k|D) = \frac{\Pr(M_k) \times \Pr(D|M_k)}{\sum_{i=1}^K \Pr(M_i) \times \Pr(D|M_i)}, k = 1, \dots, K \quad (1)$$

Where, $\Pr(M_k)$ is prior probability of model M_k , $\Pr(M_k|D)$ is posterior probability of model M_k , and $\Pr(D|M_k)$ represents likelihood of model M_k given observed data D .

A common formulation for a model prediction can be written as follows:

$$y = f_k + \varepsilon_k, \varepsilon_k \sim N(0, \sigma_k^2) \quad (2)$$

Where y is a system response, and f_k is the prediction of y by a model M_k . ε_k is the error for both

bias associated with model prediction f_k of response y and measurement error. ε_k is assumed to be an independent and identically distributed normal variable with zero mean and a constant variance. σ_k is the standard deviation of the error.

Eq.(2) can be represented in a probability distribution form as

$$g_Y(y|M_k) = \frac{1}{\sqrt{2\pi\sigma_k^2}} \exp\left(-\frac{(y-f_k)^2}{2\sigma_k^2}\right) \quad (3)$$

$g_Y(y|M_k)$ is the predictive distribution of response y under model M_k . Using the above equation, the likelihood function of σ_k for each model M_k given a data set d_n is expressed by

$$\Pr(d_n|M_k, \sigma_k) = \frac{1}{\sqrt{2\pi\sigma_k^2}} \exp\left(-\frac{(d_n-f_{kn})^2}{2\sigma_k^2}\right) \quad (4)$$

Where, f_{kn} is the prediction of data d_n by model M_k .

Because experimental data are independent of one another, the likelihood of σ_k for each model M_k can be calculated by multiplying $\Pr(d_n|M_k, \sigma_k)$ in the above equation as represented by

$$\Pr(D|M_k, \sigma_k) = \left(\frac{1}{2\pi\sigma_k^2}\right)^{N/2} \exp\left(-\frac{\sum_{n=1}^N (d_n-f_{kn})^2}{2\sigma_k^2}\right) \quad (5)$$

Model likelihood $\Pr(D|M_k)$ is expressed by marginal likelihood integral as follows:

$$\Pr(D|M_k) = \int \Pr(D|M_k, \sigma_k) g(\sigma_k|M_k) d\sigma_k \quad (6)$$

In general, the maximum likelihood estimation is implemented to evaluate model likelihood $\Pr(D|M_k)$ instead of finding a direct solution of Eq.(6). That is, taking the derivative of the logarithm of Eq. (5) with respect to σ_k and setting it equal to zero, and solving

the equation for σ_k gives

$$\sigma_k^2 = \frac{\sum_{n=1}^N \varepsilon_{kn}^2}{N}, \varepsilon_{kn} = d_n - f_{kn} \quad (7)$$

By putting the above equation into the exponential term in Eq.(5), likelihood $\Pr(D|M_k)$ of each model M_k given a set of experimental data D is computed:

$$\Pr(D|M_k) = \left(\frac{1}{2\pi\sigma_k^2} \right)^{N/2} \exp\left(-\frac{N}{2}\right) \quad (8)$$

2.2 Application to Release Rates of Radionuclide

KAERI developed a GS-TSPA code for the post-closure safety assessment of a radioactive waste repository [2]. In this code, three models for the release rate of radionuclides from the waste canister are considered; annual release rate, congruent release, and surface release. The results of release rate for I-129 by three models and hypothetical experimental data are summarized in Table 1. The hypothetical experimental data are assumed to be the mean value of simulated results using three models because experimental data are not available.

Table 1. Release rates of I-129 (g/yr)

Time (yr)	Exp. Data	Annual Release	Congruent Release	Surface Release
10,000	1.60E-01	2.97E-02	2.96E-02	4.22E-01
20,000	7.65E-02	5.37E-03	4.38E-03	2.20E-01
30,000	3.02E-03	1.20E-03	1.78E-04	7.68E-03
40,000	4.50E-04	1.06E-03	2.44E-05	2.69E-04
50,000	3.59E-04	1.05E-03	1.61E-05	9.39E-06
60,000	3.55E-04	1.05E-03	1.42E-05	3.28E-07
70,000	3.53E-04	1.05E-03	1.31E-05	1.15E-08
80,000	3.53E-04	1.05E-03	1.22E-05	4.01E-10
90,000	3.52E-04	1.04E-03	1.15E-05	1.40E-11
100,000	3.51E-04	1.04E-03	1.10E-05	4.90E-13

We assumed that prior probabilities for three models are uniformly distributed. The updated posterior probabilities are summarized in Table 2. As shown in Table 2, the annual release rate model is

most likely to give closest predictions among the models considered. The significantly low posterior probability of surface release model indicates that the model fits the data very poorly.

Table 2. Prior and posterior probabilities for three models

	Annual Release	Congruent Release	Surface Release
Prior probability	1/3	1/3	1/3
Standard deviation	4.70E-2	4.72E-2	9.43E-2
Likelihood	1.30E+7	1.25E+7	1.25E+4
Posterior probability	0.51	0.49	4.88E-4

3. Conclusions

We adopted the Bayes' theorem for the quantification of model uncertainty based on model probability. According to the results of application example, we found that the Bayes' theorem can be used as an efficient tool for the quantification of model uncertainty. However, the real experimental data are necessary to obtain more exact degree of belief for models by applying Bayes' theorem.

ACKNOWLEDGEMENT

This work was supported by the National Research Foundation of Korea Nuclear Research and Development Program (2017M2A8A5014856) funded by the Ministry of Science and ICT.

REFERENCES

- [1] I. Park and R.V. Grandhi, "A Bayesian statistical method for quantifying model form uncertainty", Reliability Engineering and System Safety 129, 46-56 (2014).
- [2] Y.M. Lee and Y.S. Hwang, "A Goldsim model for the safety assessment of a HLW repository", Progress in Nuclear Energy, 51 (2009).

Statistical Approach for the Distribution of Natural Uranium in the KURT Groundwater

Jihye Jeong* and Jae-Kwang Lee

Korea Atomic Energy Research Institute, 111, Daedeok-daero 989beon-gil, Yuseong-gu, Daejeon, Republic of Korea

*yz0201@kaeri.re.kr

1. Introduction

For the high-level radioactive waste disposal facilities, it is important to evaluate the characteristics of radionuclides in groundwater and the geochemical factors that control its behavior in case of leakage of radionuclides to groundwater. So far, a number of studies have been conducted to investigated geochemical and biochemical properties of the groundwater in the KAERI Underground Research Tunnel (KURT) [1-4], but statistical approach of natural nuclides in the groundwater have not been carried out. The main aim of this contribution is to assess the distribution of natural uranium in KURT groundwater under various geochemical environments and the geochemical factors which affect existence of aqueous uranium using a statistical approach. Principal component analysis was primarily used to find out possible relationships among the examined parameters.

2. Results

2.1 Principal component analysis (PCA)

PCA is a powerful recognition technique that attempts to explain the variance of a large set of intercorrelated variables with a smaller set of independent variables-principal components. It was usually employed to compare the compositional patterns between the examined water samples and to

identify the factors influencing each one [5].

The treatment of dataset with PCA showed two factors interpreting the 64.86% of variance (PC1 36.49%, PC2 28.37%). The PCA plot of PC1 against PC2 is illustrated in the Fig.1. Three groups of KURT groundwater are observed: group A (oxidized high uranium group) with PC1 scores < 0, group B (weak granitic weathered group) with PC2 scores < 2 and group C (high granitic weathered group) with PC1 > 0.

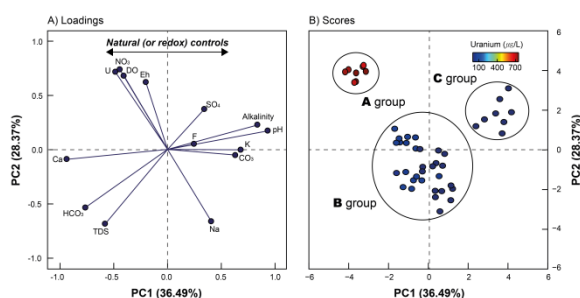


Fig. 1. First vs. second principal component from PCA analysis: A) loadings of the major parameters, B) scores of the natural groundwater samples.

2.2 Hydrochemical characteristics

These three groups represent significant different hydrochemical characteristics according to non-parametric Kruskal-Wallis test. The group A exhibited the high concentrations (or values) of U, DO, Eh and NO_3 and low pH, Na, alkalinity and F. However, groundwater samples in group C showed relatively high concentrations of pH, alkalinity, Na, F and TDS whereas low concentrations of DO and Ca.

The group B samples has high Ca, Na, alkalinity and F. Groundwater from group C is mainly of Na-HCO₃ type, whereas groundwater in groups A and B are Ca-HCO₃ type.

3. Conclusions

The groundwater in KURT was analyzed using the PCA technique to explain the variance of the hydrogeochemical relationship of a large different data. Three major groundwater groups were divided. Group A showed positive correlation with U, DO, Eh and NO₃ indicating mobile property of uranium under oxidized condition. Groundwater in group B was suffered relatively low water-rock interaction and the groundwater type of groups A and B is included in Ca-HCO₃. The C group groundwater is a high granitic weathered group and show positive correlation with F, Na, alkalinity and TDS. And, the water quality type is Na-HCO₃ indicating high interaction between groundwater and contact rock.

ACKNOWLEDGEMENT

This work was supported by the Ministry of Science and ICT within the framework of the national long-term nuclear R&D program (2017M2A8A5014859).

REFERENCES

- [1] J.-H. Ryu, J.-S. Kwon, G.-Y. Kim, and Y.-K. Koh, "Geochemical Characterization of Rock-Water Interaction in Groundwater at the KURT Site," J. Nucl. Fuel Cycle Waste Technol., vol. 10, no. 3, pp. 189–197, 2012.
- [2] N.-Y. Ko, K. W. Park, K. S. Kim, and J. W. Choi, "Groundwater Flow Modeling in the KURT site for a Case Study about a Hypothetical Geological Disposal Facility of Radioactive Wastes," J. Nucl. Fuel Cycle Waste Technol., vol. 10, no. 3, pp. 143–149, 2012.
- [3] J.-H. Lee, H. Jung, E. Lee, and S. Kim, "Estimation of groundwater level fluctuation of the crystalline site using time series analyses in south Korea," J. Nucl. Fuel Cycle Waste Technol., vol. 11, no. 3, pp. 179–192, 2013.
- [4] S. Y. Lee, Y. Roh, and J. T. Jeong, "Changes of the Oxidation/Reduction Potential of Groundwater by the Biogeochemical Activity of Indigenous Bacteria," Econ. Environ. Geol., vol. 47, no. 1, pp. 61–69, 2014.
- [5] Kouras, A., I. Katsoyiannis, and D. Voutsas. "Distribution of arsenic in groundwater in the area of Chalkidiki, Northern Greece." Journal of Hazardous materials 147.3 (2007): 890-899.

Preliminary Shielding Analysis for Review of Multipurpose Utilization of PWR Spent Nuclear Fuel Disposal Canister

Ho-Seog Dho* and Taeman Kim

Korea Radioactive Waste Agency, 174, Gajeong-ro, Yuseong-gu, Daejeon, Republic of Korea

*ehghtjr@korad.or.kr

1. Introduction

Most of countries are developing and using a variety types of Cask for efficient and safe management of Spent Nuclear Fuel (SNF). In particular, the Disposal Cask used in the final management phase provide a primary barrier to isolate spent fuel and maintains leak tightness in deep environments during its design lifetime to prevent leakage of internal radioactive nuclide.

There is no domestic technical standard for disposal casks and according to the overseas disposal cask shielding design requirement, the maximum absorbed dose rate in the surface structure of the disposal container must be kept below 1 Gy/h to prevent corrosion due to radiolytic products on the outer surface of the cask [1][2].

The purpose of this study is to evaluate the thickness of a multi - purpose canister for transport - storage - disposal that meets the shielding design standard, for bentonite used as a structure around the disposal cask.

2. Method and Assumption

2.1 General Information of disposal cask

The inserting channel of SNF was designed with a width of 23.5 cm and a height of 454.8 cm, which can facilitate WH fuel (width 21.4 cm, height 406 cm), and CE fuel (width of 20.7 cm, height of 453 cm). The loading capacity of SNF is 4 bundles to made of corrosion resistant copper outside and cask nodular iron inside.

2.2 General assumptions

Based on the study by the KORAD (Korea Radioactive Waste Management Corporation), the design basis fuel for the shielding analysis is selected as CE type PLUS7 with the initial concentration of 4.0%, the emission combustion of 45 GWD/MTU and the cooling period of 40 years [3].

The analytical conditions are as follows; finding absorbed dose rate of bentonite used as external structure of the disposal cask in the normal condition by increasing the thickness of the multi-purpose canister. The MCNP6 was used to evaluate the shielding. The relative error and reliability of the calculation results were confirmed by the 10 statistical errors provided in the MCNP6 output file.

2.3 Special assumptions

In this study, the IRON INSERT of the disposal cask in the previous research is named 'internal canister'. Furthermore, in order to utilize it for transportation or storage, some assumptions are established with its inside structural change as shown in Fig. 1.

- To reduce the weight, the inside of the canister was changed to an empty space, and the assembly basket filled with the fuel
- To alter material of the changed inner canister to stainless steel, and to maintain the upper thickness of 5 cm and the lower thickness of 8 cm.
- The cask shell is made of copper to maintain a proper thickness of 5 cm to prevent corrosion.
- For the above conditions, an SNF gap of 7cm and 78 cm in inner diameter satisfying the critical condition is applied.
- Calculation of the absorbed dose rate for bentonite,

which is an outer structure of the disposal cask, is applied at a depth of 1 cm.

3. Results

The calculated gamma - ray and neutron absorbed doses rate of bentonite on the top and bottom of the disposal cask were estimated to be 0.391 Gy/h and 0.00003 Gy/h, respectively. In case of the side thickness of the inner canister was 1 cm, the absorbed dose for gamma rays of the bentonite was 1.445 Gy/h and the neutron was 0.00005 Gy/h. The absorbed dose for 3 cm was estimated to be 0.627 Gy/h for gamma rays and 0.00004 Gy/h for neutrons. Finally, in case of the thickness of the inner canister is 4 cm, the absorbed dose is estimated to be 0.379 Gy/h for gamma rays and 0.00003 Gy/h for neutrons, which does not exceed the shielding design standard of 1 Gy/h Respectively.

4. Tables and Figures

4.1 Figures

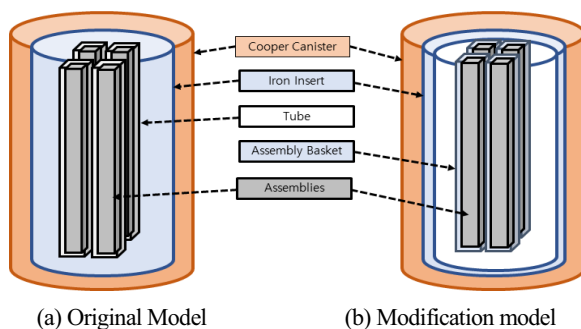


Fig. 1. Design modify of Disposal cask and Canister.

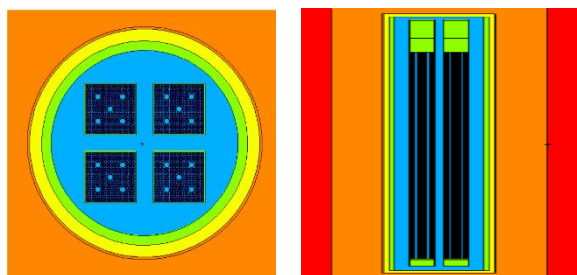


Fig. 2. MCNP modeling of Modification Model.

4.2 Table

Table 1. Absorbed dose of bentonite structure

[Unit : Gy/h]			
	Width	Gamma ray	Neutron
Side	1 cm	1.445	0.00005
	2 cm	0.813	0.00004
	3 cm	0.627	0.00004
	4 cm	0.379	0.00003
Top & Bottom		0.391	0.00003

5. Conclusion

The preliminary shielding evaluation was carried out to examine the multi - purpose utilization by changing the internal structure of the 4 bundles disposal cask developed by the existing research. As a result of the evaluation, when the thickness of the inner canister was 3 to 4 cm, the absorbed dose to the side of the cask and the top & bottom bentonite did not exceed the design standard of 1 Gy/h.

With the Shielding analysis method, it is possible to derive the basic specifications of the canister meeting all the transportation, storage and disposal standards. Also, it is considered that the optimum multi-purpose canister can be developed by analyzing the heat and structure.

ACKNOWLEDGEMENT

This work was supported by the Korea Institute of Energy Technology Evaluation and Planning (KETEP Project No. 20171720201000) and the Ministry of Trade, Industry & Energy (MOTIE) of the Republic of Korea.

REFERENCES

- [1] U.S. NRC, 10CFR60 Disposal of High Level Radioactive Waste in Geologic Repositories, (2012).
- [2] POSIVA 2005-02, "Disposal Canister for Spent Nuclear Fuel Design Report", July, 2005, Posiva Oy.
- [3] Korea Radioactive Waste Agency, Development of Engineering Barrier System for Disposal of Spent Nuclear Fuel, KORAD/EBS-TR/2014-06, (2014).

Fracture Stress Condition and its Relationship With Hydraulic Conductivity in the KURT Site

Yeonguk Jo*, Kyung-Woo Park, and Sung-Hoon Ji

Korea Atomic Energy Research Institute, 111, Daedeok-daero 989beon-gil Yuseong-gu, Daejeon, Republic of Korea

*joy@kaeri.re.kr

1. Introduction

The hydraulic conductivity of a rock fracture generally depends on the aperture size, surface roughness and contact area, all of which are functions of the stress which acts on the fracture plane [1]. Thus the stress condition on the fractures is an important factor affecting hydraulic properties of fractured rock mass. In this study, we investigated the stress conditions of the natural fractures in KURT site based on the reviewed in situ stress states and fracture observations, and compared them with estimated from a series of in situ borehole tests to observe relationship between the stress condition and hydraulic conductivity.

2. Fracture Stress Conditions and Hydraulic Conductivity

2.1 Fracture observation

We investigated distributions of natural fractures, which cross boreholes at KURT site, using borehole images from acoustic and optical image wireline-loggings. Natural fractures are ubiquitously distributed with depths, and randomly oriented. The fracture density is defined as number of all fractures at a 9.2-10 m interval, which corresponds to interval length of the hydraulic tests.

2.2 Stress condition on the fracture plane

The condition of stress on the fracture plane are generally described as slip tendency (μ), which is the ratio of effective normal stress (σ_n) to shear stress (τ). The stress components, normal and shear stress, are a function of in-situ stress states and fracture orientations (Fig. 1).

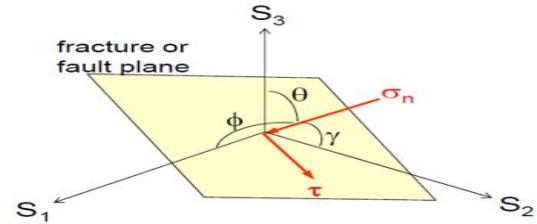


Fig. 1. Effective normal and shear stress conditions on the fracture plane.

The S_1 , S_2 and S_3 are maximum, intermediated and minimum principal stress, respectively. Since the stress regime at KURT site is favored to thrust-faulting [2], the S_1 should be maximum horizontal principal stress (S_{Hmax}). Then S_2 and S_3 are minimum horizontal principal stress (S_{Hmin}) and vertical stress (S_v), respectively.

About the poles of individual fractures, direction cosines of normal vectors are given below:

$$n_1 = \cos\phi, \quad n_2 = \cos\gamma, \quad n_3 = \cos\theta \quad (1)$$

Effective normal stress (σ_n) and shear stress (τ) can be calculated in terms of principal stresses, normal vectors and formation pore pressure (P_p):

$$\begin{aligned} \sigma_n &= n_1^2 S_1 + n_2^2 S_2 + n_3^2 S_3 - P_p \\ \tau &= \sqrt{(n_1 S_1)^2 + (n_2 S_2)^2 + (n_3 S_3)^2 - \sigma_n^2} \\ \mu &= \tau / \sigma_n \end{aligned} \quad (2)$$

All natural fractures have slip tendency, a range between 0.1-0.5 with its value significantly varying with their orientations (strike and dip).

2.3 Hydraulic conductivity

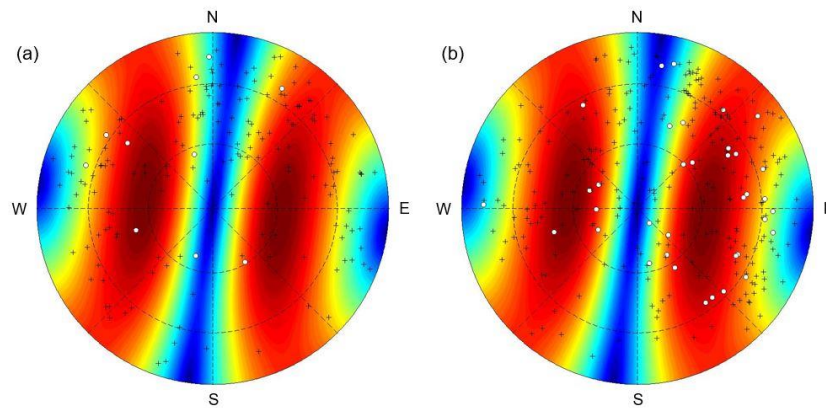


Fig. 2. Stereonets showing poles of natural fractures in the intervals of HRD (a) and HCD (b). White-circle and cross symbols denote fractures with aperture > 5 mm and all other fractures, respectively. Background color expresses slip tendency (ratio of shear to effective normal stress) acting natural fractures in different orientations.

The hydraulic conductivity was determined by a series of constant head injection tests in the boreholes (YS-area) located in the KURT site. Double packer system with an interval length of 9.2 to 10 m was used in the in situ borehole tests. Estimated hydraulic conductivities (K) at individual intervals have a range between 10^{-6} and 10^{-12} m/sec. Then we classified HRD as the interval where $\log K$ values are less than -10, and HCD as the intervals where intervals of $\log K$ are relatively higher.

2.4 Fracture distribution characteristics in HRD/HCD intervals

To observe relationship between fracture distributions and hydraulic conductivity, we plotted natural fractures in the stereonet showing slip tendency of individual fractures (Fig. 2).

All natural fractures, which are quite randomly oriented, have significantly different slip tendency depending on their geometry. There are some wide natural fractures (aperture size > 5 mm) in HCD intervals and they especially have relatively high slip potential under the in situ stress conditions.

3. Conclusion

In this study, we observed fracture distribution features and their stress conditions in the HRD and HCD intervals. We think that fracture types and fracture stress conditions are important factors

affecting water flow in fractured intervals.

ACKNOWLEDGEMENT

This work was supported by the Ministry of Science, ICT and Future Planning within the framework of the national long-term nuclear R&D program (NRF-2017M2A8A5014858).

REFERENCES

- [1] I. W. Yeo, M. H. de Freitas, and R. W. Zimmerman, "Effect of shear displacement on the aperture and permeability of a rock fracture," *Int. J. Rock Mech. Min. Sci.*, vol. 35, no. 8, pp. 1051–1070, 1998.
- [2] Y. Jo, C. Chang, S.-H. Ji, K.-W. Park, "In situ stress states at KURT, an underground research laboratory in South Korea for the study of high-level radioactive waste disposal", *Eng. Geol.*, under review.

Interpretation of Geological Deformation History Using Flat-cutting Surfaces of the Inner Wall of KURT

Soolim Jung*, Sung-Hoon Ji, and Kyung-Su Kim

Korea Atomic Energy Research Institute, 111, Daedeok-daero 989beon-gil, Yuseong-gu, Daejeon, Republic of Korea

*sljung@kaeri.re.kr

1. Introduction

In order to prevent the effect of radioactive waste on the ecosystem, it is important to understand the deep geological environment where the repository will be located. Especially, it is necessary to identify evolution processes and evaluate long-term stability of the deep geological environment so that the repository can be isolated from accessible biosphere during the long-term geological evolution. The KAERI Underground Research Tunnel (KURT) was constructed in 2006, and has been operated for site characterization research in terms of safety assessment of nuclear waste disposal. In this study, we will interpret the long-term brittle deformation history around the KURT site using flat-cutting surfaces and exposed outcrops of the inner wall of the Tunnel.

2. Study area

The KURT is located in the boundary between Okcheon Belt and Kyunggi Massif. The area is composed mainly of the Mesozoic granitoids, which is intruded in the north-east direction[1]. Regional scale area around KURT site includes various type of granitic rock such as biotite granite, two-mica granite, granite porphyry, and alkaline granite, which is evidence of continuous volcanic activity and dyke intrusion.

According to previous field survey, the major rock composition of the KURT site is two-mica granite. Weakly foliated biotite granite was also observed.

3. Methods

To understand the geological information around the research area, various geological surveys were conducted, including a literature survey, surface geophysical survey, geological lineaments analysis, field observations, borehole investigations, chemical analyses, age dating of the rock samples, and a structural analysis of the exposed outcrop and flat-cut surface inside KURT. In this paper, we focus on the results of field work and observations along the tunnel.

Two flat-cut sections were constructed to aid in the research of geological structures in the tunnel. The sections are rectangular cut surfaces measuring 5m in width and 2.5m in length. By analyzing these surfaces where the geological structure is evident, it is possible to understand the texture of rock masses and to estimate the cross-cut relationship of each structure. In addition to the surfaces, relatively fresh outcrops located in the several research modules of the KURT were observed to interpret the history of brittle deformation.

4. Results

From the study on the fracture system observed in the tunnel and the chemistry using samples from the flat-cutting surfaces, five sets of joints, two directions of major faults and three dominant rock types are identified. Although some relative ages are not yet clear, the simplified deformation history can

be interpreted as follows. The basement rock of the research area was intruded by Jurassic granite. The granite was mylonitized at deep depth and intruded by another Jurassic granite. During the cooling, pegmatitic dykes were intruded. Uplifting and volume change of rock mass caused brittle deformation. Several sets of joints formed under local stress fields. Mafic dykes were intruded along the joint surfaces. Faults occurred and crosscut mafic dykes.

REFERENCES

- [1] H.-I. Park, J.-D. Lee, J.G. Jeong, "Geological map of Korea: Yuseong sheet", Korea Institute of Geoscience and Mineral Resources (1977).

Preparation of Anoxic Corrosion Test of Canister Materials in a Deep Borehole

Minsoo Lee*, Kyung-Woo Park, Yeounguk Jo, Jihye Jeong, Jang-Soon Kwon, and Sung-Hoon Ji

Korea Atomic Energy Research Institute, 111, Daedeok-daero 989beon-gil, Yuseong-gu, Daejeon, Republic of Korea

*minm@kaeri.re.kr

1. Introduction

It is very important to verify the corrosion behavior of a disposal canister in a regional deep geologic environment. KAERI launched long term corrosion test cells in Oct. 2010 at KURT site. The launched corrosion test is undergoing in oxic condition. Recently anoxic corrosion test is planned since it is presumed that the canister corrosion in the most of the disposal period occurs in anoxic condition.

Anoxic corrosion test in a borehole is progressing in GTS, Swiss as a name of 'MACOTE; MATERIAL CORrosion TEST'[1]. The KAERI anoxic corrosion test is recently planned in one of old exploration boreholes near KURT site like MACOTE.

2. Experiment

2.1 Borehole Selection

The borehole depth is only 10 m in the MACOTE since GTS is located in anoxic granic rock bed. But the depth of a test borehole in this study will be around 300 m from ground. Several old exploration boreholes in KAERI site was studied, and then a borehole designated as YS-03 was selected since its Eh value was enough low (-247 mV) to be reductive to copper and closely located near security trail.

2.2 Borehole Conditioning

A single packer was installed at 250 m depth in YS-03, and the underground water below the packer has been extracted to about 9 liter every week through a H55 m long and ID15 mm Pipe line. The characteristics of extracted water from YS-03 were summarized in Table 1.

Table 1. Characteristics of YS-03 underground water

	Name	pH	EC, uS/cm	DO, mg/L
YS-03	Old(2004)	10.0	144	1.9
	5/23(2018)	9.36	140.6	0.14
	7/10(2018)	9.47	141.7	0.16
	8/24(2018)	9.39	128.7	0.15
	KURT Test	8.57	144.8	4.62

The oxygen concentration measured in 2018 is very lower, and the pH is higher than the old one. The YS-03 also showed clearly different water properties from the feed water supplied to the KURT corrosion test. As a result of ion concentration analysis, Cl^- is 2 ppm, SO_4^{2-} is 6 ppm, but the HCO_3^- is 36 ppm in the YS-03 underground water. It was certain that the YS-03 has been well isolated from the oxygen rich sub-surface water.

2.3 Corrosion Module Design

The YS-03 is 300 m deep and NX size (D76 mm) borehole. Some mud or debris by wall spallation may sink on the borehole bottom, so a rigid base support should be installed before the module installation. The corrosion module was designed in BX size (D60 mm) cylindrical container to fit in the NX size

borehole. Nine bentonite blocks of 10 mm thick is packed in the module, and 6 kinds of candidate metals (D15 mm, t1 mm) are inserted between the block layers as seen in Fig. 1. The test metals are to be cold sprayed coating Cu, compressed Cu, SKB forged Cu, Titanium, Stainless steel, and cast nodular iron. There are 10 μ m pore metal filters at the inside top and bottom of the module for water flow-in but blocking of bentonite extrusion

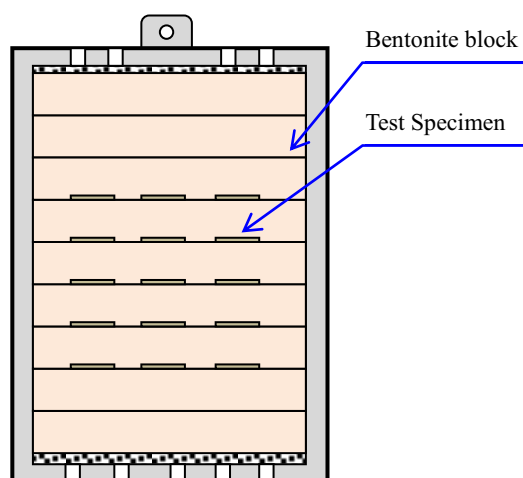


Fig. 1. Conceptual illustration of a corrosion module for a borehole corrosion test.

The emplacement of corrosion modules is quite troublesome because the lowering distance is 300 m, and its retrieval must be possible after long days. Several emplacement methods were considered as connection and disconnection method, single rotary wire connection, and respective cord connection for each module. Then the respective cord connection was chosen as an emplacement method because it is very reliable and less obstructive for the packer installation after the module emplacement.

3. Conclusion

The installation of corrosion module is planned in

2019 after several demonstration tests. And the module will be extracted after 1-2-3-4-7-10 years respectively. Actually, the extraction process is more important than the installation process because the extracted module should be kept not to contact with oxygen. Thus the design of a transportation bag for the carrying and a glove box for the dismantling of the module is necessary after the module launching in 2019.

ACKNOWLEDGEMENT

This work was supported by the Ministry of Science, ICT and Future Planning within the framework of the national long-term nuclear R&D program (NRF-2017M2A8A5014858).

REFERENCES

- [1] Grimsel Test Site, "The Material Corrosion Test (MaCoTe) Introduction", Accessed Sep. 5 2018. Available from: <http://www.grimsel.com/gts-phase-vi/macote-the-material-corrosion-test/macote-introduction>.

Synthetic Study Between Mechanical and Geological Characteristics in Crystalline Rock

Kyung-Woo Park*, Younguk Jo, Sung-Hoon Ji, and Kyung-Su Kim

Korea Atomic Energy Research Institute, 111, Daedeok-daero 989beon-gil, Yuseong-gu, Daejeon, Republic of Korea

*woosbest@kaeri.re.kr

1. Introduction

The KURT (KAERI Underground Research Tunnel) is a research tunnel which is located in KAERI (Korea Atomic Energy Research Institute). Recently, the KURT was extended to obtain the more research modules, and following researches such as engineering and natural barrier system, which are the most important factors for geological repository has been conducted in KURT. To identify the KURT site characteristics, several field tests were carried out since 2007. From the result of field investigations, the site descriptive model around KURT area was finally constructed in 2016. This paper describes the synthetic understanding between rock mechanical and geological properties in crystalline rock around KURT area. In addition, the hydrogeological characteristic can be explained by the rock mechanical understanding.

2. Site characteristics

2.1 Geo-structural characteristic-Fractures

One of the most important geo-structural characteristic is the discontinuities (fractures) in crystalline rock. Orientation of fractures, which was logged in boreholes and KURT inside could be classified with 4 groups by cluster analysis, which are NS, EW, NW and log-angled fracture groups.

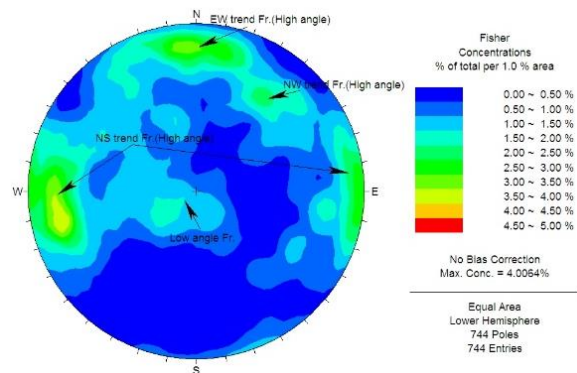


Fig. 1. Orientation of fractures around KURT.

2.2 Hydrogeological characteristic

In-situ hydraulic tests were carried out to focus on the fracture zones in study area. The transmissivities of fracture zones varied from 10^{-3} m²/sec to 10^{-7} m²/sec and showed the bimodal distribution (Fig. 2).

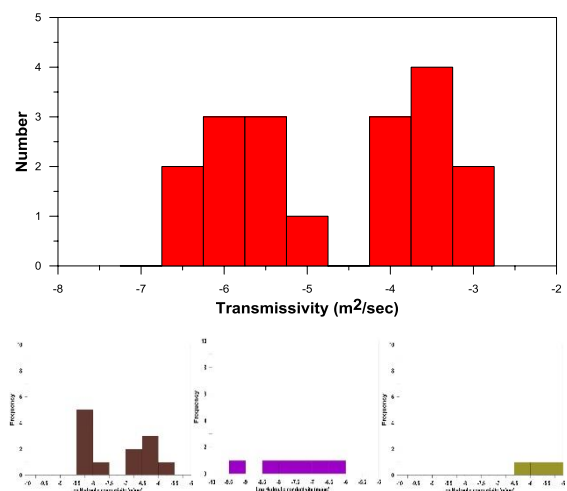


Fig. 2. Transmissivity distribution around KURT.

2.3 Rock mechanical characteristics.

Rock mechanical properties such as orientation and magnitude of in-situ stress were estimated by the hydro-fracturing and DITF measurement test. At results, the orientation of S_{Hmax} was determined as EW trend.

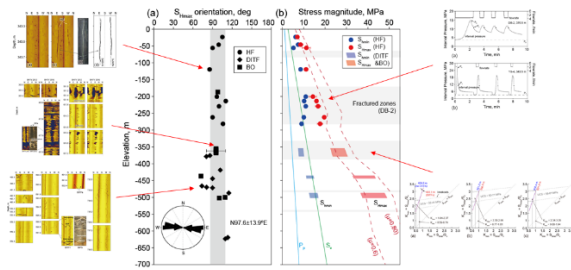


Fig. 3. Rock mechanical properties in DB-2 around KURT.

3. Geo-synthetic understanding

Based on the geological properties, we could assume that two major rock stresses were applied around KURT area in previous. The hydro-geological characteristics told us that there are two fracture zones, which have different hydrogeological properties. That is, the EW trend fracture zone has more permeable than NS and NW fracture zone. These geological and hydrogeological characteristics can be explained by rock mechanical characteristics. EW trend of S_{Hmax} had potential role to make the fracture zone with perpendicular orientation of NS and EW. Also, it could occur the EW tensile fractures, which has relatively higher permeability compared with other fractures with different orientation.

4. Conclusion

The site characteristics around KURT area were

described as site description model. Geological, hydrogeological and geo-mechanical model were constructed on the basis of the field investigations. From the results of site characteristics, we can explain that the orientation of fractures and transmissivity of fracture zones are related with the rock mechanical characteristics.

These geo-synthetic approach can help the more understanding of several geo-environmental phenomena.

Mechanical Constitutive Models of Unsaturated Expansive Clays: A Review of BExM

Jae Owan Lee*, Seok Yoon, and Geon Young Kim

Korea Atomic Energy Research Institute, 111, Daedeok-daero 989beon-gil, Yuseong-gu, Daejeon, Republic of Korea

*jolee@kaeri.re.kr

1. Introduction

Expansive clays (ex., bentonite) is favored as a buffer material for an HLW repository. When the expansive clay is installed for the buffer, it remains unsaturated for a certain period of time after installation. Mechanical constitutive models of unsaturated expansive clays are essential for the performance assessment and design of engineered barrier system (EBS) in the repository. Mechanical constitutive models of unsaturated expansive clays have been studied by many researchers. Among them, the BBM (Barcelona Basic Model) presented by Alonso et al. [1] has been widely used. It is a model for nonexpansive or slightly swelling clays, considering only the macrostructural level responsible for major structural rearrangement and also allowing for the small reversible swelling in the elastic zone. However, it has been pointed out that the BBM has limitations in applying to expansive clay with large swelling strain. The BExM (Barcelona Expansive Model), which overcomes the limitations of the BBM, has been used to describe the mechanical behavior of unsaturated expansive clays. The present paper reviews the model concept and mathematical formulation of the BExM and intends to provide the technical knowledge and information needed to test and model the mechanical behavior of the bentonite buffer for the KRS repository.

2. Model Concept

The BExM [2] is an extension of BBM in order to apply to the expansive clays with large swelling. It is based on the consideration of two levels of structure (Fig. 1 and 2): macrostructural level for major structural rearrangement and microstructural level at which the swelling of active minerals take place. The BExM takes account into the large irreversible volumetric change in the expansive clays as well as

small reversible swelling in the elastic zone.

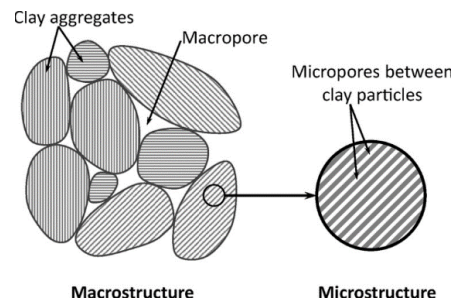


Fig. 1. Macrostructure and microstructure in expansive clays.

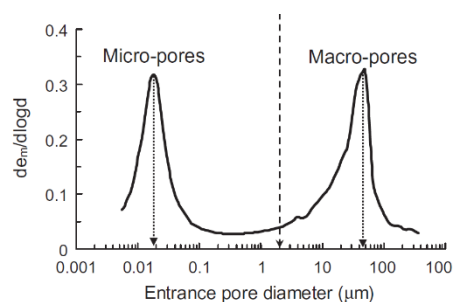


Fig. 2. Pore size distribution of the compacted expansive clays.

The following assumptions are made in this model: 1) excessive volume change tendency of expansive clays is mainly attributed to the presence of highly expansive clay minerals; 2) the microstructural level is mainly saturated and the effective stress concept holds and the microstructural behavior is elastic and volumetric; 3) mechanical, hydraulic and chemical equilibrium exists between microstructure and macrostructure; 4) coupling between microstructure and macrostructure results in possible build-up of macrostructural elastoplastic strains when elastic microstructural strains take place. Many experiments have shown that the volume change behavior is controlled by many factors including the type of clay minerals, the current degree of saturation, past wetting-drying cycles, fabric and structure created during the compaction, presence of non-expansive

minerals, their sizes, percentages and distribution in the matrix. The BExM encompasses these factors, thereby allowing predicting the mechanical behavior of expansive clays under various disposal conditions.

3. Mathematical Formulation

The BExM accounts for two levels of clay structure. The microstructural level corresponds to the aggregates of active clay mineral particles with intra-aggregate pores, whereas the macrostructural level corresponds to the larger scale clay structure.

The microstructural elastic volumetric strain is calculated as follows:

$$d\varepsilon_{vm}^e = \frac{de_m}{1 + e_m} = \frac{d(p + s)}{K_m}$$

$$K_m = \frac{\exp[\alpha_m(p + s)]}{\beta_m}$$

The macrostructural elastic volumetric strain is expressed as a function of mean net stress and suction:

$$d\varepsilon_{vM}^e = \frac{de_M}{1 + e_M} = \left(\frac{k}{1 + e_M} \right) \frac{dp}{p} + \left(\frac{k_s}{1 + e_M} \right) \frac{ds}{s + p_{atm}}$$

The variation of preconsolidation mean net stress (p_0) with suction is given by an LC (loading and collapse) yield curve function:

$$\frac{p_0}{p_c} = \left(\frac{p_0^*}{p_c} \right)^{\frac{\lambda(0) - k}{\lambda(s) - k}}$$

$$\lambda(s) = \lambda(0)[r + (1 - r) \exp(-\beta s)]$$

Macrostructural plastic strain resulted by mechanical loading:

$$d\varepsilon_{vML}^p = \frac{\lambda(s) - k}{1 + e_M} \frac{dp_0}{p_0}$$

Macrostrutural plastic strain induced by microstructural strain:

$$d\varepsilon_{vMSI}^p = f_I d\varepsilon_{vM}^e$$

$$d\varepsilon_{vMSD}^p = f_D d\varepsilon_{vM}^e$$

where f_I and f_D are the interaction functions between microstructural and macrostructural levels in case of suction increase and suction decrease, respectively (refer to Fig. 3).

Incremental total macrostructural strain:

$$d\varepsilon_{vM}^p = d\varepsilon_{vML}^p + d\varepsilon_{vMSI}^p + d\varepsilon_{vMSD}^p$$

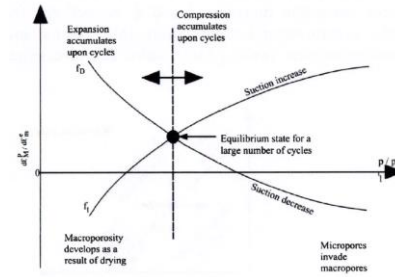


Fig. 3. Interaction and coupling functions in BExM.

4. Summary and Conclusions

More researches have been carried out for the development and enhancement of the unsaturated non-expansive clays models, while much lesser contributions have been made for the expansive clay modelling. The BExM is a representative constitutive model which may be used to predict the mechanical behavior of expansive clays. The microstructure in the constitutive model had a central role in the overall behavior of the expansive clays. The HLW repository uses as a buffer material the expansive clays (i.e., bentonite) with large swelling. The BBM may have a limitation in its application, and thus the BExM is strongly suggested to use for understanding and predicting the mechanical behavior of bentonite buffer with high reliability.

REFERENCES

- [1] Alonso, E.E., Gens, A., and Josa, A., "A constitutive model for partially saturated soils," *Geotechnique* 40(3), 405-430 (1990).
- [2] Alonso, E.E., Vaunat, J., Gens, A. "Modeling the mechanical behavior of expansive clays," *Engineering Geology* 54, 173-183 (1999).

A Conceptual Development of Coupled Thermo-hydro-mechanical Damage (THM_D) Model in a Nuclear Waste Repository

Jin-Seop Kim^{1)*}, Jun-Seo Jeon²⁾, Min-Seop Kim²⁾, and Geon-Young Kim¹⁾

¹⁾ Korea Atomic Energy Research Institute, 111, Daedeok-daero 989beon-gil, Yuseong-gu, Daejeon, Republic of Korea

²⁾ Korea Advanced Institute of Science and Technology, 291, Daehak-ro, Yuseong-gu, Daejeon, Republic of Korea

*kjs@kaeri.re.kr

1. Introduction

Damage evolution in a nuclear waste disposal system is one of the important issues from the perspective of a long-term safety concerns. Accumulation of damage induces changes in the mechanical, hydraulic, and thermal properties of a near-field rock [1].

The objective of this study is to propose the coupled thermo-hydro-mechanical damage (THMD) model to simulate the time-dependent long-term behaviors of disposal system.

2. Approach

2.1 General approach

Mazars damage model was applied to THM_D model development with regard to the damage evolution of rock [2]. The Bacerona Basic Model (BBM) was used to simulate unsaturated and partially saturated bentonite by incorporating an extra state variable for the pore suction. The general approach for THM_D model development is presented in Fig. 1. The primary code in use was Comsol MultiPhysics Ver. 5.3a.

2.2 Mass balance equations [3]

Solid

$$\frac{(1-n)}{\rho^s} \frac{D^s \rho^s}{Dt} - \frac{D^s n}{Dt} + (1-n) \text{div } \mathbf{v}^s = 0$$

Liquid water

$$\left(\frac{\alpha-n}{K_s} S_w^2 + \frac{nS_w}{K_w} \right) \frac{D^s p^w}{Dt} + \frac{\alpha-n}{K_s} S_w S_g \frac{D^s p^g}{Dt} + \alpha S_w \text{div } \mathbf{v}^s - \beta_{sw} \frac{D^s T}{Dt} + \left(\frac{\alpha-n}{K_s} p^w S_w - \frac{\alpha-n}{K_s} p^g S_w + n \right) \frac{D^s S_w}{Dt} + \frac{1}{\rho^w} \text{div} \left\{ \rho^w \frac{\mathbf{k} k^{rw}}{\mu^w} \left[-\text{grad} p^w + \rho^w (\mathbf{g} - \mathbf{a}^s - \mathbf{a}^{ws}) \right] \right\} = -\frac{\dot{m}}{\rho^w}$$

Gas

$$\frac{\alpha-n}{K_s} S_w S_g \frac{D^s p^w}{Dt} + \frac{\alpha-n}{K_s} S_g^2 \frac{D^s p^g}{Dt} - \left(n + \frac{\alpha-n}{K_s} p^g S_g \right) \frac{D^s S_w}{Dt} - \beta_s (\alpha-n) S_g \frac{D^s T}{Dt} + \alpha S_g \text{div } \mathbf{v}^s + \frac{nS_g}{\rho^g} \frac{D^s}{Dt} \left[\frac{1}{\theta R} (p^{gw} M_a + p^{gw} M_w) \right] + \frac{1}{\rho^g} \text{div} \left\{ \rho^g \frac{\mathbf{k} k^{rg}}{\mu^g} \left[-\text{grad} p^g + \rho^g (\mathbf{g} - \mathbf{a}^s - \mathbf{a}^{gs}) \right] \right\} = \frac{\dot{m}}{\rho^g}$$

2.3 Momentum balance equations

$$-\rho \mathbf{a}^s - n S_w \rho^w [\mathbf{a}^{ws} + \text{grad } \mathbf{v}^w \cdot \mathbf{v}^{ws}] - n S_g \rho^g [\mathbf{a}^{gs} + \text{grad } \mathbf{v}^g \cdot \mathbf{v}^{gs}] + \text{div } \boldsymbol{\sigma} + \rho \mathbf{g} = 0$$

2.4 Enthalpy balance equations

$$(\rho C_p)_{\text{eff}} \frac{\partial T}{\partial t} + (\rho_w C_p^w \mathbf{v}^w + \rho_g C_p^g \mathbf{v}^g) \cdot \text{grad } T - \text{div}(\chi_{\text{eff}} \text{grad } T) = -\dot{m} \Delta H_{\text{vap}}$$

$$\text{where } (\rho C_p)_{\text{eff}} = \rho_s C_p^s + \rho_w C_p^w + \rho_g C_p^g, \chi_{\text{eff}} = \chi^s + \chi^w + \chi^g$$

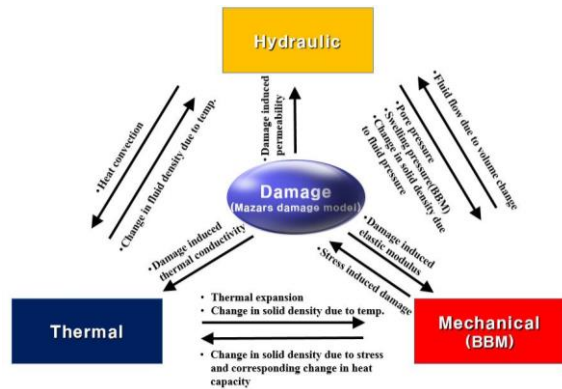


Fig. 1. A concept of coupled THM_D model development.

3. Model setup

The material properties and model constants used in THM_D modeling are listed in Table 1-3 below. Fig. 2 shows the model geometry and dimensions used for the developed model application.

Table 1. Material properties used in THM_D model

Parameter	Bentonite	Rock	plug	Heater
Density of solid particle	2740	2650	2367	7850
Dry density [kg/m ³]	1600	2650	2367	7850
Biot's coefficient	0.8	1.0	0.8	1.0
porosity	0.41	0.01	0.15	0.0001
Residual porosity	-	0.009	-	-
Young's modulus [GPa]	-	22.8	20.0	155.0
Poisson's ratio	0.4	0.2	0.19	0.285
Intrinsic permeability [m ²]	6e-20	1e-19	1e-19	-
P_0 [MPa]	3.8	1.5	1.5	-
m	0.25	0.595	0.595	-
S_{lr}	0	1	1	-
S_{ls}	1	0.01	0.01	-
λ	3	0.595	1	-
Thermal conductivity [W/mK]	1.299	3.3	1.2	52.5
Specific heat capacity [J/kg/K]	1000	1210	964	440
Thermal expansion Coefficient [1/K]	2.5e-5	7.5e-6	4.3e-6	0

Table 2. Constants in Mazars Damage Model

Rock type	ϵ_{d0}	A_c	B_c	A_t	B_t
Granite	3.7e-4	1	120	2	90

Table 3. Constants in Barcelon Basic Model

Bento nite	p_c [MPa]	p_o^* [MPa]	$\lambda_{(0)}$	r	β	κ_{io}	α_i
FEBEX project	0.1	14	0.15	0.75	0.05	0.05	-0.003

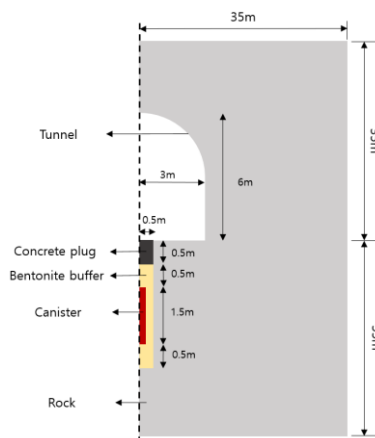


Fig. 2. Model geometry and dimensions.

4. Main Results

The variation of pore pressure, temperature and swelling pressure of bentonite with time are presented in Fig. 3-4. It is anticipated that the full saturation of bentonite is obtained after about 40 years.

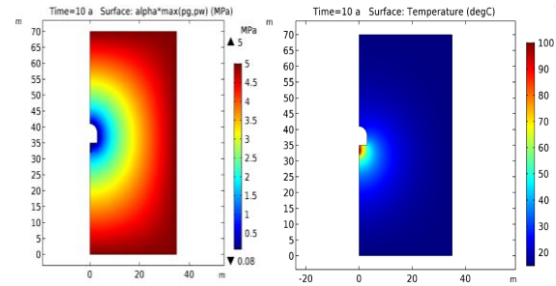


Fig. 3. Variations of pore pressure and temperature after 10 years.

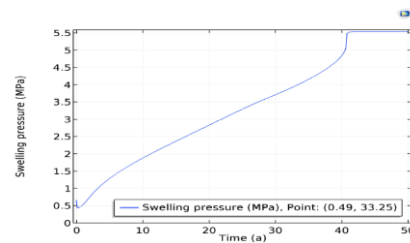


Fig. 4. Swelling pressure for 50 years.

5. Conclusion

The THM_D model was conceptually developed and successfully applied to a nuclear waste repository based on the consideration of damage evolution of rock and bentonite resaturation. It is necessary to validate the developed THM_D model from further study.

REFERENCES

- [1] C. Wei, W. Zhu, S. Chen and P.G. Ranjith, "A coupled Thermal-Hydrological-Mechanical damage model and its numerical simulations of damage evolution in APSE", Materials, 9(841), 1-19 (2016).
- [2] J. Mazars, "A description of micro-and macroscale damage of concrete structures", Engineering Fracture Mechanics, 25(5/6), 729-737 (1986).
- [3] R.W. Lewis and B.A. Schrefler, "The finite element method in the static and dynamic deformation and consolidation of porous media", John Wiley & Sons, England, 1998.

Alternative Concepts of Deep Geological Disposal for Spent Fuels

Jong-youll LEE*, Heui-joo CHOI, Hyun-a KIM, and Dong-keun CHO

Korea Atomic Energy Research Institute, 111, Daedeok-daero 989beon-gil, Yuseong-gu, Daejeon, Republic of Korea

*njylee@kaeri.re.kr

1. Introduction

For the spent fuels or high level radioactive waste, a deep geological disposal (DGD) concept is considered as the safest method with the best available technology at present time to isolate them from the biosphere. But there are lots of methods as alternative concepts to the KBS-3V(Vertical) type deep geological disposal technology which is considered as a reference concept and currently under the stage of licensing. They can be KBS-3H(Horizontal) type disposal concept and deep geological disposal system after long-term storage. In this study, reference disposal concepts for two types of spent fuels were described and two types of disposal concepts as alternative concepts were developed and analyzed preliminarily.

2. Disposal Concept for Spent Fuels

According to the Site specific activity, engineering design development was shown in the Figure 1.

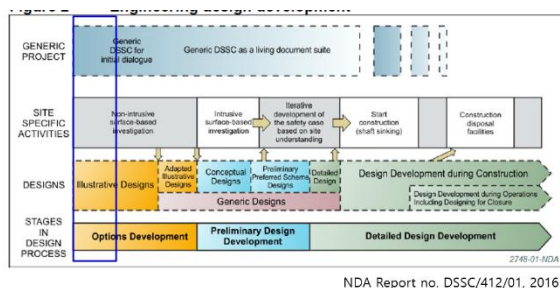


Fig. 1. Engineering Design Development.

2.1 Reference Concepts

A reference deep geological disposal concepts for PWR spent fuels and CANDU(PHWR) spent fuels were shown in the Figure 2. The thermal analyses for

the disposal systems to check the design requirement were carried out and figure 3. Showed the results the analyses.

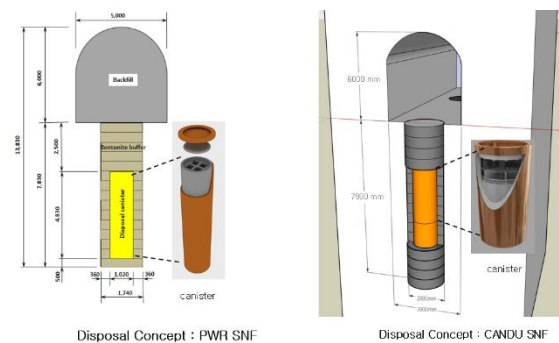


Fig. 2. Reference disposal concepts.

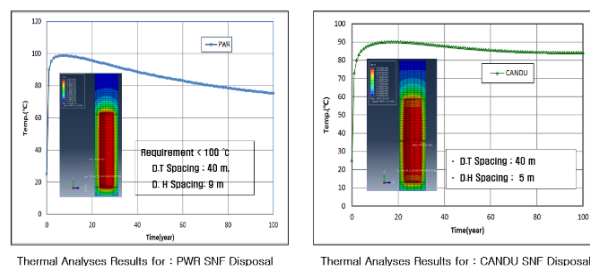


Fig. 3. Thermal analyses results for reference concepts.

2.2 Alternative concepts

2.2.1 KBS-3H. A KBS-3H type disposal concept was horizontal type disposal concept. In this concept, a Super-container which was combined with bentonite block was emplaced in the disposal tunnel horizontally. Figure 4 showed the concept of Super container and Figure showed the disposal tunnel concept with super-container.

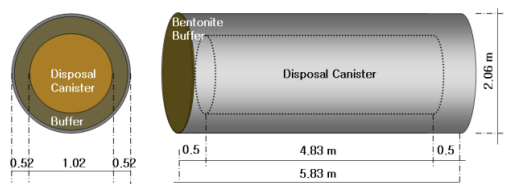


Fig. 4. Super-container concept.

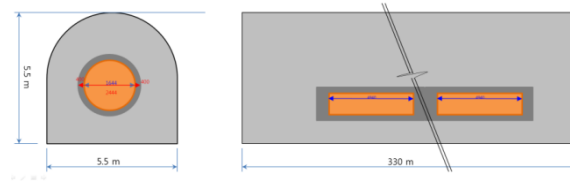


Fig. 7. Disposal concept after long-term.

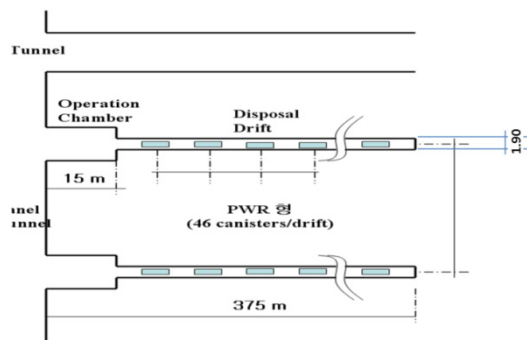


Fig. 5. KBS-3H type disposal concept.

2.2.1 Disposal concept after long-term storage.

Another alternative disposal concept can be the deep geological disposal after long-term decay storage for the spent fuels. Figure 6. showed a concept of disposal canister which had the capacity of 21 PWR spent fuels.

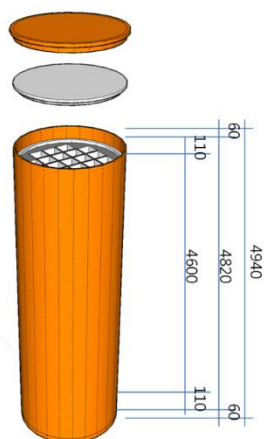


Fig. 6. 21-PWR spent fuels disposal canister.

With this 21-PWR disposal canister, firstly, the canisters were stored during about 200-300 years to reduce the decay heat. After then, the disposal tunnel would be backfilled and closed with plugs. Figure 7 showed the disposal concept after long-term storage.

3. Conclusion

There are lots of methods as alternative concepts to the KBS-3V(Vertical) type deep geological disposal technology which is considered as a reference concept and currently under the stage of licensing. They can be KBS-3H(Horizontal) type disposal concept and deep geological disposal system after long-term storage. In this study, reference disposal concepts for two types of spent fuels were described and two types of disposal concepts as alternative concepts were developed and analyzed preliminarily.

The results of this study can be used as an input data for establishment of national policy on spent fuel management.

ACKNOWLEDGEMENT

This work was supported by the Ministry of Science and ICT within the framework of the national long-term nuclear R&D program (NRF-2017M2A8A5014856).

REFERENCES

- [1] NDA, DSSC/412/01, NDA report (2016).
- [2] SKB, Final Storage of Spent Nuclear Fuel-KBS-3, SKB, Sweden (1983).
- [3] US DOE, Yucca Mountain Science and Engineering Report, DOE/RW-0539-1, US DOE (2002).
- [4] E.L. Hardin, D. J. Clayton, et al., Preliminary Report on Dual-Purpose Canister Disposal Alternatives, SNL, FCRD-UFD-2013-000171 Rev.1, (2013).

Characteristics of Water Retention Capacity for Korean Compacted Bentonite

Seok Yoon*, Changsoo Lee, Jae-Owan Lee, Won-Jin Cho, and Geon-Young Kim

Korea Atomic Energy Research Institute, 111, Daedeok-daero 989beon-gil, Yuseong-gu, Daejeon, Republic of Korea

*syoon@kaeri.re.kr

1. Introduction

Engineered barrier system (EBS) is suggested to dispose high level radioactive-waste (HLW). EBS is composed of a disposal canister, a buffer material, a backfill material, and a near field rock mass. The compacted bentonite buffer is one of the most important components of EBS for the disposal of HLW. As the compacted bentonite is located between a disposal canister with spent fuels and host rock, it is indispensable to assure the disposal safety of HLW. It can restrain the release of radionuclides and protect the canister from the inflow of groundwater. Because of inflow of groundwater into the compacted bentonite, it is essential to investigate water retention capacity of the compacted bentonite in order to evaluate the entire safety performance of EBS. Therefore, this paper conducted laboratory experiment in order to evaluate water retention capacity of Korean compacted bentonite, and compared previous researches.

2. Results and discussion

In Korea, Ca bentonite buffer materials have been produced in Gyeongju by CLIRIANT KOREA. Ca bentonite is named as KJ-I produced before 2015, and KJ-II after 2015 [1]. Table 1 shows geotechnical properties considering the Atterberg limit [2], and Korean bentonite is classified as CH with very high plasticity based on the unified soil classification system (USCS) [3].

WP4C equipment (decagon devices Inc., USA) was used to investigate water retention capacity for

Korean compacted bentonite. The WP4C equipment is based on the chilled-mirror dew point temperature condensation principle to measure total suction, it measures water potential by equilibrating the liquid phase water of the bentonite with the vapor phase water of the chamber. Total suction can be calculated using Kelvin equation, which is the thermodynamic relationship between total suction and relative humidity of the vapor space in the bentonite [4]. The water retention capacity for KJ-II bentonite was measured under the partially confined condition with initial dry density of 1.72 g/cm^3 . Fig. 1 shows the wetting and drying path. The suction of drying path showed higher than that of wetting path because of several reasons such as the inhomogeneous geometry of bentonite pores and the structural change due to the swell and contraction of bentonite. Fig. 2 shows different water retention curve (WRC) with previous research [5] using KJ-I bentonite.

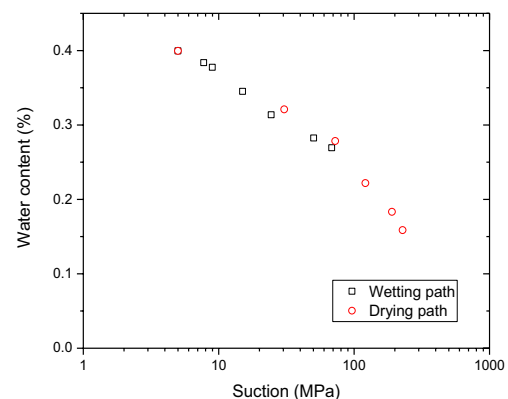


Fig. 1. Retention curve in a wetting and drying path for KJ-II .

Table 1. Geotechnical properties of Korean bentonites

	Specific Gravity	Liquid Limit (%)	Plastic Limit (%)	Plastic Index (%)	USCS
KJ-I	2.74	244.5	46.1	198.4	CH
KJ-II	2.71	146.7	28.4	118.3	CH

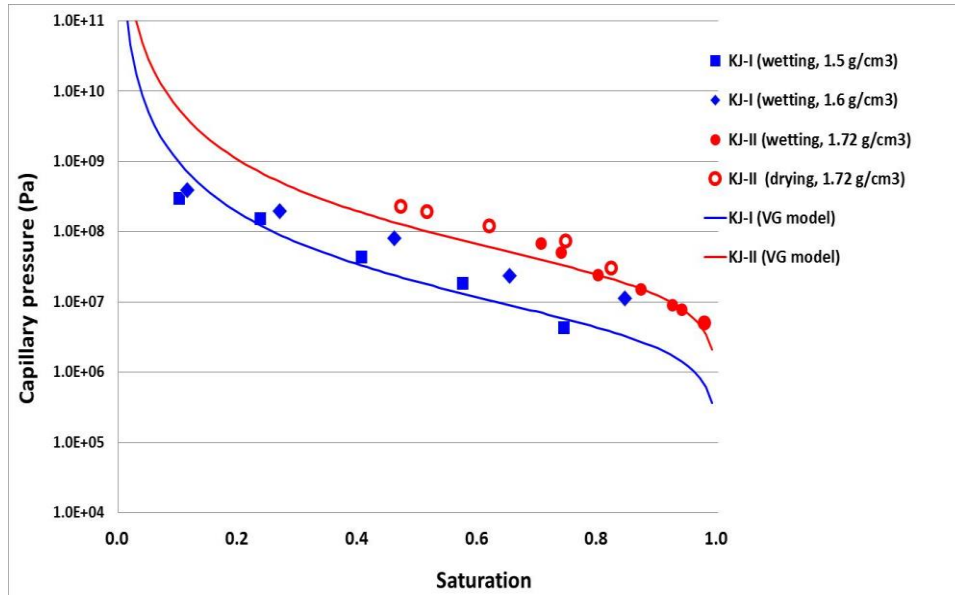


Fig. 2. Retention curve for KJ-I and KJ-II bentonites.

3. Conclusion

This paper investigated water retention capacity for Korean compacted bentonites such as KJ-I and KJ-II. Since hysteric behavior of compacted bentonite buffer in a real repository system is important, WRC was derived in a wetting/drying path for KJ-II, and various retention curves were investigated with different initial dry density. It is though that retention curves of compacted bentonites are determined according to the drying or wetting path, dry density or void ratio, and so on. Therefore, it is necessary to evaluate retention curves considering various affecting factors.

ACKNOWLEDGEMENT

This research was supported by the Nuclear Research and Development Program of the National Research Foundation of Korea (NRF-2017M2A8A5014857), funded by the Ministry of Science and ICT.

REFERENCES

- [1] You, M., Choi, H.J., Lee, M.S., Lee, S.Y., Chemical and mineralogical characterization of domestic bentonite for a buffer of an HLW repository, KAERI/TR-6182(2015).
- [2] Andrade, F.A., Al-Qureshi, H.A., Hotza, D., Measuring the plasticity of clays: a review. Appl. Clay Sci. 51(2011), 1-7.
- [3] ASTM D2487/17, Standard practice for classification of soils for engineering purpose (unified soil classification system). 2017.
- [4] Nguyen-Tuan, L., Coupled thermo-hydro-mechanical analysis: experiment and back analysis. Ph.D Thesis, Ruhr-Universität Bochum.
- [5] Lee, J.O., Choi, H.J., Lee, M.S., Lee, S.Y., Chemical and mineralogical characterization of domestic bentonite for a buffer of an HLW repository, KAERI/TR-6182(2015).

Implementation of Non-isothermal Two-phase Flow Model Into COMSOL Multiphysics

Jaewon Lee*, Jung-Woo Kim, and Dong-Keun Cho

Korea Atomic Energy Research Institute, 111, Daedeok-daero 989beon-gil, Yuseong-gu, Daejeon, Republic of Korea

*jwl@kaeri.re.kr

1. Introduction

In the case of a repository for radioactive waste, flow of ground water and gas is the key issue for the integrity of engineered barrier system (EBS). The intention of disposal is to provide sufficient isolation of radioactive wastes from reaching humans and the environment as long as possible. In order to fulfill such a strenuous criterion successfully, the evaluation of the combined effects of groundwater flow through the EBS and thermal loading from the decaying waste on the performance of the repository is important [1].

Recently, KAERI proposed the concept of the process-based total system performance assessment model for a geological disposal system which is called APro (Advanced Process-based total system performance assessment framework for a geological disposal system) [2]. Because COMSOL Multiphysics is one of the main code for APro, thermal-hydraulic model using COMSOL Multiphysics should be required.

Therefore, in this study, we implemented non-isothermal two-phase flow model into COMSOL Multiphysics and verified the numerical model compared with the results of TOUGH2.

2. Governing equation

2.1 Basic assumptions

Basic assumptions for the governing equation of non-isothermal two-phase fluid flow are defined as follows:

- Local thermodynamic (mechanical, thermal, and chemical) equilibrium
- Rigid solid phase
- Two-phase flow consisting of a liquid phase and a gas phase
- Two components being present in each phase: water and air

- Compositional model which allows a transfer of components from one phase into the other
- Negligible influence of dispersion and diffusion

2.2 Mass balance equation

Mass balance equation for arbitrary subdomain V_n of the flow system which is bounded by the closed surface Γ_n is as follows:

$$\frac{d}{dt} \int_{V_n} M^\kappa dV_n = \int_{\Gamma_n} \mathbf{F}^\kappa \cdot \mathbf{n} d\Gamma_n + \int_{V_n} q^\kappa dV_n \quad (1)$$

where κ is the mass component (water and air).

Mass accumulation term M^κ is as follows:

$$M^\kappa = \phi \sum_{\beta} S_{\beta} \rho_{\beta} X_{\beta}^{\kappa} \quad (2)$$

where β is fluid phase (liquid and gas), ϕ is porosity, S_{β} is saturation of phase β , ρ_{β} is density of phase β , and X_{β}^{κ} is mass fraction of component κ present in phase β .

Only advection is considered for mass flux term F^κ based on multi-phase Darcy's law.

$$\mathbf{F}^\kappa \Big|_{adv} = \sum_{\beta} X_{\beta}^{\kappa} \mathbf{F}_{\beta} \quad (3)$$

$$\mathbf{F}_{\beta} = \rho_{\beta} \mathbf{u}_{\beta} = -k \frac{k_{r\beta} \rho_{\beta}}{\mu_{\beta}} (\nabla P_{\beta} - \rho_{\beta} \mathbf{g}) \quad (4)$$

where u_{β} is Darcy velocity (volumetric flux) in phase β , k is absolute permeability (intrinsic permeability), $k_{r\beta}$ is relative permeability to phase β , and μ_{β} is viscosity in phase β .

2.3 Energy balance equation

The form of energy balance equation is similar with the Eq. (1).

Heat accumulation term M^H is as follows:

$$M^H = (1 - \phi) \rho_R C_R T + \phi \sum_{\beta} S_{\beta} \rho_{\beta} u_{\beta} \quad (5)$$

where Φ is porosity, ρ_R is grain density of rock mass, C_R is specific heat of rock mass, and u_{β} is specific internal energy in phase β .

Heat flux term F^H is as follows:

$$\mathbf{F}^H = -\lambda \nabla T + \sum_{\beta} h_{\beta} \mathbf{F}_{\beta} \quad (6)$$

where λ is thermal conductivity, and h_{β} is specific enthalpy in phase β .

3. Verification

We verified COMSOL Multiphysics compared with TOUGH2 results using 1D unsaturated domain. Fig. 1 shows the geometry, initial condition, and boundary conditions of 1D unsaturated flow model.

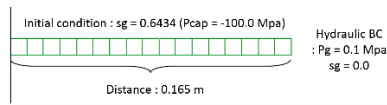


Fig. 1. Schematic view of 1D unsaturated domain.

Table 1 shows properties of the unsaturated domain.

Table 1. Properties of the unsaturated domain

Properties		Value
Porosity		0.438
Permeability (m ²)		6.4E-21
Pore compressibility (Pa ⁻¹)		1.0E-10
Relative permeability (Corey's curve)	$k_{r_i} = \hat{S}^4$	S_{lr} 0.0
	$k_{r_g} = (1 - \hat{S})^2 (1 - \hat{S}^2)$	S_{gr} 0.0
		λ 4.0
		λ 0.3
Capillary pressure (Van Genuchten curve)	$P_c = -P_0 ([\hat{S}^*]^{-1/\lambda} - 1)^{1-\lambda}$	S_{lr} 0.0
		P_0 1.08e-7
		P_{max} 1.0E+15

Fig. 2 shows the distribution of liquid saturation in 1D unsaturated flow model. Dot means TOUGH2 results and line means COMSOL Multiphysics results. As shown in Fig. 2, the results of COMSOL Multiphysics are well matched with the results of TOUGH2.

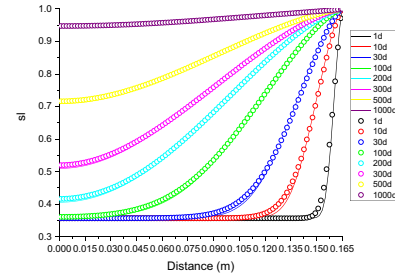


Fig. 2. Distribution of liquid saturation in 1D unsaturated flow model.

4. Conclusion

In this study, we implemented non-isothermal two-phase flow model into COMSOL Multiphysics and verified the numerical model compared with the results of TOUGH2 using 1D unsaturated domain. For further work, more comprehensive verifications and validations will be conducted. After verifications and validations, we will embed this model in the process-based total system performance assessment model for a geological disposal system (APro).

ACKNOWLEDGEMENT

This work was supported by the Nuclear Research and Development Program (No. 2017M2A8A5014856) of the National Research Foundation of Korea (NRF) funded by the Ministry of Science and ICT (MSIT).

REFERENCES

- [1] K.B. Min et al., "Thermally-induced mechanical and permeability changes around a nuclear waste repository - a far-field study based on equivalent properties determined by a discrete approach", International Journal of Rock Mechanics and Mining Sciences, 42, 765–80 (2005).
- [2] J.-W. Kim et al., "Development of Modeling Interface for a Process-Based Total System Performance Assessment of a Geological Disposal System", Proceeding of 2018 KRS Spring Meeting (2018).

Numerical Analysis of In-situ Flow Tests for Locally Variable Hydraulic Property on a Borehole

Nak-Youl Ko* and Sung-Hoon Ji

Korea Atomic Energy Research Institute, 111, Daedeok-daero 989beon-gil, Yuseong-gu, Daejeon, Republic of Korea

*nyko@kaeri.re.kr

1. Introduction

If deposition holes for high-level wastes in the deep geological disposal are damaged by excavation of the holes, flow and transport resistance at the near-field can be degraded. In this study, numerical analysis for in-situ flow with a double chamber (dipole) structure in single borehole was conducted [1].

2. Method

Numerical simulations for dipole flow tests were performed in discretized subsurface medium with hydraulic properties observed at KURT Research Gallery #6. First of all, the effect of anisotropic hydraulic conductivity on groundwater flow was examined. Then, a locally variable hydraulic conductivity, which represents local flow structures or damaged zone, was applied between the upper and lower chamber.

2.1 Modeling Domain for Numerical Simulations

For numerical simulations, discretized modeling domain was constructed (Fig. 1). Hydraulic conductivities were applied as the estimations obtained by field tests in KURT (Fig.2)

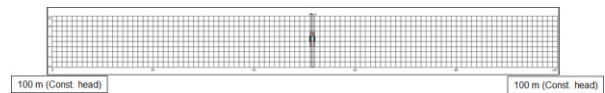


Fig. 1. Discretized modeling domain.

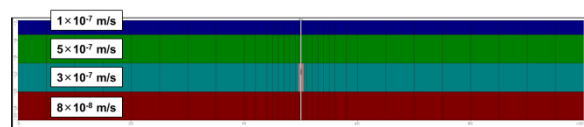
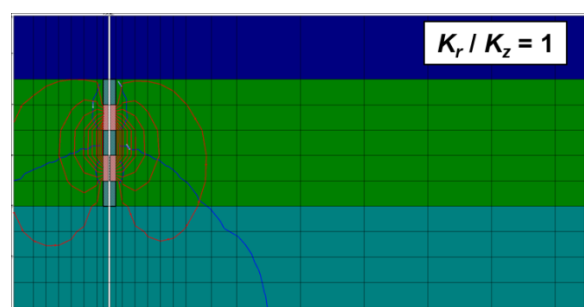


Fig. 2. Distribution of Hydraulic conductivity in the modeling domain.

3. Results

3.1 Effect of Anisotropy

Anisotropic hydraulic conductivity ($K_x / K_z = 10.0$) was applied and the simulation results were compared with that of isotropic case ($K_x / K_z = 1.0$). In the anisotropic case, groundwater flow path was extended more laterally than that of isotropic case. Therefore, travel time of groundwater also increased. If high anisotropy is observed or expected in test area, enough test time will be required to analyze groundwater flow conditions more accurately.



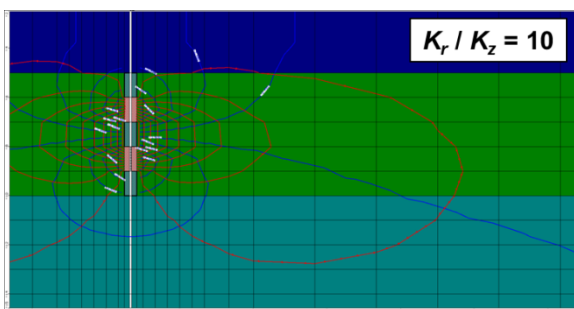


Fig. 3. Difference of groundwater flow path by anisotropy of hydraulic conductivity.

3.2 Effect of Local Structure

A high hydraulic conductivity zone between the upper and lower chamber was assumed and groundwater flow was simulated under anisotropic condition (Fig. 4). From the results, groundwater flow path became smaller and more than 50% of injected water at the lower chamber reached upper chamber throughout the high conductivity zone, which had 10-100 times higher hydraulic conductivity than other part of modeling domain.

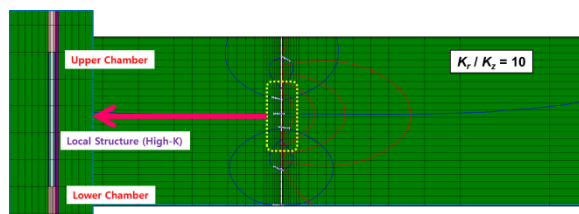


Fig. 4. Changes of groundwater flow path by local structure.

4. Conclusions

To investigate an effect of locally variable hydraulic conductivity on groundwater flow, numerical simulations were performed. The simulation results show that anisotropic distribution of hydraulic conductivity and locally variable hydraulic conductivity have much influence on

groundwater flow path and travel time. These results and analysis can be helpful to design in-situ field test of dipole tracer test, which may shows directly an effect of short-cut transport via local damaged zone.

ACKNOWLEDGEMENT

This work was supported by the Ministry of Science, ICT and Future Planning within the framework of the national long-term nuclear R&D program (NRF-2017M2A8A5014858).

REFERENCES

- [1] Z.J. Kabala, "The dipole-flow test: a new single-borehole tests for aquifer characterization," Water Resources Research, 29(1), 99–107 (1993).

4분과

중저준위폐기물관리 (Oral)



Necessity of Reasonable Consideration About Disposal Condition for VLLW (Very Low Level Radioactive Waste) of NPP Decommissioning

Hyun-Tae Choi*, Byeoung-Kug Lee, Hyun-Keun Shin, and Jun-Ki Yum
Korea Hydro & Nuclear Power Co., Ltd., 1655, Bulguk-ro, Gyeongju-si, Gyeongsangbuk-do, Republic of Korea
*brilliant@khnp.co.kr

1. Introduction

Change of government's energy policy have effected on nuclear industry. The first commercial NPP (Nuclear Power Plant) in Korea, Kori-1, will be decommissioned and Wolsung-1 will take a step for permanent shutdown and decommissioning. Under this situation, It is possible to predict that the radioactive waste will increase during the NPPs (Nuclear Power Plant) decommissioning period. Therefore, radioactive waste disposal will be a major problem without proper disposal criteria. Especially, it is necessary to consider more effective method to dispose Very Low Level Radioactive Waste (VLLW) which is the largest amount of radioactive Waste. To do this, the reasonable disposal criteria for VLLW should be established based on experience and technical knowledge. The purpose of this study is to suggest necessity of appropriate disposal criteria and treatment for VLLW of NPP decommissioning

2. Current state about VLLW disposal

2.1 Properties of decommissioning waste

Kori unit 1 will be decommissioned in several years. Then, large amount of waste generation will be expected during the decommissioning. Therefore, proper management for decommissioning waste is able to effect on result of decommissioning. For this objective, properties of decommissioning waste should be analyzed. Table 1 shows the properties of waste of NPPs decommissioning

Table 1. The properties of decommissioning waste [1]

Properties	Description
Kinds of waste	· Almost is industrial waste · Most of radioactive waste is VLLW · Just few of ILW and LLW
Amount	· Large volume of waste · Generated in short time
Applicable Management	· Extension of Self disposal · Recycling for metallic waste

As shown in Table 1, decommissioning waste has many kinds of properties. Moreover, it will be able to affect decommissioning strategy. Therefore, analyzing result of decommissioning effect which is considering decommissioning waste properties are very important to perform decommissioning successfully.

2.2 Generation ratio of VLLW of NPP decommissioning.

The amount of waste is important factor to establish decommissioning strategy because it is possible to affect economics of decommissioning due to the high cost for waste disposal. Therefore evaluation for exact prediction of waste amount is important. However, it is difficult to predict exact amount of radioactive waste during the NPP decommissioning. For example, real waste quantity is more than expected quantity decommissioning in USA due to increase of contaminated soil [2]. Since, there is no standard to predict exact quantity of radioactive waste during NPPs decommissioning. Moreover, amount of radioactive waste can be affected by government policy, decommissioning strategy and regulations [3]. According to the revised classification criteria of IAEA total amount of waste will be 14,000 (200 L Drum) during the NPPs decommissioning of 900 ~ 1,300 MWe PWR type. Table 2 shows the predictive VLLW amount of other countries.

Table 2. Prediction about VLLW amount of countries [4]

Country	Total Waste	VLLW(%)
Korea	14,500 Drum	6184 Drum(42.6%)
France	85,500 Drum	50,000 Drum (58.5%)
Japan	4.213 ton	2,823 ton (67%)

2.3 Consideration of Treatment for Particulate VLLW

The cost of waste management is the largest portion of total decommissioning budget.(225,577 M USD, 39%) Therefore, the effective management plan for waste should be established to implement decommissioning NPPs economically. In particular, it needs appropriate evaluation about VLLW waste. Since, as shown in Table 2, VLLW is the largest volume of waste. It means that if we can decrease the cost of disposal for VLLW, total cost of decommissioning will be decreased. Moreover, as shown Table 3, cost for disposal has increased. Thus, it is possible to foresee the total cost of NPP decommissioning will increase in future.

Table 3. Change of cost for disposal waste

Years	2010	2012	2015
Cost for drum	6,600 USD	10,650 USD	13,700 USD

In addition, additional treatment for VLLR such as immobilization or stabilization and etc, is another factor which can raise the disposal cost. For example, concrete and soil occupy the large amount of decommissioning waste. According the Korean waste acceptance criteria,

these kinds of waste are should be immobilized or solidified by specific matrix like a Polymer, Paraffin or using vitrification. And also, the homogeneous waste like a spent resin, soil, concentrated waste fluid should be solidified and hetero generous waste such a concrete and metal scrap have to be immobilized. These additional treatments can lead volume increase of waste drum for VLLW. As a result of that, total cost of decommissioning can increase. Table 4 shows the comparison of the additional treatment including cost and volume increase.

Table 4. Comparison of treatment cost for VLLW

Treatment	Vinyl Package	Cement Solidification	Polymer Solidification
Volume Increase	-	100%	50%
Cost Increase	120 USD	30,000 USD	23,000 USD

2.4 Particulate VLLW Treatment of foreign case

The acceptance criteria in Korea for particulate VLLW is more ambiguous than other country. So, it is difficult to dispose particulate VLLW efficiently without specific conditions of treatment for VLLW such as stabilization, solidification. Many other countries have their own acceptance criteria for VLLW. The acceptance criteria has established according to properties of VLLW and disposal facility. Table 2 shows various VLLW treatment of foreign country. Thus, they can improve the effectiveness of waste disposal by applying various acceptance criteria such a characteristic of physical and chemical, package for radioactive waste. Therefore, it is necessary to analyze method of VLLW treatment in foreign countries to establish more effective and reasonable acceptance criteria for VLLW.

Table 5. VLLW treatment of foreign country

Country	USA	SPAIN	UK
Waste Class	Class A	VLLW	VLLW
Treatment	No Stabilization	Without solidification pretreatment	No additional Treatment
Package	Soft-bag	Flexible Package	Soft-side

3. Proposal to overcome difficulties

There are multifarious considerations to establish reasonable acceptance criteria for VLLW. Since, there is no exact information of decommissioning waste in Korea. Consequently, lots of opinion could be raised by various expert groups [5]. Therefore, to establish reliable and effective acceptance criteria for VLLW, continuous efforts, as following challenges, are needed.

- Radioactive effects of VLLW should be evaluated by adapting more advanced technique which can predict exact VLLW amount and environmental effect

- It needs sufficient research and review about foreign case when adjust acceptance criteria for VLLW.
- The communication among NPPs operator, disposal facility agent, the public and government has to be taken actively to apply effective and economical waste treatment.

Careful and steady research of foreign case, applying new technology, smooth communication system can be a core requirement to establish reasonable acceptance criteria for VLLW.

4. Conclusion

Government has tried to enforce safety regulation to satisfy people's sympathy against radioactive concern. In addition, government is concerning the disposal of radioactivity waste, because of resent social issue related Radon mattress. As a result of that, the worry about radioactivity waste has been increased much more than before. In this state, it is essential to consider various methodologies to improve economics and safety of decommissioning for Kori-1. Particularly, reasonable acceptance criteria and effective VLLW treatment will be a key factor to perform efficient and safe decommissioning. This paper suggested proposal to incarnate VLLW disposal condition by comparing and analyzing various data. Reliable and effective VLLW waste disposal could be achieved by adopting reasonable disposal criteria and researching enormous information including foreign case. And also, active analysis and steady effort to develop advanced methodology will be able to reduce potential risk of the radioactive waste amount and its environmental effect. These suggestions of this paper can be used as meaningful data to specify effective acceptance criteria and reasonable policy for radioactive waste of NPPs decommissioning.

ACKNOWLEDGEMENT

This work was supported by the Research Fund of the Korea Hydro & Nuclear Power (KHNP), Republic of Korea.

REFERENCES

- [1] C.L. KIM, Trend of Management for NPPs Decommissioning waste, Konetic Report, 138, 2016.
- [2] EPRI, Maine Yankee Decommissioning Experience Report, 1997~2004, 2005.
- [3] J.S. Song, Y.K. Kim, and S.H. Lee, A Pre-Study on the Estimation of NPP Decommissioning Radioactive Waste and Disposal cost for Applying New Classification Criteria, Journal of Nuclear Fuel Cycle and Waste Technology, 15(3), 257-264, 2017.
- [4] Korean Radioactive waste Society, Analysis of Decommissioning Radioactive Waste management scenario, Journal of Nuclear Fuel Cycle and Waste Technology, 2013.
- [5] C.W. JUNG, J.H. Kim, Waste Immobilization after Dismantling of Radioactive Facilities, Concrete Journal, 28(5), 27-34, 2016.

Surface Complexation Modeling of Nickel Sorption Under Varying Geochemical Conditions at the Wolsong Repository Site.

Jongkul Park and Wooyong Um *

Pohang University of Science and Technology, 77, Cheongam-ro, Nam-gu, Pohang-si, Gyeongsangbuk-do,
Republic of Korea

*wooyongum@postech.ac.kr

1. Introduction

Radioactive nickels (^{59}Ni , ^{63}Ni) are one of the significant radionuclides, because they have relatively long half-life (76,000 and 96 years, respectively) and show high portion of radioactive wastes generated from nuclear power plants (NPPs). Nickel is an important constituent in a wide range of corrosion-resistant metal alloys including stainless steels, inconels, and monels, which are mainly used as structural materials in nuclear power reactor. Radioactive nickel isotopes are produced by neutron activation of these materials, resulting in a major part of radioactive wastes generated during the operation and decommissioning of the NPP.

Low-and-intermediate-level (LILW) radioactive wastes generated from NPPs will be disposed in the Wolsong repository site in Gyeongju, which has been built as underground concrete silo type and operated since 2015. For a long-term safety assessment of the repository, reactive transport models utilize the distribution coefficient (constant- K_d) modeling approach to describe the mobility of radionuclides in the subsurface environments. However, K_d values are very sensitive to the varying environmental conditions, specially by different pH conditions due to the reaction between groundwater (pH: ~8) and cement (pH: ~12). Wolsong repository utilizes lots of cementitious materials by engineered barrier system, backfill, and solidified materials. After closure of repository, these cementitious materials will interact with groundwater, then will buffer the pH to hyper-alkaline conditions (pH 10.5-13.1) [1].

In contrast to the constant- K_d approach, surface complexation models (SCM) can describe changes in nickel's sorption onto minerals as environmental

conditions vary. A lot of literatures on SCM indicated that the SCM approach has been successfully applied to predict sorption of contaminants (metal and radionuclide ions) on soils and sediments.

Therefore, in this study, nickel sorption onto minerals was studied in batch experiments as a function of pHs and different initial nickel concentrations. Then, in order to enable further predictive simulations, the experimental data were used to develop the surface complexation models.

2. Materials and Methods

2.1 Groundwater and mineral samples preparation

The mineral sample was collected from Wolsong repository site taking into account the location of the silos and the direction of groundwater flow. Specific surface area was determined by N_2 -BET method.

Artificial groundwater was synthesized to simulate the major ion compositions of the repository groundwater.

2.2 Batch sorption experiments

Three different initial concentrations of non-radioactive nickel (10, 50 and 100 ppb) were spiked into artificial groundwater. The pH range of solution was adjusted from pH 4 to pH 12 using HNO_3 (1M) or NaOH (1M). After 24 hours of reaction, supernatants were separated using a syringe filter (0.45 μm) and sampled for nickel concentration measurements using ICP-MS.

2.3 Surface complexation model (SCM)

A generalized composite surface complexation model (GC-SCM) was used to fit nickel sorption data using FITEQL 4.0 software. For simplicity, a non-electrostatic model (NEM) was used, which do not consider electric double layer (EDL).

3. Results and discussion

3.1 Nickel speciation in disposal condition

Ni^{2+} , NiOH^+ and $\text{Ni}(\text{OH})_{2\text{aq}}$ are the main nickel species in acidic and neutral pH conditions. However, above pH 12, the negatively charged complex $\text{Ni}(\text{OH})_3^-$ and $\text{Ni}(\text{OH})_4^{2-}$ are becoming more dominant species (Fig. 1).

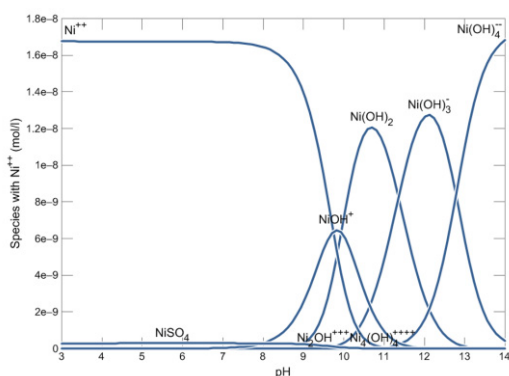


Fig. 1. Nickel speciation distribution in different pHs.

3.2 Nickel sorption experiment results

The sorption of nickel (or K_d value) is strongly influenced by the variable pH conditions. As expected, the amount of nickel sorption increased with increasing pH. However, although the surface of the mineral is negatively charged at high pH and negatively charged nickel species prevail, almost 100% of nickel sorption occurred (Fig.2a) at high pH (>8.0). Considering the solubility modeling result, these high sorption removals at hyper-alkaline condition is expected to result from $\text{Ni}_2\text{SiO}_4(\text{s})$ precipitation.

A non-electrostatic GC-SCM approach simulated the measured nickel sorption data very well as well as predicted the sorption at high pH (Fig. 2b).

Without SCM model prediction, simple batch sorption tests may mislead the nickel sorption removal, especially at high pH condition.

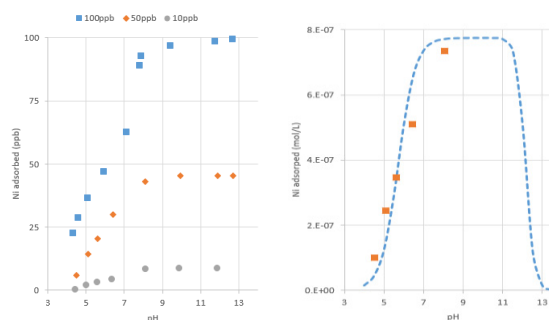


Fig. 2. a) Nickel sorption as a function of pHs at three different initial concentrations. b) SCM result.

4. Conclusion

The sorption of nickel is strongly influenced by the variable pH conditions. GC-SCM (NEM) approach simulates the experimental data very well, therefore it can be also applied to predict sorption behavior of nickel as disposal conditions vary.

ACKNOWLEDGEMENT

A portion of this research was supported by Advanced Nuclear Environment Research Center (ANERC) from the National Research Foundation of Korea (NRF), NRF-2017M2B2B1072374 and NRF-2017M2B2B1 072404.

REFERENCES

- [1] Timothy A. Marshall, Katherine Morris, Gareth T. W. Law, J. Frederick W. Mosselmans, Pieter Bots, Stephen A. Parry, and Samuel Shaw, "Incorporation and Retention of 99-Tc (IV) in Magnetite under High pH Conditions", *Environmental Science and Technology*, 48, 11853-11862 (2014).

Development of Radioactive Waste Drum Cutting System Using STD-11 Cutter

Jin Ho Ha*, Hyun Chae Song, and Myeong Ho Kim

Hana Nuclear Power Engineering Co., Ltd., 804, Hanam-daero, Hanam-si, Gyeonggi-do, Republic of Korea

*dewsky04@nate.com

1. Introduction

The radioactive waste drum is generated during the drum treatment of the radioactive waste. Especially, in the process of repacking after the integrity test (harmful substance and free moisture content) of the produced drum, the drum is broken and a lot of waste drum is generated. The waste drums produced in this way are packaged and stored in a designated place in accordance with the regulations on radioactive waste disposal or recycled through self-disposal process after decontamination process.

As a conventional disposal method, there is a method of reducing the volume by cutting the drum using oxygen welder, plasma cutting machine, grinder, etc. However, cutting method using this sort of things invariably accompanies flames, smokes and dusts which can cause high risk of fire hazard and safety concern as well as diffusion of contamination by secondary waste. In addition to that, it also has disadvantage of difficulties in securing analytical reliability owing to self-shielding effect of representative sample caused by fusion of sample's cutting surface.

In order to solve the problems of the conventional cutting method a safe cutting device has been developed.

2. Development of Radioactive Waste Drum Cutting System using STD-11 Cutter

2.1 Basic structure and cutting principle of cutting device

Basic configuration of the cutting apparatus is as follows;

- Lower rotary shaft fitting with lower cutter for cutting the drum and upper rotary shaft fitting with upper cutter
- Guide roller mounted between lower rotary shaft and upper rotary shaft for supporting peripheral of drum from bottom side
- Rotary drive mechanism for rotating the lower rotary shaft and the guide roller

The lower cutter and upper cutter are each

composed of first and second cutting elements arranged at predetermined interval on the respective lower rotary shaft and upper rotary shaft.

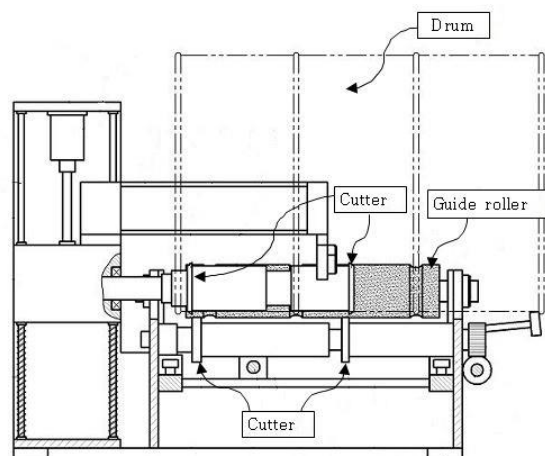
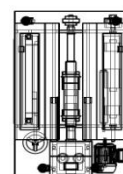
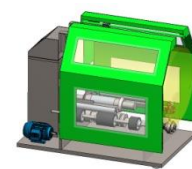


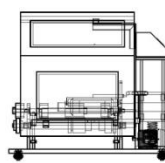
Fig. 1. Basic configuration of cutting device.



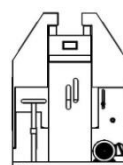
(d) Floor plan



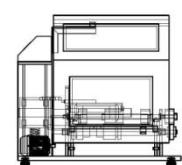
(e) Stereoscopic view



(b) Left side view



(a) Front view



(c) Right side view

Fig. 2. Outline drawing of cutting device.

The working principle of the cutting apparatus is that a waste drum is mounted between the lower cutter and the upper cutter to lower the upper cutter to the cutting position and simultaneously rotate the lower cutter and the waste drum to cut the drum in the circumferential direction.

Two pairs of the lower cutter and the upper cutter

are provided so that cutting is performed for the two portions in one-time driving, so that the operation can be performed quickly.

During drum cutting operation, the drum is rotated and at the same time, the position of the guide roller which supports peripheral of the drum at the bottom side can be adjusted by linear moving mechanism. This will enable this cutting apparatus to cut the waste drum in various sizes.

2.2 Cutting device and cutting drum Specification

Table 1. Cutting device specification

division	Prototype	Finished
size (m)	1.5(W)×1.4(D)×1.2(H)	1.3(W)×0.8(D)×1.2(H)
weight (kg)	About 800 kg	About 600 kg
motor	1,700 rpm (Gear ratio 1/10)	1,440 rpm (Gear ratio 1/60)
Power supply	220V / 380A	220V / 380A
noise	Average 60 dB	Average 60 dB
Cutter Material	STD-11	STD-11

Device Photos



Table 2. Cutting Drum Specifications

division	Design specification	
	320 L	200 L
thickness (mm)	Galvanized steel sheet 1.2(KSD 3506)	Cold rolled steel plate 1.2 (KSD 3512-SPCC)
size (mm)	ø660(inner diameter) × 955(height)	ø567(inner diameter) × 884(height)

3. Characteristics and composition of Cutter (STD-11)

STD-11 is a KS (Korean Standard) symbol, and JIS (Japanese Standard) symbol SKD-11 is also used. STD is an abbreviation of 'Steel Tool Dies'. It is a classification symbol for cold-alloy tool steel on material classification, and 11 means type.

Unlike carbon tool steels, cold alloy tool steels generally contain a small amount of silicon, manganese, nickel, chromium, tungsten, and vanadium in addition to carbon in an amount of 2 to 3%. Alloying elements improve wear resistance by forming carbides.

Table 3. Chemical composition (wt. %)

C	Si	Mn	P
1.40 ~ 1.60	≤0.40	≤0.60	≤0.030
S	Cr	Mo	V
≤0.030	11.00~13.00	0.80 ~ 1.20	0.20 ~ 0.50

Table 4. Heat treatment temperature (°C) and hardness

Heat treatment temperature (°C)			Hardness	
Annealing	Quenching	Tempering	Annealing	Tempering
800~870	1000~1050	550~680	≤255	≥58

4. Conclusions

Newly developed Radioactive Waste Drum Cutting System using STD-11 cutter makes it possible to do drum cutting job cleanly and safely without risk of fire hazard and accident experienced in the conventional cutting method due to flame, smoke, dust, noise, etc. Its clean cutting operation can also make it possible to reduce rad-waste by increasing the probability of being recycled as self-disposal after decontamination for relatively low polluting waste drums.

In addition, since operation of the device is designed easily, cutting operation is very convenient and simple, and working efficiency can be improved. Further more, the device is compactly designed and thus, working space can be sufficiently secured without any difficulty.

REFERENCES

- [1] Nuclear Safety Commission Notification No. 2014-3 (Regulation on Classification of Radioactive Waste and its Disposal Standards).
- [2] The 14th Radiation Management Cooperation Company Technology Development Case Presentation, Radioactive Waste Drum Cutting Equipment Development (2017.11.09 ~ 10), Daegu.
- [3] Korea Hydro & Nuclear Power Co., Ltd. Electronic Bidding, Radioactive Waste Drum Technical Specification, (Specification No: 10094407).
- [4] Korea Hydro & Nuclear Power Co., Ltd. Electronic Bidding, Radioactive Waste Repacking Drum Technical Specification, (Specification No: 10618080).
- [5] Sehwa Editorial, "Chemical Dictionary", Alloy Tool Steel (May 20, 2001).

Preliminary Safety Assessment for the Disposal of Neutron Activated Concrete Waste

Sol-Chan Han¹⁾ Tae-Hyeong Kim²⁾, Yongheum Jo¹⁾, Chang Je Park³⁾, and Jong-Il Yun^{1),*}

¹⁾ Korea Advanced Institute of Science and Technology, 291, Daehak-ro, Yuseong-gu, Daejeon, Republic of Korea

²⁾ Korea Atomic Energy Research Institute, 111, Daedeok-daero 989beon-gil, Yuseong-gu, Daejeon, Republic of Korea

³⁾ Sejong University, 209, Neungdong-ro, Gwangjin-gu, Seoul, Republic of Korea

*jiyun@kaist.ac.kr

1. Introduction

On the 9th of June 2017, the Korean Nuclear Safety and Security Commission (NSSC) approved the permanent shutdown of Kori unit 1 (Kori-1), which is the first commercial nuclear power plant (NPP) in Korea. In accordance with the 5th Comprehensive Nuclear Energy Promotion Plan, Kori-1 will be decommissioned by means of an immediate dismantling strategy. Including two years of preparation period, decommission of NPP would be completed within 15 years.

For safe and efficient decommissioning of NPP, not only appropriate decontamination/decommissioning techniques but also radioactive waste management strategy are needed. In particular, the disposal method for the concrete waste, which is expected to be the predominant radioactive waste that will be generated during decommissioning [1], should be prepared.

There are two major types of decommissioned radioactive concrete waste: contaminated concrete and activated concrete. Activated concrete may contain various kinds of radionuclides [2], which are difficult to be removed, while contaminated concrete is relatively easy decontaminated [1]. Therefore, activated concrete waste might be directly disposed of in a repository without decontamination process. In this study, the preliminary post-closure safety assessment is conducted for the LILW silo repository which is disposed of activated concrete waste (biological shield).

2. Model Description

2.1 Radionuclide inventory of activated concrete waste

During the operation of NPP, various radionuclides are produced within the biological shield through the neutron-induced activation process. The sort of radionuclides, which can be produced during the NPP operational period, and its inventories were calculated

by the ORIGEN-S code [3]. Impurities (i.e. europium and cobalt), which might be present in concrete, were also considered in the calculation. The assumed elemental composition of concrete by weight in percentage is listed in Table 1.

Table 1. Elemental composition of concrete

Element	Weight %	Element	Weight %
H	1	K	1.3
C	0.1	Ca	4.4
O	52.9	Fe	1.4
Na	1.6	Eu	1×10^{-3}
Mg	0.2	Co	1×10^{-2}
Al	3.4	Total	100
Si	33.7		

In the calculation, the neutron flux and the irradiation time were assumed as 1×10^{10} n/cm²·s and 40 years, respectively, and the results are summarized in Table 2.

Table 2. Radionuclide inventories in activated biological shield (cooling time: 0.01 year)

Radionuclide	Activity Concentration (Bq/g)	Radionuclide	Activity Concentration (Bq/g)
Ar-39	5.72×10^4	Mn-54	1.71×10^4
Fe-55	1.11×10^5	C-14	1.69×10^2
Eu-152	4.59×10^3	Ca-45	6.56×10^4
Co-60	4.14×10^3	Na-22	5.18×10^1
Eu-154	8.29×10^2	Cl-36	7.13
Ca-41	3.90×10^2	H-3	4.41

2.2 Safety assessment model

Basic template of the safety assessment model, used in this study, is identical to that used in the previous study [4]. Only the source-term modeling was modified to apply changes in inventory according to the disposal of activated biological shield.

3. Modeling Result

Prior to assessing the safety for the disposal of an activated biological shield, the safety assessment was conducted for the silo repository system, where only ordinary radioactive waste is disposed without activated concrete waste, as shown in Fig. 1 (base case). The maximum annual dose rate is dominated by C-14 and isotopes of iodine and technetium appeared as important radionuclides in view of the long-term safety.

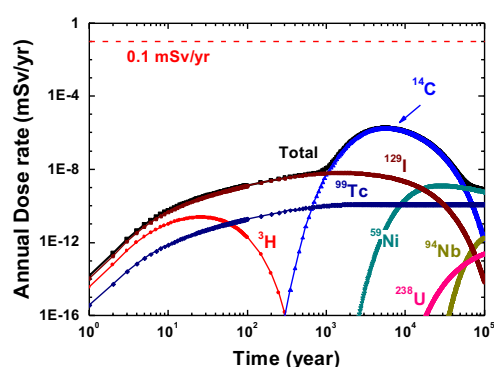


Fig. 1. Annual dose rate from the base case.

The safety assessment for the disposal of activated concrete waste in a silo repository is shown in Fig. 2. In comparison with the base case, Cl-36 and Ca-41 additionally appeared to be predominant radionuclides with respect to the long-term safety. However, no significant difference in the maximum annual dose rate is observed. In addition, the maximum annual dose rate is calculated as 1.6×10^{-6} mSv/yr, only 0.0016% of regulatory criteria.

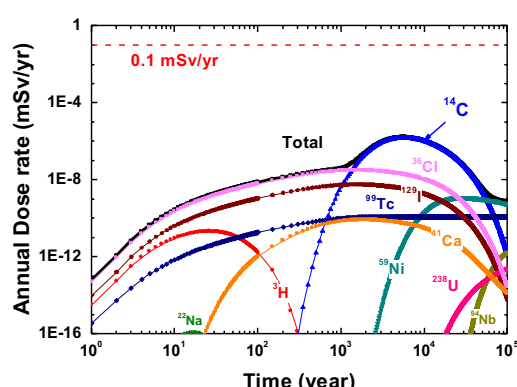


Fig. 2. Safety assessment results for the disposal of the activated biological shield.

ACKNOWLEDGEMENT

This work was supported by the Nuclear Safety Research Program through the Korea Foundation of Nuclear Safety (KOFONS), granted financial resource from the Nuclear Safety and Security Commission (NSSC), Republic of Korea (No. 1305032), and a grant from the Nuclear R&D Program of the National Research Foundation of Korea funded by the Korean Ministry of Science and ICT (Grant code: 2017M2A8A5014796).

REFERENCES

- [1] C.-S. Cheon and C.-L. Kim, "The Dismantling and Disposal Strategy of a Biological Shield for Minimization of Radioactive Concrete Waste During Decommissioning of a Nuclear Power Plant", *Journal of Nuclear Fuel Cycle and Waste Technology*, 15(4), 355-367 (2017).
- [2] G.Y. Cha, S.Y. Kim, J.M. Lee, and Y.S. Kim, "The Effects of Impurity Composition and Concentration in Reactor Structure Material on Neutron Activation Inventory in Pressurized Water Reactor", *Journal of Nuclear Fuel Cycle and Waste Technology*, 14(2), 91-100 (2016).
- [3] O.W. Hermann, R.M. Westfall, ORIGEN-S: SCALE System Module to Calculate Fuel Depletion, Actinide Transmutation, Fission Product Buildup and Decay, and Associated Radiation Source Terms, ORNL/NUREG/CSD-2/V2/R6, Oak Ridge National Laboratory, 1998.
- [4] Y. Jo, S.-C. Han, S.-I. Ok, S. Choi, and J.-I. Yun, "Radiotoxicity flux and concentration as complementary safety indicators for the safety assessment of a rock-cavern type LILW repository", *Nuclear Engineering and Technology*, in press (2018).

Competitive Sorption and Desorption Modeling of Sr Under the Binary Exchange System

Seeun Chang^{1),2)} and Wooyong Um^{1),*}

¹⁾ Pohang University of Science and Engineering, 77, Cheongam-ro, Nam-gu, Pohang-si, Republic of Korea

²⁾ Korea Atomic Energy Research Institute, 111, Daedeok-daero 989beon-gil, Yuseong-gu, Daejeon, Republic of Korea

*wooyongum@postech.ac.kr

1. Introduction

The transport behavior of radioactive strontium (^{90}Sr , a pure β -emitter with $t_{1/2}=28.1$ y), which can be released into the subsurface environment during operation of NPPs and decommissioning/decontamination of old NPPs, is greatly affected by the degree of Sr sorption and desorption at the solid-solution interface. The sorption reaction of Sr is commonly controlled by outer-sphere complexation of hydrated Sr ion onto the solid surface. However, if major cations (Na^+ , K^+ , Ca^{2+} , and Mg^{2+}) coexist with Sr due to seawater intrusion to groundwater, the sorption behavior of Sr will be significantly affected by the cation-exchange reaction. Therefore, we investigated the competitive sorption and desorption of Sr as a function of Sr and other cations' concentrations with the ion-exchange model using the GWB software (v.12 with thermos.dat database) from batch binary exchange reactions.

2. Experiments

2.1 Materials

Core rock samples were collected at the Shin-Kori #3 and 4 nuclear reactor sites in South Korea. According to XRD data, quartz and feldspar are the dominant minerals with about 13% of mica and 4.5% chloride as clay mineral. The determined exchangeable values were 0.05, 1.13, 1.00, 8.66, and 17.0 meq/kg for Sr^{2+} , K^+ , Na^+ , Mg^{2+} , and Ca^{2+} , respectively, and the sum of these values was used as the total CEC value (28.00 meq/kg) of the solid material in all experiments.

2.2 Competitive sorption and desorption of Sr

The exchangeable batch sorption experiment was conducted in binary cation system at a constant pH (pH 7). Various solution concentrations of Sr^{2+} from 10^{-6} to 10^{-1} M were prepared with deionized water. The batch experiment was conducted in an individual 15 mL polypropylene centrifuge tube by mixing the sorbent and Sr-spiked solution. Sorbent (0.1 g) and 10 mL solution were reacted in the tubes on a slow moving platform shaker at 200 rpm for 12 hours. Then suspensions were centrifuged at 10,000 rpm for 30 minutes and supernatants were filtered through 0.45 μm PVDF syringe. Sorption of Sr^{2+} on the test tubes was reported to be negligible, and the final concentrations of Sr^{2+} , K^+ , Na^+ , Mg^{2+} , and Ca^{2+} in the filtered effluent solutions were determined using ICP-OES. For this experiments, nitrated form of Sr, $\text{Sr}(\text{NO}_3)_2$ solutions were prepared using analytical grade salts.

For the desorption experiments of Sr, the desorption solution concentration of the respective background cation ranged from 10^{-6} to 10^{-1} M in pH 7 for K^+ , Na^+ , Mg^{2+} , and Ca^{2+} , respectively. The sorptive and exchangeable Sr^{2+} on the solid surface would be replaced with simultaneous sorption of respective cation in solution. The experiment procedure was the same as exchangeable sorption of Sr experiment as binary cation exchange reaction. For the experiments, KNO_3 , NaNO_3 , $\text{Mg}(\text{NO}_3)_2$, and $\text{Ca}(\text{NO}_3)_2$ were used to prepare for the respective desire concentrations in solution. The selectivity coefficients (K_{sel}) of binary ion exchange reaction were calculated by using Gaines-Thomas exchange convention over a large range of concentrations.

3. Results and discussion

When Sr^{2+} reacts on the surface of solid sample, the mineral precipitation, surface hydroxyl sorption as non-specific sorption, or ion exchange reaction with major cations controls Sr^{2+} surface reaction. The exchange affinity of major cations toward Sr^{2+} was in order of $\text{Ca}^{2+} > \text{Mg}^{2+} > \text{K}^+ > \text{Na}^+$ under both binary Sr^{2+} sorption and desorption reactions.

3.1 Competitive Sr sorption with modeling

The experimental and model fit results are shown in Fig. 1. The red dots are the exchangeable sorption amount of Sr^{2+} and dotted line is the best fit results. The K_{sel} value from exchange reaction between Sr^{2+} and CaX_2 (Ca^{2+} on the solid surface) was exceedingly valuable at relatively low ionic strength ($\sim 5 \times 10^{-2}$ M), however, as increasing the equilibrium ionic strength the other exchange reactions must be applied to fit the data. Thus considering only ion exchange reaction is enough to observe the sorption behavior of Sr under low ionic strength condition. However, as the ionic strength increased, the additional sorption mechanism such as precipitation, non-specific surface sorption, or ion exchange reaction (even all major kind of cation exchange reaction) must be considered to describe Sr sorption behavior much more correctly.

3.2 Desorption of Sr with modeling

The exchangeable amounts of Sr^{2+} onto the solid surface after Sr^{2+} desorption reaction are shown in Fig. 2. As a result, the Sr^{2+} amount on the solid surface was decreased with increasing the equilibrium IS (Ionic Strength) for all the reactive cations. However, when SrX_2 (Sr^{2+} on the solid surface) reacted with Na^+ at 0.1 M of equilibrium IS condition, the exchange reaction between SrX_2 and Na^+ reached the equilibrium state. Therefore, approximately 4.5×10^{-2} $\mu\text{eq/kg}$ of Sr^{2+} was considered as the maximum desorption amount of

exchangeable Sr^{2+} from the solid surface. The order of relative mean square is Ca^{2+} (0.0004) > Mg^{2+} (0.033) > K^+ (0.454) > Na^+ (1.000). Thus, we can make the best description and predict the desorption behavior of Sr^{2+} from the solid surface by using divalent data (Mg^{2+} and Ca^{2+}) with the modeling works.

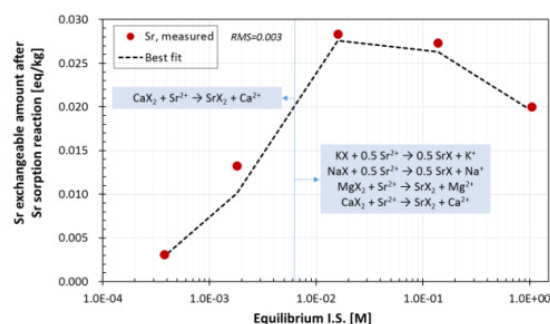


Fig. 1. The measured exchangeable Sr^{2+} amount with the best model fit.

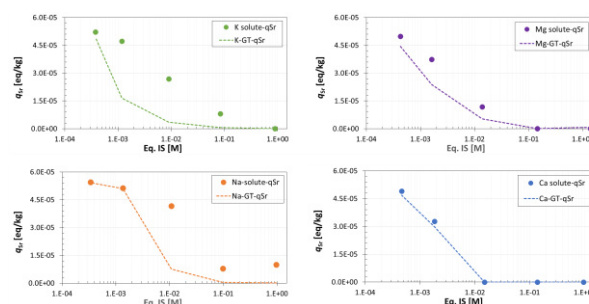


Fig. 2. The modeling fit results of exchangeable Sr^{2+} amount on the solid surface with respect to major cations.

ACKNOWLEDGEMENT

This work was supported by the National Research Foundation of Korea [NRF-2013R1A1A2063649] funded by the Ministry of Education, Science, and Technology, and by the Nuclear Core Technology of the Korea Institute of Energy Technology Evaluation and Planning (KETEP) grant funded by the Korea government Ministry of Trade, Industry and Energy [No.20171510300670].

Preliminary Studies on Lower Limits of Detection for Gaseous Radioactive Effluent Based Upon Risk-based Approach

Na Yoon Choi and Jae Hak Cheong*

Kyunghee University, 1732, Deokyoung-daero, Giheung-gu, Yongin-si, Gyeonggi-do, Republic of Korea

*jhcheong@khu.ac.kr

1. Introduction

Nuclear power plant ("NPP") generate various types and amounts of radioactive waste during operation. Liquid and gaseous radioactive wastes are treated in each system and released into the environment in the form of effluents. Discharged liquid and gaseous radioactive effluents cause exposure to populations to various exposure pathway. In order to regulate the effects of radioactive effluents, the provisions of radioactivity concentration and offsite dose are used in domestic and abroad.

In order to obtain the reliability of the measured radioactivity concentration and offsite dose, the sensitivity of the Lower Limit of Detection (LLD) should be secured at a certain level or more. If radioactivity concentration or offsite dose measured using LLD which is not secure the appropriate sensitivity, the accuracy of results cannot have sufficient reliability. For the proper monitoring of the released each nuclide, LLDs are prescribed in domestic and abroad. LLDs for each nuclide are defined in Korea Hydro and Nuclear Power Co. Ltd. (KHNP), Radiological Effluent Control Plan for Younggwang NPP Units 5 and 6 in case of domestic and defines in USNRC (United States Nuclear Regulatory Commission) NUREG-1301 in case of United States [1, 2]. But the values are uniform values that do not take into account the characteristics of the NPP, radioactive effluent and that effects.

In 2017, Cheong proposed the deriving methodology of risk-based detection limits for liquid radioactive effluents [3]. That methodology derives the risk-based detection limits using the level of contribution to both radioactivity concentration and offsite dose.

In this study, proposing the deriving methodology of risk-based LLD for gaseous radioactive effluent. Also, deriving the risk-based LLD and confirm the validity of risk-based LLD and present LLD using the APR1400 case.

2. Method

The risk of gaseous radioactive effluent is defined by totally six criteria, the radioactivity concentration and five kinds of offsite dose (Gamma air dose, Beta air dose, Total body dose, Skin dose by noble gases

and Organ dose by radioiodine and particulates). In this study, six values were calculated using the releasing of the gaseous radioactive effluent and the virtual environment data in the APR1400 Design Control Document tier 2 (DCD).

As the mentioned at the prior research, the methodology for gaseous radioactive effluent based upon risk-based approach is divided 2 steps. First, in a single nuclide condition, deriving the risk-based LLDs for each risk (six criteria). Second, in the multiple nuclides condition, evaluating the sensitivity of the gaseous radioactive effluent totally.

First of all, in order to derive the risk-based LLD for each risk, specifies the minimum margin for risk when the radioactivity concentration which will be measured at the monitoring tank is same with the LLD. This value is called the safety factor (s). Safety factor means that it is necessary to have a sensitivity which can measure within the range of not exceeding designated value (i.e., $0 < s < 1$) of risk value by nuclides in the single nuclide condition. It can be calculated each risk-based LLD with the designated margin. The smallest values for each nuclide among the calculated LLD become the risk-based LLD.

In this case, target nuclide is all nuclides (37) in the gaseous radioactive effluent to be discharged. Equations for deriving risk-based LLDs are in Table 1.

Table 1. Equations for deriving the risk-based LLD under the single nuclide condition

Condition	Equation
Radioactivity concentration	$LLD_{ECL,i} \leq \frac{s}{f \cdot (X/Q)} \times ECL_i$ (1)
Offsite dose	$LLD_{D,i} \leq \frac{s}{f} \times \frac{DC_D}{PDF_{D,i}^{path}}$ (2)

After that, evaluate the risks due to gaseous radioactive effluents totally when using risk-based LLDs as radioactivity concentration according to confirm the sensitivity of the used LLDs as a monitoring standard. Standard level in multiple nuclides condition is also called safety factor (S) and it also means that in order to evaluated as LLD which is have designated sensitivity, it is need to be able to measure within the range of not exceeding designated value (i.e., $0 < s < S < 1$) of risk value caused by all nuclides in the multiple nuclides condition. If values calculated in each risk greater than safety factor, it

can judge that used LLDs do not have sufficient sensitivity to measure the radioactivity concentration in risk-based point of view. The application of a risk-based approach for gaseous radioactive effluent under the multiple nuclides condition can be obtained by extending the prior study, which deals the methodology of deriving the risk-based LLD for liquid radioactive effluent.

3. Results

3.1 Risk-based LLD of APR1400 in Single Nuclide Condition

Based on the gaseous radioactive effluent discharged from APR1400 nuclear power plant, risk-based LLDs for each nuclide is shown in Figure 1. Present LLDs in NUREG-1301 are indicated by a solid red line and the risk-based LLDs derived by six criteria (radioactive concentration, Gamma air dose, Beta air dose, total body dose, skin dose by noble gases and organ dose by radioiodine and particulates) are expressed as a various notation.

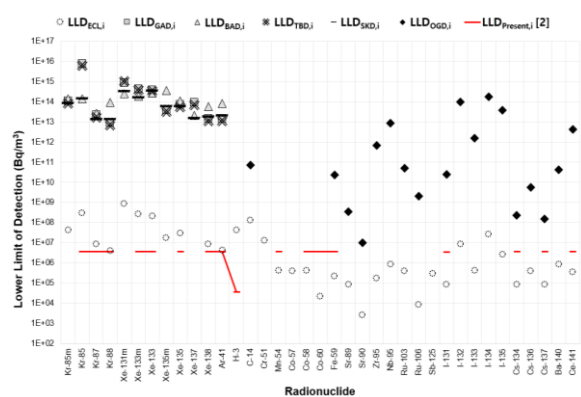


Fig. 1. Present and derived Risk-based LLD in single nuclide condition by Equation (1) and (2).

As mentioned like, risk-based LLD for each nuclide is determined as the smallest value among derived LLDs nuclide. Respectively, risk-based LLDs are determined by the radioactivity concentration for 36 nuclides and by the skin dose due to noble gas for only 1 nuclide. Also among 17 nuclides which present LLDs values are specified, 9 nuclides have lower value (i.e., more sensitivity) than the derived risk-based LLDs in radioactivity concentration and four offsite doses by noble gas and 0 in radioactivity concentration and one offsite dose by radioiodine and particulates. The nuclide representing the most significant difference between present LLD and risk-based LLD is ^{60}Co , and the risk-based LLD is about 170 times lower. This indicates for single nuclide that all risks due to noble gas can be measured with sufficiently sensitivity and it can have confidence to results. On the other hand, the risk due to radioiodine and particulates, especially the radioactivity concentration denotes a possibility that the present LLDs cannot be

performed sufficiently measurement from the risk-based point of view.

In multiple nuclides condition, safety margin which is relevant with safety factor can be calculated by methodology in previous study. Results calculated by previous study, risk-based LLDs have enough sensitivity to all risk except the radioactivity concentrations. It can also be deduced that this value is lower than the value derived by using present LLD.

4. Conclusion

In this study, derivation methodology of risk-based LLD derivation method for gaseous radioactive effluent is proposed. The risk-based LLD allows detecting of the nuclides graded by contribution, taking into account the environmental impact of the effluent on the radioactive concentration and contribution to offsite doses. A case study was conducted based on the gaseous radioactive effluent and the hypothetical condition in APR1400 DCD. Risk-based LLD was derived for 37 nuclides. Respectively, risk-based LLD for 36 nuclides for the radioactivity concentration, and 1 nuclide for the skin dose due to radioiodine and particulates are determined. Also, among 17 nuclides which specified the present LLD values already, 8 nuclides have lower risk-based LLD values than present LLD. All 8 nuclides are radioiodine and particulates. It represents the probability that risk cannot be got confidence when measured by using present LLD for radioiodine and particulates.

ACNOWLEDGEMENT

This work was supported by the Nuclear Safety Research Program through the Korea Foundation Of Nuclear Safety (KOFONS), granted financial resource from the Nuclear Safety and Security Commission (NSSC), Republic of Korea (No. 1605008).

REFERENCE

- [1] Korea Hydro and Nuclear Power Co. Ltd. (KHNP), Radiological Effluent Control Plan for Younggwang NPP Units 5 and 6, 2000.
- [2] Nuclear Regulatory Commission (NRC), Offsite Dose Calculation Manual Guidance: Standard Radiological Effluent Controls for Pressurized Water Reactors, NUREG-1301, 1991.
- [3] J.H. Cheong, "Calculation of Risk-Based Detection Limits for Radionuclides in the Liquid Effluents from Korean Nuclear Power Plants," Journal of Nuclear Science and Technology, 54(9), pp.957-968, 2017.

Effect of Permanent Shutdown on the Characteristics of Radioactive Effluent Discharges From European and Japanese Nuclear Power Plants

Ji Su Kang, Na Yoon Choi, and Jae Hak Cheong*

Kyunghee University, 1732, Deokyoung-daero, Giheung-gu, Yongin-si, Gyeonggi-do, Republic of Korea

*jhcheong@khu.ac.kr

1. Introduction

Since the provision for notification of the intent of decommissioning was first introduced into the Atomic Energy Act in 1982, the obligation to submit the decommissioning plan was given to the operator in 1995. As detailed items to be stipulated in the decommissioning plan were specified in the Enforcement of the Nuclear Safety Act in 2015, the decommissioning activities have been considered starting from the construction stage [1]. Despite these institutional improvements, most of the nuclear safety standards are mainly specified for construction and operation phases of nuclear power plants rather than post shutdown phase. Since Kori Unit 1 was permanently shutdown and entered the transition phase in June 2017, the need to establish more detailed and specific regulatory guidance for transition and decommission phases has been emphasized.

Detailed safety standards for permanent shutdown phase should be applied to all of the back-end of cycle of NPPs including control of radioactive materials released to the environment in, liquid and gaseous effluents. In addition, there have been no clear provisions on effluent control of radioactive discharges from NPPs decommissioning after permanent shutdown. Therefore, the authors investigate and analyze the characteristics of radioactive effluents released from permanent shutdown NPPs in the world, and suggest implications for effective regulatory control of radioactive effluents after permanent shutdown. In this regard, a case study for the radioactive effluent discharges from a few US NPPs were reported in June 2018 that had been permanently shutdown [2]. In this study, the authors analyzed the characteristics of radioactive effluents of shutdown NPPs in Europe and Japan.

2. Method

Liquid and gaseous radioactive effluent data for European NPPs are provided from radioactive protection publications covering reactor effluent data for each of 1995-1999, 1999-2003 and 2004-2008 in the European Union (Radioactive effluents from nuclear power stations and nuclear fuel reprocessing sites in the European Union, EC-RP-127/143/164). The reports provide radioactive materials emission by nuclide, for NPPs in operation or permanent shutdown. Liquid radioactive effluents are classified into four categories: fission products or activation products, tritium, dissolved gas, and alpha-emitters. In case of gaseous radioactive effluents, it is further categorized

into fission products, tritium, radioactive iodine, particulates, and alpha-emitters. In Japan, the liquid radioactive discharge is divided to two categories of radioactive materials except tritium and tritium. The gaseous radioactive discharge is grouped into two categories: radioactive materials except radioactive iodine and radioactive iodine. The effluent data for Japanese NPPs were collected for the period from 1994 to 2016. The effluent data for OBRIGHEIM and STADE NPPs in Germany and JOSE CABRERA NPP in Spain were analyzed for the period from 1995 to 2008. The authors analyzed effluent data from 2004 to 2008 for BOHUNICE Unit 1 in Slovakia, since the past data are not available in the report. For GENKAI Unit 1 and MIHAMA Unit 1, power generation was stopped in 2011. For MIHAMA Unit 2 and IKATA Unit 1 were stopped in 2012. Table 1 show the permanent shutdown NPPs considered in this study.

Table 1. Shutdown NPPs Analyzed in This Study

Country	Reactor Name	Shutdown Date
JAP	GENKAI-1	27 Apr. 2015
JAP	MIHAMA-1,2	27 Apr. 2015
JAP	IKATA-1	10 May. 2016
DEU	OBRIGHEIM	11 May. 2005
DEU	STADE	01 Nov. 2003
SVK	BOHUNICE-1	30 Apr. 2006
ESP	JOSE CABRERA	30 Apr. 2006

3. Results

3.1 Characteristics of liquid effluent from NPPs in decommissioning

Figure 1 shows the discharge characteristics of liquid effluents from permanently shutdown NPPs in Germany. The amount of fission products or activation products in the liquid radioactive effluent does not tend to decrease after the permanent shutdown. In case of tritium from OBRIGHEIM NPP, the emission has been reduced since its permanent shutdown. However, for STADE NPP, the tritium emission has not been decreased after the year of its permanent, 2003, but started to decrease around 2008. Dissolved gas was discharged to a level below the detection limit of both NPPs. JOSE CABRERA NPP in Spain, and does not show a trend of decrease of fission products or activation products in the liquid radioactive effluent after the permanent shutdown. The tritium discharge has been decreased like that for OBRIGHEIM and Japanese NPPs. Both dissolved gas and the alpha-emitters were discharged below the detection limit.

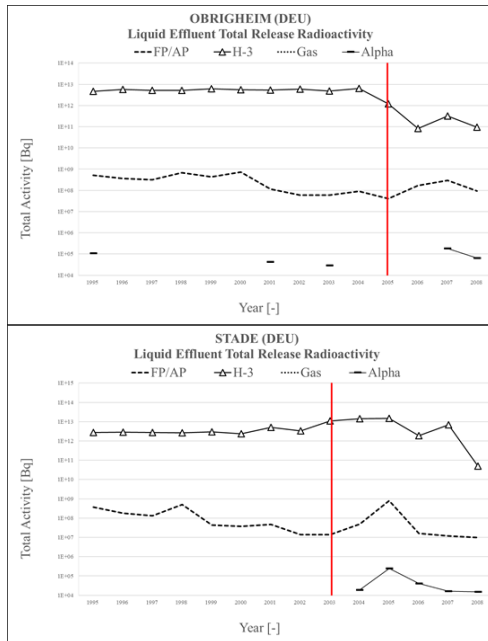


Fig. 1. Total Radioactivity in Liquid Effluent from German NPPs (OBRIGHEIM and STADE) from 1995 to 2008.

3.2 Characteristics of gaseous effluent from NPPs in decommissioning

Figure 2 shows the discharge characteristics of gaseous radioactive effluents from permanently shutdown NPPs in Germany. Fission products (noble gases) can be seen to remain similar to their past emission data after the permanent shutdown. Unlike tritium in liquid radioactive effluents, gaseous tritium has no significant change in emission after the permanent shutdown. There is no specific correlation between reactor operation and tritium emission. In the case of radioactive iodine and alpha-emitters, there was no specific change in emission even before and after the permanent shutdown. For BOHUNICE NPP in Slovakia, it is difficult to identify any characteristics of the emission pattern before and after the permanent shutdown of a single unit. In JOSE CABRERA, fission products were not detected after the permanent shutdown. In the case of tritium, radioactive iodine and particulates, however, no specific pattern of emission was identified before and after the permanent shutdown. In Japanese NPPs, radioactive iodine did not show a decreasing tendency. In case of except radioactive iodine, however, were discharged below the detection limit.

4. Conclusion

In this study, GENKAI Unit 1, MIHAMA Units 1 and, 2 and IKATA Unit 1 in Japan, OBRIGHEIM and STADE in Germany, BOHUNICE Unit 1 in Slovakia and JOSE CABRERA in Spain were analyzed. Fission products or activation products in the liquid radioactive effluent did not show a decreasing tendency in German and Spanish NPPs.

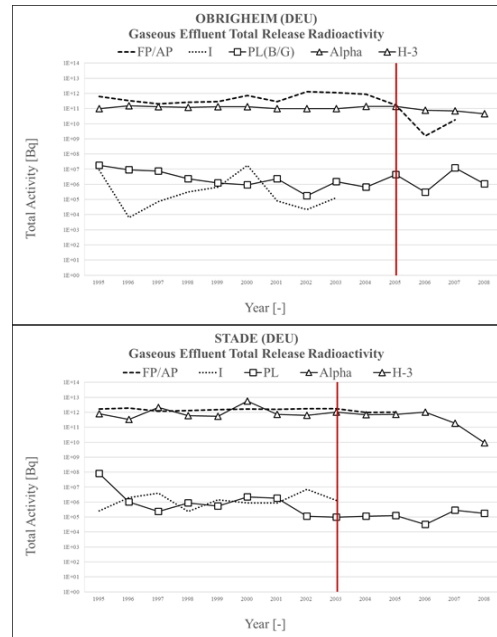


Fig. 2. Total Radioactivity in Gaseous Effluent from German NPPs (OBRIGHEIM and STADE) from 1995 to 2008.

In case of tritium, however, overall emissions were reduced from all NPPs. In the case of gaseous radioactive effluents, unlike liquid radioactive effluents, tritium discharge did not change significantly after the permanent shutdown. For radioactive iodine, there was no specific emission trend even after the permanent shutdown of both European and Japanese NPPs. The emission was not detected after the permanent shutdown. As a result, the authors identified a difference in the characteristics of the radioactive effluents emitted during the operation of the NPP and after the permanent shutdown. Therefore, it is necessary to study further more specific effluent control plan, and the regulatory requirements for the effluents from NPPs in decommissioning phase.

ACKNOWLEDGEMENT

This work was supported by the Nuclear Safety Research Program through the Korea Foundation Of Nuclear Safety (KOFONS), granted financial resource from the Nuclear Safety and Security Commission (NSSC), Republic of Korea (No. 1605008).

REFERENCES

- [1] Nuclear Safety and Security Commission, Regulations of Nuclear Facilities Decommissioning Plan, Notice 2015-8.
- [2] Na Yoon Choi, "Comparison of Characteristics and Implications for Radioactive Discharges before and after the Post-shutdown of Nuclear Power Plants in United States", Proc. of the KRS 2018 Spring Conference, May 30-June 1, 2018, Busan.

Review on Characteristics of Decommissioning Waste Generation in Foreign Nuclear Power Plants and Potential Waste Characterization Issues

Ki Nam Kwon, Sae Geun Lee, and Jae Hak Cheong*

Kyunghee University, 1732 Deokyoungdaero, Giheung-gu, Yongin, Gyeonggi-do, Republic of Korea

*jhcheong@khu.ac.kr

1. Introduction

Kori unit 1 was shut down in June 2017 and is scheduled to begin decommissioning in 2022. There is no decommissioning experience with commercial nuclear power plants (NPP) in Korea. And considering the characteristics of decommissioning waste (DW) current regulatory guidelines are not sufficiently prepared.

In the United States and Europe, which have operated NPPs for a long time before Korea, decommissioning of NPPs whose lifetime is over or commerciality is low has been in progress and some NPPs already had been decommissioned [1-3]. Therefore, if the characteristics of the DW are arranged in advance through analysis of the decommissioning experiences of abroad, it can be used as a basis for developing the regulatory guidelines on DW.

This study investigated the decommissioning experience of abroad and related cases including Kori Unit 1 estimated case [4]. And through the analysis of the characteristics of DW confirmed whether there may be have potential issue in the currently regulation of radioactive waste (RW).

2. Investigation and analysis of decommissioning waste characteristics

This study investigated the cases of generation of DW were reported due to the decommissioning of NPPs. A total of 23 cases were collected through the survey. However, the report criteria for DW

generation varied according to the case. Among them, 6 cases reported DW generation based on the type of material. DW was classified as concrete, metal, soil, mixed waste, resin and dry waste, and ETC. And the range and average values of the types of DW are shown in Fig 1. Only the generation classified as RW in DW was used for the Fig 1.

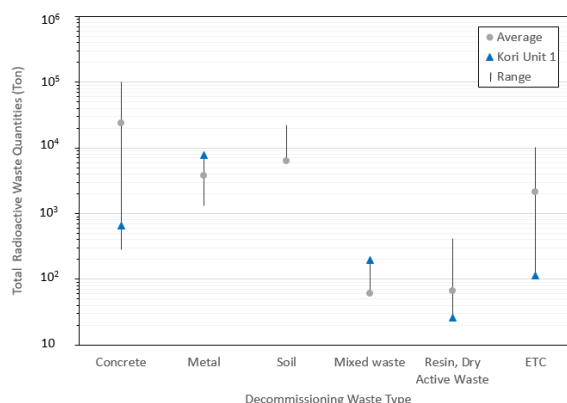


Fig. 1. Quantities of decommissioning waste.

The average generation of concrete was the highest, and there is a large difference in generation depending on the case. Average generation of metal is the third high of them. Soil was generated in only 2 of 6 cases. The range and average values in Figure 1 were used only data of 2 cases. Although it was generated only in 2 cases, average generation of soil is the second high when if it is generated. Mixed waste, resin and dry active waste had a lower average generation than other types of DW. ETC is a combination of hard-to-distinguish waste. Therefore, the generation was varied depending on the case.

Next, this study summarized the generation characteristics of each type of DW.

Concrete is used as building materials and Bioshield for NPPs. Considering the total amount of combined radioactive and non-radioactive concrete, it accounts for most of the total amount of DW. Most of the concrete is low radioactivity, it is classified as low level RW or exempt waste.

Metal is used as building materials and components for NPPs. Some components around the reactor are activated due to the activation reaction. Some of these activated components are highly activated and become intermediate level RW. And some components are large size, so they are generated large size waste. And some metal pipes are internal contaminated.

Mixed waste is a waste with both radiological and non-radiological hazards. The asbestos used as the structural material of the building can be inhaled into the respirator of the worker at building dismantling process. Chelating agents used as decontamination and they can affect the mobility of radionuclides.

Contaminated soil can be generated from decommissioning. It may not be confirmed before decommissioning [1-2].

The currently RW regulation may have potential issue regarding these DW. Table 1 shows the potential issue regarding DW.

Table 1. The potential issue of the currently RW regulation regarding DW

Waste type	Potential issue
Concrete	Generated in large quantities in a short period of time when the building dismantles. And type of contamination or contamination level is not uniform.
High activated metal	Difficult to in-situ measure due to high radioactivity and volumetric contaminated. Therefore, Indirect measurement and theoretical measurement are required.
Large components	Currently standard RW package is 200-L drums. It is necessary to consider the characteristics that generate in large size.
Contaminated pipes	A proven technique to measure internal contamination is needed.

Asbestos	Fatal impact on inhalation, but there is no regulation for radioactive asbestos.
Chelating agent	There is no detail list of chelating agents at RW regulation.
Contaminated soil	The Kori unit 1 case does not consider the occurrence of contaminated soil. It can generate unexpectedly, so need to be prepared for the generation.

3. Conclusion

In this study investigated the decommissioning experiences and related cases and classified the DW by types. Also summarized the generation characteristics of each types of DW and analyzed the potential issue regarding DW. Considering these, it is necessary to develop the DW management plan and regulation.

ACKNOWLEDGEMENT

This work was supported by the Nuclear Safety Research Program through the Korea Foundation Of Nuclear Safety (KOFONS), granted financial resource from the Nuclear Safety and Security Commission (NSSC), Republic of Korea (No. 1605008).

REFERENCES

- [1] EPRI, "Main Yankee Decommissioning Experience Report", (2005).
- [2] EPRI, "Connecticut Yankee Decommissioning Experience Report", (2006).
- [3] Per-Ole Nielsen, "Waste from Decommissioning of Nuclear Power Plants". SKI-TR 92:17, (1992).
- [4] K.M Lee, J.H. Kim, and S.H. Kang, "Preliminary Evaluation of Decommissioning Wastes for the First Commercial Nuclear Power Reactor in South Korea", International Journal of Nuclear and Quantum Engineering Vol:11, No:8 (2017).

4분과

중저준위폐기물관리 (Poster)



Development of Plasma Melter for Melting & Volume Reduction

Mi-Hyun Lee* and Hyun-Je Cho

Korea Hydro & Nuclear Power Co., Ltd. Central Research Institute, 70, Daedeok-daero 1312beon-gil, Yuseong-gu, Daejeon, Republic of Korea

*mihyun.lee@khnp.co.kr

1. Introduction

KHNP-CRI has been developed the plasma melter to reduce disposal costs and safely dispose of radioactive waste, which is instrument to treat the combustible and non-combustible waste as large-capacity plasma melting system with 1.5MW torch power. This melter which can efficiently treat various types of waste in large amounts was developed for treating 200 L drum, directly. The appearance of the melter comprises an inclined upper surface having a slope with respect to the horizontal upper surface, a pouring portion formed through a bottom surface of the melter for discharging molten material there through, and an 200 L drum input apparatus having a slope for pushing waste into the melter, and plasma torch installed on the inclined upper surface with a slope for generating melting heat in the melter.

2. Melt and Volume Reduction

2.1 Treatment of Target Waste

Plasma melter is typically used to dispose of radioactive waste generated from nuclear power plants. In general, the medium and low level wastes generated in nuclear power plants are stored in a closed 200 L drum container. The wastes stored in drums are collected and stored in various forms, and the wastes comprise a variety of components having characteristic such as flammable, inorganic, etc. Therefore, it is difficult to separate and treat the radioactive waste stored in the 200 L drum separately because of the concern on secondary contamination. Therefore, it is very important that a series of stabilization treatments such as waste input, crushing, combustion and melting, etc. should be continuously made in a melter. The plasma melter has advantage to melt non-combustible materials such as metals, concrete, and so on, thereby reducing the volume.

2.2 Status of Operation on Commercial Facility

Recently, the plasma torch melter facility in the Kozloduy Nuclear Power Plant on Bulgaria was finished the pre-operation test on July, 2018 and commercial operation from August started for volume reduction of radioactive waste generated during NPP operation. This melter is discharging molten material with a method by tilting like as plasma facility on Zwilag in Switzerland. In case of Tsuruga nuclear power plant, the pouring of molten is using heating method with an induction heating device on around an outlet of the melter. An induction heating tool is an outlet positioned at the center of the bottom of the cone type.

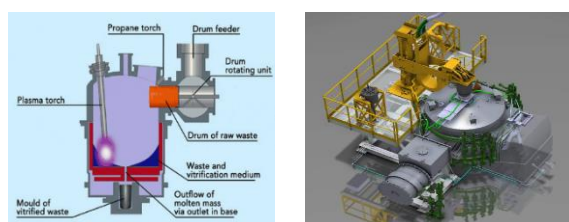


Fig. 1. (a) Tilting Type Plasma Melter of Zwilag, (b) Bulgaria Plasma Melter System.

3. Status of KHNP

KHNP-CRI through the present research developed a large-capacity melter to treat combustible and non-combustible wastes. A large-sized melter for directly processing a 200 L drum scale is used to increase the throughput of a target material, and a megawatt(MW) scale plasma torch is applied in consideration of the heat loss in the melter and the torch. In a plasma melter developed from present research, the upper surface on which the plasma torch is installed is provided with a constant inclined surface. Accordingly, the torch in melter is smoothly operated, and plasma heat source generated by the torch can easily keep balanced up to the upper

portion of the melter. The waste input on upper portion of melter is provided by a small-diameter (approximately 20 cm) inlet pipe and non-drum-shaped combustible waste can be input. The large-scale inlet apparatus is installed at the lateral inlet formed through the side of melter such that the waste drum of 200 L is directly inputted. The drum waiting portion is provided to have a gentle slope in a range of approximately 20 to 45 degrees so that the waste drum is inputted along the inclined bottom surface. Accordingly, the waste drum is input into the melter along a gently inclined surface, thereby minimizing the impact that may be applied to the melter body. The drum waiting portion comprises a slide gate provided on the upper portion which is sliding openable; and an input gate for spatially separating the drum waiting portion and the guide support and being vertically openable.

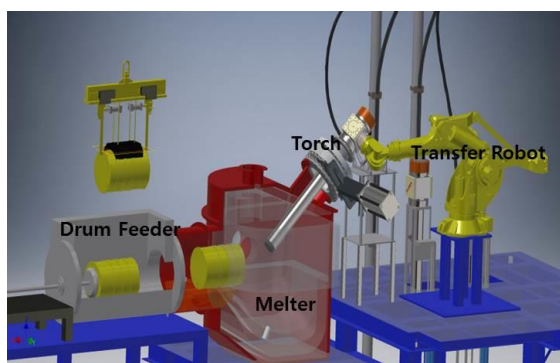


Fig. 2. KHNP Plasma Torch Melter Outline.



Fig. 3. Large-capacity KHNP Plasma Melter.

4. Result and Conclusion

The plasma melter comprises a discharge portion formed through a lower portion of inside body and at

least two lateral discharge gates provided on the side of the melter at different heights for discharging the molten material. The melter body was made using a material with a high thermal stability such as heat-resistant bricks, and a cooling channel is formed in the inside of the melter.

The refractories inside melter were comprised with B-5, alumina brick, SAL/WMCT-10CR($\text{Al}_2\text{O}_3\text{-Cr}_2\text{O}_3$ brick), MgO-C brick(YGM-15S1), MgO-C ramming (MgO-C) and so on. There are used with B-5 as an insulating material, MgO-C and MgO- Cr_2O_3 bricks as fireproof, MgO-C plastic as filling material around electrode inserted on melter bottom and castable of HACT-170. Accordingly, the outer surface of the melter can be cooled and maintained at a proper temperature below 60 degree by circulation of cooling water. The plasma torch is installed at the upper end of the melter which is operated with transferred or non-transferred mode. Electrodes for transferred operation were provided at the lower portion of inside melter.

REFERENCES

- [1] Frederik Nachtrodt, "Development of a Method for Plasma", ING-IND/18, 2013.
- [2] Jan Deckers, "The Innovative Plasma Tilting Furnace for Industrial Treatment of Radioactive Waste", WM2014 Conference, March 2-6, 2014, Phoenix, Arizona, USA.
- [3] H.J., CHO, "Comparison to Thermal Properties using Computational Fluid Dynamics of Melter Refractory", Autumn Symposium of Chemical Society, DCC, October 25~27, Daejeon, Korea, pp69, 2017.

A Preliminary Study of Hydraulic Performance Assessment of a Multi Barrier System in Near Surface Disposal Facility

Se-Ho Choi*, Mi-Jin Kwon, and Jae-Yeol Cheong

Korea Radioactive Waste Agency, 174, Gajeong-ro, Yuseong-gu, Daejeon, Republic of Korea

*seho0405@korad.or.kr

1. Introduction

The radioactive waste repository has been operated to store low and intermediate-level radioactive waste at the Wolsong site in South Korea. The second stage repository is planned to be built in shallow depth conditions at the same Wolsong site. The multiple engineered barrier cover system will be constructed to protect the near-surface disposal facility. After a long term period of time, the barrier cover system may lose integrity and precipitation may infiltrate into the concrete vaults. Therefore, the barrier cover system should be maintained for a long period of time and should be minimized when the performance is lost.

In this paper, rainfall infiltration through the multiple barrier cover will be approached and assessed using 2-dimensional groundwater flow modeling.

2. Materials and Methods

2.1 Design of multiple engineered barrier cover system

The primary objective of the barrier cover is to limit the amount of water that passes through the cover and the amount of water potentially contacting wastes. The cover of the second stage disposal facility is composed of different layers : surface layer, drainage layer, and barrier layer. The configuration of the cover is shown in Fig. 1 [1].

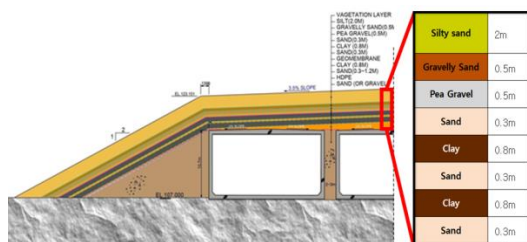


Fig. 1. Configuration of multiple engineered layer cover in Wolsong LILW 2nd stage disposal facility.

2.2 Concept model

The second stage near-surface disposal facility at ground level is 171 m wide and 67 m high, which corresponds to 10,209 m². The groundwater table located approximately 50m from the bottom of the concrete vaults [1].

It is assumed that the cover maintains its function for 300 years, and then the properties of all layers change to sand or clay.

2.3 Rainfall conditions

To set the rainfall conditions, the recharge amount of the disposal cover was estimated by applying the daily precipitation based on of Ulsan's annual precipitation for 30 years. In the case of 300 years, 10 sets of 30-year rainfall were applied.

2.4 Hydraulic properties of cover

The hydraulic properties of silty sand, gravelly sand, pea gravel, sand, clay, and concrete vault are listed in Table 1[2]. The hydraulic conductivities of the unsaturated zone were applied to the results of discrete fracture network modeling.

Table 1. Properties of multi-barrier cover materials

Layer	Water Content		Van Genuchten Parameters		Saturated Hydraulic Conductivity (cm/s)
	Residual	Saturated	α (cm ⁻¹)	n	
Silty sand	0.1	0.47	0.044	1.523	1.00e-04
Gravelly sand	0.02	0.32	0.1008	2.922	1.00e-02
Pea gravel	0.03	0.26	4.695	2.572	1.00e+00
Sand	0.045	0.37	0.0683	2.08	3.00e-02
Clay	0.0001	0.36	0.0016	1.203	1.00e-07
Concrete Vault	0.08	0.40	0.0063	1.08	1.00e-8

3. Results

The change of saturation distribution over 1,000 years is shown by Fig. 2 and 3. As the saturation continued for 300 years, Infiltrated water collected in the sand layer at the lower-most part of the drainage layer, and most of the infiltrated water flowed down the slope.

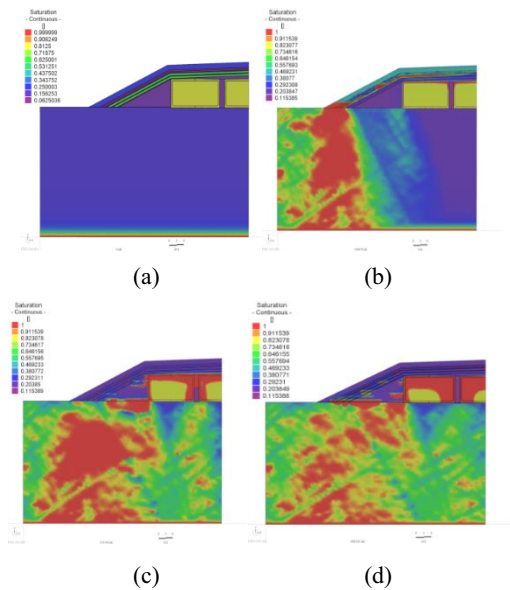


Fig. 2. Saturation distribution of changing to sand properties after (a) 0, (b) 300, (c) 600, (d) 1000 years, respectively.

When the performance of the multiple barrier cover was compromised, the rainfall came in contact with the concrete storage well. As a result of checking path lines distributions, it was found that the infiltration water to the inside of storage is extremely small compared with the precipitation amount, which was confirmed by calculation of the infiltration volume.

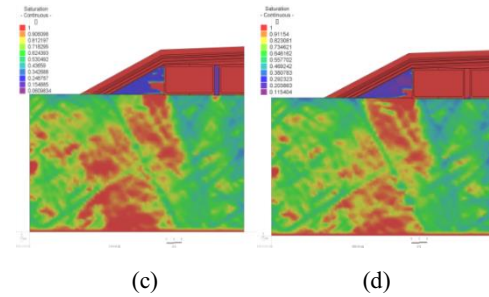
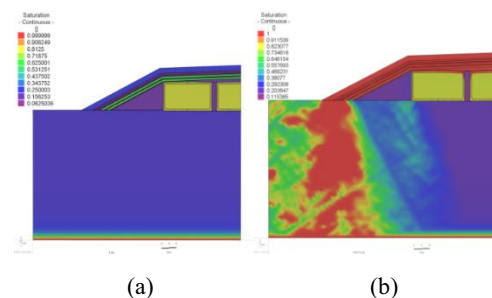


Fig. 3. Saturation distribution of changing to clay properties after (a) 0, (b) 300, (c) 600, (d) 1000 years, respectively.

4. Conclusion

After a long time period, even if all the layers had the properties of sand or clay, the infiltration rate was low. In order to improve the reliability and validity of the simulation results, various future studies such as estimation of recharge amount and degradation of concrete, are required.

REFERENCES

- [1] Mi-Jin Kwon and Ki-Jung Kwon, "Barrier of near-surface LILW disposal facility in Korea : hydraulic model development", 6th EA Forum on Radwaste Management Conference (2017).
- [2] Nuclear Regulatory Commission, "Application of an infiltration evaluation methodology to a hypothetical low-level waste disposal facility", NUREG/CR-6114 PNL-8842 Vol.1 (1993).

The Economic Evaluation of Solid Radioactive Waste Treatment Units for Centralized Radioactive Waste Treatment Facility

Jin-Kyu Choi*, Young-Hwan Kim, and Eun-Young Kim

Korea Electric Power Corporation E&C, 269, Hyeoksin-ro, Gimcheon-si, Gyeongsangbuk-do, Republic of Korea

*cjk@kepc-co-enc.com

1. Introduction

Economical and safe processing of radioactive waste is one of the major element to enhance the safety and reliability of operation of nuclear power plant (NPP). Since radioactive waste treatment technologies are constantly developing, it is necessary to perform the economic evaluation considering various situation and technologies for the optimization of waste treatment.

This paper performed an economic evaluation for solid waste processing technologies in a centralized radioactive waste treatment facility assuming that several NPP operates in the same area such as Ulchin, Haiyang (China), and Barakah (U.A.E.).

In case of generating the large amounts of radioactive waste from multiple units, the results of this paper are expected to provide a technical basis for how to construct an optimal solid waste treatment system. The facility is assumed to handle solid radioactive waste generated from six 1,400 MWe PWR units.

2. Case Selection & Waste Drum Estimation

The spent resin generated from ion exchange bed, concentrate generated from filtering or evaporating process, and Dry Active Waste (DAW) are the major solid radioactive waste from NPP. These wastes are required to be packaged suitable for disposal by using appropriate treatment system. The solid radioactive waste treatment systems used in Korea are as follows:

Table 1. List for the Treatment Units

Waste Type	Treatment Unit
Spent Resin	- Spent Resin Drying System
	- Cementation System
	- Polymer Solidification System
	- Vitrification System
Concentrate	- Cementation System
	- Polymer Solidification System
	- Vitrification System
DAW	- Compactor
	- Vitrification System

Among the solid radioactive waste treatment unit in Table 1, three cases can be considered for solid radioactive waste treatment unit suitable for the centralized radioactive waste treatment facility.

- Case 1 : Cementation
- Case 2 : Polymer Solidification
- Case 3 : Vitrification

Since the radioactive waste generation data for 1,400 MWe PWR has not been available yet, the expected generation rate of 950 MWe unit in Korea (Kori 3&4) is used for estimating waste drum. The total scale-up value of 9 is applied. The estimated waste volume for six 1,400 MWe PWR is shown in Table 2.

Table 2. Estimated Waste Volume (Drums/yr-6unit)

Waste Type	Case 1	Case 2	Case 3
Spent Resin	477	239	9
Concentrate	1,314	132	438
DAW	2,601	2,601	220
By-product of Vitrification	-	-	40
Total	4,491	3,071	806

3. Economic Evaluation for each Case

Economic evaluation is performed to estimate the total cost for each case during 40 years operation. The parameters considered for the evaluation are as follows:

Table 3. The Input Parameters for each Case

Case 1 (By Cementation)				
Parameter	Unit	Conce- ntrate	Spent Resin	DAW
Purchasing Cost	\$		3,382,800	
Disposal Cost	\$		13,774 (Identical to Case 1~3)	
Personnel Expenses	\$/hr		25 (Identical to Case 1~3)	
Electric Cost	\$/kWh		0.07 (Identical to Case 1~3)	
Agent Cost	\$/m ³	152	152	0
Operating Time per Year	Hr	36	1,056	2,336
Manpower	Man	1	1	1
Electricity	kWh	8.4	8.4	10
Drum Cost	\$	120	120	120
Case 2 (By Polymer Solidification)				
Purchasing Cost	\$		3,482,800	
Agent Cost	\$/m ³	32,528	32,528	0
Operating Time per Year	Hr	72	1,056	2,336
Manpower	Man	2	1	1
Electricity	kWh	49.9	8.4	10
Drum Cost	\$	120	120	120
Case 3 (By Vitrification)				
Purchasing Cost	\$		39,732,800	
Agent Cost	\$/m ³	77,042	77,042	77,042
Operating Time per Year	Hr	240	2,080	1,756
Manpower	Man	3	3	4
Electricity	kWh	165	165	175
Drum Cost	\$	120	120	120

4. Conclusion

The result of economic evaluation for each case is shown in Fig. 1. The Figure shows the cost comparison for each case by the basis of waste type and the total cost for each case. As a result, the Case 3 by vitrification is evaluated as the most economical waste treatment unit for centralized radioactive waste treatment facility.

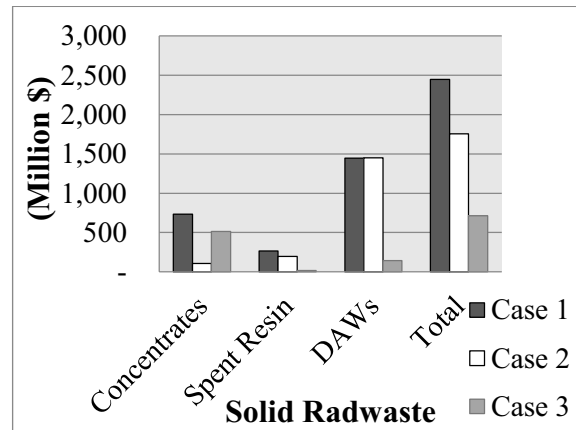


Fig. 1. The Result of Economic Evaluation.

REFERENCES

- [1] B.S.Lee, Radwaste Stabilization, Radwaste Volume Reduction Technology and Economic Evaluation Methodology Study, KEPSCO E&C, 2012.
- [2] H.J.Yoon, Design and Development of Centralized Radioactive Waste Disposal Facility, KEPSCO E&C, 2012.

Optimum Method for Accommodation of Fire-Fighting Water in Control Building of 2nd LILW Disposal Facility

Mu-gap Shin* and Young-hwan Kim

Korea Electric Power Corporation E&C, 269, Hyeoksin-ro, Gimcheon-si, Gyeongsangbuk-do, Republic of Korea

*mgshin@kepc-co-enc.com

1. Introduction

According to the NFPA801 (Fire Protection for Facilities Handling Radioactive Materials), the drainage of fire-fighting water from the fire suppression system has been considered in the design on the basis of accommodating maximum generation rate. In addition, minimum requirements for design of related equipment (e.g. pit, sump, sump pump) has been also described in the NFPA 801. For this reason, three options on how to accommodate and handle the fire-fighting water caused by fire in the control building of 2nd LILW Disposal Facility have been reviewed.

2. Method for Accommodation of Fire-fighting Water

2.1 Liquid Waste Generated in the Control Building

According to the NFPA 801.5.10.2, the provisions for drainage design involved in handling radioactive materials in an area and associated drainage facilities shall be sized to accommodate the following.

- The credible volume of discharge by the suppression system operation for 30 minutes where automatic suppression is provided throughout.
- The volume based on a manual fire-fighting flow rate of 500 gpm for 30 minutes where automatic suppression is not provided.

The required capacity to accommodate drainage of fire-fighting water is 56 ton (500 gpm x 30 min) because there is no automatic suppression facility in

the control building.

2.2 Option 1 – Transfer to Infiltration Waste Storage Sump

Option 1 is an active design and illustrated in Fig. 1. The capacity of the Control Building Drain Sump and Infiltration Water Storage Sump is respectively 5 ton and 125 ton. As the Infiltration Water Storage Sump can accommodate maximum generation rate of fire-fighting water, an operator can transfer fire-fighting water to the infiltration water storage sump by the change of flow direction in the discharge using remote control valve when the fire suppression system has been operated. In this case, it is necessary to increase the capacity of the control building drain sump pump, and flame retardant cable for the pumps and valves shall be adapted and guaranteed up to two hours in accordance with the fire retardant requirements. In addition, the operator shall additionally monitor the water level of control building drain sump even when a fire has occurred.

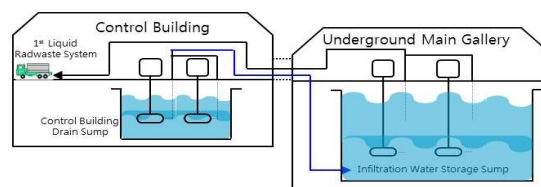


Fig. 1. Active Transfer to the Main Gallery.

2.3 Option 2 – Gravity Drainage to Infiltration Water Storage Sump

Option 2 is a passive design and illustrated in Fig. 2. As the floor elevation of the control building is 0.5 m higher than that of the underground main gallery,

fire-fighting water can be drained from the control building to the underground main gallery through embedded piping by gravity at a flooding condition. Because the embedded piping is continuously sloped, the operator does not need to take any action. However, it is expected that the drain effect by gravity is low due to the little floor level difference between control building and underground main gallery considering the length of embedded piping (about 150 m). In addition, the control building, the underground main gallery and the connection tunnel are designed as individual basic structures and connected to the expansion joints between buildings. For this reason, the construction of structure adapting embedded piping is almost impossible because stress concentration is expected to be generated to the embedded piping when the earthquake or the ground subsidence is occurred.

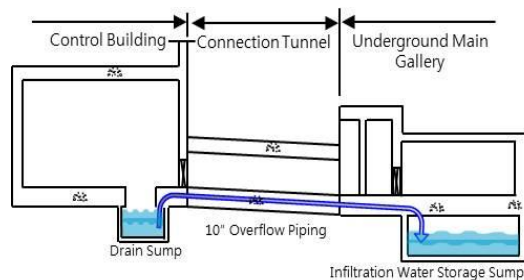


Fig. 2. Passive Transfer to the Main Gallery.

2.4 Option 3 – Accommodation in the Control Building Drain Sump

Option 3 is an accommodation design and illustrated in Fig. 3. To accommodate the maximum generation rate of fire-fighting water within the control building, independent and large sump pit is additionally constructed near the control building drain sump. The capacity of the sump pit is determined about 70 ton, considering the design and engineering margin. The fire-fighting water drained to the sump pit can be pumped using the flexible hose through manhole. As the sump pit is located below the sump pump room and equipment decontamination room, the fire-fighting water can be

accommodated within the controlled area of the control building and it prevents the spread of potential radioactive material.

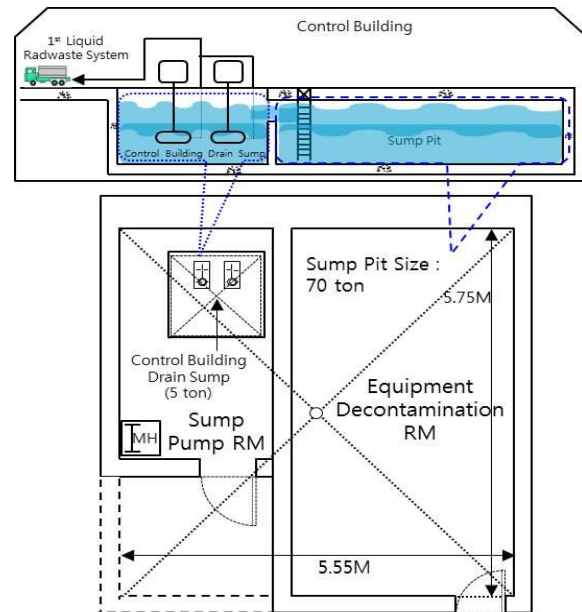


Fig. 3. Accommodation in the Control Building.

3. Conclusion

To meet the requirements of NFPA 801(Standard for Fire Protection for Facilities Handling Radioactive Materials), three options to accommodate of fire-fighting water have been reviewed. The Installation of independent sump pit (Option 3) is the best because construction is relatively easy and there is no possibility of potential radioactive material release to the environment.

REFERENCES

- [1] Matterymarch Park, “Standard for Fire Protection For Facilities Handling Radioactive Materials”, NFPA 801, Chapter 5 (2014).
- [2] H.J. Na, M.G. Shin, Disposal Facility Operating Plan, KEPCO-E&C (2015).

Treatment of Spent Uranium From Medical Radioisotope Production

Seung-Kon Lee*, Suseung Lee, Myunggoo Kang, Kyungsoek Woo, and Junsig Lee

Korea Atomic Energy Research Institute, 111, Daedeok-daero 989beon-gil, Yuseong-gu, Daejeon, Republic of Korea

*seungkoonlee@kaeri.re.kr

1. Introduction

Technetium-99m (Tc-99m), daughter isotope of Molybdenum-99 (Mo-99), is the most commonly used medical radioisotope for nuclear diagnostics. Majority of Mo-99 has been produced by the fission of U-235 in research reactors with highly enriched uranium (HEU) targets, historically. [1] However, to reduce the use of HEU in the civilian sector for non-proliferation purpose, all producers are being forced to use low enriched uranium (LEU, 19.75% U-235 enrichment) targets. Use of LEU targets, instead of HEU, significantly increases overall cost for the production. It is not only because of the lower production yield, but also because of the increased radioactive waste by 200%. Therefore, development of modified Mo-99 production process optimized for the use of LEU with decreased radwaste generation is required. [2, 3]

2. Fission Mo-99 Production

2.1 Fission Mo-99 Target

Target with uranium aluminide (UAl_x) meat and aluminum cladding is commonly used for the production of fission-based Mo-99 in commercial scale. Alkaline digestion of the aluminum-based targets with various shapes has been preferred process for production. KAERI developed plate-type LEU target composed of UAl_3/UAl_4 meat dispersed in Al-6061 cladding. LEU powder with spherical morphology was produced using centrifugal atomization technique. Each target plate contains 14.95 g LEU and uranium density of the meat is 2.6 g U/cm^3 .

2.2 Irradiation of Target and

The target were irradiated in the research reactor HANARO for three days, and cooled for two days in the reactor pool. Then transferred to the hot cell in the irradiated material examination facility (IMEF) for processing.

2.3 Fission Mo-99 Process

Irradiated targets are dissolved in sodium hydroxide solution for processing. Fission products other than Mo-99 are removed from the solution using multiple separation steps, as shown in the figure 1. Then Mo-99 is eluted and purified to meet international pharmacopoeia standard. [4, 5, 6]

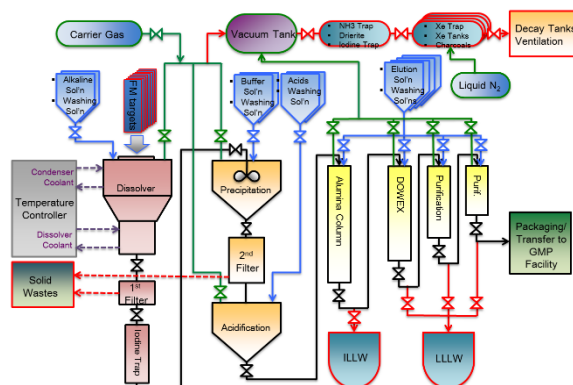


Fig. 1. FM process scheme and processing equipment.

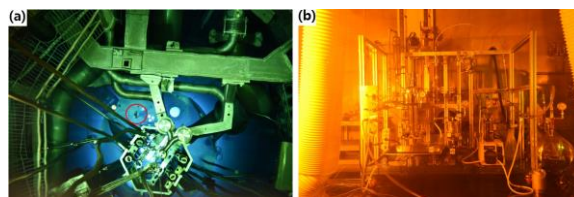


Fig. 2. (a) Irradiation of the FM target in HANARO reactor core. (b) System for target dissolution and processing.

3. Treatment of Spent Uranium in FM Production

3.1 Target Dissolution and Uranium Separation

Irradiated FM targets are dissolved by alkaline solution in a dissolver. This is the first chemical process for Mo-99 production. Uranium aluminide in the target meat transforms to the insoluble oxide forms during dissolution. Most of the uranium and insoluble impurities containing transition metals, part of alkaline earth metals and transuranium elements form colloidal particles. In alkaline solution, aluminum elements originated from the target form soluble sodium aluminide ions. But eventually, it transformed to insoluble aluminum oxides. Therefore, unreacted uranium, transuranium elements and majority of insoluble products can be separated by timely filtration right after dissolution.

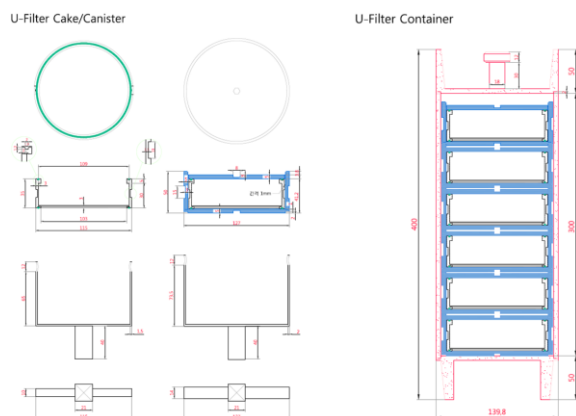


Fig. 3. Drawing for uranium filter, filter canister and filter container with manipulator handling tool.

3.2 Handling of Spent Uranium

The insoluble precipitates is separated as a form of filter cake in the uranium filter. The filter is packed in a canister. The uranium filters are temporarily stored to decay their heat and radioactivity. In a hot cell. The canister shall be stored in a cooling rack for several months to dissipate decay heat. After enough decay, six

uranium canisters are sealed in a container and stored in a pit of storage room for up to 50 years.

4. Conclusion

Development of radwaste treatment program for the FM production is one of the most essential piece for the successful construction, licensing and operation of the new research reactor (KJRR), which is being constructed in Gijang, Busan, Korea.

To achieve production objective (2,000 Ci/week) of Mo-99 in KJRR, to cover 100% domestic and 20% of international demand, 10 kg of spent uranium should be treated, every year.

ACKNOWLEDGEMENT

This work was supported by the National Research Foundation of Korea (NRF), funded by the Ministry of Science and ICT (NRF-2012M2A2A6009866).

REFERENCES

- [1] International Atomic Energy Agency, "Non-HEU Production Technologies for Molybdenum-99 and Technetium-99m", IAEA Nuclear Energy Series No. NF-T-5.4, 2013.
- [2] International Atomic Energy Agency "Fission Molybdenum for Medical Use", IAEA-TECDOC-515, 1989.
- [3] International Atomic Energy Agency, "Management of Radioactive Waste from 99 Mo Production", IAEA-TECDOC-1051, 1998.
- [4] M. V. Wilkinson, A. V. Mondino, A. C. Manzini, J. Radionanl. Nucl. Chem., 256, 413, 2003.
- [5] R. Muenze, G. J. Beyer, R. Ross, G. Wagner, D. Novotny, E. Franke, M. Jehangir, S. Pervez, A. Mushtaq, Sci. and Tech. of Nuclear Installations, 932546, 9, 2013.
- [6] S. Dittrich, Sci. and Tech. of Nuclear Installations, 514894, 9, 2013.

Analysis of Strengths of Korean Vitrification Technology Comparing to UK

K.H.Lee*, U.J.Lee, S.W.Chung, and D.H.Kim

ORION EnC Co., Ltd., 37, Seongsui-ro 22-gil, Seongdong-gu, Seoul, Republic of Korea

*khlee@orionenc.com

1. Introduction

So far Sellafield Waste Vitrification Plant (WVP) in UK performed a stable and durable waste vitrification progress for long-term storage and subsequent disposal towards high radioactive liquid waste generated from reprocessing of spent fuel. WVP used a two stage design based on the continuous French AVH (Atelier de Vitrification de la Hague) process. Instead Korean vitrification technology developed by KHNP inherently used cold crucible melter with 300 kW high frequency generator (frequency: 300 kHz) and 200 kW plasma torch system for low level and intermediate level waste [1]. This paper shows the strengths of Korean vitrification technology comparing to UK in economic, technical and social point of view because many foreign countries including Japan plans to adopt it due to much merits.

2. Korean Technology Merits

Vitrification technology is focused on high radioactive waste for stabilizing and subsequent safe disposal because of the use of expensive glass, etc. comparing to other waste stabilizing and treatment technologies. The patent information searching service site (KIPRIS) also shows the utilization trend of vitrification technology targeting high radioactive waste [2].

2.1 History of technology development between Korea and UK

The history of UK technology is shown in Table 1.

Table 1. History of UK vitrification technology

Division	year
Research into vitrification started	1950s
Fingal developed by UKAEA laboratories, Harwell	1960-1962
Operation(72 glass-making runs)	1962-1966
Review decision to continue for HARVEST process	1972
Detailed comparison of HARVEST And French AVM process	1979-1980
Decision of implementation of AVM process	1980
Full scale inactive facility(FSIF) replica of AVM process built	1981-1983
Operation	1983-1991
Commission of WVP	1989-1990
Operation Line 1,2 and (3)	1990-date (2002-date)
Vitrification Test Rig(VTR) constructed	2002-2004
VTR operation	2004-date

UK have accumulated long-term experiences since 1950s. But Korea started the feasibility R&D in 1991 for 5 years, and constructed commercial facility from 2002 till 2006 at Uljin after accomplishing pilot plant R&D and commercial plant design, etc. Especially Korean technology also cooperated with SGN (Areva's subsidiary Company) during pilot plant R&D (1997-1998).

2.2 Description of Vitrification Technology

Fig. 1 shows the UK progress for HLW [3].

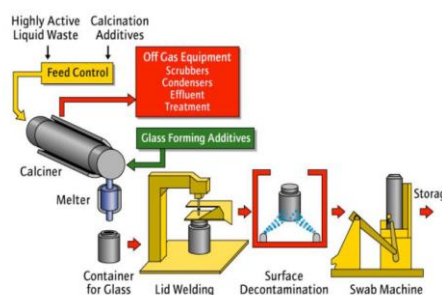


Fig. 1. UK vitrification technology at Sellafield.

High active liquid waste is combined with sugar solution (to reduce ruthenium volatilization and enhance de-nitration) and the produced dry power is heated to $\sim 1,050^{\circ}\text{C}$ at induction-heated melter. The used glass was by UK in itself to maximize the waste incorporation whilst meeting the process requirements (easy of manufacture, melter residence time and viscosity) and having acceptable chemical durability and thermal stability. Finally two mixture windscale (MW) compositions for base glass were selected as shown in Table 2.

Table 2. Composition of base glasses

Base glass type	SiO ₂	B ₂ O ₃	Na ₂ O	Li ₂ O
MW	61.75	21.88	11.05	5.33
MW-1/2Li	63.42	22.50	11.35	2.74

Instead KHNP targeted vitrification technology development targeting LLW waste in consideration of disposal site aspects. Fig. 2 shows the schematic of Korean vitrification plant installed at Uljin. The main characteristics of the technology are; 1) combined process (induction-heated cold melter and plasma torch melter) is adopted, 2) dust collection, dioxin dissolution device, acid gas removal device and de-NO_x device are installed in consideration of environmental problems, 3) vitrification process in which the simultaneous loading of wastes (for example; W1 wastes including DAW, low radioactive spent resin, Zeolite and high temperature filter dust as well as W1 & high radioactive spent resin) applied is possible, and 4) high performance glass is used, etc.

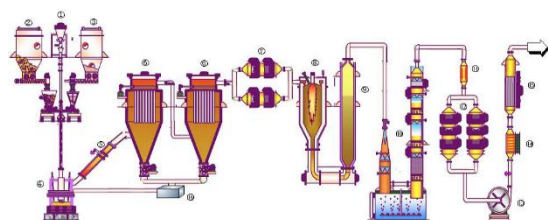


Fig. 2. Vitrification System installed at Uljin NPP.

2.3 Merit of Korean vitrification technology

KHNP's vitrification technology has much merits such as operation easiness, easy adaptability to high radioactive waste with cold crucible melter application and various adaptability towards LLW targeting D&D, especially Fukushima site in Japan and Kori #1, etc. in technical point of view, and also has the environmental and economic excellence because environment-friendly exhaust gas treatment process is equipped, and the construction and maintenance cost are cheap.

3. Conclusion

Korean vitrification technology is compared with UK's in technical, social and economic point of view. As shown in this paper Korean vitrification technology was targeting LLW treatment and stabilization in consideration of Korean disposal site aspect and disposal policy. But it was positively reviewed by foreign countries such as USA, Canada and Japan, etc. to import it because of much merits, and it was also adopted as TCP (technical Cooperation Program) by IAEA. The vitrification technology acceptability can contribute to D&D project towards Kori #1 as well as Fukushima site if the merits of Korean vitrification technology is revealed and noticed around the world as a good choice of stabilizing method for LLW.

REFERENCES

- [1] KHNP, "Seminar on performance of vitrification technology development for LLW & MLW (2012).
- [2] KIPRIS, "Patent Information Searching Service System" (2018).
- [3] Mike T. Harrison, "Vitrification of High Level Waste in the UK", *Procedia Materials Science* 7 (2014).

Waste Management of Dismantling North Korean Nuclear Facilities: Investigation of Facilities Subject to Vitrification for Decommissioning Waste

Kyungho Lee*, Sewon Chung, Unjang Lee, and Dohyung Kim
ORION EnC Co., Ltd., 37, Seongsui-ro 22-gil, Seongdong-gu, Seoul, Republic of Korea

*khlee@orionenc.com

1. Introduction

For the settlement of peace on the Korean peninsula, the complete dismantlement of all North Korean nuclear facilities should be prioritized. However, for the complete denuclearization of North Korea, managing dismantled waste is more important than dismantling North Korean nuclear facilities. In this study, the status of dismantling waste of North Korean nuclear facilities and the treatment method according to waste type are reviewed. On the other hand, investigation for the overseas cases of radioactive waste disposal by vitrification is performed, and the facilities applicable to vitrification for management of waste generated by dismantling North Korean nuclear facilities are investigated. In addition, the necessity of preliminary research is suggested so that the technology of vitrification facilities at Uljin Power Station can be utilized in the dismantlement of reprocessing facilities in North Korea.

2. Status of waste generation and classification of waste in the dismantling of North Korean nuclear facilities

2.1 Status of waste generation by the dismantlement of North Korean nuclear facilities.

In this study, the major facilities directly related to nuclear weapon development among the nuclear facilities concentrated in the Yongbyon area are investigated. Among them, the IRT-2000 research reactor, 5MWe graphite moderated reactor, ELWR and reprocessing facility are limitedly considered. Figure 1 shows a view of North Korea's nuclear facilities in Yongbyon.

Table 1 summarizes the types and quantities of waste generated when these facilities are dismantled, based on previous research [1].



Fig. 1. A view of Nuclear Facilities in Yongbyon
(source: <http://blog.naver.com/vkfs0732>).

Table 1. Decommissioning Wastes of North Korea's Nuclear Facilities[1]

Facilities	Type of Waste	Quantity
IRT-2000	Activated Concrete	18 m ³
	Metal Waste	23.8 m ³
	Spent Fuel	10-12 bundles/year
5MWe Graphite Moderated Reactor	Graphite	600 ton
	Concrete(Including Shielding Concrete)	6744(144) ton
	Metal(Including Pressure vessel)	491(164) ton
	Spent Fuel	3850 bundles
ELWR (Experimental LWR)	Concrete	86 ton
	Metal Waste	77 ton
Radiochemistry Laboratory (Reprocessing Facility)	Concrete	36,994 ton
	Metal Waste	2,252 ton
	HLW(Liquid)	562,000 ~ 1,498,000 m ³
	ILW(Liquid)	472 m ³

2.2 Classification and disposal method of wastes

As shown in Table 1, the dismantled wastes of North Korea's nuclear facilities can be classified into four types, such as spent nuclear fuel, concrete waste, metal waste, and special waste including liquid waste and graphite. In the end various types of dismantled wastes must eventually be converted into a manageable form that is suitable for movement, storage and final disposal. The choice of treatment measures for the management is dependent on the level of activity and the type of waste. Table 2 shows types of waste and brief treatment processes and measures.

Table 2. Treatment Measures of Types of Waste

Type of Waste		Treatment Measures
Spent Fuel		The spent fuel is stored in a sealed canister after a sufficient cooling period.
Concrete		The contaminated part is stored after decontaminated by grinding, and most of the waste is treated as industrial waste
Metal Waste		Contaminated metal waste is recycled after decontamination using melting and decontamination techniques such as ultrasonic, chemical and blasting.
Special Waste	Graphite	Separate classification and management required. Current treatment plan is under study
	ILW/HLW (Liquid Waste)	Solidification is necessary and vitrification is the most stable method.

3. Investigation of North Korea's nuclear facilities applicable to vitrification

3.1 Vitrification condition and process

The key to dismantling waste management is how to manage high-level waste. In fact, most HLW, other than spent fuel itself, arises in a liquid form from the reprocessing of spent fuel, shown in Table 1. The immobilization of HLW requires the formation of an insoluble, solid waste form without leaching that will remain stable for many thousands of years. In general borosilicate glass has been chosen as the medium for dealing with separated HLW. This HLW comprises highly radioactive fission products and some transuranic elements with long-lived radioactivity. To allow incorporation into the glass matrix the waste is initially dried to a granular

powder. The product is then incorporated into molten glass, poured into a robust stainless steel canister, and allowed to cool, forming a solid matrix. The containers are then welded closed and are ready for storage and final disposal.

3.2 Application of vitrification and evaluation of applicability to North Korean nuclear facilities

Vitrification was found to be most suitable for the management of high level liquid waste generated in reprocessing facilities. For example, the Sellafield Waste Vitrification Plant(WVP) and AVH(Atelier de Vitrification de la Hague)[2], Hanford VIT Plant, etc., are the representative systems to treat the high radioactive liquid waste generated from reprocessing facilities. Of course vitrification system in Uljin NPP can treat both combustible and non-combustible LLW[3]. But foreign vitrification facilities have been mostly used to treat the liquid waste of reprocessing process. Thus vitrification can be also used for management of the waste by dismantlement of North Korean reprocessing facility.

4. Conclusion

As shown in Table 1, among the waste produced from dismantling of North Korean nuclear facilities, particular waste is high-level liquid waste from reprocessing facility. In order to safely manage these wastes for thousands of years, we can conclude that the best management practices for dismantling wastes of this facility must be vitrification, as can be seen in decades of experience in foreign countries. In addition Korean government should recognize that it is necessary to advance the technology of Uljin vitrification plant through further research for utilization in the dismantling of North Korea reprocessing facility.

REFERENCES

- [1] J.H.Son, "Management Alternatives for decommissioning waste of the North Korean nuclear facilities" M.S.thesis of Graduate School of Kyung Hee University (2016).
- [2] Mike T. Harrison, "Vitrification of High Level Waste in the UK", *Procedia Materials Science* 7 (2014).
- [3] KHNP, "Seminar on performance of vitrification technology development for LLW & MLW(2012).

Safety Considerations for Optimal Development of National LILW Repository Complex

Chan Woo Jeong*, Eun Jin Seo, Ayeong Kim, Jeheon Bang, Hyo Sook Jung, and Jinyong Park
Korea Institute of Nuclear Safety, 62, Gwahak-ro, Yuseong-gu, Daejeon, Republic of Korea
*jcw@kins.re.kr

1. Introduction

Gyeongju repository is the national radioactive waste management center where all the domestic LILW is to be disposed of throughout this century. The repository has been developing underground silos (2006~) and near-surface vaults (2012~), and it is now setting about landfill disposal. In such a complex development, diverse steps or situations will proceed concurrently for different disposal facilities. This paper considers some safety points for overall development of the unique repository complex.

2. Step-by-step safety case approach

A disposal system and the relevant safety case should be optimized step by step based on the previous experience, the latest data and best available techniques, and updated contents of the next steps [1]. Such a point should be emphasized for the repository complex. Fig. 1 shows a range of steps and important elements to be reflected at each step for this purpose.

Steps	Development scheme	Basic design	Detailed design	Operation	Closure	Post-closure
Items						
Disposal system	Site	Site characterization	Safety elements characterization	Site monitoring		Post-closure control
	Facility	Alternative concept-meth	EBS construct / Safety elements characterization	EBS optimize		
	EBS	Proposed method-organization	EBS engineered barrier system	Operation method		
	Container	Alternatives	Proposed	Design / Performance		
	Waste			Waste acceptance criteria		
Safety case (SC)						
Disposal system development						
System-Safety construct						
P_SAR						
SAR_amend						
Periodic Safety Review (PSR)						
Closure SC						
Final SC						
PC_PSR						

Fig. 1. Overall considerations for repository development.

For example, all the steps and components should be considered for new development, and operational safety and the succeeding processes should be considered for the underground facility in operation.

The repository complex should be developed based on an appropriate safety case to the situation with an overall sketch of the development. The safety case should be constructed progressively even till post-closure phase, which is also important for future introduction of similar hazardous applications [2,3].

3. Systems analysis for overall optimization

Improper processes of development, including

incongruity between disposal demand and repository provision, may have a significant impact on the predisposal management as well as on the disposal safety. Therefore, a due arrangement is needed between the overall schedule and the steps implementation. In this sense, relevant regulatory activity should also include a review, in terms of radiological safety, on the overall development program with connection to predisposal management.

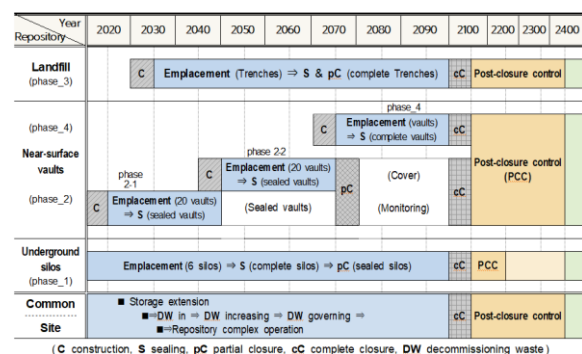


Fig. 2. An overall development plan for the complex.

Fig. 2 is an example of the overall development, which reconstructs one of the recent drafts by the developer. Such a schema may bring an overview of the whole development. Again, the safety review at each point should judge, in terms of optimization, congruity of the step with the overall program.

Fig. 3 illustrates a mathematical system optimizing the complex development.

Step 1. Overall scheduling. Make out an overall schedule from the following expressions producing annual demand of disposal and long-term storage.

$$Q(t) \geq W_d(t)$$

$$S(t) \geq W_s + w_d(t)$$

W = cumulative waste generation; W_d = portion of W to be disposed of; W_s = portion of W to be stored for a long time; w = annual waste generation; w_d = portion of w to be disposed of; Q = disposal capacity; S = storage capacity.

The schedule should include points of time and duration, disposal methods and capacities, and an arrangement of steps. The contents can be more specified with more detailed information on the waste in terms of generation and property.

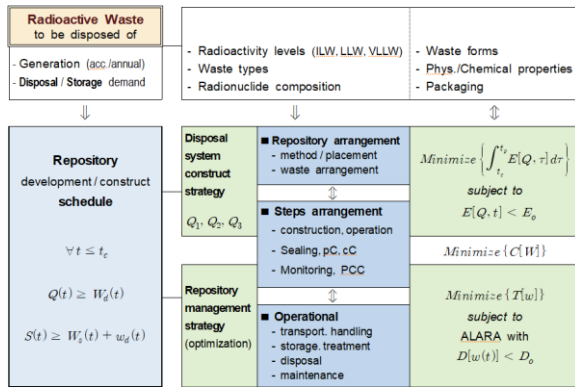


Fig. 3. An optimization scheme of systems analysis for planning the overall development of repository complex.

Step_2. Disposal system arrangement. Through the following expression, put the disposal method, disposal/storage capacity and the waste property from Step_1 into the disposal site to produce locations of the facilities from which the radiological consequence, E , is to be minimized:

$$\text{Min. } \int_{t_c}^{t_p} E[Q, \tau] d\tau \text{ subject to } E[Q, \tau] < E_o$$

t_c = facility closing year; t_p = performance required period; E_o = performance objective (e.g., 0.1 mSv/y).

Through this manipulation, some rearrangement may occur among capacities, methods, and facilities.

Step_3. Optimizing the repository operation. For the temporary setting through Steps_1 & 2, optimize the procedures and methods on an annual basis. This can be carried out by arranging individual elements in such a way that minimizes the total necessary time:

$$\text{Min. } \{T[w]\} \text{ subject to } D[w] < D_o$$

D_o = annual dose constraint.

Step_4. Optimizing the complex development. In the repository complex, different steps of development may occur together with different facilities. Such situations also need optimizing throughout the overall repository period. For example, in the sense of efficient site management, they may be optimized in terms of the required cost, e.g., by minimizing $C[W]$ in such a comprehensive way that minimizes

$$\oint T[w(t)] dt,$$

where the line integral indicates that it should be performed via all steps during the overall development.

The output from Step_4 may be fed back into Step_1 to modify the draft schedule. Again, the result may be fed back repeatedly into Step_2, Step_3 and Step_4 for the overall rearrangement.

4. Constructing the reliable safety

Defense-in-depth arguments should be more emphasized for safety of the repository complex. For this purpose, understanding of the site characteristics should be enhanced throughout the repository development to find and upgrade the safety elements [2,3,4]. In order to assess safety features of the complex disposal system, it should be prerequisite to predict distributions of the contaminants over the site with the system evolution, which is required for an integrated compliance assessment with the safety objectives. In addition, it should be remembered that credible information on the waste is an essential element for a valid development and the safety case. For example, relevant arrangement between disposal facilities and the dynamic properties of waste forms may result in less consequence with less uncertainty.

5. Concluding remarks

Gyeongju repository is a national infrastructure for the sustainable application of nuclear energy. A systematic safety case based on timely consideration of safety elements is necessary for the prosperous complex development. For this purpose, the overall program optimization should continue step by step with updated characteristics of the waste and the site. The considerations discussed here may provide some ideas for establishing a solid overall development program and for its optimization.

ACKNOWLEDGEMENT

This work was supported by the Nuclear Safety Research Program through the Korea Foundation of Nuclear Safety(KoFONS), granted financial resource from the Nuclear Safety and Security Commission (NSSC), Republic of Korea (No.1703005). Regulatory points discussed here are the authors' opinion in the process of research.

REFERENCES

- [1] SSR-5, Disposal of Radioactive Waste, IAEA.
- [2] Jeong *et al.*, KRS Proc. 9(1) 349-350 (2011).
- [3] KINS/RR-1223, Safety criteria & safety assessment for complex repository (2014).
- [4] Jeong *et al.*, KRS Proc. 7(1) 165-166 (2009).

A Safety Concept of Landfill Disposal for National LILW Repository Complex

Chanwoo Jeong*, Jinyong Park, Jungjin Kim, Yohan Kim, and Sang Myeon Ahn
Korea Institute of Nuclear Safety, 62, Gwahak-ro, Yuseong-gu, Daejeon, Republic of Korea
*jcw@kins.re.kr

1. Introduction

Korea Radioactive Waste Agency (KORAD), which has been developing underground silos (2006~) and near-surface vaults (2012~) in the Wolseong site, is now setting its third phase of development for landfill disposal (LD) of very low-level waste (VLLW) in the same site. In order to develop the LD system properly, it is essential to consider its safety features with the disposal site as well as the generic characteristics. This paper discusses the proper concept of landfill disposal for the repository complex and the corresponding implementation.

2. The concept of landfill disposal

The NSSC Notice on the classification of radioactive waste defines LD as “disposing of radioactive waste with natural barrier near the surface of the earth” and allows it to accommodate VLLW. This concept of LD could be extended as “disposing of waste near the surface of the earth in such a way that the safety does not rely on engineered barrier.” The LD thus has its meaning in a set of the relevant structure of natural barrier and a range of waste disposed of. Correspondingly, an LD system may hold as a disposal “method”, not as an engineered “facility.”

With some favorable properties of the repository and its structure and arrangement, the natural elements could construct the required safety functions for a limited range of VLLW plus containers without any help of engineering elements. This corresponds to a pure LD system. More generally, an LD system may adopt engineering elements partly to enhance the safety. In this case, the system still could be put into a category of LD as far as the natural elements construct the required safety functions. If such safety features are reliable, it is not necessary to impose some performance criteria to the applied engineering elements. In this relation, supplementary material such as polymer membrane and clay may also be constituent of LD system. On the other hand, if there is an engineering element participating in compliance with the safety objectives, the element should meet the relevant performance requirement like that to near-surface disposal facility. In this case, the repository should actually be considered as a near-

surface facility for disposal of VLLW.

3. Technical criteria for landfill disposal

In relation with the control of precipitation during operation, LD may be divided into two types: (1) The whole base of repository are formed first to fill waste packages openly, which is suitable for dry sites. (2) The repository is developed gradually with shelters, where trenching, emplacing waste packages, backfilling and covering may proceed little by little. The Wolseong site seems to apply the latter system since it has much rain.

Among the existing technical criteria for near-surface disposal, the following are needed to review in terms of the landfill: siting, structure and equipment, considerations for natural phenomena, and drainage. Since the current standards are basically covering the concept of LD, they may apply properly to LD in terms of the potential hazard. With shaping the development, however, some details may be necessary for some items to discern between engineered facility and landfill.

4. Constructing the safety of landfill disposal

The realization of an LD system depends largely on the characteristics of waste and radionuclides involved as well as site characteristics and landfill method. In this context, the safety considerations for development of the LD system on Wolseong site should place the focus on the following issues.

4.1 Does the proposed disposal system belong to landfill?

The case should be examined with due consideration on characteristics of the VLLW including the radionuclide composition. Taking the concept of landfill into consideration, it is desirable to restrict long-lived radionuclides regardless of the waste forms for defense in depth in addition to compliance with the safety objectives.

4.2 Is the system making the best use of safety features of LD?

The safety features of LD may again become

different for different designs and different ways of development. So, it should be confirmed continuously from the beginning to the final phase that the system is to reflect the essential safety features. In particular, for the case of gradual development, the overall validity should be judged in the initial review for permission of the construction and operation and be checked throughout the following phases.

4.3 Are the functions of drainage and percolated water collection assured?

As shown in Fig. 1, an LD system may use collectors to collect percolated water after covering till the final closure. In addition, it practically has ditches around the mound for surface drainage, which still may be maintained after the repository closure. Since most radionuclides in the VLLW should be short-lived, the performance of landfill disposal may depend greatly on such water control functions. Therefore, the relevant design shall be demonstrated in advance to assure the expected performance, the installation and covering or (partial) closure be carried out so as to realize the performance, and the function be continuously monitored and (if necessary) corrected throughout the required period. For this purpose, the relevant design and operational specifications shall contain the follow-up measures.

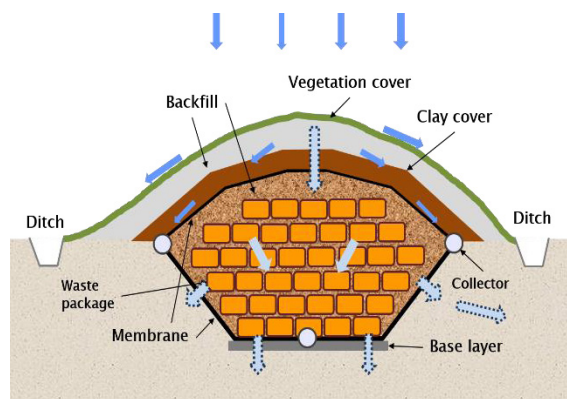


Fig. 1. A typical shape of landfill disposal.

4.4 Is there no problem with opening the site after post-closure control?

From its basic idea, MD is rather appropriate to be considered as a practice of “work” than as a “facility.” In this context, it is not reasonable to apply the post-closure safety objectives and the related scenario approaches for compliance assessment to the LD in the same way as to the other types of disposal facilities. For example, after the post-closure control,

a landfill repository will be faced with a situation of human intrusion as it is on the surface, while other types of repository still have their engineered facilities underground for which the intrusion may be limited considerably. In this sense, the site release approach, as to decommissioning, is more pertinent to a landfill repository. So, the future Wolseong repository complex containing LD should be developed in such a way that it satisfies not only the post-closure safety objectives but also the site release criteria (e.g., 0.1 mSv/y). This indicates again that a limited range of VLLW should be introduced into the landfill. In other words, an insignificant amount of important radionuclides should remain on the site surface after the post-closure control phase.

4.5 Does the safety assessment support the safety arguments, mentioned above for LD?

The safety assessment for LD should be based on the concrete description on how the waste will evolve and how the radionuclides will behave. In short, it is essential to predict the distribution of radionuclides around the landfill with time. Accordingly, it should be emphasized that unrealistic simplifications, such as all the radionuclides released from the landfill will come into the groundwater, cannot lead to a valid argument on the safety of the landfill and thus the repository complex.

5. Concluding remarks

In view of radiation protection, disposal is just an option for managing radioactive waste safely. If we are to adopt LD as the ultimate phase, we have to understand its safety features and develop the disposal system making their best use. The safety concept discussed here may be a basis for developing the domestic landfill repository.

ACKNOWLEDGEMENT

This work was supported by the Nuclear Safety Research Program through the Korea Foundation of Nuclear Safety(KoFONS), granted financial resource from the Nuclear Safety and Security Commission (NSSC), Republic of Korea (No.1703005). Regulatory points discussed here are the authors’ opinion in the process of study.

Leaching Test for Polymer Waste Form of Spent Ion-exchange Resins

Seongye Kwon, Won-Seok Kim, and Wooyong Um*

Pohang University of Science and Technology, 77, Chungam-ro, Nam-gu, Pohang-si, Gyeongsangbuk-do, Republic of Korea

*wooyongum@postech.ac.kr

1. Introduction

Spent ion-exchange resin is generated through the purification of primary system of nuclear power plant. The proper solidification of spent resin is urgent issues and needs to be developed because spent resin is consisted of organics which can generate the gas. Spent ion-exchange resin is considered to be problematic waste so that, in many case, it requires special approaches and precaution during their solidification to meet the acceptance criteria for disposal. In this study, the polymer was used as a solidification material to improve the waste content and reduce the leachability in solidification. Despite this, the reference data for leaching test is still limited.

The objective of this study is to evaluate the polymer wasteform solidified spent ion-exchange resin waste. In fact, the leaching test (ANSI/ANS16.1) and compressive strength test are performed to meet the acceptance criteria for disposal facility.

2. Experimental section

2.1 Development of polymer waste form

Polymers vary in characteristics depending on chemical and physical structure and range of strength, durability required for the purpose of use. Therefore, physical properties can be enhanced by the selection of suitable polymers that meet the criteria of a polymer and by adding additives as needed. Polymer (Polyester Epoxy) was used as solidification ingredient and added with ion exchange resin (GRAVEX GR 3-16 N, mixed bed resin) to develop polymer waste form. The ion exchange resin was dried and crushed in advance, and added after

removing air gap (Fig. 1).

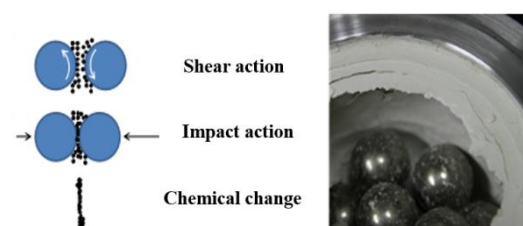


Fig. 1. Crushed ion exchange resin by ball mill.

In this study, the polymer solid waste form (Type A) was prepared as cylindrical. In comparison, polymer waste form (Type B) containing only Co without resin was prepared. The characteristics of polymer waste form A and B are shown in Table 1. The compressive strength of polymer waste form was analyzed by the universal testing machine (SALT model ST-1001).

Table 1. The characteristics of waste form A and B

Waste form type	A	B
Containing	Co adsorbed ion-exchange resin	Co chemicals
Average diameter	4.6 cm	4.6 cm
Average height	9.4 cm	9.4 cm
Surface area	169.1 cm ²	169.1 cm ²
Initial weight	218.1 g	219.0 g
Initial concentration	1569.7 µg/g	27983.2 µg/g

2.2 Leaching test

The leaching test was conducted according to ANSI/ANS16.1 method. A total sampling time was 10 times with 2 hr, 7 hr, 1 day, 2 days, 3 days, 4 days, 5 days, and 19 days. The 8 times out of 10 times. The sampling is scheduled for 49 days and 90 days. The reactor of leaching test is shown in Fig.2. Polymer waste form was soaked in deionized DIW (deionized water) with 9.0±1.0 ratio of total volume of DIW

waste to surface area of waste form. The whole of leachate was replaced at every sampling time.



Fig. 2. ANSI/ANS 16.1 test of 19 days.

After each sample collection, the leachate was analyzed by Inductively Coupled plasma-mass spectrometry (ICP-MS) to determine the leachability of the elements of interest. The leachability index (LI) was calculated by Eq. (1).

$$L_i = \frac{1}{n} \cdot \sum_{i=1}^n [\log(\beta/D_i)] \quad (1)$$

where L_i : The leachability index of a nuclide, i
 n : Total sampling days
 β : A defined constant ($1.0 \text{ cm}^2/\text{s}$)
 D_i : The effective diffusivity of nuclide

3. Results and discussion

The measured compressive strength was 65 Mpa (A) and 28 Mpa (B), respectively. It is higher than 3.44 Mpa which is the acceptance criteria for waste form in repository.

Effective diffusivity of Co is shown in Fig. 3.

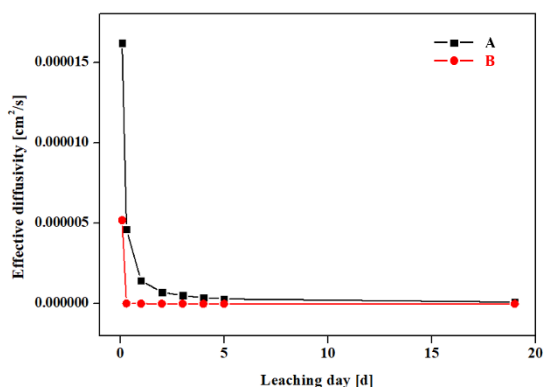


Fig. 3. Leaching test results of A and B.

The Leachability Index for A and B was calculated as 6.04 and 8.35, respectively. The leachability index of sample A and B were appropriate to the radioactive waste criteria.

4. Conclusion

Polymer waste form was developed using polyester epoxy. The leaching test for two polymer waste form specimens were conducted by ANSI/ANS16.1 method. The leachability indexes of sample A and B were appropriated to be accepted for disposal. In order to optimize the solidification of resin waste for acceptance to repository, additional additives or formulation should be developed to increase the LI for acceptance to repository.

ACKNOWLEDGEMENT

This work was supported by the Korea Institute of Energy Technology Evaluation and Planning (KETEP) granted financial resource from the Ministry of Trade, Industry & Energy, and Republic of Korea (No. 20171520000410).

REFERENCES

- [1] ANS 16.1, "Measurement of the Leachability of Solidified Low-Level Radioactive Wastes by a Short-Term Test Procedure", 1986.

Development of Low-contaminated Sludge Separation Technology

HeeJin Ahn*, MiHyun Lee, and KangOk Cho

Korea Hydro & Nuclear Power Co., Ltd Central Research Institute, 70, Daedeok-daero 1312beon-gil,
Yuseong-gu, Daejeon, Republic of Korea
*cowahn61@khnp.co.kr

1. Introduction

When nuclear power plants are dismantled, radioactive waste of various kinds and levels such as metal, concrete, and soil is generated in a very short period of time. If the appropriate waste management plan is not applied from the beginning of the decommissioning project, it will cause enormous hindrance to the decommissioning business such as increase of the disposal cost. In particular, disposal alternatives are not available due to insufficient treatment technology for disposal unsuitable wastes generated during decommissioning of nuclear power plants such as sludge wastes.

As a part of the development of radioactive waste disposal technology and special waste treatment technology, we conducted a survey on the status of low - contaminated sludge and the case of sludge separation technology at Hanbit 3 power plant. In addition, samples of low - contaminated sludge from Hanbit 3 power plant, radionuclide analysis and chemical characteristics analysis were performed.

2. Survey of low-contaminated sludge and sludge separation technology

2.1 Survey on the status of low-contaminated sludge

A large amount of radioactive waste was generated at the sewage treatment plant due to the contamination of demineralized water supply system of Hanbit Unit 5. It was collected and stored in 220 pieces of 1 ton reinforced plastic cylinders. The contaminants on the upper part of the slurry were dried and stored in a bag of 40 kg. The sludge on the floor is stored in a 689 sack bag of 40 kg capacity and is located 147 feet from the radioactive waste disposal facility. It is expected that the pollution degree of the sludge and the filter material collected at the wastewater treatment plant is very low. Therefore, it is necessary to take measures to properly dispose of these radioactive wastes below the disposal limit in accordance with legal procedures, rather than drum-disposing them.

2.2 Sludge separation technology case study

The main purpose of the sludge separation technology is to minimize the radiation effects. The key to the treatment technology is separation and concentration. Radioactive waste, which has become very low in concentration through separation, is disposed of itself, and enriched is isolated from the living environment through solidification treatment

after volume reduction for efficient storage and management. The method of treatment of radioactive waste should be selected according to the radioactive level of radioactive waste, physical and chemical conditions, kinds of radionuclides contained in radioactive waste, and so on. As a result of the survey, the radioactive sludge generated from the nuclear power plant was partially treated for solidification, but no radioactive material was removed through the separation of nuclides. However, related research is ongoing in the United States and Japan [1].

3. Sampling of low-contaminated sludge, analysis of radionuclides and chemical characterization

3.1 Results of low-contamination sludge radionuclide analysis

Radionuclides of low - contaminated sludge were analyzed. As a result, the radionuclides above the reference concentration were Mn-54, Co-58, Co-60, Cs-137 and Nb-94.

The Concentrations of nuclides in waste types were up to 17 times higher than that of Co-60, but other nuclides were 2 ~ 3 times higher than self-disposal concentration or slightly higher than the reference value. Table 1 shows the nuclide analysis results for self-disposal evaluation.

4. Nuclide removal experiment of low-contaminated sludge

4.1. Washing treatment and ultrasonic treatment

Experiments were conducted to remove the nuclides above self-disposal standards.

As a method of removing nuclides, a washing treatment method and an ultrasonic treatment method were used. In the washing process, 250 cc sample was placed in a 500 cc sample bottle, and 250 cc of deionized water was filled in the sample bottle, followed by washing and ultrasonic treatment. As a result of the nuclides removal treatment, Cs-137 was completely removed. Co-60 was removed to about 1/2 to 1/5 level. This suggests that it was moved to a pH alkaline area by OH⁻ ions present on the surface of sludge. And radioactive cobalt that must be leached are present as sediment in Co(OH)₂ and were not leached.

4.2 Chemical elution and substitution

4.2.1 Radiochemical properties of Co-60. Cobalt has oxidation states of 0, +2 and +3, and Co²⁺ & Co³⁺

coexist in a stable state as Co^{2+} ion in aqueous solution. The Cobalt chemical species are absorbed into small particles in the water, settled down to rocks or sand, or are directly absorbed into materials such as sand and gravel [2].

This degree of adsorption depends on the pH, the oxidation-reduction atmosphere, and the concentration of dissolved organic matter. When a strong oxidizing agent is present in the aqueous solution, the cobalt ions are present in the oxidized state of Co^{3+} and exist in the form of a precipitate of $\text{Co}(\text{OH})_3$ over the acidic and alkaline regions. In the absence of oxidant, cobalt ions exist in the form of Co^{2+} , and exist in the form of precipitates of $\text{Co}(\text{OH})_2$ from alkaline near neutral to strongly alkaline.

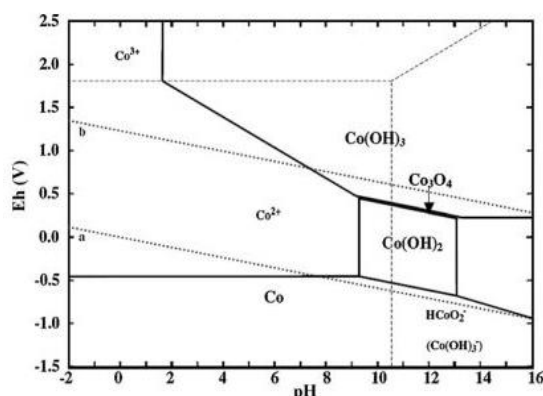
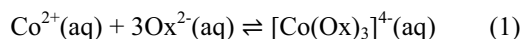


Fig. 1. Eh-pH Diagram for Cobalt Ion.

4.2.2 Co-60 elution experiment using strong acid. It is believed that the Co-60 are absorbed onto their surfaces due to the presence of large amounts of iron and manganese in the sludge contents, to remove the co-60 that is absorbed on the surface, use acid solutions such as HCl , $\text{HCl}+\text{HNO}_3$, $\text{HCl}+\text{H}_2\text{SO}_4$, $\text{HCl}+\text{HClO}_4$ to dissolve iron or manganese[3]. In this experiment, 0.5 M HCl was used, and three kinds of reducing agent such as oxalic acid ($\text{C}_2\text{H}_2\text{O}_4$), chloride tin (SnCl_2), and hydroxyl amine ($\text{NH}_2\text{OH}\cdot\text{HC}$) were used for elution of Co-60[4].



In particular, chloride annotations (SnCl_2) were used to replace eluted Co-60 with Sn. To check the time effect of elution and substitution, stirred it for 10 minutes, 1 hour, 6 hour and 24 hours, respectively.

5. Conclusion

In order to reduce the amount of radioactive waste generated due to contamination of the desalination water supply system of Hanbit Unit 5, a self-disposal plan was sought. The types of wastes were ground sludge of sedimentation tank, gravel used as filtration media, sand, activated carbon anthracite. As a result of the analysis of radionuclides in low-contaminated radioactive wastes, radionuclides exceeding the self-

disposal standard values were analyzed as Mn-54, Co-58, Co-60, Cs-137 and Nb-94. Concentrations of nuclides in waste types were up to 17 times higher than that of Co-60, but other nuclides were 2 ~ 3 times higher than self-disposal concentration or slightly higher than the reference value. In order to confirm the possibility of self-disposal of radioactive waste, a nuclide elimination experiment in radioactive waste was conducted.

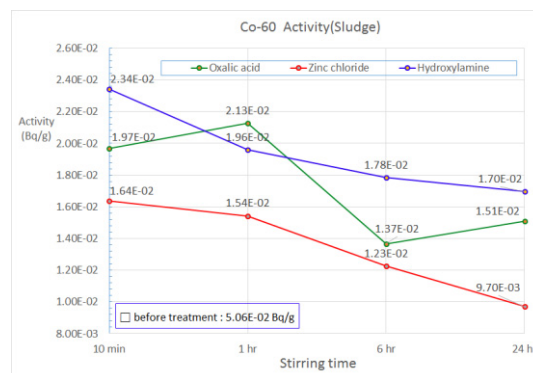


Fig. 2. Co-60 activity in Sludge after treating nuclide removal.

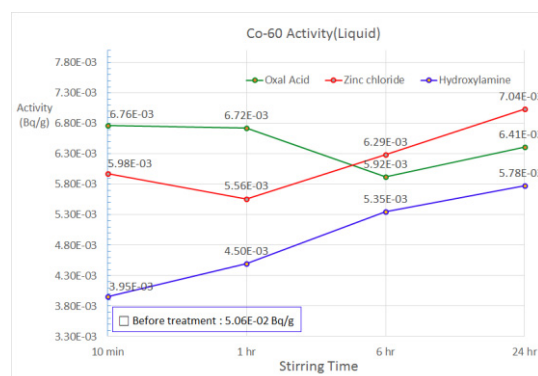


Fig. 3. Co-60 activity in Liquid after treating nuclide removal.

The biggest effect of removing nuclide was in case of chloride annotations were treated as reductants when the analysis of sludge nuclides after treating nuclide removal.

The elimination rate of nuclide was treated up to about 20%, which is equivalent to 1/10 of the criteria for self-disposal and, it is sufficient level self-disposal.

REFERENCES

- [1] ANDRA, "National Inventory of Radioactive Materials and Waste", 2012.
- [2] M. Pourbaix, "Atlas of Electrochemical Equilibria in Aqueous Solutions", National Association of Corrosion Engineers, Houston, Texas, USA, p. 325. 1974.
- [3] Sahuquillo et al, Analytica Chimica Acta, 382(3), 317 ~ 327, 1999.
- [4] McLaren et al., Journal of Soil Science, 37(2), 223 ~ 234, 1986.

A Plan to Build a Total Radwaste Management, STAR (Storage and Treatment of All Radwastes in KAERI) Facility

Jeong Guk Kim*, Jongjin Kim, Won Hyuk Jang, Hongrae Jeon, and Dae Seok Hong

Korea Atomic Energy Research Institute, 111, Daedeok-daero 989beon-gil, Yuseong-gu, Daejeon, Republic of Korea

*jungkim@kaeri.re.kr

1. Introduction

KAERI has a plan to build a total radioactive waste management facility, STAR (Storage and Treatment of All Radwastes in KAERI) by 2021, as an alternative for the present waste storage buildings and radwaste treatment facility. This new radwaste management facility will significantly contribute to reduce the radwaste inventory in KAERI site.

2. Radioactive Waste

2.1 Radwaste Inventory in KAERI

The inventory of low- and intermediate-level radwaste in KAERI site is about 20,000 drums (based on 200-liter drum), as of June, 2018, as shown in Table 1.

Table 1. Radwaste Inventory in KAERI Site
(Basis 200-liter drum, As of June, 2018)

	Storage (drum)	Storing ratio, % (storage/capacity)
Waste from R&D	8,848	55.2
Waste from Decommissioning	11,677	59.6
Total	20,525	

2.2 Waste Reduction Plan

KAERI is now trying to reduce the radwaste inventory, and has a plan to reduce the present inventory to a half by 2027. Considering an annual generation of about 500 drums, the amount of the treatment and the transportation to disposal site should be increased more than now. To achieve this goal, the STAR facility, which would have a store and treatment processes for radwaste, will significantly contribute to reduction.

3. Clearance Level Waste

Recently, the clearance level (literally self-disposable) waste [1] has been a hot potato. According to regulations, all things, whether waste or not, in radiation zone are limited from taking out freely. Therefore, a lot of potential radwastes are being accumulated in the radiation zone. Of cause there is a regulation [2] to dispose such clearance level waste, but the procedure to show its safety requires time and endeavor.

3.1 Estimated Inventory of Clearance Level Waste

The amount of clearance level waste was estimated about 900 tons, containing equipments, as of March, 2017. Most of these wastes are expected to be self-disposed after admission of NSSC (Nuclear Safety and Security Commission).

3.2 Plan to Manage Clearance Level Waste

Before treatment of clearance level waste, the essential step is a check for radioactive waste or not. So, a representative sampling, analysis, and confirming to radwaste are significantly important steps in management of clearance level waste. And then, the process to show harmlessness to environments is essentially proceeded. Therefore, some analytical equipments are also needed in the STAR facility.

4. Treatment Processes in STAR

4.1 Treatment Processes in STAR Facility

The STAR facility is now being designed for construction. This design includes writing and applying for licensing documents. The STAR facility will contain radioactive waste storage and some treatment processes such as pre-treatment, metal melting, compression, re-packing, and cement solidification. It also contains radionuclide sampling and analysis, and radiation dose measurement and evaluation room.



Fig. 1. A bird's eye view of the STAR facility.

5. Conclusion

The STAR (Storage and Treatment of All Radwaste in KAERI) facility, a total radwaste management facility, is now being designed and will be constructed by 2021. The STAR facility, including a radwaste storage and some management processes, will contribute to reducing radwaste the present inventory by half.

REFERENCES

- [1] IAEA-TECDOC-855, "Clearance levels for radionuclides in solid materials", Application of exemption principles, International Atomic Energy Agency (1996).
- [2] Notice of Nuclear Safety and Security Commission No. 2014-003, "Regulations on the Classification and Self-disposal of Radioactive Waste", Sep. 15, 2014.

Selective C-14 Stripping Method From Waste Resin Generated From HWR via Microwave Treatment

Ki-Rak Lee^{a)*}, Hyeon-Oh Park^{b)}, Geun-Il Park^{a)}, Hwan-Seo Park^{a)}, Hong-Joo Ahn^{a)}, Jung-Hoon Choi^{a)},
Seung-Youb Han^{a)}, and Young-Ku Choi^{b)}

^{a)} Korea Atomic Energy Research Institute, 111, Daedeok-daero 989beon-gil, Yuseong-gu, Daejeon, Republic of Korea

^{b)} Sunkwang T&S Co.,Ltd., Sunkyung Officetel 20F, 3, Gongwon-ro, Guro-gu, Seoul, Republic of Korea

*kirakki@kaeri.re.kr

Inorganic and organic ion exchange materials were generally applied to liquid processes in nuclear reactor. In the case of heavy-water reactor (HWR), zeolite, active carbon, anion resin, and cation resin were used to treat liquid processes such as reactor primary coolant cleanup and liquid radioactive waste management system. Then, used ion exchangers were stored at storage tanks. Various kinds of nuclides were adsorbed in ion exchange materials. Especially, C-14, long half-life nuclide, was highly concentrated in anion resin, and waste resin was treated as intermediated level radioactive waste (ILW).

In KOREA, 4 units of heavy-water reactor are operated and a lot of spent resins are generated. Until now, 580 m³ of waste resins were generated from Wolsung HWR unit 1 and 2 and stored at storage tank (storage tank capacity of Wolsung HWR unit 1 and 2: 986 m³). Enormous cost will be expected to dispose this radioactive waste if there is no process treating this waste.

Conventional process to treat radioactive wastes is not suitable for treating spent resin. To solve this problem, various kinds of processes were developed such as acid stripping, PLO process, activity stripping, thermal treatment, and etc. In this study, new process using microwave, is suggested. Basic properties of anion and cation were characterized by using surrogate waste resin. Removal efficiency of

C-14 via microwave method was evaluated with active waste resin generated from Wolsung HWR.

Surrogate waste resin was synthesized by using anion resin absorbed HCO₃⁻ ion. Surrogate waste resin was treated by microwave under different time condition from 1 min to 30 min. Treated surrogate waste resin was characterized by C NMR to confirm a stripping of adsorbed HCO₃⁻ without damage of main chain in resin. After 20 min microwave treatment, ammonium functional group was perfectly changed to amine group. It means that of adsorbed HCO₃⁻ was removed. Additionally, main chain and benzene group were detected at even 30 min treated sample.

Surrogate C-14 nuclide was perfectly removed from waste anion resin without damage of resin.

Active waste resin was treated under 1 kW microwave condition with and without additional DI water. More than 94% of C-14 from active waste resin were desorbed.

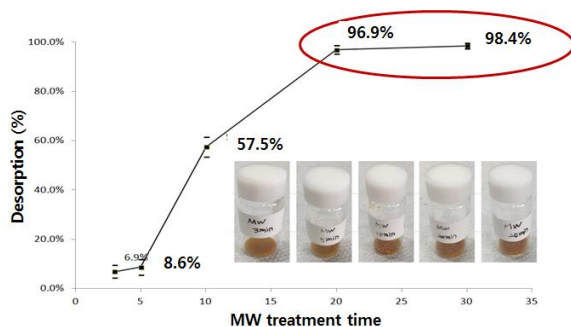


Fig. 1. Desorption efficiency of microwave treatment with surrogate waste resin.

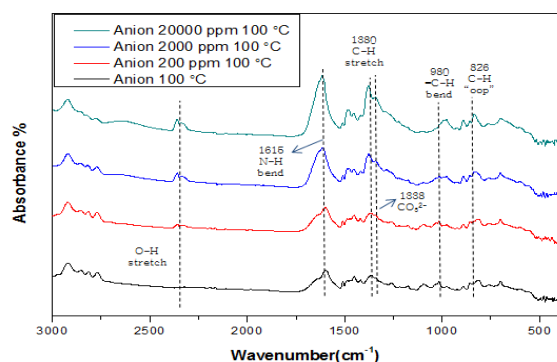


Fig. 2. IR results of surrogated anion resin treated by microwave.

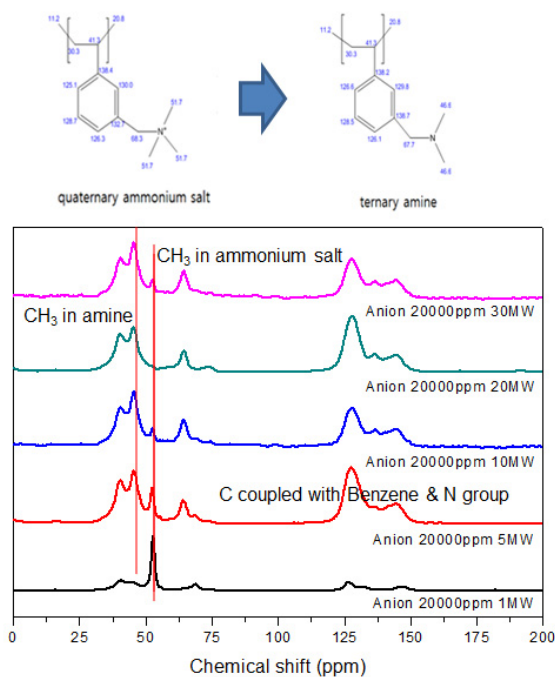


Fig. 3. C NMR results of surrogated anion resin treated by microwave.

REFERENCES

- [1] Technical Reports Series no. 408, Application of ion exchange processes for the treatment of radioactive waste and management of spent ion exchangers, IAEA, Vienna, 2002.
- [2] M. Matsuda, K. Funabashi, T. Nishi, H. Yusa, M. Kikuchi, "Decomposition of ion exchange resins by pyrolysis", Nuclear Technology, 75 (1986), 187-192.

Corrosion Properties of Metal Waste Alloys for Long-lived Radionuclides Immobilization

Seungyoub Han*, Junghoon Choi, Kirak Lee, and Hwanseo Park

Korea Atomic Energy Research Institute, 111, Daedeok-daero 989beon-gil, Yuseong-gu, Daejeon, Republic of Korea

*hsy@kaeri.re.kr

1. Introduction

Technologies used in solidification processing by melting spent nuclear fuel assembly materials and hulls for metal waste reduction that occurs during the pyro-processing have been studied, mainly in the United States [1-3]. A cladding hull in a spent fuel assembly to be applied to a domestic PWR is composed of a metal alloy such as Zircaloy-4, ZIRLO accounts for the highest volume and weight ratio in the generation of process waste. Recently, at KAERI, we have been conducting research on the recycling of a cladding hull as a solidification host matrix in order to solidify and handle highly radioactive anode sludge residue including noble metal (NM) that occurs from electro-refining from pyro-processing. If we produce an MWF (Metallic Waste Form) by adding and melting the alloying elements and anode sludge in the cladding hull, the effect on the volume reduction and weight loss can be maximized because the cladding hull can be 100% recycled to the solidification host matrix of MWF. According to the existing results of MWF alloys manufactured in the US, although a stable production of MWF is possible with SS-15Zr alloy, it is disadvantageous in terms of the domestic cladding hull recycling efficiency, because the Zr content is low. In addition, the mechanical stability and corrosion resistance of Zr-8SS is relatively low [3]. As a result of the new composition with Zr-Cr-Si-NM in KAERI, a stable MWF was formed without cracks. Moreover, it was possible to confirm the possibility that the cladding hull and anode sludge generated from the pyro-processing can be fabricated MWF alloy with an excellent corrosion resistance.

2. Experimental Results

The ZIRLO-SS304-INCONEL718 composition of the 9 kinds of solidification host matrix compositions has the eutectic point composition. All specimens were fabricated by high frequency induction heating in a silica crucible in an Ar atmosphere after forming a vacuum of 5×10^{-5} torr. To ensure the integrity of the specimen, it was held at 1600 to 1800 °C for 5 minutes. After forming the melt completely, it was kept at 1350 °C for about 15 minutes, furnace cooling was then applied to reduce the solidification shrinkage cracks and porosity. All prepared specimens were cut and polished, and XRD, SEM, and EDS analyses were performed for a microstructure and phase analysis.

For an evaluation of the corrosion properties, potentiodynamic (PD) and potentiostatic (PS) tests were carried out in the acidic brine aqueous solution condition ($0.0001 \text{ mol} \cdot \text{kg}^{-1} \text{ H}_2\text{SO}_4 + 0.01 \text{ mol} \cdot \text{kg}^{-1} \text{ NaCl}$ in demineralized water, pH). The main phases composing the Zr-Cr-Si-NM alloy consist of α -Zr, ZrCr_2 , and Zr_2Si . The eutectic structure and ZrCr_2 phase increased with increasing Cr content. Pd was concentrated on α -Zr, Ru on α -Zr and ZrCr_2 , Re on Zr_2Si phase. Electrochemical accelerated corrosion tests such as PD and PS were carried out on the Zr-Cr-Si and Zr-Cr-Si-NM alloys prepared in this study. The Zr-Cr-Si-NM alloys exhibited a high corrosion resistance and low corrosion rate owing to their low I_{corr} values with high E_{corr} values compared to conventional materials. As a result of the analysis of the composition of the leachate after the PS test, there was no NM element leaching below 500 mV, or leaching of the elements excluding Re, which is a surrogate Tc at 800 mV. In particular, the Zr_2Si

phase, which is encapsulating phase of Re, was very stable, and showed no shape change or leaching of Re after the corrosion test, suggesting that the Tc immobilization ability is excellent.

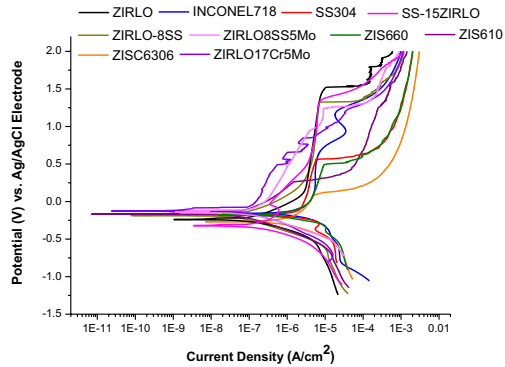


Fig. 1. Potentiodynamic test results of all specimens.

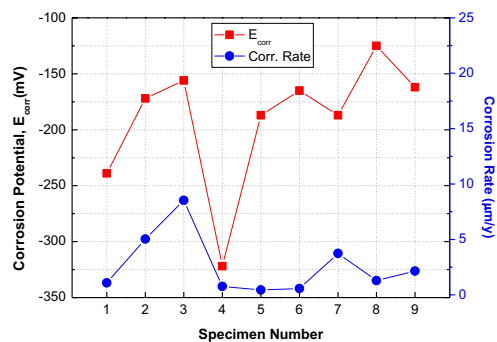


Fig. 2. Corrosion potential and Corrosion rate values of all specimens.

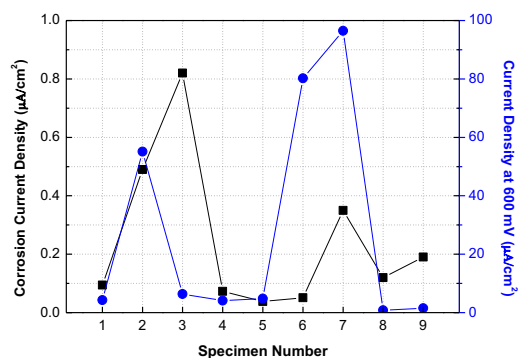


Fig. 3. Corrosion current density and current density at 600 mV of all specimens.

3. Conclusion

The main phases composing the Zr-Cr-Si-NM alloy consist of α -Zr, ZrCr_2 , and Zr_2Si . The eutectic structure and ZrCr_2 phase increased with increasing Cr content. Pd was concentrated on α -Zr, Ru on α -Zr and ZrCr_2 , Re on Zr_2Si phase. Electrochemical accelerated corrosion tests such as PD and PS were carried out on the Zr-Cr-Si and Zr-Cr-Si-NM alloys prepared in this study. The Zr-Cr-Si-NM alloys exhibited a high corrosion resistance and low corrosion rate owing to their low I_{corr} values with high E_{corr} values compared to conventional materials.

REFERENCES

- [1] D. D. Keiser Jr, D. P. Abraham, and J.W Richardson Jr, "Influence of technetium on the microstructure of a stainless steel-zirconium alloy", J. Nucl. Mater, 277(2-3), 333-338 (2000).
- [2] S. M. McDevitt, D. P. Abraham, and J. Y. Park, "Evaluation of stainless steel-zirconium alloys as high-level nuclear waste forms", J. Nucl. Mater, 257(1), 21-34 (1998).
- [3] W. L. Ebert and D. Kolman, Alloy Waste Form Testing Strategy Roadmap, U.S. Department of Energy Report, FCRD-SWF-2013-000226 (2013).

Research and Development of High-dose Radioactive Material Transport Wagon Using Water Shielding

Dong Hyun Park, Sang Tae Lee, Myeong Ho Kim, Jeon Joon, and Sung Jun Hong
HANA Nuclear Power Engineering, Co., Ltd., 804, Hanam-daero, Hanam-si, Gyeonggi-do, Republic of Korea
*pdh200@hanarad.com

1. Introduction

During the Overhaul(outage) period of Nuclear Power Plant(NPP), generated high dose radioactive materials in reactor buildings and elsewhere are transport to attenuation storage areas or waste treatment rooms for radiation dose reduction or waste treatment. Therefore, lead shielding has been used to reduce the radiation exposure of workers or movement path during high-dose radioactive material movement. However, due to the characteristics of the lead shield, the lead weight is too heavy to handle and it is difficult to fix the shield to the wagon. In addition, there is a possibility that the wagon may be shaken due to various equipments or protrusions installed on the movement route, or the lead shielding body may be dropped by some impacts. To solve these problems, we have developed a carriage wagon that relatively light and easy to handle, and can move stably even under the harsh route conditions for high dose radioactive materials that frequently generated in reactor building of NPP.

2. Production of shielded wagon

The shielded wagons should have shielding capacity of 70 ~ 80% based on the radiation dose rate for high dose radioactive materials and should be more efficient than the existing transportation method. Therefore, the method of filling water for shielding in cavity structure made of a double SUS material outside of a wagon that having a space in which radioactive materials can be sufficiently store was selected in this study. In addition, the water for shielding is designed to be easy to fill and drain if necessary. It is designed to be drained state when moving to the area for loading radioactive materials to be easily moving. And It can be shielded by adding water before loading high dose radioactive materials. Also, in order to minimize the impact caused by the obstruction of the moving path or the protrusion of some equipments, the wheel was used as a shock absorber wheel. This proved its effectiveness in actual field applications.

Since water is used as a shielding material, all materials used are SUS 304, which has high corrosion resistance against water. And, in order to prepare for higher radioactive material than anticipated, connection rings were equipped to outside of the shielded wagon for the existing lead blanket could be attached. This connection rings are designed to be securely fixed to wagon. It differs from the existing method of temporarily using a lead shield in wagons.

2.1 Estimated shielding ability calculation

Designed to attenuate more than 72%

$$I_{\text{total}} = 0.755(\text{shielding ability of wagon}) \times 0.370(\text{shielding ability of water}) = 0.279$$

Therefore, the shielding effect,

Dose before shielding \times 0.279(shielding ability of shielded wagon) = Dose after shielding

$$I = I_0 e^{-\frac{0.693t}{T}} \quad (1)$$

I : Radiation intensity after shielding,
I₀ : Radiation intensity before shielding
T : Half-value layer thickness,
t : Thickness of shielding material

Shielding ability of wagon material (applied steel plate)

$$\begin{aligned} &[\text{Density(g/cm}^3\text{)} : \text{steel}=7.87, \text{SUS 304}=7.90] \\ I_{\text{SUS}} &= 100\% \quad e^{-\frac{0.693 \times 0.60\text{cm}}{1.48\text{cm}}} = 75.5\% \\ &(\text{T} : 1.48 \text{ cm}, \text{t} : 0.6 \text{ cm}) \end{aligned}$$

Shielding ability of water

$$\begin{aligned} I_{\text{water}} &= 100\% \quad e^{-\frac{0.693 \times 14\text{cm}}{9.8\text{cm}}} = 37.0\% \\ &(\text{T} : 9.80 \text{ cm}, \text{t} : 14.0 \text{ cm}) \end{aligned}$$

2.2 Estimated weight of shielded wagon

The weight was calculated using the amount of SUS used and the density (7.9 g/cm^3) used in the shielded wagon with reference to the production drawings. The weight of the SUS used in the shielded wagon body is about 68 kg, and the amount of water to be filled with the shielding is 128 liters, and 20 kg is added by wheels, reinforcements and handles. Therefore, the weight of the shielded wagon that was filled with water was estimated to be about 216 kg.

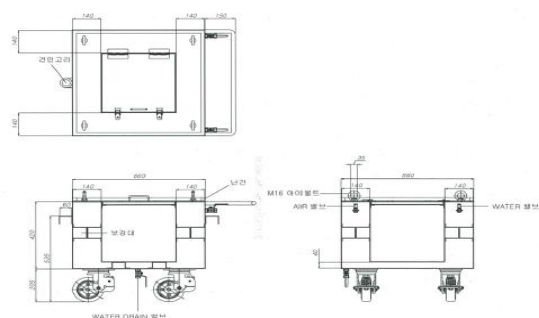


Fig. 1. Drawings of shielding wagon.

3. Field Application Results

The actual shielded wagon, which was actually made, weighed about 224 kg when water was injected, it is 8 kg heavier than expected. However, it was considered that there would be no problems for safely moving from the reactor building to the attenuation storage area or the waste treatment room. The shielded wagon tested the shielding ability before application in field. As a result of storing radioactive materials with a surface radiation dose rate of 2 mSv/h in the shielded wagon, it was confirmed that they had a shielding ability of about 90%.

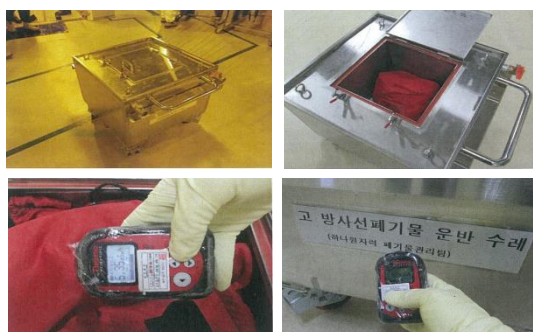


Fig. 2. Field applied Shielded wagon.

The results of field application after shielding ability test are as follows.

Table 1. Field application results of water shielded wagon

Radio active waste	Surface radiation dose rate (mSv/h)		1m Radiation dose rate (mSv/h)		Shielding ability (Based on surface)
	Before shielding	After shielding	Before shielding	After shielding	
Concentrated waste liquid granules	4	0.5	0.13	0.027	87.5%
Concentrated waste liquid granules	2	0.13	0.05	0.006	93.5%
VGS Decontamination waste	7	0.8	0.2	0.05	88.6%
Cavity Decontamination waste	5	0.6	0.14	0.003	88.0%
Cavity Decontamination waste	1.6	0.2	0.06	0.008	81.3%
ICI working waste	8	1	0.4	0.06	87.5%
ICI working waste	4.8	0.6	0.2	0.037	87.5%
Cavity Bottom sludge	20	2.1	-	0.3	89.5%

4. Conclusion

The purpose of this study was development the shielded wagon that can effectively and safely carrying for high dose radioactive materials, which are frequently generated in reactor buildings, during overhaul period of NPP. This includes reducing radiation exposure of workers and radiation of movement path during high-dose radioactive material movement. We have developed the 'water-shielding wagon' by improving the existing universal method of loading radioactive material on a wagon and shielding it with a lead shield temporarily. This will contribute to the reduction of the radiation workers' exposure and quality improvement of radiation safety management.

REFERENCES

- [1] Radiation protection standards Notification 2014-034).
- [2] Regulations on packaging and transportation of radioactive materials (Notification 2014-050).
- [3] Metal material comparison handbook "Published by Gold" (Lee eui jong).
- [4] Nuclear Safety Commission Act and Radioactive Waste Management Act.

Characteristics of the Precipitate From Cs⁺ Extraction Using Ionic Liquids

Jungweon Choi*, Hayeon Ryu, Wonzin Oh, and Sang-June Choi

Kyungpook National University, 80, Daehak-ro, Buk-gu, Daegu-si, Republic of Korea

*jungweon@knu.ac.kr

1. Introduction

The chemical and physical properties of precipitates from Cs⁺ extraction process using ionic liquids (ILs) [1] were investigated. The chemical form was Cs⁺•Tf₂N⁻•DCH18C6 which is a Cs ionic solid extracted by the extractant of DCH18C6. The solid liquid separability of the precipitates were also studied by using the physical properties including density and thermal stability.

2. Experimental

2.1 Materials

Cesium nitrate (CsNO₃, 99%) and the extractant, dicyclohexano-18-crown-6 (DCH18C6, 98%) were purchased from Sigma-Aldrich Chemical Co. (Germany). The ionic liquids, 1-ethyl-3-methylimidazolium bis(trifluoromethylsulfonyl)imide (C₂mimTf₂N) was purchased from C-TRI Co. Ltd. (Korea).

2.2 Method

CsNO₃ simulated waste solution was prepared at 30 mM concentration. And then 0.6 mM DCH18C6 was dissolved in 0.6 mmol C₂mimTf₂N. These aqueous phase and organic phase was mixed for 2 hours at 25°C. After extraction, the precipitate was separated. To get the dried precipitate, the precipitated was placed in the oven at 80°C. The precipitate was analyzed by SEM, PSA, TGA, DSC and XRD.

3. Results

We found that the new phenomenon, the precipitate is formed when the amount of ILs was reduced [1]. We confirm that the precipitate consist of Cs⁺•Tf₂N⁻•DCH18C6 by SEM-EDS as shown in Fig. 1(c).

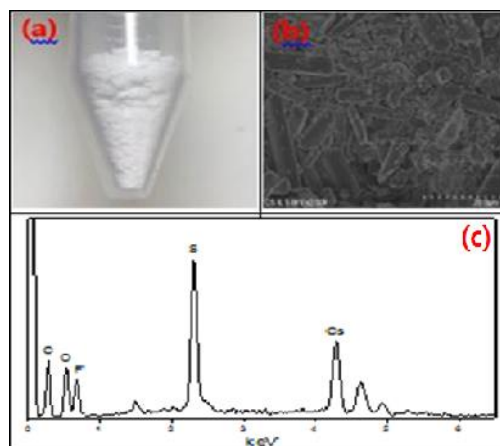


Fig. 1. Experimental image (a), FE-SEM image (b), SEM-EDS spectrum (c) of the precipitate.

From now on, it is the result of sediment size analysis and thermal analysis to judge whether the solid-liquid separation of cesium is applicable.

3.1 Size distribution of the precipitate

The particle size of the precipitate was analyzed to be 171.7 μ m on average and most of the precipitates were evenly distributed between 100 and 400 μ m. Even, small particles are of a size (over 10 μ m) enough to separate with conventional MF filter.

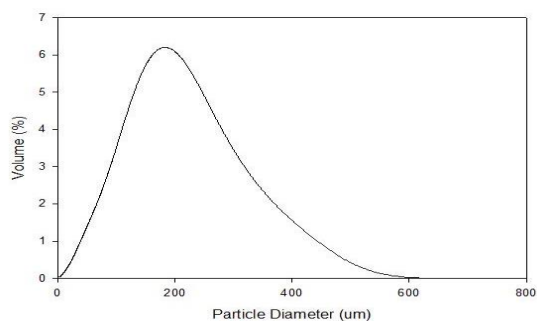


Fig. 2. PSA result of the solid precipitate.

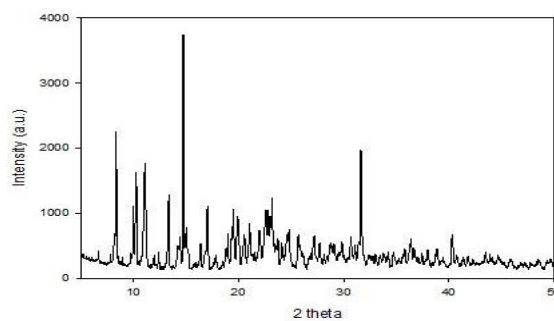


Fig. 5. XRD result of the solid precipitate.

3.2 Physical properties depending on temperature

These graphs indicate that the melting point and weight loss of the precipitate respectively. The precipitate was dissolved at 91.1°C, it takes 28.20 W/g (Fig. 4). The precipitate is stable up to 300°C.

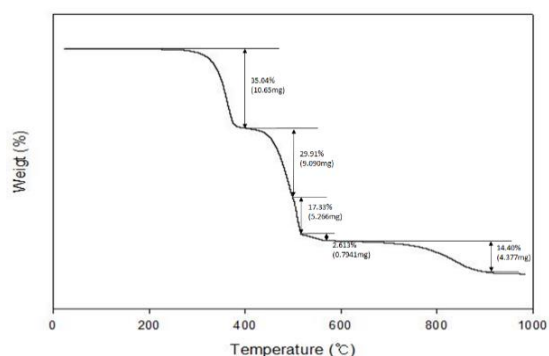


Fig. 3. TGA curves of the solid precipitate.

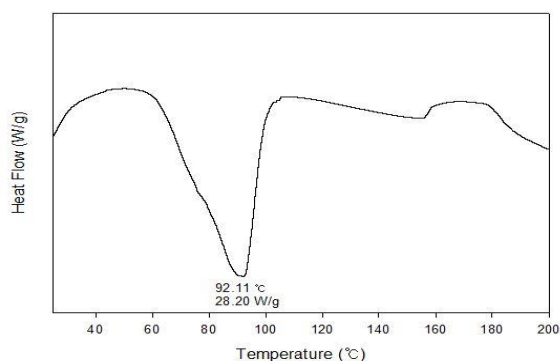


Fig. 4. DSC curves of the solid precipitate.

The XRD results of the precipitate showed numerous sharp peaks, indicating that the precipitate was crystalline ordered structure.

4. Conclusion

Through the studies on the precipitates from Cs^+ extraction process using ionic liquids (ILs), the following conclusions were obtained within the experimental ranges.

- 1) By analyzing the size of the precipitate, it was confirmed that it is easy to separate from the waste solution in the actual process. Also, the density of precipitate has 1.315 g/cm^3 value.
- 2) Through analysis, it was confirmed that the thermal stability of precipitate was not degraded up to 300°C. The precipitate was melted at 91.1°C, and the precipitate had a crystalline structure.

ACKNOWLEDGEMENT

This research was supported by Nuclear Energy Development Program through the National Research Foundation of Korea (NRF) funded by the Ministry of Science and ICT (2018M2B2B1065631).

REFERENCES

- [1] K. Sumin et al., "A novel method for separating Cs^+ from liquid radioactive waste using ionic liquids and a selective extractant", J Radioanal Nucl Chem 311:1605–1611 (2017).

A Study on Characteristics for Manufacturing the Sintered Green Body of Moist Particulate and Sludge-type Radioactive Waste

Hyoungmin Park²⁾, Yongho Hong^{1)*}, Minsu Kim¹⁾, Heekyung Kim¹⁾, Eunsuk Choi¹⁾, Dongchul Kim¹⁾, Taekyu Lee¹⁾, Byunggu Lee²⁾, Seonghun Yoon²⁾, and Jeongsu Kim²⁾

¹⁾ ACT Co., Ltd., 406, IT Venture Town, 35, Techno9-ro, Yuseong-gu, Daejeon, Republic of Korea

²⁾ TAEKWANG Co., Ltd., 68, Bugok-ro, Nam-gu, Ulsan, Republic of Korea

*hyh@actbest.com

1. Introduction

It is a study on characteristics and the suitability of disposal for a sintered green body by using the simulated sample of the moist particulate and sludge-type radioactive waste. The moist particulate and sludge-type radioactive waste contain glass components, so cerium oxide (CeO_2) was added to samples in order to maintain molding conditions in the high -temperature furnace at 1100°C . As a result, it was confirmed that the samples had sufficient compressive strength, no harmful substance and were isotropically shrunk.

2. Main Title

2.1 Process of manufacturing the green body

As shown in the table 1, it is the comparative analysis of composition between the original sample and simulated sample.

Table 1. The comparative analysis of composition between the original sample and simulated sample(ppm)

	Si	Sb	Mo	Fe	Al	Cu	Zn	P	Ca	Mg	B	Ti
O.S*	22.3	2.58	332	27.04	35.21	-	1.33	2.27	698.7	21	61.85	0.38
S.S**	34.2	3.39	839.6	37.76	97.8	70.9	2.24	61.86	1704	52.9	123.7	1.69

*O.S : Original Sample **S.S : Simulated Sample

To manufacture the sintered green body, the sample was dried in the dryer to remove moisture, and then put into a super-mixer to make a homogeneous powder. After that, the powder was put into the molding machine and sintered in the high-temperature furnace.

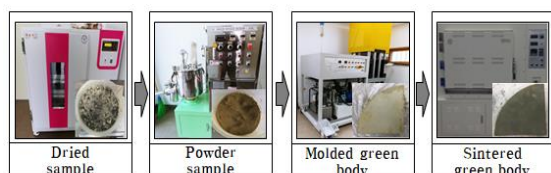


Fig. 1. The process for Manufacturing sintered green body.

According to the optimum condition of the sintering process, the molded green body was put into the furnace at 200°C for 2 hours and at 300°C for

1 hour to remove the moisture of the green body. After that, temperature was elevated to 1100°C and maintained for 3 hours in the furnace to remove the harmful substance in the green body.

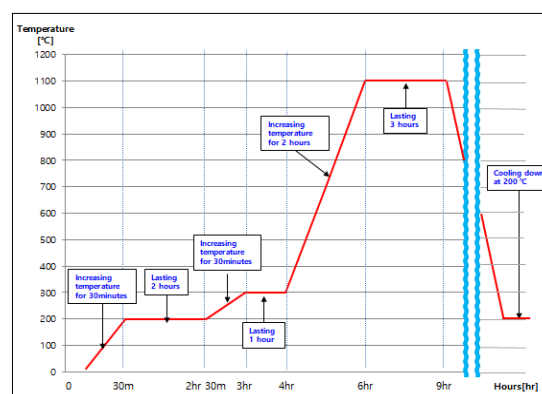


Fig. 2. Temperature and setting time to manufacture the sintered green body.

As shown in Fig. 3, it was sintered green body with the glass-ceramic shaped structure.

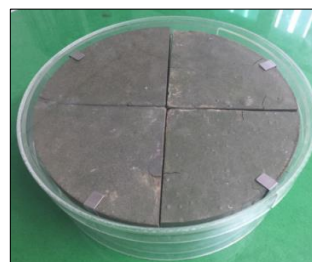


Fig. 3. The fan-shaped disk type of sintered green body.

2.2 Compressive strength test

The compressive strength test is to confirming the structural integrity in the solidification of radioactive waste to satisfy the acceptance criteria of KORAD. In order to confirm the structural stabilities of the sintered green body, it made the specimens which were SB1, SB2. And then, evaluate the compressive strength of the specimens as shown in Fig. 4.

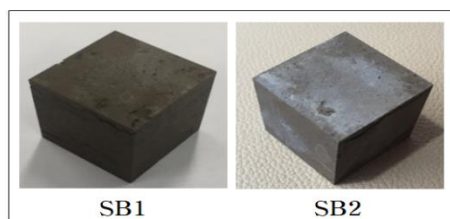


Fig. 4. The specimens of sintered green body.

Table 2. The result of compressive strength test

Compressive Strength test				
Solidification of radioactive waste		Sintered Green body		
Acceptance Criteria of KORAD	psig	Result	Specimen	psig
500			SB1(Sample 1)	8,267
			SB2(Sample 2)	28,282

The compressive strength test of the specimens showed about 16 ~ 57 times higher than that of acceptance criteria of KORAD. Consequentially, it was observed that the sintered green body had sufficient compressive strength.

2.3 Analysis of composition in sintered green body

As shown in Fig. 5, it is the analysis of composition in the sintered green body by using the XRD. It was confirmed that Sb_2O_3 , which is a harmful substance, was oxidized to Sb_2O_5 in the sintering process.

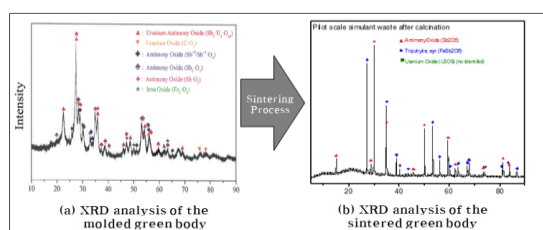


Fig. 5. Analysis composition of sintered green body by using XRD.

According to the analysis results, Sb^{+3} , Sb^{+5} were included in the samples, but after sintering the samples, it was observed that Sb^{+5} was only presented in the samples.

2.4 Evaluation of volume reduction and isotropic shrinkage in sintered green body

As shown in Fig. 6, the length of the sample was reduced by 13% on average and it was confirmed that the volume of the sample was reduced by 35% and was isotropically shrunk.

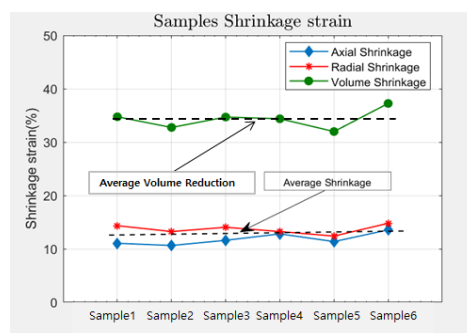


Fig. 6. The result of volume reduction and isotropic shrinkage for the sintered green body.

3. Conclusions

As stated above, it studied the characteristics for manufacturing the sintered green body. The compressive strength of the sintered green body is harder than the acceptance criteria which is 500 psig applied to the solidification of radioactive waste in KORAD. In addition, it was confirmed that harmful substance of Sb^{+3} in the molded green body was removed after the sintering process. Therefore, it is expected that the result of this study will provide the basis for satisfying the acceptance criteria of low-intermediate level radioactive waste in KORAD and it can be applied to the commercial scale design for manufacturing the sintered green body of moist particulate and sludge-type radioactive waste.

ACKNOWLEDGEMENT

This study is the result of conducting the research for securing safety and satisfying the transportation requirements of radioactive waste in Taekwang industry.

REFERENCES

- [1] KAERI. Development of Technology for Volume Reduction of Depleted Uranium Waste (2017).
- [2] ACT co., Ltd., Development of the Process for Disposal of Radioactive Waste in TK Petrochemical Factory 3 (2018).
- [3] ACT co., Ltd., A Study on Characteristics for Manufacturing Immobilization of Green Body for the Moist Particulate and Sludge-type Radioactive Waste (2018).

Development of a 200 Liter-disposal Container (Drum) Cutting Machine for Nuclear Facilities

SeungGeon An*, SeakJun Yoo, Seongil Cho, JungSik So, and DaeHwan Kim

Sunkwang T&S Co.,Ltd., Sunkyung Officetel 20F, 3, Gongwon-ro, Guro-gu, Seoul, Republic of Korea

*seunggeonan@hotmail.com

1. Current technology status

In nuclear facilities, as for the same specifications as the disposal container, the drum has a upper band on the upper part and the bottom part of the drum is also ringed with a solid band. Disposal target drums are stored separately from permanent waste and clearance waste¹⁾ according to the radiation dose rate and surface contamination throughout scan survey. Clearance waste level drums are kept separately in a certain place. Both clearance and permanent waste drums are cut into appropriate sizes for disposal.

Clearance waste drums are then carry out decontamination and sampling process and permanent waste are stored in disposal drum. We normally use drum scissors, hydraulic scissors when cutting the drum which requires a lot of manpower since it is done manually. In this paper, we described the drum cut-off device that can be safely and efficiently cut to solve the problem of cutting the existing disposal drums.

2. Basis for development

Drum cutting machine is developed into two types. Curved cutter is designed to cut curved part of the drum and plane cutter is able to cut flat part of the drum. Also our drum cutting machine is designed to facilitate consumable replacement and maintenance, making it easy to maintain.

Furthermore, with simple education, workers can use the device easily, reduce work time and also cut drum in even sizes suitable for clearance waste requirement and disposal container size.

3. Development content

3.1 Curved Cutter (SKDC2 150A) specification



- 1) Operation system: Electricity, air (semi-auto)
- 2) Weight: 258 kg
- 3) Size: 1,300 W x 900 D x 1,300 H
- 4) Operation condition: 220 V (single phase), air compressor
- 5) Cutting motor: 1,800 W
- 6) Blade used: 9" (blade, tip-saw blade)
- 7) Rotator motor: BLDC 180 W
- 8) Airbag: tube extension up to 1.8~2 psi
- 9) Mobility: wheel movement
- 10) Cutting target: 200 L, 100 L, 50 L steel drum
- 11) Cutting speed: 1 drum/5 min (200 L base)

3.2 Plane cutter (SKDC2 150B) specification

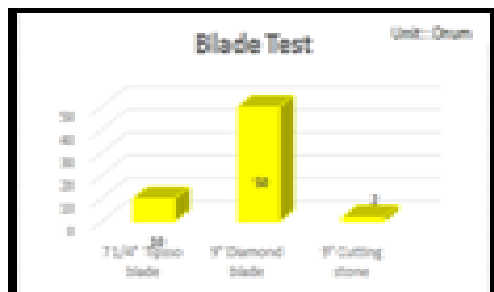


- 1) Operation system: manual
- 2) Weight: 166 kg
- 3) Size: 1,300 W x 900 D x 1,300 H
- 4) Operation condition: 220 V (single phase)
- 5) Cutting motor: 1,200 W (round saw)
- 6) Blade used: 7 1/4" (blade, tip-saw blade)
- 7) Mobility: wheel movement

- 8) Cutting target: 200 L, 100 L, 50 L steel drum
- 9) Cutting speed: 1 drum/5 min (200 L base)

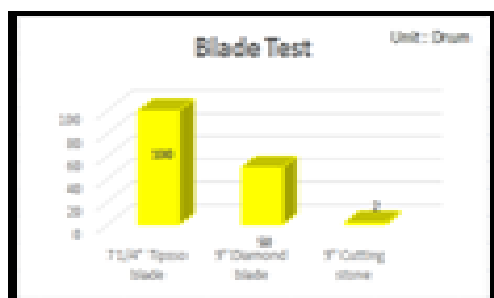
3.3 Blade test Result (200 L base)

- No. Of drum cut by different blade



*Curved cutter (5.4 m/drum)

*Used self-manufactured diamond blade



*Plane cutter (2.58m/drum)

*plane cutter: used tip-saw blade

3.4 Curved / plane cutter advantages



- ① Active design (fast replacement of consumable supplies)
 - Easy to repair when trouble
 - Easy to disassemble which makes decontamination more comfort
- ② User-centered design
 - With simple education, users can operate the machine easily and save time

- ③ Scatter-free cover by using 3 mm iron plate for safety purpose (reduce scattering to prevent contamination)
- ④ Accurate cut performance and blade efficiency (1 blade to cut 90 or more drum)
- ⑤ reduce consumable supplies
- ⑥ ensure consistent cutting and even cutting sizes
- ⑦ Minimize exposure time in hazardous material space

4. Expectation and future application

4.1 Expectation

① By cutting disposal drums into appropriate size, we can reduce the porosity and number of the permanent waste drum.

Furthermore, as we can cut drums in appropriate shape for disposal, we can reduce the time and man-power spent on the operation.

② As to make radioactive-waste drums into clearance waste, we can cut drums into easy-decontamination and easy-sampling size, which will lead to reduction of the permanent waste.

③ By making scatter-free cover in the device, working place can be more safe to prevent any negligent accident.

4.2 Application plan

Applicable to other nuclear power plants and also general industry.

REFERENCES

- [1] The Solid Nuclear Wastes Management (SK-U2-radiation-200, 2017).
- [2] Clearance of Metal Nuclear Wastes (SK-U2-radiation-204, 2017).
- [3] Notify for Classification and Clearance of Nuclear Wastes (Nuclear Safety and Security Commission Notify, 2017-65).

Examination on Electrochemical Behaviors of Niobium Chloride in Molten LiCl-KCl by Cyclic Voltammetry

Gwan Yoon Jeong and Jaeyeong Park*

Ulsan National Institute of Science and Technology, 50, UNIST-gil, Eonyang-eup, Ulju-gun, Ulsan 44919, Republic of Korea

*jypark@unist.ac.kr

1. Introduction

Niobium (Nb) is one of the major alloying elements which has been widely utilized in nuclear industry to enhance corrosion resistance under high temperature and pressure (e.g., fuel cladding and CANDU pressure tube). In addition, it is also contained in various types of nuclear structural materials like stainless steel, Inconel. Niobium is monoisotopic elements with ^{93}Nb , but a long lived radioisotope, ^{94}Nb , is generated and accumulated in the materials during irradiation inside or near a nuclear reactor. This radioisotope is often the key element, elevating the radioactive waste hierarchy of the activated materials from the low level waste (LLW) to the intermediate level waste (ILW) because the ^{94}Nb concentration limit for the LLW in Korean radioactive waste classification system is low as 111 Bq/g.

Electrorefining in LiCl-KCl has been widely utilized not only in nuclear industry but also in rare earth and refractory elements industry to separate target elements from the ore and waste. The chloride-based separation technique would also be applied for the Nb contained metallic radioactive waste. Electrochemical behaviors of Nb has to be fully understood during electrorefining to monitor and manage the anode and cathode potential utilized to suppress dissolution and deposition of Nb on the anode and cathode respectively. In LiCl-KCl, it has been identified that Nb has various oxidation states (Nb^{5+} , Nb^{4+} , Nb^{3+} , Nb_xCl_y , Nb), but the number of reports regarding redox mechanism of the states in LiCl-KCl is limited [1][2].

In this study, the electrochemical redox behaviors of Nb in LiCl-KCl-NbCl₅ (1wt.%) at 450°C are examined by cyclic voltammetry (CV) which is the most widely used technique for qualitative and quantitative analysis for electrochemical redox mechanism and properties. Diverse scan rates, scan ranges at the fixed concentration and temperature are investigated, and the redox reactions of Nb for each redox peaks of cyclic voltammograms are suggested by the peak shapes with comparison to the reported papers. The identified Nb behavior will be utilized to design an electrochemical decontamination process for lowering the Nb contained waste hierarchy.

2. Experimental

The reagent of LiCl-KCl-1wt.% NbCl₅ for the CV experiments were prepared with LiCl-KCl eutectic and NbCl₅ of 99.9% purity from Alfa Aesar. All experimental procedures from the reagent preparation to the CV experiment were performed within the glovebox which is designed to limit oxygen and moisture concentrations to be < 0.1 ppm under Ar gas (99.99%) environment.

The electrochemical cell with the diameter of 13 mm for the CV experiments was placed in the electric resistance furnace installed by connecting to the bottom surface of the glovebox module as shown in Fig. 1. A temperature measuring quart tube containing only eutectic LiCl-KCl molten salt with the identical size of the CV experiment tube was additionally placed right next to the CV cell to predict the temperature of the CV cell indirectly. The temperature of LiCl-KCl in the temperature cell was measured by a K-type thermocouple.

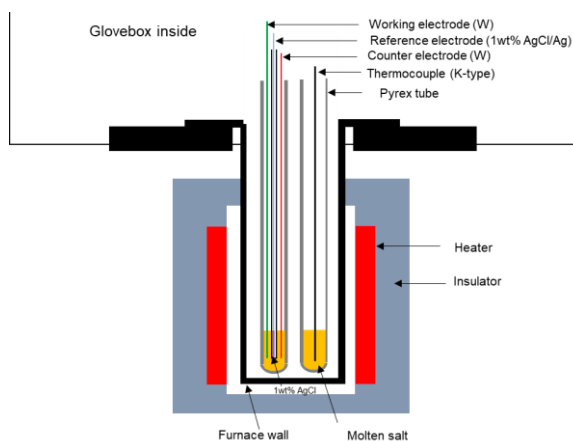


Fig. 1. A schematic showing an experimental setup for cyclic voltammetry.

Inert working and counter electrode made of tungsten wire with the diameter of 1 mm was inserted into the molten salt. The surface areas of the electrodes were determined by measuring the immersed depth of the electrode after the CV experiment, and the wetted depth was measured as about 13 mm. The reference electrode was the Ag/AgCl electrode, in which Ag metal wire with a diameter of 1 mm and purity of 99.99% was placed within the LiCl-KCl-AgCl (1wt. %) solution.

CV was performed with different scan rates (20 ~ 1500 mV/sec) and scan ranges (-1.1 ~ 1.0 V) to identify possible redox peaks.

3. Results

Fig. 2 shows cyclic voltammograms with different scan rates in the scan range from 1.0 to -1.1 V (vs. 1 wt.% Ag/AgCl). Due to the complexity from multiple oxidation states of Nb ion, multiple cathodic and anodic peaks were found. They were identified by referring to the literature data published by Lantelme *et al.* as summarized in Table 1 with major reactions which can contribute to each current peak [3].

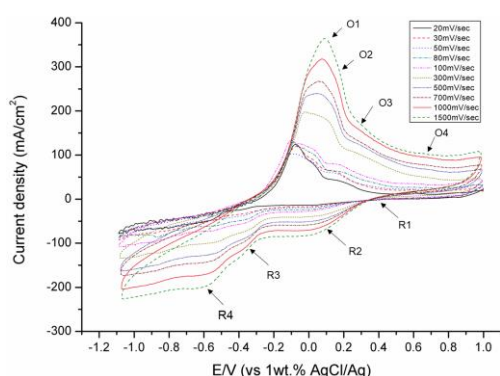


Fig. 2. Cyclic voltammograms showing the major redox reactions with different scan rates at 450°C.

Table 1. Comparison of possible reactions for CV peaks in LiCl-KCl-NbCl₅ system

Peak	This study (possible major reactions)	Lantelme (450°C, 5·10 ⁻² mol/L NbCl ₅ , molybdenum electrode) [3]
R1	Nb(V) + e ⁻ → Nb(IV)	Nb(V) + e ⁻ → Nb(IV)
R2	Nb(IV) + e ⁻ → Nb(III)	Nb(IV) + e ⁻ → Nb(III)
R3	Nb(III) + e ⁻ → Nb _x Cl _y (major)	Nb(III) + e ⁻ → Nb _x Cl _y
R4	Nb(III) + 3e ⁻ → Nb	Nb(III) + 3e ⁻ → Nb
O1	Nb → Nb(III) + 3e ⁻	Nb → Nb(III) + 3e ⁻
O2	Nb _x Cl _y → Nb(III) + e ⁻	
O3	Nb(IV) + e ⁻ → Nb(III)	Nb(III) + e ⁻ → Nb(IV)
O4	Nb(V) + e ⁻ → Nb(IV)	Nb(V) + e ⁻ → Nb(IV)

Peak potentials and corresponded redox reactions were consistent with CV results including peak shapes reported by Lantelme *et al.* [3]: Cathodic peaks for R3 and R4 were due to the formation of niobium subchloride (i.e., NbCl_x, x~2.33) and Nb metal deposition.

Fig. shows cyclic voltammograms with different scan ranges at the fixed scan rate of 100 mV/sec. It is noticed that the height for peak O1 increased as the negative potential limit became more negative since

the formation of metallic Nb is predominant by direct reduction of Nb(III) rather than the subchloride formation. The reaction for O2 peak is not clearly identified, but it is possibly due to the oxidation of niobium subchloride since the peak height for O2 increased as that for R3 increased as the negative potential limit became less negative with the preferential formation of the niobium subchloride.

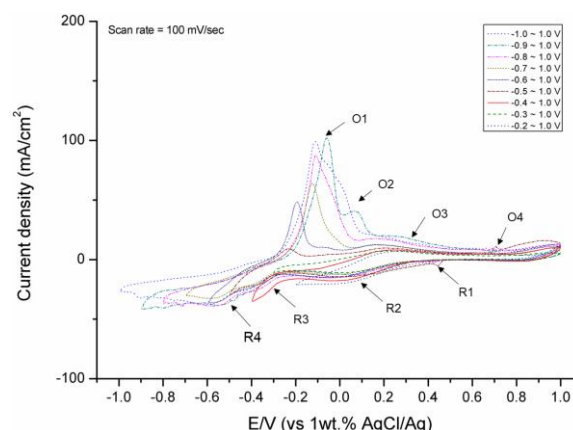


Fig. 3. Cyclic voltammograms with different scan ranges at the fixed scan rate of 100 mV/sec.

4. Summary

Electrochemical behaviors of Nb ion in the LiCl-KCl-NbCl₅ molten salt were examined. Cyclic voltammograms with different scan rates and scan range at 450°C showed possible electrochemical redox reactions which were identified by comparison to the literature data. Peak potentials for each redox reaction were consistent with the literature, but some redox reactions were not clearly defined due to the formation of subchloride compound in chloride salt. The electrochemical behaviors of Nb ion related to the subchloride formation as well as Nb metal deposition will be investigated for the future work.

REFERENCES

- [1] F. Lantelme, Y. Berghoute, Transient Electrochemical Techniques for Studying Electrodeposition of Niobium in Fused NaCl-KCl, *J. Electrochem. Soc.*, 141 (12) (1994) 3306-3311.
- [2] M. Mohamedi, Y. Sato, T. Yamamura, Examination of niobium electrochemistry from the reduction of Nb₃Cl₈ in molten LiCl-KCl eutectic, *Electrochimica Acta*, 44 (1999) 1449-1565.
- [3] F. Lantelme, A. Barhoun, J. Chevalet, Electrochemical Behavior of Solutions of Niobium Chlorides in Fused Alkali Chlorides, *J. Electrochem. Soc.*, 140 (2) (1993) 324-331.

Estimation and Measurement of Centerline Temperature of the Glass Waste Form

Jung-Hoon Choi*, Ki-Rak Lee, Seung-Youb Han, and Hwan-Seo Park

Korea Atomic Energy Research Institute, 111, Daedeok-daero 989beon-gil, Yuseong-gu, Daejeon, Republic of Korea

*mrchoijh@kaeri.re.kr

1. Introduction

High level glass waste forms are to be stored in the storage building before final disposal. The waste form storage vault should be operated using mechanically induced cooling system to remove the decay heat preventing overheating of the vault and devitrification of glass waste form in the canister [1,2]. However, even with the air cooling system in the storage vault, when the waste loading of heat generative nuclides are high, the centerline temperature of a glass waste form could exceed its glass transition temperature, leading to the increase of leaching rate of radioactive nuclides due to the devitrification of glass waste form [3]. Therefore, the estimation of centerline temperature of glass waste form for each waste stream is very essential in the period of storage. Also, the centerline temperature is important when a molten glass waste form is drained from vitrification equipment to a metal canister because the glass can be devitrified if the temperature profile from melting to room temperature is slow. Here, the centerline temperature of rare earth glass waste form generated from pyrochemical process has been estimated [4] and the temperature profile after drain process was measured.

2. Experimental

2.1 Fabrication of rare earth glass waste form

The rare earth glass waste form was fabricated using a $\text{SiO}_2\text{-Al}_2\text{O}_3\text{-B}_2\text{O}_3$ glass frit and $\text{Nd}_2\text{O}_3/\text{Gd}_2\text{O}_3$ as a surrogate waste material of rare earth fission products. For a vitrification of mixed oxides, the crucible was heated to $1,450^\circ\text{C}$ with a heating rate of $6^\circ\text{C}/\text{min}$ and maintained at $1,450^\circ\text{C}$ for 4 hours.

Thermal conductivity that is required in the centerline temperature calculation was measured using NETZSCH-LFA457 under an Ar atmosphere with a sample size of 12.7 mm in diameter and 2 mm in thickness.

2.2 Centerline temperature calculation

Centerline temperatures of waste forms for each transuranic elements (TRU) recovery ratio in the electrowinning process of the pyrochemical process were calculated using steady-state conduction equation (see equation (1) and (2)) in a long and solid cylinder with uniform heat generation and constant thermal conductivity. The heat generations of the waste form for each TRU recovery ratio were calculated using ORIGEN-S code.

$$\frac{1}{r} \frac{\partial}{\partial r} \left(kr \frac{\partial T}{\partial r} \right) + \frac{1}{r^2} \frac{\partial}{\partial \phi} \left(k r^2 \frac{\partial T}{\partial \phi} \right) + \frac{\partial}{\partial z} \left(k \frac{\partial T}{\partial z} \right) + \dot{q} = \rho c_p \frac{\partial T}{\partial t} \quad (1)$$

$$T_c = T(r = 0) = \frac{-A + \sqrt{A^2 + 2B \left(AT_s + \frac{B}{2} T_s^2 + \frac{\dot{q}}{16} D^2 \right)}}{B} \quad (2)$$

2.3 Measurement of centerline temperature

Centerline temperature profile was measured by metal canister having R-type thermocouples that can measure temperature profiles at characteristic points. Test glass (general borosilicate glass) was poured into the metal canister (cylinder type, 300 mm diameter) and the centerline temperature profile from melting temperature to room temperature was obtained.

3. Results and Discussion

During the pyrochemical process, TRUs could be

involved in the rare earth waste owing to the TRU recovery ratio (hereafter TRR) in the electrowinning process. The nuclide formulation of each waste form after electrowinning process was calculated according to the TRR, where TRR-100 indicates 100% TRU recovery ratio. TRR-99, TRR-95, TRR-90, TRR-85, and TRR-80 indicate TRU recovery ratio of 99%, 95%, 90%, 85%, and 80%, respectively.

The centerline temperatures of each waste form having 0.3 m diameter were calculated according to the scheme in Fig. 1. In case of TRR-100, when there are no TRUs in the rare earth waste, the centerline temperature was 138.34°C at the initial stage of storage. The centerline temperature was increased according to the decrease of TRU recovery ratio, however, even the TRR-80 case showed the centerline temperature of 201.62°C, which is far below the glass transition temperature of the rare earth glass waste form ($T_g=769.46^\circ\text{C}$). Therefore, it is concluded that thermal stability of waste form in case of 0.3 m diameter is not affected by the TRU recovery ratio (even with the TRR-80 case) in the electrowinning process.

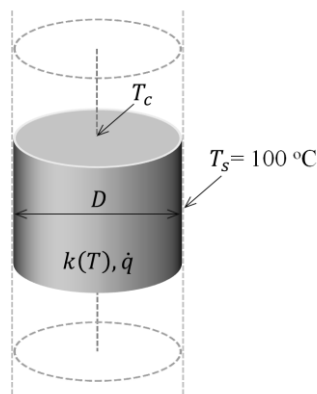


Fig. 1. Scheme of centerline temperature (T_c) calculation (T_s : surface temperature, k : thermal conductivity, q : heat generation, D : diameter).

Meanwhile, the centerline temperature after drain process was obtained using metal canister with 300 mm diameter. It was found that the molten glass poured at $1,350^\circ\text{C}$ was cooled to room temperature within 12 hours.

4. Conclusion

In order to determine thermal stability of the waste form immobilizing rare earth waste generated from the electrowinning process of the pyrochemical process, the centerline temperature of the rare earth glass waste form was calculated using steady-state conduction equation in a long and solid cylinder type waste form of constant thermal conductivity and uniform heat generation. To verify the effects of TRU content in the rare earth waste on the centerline temperature, the TRU recovery ratio (TRR) was varied from 80% to 100%. It was revealed that thermal stability of waste form in case of 0.3 m diameter was not affected by the TRU recovery ratio in the electrowinning process, meaning that the waste form size is thermally reasonable due to the low centerline temperature being far below the glass transition temperature of the rare earth glass waste form. Also, the devitrification tendency with current size waste form in the fabrication process can be assessed using temperature cooling profile obtained from current study.

REFERENCES

- [1] R. Rainisch, Alternative design concept for the second glass waste storage building, WSRC-TR-92-466 (1992) 1-23.
- [2] B.J. Hardy, Temperatures in DWPF glass waste storage building, WSRC-RP-93-1177 (1993) 1-10.
- [3] D.B. Spilman, L.L. Hench, D.E. Clark, Devitrification and subsequent effects on the leach behavior of a simulated borosilicate nuclear waste glass, Nucl. Chem. Waste Man. 6 (1986) 107-119.
- [4] J.H. Choi, H.C. Eun, T.K. Lee, K.R. Lee, S.Y. Han, M.K. Jeon, H.S. Park, D.H. Ahn, J. Nucl. Mater. 483 (2017) 82-89.

Database Design for Development of Waste Management Program for Clearance Level Waste

Gyo Hyeok Song¹⁾, Ji Young Song¹⁾, Seung Cheol Oh²⁾, Bo Haeng Lee¹⁾, and Kwang Pyo Kim^{1)*}

¹⁾ Kyunghee University, 1732, Deokyoungdae-ro, Giheung-gu, Yongin-si, Gyeonggi-do, Republic of Korea

²⁾ Korea Institute of Nuclear Safety, 62, Gwahak-ro, Yuseong-gu, Daejeon, Republic of Korea

*kpkim@khu.ac.kr

1. Introduction

The Kori Nuclear Power Plant unit 1 was permanently shut down in 2017. From now on, as the decommissioning proceeds, it is expected that a substantial amount of the radioactive waste will be generated. Most of waste generated during decommissioning are clearance level waste. This is approximately 90% generated decommissioning waste.

To dispose the clearance level waste, it should meet the legal requirements. In terms of self-disposal, nuclear operator should consider whether they obey clearance level waste legal standards and whether they effectively manage the clearance level waste. Thus it is necessary to develop program for effective management.

In this study, we performed database design of the management program for clearance level waste. To design the database, we investigated the legal requirements and management requirements. Based on this, database design was performed.

2. Investigation of data items

2.1 Legal requirements

To develop clearance level waste management program, data items of legal requirements should be reflected. In this study, data items of legal requirements reflected article 9, 10 and 11 of the in NSSC (Nuclear Safety and Security Commission) No. 2017-65. A total of 17 data items was derived NSSC

No. 2017-65. For example, there are radioactive concentration by radionuclides, alpha/beta radioactive concentration, individual dose and collective dose. This is shown in Fig.1.

2.2 Management requirements

To design the database, data items of management requirements should be required as well as legal requirements. Data items of management requirements reflected the data items required in terms of maintaining counter traceability, waste tracking management, radioactive concentration calculation, sample management and record management.

Data items of the maintaining counter traceability include validity period of the counter calibration, the counter efficiency etc. Data items of the waste tracking management consist of management number. Data items of the radioactive concentration calculation include information of measurement time, and count rate etc. Data items of the sample management are information on the sample mass and management number etc. Data items of the record management consist of the person in charge of information and record date. There are a total of 71 data items of management requirements. This is shown in Fig.1.

Legal requirements data (17)	Management requirements data (71)
<ul style="list-style-type: none"> •Existence of nuclides •MDA by radionuclides •Radioactive concentration by radionuclides •Permissible concentration by radionuclides •Fraction by radionuclides •Gross alpha radioactive concentration •Gross alpha MDA •Gross beta radioactive concentration 	<ul style="list-style-type: none"> •Weight scale information (5) •Radionuclide analyzer information (6) •Low level alpha/beta counter (6) •Inspection step information (16) •Dose rate detector information (6) •Alpha/beta measurement step information (28) •Dose assessment step information (4)
<ul style="list-style-type: none"> •Gross beta MDA •Waste type •Waste weight •Waste disposal method •Individual dose •Collective dose •Surface dose rate •Dose satisfaction •Calculation Program 	

Fig. 1. Data items for legal and management of clearance level waste.

3. Database design for developing system

In this study, to structuralize the data items and translate that into programming language, we grouped data items and defined their relationships. Data items were grouped into equipment data and input data. The equipment data is the detector and the weight scale information. There are three categories of input information: radioactive concentration calculation, alpha/beta radionuclide measurement, and dose assessment in accordance with the legal requirements of clearance level wastes.

To define the relationships of grouped data, we analyzed characteristic of grouped data. The equipment data can be made into a library and necessary data items can be loaded from the input data. The equipment data required to calculate radioactive concentration: weight scale, radionuclide analyzer and radiation dose rate equipment. To measure alpha/beta radionuclides, equipment data with weight scale and low level alpha/beta counter can be loaded. For dose assessment, data on the radioactive concentration derived earlier can be loaded. This relationship is shown in Fig.2.

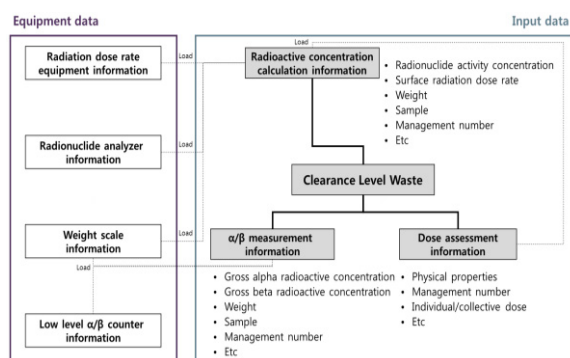


Fig. 2. Database design between equipment data and input data.

4. Conclusion

In this study, we structured database to develop clearance level waste management program. To proceed with the structure design, data items were derived by investigation the legal requirements and management requirements for clearance level waste. The derived data items were grouped, we performed relationship design defining the relation among the grouped data items. This study will be used to develop a radioactive waste management program when nuclear facilities are decommissioned.

ACKNOWLEDGEMENTS

This work was supported by the Korea Institute of Energy Technology Evaluation and Planning (KETEP) and the Ministry of Trade, Industry & Energy (MOTIE) of the Republic of Korea (No. 20171510300580).

REFERENCES

- [1] IAEA, "Waste inventory record keeping systems (WIRKS) for the management and disposal of radioactive waste", International Atomic Energy Agency, IAEA-TECDOC-1222, (2001).

A Study on ^{14}C Desorption From Spent Activated Carbon of Air Cleaning Units in Domestic Nuclear Power Plants

HangRae Cho* and Cheon-Woo Kim

Korea Hydro & Nuclear Power Co., Ltd. Central Research Institute, 70, Yuseong-daero 1312beon-gil, Yuseong-gu, Daejeon, Republic of Korea

*hrcho6795@khnp.co.kr

1. Introduction

There are many air cleaning units (ACUs) that purify the exhaust air containing radioactive iodine compounds and micro particles such as organic/inorganic carbon compounds in the radiation controlled area buildings of nuclear power plant (NPP).

The TEDA impregnated activated carbon has numerous pores and adsorbs inorganic carbon dioxide (CO_2) and volatile organic compounds ($\text{C}_n\text{H}_{2n+2}$) containing ^{14}C . The iodine removal efficiency of the activated carbon filters are checked periodically every over-haul of NPP under strict regulation. When the removal efficiency is lower than design value, the activated carbon filters are replaced by new activated carbon and spent activated carbon (SAC) is generated in bulk [1].

It is expected to cost enormous money to dispose of the SAC as intermediate and low level radioactive waste because almost all SAC contains ^{14}C exceeding the severe limit concentration (1Bq/g) for clearance level.

Therefore, we began a study on the ^{14}C desorption from SAC and performed a lot of experiments to seek the best condition for efficient removal of ^{14}C from the pore space and wall surface of SAC.

2. Experiment for ^{14}C desorption

A thermal desorption device of laboratory scale by micro-wave was used with vacuum pump, nitrogen (N_2) purge gas and mass flow controller (MFC, 0~20 SLPM), steam generator and PLC/MMI control system to derive an optimal conditions for almost perfect desorption of hydrocarbon compound containing ^{14}C .

2.1 Physicochemical characteristics of activated carbon

The result of moisture desorption test, thermal gravimetric analysis (TGA), py-GC/MS analysis, SEM-EDS analysis on SAC and new activated carbon showed that the gaseous molecules containing ^{14}C are likely to be adsorbed physically on the surface of pore by van der Waals force [2].

2.2 Preparation of sample for experiment

Three samples among thirty four SAC samples taken from domestic NPPs were selected as representatives of three kinds of ^{14}C concentration

level (low, intermediate, high). The ^{14}C concentrations of representative samples were 1.73, 35.2, 128 Bq/g respectively. Each selected sample of 4,000 mL was prepared respectively in consideration of the sample volume of 200 mL per batch and twenty times of experiments for several levels of various parameters such as heating temperature, temperature ramp rate, flow rate of N_2 purge, amount of water injection, reduced pressure during heating and after heating.

2.3 Establishment of experimental strategy

Three steps of heating temperature range was decided on the basis of the physicochemical characteristics of activated carbon.

At the first step, sample was heated by near 150°C and kept for 1 hour under reduced pressure for removal of CO_2 and moisture, various organic compound adsorbed physically in the pores of activated carbon because physically adsorbed material could react with functional group or TEDA at high temperature over 200°C .

At the second step, the heating temperature was increased by the temperature range of $550\sim 600^\circ\text{C}$ for desorption of the organic compound captured by functional group on the surface of pore and the impregnated TEDA.

At the final step, the heating temperature was increased up to 850°C with small amount of water oxidant to oxidize partially the wall surface of pores for removal of the ^{14}C bonded chemically to carbon skeleton itself or adsorbed at the edge of carbon skeleton. The water oxidant was injected into the N_2 purge gas supply line by the differential pressure between the microwave heating chamber and atmosphere. This step is similar to a reactivation process to regenerate the spent activated carbon.

3. Result of experiment

3.1 Low-concentration sample

The ^{14}C concentration of sample below 2 Bq/g was decreased below 1 Bq/g by single step heating for 60 minutes under the temperature of 400°C and the reduced pressure of 400 mmHg getting the decontamination factor (DF) of 3.8 higher than the demanded DF of 2 as shown in Fig. 2 and Fig. 3.

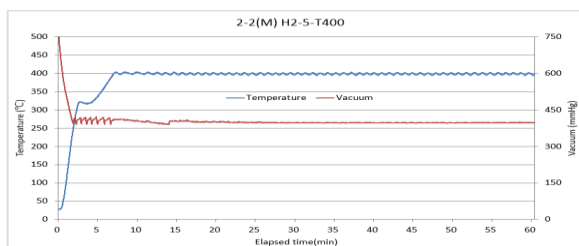


Fig. 1. The graph of single step heating (400 °C).

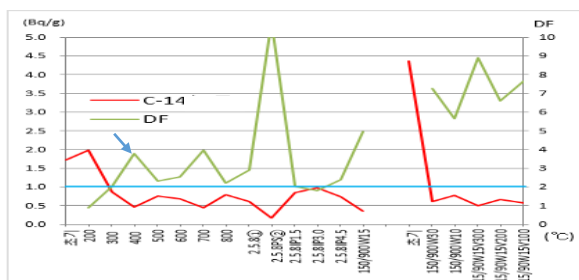


Fig. 2. ¹⁴C desorption trend of low concentration sample.

3.2 Medium-concentration sample

In case of medium concentration sample (35.2 Bq/g), the ¹⁴C decontamination factor over 50 was demanded to decrease the concentration below 1 Bq/g. However, the DF only reached up to 16 by 3 step heating for 90 minutes under the condition of temperatures of 200 °C, 500 °C, 800 °C and reduced pressure of 400 mmHg, continuous purge, steam supply at 800 °C as shown in Fig. 3 and Fig. 4.

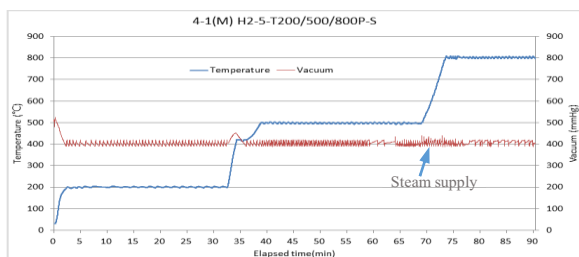


Fig. 3. The graph of 3 step heating (200, 500, 800 °C).

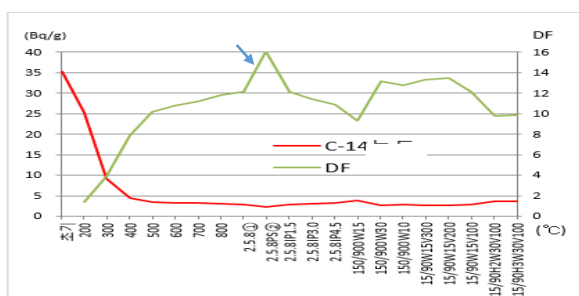


Fig. 4. ¹⁴C desorption trend of medium concentration sample.

3.3 High-concentration sample

The ¹⁴C DFs of high concentration sample were in the range of 1.5 ~ 19.4 according to the progression of experiment as shown in Fig. 6. In case of high concentration sample (128 Bq/g), the DF of 200 was demanded to decrease the concentration below 1

Bq/g. The maximum DF reached by 2 step heating for 210 minutes under the condition of temperatures of 150 °C, 800 °C and reduced pressure of 300 mmHg during heating as shown in Fig. 5 and intermittent purge, water injection at 700 °C and 800 °C, reduced pressure of 100 mmHg after heating.

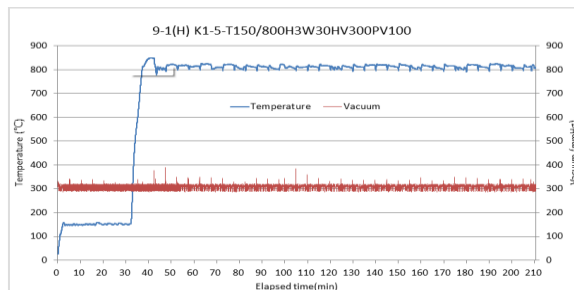


Fig. 5. The graph of 2 step heating (150, 800 °C).

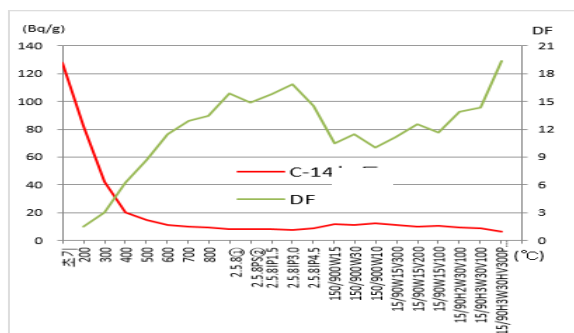


Fig. 6. ¹⁴C desorption trend of high concentration sample.

4. Conclusion

The experiments for ¹⁴C desorption from SAC were performed with a thermal desorption device by microwave and SAC samples of domestic NPPs to ascertain the possibility to dispose the spent activated carbon as a clearance level waste.

As a result of the experiments, it is expected that SACs below 15 Bq/g in ¹⁴C concentration can be changed easily to the clearance level waste by the thermal desorption technology with reduced pressure and appropriate moisture.

However, the last experiment implied that the ¹⁴C DF will be more enhanced by the increased heating temperature up to 1,000 °C and more reduced pressure below 200 mmHg and extended heating time.

REFERENCES

- [1] U.S. NRC, "Design, Inspection and Testing Criteria for air Filtration and Adsorption Units of Post-accident Engineered-safety Feature Atmosphere Cleanup System in Light-water-cooled NPPs", Regulatory Guide 1.52 Rev. 4 (2012).
- [2] Roop Chand Bansal et al., Activated carbon Adsorption, CRC Press, p.3-10 (2005).

The Guideline for Low and Intermediate Level of Radioactive Waste Management Life Cycle – A Reference for Waste Tracking System (WTS) and Waste Certification Program (WCP)

Kwangyoung SOHN*, ChangHwan CHO, and Sungjong KIM
MIRAE-EN Co., Ltd., RN803, 72, Technojungang-ro, Yuseong-gu, Daejeon, Republic of Korea
*kwangyoung.sohn@mirae-en.co.kr

1. Introduction

Recently each organization is preparing the decommissioning of nuclear power reactor. Thus government and Korea Hydro & Nuclear Power (KHNP) has recognized the need of support to manage all the data generated in the decommissioning and decontamination process. With the support of Korean Energy Technology Evaluation and Planning (KETEP), the project called radioactive WTS [4] was organized to develop the database system with friendly User Interface (UI), managing all the internal and external data generated from waste generation up to disposal process. Now detail software design specification is being refined step by step.

Most of requirements for WTS are based on the IAEA TECDOC [1][2][3], decommissioning plan, and examples of foreign experiences and a sort of specific needs from utility. In addition to those resources, MIRAE-EN Co., Ltd. is suggesting the ISO TC85 SC5 WG5 standard describing the requirements of radioactive waste management life cycle, which could be also obviously requirements for WTS development and would be good aids and basis for waste certification for disposal. This paper addresses the story of this standard proposal, which is virtually design concept of WTS.

2. Main content of the guideline

When implementing the radioactive waste management process, there are many important technologies such as identification of radionuclides by scaling factor, collection and segregation, waste treatment and conditioning like solidification, incineration, vitrification and etc., container, and transport. All these detail technologies could be the scope of a general standards under this umbrella description, meaning that this proposal just figures out the general requirements of overall process of radioactive waste management life cycle.

The structure of this proposal is to provide the 1) guidance or requirements, 2) activities, and 3) outcome of each radioactive waste management process.

It is expected that this proposal could be a strategic guideline for radioactive waste management process. The standard proposed to ISO TC85 SC5 WG5 “Characteristics and waste management” has the following contents;

2.1 Conceptual structure

This proposal is organized in accordance with strategy in Figure 1, and this process structure could be flexible and used in selective manner in each waste stream and characteristics. Things interesting is that this includes the process for the radioactivity hazard and impact analysis for safe and transparent waste management before commencing the radioactive waste management process.

2.2 Contents in proposal

Table 1. The content of proposal

4	General principles
4.1	Waste management life cycle process requirements
4.1.1	Waste management planning process
4.1.2	Radioactive waste generation process
4.1.3	Radioactive waste treatment process
4.1.4	Waste characterization process
4.1.5	Radioactive waste classification process
4.1.6	Radioactive waste conditioning process
4.1.7	Radioactive waste packaging process
4.1.8	Radioactive waste transport process
4.1.9	waste delivery and maintenance process
5.	Documentation
5.1	Required data
5.2	Record plan/procedure
5.3	Data traceability

Also since the generation of radioactive waste of low and intermediate level, a couple of organization is trying to minimize the waste volume increase during the treatment process mainly due to the disposal cost and safety in disposal infrastructure. Thus various treatment and conditioning technologies could be used to achieve this goal, which implicates the use of possible technologies is dependent on the position of national regulation or practices.

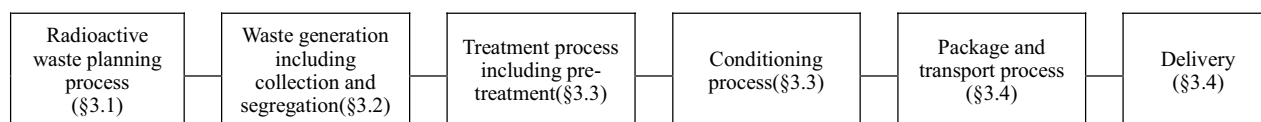


Fig. 1. Umbrella process for waste management.

A solidification by Portland and Calcium Aluminate cement, Paraffin and Polymer, vitrification, and incineration could be one of the samples for those technologies.

2.3 Quality management Issues

First of all, the main objective of this proposal is to maintain the traceability of radioactive waste from waste generator to disposal, which ultimately to achieve the safety of radioactive waste management. In order to achieve this final objectives, the quality system should be established to support the integrity of radioactive waste management with respect to staffs, organization and other stakeholder with integral documentation of process history.

3. Technical management for processes

3.1 Radioactive waste management planning

According to the proposal, the conceptual planning for management shall be established for systematic and transparent guideline as a basis for managing radioactive waste life cycle. It needs to provide the comprehensive waste management and certification that should be adhered to throughout the waste management process. Also all the risks and its emergency, mitigation or recovery plan shall be considered and prepared to cope with the unexpected events during radioactive waste management life cycle.

3.2 Waste segregation and collection

This could be an actual step occurring just after waste generation process, which also could be divided into sub-process such as pre-treatment and treatment process depending on the specific waste stream. It may involve collection, segregation, decontamination and chemical adjustment for waste collection. However this section describes the requirements of those processes as one single topic.

The characteristics of raw radioactive waste treatment process need to be well defined with care in a sense that the various type of characteristics of raw waste stream is able to determine a series of treatment process such as burning as incineration, pyrolysis and solidification by eliminating a liquid, gaseous and pyrophoric compound etc., and of characteristic performance testing for conformity. All the data gathered in this process need to be recorded and reviewed for approval.

3.3 Waste treatment and condition

According to the waste stream and characteristics, the numerous waste treatments such as cutting, chemical adjustment and decontamination which includes decontamination by sand, smear, chemical compound, ultrasonic, electrolytic and sand polishing etc. and centrifugal separator, decompressive evaporator, enrichment etc. could be selected and applied for treatment. All the information gathered during this process need to be recorded and reviewed for approval.

3.4 Radioactive waste packaging and delivery

According to the international comments, these two (2) processes has been already mentioned in another working group under TC5 so that these topics are left out in this proposal.

4. Supporting tool and environment

All of information produced through these activities shall be managed and maintained through integrated WTS systematically and electronically.

5. Conclusion

It is expected that there're lots of requirements for specific technologies for waste management that could be one of the technologies under this whole umbrella process requirements. Hopefully this could be utilized for process establishment and implementation for WTS in selective manner that is compliant to each waste stream and application.

All the topics mentioned so far is an attempt to achieve the traceability and safety of radioactive wastes management regardless of the waste stream and level of activity. Thus Section 5 in Table 1 emphasizes on any kind of documentation, which plays a great role of requirements ensuring the integrity of waste acceptance criteria (WAC), and then the appropriateness of waste certification or accreditation system of radioactive waste management system. Also there is plan to expand this proposal into WTS and WCP if consented by ISO TC85 SC5 WG5 Member States in the future (See Figure 2).

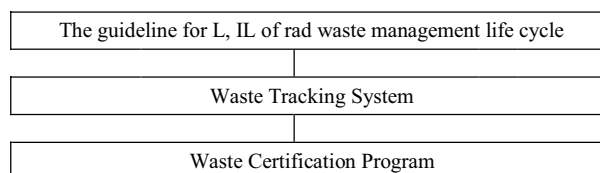


Fig. 2. ISO standardization plan.

REFERENCES

- [1] No. SSG-40, Predisposal Management of Radioactive Waste from Nuclear Power Plants and Research Reactors.
- [2] No. SSG-41, Predisposal Management of Radioactive Waste from Nuclear Fuel Cycle Facilities.
- [3] GS-G-3.3, the management system for the Processing, Handling, and Storage of Radioactive waste.
- [4] Radioactive Waste Tracking System for Nuclear Power Plants Decommissioning and Non-Reactor Nuclear Facilities (NRNF), PN: 20171510300710, the project proposal by MIRAE-EN Co., Ltd., KETEP.

Radioactive Waste Tracking System (WTS) for the Decommissioning of Nuclear Power Plants

Sungjong KIM*, Kwangyoung SOHN, and Changhwan CHO

MIRAE-EN Co., Ltd., RN803, 72, Technojungang-Ro, Yuseong-gu, Daejeon, Republic of Korea

*sungjomg.kim@miraen.co.kr

1. Introduction

With the advent of decommissioning and decontamination of nuclear power plants, Korean Energy Technology Evaluation and Planning (KETEP) has organized the project called radioactive Waste Tracking System (WTS) [2] to develop the database system with friendly User Interface (UI) in 2017, which is to manage all the internal and external data generated from waste generation up to disposal process for nuclear power plant decommissioning. WTS will be developed during 4 years, actually 36 months. Now detail software design specification is being prepared and refined step by step.

Most of requirements for WTS for nuclear power plants are based on the IAEA TECDOC, decommissioning plan, and examples of foreign experiences and a sort of specific needs from utility. In addition to those resources, MIRAE-EN Co., Ltd. is suggesting the ISO TC85 SC5 WG5 standard[1] describing the requirements of radioactive waste management life cycle, which is also obviously crystal guideline for WTS development and would be good aids and basis for waste certification for disposal. This paper addresses the development progress of WTS based on [2].

2. Development strategy for WTS

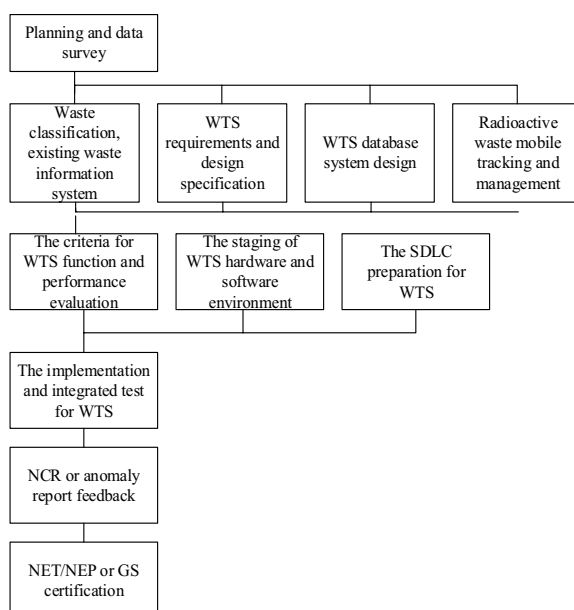


Fig. 1. A strategy for WTS development.

Especially for survey of site waste management system and experiences of oversea waste management, Project leading group has visited the Ulchin 5&6 site and reviewed the management system for Ulchin 1 & 2 NPP, and had a workshop in the title of “WTS – Waste Acceptance Criteria (WAC) and Waste Certification Program (WCP)” with TÜV SÜD operating the Reststoff-Verfolgungs und Kontrollsystem (RevK), the WTS for decommissioning of nuclear power plants. In addition to this, this project has reviewed IAEA and BRIMS in UK and many others also.

3. WTS development life cycle (SDLC)

3.1 Documents development

For the development of SDLC documents, project leader has document production schedule selectively from IEEE 1012. Those are as below with standard reference, and not limited to this;

- 1) WTS software system development plan (IEEE 1074),
- 2) Configuration plan and procedure (IEEE 828),
- 3) Software verification and validation plan (IEEE 1012),
- 4) Software requirement specification (IEEE 830),
- 5) Software Design Specification (IEEE 1016),
- 6) Unit test procedure and report (IEEE 829),
- 7) Site conformance test and report (as necessary),
- 8) The 3rd party independent verification and validation report
- 9) Operational guideline and manual (including others)

Especially the plan/procedure and the report of verification and validation is to be conducted by separate organization independent technically as well as organizationally

3.2 WTS hardware staging

The selection of WTS DB system hardware and software environment is a critical factor to implement and operate for a long time while decommissioning. Thus the most important factor to select the commercial hardware and software is the market share, and then ease of use and maintenance, and performance has been considered for long time operation and maintenance.

Operating System (OS) for WTS DB system will be using Linux series of open sources, Oracle Database Management System (DBMS) as a skeleton

platform, and other application software like Visual Basic and C# and graphic tools.

3.3 WTS DB implementation

The critical design of WTS is the establishment of DBMS based on the procedure below;

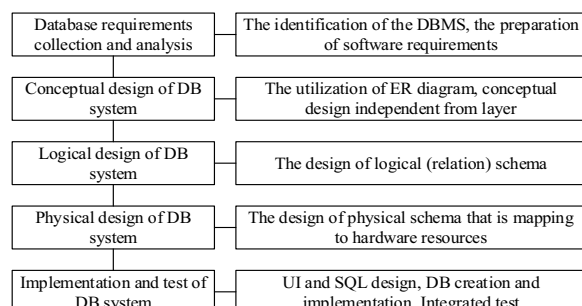


Fig. 2. WTS DB implementation flow.

In addition to this implementation flow, UI include the function of graphic, chart, data calculation and composing and statistics for report generation and other purposes. Also in case of integration with conventional waste information system already operated in each organization, data import and export UI will be available too.

As we all aware of, the design and operation of UI is one of the typical criteria of WTS, which means UI should be implemented as friendly, ease of use and efficient for easy access and navigation.

4. Design considerations

4.1 META data implementation [3]

Typically radioactive waste management life cycle requires large amounts of data across multiple disciplines (e.g. engineering, geoscience, waste management) and for multiple purposes (e.g. site characterization and selection, numerical modelling, licensing, repository design, construction and operation, waste packaging, safety case, environmental impact assessment etc.). Thus *contextual and detail meta data*, “data about data”, plays a fundamental role in the long-term management of waste management data

4.2 Constant DB implementation and management

In order to operate the WTS, there are many constant DB implementation and management for information such as classification of isotopes and their half-lives, the type of containers and etc. Thus the information shall be provided for easy access of WTS also.

4.3 Other technical issues

4.3.1 On-line direct upload of waste process data. This topic is not the scope of this project. But

judging from the past experiences from the characteristics testing in solidified radioactive waste, there are a lots of test and measure results that is not currently directed to WTS server. It means the test and measure data is logged in excel file temporarily at first time, and put in the WTS server database manually, which causes a waste of time in WTS data management. Considering the amount of data generated during radioactive waste management life cycle, thus it is highly recommended that the communication middleware between radioactive measuring instruments and WTS server to directly upload the test and measured data into WTS server should be implemented and equipped with system.

4.3.2 WCP activation by WTS and repository information. In a sense that this WTS is intended for KHNP to track the radioactive waste management data in nuclear power plant decommissioning, the view of repository owner (e.g. KORAD) is after delivery is not a critical requirements of this WTS. However considering that this WTS needs to provide the radioactive waste tracking information, those two systems sometime might interface for complete mission of national radioactive waste management with the activation of WCP utilizing this WTS.

5. Conclusions

As of today, conducting the 2nd year of KETEP project it is expected that there're lots of requirements for specific technologies for waste treatment, process and management, and for a specific needs from utility (waste generator). Thus the iterative consultations, meetings and evolutions of WTS is a corner stone of WTS success.

ACKNOWLEDGEMENT

This work is supported by the KETEP granted financial resource from the Ministry of Trade, Industry and Energy, Republic of Korea (No. 20171510300710)

REFERENCES

- [1] The guideline for low and intermediate level of radioactive waste management life, MIRAE-EN Co. Ltd., sungjong KIM, kwangyoung SOHN, changhwan CHO, KRS Conference, Jeju in Autumn.
- [2] Radioactive Waste Tracking System for Nuclear Power Plants Decommissioning and Non-Reactor Nuclear Facilities (NRNF), PN: 20171510300710, the project proposal by MIRAE-EN Co., Ltd., KETEP.
- [3] OECD/NEA RepMet(Radioactive Waste Repository Metadata Management) Initiative, Massimo Ciambrella, RepMet Technical Secretary, IAEA Third International Conference on Nuclear Knowledge Management, 7-11 November 2016.

Overview of Radioactive Waste Acceptance Criteria for Treatment and Management of Radioactive Waste

Won-Seok Kim, Jaeeun Kang, and Wooyong Um*

Pohang University of Science and Technology, 77, Chungam-ro, Nam-gu, Pohang-si, Republic of Korea

*wooyongum@postech.ac.kr

1. Introduction

To use nuclear energy as a sustainable energy source, the treatment of radioactive waste generated from the nuclear fuel cycle including nuclear power plant (NPP) decommissioning is of great importance. The establishment of acceptance criteria for radioactive waste from decommissioning nuclear power plant is seemed to play a key role for safe radioactive waste disposal strategy. This research compiles the acceptance criteria of low-and-intermediate level radioactive waste in the world and provides various cases for radioactive waste disposal from decommissioning of NPP. These materials give information to use in the new radioactive waste repository. Appropriate waste acceptance criteria for radioactive waste are essential component of facility design and operation, and should be developed for different conditions. Physically suitable standards for waste disposal facilities should be ensured, and the repository is controlled with relevant monitoring and requirement for a long-term safe performance assessment.

Clearance levels and acceptance criteria specifications are under the authority of national regulators. Although several international organizations, like the IAEA— International Atomic Energy Agency and the EC— European Commission, have their own acceptance criteria, but the differences are still significant. In this study, the standard and differences of waste acceptance criteria in national and international for radioactive waste was arranged. Radioactive waste acceptance criteria were overviewed and compared, which can be used to support radioactive waste management for the wastes from the NPP decommissioning in Korea.

2. Research Procedure

2.1 International recommendation on radioactive clearance levels and acceptance criteria

In general, radioactive waste acceptance criteria are related to the geological environment and repository condition. Although it is not possible to establish generally quantitative waste acceptance criteria because the geological environment and the engineering concept at each repository is different, the overview of international recommendation on radioactive clearance levels and acceptance criteria is required to oversee an evaluation of suitable long-term management in repository.

2.2 Derivation of radioactive waste acceptance criteria for radioactive waste in different countries

The difference and derivation of criteria for radioactive waste acceptance in each country was investigated, overviewed, and arranged. The information of criteria in each country can be used as a general guideline to the repository.

2.3 Waste acceptance process

Waste acceptance criteria have to be developed to specify the radiological, mechanical, physical, chemical and biological characteristics of waste packages and unpackaged waste that are to be processed, stored, or disposed in repository. For example, radionuclide type, content or activity limits, heat and radiation output, and the properties of the waste form and package type should be considered prior to disposal.

3. Results and discussion

Important parameters characterizing radioactive waste are shown in Table 1. [1]

Table 1. Important parameters characterizing radioactive waste (IAEA)

Package identifier or number
Type and version
Specification
Name of the conditioning facility and site
Date of conditioning
Content of raw waste and details
Details about the container
Details about the immobilizing matrix
Details about the capping matrix
Activity content
Does rate
Heat rating
Surface contamination
Overall package weight

In most countries which have radioactive waste repository, they have their own radioactive waste acceptance criteria depending on characteristics of repository. In order to meet the waste acceptance criteria, wastes need to have allowable activities and concentration of specific radionuclides, and use acceptable waste form and container requirements.

Table 2 shows the radioactive waste acceptance criteria in South Korea. Specific test methods for radioactive acceptance criteria are following the NRC method in USA [2].

Table 2. The radioactive waste acceptance criteria of South Korea

Classification	Test Item	Relative Standards	
		Hard solidification	Soft solidification
Structural safety	Compressive	KS F2405	KS F2351
	Immersion	NRC "Technical Position on Waste Form, Rev.1"	
	Thermal cycling	ASTM B553	
	Radiation	NRC "Technical Position on Waste Form, Rev.1"	
Leachability	Leaching	ANS 16.1 (or EPA 1315 Method)	
Free water measurement	Actual size	ANS 55.1	
	Specimen and waste	EPA Method 9095B (PAINT Filter Liquid Test)	

4. Conclusion

The information of radioactive waste acceptance criteria in nation/international can support to radioactive waste acceptance to repository in order to store safely. The purpose of waste acceptance criteria development is for the safe transportation, handling, storage, and disposal of waste packages, and it can help to develop the criteria for the decommissioning waste in Korea. Waste acceptance criteria are facility-specific and can be also different from the package type. It is the common responsibility for the repository operator and the national regulatory bodies to establish the appropriate acceptance criteria for various wastes to any type of disposal facility.

ACKNOWLEDGEMENT

This work was supported by the Korea Institute of Energy Technology Evaluation and Planning (KETEP) granted financial resource from the Ministry of Trade, Industry & Energy, and Republic of Korea (No. 20181510300870).

REFERENCES

- [1] IAEA, "Requirements and Methods for Low and Intermediate Level Waste Package Acceptability", IAEA-TECDOC-864, Vienna. 1996.
- [2] "The Report of Safety Assessment of Low- and Intermediate-level Radioactive Waste Disposal Facility in Korea", KORAD. 2011.

Introduction on Revised Technical Standard for LILW Incineration in Korea

Jungjoon Lee, Kyungwoo Choi, and Sangmyeon Ahn

Korea Institute of Nuclear Safety, 62, Gwahak-ro, Yuseong-gu, Daejeon, Republic of Korea

*k720ljj@kins.re.kr

1. Introduction

Incineration Criteria for Low- and Intermediate-Level Radioactive Wastes was promulgated in 1997. This technical standard is giving the information about application scope, design criteria for incineration equipment, waste acceptance criteria, operation criteria during the operation of incineration equipment such as incineration method, emergency response, etc. The management by monitoring and measuring the effluent gas discharged from incineration equipment is very important not only for radionuclides but also for air pollution substances.

This study shows the introduction on recently revised guidelines Technical Standard for LILW Incineration (NCCS Notice No. 2017-6), in order to provide the exact information on technical criteria for LILW incineration for the operator of related facilities and for the licensee who is going to have a plan to get an issue for LILW incineration.

2. Incineration criteria

2.1 Purpose & Scope of Application

The purpose of this notice is to specify technical standards for ensuring the safety of incineration facilities and the incineration of radioactive wastes pursuant to Subparagraphs 4 (d) and 10 (a) of Article 10, Subparagraph 3 of Article 22, Subparagraph 4 (c) of Article 40, and Subparagraphs 4 (d) and 10 (a) of Article 87 of the Regulations on the Technical

Standards for Radiation Safety Control, Etc [1].

The standards on incineration facilities of solid or liquid combustible LILW provided in the Regulations on the Technical Standards for Radiation Safety Control, Etc. shall be applied [1].

2.2 Design Standards of Incineration Facilities

The incineration facilities shall consist of the following equipment and shall be designed to ensure structural safety: pre- treatment equipment (if pre-treatment is required), incinerator equipment, off-gas treatment equipment, liquid effluent collection equipment (treatment equipment included if treated in house), ash collection equipment (treatment equipment included if treated in house), equipment for monitoring processes and off-gases, ventilation equipment, and other subsidiary facilities.

2.3 Off-gas Treatment Equipment

The weekly average radioactive concentration of gases and the annual average exposure to the residents living around the facility to release gases, emitted from the incinerator into the air, shall satisfy the Notice of the Nuclear Safety and Security Commission (Standards for Radiation Protection, Etc.) outside the boundary of the exclusion area.

The off-gas generated from the incinerator into the air after their proper treatment shall be satisfied with effluent quality standard such as SO_x, NO_x, CO, HCl and dust, etc.

Table 1. Applying facilities for incineration criteria

Name	KAERI Treatment facility for combustible RW	Hanul Vitrification equipment
Location	KAERI, Daejeon	Hanul NPP, Uljin
Radioactive Waste	Combustible LILW generated from KAERI decommissioning project (Uranium conversion facility and Research reactor 1&2)	Combustible LILW including spent resin generated from Uljin NPP operation
Treatment technology	Incineration	Incineration & vitrification
Treatment capacity	~25 kg/h	~25 kg/h

Table 2. Main changes in revision of incineration criteria

Contents	Before revision	After revision
effluent quality standard following as treatment capacity	None	- Quotation of standards from 3 related legislations - [Special provision] Applying the nearby treatment capacity regulated in 3 related legislations
Contents and concentration of effluent quality standard	Provided as Table 1 in NSSC Notice	Quotation of standards from 3 related legislations

3. Revision of technical standard

There was no effluent quality standard for incineration capacity in previous standard. And, effluent quality standard has never been revised since the promulgation of NSSC Notice, while effluent quality standard which is quoting in NSSC Notice has been revised in every 5 years. The 3 related legislations are as follows; Enforcement Regulations for Clean Air Conservation Act [2], Enforcement Regulations for Persistent Organic Pollutants Control Act [3], and Enforcement Regulations for Malodor Prevention Act [4].

For these reasons, NSSC Notice was revised in April 2017. The 2 facilities, KAERI treatment

facility for combustible radioactive waste and Hanul vitrification equipment (Table 1), shall meet the revised criteria according to the NSSC Notice, especially, for the effluent quality standard.

Main changed in revised incineration criteria are shown in Table 2.

4. Conclusion

Recently revised technical standard for LILW incineration (NSSC Notice No.2017-6) was introduced in this study. Additional operation manual of related facility could be prepared and modified for the application of the revised incineration criteria, especially, with regarding to the measurement period of each effluents and management method including abnormal operation.

ACKNOWLEDGEMENT

This work was supported by the Nuclear Safety Research Program through the Korea Foundation of Nuclear Safety (KoFONS) using the financial resource granted by the Nuclear Safety and Security Commission (NSSC) of the Republic of Korea (No. 1605008).

REFERENCES

- [1] NSSC Notice No.2017-6, "Incineration Criteria for Low- and Intermediate-Level Radioactive Wastes" (2017).
- [2] Enforcement Regulations for Clean Air Conservation Act (2018).
- [3] Enforcement Regulations for Persistent Organic Pollutants Control Act (2018).
- [4] Enforcement Regulations for Malodor Prevention Act (2018).

KO-CN Tritium Analysis Benchmark for HCCR and HCCB TBS

Hyung Gon Jin^{a),*}, Dong Won Lee^{a)}, Jae Sung Yoon^{a)}, Suk Kwon Kim^{a)}, Eo Hwak Lee^{a)}, Seong Dae Park^{a)},
Chang Wook Shin^{a)}, and Seungyon Cho^{b)}

^{a)} Korea Atomic Energy Research Institute, 111, Daedeok-daero 989beon-gil, Yuseong-gu, Daejeon, Republic of Korea

^{b)} National Fusion Research Institute, 169-148, Gwahak-ro, Yuseong-gu, Daejeon, Republic of Korea

*jhg@kaeri.re.kr

1. Introduction

Korea has been developing a Helium Cooled Ceramic Reflector (HCCR) TBM to be tested in the ITER [1]. It consists of two major systems, which are HCS (Helium Cooling System) and TES (Tritium Extraction System) (figure 1). Tritium is one of the most highly permeable molecules on earth, therefore tritium permeation takes place from TES to HCS in the TBM. Permeated tritium migrates along the system pipes, thus tritium inventory should be considered with respect to entire TBS. Simplified steady state tritium analysis models and codes were developed by TBM teams, including KO and CN, for the analysis of tritium balance and tritium permeation release from TBSs. Considering the importance of the tritium data for the safety analysis of TBSs, the quality of the calculation should be ensured and verified.

HCCR and HCCB TBSs both consist of helium cooled ceramic breeder TBM, helium cooling system, tritium extraction system using low pressure helium, and coolant purification system. With these similarities, the developed model for one TBS can be easily used to the tritium analysis for another TBS. This allows good opportunities for a benchmark between 2 models. This paper presents comparison results of the analysis.

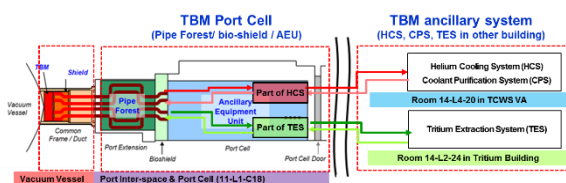


Fig. 1. Schematics of HCCR-TBS.

2. Progress of Benchmark Activities

The KO-CN Tritium Permeation Model Benchmark Analysis was proposed by CN on 2016.11.29, and was agreed by KO on 2016.12.02. Input data sets was exchanged between each other during December 2016. CN finished calculation for HCCR TBS using CN code and KO input data in

March 2017. The results were compared with KO HCCR calculation. The results were in same order of magnitude, but with some differences. In order to solve the differences piece by piece, several kinds of hand calculation verifications were proposed by CN. After discussions through video-meetings and e-mails in March and April. KO updated the calculation and the results are almost consistent now. KO finalized benchmark analysis and presented the result during KO-CN TBM workshop on May 2018.

3. Characteristics of the codes

The simplified KO and CN tritium models have following characteristics:

TBS sub-systems fully interconnected, the tritium concentration, tritium generation and losses are calculated together for all concerned sub-systems. The tritium mass conservation is ensured. Tritium is assumed in T2 form in all fluid, and tritium transport mechanisms in solid materials limited to the diffusive regime, which means the surface phenomena is not taken into account. The system is modelled as connection networks of volumes. 0-D lumped model is used, which means the interior properties like tritium concentration, temperature, pressure etc. are assumed to be uniform in each volume. Steady state assumption, which means the generation and loss of tritium are in balance, all the parameters do not change by time. No multi-physics phenomena modelled, the flow distribution of main fluid and temperature distribution in structure materials are inputs of the analysis.

4. Input data set of the Benchmark

Table 1 is summary of boundary condition which is applied to HCCR TBS calculation and Figure 2 is pipe length and operational temperature information of each room which HCCR-TBS is allocated. Design of HCCR-TBS is evolving and this data reflects recent update of PD-1 phase.[2]

Table 1. Summary of boundary condition

Tritium Production Rate	25.9 mg/day (continuous back to back with duty 0.25)
PI/PC Volume	280.264 m ³
TCWS VA Volume	500 m ³ (considering occupied by HCCR HCS/CPS)
TES Pipe Thickness	3.68 mm
HCS Pipe Thickness	8.56 mm (Vertical shaft pipe thickness 8.56 mm)
BZ Pipe Thickness	4.0 mm
N-DS at PI/PC	40 m ³ /h
HVAC at TCWS	1 Vol/hr, i.e. 500 m ³ /h

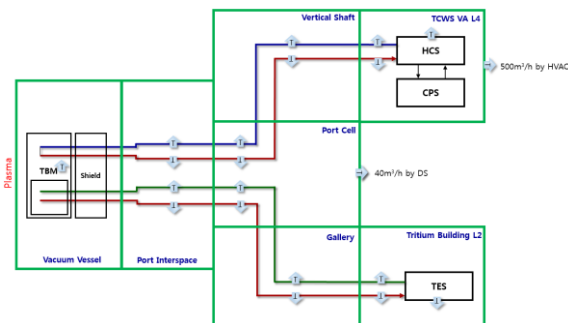


Fig. 2. Pipe length and temperature of HCCR-TBS.

5. Comparison Results

This result is one of outcomes of KO-CN collaboration which includes tritium release, inventory and benchmark analysis. Table 2 and 3 are a summary of the results which consists of KO and CN calculation results and its comparison.

KO provided HCCR TBS's design information (pipe length, diameter and etc.) to CN. CN performed tritium release analysis of HCCR TBS by using CN tritium release code. Both two codes show good agreement with each other, which result is shown in the table 2.

Table 2. Tritium Analysis Benchmark for HCCR TBS

Rooms	CN results (mg/day)	KO results (mg/day)	KO/CN
HCS to Port Interspace	2.89E-02	3.14E-02	1.09
TES to interspace	1.04E-01	1.06E-01	1.02
HCS to Port Cell	2.19E-02	2.39E-02	1.09
TES to port cell	1.05E-08	1.10E-08	1.05
V18-L1	1.71E-02	1.73E-02	1.01
V18-L2	1.67E-02	1.70E-02	1.02
L3-03E	3.92E-02	4.00E-02	1.02
L4-04	6.82E-02	7.00E-02	1.03
L4-21	5.84E-03	6.00E-03	1.03
L4-20	1.37E-01	1.42E-01	1.04
Gallery 11-L1-02E	5.12E-08	5.21E-08	1.02
Gallery 11-L1-02E	2.14E-08	2.17E-08	1.02
14-L2-24	2.20E-07	2.25E-07	1.02

The other way around, CN provided HCCB TBS's design information (pipe length, diameter and etc.) to KO. KO performed tritium release analysis of HCCB TBS by using KO tritium release code. Both two codes show good agreement with each other. Based on these results, technical memo will be reported to IO.

Table 3. Tritium Analysis Benchmark for HCCB

CN	CN results (mg/FPD)	KO results (mg/FPD)	KO/CN
Interspace	7.12E-02	7.02E-02	0.986
Interspace	2.84E-02	2.86E-02	1.009
Port Cell	1.62E-01	1.60E-01	0.985
Port Cell	6.50E-02	6.53E-02	1.006
Vertical Shaft	2.51E-01	2.48E-01	0.986
TCWS VA	4.72E-02	4.65E-05	0.986
TCWS VA	9.77E-04	9.67E-04	0.989
TCWS VA	8.35E-06	8.30E-06	0.993
Gallery	1.04E-07	1.06E-07	1.018
TES Room	2.50E-08	2.54E-08	1.018

6. Conclusion

Tritium benchmark analysis has been done successfully, which shows less than 10% and most of cases less than 5% deviation between two countries. One important thing for this result is degree of conservatism/margin of estimated tritium release is huge because detail logic of each code is different. Specially pipes which is high temperature during operation generate bigger deviation. KO and CN have long term tritium research plan for their TBSs and this type of benchmark analysis can help demonstrate safety of the systems.

ACKNOWLEDGEMENT

This work was supported by the R&D Program through the National Fusion Research Institute (NFRI) funded by the Ministry of Science and ICT of the Republic of Korea (NFRI-IN1803).

REFERENCES

- [1] D.W. Lee, et. al., "Current Status and R&D Plan on ITER TBMs of Korea," Journal of Korean Physical Society, 49 S340-S344 (2006).
- [2] I. Ricapito, TBM Project team, F4E "Guideline for the Benchmark Exercise on Tritium Modelling of TBSs", TM9J3Q (2016).

Development of Cement Form an Enhancement for Leaching Resistance

Gi Yong Kim, Won Hyuk Jang, Junhyuck Im, Dae Seok Hong, and Jong Sik Shon*

Korea Atomic Energy Research Institute, 111, Daedeok-daero 989beon-gil, Yuseong-gu, Daejeon, Republic of Korea

*njsshon@kaeri.re.kr

1. Introduction

Currently, the Korea Atomic Energy Research Institute (KAERI) is planning to build the Ki-Jang Research Reactor (KJRR) in Ki-Jang, Busan. One of the efficient way to treat radioactive waste is cement solidification. Thus, this study was focused on the development of cement for an enhancement of cesium leaching resistance. We used zeolite to improve the cesium leaching resistance of KJRR cement containing KJRR simulated liquid waste. We confirmed that zeolite successfully isolates KJRR cement based on an SEM-EDS spectrum analysis. A leaching test was carried out using KJRR simulated liquid waste containing 3000 mg / L of cesium for 90 days. Zeolite showed that KJRR cement made cesium leaching resistance 27.9% higher than the control value.

2. Methods and Results

2.1 Materials

Portland cement and zeolite were purchased from SSangyong, Zeobuilder. NaCl and Na₂SO₄ were purchased from Sigma-Aldrich (Mo, USA). All other chemicals used are of analytical or research grade.

2.2 Component of KJRR simulated liquid waste

The KJRR (Ki-Jang Research Reactor) simulated liquid waste constituents are as follows: NaCl 64.28 g L⁻¹, Na₂SO₄ 106.53 g L⁻¹, and Cs⁺ 3000 mg L⁻¹ [1].

2.3 Manufacture of KJRR cement

The KJRR cement (including KJRR simulated liquid waste) were manufactured in accordance with the Korean Industrial Standard (KS-L-5109) [2]. The mechanical mixer was purchased from JI-206 (Jeil Precision, Korea). KJRR cement was made to find the optimal mixing rate (W/C, where W is water and C is cement) from 0.45 to 1.30. In addition, we added zeolite to improve the cesium leaching resistance of KJRR cement (S/C S; zeolite, C; cement) from 1, 5, and 10 wt.%. KJRR cement solidified while curing at room temperature with relative humidity of 40 to 60 % for 28 days (Fig. 1). After 28 days, the uniformity of the surface of the KJRR cement was visually confirmed.

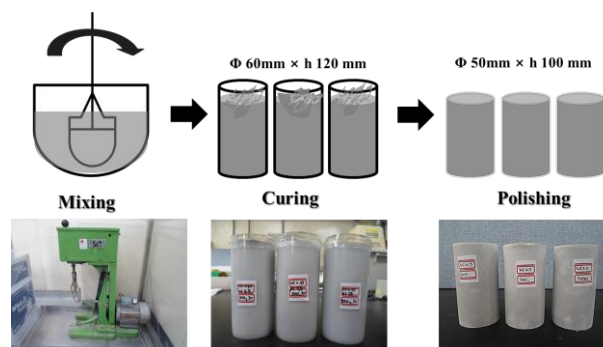


Fig. 1. Schematic diagram showing manufacture of KJRR cement.

2.4 Characterization of KJRR cement

The component of KJRR cement was analyzed using SEM-EDS. As shown in Table 1, it can be seen that (Na, Al, Si, Ca) ions, which are the main components of zeolite, increase with the zeolite content of KJRR cement.

Table 1. Component of zeolite and KJRR cement form

Element	Zeolite	KJRR (Without Zeolite)	KJRR (Zeolite 5%)	KJRR (Zeolite 10%)
	Weight (%)	Weight (%)	Weight (%)	Weight (%)
C	7.90	2.83	3.55	4.16
O	42.34	42.19	42.26	45.75
Na	15.48	2.60	4.81	5.86
Al	17.27	1.57	2.13	3.95
Si	16.80	6.50	7.49	9.50

2.5 Leaching test of KJRR cement

The Cumulative fraction leach (CFL) of cesium according to the change of zeolite content was calculated using the ANS 16.1 test method from USA. The leaching resistance was determined by considering the degree of cesium ions leached during the leaching test, and the cumulative fraction leach was defined as the equation below [3]

$$CFL = \frac{\sum A_i}{A_0}$$

A_i = Cumulative leaching amount of material A during the leaching interval

A_0 = Initial content (g) of the material A.

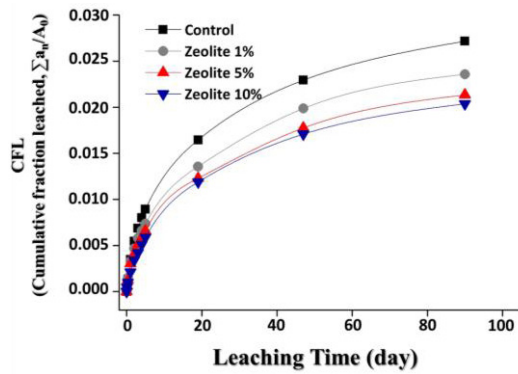


Fig. 2. Cumulative fraction of Cs⁺ leached in zeolite KJRR cement.

It was confirmed that KJRR cement containing zeolite was less Cs⁺ leaching than the control sample(KJRR cement, without zeolite) (Fig. 2). In addition, the leachability index can be obtained through by the following equation.

$$D_e = \pi \left[\frac{a_n/A_0}{(\Delta t)_n} \right]^2 \left(\frac{V}{S} \right)^2 T$$

D_e = Effective diffusion coefficient (cm² s⁻¹)

V = Volume of KJRR cement (cm³)

S = Surface area of KJRR cement (cm²)

T = n leaching time, which means the average time of the n th leach.

The leachability index (Li) was determined from the effective diffusion coefficient obtained from the above equation using the following equation.

$$L_i = -\log D_e$$

L_i = Leachability index

As shows in Table 2, it was confirmed that the leaching index was larger than 6, which means the leaching test meets the satisfied acceptance criteria for the final disposal facility. In addition, it was observed that the KJRR cement containing zeolite showed a cesium leaching resistance 27.9% higher than the control.

Table 2. Cesium Leachability index and leaching resistance of zeolite KJRR cement

Component	Leachability index of Cesium	Leaching resistance of Cesium (%)
Control	9.26	-
Zeolite 1%	9.40	12.6
Zeolite 5%	9.49	21.5
Zeolite 10%	9.52	27.9

2.6 Compressive strength test of KJRR cement

Table 3 shows the compressive strength results of the KJRR cement and zeolite KJRR cement. All

experiment groups were satisfied with the final disposal facility.

Table 3. Compressive strength test of KJRR cement and zeolite KJRR cement

Compressive strength (Mpa)*		
Component	Number	Results
Control	1	27.60
	2	26.80
	3	25.30
Zeolite 1%	1	21.50
	2	20.80
	3	20.90
Zeolite 5%	1	24.80
	2	36.20
	3	30.50
Zeolite 10%	1	25.20
	2	24.10
	3	26.20

* Compressive strength acceptance criteria ≥ 3.45 MPa [3]

3. Conclusions

In this study, we made a KJRR cement with KJRR simulated liquid waste. In addition, we used zeolite to improve the cesium leaching resistance of KJRR cement. We demonstrated that zeolite successfully isolated the KJRR cement based on an SEM-EDS spectrum analysis. A leaching test was carried out using simulated KJRR liquid waste containing 3000 mg / L of cesium. Zeolite KJRR cement achieved a cesium leaching resistance 27.9% higher than the control value. In addition, all experimental groups were satisfied with the final disposal facility, such as the compressive strength and leaching test.

REFERENCES

- [1] J.S. Shon, J.G. Kim, D.S. Hong, and C.G. Seo, "Treatment and Disposability of Intermediate Level Liquid Radwastes generated by Fission Moly Production", Proc. of the Korean Radioactive Waste Society, 15(1), 271-272 (2017).
- [2] W.H. Jang and J.H. Hyun, "A Study on Operating Range of Cement Solidification for Final Disposal of Radioactive Soil", Journal of Korea Society of Waste Management, 34(1), 34-40 (2017).
- [3] Y.J. Lee, D.S. Hwang, K.W. Lee, G.H. Jeong, and J.K. Moon, "Characterization of Cement Waste Form for Final Disposal of Decommissioned Concrete Waste", Journal of Nuclear Fuel Cycle and Waste Technology, 11(2), 271-280 (2013).

Application of Averaging Representative Sampling for a Various Surface Contaminated Wastes

MalGoBalGaeBitNaLa Yoo*, WonHyuk Jang, and JeongGuk Kim

Korea Atomic Energy Research Institute, 111, Daedeok-daero 989beon-gil, Yuseong-gu, Daejeon, Republic of Korea

*yoo1707@kaeri.re.kr

1. Introduction

According to Nuclear Safety Commission Notice No. 2017-65, a waste of clearance level can be managed by incineration, landfill or recycle. The artificial radionuclides for clearance in the Nuclear Safety Act (NSA) have 257 radionuclides with reference to IAEA RS-G-1.7, of which 138 short-lived radionuclides are included in the exemption levels of Schedule I of the Basic Safety Standards [1, 2]. In the case of fuel cycle facilities, contaminated waste may be generated by trace amounts of isotope uranium (U-234, U-235 and U-238) and their progeny; however, there is no definite clearance criterion for natural radionuclides domestically. Also, detailed guideline is needed to establish representativeness of various types of waste samples that can occur within radiation controlled area.

This paper describes in representative averaging sampling of surface contaminated waste refer to the domestic and international guidance.

2. Domestic clearance guidance

Clearance means the radioactive materials or items do not require any further regulatory control by the NSA. The solid wastes of very low radioactivity concentration that should be below the regulated activity concentration value of radionuclides or exposure dose level can be disposed of to landfill, incineration or recycling. The values of activity concentration should be derived from homogeneous

and averaged for representative sampling [Table 1.].

Table 1. Guideline for representative sampling of clearance level wastes

Authority	Acceptable range
Korea Institute of Nuclear Safety	- Averaged over at least 1 m ³ for solid wastes. - Averaged over 200 kg for solid wastes (including surface contaminated waste).

This procedure also applies to all disposal of non-contaminated items in radiation controlled area. For examples, there are a wide variety of items such as furniture, computer system, large equipment, and device control box. Surface contaminated wastes under domestic clearance regulatory guideline should be proved using direct and indirect surface contamination verification and scenario assessment; however, regulatory body ends to make a conservative approach as volumetric contaminated waste that samples 1 kg per 200 kg. Averaging is essential but very difficult to obtain representativeness for the radiological characterization of the surface contaminated items, when assuming a volumetric waste.

3. International clearance guidance

According to IAEA RG-S-1.7 of the concept of exclusion and ANSI/HPS N13.12 of the concept of clearance [3], the radioactivity concentration for K-40 is 10 Bq/g, and the remaining natural radionuclides are 1 Bq/g. In the event of a mixture of

radionuclides of natural and artificial origin radionuclides, the each natural radionuclides should be less than the value of activity concentration and the sum of the fraction of artificial radionuclides should be less than 1, and both conditions should be met. ANSI/HPS N13.12 refers to USNRC's mass to surface information for various surface contamination materials and provides additional typical items summary to apply volume-to-surface ratios [Table 2.].

Table 2. Mass to surface ratios for typical items

Item	Mass to surface ratio(g/cm ²)
Notebook computer	0.45 – 0.66
Plywood sheet	0.21 – 0.61
Lead acid battery	12.2

It is very significant to secure the representative samples for radioactivity analysis of the clearance level wastes. For this reason, there are guidelines for securing the averaging of samples outside the country as well as ANSI/HPS N13.12 [Table 3].

Table 3. Criteria for averaging both mass and surface of contaminated wastes

Authority	Acceptable range
Nordic council of minister	-Averaged over a maximum area of 300 cm ² for a metal.
	-Averaged over a maximum mass of 1000 kg for a metal.
European commission Radiation Protection	-Averaged over a mass of few 100 kg for a metal. (or several 100 cm ² respectively).
	-Averaged over a surface area of 1 m ² for a reuse of buildings
	-Averaged over a mass of 1000 kg for a building rubble.

4. Conclusion

Nuclear Safety Act requires that all items used in the radiation controlled area are counted as potential radioactive wastes and treated as clearance level wastes. In fact, there are many items that do not have

directly contact with radioactive material and that are difficult to dismantle. Actually, it is necessary to develop a domestic guideline of converting the surface contamination level to the concentration per unit volumetric for the surface contaminated wastes that meet the transfer criteria from the radiation controlled area. It is appropriate to consider the development of clearance standards for surface contaminated wastes adequate for domestic circumstance, because many countries such as Belgium, UK, and France are applying case-by-case assessments of clearance wastes. In addition, additional clearance criteria are likely to be required since natural radionuclides may be included in the regulated facilities or substances.

In the near future, it is expected that large-scale clearance wastes will be generated due to the dismantling of the Kori 1 nuclear power plant and the TRIGA MARK II&III research reactors as well as an aged building or area in the radiation controlled zone. Therefore, it is necessary to subdivide and continually amend the guidelines and regulations based on international safety standards and domestic clearance regulation.

REFERENCES

- [1] International Atomic Energy Agency, Application of the concepts of exclusion, exemption and clearance. Vienna, Austria, IAEA Safety Standards Series No. RG-S-1.7, 2004.
- [2] International Atomic Energy Agency, Derivation of activity concentration values for exclusion, exemption and clearance, Vienna, Austria, IAEA Safety Reports Series No.44, 2005.
- [3] Approved American National Standard/Health Physics Society, Surface and volume radioactivity standards for clearance, ANSI/HPS N13.12, 2013.

A Strategy of Soil Washing Water Purification Using Selective Media

DamHyang Kim*, Pil-yong Jeon, Woo-hyeon Rhee, Seung-il Kim, Deok-won Kang, and Joon-seok Lee
Elim-Global Co., Ltd., 767, Sinsu-ro, Suji-gu, Yongin-si, Gyeonggi-do, Republic of Korea
*damhyang.kim@elim-global.com

1. Introduction

After permanent shutdown of Kori #1, Korea has developed various decontamination and decommissioning technologies. Due to the long period operation, Kori NPP's would be a little contaminated with radioactive material. Thus, it is necessary to develop the technology of soil washing and contaminated water purification. For this, Elim Global Inc. is developing the decontamination technology for contaminated soil management. This study introduced the characteristic of zeolite adsorbents and application of ion-exchange fibers for effective removal of activity.

2. Tech. of soil washing water purification.

Among of several technology such as sorption, ion-exchange, chemical precipitation, coagulation/flocculation and membrane separation, adsorption technology is noticeable technology because of no preparation, small amount of sludge and simple process without any energy consumption from the outside.

2.1 Zeolites as radioactive material adsorbents

Many studies have been carried out on decontamination of radioactive material in water using zeolite because natural zeolites as well as synthetic zeolites have good sorption capability, strong affinity for alkaline metal and high stability under high temperature. In addition, Previous study shows that the adsorption characteristics depend on the type and structure of zeolite. Thus, Zeolites that have good adsorption selectivity for radio-nuclides have been chosen through assessment for zeolite properties and assessment for sorption capability

using simulated wastewater.

As shown in Fig. 1, zeolites are made of silicon dioxide and aluminum oxide. Si has a charge balance, but Al has a negative charge because it is trivalent. Adsorption takes place in an environment surrounding oxygen. (Fig.2).

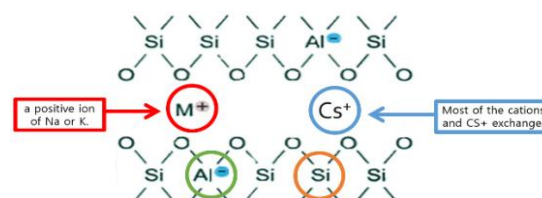


Fig. 1. Mechanism of cation adsorption of zeolite.

2.2 Natural Zeolite

Zeolites present in nature are cheaper than synthetic zeolites, but are a mixture of various natural zeolites and minerals. Adsorption study using rocks including zeolites can't represent the properties of a particular zeolite. Until this time, a study of various selective adsorption has assessed adsorption capability of particular natural zeolites through the systematic study. As reportedly did, natural zeolites have less adsorption capability than synthetic zeolite due to the inside impurities.

2.3 Manufacture of synthetic zeolite

Hydrated radius of ion influences cation sorption capability in water. Thus, the synthetic zeolite itself can be an adsorbent by synthesizing the structure that the hydrated radius of the adsorbate and size of the zeolite pores are similar. and then zeolites have high affinity with the adsorbate.

Even though powdered zeolites have an excellent sorption capability because of wide surface contact

area. These powdered zeolites are difficult to separate from wastewater. So, Zeolites is made in bead type through the immobilizing with polyvinylalcohol (PVA). Metal Ferrocyanide (MFC), which has highly adsorbent on Cs nuclide, is made of small particle (about 30 nm) and exists in colloidal into water. So MFC has weakness of remarkably reducing the liquid to solid separation efficiency. But, Numerous pores of zeolites has a merit as supporter for other materials. And also, after adsorption and separation of nuclides using zeolite, it can be insolubilized by immobilization of radionuclides through pyrolysis at high temperature. So, if we could develop the technology of impregnation of selective media on zeolite material, we could use the various nuclides using high efficiency adsorbent.

3. Master plan for experiments

3.1 Adsorption experiments using zeolite

Adsorption capability will be assessed by lab-scale adsorption experiment using non-radioactive material after providing under the manufacturing method using ^{133}Cs of non-radioactive. The adsorption capability assessment uses Cs isotope because particular zeolites have a good adsorption capability for ^{137}Cs (half-life ≈ 30.1 yr). [2]

Zeolites immerse in 50 mL of simulated wastewater polluted by the stable isotope, ^{133}Cs , and stir for 2.5 h. The wastewater then passes through a 0.20 μm membrane filter, and the Cs^+ concentration measures by inductively coupled plasma mass spectrometry. [2]

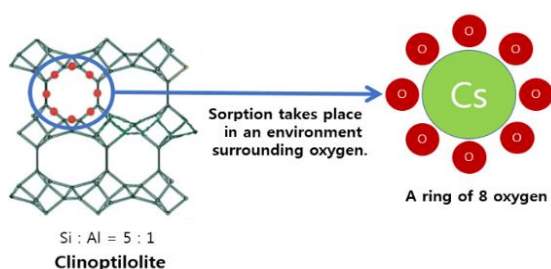


Fig. 2. Adsorption behavior of Cs.

3.2 Adsorption experiment on other nuclides

In the long term, adsorption technology for various nuclides besides Cs is required for water purification. Selected adsorbent by removal experiment using non-radioactive material will be used at hot laboratory for real testing. And also adsorption capability for the β -nuclides such as ^3H , ^{14}C and γ -nuclides will be assessed by LSC and HPGe Detector. Finally, removal efficient testing of contaminated soil will be carrying out to evaluate the purification capability using selected adsorbent.

4. Conclusion

Next researches talk about synthesizing zeolite that has good adsorption capability for particular radionuclides and develop hybrid-treatment device of the synthesized zeolite and ion-exchange fibers and perform treatment experiments of wastewater from decontaminated soil-washing.

ACKNOWLEDGEMENT

This work was supported by the Korea Institute of Energy Technology Evaluation and Planning (KETEP) granted financial resource from the Ministry of Trade, Industry and Energy, Republic of Korea. (No. 20181510300800)

REFERENCES

- [1] Seok-Chul Kim, et al., "Sorption Behavior of Cesium-137, Cerium-144 and Cobalt-60 on Zeolites", Journal of radiation protection and research, 10(1), 3-13(1985).
- [2] Endo, et al., "The removal of cesium ion with natural Itaya zeolite and the ion exchange characteristics", Journal of Chemical Technology & Biotechnology, 88(9), 1597-1602.

An Experimental Study on the Melting Decontamination for Radioactive Metal Waste Treatment Using Nuclide Coated Specimens

MinHwan Mo*, YongHo Cho, NakJeom Kim, and SangHun Choi

Korea Electric Power Corporation Plant Service & Engineering Co., Ltd, 211, Munhwa-ro, Naju-si, Jeollanam-do, Republic of Korea

* saintmo@kps.co.kr

1. Introduction

Melting decontamination process is applied widely for radioactive metal waste treatment because melting process make the pollutants of metal waste uniformly and make easier to measure the residual radioactivity[1].

In this paper, to develop optimal melting decontamination process of radioactive metal waste evaluated the removal rate of Co-60, Cr-51, Cs-137 nuclides according to melting parameters through the melting experiment using induction furnace. For this experiment, we investigated the main radioactive nuclides using thermal insulator which covered RCS (Reactor Coolant System) Loop of KORI unit1 and made the specimens coated with investigated nuclides.

2. Methods and Results

2.1 Nuclides Investigation of RCS Loop

In order to investigate the main radioactive nuclides of the RCS Loop of KORI unit1, we took measurement samples at inside and outside of the thermal insulator of the RCS equipments and pipes(fig.1). In the results of analysis, Co-60, Cr-51 and Xe-133 were detected on the inside of the thermal insulator and Co-60 and Cs-137 were detected on the outside of the thermal insulator at all sampling locations. The nuclides and their

radioactivity found in measurement samples are summarized in table 1.

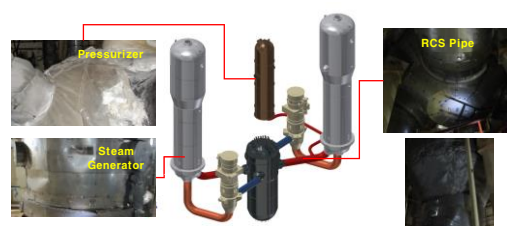


Fig. 1. Sampling locations of RCS Loop.




Table 1. Nuclide Distribution of Insulation of RCS Loop

Sampling Location		Nuclide	Activity(Bq/g)
Steam Generator	Inside Insulation	CR-51	1.22E+01
		CO-60	8.89E+00
		XE-133	5.71E+00
	Outside Insulation	CO-60	3.14E+00
		SB-124	1.42E+00
		XE-133	1.01E+00
RCS Pipes	Inside Insulation	CS-137	3.98E+00
		CR-51	7.58E+00
		CO-60	4.14E+00
	Outside Insulation	XE-133	2.97E-01
		CO-60	1.37E+00
		XE-133	5.36E-01
Pressurizer	Inside Insulation	CO-60	4.99E-01
	Outside Insulation	CS-137	3.35E-01

2.2 Melting Decontamination Experiment

We experimented melting decontamination effect of Co-58/60, Cr-51 and Cs-137 nuclides using induction furnace while varying the melting parameters(slag weight, composition, basicity). We prepared metal specimens coated with each nuclide as shown in table 2.

Table 2. Nuclides Coated Specimen

Nuclide Coating	Co3O4	Cr2O3	CsCl
Coating times	3 times	3 times	3 times
Solidification temp	200 °C	200 °C	Room Temp'
Solidification time	30 min	30 min	180 min
Resin ratio	50w%	50w%	50w%
Specimen image			

We melted the nuclide coated specimens and slag in a graphite crucible (purity: 99% more) using the induction furnace. Information of slag added to remove nuclides from specimens is as shown in table 3. Weight changes before and after melting are as shown in table 4.

Table 3. Test parameters for induction melting test.

Sp. No	Coated Nuclide		Slag		B ratio
	kind	Weight	Composition (W%)	Weight	
1	Co-58/60	1.39 g	SiO2(50)-CaO(30)-Al2O3(20)	72 g	0.6
2	Co-58/60	1.10 g	SiO2(50)-CaO(30)-Al2O3(20)	36 g	0.6
3	Co-58/60	1.43 g	SiO2(50)-CaO(30)-Al2O3(10)-Fe2O3(10)	36 g	0.6
4	Cr-51	2.33 g	SiO2(50)-CaO(30)-Al2O3(20)	72 g	0.6
5	Cr-51	2.09 g	SiO2(50)-CaO(30)-Al2O3(20)	36 g	0.6
6	Cr-51	2.09 g	SiO2(50)-CaO(30)-Al2O3(10)-Fe2O3(10)	36 g	0.6
7	Cs-137	4.88 g	SiO2(50)-CaO(30)-Al2O3(20)	72 g	0.6
8	Cs-137	3.72 g	SiO2(50)-CaO(30)-Al2O3(20)	36 g	0.6

Table 4. Weight information before/ after melting

Sp. No	Before melting(g)			After melting(g)		
	Specimen	Slag	Coated Nuclide	Specimen	Slag	Nuclide in slag
1	356.7	72	1.39 g	352.9	85.2	0.192
2	355.1	36	1.10 g	352.1	53.9	0.118
3	356.4	36	1.43 g	352.5	50.4	0.035
4	364.8	72	2.33 g	358.0	92.1	1.65
5	362.3	36	2.09 g	356.2	55.3	1.91
6	362.9	36	2.09 g	356.8	48.2	1.93
7	364.8	72	4.88 g	358.0	83.22	0.47
8	362.3	36	3.72 g	356.2	61.82	0.36

We separated the molten metal and slag after melting, and then analyzed the weight percent of Co,

Cr, Cs nuclides in the slag by XRF. The removal rates of nuclides are calculated using the equation (1) and the results are as shown in table 5.

$$D(\%)=w^0 \times m(g)/M(g) \quad (1)$$

(D(%):Removal rate, w%:Nuclide weight percent in the slag, m(g):Weight of slag after melting, M(g):Weight of nuclide coated on the specimen)

Table 5. Nuclide removal rate by Slag after melting

Sp.No	Coated Nuclide	Weight(g) (in Specimen)	Weight(g) (in Slag)	Removal rate(w%)
1	Co-58/60	1.39	0.192	13.8
2	Co-58/60	1.10	0.118	10.9
3	Co-58/60	1.43	0.035	2.24
4	Cr-51	2.33	1.65	70.8
5	Cr-51	2.09	1.91	91.3
6	Cr-51	2.09	1.93	92.3
7	Cs-137	4.88	0.47	9.9
8	Cs-137	3.72	0.36	10.0

3. Conclusion

We carried out decontamination experiments of the metal waste coated the field nuclides which investigated in the RCS Loop of KORI Unit1 using induction furnace. In the experiment, we got 2.2 ~ 13.8% removal rate of Co, 70.8 ~ 92.3% removal rate of Cr and 10.0% removal rate of Cs according to the change of slag composition and weight. But we need more experiment for increasing removal rate of Co and Cs.

REFERENCES

- [1] Park Jin Ho, et al., "Development of post-decontamination process after integrated EPN treatment", Korea Atomic Energy Research Institute, (2010).

Manufacture of KJRR Cement Waste Form for Enhancement of Cesium Leaching Resistance

Won Hyuk Jang, Gi Yong Kim, Dae Seok Hong, Jeong Guk Kim, and Jong Sik Shon*

Korea Atomic Energy Research Institute, 111, Daedeok-daero 989beon-gil, Yuseong-gu, Daejeon, Republic of Korea

*njsshon@kaeri.re.kr

1. Introduction

KAERI has a plan to build KRJJ (Ki-Jang Research Reactor) in Ki-Jang, Busan by 2022. It is important to safely dispose of low and intermediate level liquid radioactive waste from operation of the research reactor. One of the efficient ways to treat liquid radioactive waste is cement solidification. The cement solidification is more simple and efficient than other solidification method, but has relatively lower leaching resistance. Therefore, this study focused on the development of cement solidification for an enhancement of cesium leaching resistance. We used loess to improve the cesium leaching resistance of KJRR cement form containing KJRR simulated liquid waste (Loess KJRR cement waste form). A leaching test was carried out using KJRR simulated liquid waste containing 3 g/L of cesium for 90 days. KJRR cement waste form containing loess showed cesium leaching resistance was 21.1% higher than KJRR cement form without loess (KJRR cement waste form).

2. Methods and Results

2.1 Materials

Portland cement and loess were purchased from SSangyong and Greenbio respectively. NaCl, Na₂SO₄ and CsCl were purchased from Sigma-Aldrich (Mo, USA). All other chemicals used are of analytical or research grade.

2.2 KJRR simulated liquid waste

The KJRR (Ki-Jang Research Reactor) simulated liquid waste constituents are as follows: Na₂SO₄ 106.53 g/L, NaCl 64.28 g/L, and Cs⁺ 3 g/L [1].

2.3 Manufacture of KJRR cement waste form

The KJRR cement waste form were simulated in accordance with the Korean Industrial Standard (KS-L-5109) [2]. The mechanical mixer was purchased from JI-206 (Jeil Precision, Korea). KJRR cement waste forms were made to find the optimal mixing rate (W/C, W: water, C: cement) from 0.4 to 1.3 (Fig. 1a). The KJRR cement waste forms were made by W/C 0.7 considering the result of the workability test (Fig. 1b). And we added loess to improve the cesium leaching resistance of KJRR cement (S/C, S: loess, C: cement) from 1, 5 and 10wt.% (Fig. 1c). And KJRR cement was solidified while curing at room temperature with relative humidity of 40 to 60% for 28 days. After 28 days, the uniformity of KJRR cement waste form was visually confirmed.

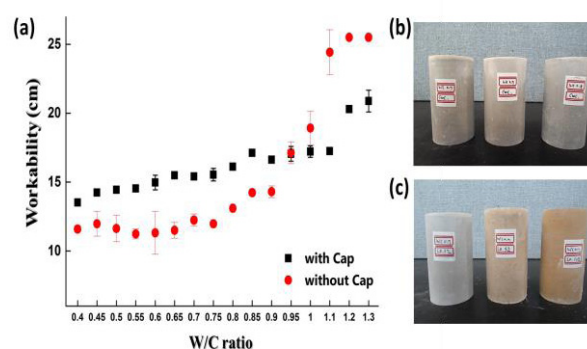


Fig. 1. (a) Workability of KJRR cement waste form according to W/C ratio (b) KJRR cement waste form (c) Loess KJRR cement waste form.

2.4 Characterization of KJRR cement waste form

The component of KJRR cement waste form was analyzed using SEM-EDS. As shown in Table 1, it can be seen that (Fe, Al, Si) ions, which are the main components of loess, increase with the loess content of KJRR cement waste form.

Table 1. Weight percent (wt. %) of loess elements according to loess contents of KJRR cement waste form

Elements	Loess	KJRR (Without Loess)	KJRR (Loess 5%)	KJRR (Loess 10%)
O	48.84	42.19	36.64	43.64
Al	17.87	1.57	2.30	3.00
Si	24.69	6.50	6.66	7.96
Ca	0.41	37.25	40.84	30.43
Fe	7.62	1.57	3.90	4.24

2.5 Leaching test of KJRR cement waste form

As shown in Fig 2. We analyzed pH and electronic conductivity of KJRR cement waste form with a leaching time. It was confirmed that the pH and Eh increased with loess content of KJRR cement waste form.

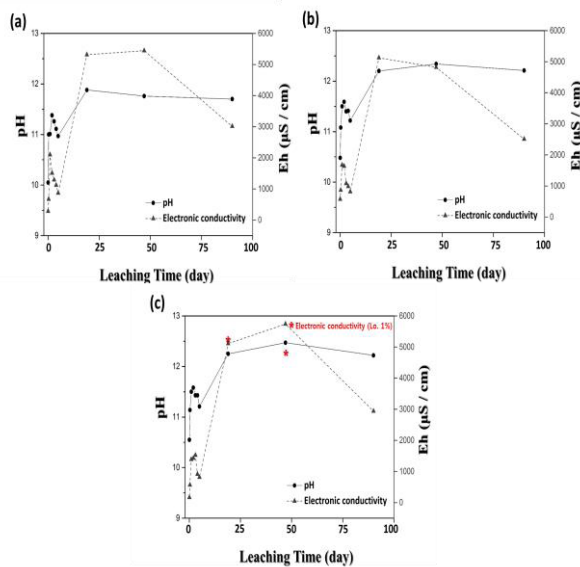


Fig. 2. pH and electronic conductivity with a leaching time (a) control, (b) Loess in KJRR cement waste form (S/C 1.0 wt.%) and (c) (S/C 10 wt.%).

The cumulative fraction leached (CFL) of cesium according to the change of loess content was calculated using the ANS 16.1 test method from USA. The leaching resistance was determined by considering the degree of cesium ions leached during the leaching test, and the cumulative fraction leach was defined as the equation below [3]

$$CFL = \frac{\sum A_i}{A_0} \quad (1)$$

A_i = Cumulative leaching amount of material A during the leaching interval

A_0 = Initial content (g) of the material A

It was confirmed that KJRR cement waste form containing loess was lower Cs^+ leaching rate than control sample(KJRR cement waste form, without loess) (Fig. 3).

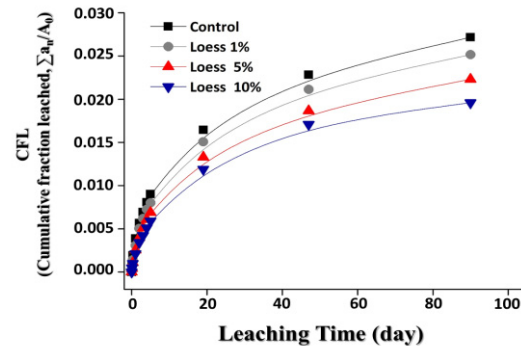


Fig. 3. Cumulative fraction of Cs^+ leached in loess KJRR cement waste form.

3. Conclusions

In this study, we made a KJRR cement waste form with KJRR simulated liquid waste. In addition, we used loess to improve the cesium leaching resistance of KJRR cement waste form. We proved based on SEM-EDS spectrum analysis that loess was successfully isolated with the KJRR cement waste form. A leaching test was carried out using simulated KJRR liquid waste containing 3 g/L of cesium. Loess KJRR cement waste form achieved a cesium leaching resistance 21.1% higher than the control value. In addition, all experimental groups were satisfied with acceptance criteria of the final disposal facility such as the compressive strength and leaching rate.

REFERENCES

- [1] J.S. Shon, et al., "Treatment and Disposability of Intermediate Level Liquid Radwastes generated by Fission Moly Production", Proc. of the Korean Radioactive Waste Society, 15 (2017).
- [2] W.H. Jang, et al., "A Study on Operating Range of Cement Solidification for Final Disposal of Radioactive Soil", Journal of Korea Society of Waste Management, 34 (2017).
- [3] Y.J. Lee, et al., "Characterization of Cement Waste Form for Final Disposal of Decommissioned Concrete Waste", Journal of Nuclear Fuel Cycle and Waste Technology, 11 (2013).

Design Factor Analysis of the Treatment Equipment for the Spent Resin Mixture From Pressurized Heavy Water Reactor

Kyu-Tae Park*, Jung-Min Yoo, Hyeon-Oh Park, Ki-Hyun Kown, and Young-Ku Choi
Sunkwang T&S Co., Ltd., Sunkyung Officetel 20F, 3, Gongwon-ro, Guro-gu, Seoul, Republic of Korea
*paradoxno1@hanmail.net

1. Introduction

The annual average amount of spent resin mixtures, generated in domestic PHWR (Pressurized Heavy Water Reactor) nuclear power plants, is 124,560 L. They are stored in 200 m³ concrete storage tanks located inside the nuclear power plants.

PHWR spent resin has high specific radioactivity of C-14, and as the total radioactivity is about 10 times higher than the total amount limit (3.04×10^{14} Bq) of the underground repository, it is absolutely necessary to remove C-14 in the spent resin for permanent disposal of spent resin mixtures.

This study separated spent resin from the spent resin mixture, deposited C-14, collected it in $\text{Ca}(\text{OH})_2$ or $\text{Ba}(\text{OH})_2$, and analyzed the factors that must be considered when designing a commercial device for treating PHWR spent resin mixtures based on the on-site verification experiment conducted to review the validity of recycling.

2. Body

PHWR spent resin mixture treatment equipment consists of 4 stages, i.e. the spent resin mixture transfer process, the resin separation process, the C-14 desorption process, and the C-14 adsorption process, and the authors analyzed the factors necessary for designing the device in consideration of the characteristics of each process.

2.1 Treatment capacity

The total capacity of the spent resin storage tanks of Wolsong Nuclear Power Plants 1 and 2 is 1,786 m³. Assuming that spent resin is stored at up to 80% of the total capacity in consideration of safety, the total amount of spent resin mixtures to be treated is 1,428,800 L, and assuming that all stored spent resin mixtures are treated in the next 3 years after permanent shutdown according to the NPP decommissioning plan, the daily treatment capacity was calculated as 1000 L/day. Based on this, the treatment capacity of each process was calculated as shown in Table 1.

Table 1. Treatment capacity of each process

	Classification	Design capacity	Treatment capacity
Transfer	SUMP HOPPER	850 L	600 L
	1 st separation tank A, B	1000 L	600 L
Separation	Zeolite+activated carbon recovery tank	2390 L	1910 L

	RESIN BUFFER TANK	2390 L	1910 L
	RESIN DAILY TANK	1550 L	850 L
	2 nd separation tank	300 L	150 L
	Constant SCALE HOPPER	150 L	130 L
	Constant FEEDER	30 L/min	30 L/min
Desorption	MW REACTOR A, B	380 L	125 L
Adsorption	C-14 adsorption tower A	12 L	6 L
	C-14 adsorption tower B	9 L	3 L

2.2 Treatment time

The pretreatment process for treating spent resin mixtures, i.e. the 'concrete storage tank→SUMP HOPPER→1st separation tank A, B→RESIN BUFFER TANK→RESIN DAILY TANK' process, is operated automatically by the level sensor attached to each tank, and it is constantly operated separately from back-end processes.

The separated spent resin treatment process has a closed circulatory structure consisting of 'feeding spent resin→C-14 desorption→removing moisture→C-14 adsorption→discharging spent resin after reaction,' and the treatment time for all processes is 2 hr/Batch. The spent resin treatment process is operated 4 batches a day, and 8 hours of operation treats 800 L of spent resin.

2.3 Removing spent resin mixtures

Stored spent resin is stored in liquid waste in the form of a mixture of zeolite, activated carbon and spent resin. Depending on their location, part of mixtures, which have been stored for a long time, may be hardened. So there must be a way to crush them before removal. Propeller-type equipment with a digging function will be used to crush the hardened parts, and transfer them to the Sump Tank through the Resin Outlet.

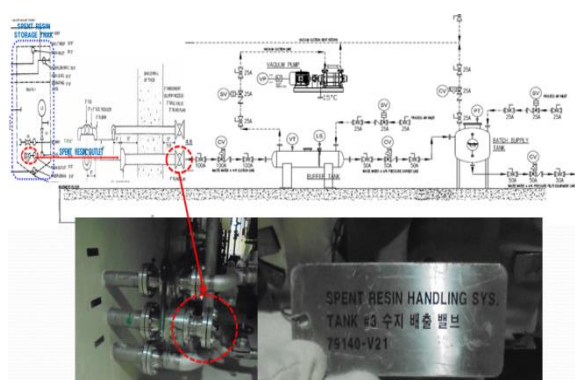


Fig. 1. Spent resin mixture removal process.

2.4 Separation of spent resin

The spent resin mixture, transferred to the SUMP TANK, will be transferred to the 1st separation tank, and passes through multi-stage mesh in the liquid stage, and it is separated into 'zeolite+activated carbon' and 'spent resin.' The separated 'zeolite+activated carbon' will be transferred to the recovery tank, and the spent resin will be transferred to the BUFFER TANK for storage.

2.5 C-14 desorption

1 kW Magnetrans (26) will be used to generate electromagnetic waves (2.45 GHz) in the cylindrical reactor, designed with optimization simulation that has a treatment capacity of 100L/Batch, and C-14 is desorbed in the form of $^{14}\text{CO}_2$ gas due to functional group pyrolysis.

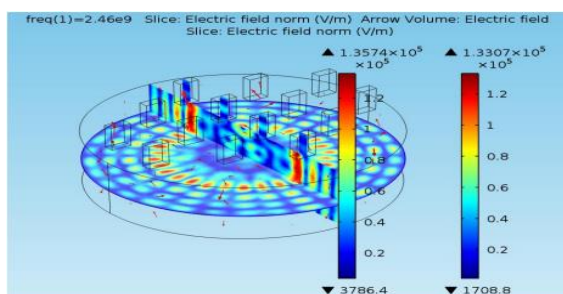


Fig. 2. Optimization simulation.

2.6 C-14 adsorption and recycling

$^{14}\text{CO}_2$, which passed the heat exchanger and had moisture removed, was designed as a lattice structure to maximize the reaction efficiency of the adsorbent and the surface area, and the CO_2 adsorbent (Ca or Ba series) will be loaded in each stage, and C-14 will be adsorbed.

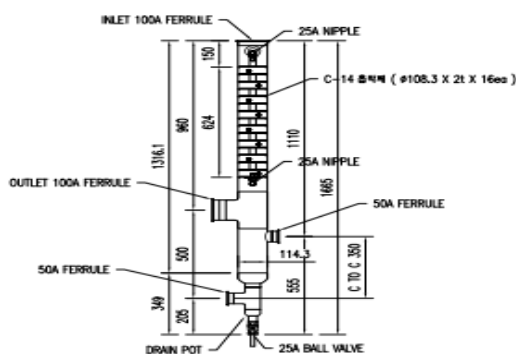


Fig. 3. lattice structure's adsorption tower.

C-14, recovered in the adsorbent, is an expensive resource. The authors are planning to find a method of concentrating and recycling it in the adsorption process so that it satisfies the commercial standard (50mCi/mmol) for manufacturing labeled compounds.

2.7 Disposal of wastes

The 'zeolite+activated carbon,' recovered in the spent resin mixture separation process and the 'post-treatment spent resin' will be stored in their respective storage tanks, and put in their respective containers using the automatic packing system, and treated according to plan.

2.8 Radiation protection

To minimize the influence of radiation on the workers operating the PHWR spent resin mixture treatment device, workers' exposure was minimized through modeling with the VISIPLAN code, and risk factors were verified.

2.9 PHWR spent resin mixture treatment process

Design factors of each key process were analyzed, and a device, capable of treating 1000 L of spent resin mixtures (zeolite+activated carbon+spent resin+stored liquid waste) per day, was designed. The design standard of each process is a capacity that can treat 800 L of pre-reaction spent resin (moisture content about 50%) in view of the component ratio (spent resin 80%) of spent resin mixtures.

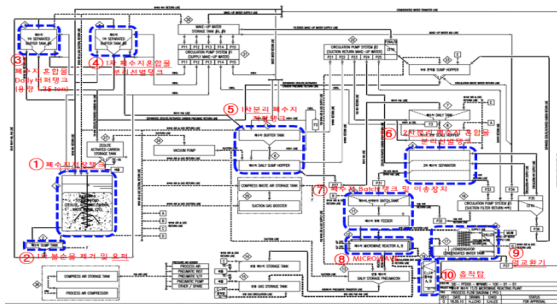


Fig. 4. PHWR spent resin mixture treatment process.

3. Conclusion

The 'PHWR spent resin mixture treatment commercialization equipment,' designed in this study, can be used to secure the safety of radioactive waste disposal. Also, it is believed that the disposal costs will be reduced as the volume of the wastes, generated by NPPs, is reduced, and economic gains will be generated through the recycling of expensive resources. But it is necessary to reflect the inadequacy of the current system and the regulatory agency licensing process.

ACKNOWLEDGEMENT

This work was supported by a Korea Institute of Energy Technology Evaluation and Planning (KETEP) grant funded by the Korean government (No. 20151520302120).

Analysis of International Standards and Guidelines for Optimal Management of Decommissioning Waste and Its Implication

Ji Woo Lee, Wang Hyeon Lee, and Jae Hak Cheong*

Kyunghee University, 1732, Deokyoungdaero, Giheung-gu, Yongin, Gyeonggi-do, Republic of Korea

*jhcheong@khu.ac.kr

1. Introduction

June 2017, as the first commercial Nuclear Power Plant(NPP) Kori Unit 1 is permanently suspended, it is expected that the preparation for the decommissioning of NPPs in Korea will needed. KHNP is proposing a challenging goal of disposing 14,500 drums per Unit through minimization of Decommissioning Waste(DW).

Nuclear-related institutions and national regulatory agencies are establishing regulation for optimal managements of DW and responsible for ensuring that the needs of the operator can meet legal requirements through rules and guidelines. Therefore, this study proposes measures to facilitate decommissioning by researching and analyzing the regulations of 8 institutions and countries for optimal management of DW from generation to disposal.

2. Analysis of Relevant Regulations

In this study, prior research of the optimal regulatory management of DW by major institutions and countries were investigated and analyzed them in three categories. The state of application of each institutions and countries is shown in Table 1 below and in Korea, regulations are managed to the same level as the IAEA's recommendation on DW through laws and regulatory agencies [1][2].

Table 1. The State of Application for Institutions/Countries

	IAEA	EC	WENRA	USA	UK	FR	JP	KR
RW Source Reduction	○	○	○	○	○	○	○	○
Prevention of Contamination Spread	○	○	○	○	○			○
Recycle and Reuse	○	○			○	○	○	○

2.1 Radioactive Waste(RW) Source Reduction

Minimizing waste generation means minimizing the generation of radioactive waste during operation and decommissioning phase through proper design and operation. All 8 institutions and countries surveyed have specified the minimization of waste generation through guidelines and recommendations

2.2 Prevention of Contamination Spread

Prevention of contamination spread is to prevent the spread of radioactive contamination, thereby reducing the needs for decontamination and minimizing the generation of secondary wastes including byproducts from treatment process. As shown in Table 1, 6 out of 8 institutions and countries specify the prevention of contamination spread.

2.3 Recycle and Reuse

6 Institutions and countries, including IAEA,

specify recycling and reusing in their guidelines and recommendations, and suggest that recycling and reusing through characterization is one of the most important strategy in terms of minimizing DW. In the case of France and Japan in particular, it aims for restrict recycling and reusing in the nuclear industry.

3. Results and Discussion

3.1 DW Management Flow Chart

Based on the DW management flow chart proposed by the optimal regulation management for each institution and country, this study propose a flow chart for DW management considering the domestic situation, and some of them are shown in Figure 1 [3].

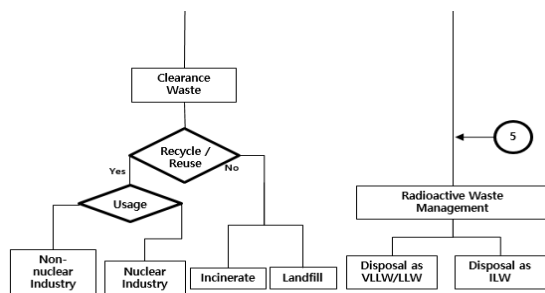


Fig. 1. DW Management Flow Chart (Extract).

3.2 History Management System linked with Configuration Management(CM)

To ensure facilitate of decommissioning, history management is required from the design and operation stage to characterize the DW. KHNP carries out CM through Equipment Master Data of material and equipment IT system to ensure safe operation of NPP and prevent irregularities, it is considered that some of the CM items managed during operation can be utilized in the history management system for DW at the decommissioning stage.

4. Conclusion

This study investigates and analyzes the regulations of eight institutions and countries for the optimal management of DW and proposes the methods to improve the facilitate of decommissioning as a flow chart of DW management for minimizing wastes and a history management system for DW that linked with CM for the efficient waste characterization.

On the other hand, there is case where asphalt using materials below the clearance levels is removed (Songpa-gu, Seoul) and controversy over the recycling of Non-RW to road paving foundations (Uiwang, Pocheon). Therefore, it is necessary to consider way of recycling the items with low average frequency of exposure to the public through recycling in the nuclear industry considering public acceptance.

ACKNOWLEDGEMENT

This work was supported by the Nuclear Safety Research Program through the Korea Foundation Of Nuclear Safety (KOFONS), granted financial resource from the Nuclear Safety and Security Commission (NSSC), Republic of Korea (No. 1605008).

REFERENCES

- [1] IAEA, "Methods for the Minimization of RW from Decontamination and Decommissioning of Nuclear Facilities", TRS 401 (2001).
- [2] Regulations on Technical Standards for Nuclear Reactor Facilities, Etc (2016).
- [3] EC, "Material Management and Characterisation Techniques", EC-CND (2008).

Development of Radioactive Contaminated Waste Filter Disposal System in NPP

YongHo Cho*, NakJeom Kim, HeeCheol Yoon, MinHwan Mo, and SangHoon Choi

Korea Electric Power Corporation Plant Service & Engineering Co., Ltd., 211, Munhwa-ro, Naju-si,
Jeollanam-do, Republic of Korea

*yongho_jo@kps.co.kr

1. Introduction

The HVAC (Heating, Ventilation, and Air conditioning) system of a nuclear power plant is equipped with a filter that passes air through a porous filter media to filter out foreign substance and dust. The types of filter used consist of HEPA(High efficiency particulate air)filter and medium filter.

More than 300 to 400 filters are exchanged per 1 unit in a nuclear power plant every year.

This working process is carried out when differential pressure is occurred and waste HEPA filters should be separated for disposal.

In the primary system, the separation work is performed by manual process to sort out the material, and it needs high intensity of labor and takes a long time.

Therefore, it is necessary to develop the automatic equipment that separates contaminated HEPA filter.

This paper presents the results of a separation condition test for developing a waste filter disposal system.

2. Methods and Results

2.1 Development background

Waste HEPA filter disposal contaminated with radiation from a nuclear power plants requires complete separation as shown in Figure 1. (Filter frame, Adhesive, Separator, Filter media) Therefore, separation process of one waste filter required 0.8 M/D(Man/Day), and the serious problem is that unprocessed filters keep accumulating inside

the primary system.

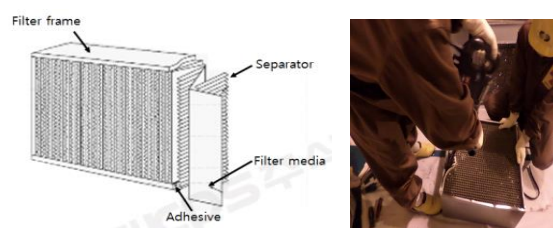


Fig. 1. waste filter composition and manual process.

Also, if we try to develop the equipment that can automatically remove a filter from a frame, there is no clear standard about the width and tolerance of the filter frame, which makes it difficult to develop standardized equipment.

2.2 principle of equipment

Figure 2 is a device for separating the filter from the frame by mechanical pressure method.

This device is fixed with left side of the frame as a reference and tighten the right side of the frame inward. Thereafter the cutter moves up and down in the vertical direction to separate the adhesives and Filter frame.

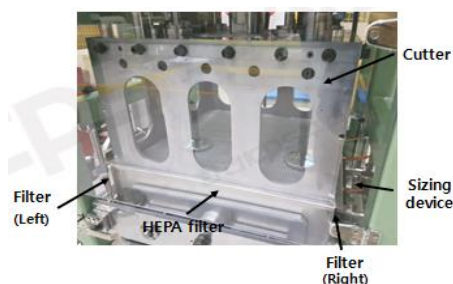


Fig. 2. Separating system.

In Table 1, this filter has no clear standard for outside and inside of “Before Sizing” with some tolerance at least 1~3mm, so this filter disposal system applied the standardized size for each Outside and Inside of “After Sizing” by Experimental Verification.

Table 1. HEPA Filer Size & Sizing dimension(mm)

Sample		Before sizing		After Sizing	
		Outside	Inside	Out side	Inside
HEPA Filer	Double-turned flange Type	577.8	573.8	576.6	572.6
		577.1	573.1	576.6	572.6
		577.3	573.3	576.6	572.6
		576.7	572.7	576.6	572.6

2.3 Mock-up Test

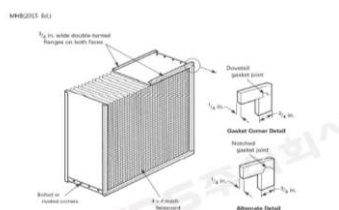


Fig. 2. HEPA Filter Double-turned flange Type.

In this Mock-up Test, the filter in Figure 2 is used. For the performance test, 4EA Filters of different sizes within HEPA Filter Nominal Size in Table 1 were arbitrarily selected, and the pressure and speed of the Hydraulic cylinder were set to the same condition in Table3 to confirm the effect of sizing.

Table 3. Main & Sub Cylinder Operation Speed & Pressure

Speed(mm/s)		Pressure (kgf/cm ²)	Gauge (kgf/cm ²)
Main(1 st)	Sub(2 nd)		
7	20	100	60

2.4 Result of Mock-up Test

Outside		picture of test		Result
Before Sizing	After Sizing	Filter frame	Adhesive, Filter media	
577.8mm	576.6 mm			Very satisfied
577.1mm	576.6 mm			Very satisfied
577.3mm	576.6 mm			Very satisfied
576.7mm	576.6 mm			Very satisfied
577.8mm	577.8mm (unapplied)			Unsatisfied

Fig. 3. result of test.

As a result, we could confirm that all 4 tests were cleanly separated by applying “After sizing”. On the contrary, when sizing is not applied, the separation of the adhesives is not cleaned due to the widening of the Filter frame.

3. Conclusion

In the development of the waste HEPA filter disposal equipment the mock-up performance test using the unified sizing method showed that the work time was reduced by 90%. It is expected that by reducing the waiting time in the primary system where the work is done, the amount of radiation exposure can be significantly reduced. In the future, we intend to improve the completeness of this equipment by applying it to the field of waste HEPA filter disposal in a nuclear power plants.

Performance Evaluation of Ca-based Adsorbent for C-14 Trapping

In-Hak Cho^{1)*}, Hwan-Seo Park²⁾, Ki Rak Lee²⁾, In-Tae Kim²⁾, Geun-Il Park²⁾, and Young-Seok Lee¹⁾

¹⁾ Chungnam National University, 99, Daehak-ro, Yuseong-gu, Daejeon, Republic of Korea

²⁾ Atomic Energy Research Institute, 111, Daedeok-daero 989beon-gil, Yuseong-gu, Daejeon, Republic of Korea

*choinhak@kaeri.re.kr

1. Introduction

Generally ion-exchange materials were applied to liquid processes in nuclear reactor. In the case of heavy-water reactor, zeolite, active carbon, anion resin, and cation resin were used to treat liquid processes such as reactor primary coolant cleanup and liquid radioactive waste management system. Then, spent ion exchangers were stored at storage tanks. Spent ion-exchange resins contaminated with the C-14 radioisotope influences the strategy for the disposal of the spent resin. In order to overcome the disposal concentration limit of the spent resin loaded with C-14, it is recommended that the removal of C-14 from spent resin and its concentration to solid adsorbents become a desirable feature which can be disposed of as intermediated level radioactive waste (ILW). Therefore, develop of technology for effective desorption of C-14 from spent ion-exchange resin and its treatment is needed. In this study, evaluates the performance of CO₂ trapping according to the manufacture conditions of adsorbent. The CO₂ trapping performance according to the effect of alcohol added to the adsorbent and the heat treatment temperature of the adsorbent was examined.

2. Experimental

2.1 Materials and methods

The adsorbent was prepared by using calcium acetate monohydrate (Ca(CH₃COO)₂·H₂O, Shinyo 98%), calcium hydroxide (Ca(OH)₂, Junsei, 96%),

ethylene glycol (C₂H₆O₂, Daejung, 99%), isopropyl alcohol (C₃H₈O, Daejung, 99.7%). The calcium acetate monohydrate dissolved in D.I. water and then added ethylene glycol in the solution while stirring. By adding calcium hydroxide powder was produced paste form the solution. After adding isopropyl alcohol, it can be extruded a pellet form by aging for a day. Finally, Ca-based adsorbent is prepared through heat treatment from 110 to 900 degrees Celsius. The batch composition of Ca-based adsorbent was indicated in table 1.

Table 1. The batch composition of Ca-based adsorbent

	C-1	C-2	C-3
D.I. Water	45(ml)	45(ml)	45(ml)
Calcium acetate monohydrate	15(g)	15(g)	15(g)
Ethylene glycol	13(g)	13(g)	13(g)
Calcium hydroxide	80(g)	80(g)	80(g)
Isopropyl alcohol	-	10(ml)	200(ml)
Heat treatment	110~900(°C)		

2.2 Performance evaluation

The performance evaluation of the Ca-based adsorbent was determined by the trapping of CO₂ and shown in Fig. 1. In order to remove CO₂ using a Ca-based adsorbent, the moisture in the gas must be 85% or more to enhance the CO₂ removal efficiency. Nitrogen gas is supplied to the humidify generator to control a gas condition of 85% relative humidity, using a 10% CO₂ cylinder supply the desired flow rate and mix the two gases in the mixing tank.

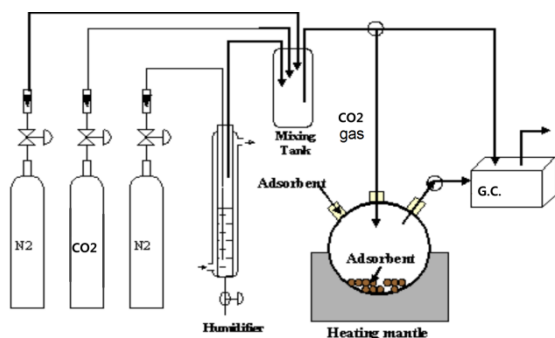


Fig. 1. Batch type test equipment of CO₂ adsorption.

3. Result

The changes in CO₂ concentration according to the conditions of adsorbent manufacturing are shown in Fig. 2, and when isopropyl alcohol was added 200 ml, the rate of removal was the fastest. The alcohol added to the adsorbent increases the porosity in the adsorbent, and is considered to have excellent CO₂ removal efficiency. The concentration variation of CO₂ by adsorption heat treatment temperature of adsorbent is shown in Fig. 3, and the rate of removal of CO₂ was the fastest when the heat treatment temperature was 900°C. As carbon attached to the surface of the adsorbent is removed at a heat temperature of 900°C or higher, the adsorption rate of the adsorbent seems to have increased.

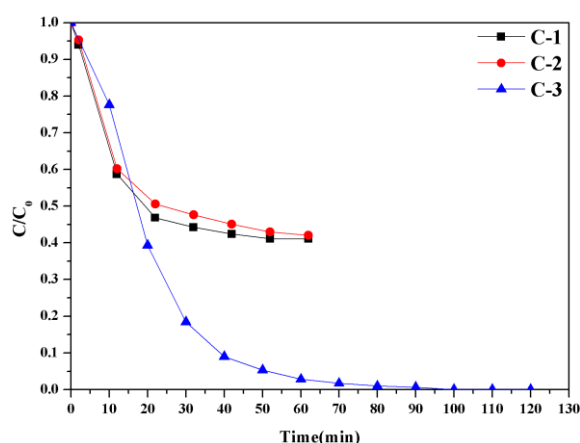


Fig. 2. Variation of CO₂ concentration according to adsorbent manufacturing conditions.

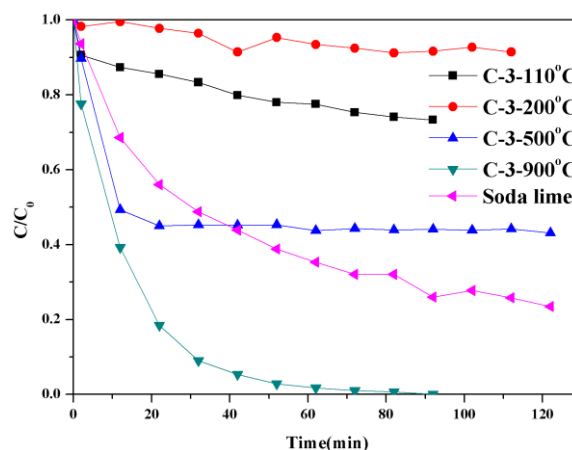


Fig. 3. Variation CO₂ concentration with heat treatment temperature of adsorbent.

4. Conclusion

In high concentration CO₂ conditions, Ca-based adsorbent has been found to have excellent adsorption performance compared to soda lime.

REFERENCES

- [1] Chew, V. S., Cheh, and Glass, R. W., "Mechanism or the CO₂-Ca(OH)₂ reaction" 17th DOE Nuclear Air Cleanig Conference, 400-413.
- [2] Gregg, S. J., Sing, K. S. W., "Adsorption, Surface Area and Porosity", Academic Press, New York, 1982.

Radiological Impact Assessment for the New Radioactive Isotope Wastes Land Transportation Route Using RADTRAN

Hyeon-Oh Park^{1)*}, Bong-Ki Ko¹⁾, Kyu-Tae Park¹⁾, Ki-Hyun Kwon¹⁾, Young-Ku Choi¹⁾
Myunghwan Seo²⁾, and Jin Beak Park²⁾

¹⁾ Sunkwang T&S Co., Ltd., Sunkyung Officetel 20F, 3, Gongwon-ro, Guro-gu, Seoul, Republic of Korea

²⁾ Korea Radioactive Waste Agency, 174, Gajeong-ro, Yuseong-gu, Daejeon, Republic of Korea

*pho1428@hanmail.net

1. Introduction

Since the operation of Wolsong Low and Intermediate level Radioactive Waste Disposal Center had been approved in 2014, the operation of the disposal facility began. From 2015, Korea Radioactive Waste Agency (KORAD) carries out transporting the radioactive isotope wastes temporarily stored in the 'radioisotope (RI) waste management facility' to the disposal facility.

This study concerns Radiological Impact Assessment using the RADTRAN program, and will predict the estimated dose rate to workers and the publics around the transportation vehicles by applying the new land route transportation scenario for transporting RI wastes to the disposal facility, and compare the results with the legal standards of the Enforcement Decree of the Nuclear Safety Act [Presidential Decree No. 28987] for evaluation.

2. Transportation system

2.1 Wastes to be transported

The study assumed that RI wastes are transported, and the nuclides and amounts of radioactivity used for Radiological Impact Assessment are shown in [Table 1].

Table 1. Amount of radioactivity of each nuclide

Nuclide	Amount of radioactivity	Nuclide	Amount of radioactivity
H-3	1.076E+06	I-131	0.0
C-14	4.063E+07	Cs-143	3.214
Cr-51	0.0	Co-57	1.945
Co-58	1.804E+00	Fe-59	3.195E+01
Sr-90	0.0	Ca-45	7.248
P-32	5.606E-02	Y-90	0.0
S-35	8.527E+01	Cd-109	0.0
I-125	8.580E-01	Rb-86	0.0
Co-60	6.491	Ga-67	0.0
Cs-137	9.550E+06	Am-241	0.0
Pm-147	3.137E+02		

2.2 Setting the transportation route

The new land transportation route for transporting RI wastes to the disposal facility consists of expressways and general national roads. Using the new transportation route setting conditions to minimize transportation time and thus minimize exposure time and transportation accident rates was

considered.

The main route of the new transportation route, applied to this study, includes Honam Expressway, Gyeongbu Expressway, Dangjin Yeongdeok Expressway, Sangju Yeongcheon Expressway, Iksang-Pohang Expressway and Donghae Expressway. This study divided the distance of about 260km into a total of 10 transportation sections in consideration of the population density, traffic volume and accident rate of the administrative districts on the transportation route as shown in [Table 3]. The maximum value of each section was used as the population density of the transportation route in consideration of the population subject to exposure in case of an accident. Recent data, specified as information standard, was used as the statistics used for each transportation section.

2.3 Transportation scenario

This study applied the normal transportation scenario and the transportation accident scenario to the new transportation route to assess each scenario, and the number of accidents per unit distance (collision accident rate) for the number of floating vehicles was applied to access the transportation accident scenario.

3. Result of transportation safety assessment

The collective radiation dose of ordinary citizens and radiation workers (loading and unloading) during normal transportation and transportation accidents was assessed. Also, the expected population around the route and stopover sites and the assessed collective radiation dose were used to calculate the personal radiation doses, and they were compared with the legal standards.

The radiation dose of each subject of exposure during normal transportation and loading/unloading of RI wastes is shown [Table 2]. If the personal radiation dose of each subject is compared with the legal standard, the annual personal radiation dose of vehicle drivers during normal transportation was 1.59% of the legal standard, that of ordinary citizens 0.29%, and radiation workers doing the loading and unloading work 3.70%. It was confirmed that the annual personal doses of all subjects are within the dose limit.

Moreover, the estimated radiation dose was predicted according to the behavior of the radioactive

material leaked from the drum during a collision transportation accident in consideration of accident rates, and the radiation dose of each section was shown in [Table 4].

Table 2. Radiation dose by exposure subject during normal transportation

Subject	Collective dose	Personal radiation dose	Legal standard
Drivers	1.91E-01 mSv	9.55E-02 mSv	6 mSv
Ordinary citizens	9.95E+00 mSv	2.91E-03 mSv	1 mSv
Radiation workers	1.55E+01 mSv	1.85E+00 mSv	50 mSv

The personal radiation dose of each section in consideration of the radiation dose during a collision accident is $5.43\text{E-}19 \sim 8.37\text{E-}17$, and it is clear that it is a very low value compared to the annual dose limit of ordinary citizens, i.e. 1 mSv.

4. Conclusion

In this study, the Radiological Impact Assessment

of the new RI waste land transportation route using expressways and national highways was done for the two transportation scenarios, i.e. the normal transportation scenario and the transportation accident scenario. The radiation doses were lower than the legal standards in both scenarios.

If the RI wastes and radioactive wastes are transported using the new land transportation route, proposed in this study, it is believed that assessment that reflects radiation shielding and the nuclide inventory of actual radioactive wastes must be conducted.

REFERENCES

- [1] M. H. Seo, S. W. Hong and J. B. Park, "Radiological Impact Assessment for the Domestic On-road Transportation of Radioactive Isotope Wastes", JNFCWT vol 14, No.3, pp279-287, September 2016.
- [2] 2017, Traffic Accident Analysis System (TAAS)
- [3] Korean Statistical Information Service (KOSIS), Available from: <http://kosis.kr/index/index.do>.

Table 3. Population and traffic data by section

Section number	Starting and End Points of the Sections	Distance Of section (km)	Adapted Population Density [people/km ²]	Daily vehicle accident occurrence [Acc/day]	Daily traffic [Car/day]	Vehicle accident rate [Occurrence/km Car]
1	Bukdaejeon IC ~ Hoedeok JC	15.64	2,866	2.47E-02	74,643	6.12E-09
2	Hoedeok JC ~ Cheongju JC	9.04	(Daedeok-gu)	5.48E-01	119,200	1.11E-08
3	Cheongju JC ~ Boeun IC	29.3	885 (Cheongju-si)	2.74E-03	38,718	2.54E-10
4	Boeun IC ~ Nakdong JC	50.73	82 (Sangju-si)	2.74E-03	38,718	2.54E-10
5	Nakdong JC ~ Gunwi JC	39.82	682 (Gumi-si)	8.22E-03	23,591	3.71E-09
6	Gunwi JC ~ Hwaseon JC	33.77	110 (Yeongcheon-si)	8.22E-03	23,591	3.71E-09
7	Hwaseon JC ~ Pohang IC	40.5	460	1.64E-02	32,954	3.83E-09
8	Pohang IC ~ Nampo Port IC	14.7	(Pohang-si)	1.10E-02	9,157	8.14E-08
9	Nampo Port IC ~ Donggyeongju TG	20.9	196	1.37E-02	17,769	4.38E-09
10	Donggyeongju TG ~ Disposal Facility	7.8	(Gyeongju-si)	2.74E-03	6,778	5.18E-08

Table 4. Personal radiation dose in a collision accident (considering accident rates)

Section number	Inhalation [mSv]	Resuspension [mSv]	Cloud shine [mSv]	Ground shine [mSv]	Total [mSv]
1	1.81E-17	1.51E-19	1.54E-19	1.84E-18	2.03E-17
2	1.90E-17	1.58E-19	1.61E-19	1.93E-18	2.13E-17
3	4.86E-19	4.04E-21	4.12E-21	4.93E-20	5.43E-19
4	8.41E-19	6.99E-21	7.14E-21	8.54E-20	9.41E-19
5	9.64E-18	8.01E-20	8.01E-20	9.79E-19	1.08E-17
6	8.18E-18	6.82E-20	6.95E-20	8.31E-19	9.16E-18
7	1.01E-17	8.42E-20	8.59E-20	1.03E-18	1.13E-17
8	7.81E-17	6.49E-19	6.63E-19	7.93E-18	8.37E-17
9	5.98E-18	4.97E-20	5.08E-20	6.07E-19	6.68E-18
10	2.63E-17	2.19E-19	2.24E-19	2.68E-18	2.95E-17

An Experiment on Pellet Manufacturing Using the High-Volume-Reduction Forming Device Based on the Roll Compaction System

Jong Soon Song, Min Young Jung, and Sang Hyun Lim*

Chosun University, 309, Pilmun-Daero, Dong-gu, Gwangju, Republic of Korea

*1991sanghyun@naver.com

1. Introduction

If powdered radioactive wastes are compacted into high-density pellets of the same size, pores will be formed between particles, and polymers can penetrate them more easily, and even in case of solidifying the wastes by filling the pores with liquid agents, the volume will not increase. Rather, this roll compaction system, which reduces the bulk density of radioactive wastes first and further reduces the volume by improving the filling rate in the drum, can drastically improve the operation of the conventional solidification process, and greatly reduce the cost of disposal. Accordingly, to form particulate fine powder into pellets, the Roll Compaction System was used to make the high-volume-reduction forming device [1]. This study will select the optimal operating standards for the high-volume-reduction forming device to improve the filling rate during solidification, and conduct a preliminary experiment to ensure the soundness of the compression-molded pellets.

2. Experiment

2.1 Experimental materials and equipment

The particle powder in use is Active bentonite sold by company L. Its particle size is $85 \sim 100 \mu\text{m}$. The particle size distribution and the shape of the powder are as shown in Fig. 1.

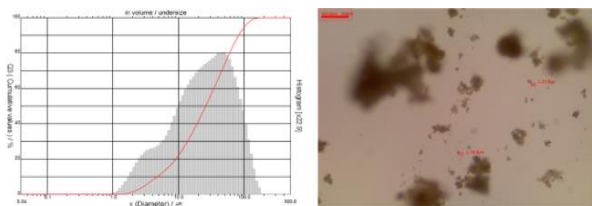


Fig. 1. Particle size distribution (L) and form of powder (R).

To make the particulate fine powder into rectangular pellets, the high-volume-reduction forming device in Fig. 2 was used.

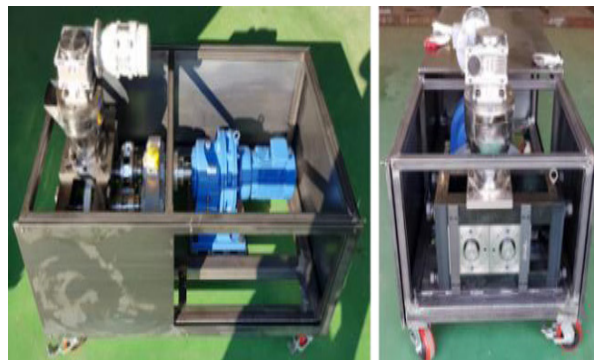


Fig. 2. Pellet forming device – side (L), front (R).

2.2 Experimental method and details

To determine the device operating standards, operating variables, such as the rotational speed of the roll, the powder supply speed, and the forming compression, were changed to check the changes in the mass of the pellets and their status depending on the situation.

2.2.1 Roll Speed. If the rotational speed increases, the amount of the powder injected into the pocket will decrease, and the weight of the pellets cannot but be reduced as shown in Fig. 3. Accordingly, the powder supply speed had to be increased as well to increase the amount of processing per unit time.

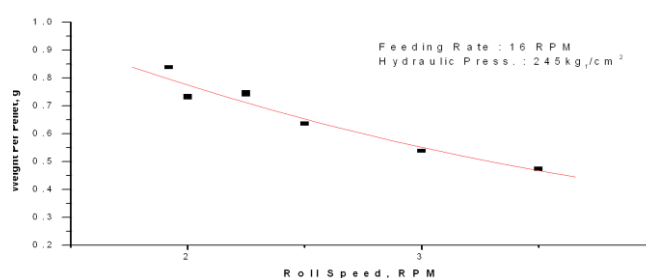


Fig. 3. Changes in the mass of the pellets depending on the variables - Roll Speed.

2.2.2 Feeding rate. Fig. 4 shows that the increased powder supply speed is proportional to the weight of the pellets. Due to the limitations in equipment design, however, if the powder supply speed is 19 rpm or higher, the torque of the motor will not be able to withstand the force, and stop [2].

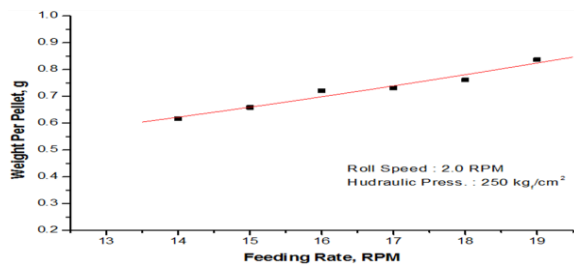


Fig. 4. Changes in the mass of the pellets depending on the variables - Feeding Rate.

2.2.3 Hydraulic Pressure. As the powder supply speed increases, the amount of powder supplied to the pocket will increase. At this time, the hydraulic pressure must be increased so that the force keeping the gap between rolls can be maintained as shown in Fig. 5.

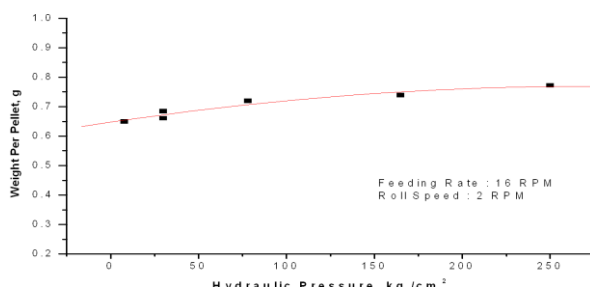


Fig. 5. Changes in the mass of the pellets depending on the variables - Hydraulic Pressure.

3. Result and discussion

The experiment found that forming compression was very important to ensure the soundness of the pellets while increasing the amount of processing of the forming device per unit time and the powder reduction ratio, and Fig. 6 illustrates that as hydraulic pressure increases, the compression state of the pellets and the widening of the gaps will be improved.

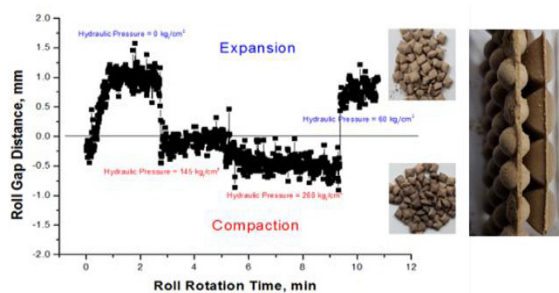


Fig. 6. Gap distance and compaction depending on the compressive force.

As a result, the optimal operating standards of the forming device were selected as roll speed 2 rpm, powder supply speed 14.0 rpm, and hydraulic pressure $245 \text{ kg}_f/\text{cm}^2$. The shape of the pellets made under these conditions is shown in Fig. 7, and the per-unit-time processing amount of the forming device can be expressed by Formula (1), and the

volume reduction ratio of powder pelletization by Formula (2).



Fig. 7. The appearance of the pellets – Tertragonal shape (L), Circular shape (R).

$$\left(\frac{0.5847\text{g}}{\text{Pellet}}\right) * \left(\frac{264\text{Pellets}}{\text{Roll}}\right) * \left(\frac{2\text{RPM}}{\text{min}}\right) * \left(\frac{60\text{min}}{\text{hr}}\right) = 18.374 \text{ Kg/hr} \quad (1)$$

$$\frac{\text{Density of the pellet}(2.00 \text{ g/cm}^3)}{\text{Density of the powder}(0.87 \text{ g/cm}^3)} = 2.30 \quad (2)$$

4. Conclusion

The result of the experiment shows that the optimal operating standards of the high-volume-reduction forming device were applied, and high-quality pellets with a 2.3 times higher volume reduction rate could be made. If additional experiments on the influence of the particle size of the powder and the particle size distribution, and the influence of moisture contents on pellet formation are conducted and the soundness of formed pellets is secured, a high filling rate will be secured during solidification of powdered wastes, and excessive disposal costs and saturation problems will be solved.

ACKNOWLEDGEMENT

This paper is a research project funded by Ministry of Commerce, Industry and Energy, which was conducted with the help of the Korea Institute of Energy Technology Evaluation and Planning. (No. 20171520101630) and supported by the National Research Foundation of Korea (NRF) funded by the Ministry of Science and ICT (The grant number: NRF-2018M2B2B1065636).

REFERENCES

- [1] J.S. S, M.Y. J, S.H. L, et al., "An Experimental Study on the Pelletization of Powdered Radioactive Waste Using the Roll Compaction System", Proc. of KRWS 2018 Spring, pp. 190-1, 2018.
- [2] Johanson, J.R, 1965. A rolling theory for granular solids. J. Appl. Mech. 32, 842-848.
- [3] Solidification Radwaste structural soundness verification of examination, LILW-Operate-Radiation-048, Korea Radioactive Waste Agency.

Structural Design and Stability Simulation of Polymer Sponge for TBP and Dodecane Separation in Liquid Waste

Junhyuck Im^{1),*}, Jongjin Kim¹⁾, Hyungwoo Kim²⁾, and Donghoon Seoung²⁾

¹⁾ Korea Atomic Energy Research Institute, 111, Daedeok-daero 989beon-gil, Yuseong-gu, Daejeon, Republic of Korea

²⁾ Chonnam National University, 77, Yongbong-ro, Buk-gu, Gwangju, Republic of Korea

*jhim@kaeri.re.kr

1. Introduction

As organic liquid waste, one of the hardly disposable radioactive wastes, has not been established for its treatment technology, the waste is temporarily stored in the research organizations or facilities. Although the use of incineration technology is known to be effective for the treatment of organic radioactive wastes, it is not possible for the general public to accept the environmental pollutants such as process corrosion and dioxin generated during the high temperature incineration process.^[1] Alternative oxidation technologies (AOTs) have been developed since the 1980s to improve various incineration processes. Typical incineration alternatives include catalytic chemical decomposition processes, direct chemical decomposition, oxygenation, steam reforming, gas phase reduction, and a method for the oxidation of hydrochloric acid.^[2]

However, despite the long-term research of these treatment methods, about 14 tons of organic radioactive waste, including TBP, dodecane, cutting oil, waste oil, alcohol, and etc., which were generated during the operation of the research institute, were temporarily stored in the Radioactive Waste Disposal Facility (RWTF) at Korea Atomic Energy Research Institute (KAERI). Therefore, in order to treat these radioactive liquid wastes, we have recommended the treatment method using a sponge filter made of

polymer or graphene which have micro- and macro-pores completely different from the conventional treatment methods. If the organic compounds can be separated from the organic radioactive wastes, it is possible to effectively treat the organic radioactive wastes with minimization of further occurring radwastes.

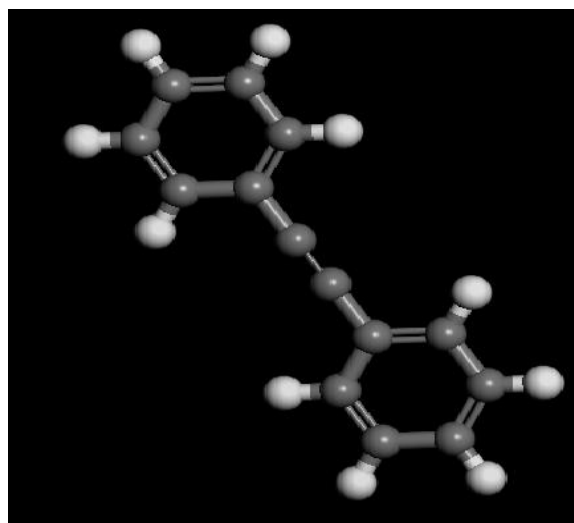


Fig. 1. Molecular structure of designed polymer sponge material.

2. Polymer Sponge Design

To selectively adsorb organic compounds such as TBP and dodecane in liquid wastes, several candidates of polymer sponge materials were selected. Fig. 1 shows one of the selected molecular structure among the polymer sponge candidates. Various factors like large adsorption

capacity for TBP and dodecane compounds, hydrophobicity, structural stability and etc. are considered in this polymer sponge.

3. Structural Simulation

In order to understand the structure and characteristics of synthesized candidates, Density of state (DOS), Bandstructure and Optimized structure were calculated by using Density Functional Theory (DFT) calculation technique. As a result of the calculations, it was found that the most stable form of the polymer sponge composed of honeycomb structure among all the polymer sponge candidates was observed. The geometry optimization of the polymer sponge was conducted due to confirmation of structural stability and geometry energy of about 20 kcal/mol after 40 calculation cycles was obtained (Fig. 2).

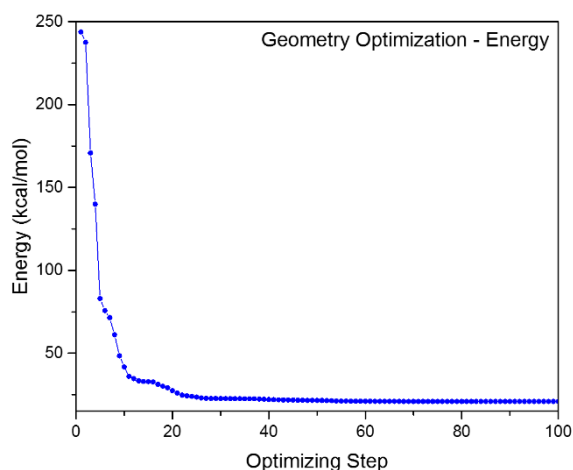


Fig. 2. Geometry energy optimization of designed polymer sponge material.

4. Conclusions

Through this study, a structure model of the polymer sponge is designed and its structural stability can be demonstrated by using DFT calculation. The structure of polymer sponge,

which is expected to be the most stable among other candidates, has a honeycomb structure and it has a geometry energy of 20 kcal/mol which is quite low. The results of this research will provide important information for designing the most efficient and stable polymer sponge materials in the theoretical way, and will be able to transmit the key factors for the treatment of organic liquid wastes when using the polymer sponge materials.

REFERENCES

- [1] K.-W. Lee, H.-B. Yang and S.-H. Na, "Development of Technology of Advanced Oxidation Process (AOP) for Radioactive Organic Wastes", KAERI Research Report (2012).
- [2] D.-Y. Chung and et al., "Development of technologies for treatment of decommissioning wastes", KAERI Research Report (2017).

A Preliminary Experiment on the Disposal Compatibility of the Polymer Solidification Incorporating Pellets

Jong Soon Song, Sang Hyun Lim, and Min Young Jung*
Chosun University, 309, Pilmun-Daero, Dong-gu, Gwangju, Republic of Korea
*1991sanghyun@naver.com

1. Introduction

To reduce the volume of powdered radioactive wastes and solidify them by using the high-volume-reduction forming device based on the Roll Compaction System to pelletize and granulate them, they can be filled with liquid solidifying materials like epoxy to convert them into a disposable shape. But to deliver then to the disposal facility, Waste Acceptance Criteria (WAC) must be satisfied, and to assess the disposal fitness of solidifications, the Waste Acceptance Criteria testing method and judgment criteria are presented[1]. In this study, a preliminary experiment to measure compressive strength will be conducted according to the KS F-2405 test standard to check if the polymer solidification incorporating pellets, introduced above, satisfy the Waste Acceptance Criteria.

2. Experiment

2.1 Preparing samples

The high-volume-reduction forming device was used to pelletize particulate powder into rectangular pellets, and they were incorporated to make the polymer solidification samples. They are 50 mm in diameter, and 100 mm high. The shape of the sample is shown in Fig. 1. Surface processing was done to measure compressive strength, and the details of the samples are shown in Table 1.



Fig. 1. Produced pellets (L) and polymer solidification samples (R).

Table 1. Technical specifications by type – before the experiment

Sample No.	Curing temperature	Sample Size (mm)	Weight(g)			Sample volume (cm ³)
			powder	Epoxy	Total	
A1	Room temperature	H=97.59 D=49.87	215.27	93.7	308.98	190.57
A2	Room temperature	H=97.58 D=49.99	215.54	94.14	309.68	191.44
B1	50℃	H=97.66 D=49.79	215.7	89.55	305.25	177.62
B2	50℃	H=98.59 D=48.13	215.4	91.49	306.89	191.87
C1	75℃	H=98.26 D=49.97	232.8	90.16	322.96	192.66
C2	75℃	H=100.03 D=49.90	242.96	91.2	334.16	195.58

Also, as thermocouples are inserted when temperature is measured, only the diameter and height of the samples used for measuring temperature were changed to 100 mm and 150 mm respectively, but the pellet incorporation ratio and the epoxy resin mixing ratio are the same, i.e. YD-128-epoxy/G1034-hardener/LGE-diluent = 57.5/31/11.5 (Weight %) respectively[2].

2.2 The heat-generating temperature of the solidification depending on the curing temperature

To examine the internal temperature of the solidification during curing, the center and diameter of the samples were trisected, and a total of three thermocouples were installed at 1/3 and 2/3 height from the floor, and the Data Logger was used to measure the temperature, and the forced convection oven, made by Company I, was used to vary the temperature.



Fig. 2. Measuring the heat-generating temperature of the solidification depending on the curing temperature– Room temperature (L), 50℃ atmosphere (R).

2.3 Measuring compressive strength

To measure compressive strength, the DTU-900HC Series (DT&T, Capacity: 50 ton) equipment, owned by the Korea Atomic Energy Research Institute was used. As illustrated in Fig. 3, the curing temperature was varied, and the compressive strength of the 3 manufactured samples was measured.

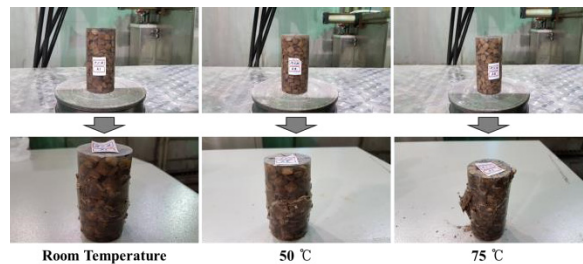


Fig. 3. Measuring the compressive strength of the solidification.

3. Results and discussion

The result of measuring the heat-generating temperature of the solidification by the curing temperature showed that as the ambient temperature rises, curing is accelerated, and as the difference between the ambient temperature and the curing temperature is small, the polymer solidification did not have any crack. Compared to the data in Fig. 4-5, it can be inferred that the curing time at 50 °C is 1/2 shorter than the curing time at room temperature, and accordingly it can be said that the curing at 50 °C is more advantageous in terms of working time.

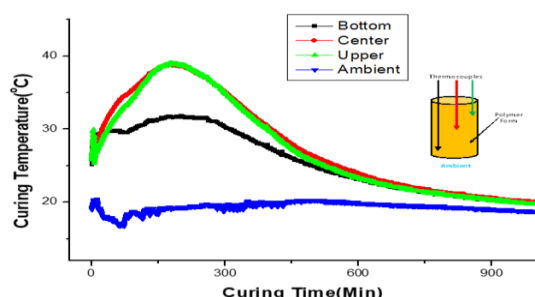


Fig. 4. The heat-generating temperature data by temperature – Room temperature.

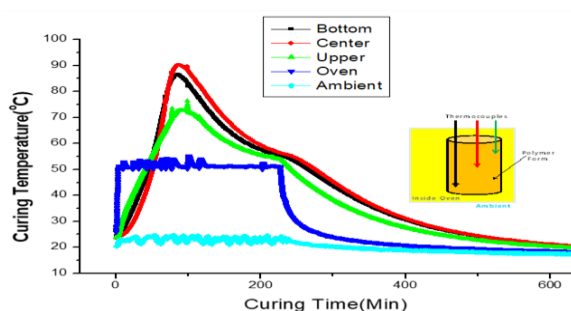


Fig. 5. The heat-generating temperature data by temperature –50 °C atmosphere.

Also, in the compressive strength measurement test, the failure mode showed a typical rigid type. The compressive strength was 200 kg_f/cm^2 or greater regardless of the curing temperature, and the measurement result at 50 °C was most excellent, and the details are shown in Table 2 and Fig. 6.

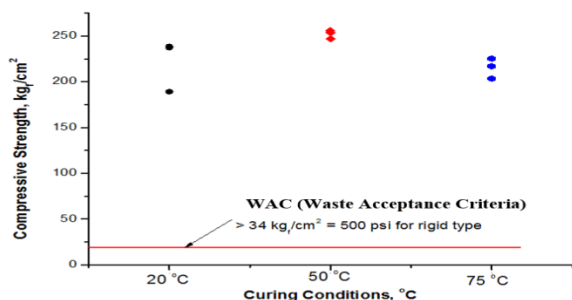


Fig. 6. Compressive strength of the solidification depending on the curing temperature.

Table 2. Technical specifications by type – after the experiment

Sample No.	Curing temperature	Sample size (mm)			Weight (kg_f)	Compressive strength (kg_f/cm^2)
		Diameter (mm)	Height (mm)	Cross-sectional area (cm^2)		
A1	Room temperature	4.99	9.76	19.53	4,660.71	238.64
B1	50 °C	4.81	9.77	18.19	4,912.69	256.00
C1	75 °C	4.97	9.82	19.61	4,419.97	225.39

4. Conclusion

The result of the preliminary experiment on the disposal suitability of the polymer solidification incorporating pellets far exceeds the Waste Acceptance Criteria ($34 kg_f/cm^2$) through the compressive strength KS F-2405 test standards. Accordingly, if additional experiments are conducted according to the strength depending on the moisture contents of the pellets, the epoxy mixing ratio and the solidification judgment criteria, and shortcomings are improved, it is believed that this technology can be applied to solving the problems of excessive wastes and saturation.

ACKNOWLEDGEMENT

This paper is a research project funded by Ministry of Commerce, Industry and Energy, which was conducted with the help of the Korea Institute of Energy Technology Evaluation and Planning. (No. 20171520101630) and supported by the National Research Foundation of Korea (NRF) funded by the Ministry of Science and ICT (The grant number: NRF-2018M2B2B1065636).

REFERENCES

- [1] M.Y. J, S.H. L, J.S. S, et al., “Development of Treatment Technology of Non-Disposal Radwastes for the Increase of Their Volume at Disposal Site”, Proc. of KRWS 2017 Fall, pp. 171-2, 2017.
- [2] J.S. S, M.Y. J, S.H. L, et al., “An Experimental Study on the Pelletization of Powdered Radioactive Waste Using the Roll Compaction System”, Proc. of KRWS 2018 Spring, pp. 190-1, 2018.
- [3] Radwaste Acceptance Criteria, LILW –Operation-Radiation-028, Korea Radioactive Waste Agency.
- [4] Solidification Radwaste structural soundness verification of examination, LILW-Operate-Radiation-048, Korea Radioactive Waste Agency.

Sampling Design for Defluorination of D-UF₆

Jongjin Kim*, Jeongwook Moon, Yunjeong Hong, Jeong-guk Kim, and Dae-Seok Hong

Korea Atomic Energy Research Institute, 111, Daedeok-daero 989beon-gil, Yuseong-gu, Daejeon, Republic of Korea

*kjj@kaeri.re.kr

1. Introduction

In 1986, as part of securing resources for the PWR fuel localization project, KAERI imported about 200 tons of D-UF₆ (a byproduct of fuel production) after concentrating as free of charge. Some of them were used for research activities

Currently, The D-UF₆ being stored in large cylindrical steel cylinders 48 inches in diameter (48Y type) each holding up to 12.5 tons, totally, 185 tons of D-UF₆ are being stored and managed in the storage building.

KAERI has a plan to deconvert D-UF₆ into a stable compound like U₃O₈ to improve storage safety [1-3]. In domestic, there are no facility that can handle the D-UF₆ in 48Y cylinders and deconvert it. Therefore, the D-UF₆ have to be transported to other countries which have suitable facilities and skills.

In order to transport the D-UF₆ to other countries, and to load the facilities, it is necessary that precious information about chemical composition, enrichments and purity. That is, the sampling process is necessary and it should be performed before transportation to other country.

In this study, the draft design of the sampling equipment and sampling process will be discussed.

2. Design and procedure of D-UF₆ sampling

The sampling equipment will be manufactured at ORANO Cycle which has great technique and

knowhow about the deconversion of UF₆

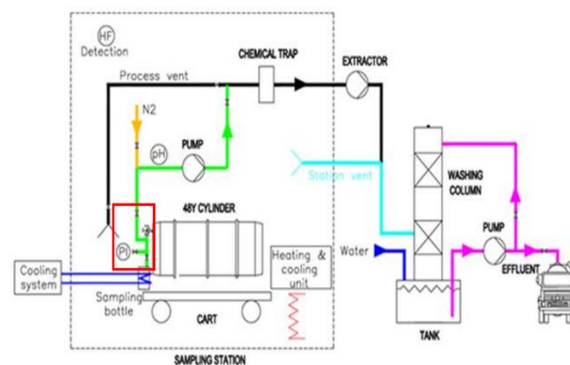


Fig. 1. Schematics of the sampling equipment.

Figure 1. shows the schematics of the sampling equipment consists with chemical traps, heat and cooling system for the cylinder, ventilation system, carts for the cylinder loading/unloading and big shield to protect the UF₆ release.

Figure 2 shows the magnified images of the valves parts (red box in Figure 1.)

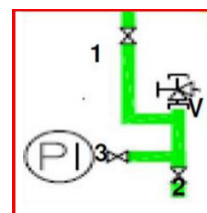


Fig. 2. Magnified images of valves part (red box in Figure 1.).

The sampling procedure is followings.

First, start with all valve is closed. For the valve mechanical test, open V and close V. in order to remove of non-condensable gas, open valve V & 1.

Pumping out until reaching below P_{atm} pressure during limited time to be defined, then close V & 1. Heat the cylinder to make gas condition of UF_6 , around 50°C , the temperature to be define considering safety issues. Then, Open V and 2 to sampling. During the sampling, the sample bottle will be cool down by cooling system in order to UF_6 crystallization. Several time will be needed for the right quantities.

All equipment and relevant works will be set up and be performed inside of current storage building at KAERI. The storage building is designated as a radioactive controlled area, however, it has a license for the nuclear materials to storage and management only. The evaluation of the environmental effects of these radioactive works and accident analysis will be performed in order to acquire relevant license from Nuclear Safety and Security Commission.

3. Summary

KAERI has about 185 tons of D- UF_6 from 1986 and it being stored 16 48Y type cylinders inside of storage building. The D- UF_6 cylinders should be transported to other countries for the deconversion into stable materials such as U_3O_8 in order to enhance the storage safety and disposal.

For the transportation to other country and loading the cylinders to the deconversion facility, the sampling process is essential. The design and procedure for the sampling are now developing, and environmental effect evaluation and risk evaluation works will be performed to acquire license for the sampling.

REFERENCES

- [1] <http://www.world-nuclear.org>.
- [2] <http://www.arenvgroup.com>.

- [3] P.D. Wilson (Ed). The Nuclear Fuel Cycle – From Ore to Wastes, Oxford University Press. Oxford. UK, 1996.

Measurements of Two Dimensional Gamma Ray Distributions of Low and Intermediate Level of Radioactive Wastes Using Fiber-Optic Radiation Sensors

Si Won Song¹⁾, Sang Hun Shin¹⁾, Hyun Young Shin¹⁾, Hyungi Byun¹⁾, Cheol Ho Pyeon²⁾, Bongsoo Lee^{1), *}

¹⁾ Chung-Ang University, 84, Heukseok-ro, Dongjak-gu, Seoul, Republic of Korea

²⁾ Kyoto University, 606-8501, Yoshida-honmachi, Sakyo-ku, Kyoto, JAPAN

*bslee@cau.ac.kr

1. Introduction

Large amounts of low and intermediate level waste (LILW) are generated when nuclear power plants operate. In order to transfer such LILW to the radioactive waste disposal site, it is essential to analyze the radioactivity of radionuclides in the radioactive wastes according to the Nuclear Safety Act (Article 70, Enforcement rule 98) and the Nuclear Safety And Security Commission Notice (No. 201760) [1]. Therefore, the nuclear waste disposal facility should operate the radwaste drum assay system for permanent disposal of LILW drums, and it is important to develop technology and evaluation method to maintain the radwaste drum assay system. In this case, it is very important to monitor possible leaks of radioactive material from the radwaste drum and to reduce the risks of contamination for the operators and for the environment [2].

In this study, we fabricated nine fiber-optic radiation sensors to monitor LILW remotely and in real-time with measuring its dose distribution. The LILW are generated during the operation of the research reactor at Kyoto University Research Reactor Institute.

2. Materials and Methods

The sensing probe consists of inorganic scintillators and plastic optical fibers. Nine LYSO:Ce (cerium-doped lutetium yttrium silicate) inorganic scintillators are arranged in a 3 x 3 array on the square plastic plate with a shape of a rectangular parallelepiped. The size of an inorganic scintillator is $3 \times 3 \times 15 \text{ mm}^3$ and the diameter of a plastic optical fiber is 1.5 mm. The LYSO:Ce inorganic scintillator has a peak wavelength emission of 420 nm, the output is well matched to the peak sensitivity wavelength of multi-pixel photon counter (MPPC) module.

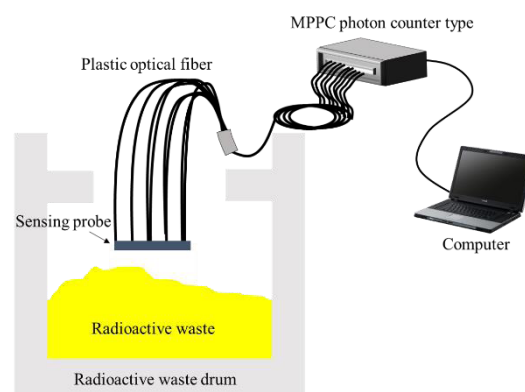


Fig. 1. Experimental setup.

Figure 1 shows an overall experimental setup for measuring dose distribution of LILW with nine fiber-optic radiation sensors. The scintillation light signals generated from the sensing probe are transmitted to the light-measuring device through the 5 m long step-index plastic optical fibers. The light-measuring device used in this experiment is the MPPC module

(C13368-5381, Hamamatsu Photonics). MPPC module has a total of 16 channels, the peak sensitivity wavelength is about 450 nm and measurable wavelengths is from 320 nm to 900 nm.

3. Results

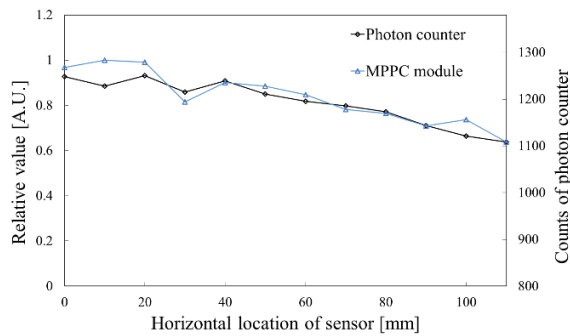


Fig. 2. Gamma ray distributions of LILW using nine fiber-optic radiation sensors.

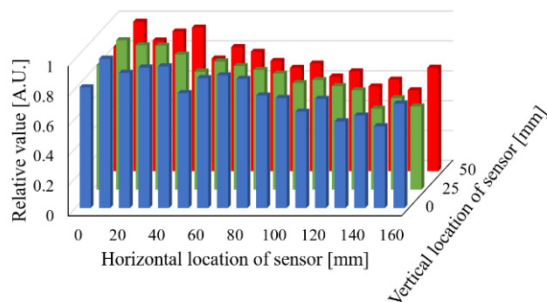


Fig. 3. Two dimensional gamma ray distribution of LILW using nine fiber-optic radiation sensors.

Figure 2 shows Gamma ray distributions of LILW using nine fiber-optic radiation sensors. The sensing probe was horizontally moved by 1 cm to the left and right from the center of the upper entrance of LILW drum. In this experiment, we used two kinds of light measuring devices such as a MPPC and a photon counter (H11890-210, Hamamatsu Photonics). The measured values using a MPPC are averaged and compared with those of a photon counter.

As shown in Fig. 3, two dimensional gamma ray distribution of LILW was obtained by using nine

fiber-optic radiation sensors. It is possible to monitor the leaks of radioactive material from the radwaste drum using an array of fiber-optic radiation sensors remotely and in real-time.

4. Conclusion

In this study, nine fiber-optic radiation sensors were fabricated using LYSO:Ce scintillators, plastic optical fibers and a MPPC module for remote and real-time monitoring of LILW. We measured two dimensional gamma ray dose distribution of LILW in a real radwaste drum. It is expected that the developed fiber-optic radiation sensors can be used to monitor the leaks of radioactive material in the radioactive waste disposal site.

ACKNOWLEDGEMENT

This research has supported by the National Research Foundation of Korea (NRF) grant funded by the Korea government (MSIT) (No. 2017R1A2B2009480, 2016M2B2B1945255) and this research was supported by Basic Science Research Program through the National Research Foundation of Korea (NRF) funded by the Ministry of Education (No. 2018R1D1A1B0704115).

REFERENCES

- [1] K.M. Lee, et al., "Radioactive Wastes Assay Technique & Equipment", Journal of Nuclear Fuel Cycle and Waste Technology, KAERI/TR-2879/2004 (2004).
- [2] C. Cali, et al., "On-line remote monitoring of radioactive waste repositories", EPJ Web of Conference 79, 03007 (2014).

minimum of up to 0.1 μm .

4. Results

Adsorption results of Co and Cs on IER were confirmed by using inductively coupled plasma mass spectrometry (ICP-MS). Compressive strength of produced solidification was tested, which met the acceptance criteria. Fig. 2 shows the change in color after adsorbing Co and Cs to the IER.

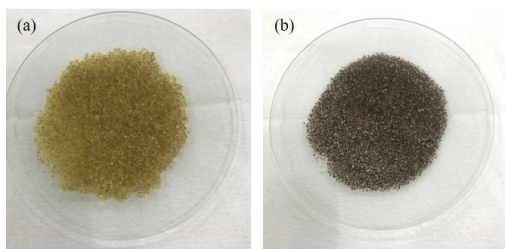


Fig. 2. The pictures of (a) non-treated IER, (b) Co and Cs adsorbed IER.

Table 1. The characteristics of MB-106

Resin	T-46	A-33
Interacting ion	H ⁺	OH ⁻
Ion exchange capacity	>1.8 eq/L (H ⁺)	>1.0 eq/L (OH ⁻)
Average diameter	0.3-1.2 mm (95%)	0.3-1.2 mm (95%)
Water contents	52%	60%
Volume ratio	1	2

In the compressive strength test of solidifications according to the KS-F-2351 test method, the epoxy resin met the acceptance criteria (ASTM C39, D1074, ≥ 0.34 MPa).

A leaching test of Co and Cs is currently in progress according to the ANSI/ANS-16.1 test method.

Fig. 3 shows a schematic diagram of the continuous treatment system of spent resins using mechano-chemistry process, which is the combination of the mechanical volume reduction process using ball mill and solidification process using chemical binders.

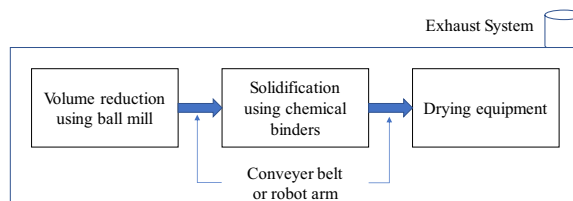


Fig. 3. schematic diagram of continuous mechano-chemistry treatment system.

5. Conclusion

Bisphenol A type epoxy was used to produce a solidified resin. In the compressive strength test, the epoxy resin met the acceptance criteria. A leaching test of Co and Cs is currently in progress.

For the treatment of spent resins, the mechano-chemistry processing system is the first attempt at home and abroad, and will be a way to reduce the treatment cost and to prove the chemically unstable characteristic of spent resins.

ACKNOWLEDGEMENT

This work was supported by the Korea Institute of Energy Technology Evaluation and Planning (KETEP) granted financial resource from the Ministry of Trade, Industry & Energy, and Republic of Korea (No. 20171520000410).

REFERENCES

- [1] Kim.J.M., "Relationship between Compressive Strength and Dynamic Modulus of Elasticity in the Cement Based Solid Product for Consolidating Disposal of Medium-Low Level Radioactive Waste", Journal of the Korea Concrete Institute, 25 (3), 2013, pp.321 ~ 329.
- [2] J. F. Li, J. L. Wang, "Advances in cement solidification technology for waste radioactive ion exchange resins: A review", Hazard. Mater, 135 (1-3), 2006, pp. 443-448.
- [3] I. Plecas, A. Peric, S. Glodic, A. Kostadinovic., "Comparative leaching studies of ⁶⁰Co from spent radioactive ion-exchange resin incorporated in cement" Cement Concrete Res., 25 (2), 1995, pp.314-318.
- [4] Noboru Moriyama, Shigeru Dogiri, Tadahiro Honda, "Solidification of powdered ion exchange resins with polyethylene", Nuclear and chemical waste management, 3, 1982, pp.131-137.

Study on Modification of Solid Radioactive Waste Management System at KAERI

Dong-Ju Lee*, Il-Sik Kang, and Dae-Seok Hong

Korea Atomic Energy Research Institute, 111, Daedeok-daero 989beon-gil, Yuseong-gu, Daejeon, Republic of Korea

*dongju15@kaeri.re.kr

1. Introduction

The Operational Radwaste Control Team at Korea Atomic Energy Research Institute (KAERI) manages various types of radioactive wastes generated during the operation of nuclear facilities (nuclear cycle facilities, HANARO, RI production facility, nuclear R & D facilities, etc.) [1]. The radioactive waste from the waste generation department is repackaged at the Radioactive Waste Treatment Facility (RWTF) and a sample representing their generation characteristics is taken. After identifying the concentration of radionuclide using the representative samples and reviewing the waste characteristics, wastes meeting waste acceptance criteria will be delivered to the final disposal site.

As the safety of radioactive waste management becomes more important, the importance of transparent history management in the treatment and disposal of waste is also increasing.

In this paper, we reviewed the current solid radioactive waste management system for improvement. Based on the technical review, we plan to establish a transparent management system for solid radioactive waste at KAERI.

2. Solid radioactive waste management system

2.1 Procedure of solid radioactive waste management

Presently, generated radioactive waste is classified into major categories (combustible, non-combustible, waste filter, waste resin, etc.) and collected in packaging containers (200 L drum, 100 L plastic pack, 50 L container, etc.) [2]. When collecting waste drum from the generation department, the waste management department requires the list of items for waste management. The radioactive waste management department manages the waste after it is loaded into the radioactive waste storage, and from this time, history management for waste drum begins.

For treatment, waste drum at storage is sent to RWTF. At the RWTF, the waste drum is repacked. It is also included in the history management.

Table 1 shows an example of the list of generated waste drum.

Table 1. List of the Generated Waste Drum

Waste type	Volume (L)	Serial Number	Major Nuclide	Waste Contents
Combustible	200	가-001	Co-60, Cs-137	Vinyl, Paper

2.2 Issues of current solid radioactive waste management system

Through final disposal was begun in 2015, there are still lots of issues for waste characterization as follows.

First, it is difficult to trace the history of repackaged waste by contents and prove the representativeness of the waste samples, because the history management through classification of the waste contents (vinyl, paper, plastic, etc.) is not performed in the waste generation department.

Second, in the case of facilities where radioactive wastes are generated intermittently, it is necessary to store the wastes in the radiation area for a long time to fill a 200 L drum with one type of radioactive waste which may cause problems such as workers' radiation exposure and possibility of waste loss.

Third, the waste management system linked through related departments is not established. As the relevant departments performing waste disposal work manage the history data separately, it is difficult to trace the history of the waste for disposal.

3. Plan for modification of management system

3.1 Introduction of small sub-package

The waste generation department uses small sub-packages to collect wastes with the same generation characteristics. The same generation characteristics refer to wastes generated from same radiation work at a facility and with same contents. That is, the waste generation department collects waste with same generation characteristics in several small packages and packs them in a 200 liter drum. Then record the waste characteristics (weight, contents, nuclides, etc.) so that the traceability of the generated waste is possible.

Figure 1 shows the management items for small sub-package.

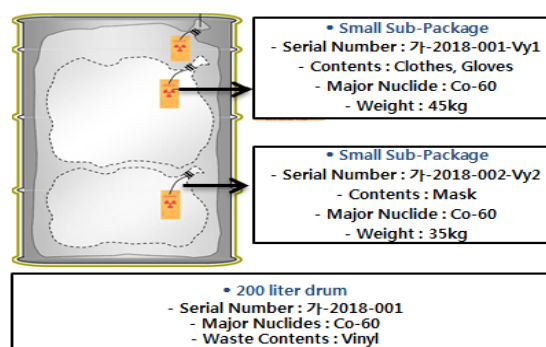


Fig. 1. Example of Management items for Small Sub-Package.

The main difference of this system from current management systems is that serial number and weight management are performed based on a small sub-package.

3.2 Management of mixed waste with different generation characteristics

Radioactive waste generated in small-scale laboratories where wastes are generated intermittently or generated by collecting residual wastes during waste treatment process can be sorted into contents according to the small sub-package waste management system of Section 3.1 and collected in one drum. That is, even if the generation characteristics are different, it can be collected in one drum, and the history can be clearly managed. This will enable the waste management department to perform accurate repacking and representative sampling of mixed waste.

3.3 Integrated history management

While the waste generation department carries out the history management of the wastes based on small sub-package, the waste management department receives the waste data and also performs the waste history management (repackage, waste sampling, etc.) based on 200 liter drum. Based on the collected representative samples and history information, the radiochemical analysis department analyzes the radiological characteristics of each drum. In this process, data on waste characteristics are managed from generation, treatment, analysis and finally to disposal.

Figure 2 shows the example of history data on waste characteristics.

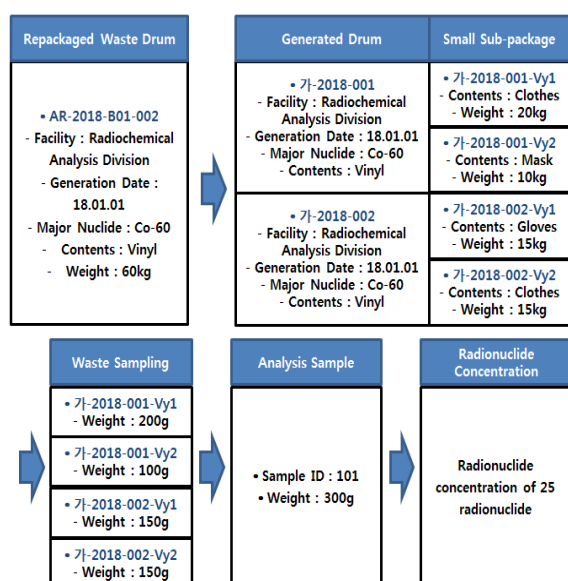


Fig. 2. Example of History data on waste characteristics.

4. Conclusion

In this paper, we reviewed the plan to modify the management system of solid radioactive waste at KAERI. The effects of the modified radioactive waste management system are as follows.

First, it can shorten the waste packaging period at the generation site. Waste generation department will collect the waste with the same generation characteristics in units of small sub-packages and deliver the packaged drums to the waste management department immediately. Through this, it is possible to solve the issues on workers' radiation exposure and loss of waste.

Second, it is easy to review waste generation characteristics. By performing life time waste management from generation to final disposal, it will be possible to accurately record the generation characteristics of each drum and to utilize it to review the waste generation characteristics for preparing final disposal.

Third, transparent history management of the waste becomes possible. The contents and weight of the waste can be finely controlled in units of small sub-packages. Also, repacking history and analysis information also can be reviewed appropriately.

Through this modified waste management system, it is expected that more safe and efficient waste management, treatment and disposal process will be established at KAERI.

REFERENCES

- [1] Korea Atomic Energy Research Institute, "Operation of Radioactive Waste Treatment Facility", KAERI/MR-609 (2017).
- [2] Korea Atomic Energy Research Institute, "Regulations for Radioactive Waste Management", 2-14.24.

Physicochemical Properties of Cation Exchange Resin and Binary Cation Exchange Selectivity

Hyun Kyoung Ahn¹⁾, Yean Ju Lee¹⁾, Jieun An¹⁾, Ki-Bang Sung²⁾, and In Hyoung Rhee^{1),*}

¹⁾ Soonchunhyang University, 22, Soonchunhyang-ro, Sinchang-myeon, Asan-si, Chungcheongnam-do, Republic of Korea

²⁾ Korea Hydro Nuclear Power Co., Ltd. Central Research Institute, 70, Yuseong-daero 1312beon-gil, Yuseong-gu, Daejeon, Republic of Korea

*ihrhee@sch.ac.kr

1. Introduction

Ion exchange resins are being used to remove impurities through industries, such as water treatment, chemicals, and power plants. In the de-ionizer of the secondary system of the nuclear power plant, ion exchange resin is used to remove impurities.

In the secondary system of the nuclear power plant, a pH control agent (amine) is used to reduce the corrosion of metallic components. The pH control agent currently used at industries saturates the ion exchange resin of the secondary system de-base early. Therefore, it is difficult to maintain the pH of the secondary system at a high level. In order to solve this problem, the de-base operation can be changed to an amine saturation operation. However, the impurities trapped in the ion exchange resin may be released.

In this study, the physicochemical properties of cation exchange resins and the ion - exchange selectivity of amine - saturated resins were investigated in order to characterize the amine saturation operation under systemic conditions.

2. Test methods and results

2.1 Physicochemical Properties of Cation Exchange Resin in Nuclear Power Plant Secondary System Condition

The water retention capacity, backwashed and settled density, particle size distribution and total

cation exchange capacity of the cation exchange resin were experimented by the ASTM D2187-17[1] method in the secondary system conditions of the nuclear power plant (Table 1).

Table 1. system conditions

Temperature (°C)	25, 60
Impurities (ppm)	50(Fe, Cu, Cl ⁻)
Deterioration time (day)	5
Stirring speed (rpm)	250

Experimental results showed that water retention capacity, backwashed and settled density, particle size distribution and total cation exchange capacity of cation exchange resin did not affect the deterioration. Table 2 shows the difference in the characteristics of cation exchange resins.

Table 2. Cation Exchange Resin Type (water content, sedimentation density, cation exchange capacity, effective diameter, homogeneity factor)

		A	B	C	D
water retention capacity (%)		34.36	41.57	51.89	36.24
backwashed and settled density (g/ml)		0.866	0.870	0.858	0.814
Cation exchange capacity	meq/g wet	3.32	3.31	2.66	3.41
	meq/g dried	4.16	4.62	4.42	4.28
Particle size distribution	Effective diameter(μm)	602	520	545	429
	Homogeneity coefficient	1.07	1.23	1.24	1.07

2.2 on exchange selectivity of amine saturated resins

Figures 1 to 6 show the results of binary cation

exchange selectivity experiments.

Figure 1 shows the selectivity of cation exchange resin in H-Na. The selectivities of cation exchange resins were $B > C > A > D$.

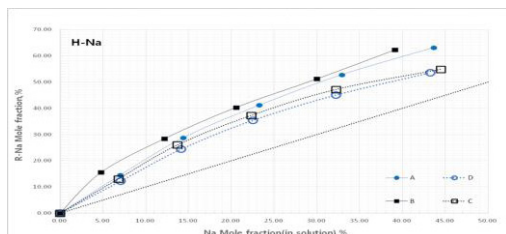


Fig. 1. H-Na Binary cation exchange.

Figure 2 shows the selectivity for ETAH-Na, Figure 3 for H-NH₄, Figure 4 for ETAH-NH₄, Figure 5 for H-ETAH and Figure 6 for ETAH-H. The selectivity varied with mole fraction.

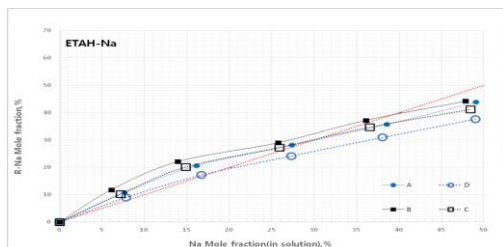


Fig. 2. ETAH-Na Binary cation exchange.

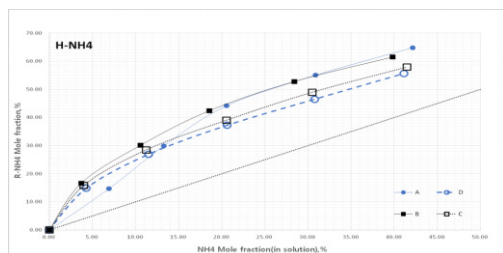


Fig. 3. H-NH₄ Binary cation exchange.

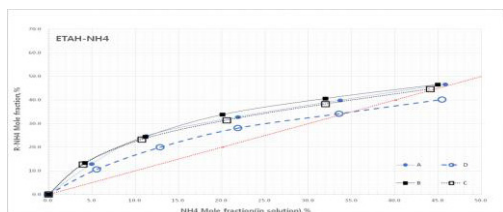


Fig. 4. ETAH-NH₄ Binary cation exchange.

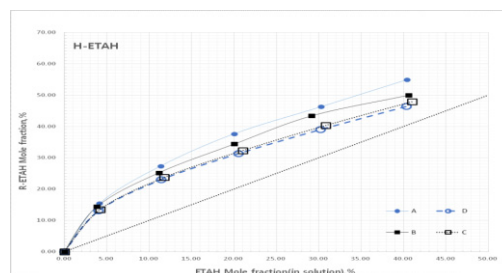


Fig. 5. H-ETAH Binary cation exchange.

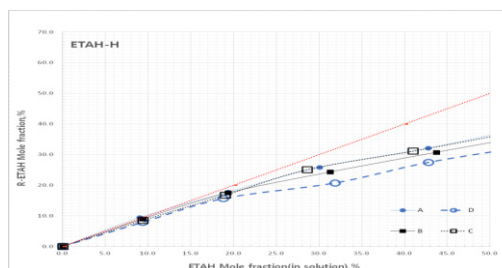


Fig. 6. ETAH-H Binary cation exchange.

3. Conclusion

There were no significant differences in physicochemical properties between resin products in the second system condition of the nuclear power plant.

The selectivity of cation exchange resin varied with the molar fraction, but the selectivities of products B and A were high. Product D showed the lowest selectivity. Productivity of products B and A will be high if we select cation exchange resins.

ACKNOWLEDGEMENT

This work was supported by KOREA HYDRO & NUCLEAR POWER CO., LTD (KHNP).

REFERENCES

- [1] Standard Test Methods and Practices for Evaluating Physical and Chemical Properties of Particulate Ion-Exchange Resins1, ASTM D2187-17.

Investigation of Leakage Trend by Ion Exchange Column Experiment in Secondary System of Nuclear Power Plant

Hyun Kyoung Ahn¹, Yoon Soo Kim¹, Woo Chan Ahn¹, Kyung Hee Lee², In Hyoung Rhee^{1*}

¹Soonchunhyang University, 22, Soonchunhyang-ro, Sinchang-myeon, Asan-si, Chungcheongnam-do, Republic of Korea

²Korea Hydro & Nuclear Power Co., Ltd. Central Research Institute, 70, Yuseong-daero 1312beon-gil, Yuseong-gu, Daejeon, Republic of Korea

*ihrhee@sch.ac.kr

1. Introduction

In the secondary system of the nuclear power plant, a pH control agent (e.g., amine) is being used to reduce the corrosion of components. It is well known to be difficult to maintain the pH of the system just by injecting a pH control agent at high level by means of saturating the ion exchange resin of the secondary system de-ionizer early. In order to solve this issue, it is possible to operate the amine-breaker by operating the desalter. However, when the amine saturation operation is carried out, impurities trapped in the ion exchange resin may be released.

In this study, a cation exchange column experiment was conducted to observe the tendency of leaking impurity concentration by two different cation exchange resins.

2. Test methods and results

2.1 Impurity Leakage Tendency in Amine Saturated Resin

In the ion exchange column experiment [1], two types of column experiments were conducted as illustrated Figures 1 and 2. The experimental conditions of the injection solution are shown in Table 1.

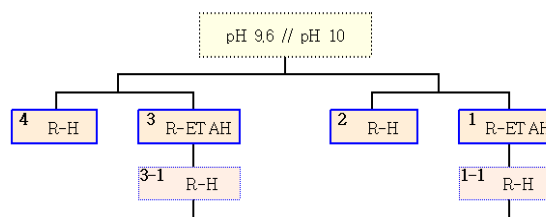


Fig. 1. R-H resin vs. R-ETAH resin(column experiment).

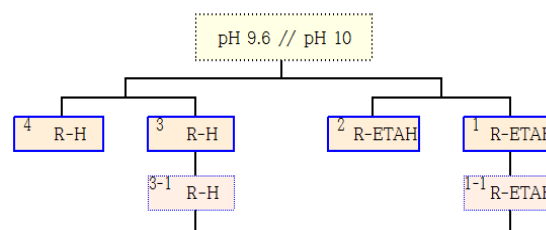


Fig. 2. R-H resin and R-ETAH resin(column experiment).

Table 1. Injection solution

	ETA		NH ₃		NaCl	
	eq/L	ppb	eq/L	ppb	eq/L	ppb
pH 10	2.45 $\times 10^{-4}$	14945	2.90 $\times 10^{-4}$	4,930	0 /3.42 $\times 10^{-4}$ /8.55 $\times 10^{-3}$	0 /20 /500
pH 9.6	5.00 $\times 10^{-5}$	3,050	6.00 $\times 10^{-5}$	1,020	0 /1.71 $\times 10^{-4}$ /1.71 $\times 10^{-3}$	0 /10 /100

The results of the leaching tendency of R-ETAH resin versus R-H resin are shown in Figure 3, indicating that the leakage rate of the cation exchange resin product D was lowest.

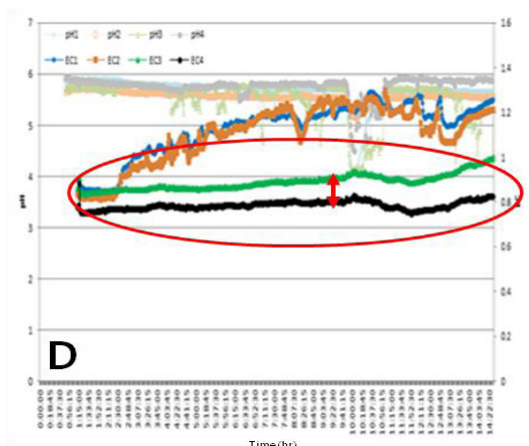


Fig. 3. Leakage trend(Product D).

The results of the leakage tendency of R-H resin product C and R-ETAH resin product D are shown in Figures 4 and 5, respectively. The leaching tendency of R-H resin (pH 10) was on product D, but Leakage tendency of product C was highest.

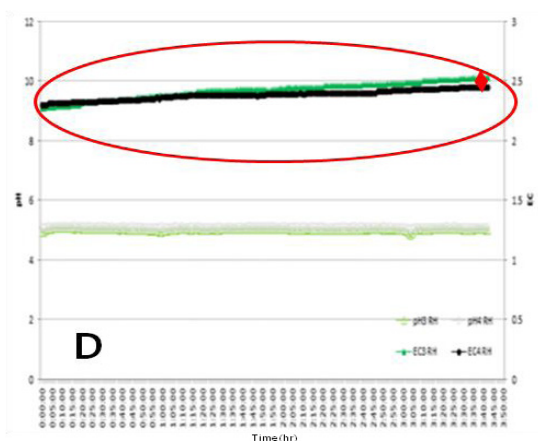


Fig. 4. Leakage trend(pH 10, Product D).

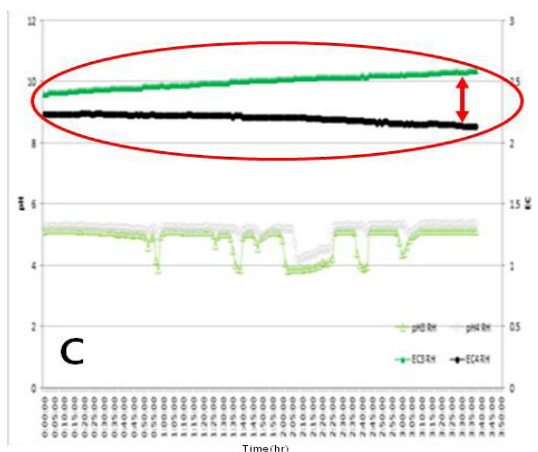


Fig. 5. R-H Leakage trend(pH 10, Product C).

3. Conclusion

Comparison of the leakage tendency of R-ETAH resin versus R-H resin was studied in pH 9.6 and 10(Injection solution conditions Table 1) to evaluate the efficiency of different resin products. It is clearly observed that the leakage tendency of product D is significantly smaller than that of other products. Based on the current test methods and results the product D provides the most efficient quality in the amine saturation operation.

ACKNOWLEDGEMENT

This work was supported by KOREA HYDRO & NUCLEAR POWER CO., LTD (KHNP).

REFERENCES

- [1] Standard Test Methods and Practices for Evaluating Physical and Chemical Properties of Particulate Ion-Exchange Resins1, ASTM D1782-17.

Treatment of Ethanolamine and Hydrazine in CPP Regeneration Wastewater Using Zero-valent Iron Nanoparticle and Hydrogen Peroxide

Jun Hee Lee^{1),*}, Ki-Bang Sung²⁾, Jung Yeul Lee¹⁾, So Yeon Park¹⁾, and Byoung Ho Lee³⁾

¹⁾ Michigan Technology Co., Ltd., B502, 15 Jongga-ro, Jung-gu, Ulsan, Republic of Korea

²⁾ Korea Hydro & Nuclear Power Co., Ltd. Central Research Institute, 70, Yuseong-daero 1312beon-gil, Yuseong-gu, Daejeon, Republic of Korea

³⁾ University of Ulsan, 93, Daehak-ro, Nam-gu, Ulsan, Republic of Korea

*Junhl70@gmail.com

1. Introduction

Ethanolamine is a main substance of wastewater produced from regeneration process of the condensate polishing plant (CPP). Ethanolamine (ETA) is an alkali pH controller in order to sustain pH to prevent metal piping from corrosion in the secondary cooling system within power plants. It is known as refractory by physicochemical and biological treatment process. Furthermore, the wastewater also contains hydrazine, a dissolved oxygen scavenger to prevent pipe corrosion, and is toxic to human health and environment. Best available technology (BAT) to treat ETA has not been yet fully established. This research poster shows complete degradation of ETA and hydrazine by oxidation reaction using nano-particulate zero valent iron (nZVI) and hydrogen peroxide. And a biological treatment process, PPFBR (pseudo plug flow bioreactor), was employed as a post-treatment to down the level of COD and total nitrogen to legal discharge limit.

2. Background

2.1 Characteristics of wastewater from CPP regeneration

The major pollutants in the wastewater are ETA, Hydrazine, and sulfate ion. The concentration of ETA (C_2H_7ON) ranges from 5,000 to 9,000 mg/L which results in elevated COD level, 6,000 to 13,500 mg/L.

ETA is highly stable substance both chemically and biologically. The ratio of COD_{Cr} to COD_{Mn} was more than 7. Degradation of ETA produces high total nitrogen concentration, mainly ammonia.

Hydrazine (N_2H_4) also induces high ammonia concentration after degradation. The total nitrogen concentration of the wastewater ranges from 2,000 to 3,500 mg/L and ammonia 500 to 1,500 mg/L.

Huge amount of sulfuric acid is used to regenerate cation exchange resin resulting in sulfate ion concentration as high as 60,000 mg/L. Extremely low pH requires huge chemicals for neutralization.

2.2 Previous Researches

One of the most effective technique for ETA removal is Fenton oxidation⁽¹⁾ using ferrous salt. Dutta et al (1) reported that as high as 55% of ETA was removed using ferrous iron ($FeSO_4$) and hydrogen peroxide. This most highest removal rate achieved at high initial ETA concentration, 13,000 mg/L as COD, at extreme high chemical dose such as 8,100 mg/L $FeSO_4 \cdot 7H_2O$ and 212 mL of 35% H_2O_2 . However, as the initial ETA concentration decreases, removal rate decreased.

3. Oxidation using nZVI and Peroxide

3.1 ETA Degradation using nZVI

nZVI and hydrogen peroxide was employed to

degrade ETA in this research. 1 g/L of nZVI and 150 mL/L of 35% H_2O_2 was removed ETA from 9814 mg/L to 290 mg/L for 24 hours reaction. Removal rate was 97%. Fig. 1 shows ETA removal by reaction time as COD.

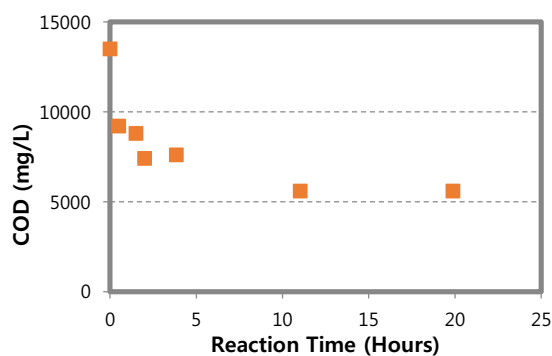


Fig. 1. The effect of reaction time of ETA removal using 1 g/L nZVI and 150 mL/L 35% H_2O_2 .

The effect of dose of hydrogen peroxide was examined from 10 to 150 mL/L, and showed proportional relationship. The optimum dose was identified at 50 mL/L dose in the economical aspect. The effect of nZVI was also tested from 10 mg/L to 1,000 mg/L. At 10 mg/L of nZVI also showed 60% COD removal. Optimum pH was observed at pH 3.

Hydrazine was removed 99.8% from 1520 mg/L to 3.2 mg/L with 10 mg/L of nZVI and 50 mL/L H_2O_2 .

4. Biological Treatment using PPFBR process

Pseudo Plug Flow Bioreactor (PPFBR) is a patented bioreactor designed for advanced fast nitrification. Fig. 2 shows COD and ammonia removal by PPFBR. After oxidation of ETA wastewater, COD and ammonia were 3,800 and 1,720 mg/L, respectively. After 200 hours of retention time COD and ammonia was 90 and 1.7 mg/L, respectively.

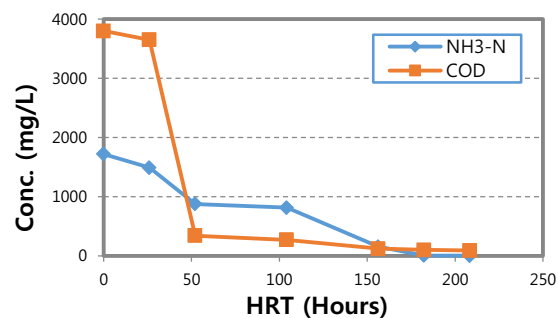


Fig. 2. COD and ammonia removal by Pseudo Plug Flow Bioreactor (PPFBR).

5. Conclusion

Zero-valent iron nano-particulate (nZVI) and hydrogen peroxide effectively degrades ethanolamine. After 97% degradation of ETA and 99.8% degradation of hydrazine by nZVI oxidation, the remaining COD and total nitrogen were effectively degraded by biological treatment to below of legal discharge limit.

ACKNOWLEDGEMENT

This research is funded by KCLOUD of KHNP.

REFERENCES

- [1] Dutta BK., Ariff IF., Chakrabarti, S, and Vione D, "Degradation of Monoethanolamine in Aqueous Solution by Fenton's Reagent with Biological Post-Treatment", Water Air and Soil Pollution, 211, 273-286 (2010).
- [2] Lee SD, Mallampati SR, Lee BH, "Hybrid nano zero-valent iron initiated novel oxidation process for the enhanced removal of ethanolamine from secondary system of nuclear power plant wastewater", Environ Sci Pollut Res Int., 24(21), 17769-17778, 2017.

5분과

제염해체 (Oral)



Critical Factors for Creating Effective Relations With Stakeholders During Decommissioning of Nuclear Facilities

KwanSeong Jeong *, SeungKook Park, DaeSeo Koo, InHye Hahm, SangBum Hong, and BumKyoung Seo
Korea Atomic Energy Research Institute, 111, Daedeok-daero 989beon-gil, Yuseong-gu, Daejeon, Republic of Korea

*ksjeong1@kaeri.re.kr

1. Introduction

Taking into account that the decommissioning is rather complicated and long term process, stakeholders have an important (sometimes governing) influence on it. It is important to balance the impacts of any particular stakeholder, in as much as they can have positive and negative impacts. The key to good stakeholder management is to maximize and develop the positive aspects and minimize the impact of the negative aspects, without undermining any group's confidence in the decommissioning process.

2. Understanding the influence of stakeholder involvement during decommissioning of nuclear facilities

Taking into account that the decommissioning is rather a complicated and long term process, stakeholders have an important (sometimes governing) influence on it. The areas of influence depend on the categories of stakeholders.

Table 1 presents four typical steps in the involvement of stakeholders in a project.

Table 1. Types of stakeholder involvement

Approach	What is meant by this	Aim
Information giving	Where we give information to people, for example, raising awareness of an issue,	To ensure that those who want or need it are in receipt of

	alerting people to opportunities for getting involved, telling people of a decision.	relevant information.
Information gathering	Using survey methods to gather information. Usually used where we need to understand the opinions of a large number of people.	To generate information to inform the decision-making process.
Consultation	Giving people the opportunity to consider and respond to proposals, issues and options that we have developed.	To generate clearer understanding of people's concerns and opinions
Dialogue	Where we bring smaller numbers of key stakeholders together to discuss and deliberate together with us, before decisions are made.	To create opportunities to build shared understanding and agreement

3. Critical success factors for creating effective relations with stakeholders during decommissioning of nuclear facilities

Critical success factors for creating effective stakeholder relations are organizational readiness, planning, stakeholder relations and communications, openness and transparency, developing effective process, and evaluation.

In decommissioning projects, the primary decision-making criteria are protection of human health and environment, compliance with legal requirements, and costs. Other factors include but are not limited to schedule impacts, local economic impacts, institutional preferences, local social preferences, and environmental.

4. Conclusions

Stakeholder involvement should be an integral part of the management of nuclear facilities/program from their conception through final closure and decommissioning. Regardless of the scope of adjustment, nuclear communication with stakeholders must continue to be implemented even while it is continually adjusted in a disciplined and deliberate manner. The cycle of planning, implementing, evaluating and adjusting can be represented in many ways, such as represented in Fig. 1.



Fig. 1. The learning cycle of stakeholder engagement.

Decisions regarding any type of nuclear facility have typically received considerable attention of the public and other stakeholders. Regardless of the stage in the life cycle of the nuclear program, properly addressing stakeholder needs and concerns improves the probability of program success. Engaging stakeholders as early as possible and with ongoing attention is essential, including helping stakeholders to understand the extent of their involvement and responsibility in decision making processes regarding these nuclear facilities/program.

Continual assessment of the stakeholder involvement program is necessary to ensure that it

continues to achieve its goal and objectives, as well as to determine if these objectives continue to be relevant. Active involvement of stakeholders in evaluation of the program is strongly encouraged

ACKNOWLEDGEMENT

This work was supported by the Nuclear Research and Development Program through the National Research Foundation of Korea funded by the Ministry of Science and ICT.

Design and Experimental Setup for In-situ Underwater Beta Monitoring System

UkJae Lee*, Woo Nyun Choi, and Hee Reyoung Kim

Ulsan National Institute of Science and Technology, 50, UNIST-gil, Eonyang-eup, Ulju-gun, Ulsan, Republic of Korea

*dldnrwp@unist.ac.kr

1. Introduction

Monitoring of groundwater is necessary for decommissioning of nuclear facilities because it contains the beta radioactive nuclides which include tritium. These nuclides must be managed from a health physics standpoint, but it is hard to detect because of its short range. Therefore, it is necessary to have a technique for detecting short range beta nuclides and quickly grasping the degree of contamination.

2. Methods

2.1 Concept of in-situ beta monitoring with scintillator

The detecting system was designed that directly contacts the radiation source with the scintillator for detecting short range beta ray[2]. Based on the design of detection part, detecting time can be reduced due to the increased detection efficiency. Fig. 1 shows schematic diagram for in-situ beta monitoring system.

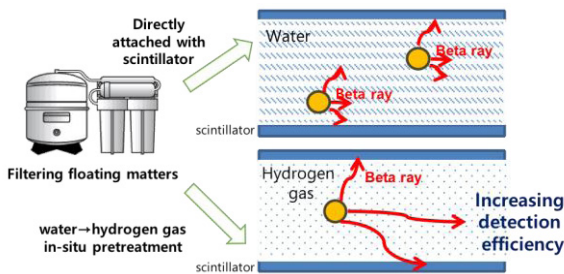


Fig. 1. Schematic diagram for in-situ beta monitoring system.

2.2 Experimental setup

The electronics are designed based on coincidence circuit for the background reduction and noise elimination. The details about each component are described at Fig. 2.

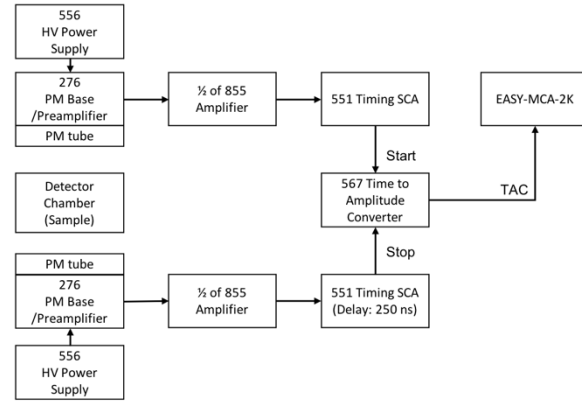


Fig. 2. Experimental setup of coincidence circuit electronics for beta detection.

2.3 Data analysis

Experiments on flow rate and amplification of electronics were carried out. The results were evaluated in relation to MDA (Minimum Detectable Activity). The MDA is defined as equation (1).

$$MDA = \frac{2.71 + 4.65 \times \sqrt{B}}{T \times \epsilon \times 100 \times V_c} \quad (1)$$

Where,

B = Background sum (#)

ϵ = Efficiency (%)

T = Sample measurement time (sec)

V_c = Volume of sample (g/cm^3)

3. Results

The count rate measurement results according to radioactivity concentration were confirmed. The flow rate and the amplification of the electronics system are defined as parameters for the measurement and the results are described in this section.

3.1 Linearity to activity concentration

The linearity test between activity concentration and count rate was performed for checking the

feasibility of the system. The linearity tests are done by the cases for radionuclides of ^3H and ^{90}Sr , amplification of 10, 20, 40. Fig. 3 shows the result for linearity test in case of ^{90}Sr at 10 amplification.

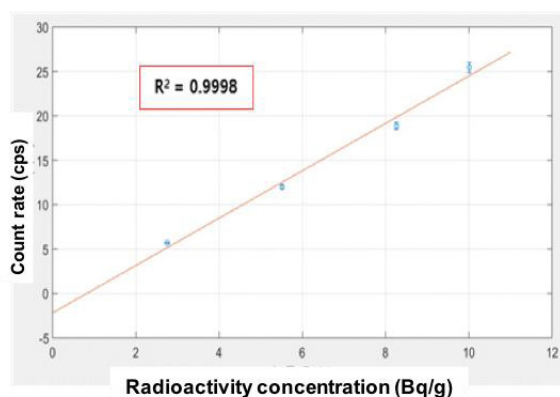


Fig. 3. The result of linearity test for radioactivity concentration to count rate (^{90}Sr , 10 amplification).

In case of ^{90}Sr , the coefficients of determination were 0.9998 at 10 amplification, 0.9992 at 20 amplification and 0.9954 at 40 amplification. In case of ^3H , the coefficients of determination were 0.9992 at 10 amplification, 0.9771 at 20 amplification and 0.9934 at 40 amplification. It was confirmed that all the results showed good accordance between radioactivity concentration and count rate with coefficients of determination which are bigger than 0.9.

3.2 Effect of flow rate

The flow rate was defined as 0, 600, 800, 1000 for the evaluation of the influence of the amount of water sample in the measurement part. The flow rate was varied, and the background counting rate was measured. The results were in Table 1. It was confirmed that the measured value did not change with respect to the change of the flow rate.

Table 1. Background counting rate per flow rate

0 mL/min	600 mL/min	800 mL/min	1,000 mL/min
31.12 ± 0.23 cps	31.12 ± 0.17 cps	31.39 ± 0.12 cps	31.24 ± 0.19 cps

3.3 Effect of amplification

The target MDA was set to 1/10 of the initial activity concentration, and the amplification was

varied to derive the required time for the measurement. The results were described at Fig. 4. It was checked that as the amplification degree increases, the required measurement time decreases.

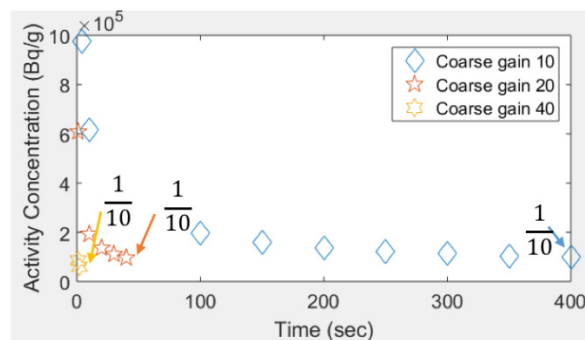


Fig. 4. Time to reach MDA by amplification difference.

4. Conclusion

The monitoring system for in-situ beta in water sample was designed and constructed. It was confirmed that the change of radioactivity concentration had a certain influence on the counting rate and the feasibility was secured to. The process for quantizing minimum detectable activity corresponding to a flow rate and amplification was performed. There was no effect on the flow rate, and it could be expected that the time for reaching the MDA could be reduced by optimizing the amplification and it can be applied to rapid monitoring system.

ACKNOWLEDGEMENT

This work was supported by the National Research Foundation of Korea (NRF) grant funded by the Korea government (Ministry of Science and ICT) NRF-2016M2B2B1945082, NRF-22A20153413555.

REFERENCES

- [1] Stephen W. Duce, Amir H. Mohagheghi, Mark L. Miller, Robert R. Reese, and David R. Miller, "In-situ radiation detection demonstration", WM'00 Conference, February 27-March 2, 2000, Tucson, AZ.
- [2] Thomas Theakston Alton, Stephen David Monk, and David Cheneler, "Beta particle energy spectra shift due to self-attenuation effects in environmental sources", Nuclear Engineering and Technology, 49, 1483-1488 (2017).

Efficiency Analysis for In-situ Beta Measurement System in Groundwater

Woo Nyun Choi*, UkJae Lee, and Hee Reyoung Kim

Ulsan National Institute of Science and Technology, 50, UNIST-gil, Eonyang-eup, Ulju-gun, Ulsan, Republic of Korea

*Chldnsus95@unist.ac.kr

1. Introduction

Monitoring of site groundwater is required before and after decommissioning of nuclear facilities. But the range of low-energy beta radionuclide is short, so the radioactivity is analyzed through a pretreatment process after sample sampling using a liquid scintillation counter which requires much time and labor [1]. So, in-situ measurement techniques for beta radioactive contamination such as ^3H during decommissioning site are required. Design of detecting system that directly contacts the radiation source with the scintillator for detecting short range beta ray is shown in Fig. 1.

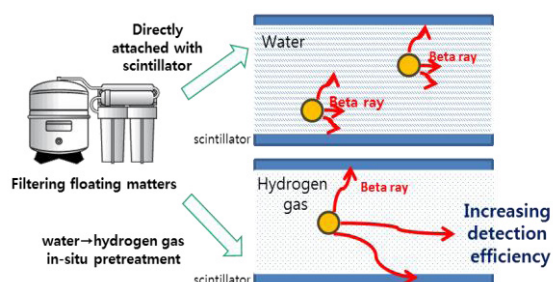


Fig. 1. Concept of in-situ beta monitoring with scintillator.

2. Method

2.1 Concept of radiation monitoring in water

The monitoring system was designed by using plastic scintillator which does not react with water. Also, PMT (Photo Multiplier Tube) based detection signal processing system was constructed. Fig. 2 shows establishment of on-site monitoring system based on time reduction with increasing detection efficiency. 556 HV Power Supply apply power to 276 PM Base/Preamplifier and then the photons amplification from 855 Amplifier. Then the photons are changed to signal by passing 551 Timing SCA & 567 Time to Amplitude Converter, after that we can check the total counts.

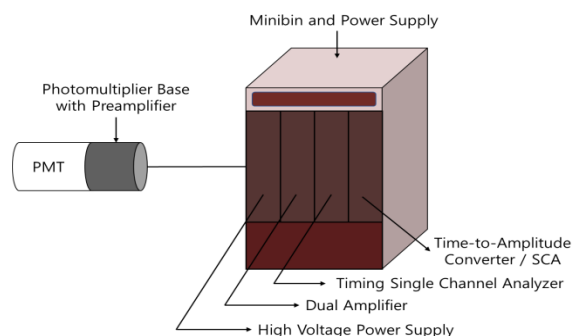


Fig. 2. Components of detecting system.

The major open beta nuclide sources such as ^3H , ^{14}C , ^{32}P and ^{90}Sr were used.

2.2 Simulation for detecting system about thickness of plastic scintillator

To calculate the efficiency of plastic scintillator with different thickness, namely 1 mm and 5 mm the MCNP simulation was used [2]. The simulated geometry for source and scintillator are shown in Fig. 3.

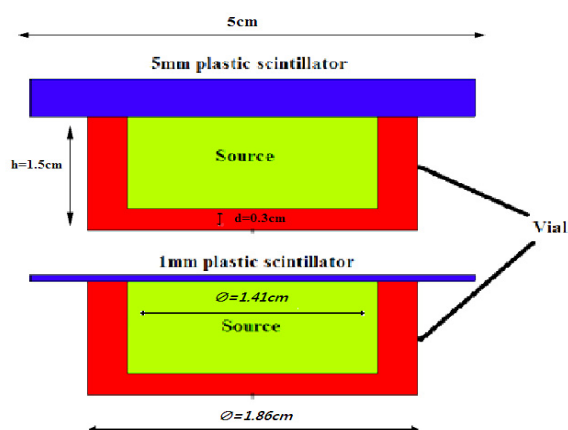


Fig. 3. Simulated geometry for source and scintillator.

2.3 Simulation for detecting system about diameter of scintillator and height of source

Detection efficiency according to diameter (2, 3, 5 cm) of scintillator and height of water sample (5, 10,

30, 50 cm) by nuclide were also calculated by MCNP. 2.4 Simulation for detecting system about thickness of air layer

Detection efficiency according to thickness of air layer (0, 0.025, 0.05, 0.1 and 0.2) was detected by MCNP.

3. Result and Discussion

A good match between the MCNP simulation and experimental results was observed on ^{32}P and ^{90}Sr showing the relative difference of 1.95% and 0.43% for ^{32}P and ^{90}Sr compared to simulation efficiency, respectively. However, beta particles have a short range in water (ex. ^3H range in air is 6 mm and in water is 6 μm), the efficiency for both ^3H and ^{14}C was rather low, and these radionuclides could not be detected or the value of relative difference was calculated little high as shown in Table 1.

Table 3. Efficiency and comparison with simulation results

Nuclides	Net counts (#)	Detection efficiency (%)	Relative difference (%)
^3H	Not available	Not available	Not available
^{14}C	241±85	0.10±0.04	6.54
^{32}P	9,224±112	5.54±0.07	1.95
$^{90}\text{Sr}/^{90}\text{Y}$	21,570±158	4.60±0.03	0.43

The efficiency was not affected by the thickness of the plastic scintillator. That is, the efficiency of 1 mm and 5 mm plastic scintillator was same. The amount of deposition energy is different, but any non-zero energy deposition of the beta particles in the scintillator is counted as one count in the F8 tally calculation.

Detection efficiency calculated according to diameter of scintillator and height of water sample by nuclide. As shown in Fig. 4 which is about ^{14}C , as the height of the water sample increases, the detection efficiency decreases and the influence of the diameter of the scintillator can be ignored. Radionuclides such as ^3H , ^{32}P and ^{90}Sr have similar results like Fig. 4.

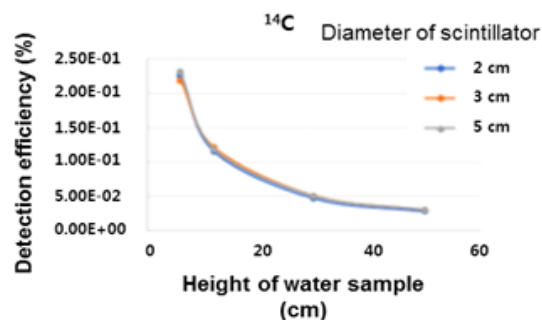


Fig. 4. Detection efficiency according to diameter of scintillator and height of water sample.

As shown in Fig. 5, low energy beta release radionuclides are strongly affected by the thickness of the air layer between the scintillator and the beta nuclide.

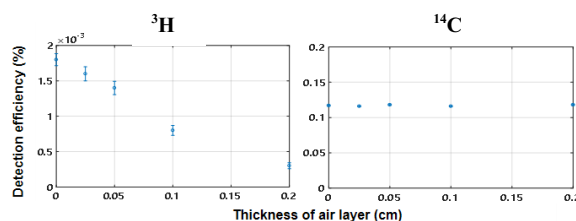


Fig. 5. Detection efficiency according to thickness of air layer.

4. Conclusion

A plastic scintillator could be used in an in-situ system as its efficiency was adequate to meet the task, for applications to monitor major beta-emitting nuclides at a decommissioning site. Further research is needed relating to the efficiency of the detection system, focusing more on radionuclides that emit weak beta particles.

REFERENCES

- [1] S. W. DUCE, et al. "In-situ radiation detection demonstration.", WM'00 Conference, Tucson, AZ, February 27-March 2 (2000).
- [2] T. GOORLEY, et al. "Initial MCNP6 Release Overview." Nuclear Technology, 180, 298-315 (2012).

On-site Analytical Laboratory During Decommissioning: Mobile Lab

Hyuncheol Kim*, Chang-Jong Kim, Mee Jang, Jin-Hyung Lee, and Jong-Myoung Lim

Korea Atomic Energy Research Institute, 111, Daedeok-daero 989beon-gil, Yuseong-gu, Daejeon, Republic of Korea

*hckim3@kaeri.re.kr

1. Introduction

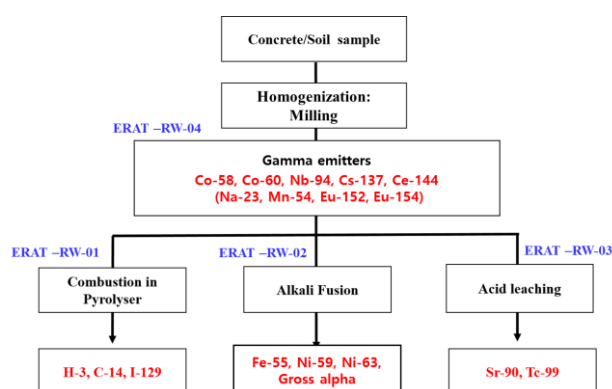
Kori-1 was decided to shut down in June 2017 and is about to be decommissioned. KHNP, the operator of the nuclear power plant, expected that the amount of radioactive wastes (RWs) produced during decommissioning is about 15,000 – 18,000 drum (200 L). The scaling factor could be applied for determining the activity of hard-to-measure (HTM) radionuclides. However, this methodology can lead to overestimate the activity of HTM radionuclides in some cases. Therefore, the direct analysis of HTM radionuclides using chemical separation should be performed.

It creates issues related to the shipment of radioactive samples from the site to the external analytical laboratory. It is complex, expensive and time-consuming, and can sometimes cause a delay in the dismantlement planning. Radiological measurements of decommissioning sample out of site is not good way to manage high throughput of samples in a timely manner. The on-site radiological characterization is a reasonable and cost-effective approach.

In this study, we conceptually designed the mobile lab for the on-site radiological characterization during decommissioning and described the analytical method and instruments which are optimized for the mobile lab.

The main characteristic of the analytical method is the sequential separation of several radionuclides from a single sample. It is resulting in less production of secondary wastes during the analysis process and reducing the analytical time. In the analytical process, lots of waste are generated than expected. All of these wastes are classified as radioactive waste and waiting for another radiological characterization to be transferred to the repository. It leads to increasing the decommissioning cost.

According to the nuclear act, the following 14 radionuclides should be analyzed: 3H, 14C, 60Co, 59Ni, 53Ni, 90Sr, 94Nb, 99Tc, 129I, 137Cs, and gross alpha. We divided them into three groups: volatile radionuclides, activated radionuclides, and fission products. The pretreatment method for each group was applied. Then, radionuclides in each group were properly separated from the sample with the extraction chromatography application.



2. Conceptual design of mobile lab

2.1 Analytical method

2.2 Characteristics of instrument

We installed instruments for the pre-treatment, chemical separation and detectors for alpha, beta, gamma radionuclides in the mobile lab. (Some of

them are made by other company and we made others.) Except some detectors such as liquid scintillation counter and low background alpha/beta counter, we have developed instruments which allow the analysis process to be simple and complete in a short time, such as pyrolyzer, automated separation system, and smart filtration system.

The developed pyrolyzer is designed for extracting the volatile radionuclides from the sample. Compared with the commercialized equipment for the same purpose, it can extract only ^3H and ^{14}C as well as ^{129}I and ^{99}Tc also. The modified combustion tube made it. The automated separation system which is called FIRST (fast and intelligent radionuclide separation technique) allows the user to separate target radionuclide from the sample with less labor and time. The filtration system can be applied for a large or small volume of liquid sample at the same time. It allows the user to produce less wastes compared with typical filtration approach.



Fig. 1. Instruments in the mobile lab (developed by KAERI).

2.3 Site planning

The on-site radiological laboratory is consisted of three containers: 1. Sample preparation lab, 2. Chemical separation lab, 3. Analysis lab. Each lab has a suitable instrument and equipment for its objective. After collection of the representative sample of each drum, it is transferred to the sample preparation lab and being homogenizing. Then, each radionuclide is chemically separated from the homogenized sample in the chemical separation lab. Finally, it is measured with proper detector in the analysis lab, and then the report on it would be produced.



Fig. 2. Schematic diagram of the mobile lab.

3. Conclusion

KAERI is a major player in the fields of research and development in the nuclear chemistry field in Korea. We have developed the on-site analytical laboratory based on mobile lab, in which most of radiological characterization work will be carried out. This mobile lab allows the prompt analysis of decommissioning wastes on the site and leads to reduce the decommissioning cost.

REFERENCES

- [1] Goudeau V., Daniel B., "Mobile laboratories: An innovative and efficient solution for radiological characterization of sites under or after decommissioning", *Journal of Environmental Radioactivity*, in press (2017): doi/10.1016/j.jenvrad.2017.04.010.

Fundamental Study on Underwater Laser Cutting for Dismantling Nuclear Facilities

Jae Sung Shin*, Seong Yong Oh, Hyunmin Park, Taeksoo Kim, Lim Lee, ChinmMan Chung, and Jonghwan Lee
Korea Atomic Energy Research Institute, 111, Daedeok-daero 989beon-gil, Yuseong-gu, Daejeon, Republic of Korea

*jsshin12@kaeri.re.kr

1. Introduction

Laser cutting has many advantages when applied to dismantling of nuclear facilities. Since the laser can be delivered by an optical fiber, it is easy to work at a long distance with only a small cutting head. In addition, laser cutting is also advantageous to control the cutting head because it is a non-contact cutting so that there is little reaction force. Moreover, laser cutting has a narrower kerf width, so the amount of secondary waste is less than that of other cuttings.

To apply laser cutting to nuclear dismantling, it is necessary to be able to effectively cut thick steels. Therefore, many researchers in this field including our group have been developing laser cutting technology [1-7]. In addition, underwater cutting is also required for dismantling nuclear facilities. Therefore, underwater laser cutting technology has been also developed [3].

In this work, fundamental study on underwater laser cutting was performed for dismantling nuclear facilities. A waterproof laser cutting head was developed for use in underwater environment. And cutting tests on thick stainless steel plates were performed with this cutting head.

2. Experimental procedure

Fig. 1 shows the view of the underwater laser cutting experiment. A 6-kW fiber laser (YLS-6000, IPG Photonics) was used as a laser source. The laser

beam was delivered by a process fiber and entered the developed underwater cutting head. A compressed air was used as an assisting gas. The gauge pressure of the assisting gas was set to be ~1 MPa and the gas flow rate was measured to be 880 L/min expressed under ANR (Atmosphère Normale de Référence) condition (20°C, 101.3 kPa, 65% relative humidity).

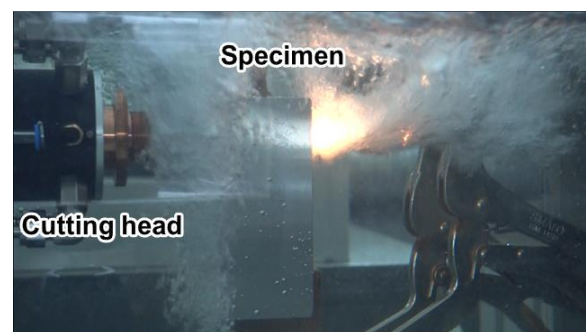


Fig. 1. View of the underwater laser cutting experiment.

50-, 60- mm thick stainless steel plates (SUS304L) were used as specimens. Some specimens were initially mechanically pierced to blow the melt easily near the start point. Cutting processes were started from the center of the hole for pierced specimens and from the side edge for non-pierced specimens. In order to evaluate the cutting performance, the maximum cutting speed of each specimen was measured by changing the cutting speeds by line-to-line.

3. Results and Discussions

When using the pierced specimens, the maximum speeds were measured to be 100 mm/min for 50 mm thickness and 40 mm/min for 60 mm thickness. In these cases, the stand-off distance were set to be 10 mm. When using the non-pierced specimens, the maximum cutting speed for 50 mm thickness was measured to be 80 mm/min. However, the 60 mm thick plates were not able to be cut. To cut the 60 mm thickness, a method of improving cutting near the start point was proposed. With this method, cutting of 60 mm thickness was also done well for the non-pierced specimen.

4. Conclusion

In conclusion, fundamental study on underwater laser cutting was performed for dismantling nuclear facilities. An underwater laser cutting head was developed and the cutting tests were performed. As results of the cutting tests, 50-, 60- mm thick stainless steel plates were effectively cut with this cutting head.

ACKNOWLEDGEMENT

This research was supported by the Nuclear Research and Development Program through the National Research Foundation of Korea (NRF), funded by the Ministry of Science and ICT (grant no.: NRF-2017M2A8A5015146), Republic of Korea.

REFERENCES

[1] K. Tamura, R. Ishigami, and R. Yamagishi, "Laser cutting of thick steel plates and simulated steel components using a 30 kW fiber laser," *Journal of Nuclear Science and Technology*, 51(6), 916-920 (2016).

[2] C. Chagnot, G. de Dinechin, G. Canneau, "Cutting performances with new industrial continuous wave ND:YAG high power lasers: For dismantling of former nuclear workshops, the performances of recently introduced high power continuous wave ND:YAG lasers are assessed," *Nuclear Engineering and Design*, 240, 2604–2613 (2010).

[3] P. A. Hilton, and A. Khan, "Underwater cutting using a 1μm laser source," *Journal of Laser Applications*, 27(3), 032013 (2015).

[4] J. S. Shin, S. Y. Oh, H. Park, C.-M. Chung, S. Seon, T.-S. Kim, L. Lee, B.-S. Choi, and J.-K. Moon, "High-speed fiber laser cutting of thick stainless steel for dismantling tasks," *Optics and Laser Technology*, 94, 244-247 (2017).

[5] J. S. Shin, S. Y. Oh, H. Park, C.-M. Chung, S. Seon, T.-S. Kim, L. Lee, and J. Lee, "Laser cutting of steel plates up to 100 mm in thickness with a 6-kW fiber laser for application to dismantling of nuclear facilities," *Optics and Lasers in Engineering*, 100, 98-104 (2018).

[6] S. Seon, J. S. Shin, S. Y. Oh, H. Park, C.-M. Chung, T.-S. Kim, L. Lee, and J. Lee, "Improvement of cutting performance for thick stainless steel plates by step-like cutting speed increase in high-power fiber laser cutting," *Optics and Laser Technology*, 103, 311-317 (2018).

[7] J. S. Shin, S. Y. Oh, H. Park, C.-M. Chung, S. Seon, T.-S. Kim, L. Lee, and J. Lee, "Cutting performance of thick steel plates up to 150 mm in thickness and large size pipes with a 10-kW fiber laser for dismantling of nuclear facilities," *Annals of Nuclear Energy*, 122, 62-68 (2018).

Digital Mock-up Update Based on 3D Scanned Environmental Information for Nuclear Facility Decommission

Ikjune Kim*, Dongjun Hyun, Jonghwan Lee, and Sungmoon Joo

Korea Atomic Energy Research Institute, 111, Daedeok-daero 989beon-gil, Yuseong-gu, Daejeon, Republic of Korea

* ikjunekim@kaeri.re.kr

1. Introduction

The dismantling of nuclear facilities takes a very long time and is a dangerous procedure. Thus, it should go through a process optimization procedure based on the process simulation [1].

And we are developing a system that performs cutting operations based on the scenarios created in the simulation system. However, existing CAD models and actual sites may differ, so that cutting activity in the scenario which is created based on the existing CAD models can be inapplicable for actual cutting operations.

So we need to acquire the actual site data and apply appropriate feedback to the simulation system to find out if there are changed parts of the existing CAD models from the real sites and then we update the models and dismantling scenarios [2].

As laser scanners become widely used in 3D data acquisition of industrial sites [3], we use a 3D laser scanner to acquire the real site data. The format of feedback data from the scanner is a 3D mesh model.

In this study, we developed the digital mock-up (CAD model) update methodology based on the dismantle simulation system, and tested the system with a sample 3d scan model on our test-bed.

update methodology which is applying transformation matrix to the CAD model calculated from the model alignment procedures.

The source point cloud is aligned to the target point cloud model. The scanned model is composed of point cloud, and the CAD model is defined by mathematical formulas. Therefore, to compare both models, we need to convert the CAD model into a point cloud model, because it's easier than vice versa.

We create a mesh model from the CAD model by tessellation. And sample the points from the tessellated model because tessellated model has boundary points only. So that we can get the point cloud of the CAD model. To enhance the alignment accuracy and shorten the processing time, we segment the scanned point cloud with the bounding box of the part of the CAD model as shown in Fig. 1.

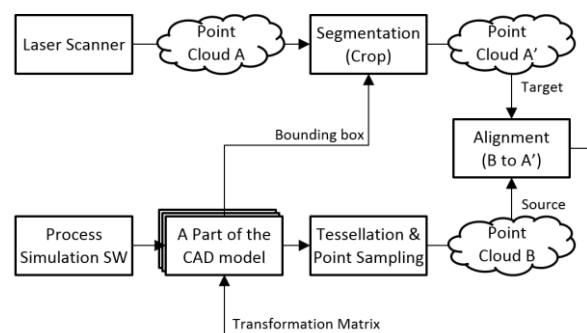


Fig. 1. CAD Model update methodology.

2. Methodology

Fig. 1 is overall scheme of the digital mock-up

We align two models in two steps, first we perform initial alignment to get the initial condition of the Iterative Closest Point (ICP) alignment. And

then we align the model with the fine alignment method (ICP) ICP gives the very fine alignment result, but it's very sensitive to the initial condition of the input models. So we roughly calculate the initial alignment before ICP.

3. Test results

We tested the model update system between the laser scanned 3D mesh model and its original CAD model as shown in Fig. 2. In the figure, we confirm that it is possible to update the CAD model based on the alignment result between the scanned point cloud model and the point cloud which is sampled from the CAD model.

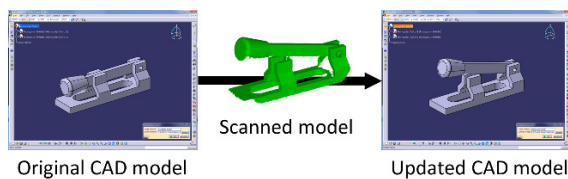


Fig. 2. Update result of sample model.

4. Conclusion

In this study, we developed the digital mock-up update system based on our process simulation software, and we tested the system on our test-bed. So far, we implemented the system for updating the location and orientation of the digital mock-up, In the future we plan to evaluate the CAD model update result numerically and develop the system that updates the shape of CAD model based on acquired point cloud model by the 3D laser scanning.

ACKNOWLEDGEMENT

This work was supported by the nuclear research and

development program through the national research foundation of Korea funded by the Ministry of Science and ICT.

REFERENCES

- [1] I. Kim, B. Choi, D. Hyun, J. Moon, J. Lee, K. Jeong, et al., A framework for a flexible cutting-process simulation of a nuclear facility decommission, *Annals of Nuclear Energy*, vol. 97, pp. 204-207, 2016.
- [2] I. Kim, B. Choi, D. Hyun, J. Lee, K. Jeong, S. Kang, S. Moon, et al., "Environmental Information Feedback Framework for Nuclear Facility Decommission", *Korean Nuclear Society Autumn Meeting*, 2017
- [3] J. Huang and S. You, "Change detection in laser-scanned data of industrial sites", in *Applications of Computer Vision (WACV)*, 2015 IEEE Winter Conference on, 2015, pp. 733-740.

Negative Impact on Radiation Safety of Workers in D&D by Nano-Scale Aerosols from Metal Cutting Process

Sungyeol Choi*, Min-Ho Lee, Wonseok Yang, and Nakkue Chae

Korea Advanced Institute of Science and Technology, 291, Daehak-ro, Yuseong-gu, Daejeon, Republic of Korea

*sungyeolchoi@kaist.ac.kr

1. Introduction

As the lifetime expiration of nuclear power plants (NPPs) constructed at the 1970s approaches, the technology of NPP decommissioning and decontamination (D&D) activities become more important. During the D&D process, the primary step is a massive amount of radioactive material such as steel containment, pipe, and concrete should be cut into small pieces. Making things work, we could use various cutting technics. However, the cutting process can cause undesirable results in generating radioactive aerosols [1].

The inhalation of a radioactive aerosol is deeply concerned about of internal exposure of workers at the D&D facility. The characteristics of aerosol such as density, shape, and aerodynamic diameter are strongly dependent on risk assessment of worker's internal dose. Especially, activity median aerodynamic diameter (AMAD) is a critical factor for accurate internal exposure assessment [2].

Therefore, in this study, we designed the aerosol measurement system at a metal cutting condition. The experimental data of aerosol distribution could be helpful for the risk assessment of internal dose.

2. Methods and Experimental setup

2.1. Automatic metal cutting system

In laboratory experiments, Plasma cutter (Powermax 125, Hypertherm) was used to cut stainless steel plate. The plasma cutter was fixed in the center of the chamber ceiling. The plasma cutting device operated at 75A current with supplying compressed air. The movable table controlled by sub-motor system helped to control the metal cutting speed automatically (Fig.1).

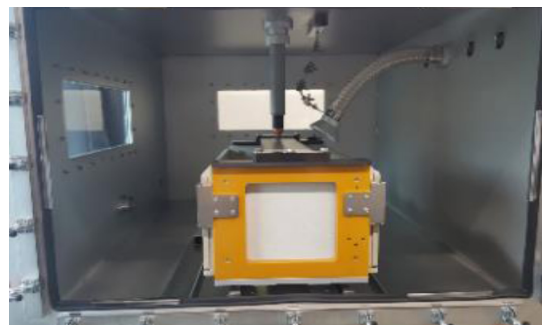


Fig. 1. Plasma cutting device (Powermax 125, Hypertherm) and movable table controlled by sub-motor system.

2.2. Aerosol distribution measurement

We designed the isolated aerosol chamber for collecting generated aerosol particles without leakage outside (Fig. 2). The measurement of the aerosol is performed using the electrical low-pressure impactor (ELPI®, DEKATI). All aerosol particles which have the size from 6 nm up to 10 μm collected at each 14 different size stages.



Fig. 2. The system for aerosol measurement from metal cutting in KAIST Nuclear Fuel Cycle Lab.

3. Results and Discussion

3.1 Internal dose depending on aerodynamic diameter

The activity median aerodynamic diameter (AMAD) which is the half of the radioactivity in the cumulative size distribution. In general, as decreasing aerodynamic diameter, committed effective doses for aerosol inhalation became increasing more [3]. In the

previous study for measurements of aerosol at nuclear workplaces, recommended AMAD is in the region of 5 μm . However, it is the better assessment to use real experimental data [4].

3.2 Number and mass aerodynamic diameter distribution

Fig. 3 shows the number and mass aerodynamic diameter distribution when stainless steel samples were cut using the plasma arc. The peak value in number distribution was observed near 100 nm. On the other hand, the mass of aerosol tended to increase with increasing AMAD.

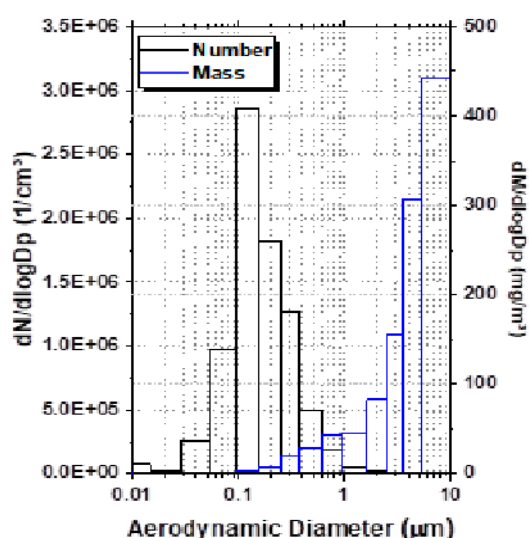


Fig. 3. Counted number and mass aerodynamic diameter distribution of stainless steel cut with plasma cutter.

3.3 Radioactive aerosol captured at the HEPA filter depending on particle size.

The nuclear facilities including the D&D workplace usually used HEPA filters to prevent radioactive aerosol leakage and to keep workers safe. Most of the aerosols do not pass through the filter. However, the aerosol particles around 100 nm in size cannot be completely removed by a filter because of HEPA filters have the lowest filtration efficiency in a 100 nm size region [5].

Therefore, the radiation risks of public and environment are not under consideration when HEPA filter works well for this expectation. However, it is still a risk for the internal exposure of the worker [6].

4. Conclusion

It is significant to fully understand the distribution of radioactive aerosols during the D&D process. The experimental data of aerosol distribution could be helpful for the risk assessment of internal dose. Although the protection system managed the internal dose admirably, dispersion behavior and generation of very small aerosol under 0.1 μm should be considered from a worker's safety standpoint. To put it in a nutshell, nano-scale aerosols from the metal cutting process could have a negative impact on the worker in D&D.

ACKNOWLEDGMENT

This work was financially supported by the National Research Foundation of Korea (NRF) by a grant funded by the Ministry of Science and ICT, Republic of Korea (Grant No. NRF-2017M2A8A4018596).

REFERENCES

- [1] M. Ebadian, S. Dua, and H. Guha, "Size Distribution and Rate of Production of Airborne Particulate Matter Generated During Metal Cutting," (2001).
- [2] M.D. Dorrian, and M. Bailey, "Particle Size Distributions of Radioactive Aerosols Measured in Workplaces," *Radiation protection dosimetry*, 60(2), 119-133 (1995).
- [3] S.Y. Kim, C.K. Choi, Il Park, Y. G. Kim, W. C. Choi, and K. P. Kim, "Assessment of Inhalation Dose Sensitivity by Physicochemical Properties of Airborne Particulates Containing Naturally Occurring Radioactive Materials," *Journal of radiation protection and research*, 40(4), 216-222 (2015).
- [4] ICRP, "Human Respiratory Tract Model for Radiological Protection, Publication 66," ICRP 24(1-3), (1994).
- [5] Kowalski WJ, Bahnfleth WP and Whittam TS, "Filtration of airborne microorganisms: modeling and prediction," *ASHRAE Trans* 105(2), 4-17 (1999).
- [6] Taro Shimada and Tadao Tanaka, "Characterization on the radioactive aerosols dispersed during plasma arc cutting of radioactive metal piping," *J Radioanal Nucl Chem*, 303,1345–1349 (2015).

Ceramicrete Solidification of Concrete Wastes From Nuclear Power Plants Decommissioning

Jae-Young Pyo* and Jong Heo

Pohang University of Science and Technology, 77, Cheongam-ro, Nam-gu, Pohang-si, Gyeongsangbuk-do, Republic of Korea

*vywodud@postech.ac.kr

1. Introduction

Large amount of radioactive concrete wastes are generated during the decommissioning of nuclear power plants. Most of the radionuclides are easily separated from the aggregates and enter mainly into the cement pastes during the heating and grinding process [1]. Powdered wastes composed of cement pastes and sand of less than 1 mm in diameter are generated. The objectives of this study are to solidify these powdered wastes generated from the concrete decontamination process using ceramicrete. The ceramicrete is formed by the acid-base reaction of calcined MgO and KH_2PO_4 in aqueous solution; $\text{MgO} + \text{KH}_2\text{PO}_4 + 5\text{H}_2\text{O} \rightarrow \text{MgKPO}_4 \cdot 6\text{H}_2\text{O}$. The superplasticizer (SP) is added to the starting mixtures to improve the flowability.

2. Experimental Procedures

Concrete wastes were formulated following the composition of the concretes used for nuclear power plants constructed by the Korea Hydro & Nuclear Power Co., Ltd [2]. The simulated concretes were heated at 350°C for 3 hr and was pulverized into powder and sieved to 1 mm. The formulations of ceramicretes are shown in Table 1. The molar ratio of MgO : KH_2PO_4 : H_2O was selected as 1.5 : 1 : 5 based on the preliminary tests. Additional waster was necessary in the specimens with no SP addition due to the increase of viscosity with the addition of

wastes. 1wt.% of boric acid was added to retard the acid-base reaction of MgO and KH_2PO_4 that normally occurs quickly [3]. X-ray diffraction (XRD) patterns were recorded to analyze the formation of the ceramicrete. Compressive strengths were measured using a universal testing machine with specimens 20 mm in diameter and 40 mm in length.

Table 1. Compositions of ceramicretes prepared (wt%)

	W0	W25	W50	W25S	W50S
M/P*	1.5				
W/P**	5.00	5.23	10.78	5.00	5.00
MgO	21.05	15.57	7.72	15.58	10.31
KH_2PO_4	47.38	35.04	17.39	35.06	23.22
H_3BO_3	0.21	0.16	0.08	0.16	0.10
H_2O	31.36	24.24	24.81	23.21	15.37
Waste	0	25.00	50.00	25.00	50.00
SP	0	0	0	1.00	1.00
Total	100	100	100	100	100

*M/P is the molar ratio of MgO to KH_2PO_4 .

**W/P is the molar ratio of H_2O to KH_2PO_4 .

3. Results and Discussion

The compressive strengths of ceramicrete specimens decreased as the amount of wastes in the mixtures increased (Fig. 1). For example, when SP was not added, 28-days strength decreased from 33.25 to 7.61 MPa as waste loading increased from

zero to 50wt.%. On the other hand, the addition of SP resulted in a large increase of the compressive strengths from 7.61 to 28.78 MPa for ceramicrete containing 50wt.% wastes. The high fluidity of the mixtures reduce the pore volume and makes result in the compact ceramicretes.

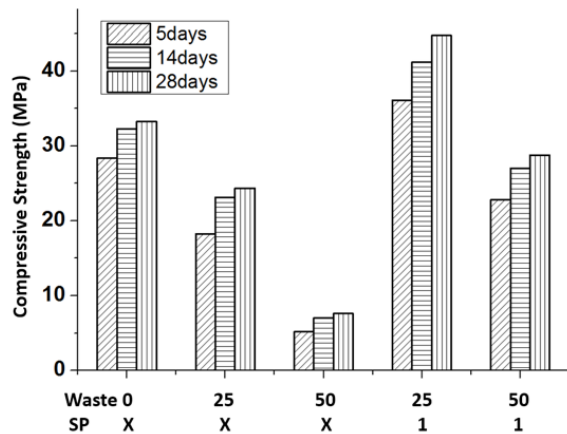


Fig. 1. The compressive strengths of ceramicrete.

The concrete wastes are usually composed of cement pastes and sands therefore, the crystalline phases are mostly calcium silicates and quartz. XRD patterns of ceramicretes containing simulated concrete wastes have peaks related to the $\text{MgKPO}_4 \cdot 6\text{H}_2\text{O}$ phases together with the residual MgO and waste components (Fig. 2).

4. Conclusion

Ceramicretes were developed to solidify the powdered wastes from decontamination of radioactive concretes. Addition of waste decreased the compressive strengths due to the increase of the viscosity. Small amount of superplasticizer (~1.0wt.%) improved the compressive strengths from 7.61 to 28.78 MPa. Formation of the ceramicrete $\text{MgKPO}_4 \cdot 6\text{H}_2\text{O}$ phase was clearly identified even when 50wt.% of the wastes were added.

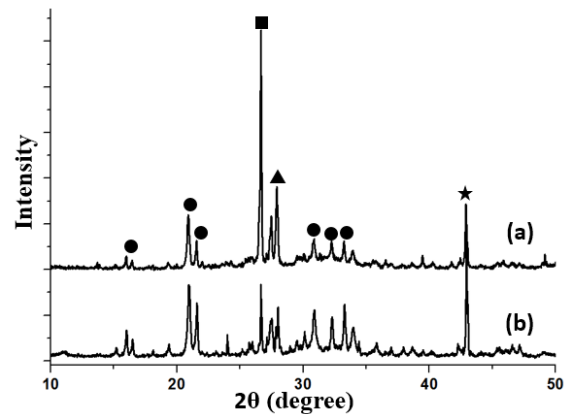


Fig. 2. XRD patterns of the ceramicrete specimens. (a) W50S and (b) W25S; circles: $\text{MgKPO}_4 \cdot 6\text{H}_2\text{O}$, stars: MgO, squares: SiO_2 , triangles: Ca_3SiO_5 .

ACKNOWLEDGEMENT

This work was supported by the National Research Foundation (NRF) grant funded by the Ministry of Science & ICT (NRF-2017M2B2B1072405).

REFERENCES

- [1] B. Min, W. Choi and K. Lee, "Separation of clean aggregates from contaminated concrete waste by thermal and mechanical treatment", ANN. NUCL. ENERGY, 37, 16-21 (2010).
- [2] J. Kim, D. Kim, S. Kang and J. Lee, "Influence of sand to coarse aggregate ratio on the interfacial bond strength of steel fibers in concrete for nuclear power plant", NUCL. ENG. DES. 252, 1-10 (2012).
- [3] A.S. Wagh, Chemically Bonded Phosphate Ceramics. Elsevier, New York (2004).

5분과

제염해체 (Poster)



Resin Treatment Using Fenton Like Process With Cu Catalysis

Wooyong Um* and M.Aamir Hafeez

Pohang University of Science and Technology, 77, Cheongam-ro, Nam-gu, Pohang-si, Gyeongsangbuk-do, Republic of Korea

*wooyongum@postech.ac.kr

1. Introduction

Ion exchange resins are playing a vital role in nuclear industry since the commercialization of Nuclear power Plants. Polystyrene divinyl benzene having sulphonic acid functional group (i.e. Amberlite INR-77 called strongly acidic resin) is used for the removal of cationic contaminants, while Polystyrene divinyl benzene possessing quaternary amine as functional group (Amberlite INR-78 called strongly basic resins) are deployed for the capturing of anionic contaminants from water used in primary heat transport and moderator circuits of nuclear power plants. Once completing their useful life, they are discarded as organic radioactive waste and known as spent ion exchange resins[1, 2]. Among other resin treatment techniques, Fenton/Fenton like oxidation process is superior technique in term of the volume/weight reduction of spent ion exchange resins. In addition, the final product of residues possessing radionuclide can easily be incorporated in stable solid matrix.

The objective of this study was to perform homogeneous Fenton like treatment using Cu as catalyst for reducing the weight of spent nuclear grade mixed Hydrogen/Hydroxide form ion exchange resin, and study the effect of Cu concentration on the efficiency of weight reduction and mineralization of the spent ion exchange resin.

2. Experimental

2.1 Material and Chemicals

All the experiments in this study were conducted under non-radioactive conditions. The IER used in this study is nuclear grade Hydrogen/Hydroxide form mixed bed Gravex GR 3-16 N Resin, product of Graver Technology USA. General physical and chemical properties of resin are shown in Table 1. All reagents including hydrogen peroxide (30% (V/V water), catalyst CuSO₄·5H₂O, H₂SO₄, and Ca (OH)₂ used in this study are equivalent to analytical grade.

2.2 Experimental Setup and Methods

Experiments were performed in a 500 mL, three necked round bottom flask with a magnetic stirrer. The reactor was immersed in oil bath placed on hotplate. Temperature of reaction mixture was kept constant at 90±3°C for all the experiment. Catalysts

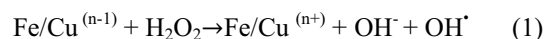
pH was adjusted around 2.80 using dilute H₂SO₄. Fresh Gravex GR 3-16 N 10 (g) was inserted in reactor and hydrogen peroxide and catalyst CuSO₄ were added using dual channel peristaltic pump with flow rate of 0.75 mL/min and 0.375 mL/min, respectively. After 2 hrs the reaction was stopped and the final pH of the solution was recorded.

Table 1. Properties of Each Resin Mixed in GR3-16N

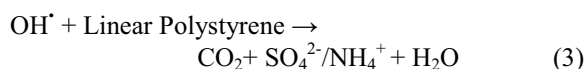
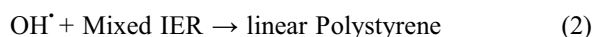
Properties	Cationic (GR2-0NG)	Anionic (GR1-9NG)
Ionic form	H ⁺	OH ⁻
Functional group	-SO ₃ H	-CH ₂ N(CH ₃) ₃ OH
Exchange capacity	2.4 eq/L	1.2 eq/L
Average Particle size	1.188 mm	1.188 mm
Mixing Volume ratio	1	2
Moisture %	36-42%	53-59%
Average Moisture of GR 3-16 N Resin		47%
Metals, Dry resin basis ppm max (Na, Fe, Cu, Pb, Al, Ca, Mg, K, Zn, SiO ₂ =50 ppm)		

2.3 Fenton /Fenton like Process

Use of Fe²⁺ as catalyst and H₂O₂ as oxidant is called Fenton reagent and reaction is known Fenton reaction. However, term Fenton like process is often used when non-ferrous metals such as Cu, Co, Ru, or Mn are used as catalyst. The Fenton process comprises the production of Hydroxyl radical (OH[•]) by the reaction of transition metals (mainly Fe/Cu) with hydrogen peroxide H₂O₂ as oxidant. Production of OH[•] is described in Eq. (1)



Attack of OH[•] On ion exchange resin (IER) initiates through free radical generation mechanism which converts complex structure to simple substrate and finally into CO₂ and H₂O as shown in Eq. (2) & (3).



Both monovalent (Cu⁺) and divalent (Cu²⁺) react with hydrogen peroxide to produce OH[•] Moreover Cu shows better catalytic activities in broad pH range from acidic to neutral conditions.

2.4 Extent of mineralization

The weight of CaCO_3 (mg) produced by reaction between captured gaseous CO_2 and saturated $\text{Ca}(\text{OH})_2$ solution was applied for assessing the amount of mineralization. Final product of $\text{CaCO}_3(\text{s})$ was filtered using $0.45\ \mu\text{m}$ Whatman nylon membrane filter paper of diameter 47 mm and dried at 70°C for 24 hrs inside an oven.

2.5 Weight Reduction of Resin

Weight reduction (%) of Gravex GR 3-16 N Resin was calculated after vacuum filtration and 72 hrs drying at 105°C in vacuum oven. Weight reduction formula is as shown in Eq. (4)

$$\% \text{ Weight Reduction} = \frac{W_0 - W_i}{W_0} * 100 \quad (4)$$

Where W_0 is weight of fresh dry resin corrected using average moisture content; W_i is weight of residue after vacuum oven drying. Weight of catalyst was ignored for weight reduction calculation.

3. Results and Discussion

3.1 Effect of Catalyst concentration on weight Reduction

Different concentrations of $\text{CuSO}_4 \cdot 5\text{H}_2\text{O}$ 30 mM to 400 mM after adjusting their pH at 2.80 were used to study the effect of percentage weight reduction of fresh Gravex GR 3-16 N Resin upon Fenton like treatment. Up to 250 mM catalyst solution directly increases the weight reduction by Fenton like reaction. It indicates that with the increment of Cu ions concentration enhances the production of OH^\cdot (Hydroxyl radical) which ultimately increases degradation of Mixed Resin as shown in Fig 1. However, when the concentration of catalyst solution increased above 250 mM to 400 mM, resin degradation were not increased further, but it started decreasing weight reduction after Fenton Treatment because of scavenging effect produced by Free radicals during reaction.

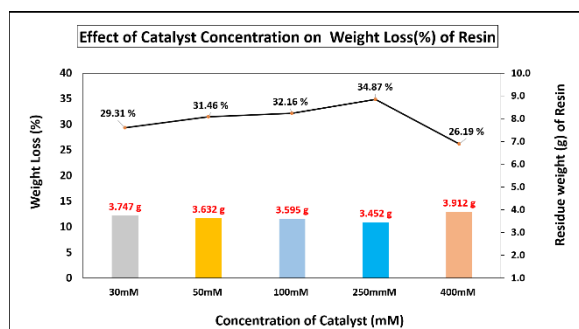


Fig. 1. Effect of Catalyst Concentration on weight reduction of resin.

3.2 Amount of CaCO_3 as indicator for mineralization

Weight (mg) of CaCO_3 precipitated after oxidative degradation during reactions is an indicator of mineralization of organic compound. Results indicates that % weight reduction and amount of CaCO_3 are directly related as shown in Table 2.

Table 2. Weight of CaCO_3 as Indicator of Mineralization

Catalyst CuSO_4 mM	Final pH	CaCO_3 (mg)	Weight Reduction (%)
30	2.94	306	29.31
50	2.88	391	31.46
100	2.92	538	32.16
250	3.01	588	34.87
400	1.92	417	26.19

4. Conclusion

Fenton like decomposition of mixed ion exchange resin was optimized using Cu^{2+} as catalyst. The experimental results indicated that maximum 35% of weight reduction and about 588 mg of CaCO_3 mineralization was achieved by using 250mM $\text{CuSO}_4 \cdot 5\text{H}_2\text{O}$ as catalyst and 30% (v/v water) as oxidant. Final products of such reactions are useful for the development of solidification techniques applied for the management of problematic spent resin wastes.

REFERENCES

- [1] Park, S.-C., et al., "A Study On Adsorption And Desorption Behaviors Of 14c From A Mixed Bed Resin". Nuclear Engineering and Technology, 46(6), 847-856 (2014).
- [2] Wang, J. and Z. Wan, "Treatment and disposal of spent radioactive ion-exchange resins produced in the nuclear industry". Progress in Nuclear Energy, 78, 47-55 (2015).

Three-dimensional MXene ($\text{Ti}_3\text{C}_2\text{T}_x$) Film for Radionuclide Removal From Aqueous Solution

Jiseon Jang and Dae Sung Lee*

Kyungpook National University, 80, Daehak-ro, Buk-gu, Daegu, Republic of Korea

*daesung@knu.ac.kr

Abstract

MXenes are a new family of 2D transition metal carbide nanosheets analogous to graphene (Lv et al., 2017; Sun et al., 2018). Due to the easy availability, hydrophilic behavior, and tunable chemistry of MXenes, their use in applications for environmental pollution remediation such as heavy metal adsorption has recently been explored (Li et al., 2017). In this study, three-dimensional (3D) MXene ($\text{Ti}_3\text{C}_2\text{T}_x$) films with high adsorption capacity, good mechanical strength, and high selectivity for specific radionuclide from aqueous solution were successfully fabricated by a polymeric precursor method using vacuum-assisted filtration. The highest removal efficiency on the films was 99.54%, 95.61%, and 82.79% for Sr^{2+} , Co^{2+} , and Cs^+ , respectively, using a film dosage of 0.06 g/L in the initial radionuclide solution (each radionuclide concentration = 1 mg/L and pH = 7.0). Especially, the adsorption process reached an equilibrium within 30 min. The expanded interlayer spacing of $\text{Ti}_3\text{C}_2\text{T}_x$ sheets in MXene films showed excellent radionuclide selectivity (Cs^+ and/or $\text{Sr}^{2+}/\text{Co}^{2+}$) (Simon, 2017). Besides, the MXene films was not only able to be easily retrieved from an aqueous solution by filtration after decontamination processes, but also to selectively separate desired target radionuclides in the solutions. Therefore, the newly developed MXene ($\text{Ti}_3\text{C}_2\text{T}_x$) films has a great potential for radionuclide removal from aqueous solution.

Keywords: MXene; Radionuclides; Polymer films; Separation; Adsorption

REFERENCES

- [1] Li, J. Yuan, X. Lin, C. Yang, Y. Xu, L. Du, X. Xie, J. Lin, J. Sun, J. (2017), Achieving high pseudocapacitance of 2D titanium carbide (MXene) by cation intercalation and surface modification. *Adv. Energy Mater.*, 7(15), 1602725.
- [2] Lv, G. Wang, J. Shi, Z. Fan, L. (2018), Intercalation and delamination of two-dimensional MXene ($\text{Ti}_3\text{C}_2\text{T}_x$) and application in sodium-ion batteries. *Mater. Lett.*, 219, 45-50.
- [3] Simon, P. (2017), Two-dimensional MXene with controlled interlayer spacing for electrochemical energy storage. *ACS Nano*, 11(3), 2393-2396.
- [4] Sun, S. Liao, C. Hafez, A. M. Zhu, H. Wu, S. (2018), Two-dimensional MXenes for energy storage. *Chem. Eng. J.*, 338, 27-45.

A Study on Decommissioning Strategy for Wolsong-1

Byeong Ik Park*, Eu Tteum Oh, Hyoung Woo Lee, Ji Han Jeon, and Chang Lak Kim
Korea Electric Power Corporation International Nuclear Graduate School, 658-91,
Haemaji-ro Seoseng-myeon Ulju-gun Ulsan, Republic of Korea
*Parkx578@email.kings.ac.kr

1. Introduction

Wolsong-1, which was licensed to extend its operation until 2022, has been permanently shutdown in June 2018. Since the shutdown of Wolsong-1 has been suddenly decided and CANDU has never been fully decommissioned, this study suggests the optimized Decontamination and Decommissioning (D&D) strategy of Wolsong-1.

2. D&D Strategy

2.1 Decommissioning Schedule

Factors considered in Fig. 1 decommissioning schedules are:

- Decommissioning Experience,
- Technical development specialized in CANDU,
- Common & adjacent facilities,
- Site remediation for soil and groundwater,
- Spent fuel management,
- Human resource management,
- Project finance.

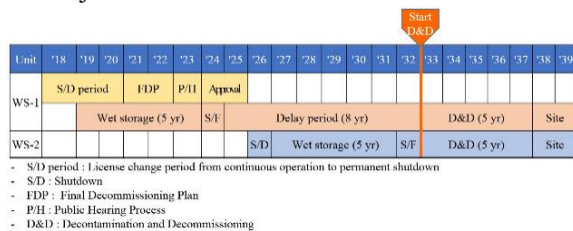


Fig. 1. D&D Schedule for Wolsong-1.

The proposed plan of Wolsong-1 (WS-1) D&D project for primary system is to start in 2032 along with Wolsong-2 (WS-2) after completion of Kori-1 D&D project. [1]

It would be necessary to develop specific technologies for CANDU reactor even though Wolsong-1 will reflect Kori-1 D&D project. Wolsong-1 has many common facilities with Unit 2 that D&D project should be carried out together to increase work efficiency and cost benefit. Due to the characteristics of CANDU reactor, Wolsong site soil and groundwater may have been more contaminated than Kori site, specifically for tritium. Thus, it is

recommended to utilize decay effect and perform site remediation for soil and groundwater for Wolsong-1, 2 together. In this study, spent fuel dry storage facilities are expected to reach its maximum capacity by 2020, which means it is required to construct additional facility in advance for the continuous operation of Unit 2,3, and 4 and removal of spent fuel from Wolsong-1 wet storage. Operational personnel of Wolsong-1 will remain during the transition period (14 yrs.) for the preparation of D&D project. Extending transition period of project will give more time for licensee to finance the D&D project fund.

3. Detailed D&D Preparation Plan

3.1 Detailed Schedule of D&D Preparation

The transition period of Wolsong D&D project will begin in 2019 after permanent shutdown of its operation. (see Fig. 2)

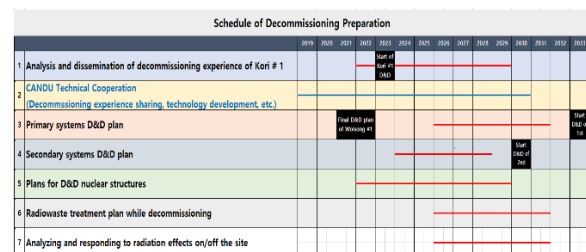


Fig. 2. D&D Prep. Schedule of Wolsong-1.

Delay period starting in 2027(see Fig. 1) is given time due to delay of Wolsong-1 D&D project based on previous consideration.

This detailed schedule consists of decontamination and dismantling of structures and equipment in details, evaluation of environmental radiation effects, and human resource management. Furthermore, lesson learned from Kori-1 D&D project is also implemented to detailed schedule of Wolsong-1 D&D project preparation.

However, CANDU has never been decommissioned, KHNP personnel have no experience in D&D project, and the uncertainties of national policy on Wolsong-1 were considered to establish a detailed schedule.

4. Spent Fuel Management

As shown in Table 1, total storage saturation level of Wolsong site already reached 87.8%. The dry storage reached saturation level of 94.9% and the remaining capacity of unit 1~4 wet storage will reach full saturation by 2020.

Table 1. Amount of Spent Fuel at Wolsong NPP Site [2]

Wolsong Site	Storage	Capacity (Bundles)	Saturation
Wet Storage Facility	Unit 1	28,168	66.4%
	Unit 2	29,768	70.2%
	Unit 3	33,048	77.9%
	Unit 4	34,496	81.3%
Dry Storage Facility	313,200	330,000	94.9%
Total Storage Capacity	438,680	499,632	87.8%

Thus, KHNP has planned to construct additional dry storage facility (MACSTOR) by 2020. [3] In this study, the spent fuel management simulation (see Fig. 3) was performed based on the plan of licensee considering follow assumptions:

- Annual production of Spent fuel per unit = 5,076 bundles (= 20,303 bundles/4 units)
- Additional Capacity = 168,000 bundles (7 modules of MACSTOR)
- Additional storage will be in operation = June 2020
- Maximum Capacity of transfer per quarter = 6,240 bundles

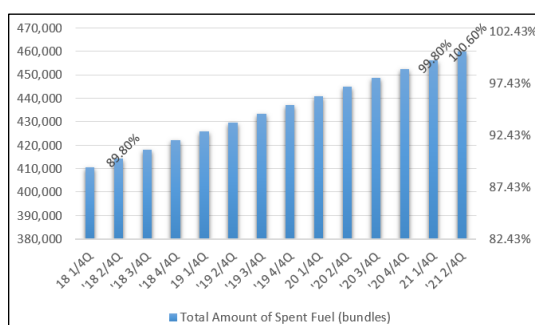


Fig. 3. Prediction of Spent Fuel Saturation without Additional Dry Storage Facility.

According to the simulation, It shows that the expected saturation of total capacity of storage is in 2021 second quarter, which is later than date stated above. It is due to the effect of early shutdown of Wolsong-1 and other maintenance work.

Until June 2020, the spent fuels in wet storage of Wolsong Unit 2, 3, and 4 will be transferred to existing dry storage to delay the saturation. Once the construction of new dry storage is finished, all the

cooled spent fuel will be transferred to newly constructed dry storage facility. The spent fuel in wet storage of Wolsong-1 will be fully removed on second quarter of 2023, which is prior to the actual D&D project. (see Fig. 4)

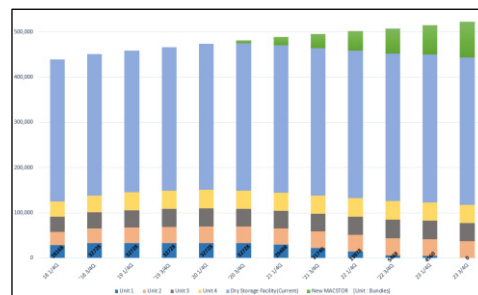


Fig. 4. Spent Fuel Management Using Additional Dry Storage Facility.

5. Conclusion

In this study, Wolsong-1 D&D project is proposed to begin after completion of Kori-1 D&D project, which plans to finish in 2032 as the first NPP D&D project of Korea. Thus, Wolsong-1 D&D project schedule is subject to change depends on Kori-1 D&D project schedule and given delay period. The construction of new dry facility (MACSTOR) is also required within the timetable to proceed Wolsong-1 D&D project. Even though many factors have been already considered, more detailed consideration on D&D strategy would be necessary to succeed in Wolsong-1 D&D project.

ACKNOWLEDGEMENT

This research was supported by the Nuclear Safety Research Program through the Korea Foundation of Nuclear Safety (KOFONS), granted financial resource from the Nuclear Safety and Security Commission (NSSC), Republic of Korea (No.1605008)

REFERENCES

- [1] MOTIE Press Releases, Ceremony Plan for permanent shutdown of Kori-1, Busan: MOTIE Press Releases, 2017.
- [2] Korea Hydro Nuclear Power, "Korea Hydro Nuclear Power Homepage," KHNP, 17 7 2018. http://khnp.co.kr/board/BRD_000179/boardMain.do?mnCd=FN051304. [access: 24/08/2018].
- [3] Y. C. Jung (KHNP), "Status of Spent fuel management," Korean Nuclear Society, Jeju, 2018.

Proposal of Decommissioning Planning for Kori Site

KiHo Cho*, YoungJu Son, EunHee Lee, JaeYeon Jung, and ChangLak Kim

Korea Electric Power Corporation International Nuclear Graduate School, 658-91, Haemaji-ro,

Seoseng-myeon, Ulju-gun, Ulsan, Republic of Korea

*khcho@email.kings.ac.kr

1. Introduction

Recently the decommissioning of nuclear power plants has been accelerated in accordance with the government's policy of phasing out of nuclear energy. In 2017, Kori Unit 1 was permanently suspended for the first time, and lately Wolsong Unit 1 was permanently shut down. With this trend, it is anticipated that the existing nuclear power plants will be permanently suspended from 2020 without any extension of Operating License. In order to dismantle the commercial NPPs, the owner (KHNP in Korea), should submit the final decommissioning plan and related documents within 5 years from the day of shut down to get approval for decommissioning from regulatory body, in accordance with Nuclear Safety Act article 28 and Para.1 of article 41-2 of the Enforcement Decree of NSA(Presidential Decree). In this study, the decommissioning plan for Kori unit 1 of KHNP is analyzed. Then possible alternative is presented. Through this, we propose an effective decommissioning plan for Kori unit 2, 3 and 4, which are expected to shut down in every year.

2. Current Schedule

For decommissioning the nuclear power plant, first of all, after the permanent stop of the power plant, cooling of the spent fuel, dismantling of the secondary system, installation of facilities for the treatment of radioactive waste management, and exporting of the cooled spent fuel must be preceded. Thereafter, dismantling of the primary system and site restoration is carried out. The minimum cooling period of the spent fuel is assumed to be seven years, and the dismantling process and the sequence between each process are considered. Based on this, the expected decommissioning plans for Kori Unit 1

through 4, including Kori 1, which has been permanently suspended for dismantling in 2017, are summarized in Fig. 1.

Unit	'17	'18	'19	'20	'21	'22	'23	'24	'25	'26	'27	'28	'29	'30	'31	'32
Kori1	Cooling							Secondary	RWMS Installation	Exporting	Primary Dismantling				Site Restoration	

Fig. 1. Expected Decommissioning Plan for Kori Unit 1.

According to Fig. 1, termination of site restoration time is expected to be 2032 in Kori Unit 1. Considering the effectiveness of transportation of spent fuel, management of professional manpower, and operation of equipment, we propose modified the Decommissioning Schedule for the effective termination of licensing.

3. Suggestions

A reasonable decommissioning schedule for Kori site was suggested in consideration of management of human resources and business efficiency. Based on several assumptions, a decommissioning plan for the Kori site and the resulting spent fuel transfer scenario have been proposed.

3.1 Assumptions

Above all, there will be no life extension for Kori unit 2, 3 and 4. And the decommissioning process and sequence will be similar to Kori 1. Also the immediate dismantling strategy will be selected. Dry storage facility for Kori site will begin its operation in 2025 and concrete cask (Model : VSC-24) will be used for storage. The capacity of a cask is 24 assemblies. Central interim Storage facility operation starts from 2035. Future projection of spent fuel production was estimated by averaging spent fuel

production from 2010 to 2017.

3.2 Decommissioning schedule for Kori site

For efficient manpower management, each phase of the decommissioning process is designed to be performed gradually for the whole units. In other words, after the completion of the spent fuel exporting of Unit 1, spent fuel exporting for Unit 2 starts. Also it is beneficial in terms of manpower management that the primary and secondary system dismantling are performed after the process of it for previous unit is progressed to some extent. The site restoration is a very important step for successful decommissioning as the last stage of the decommissioning process. So it is suggested to focus on the site restoration of the unit after site restoration of the previous unit is completed fully. Suggested decommissioning plan for Kori site is shown in Fig. 2.

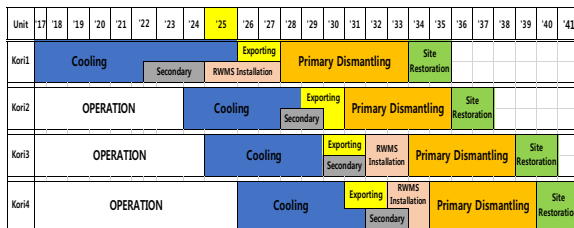


Fig. 2. Proposed Decommissioning Plan.

One of the objectives of this paper is to suggest a desirable spent fuel management scenario for the Kori site. Annual spent fuel production per year and unit is considered as 40 assemblies as estimated by averaging from 2010 to 2017. And the capacity of cask is assumed as 24 bundles. As a result of calculation, some of the spent fuel in Kori unit 2, 3, and 4 should be transferred to Shin Kori unit 1 and 2 before dry storage facility operation. After operation of it, all the spent fuel in Kori 1 should be transferred to dry storage facility just before primary system dismantling. After that, if the spent fuel in Kori 2, 3 and 4 is transferred to the dry storage facility sequentially, suggested scenario would be possible as shown in Fig. 3.

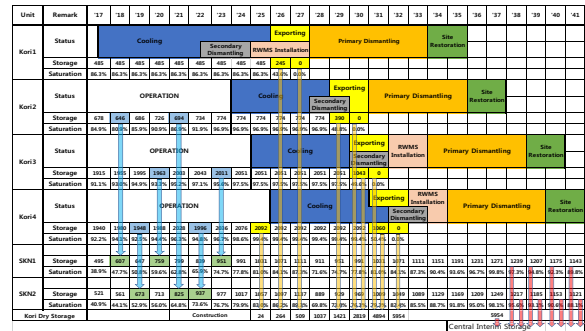


Fig. 3. Proposed Decommissioning Plan with Spent Fuel Transfer.

4. Conclusion

The suggested plan has been scheduled for an effective and successful decommissioning business aimed at 4 nuclear power plants that one (Kori unit 1) is already shut down and the others (Kori unit 2,3 and 4) will be shut down consecutively starting from 2023. Although the calculation of the damaged fuel or appropriate number of transportation cask should be considered more, our proposed decommissioning plan is expected to have significant benefits in terms of cost, management of professional manpower, and business efficiency.

ACKNOWLEDGEMENT

This research was supported by the Nuclear Safety Research Program through the Korea Foundation of Nuclear Safety (KOFONS), granted financial resource from the Nuclear Safety and Security Commission (NSSC), Republic of Korea (No.1605008)

REFERENCES

- [1] KINGS, "Project Report SU 2.1 - Decommissioning Planning," 2017.
- [2] KHNP, "Preparation Program at the Pre-Decommissioning Phase for the D&D of the Kori-1 Nuclear Power Plant_IAEA Conference," 2016.

Cerium Effect on Decontamination of Stainless Steel 304 Metal Oxide

Byung-Seon Choi* and Seon-Byeong Kim

Korea Atomic Energy Research Institute, 111, Daedeok-daero 989beon-gil, Yuseong-gu, Daejeon, Republic of Korea

*bschoi@kaeri.re.kr

1. Introduction

The primary system of the Pressurized Water Reactors (PWR) are operating in a closed cycle at a pressure of about 15 MPa and a temperature of 270~310°C. The main components of the system are consisted of zirconium alloy as fuel cladding material and inconel alloy and other major components are made of stainless steel with excellent corrosion resistance. As the operation of a nuclear power plants were increased, radioactive corrosion products (CRUD) generated by system corrosion attach to the surface of the primary system. It has known the two types of oxides that was impregnated on the system surface another oxides grown inside the metal. It is reported that the ratio of the radioactivity from these two oxides is almost the same.[1,2]

Radioactive corrosion products (CRUD) generated from the reactor coolant system are known to be composed of the magnetite and nickel ferrite (NiFe_2O_4) including various chromium oxides(FeCr_2O_4 , Fe_2CrO_4 , NiCr_2O_4). The composition of these oxide films are similar to that of nickel ferrite and is expressed as a non-stoichiometric mixed oxide of spinel structure $(\text{Fe})_{3-xy}(\text{Ni})_x(\text{Cr})_y\text{O}_4$. [3,4] The major chemical decontamination method that has been developed so far is the reduction and dissolution of Fe oxide film by a reducing agent. The chromium oxide in the corrosion oxide is oxidized to Cr (III) \rightarrow Cr (IV) and the iron oxides dissolve when reduced to Fe (III) \rightarrow Fe (II).

In this study, the cerium effect on chemical decontamination characteristics of the metal oxide film formed on the surface of the SUS 304 material

was investigated to determine the optimal conditions as function of cerium concentration and operating temperature.

2. Evaluation of Decontamination Performance

The experimental apparatus shown in Fig. 1 was fabricated to test the various reaction conditions for the dissolution of SUS 304 corrosion oxide film for the sulfuric acid-cerium decontamination. The apparatus used in this research is composed of a decontamination tank, a decontamination make-up tank, and a regeneration tank. The cylindrical type decontamination tank and the regeneration tank were made of SUS 304 and the inner surfaces were coated with Teflon to prevent corrosion. The SUS 304 corroded specimen used in the test was cut to a size of 15 mm in radius and 1.5 mm in height. The metal oxide of the test specimen were corroded for 72 hours at 45~53 kg/cm^2 under EDTA-hydrazine mixed solution by using autoclave.

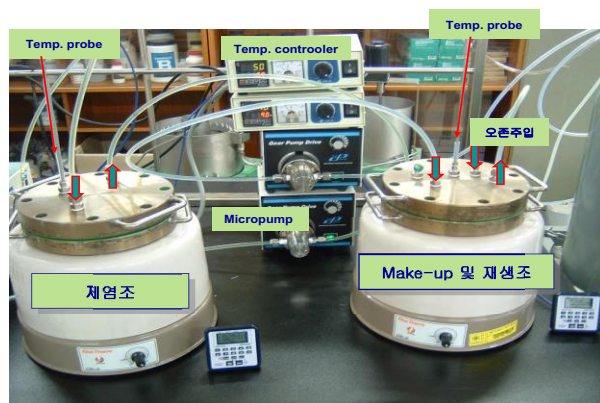


Fig. 1. Decontamination Test Apparatus.

In order to evaluate the effect of Ce(IV)

concentration on the decontamination of SUS 304 corroded oxidation specimens, the weight change of test specimen were measured at the various cerium concentration of 2, 3.5, 5 and 10 mM. As a result, the corrosion oxide film of SUS 304 was not completely removed even after the decontamination time of 6 hours at the Ce (IV) concentration of 2 and 3.5 mM, while it took 6 hours at 5 mM and 4 hours at 10 mM to remove all oxide film (Fig. 2).

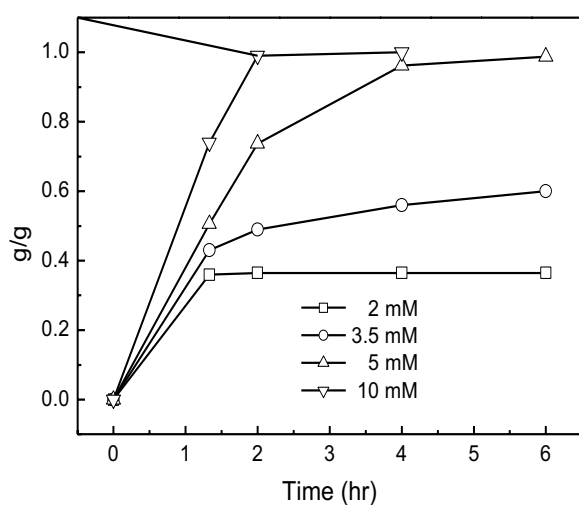


Fig. 2. Effect on the Ce(IV) on oxide removal.

The evaluate the effect of reaction temperature on decontamination were investigated at four different reaction temperatures of 60, 70, 80 and 90°C at 10 mM Ce(IV) concentration. As shown in Fig. 3, the removal rate of was tested to increase at high reaction temperature. In the case of SUS 304, the oxide film were removed within 2 hours. From these results, it is confirmed that the best decontamination efficiency was tested under the Ce (IV) concentration of 10 mM at 60°C.

3. Conclusion

The experimental tests were investigated the decontamination characteristics of the contaminated SUS 304 corrosion oxide in the primary system operating environment. solution. It was evaluated

that sufficient decontamination performance was secured under conditions of Ce (IV) concentration of 10 mM and reaction temperature of 60°C for SUS 304 corrosion oxide film removal.

REFERENCES

- [1] K. Varga, et al., *Electrochimica Acta* 46, pp. 308-379 (2001).
- [2] G. Hirschberg, et al., *J. Nucl. Mater.* 265, p273 (1999).
- [3] J. N, Saas et al., *J. Chem. Phys*, 95(1) (1998).
- [4] J.A. Wharton, et al., *J. Electrochem. Soc.* 147, p.3294 (2000).

Case Study on the Soil Remediation Experience in the U.S.

Hyoung-woo Lee*, Jung-ha Kim, Ju-youll Kim, and Chang-lak Kim

Korea Electric Power Corporation International Nuclear Graduate School, 658-91, Haemaji-ro, Seoseng-myeon, Ulju-gun, Ulsan, Republic of Korea

*hyoungwoo.lee@email.kings.ac.kr

1. Introduction

Kori-1 was permanently shutdown and the other domestic commercial nuclear power plant to be decommissioning near future. Preliminary work of Kori-1 is ongoing to prepare for D&D after the decision of permanent shutdown, June 2017 and site restoration work is scheduled on 2031 after the removal of all structures as a final phase of D&D. Korea doesn't have experience in soil remediation in commercial NPP site so it is important to develop effective remediation strategy reflecting domestic site characteristics and conditions from other cases. This paper would like to review the advanced experience about contaminated soil assessment, remediation technique in the U.S. and suggest some considerations based on site specific condition in Korea.

2. Case Study

2.1 Soil Type

Two types of soil is defined that one is 'Surface soil' which is 0 to 30 cm depth and 'Subsurface soil' represent below 30 cm until aquifer. It is important to distinguish the soil type that they have unique pre-assumptions such as; surface soil is important to the exposure pathway simulation as it is possibly excavated in the future by the activity of residence (such as resident farmer) and cause a expose to them. The other hand, subsurface soil has rare chance to be contaminated due to the depth but if subsurface soil is contaminated then it is regarded as contamination of groundwater which required comprehensive assessment and long-term monitoring.

2.2 Case Study NPP in the U.S.

Total five NPP sites in the U.S. were selected in this paper that four decommissioned sites and one delayed D&D site (see Table 1)

Table 1. Case Study NPP in the U.S.

NPP	Type	Capa. (MWt)	Op./ Shut.	Status	Site use
Big Rock Point (BRP)	BWR	240	1964/ 1997	DECON Completed	ISFSI
Dresden-1	BWR	700	1959/ 1978	SAFSTOR	-
Haddam Neck (HNP)	PWR	1,825	1974/ 1996	DECON Completed	ISFSI

Maine Yankee (MY)	PWR	2,700	1973/ 1996	DECON Completed	ISFSI
Rancho Seco (RSNGS)	PWR	2,772	1974/ 1989	DECON Completed	ISFSI

2.3 Cause and Measures of Soil Contamination

The cause and measure of contaminated soil in each site was found based on historic site assessment result (see Table 2) which is performed to identify the contamination situation in the site for the development of remediation plan.

Table 2. Soil Contamination and Measures

NPP	Area	Main radionuclide and Max. Con. (pCi/g)	Reme. measures	Note
BRP	TRN and CB ¹⁾ base soil	Cs-137 (5.29), Co-60 (0.17), H-3 (32,000 pCi/l)	Total 1,776m ² area excavated in 4m	10.7m of substructure excavated and removal water leads remediation of H-3 in groundwater
HNP	PAR and Reserve Tank Area subsurface soil	Co-60 (207.4), Cs-137 (97.14)	About 11,700m ² area excavated in Max. 12.2m	Groundwater contamination found then perform soil remediation before long-term monitoring
Dresden	Unit 2, 3 CST buried pipe	H-3 (3,200,000 pCi/L)	61m of corroded pipe was replaced and adjacent soil excavated	Groundwater contamination assessment for total 9~10 million pCi/l. result shows no remediation required (only monitoring)
MY	RRA ²⁾	-	Total 3 reserve tank area excavated in Max. 1m	Comprehensive remediation performed to the all RRA area (13 survey unit)
RSNGS	SF pool cooler	Cs-137 (941), Co-60 (6.41)	Buried pipe removal with soil excavation in 2.5m	Soil remediation performed to the several reserve tank area

1) CB : Containment Building

2) RRA : Radiological Restricted Area

Result shows that the major contamination area in this case study is concentrated in the reservoir area and buried pipeline routes in the RCA area and major radionuclides were identified as Co-60, Cs-137 and H-3.

Even though immediate remediation measures were performed to the contaminated soil, repetitive leakages in this area lead to increasing of residual activity and those high concentrate of contaminants in surface soil has been move into the subsurface soil

and groundwater (BRP, HNP and Dresden-1) as well by infiltration and leaching. [1]

In this case, the U.S. regulatory body required long-term monitoring of groundwater after soil remediation and the case of long-term monitoring of groundwater in Dresden site until permanent shutdown of Unit 2,3 shall be considered when site remediation strategy for Kori-1 is established in case of wide range of groundwater contamination is found along the Kori site.

2.4 Contaminated Soil Remediation

Excavation is commonly used in soil remediation work as it is very simple and effective remediation technology in both surface and subsurface soil. It is assumed that extensive excavation was performed to the wide area of every NPP site in this paper so that residual activity can be reduced by removal of contaminants along with the special excavation techniques for specific areas on a case-by-case basis (see Table 3);

Table 3. Special Excavation Techniques [2,3]

NPP	Contaminated Media	Depth	Applied Technology
BRP	Substructure (CB)	10.7 m	1) Slurry wall (side collapse and groundwater penetration)
			2) Pump (stagnant water)
			3) Storage basin (water treatment and discharge)
HNP	Bedrock (PAB)	12.2m	- Hydraulic Hammer (Hoe-Ram)
			- Explosive
			- High flow rate vacuum truck

Both cases were produced the huge amount of excavated soil but the U.S. regulatory body allowed on-site disposal of excavated soil to the very low level contaminated soil with certain procedure so that licensee can use less contaminated soil as a backfill for their site restoration work.

Not all the contaminated soil were exempted but some of highly contaminated soil is disposed as radioactive waste based on regulatory guideline and licensee's technical justification (see Table 4) which provides effective method for the efficient management of radioactive waste in response to the occurrence of large amounts of contaminated soil in US.

Table 4. Licensee's Justification in Dresden Site

Regulatory Body	Licensee (Exelon, Inc)
On-site disposal approval request to the U.S. NRC for the contaminated soil (6,000m ²) that only have 20% of DCGL (U.S. NRC requests environmental effect analysis)	Establish on-site disposal procedure and perform environmental effect analysis (by minimize leakage and groundwater monitoring)

Discharged contaminated liquid containing radioactive material (H-3) to the unauthorized place rather than designated discharge route (U.S. EPA issues violation letter)	Groundwater generated during excavation of soil is discharged after treatment through waste management system, and groundwater is not subject to unauthorized discharge management such as river, stream and lake
--	---

Consideration should be given for the establishment of regulatory standard about on-site disposal of excavated soil in compliance with the domestic waste management system and considering safety impact review result from the residual activity in soil.

3. Conclusion

In this study, soil remediation experience of the five NPP were reviewed in order to suggest some considerations take into account for the site specific condition in Korea. Application of long-term monitoring strategy of groundwater and establishment of on-site disposal guideline of very low level contaminated soil are suggested along with the status about major contaminated area and radionuclides in soil.

ACKNOWLEDGEMENT

This research was supported by the Nuclear Safety Research Program through the Korea Foundation of Nuclear Safety (KOFONS), granted financial resources from the Nuclear Safety and Security Commission (NSSC), Republic of Korea (No. 1605008).

REFERENCES

- [1] RETEC Group, Inc., "Groundwater Tritium Investigation Report for Dresden Generation Station", ML102420146, Chicago, 2005.
- [2] Consumers Energy Company(CE), "Big Rock Point License Termination Plan' Revision 3, ML13204A012, MI, 2013.
- [3] EPRI, "Connecticut Yankee(Haddam Neck Plant) Decommissioning Experience Report-Detailed Experience 1996~2006," FL, 2006.

Thermodynamic Analysis of Dissolution Reaction Mechanism of Magnetite in HyBRID Chemical Decontamination

Byung-Chul Lee^{1),*}, Eun-Ju Lee¹⁾, Seon-Byeong Kim²⁾, Jei-Kwon Moon²⁾, and Hui-Jun Won²⁾

¹⁾ Hannam University, 1646, Yuseong-daero, Yuseong-gu, Daejeon, Republic of Korea

²⁾ Korea Atomic Energy Research Institute, 111, Daedeok-daero 989beon-gil, Yuseong-gu, Daejeon, Republic of Korea

*bclee@hnu.kr

1. Introduction

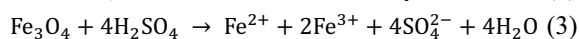
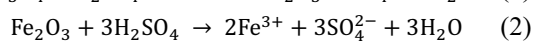
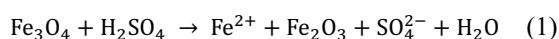
The removal of radioactive isotopes from the primary coolant system takes place with the dissolution of corrosion metal oxide layers in which radioisotopes are deposited. Chemical decontamination by oxidative and reductive dissolution is considered to be the most effective method to date. KAERI has developed the HyBRID process without using any organic acids or organic chelating agents [1, 2]. In this work we proposed the plausible reaction mechanisms of the acidic and reductive dissolution involved in the HyBRID process and studied the thermodynamic analysis of the dissolution reaction mechanisms of magnetite.

2. Mechanism of Magnetite Dissolution Reactions

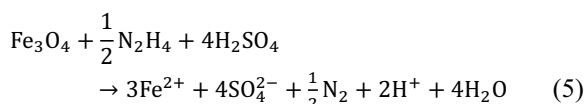
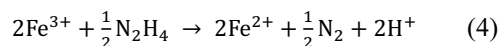
The HyBRID process uses hydrazine as a strong reducing agent and copper ion as a catalyst to form copper-hydrazine complexes which transfer electrons from Cu^+ to Fe^{3+} to be reduced to Fe^{2+} [2]. Sulfuric acid is used to control the pH of the solution. Cu^{2+} are reduced by hydrazine to produce Cu^+ . The resulting Cu^+ are oxidized to Cu^{2+} after reducing the Fe_3O_4 layer, and the Cu^{2+} are rapidly reduced to Cu^+ by hydrazine, thereby completing redox cycling. Hydrazine participates in the reaction pathway of reducing Fe^{3+} to Fe^{2+} and simultaneously regenerating oxidized Cu^{2+} into Cu^+ . [3]

2.1 Dissolution of Magnetite Using $\text{N}_2\text{H}_4/\text{H}_2\text{SO}_4$

The dissolution reactions of magnetite in aqueous solution of sulfuric acid are:

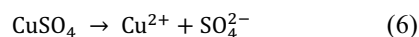


By adding hydrazine into the solution, Fe^{3+} are reduced to Fe^{2+} :

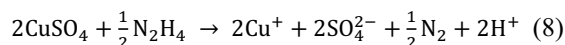
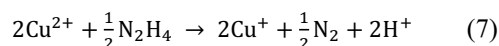


2.2 Dissolution of Magnetite Using $\text{N}_2\text{H}_4/\text{H}_2\text{SO}_4/\text{CuSO}_4$

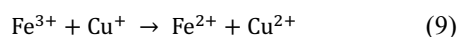
CuSO_4 dissociates in aqueous solution:



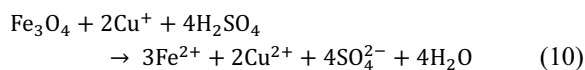
The Cu^{2+} ions are reduced to the Cu^+ ions by the coordination reaction with hydrazine:



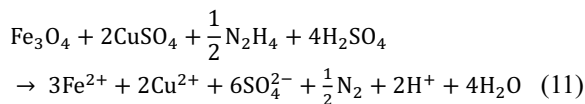
Reduction of Fe^{3+} to Fe^{2+} by oxidative regeneration of Cu^+ to Cu^{2+} is



Combining reactions (3) and (8) gives



Hydrazine facilitates the transfer of electrons to Fe^{3+} in magnetite via Cu^{n+} ions. From reactions (8) and (10), the dissolution reaction can be summarized:



3. Results and Discussion

The data of thermodynamic properties for all the species involved in the dissolution reactions of magnetite were obtained from the database of HSC Chemistry[®] version 9 by Outotec [4]. The

temperature dependence of heat capacity is given by:

$$C_{p,i}^0(T) = A_i + 10^{-3}B_iT + 10^5C_iT^{-2} + 10^{-6}D_iT^2 \quad (12)$$

Fig. 1 shows the standard heat of reaction ($\Delta H_{r,T}^0$) for individual reactions of the HyBRID dissolution of magnetite. The values of $\Delta H_{r,T}^0$ for all the reactions are negative, giving that the reactions are all exothermic. Fig. 2 shows the effect of temperature on the equilibrium constants (K) for the reactions. The K values were much greater than 1 for all the reactions and decreased with the increase of the temperature. $\ln K$ showed a nearly linear relationship to the inverse of the temperature for all the reactions.

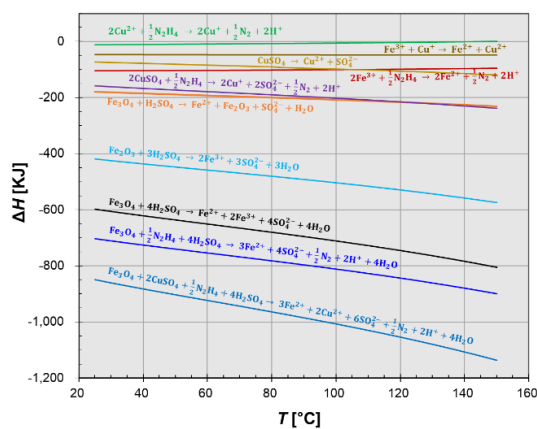


Fig. 1. Standard heat of reaction for dissolution reactions of magnetite.

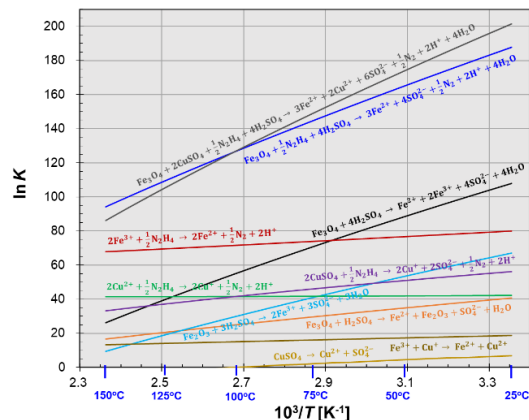


Fig. 2. Equilibrium constant for dissolution reactions of magnetite.

Table 1. Comparison of equilibrium constant (K) for three main reactions of the dissolution of oxides

Reaction No.	$\ln K$		
	25°C	60°C	95°C
(3)	107.8	81.3	58.1
(5)	187.7	156.9	130.2
(11)	201.5	164.0	131.1

The spontaneity of the main dissolution reactions for magnetite was evaluated by comparing the equilibrium constant (K), as shown in Table 1. Compared to the acidic dissolution using H_2SO_4 only, the equilibrium constant greatly increased by adding hydrazine, indicating that the reaction spontaneity improved significantly by hydrazine. The reaction spontaneity slightly increased by further addition of copper sulfate.

4. Conclusion

The chemical equilibrium of the dissolution reactions for magnetite using the HyBRID method for the decontamination of the coolant system of NPPs was investigated. Complete sets of the dissolution reaction mechanisms of magnetite were presented. For individual reactions, the standard heat of reaction, the standard entropy change of reaction, the standard Gibbs energy change of reaction, and the equilibrium constant were calculated in the temperature range of 25°C to 150°C. All the reactions were exothermic. The reaction spontaneity improved significantly by adding hydrazine and slightly increased by further addition of copper sulfate.

ACKNOWLEDGEMENT

This work has been carried out under the Nuclear R&D Program (NRF-2018M2A8 A5024102) funded by Ministry of Science and ICT.

REFERENCES

- [1] W.K. Choi, Development of Advanced Decontamination Technology for Nuclear Facilities, KAERI Report No. 2012M2A8A5025655 (2017).
- [2] W. K. Choi, H. J. Won, S. Y. Park, S. B. Kim, J. Y. Jung, J. K. Moon, "Chemical Decommissioning of a Primary Coolant System Using Hydrazine Based Solutions", Waste Management Conference, Phoenix, Arizona, USA, March 15-19 (2015).
- [3] B.T. Heaton, C. Jacob, P. Page, "Transition Metal Complexes Containing Hydrazine and Substituted Hydrazines", Coordin. Chem. Rev., 154, 193-229 (1996).
- [4] HSC Chemistry software, www.outotec.com.

Study on HyBRID Chemical Decontamination and Waste Water Treatment by Using Pilot Scale Equipment

Ki-Chul Kim*, Ju-Hyeon Park, Dong-Yeon Kim, and Jung-Hyun Lee
Korea Engineering Power Corporation Plant Service & Engineering Co., Ltd., 96-1 Gilchon-Gil, Jangan-Eup,
Gijang-Gun, Busan, Republic of Korea
*KICKIM@kps.co.kr

1. Introduction

Chemical Decontamination technology is widely used in primary system of the nuclear power plant. It is essential to develop chemical decontamination process for minimizing secondary waste along with increasing decon factor. HyBRID(Hydrazine Based Reductive metal Ion Decontamination) is chemical decontamination process using a reducing agent containing a metal catalyst without using organic acid. Most of the decontamination agent as well as the metal ions are precipitated, thereby reducing the amount of waste. This study was carried out to demonstrate HyBRID decontamination and waste water precipitation process for the pilot scale.

2. Process equipment

The chemical decontamination pilot is a 1/3 scale commercial RCP internal chemical decontamination equipment consist of decontamination tank (400L), chemical injection tank, DI water/storage tank, IX Column (4 EA), cooling tank/cooler etc. The waste water precipitation equipment consists of mixing tank (500L) and filter press to separate sludge.

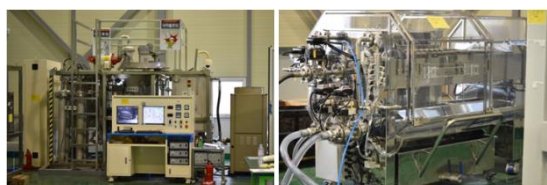


Fig. 1. Chemical decontamination pilot equipment (L).

Fig. 2. Filter press(R).

3. Experiments

3.1 Experimental method

The STS304 test specimen (50*50*2 mm, 20EA)

with 10 um oxide film that has similar composition to the PWR nuclear power plant were used for the pilot scale demonstration test. After filling 300 L DI water in the decontamination tank of the chemical decontamination pilot, the test specimens were placed in a basket and placed in the decontamination tank. The oxidation process was carried out for 3 hours after reaching the temperature 95 °C. After HyBRID chemical decontamination process, the process water was cooled and transferred to the mix tank of the waste water precipitation equipment. In the mixing tank, Precipitation process and Hydrazine decomposition process were performed, and SiO₂ was injected to grow the precipitate particle size. Precipitate in the process water was separated by using a filter press and finally purified with an ion exchange resin. The final purified water was re-used in the second HyBRID chemical decontamination process, and the chemical concentration for each step is as below.

Table 1. Chemical concentration conditions of HyBRID decontamination process

Step	Chemical	Concentration
Oxidation	H ₂ SO ₄	3.25 mM
	KMnO ₄	6.33 mM
Reduction	N ₂ H ₄ ·H ₂ O	33.77 mM
	H ₂ SO ₄	57.91 mM
	CuSO ₄	0.5 mM
Precipitation	Ba(OH) ₂ ·8H ₂ O	40 mM
N ₂ H ₂ decomposition	H ₂ O ₂	230 mM
Particle growth	SiO ₂	0.5 wt%

3.2 Experimental result

The ICP-OES analysis result of the process water sampled in HyBRID chemical decontamination

revealed that the spinel structure of the oxide film was destroyed in the oxidation Step and Cr ion was dissolved. In the reduction step, it was confirmed that the dissolved Fe and Ni ion concentration was increased and the oxide film was removed. After precipitation process, Fe^{2+} / Ni^{2+} / Cu^{2+} / Mn^{4+} ion were completely removed, but Cr^{3+} and SO_4^{2-} ion remained a little. It was confirmed that only 45.9% of K^+ ion was precipitated and remains in the process water. The remained ions in the process were mostly removed through the ion exchange resin.

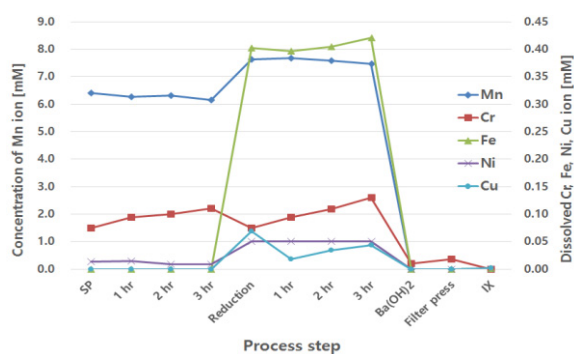


Fig. 3. ICP-OES analysis result.

Table 2. The residual ion concentration(before and after the precipitation process)

Step	K^+ [mM]	SO_4^{2-} [mM]
Reduction	6.60	43.8
Precipitation	3.572 (45.9% removal)	1.83 (95.8% removal)
After IX	0.037	0.034

4. Conclusion

In this study, HyBRID chemical decontamination was demonstrated by using a pilot scale decontamination system. As result of the test, the oxide film was removed and most of the reagent and metal ions in the process water were precipitated by the precipitation step.

It is expected that HyBRID chemical decontamination process can be applied to commercial decontamination process, if the precipitation step is improved.

ACKNOWLEDGEMENTS

This work was supported by the National Research Foundation of Korea (NRF) and the Ministry of Science and ICT (MSIT) of the Republic of Korea. (No. 2017M2A8A5041776)

REFERENCES

- [1] H. J. Won, W. S. Lee, C. H. Jung, S. Y. Park, W. K. Choi, and J. K. Moon, "A Feasibility Study on the Decontamination of Type 304 Stainless Steel by N_2H_4 Base Solution", Asian Journal of Chemistry, 26(5), 1327-1330 (2014).
- [2] S. B. Kim, H. J. Won, W. S. Lee, J. K. Moon, W. K. Choi, "Development of HYBRID-II decontamination agent ($\text{Cu}^+ / \text{N}_2\text{H}_4 / \text{H}_2\text{SO}_4$) for removal of contamination of primary radioactive materials required for nuclear dismantling", Proc. of the KRS 2014 Spring Conference, 12(1), May 07-09, 2014, Pyeongchang.

Structural Change of Non-expandable Mineral Illite by Treatment With Organic Acid (Oxalic Acid) and Extraction of Cesium

Sung Man Kim^{1),2)}, Chan Woo Park¹⁾, Il-Gook Kim¹⁾, Hee-Man Yang¹⁾, Kune-Woo Lee¹⁾, So-Jin Park²⁾, and In-Ho Yoon^{1),*}

¹⁾ Korea Atomic Energy Research Institute, 111, Daedeok-daero 989beon-gil, Yuseong-gu, Daejeon, Republic of Korea

²⁾ Chungnam National University, 99, Daehak-ro, Yuseong-gu, Daejeon, Republic of Korea

*ihyoon@kaeri.re.kr

1. Introduction

Illite has a 2:1 structure, with one octahedral sheet and two tetrahedral sheets combined. In addition, the charge balance of potassium between the interlayers causes little swelling. Illite has an FES (Frayed Edge Site) at the end of the interlayer. When this weathering occurs, the potassium may be released and replaced with other cations to desorb Cesium. Oxalic acid is a chelating agent having a carboxyl group, and a carboxyl group is bonded to a metal ion such as silicon or aluminum constituting a crystal of a clay mineral. It has the function of extracting. Therefore, crystals of clay minerals can be destroyed. This reaction can accelerate the release of cesium.

In this study, we investigated the desorption mechanism of cesium and the interlayer changes due to crystal destruction by treating oxalic acid with illite.

2. Main Title

2.1 Materials

The clay used in this study was sieved using a sieve (Mesh Size 20 μm , EF-8F020) with particle size ($> 20 \mu\text{m}$) as an illite and purchased from the clay minerals society (USA). Oxalic acid dehydrate, sodium chloride, potassium chloride, and calcium hydroxide were purchased from Sigma-Aldrich as a desorbent to remove Cs from Cesium chloride and clay. A shaking heating bath (BS-21, JEIO TECH Company, Korea) was used to conduct desorption

experiments at a temperature of 80°C.

2.2 Hydrothermal desorption of Cs-Illite

Add oxalic acid 0.015, 0.15, 0.2, 0.5, 1 and 1.5 mol/L (35 ml) to the illite (0.35 g) contaminated with CsCl in a 60 ml tube (Graduated Bottle Wide neck, PP 60 ml, Azlon®, UK). After adding 1 M KCl and 1 M NaCl to oxalic acid, add the reaction mixture to a 60 ml tube.

The reaction is carried out in a shaking heating bath (BS-21, JEIO TECH Company, Korea) for thermal desorption at 80°C for 3 days. After 3 days, the solid / liquid was separated using a centrifuge (Multi-purpose Centrifuge, Combi-514R, Hanil Science Inc., Korea), and only the supernatant was collected and filtered through a polyvinylidene fluoride (PVDF) membrane filter (pore size = 0.45 μm) The desorption rate of Cs in clay is analyzed by inductively coupled plasma mass spectroscopy (ICP-MS; ELAN DRC II, Perkin-Elmer, USA).

3. Results and Discussion

3.1 Cs desorption effect of the clay on oxalic acid

We show Cesium desorption efficiency in illite when treated with 1M concentration of oxalic acid. The reaction was carried out at 80°C for 1 day and 3 days. As shown in the chart, the desorption efficiency was 94.76% on the first day and 95.58% on the third day.

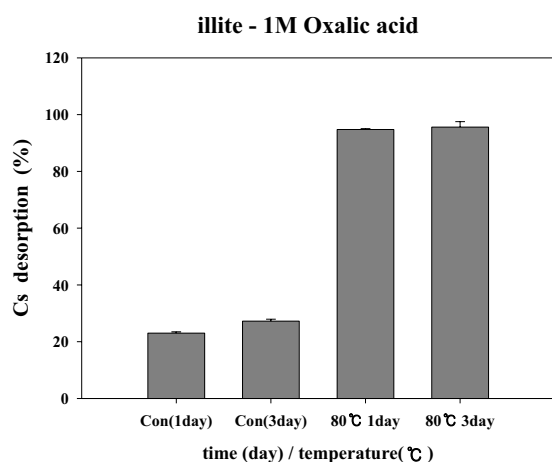


Fig. 1. Cs desorption rate using 1M Oxalic acid desorbents in illite at 80°C for 3 day.

3.2 The release of Al, Fe, K, Mg affected by the Oxalic acid concentration

This is the result of metal ion elution test for 1M treatment of oxalic acid. It shows the change of elution of metal ion with reaction time.

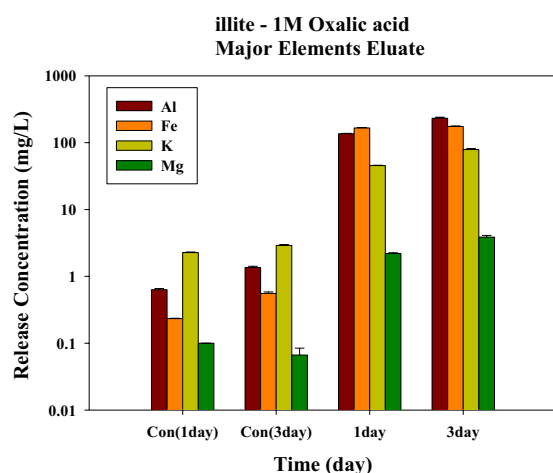


Fig. 2. Extraction of major Clay mineral component of illite by 1M Oxalic acid.

As shown in Fig. 2, when the concentration of oxalic acid was 1M, the elution was performed in the order of Al, Fe, K and Mg, and the amount of elution was greatly increased when compared to the untreated group. However, the change with reaction time did not appear much.

4. Conclusion

In conclusion, Oxalic acid (organic acid) proved to be effective in desorbing Cs from clay. Oxalic acid binds to the metal ions forming the crystal of the clay through the chelating mechanism and breaks the interlayer.

For that reason, it facilitates Cs desorption. Therefore, it can be effectively used to restore soil in a residential area that has been widely contaminated with radioactive radionuclides such as Fukushima nuclear accident.

ACKNOWLEDGEMENT

This work was supported by a National Research Foundation of Korea (NRF) grant funded by the Korean government (Ministry of Science and ICT) (No. 2017 M2A8A5015148) and the Korean government (Ministry of Science and ICT) (No. 2017M2A8A1092471).

REFERENCES

- [1] K. mingming, L. Haung, et al, "Effect of oxalic and citric acids on three clay minerals after incubation", *Applied clay Science.*, 99, 207-214 (2014).
- [2] Q. Rongliang, Z. Zeli, et al, "Removal of trace and major metals by soil washing with Na₂EDTA and oxalate", *J Soils Sediments.*, 10, 45-53 (2010).
- [3] A. de Koning, R.N. Comans, "Reversibility of radiocaesium sorption on illite", *Geochimica et cosmochimica acta.*, 68, 2815-2823 (2004).

Study on Dismantling Scenario for Large Components of Kori Unit 1

Young Hwan Hwang*, Seok-Ju Hwang, and Cheon-Woo Kim
Korea Hydro & Nuclear Power Co., Ltd. Central Research Institute, 70, Yuseong-daero 1312beon-gil,
Yuseong-gu, Daejeon, Republic of Korea
*yhhwang7@khnp.co.kr

1. Introduction

After the permanent shut down, a nuclear power plant (NPP) enters new era, decommissioning phase. The removal of radioactive components and the demolition of the building take place in this phase. The removal of radioactive component, including reactor and large components (LC), is complex, expensive, and multidisciplinary. Among large components, including steam generator (SG), pressurizer, and reactor coolant pump, in containment building (CB), the treatment of SG is the most challenging task due to its size and level of contamination [1].

Dismantling scenario for large components is studied, in terms of processability and characteristics. Optimization of processes during decommissioning is one of the important task to reduce the cost and risk. The SG is selected as a representative item among LCs. In the previous experiences, the dismantling strategy for LC is related to the site condition, such as physical dimension, public acceptance, disposal, etc.



Fig. 1. Example of Steam Generator Withdrawal in ZORITA NPP.

2. Scenario Study of Dismantling

Three scenarios, listed below, are considered in this research. Since the large components in primary circuit are activated by neutron and/or contain surface contaminants, the direct disposal without segmentation is preferred in terms of radiation reduction of workers. However, the waste acceptance criteria should be considered for the implementation of disposal.

- Direct disposal (without segmentation)
- Segmentation in containment building
- Segmentation in waste treatment building

The total height, maximum outer diameter (OD), and weight of Kori unit 1 SG are 20.7 m, 4.5 m, and 327 ton, respectively. The steam generator has more than 4,900 U-tubes, made of Inconel 690TT. The coolant of primary circuit flows through U-tube and contaminates them. The dismantling of SG includes disassemble and separation of U-tubes from SG body. The height of U-tubes from the plate is 935 cm. The chemical and physical decontamination equipment is required to remove the contaminants inside the U-tubes. It is generally understood that the space, at least around 2.5~3 times of SG total height and outer diameter, is required for the decontamination and dismantling of SG. Based on the hypothesis, the required minimum length and width are 5.2~6.2 m and 1.2~1.4 m, respectively.

Fig. 2 shows the cross sectional view of the Kori unit 1 CB. Many components, including reactor, RCP, SG, etc., are closely packed in CB. It seem that the cavity region, blue dotted rectangle in Fig. 3, could be an only option for the decontamination and segmentation.

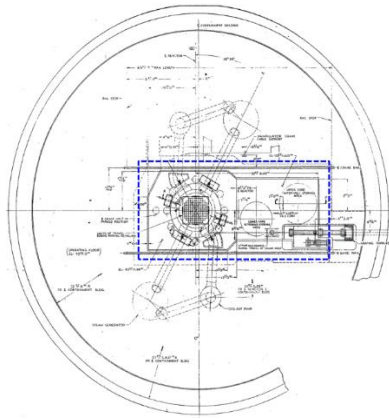


Fig. 2. Cross sectional view of Kori Unit 1 CB.

Since the SG is a massive component, weight of 327 ton, a solid plates and supporting structure should be prepared to cover the cavity region and provide sufficient force to support the SG. In addition, the safety plan from industrial hazardousness and management plan for transportation of cutting debris, particles, and aerosol should be prepared to decrease the secondary waste generation and reduce the risk.

On the other hand, decontamination and dismantling the LC at the outside of CB, for instance waste treatment facility, allows various advantages, such as conveniences in process, radiation protection of workers, packaging, etc. The sufficient space for the process allows worker prevent the unnecessary approach to the activated and/or contaminated LC. Also, higher degree of decontamination is achievable compared to implementation of the process in CB. This indicates that it is reasonable to conclude that the segmentation of LC in waste treatment building is favorable in the case of Kori unit 1.

Fig. 3 shows the suggested opening location of CB. Since the diameter of equipment hatch is smaller than OD of SG, some part of CB liner plate and concrete wall of CB. The suggested dimension of temporary opening is width and height of 6.9 m.

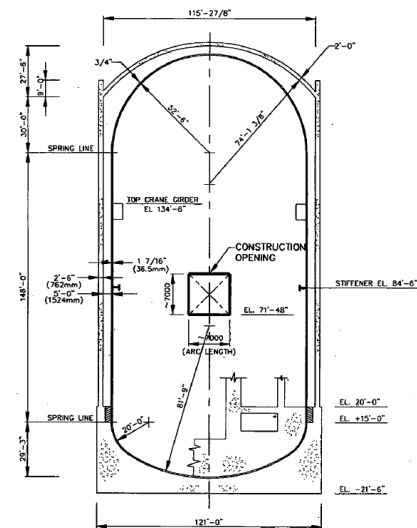


Fig. 3. Suggested Opening Location of CB.

3. Conclusion

Various scenarios for dismantling of large components are studied. Considering the status in containment building and ALARA principle, the segmentation in waste treatment building has advantages, such as radiation protection and processability.

ACKNOWLEDGEMENTS

This work was supported by the Korea Institute of Energy Technology Evaluation and Planning (KETEP) and the Ministry of Trade, Industry & Energy (MOTIE) of the Republic of Korea (20161510300430).

REFERENCES

- [1] C.-W. Kim et. al., "Technology Development for Pilot Test of Activated RV and RVI Decommissioning", Intermediate report (2018).

Modeling of Dissolution Rate of Magnetite in HyBRID Chemical Decontamination

Byung-Chul Lee^{1)*}, Eun-Ju Lee¹⁾, Seon-Byeong Kim²⁾, Jei-Kwon Moon²⁾, and Jeongsun Park²⁾

¹⁾ Hannam University, 1646, Yuseong-daero, Yuseong-gu, Daejeon, Republic of Korea

²⁾ Korea Atomic Energy Research Institute, 111, Daedeok-daero 989beon-gil, Yuseong-gu, Daejeon, Republic of Korea

*bclee@hnu.kr

1. Introduction

The removal of radioactive isotopes from the primary coolant system takes place with the dissolution of corrosion metal oxide layers in which radioisotopes are deposited. Chemical decontamination by oxidative and reductive dissolution is considered to be the most effective method to date. Recently, KAERI has developed the HyBRID process without using any organic acids or organic chelating agents [1, 2]. The solution containing hydrazine, sulfuric acid and copper sulfate provided the acidic and reductive dissolution of transition metal ions from the corrosion oxides like magnetite. In this work we investigated the modeling of the kinetic data in the dissolution of metal oxides using the HyBRID method.

2. Modeling of Kinetic Data

The experimental data of reaction rate for dissolution of Fe ion from magnetite in HyBRID decontamination were analyzed by various kinds of kinetic models reported in literature for heterogeneous reactions such as the present work. Models are generally classified based on the graphical shape of their isothermal curves (dissolution vs time) or on their mechanistic assumptions [3]. Based on their shape, kinetic models can be grouped into acceleratory, deceleratory, linear, or sigmoidal models. Based on mechanistic assumptions, models are divided into nucleation, geometrical contraction, diffusion, or reaction-order. 12 different equations for dissolution are listed in Table 1 [3, 4].

The equations can be roughly divided into two categories: diffusion and reaction controlled [4]. For diffusion, the rate determining phenomenon is the transportation of reactants of reaction products to or from the reaction site. For chemical reaction, the rate determining step is, in turn, the actual chemical reaction taking place at the reaction site. In Table 1, x is the extent of reaction at time t , ranging from 0 to 1,

k is the rate constant and a is a phase-specific constant. The x value is determined as the ratio of concentration of dissolved Fe ion to concentration of initially added Fe ion.

Table 1. Equations for modeling kinetics of dissolution

Eq. No.	Equation	Curve ¹	Physical Background	Remark
1	$x^2 = kt$	D	1D diffusion parabolic	
2	$(1-x) \ln(1-x) + x = kt$	D	2D diffusion for cylinder	
3	$[1 - (1-x^{1/2})]^2 = kt$	D	3D diffusion for sphere	shrinking core model
4	$(1 - \frac{2}{3}x) - (1-x)^{3/2} = kt$	D	3D diffusion for sphere	shrinking core model
5	$-\ln(1-x) = kt$	D	1 st order random nucleation	1 st order rate law
6	$[-\ln(1-x)]^{1/2} = kt$	V	random nucleation 2D	Avrami-Erofe'ev eq.
7	$[-\ln(1-x)]^{1/3} = kt$	V	random nucleation 3D	Avrami-Erofe'ev eq.
8	$\ln[-\ln(1-x)] = a \ln k + a \ln t$	V	modified 1 st order random nucleation	Kabai eq.
9	$1 - (1-x)^{1/2} = kt$	G	phase boundary control, shrinking disc	
10	$1 - (1-x)^{1/3} = kt$	G	phase boundary control, contracting sphere	shrinking core model
11	$x^{1/3} = kt$	A	-	cubic root law
12	$\ln x = kt$	A	-	

¹D = decelerator, V = variable, G = geometric, A = acceleratory

3. Results and Discussion

The kinetic data of dissolution of magnetite in HyBRID decontamination obtained from KAERI laboratory were correlated by all the model equations listed in Table 1. Fig. 1 shows the kinetic data of the dissolution of Ni and Fe ions from nickel ferrite (NiFe₂O₄) at five different hydrazine concentrations and at Cu ion concentration of 10-4 mol. The kinetic data of the dissolution of Fe ion from magnetite (Fe₃O₄) by the HyBRID solutions with various pH values are shown in Fig. 2.

The modeling results for the experimental data of Figs. 1 and 2 are given in Tables 2 and 3. When applying each model equation to each data set, the regression coefficient (R²) was calculated. The number of occurrences of the R² value obtained by applying the model equation to each data is classified by the range of the R² value. As shown in Table 2, the kinetic data of the dissolution of Ni and Fe ions from nickel ferrite measured at different N₂H₄ concentrations were quite well described (R² > 0.90) by the 2D diffusion model (equation 2), the modified first-order Kabai equation (equation 8), and the shrinking core model (equation 10). Table 3 shows that the kinetic data of the Fe ion dissolution from magnetite were fitted the best by the modified first-order Kabai equation. The shrinking core model, the

Avrami-Erofe'ev equation, and the cubic-root law did not adequately describe the experimental data.

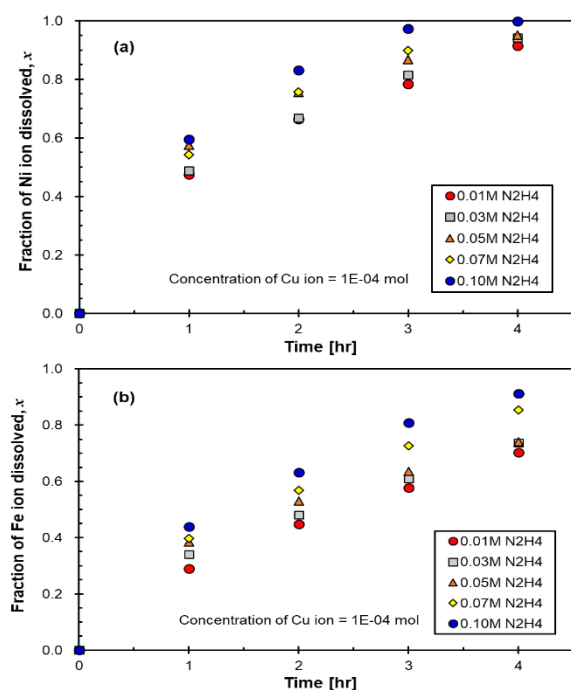


Fig. 1. Dissolution rate of Ni and Fe ions from nickel ferrite: (a) Ni ion; (b) Fe ion.

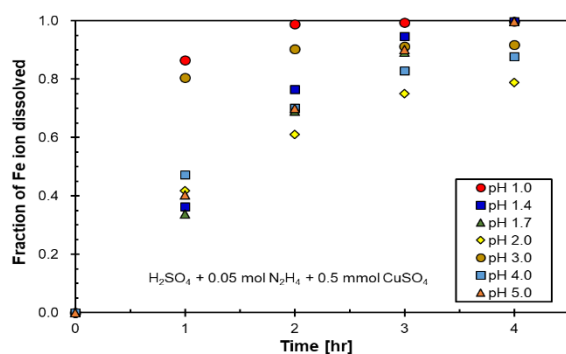


Fig. 2. Dissolution rate of Fe ion from magnetite at different pH values.

Table 2. Modeling results for the experimental kinetic data of Figure 1

Model equation	Number of data sets	Number of occurrences				
		$R^2 < 0.80$	$0.80 < R^2 \leq 0.90$	$0.90 < R^2 \leq 0.95$	$0.95 < R^2 \leq 0.99$	$R^2 > 0.99$
1	10	0	2	0	3	5
2	10	0	0	3	6	1
3	10	10	0	0	0	0
4	10	0	0	7	3	0
5	10	1	1	2	4	2
6	10	8	1	1	0	0
7	10	10	0	0	0	0
8	10	0	1	0	7	2
9	10	2	2	4	2	0
10	10	0	2	2	5	1
11	10	10	0	0	0	0
12	10	0	1	2	7	0

Table 3. Modeling results for the experimental kinetic data of Figure 2

Model equation	Number of data sets	Number of occurrences				
		$R^2 < 0.80$	$0.80 < R^2 \leq 0.90$	$0.90 < R^2 \leq 0.95$	$0.95 < R^2 \leq 0.99$	$R^2 > 0.99$
1	7	2	0	3	2	0
2	7	2	1	2	2	0
3	7	7	0	0	0	0
4	7	2	2	1	2	0
5	7	4	1	1	1	0
6	7	4	0	0	2	1
7	7	6	1	0	0	0
8	7	0	1	1	2	3
9	7	4	0	0	2	1
10	7	3	1	1	2	0
11	7	7	0	0	0	0
12	7	2	5	0	0	0

4. Conclusion

The kinetics of dissolution of magnetite and nickel ferrite by the HyBRID decontaminating agent was studied. The results showed that the concentration of hydrazine and copper sulfate and the pH of solution were of importance for the determination of the kinetics of dissolution reactions. The modeling results for the kinetic data showed that the dissolution rate data were correlated the best by the modified first-order random nucleation, represented by the Kabai equation.

ACKNOWLEDGEMENT

This work has been carried out under the Nuclear R&D Program (NRF-2018M2A8 A5024102) funded by Ministry of Science and ICT.

REFERENCES

- [1] W.K. Choi, Development of Advanced Decontamination Technology for Nuclear Facilities, KAERI Report No. 2012M2A8A5025655, March 2017.
- [2] W. K. Choi, H. J. Won, S. Y. Park, S. B. Kim, J. Y. Jung, J. K. Moon, "Chemical Decommissioning of a Primary Coolant System Using Hydrazine Based Solutions", Waste Management Conference, Phoenix, Arizona, USA, March 15-19, 2015, Paper No. 15215.
- [3] A. Khawam, D. R. Flanagan, Solid-State Kinetic Models-Basics and Mathematical Fundamentals, J. Phys. Chem. B, 110, 17315-17328 (2006).
- [4] R. Salmimies, M. Mannila, J. Kallas, A. Häkkinen, Acidic Dissolution of Hematite: Kinetic and Thermodynamic Investigations with Oxalic Acid, Int. J. Mineral Processing, 110-111, 121-125 (2012).

Grouping of Radioactive Wastes During the Decommissioning of PWR NPPs

Ji-Hoon Lee* and Kang-Ok Cho

Korea Hydro & Nuclear Power Co., Ltd. Central Research Institute, 70, Daedeok-daero 1312beon-gil, Yuseong, Daejeon, Republic of Korea

*leejihoon@khnp.co.kr

1. Introduction

Grouping of radioactive wastes is necessary to perform the more safe and efficient management of radioactive waste during decommission of NPPs. For those purpose, the generation characteristics of radioactive waste such as waste types, generation rate, radioactivity and physico-chemical characteristics should be identified and classified during decommissioning activities. It is also important to know the waste route from generation to on site, temporary storage, treatment facility, transfer and disposal site. In each step, the information of waste characterization should be known for decommissioning activities. Therefore, the concept for grouping of decommissioning radioactive waste are proposed for the efficient management of wastes during decommissioning of Kori Unit 1.

2. Grouping of Decommissioning Radioactive Waste

2.1 Grouping of decommissioning radioactive wastes by generation Characteristics

Radioactive waste will be generated by different materials and amounts, radioactivity during decommissioning of NPPs. Thus, It is essential to group the same types of waste material, shape and radioactivity so that wastes can manage efficiently during the initial step of decommissioning. There are many kinds of radioactive waste such as various type of metal, concrete, cables and the others. The Estimated waste types generated by decommissioning are shown in Table 1.

Table 1. Estimated waste generated by decommissioning

Waste Type		Radioactive level
Metal	SF storage rack	LLW, VLLW, CW
	RV/RVI	VLLW, LLW, ILW
	Large components	LLW, VLLW, CW
	Small metals	ILW, LLW, VLLW, CW

Concrete	Scabbling	LLW, VLLW
	Debris	LLW, VLLW, CW
Wire	cable	LLW, VLLW, CW
	resin	VLLW, LLW, ILW
Others	Cutting Swarf	VLLW, LLW, ILW
	filter	LLW, ILW
	DAW	VLLW, LLW

2.2 Grouping of radioactive wastes by decommissioning activities

Grouping of radioactive waste during decommissioning can be considered by management of on site and central treatment facility. From on site for decommissioning. Radioactive wastes can be grouped clearance wastes, waste to be treated, waste to be untreated. In the central treatment facility, radioactive waste can be grouped clearable waste by washing, radioactive waste which can be decontaminated by physico-chemical decontamination technologies, volume reduction waste by super compaction or melting technology and stabilization or solidification wastes for satisfying the waste acceptance criteria. Table 2 shows the concept of grouping methodology of radioactive wastes from on-site and central treatment facility.

Table 2. Grouping of radioactive waste from on-site and central treatment facility

Division		Waste Type
On Site	Clearance Waste(Non Additional process)	
	Waste to be treated	• Metals
		• Nonmetals
		• Super compaction(SG tube, Alloy)
Central Treatment Facility	Waste to be untreated	• RV/RVI
		• Activated Concrete
		• Intermediate Waste resin /filter
	Clearable waste by washing	
Radioactive Waste	Radioactive Waste	• Decontamination
		• Volume Reduction
		• Solidification

2.3 Grouping of radioactive wastes by radioactivity, site and package

Fig. 1 suggested the waste grouping concept according to radioactivity, waste management site and waste packages. Waste package will be determined regarding each waste type and its radioactivity during decommissioning. In present, only 200 L and 320 L of metal container are admitted to the radioactive disposal facility in KORAD. But decommissioning waste will be generated large amounts and various types at a short period. Thus, KORAD-KHNP have discussed the waste acceptance criteria of second and third disposal facility so that they can accept various types of waste package for the decommissioning wastes.

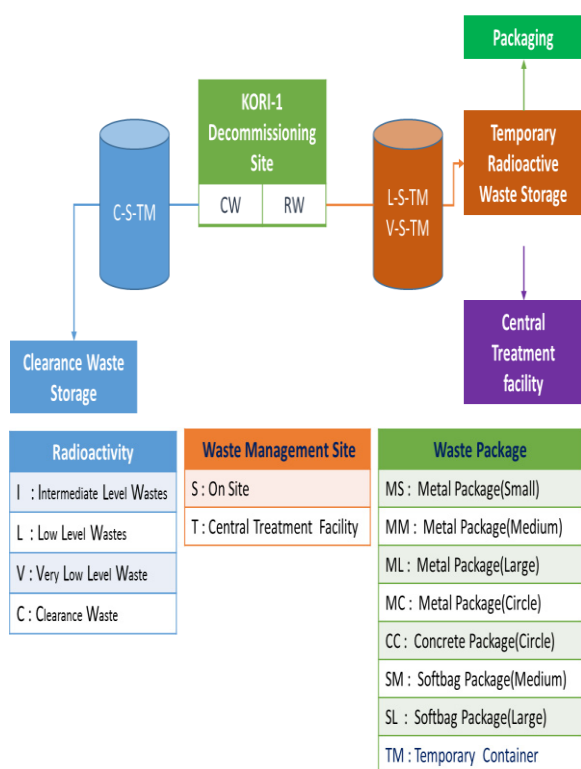


Fig. 1. Grouping of radioactive wastes according to radioactivity, site and waste package type.

KHNP will apply the appropriate size, weight and materials of packages for the different radioactivity and waste types of decommissioning wastes of KORI #1.

3. Conclusion

During decommissioning of NPPs, a lot of waste will be generated and their characteristics are varied

with different materials, shape, radioactivity and so on. It is very important to appropriate grouping of waste for minimizing and efficient management of radioactive wastes. In order to achieve this, it is necessary to investigate the waste characterization during decommissioning of NPPs.

REFERENCES

- [1] KHNP Report, "Technology Development for the Reduction of Radwastes and Treatment of problem Radwastes on D&D of Nuclear Power Plants" (2018).
- [2] KEPCO E&C Technical Report, "Evaluation of Decommissioning Source Terms and Wastes for the Pressurized Water Nuclear Power Plant and Heavy Nuclear Power Plant" (2016).
- [3] IAEA-TECDOC-1222, "Waste inventory record keeping systems(WIRKS) for the management and disposal of radioactive waste" (2001).

γ -ray Irradiation Effects on the Polypropylene Yarns

N.O. Chang^{1),2)}, H.J. Won^{1),*}, S.Y. Park¹⁾, S.B. Kim¹⁾, B.K. Seo¹⁾ and Y.S. Kim²⁾

¹⁾Korea Atomic Energy Research Institute, 111, Daedeok-daero 989beon-gil, Yuseong-gu, Daejeon, Republic of Korea

²⁾Hanyang University, 222, Wangsimri-ro, Seongdong-gu, Seoul, Republic of Korea

* nhjwon@kaeri.re.kr

1. Introduction

During the decommissioning, a chemical decontamination process is used for removing the radionuclides by dissolution of oxide layer on the primary system of nuclear power plant. It consists of oxidizing and reducing processes. As a reducing decontamination agent, N_2H_4 -Cu(I)- H_2SO_4 solution developed by KAERI can be applied. Radioactive liquid wastes produced after the decontamination process should be treated because it contains the radioactive materials. The filter press is used for the removal of radioactive materials in the radioactive liquid wastes as a solid form [1]. Polypropylene (PP) fabric is used as the filter medium. The filter press is operated up to a 1 MPa. PP filter, however, can be degraded during the treatment process due to the γ -ray exposure by the radioactive waste. In this study, the γ -ray irradiation effects on the mechanical properties of PP yarns are analyzed. The variations of surface morphology of PP yarns after inducing γ -ray are also analyzed.

2. Methods and Results

2.1 Sample preparation and γ -ray irradiation

PP yarns having a thickness of 450 deniers were cut into 200 mm. The samples were irradiated with 0, 20 and 40 kGy of γ -rays in the air condition by using a Low-dose γ -ray Irradiator (Co-60 source) in the

Jeonup City (Korea Atomic Energy Research Institute).

2.2 Mechanical properties of the PP yarns

To evaluate the mechanical properties of the PP yarns, tensile tests by the universal tester (INSTRON 4482, Instron Corporation) were carried out. The results of the tensile test are presented in Fig. 1.

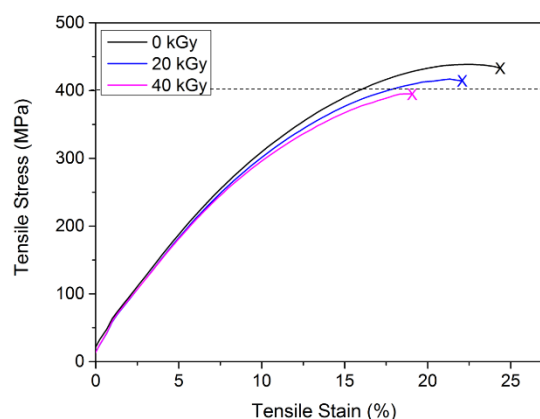


Fig. 1. Tensile Stress-Tensile Strain curves of PP yarns before and after γ -rays irradiation.

As shown in Fig. 1, the tensile stress at break (\times marks) decreases with the increase of the absorbed dose. This phenomenon occurs because of the chain scission of the C-C bonding occurs in the PP yarns. During and after the γ -ray irradiation, oxygen atoms in the air are converted to the radicals and decompose to carbonyl and hydroxyl compounds. These compounds cause the chain scission of C-C bonding in the PP yarns, which is the reason of the degradation [2].

For all the PP yarn samples, the tensile stress at break is about 400 MPa. When the PP is used as a filter, the filters receive a pressure. Therefore, the mechanical degradation of PP yarns due to the γ -ray irradiation can be ignored within absorbed doses in this study.

2.3 Surface properties of the PP yarns

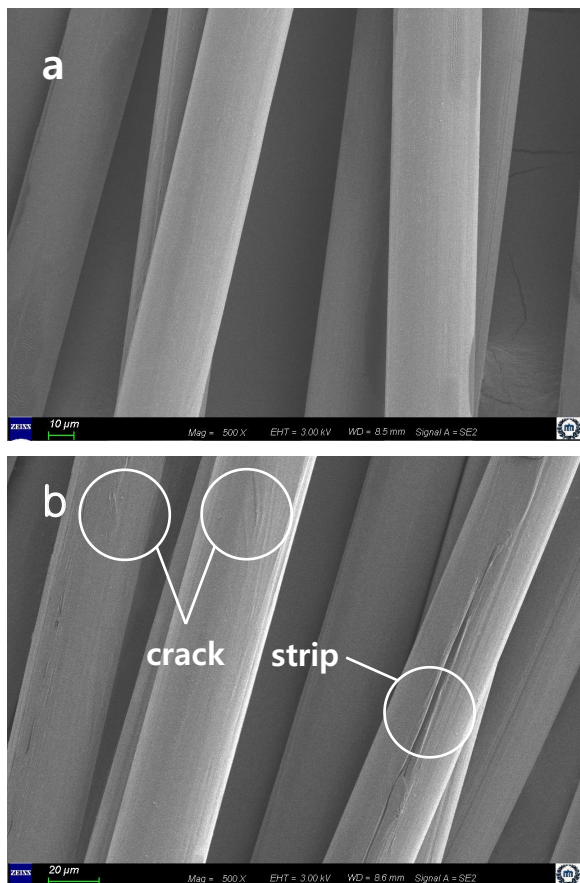


Fig. 2. Surface change of the PP yarns, (a) 0 kGy and (b) 40 kGy of absorbed dose by γ -rays irradiation.

The surface change of the PP yarns is observed by FE-SEM(JSM-7000F, ZEISS Co. Ltd) and shown in the Fig. 2. The PP filaments before irradiation have sound surface as shown in the Fig. 2a. However, after PP yarns received the 40 kGy of absorbed dose, cracks and long strips occur along the outer PP filaments. It is difficult to observe the change of the morphology on the inner PP filament. Therefore, it

can be predicted that the degradation of PP yarns occur from the outside to the inside.

3. Conclusions

During the treatment of radioactive liquid wastes, PP filters are degraded by γ -ray irradiation. This phenomenon can be explained by C-C bond scission of PP yarns. In the absorbed dose range of this study, PP yarns have the resistances against pressures up to 400 MPa. The maximum operating pressure of the filter press is 1 MPa. Comparing the maximum tensile strength and the operating pressure, it can be concluded that the negative effect by γ -ray irradiation can be neglected during the filtration. PP yarns, however, contact with water during the real decontamination process. Thus, it is necessary to study the effects of γ -ray irradiation on PP yarns in a water condition.

ACKNOWLEDGMENT

This work has been carried out under the Nuclear R&D Program (NRF-2017M2A8A5015144) funded by Ministry of Science and ICT.

REFERENCES

- [1] International Atomic Energy Agency, Application of Membrane Technologies for Liquid Radioactive Waste Processing, Technical Reports Series, No. 431 (2013).
- [2] Miroslav Mrlik and Mariam Al Ali Al Maadeed, Tailoring of the thermal, mechanical and dielectric properties of the polypropylene foams using gamma-irradiation, Polymer Degradation and Stability, No. 133, p. 234-242 (2016).

A Methodology of Selecting Potential Radionuclides for the Kori Unit 1 DCGL

Calculation

Hyung-Woo Seo*, and Dong-Hee Lee

Korea Hydro & Nuclear Power Co., Ltd. Central Research Institute, 70, Yuseong-daero 1312beon-gil, Yuseong-gu, Daejeon, Republic of Korea

*seohyungwoo@hanmail.net

1. Introduction

A potential list of radionuclides is needed to ensure that the survey and characterization techniques based on the Multi-Agency Radiation Survey and Site Investigation Manual (MARSSIM) [1] are appropriate and that doses have been assessed taking into account the radionuclides that may be present at the site. Nuclear facility operators should also ensure that the list of radionuclides developed through Historical Site Assessment (HSA) and operation history is applicable and appropriate for each contaminated materials. Therefore, a list of radionuclides should be developed for each type of material, reflecting site characteristics that are expected to remain after site remediation. The purpose of this study is to propose a methodology to make a list of potential radionuclides that will remain on the site after completion of the decommissioning of Kori Unit 1.

2. Methods

2.1 Rancho Seco Nuclear Power Station (RSNPS) case

RSNPS reviewed several NRC guidance documents in a way that theoretically defines the radionuclides that are potentially present at the decommissioning site. This includes NUREG/CR-3474, NUREG/CR-4289, and NUREG/CR-0130.

However, the potential radionuclides based on the reference document were directly not appropriate, so additional technical reviews were carried out. Several radionuclides were added using ORIGEN computer code, and the incident history illustrated in the historical site assessment was also included. Finally, detected radionuclides in the spent fuel system were added.

The list of potential radionuclides based on the above criteria includes minor radionuclides and their importance was evaluated by qualitative comparison of the total radioactivity. For the discounted radionuclides from the regulatory references and the ORIGEN code, the radionuclides of less than 0.1% of the radioactivity concentration were considered to be excluded, and the dose was confirmed to be insignificant by using DandD code. Among the discounted radionuclides, there are some not supported by the DandD code. In this case, it is confirmed that the weighted Dose Conversion Factor

(DCF) is insignificant compared with those of Co-60 and Ni-63 which have high radioactivity ratio. In addition, naturally occurring radionuclides and noble gases are discounted because they are less likely to be found at the site. Table shows the list of potential radionuclides for the RSNPS.

Table 1. Potential radionuclide list of RSNPS

H-3	C-14	Na-22	Fe-55
Ni-59	Co-60	Ni-63	Sr-90
Nb-94	Tc-99	Ag-108m	Sb-125
Cs-134	Cs-137	Pm-147	Eu-152
Eu-154	Eu-155	Np-237	Pu-238
Pu-239	Pu-240	Pu-241	Am-241
Pu-242	Cm-244		

2.2 Zion Station case

The Zion Nuclear Station also starts with a list of potential radionuclides from a theoretical list with reference to regulatory documents similar to RSNPS. They reviewed guidance document including NUREG/CR-3474, NUREG/CR-4289, and WINCO-1191. WINCO-1191 presents a theoretical list of radionuclides expected to come from PWR and BWR, and includes both fission and activation products.

In a slightly different way than the RSNPS, Zion Station analyzed and reviewed the representative radioactive waste samples collected at the site to supplement the list of potential radionuclides. A total of 19 samples analyzed were reviewed, which are based on the waste characteristics data collected after the permanent shutdown of nuclear facilities.

To eliminate minor radionuclides, Zion Station selected discounted activation products from NUREG/CR-3474 where the radioactivity fraction for Co-60 and Ni-63 was less than 0.01%. It was also excluded for noble gases that were not expected to be measured at the site. Table shows the list of potential radionuclides for the Zion Station.

Table 2. Potential list of potential radionuclides

H-3	C-14	Fe-55	Ni-59
Co-60	Ni-63	Sr-90	Nb-94
Tc-99	Sb-125	Cs-134	Cs-137
Pm-147	Eu-152	Eu-154	Np-237
Pu-238	Pu-239	Pu-240	Pu-241
Am-241	Am-243	Cm-243	Cm-244

3. Results & discussion

We reviewed a methodology for developing the initial list of potential radionuclides from the RSNPS and Zion Station. As a result, it can be seen that they first made a starting point from the data in the regulatory documents, and added supplemental data such as historical site assessment, sampling analyzed, and ORIGEN code, etc. Based on these cases, a methodology for the list of potential radionuclides of Kori Unit 1 decommissioning can be developed.

3.1 Resources for selecting potential radionuclides

First, referring to the overseas cases, the starting point is the result of the review of the radionuclides in the reference documents: NUREG/CR-3474, NUREG/CR-4289, and NUREG/CR-0130.

Next, reference to the radionuclides considered for radioactive waste for the nuclear power plants currently in operation will be possible. Therefore, it may include 14 radionuclides specified in the Nuclear Security and Safety Commission (NSSC) Notice No. 2017-60, “Regulations for the Management of Low and Intermediate Level Radioactive Waste”.

Others, as a reference to consider, may be possible by executing the ORIGEN code for the radionuclides produced in the nuclear fuel assembly that has undergone 15 years of radioactive decay after the permanent shutdown. It should also reflect the HSA data and the radionuclides detected in the future at the site.

3.2 Discounted radionuclides

For the discount methodology, first, the radionuclides specified by NUREG/CR-3474 are considered for selection of discounted radionuclide if the radioactivity fraction decayed for 15 years is less than 0.1%. In the case radionuclides selected from the ORIGEN code, in the same way, if the fraction of radioactivity is less than 0.1% of total inventory, it also can be considered for discount.

3.3 Dose evaluation for discounted radionuclides

In order to eliminate radionuclides with a radioactivity of less than 0.1% of total from those of discounted, the dose fraction of the discounted radionuclides should be less than 1% of the total dose. In case of overseas cases, the evaluation was made for radionuclides that can be supported by the DandD code. Otherwise, the weighted DCF was compared. The DandD code can be used for Kori Unit 1, but it

is also possible to use the RESRAD code because many decommissioning plants adopted RESRAD code to calculate residual activity of potential radionuclides. Therefore, it is appropriate to use RESRAD code to show the dose of discounted radionuclides is insignificant. The overall procedure can be depicted as shown in Fig. .

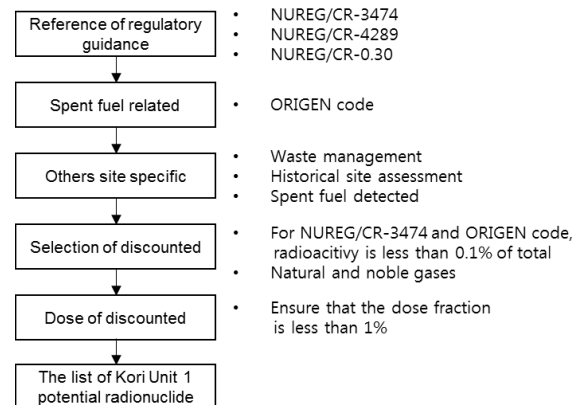


Fig. 1. Process of potential radionuclides selection.

4. Conclusion

In this paper, we reviewed the RSNPS and Zion Station cases of developing the list of potential radionuclide, and propose a methodology for Kori Unit 1 decommissioning. To summarize, starting from the regulatory guidance, the initial list is made together with referring to site history, sampling, and radioactive waste stream, and radionuclides not important are eliminated by comparing the fraction of radioactivity. And dose assessment can be performed on the discounted radionuclides to confirm that their effects are insignificant. Therefore, it is possible to select the potential radionuclides of Kori Unit 1 through this methodology.

REFERENCES

- [1] NRC, Multi-Agency Radiation Survey and Site Investigation Manual, U.S. Nuclear Regulatory Commission, 2000.

Studies on the Decomposition Behavior of Oxalate Organic Waste by UV-photo-Fenton AOP Using a Medium Pressure UV Lamp

Yoon-Ji Park^{1*}, Jin-Hee Kim¹, Hyun-kyu Lee², Sae-Binna Lee¹, Wonzin Oh², and Sang-June Choi^{1,2}

¹Kyungpook National University, 80, Daehak-ro, Buk-gu, Daegu, Republic of Korea

²Research Institute of Advanced Energy Technology, 80, Daehak-ro, Buk-gu, Daegu, Republic of Korea

*qkrdbswl2@knu.ac.kr

1. Introduction

Oxalic acid($\text{H}_2\text{C}_2\text{O}_4$) is used as reagent for reductive dissolution of metal oxide such as Fe_3O_4 . After the dissolution process, it is necessary to decompose oxalic acid into CO_2 and H_2O to reduce waste volume. In order to decompose the oxalic acid, photo-Fenton reaction, which decomposes organics by the combination of H_2O_2 , Fe^{2+} and UV, could be applied [1]. In the photo-Fenton reaction, the type of UV lamp and the irradiation density are important factors determining decomposition performance. Especially, the medium pressure UV lamp has UVA, UVB and UVC with a wavelength of 200~400 nm. [2]. In this study, the decomposition behavior of oxalic acid depending on the energy irradiation density was investigated using a medium pressure lamp. Moreover, we tried to confirm that the decomposition behavior of oxalic acid by the medium pressure lamp can be represented as a first-order reaction to the UV irradiation density.

2. Experiments

2.1 Decomposition process of oxalic acid depending on energy irradiation density

This experiment was confirmed the decomposition rate according to energy irradiation density using a medium pressure lamp. The solution was prepared by mixing 2 mM ferrous chloride and 30 mM oxalic

acid. For the Photo Fenton treatment, 1500 W medium pressure lamp was used. After injection of 30 mM H_2O_2 , the UV lamp was operated with 1700 mL/min circulation using the peristaltic pump. Comparing the volume of 17 L with the volume of 8.5 L, the decomposition behavior with time was investigated. Expt-1 was sampled at 0, 2, 4, 6, 8, 10, 15, 20 and 25 minutes, Expt-2 was sampled at 1, 2, 3, 4, 5, 6, 7, 8, 9, 10 and 15 minutes. After sampling and dilution, to investigate decomposition behavior of oxalic acid, Total Organic Carbon was measured using TOC analyzer.

Table 1. Experimental Conditions of oxalic acid decomposition of medium pressure lamp

Exp. No	Volume [L]			Q [L/min]	E [kW]
	Reactor	Tank	Total		
Expt-1	1.7	15.3	17	1.7	1.5
Expt-2	1.7	6.8	8.5	1.7	1.5

3. Results

Fig. 1 shows the residual rate of oxalic acid over time. Experimental results show that the decomposition rate was higher when the volume of oxalic acid waste was smaller (8.5 L). It was confirmed that 99% decomposition of 8.5 L took 25 minutes, and that of 17 L took 15 minutes. In this study, to identify the factors involved in decomposition behavior The energy irradiation density was calculated as follows. We also confirmed whether it fitting the first-order reaction model.

$$X = \frac{c}{c_0} \times 100[\%] \quad (1)$$

$$-\frac{dX}{dt} = kX \quad (2)$$

$$X(t) = 100 \times \exp(-kt) \quad (3)$$

$$E_{UV} = P_{UV} \times t/V_w \quad (4)$$

[E_{UV} : Energy density, P_{UV} : Lamp, t : UV irradiation time, V_w : Volume of the oxalic acid waste]

Therefore, This can be represented as shown in eq.(5)

$$X(E_{UV}) = 100 \times \exp(-k' E_{UV}) \quad (5)$$

Fig. 2 shows the result of fitting the residual rate to the UV irradiation density to the first-order reaction model equation. It was confirmed that the decomposition behavior in both experiments can be fitted well by a single graph. Therefore, it can be confirmed that the graph of the decomposition behavior of oxalic acid according to the energy irradiation density is well fitted when the first-order reaction model equation is applied.

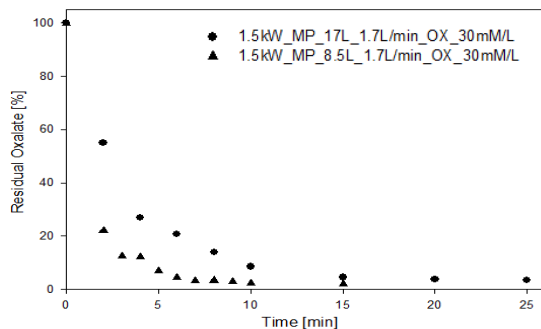


Fig. 1. Fraction of oxalic acid residual depending on time.

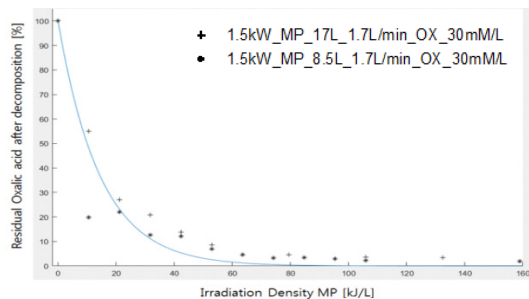


Fig. 2. Fraction of oxalic acid residual depending on energy irradiation density.

4. Conclusion

The decomposition behavior of oxalic acid by a UV-photo-Fenton AOP was investigated using a medium pressure lamp. The following conclusions were obtained within the experimental ranges.

1. The oxalate decomposition behavior by the Photo-Fenton AOP using a medium pressure lamp follows a first-order reaction.
2. The oxalate decomposition behavior is dependent on the UV energy irradiation density[kJ/L] regardless of the recirculation speed and quantities.

ACKNOWLEDGEMENT

This work was supported by the National Research Foundation of Korea(NRF) and the Ministry of Science and ICT(MSIT) of the Republic of Korea. (No. 2017M2A8A5041776)

REFERENCES

- [1] Zuo, Yuegang, and Yiwei Deng., "Iron (II)-catalyzed photochemical decomposition of oxalic acid and generation of H_2O_2 in atmospheric liquid phases.", *Chemosphere*, 35(9), 2051-2058(1997).
- [2] Oguma, Kumiko, Hiroyuki Katayama, and Shinichiro Ohgaki., "Photoreactivation of *Escherichia coli* after low-or medium-pressure UV disinfection determined by an endonuclease sensitive site assay.", *Applied and environmental microbiology*, 68(12), 6029-6035(2002).

Review of Control Methods of Full System Decontamination Operation Temperature and Decontamination Facility Inlet Temperature

Hak-Soo Kim*, and Cho-Rong Kim

Korea Hydro Nuclear Power Co., Ltd. Central Research Institute, 70, Yuseong-daero 1312beon-gil, Yuseong-gu, Daejeon, Republic of Korea

*hskim0071@khnp.co.kr

1. Introduction

System decontamination applied after nuclear power plants are permanently ceased is the technology to remove contaminated metal oxide films, or metal oxide deposits from the interior surfaces of systems or equipment using the NPP facility and decontamination facility. Since full system decontamination operation is very different from normal operation of the NPP, various operating conditions required in the operation of the actual plant can be excluded. As shown in Fig. 1, the full system decontamination of Kori-1 NPP, which was the first permanently ceased in Korea, is planned to be carried out for Reactor Pressure Vessels (RPV), Pressurizer (PZR), Steam Generators (SG), Chemical & Volume Control System (CVCS), Residual Heat Removal System (RHRS), and Reactor Coolant System (RCS) piping and system decontamination facility is planned to be connected to the RHRS.

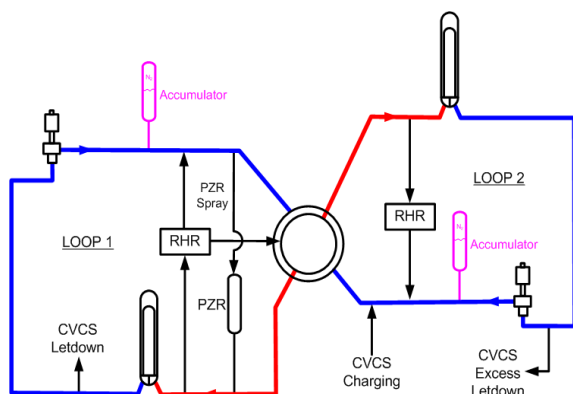


Fig.1. Schematic Diagram of WH-2 Loop PWR Reactor Coolant System.

The system decontamination operating conditions required to effectively decontaminate these systems and equipment are as follows.

- Facilities of Kori-1 NPP are operable
- Connected System decontamination facility to RHRS
- The range of system decontamination include RPV, PZR, SG, CVCS, RHRS and RCS piping
- Conditions of system decontamination operation temperature and pressure
 - Temp./Pressure in RCS : 95℃ / 25 bar
 - Inlet temperature of system decontamination facility : 40℃

This paper dealt with control method of full system decontamination operation temperature and

decontamination facility inlet temperature.

2. Control Method of System Decontamination Operation Temperature

In the case of maintaining the system decontamination operating temperature at 95℃, it is possible to operate at atmospheric pressure because the operating temperature is much lower than that of normal operation of NPP. The temperature increase for the system decontamination operation can be achieved by using PZR heater and RHR heat exchanger. However, if the PZR spray flow rate is low, it may take a long time to control the temperature, and the required time can be calculate using Equation (1).

$$T(rcs) = T_{in} + \frac{T_{rcs0} - T_{in}}{\exp\left(\frac{Min}{Mr_{cs}}\right)} \quad (1)$$

where, T_{in} : RCS temperature

T_{rcs0} : RCS initial temperature, 20℃

Min : RCS flow rate, gpm

Mr_{cs} : RCS volume

Fig. 2 shows the RCS temperature increase characteristics with the flow rate of auxiliary spray.

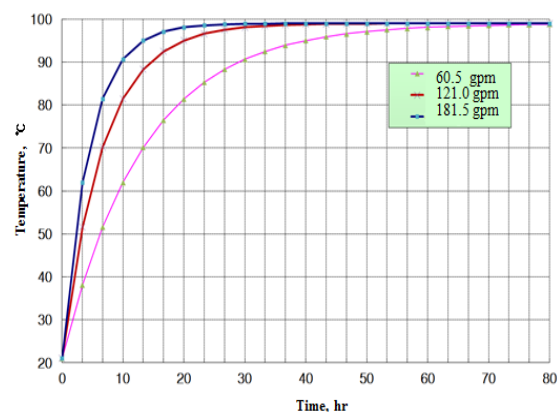


Fig. 2. RCS Temperature Increase Characteristics with Auxiliary Spray Flow Rate.

The RCS temperature characteristics are evaluated based on the PZR temperature is 99℃ and RCS temperature is 20℃. As shown in Fig. 2, it was estimated that it would take about 40 hours up to the system decontamination operation temperature, 95℃ for one charging pump operating, 20 hours for the two charging pumps, and 17 hours for the three

charging pumps. It takes a long time to increase RCS temperature to the system decontamination operation temperature but if the system decontamination operation temperature reaches, it is possible to control the system decontamination operation temperature using the PZR heater.

3. Control Method of System Decontamination Facility Inlet Temperature

The system decontamination facility consists of chemical injection system and chemical waste decomposition & treatment system to remove oxide film in the system decontamination range and to decompose the chemical waste. The temperature condition of the chemical waste flowing into the system decontamination facility after completion of the oxidation-reduction process in the RCS should be provided below 40°C considering the operation efficiency of the UVC lamp in the chemical waste decomposition & treatment system. Fig. 3 shows the efficiency of organic acid decomposition with UVC operating temperature and Fig.4 shows the location where system decontamination facility is connected to the RHRS.

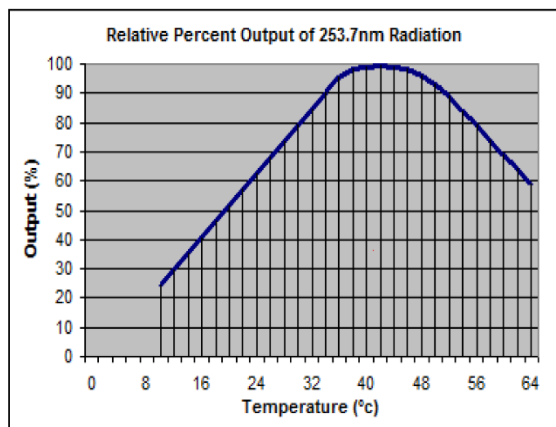


Fig. 3. Efficiency of Organic Acid Decomposition with UVC Temperature.

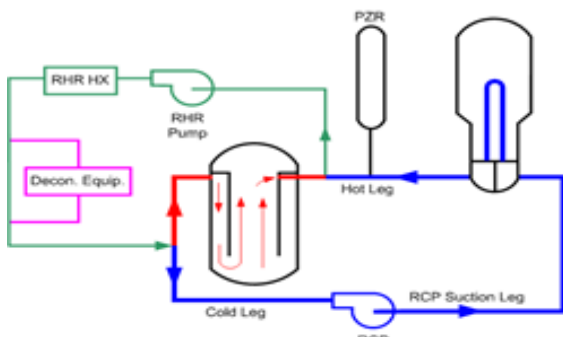


Fig. 4. Connection Location of System Decontamination Facility.

The actual operation of the RHR heat exchanger to maintain the system decontamination operation

temperature, 95°C, can be expected as shown in Table 1.

Table 1. Temperature in RHR Heat Exchanger

Items	Shell side(CC)	Tube side(RHR)
Flow Rate	600 m ³ /hr	468 m ³ /hr
Inlet Temp.	26.8°C	95.0°C
Outlet Temp.	50.6°C	64.5°C

The data in Table 1 are obtained when the RHR heat exchanger is operating for cooling the RCS. It is possible to keep the inlet temperature of the system decontamination facility below 40°C according to the current plant operation procedure. The flow rate to keep the RHR heat exchanger outlet temperature below 40°C is about 260 m³/hr and since this flow rate is about 10 times larger than the treatment capacity of the system decontamination facility, it is expected that the temperature control can be achieved by adjusting the RHR flow rate and component cooling water flow rate.

4. Conclusions

This paper dealt with control method of full system decontamination operation temperature and decontamination facility inlet temperature to effectively decontaminate the full system decontamination range. As a result, it was confirmed that the temperature increase for the system decontamination operation can be achieved by using PZR heater and RHR heat exchanger and system decontamination inlet temperature can be achieved by adjusting the RHR flow rate and component cooling water flow rate.

ACKNOWLEDGMENT

This work was supported by the Korea Institute of Energy Technology Evaluation and Planning (KETEP), granted financial resources from the Ministry of Trade, Industry & Energy(Number 20141510200310)

REFERENCES

- [1] Kori Unit 1, 'Final Safety Analysis Report of Kori Unit 1,' KHNP (2014).
- [2] H.S. Kim, C.R. Kim, 'Review of Operating Conditions for Full System Decontamination Operation Procedure Development of Kori-1 Nuclear Power Plant,' KRS Spring Conference, 2018.
- [3] H.S. Kim, C.R. Kim, 'Flow Characteristics Evaluation in Reactor Coolant System for Full System Decontamination of Kori-1 Nuclear Power Plant,' Journal of Nuclear Fuel Cycle and Waste Technology, Vol.16, No.3, 2018. 9.

US-APR1400 Design Features to Facilitate Decommissioning

Hye-Young Shin

Korea Hydro & Nuclear Power Co., Ltd. Central Research Institute, 70, Yuseong-daero 1312beon-gil,

Yuseong-gu, Daejeon, Republic of Korea

*shinehyshin@khnp.co.kr

1. Introduction

During the long history over 40 years of nuclear power generation, Korea has been experiencing a full lifecycle of nuclear power plants. While Kori Unit 1 had started its decommissioning in June 2017 for the first time in Korea, the Korean export type reactor APR1400 has been being improved to re-enter overseas since the first export to UAE in 2009. Even though Korean history of decommissioning is not so long, many foreign experiences showed that consideration of decommissioning from the design stage is very important for safety and economy of nuclear power plants because decommissioning is a work consuming large amount of both time and cost.

This paper reviews design features on US-APR1400 (APR1400 NRC-DC model) and identifies further works for construction in U.S.A from the decommissioning point of view

2. Regulatory Scheme and Application

Since the issuance of decommissioning regulations in 1997, known as LTR (License Termination Rule), lessons learned from real implementations of decommissionings revealed that decommissioning needs to be considered at all stages in the lifecycle of a NPP, especially from the planning and design stages of a NPP, even though it is the last stage. Therefore the final rule for decommissioning, Decommissioning Planning Rule (DPR), was published in 2011 [1].

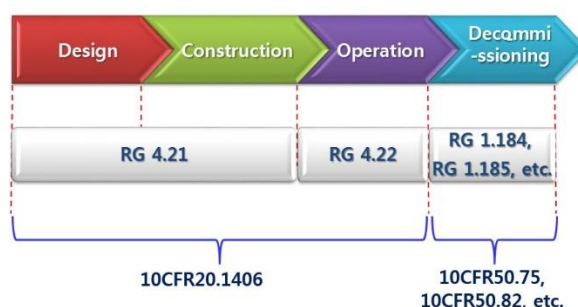


Fig. 1. Application Scope of Decommissioning-related Regulations under U.S. NRC's DPR.

Under DPR, existed or newly established several regulations and guides regarding decommissioning are closely and sequentially related by stages as shown in Fig. 1. Conformance of US-APR1400, currently targeting the standard design certification from U.S. NRC, to the related regulations is indicated in Table 1.

Table 1. Conformance with Regulatory Guides (RGs) on Decommissioning (DC) of US-APR1400

Doc. No.	Subject	Apply
RG 4.21	Minimization of Contamination and Radioactive Waste Generation	SDC ¹
RG 4.22	DC Planning During Operations	COL ²
RG 1.159	Availability of Funds	COL
RG 1.184	Decommissioning of NPPs	COL
RG 1.185	Standard Format and Content for Post-Shutdown DC Activities Report	COL
RG 1.191	Fire Protection Program	COL
RG 1.202	Standard Format and Content of DC Cost Estimates	COL

¹ SDC: Standard Design Certification

² COL: Combined license (for construction and operation)

3. Decommissioning Design Features of US-APR1400 [2]

In order to reflect the requirement of facilitation decommissioning according to Reg. Guide 4.21, US-APR1400 design has several physical design features for minimizations of the amount of residual radioactivity/waste generations, and for easy removal during decommissioning. Table 2 shows the categorized representative decommission-related design features and Fig. 2 presents a typical schematic design for piping penetrations and sleeves between buildings in order to prevent unintended contamination to the environment.

Table 2. Decommissioning Design Features to facilitate decommissioning US-APR1400

Design Features	Applied SCs
Minimization of Embedded and/or Buried Piping	Minimal: CSS, etc.(9) None: SCS, CMS, etc.(11)
Piping Sleeve/Tunnel Between Buildings with Leak Detection	SFPCCS, ESWS, CCWS, PPASS, EFDS, etc. (7)
Continuous Water Purification/Sampling/Analysis	RCS, SGBDS (2)
Smooth Surface Finishes	SIS, CSS, MSS, etc. (13)
Accessibility	RCGVS, PPASS (2)
Modular Units/Compartments /Individual Assemblies	PAR, HI, ACUs, AHU, RFFCs, etc

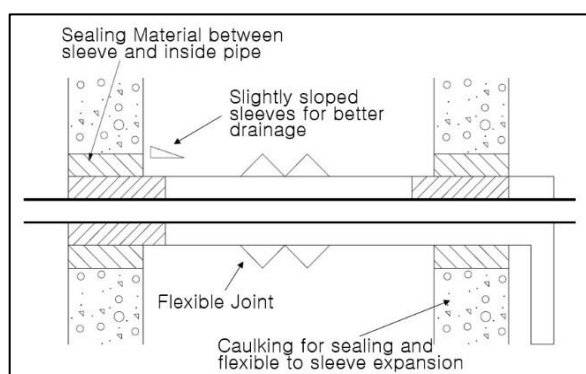


Fig. 2. Typical Design for Building Sleeves Schematic.

4. Further works for COL application

For the COL application of US-APR1400 to U.S. NRC, this means another export of APR1400, a full compliance with RG 4.21 is required. Several activities for that purpose have been identified and are indicated in Table 3.

Table 3. COL items regarding facilitation of decommissioning of US-APR1400

No	COL Activities
1	Estimate construction worker doses based on the site-specific information such as the number of operating units, meteorological conditions, etc.
2	Provide operational procedures and programs including a site radiological environmental monitoring program
3	Implement concrete tunnels coated with epoxy and equipped with sumps for piping of the system that may include underground piping
4	Maintain complete documentation regarding decommissioning planning and implementation in a centralized area for ready recovery

5. Conclusion

US-APR1400 has the improved design features for facilitation of decommissioning and is ready for an entrance to US nuclear market with the well identified decommission-related activities for the stage of construction.

REFERENCES

- [1] U.S. NRC, "Decommissioning Planning Rule," Federal Register, Volume 76, Number 117, June 17, 2011, pp. 35512-35575.
- [2] KEPSCO/KHNP, APR1400 DCD Tier 2, Chapter 12, APR1400-K-X-FS-14002-NP, Rev. 3, August, 2018, pp. 12.4-11 to 12.4-16.

Decontamination of Concrete Waste Generated From Nuclear Power Plant Decommissioning With Different Organic Solvents

Seok-ju Hong, Sangsoo Han, Seongsik Nam, Won-Seok Kim, and Wooyong Um*

Pohang University of Science and Technology, 77, Cheongam-ro, Nam-gu, Pohang-si, Gyeongsangbuk-do, Republic of Korea

*wooyongum@postech.ac.kr

1. Introduction

Contaminated radioactive concrete waste is one of the main issues in Nuclear Power Plant (NPP) decommissioning, because of its large amount and volume. Therefore, many countries are trying to reduce the volume of radioactive concrete/cement wastes.

However, the methods of decontamination process are all different in each country. For example, CITROX process uses a mixture of oxalic acid (2.5wt%) and dibasic ammonium citrate (5wt%) [1]. CORD process mainly uses oxalic acid, and CAN-DECON process which modified the CITROX process, uses ethylenediaminetetraacetic acid(EDTA), oxalic acid, and citric acid with mass ratio of 2:1:1 [2].

In this regard, Korea also needs to establish the most efficient decontamination process before starting the Go-ri 1st NPP decommissioning. Therefore, this study was conducted to find optimal decontamination condition for concrete waste with various concentrations of organic acids.

2. Materials and Methods

2.1 Simulated Concrete Coupon

Simulated concrete coupons were made with 37 g of sand, 24 g of aggregates, 21 g of Portland cement (Type I/II), 13 g of DI water and 5 g of fly ash. After complete mixing, concrete slurry was poured into a paper mold (5 cm diameter and 10 cm height) and cured for a week with high relative humidity condition (80~90%).

Cobalt nitrate hexa-hydrate ($\text{Co}(\text{NO}_3)_2 \cdot 6\text{H}_2\text{O}$) and

cesium nitrate (CsNO_3) were used to contaminate the concrete coupons. During curing, about 10,000 ppm of Co or Cs solution (0.4 mL of each) was spiked individually into the concrete coupons at a depth of 0.7 cm from the outer surface, using a glass syringe.

2.2 Thermal Deterioration

In our previous [3] study, 1 hour of deterioration at 550°C was found to be the optimal thermal treatment condition. After thermal deterioration, the samples were crushed by hammer to separate the cement paste from concrete aggregates. Concrete pastes were completely mixed for the homogeneity before use.

2.3 Chemical Decontamination

Nitric acid solution with pH 2 (DI water 40 mL + 70 uL of Nitric acid 60%) was used for based solution. To find an optimal decontamination condition, EDTA, oxalic acid, and citric acid were prepared and tested. Decontamination experiments were carried out with a concentration of 500, 1000, 2000, 4000 ppm of each organic solvent. An additional 8000 ppm was also carried out, similar to the CAN-DECON process.

After decontamination experiments, the released amounts of Co and Cs were analyzed by Inductively coupled plasma mass spectroscopy (ICP-MS).

2.4 Characterization

X-Ray Diffraction (XRD) was used to identify the type of minerals from the concrete paste. Scanning Electron Microscope (SEM) was used to observe the

surface morphology of concrete paste. Fourier Transformed Infrared Spectroscopy (FT-IR) was used to analyze the changes in chemical bonds.

3. Results and Discussions

3.1 Concrete Preparation and Deterioration

After the thermal deterioration at 550°C, concrete coupons showed severe cracks on their surfaces and the color of concrete also changed to bright.



Fig. 1. Thermal treatment at 105°C (left) and 550°C (right).

3.2 Concrete Paste Separation

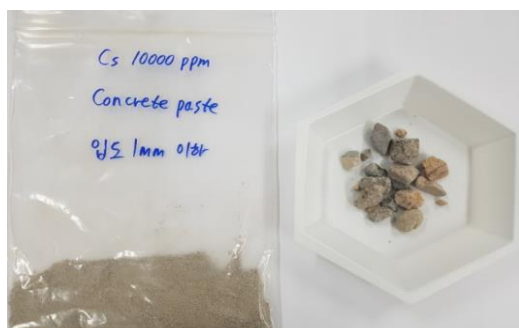


Fig. 2. Separation of concrete pastes and aggregates.

Over 95% of concrete aggregates were recovered (initial input mass: 24 g, recovered mass: 23 g~23.5 g) after the separation.

3.3 Chemical Decontamination

We could see that different types of organic acids should be used depending on the type of target nuclides. Concentration of each organic acid also has affected the efficiency of decontamination.

Table 1. Organic acids additives

	Concentration (ppm)				
EDTA	500	1000	2000	4000	8000
Oxalic acid	500	1000	2000	4000	
Citric acid	500	1000	2000	4000	

From the results, we could set the optimum organic acid type and its concentration for the best efficiency.

4. Conclusion

This study was carried out to find the optimum decontamination conditions by changing the concentrations and times of various organic acids that are commonly added to existing decontamination processes such as CITROX, CAN-DECON and CORD. The results of this study will increase our understanding of chemical decontamination process to reduce the volume of concrete wastes generated from the NPP decommissioning.

ACKNOWLEDGEMENT

This research was supported by Advanced Nuclear Environment Research Center (ANERC) from the National Research Foundation of Korea (NRF), NRF-2017M2B2B1072374 and NRF-2017M2B2B1072404

REFERENCES

- [1] John F. Remark, Fia, Plum Borough, Thomas G. Bengel et al. "Process for decontaminating a nuclear reactor coolant system", U.S. Patent No. 5,305,360, February 16th, 1993.
- [2] Petri Kinnunen, "Decontamination techniques for activity removal in nuclear environments", VTT Technical Research Centre of Finland, Research report No. VTT-R-00299-08, March 12th, 2008.
- [3] Sangsoo Han, Seok-ju Hong, Seongsik Nam, Won-Seok Kim, and Wooyong Um "Characterization and thermal treatment application for radioactive concrete wastes from nuclear power plant decommissioning", Korean Nuclear Society, May 17th, 2018.

Radionuclides Removal Using Cancrinite and Chalcogel Sorbents

Sangsu Park*, Jaehyuk Kang, and Wooyong Um

Pohang University of Science and Technology, 77, Cheongam-ro, Nam-gu, Pohang-si, Gyeongsangbuk-do, Republic of Korea

*pss33823012@postech.ac.kr

1. Introduction

Oxidation layer of primary system of nuclear power plant consists of radionuclides and metals like Fe, Ni, Cr etc. The layer is generally removed by chemical oxidation-reduction decontamination (CORD) process which is a kind of chemical decontamination method. Then, the remaining contaminants (radionuclides and metals) in waste solution is treated by passing ion exchange resin to remove the metal ions. However, the spent resin is not easy to dispose because of the presence of some organic materials and large volume of the spent resin which is about 4500 L. Therefore, it is necessary to reduce the volume of the waste resin and develop the inorganic sorbents which can be easily used for waste form and disposal in repository.

In this study, we synthesized cancrinites and chalcogel to remove the radionuclide and metal ions in simulated CORD waste solution condition. Cancrinites were expected to have high ion exchange capacity for heavy metal cations and anions due to its low Si/Al ratio and the presence of exchangeable anions in cage structure [1]. In addition, chalcogel was investigated to have high specific surface areas and multifunctional characteristics for use of sorbent. Our main objective is to synthesize inorganic sorbents (cancrinites and chalcogel) for removal of radioactive wastes in CORD waste solution and understand the removal mechanism.

2. Experimental section

2.1 Synthesis of cancrinites

Cancrinites were synthesized using hydrothermal synthesis method at low temperatures of 200 °C and autogenous pressure in 125 mL Teflon-coated steel Parr reactor. For carbonate cancrinite, 4 g of kaolinite($\text{Al}_2\text{O}_3\cdot\text{Si}_2\cdot 2\text{H}_2\text{O}$) and 0.5 M of sodium carbonate were mixed in 90 mL of 8 M of sodium hydroxide solution. The synthesis was performed for 45 h inside an oven. All the final products were centrifuged by 3000 rpm for 10 min, washed to decrease pH to around 7 using deionized (DI) water and dried for 24 h at 80 °C. The final white powder products were analyzed by X-ray diffraction for mineral identification. In case of nitrate cancrinite, 1 M of sodium nitrate and 72 h heating was used instead of sodium carbonate and 45 h heating process for carbonate cancrinite synthesis.

2.2 Synthesis of chalcogel

Chalcogel was synthesized using Sol-Gel method. For synthesis of Co-Pb-MoS chalcogel, 0.14 mmol of $\text{Co}(\text{NO}_3)_2\cdot 6\text{H}_2\text{O}$ and 0.06 mmol of $\text{Pb}(\text{CH}_3\text{COO})_2\cdot 3\text{H}_2\text{O}$ were dissolved in 4 mL of formamide. Ammonium tetrathiomolybdate (0.2 mmol) was dissolved in 2 mL of formamide. Then, Co-Pb precursor solution was added into the tetrathiomolybdate solution without stirring or heating for 7 days. Then, mixed solution was

decanted and the chalcogel was washed by DI water for 5 days to remove the residual ions with changing the DI water every 24 h. Then, the chalcogel was divided to two parts of particles. One was dried using Freeze dryer (0.1 mBar, -50°C), while another was dried at room temperature without oven.

3. Results

The XRD results of synthesized cancrinites are shown in Fig. 1 and 2. The XRD patterns of synthesized cancrinites (nitrate and carbonate) well match with the references. Synthesized chalcogel shows black color as shown in Fig. 3. After the freeze drying process, the chalcogel becomes powder which makes the surface area increased. Additional analysis (SEM-EDS, BET, etc.) is also planned for chalcogel characterization.

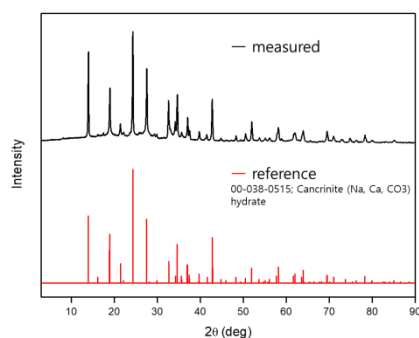


Fig. 1. XRD pattern of the carbonate cancrinite with reference.

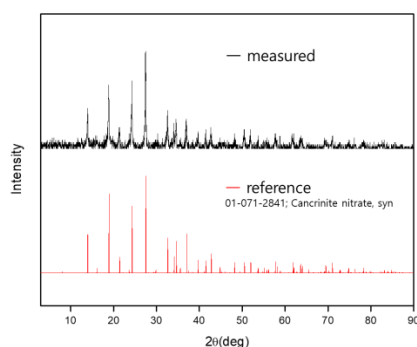


Fig. 2. XRD pattern of the nitrate cancrinite with reference.

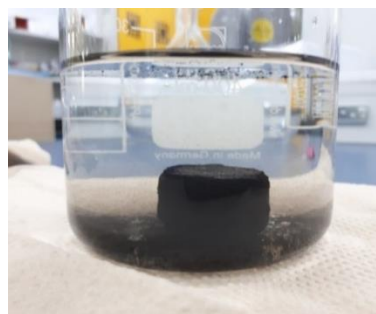


Fig. 3. Solvent exchanging process of the chalcogel.

4. Conclusions

The adsorption using the synthesized cancrinites and chalcogel would be conducted under the aqueous condition prepared to mimic the CORD waste solution. In carbonate cancrinite, because of carbonate ion playing a role for a pH buffer, the carbonate cancrinite was still stable and could be used even at low pH conditions ($\text{pH}=1-3$), while nitrate cancrinite was dissolved in low pH condition. For the chalcogel, ability to stand at low pH should be tested. In addition, both of the inorganic sorbents would be investigated for removal of radionuclides.

ACKNOWLEDGEMENT

This work was supported by KOREA HYDRO & NUCLEAR POWER CO., LTD (No. 2017-Tech-07)

REFERENCES

- [1] Hackbarth, K. et al., "Synthesis and crystal structure of carbonate cancrinite $\text{Na}_8[\text{AlSiO}_4]_6\text{CO}_3(\text{H}_2\text{O})_{3.4}$, grown under low-temperature hydrothermal conditions.", *Microporous and Mesoporous materials*, 1999. 30(2-3): p.347-358.

Treatment of Radionuclide From CRUD Using Underwater Microwave Plasma

Seongsik Nam and Wooyong Um*

Pohang University of Science and Technology, 77, Cheongam-ro, Nam-gu, Pohang-si, Gyeongsangbuk-do, Republic of Korea

*wooyongum@postech.ac.kr

1. Introduction

As nuclear power plants (NPPs) are getting older, the levels of radioactive contamination are also increased. CRUD (Chalk River Unidentified Deposit) is a kind of corrosion product accumulated on the metal surfaces of NPP as the operation time goes by. Decontamination of CRUD is really important task because radionuclides such as ^{60}Co (γ -emitter) can be deposited and react with the constituents of CRUD. The objective of this study is to decontaminate radionuclides such as ^{60}Co from the CRUD waste using microwave plasma approach in underwater system. In comparison with other techniques, microwave plasma in water technique was developed to provide high reliability for the environmental aspect using, efficient generation of plasma and high frequency radical.

2. Materials and Methods

2.1 Experimental setups of underwater plasma system

The experimental set-up of CRUD decontamination by underwater plasma system is described in Fig. 1. It includes argon and hydrogen supply system, microwave plasma torch, high voltage power supply and radical analysis (optical emission spectrometer) instruments. This system can generate microwave plasma that can react with synthesized CRUD samples inside of the acid solution.

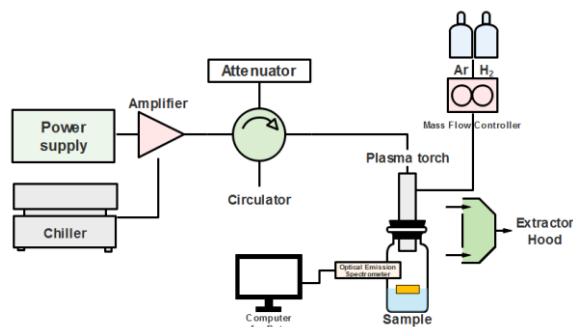


Fig. 1. Schematic diagram of Underwater Microwave Plasma system.

Inside of acid solution, typical chelate agent, EDTA was added to synthetic decontamination liquid waste and measured the kinds of generated radical at the same time with optical emission spectrometer. In addition, UV-VIS spectrometer was used to measure the oxidation state of cobalt ions.

2.2 Synthesis of Co-doped simulated CRUD

A doping method was used to deposit CRUD on stainless steel SUS 304 (Ni: 8~11%, Cr: 18~20%, Fe). The surfaces of metallic (SUS 304) samples were abraded using silicon carbide paper (#1200), then washed in acetone (99.5%, KANTO) with ultrasonic cleaner (BRANSON 1510) for 5 min. After that, 0.25 mL of cobalt nitrate solution (150 g/mL) was spread on the metallic coupon and dried at 100 °C. This procedure was repeated four times. Finally, 1 mL of cobalt nitrate was doped on the metal coupon. To form an oxide layer on the coupon surface, it was heat treated at 700 °C for 24 h. XRD and XPS were conducted to characterize CRUD samples.

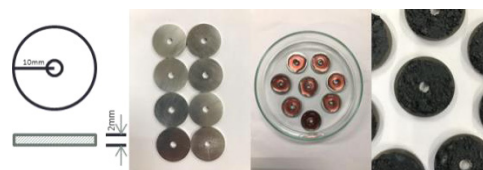


Fig. 2. Schematic diagram and doped metal coupon.

3. Results & Discussion

To see the effect of plasma, the synthesized simulated CRUD samples were characterized using x-ray diffraction (XRD) to identify the mineralogy. Compared with original data, the intensity of cobalt ferrite was reduced when it was treated by H₂ gas plasma. In details, Co²⁺ and Fe³⁺ changed their oxidation state to reduced state or elemental metal ions such as Co⁰, Fe⁰, and Fe²⁺ respectively.

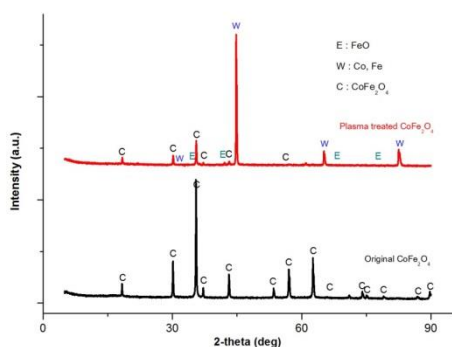


Fig. 3. XRD patterns of original CoFe₂O₄ (black) and after treatment with H₂ gas plasma (red).

The chemical composition of the samples is further studied using XPS analysis. The counts of Co, Fe, and O elements are decreased after H₂ plasma treatment (Fig.4).

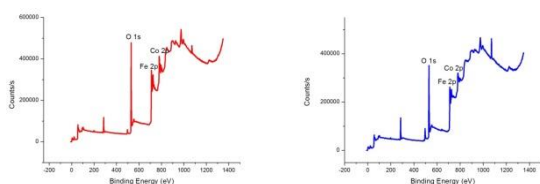


Fig. 4. XPS spectra of the CRUD (a) survey spectrum, (b) survey spectrum treated with H₂ gas plasma.

Additional microwave plasma generated by argon gases in the liquid condition was applied and the oxidation number of cobalt(II) was changed to oxidized state, Co(III), which is different from the result of plasma with H₂ gas condition. Reference peaks of cobalt(III), 382 nm and 530 nm increased with reaction time (Table 1). Cobalt(II)-EDTA complex was also found in the solution. According to Table 1, oxidation state of cobalt ions is changed to

2⁺ to 3⁺, during the argon microwave plasma reacted with simulated CRUD.

Table 1. Change of UV absorbance at 532 nm with increasing reaction time

Time	Absorbance at 532 nm wavelength
5 min	0.103
10 min	0.115
20 min	0.132
30 min	0.147

4. Conclusion

The microwave plasma in underwater system can be applied to decontamination process for the selective decontamination and volume reduction of the metal wastes. Further study will be investigated with varying decontamination reagent, power, temperature, ion conductivity, and pH. Development and application of our results will contribute to make an effective and safe decontamination process of nuclear power plants.

ACKNOWLEDGEMENT

This work was supported by Nuclear Research & Development Program of the National Research Foundation (NRF) grant (NRF- 2018M2B2A906 5874) funded by the Korean government (MSICT).

REFERENCES

- [1] Kim W-S, Nam S, Chang S, Kim H, Um W. Removal of Chalk River unidentified deposit (CRUD) radioactive waste by enhanced electrokinetic process. Journal of Industrial and Engineering Chemistry, 7:89-96, 2015.
- [2] NEA, The Decommissioning and Dismantling of Nuclear Facilities, 2002.

Review on the Liquid Radioactive Material Leakage Accidents in the U.S.

Jung-ha Kim *, Hyoung-woo Lee, Ju-youl Kim, and Chang-lak Kim

Korea Electric Power Corporation International Nuclear Graduate School, 658-91, Haemaji-ro, Seoseng-myeon,
Ulju-gun, Ulsan, Republic of Korea

*jjjjjung0920@hanmail.net

1. Introduction

Korean nuclear power plants (NPPs) are expected to enter the phase of permanent shutdown in the 2020s if there is no extension of their design life. Kori unit 1 is in the process of preliminary work to prepare for decommissioning after the decision of permanent shutdown in June 2017, and the on-site restoration work is scheduled in 2031. Korea has no experience of decontamination of groundwater and soil pollution in NPP site, therefore, it is useful to review previous experiences of other countries for establishing strategies for restoration of groundwater and it is important to develop effective remediation strategies based on the analysis of groundwater and soil pollution decontamination cases from operating NPPs in the U.S. The purpose of this study is to investigate the contamination case from operating NPPs in the U.S. and to propose some valuable considerations.

2. Case Study on Liquid Leakage Accidents

A total of 14 operating NPPs that experienced contamination with leaked liquid radioactive materials were investigated as shown Table 1.

Table 1. NPPs where liquid radioactive materials were leaked during operation

NPP	Type	Op./Shut.	Capacity (MWt)
Oyster Creek	BWR	1969/2018	1,930
Brunswick Unit 1	BWR	1977/undecided	938
Brunswick Unit 2	BWR	1975/undecided	920
Quad Cities Unit 1	BWR	1973/2018	908

Quad Cities Unit 2	BWR	1973/2018	911
Callaway	PWR	1984/undecided	1215
Braidwood	PWR	1988/undecided	1194
Palo Verde Unit 2	PWR	1986/undecided	1314
Palo Verde Unit 3	PWR	1988/undecided	1312
Byron	PWR	1985/undecided	1164
Indian Point Unit 1	PWR	1962/1974	615
Indian Point Unit 2	PWR	1974/undecided	3216
Point Beach	PWR	1970/undecided	591
Three Mile Island	PWR	1974/undecided	2568
Watts Bar	PWR	1996/undecided	3459

Table 2 lists the causes of the liquid radioactive materials leakage accidents in operating NPP and the countermeasures.

Table 2. Summary of Leakage Accidents in NPPs

NPP	Leak Detection		Nuclide	Cause	Countermeasures
	Date	point			
Oyster Creek	2009. 04.15	Condensate Transfer System	H-3	Leakage from pipelines of 8 and 10 inch diameter between facility and Condensate Storage Tank	Pipeline Replacement
Brunswick	2007. 05.07	Manhole near Storm Drain Storage Pond	H-3	Leakage from Storm Drain Storage Pond	Continuous analysis of concentration after installing additional tube well for sampling
Quad Cities	2007. 10.12	Tube well newly installed in site	H-3	Suspected underground pipeline connected to Condensate Storage Tank	Inspection of underground pipeline connected to Condensate Storage Tank and installation of additional tube well for concentration monitoring

Callaway	2006.06.14	Surface toil inside manhole where drainage valve is installed	H-3 Cs-134 Cs-137 Co-58 Co-60	Leakage through vacuum breaker valve during discharge of liquid radioactive materials through drainage pipeline	Suspension of discharge of drainage pipeline and installation of Collecting Pond below valve to capture leakages
Braidwood	2005.03	Well near NPP	H-3	Leakage through openings of vacuum breaker valve in circular water drainage pipe and drainage cooler protection valve in Feed Water System	decontamination of H-3 after installation of additional tube well for identifying contaminated area
Palo Verde	2006.03.01	Groundwater in Unit 3 area	H-3	Gas leakage from Boron Concentrating System	Installation of new tube well and continuous monitoring and evaluation
Byron	2006.02.10	Storage room for vacuum breaker valve	H-3	Leakage from Vacuum Breaker Valve	Determination of contaminate area and leakage monitoring
Indian Point	1992	Spent Fuel Pool Water	H-3, Ni-63, Cs-137 Sr-90 Co-60	Welding defect in SFP Stainless Liner	Isolation of leakage area (Installation of Collecting Pond))
Point Beach	1975.02	Pond in site	H-3 Cs-137	Rupture of Steam Generator tube	Groundwater monitoring and submission of site-specific report on contamination
Three Mile Island	1999	Condensate Storage Tank	H-3	Rupture of ice-making pipeline	Continuous and enhanced monitoring of groundwater
Watts Bar	2004.12.29	Shield Building annulus in Unit 2	H-3	Waste discharge pipeline and temporary radioactive waste pipeline	countermeasure to remove contaminate soil

Table 2 showed that the contamination-related nuclear species were Cs-137, Co-60 and H-3, and where H-3 was dominant. The causes of contamination were valve defects, operational accidents by operator and welding defects during repair work with leakage through valve rupture of pipeline being dominant. In the United States, countermeasures were replacement or repair of the pollutant valve and no specific decontamination activity on soil contamination was performed. In the case of groundwater, the management activities were continuous monitoring not to exceed 20,000 pCi/L

which is a EPA criterion for drinking groundwater. In Korea, the fact that the groundwater in decommissioned NPP site is not used as drinking water should be considered in establishing evaluation and decontamination criteria, and the restoration methods should be selected based on the analysis of the contamination range of groundwater and soil in the NPP sites to be decommissioned.

3. Conclusion

This study reviewed groundwater and soil pollution cases of NPPs in the U.S. We proposed several considerations specific for conditions in Korea. It was found that the investigation of major contaminated area, currents status of a radionuclide H-3 distribution, and development of continuous monitoring plan and evaluation guide of groundwater are needed.

ACKNOWLEDGEMENT

This research was supported by the Nuclear Safety Reserch Program through the Korea Foundation of Nuclear Safety (KOFONS), granted financial resources from the Nuclear Safety and Security Commission (NSSC), Republic of Korea (No. 1605008).

REFERENCES

- [1] Liquid Radioactive Release Lessons Learned Task Force Final, U.S.NRC.
- [2] Groundwater Events Sorted by Location, U.S. NRC.
- [3] Exelon Generation Co., Tritium Leakage, PNO-RIII-06-004, 2006.

Application of a Logistical Simulation Model to Planning of Soil Washing Process

Jihan Jeon*, Jaeyeon Jung, Eutteum Oh, David S. Kessel, and Changlak Kim

Korea Electric Power Corporation International Nuclear Graduate School, 658-91, Haemaji-ro, Seosaeng-myeon, Ulju-gun, Ulsan, Republic of Korea

*jihana@emal.kings.ac.kr

1. Introduction

Soil washing is one of the decontamination techniques to remove radioactive materials from the surrounding soil of nuclear power plants in the soil remediation stage. The nature of this work is repetitive and requires significant resources, and it has uncertainty due to lack of domestic experience.

However, modeling the soil washing process using the simulation tools at the planning stage can make the process more predictable and more efficient. This study suggests the application of a discrete event simulation model to the site remediation work, especially the soil washing process.

2. Soil Washing Process

2.1 General

Soil washing is an ex-situ, water-based remediation process that removes surface contaminants of soils by separation and treatment of soils. Soil washing is based on the principle that contaminants are generally bound more tightly to the fine soil particles (silts and clays) and not to larger grained sand and gravel [1].

In other words, soil washing is used to separate contaminated fine particles and wash water from the washed coarse particles. A low ratio of silt and clay in the soil will generally reduce the solid waste requiring disposal as radioactive waste. Soil washing must be used with other treatments, such as precipitation, filtration and/or ion exchange. Through the operation, the contaminated residuals (fine particles and washing solution) are treated or disposed of, and the cleaned soil is returned to the site and reused as backfill.

2.2 Procedure

The soil washing process is normally accomplished by physical methods depending on the soil particle size. Fig. 1 below illustrates the general soil washing process.

Soil washing systems usually consist of the following 6 units: [2]

- i) Pretreatment
- ii) Separation
- iii) Coarse grained treatment
- iv) Fine grained treatment
- v) Process water treatment

vi) Residuals management

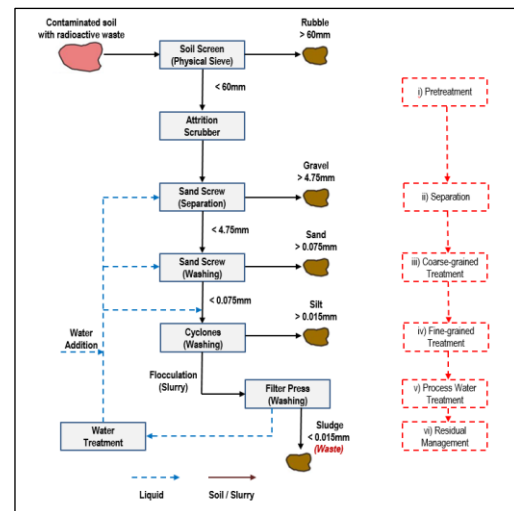


Fig. 1. Soil Washing Procedure.

3. Simulation Model using Flexsim

3.1 Flexsim

A soil washing process was modeled and simulated using the Flexsim software which is widely used in industries such as material handling, manufacturing, logistics, transportation and mining [3].

FlexSim enables implementation of discrete-event simulation (DES). In a DES model, specific events affect the state of system at a specific point in time. DES can be applied to the soil washing process and used as part of site remediation project planning.

3.2 Input Data

The input data used in the soil washing simulation model are the soil excavation rates and the particle size distribution of the soil.

The soil particle size distribution obtained from current soil remediation studies at the Kori nuclear power plant site [4] was used in the simulation model as a source of input data for the soil washing system. Table 1 specifically lists raw data and input data by soil particle size.

Table 1. Input Data of the Model

Parameters	Raw Data		Input Data	
	Type	Value	Type	Value
Excavation Rate	-	-	-	15.0 ton/hr

Particle Size of Soil	Gravel (>4.75 mm)	6.3%	Gravel (>60 mm)	1.0%
			Gravel (60~4.75 mm)	5.3%
	Sand (4.75~0.075 mm)	83.4%	Sand (4.75~0.075 mm)	83.4%
			Silt (0.075~0.015 mm)	3.9%
	Silt & Clay (<0.075 mm)	10.3%	Clay (<0.015 mm)	6.4%
Cleanup Process Rate	-	-	-	10.0 ton/hr

3.3 Simulation Model

The soil washing procedure is modeled based on the conceptual design of process in Fig. 1, and the process rate and logic are programmed based on input data in Table 1. In the model, soil at the project site is the logistics target. The Flexsim model allows 3D visualization of the throughput of soil through the process and detailed flow of soil within the soil washing system. Furthermore, detailed processing data can be shown and extracted as numerical tables or graphical charts.

Fig. 2 shows a screen shot of the 3D simulation model in Flexsim at 5 hours of operation. The excavated soil is fed to the feed hopper on the left side of figure, and the soil that has been cleaned by operation is sent to each sink according to the grain sizes such as rubble, gravel, sand, silt and sludge/clay(waste). Wash water is circulated in the water system placed in the upper part of the figure, and a certain portion of the wash water is discharged into the sink as process waste.

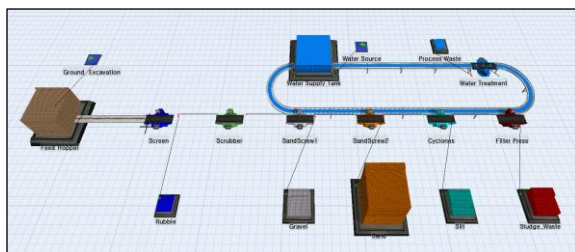


Fig. 2. Logistical Simulation of Soil Washing Process.

3.4 Result

Through the simulation, we can see the visualized soil washing process and throughput. Once the simulation starts, 15 tons of soil per hour are supplied to the feed hopper and the soil washing system operates at 10 tons per hour. Due to difference between the soil excavation rate and process rate, soil

stock is increased in the feed hopper. Table 2 contains the process results after 5 hours of operation. The results show that the amount of process output is approximately close to the input data, which means that the simulation is correctly modeled based on procedure in Fig. 1 and is operating correctly according to the intended logic.

Table 2. Simulation Results at 5-hour-operation

Queue	Rubble	Gravel	Sand	Silt	Sludge	Total
Processed Soil (ton)	0.537	2.666	41.685	1.946	3.134	49.968
Ratio	1.07%	5.34%	83.42%	3.89%	6.27%	100%

4. Conclusion

In this study, we investigated the applicability of a simulation model of soil washing process used in the site remediation project. Although safety against dose exposure is the primary concern in soil remediation, efficient allocation of resources and efficient waste management including volume reduction are also the main objectives in the soil remediation process.

These objectives can be achieved by use of logistical simulation model in the planning stage. Detailed input data are required for more accurate and optimized planning, and it is expected to obtain practical operating data through the management of various properties and parameters in the model.

ACKNOWLEDGEMENT

This research was supported by the International Cooperation Program for Nuclear Energy through the Nation Research Foundation of Korea (NRF), granted financial resources from the Ministry of Science and ICT (MSIT), Republic of Korea (No. NRF-2017M2A8A1092470).

REFERENCES

- [1] US EPA, "Technology Reference Guide for Radioactively Contaminated Media", EPA 402-R-04-004, Washington, D.C., 2007.
- [2] US EPA, "Innovative Site Remediation Technology", EPA 542-B-93-012, Washington, D.C., 1993.
- [3] Flexsim Software Products, Inc., "Flexsim User Manual 2017 Update 1", 2017.
- [4] Seo, Bumkyung, et. al, "Development of Site Remediation Technology for Decommissioning and Contaminated Site," Korea Atomic Energy Research Institute, KAERI/RR-4233/2016 (2016).

The Study for Method of Full System Decontamination to Remove the Inner CRUD Layer on the Primary Piping

Dong-Kyun Ko^{1)*}, Eui-Dong Lee¹⁾, Geon-Hwa Lee¹⁾, Sung-Jun Hong¹⁾, Chang-Sik Kong²⁾, and Kwang-Soo Park²⁾

¹⁾ Hana Nuclear Power Engineering Co., Ltd., 804, Hanam-daero, Hanam-si, Gyeonggi-do, Republic of Korea

²⁾ Doosan Heavy Industries & Construction, 22, Doosan Volvo-ro, Seongsan-gu, Changwon-si, Gyeongsangnam-do, Republic of Korea

*kodk07@naver.com

1. Introduction

In preparation for dismantling Kori Unit 1 nuclear power plant, various parts should be considered on worker's exposure and waste reduction. In order to satisfy this requirement, a full system decontamination, mainly chemical decontamination, is used before the actual decommissioning activities. Generally, widely known full system decontamination methods over the world are CORD-UV, NITROX-E, and ASDOC D-MOD.

In this experiment, chemical decontamination method (Oxidation and Reduction process) is applied to find a way to decontaminate the inner surface of pipe system. From the test, we evaluate decontamination performance of this method.

The specimens are selected to chromium-nickel alloy stainless steels used for RCS pipe material and component material. The expected properties of the crud are selected as metal oxides such as iron and chromium based on Reference [1].

2. Experiment

2.1 Experimental equipment and reagents

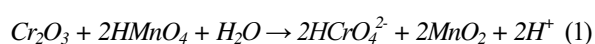
The experimental equipment consisted of a closed system using a circulation pump to circulate the aqueous solution in the reaction tank, and the temperature of the aqueous solution is maintained at 80 °C by a heating controller.

Two reagents are used for the experiment : potassium permanganate(KMnO₄) for oxidizing decontamination process, and oxalic acid(C₂H₂O₄) for reducing decontamination process

2.2 Experimental method

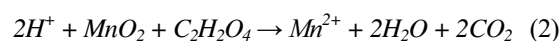
2.2.1 Preparation. Put the specimen and potassium permanganate aqueous solution (4 L, 300 ppm) in the reaction tank and keep the temperature of the aqueous solution at 80 °C by using the heating controller.

2.2.2 Oxidizing Process. HMnO₄ acts as an oxidant, and oxidizes and removed the insoluble Cr₂O₃ layer to soluble CrO₄²⁻.



2.2.3 Preparation for reducing process. After the oxidizing process, the excess amount of C₂H₂O₄ is added and the reaction is repeated for 3 hours. At this time, the same amount of C₂H₂O₄ is further injected once per hour.

C₂H₂O₄ is required to maintain a certain concentration because it plays a role of reducing MnO₂ to Mn²⁺ and reducing iron in the next step



2.2.4 Reducing process. Fe₃O₄ is reduced and

removed as soluble Fe^+ .



The Fig. 1 shows the changes in the oxidizing process and the reducing process when the reagents are added.



Fig. 1. Oxidizing process (Left), Reducing process (Right).

2.3 Results and discussion

After the test, the surface of the specimen is observed with a scanning electron microscope. Fig. 2 is the scanning electron microscope (SEM) image that the uncoated base material (Blank) and before/after decontaminated specimen. Before decontamination, the surface is plated with chromium and a smooth surface is observed. After the decontamination, the plated chrome is peeled off and the surface on which the base material was exposed is observed.

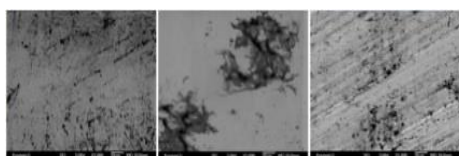


Fig. 2. Scanning Electron Microscope image.
[Blank (Left), Before Decontamination (Mid), After Decontamination (Right)]

Fig. 3 is a photograph of the specimen after chemical decontamination. As shown in the Fig. 3, the base material is visible in the area where the chemical reaction occurs, but in the other side, the chromium plating remains. It is considered that a sufficient reaction time and more decontaminating

agent are required to achieve higher decontamination efficiency

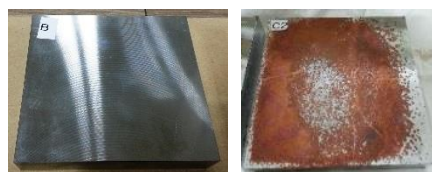


Fig. 3. Specimen before (Left) decontamination and after (Right) decontamination.

3. Conclusion

As shown in the above test results, we know that chemical decontamination method(oxidation and reduction process) can applied to decontaminate the contaminated area such as the crud layer of the surface, and it is confirmed that the direct contact of the worker is minimized.

REFERENCES

- [1] IAEA, Lawrence, E. Boing, 10. 2006, "Decommissioning of nuclear facilities – Decontamination technologies".
- [2] Final report on Application of Decontamination & Dismantling Technology for Old Steam Generator.

A Study on the Reduction Behavior of the Ferric Ion From Phosphoric Electrolyte by Hydrazine

Sae-Binna Lee*, Hyun-Kyu Lee, June-Hyun Kim, Jin-Hee Kim, Yoon-Ji Park, Seung-Won Lee, Won-Zin Oh, and Sang-June Choi

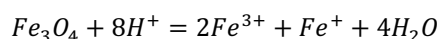
Kyungpook National University, 80, Daehak-ro, Buk-gu, Daegu, Republic of Korea

*dltoqlcsk@knu.ac.kr

1. Introduction

In the phosphoric acid electrolytic decontamination process, accumulation of metal ions including Fe(2+), Fe(3+), Ni(2+), Cr(3+) takes place in the electrolyte. Regeneration of the electrolyte by removing these metal ions has been carried out in the study. The precipitation of metal ions in the form of ferrous oxalate is the process of removing the metal ions in the waste solution.

On the other hand, electrolytic decontamination of the magnetite formed by the internal of the nuclear reactor generates Fe³⁺ and Fe²⁺. The decomposition process of magnetite is as flows.



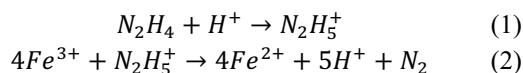
Since Fe³⁺ reacts with oxalic acid used in the precipitation process to form chelate, a reduction process using hydrazine is necessary.

In this study, the reduction behavior of hydrazine, which is a typical material for reducing Fe³⁺ to Fe²⁺ was researched.

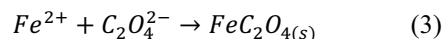
2. Experimental details

2.1 Experimental theory

The Fe³⁺ reduction reaction of hydrazine (N₂H₄) is as follows.



The precipitation reaction of reduced Fe²⁺ is as follows.



2.2 Hydrazine reduction experiment

At first, set the FeCl₃ 0.15 M/L, N₂H₄-dehydrate 0.075 M/L (double concentration of a standard capacity). Then, progress reduction reaction 1hr at 25 °C and 90 °C with N₂H₄. Cool down the temperature until 25 °C, and add the oxalic acid 0.3 M/L and react the precipitate reaction for 5hr at 25 °C.

The Fe ions were analyzed by ICP-OES after filtering the supernatant and initial solution of the precipitate with 0.2 nm filter. And the components of the sediment were analyzed by FE-EPMA and PSA.

3. Results and discussion

In the case of Fe, the removal rate in the case of using hydrazine was 29.12% in RT, and the removal rate was not significantly increased as compared with the case of not using hydrazine. It can be interpreted that hydrazine does not sufficiently reduce Fe³⁺ to Fe²⁺ at RT. However, when hydrazine was used at 90°C, the removal rate reached almost 80%, indicating that the reduction process using hydrazine

requires a heating process

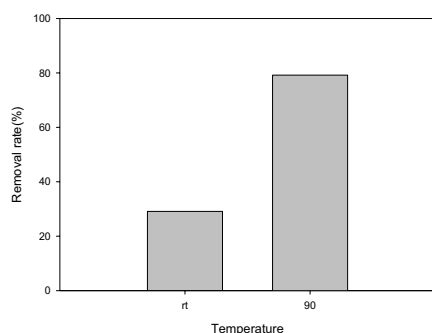


Fig. 1. Fe Removal rate depending on temperature at 4 M/L H_3PO_4 , 0.075 M/L hydrazine.

The analysis of the precipitation is as follows.

Table 1. Result of the precipitation of FE-EPMA

Element	Atom (%)
C	18.2300
O	69.9433
Fe	9.2847
P	2.5421

Since the particles are formed in the phosphoric acid solution, P is the impurity due to this, and the composition for the remaining elements except P is recalculated as follows. C : 18.7055%, O : 71.7676%, Fe : 9.5268%. From this, Fe: C: O = 1: 1.96: 7.5332 ratio can be obtained. It indicate that the precipitate formed $FeC_2O_4 \cdot 2H_2O$.

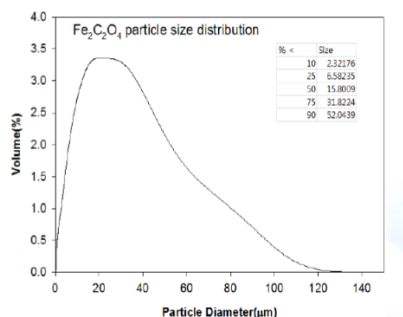


Fig. 2. PSA result of precipitate Fe-Oxalate.

Fig. 2 is the PSA result for sediment. As a result, the Fe oxalate precipitate was more than 25 μm

above 91.2%, which suggests that the precipitate can be removed by filtration and centrifugation.

4. Conclusion

Through the study on regeneration of phosphate electrolyte decontamination solution, we obtained the following conclusion in the experimental range:

1. The hydrazine reduction rate of ferric ions to ferrous increases with temperature..
2. The phosphate electrolyte decontamination solution can be successfully regenerated by hydrazine reduction and oxalate precipitation

ACKNOWLEDGEMENT

This work was supported by the National Research Foundation of Korea (NRF) and the Ministry of Science and ICT(MSIT) of the Republic of Korea. (No. 2017M2A8A5041776)

REFERENCES

- [1] Andre Angermann et al., "Synthesis of magnetite nanoparticles by thermal decomposition of ferrous oxalate dihydrate", Journal of Materials Science, pp 5123–5130 (2008)

A Study on the Radioactive Decomposition Characteristics of Oxalic Acid Using Metal Catalysts

Dongwoo Kim^{1),2)}, Kang Lee¹⁾, Tak-hyun Kim¹⁾, and Seungjoo Lim¹⁾

¹⁾ Korea Atomic Energy Research Institute, 29, Geumgu-gil, Jeongeup-si, Jeollabuk-do, Republic of Korea

²⁾ Jeonju University, 303, Cheonjam-ro, Wansan-gu, Jeonju-si, Jeollabuk-do, Republic of Korea

* seungjoolim@gmail.com

1. Introduction

Oxalic acid radiators, boilers and other major components are as follows. Textile manufacturing, dyeing, metal extraction and purification, bleaching of leather or leather. Another source of energy is the element containing the eliminating element.1-2)

Oxalic acid such as potassium permanganate or chromic acid may be used to treat oxalic acid remaining in the wastewater for various purposes. However, new researches are underway to remove oxalic acid because of the disadvantages of a large amount of chemicals and a relatively large amount of residual wastes.1-3)

Recently, a method of treating oxalic acid using AOP (Advanced Oxidation Process) has been attempted. In AOP, OH radicals (OH·, Potential difference: 2.8 V) is generated to treat the organic matter.

In the general AOP method, a method of adding ozone, hydrogen peroxide, or the like in parallel is already well known. Several researchers have also introduced a process to improve the TOC removal effect by applying sulfate salts and metal salts in the form of sulfate in the ozone / catalyst process.1-4)

In this study, sulphate type Fe (II), Cu (II) and Ni (II) were used to apply ionizing radiation (electron beam) / metal catalyst process. Experiments were carried out to remove oxalic acid in water by using OH radicals in water by acting electron beam and a small amount of transition metal ions like catalyst.

2. Main subject

2.1 Materials and methods, analysis

2.1.1 Sample preparation. The initial concentration of oxalic acid (Oxalic Acid, 99 +%, 144-62-7, Aldrich Chemical Company, Inc.) was set at 2 mM and the total volume of the sample was fixed at 10 mL.

2.2 Radiation (electron beam) irradiation

All the irradiation experiments were carried out with the electron beams of the electron beam accelerator units 2 and 4 of EB-Tech (170-9, Techno 2-ro, Yuseong-gu, Daejeon, 34028, KOREA). The maximum electron energy is 2.5 MeV. All investigations were carried out at room temperature. The absorbed dose of radiation was 5, 10, 30, 50 kGy.

The sample was allowed to have a depth of 0.7 cm in a beaker (150 mL of glass beaker) so that the electron beam could be irradiated uniformly.

2.3 Experimental apparatus and analysis apparatus

The concentration of oxalic acid was analyzed using High Performance Liquid Chromatography (HPLC) (Agilent Technologies, 1200 series). Rezex ROA-Organic Acid H + (8%) (300 × 7.8 mm) was used as the column. The mobile phase used 0.005 N sulfuric acid. TOC-VCSN TOC analyzer (Shimadzu, Kyoto, Japan) was used to measure total organic carbon.

3. Result

Fig. 1 shows the results of decomposition of oxalic acid by radiation (electron beam) irradiation.

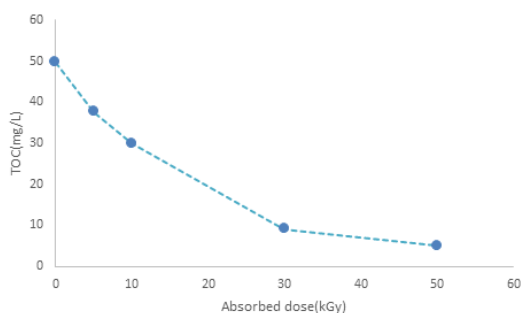


Fig.1. Total Organic Carbon change of oxalic acid by electron beam.

Fig. 2 and 3, show the results of irradiation of the metal catalyst (Cu, Ni) added to oxalic acid.

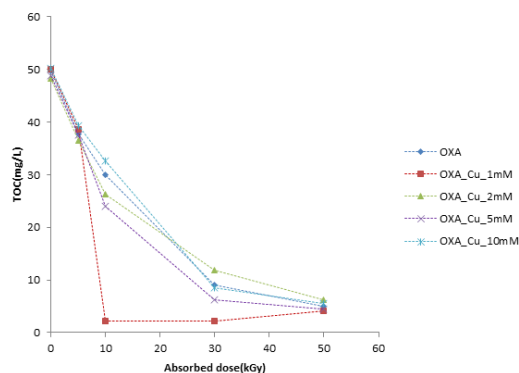


Fig.2. TOC change of oxalic acid by electron beam (Cu addition).

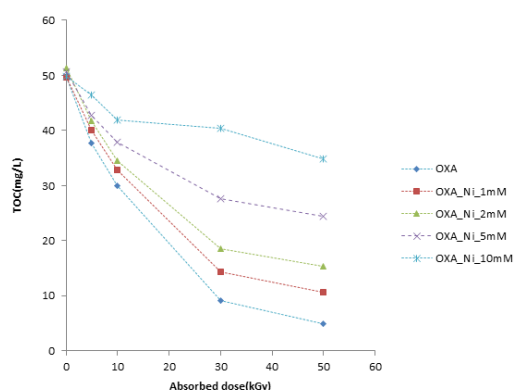


Fig.3. TOC change of oxalic acid by electron beam (Ni addition).

4. Conclusion

The following conclusions were obtained through the electron beam irradiation process and the electron beam irradiation process with various chloride metal

salts added. Compared with the case of using only the electron beam without using the metal catalyst and the process using the metal catalyst, the addition of Fe and Ni to oxalic acid resulted in a decrease in the decomposition rate of oxalic acid.

However, in the case of Cu, before the electron beam irradiation, the TOC was decomposed according to the change in the concentration of Cu, and it was found that the efficiency was improved when the electron beam was irradiated. Therefore, it is expected that the process of adding Cu as a metal catalyst to the decomposition process of irradiating the electron beam to oxalic acid will have a decomposition effect.

REFERENCES

- [1] Dong Yun Ha, Soon Haing Cho, Young Soo Choi, Gyu Seok Kyung, and Dong Hyun Kim, "Degradation Characteristics of Oxalic Acid and Citric Acid by UV/H₂O₂ Oxidation", Korean Society of Environmental Engineers, 22(7), 1307~1318 (2000).
- [2] Eung Ho Kim, Young Hwan Kim, Dong Yong Chung, and Jae Hyung Yoo, "Decomposition of Oxalic Acid in Nitric Acid by UV Radiation", Applied Chemistry for Engineering, 8(1), 108~113 (1997).
- [3] Gyu Seok Kyung, Soon Haing Cho, Young Soo Choi, Dong Hyun Kim, and Dong Yun Ha, "Degradation Characteristics of Oxalic Acid and Citric Acid by TiO₂ Photocatalytic Oxidation", Korean Society of Environmental Engineers, 25(3), 393~400 (2003).
- [4] Seung Ju Song and Joon Wun Kang, "Degradation of Oxalic Acid by Homogeneous Catalytic Ozonation using Various Metallic Salt", Korean Society of Environmental Engineers, 26(5), 588~593 (2004).

The Analysis for Corrosion Products in Primary Circuit Structures to Increase FSD (Full System Decontamination) Efficiency

HeeDong Sohn^{a)*}, KwangSoo Park^{a)}, HaeWoong Kim^{a)}, HanSol Im^{a)}, and ChangJe Park^{b)}

^{a)}Doosan Heavy Industries & Construction, 22, Doosan Volvo-ro, Seongsan-gu, Changwon-si, Gyeongsangnam-do, Republic of Korea

^{b)}Sejong University, Department of Nuclear Engineering, 209, Neungdong-ro, Gwangjin-gu, Seoul, Republic of Korea,

*heedong.sohn@doosan.com

1. Introduction

During the operation of nuclear power plant, lots of corrosion products are produced in primary circuit structures, especially, inner surface of reactor pressure vessel and head, inside wall of steam generator tube, and primary piping, etc. They are usually activated products and fuel clad corrosion ones (CRUD. Chalk River Unidentified Deposits). Some are ionic, some are particle and others are soluble. Therefore, to increase primary circuit full system decontamination efficiency, the exact analysis for corrosion products are necessary and to find out the best way to remove them efficiently.

In this paper, various sources of corrosion products in the primary coolant are explained with formation mechanism and deposition behavior.

2. Analysis for Corrosion Product Source

2.1 Activated Productst

Activated O^{16} included in primary coolant is changed to N^{16} through the (n,p) reaction, which emits high energy γ -rays of 6.1 MeV and 7.1 MeV. So, it becomes the main radioactive source with the short half-life of 7 seconds. Ar^{41} which also emits γ -ray is produced with the reaction of neutron capture (n, γ) by Ar^{40} soluble in primary coolant. Ag^{110m} released from the position of fuel clad crack is the important radioactive source in steam generator, especially, deposited nearby the inlet nozzle. Sb^{124} is also the important source in the reactor coolant pump and it is produced caused by the corrosion of neutron source clad which includes Sb-Be.

2.2 Fuel Clad Corrosion Products (CRUD)

CRUD, Ni-Fe series corrosion product, is deposited on the surface of high temperature fuel clad. Its thermal conductivity is lower than the one of zirconium clad and it includes Lithium and Boron. Even though the stream of porosity in CRUD is slow, it helps to develop the nickel ferrite oxidation ($NiFe^2O^4$).

Usually, in pressurized water reactor, the CRUD thickness is about 100 μm , Fig. 1 depicts the SEM for CRUD formation in reactor pressure vessel and Fig. 2 for CRUD cross section image.

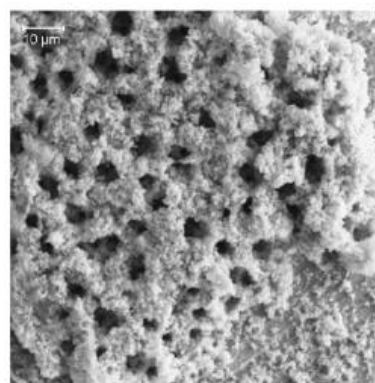


Fig. 1. CRUD Formation [1].

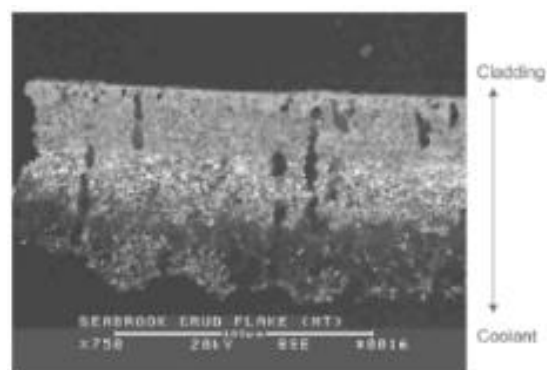


Fig. 2. CRUD Formation (Cross Section) [1].

As the CRUD formation is proceeded continuously, the inner corrosion of clad is increased and eventually, damaged clad will be incurred (CILC. CRUD Induced Localized Corrosion).

2.3 Activities in Corrosion Products

Corrosion and erosion are the main mechanisms to produce the corrosion products. They are transported as being soluble in coolant, the type of colloid or particle and deposited on the surface of oxidized layer in structures and finally activated. It is easier for particles to be deposited on the area of low fluid velocity or horizontality [4]. They will become the major radioactive sources around the lower part of reactor pressure vessel and on the steam generator tubes.

In case of PWR nuclear power plant, long half-life nuclides – Cr⁵¹, Co⁵⁸ and Co⁶⁰ – which are included in corrosion products caused by activation of stainless steel structures are the main radioactive sources. Among the isotopes of Cobalt, Co⁵⁸ is produced by the activation of Ni⁵⁸ which are produced in Ni alloy or steam generator tubes. Co⁵⁹ is produced from Co⁵⁸ and Co⁶⁰ is produced from Co⁵⁹ with the reaction of neutron capture.

Table 1 describes the results of measured specific activity for each nuclide for the condition of normal operation and shutdown with proceeding oxidation. In case of normal operation, the main nuclides are Co⁵⁸ and Co⁶⁰, however, after shutdown, Co⁵⁸ is the main one and Sb¹²⁴ and Ab^{110m} are the minor radioactive sources with decreasing nuclide of Co⁶⁰.

Table 1. Measured Specific Activity in Primary Circuit [3]

Specific Activity	Co ⁵⁸	Co ⁶⁰	Sb ¹²⁴	Ag ^{110m}
Normal (MBq/t)	10~100	1~10	-	-
Shutdown (MBq/t)	100,000	3,000	10,000	2,000

3. Conclusion

The main radioactive sources inside structures in primary circuit are Cobalt series nuclides of

corrosion products with about scores of um thickness which emit γ -rays. CRUD is deposited on the surface of clad and it is composed of Ni-Fe based material. To perform full system decontamination efficiently, analysis for corrosion product producing mechanism is very important, because various kinds of corrosion products are deposited on the surface of complex structures with various thicknesses. And it is necessary to make optimized decontamination process, design facilities and prepare reagents to remove them and to increase decontamination factor up to the target based on the corrosion product analysis.

Acknowledgement

This work was supported by the National Research Foundation of Korea (NRF) granted financial resource from the Ministry of Science and ICT, Republic of Korea (NRF-2017M2A8A5041777).

REFERENCES

- [1] J. Deshon et al., "Pressurized Water Reactor Fuel Crud and Corrosion Modeling", Journal of Materials, 63(8), 64-72 (2010).
- [2] IAEA, Modeling of Transport of Radioactive Substances in the Primary Circuit of Water-Cooled Reactors, IAEA TECDOC-1672, 2012.
- [3] H. Provens, Primary Circuit Contamination in Nuclear Power Plants: Contribution to Occupational Exposure
- [4] M. Vepsalainen, Deposit Formation in PWR Steam Generators, VTT-R-00135-10, VTT Technical Research Centre of Finland, 2010.

Selective Adsorption of Aquatic Strontium Using Monosodium Titanate Species

Gyuhyeon Kim^{a)}, Dae Sung Lee^{b)}, and Jong Moon Park^{a)*}

^{a)} Pohang University of Science and Technology, 77, Cheongam-ro, Nam-gu, Pohang-Si, Gyeongsangbuk-do, Republic of Korea

^{b)} Kyungpook National University, 80, Daehak-ro, Buk-gu, Daegu, Republic of Korea

*jmpark@postech.ac.kr

1. Introduction

The most uprising issue of nuclear safety is how to decontaminate and decommission expired nuclear facilities effectively and economically. During the decontamination and decommissioning process, hazardous mobile radionuclides can be discharged through air and streams. ⁹⁰Sr and ⁸⁹Sr are most abundant contaminants in radioactive waste owing to their high specific radioactivity, high mobility, high water solubility, and long half-life [1]. Selectively adsorption of strontium in mixed solution using monosodium titanate synthesized by Hobbs's method was performed [2]. Physical characteristics of sodium titanate and strontium adsorption rate were also examined for effective aquatic strontium adsorption by sodium titanate.

2. Experimental Results

2.1 Properties of Synthesized Sodium Titanate

The structure and morphology of the synthesized monosodium titanate (MST) was analyzed by using SEM. Synthesized sodium titanate showed amorphous and aggregated structures with microporous property. (Fig. 1)

Stoichiometry of synthesized MST was also examined by using EDAX. Chemical composition of synthesized MST was verified as NaTi₂O₇. (Fig. 2)

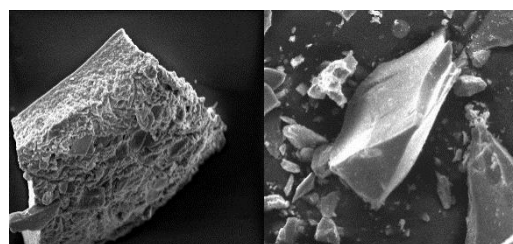


Fig. 1. SEM picture of synthesized sodium titanate (Left: vacuum dried form; right: grinded from vacuum dried form).

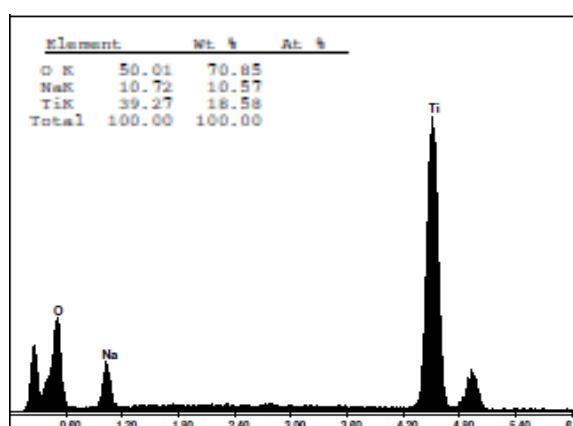


Fig. 2. EDAX result of synthesized MST.

Physical characteristics of MST such as surface area, mean pore diameter and pore volume were calculated via Brunauer-Emmett-Teller (BET) experiments, as summarized in Table. 1

Table 1. Physical characteristics of MST by BET

Sample	MST
BET total surface area (m ² /g)	244.17
BJH mean pore diameter (nm)	10.344
BJH total pore volume (cm ³ /g)	0.0563

2.2 Strontium Adsorption rates

Aquatic strontium adsorption experiments from

1mM strontium and cesium containing solution using synthesized MST were conducted. 99% of 1mM strontium was adsorbed in MST within 3 hours. Otherwise, about 40% of 1mM cesium was adsorbed in MST during 24 hours.

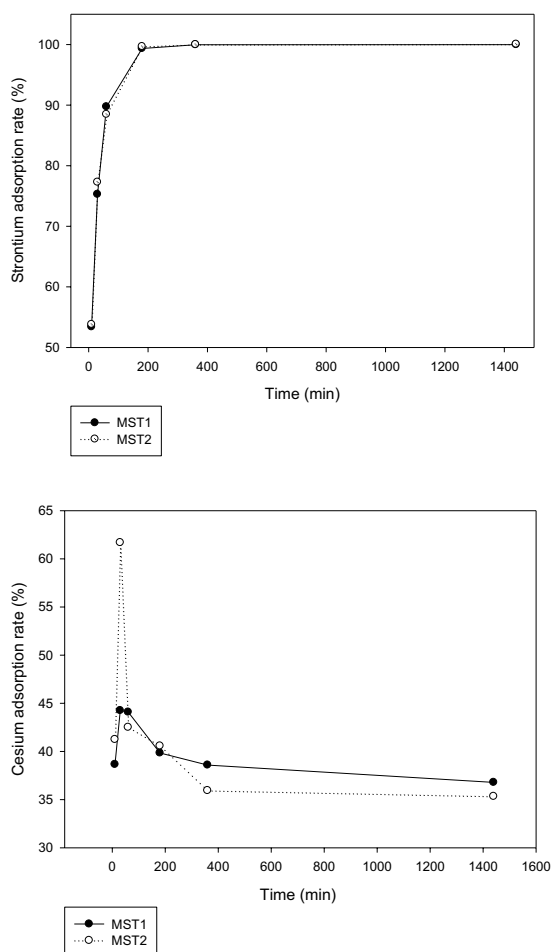


Fig. 3. Strontium and cesium adsorption rate by MST during 24 hours (conditions: temp = 25°C, initial strontium and cesium concentration = 1 mM; weight of adsorbent = 0.1 g; volume of solution = 0.1 L; shaking speed = 200 rpm; duplicate).

3. Conclusions

Monosodium titanate NaTi_2O_7 were successfully synthesized by a simple hydrothermal method. Synthesized MST got high surface area, pore diameter, and pore volume which affect high strontium adsorption capacity, and its amorphous,

microporous structures also affect high strontium adsorption ability. Synthesized MST showed good selectivity for strontium ions in the presence of cesium which means selective strontium adsorption in mixed radionuclide solution. Although various sodium titanate species were synthesized and utilized in nuclear industries [3], our MST can be good method to adsorb strontium selectively during decontamination and decommission of nuclear facilities.

ACKNOWLEDGEMENT

This research was supported by the National Research Foundation grant from the Korean government (MSIP) (NRF-2015M2A7A1000194).

REFERENCES

- [1] Jang, Jiseon, and Dae Sung Lee. "Three-dimensional barium-sulfate-impregnated reduced graphene oxide aerogel for removal of strontium from aqueous solutions." *Journal of Nuclear Materials* 504 (2018): 206-214.
- [2] D. T. Hobbs and M. D. Nyman. "Preparation and Use of Dried Monosodium Titanate", Technical Report, WSRC-TR-2003-00546, Westinghouse Savannah River Company, (2003).
- [3] K. M. L. Taylor-Pashow, D. M. Missimer, A. Jurgensen and D. T. Hobbs. "Characterization of Modified Monosodium Titanate – An Improved Sorbent for Strontium and Actinide Separations" *Separation Science and Technology*, 46:7 (2011): 1087-1097.

Mineralization of Oxalic Acid by Ni(II) With Gamma Radiation

Kang Lee, Dongwoo Kim, TaeHun Kim, Tak-hyun kim, and Seungjoo Lim*

Korea Atomic Energy Research Institute, 29, Geungu-gil, Jeongeup-si, Jeollabuk-do, Republic of Korea

*seungjoolim@gmail.com

1. Introduction

Various organic solvents are used in many countries' nuclear industries to eliminate the metal scales produced in cooling pumps, piping, etc [1]. Organic acids such as oxalic acid, citric acid, and formic acid are commonly used, and various studies are being conducted to remove organic acids that advanced oxidation processes (AOPs) [2]. Highly reactive species are generated in water radiolysis using gamma radiation. Then, hydroxyl radical ($\bullet\text{OH}$) and sulfate radical ($\text{SO}_4^{\bullet-}$) can be formed by the Ni(II) and potassium persulfate (PDS). The objectives of this study is to form hydroxyl radical and sulfate radical by combining Ni(II)/PDS with gamma radiation.

2. Materials and methods

2.1 Materials and sample preparation

Oxalic acid, $\text{NiSO}_4 \cdot 6\text{H}_2\text{O}$, $\text{K}_2\text{S}_2\text{O}_8$ (PDS) were purchased from Sigma-Aldrich. Oxalic acid solution of 2 mM was irradiated for effect of Ni(II):PDS on oxalic acid degradation. Fixing the initial Ni(II) concentration at 1 mM and varying the PDS concentration to obtain molar ratio of 1:0, 1:1, 1:2 and 1:5.

2.2 irradiation sources

The samples were irradiated at the absorbed doses

from 5 to 50 kGy and dose rate of 10 kGy/hr. Gamma radiation was achieved using a ^{60}Co source (Nordion Inc., Canada) at the Korea Atomic Energy Research Institute (KAERI, Korea).

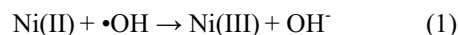
2.3 Analysis methods

Total organic carbon (TOC) for mineralization was determined using a TOC-VCSN TOC analyzer (Shimadzu, Kyoto, Japan). A digital pH meter was used for pH measurement (Orion, Singapore).

3. Result and discussion

3.1 Effect of Ni(II) on the mineralization of oxalic acid

Fig. 1 shows that the effect of various Ni(II) on the degradation of oxalic acid by gamma radiation. The degradation efficiency of oxalic acid was increased with the addition of Ni(II), and was decreased when excessive concentration of Ni(II) was added. The decreased efficiency with the addition of Ni(II) can be explained by the following equation:



Excess concentration of Ni(II) occurs due to the hydroxyl radical scavengers.

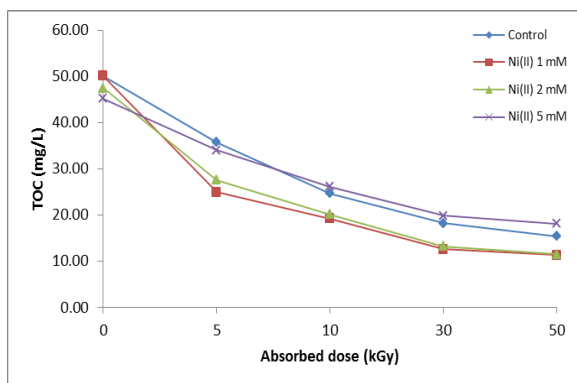


Fig. 1. Effect of different Ni(II) concentration on oxalic acid ($C_0 = 2$ mM) degradation using gamma radiation.

3.2 Effect of Ni(II) and PDS on the mineralization of oxalic acid

Fig. 2 shows the degradation of oxalic acid at different molar ratios of Ni(II) to PDS using gamma radiation. The degradation efficiency increased with an increase in PDS concentration. When 5 kGy of an absorbed dose, TOC of oxalic acid was removed about 88% at the Ni(II):PDS = 1:5 molar ratio. The initial TOC of oxalic acid was decreased before gamma radiation.

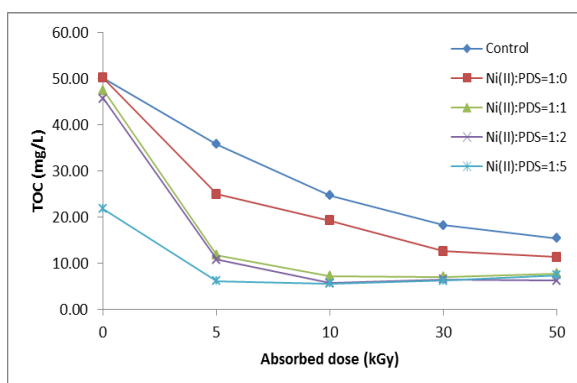


Fig. 2. Effect of 1 mM Ni(II) and various PDS concentration from 1 to 5 mM on oxalic acid ($C_0 = 2$ mM) degradation using gamma radiation.

The reason is considered to be an oxidation reaction by the Fenton-like reaction. The hydroxyl radical and sulfate radical were formed by a reaction

of Ni(II) and PDS. Oxalic acid is removed by the effect of hydroxyl radical and sulfate radical. But, excess PDS addition resulted in a decrease of degradation efficiency.

4. Conclusion

The mineralization of oxalic acid was investigated combining Ni(II)/PDS with gamma radiation. The this study, the Ni(II)/PDS/gamma radiation process shows a high dependency on the concentration of Ni(II) and PDS. Ni(II)/PDS/gamma radiation process is more effective than the gamma radiation or Ni(II)/gamma radiation process.

REFERENCES

- [1] Enda, Masami, et al. "System and method for chemical decontamination of radioactive material." U.S. Patent No. 7,087,120. 8 Aug. 2006.
- [2] Thomas, Daniel A., et al. "Real-time studies of iron oxalate-mediated oxidation of glycolaldehyde as a model for photochemical aging of aqueous tropospheric aerosols." *Environmental science & technology* 50.22 (2016): 12241-12249.

Decomposition of Oxalic Acid by Gamma-ray Irradiation

Seung Joo Lim*, Kang Lee, and Dong Woo Kim

Korea Atomic Energy Research Institute, 111, Daedeok-daero 989beon-gil, Yuseong-gu, Daejeon,
Republic of Korea

* seungjoolim@kaeri.re.kr

1. Introduction

Recalcitrant organic compounds are used to decontaminate oxide films or oxide deposits in various nuclear power systems. Oxalic acid was usually used for decontamination of water-cooled reactors such as pressurized power reactor and boiled water reactor. To remove chemical agents, advanced oxidation processes by radicals were used [1, 2]. This study focused on radiolytic decomposition of oxalic acid by gamma irradiation.

2. Materials and Methods

2.1 Chemicals

All of chemicals were high-purity analytical grade. The initial concentrations of oxalic acid prepared at 1, 2, 5 and 10 mM. The initial pH was 3-4 at each test condition.

2.2 Irradiation

Gamma irradiation was performed using a high-level ^{60}Co source at the Korea Atomic Energy Research Institute. The radiation activity of source was 1.47×10^{17} Bq with dose rate of 10 kGy/hr. Absorbed doses were 5, 10, 20, 30 and 50 kGy, and measured by the alanine-EPR dosimetry system. All tests were carried out at room temperature.

3. Results and Discussion

3.1 Radiolytic decomposition of oxalic acid

Degradation of contaminants by ionizing radiation is initiated by the primary products of water radiolysis. The efficiency of gamma irradiation in the degradation of oxalic acid was compared between percentage removal and G-value. The results obtained are shown in Fig. 1. The G-Values for radiolytic decomposition of oxalic acid at 10 mM were 19.3, 9.7, 4.8, 3.2, and 1.9 for absorbed dose of 5, 10, 20, 30, and 50 kGy, respectively. The G-value increased with the initial concentration of oxalic acid. Interestingly, the G-value decreased with accumulated radiation dose but the removal increased. The removal of oxalic acid at 10 mM was 16.6, 36.5, 69.5, 83.4, and 92.2% for absorbed dose of 5, 10, 20, 30, and 50 kGy, respectively. According to these results, the efficiency of gamma irradiation process decreases with longer gamma exposure time.

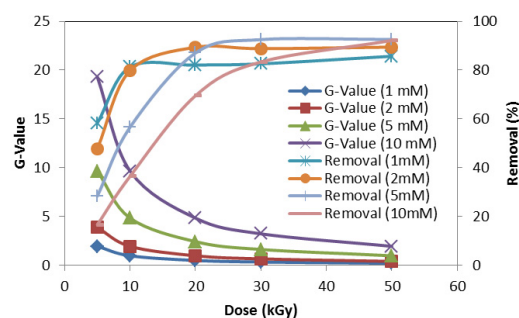


Fig. 1. G-Value and removal of oxalic acid using gamma irradiation.

3.2 Decomposition characteristics of oxalic acid

The dose constant, k , at different initial concentration was shown in Fig. 2. Oxalic acid removal efficiency can be quantitatively described in terms of two parameters, G-value and k . The G-values at 50 kGy were proportional to oxalic acid concentration. The G-values for radiolytic decomposition of oxalic acid at 50 kGy were 0.2, 0.4, 1.0, and 1.9 for initial concentration of 1, 2, 5, and 10 mM, respectively. Meanwhile, dose constant decreased with G-value. Dose constants for initial concentration of 1, 2, 5, and 10 mM were 0.1695, 0.1221, 0.0904, and 0.0536 kGy^{-1} , respectively.

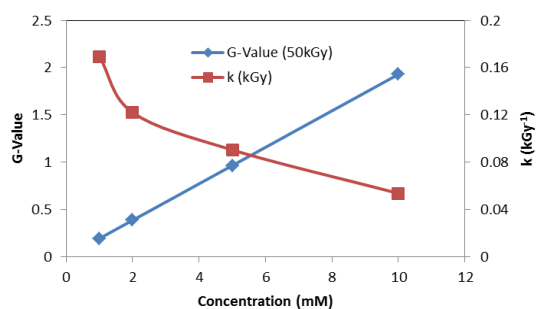


Fig. 2. Oxalic acid gamma irradiation at different initial concentrations.

The dose constant, k , was used to calculate the dose required to produce 50% and 90% oxalic acid degradation ($D_{0.5}$ and $D_{0.9}$ values). The variation of $D_{0.5}$ values was not too high. $D_{0.5}$ values increased from 4.1 to 12.9 kGy for initial concentration of 1 to 10 mM. Meanwhile, To obtain 90% removal at oxalic acid 10mM, 43.0 kGy was required. $D_{0.9} - D_{0.5}$ values for initial concentration of 1, 2, 5, and 10 mM were 9.5, 13.2, 17.8, and 30.0 kGy, respectively. This shows that the mineralization of oxalic acid at higher concentration was difficult more than that at lower concentration because of a great number of generated intermediates.

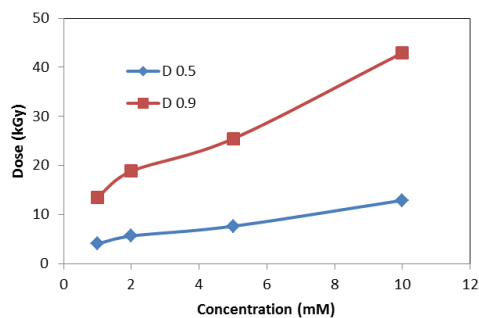


Fig. 3. D_{50} and D_{90} of oxalic acid gamma irradiation at different initial concentrations.

4. Conclusions

Oxalic acid was successfully degraded by gamma irradiation. 92% removal was obtained at initial concentration of 10 mM. Dose constant ranged from 0.1695 to 0.0536 kGy^{-1} at different initial concentrations. G-value was inversely proportional to dose constant.

ACKNOWLEDGEMENT

This work was supported by a Nuclear Research & Development Program through an NRF grant funded.

REFERENCES

- [1] N. Davis et. al., "Enhanced chemical cleaning: A new process for chemically cleaning Savannah river waste tanks-9100", Proc. of WM2009 Conference, March 1-5, 2009, Phoenix.
- [2] H. Lee et. al., "Degradation kinetics of recalcitrant organic compounds in a decontamination process with UV/H₂O₂ and UV/H₂O₂/TiO₂ processes" Korean Journal of Chemical Engineering, 20(3), 503-508 (2003).

Development of Gamma Scanning System for Irradiated Materials

Young-Jun Kim*, Seung-Je Baik, and Ki-Soo Heo

Korea Atomic Energy Research Institute, 111, Daedeok-daero 989beon-gil, Yuseong-gu, Daejeon, Republic of Korea

*yjkim05@kaeri.re.kr

1. Introduction

Various post-irradiation examination (PIE) of fuels and materials irradiated in HANARO research as well as commercial reactor have been performed in Irradiated Materials Examination Facility (IMEF). In particular, there is steady PIE demand for materials irradiated a commercial reactor to analyze defects or produce basic data for decontamination and decommissioning.

A gamma scanning is one of the basic non-destructive test and it is used to analyze gamma emission nuclides and a specific activity. The existing gamma scanning system installed in IMEF is separated into a detector part and a specimen part because of a high radioactivity of an irradiated fuel [1]. However, the gamma scanning system is not suitable for measuring irradiated materials which have relatively low radioactivity because the hotcell wall which separate the two parts is too thick. Therefore the gamma scanning system for the irradiated materials was developed.

The gamma scanning system for the irradiated materials and test results using the system are introduced in this paper.

2. Methods and Results

2.1 Gamma Scanning System

Fig. 2 shows the gamma scanning system for the irradiated materials. The system is composed of the

HPGe detector, the shielding material, the collimator, and the shielding for specimen. The shielding materials and the collimator were made of a lead to reduce a radiation exposure of a researcher. And it can reduce an influence of a background caused by contaminants in the service area. The system was designed to adjust a dead time of the detector using the collimator and to able to measure by position using bench that can move in X,Y,Z-axis.

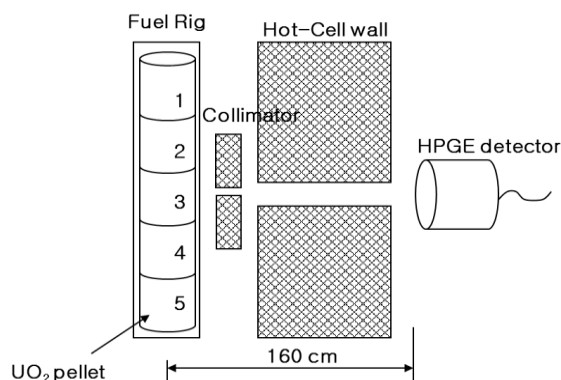


Fig.1. Schematic diagram of existing gamma scanning system installed in IMEF.

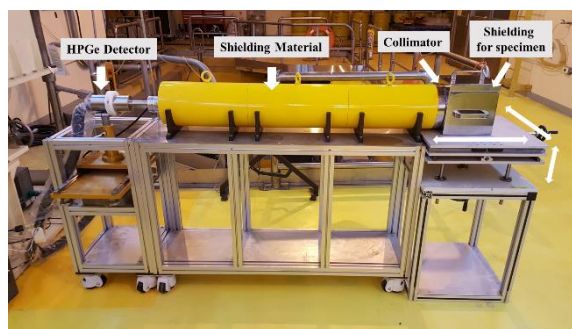


Fig. 2. Gamma scanning system for irradiated materials.

2.2 Evaluation of background influence

The shielding materials were used to minimize the influence of the background caused by contaminants

in the service area. Gamma scanning was performed to compare the background effects before and after use of the shielding materials.

An energy calibration was performed using standard sources of Co-60 and Cs-137 before the measurement. The measurement was carried out for 3,600 s (Live time) and the gamma scanning results of the background before and after use of the gamma scanning system are shown in Table 1. Although some gamma emission nuclides were still detected, the background effects were reduced by more than 97%.

Table 1. Gamma scanning results of background

Nuclide	Energy	without system	with system
Co-60	1173.23 keV	57197±277	1416±44
Co-60	1332.51 keV	52777±250	1415±40
Cs-137	661.62 keV	65369±308	1632±65

2.3 Measurement of radioactive sample

Gamma scanning of a radioactive sample was performed for 3,600 s (Live time). The radioactive sample is a filter collected from a spent fuel pool of a nuclear power plant using an ultrasonic cleaner and it has various gamma emission nuclides.

As the results of the gamma scanning, Co-57, Co-58, Co-60, Mn-54, Nb-95 and so on were detected as shown in Fig. 3. The detected radionuclides are mainly found in a primary coolant of a nuclear power plant. Especially, Co-58, Co-60, Mn-54 and so on are main factors that increase the dose rate of a reactor system and they are main source of radiation exposure when workers approach the system for maintenance and inspection in a radiation area. Also, Co-60 which has a long half-life is nuclide that require a special attention when handling and disposing of a radioactive wastes.

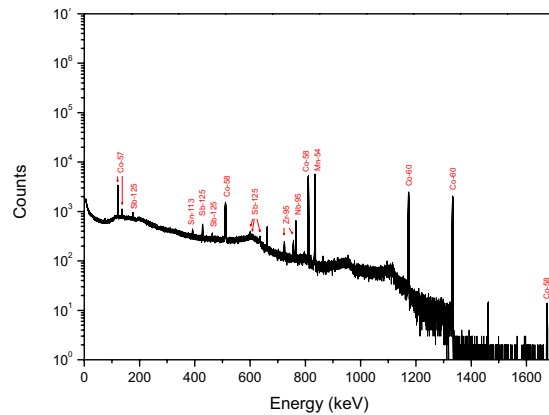


Fig. 3. Gamma scanning result of radioactive sample.

3. Conclusion

The gamma scanning system was developed for various PIE demand of materials irradiated in the commercial reactor. The gamma scanning system was designed to minimize the background influence and produce the reliable data. As the results of measuring the radioactivity sample, gamma emission nuclides can be clearly confirmed without the background influence. In the future, the specific activity measurement of a radioactive sample will be performed by establishing an efficiency calibration procedures appropriate to the gamma scanning system.

REFERENCES

- [1] H.M.Kim, S.J.Baik, B.O.Yoo, Y.S.Choo, and W.S.Ryu, "Technical Development of Gamma Scanning for Irradiated Fuel Rod after Upgrade of System in Hot-cell", KAERI/TR-3425/2007.

Purolite S957 Ion Exchange Resin for Uranium Removal From Effluents Generated During a Spent Catalyst Treatment Process: Real Waste Uptake and Elution Studies

Richard I. Foster^{1)*}, James T. M. Amphlett^{2),§}, Keun-Young Lee¹⁾, and Kwang-Wook Kim¹⁾

¹⁾Korea Atomic Energy Research Institute, 111, Daedeok-daero 989beon-gil, Yuseong-gu, Daejeon, Republic of Korea

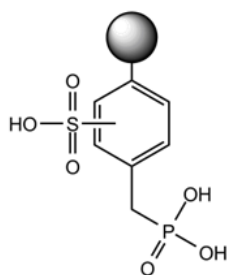
²⁾University of Manchester, Oxford Rd, Manchester M13 9PL, United Kingdom

*rifoster@kaeri.re.kr, §j.amphlett@sheffield.ac.uk

1. Introduction

A large volume of problematic uranium waste in the form of a spent catalyst is in temporary storage in Korea. Recently the Korea Atomic Energy Research Institute (KAERI) has developed an appropriate method for the treatment, segregation and ultimately safe disposal of this waste.[1-5] This research has led to the development of a process involving multiple unit steps including heat treatment, dissolution, selective precipitation and filtration. The process relies on the treatment of generated effluents via a uranium precipitation method.[1,4] While effective, recording decontamination factors greater than 8000, the generation of large floc volumes is not ideal for final volume reduction. Further, there is currently no back-up system in the event of mal operation should there be a process failure during uranium precipitation.

Recently we have reassessed, in collaboration with the University of Manchester (UoM), the treatment options available for the generated effluents. The goal was to explore alternative treatment methods and develop a back-up strategy based on ion exchange (IX) in the event of mal operation. It is shown that Purolite S957 (**Figure 1**), a phosphonic sulfonic acid chelating/anion exchange resin, outperforms all other tested resins during screening trials.[6] In this study we present the results from real waste tests focusing on laboratory scale uranium removal and elution. We have assessed the viability of S957 for the selective removal of uranium from the real process effluent.



S957

Fig. 1. Structural diagram of Purolite S957.

2. Experiment

2.1 Materials

Purolite S957 is a macroporous styrene DVB 8%

crosslinked phosphonic sulfonic acid chelating/anion exchange ion exchange resin. The resin was supplied by Purolite. The effluent was produced during the treatment of the catalyst and stored in 20 L plastic drums before use. All other chemicals were purchased from Sigma-Aldrich and used as supplied. A complete description of the spent uranium catalyst and dissolution process has been previously reported.[1]

2.2. Method

U Removal: Dynamic tests with the real waste (~30 ppm U) were conducted at the laboratory scale using variable flow rates (12.5, 7.4, 4.7 or 1.3 BV Hr⁻¹) and 1 mL of WSR loaded in a sealed plastic column in an upflow configuration.

U Elution: Elution tests were performed under the same configuration as the removal tests. The elution media was passed through the resin at 1.3 BV Hr⁻¹. Four eluents were tested, 0.1 M H₂SO₄, 2.5 M H₂SO₄, 0.1 M Na₂CO₃ in 2 M Na₂SO₄ and 0.1 M FeCl₃. Five BV of deionised water was passed over the resin bed prior to the eluent media. A total of 100 BV of eluent was used. Uranium concentration was determined via ICP-OES analysis in a 5% nitric acid carrier-media.

3. Results and discussion

3.1 Screening studies & IXR Selection (UoM)

Uranium loading tests showed Purolite S957 to be the most effective at high [H⁺]; synonymous to the real waste. Purolite S957 was also found to have the highest loading capacity of all the resins tested (96.15 mg g⁻¹) in batch and dynamic testing. The superior performance of S957 also carried across to the dynamic testing studies with the simulant waste. Purolite S957 was found to show the highest uranium breakthrough capacity at the slower flow rate of 88.73 mg g⁻¹ at a flow rate of 7.5 BV hr⁻¹. [6]

3.2 Real waste tests – Uranium Removal (KAERI)

Tests with the real waste were performed with Purolite S957. Removal of uranium was successful across all flow rates tested (**Figure 2**). However, the breakthrough capacity of Purolite S957 under real waste conditions is significantly lower at 12.2 mg g⁻¹ under a flow of 1.3 BV Hr⁻¹ when compared to 88.73 mg g⁻¹ at a flow of 7.5 BV Hr⁻¹ for the simulant waste.

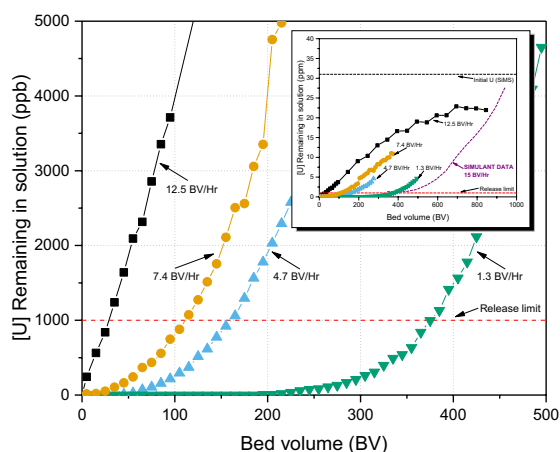


Fig. 2. Breakthrough curves for S957 at various flow rates.

3.3 Real waste tests – Uranium Elution (KAERI)

Elution of uranium was achieved with four different elution media (**Figure 3**). Sulfuric acid, regardless of concentration, was poor for the elution of uranium. At 2.5 M H_2SO_4 after 100 BV residual uranium remained on the resin which accounted for approximately 20% by difference (**Figure 3 B**). Iron chloride showed a significant improvement with an initial sharp rise in eluted uranium, but this was followed with a long and drawn out tail (**Figure 3 D**). A mix of sodium sulfate and sodium carbonate yielded the most promising results with a sharp elution profile over 15 - 20 BV (**Figure 3 C**). It is well known that uranium forms highly soluble carbonate species, a fact which is leveraged for the purposes of elution in this study.

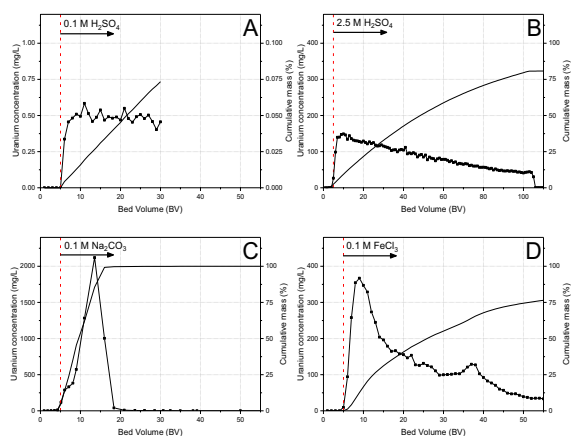


Fig. 3. Uranium elution curves for S957 using various eluents.

The use of a carbonate-based elution media offers the possibility of recycling the S957 resin, thus enabling significantly more effluent through the resin before final exhaustion and disposal. Such an approach would reduce costs and potentially overcome the issue of reduced breakthrough capacity as seen compared to the simulant studies.[6] However, not only is the uranium eluted off the column but so too are the other major contaminants (**Figure 4**). This has potential to further complicate effluent handling post-column as the effluent would require final treatment.

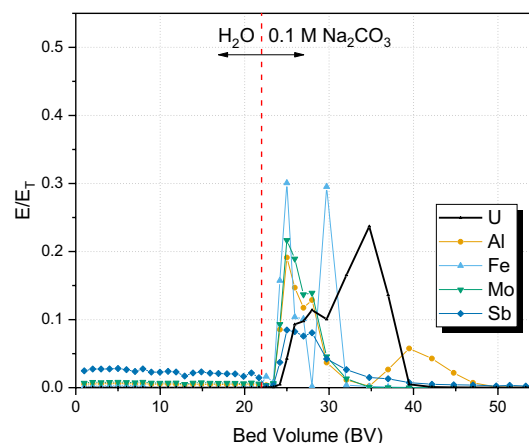


Fig. 4. Elution profile of all contaminants with H_2O and Na_2CO_3 .

4. Conclusions

Despite promising results with the simulant S957 showed poorer performance under real waste tests with approximately 376 BV being treated before breakthrough at the lowest flow rate of 1.3 BV Hr^{-1} . This was accompanied by a significantly lower breakthrough capacity of only 12.2 mg g^{-1} . Evidence suggests uranium elution is possible with a carbonate elution media, however, this is accompanied by the elution of the other contaminants which poses issues for final effluent treatment. Therefore, implementing a uranium absorption column loaded with S957 for the treatment of the effluent as a direct replacement for the phosphate precipitation method[4] would not be recommend. However, there is evidence to suggest that incorporating such a column into the process flow sheet in the event of mal-operation is still possible.

REFERENCES

- [1] K. W. Kim *et al.*, "The development of a process for the volume reduction of uranium catalyst waste used for production of acrylonitrile", In Press, (2018).
- [2] K.-W. Kim *et al.*, "Treatment method of spent uranium catalyst", U.S. Patent 9181605 B2, 2015.
- [3] R. I. Foster *et al.*, "The removal of uranium from aqueous effluents via meta-ankoleite formation", KRS, (2017).
- [4] R. I. Foster *et al.*, "The Selective Removal of Uranium via Phosphate Addition for the Treatment of Uranium Laden Effluents", In Press, (2018).
- [5] H. H. Sung *et al.*, "An Evaluation on the Glass-Ceramic Solidification Characteristics of Uranium catalyst waste by Green body Pressure", KRS, (2017).
- [6] R. I. Foster *et al.*, "Ion-Exchange as an Alternative Treatment Method for Uranium Effluents Generated as part of a Spent Uranium Catalyst Treatment Process", International Conference on Ion Exchange, Indonesia, (2018).

Task Analysis of Decommissioning Activities in Nuclear Power Plants

Hyun-Jae Yoo*, Chang-su Nam, and Byung-Sik Lee

Dankook University, 119, Dandae-ro, Dongnam-gu, Chunan-si, Chungcheongnam-do, Republic of Korea

*72170449@dankook.ac.kr

1. Introduction

At present, the decommissioning of Unit 1 of Kori Nuclear Power Plant in Korea is being prepared for a safe and economical decommissioning. As the decommissioning operation progresses, it is judged that accidents due to human errors will occur frequently. Therefore, to reduce the cause of human error, the Human Reliability Analysis (HRA) for the decommissioning activity of Unit 1 of Kori is required.

Reactor Pressure Vessel Internal is dangerous because of the highest radioactivity level among the decommissioning activities of Unit 1 of Kori, and because the dismantling operation of RPVI is performed in the water, depending on remote equipment and visual system, which occur a lot of human error possibility. Therefore, Task Analysis that should be important in the qualitative analysis of HRA is performed for RPVI decommissioning activities of Unit 1 of Kori.

2. Task Analysis

Task Analysis is an initial stage for evaluating human error, and it is a task to analyze the task objective, method, content and procedure and to identify task characteristics, vulnerabilities and propriety [1].

Among various TA, Hierarchical Task Analysis is a systematic and detailed task analysis method, which is a suitable method to identify detailed task compositions and conditions and to express complex task steps in a hierarchical structure [2]. Therefore, the HTA can identify information about physical characteristics, HMI, and possible accidents, etc. so it used this to perform TA for decommissioning activities. The format for task analysis of decommissioning activities was established using tabular format of HTA [3].

The purpose of this Task Analysis is to identify the characteristics, procedures and information of RPVI dismantling operation, and to identify possible human errors and performance shaping factors of decommissioning activities.

3. Task Analysis Application

As mentioned above, the target of task analysis is RPVI that the most complicated and have the highest radioactivity level in Kori 1. The following figure shows the internal components for the RPV of Unit 1 of Kori.

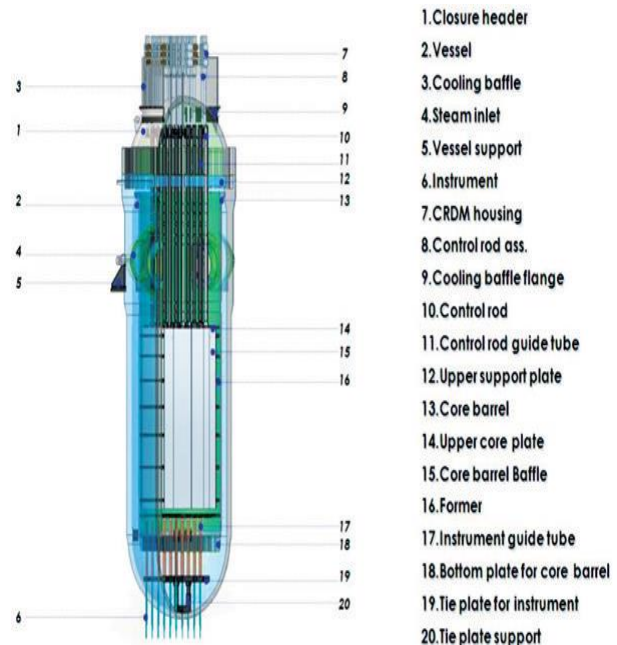


Fig. 1. Internal components for the RPV of Unit 1 of Kori [4].

RPVI dismantling operation was selected from Control Rod Guide Tube Upper Area Cutting Packaging to Lower Internal Structure Assembly Cutting and Packaging, and as shown in the following table 1, the sub tasks of RPVI dismantling operation are classified into 10 activities.

Table 1. Sub Tasks for the RPVI Dismantling Activity

No	Sub Task
1	Control Rod Guide Tube Upper Area Cutting and Packaging
2	Control Rod Guide Tube Lower Area Cutting and Packaging
3	Upper Plate Cutting and Packaging
4	Baffle Fixed Bolt Head Cutting
5	Baffle Cutting and Packaging
6	Former Separation
7	Barrel Upper Area Cutting and Packaging
8	Thermal Shield Cutting and Packaging
9	Barrel Lower Area Cutting and Packaging
10	Lower Internal Structure Assembly Cutting and Packaging

4. Task Analysis Results

Task Analysis was performed on 10 sub-tasks of RPVI dismantling operation shown in table 1 according to the HTA format, Task analysis results for RPVI dismantling operation are as follows.

- In general, in the decommissioning of nuclear power plants, the cutting of parts in the RPVI is the most complicated and difficult task during the dismantling process. Therefore, the influence on the internal factors of the workers was evaluated in order to have a relatively high value in terms of operator internal response.
- In general, RPVI dismantling operation is the most complicated and difficult task in the decommissioning process of nuclear power plant. Therefore, it was evaluated that the influence of 'operator internal response' on the internal factors of the operator was significant. However, in case of general decommissioning operation, the work procedure is not complicated when compared with the operation of NPP, and it is necessary to understand and acquire information such as equipment and workplace preparation. Therefore, the impact on internal factors of decommissioning operator will not be relatively large.
- Decommissioning operation is required high accuracy and reliability. Therefore, when the dismantling operation is performed, the influence on the internal and external factors of the operator is significantly large, so that sufficient training and education is required. However, the operation principle and method of these cutting equipment and device (cutting equipment, auxiliary equipment, display, remote control device, etc.) are not complicated and it is easy to operate them. Therefore, the operator is not required to have significant experience in using them.
- In advance, the dismantling operation should be planned in consideration of the work characteristics (the cutting target, equipment and facilities, and clothing according to work environment, etc.), a detailed work plan should be established in advance. Therefore, the work plan should be established for many times, so the psychological and physical effects that the supervisor and the operation can receive are considerable.
- Dismantling operation is not only dangerous, but it is carried out for a long time. Therefore, the operator carries out operation during day time/night time. In this case, various difficulties (such as break time, discomfort of clothes, and physiological factor) are generated. Since these difficulties have a significant impact on the internal/external factors of the operator, cooperation and communication is required

between the supervisor and the operator in this working environment.

- The physical environment (radiological, under water environment) of the workplace is the major risk factors for the operators, and the influence of these environments on the internal and external factors of the operators was considerable.
- Decommissioning operation of nuclear power plant is not often performed work. Therefore, operators may have insufficient education, training and experience. Therefore, it is necessary to feedback the results of the decommissioning operation and to be reflected in the necessary work procedure and to be managed it as experience data.

5. Conclusion

Task analysis, which is the initial step of HRA for human error reduction, was performed. TA format was established using HTA which is one of task analysis methods. Also, complex and dangerous RPVI dismantling operation among the decommissioning activities of Unit 1 of Kori were classified into 10 activities. The results of task analysis were derived by applying these to TA format.

The results of the TA, the detailed planning, the difficulties during the work, the experience of the decommissioning, the physical environment (radiological environment, underwater operation) influenced the internal and external factors of the operator. Therefore, if these factors are identified and used, it will help to reduce the human error and to identify the cause.

ACKNOWLEDGMENT

This work was supported by the National Research Foundation of Korea (NRF) grant funded by the Korean government, Ministry of Science, ICT and Future Planning (No. 2017M2A8A5015148 and No.2016M2B2B1945086).

REFERENCES

- [1] Jung-Kyung Hee: Development of a Human Reliability Analysis Model for the Reduction of Human Errors, Kyunghee University (2010).
- [2] Center for Chemical Process Safety: Guidelines for Preventing Human Error in Process Safety (1994).
- [3] Byung-Sik Lee, Hyun-Jae Yoo: PSF Derivation by Task Analysis for the Human Reliability in Decommissioning Activities, Dankook University (2018).
- [4] KAERI: Dismantling technology development of the major equipment in the nuclear power plant (2013).

Preliminary Study on the Heating and Grinding Method for Volume Reduction of Radioactive Concrete Waste From Decommissioning Process

Maeng-Kyo Oh^{1),2)}, Keun-Young Lee^{2),*}, Richard I. Foster²⁾, and Chang-Ha Lee^{1),*}

¹⁾Yonsei University, 50, Yonsei-ro, Seodaemun-gu, Seoul, Republic of Korea

²⁾Korea Atomic Energy Research Institute, 111, Daedeok-daero 989beon-gil, Yuseong-gu, Daejeon, Republic of Korea

* lky@kaeri.re.kr, leeche@yonei.ac.kr

1. Introduction

Nuclear facilities, which lost utility value, will be safely returned to society after a period of about 10~20 years of decommissioning processes including preparation, characterization, decontamination, dismantling, waste treatment and environmental remediation.

Various types of decommissioning wastes are generated during the decommissioning of nuclear facilities. Concrete, which is the main building material of a nuclear facility, is contaminated and activated during its operation, resulting in a large amount of radioactive waste. The amount of radioactive concrete waste generated varies significantly depending on the type of facility, method of decommissioning and volume reduction treatment that has a huge impact on the cost of decommissioning. In Korea, the volume of radioactive concrete must be reduced. Because strict and high standards are applied to classification, treatment and disposal of radioactive wastes, also the disposal cost for radioactive waste is very high.

Most radionuclides found in radioactive concrete waste are present in cement component [1]. Heating and grinding technology is a typical radioactive concrete waste treatment technology using to separate the cement and aggregate components, thus separating radioactive and non-radioactive waste[2,3]. It has been confirmed through previous researches that most of cement paste is separated from the aggregate, thus achieving an effective volume reduction of concrete waste. However, it is unclear that separated aggregate could be released after heating and grinding treatment,

and further studies are required to meet regulation criteria for free-release.

In this study, basic studies were conducted to improve the separation efficiency of aggregates and cement by using heating and grinding technology for the volume reduction of radioactive concrete waste.

2. Materials and Methods

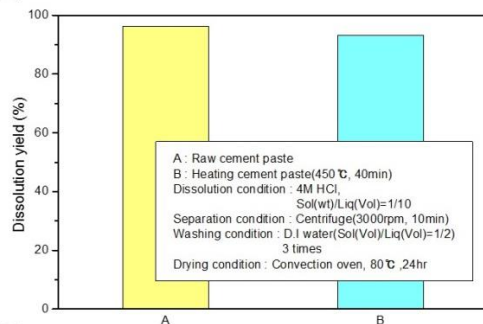
The concrete simply crushed to 10~40mm diameter was obtained from a construction waste disposal company.

During the heating and grinding experiment, 150~200 g of concrete was heated at 400~700°C for 10~120 minutes using muffle furnace(MF-12GH, JEIO-TECH). The concrete was then cooled naturally before the grinding. Concrete grinding was completed using a ball mill (LM-BD4530, LK LAB KOREA) that was most commonly used in the industry. The pre-heated concrete along with grinding balls (Alumina ball, D: 0.5~40 mm) were placed in the mill pot (Porcelain, 500 ml) and ground for a certain time at 300 rpm/mill roller speed. The ground concrete was separated into aggregate and cement paste by using a 1mm test sieve and the weight of each parts were measured to confirm the classification rate.

The difference in weight before and after grinded concrete using acid dissolution were confirmed the separation rate of cement and amount of residual cement in aggregate. This method is an analytical method using difference of solubility of aggregate and cement in acid solution. Each component was dissolved using 4 M hydrochloric acid (HCl, Merck) as shown in Fig.1. Since aggregate was almost

insoluble and cement has a high solubility, which was easy to analyze the residual amount of cement.

(1)



(2)

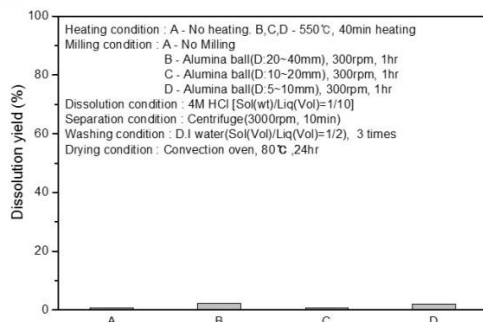


Fig. 1. Dissolution yield of (1) Cement, (2) Sand.

3. Result and discussion

Fig. 2 shows the results of 5 min ~ 24 hrs for grinding condition using ball mill after heat treatment at 450℃ in 40 minutes.

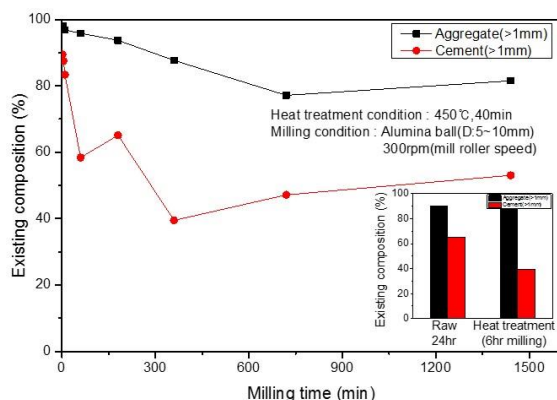


Fig. 2. Result of heating and grinding experiment.

In the case of raw concrete, that 65% cement component was remains in the aggregate of 1mm or more after 24hours grinding. However, heat-treated concrete was about 45% cement component remains in the aggregate at the 6hours grinding. Because of the

bonding strength between the cement and aggregate was reduced by heating above 450℃.

Aggregate and cement will be separated more effectively by optimizing the heating temperature with time and grinding condition like a ball size, combined grinding medium and filling method.

4. Conclusion

This study was to improve the separation efficiency of the heating and grinding technology for radioactive concrete waste. In the case of concrete, it was found that the separation rate was increased by first weakening the bond between the cement and aggregate by heat treatment. If the heat treatment conditions, temperature, time and grinding condition, are optimized, it could be expected that a lot of volume reduction can be achieved.

ACKNOWLEDGEMENT

This work was supported by the National Research Foundation of Korea grant (No. NRF-2017M2A8A5015147) funded by Ministry of Science and ICT.

REFERENCES

- [1] K.Y. Lee, M.K. Oh, J.M. Kim, E.H Lee, I.S Kim, K.W. Kim, D.Y Chung, B.K Seo, "Trends in technology development for the treatment of radioactive concrete waste", Journal of Nuclear Fuel Cycle and Waste Technology, 16(1), 93-105 (2018).
- [2] B.Y Min, W.K. Choi, K.W Lee, "Separation of clean aggregates from contaminated concrete waste by thermal and mechanical treatment", Annals of Nuclear Energy, 37, 16-21 (2010).
- [3] I.P. Binkhorst, H.A.W. Cornelissen, "Technology for reuse of contaminated concrete constituents", IAEA-TECDOC-1022 (1998).

Weighting Factors of the Performance Shaping Factors for the Segmentation of Reactor Pressure Vessel Internals Using Fuzzy AHP

Chang-Su Nam*, Hyun-Jae Yoo, and Byung-Sik Lee

Dankook University, 119, Dandae-ro, Dongnam-gu, Chunan-si, Chungcheongnam-do, Republic of Korea

*72180291@dankook.ac.kr

1. Introduction

In recent years, the development of technology for multiplicity and protection has reduced the incidence of accidents due to technical problems. However, it is impossible to say that the system is reliable without mentioning the failure rate of all system components, especially the impact of one of the components, Human Errors, on the system. For this reason, in order to reduce the human error, job analysis and related performance factors of reactor pressure vessel internal structure cutting work were derived. In this paper, we use Fuzzy-AHP to derive the weighting factors of performance shaping factors to understand the importance of performance impact factor items.

2. Fuzzy-AHP

Fuzzy theory, initiated by Zadeh in 1965, has been used in many fields as a mathematical model for analyzing uncertainty involving ambiguity based on the fuzzy set theory. Especially, it is useful for risk analysis in situations where ambiguity due to the subjective perception of the human being can't be handled stochastically.

2.1 Fuzzy-AHP decision step

The decision steps of Fuzzy-AHP are as follows.

- Step 1 : Form a hierarchy
- Step 2 : Pairwise Comparison of evaluation items by expert questionnaire
- Step 3 : Construct a pairwise comparison matrix using a fuzzy membership function
- Step 4 : Calculation of final weighting by normalization after calculating fuzzy weighting
- Step 6: Evaluate the preferences of the alternatives for the sub-items
- Step 7: Convert to consider the preference of each alternative by weighting and Final selection

2.2 Advantages of Fuzzy-AHP

Fuzzy-AHP is effective in describing uncertain

phenomena in actual field by introducing fuzzy theory which reflects many similarities and characteristics of natural language which represents human thought. Although the data used for risk assessment are mostly ambiguous language expressions, the pairwise comparison values of Fuzzy-AHP can be more accurate using three values rather than having one value per interval on nine interval scales.

2.3 Deriving Weighting factors, Using Fuzzy-AHP

The order of weight derivation using Fuzzy-AHP is as follows.

- 1) Derive the comparison fuzzy membership function by AHP weighting
 - Compute pair of fuzzy matrices using the 9 - factor significance table applied Ishizaka 's relative important fuzzy membership function.
- 2) Derivation of the mean value of the pairwise fuzzy matrix
 - Find the trigonometric fuzzy function from multiple experts and derive the average value using the fuzzy averaging method (arithmetic mean).
- 3) Derivation of Fuzzy Synthetic Extent Value
 - Compute the fuzzy synthesis extension value to obtain the degree of possibility (V, Degree of Possibility) for given information.
- 4) Calculate the degree of possibility (V) and weighting
 - Calculate the degree of possibility and use it to derive a weighting.
- 5) Weighting vector conversion
 - Normalize the derived weighting.

3. Performance Shaping Factors

Human error probability (HEP) is calculated based on the worker's activity. Much human reliability analysis (HRA) methodologies use performance shaping factors (PSFs) to obtain quantitative estimates from calculated HEPs. Because it can

characterize important aspects of human error and provide numerical criteria that can be adjusted to nominal HEP levels.

The performance shaping factors derived from the reactor pressure vessel cutting process are as follows.

Table 1. Performance shaping factors (Level 1, Level 2) affecting reactor pressure vessel internal structure cutting

Level 1	Level 2
Human	Psychological State
	Physical State
	Performance Capability
Operation	Organizational Factors
	Task Management
	Procedure and Information
Ergonomic System	HMI
	Workplace Design
	Workplace Physical Environment

Table 2. Performance shaping factors(Level 2, Level 3) affecting reactor pressure vessel internal structure cutting

Level 2	Level 3
Psychological State	Stress
	Emotional State
	Safety Awareness
Physical State	Fatigue
	Physical Capability
	Discomfort
Performance Capability	Task Knowledge and Memory
	Experience
	Personal capability
Organizational Factors	Overall Planning
	Supervision of Management
	Team Factors
Task Management	Work Process Design
	Workload Management
	Problem Identification and Solution
Procedure and Information	Communication Availability and Quality
	Availability
	Complexity
HMI	Accuracy and Completeness
	Feedback and Recency
	Interaction Element
Workplace Design	Familiarity of Controller and Display
	Complexity of Controller and Display
	Maintenance
Workplace Physical Environment	Physical Access to Work Items
	Warning Sign
	Arrangement of Functional Areas
	Safety Device
	Noise
	Lighting
	Temperature
	Radiation Level

4. The results of derived Performance effect factor weighting

The weighting factors for the performance shaping factors derived from the reactor pressure vessel internal structure were derived using Fuzzy-AHP. A total of 32 Level 3 performance shaping factors' weighting were derived. Typically derived weightings are Task Knowledge and Memory 0.16, Stress 0.10, Personal Capability 0.09, Emotional State 0.05, Fatigue 0.06, Safety Device 0.04, Radiation Level 0.03. As a result, it is possible to reduce the possibility of human errors by improving the knowledge and ability of the individual through continuous education and training programs. In addition, if the environment is well maintained and managed, it will be effective to prevent human errors in cutting the internal structure of the reactor pressure vessel.

5. Conclusion

It is difficult to predict the probability and type of human errors that can occur between jobs, if the overall characteristics of the worker's job performance can't be accurately grasped, or if the decision process and job characteristics of the worker are not completely known. In order to mitigate such human error, the importance of performance factors related from the cutting work of the reactor pressure vessel internal structure was grasped, and it was considered necessary to manage the items with high importance among the items.

ACKNOWLEDGEMENT

This work was supported by the National Research Foundation of Korea (NRF) grant funded by the Korean government, Ministry of Science, ICT and Future Planning (No. 2017M2A8A5015148 and No.2016M2B2B1945086).

REFERENCES

- [1] Lee, Dong-un, A Study on the Cost risk Analysis for Construction Projects using fuzzy-AHP Method, 2003.
- [2] Lee, Seungchan, A Study on the Solution Selection Model of Information Systems Using Fuzzy AHP, 2005.
- [3] Cognitive Modeling and Dynamic Probabilistic Simulation of Operating Crew Response to Complex System Accidents Part 2 IDAC Performance Influencing Factors Model, 2006.

Dismantling Process Development of the Containment Building of Nuclear Power Plant

Myungduck Yang*, Wanil Jung, and Junhee Lee

Korea Electric Power Corporation E&C, 111, Daedeokdaero 989beon-gil, Yuseong-gu, Daejeon, Republic of Korea

*yangm@kepco-enc.com

1. Introduction

Containment Building (CB) is expected to take the longest time to dismantle power block buildings of nuclear power plant, which is the most technologically complex building. Therefore, this paper is to understand the dismantling method of the CB, the sequence of work, advantages and disadvantages of each method. And the studies of daily workload to estimate the time required for the dismantling of the CB have been followed, based on domestic and foreign references.

2. Demolition method

Two types of construction methods can be considered: demolition of the CB from top to bottom and demolition from bottom to top.

2.1. Top-down demolition method

All the equipment in the CB will be demolished including SG/RCP/Pressurizer & RV. And decontamination of the building will be followed by Cavity drainage and cleaning. The demolition of the concrete starts from the roof of the CB, sequentially from top to bottom.

[Sequence of the work]

- Concrete & Liner Plate Demolition of CB Dome & Upper Part of Exterior Wall (up to Polar Crane Rail, Top. ~ El. 135')
- CB Polar Crane and Girder Demolition
- Liner Plate Demolition of the Middle Section of CB Wall (Polar Crane Rail Location ~ El. 72')
- Concrete Demolition of the Ground Part of the Surrounding Buildings including Aux. Bldg. (Roof ~ El. 17' Foundation)
- Concrete Demolition of CB Exterior Wall above Ground (El. 135' ~ El. 20')
- CB Internal Concrete Demolition (whole)
- CB Liner Plate Lower and Bottom Part Demolition
- Concrete Demolition of Underground Part of the Surrounding Buildings & CB (El. 17' or less)

The advantage of this method is a less difficulty to work and relatively short construction period because it is crushed sequentially from the top. The disadvantage is the availability of high-crushing equipment and scattering of crushed materials

- A medium-sized backhoe breaker is mounted on a dome with the large crane to crush, which can be broken except for the edge of the dome (SONGS-1 application method)
- The edge of the dome and upper part of outer wall are crushed by using the breaker and the wire saw (SONGS-1 application).
- When demolishing CB Polar Crane and Girder, these are pulled out from the outside with a large crane.

2.2. Bottom-up demolition method

The top elevation of the CB is 220' high, with a ground level 20'. Thus in case crushing from the top is inadequate, crushing the outer wall from the bottom-up might be alternatively considerable.

[Sequence of the work]

- Concrete Demolition of the Ground part of the surrounding buildings (Roof ~ El. 17' foundation)
- CB Internal Concrete Demolition (down to El. 20')
- CB Polar Crane and Girder Demolition
- CB Liner Plate & Concrete Wall Demolition (Top ~ down to El. 20')
- CB Liner Plate & Internal Concrete Underground Demolition (El. 20' ~ Bottom Plate)
- CB Foundation Concrete Demolition (El. 20' or less)
- Concrete Demolition of the Underground part of the surrounding buildings (El. 17' or less)

The disadvantages of this method are inefficient and time consuming due to pre-dismantling of the internal concrete structure.

- In the Maine Yankee's case, many parts of the outer wall were broken with a breaker, and the remaining outer walls were demolished by blasting.
- An important precondition for this shall be established in a way that the surrounding buildings, the inside concrete structures of the CB and the Polar Crane and Liner Plate must be removed, in

advance before the crushing of the outer wall.

3. Daily workload for demolition of CB

Based on the two demolition methods, the amount of work and the required time for each detailed work will be estimated assuming the work speed. The daily workload is estimated by reference to the domestic construction standard and foreign data, and it can be adjusted according to the improvement of the equipment efficiency or the actual data of similar work process in the future as below.

[Reference for Daily Workload]

- Reference 1: Domestic Standard of Construction Estimate (Chapter 9 Mechanization Construction)
 - 9-14 : Large Breaker
 - Combination Machine: Large Breaker + Excavator $0.6 \sim 0.8 \text{ m}^3$

(m³/hr)

Item	Reinforced Structure
Average thickness of structure over 30cm	1.4 ~ 2.7

- Reference 2: DeCAT, Decommissioning Cost Analysis for the Korean pressurized Water Nuclear Power Plant
 - UCF 915, Removal of Reinforced Concrete by Diamond Wire Cutting
 - Workload : $3.3 \text{ m}^3/\text{day}$
 - Maine Yankee Performance : 20 ton/20 hour
- Reference 3: AIF/NESP-036 Guidelines for Producing Commercial NPP Decommissioning Cost Estimates
 - Work Type : Removal of Standard Reinforced Concrete
 - ✓ Work Method : Removing with Backhoe mounted demolition hammer, and shredded concrete removed with backhoe, 8 hours work a day
 - ✓ Workload : 9.5 cubic yard / day (= $7.26 \text{ m}^3/\text{day}$)
 - Work Type : Removal of Grade Slab Concrete
 - ✓ Work method : Removing with the Air powered tool, 8 hours work a day
 - ✓ Workload : 25 cubic yard / day (= $19.11 \text{ m}^3/\text{day}$)

[Review Result for Daily Workload]

- Domestic Standard of Construction Estimate (Civil Sector) classifies reinforced and non-reinforced structures. It suggests workloads under various

conditions taking into account working conditions, including work areas and obstacles.

- DeCAT, UCF 915 is likely to be applicable on some special parts, including RPV and SG bottom by wire cutting method.
- Therefore, it is reasonable to apply the average workload considering the use of equipment with large breaker in hydraulic backhoe and "over 30 cm thick reinforced structure" according to the Domestic Standard of Construction Estimate.
- This is similar figure to the average of the two standard values for concrete removal work proposed in AIF/NESP-036.

4. Conclusion

In order to establish the plan for demolition process of the Kori Unit 1 entire buildings, the demolition method and process of the containment shall be preferentially considered. And then it is reasonable to firstly review the demolition process of CB, secondly the surrounding buildings. The top-down demolition method is recommended to have more advantages than the bottom-up demolition, when it comes to the structure inside the CB, the Polar Crane demolition, and safety of the workers. Next step to review is that-the dismantling of the CB will be inefficient in case of the traditional crushing method due to the high-strength concrete and the complexed reinforcement bars. In addition working space and the work efficiency should be carefully regarded for the "work at height" and its equipment selection when estimating the daily workload.

REFERENCES

- [1] Domestic Standard of Construction Estimate, Construction Research Institute, 2018.
- [2] RSCS, KEPCO E&C, Decommissioning Cost Analysis for the Korean pressurized Water Nuclear Power Plant (DeCAT), Final Report, 2009.
- [3] AIF/NESP-036, "Guidelines for Producing Commercial Nuclear Power Plant Decommissioning Cost Estimates", 1986.5.

An Approach to the Inventory Assessment for Decommissioning Design of Nuclear Facilities

Su Jung Min^{a),*}, Kwan Seong Jeong^{a)}, Seung Kook Park^{a)}, San Chae^{b)}, and Kyung Min Kim^{b)}

^{a)} Korea Atomic Energy Research Institute, 111, Daedeok-daero 989beon-gil, Yuseong-gu, Daejeon, Republic of Korea

^{b)} Hanyang University, 222, Wangsimni-ro, Seongdong-gu, Seoul, Republic of Korea

*maymsj1118@gmail.com

1. Introduction

Decommissioning project of nuclear facilities is one of the biggest projects around the world. The management and tracking of decommissioning wastes generated from nuclear facilities should be carried out from their operation to final disposal phase.

In order to prepare a decommissioning plan for a nuclear facility, physical and radiological inventory evaluation should be performed. It is very important to investigate and identify the characteristics of a nuclear facility for decommissioning cost evaluation.

In this study, a method for configuration/system development of decommissioning waste management and assessment was studied for continuous management of commercial nuclear reactors (PWR, CANDU), research reactors (KRR-1&2, HANARO) and fuel cycle facilities (Post-Irradiation Examination Facility, Advanced Fuel Science Building).

2. Methods of Decommissioning waste inventory assessment

2.1 Differences from existing system

A similar system that builds characterization data of nuclear facilities is DEFACS (Decommissioning Facility Characterization DB System) of KAERI. The difference between DEFACS and the other system to be developed in this study is shown in the Table 1.

Table 1. Difference between system to be developed and existing system

	DEFACS	Development System
Concept	Facility characterization management	Waste history / Tracking management
Applicable facilities	KRR 1&2, UCP	Commercial reactor, Research reactor, Fuel cycle facilities
Input	Material, Size, Quantity, Shape, WBS code, Pictures, Surface contamination etc.	Building/Equipment/ Material ID, ISDC NO, Size, Radioactivity measurement data etc.
Output	Waste volume, Weight, Contamination /radioactivation rate etc.	Waste quantity, Radioactivity, Radioactive level of waste etc.

2.2 Methods of decommissioning waste inventory assessment for nuclear facilities

Fig 1 shows the schematic diagram of the analysis and assessment system of decommissioning waste inventory, which consists of PIAM, RIAM and DWAM. PIAM (Physical Inventory Assessment Module) is a module for evaluating the physical inventory of nuclear facilities using drawings and license data of each nuclear facility. RIAM (Radiological Inventory Assessment Module) is a module that evaluates radiological inventory through dose values (uSv/h, Bq/m²) and MCNP modeling results based on nuclides derived from PIAM. DWAM (Decommissioning Waste Assessment

Module) is a module for evaluating the physical and radiological characteristics of waste by applying a radioactive waste ratio calculation. Through the proposed 3 methodologies, it is possible to determine the necessity of decontamination, to confirm the effect on the worker and the environment, and to evaluate the cost based on decommissioning processes.

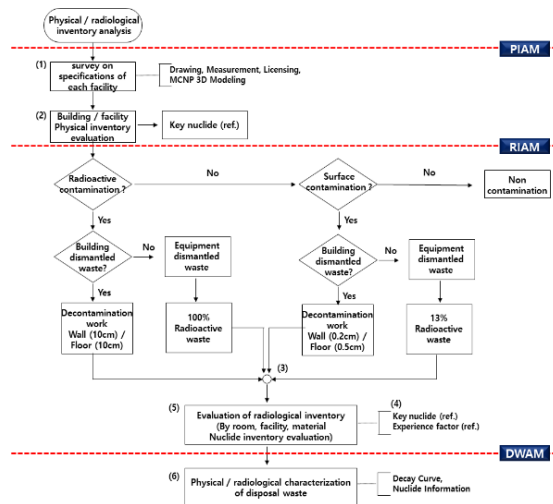


Fig. 1. Algorithm for analysis and assessment of waste inventory of nuclear facilities.

2.3 Derivation of input and output factor to build the waste assessment system

In this study, the input and output factors of system code were derived through the analysis of the existing decommissioning waste history management and assessment system. The building/system/material ID were designed to manage the physical inventory data of waste. The radiological input and output factors were distinguished by surface contamination and radioactivation, and in case of radioactivation, contamination measurement information through simulation was added. Table 2 shows the input and output factors to build the waste assessment system.

Table 2. Input and output factors for decommissioning waste assessment system

	Physical	Radiological
Input	Building/system/ Equipment/ Material ID,	Isotope information (Half-life, Decay constant etc.)
	Room/Equipment Information (Size, Material, area, Volume etc.)	Detection type (Direct, Indirect)
		Simulation(in case of radioactivation)
Output	ISDC No.	Radioactivity measurement data
	Waste quantity (ISDC NO, material, position)	Initial/Specific radioactivity data
	Waste Level	Decay curve

3. Conclusion

In order to develop the characteristics and history management system for decommissioning waste, the existing assessment system of the nuclear facilities was analyzed and the configuration/system classified into 3 categories (PIAM, RIAM, DWAM) were derived. The proposed inventory assessment methods and factors can be applied for the decommissioning of waste history management and assessment system as basic information and also can be used for the evaluation on decommissioning projects of the commercial reactors, research reactors and fuel cycle facilities.

ACKNOWLEDGEMENT

This work was supported by the Nuclear Research and Development Program through the National Research Foundation of Korea funded by the Ministry of Science and ICT.

REFERENCES

- [1] SK Park, et al., "The Decommissioning Facility Characterization DB System (DEFACS)", KAERI/TR-4128(2010).

Effective Decontamination Treatment Process of Steam Generator

Daeseo Koo*, Sang Bum Hong, In Hye Hahm, Jea Hyun Ha, Seung-Kook Park, Kwan Seong Jeong, Bum Kyoung Seo, and Kook-Nam Park.
Korea Atomic Energy Research Institute, 111, Daedeok-daero 989beon-gil, Yuseong-gu, Daejeon, Republic of Korea
*ndskoo@kaeri.re.kr

1. Introduction

The decommissioning of a nuclear power plant requires a large amount of time and cost. The treatment and disposal of radioactive waste also requires significant costs. The quantity of radioactive waste is to be diminished using several selective combinations of decontamination and treatment. The workers must be safe from exposure to radiation [1-3].

In this study, to design an effective treatment process for decommissioning radioactive waste, effective decontamination techniques for decommissioning radioactive waste were selected with their application to decommissioning radioactive waste of the steam generator. The three treatment processes were discussed with decommissioning radioactive waste of the steam generator.

2. Planning of Treatment Process for Decommissioning Steam Generator

2.1. Treatment Process for Decommissioning Steam Generator

Table 1 shows application techniques for selecting decontamination method.

Table1. Application Techniques for Selecting Decontamination Method

Part of Steam Generator	Application of Decontamination Techniques and Decontamination Effect
Outer Surface	* Outer Surface is slightly Contaminated with Radioactive Nuclide. *Selected Decontamination Techniques for Treatment Process of Outer Surface Radioactive Waste are to be Blasting Abrasive and HF series Chemical Decontamination (KAERI/RR-3478/2010). *Application of Blasting Abrasive and HF series Chemical Decontamination to Outer Surface Radioactive Waste with Decontamination Factor 80.
Water Chamber	*Radioactive Contamination of Water Chamber is Higher about 100 times than that of Outer Surface (Sweden Ringhals3). *Selected Decontamination Techniques for Treatment Process of Water Chamber Radioactive Waste are to be Electro-Chemical (German KRB-A) and MEDOC(Belgium BR3). *Application of Electro-Chemical and MEDOC ⁺ to Water Chamber Radioactive Waste with Decontamination Factor 100. Application of Melting to Water Chamber. *Application Electro-Chemical Decontamination Technique (German KRB-A) to Water Chamber Radioactive Waste. -Its Effect: Reduction from Initial Surface Contamination (20,000Bq/cm ²) to unlimited Release Level and Generation of 1.5% Radioactive Waste from Initial Radioactive Waste. *Application MEDOC

	Decontamination Technique (Belgium BR3) to Water Chamber Radioactive Waste. - Its Effect: Reduction from Initial Radioactivity of Metal Radioactive Waste (80%) to 0.1Bq/g.
U-type Tubes	*Radioactive Contamination of U-type Tubes is Higher about 100 times than that of Outer Surface (Sweden Ringhals3). *Selected Decontamination Techniques for Treatment Process of U-type Tubes Radioactive Waste are to be Dry Blasting Abrasive (Sweden Ringhals3) and Loop Chemical Decontamination (Kori3). *Application super Compression (272-14,965 ATM) to activated U-type Tubes Radioactive Waste. -Its Effect: Reduction from Initial Volume of Radioactive Waste to 1/7 Volume of Radioactive Waste. *Application of Dry Blasting Abrasive and Loop Chemical Decontamination to U-type Tubes Radioactive Waste with Decontamination Factor 100. *Application Dry Blasting Abrasive Decontamination Technique (Sweden Ringhals) to U-type Tubes Radioactive Waste. -Its Effect: Reduction from Total Radioactivity (650GBq) of Steam Generator to 510GBq (85%) of U-type Tubes Radioactive Waste. *Application high Frequency Furnace Melting Technique to Remnant Radioactive Waste. -Its Condition: Ingot: ~ 95%, Slag: ~2-3%, Sampling & Vapor: very small Quantity.

*Metal Decontamination by Oxidation with Cerium

3. Results of Effective Treatment Process for Decommissioning Steam Generator

3.1. Treatment Process for the Decommissioning Radioactive Waste of Outer Surface of Steam Generator

From Table 2, the outer surface of the steam generator is to be estimated as clearance waste (about 100%) through decontamination.

3.2. Treatment Process for the Decommissioning Radioactive Waste of Water Chamber of Steam Generator

The water chamber of the steam generator is to be estimated as partial clearance waste and partial radioactive waste through decontamination and melting.

3.3. Treatment Process for Decommissioning Radioactive Waste of U-Type Tubes of Steam Generator

The u-type tubes of the steam generator is to be estimated as partial clearance waste and partial radioactive waste through decontamination, melting [3-4], and compression process [5].

Table 2. Results of Treatment Process of Steam Generator

Part of SG	Treatment Process	Results of Treatment Process
Outer Surface	Decontamination	*Outer Surface of Steam Generator is slightly Contaminated with Radioactive Nuclide. *Application selected Blasting Abrasive Decontamination Process and HF Series Chemical Decontamination Process to Outer Surface Radioactive Waste of Steam Generator with Decontamination Factor 80 is to be Estimated as Clearance Waste (about 100%).
Water Chamber	Decontamination	*Radioactive Contamination of Water Chamber of Steam Generator is higher about 100 times than that of Outer Surface. *Application selected Electro-Chemical Decontamination Process and MEDOC Process to Water Chamber Radioactive Waste of Steam Generator with Decontamination Factor 100 is to be Estimated as Partial Clearance Waste (>70%) and Partial Radioactive Waste(<30%).
	Melting	*Remnant Radioactive Waste is to be Estimated as Partial Clearance Waste (>20%) and Partial Radioactive Waste (<10%) through Melting Process.
U-Type Tubes	Decontamination	*Radioactive Contamination of U-Type Tubes is higher about 100 times than that of Outer Surface. *complicated U-Type Tubes is Activated due to Erosive Oxidation. *Application selected Dry Blasting Abrasive Decontamination Process and Loop Chemical Decontamination Process to U-Type Tubes Radioactive Waste of Steam Generator with Decontamination Factor 100 is to be Estimated as Partial Clearance Waste(>50%) and Partial Radioactive Waste(<50%).
	Melting	*Application Melting Process to Remnant Radioactive Waste from Water Chamber and U-Type Tubes is to be estimated as Partial Clearance Waste, Partial Recycling Waste(>20%) and Partial Radioactive Waste(<10%).
	Compression	*Application Super Compression on the activated Waste from Water Chamber and U-Type Tubes is to be estimated as Radioactive Waste(<20%).

4. Conclusion

Effective decontamination techniques for decommissioning metal radioactive waste were selected with their application to outer surface, water chamber, and u-type tubes of the steam generator. The outer surface of the steam generator is to be estimated as clearance waste (about 100%). The water chamber of the steam generator is to be estimated as partial clearance waste (>70%) and partial radioactive waste (<30%) through decontamination process, partial clearance waste (>20%) and partial radioactive waste (<10%) through melting process. The u-type tubes of the steam generator is to be estimated as partial clearance waste (>50%) and partial radioactive waste (<50%) through

decontamination process, partial clearance (>20%) and partial radioactive waste (<10%) with melting process, and radioactive waste (<20%) through compression.

ACKNOWLEDGEMENT

This work is supported by the Ministry of Science and ICT (No. 2017M2A8A5015143) of the Republic of Korea.

REFERENCES

- [1] K. W. Lee, et al., "Development of Volume Reduction and Self-Disposal Technology for Large Metal Wastes including Steam Generator Produced from the Nuclear Power Plants", KAERI/RR-3478/2010.
- [2] S. H. Park, et al., "Investigation on the Operation History of Domestic NPPs for the Evaluation of Radionuclide Stream in the Historical Radioactive Wastes", KAERI/CM-2446/2017.
- [3] B. Y. Min, P. S. Song, J. H. Ahn, W. K. Choi, C. H. Jung, W. Z. Oh and Y. Kang, "Melting Characteristics for Radioactive Aluminum Wastes in Electric Arc Furnace", Journal of the Korean Radioactive Waste Society, 4(1), 33-40 (2006).
- [4] R. Xinwen, L. Wencang, Z. Yuan, "Melt Refining of Uranium Contaminated Copper, Nickel, and Mild Steel", China Institute for Radiation Protection, pp. 110-117.
- [5] J. W. Park, D. S. Kim and D. E. Choi, "A Study on Optimized Management Options for the Wolsong Low-and Intermediate-Level Waste Disposal Center in Korea-13479", WM2013 Conference, February 24-28, 2013, Phoenix, Arizona, USA.

System for Measuring Characteristic of Aerosol From Metal Cutting

Wonseok Yang*, Nakkyu Chae, Minho Lee, and Sungyeol Choi

Korea Advanced Institute of Science & Technology, 291, Daehak-ro, Yuseong-gu, Daejeon, Republic of Korea

*abw94@kaist.ac.kr

1. Introduction

In the process of dismantling nuclear facilities, radioactive materials are released in various form. To plan decommissioning nuclear power plant safely, it is important to fully understand the forms and quantities of radioactive materials.

Radioactive airborne particles are one of form of by-product which produced during the cutting radioactive materials, such as activated metal. Inhalation of radioactive aerosols can adversely affect worker's health during dismantling [1]. The aerodynamic distribution of radioactive aerosols will determine the impact of internal exposure [2]. Therefore, the size distribution of aerosols, which produced during cutting, need to be studied. This paper presents the aerosol system for the measurement of physical and chemical characteristics of aerosol from metal cutting.

2. The system for the measurement of characteristics of aerosol from metal cutting.

In a laboratory experiments, we use a plasma arc torch (powermax125, Hypertherm) for cutting metal. Electrical low pressure impactor (ELPI+, Dekati) is used for a measurement of aerosols.

2.1 Chamber and automated cutting system

For safety of researcher, we installed the isolated aerosol chamber. The chamber size is 1.2*1*0.65[m]. There is a HEPA filter inlet for air flow. For reproducibility, it has automated cutting system. The automated cutting system is made up of x-moving stage with servo motor and a control box for plasma and x-stage movement. The control box can set the cutting start point, the cutting end point, a speed and a length of cutting.



Fig. 1. The aerosol system for the measurement of physical and chemical characteristics of aerosol.

2.2 Sampling and measurement system

ELPI+ measures aerodynamic diameter distribution and its concentration in real time. It measures the size range of 6 nm – 10 μ m with 10 Hz sampling rate. After the measurement it is possible to collect size classified particles in 14 stages for chemical analysis. For chemical analysis we will conduct ICP-MS and SEM-EDS to know composition of aerosols and morphological characteristic. At sampling pipe, there are two sampling lines, velocity lines and pressure lines. The velocity and pressure are measured at sampling point (center of the sampling pipe).



Fig. 2. Sampling pipe and measurement lines.

3. Metal cutting test

3.1 Isokinetic sampling

To minimize distortion aerodynamic distribution during the sampling, isokinetic sampling is important. For isokinetic sampling, the velocity of air in sampling pipe and sampling port must be matched [3].

For matching the velocity of air during sampling, we measured velocity through velocity line at sampling pipe with probe thermometer (Testo110, Testo). According to the measured velocity we chose sampler head diameter (5-10 mm).



Fig. 3. Sampler with sampler head.

3.2 Metal cutting test setting

For test we used stainless steel plate 10mm thick. We cut metal plate with plasma arc torch (Current 75 A) with air. We set the cutting speed (10 mm/s) and cutting length (50 mm). We set the cutting speed and plasma arc torch current which can cut the metal completely. Measuring time was 30 minutes because 30 minutes after cutting, the number concentration falls off similar to background number concentration ($\sim 10^2 \text{ m}^{-3}$).

3.3 The metal cutting result

Fig 4 is the result of the test cut a 10 mm thick stainless-steel plate at 10 mm/s speed with plasma arc torch (current: 75 A) for 5 seconds

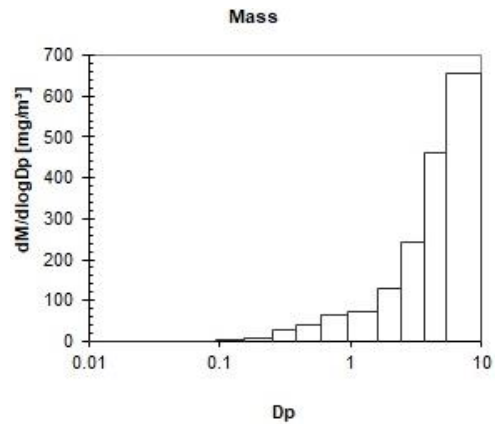


Fig. 4. The mass distribution in response to the aerodynamic distribution.

4. Conclusion

We set the aerosol system for measurement of physical and chemical characteristics of aerosols from metal cutting. With this system, we will experiment different power, speed and different kinds of metal that uses in nuclear power plant. The result is aerodynamic distribution of aerosols and chemical composition of each stage. With our experiment result, we expect to suggest optimum way to cutting radioactive waste to minimize internal dose of worker.

ACKNOWLEDGEMENT

This work was financially supported by the National Research Foundation of Korea (NRF) by a grant funded by the Ministry of Science and ICT, Republic of Korea (Grant No. NRF-2017M2A8A4018596).

REFERENCES

- [1] Ebadian, MA, SK Dua, and Hillol Guha, "Size Distribution and Rate of Production of Airborne Particulate Matter Generated During Metal Cutting." National Energy Technology Lab., Pittsburgh, PA (US); National Energy Technology Lab., Morgantown, WV (US), (2001).
- [2] ICRP, "Human Alimentary Tract Model for Radiological Protection. ICRP Publication 100." Ann. ICRP 36, 1-2, 25-327 (2006).
- [3] Vincent, James H, "Aerosol Sampling. Science and Practice." JOHN WILEY & SONS LTD., NEW YORK, NY(USA). (1989).

Gamma Spectroscopy System With Automatic Sample Feeder in Mobile Laboratory

Mee Jang, Chang Jong Kim, Hyunchul Kim, Jinhyung Lee, and Jong Myoung Lim

Korea Atomic Energy Research Institute, 111, Daedeok-daero 989beon-gil, Yuseong-gu, Daejeon, Republic of Korea

*mjang@kaeri.re.kr

1. Introduction

In the process of decommissioning, it is very important to evaluate the radiation characteristics of radioactive waste. In case of nuclear power plant decommissioning project where large amount of radioactive waste can occur, the efficiency of analysis processing is directly related to the time required for decommissioning process, which in turn affects the decommissioning cost. In Korea, it is necessary to analyze 14 radionuclides basically, and additional radionuclide analysis may be required depending on the operation history. Therefore it is necessary to develop the onsite mobile lab and automate the analysis system for alpha, beta and gamma radionuclide. In this study, we designed a gamma spectroscopy system with automatic sample feeder and evaluated the applicability for decommissioning waste.

2. Methods and Results

2.1 Design of the sample feeder

When the radioactive waste is transported from the decommissioning site, it is pulverized and mixed through a crusher and classified using the automated system of separation and sampling for radioactivity level. Some quantities of classified waste are collected as representative samples. These representative samples are transferred to the mobile laboratory to conduct alpha, beta and gamma

radioactivity analysis. To increase the analysis efficiency of gamma radioactivity, it is necessary to automate sample change. Therefore, we designed the automatic sample feeder for gamma spectroscopy system as shown in Figure 1.



Fig. 1. Automated sample feeder for gamma spectroscopy system.

Generally, the gamma spectroscopy system enclosed by a thick lead shield to shield the radiation coming from the surrounding environment and satisfy the minimum detectable activity (MDA). And, the lead lid is manually opened and closed to replace the sample in laboratory. However, this manual method has the problem that the analyst has to replace the sample every time the analysis is finished, the analysis processing efficiency may be lowered when the number of sample is large. We made a hole at the upper part of the lead shield and the sample was designed to be vertically replaced by a vacuum pump or a grip.

2.2 Applicability for decommissioning waste

To evaluate the applicability of gamma spectroscopy with automatic sample feeder for decommissioning waste, we checked the space suitability for mobile lab and the minimum detectable activity change by the absence of some lead shielding. As shown in Figure 2, vertical sample exchange is more suitable for mobile laboratory than horizontal sample exchange because of the narrowness of the space.



Fig. 2. Space suitability for mobile laboratory.

We evaluated the MDA change according to the degree of lead lid opening and the results are shown in Table 1 using equation (1).[1]

$$MDA = \frac{2.71 + 4.65 \sqrt{\mu_B}}{\epsilon \times m \times t} \quad (1)$$

Where, μ_B , ϵ , m and t are background count, measurement efficiency, sample weight and measurement time, respectively. As shown in results, it is considered that the target MDA for radioactive decommissioning waste can be satisfied.

Table 1. MDA change according to the degree of lead lid opening

Degree of opening	Background increase	MDA increase
100%	5.8	2.4
50%	2.5	1.6
25%	2	1.4

3. Conclusion

In this research, we designed the gamma spectroscopy system with automatic sample feeder and the system are suitable for mobile laboratory of decommissioning onsite.

REFERENCES

- [1] L.A Currie, "Limits for qualitative detection and quantitative determination", Anal. Chem., 40(30), pp.586-593, 1968.

Case Study of Soil Characterization Techniques at Decommissioning Nuclear Power Plants

Donghee Lee*, Wook Shon, Suk Bon Yoon, and Suhee Lee
Korea Hydro & Nuclear Power Co., Ltd Central Research Institute, 70, Yuseong-daero 1312beon-gil,
Yuseong-gu, Daejeon, Republic of Korea
*donghee.lee@khnp.co.kr

1. Introduction

Developing the remediation for soil contaminated with radionuclides at decommissioning sites is one of the challenging tasks. Many sites have discovered additional site requiring remediation toward the end of remediation projects and were forced to extend the decommissioning schedules. In order to minimize this maintain decommissioning project schedule, effective characterization of the soil and site of the contamination is needed [1].

In this paper, describes the investigation results for the characterization techniques and overseas cases in order to effectively perform the soil characterization.

2. Soil Characterization Techniques

There are a number of techniques that can be used to collect soil samples. The method chosen is driven by the data needed from the sample and the cost of the sample technique [2].

2.1 Grab Sampling

Grab sampling is the most simple and least costly among the soil sampling techniques and is typically used for surface soil sampling. However, this method is limited for use collecting surface soil samples up to 6 inch [15 cm] in depth. Generally at least 2 liters of sample must be collected per individual sample location to insure adequate material for the subsequent laboratory analyses.

2.2 Split Spoon Sampling

Split spoon sampling is generally limited to fairly loose granular material and to a total sample depth of approximately 0.5 meter. It is a relatively inexpensive method and can be useful in determining if subsurface contamination (i.e. greater than 6 inches [15 cm]) is present in a site.

2.3 Direct Push Sampling

Direct push sampling is generally used when analysis of soil located greater than 0.9 meter below the surface is needed. Samples are generally taken at 1.2 meter increments by adding additional 1.2 meter sections of push rod to the hydraulic drive head. Dividing the sample into shorter lengths would provide a more detailed contamination depth profile but may result in additional laboratory analysis complexity (and cost) due to the limited amount of material from the shorter lengths.

2.4 In situ Gamma Spectroscopy

In conducting the Final Status Survey (FSS) of site at a number of plant decommissioning projects, in-situ gamma spectroscopy equipment such as the In Situ Object Counting Systems (ISOCS) has been used. This method allows relatively large areas to be assessed with one count in place of more time consuming conventional scanning of the decommissioning site. During an FSS, in situ surveys have been used at some sites along with soil sampling to ensure compliance with the site release criteria. In situ gamma spectroscopy could be used during site characterization to determine if significant soil contamination exists in the site or to survey the inside of an excavation otherwise inaccessible from a personnel safety standpoint.

3. Cases of Soil Characterization at Overseas

3.1 Maine Yankee [3]

Maine Yankee site did not have high levels of groundwater contamination. This result would be anticipated based on the soil radionuclide fractions shown in Table 1. The very soluble radionuclide H-3 is present as a low fraction in soil and was measured in relatively low concentrations in groundwater. The somewhat less soluble Sr-90 was not measured in either soil or groundwater. Table 2 shows the summary of the soil characterization results for Maine Yankee. The data in Table 2 are from areas where soil concentrations were above or approaching

the Maine Yankee soil DCGLs. It should be noted that samples were taken in all areas of the site but are not shown here as they were generally below the soil DCGLs.

Table 1. Radionuclide Fraction in Soil at Maine Yankee

Radionuclide	Average Fraction of Total Activity
H-3	0.053
Ni-63	0.048
Co-60	0.009
Cs-137	0.890

Table 2. Summary of Soil Characterization Result at Maine Yankee

	RCA West	RCA East	Roof Drains	RCA Areas	LLW Storage Bd.
# of Samples	58	35	7	8	30
# of Positive for Co-60	23	12	4	3	0
Mean Co-60 (pCi/g)	0.62	0.28	4.09	11,213	N/A
Max Co-60 (pCi/g)	3.29	1.94	11.2	33,600	N/A
# of Positive For Cs-137	55	33	6	7	5
Mean Cs-137 (pCi/g)	10.99	4.88	0.33	0.13	0.1
Max Cs-137 (pCi/g)	156	133	0.53	0.21	0.13

3.2 Rancho Seco [4]

Rancho Seco had not experienced widespread soil contamination during the operation of the plant. The only areas that exhibited significant levels of contamination were the following:

- Spent Fuel Pool(SFP) Cooler Pad
- SFP-Turbine-Diesel Generator Room Gap
- West Tank Farm Area
- South Tank Farm Area

• Effluent Stream(Corridor) & Depression Area

Table 3 shows the results for the soil samples with the highest radionuclide concentrations. The highest samples from the first three areas listed Cs-137 concentrations that were 18, 14, and 2 times higher, respectively, than the Rancho Seco industrial worker DCGL for CS-137. The highest samples from the other two areas were in the range of 40 to 70% of the DCGLs when both Co-60 and Cs-137 results were included.

Table 3. Rancho Seco Soil Characterization Results

Radio-nuclide	Highest 6 samples soil concentration range pCi/g	Rancho Seco industrial worker DCGL pCi/g	Maximum dose contribution from any one sample or percent of soil DCGL
H-3	4.0 ~ 10.2	-	4.6E(-4)
C-14	1.7 ~ 10.0	8.33E(+6)	0.00012 %
Co-60	0.3 ~ 6.5	12.6	52 %
Ni-63	37 ~ 170	1.52E(+7)	0.00011 %
Sr-90	1.3	6,490	0.02 %
Tc-99	4.5 ~ 5	-	8.7 E(-2)
Cs-134	0.21	22.4	0.9 %
Cs-137	8.0 ~ 942	52.8	17.8

4. Conclusion

This paper describes four types of the techniques for characterization of soils. Among these, in situ Gamma Spectroscopy is generally used for decommissioning. In the case of the overseas, the characterization was performed by using the above technologies. The results of this paper, therefore, would be useful information and experiences for their future application at other nuclear power plant decommissioning including Kori-1 in the characterization of soil.

REFERENCES

- [1] NUREG-1575/EPA 402-R-97-016, "Multi-Agency Radiation Survey and Site Investigation Manual (MARSSIM).
- [2] EPRI Report 1019228, "Characterization and Dose Modeling of Soil, Sediment and Bedrock during Nuclear Power Plant Decommissioning, 2009.
- [3] Maine Yankee License Termination Plan, Revision 3, dated October 15, 2002.
- [4] Rancho Seco License Termination Plan, Chapter 6, Revision 0 dated April 2006.

Study on Metal Ions Treatment From Electro-Decontamination Wastes Using Pilot Scale Equipment

Jung-Hyun Lee*, Dong-Yeon Kim, and Ki-Chul Kim

Korea Electric Power Corporation Plant Service & Engineering, 96-1 Gilchon-Gil, Jangan-Eup, Gijang-Gun, Busan, Republic of Korea

*2jh@kps.co.kr

1. Introduction

The Regenerable Electro Decontamination is easy to regenerate electrolyte by using a precipitation process to remove metal ions. The generated metal precipitates can be converted from oxalate to oxide through a calcination process and treated as a safe compound. In this study, the regenerable electro decontamination process was evaluated by the pilot scale equipment.

2. Experiment

2.1 Experiment method

The liquid waste from electro decontamination was used to regenerate electrolyte through a waste regeneration process. The experiment was carried out the following conditions.

Table 1. Process condition

Process	Agent	Con.	Time	Temp.
Reduction	N_2H_4	0.08 M	1 hr	90 °C
Precipitation	$C_2H_2O_4$	2.75 M	6 hr	RT
Calcination	-	-	-	300 °C

2.2 Equipment

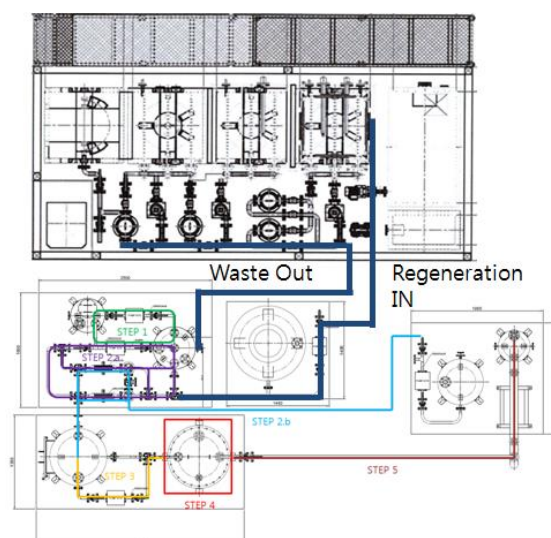


Fig. 1. Lay out of Regenerable Electro Decontamination pilot equipment.

The regenerable electro decontamination pilot equipment consist of two sub system; electro decon pilot and waste regeneration pilot.

As shown in the fig 1, the liquid waste is discharged into regeneration pilot and precipitation process is carried out. After the precipitation, metal precipitates are filtered using the multiple size of filters and calcined by a thermolysis equipment.

3. Results and Analysis

3.1 Metal precipitates analysis

Metal precipitates were sampled and analyzed for

constituents before and after calcination.

The following figures show pre-calcination and post-calcination precipitates.

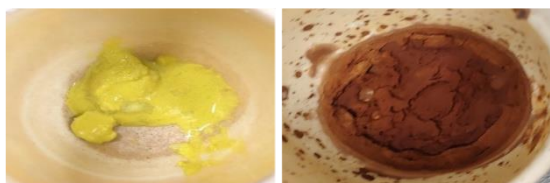


Fig. 2. Before calcination of metal precipitates (L).

Fig. 3. After calcination of metal precipitates (R).

Table 2. FE-EPMA analysis results

Element	Atom(%)	
	Before	After
Fe	39.61	30.82
Ni	6.87	5.25
O	49.38	63.85
Cr	N.D	0.06
C	4.12	N.D

As a result of FE-EMPA analysis, it was confirmed that before precipitates were form of oxalate containing carbon. After calcinations, carbon was not detected in precipitates. The element ratio Metal : O of precipitates after calcination is 1 : 1.7, which is similar to the ratio 1 : 1.5 of Fe_2O_3 and Ni_2O_3 . This result shows that precipitates have converted from oxalate to oxide.

3.2 Regenerated Electrolyte analysis

The removal rate of metal ions was analyzed by comparing the metal ions in the electrolyte. The removal rate of Fe ions was about 80% and all of Ni ions were precipitated. In case of Cr ion, It was not precipitated with oxalic acid. So Cr ions concentration was remained.

Table 3. Metal ion concentration in Electrolyte(ICP-OES)

Element	Concentration(ppm)		
	Fe	Cr	Ni
Before	150.24	34.18	20.37
After	27.32	28.35	N.D

4. Conclusion

As a result, most of the results were similar with lab scale tests. With this result, it can be conferred that the regenerable electro decontamination can remove nuclides in the base material and lower the radioactivity level. The liquid waste can be used for a longtime through the regeneration process and the solid waste can be easily treated by removing the chelate agent from the metal precipitates. Through this study, we expect that this process will contribute to not only decontamination but also waste volume reduction.

ACKNOWLEDGEMENTS

This work was supported by the Korea Institute of Energy Technology Evaluation and Planning (KETEP), granted financial resources from the Ministry of Trade, Industry & Energy, Republic of Korea (Number 20141510300310)

REFERENCES

- [1] S.W, Lee et. al., "Thermal Decomposition Characteristics of Metal Oxalate Dyedrate formed by the precipitation of the phosphoric acid solution", Proc. Of the KRS 2016 Fall Conference,14(1), Oct 12-14, 2016 Jeju.

Study on the Dissolution of Concrete for Volume Reduction of Radioactive Concrete Waste

Iksoo Kim*, Maengkyo Oh, and Keunyoung Lee

Korea Atomic Energy Research Institute, 111, Daedeok-daero 989beon-gil, Yuseong-gu, Daejeon, Republic of Korea

*niskim@kaeri.re.kr

1. Introduction

Concrete waste accounts for about 80% of the various types of waste generated from the dismantling of nuclear facilities [1]. Considering the stringent classification criteria and the high disposal cost of radioactive waste in Korea, volume reduction treatment is inevitably necessary to reduce the amount of radioactive concrete waste. The purpose of this research is to develop a technology for the volume reduction of radioactive concrete wastes. As the first step, this research aims to develop a process to dissolve concrete waste and a separation process of dissolved radionuclides. For this purpose, the physico-chemical properties of cement, mortar, and concrete waste powder were investigated, and the dissolution characteristics of concrete powder by nitric acid and hydrochloric acid solution were examined. The optimum conditions for the dissolution of concrete waste powder and radioactive concrete samples contaminated with radioactive isotopes were determined.

2. Experimental

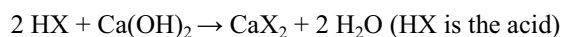
Concrete waste was obtained from a local construction company. This <4 mm pulverized concrete powder was then sieved into 6 sizes (+200 mesh ~ -16 mesh) for use throughout the experiment. For the preparation of radioactive contaminated concrete, standard solutions of radioisotopes (^{60}Co , ^{137}Cs , and ^{90}Sr) were diluted and aliquots of these radioisotopic solutions were injected in concrete powder to have 300 Bq/g radioactivity. These samples were dried for 50 days at room temperature.

After measuring the radioactivity of contaminated concrete powder by using MCA and beta counter, concrete powder was dissolved by adding hydrochloric acid or nitric acid solution of the desired concentration. Undissolved concrete powder were filtered and dried. The weight and radioactivity of undissolved powder was measured again. The residual radioactivity of concrete powder was calculated from the measured radioactivity before and after dissolution.

3. Results and discussion

3.1 Dissolution characteristics of cement based materials

Concrete is a composite material which is made up of filler and binder. The binder (cement paste) glues the filler together to form a synthetic conglomerate. The constituents used for the binder are cement and water, while the filler can be fine or coarse aggregate. Concrete is reacted with acid because of its alkaline nature. Most pronounced is the dissolution of calcium hydroxide which occurs according to the following reaction:



The decomposition of the concrete depends on the porosity of the cement paste, on the concentration of the acid, on the solubility of the acid calcium salts (CaX_2), and on the fluid transport through the concrete. Acids such as nitric acid and hydrochloric acid are very reactive with concrete as their calcium salts are readily soluble. On the other hand, sulphuric acid is relatively unreactive because of low solubility of its calcium salt. Therefore, in this study, dissolution of concrete was carried out by using nitric acid and hydrochloric acid.

3.2 Dissolution of concrete powder

In order to investigate the dissolution behavior of concrete waste in acidic solution, concrete powder, cement, and mortar were dissolved in 2 M nitric acid solution for 2 hours. About 30wt% of the concrete was dissolved, but more than 93wt% of the cement and 90wt% of the mortar were dissolved. Fig. 1 shows the composition of the dissolved components analyzed by ICP after dissolving the cement, mortar, and concrete in 2 M nitric acid. As shown in figure,

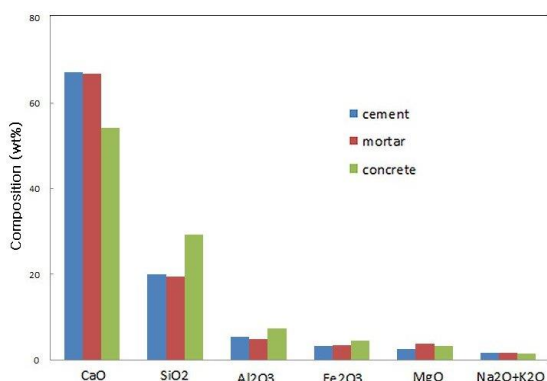


Fig. 1. Chemical composition of dissolved fraction of cement, mortar, and concrete.

the composition of the dissolved solution of cement and mortar is almost the same, and also the composition of the dissolved solution of concrete is similar to those of cement and mortar. In particular, the composition of each chemical component closely coincides with that of Ordinary Portland Cement (OPC). The dissolution ratio of concrete powder in nitric acid solution is about 30wt%, and about 70wt% of the undissolved materials are mostly sand and coarse aggregate. The composition of the dissolved material is almost the same as that of OPC.

The effects of acid concentration and temperature on the dissolution rate of concrete waste powder were examined using hydrochloric acid and nitric acid to determine the optimal dissolution conditions. The weight loss ratio of concrete powder is about 30% on average, which is almost constant even when the acid concentration increases. When the acid concentration is 0.5 M or less, the weight loss ratio increases in proportion to the acid concentration. This indicates that acid is the limiting reactant in the reaction with cement components such as CaO, Al₂O₃, and Fe₂O₃. It was calculated that 0.5 mole of acid was required to completely react with 1 kg of concrete powder.

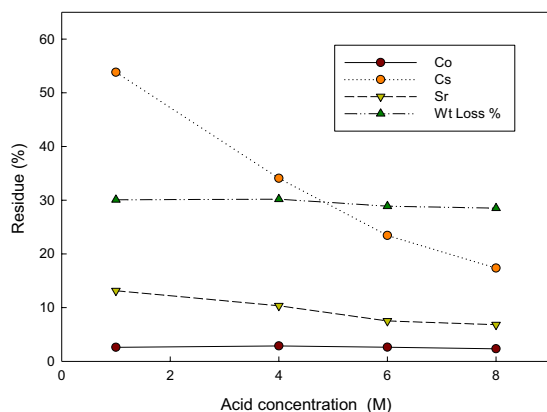


Fig. 2. Decontamination ratio of radioisotopes.

3.3 Dissolution of contaminated concrete powder

Fig. 2 shows the weight loss ratio and the radioactivity residue of the undissolved powders remaining from nitric acid dissolution of the radioactively contaminated concrete powder. Contaminated concrete powder also shows a weight reduction rate of about 30% regardless of the concentration of nitric acid solution when the concentration of nitric acid solution is 0.5 M or higher. The residual ratio of cobalt is constant regardless of the nitric acid concentration, but those of cesium and strontium decrease gradually as the nitric acid concentration increases. However, the radioactive residual ratio of cesium and strontium is higher than that of cobalt even at nitric acid concentration of 8 M.

Dissolution was carried out by increasing the dissolution temperature when the contaminated concrete powder was dissolved again in order to reduce the radioactive residual ratio. Dissolving the primary undissolved powders in 4 M nitric acid solution again for 1 hour, the radioactive residue ratio decreased drastically as the dissolution temperature increased. At 100 °C, the radioactivities of cobalt, cesium, and strontium were reduced to less than 3% as compared with the first undissolved powder. The weight loss ratio of the undissolved concrete powder was about 4wt% as compared with that of the first undissolved powder. The total radioactivity retention by primary and secondary dissolution was less than 1% at 100 °C as compared with that of the initial contaminated concrete powder.

ACKNOWLEDGEMENT

This work was supported by the National Research Foundation of Korea (NRF) Grant funded by Korea government(MSIT) (no.NRF-2017M2A8A5015147).

REFERENCES

- [1] K. Y. Lee et al., "Trends in Technology Development for the Treatment of Radioactive Concrete Waste", JNFCWT, 16(1), 93-105 (2018).

A Study on the Assessment of Internal Exposure Effect by Radioactive Aerosol Generated During Melting Facility of NPPs Using Internal Exposure Code

Sun Il Kim, Hak Yun Lee, and Jong Soon Song*

Chosun University, 309, Pilmun-daero, Dong-gu, Gwangju, Republic of Korea

*jssong@chosun.ac.kr

1. Introduction

The radioactive aerosols, which are generated during the decommissioning of a nuclear power plant, are inhaled by workers and deposited in the respiratory organs and other vital organs in their body and cause internal exposure. Also, as internal exposure is difficult to measure directly unlike external exposure, it is necessary to assess internal exposure in advance, and derive the optimal working hours and select working conditions for preventing workers' overexposure caused by radioactive aerosols.

2. Assessment factors during internal exposure assessment

2.1 Quantity of each nuclide

As the quantity of each nuclide is directly related to workers' intake as well as respiratory rate, it must be determined first before conducting internal exposure assessment. In this study, the nuclide data, collected in the process of melting the structures decommissioned by the Kozloduy NPP, was used as the data on the quantity of nuclides. This paper applied the quantity of ^{60}Co , the representative considered nuclide, and actually it is the most considered nuclide or the nuclide to be decontaminated during the decommissioning of a nuclear power plant. The quantity of ^{60}Co is 3.44MBq.

2.2 Particle size (AMAD)

The distribution of the particle sizes of the radioactive aerosols is an important factor that affects the internal exposure dose due to workers inhalation. As the fine particles of radioactive aerosol stay longer inside the body than the relatively bigger particles of radioactive aerosols, they cause long-term exposure in the whole body or organs. Like this, as the effects on the human body vary depending on particle sizes, to assess the internal irradiation dose due to the decommissioning site workers inhalation of aerosols, the distribution of particle sizes must be determined. As this study failed to secure measurement data of radioactive aerosols, however, 5 μm , recommended by ICRP, was used.

3. Input Data computation

To enter the data on the quantity of each nuclide, mentioned in Section 2, in the BiDAS code, a series of conversion processes are necessary. This section described the computation process necessary for applying the data secured by the author to the BiDAS computer code, and the assessment interval was daily, and one year of internal exposure dose was assessed.

3.1 Using the concentration and respiratory rate to assess intake

Workers internal radioactivity level can be derived from the intake yield and intake. The period from the

intake start date to the intake end date is expressed as T , and $M(t)$, the measurement value at t , a certain number of days from the intake start date, will be expressed as shown in the following formula. $m(u)$ refers to the intake yield at u , a certain time after intake, and I refers to the total intake from the intake start date to the intake end date.

$$M(t) = \frac{I}{T} \int_{t-T}^t m(u) du \quad (1)$$

As the Kozloduy PMF facility is operated for 40 weeks a year, computation was done assuming 280 days (40 weeks), and the level of radioactivity in a total of 4 organs, i.e. the body, the lung, urine and feces, were derived 1,120 times for Type M and S respectively, i.e. a total of 2,240 times.

4. Internal exposure assessment

The results of internal exposure assessment are 0.0341 mSv and 0.0909 mSv respectively. The difference in committed effective dose for Type M and Type S is 0.0568 mSv, about 2.70 times different. It is believed to be because as the particles are dissolved faster in the respiratory organ, the time they stay in the lung is reduced, and the particles move fast to the blood, whereas as the particles are dissolved more slowly, they stay longer in the lung and thus the exposure radiation dose of the lung increases.

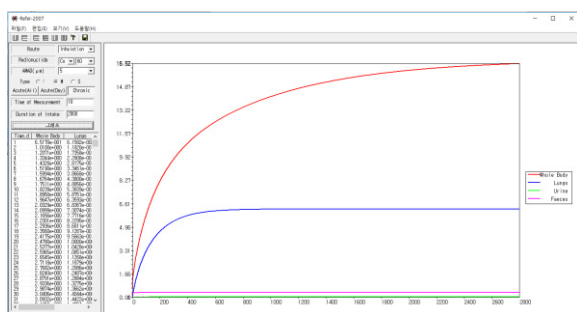


Fig.1. Fraction of intake of ^{60}Co .

5. Conclusion

The BiDAS computer code was used to assess the committed effective dose. Workers' committed effective dose due to ^{60}Co was 0.0341 mSv for Type M, and 0.0909 mSv for Type S. Compared to the annual permissible dose of Korea, the committed effective dose was insignificant 0.17% and 0.45% respectively. So it was concluded that when metals are melted, the overexposure from the viewpoint of internal exposure due to radioactive aerosols is not to be feared.

ACKNOWLEDGEMENT

This work was supported by a Nuclear Technology & Development Program of the National Research Foundation of Korea (NRF) grant funded by the Ministry of Science and ICT (MSIT) (Grant No. NRF-2017M2A8A4018598)

REFERENCES

- [1] EWN, "Experience from Greifswald NPP Decommissioning in Germany", EWN Final Report, P5cDel03Rev02-EIA-R-Chapter11(2013).
- [2] ICRP, "Individual Monitoring for Internal Exposure of Workers (Preface and glossary missing), Publication 78, Ann. ICRP 27(1997).
- [3] EWN, "Environmental Impact Assessment Report for the Facility for Treatment and Conditioning of Radioactive Waste with a High Volume Reduction Factor at Kozloduy Nuclear Power Plant", EWN Final Report, P5Cd03Rev.02-EIA-R-Chapter 4(2013).

A Study on Sign Test Procedure in MARSSIM Used to Site Release of Haddam Neck Nuclear Power Plant

Jong Hyun Kim*, Ji Young Koo, and Yong Soo Kim

Hanyang University, 222, Wangsimni-ro, Seongdong-gu, Seoul, Republic of Korea

*jhyun0064@gmail.com

1. Introduction

In order for the nuclear power plant to ultimately be released after the completion of dismantling work, licensee must demonstrate that the level of residual radioactivity at the site meets the criteria for site release. This demonstration can be carried out by MARSSIM (Multi-Agency Radiation Survey and Site Investigation Manual) (NUREG-1575). According to the site condition, MARSSIM proposes WRS test and Sign test as the methods to confirm whether residual radioactivity concentration level at the site satisfies DCGL (Derived Concentration Guideline Level), which is a measurable value corresponding to the site release criteria. This paper describes Sign test process of the US Haddam Neck Nuclear Power Plant (HNP), which completed the site release by performing Sign test.

2. Purpose of the Sign test

The Sign test is a non-parametric statistical test used where concerned radionuclides are not at the site. Through the equation of the Sign test, the required number of sample measurements for the survey unit, which is a physical area configured to the specified size, is obtained and the concentrations of the samples are compared with DCGL to determine whether the residual radioactivity of the site meets the site release criteria.

3. Methods

The survey unit measurements N can be obtained as shown in Equation (1) below.

$$N = \frac{(Z_{1-\alpha} + Z_{1-\beta})^2}{4(\text{Sign } p - 0.5)^2} \quad (1)$$

$Z_{1-\alpha}$ and $Z_{1-\beta}$ are percentiles represented by the selected decision error levels, α and β respectively (see NUREG-1575 Table 5.2), where α is the

probability of incorrectly permitting releasing a survey unit and β is the probability of incorrectly failing to release a survey unit. Sign p is the estimated probability that a random measurement from the survey unit will be less than the DCGL when the survey unit median is actually at the LBGR (see NUREG-1575 Table 5.4), where LBGR (Lower Bound of the Gray Region) is a site-specific parameter and Initially selected to equal one half the DCGL.

The spacing, L between samples can be obtained by applying the area A and the number of samples N into the following equation (2).

$$L = \sqrt{\frac{A}{0.866N}} \quad (2)$$

The main steps of the Sign test can be listed [1]: (1) List the survey unit measurements, X_i , $i = 1, 2, 3 \dots, N$. (2) Subtract each measurement, X_i , from the DCGL to obtain the differences: $D_i = \text{DCGL} - X_i$. (For multiple nuclides, DCGL is set to 1 by unity rule and the measurements of the survey unit are replaced by weighted sums, WS) (3) Discard each difference that is exactly zero and reduce the sample size, N , by the number of such zero measurements. (4) Count the number of positive differences. The result is the test statistic S^+ . (5) Large values of S^+ indicate that the survey unit does not exceed the release criterion. The value of S^+ is compared to the critical values (see NUREG-1575 Table I.3). If S^+ is greater than the critical value, k , in that table, the survey unit is released.

4. Result & Conclusion

The Sign test was applied to survey unit 9312-0002 (Southwest 115kV Switchyard, 1,486 m²), which was found to be highly polluted in HNP



Fig. 1. The location of 9312-0003 in HNP.

Cs-137, Co-60 and Sr-90 were selected as the concerned radionuclides in the HNP site through the Historical Site Assessment [2]. These were considered to be able to exceed the site release criteria through preliminary investigation and the required number of samples for the survey unit was determined in order to confirm the availability of site release.

The value of Sign P is 0.977250 and the percentiles $Z_{1-\alpha}$ and $Z_{1-\beta}$ corresponding to the site-specific decision errors α and β of 0.05 of HNP are found to be 1.645. The number of 15 required soil samples, which are rounded values increased by 12 to 20%, were calculated, because of uncertainties such as missing samples expected to occur in the survey unit. In addition, the site history and characteristics survey data were reviewed, and three samples were further collected by judgment.

The sample spacing L was 10.73 m by applying the survey unit area, A 1,486 m² and the number of sample, N 18. The location of the 15 samples was specified using AutoCAD-LT software, and the location of 3 samples by judgment were specified based on the results of the previous survey.

The locations of 18 samples in 9312-0003 are shown in Fig. 2 below.

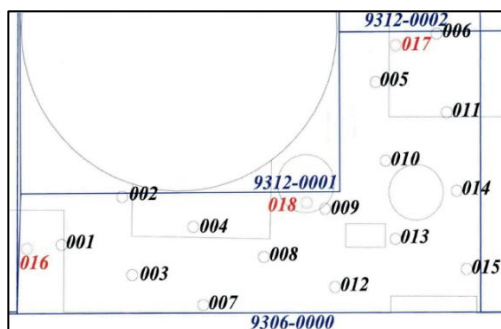


Fig. 2. The location of the samples in 9312-0003.

As a result of the analysis, Cs-137, Co-60 and Sr-90 were not identified in the three judgement samples and the Sign test results for 15 samples are shown in the following table.

Table 1. Sign test result for 9312-0003

Nuclide	CS-137	Co-60	Sr-90		
DCGL	4.75E+00	4.75E+00	9.30E-0.1		
CS-137 (pCi/g)	Co-60 (pCi/g)	Sr-90 (pCi/g)	Ws	1-Ws	Sign
-6.38E-02	6.35E-03	-1.38E-02	-0.03	1.03	+1
-1.90E-03	6.19E-03	-2.55E-03	0.00	1.00	+1
-1.28E-02	1.83E-03	1.20E-02	0.01	0.99	+1
1.19E-02	-2.21E-02	1.91E-02	0.01	0.99	+1
-9.37E-03	1.78E-02	3.25E-03	0.01	0.99	+1
-3.58E-03	-2.86E-03	-1.19E-02	-0.01	1.01	+1
-1.38E-02	1.06E-02	3.65E-02	0.04	0.96	+1
2.25E-02	-7.12E-03	-1.60E-03	0.00	1.00	+1
-8.06E-04	4.92E-03	1.08E-03	0.00	1.00	+1
1.21E-02	1.60E-02	4.06E-03	0.01	0.99	+1
-3.38E-02	-4.28E-03	1.54E-02	0.01	0.99	+1
-6.57E-02	-1.55E-02	1.98E-03	-0.02	1.02	+1
-6.68E-02	1.09E-02	-5.04E-04	-0.01	1.01	+1
-5.37E-02	4.24E-03	-8.62E-03	-0.02	1.02	+1
-3.55E-02	-2.82E-03	-2.50E-03	-0.01	1.01	+1
The number of positive differences (S+)					15
Critical Value : 11			Survey Unit : Meets Release Criterion		

As a result of the Sign test for 9312-0003, the number of difference (S+) in the amount between DCGL 1 and the weighted sum of the measurements is 15 and this is larger than the critical value 11. Therefore, 9312-0003 has been found to meet the release criteria.

REFERENCES

- [1] NRC, "Multi Agency Radiation Survey and Site Investigation Manual (MARSSIM) Revision 1", NUREG-1575, 2000.
- [2] Connecticut Yankee Atomic Power Company, "Final Status Survey Final Report Phase VII", Haddam, 2006.

Review of MARSSIM Methodology for Nuclear Decommissioning Site Restoration and Environmental Impact Assessment

Young-hyun Lee*, Hyun-jin Park, and Je-geun Jeon*
Ujuenertech, 222, Wangsimni-ro, Seongdong-gu, Seoul, Republic of Korea
*820123j@naver.com

1. Introduction

According to Article 4 “Application for Construction Permit” of the Korean Enforcement Regulation of the Nuclear Safety Act, the content is mentioned, which should be drawn up according to what are set and announced by the Committee in a plan for the decommissioning of a reactor facility in accordance with Clause 2, Article 10. However, since no concrete methodology of that is mentioned, this study would review the methodologies of nuclear decommissioning site restoration and environmental impact assessment used in foreign countries.

South Korea already had a lot of experience of Final Status Survey (FSS), through the U.S. Multi-Agency Radiation Survey and Site Investigation Manual (MARSSIM) that presents standards for various reactors decommissioning procedures, regulations and technologies for the decommissioning and site restoration of small low radiation facilities such as Research Reactors No. 1 and No. 2 and uranium conversion facilities.

MARSSIM refers to standard guidelines jointly agreed by all state agencies related to nuclear facilities in the U.S., such as Nuclear Regulatory Commission (NRC), Environmental Protection Agency (EPA), Department Of Energy (DOE) and Department Of Defense (DOD) for site environmental radioactivity survey according to nuclear facility decommissioning, which is methodologies and standard procedures based on dose or risk for the relevance judgment with regulatory requirements.

MARSSIM procedures suggest methods for fulfilling planning, performance, assessment and decision to determine whether radioactive contamination on the ground and building surface meets the standard value in each site in providing comprehensive guidelines for the processes of the measurement and decision on contaminated soil and building. In addition, it is recommended to set a plan of survey on the site with contaminated ground and building surface, investigate the scope of the performed work, characteristic technologies, restoration measures and final status and perform

quality assurance and management necessary for assessment of nuclear facility sites that have long operated and the acquisition and analysis of data. The purpose of FSS suggested by MARSSIM is to prove that residual contamination is less than Derived Concentration Guideline Level (DCGL) in nuclear facility decommissioning based on the standard for judging the satisfaction with regulatory requirements according to dose or risk at the stage of FSS.

2. Methodology

2.1 Procedures of environmental impact assessment in decommissioning nuclear facilities

MARSSIM limits the range just through a characterization assessment for the contamination of the surface of a building and the soil within 15cm under the topsoil and usually suggests guidelines for FSS. According to Radiation Survey and Site Investigation Process (RSSI) suggested by MARSSIM, it is recommended to conduct a Historical Site Assessment (HSA) first. Later, scoping survey through field investigation, check characterization survey showing the detailed contents of the contamination level and remedial action support survey are conducted. For FSS, the class of the irradiation area is modified. The location of sampling and the number of samples for accurate measurement are determined, and then, the contamination level of the relevant site is measured.

HSA determines the present status of the site of the decommissioned nuclear facility and classifies the contamination area according to the potential contamination. Through an assessment of the mobility of contaminants, classes are divided according to the latent contamination level of residual radioactivity, as shown in Table 1 below.

Table 1. Division of classes according to the contamination level

Contamination area	Classification
Class 1	An area with a contamination level higher than DCGL based on the latent

	radioactive contamination level according to the operating history or the previous radiation measurement
Class 2	An area with contamination based on the latent radioactive contamination level according to the operating history or the previous radiation measurement but with the contamination level not exceeding DCGL
Class 3	An area without any residual radioactivity or with a residual radioactivity level much lower than DCGL

The classes divided based on HSA may be changed through a detailed activity of survey on the pollutant range.

After measuring natural radioactivity to measure the accurate radiation level, it is necessary to refer to the grid coordinates provided by MARSSIM for the survey site.

In general, since the Decontamination and Decommissioning (D&D) activity is contaminated with multiple nuclides, it is necessary to know a relative radioactivity ratio of each nuclide to induce DCGL of most nuclides in DCGL for each nuclide. Generally, it can be known through alpha and gamma spectroscopy analysis.

In South Korea, as for the dose standard to open a site, the level of individual radiation exposure to residual radioactivity in a critical group should not exceed 0.1 mSv (effective dose) per year. This standard for exposure dose should be applied in order to draw DCGL. Especially, to prove that this condition of exposure dose is met, it is necessary to classify survey areas into a large number and conduct the survey according to the procedures according to potential contamination and expected residual radioactivity level based on the records of the operation of facilities like a site after decommissioning, records of decommissioning and records of radiological environment survey.

It is necessary to judge whether to open facilities by calculating DCGL applying a standard value and compare the FSS result with the DCGL based on all exposure pathways and scenarios that may actually occur if the relevant site is opened after the permanent suspension of the related facilities including nuclear facilities through these methodologies.

3. Conclusion

As a result of a review of NRC MARSSIM

methodologies, the examples of the application of FSS in decommissioning the facilities utilizing nuclear power are as follows:

1. Preparing a survey
2. Checking source terms
3. Calculating DCGLw
4. Classifying contamination areas
5. Differentiating survey units (Building/soil)
6. Selecting measuring instruments
7. Selecting a representative referential area
8. Removing machinery/equipment from the measuring area
9. Designing a survey
10. Conducting a survey
11. Evaluating survey results

It is judged that it would be desirable to apply the regulations and technologies (procedures) proposed in NRC MARSSIM, taking into account that there is a nuclear decommissioning-related law in South Korea, but it is insufficient, and it is expected that many studies would be conducted in decommissioning the facilities utilizing nuclear power and developmental methodologies would come out.

ACKNOWLEDGEMENT

This study is being conducted with support for the project of Korea Institute of Energy Technology Evaluation and Planning.

REFERENCE

- [1] NRC et al., "Multi-agency Radiation Survey and Site Investigation Manual, Revision 1" (2000).
- [2] S.Y. Jo, "Dose Assessment using RESRAD-BUILD Code for Decommissioning of Nuclear Fuel Cycle Facility" (2011).
- [3] J.S. Min, K.W. Lee, H.R. Kim & C.W. Lee, "Radiological Assessment of the Decontaminated and Decommissioned Korea Research Reactor-1 Building", Nuclear Engineering and Design, 322 (2017) 492-496.
- [4] S.B. Hong, D.S. Hwang, G.W. Lee & J.K. Mun, "Drawing the Opening Standard after decommissioning Uranium Conversion Plant", Annual Spring Conference of The Korean Association for Radiation Protection, (2011).
- [5] E. W. Abelquist, Decommissioning Health Physics: A Handbook for MARSSIM Users, CRC Press, (2013).

Regulatory Framework for Decommissioning of Nuclear Facilities in Japan

Jungjoon Lee* and Kyungwoo Choi

Korea Institute of Nuclear Safety, 62, Gwahak-ro, Yuseong-gu, Daejeon, Republic of Korea

*k720ljj@kins.re.kr

1. Introduction

Decommissioning has recently become an issue highlighted in Korea due to the permanent shutdown of Kori-1 Unit 1 which is the first PWR (Pressurized Water Reactor) NPP commissioned in 1978 and was put on permanent shutdown for decommissioning on June 2017, after 40 years of operation. Operation license of Kori Unit 1 was expired in 2007 after 30 years of design life and Kori Unit 1 received a 10 years of 1st continued operation from the government until June 2017. In June 2015, Kori Unit 1 was decided to be permanently shutdown without applying its 2nd continued operation and becomes the first NPP be decommissioned in Korea.

KHNP, the operating licensee of Kori unit 1, is now preparing final decommissioning plan (FDP) for decommissioning approval by June 2022, within 5 years from its permanent shutdown, according to the recently revised Nuclear Safety Legislations. KINS is on processing the development of review guideline of FDP by conducting R&D project.

This study shows the introduction on regulatory framework for decommissioning of nuclear facilities in Japan, in order to refer to the development of review guideline of FDP.

2. Regulatory framework

2.1 NPPs under decommissioning

There are 11 nuclear power reactors under decommissioning in Japan as of Aug. 2018 as shown in Table 1.

Table 1. NPPs under decommissioning in Japan [1]

Reactor	Start of operation	Appl. For decom. plan	NRA's approval of decom. plan
Tokai	Jul. 1966	Mar. 2006	Jun. 2006
Fugen (ATR)	Mar. 1979	Nov. 2006	Feb. 2008
Hamaoka Unit 1&2	Mar. 1976 Nov. 1978	Jun. 2009	Nov. 2009
Genkai Unit 1	Oct. 1975	Dec. 2015	Apr. 2017
Tsuruga Unit 1	Mar. 1970	Feb. 2016	Apr. 2017
Mihama Unit 1&2	Nov. 1970 Jul. 1972	Feb. 2016	Apr. 2017
Shimane Unit 1	Mar. 1974	Jul. 2016	Apr. 2017
Ikata Unit 1	Sep. 1977	Dec. 2016	Jun. 2017
Monju	Sep. 1991	Mar. 2018	Mar. 2018

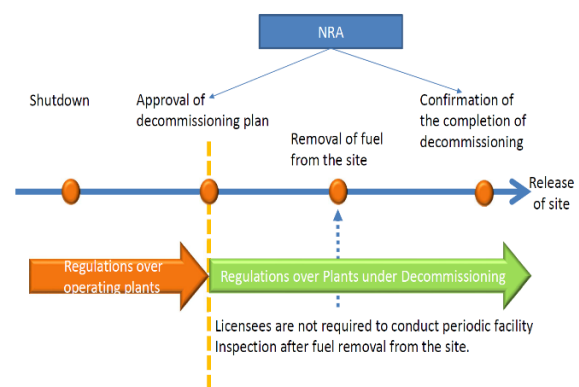


Fig. 1. Regulatory framework for decommissioning [1].

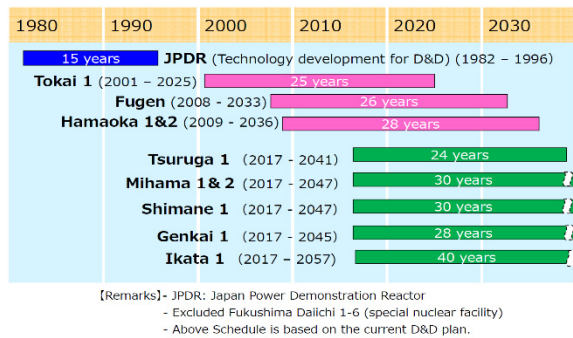


Fig. 2. Decommissioning Project Schedule of NPPs in Japan [2].

2.2 Regulatory framework for decommissioning

NRA (Nuclear Regulation Authority in Japan) review decommissioning plan whether it is proper to meet the review standard for decommissioning pf nuclear power reactor [3], when licensee submit decommissioning plan with related documents according to “Reactor Regulation Act” and other relevant acts.

3. Conclusion

Regulatory framework for decommissioning of nuclear facilities in Japan was introduced in this study. Analysis of Japanese regulatory system and review standard for decommissioning of nuclear power reactor could be a good reference during the development of review guideline for FDP of nuclear facilities in our country.

ACKNOWLEDGEMENT

This work was supported by the Nuclear Safety Research Program through the Korea Foundation of Nuclear Safety (KoFONS) using the financial resource granted by the Nuclear Safety and Security Commission (NSSC) of the Republic of Korea (No. 1605008).

REFERENCES

- [1] M. Aoki, “Regulatory Framework for Decommissioning of Nuclear Power Plants in Japan”, International workshop on decommissioning of NPPs, Tokyo, Japan (2017).
- [2] T. Yamauchi, “Current Status and Issues of D&D of Nuclear Power Plants in Japan”, International workshop on decommissioning of NPPs, Tokyo, Japan (2017).
- [3] Japanese review standard for decommissioning of nuclear power reactor (2013).

Full System Decontamination by ASDOC_D-MOD Method

HanSol Im^{a),*}, Laura Schneider^{b)}, ChangSig Kong^{a)}, HeeDong Sohn^{a)}, and KyuHo Chang^{a)}

^{a)}Doosan Heavy Industries & Construction, 22, Doosan Volvo-ro, Seongsan-gu, Changwon-si, Gyeongsangnam-do, Republic of Korea

^{b)}Siempelkamp NIS Ingenieurgesellschaft mbH, Industriestrasse 13, 63755 Alzenau, Germany

*hansol.im@doosan.com

1. Introduction

In dismantling nuclear power plant, high level radiation limits safe and efficient decommissioning. The chemical decontamination is an effective process to reduce the amount of radioactive contaminants on the inner surface of the primary circuit which has complicated shape and hard-to-reach area before dismantling. Popular chemical decontamination methods such as CORD UV and NITROX-E generally use permanganic acid (HMnO₄) and oxalic acid (C₂H₂O₄) to redox. These methods can effectively remove the contaminated layer on the surface of primary circuit through several decontamination cycles with high concentration chemicals. It could occur the corrosion of the base material which could lead to leak out of the primary circuit, and hydrogen generation when excess oxalic acid reacts with base material, which may cause safety concern.

Then we introduce the ASDOC_D-MOD (Advanced System Decontamination Oxidizing Chemistry Modified), the method which complements disadvantages of popular chemical decontamination by using low concentration of permanganic acid and oxalic acid and adjusting the pH by using additives.

2. ASDOC_D-MOD Method

2.1 Process of decontamination

Basically ASDOC_D-MOD use permanganic acid and oxalic acid for redox same as conventional methods, but it use low concentrated agent and additive to complement the reduced reactivity. For the additive, MSA(Methane Sulfonic Acid, CH₃SO₃H) is used to facilitate redox. Also, ASDOC_D-MOD is economical because it does not need an external decontamination equipment, so it eliminates the risk of secondary contamination by external equipment.[3]

ASDOC_D-MOD starts with oxidation process using permanganic acid, and oxidation → removal of permanganic acid → reduction with oxalic acid → removal of oxalic acid becomes 1 cycle.

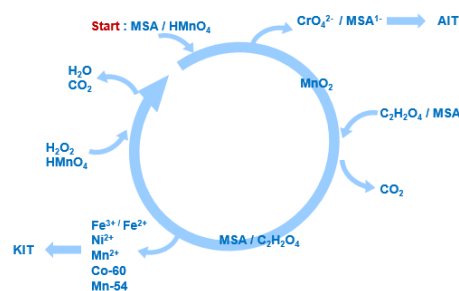


Fig. 1. ASDOC-D-MOD Process.

The oxidation process removes the chromium oxide layer (2 ~ 10 μm) using permanganic acid and the removed chromium oxide ions are filtered on the anion exchange resin. After the oxidation process, oxalic acid is injected to process a reduction and it decompose the manganese dioxide(MnO(HO)₂) generated in the oxidation process and unreacted permanganate (MnO₄⁻) after the oxidation process. The metal ions, which build oxalate-complexes with oxalic acid, are filtered out on the cation exchange resin. The rest oxalic acid is decomposed on the oxidant input of the next cycle.

The MSA added during the redox adjusts the pH to promote the reaction and increases the solubility of metal ions by its complex generating properties.

2.2 Decontamination efficiency

ASDOC_D-MOD is expected to complement disadvantages such as leakage of external equipment connection, high generation of secondary liquid waste, damage of base material and hydrogen generation by using low concentration chemical agent. In order to confirm the improvement effect of ASDOC_D-MOD, the test was carried out at the scale down model.

Fig. 2 shows the potential and pH measured during the test. Similar redox potentials were measured for each decontamination cycle, and the pH was maintained at a similar level. The MSA maintains the pH condition that suppresses the reprecipitation of oxalate and hydroxide as well as maintaining proper redox reaction for the decomposition of the corrosion oxide layer even with a low concentration of decontaminating agent.

The use of a low concentration agent can also have the effect of inhibiting excessive decomposition of base material and production of hydrogen. Fig. 3 shows the amount of Fe ion change with time. Fe ion excessive decomposition and hydrogen production are always a phenomenon followed by high concentration of oxalic acid injection, which increases with the amount of oxalic acid injected [2]. There is no direct safety problem with the excessive decomposition of Fe ions, but it induces spalling phenomenon near the injection site, disturb uniform decontamination, and rapidly increases hydrogen emission. Hydrogen generation is associated with direct safety issues.[1]

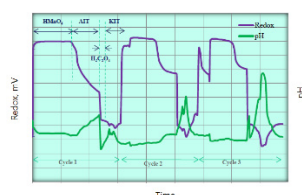


Fig. 2. Decontamination test results of ASDOC-D-MOD.

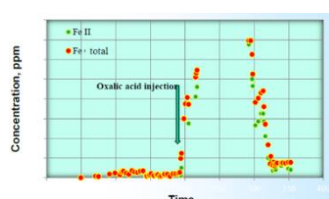


Fig. 3. Characteristics of Iron-Burst.

2.3 Decontamination equipment

ASDOC_D-MOD decontamination has the effect of reducing the cost of production of external equipment and facility manpower by using the same pump and piping as the conventional operation without using an external decontamination facility. There is no need to take risk of the connection with the external equipment which can be a weak point. The primary system operation can be carried out in

the same way as that performed by the existing operation personnel of the power plant, and only the production of the permanganate production facility, the chemical injection tank / piping, and the test loop can be done. Also, the permanganic acid production facility can be installed outside the restricted area and is not limited by the radiation exposure.

3. Conclusion

ASDOC_D-MOD, a low - concentration chemical decontamination method for primary circuit decontamination was introduced. As the results of scale down model test, ASDOC_D-MOD enables the stable, uniform decontamination, suppresses the risk of base material corrosion, hydrogen generation, and reduces the amount of waste. Also the system facility and operation manpower of power plant are used as they have being, it is possible to perform stable and economical decontamination. However, in order to perform successful, quick and safety full system decontamination, close cooperation between the radiation workers, radiation safety management personnel, chemical decontamination personnel, radiological safety, chemical safety management personnel, and their respective supervisors must be carried out.

Acknowledgement

This work was supported by the National Research Foundation of Korea (NRF) granted financial resource from the Ministry of Science and ICT, Republic of Korea (NRF-2017M2A8A5041777).

REFERENCES

- [1] IAEA, Safety in decommissioning of research reactors. Safety ser., 1986.
- [2] H. W. Park, Decontamination and Decommissioning Technology Development of Nuclear Facilities, KAERI/RR-705/87, 1988.
- [3] Andreas Loeb, Chemical System Decontamination at PWR Power Stations Biblis A and B by Advanced System Decontamination by Oxidizing Chemistry (ASDOC_D) Process Technology, 2013.

Introduction to Decontamination Technology of Soil in Decommissioning NPP

Seungil Kim*, Dam-hyang Kim, Pil-yong, Jeon, Woo-hyeon Rhee, Deok-won Kang, and Joon-seok Lee

Elim-Global Co., Ltd., 767, Sinsu-ro, Suji-gu, Yongin-si, Gyeonggi-do, Republic of Korea

*seungil.kim@elim-global.com

1. Introduction

Various studies have been carried out for securing the source technology related to decommissioning of NPP after permanent shut-down of Kori #1[1]. Soil decontamination technology must also be secured before decommissioning. This project is being carried out to develop the soil decontamination technology in preparation for decommissioning of Kori #1. The purpose of this project is to develop the pilot scale (1.2 m³/hr) automatic soil decontamination system that decontaminates the contaminated soil and purifies the wastewater based on the high pressure washing and ultrasonic process after classification of contaminated soil. In this paper, the soil decontamination cases and techniques in Japan and an overview of the whole process of the automatic soil decontamination system to be developed is introduced.

2. Case Study

2.1. Characteristics of soil around Fukushima area

Because of the nuclear accident, the soil around Fukushima in Japan has been extensively contaminated. At present, more than 70 decontamination companies are involved in soil decontamination and their technology has already reached a considerable level of skill. Recently they reached up to the level of recycling the decontaminated soils.

Most of the contaminated soil around Fukushima area was found to be accumulated within 1cm depth. The result of radioactivity measurement after classified into 9 levels by particle size shows that most of the radioactivity is concentrated in fine soil

with less than 75 μm diameter. (Fig. 1)

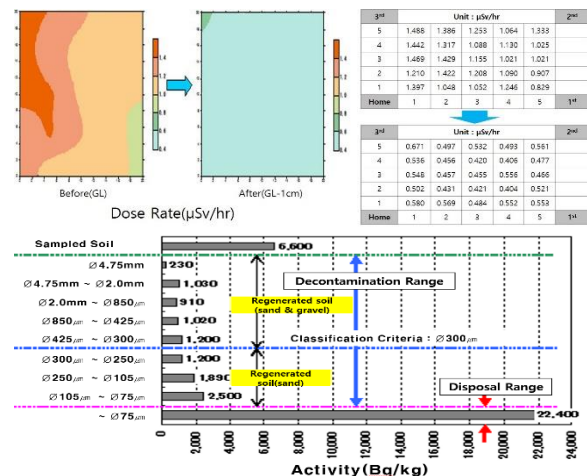


Fig. 1. Radioactivity of soil around Fukushima area.

After classifying the soil into 9 levels based on their particle size, the soils containing high radioactivity concentration, including micro-soils, are separately storing at temporary site before sending to final disposal site and the soil containing relatively low concentration are decontaminated using special decon. technology.

2.2 Decontamination technology in Japan

In Japan, various physical and chemical methods have been developed and applied to the soil decontamination. Especially, in addition to the soil decontamination technology, Japan has also developed technologies to treat organic matter such as fallen leaves and vegetation through fermentation/decomposition, decontamination technology for river and reservoir soils, wall decontamination technology using robots, volume reduction technology using biomass and adsorption technology in contaminated water using zeolite, etc., and it contains all necessary

technologies for restoration of most environments. Fig. 2 shows an example of soil decontamination process in Japan.



Fig. 2. Soil decontamination process in Japan.

3. Pilot scale soil decontamination system

To acquire the reliability results, we are planning to take a sample from Kori site. Sample composition, particle size distribution and radiological characteristics of the soil will be evaluated first, and the decontamination range of the target soil is selected according to the result. Because various unpredictable situations can occur in decommissioning the NPP, the soil decontamination system will be developed to decontaminate for all of the generated soil during decommissioning period. The soil is firstly decontaminated by high-pressure vortex washing process, and considering the contamination degree of each soil classified by particle size, the soil with high radioactivity is additionally subjected to the combined process of ultrasonic & degassing membrane process to carry out entire decontamination.

The wastewater generated during soil decontamination is purified to minimize the generation of secondary waste by a pressurized floatation separation process with microbubble, an oil filtration process to remove trace oil in the wastewater, a coagulation & precipitation process using high functional coagulant, a wastewater treatment process using submerged MF membrane or multi-stage electric deionization, an ionic radioactive material removal process such as ion-exchange fiber or zeolite

and so on. Fig. 3 shows a schematic diagram of the soil decontamination process to be developed.

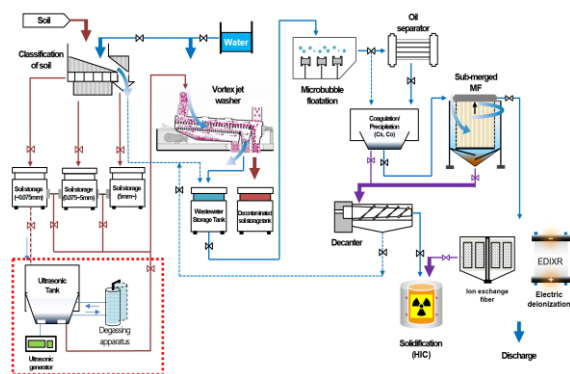


Fig. 3. Schematic Diagram of Pilot-scale Soil Decontamination Process.

4. Conclusion

Since the NPPs in Korea are expected to be gradually decommissioned, securing the source technology for decommissioning is becoming more important. Through this project, it is expected that the development of a soil decontamination system optimized for decommissioning NPP will be able to meet the domestic market demand and lay the foundations for entering the decommissioning market in the world

ACKNOWLEDGEMENT

This work was supported by the Korea Institute of Energy Technology Evaluation and Planning (KETEP) granted financial resource from the Ministry of Trade, Industry and Energy, Republic of Korea (No. 20181510300800)

REFERENCES

- [1] Sang-min Park et al., "Influence of Physico-chemical Properties on Cesium Adsorption onto Soil", Journal of Soil Groundw. Environ., 22(1), 27-32 (2017).

Analysis of Oxide Layer by Simulating NiFe_2O_4 Film on Stainless Steel, Incoloy-600 and Carbon Steel

Ayantika Banerjee^{1,2)}, Yangil Jung¹⁾, Wangkyu Choi¹⁾, Mansoo Choi¹⁾, and Seonbyeong Kim^{1)*}

¹⁾Korea Atomic Energy Research Institute, 111, Daedeok-daero 989beon-gil, Yuseong-gu, Daejeon, Republic of Korea

²⁾University of Science & Technology, 217, Gajeong-ro, Yuseong-gu, Daejeon, Republic of Korea

*sbkim@kaeri.re.kr

1. Introduction

Decontamination is one of the important technology that are applied during the decommissioning process of nuclear power reactors to secure the worker's safety and minimization of the secondary waste amount [1]. Thus dissolving or removing oxide films can release the radionuclides into solution and decontamination process follows this principle. Stability of oxide layer is mainly caused by the presence of chromium in trivalent state. Even though the reducing water chemistry for operating nuclear power plant, it is found that the oxide consisted of a dual layer, an external thick layer containing mostly iron oxide and a thinner internal layer rich in chromium oxide, is formed on the surface of system. In PWR, typical film thickness of Stainless Steel(SS) surface are 2-3 μm while those Inconel surfaces are closer to 1-2 μm but in CANDU-PHWRs surfaces is about 75 μm due to the presence of carbon steel as the primary system piping. Oxidation behaviour on different materials depends on their chemical structure and compositions of base metal. It is important to characterize the oxide formed on different kinds of materials for the better understanding of its environmental sustainability in nuclear reactors.

The main objective of this study is to understand the different composition of oxide layer based on the difference of metal. Other objectives include dissolving the oxide layer by using or developing of different types of decontamination processes based on the chemical composition of oxide layers. In this study, we prepared the NiFe_2O_4 on Stainless Steel, Inconel-600 and Carbon Steel using E-beam evaporation technique.

2. Experimental

NiFe_2O_4 thin film was deposited on Stainless Steel-SUS 304 (Ni- 9.25Cr- 19.00, Fe- Balance), Inconel-600 (Ni- 72.0, Cr-14.0-17.0, Fe- 6.00-10.00,

Carbon- 0.15) and Carbon Steel (Ni- 30.0-35.0, Cr- 19.0-23.0, Fe- 39.5) by using an electron beam evaporation system at room temperature [2]. Those three substrates were polished in order to remove the pre-existing oxide layers. NiFe_2O_4 pellet (purity 99.9%) was used as a target. The deposition rate and thickness of NiFe_2O_4 thin film were 0.7 $\text{\AA}/\text{s}$ and about 0.5 μm monitored by a thickness sensor during the evaporation process. The substrates were sputter-etched with Ar ions for 5 min before deposition in order to remove any oxide layer on metal surfaces. For the high crystallinity of NiFe_2O_4 thin film, as-deposited sample was annealed at 600°C for 1 h in Ar atmosphere. The morphology of the different substrates of NiFe_2O_4 thin film was investigated by a field emission scanning electron microscopy (SEM, S-4800, Hitachi) working at 30 kV. The thin film X-ray diffraction (XRD, X-pert PRO MRD, Philips) pattern was conducted with Cu, Ka radiation (1 $\frac{1}{4}$ 1.5406 \AA) operating at 40 kV and 30 mA between 10° and 90° at a scan rate of 0.01°/min. The XPS, X-ray photoelectron spectroscopy (Kalpha, Thermo VG Scientific) analysis was performed to evaluate the chemical status of each elements of the thin films and the binding energy was referenced to the C 1s peak from carbon at 284 eV.

3. Results and Discussions

The surface morphology of three kinds of substrates was observed by SEM. Fig. 1 shows the SEM images of those substrates, respectively. The crystallographic structure of the NiFe_2O_4 thin film on SUS-304, Inconel-600, Carbon Steel after annealing was characterized by X-Ray Diffraction. Fig. 2 shows the XRD patterns of NiFe_2O_4 thin film after heat treatment at 600°C for 1h under Ar atmosphere. When the

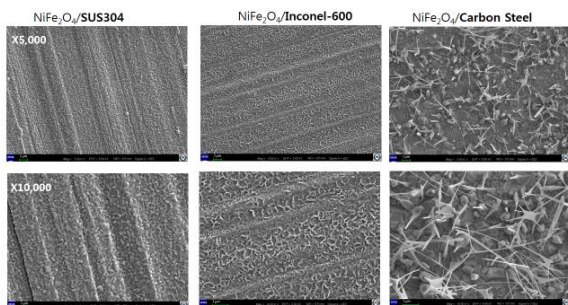


Fig. 1. SEM surface images of SUS304, Inconel-600 and Carbon Steel after NiFe_2O_4 deposition and annealing at 600°C .

samples were heated at 600°C , the film began to be crystallized as indicated by the NiFe_2O_4 peak. Three XRD peaks for SUS-304, Inconel-600, Carbon Steel have showed similar peak index. This is assigned to those of the NiFe_2O_4 cubic spinel, which could be indexed to the inverse spinel. The peak at 33° has showed higher intensity in Carbon Steel. After the heat treatment, the reflections become narrower with an increase of crystallite size. Later, we will find why the carbon steel sample shows different XRD peaks regarding crystal structure. More study will be conducted in the future.

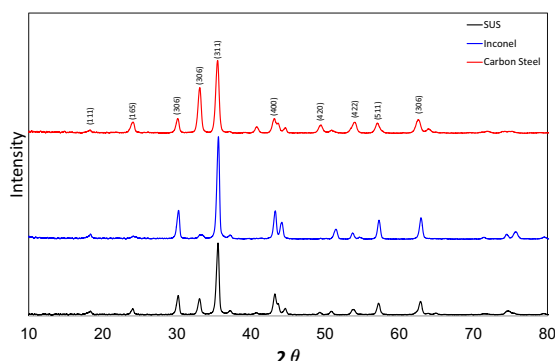


Fig. 2. XRD profiles of SUS304, Inconel-600, Carbon Steel.

XPS has been studied to observe the chemical state of each element and also for understanding the depth profile. Fig. 3 shows the XPS graph of SUS304, Inconel-600, Carbon Steel, respectively. In SUS304, Nickel was observed at 846.22 eV with a satellite peak, which is characteristic of material $\text{Ni } 2p_{3/2}$. Due to spin orbit coupling $\text{Fe } 2p$ peak always split into two (709.68 eV , $2p_{3/2}$ and 722.92 eV , $2p_{1/2}$) and describe the presence of Fe^{2+} and Fe^{3+} . This is indicating the different oxidation state of iron in SUS304 material. Both in Incoloy-600 and Carbon

Steel Fe is present in Fe^{2+} state. Chromium presents in Cr^{3+} state in all three materials. In the case of NiFe_2O_4 deposition on Incoloy-600 the concentration iron has increased with the etch time but presence of nickel goes down. The presence of chromium found high with etch time in SUS304. Nickel has deposited in the uppermost layer on SUS304.

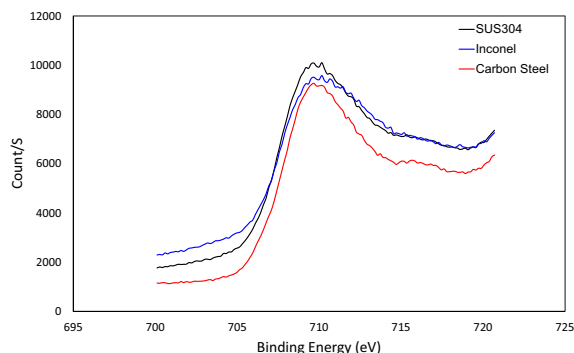


Fig. 3. XPS Spectra for Fe on SUS304, Inconel-600, Carbon Steel respectively.

4. Conclusion

The NiFe_2O_4 thin film has been deposited on substrates of Stainless Steel, Inconel and Carbon Steel by using an electron beam evaporation system. The reaction between Nickel Ferrite with different metal ions makes different composition of oxide layers. The phase, structure and morphology of materials were confirmed by SEM, XRD and XPS analysis. By analyzing these oxide layers it can be possible to determine the decontamination procedure for these metals, in future.

REFERENCES

- [1] Wang-Kyu Choi et al. "Development of Advanced Decontamination Technology for Nuclear Facilities", KAERI/RR-3964/2014 (2015).
- [2] Mansoo Choi et al., "The high capacity and cycle stability of NiFe_2O_4 thin film prepared by E-beam evaporation method for lithium ion batteries" Journal of Alloys and Compounds, 729, 802-808 (2017).

Assessment of Co and Cs Removal From Nuclear Power Plant Soil Using *Acidithiobacillus Thiooxidans*

Young-Gwang Kim¹⁾, Myoung-Soo Ko²⁾, and Kyoung-Woong Kim^{1),*}

¹⁾Gwangju Institute of Science and Technology, 123, Cheomdangwagi-ro, Buk-gu, Gwangju, Republic of Korea

²⁾Kangwon National University, 1, Gangwondaehak-gil, Chuncheon-si, Gangwon-do, Republic of Korea

*kwkim@giat.c.kr

1. Introduction

In nuclear power plants, many kinds of radioactive waste are produced such as evaporator bottoms, filter sludge and spent resins. During post treatment and storage of these wastes, radionuclides like Co and Cs can be leaked into surrounding soil and groundwater. Because the γ -rays emitted by radionuclides can cause chromosomal problem, radionuclides in soil must be removed. Recently, *Acidithiobacillus thiooxidans* has been applied to soil metal removal, which is known as bioleaching. Since bioleaching of Co and Cs from contaminated soil hasn't been reported, in this study the growth properties of *A.thiooxidans* exposed to Co and Cs was determined. And removal efficiency of Co and Cs by bioleaching was estimated.

2. Assessment of Co and Cs removal from nuclear power plant soil using *A.thiooxidans*

The growth character of *A.thiooxidans* in exposure of Co and Cs was measured. Based on this result, we applied this bacterium to bioleaching of Co and Cs contaminated soil.

2.1 Growth characteristic of *A.thiooxidans* in the exposure of Co and Cs

In this study, *A.thiooxidans* was incubated in the presence of Co and Cs with concentration ranging from 10 mg/L to 1000 mg/L and negative effects of Co and Cs on its growth was determined. Because *A.thiooxidans* produce SO_4^{2-} during its growth, concentration change of SO_4^{2-} was measured to

estimate the activity of *A.thiooxidans*.

Variation of SO_4^{2-} concentration was increased at Co free and 10 mg/L experiments. This result indicated *A.thiooxidans* can be metabolized at below 10 mg/L of Co condition.

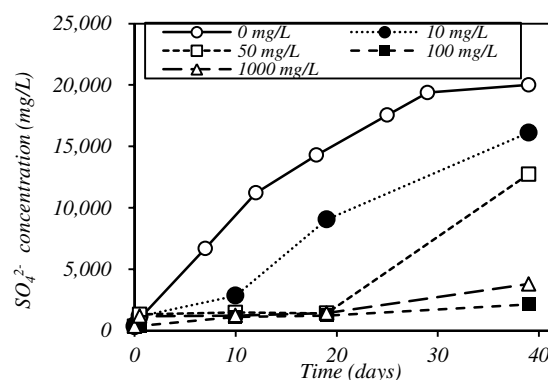


Fig. 1. Variation of SO_4^{2-} concentration with various Co concentration.

However, the *A.thiooxidans* generated SO_4^{2-} in all Cs exposure experiment, reflecting that *A.thiooxidans* can be applicable to bioleaching regardless of Cs concentration.

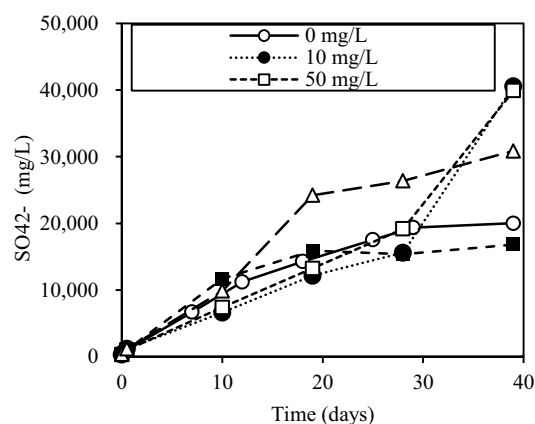


Fig. 2. Variation of SO_4^{2-} concentration with various Cs concentration.

2.2 Bioleaching of Co and Cs from artificially contaminated soil

A. thiooxidans was applied for bioleaching of Co and Cs. In the 200 mL of medium 125, 3 g of contaminated soil was added and incubated for 30 days. The Co and Cs concentration in medium and soil was measured using ICP-MS.

Figure 3. shows the result of Co bioleaching from contaminated soil. The extraction of Co was increased with time at *A.thiooxidans* inoculated experiments. The Co concentration in soil was dramatically decreased from 0.194 mg/g to 0.003 mg/g by bioleaching process.

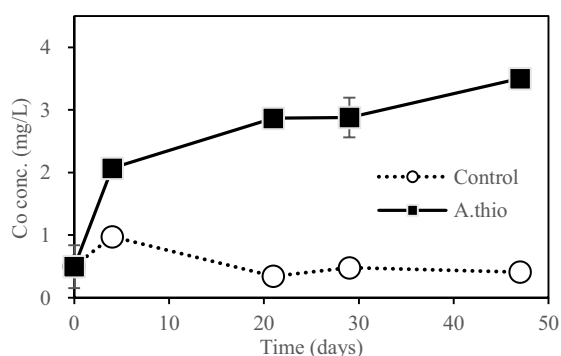


Fig. 3. Variation of Co concentration in solution during bioleaching process.

Figure. 4 shows the variation of Cs concentration during the bioleaching process. The Cs extraction from soil take place by the application of bioleaching. In addition, the Cs concentration in soil was decreased from 0.303 mg/g to 0.033 mg/g.

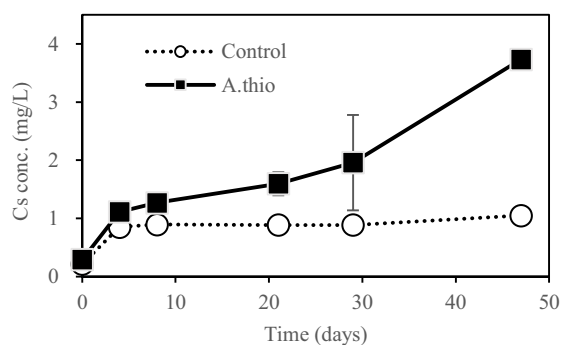


Fig. 4. Variation of Cs concentration in solution during bioleaching process.

3. Conclusion

The results indicated that the bioleaching process can be applied within 10 mg/L of Co exposure conditions. The *A.thiooxidans* was able to grow in the presence of Cs. Therefore, *A.thiooxidans* can be applied to bioleaching regardless of the Cs concentration. The extraction results of Co and Cs from soil using *A.thiooxidans* implied that the bioleaching is an appropriate process for soil recovery at decommissioning of nuclear power plant soil.

ACKNOWLEDGEMENT

This work was supported by Nuclear Energy Research Infrastructure Program grant funded by the National Research Foundation of Korea (NRF-2017M2B2B1072408) in 2018.

Technical Status of Remediation Technologies in Radionuclide-contaminated Groundwater of Nuclear Facilities

In-Ho Yoon*, Hee-Man Yang, Chan-Woo Park, Ilgook Kim, Sung-Man Kim, and Kune-Woo Lee
Korea Atomic Energy Research Institute, 111, Daedeok-daero 989beon-gil, Yuseong-gu, Daejeon, Republic of Korea
*ihyoon@kaeri.re.kr

1. Introduction

It was recently reported that radionuclides are contaminated in groundwater at nuclear power plants and nuclear facilities in the United States. The main radionuclides in the groundwater were analyzed as strontium, tritium, cesium, and cobalt. Many institutes have conducted the research development for the monitoring and remediation of radionuclides in groundwater. The pump and treatment (P&T) were applied to remove the radionuclides in the groundwater in various nuclear sites [1,2]. At the Hanford site, strontium in the groundwater was removed using a permeable reactive barrier (PRB) containing the apatite as adsorbent [3]. It was recently reported that the flow of the groundwater is obstructed using the funnel-and-gate method, and contaminated iodine was removed through precipitation using silver chloride at the Savannah River Site [1,2]. This study analyzed the radionuclide contamination and the recent remediation technology used for the groundwater in nuclear facilities.

2. Remediation technology of radionuclide-contaminated groundwater

2.1 Savannah River Site, USA

In 2004, the pump and treatment (P&T) system was replaced by a hybrid funnel-and-gate system that was installed about 1,000 feet upgradient from Fourmile Branch. The purpose of the funnel-and-gate is to slow migration of contaminated groundwater and to funnel it through in situ treatment zones at the gates. Extensive geologic characterization showed that much of the plume migrated along “troughs” at the top of the clay layer that confines the lower aquifer. The walls (or engineered subsurface barriers) were installed across these features to slow contaminant migration and force it through the gates

(Figure 1).

The treatment zones at the gates attenuate migration of uranium, Sr-90, and I-129 by sorption or precipitation. Tritium migration is slowed by the walls and additional decrease in tritium concentrations is achieved when the stratified plume mixes with less contaminated groundwater as it migrates up through the gates.

Treatment zones for uranium and Sr-90 at the gates are maintained by neutralizing acidity of the groundwater and mineral surfaces with injections of an alkaline solution. This treatment causes sorption of the contaminants and precipitation of uranium phases. Periodic injections are performed, with the frequency at each gate dictated by sentry monitoring wells located downgradient [1,2].

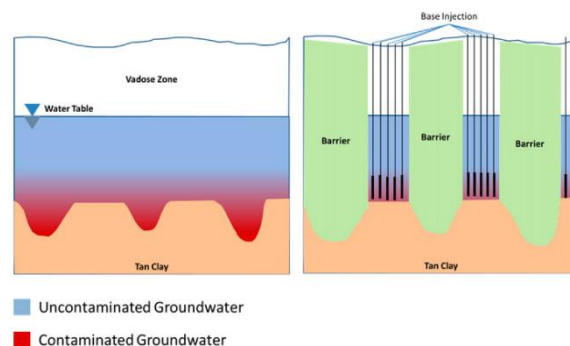


Fig. 1. Cross-sectional conceptual model of funnel-and-gate with base injection system before (left) and after installation [2].

2.2 Hanford site, USA

Apatite is a type of calcium phosphate that attracts strontium. In 2006 a test was conducted to see if apatite, in the form of fish bones, could prevent strontium from entering the Columbia River. Apatite was pumped into the ground and the water table along 300 feet of shoreline. It created a sort of curtain through which groundwater passes. As the water passes through, strontium attaches to the calcium phosphate holding it in place.

The strontium concentrations are highest within several feet of the water table. When the river rises, it pushes into the hyporheic zone, elevating the water table and allowing the apatite to capture more strontium. The 2006 test was extremely successful. Since then, more apatite has been injected along the shoreline. Eventually apatite will be injected into about 2,500 feet of shoreline [3].

2.3 Fukushima site, Japan

In Fukushima site, Water used to cool molten fuel during the accident and groundwater have mixed, generating approximately 300 tons of contaminated water per day. Countermeasures are being implemented based on the following three basic policies.

Isolating (groundwater from contamination sources) - Impermeable walls of frozen soil (land side) is that groundwater flows into the buildings are prevented by using ice walls created by freezing soil in the ground around the buildings. Pumping up groundwater (groundwater bypass and sub-drains) is that wells (sub-drains) near the buildings and wells installed in the hills (groundwater bypass) pump up groundwater, minimizing inflows of groundwater into the buildings and the quantity of contaminated water generated.

Preventing leakage of contaminated water - Impermeable steel wall (sea side) is that a 780-meter-long wall of 30-meter-tall steel pipes was constructed on the sea side of Units 1 through 4, which has been gradually improving the water quality in the surrounding sea area. Installation of additional water tanks is that water tanks for storing contaminated water are being systematically installed to ensure adequate storage capacity.

Removing contamination sources - Removal of radioactive materials was focused on cesium and strontium. Removal of radioactive materials other than tritium (hydrogen-3) was conducted and stored in water tanks after removal of radioactive materials other than tritium. The water stored in the tanks has been treated to purification. The question of how to handle the purification treatment water in the tanks is being considered in close consultation with local communities and experts [4].

3. Conclusions

Many institutes have conducted the research development for the monitoring and remediation of radionuclides in groundwater. The pump and treatment (P&T) were applied to remove the radionuclides in the groundwater. However, the treatment cost was sharply increased in the case of long-term operation. The groundwater remediation method should be applied according to the characterization of the nuclear site. In Savannah River site, P&T method was applied in high contaminated site, and Funnel & gate was installed in intermediate contaminated site. In low contaminated site, natural attenuation method was applied with monitoring method. In Koir-1 NPP, the groundwater remediation method (P&T, Funnel & gate, and natural attenuation) will be applied according to characterization of the nuclear site (groundwater flow, geological characteristics, unsaturated zone, saturated zone, and radionuclide).

ACKNOWLEDGEMENT

This work was supported by a National Research Foundation of Korea grant funded by the Korean government (MSIP) (No. 2017M2A8A1092471).

REFERENCES

- [1] Remediation Management of Complex sites. RMCS-1. Washington, D.C.: Interstate Technology & Regulatory Council (ITRC), 2017.
- [2] Eddy-Dilek, C., K. Kostelnik, and M.E. Denham. 2016. "The Challenge of Moving Science into Practice: Lessons Learned and New Approaches." Waste Management Symposium, Phoenix, Arizona, March 6-10.
- [3] Cleaning Hanford's Groundwater & Protecting the Columbia River, Publication Number: 08-05-001.
- [4] Important Stories on Decommissioning, Fukushima Daiichi Nuclear Power Station, now and in the future, 2017.

Radiation Shielding Analysis for Conceptual Design of Reactor Coolant System Decontamination Equipment of Kori Unit 1

Jonghoa Kim*, Kyeongho Han, Homin Jeon, and Yongsik Kim

Sae-An Engineering Co., Ltd., 184, Gasan digital 2-ro, Geumcheon-gu, Seoul, Republic of Korea

*jhkim4198@sae-an.co.kr

1. Introduction

Kori Unit 1 was permanently shutdown suspended at 24:00 on June 18, 2017. KHNP will conduct chemical decontamination of the reactor coolant system in order to minimize worker dose and radioactive waste in decommissioning of Kori Unit 1. In this study, radiation shielding analysis was performed on ISOCS and MicroShield[®] computational program for the filter which primarily removes the crud particles after chemical decontamination of the reactor coolant system of Kori Unit.1.

2. Materials and Methods

2.1 ISOCS

Unlike fixed semiconductor detectors, ISOCS does not use standard calibration sources for calibration. ISOCS performs the efficiency calibration by modeling the measurement object with the source. ISOCS can evaluate nuclides and radioactivity quantitatively regardless of the size of the target. The ISOCS detector used in this study is a high purity germanium detector manufactured by CANBERRA. The detector relative efficiency is 20% and the energy resolution is 1.8 keV at ⁶⁰Co of 1.33 MeV[1, 2].

2.2 MicroShield[®] Computer Program

The MicroShield[®] computer program uses 16 fixed

geometry models for radiation shielding evaluation of point sources, line sources, and volume sources using the Point Kernel method. The basic concept of the Point Kernel method is to divide the volume source into a large number of small point sources and regard each as a point source, and add up the respective contributions. The fixed geometry model approach reduces the effort required to express the geometry numerically for shielding evaluation, and can be applied to most problems, except when an accurate evaluation of complex geometry is required[3,4].

2.3 Design Guidelines for the Shields

In this study, the design guidelines for the shields are 2.50E-02 mSv/h specified in the Nuclear Safety Commission Notice No. 2017-36 (Radiation Protection Standards).

3. Results and Discussions

3.1 Kori Unit 1 Reactor Coolant System Radioactive Inventory

As of March 27, 2018, the total radioactivity inventory of the Kori Unit 1 reactor coolant system, calculated using the ISOCS and MicroShield[®] computational programs, is 4.1930×10^{11} Bq. The nuclide inventories are ⁵⁸Co 58 4.2703×10^{11} Bq, ⁶⁰Co 3.4385×10^{12} Bq and ⁶⁵Zn 3.2748×10^{11} Bq.

3.2 Radiation Shielding Analysis of Filter

Fig. 1 shows the geometry model for the radiation shielding analysis of the filter with the MicroShield[®] computer program.

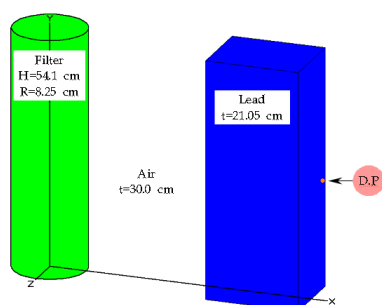


Fig. 1. Filter schematics showing models built in Microshield[®] Computer Program.

The contact exposure rate of the filter calculated by the MicroShield[®] computer program is $2.817\text{E}+05$ mSv/h. The minimum shielding thickness of lead satisfying the design criteria of shielding $2.50\text{E}-02$ mSv/h is 21.05 cm. The results of the radiation shielding analysis for the filter are shown in Fig. 2.

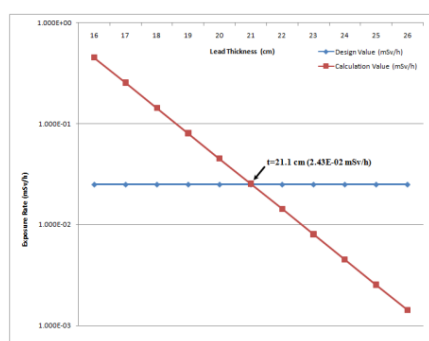


Fig. 2. Lead thickness vs. exposure rate.

4. Conclusion

In this study, the radiation shielding analysis was performed on the filter which is one of the decontamination equipment components of the Kori unit 1 reactor coolant system.

The total nuclide inventories of the Kori Unit 1 reactor coolant system are ^{58}Co $58\ 4.2703 \times 10^{11}$ Bq, ^{60}Co 3.4385×10^{12} Bq and ^{65}Zn 3.2748×10^{11} Bq. The minimum shield thickness of lead for filters meeting the design criteria of shielding material $2.50\text{E}-02$ mSv/h when calculated with the MicroShield[®] computer program is 21.05 cm. Verification of the evaluation results will be made using ISOSHLD or EasyQAD computer program.

ACKNOWLEDGEMENT

This study was conducted as part of the "Development of Decontamination Technology of Reactor Coolant System and Dismantled Equipment for NPP Decommissioning" project supported by the MOTIE (Ministry of Trade, Industry and Energy) and the KETEP (Korea Institute of Energy Technology Evaluation and Planning (Project Number: 20141510300310)).

REFERENCES

- [1] CANBERRA, In-Situ Object Counting Systems, 2012.
- [2] CANBERRA, Genie 2000 Spectroscopy Software Operation Manual, 2013.
- [3] Grove Software, "MicroShield ver. 10.03", 2015.
- [4] Grove Software, "MicroShield[®] User's Manual", 2015.

Removal of ^{60}Co and ^{152}Eu in Wastewater From Volume Reduction Treatment of Activated Concrete Waste

Woojung Shon^{1), 2)}, Maeng-Kyo Oh²⁾, Richard I. Foster²⁾, Keun-Young Lee²⁾, and Kwang-Wook Kim^{2),*}

¹⁾ University of Science and Technology, 217, Gajeong-ro, Yuseong-gu, Daejeon, Republic of Korea

²⁾ Korea Atomic Energy Research Institute, 111, Daedeokdae-ro 989beon-gil, Yuseong-gu, Daejeon, Republic of Korea

*nkwwkim@kaeri.re.kr

1. Introduction

When Co, Eu, etc elements, which are inherently present in the cement phase of concrete, are irradiated by neutron, ^{60}Co and ^{152}Eu are known to be generated, and are major nuclides in the irradiated concrete waste[1]. It is known that the concrete usually consist of aggregate (gravel and sand) and cement and the radioactive nuclides exist in the cement phase. Accordingly, if the aggregate part is completely removed from the concrete, the volume of concrete waste to be disposed can be greatly reduced. The separation of cement and aggregate is known to be carried out by thermally-assisted mechanical way[1,2]. However the method known so far is practically difficult to separate the clean aggregate enough to be released to environment as clearance. Accordingly, the KAERI process considers chemical washing by using acid after the mechanical treatment concrete waste. In that case, all the cement remained on the aggregate surface should be dissolve, which results in the generation of a lot of wastewater. Also KAERI is considering even the separation of the radionuclides of ^{60}Co and ^{152}Eu from the cement phase by chemical way for possibility of further volume reduction yield of the concrete waste, which should generate the same wastewater as the above-mentioned wastewater, as well. The elements to be studied in this work were determined as major elements found in the solution prepared from actual dissolution of ordinary concrete including Co and Eu, as shown in Table 1. The radionuclides existing in the wastewater should be

removed from the solution for the separated solution to be released to environment. The nuclides in the solution, of which concentrations are extremely low and lower than their solubilities, are known to be separated by coprecipitation using HFO (Hydrous Ferric Oxide) material and HAIO (Hydrous Aluminum Oxide)[3]. For that, it is necessary to understand exact hydro-chemical behavior of all the elements included in the wastewater. This work studied the thermodynamic behaviors of the major elements in the wastewater generated from the volume reduction process of concrete waste.

Table 1. Concentration of elements from cement paste with Co and Eu

Element	Concentration (mg/L)	Element	Concentration (mg/L)
Al	1200	Ca	20000
Mg	600	Si	3700
Fe	900	K	500
Na	100	Co	10
Eu	1		

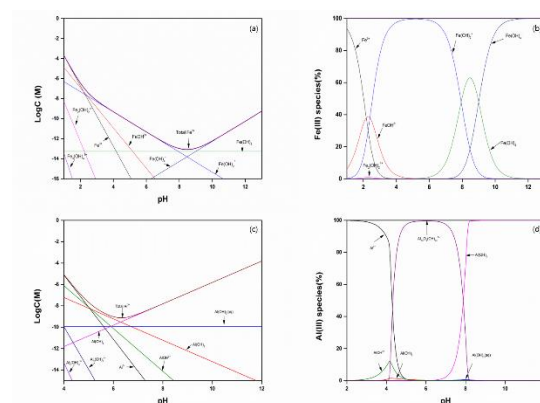


Fig. 1. Equilibrium solubility diagram and distribution of hydrolysis speciation of Fe(III)(a,b) and Al(III)(c,d).

2. Result and discussion

For the removal of elements, which exist in the concentration below their solubilities, by the HFO and HAIO, it is necessary to evaluate exact speciation of major elements as well as Al and Fe in solution. The distribution of Fe^{3+} and Al^{3+} ion species and their total solubilities were evaluated by using a chemical equilibrium modeling code of MINEQL 5.0 with relevant thermodynamic data and their results are shown in Fig. 1 Fe^{3+} and Al^{3+} forms various hydrolysis species with pH. Fe and Al has the lowest solubility around pH 8 and pH 6 with dominant species of $\text{Fe}(\text{OH})_3$ and $\text{Al}(\text{OH})_3$, respectively. It is necessary to evaluate coprecipitation of target elements by HFO and HAIO. For the experiment, precipitation of the solutions of Table 1 was conducted at pH 6, 7, 8 and 9. Concentration of Ca, Al, Fe, Co and Eu in the solution were analyzed by ICP-OES. Figure 2 shows the removal yield of each element. The Co and Eu could be removed from the solution together by more than 99% at pH 8.

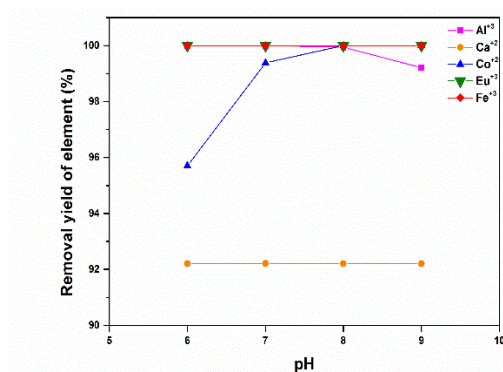


Fig. 2. Removal yields of elements(Al, Ca, Co, Eu and Fe) at pH 6, 7, 8 and 9.

3. Conclusion

The hydro-chemical behavior of all the major elements of wastewater generated from concrete waste treatment were evaluated. The nuclides of Co and Eu included in the cement phase of concrete

waste were confirmed to be removed from the solution by HFO and HAIO with $\text{DF } 2 \times 10^4$.

ACKNOWLEDGEMENT

This work was supported by the National Research Foundation of Korea grant (No. NRF-2017M2A8A5015147) funded by Ministry of Science and ICT.

REFERENCES

- [1] K.Y. Lee, M.K. Oh, J.M. Kim, E.H. Lee, I.S. Kim, K.W. Kim, D.Y. Chung, B.K. Seo, "Trends in Technology Development for the Treatment of Radioactive Concrete Waste", JNFCWT, V16(1), 93-105 (2018).
- [2] Y.M. Min, P.J. Woo, W.K. Choi, K.W. Lee, "Separation of Radionuclide from Dismantled Concrete Wastes", J.of KRWS, V7(2), 79-86 (2009).
- [3] N. Bader, A. A. Benkhayal, B. Zimmermann, "Co-precipitation as a sample preparation technique for trace elements analysis, I. Chem. Sci., 12(2), 519-525 (2014).

A Study on the Post-Treatment Process of Decontamination Waste of Nuclear Power Plant System

Seon-Byeong Kim*, Jun-Young Jung, Hui-Chul Eun, Sang-Yoon Park, and Bum-Kyoung Seo
Korea Atomic Energy Research Institute, 111, Daedeok-daero 989beon-gil, Yuseong-gu, Daejeon, Republic of Korea

*sbkim@kaeri.re.kr

1. Introduction

Decontamination of the radiologically contaminated system is essential for dismantling or maintenance of nuclear power plants to least the radiological exposure of workers. Chemical decontamination is mainly carried out to dissolve the metal oxide film containing a radionuclide formed inner side of the nuclear power plant system. In the dissolution of metal oxide, it combines typically oxidation and reduction to deal with the dissolution of Cr-rich and Fe-rich oxide respectively.

In HyBRID process, different from the other processes found in many applications using organic acid, only contains inorganic chemicals, which enables the secondary waste to be treated with precipitation process minimizing ion-exchange resin [1]. After decontamination of HyBRID process turns to second stage of process which treats decontamination solutions to be precipitated by the addition of $\text{Ba}(\text{OH})_2$. Any metal ions including radionuclides except potassium ions are removed by this process and the decomposition of N_2H_4 follows by the addition of H_2O_2 .

In this study, the removal characteristics of metal and sulfate ions in the simulated post-decontamination solution and the decomposition characteristics of N_2H_4 were evaluated through the precipitation process with $\text{Ba}(\text{OH})_2$ addition and it will be utilized in the design and development of post-treatment process.

2. Preparation of simulated post-decontamination solution

The simulated decontamination wastewaters to be used in decomposition and precipitation were prepared. The detailed composition is shown in Table 1.

Table 1. Chemical components and concentration of post-decontamination solution

	Components	Concentration [ppm]
SP-HyBRID decontamination agents	KMnO_4	1,000
	H_2SO_4	3,630
	N_2H_4	1,856
	CuSO_4	80
Metal ions	Fe, Cr, Ni, Cu, Zn, Co	50-200 (respectively)

3. Removal and decomposition of contaminants in simulated waste solution

The removal of metal and sulfate ions was carried out by the precipitation of $\text{M}^{++}(\text{OH})_x$ and BaSO_4 with the addition of $\text{Ba}(\text{OH})_2$. Before the experiment, $\text{Ba}(\text{OH})_2$ solution was prepared by dissolving its powder in 80 ml of distilled water by heating at 80°C in consideration of the property that $\text{Ba}(\text{OH})_2$ does not dissolve homogeneously in water at room temperature. The concentration of added $\text{Ba}(\text{OH})_2$ was determined at the level of 0.98 of the those of sulfate ion and it was mixed at the rate of 500 rpm.

The N_2H_4 decomposition experiment was performed to compare the residual concentration by H_2O_2 injection while adjusting the pH from 3 to 12 using $\text{Ba}(\text{OH})_2$ considering the characteristics of

N₂H₄, Respectively. At this time, the stirring speed was changed to 100-500 rpm, and the influence of the stirring speed was also evaluated. The concentration of N₂H₄ and sulfate remaining in the solution after the precipitation and decomposition was analyzed by UV spectroscopy and metal ions after precipitation was measured by the ICP-OES.

4. Results and discussion

The metal and sulfate ions in the simulated decontamination waste solution by Ba(OH)₂ addition were effectively removed. Especially, it was confirmed that the metal ions can be removed to the satisfactory level of drinking water quality standards even if the concentration of each metal ion increases from 50 to 200 ppm (Table 2).

Table 2. Concentration of reagents after precipitation process

Analyzer	Items	Concentration of metal ions (ppm)				Detection limit (ppm)	Drinking water standards (ppm)
		50	100	150	200		
UV-VIS spectroscopy	SO ₄	ND	1	1	8	2	200
	K	165	147	165	178	0.0079	12
	Mn	ND	ND	ND	ND	0.0003	0.05
	Fe	ND	ND	ND	ND	0.01	0.3
ICP-OES	Cr	ND	ND	ND	ND	0.04	0.05
	Ni	ND	ND	ND	ND	0.0037	0.01
	Cu	0.75	0.1175	0.0683	0.0784	0.0072	1.0
	Zn	0.01	0.0406	0.0057	0.0055	0.0015	3.0
	Co	ND	ND	ND	ND	0.0032	-
	Co	6×10 ⁴	-	-	-	1.7×10 ⁻⁶	-

The decomposition of N₂H₄ in simulated decontamination wastewater was confirmed to be most effective at around pH 9 as shown in Fig 1. This is because N₂H₄ at pH 9 or higher keeps its composition as N₂H₄ in the solution but changed to N₂H₅⁺ at the acidic condition [2]. Since the decomposition reaction with H₂O₂ is more effective in N₂H₄ form, and therefore the decomposition rate increased at higher pH.

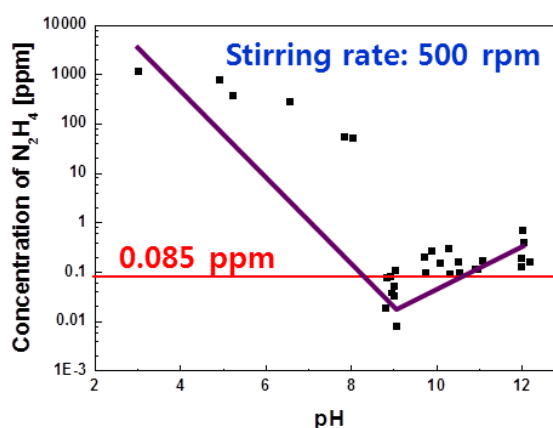


Fig. 1. Characteristics of N₂H₄ decomposition with pH change.

5. Conclusions

Removal of post-decomposition waste water of the reactor coolant system can be effectively performed by combining the precipitation process using Ba(OH)₂ and the decomposition process using N₂H₄ using H₂O₂. This process may reduce the final volume of secondary waste up to level of 30% of those generated from the process using ion exchange. The removal of all metal ions except potassium ion and sulfate salt remained in HyBRID were confirmed by precipitation and filtration. A series of scaled up experiments will be conducted in the future to elucidate the proposed combinatorial process to be reliable.

REFERENCES

- [1] H. J. Won et al. "A Feasibility Study on the Decontamination of Type 304 Stainless Steel by N₂H₄ Base Solution", Asian Journal of Chemistry, 26(5), 1327-1330 (2014).
- [2] H. Nakui et al., "Hydrazine degradation by ultrasonic irradiation", Journal of Hazardous Materials, 146, 636-639 (2007).

Development of Automated System of Classification and Sampling on Radioactive Wastes

Chang-Jong Kim*, Jin-Hyung Lee, Mee Jang, Hyuncheol Kim, and Jong-Myoung Lim

Korea Atomic Energy Research Institute, 111, Daedeok-daero 989beon-gil, Yuseong-gu, Daejeon, Republic of Korea

*cjkim@kaeri.re.kr

1. Introduction

In Korea, radioactive wastes (RWs) of the low and intermediate level can be transferred to RWs repository of deep geological disposal (Wolsung Low and Intermediate Level Radioactive waste Disposal Center). For transfer of RWs to repository, it is necessary to evaluate radiological characteristic which is radioactivity concentration of regulated radionuclides; ^3H , ^{14}C , ^{55}Fe , ^{59}N , ^{63}Ni , ^{90}Sr , ^{94}Nb , ^{99}Tc , ^{129}I , ^{60}Co , ^{58}Co , ^{144}Ce , ^{137}Cs and gross alpha.

In order to evaluate the activity concentration of radionuclides, the most important issue is to prove that it is representative value for each waste drum. Previously, representative samples were collected after re-opening the packaged RWs. This approach can cause cross contamination during the re-opening process, and leads to an increase in disposal costs. In addition, it is fundamentally difficult to collect a representative sample from the packaged RWs without classification of radioactivity level because radioactivity concentration of packaged RWs is not uniform in waste drum. Therefore, an automated system has been developed to classify the radioactive level of and collect representative samples for RWs of concrete and soil which occupy a large volume of low and intermediate level wastes.

into particles about 10 mm, 2) transfer (Fig.2.); for moving a certain amount of wastes to each step and distributing to packaging containers, 3) classification (Fig. 3.); for classifying radioactive level of RWs as clearance, very low, low and intermediate level applying gamma spectroscopy which is used scintillation or semiconductor detector and 4) representative sampling (Fig. 4.); for sampling when distributing to packaging containers.

The number and volume of sampling can be determined according to degree of representation. In relation to this, the volume of transfer container and representative sample container are also determined. And all steps are automated and proceeded sequentially.

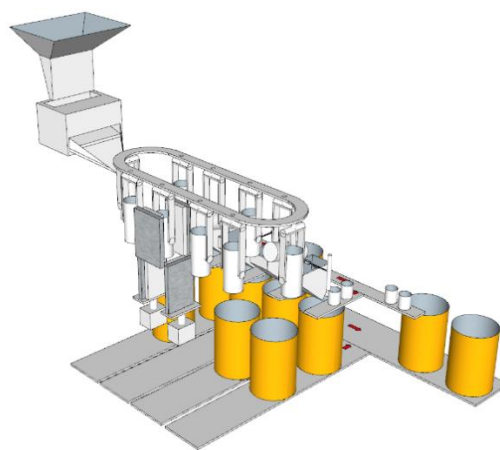


Fig. 1. Automated system of classification and sampling.

2. Conceptual design of automated system

The system consists of four steps which are 1) crushing and mixing; for making concrete and soil

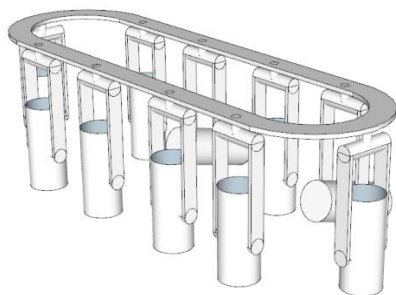


Fig. 2. Part for transfer containers.

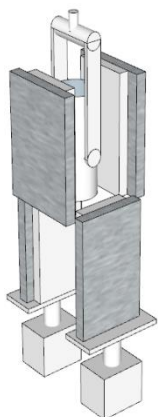


Fig. 3. Part for classifying radioactive level.

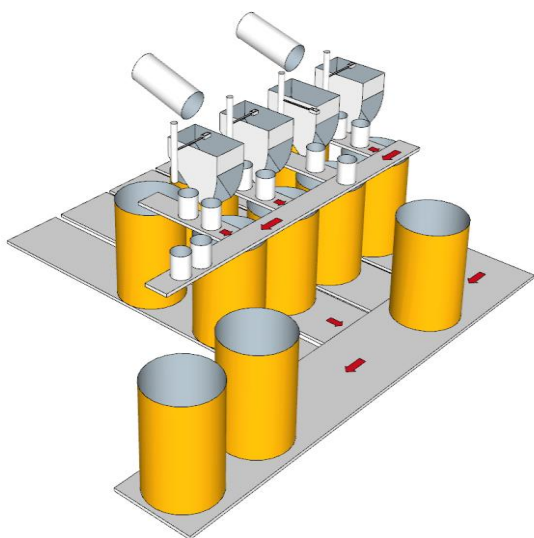


Fig. 4. Part for representative sampling.

3. Conclusion

It is possible to solve the previous problems for representativeness of sampling and to provide statistically reliable value by applying a sequential sampling method from wastes classified as clearance,

very low, low and intermediate level. The radioactivity level classifying technique of this system can contribute to the reduction of the amount of waste and the cost of nuclear decommissioning by classifying the clearance level wastes out of the mixed low and intermediate level wastes. In the nuclear decommissioning market which the disposal cost of RWs is about 40% of the total cost, this study will contribute economically by improving the treatment efficiency of RWs and lowering disposal costs.

Behavior Diagram Analysis to Define Requirements on Site Clearance and Remediation

Yunjeong Hong*, Heeseoung Park, and Jeongguk Kim

Korea Atomic Energy Research Institute, 111, Daedeok-daero 989beon-gil, Yuseong-gu, Daejeon, Republic of Korea

*hong814@kaeri.re.kr

1. Introduction

In the decommissioning of nuclear facilities, the final task of the project is clearance and remediation of the site. Behavior diagram was used to analyze the site clearance and remediation process, and designed the system environment using system engineering(SE) technology. Using the Nuclear Safety Act by the clearance and remediation of the site, decommissioning regulation, project performance and technical requirements, and criteria were derived.

2. Requirements definition for decommissioning activities

The decommissioning regulatory requirements extracted from the nuclear law were analyzed and simplification work was conducted as project requirements. The simplification was classified according to 19 major decommissioning activities. Requirements were defined through a method of identifying one clear project. In addition, by using the complement of the SE process, we have studied the application of the requirements-WBS-process and configured it to be used to define the missing requirements.

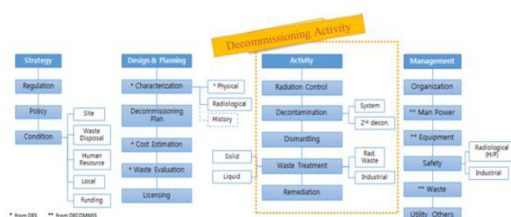


Fig. 1. The classification and scope of requirements management for decommissioning procedure.

2.1 Process analysis and behavior diagram

Decommissioning activity behavior diagram analysis refers to logically modeling the order of processes and inter-process interfaces when performing a specific decommissioning activity. The detailed activities of the decontamination and decommissioning module identified through the behavior diagram analysis ensure the requirements and traceability, and those complemented each other.

Process analysis and behavior diagramming purposes have four main purposes. First, it is to facilitate communication by reducing interpretation errors due to each background among stakeholders. Second, it can be added/refined the requirements as missing requirements is possible to identify through traceability between processes and requirements. Third, it can support WBS development that reflects the requirements of decommissioning procedure and major work process through ensuring traceability between process and WBS. Finally, the defined standard process can be used as a reference for defining the decommissioning detailed procedures of specific project.

3. Environment design and implementation to reflect scenario of SE for site clearance and remediation

3.1 Data collecting and definition of requirements on site clearance and remediation

The requirements related to the site clearance and remediation in decommissioning activity were

[illegible]

3.2 Implementation examples of requirements definition scenario on site clearance and remediation

3.3 Environment design and implementation to reflect scenario of SE for site clearance and remediation

[illegible]

4. Conclusion

REFERENCES

- 2018 한국방사성폐기물학회 춘계학술대회 논문요약집 489

Removal of Corrosion Oxide Film Using Acidic and Reductive Decontamination Foams

Wangkyu Choi*, Seungeun Kim, and Seonbyeong Kim

Korea Atomic Energy Research Institute, 111, Daedeok-daero 989beon-gil, Yuseong-gu, Daejeon, Republic of Korea

*nwkchoi@kaeri.re.kr

1. Introduction

Foam decontamination process has a potentially wide application in the removal of contaminants from large components with complex shapes or large area or large volumes. This process can be applied to any direction regardless of walls, floors and ceilings, and basically it has the advantage of generating less secondary wastes [1]. It is also easy to perform remote decontamination using injection or spray nozzles and equipment to generate the foam. However, foam decontamination has a disadvantage of relatively low decontamination factor (DF) [2]. In order to overcome this problem, it is suggested to introduce a decontamination foam containing an aggressive chemical agent and to increase the stability of the foam to increase the contact time between the decontamination foam and the contaminated surface [3].

In this study, the removal performance of nickel ferrite (NiFe_2O_4) film coated on the surface of stainless steel 304 was investigated as one of the models of fixed contamination using acid and reductive decontamination foams with various kinds of added chemicals and acidity of complex fluid.

2. Materials and Methods

2.1 Preparation of Decontamination Foam

The decontamination foams used in this study were prepared by combining surfactants, silica nanoparticles, inorganic acids such as HNO_3 , H_2SO_4 and HF, and reductive chemical reagent, HyBRID developed for primary cooling system of NPP [5, 6].

In order to evaluate the removal performance of the oxide film, two kinds of decontamination foams such as acidic foam (AF) and reductive foam (RF), were prepared and summarized in Table 1.

2.2 Performance Test with Decontamination Foam

The oxide removal performance tests were carried out by applying various decontamination foams as shown in Table 1 to the simulated specimens coated with nickel ferrite as a model fixed corrosion oxide film.

Table 1. Composition of Various Decontamination Foams

Foam Type	Chemical Composition
AF-1	1wt% EM100 ¹⁾ + 1wt% M-5 ²⁾ + 2M HNO_3 (pH \approx 0.7)
AF-2	1wt% EM100 + 0.5M HF + H_2SO_4 (pH=3)
AF-3	1wt% EM100 + 0.5M HF + 0.5M HNO_3 (pH \approx 1.2)
RF-1	1wt% EM100 + HyBRID ³⁾ (pH=3)
RF-2	1wt% EM100 + HyBRID + 0.2M HF (pH=3)
RF-3	1wt% EM100 + HyBRID + 0.5M HF (pH=3)

1) Nonionic surfactant, ELOTANT Milcoside 100, C08-10 alkyl polyglucoside

2) CAB-O-SIL[®] M-5 Fumed Silica Nanoparticle

3) 50 mM N_2H_4 + 0.5 mM Cu^{2+} (pH 3 adjusted by H_2SO_4)

The nickel ferrite coated specimens having a thickness of 500 nm were prepared by the E-beam evaporator system using the oxide target with the same composition at a deposition rate of 0.7 Å/s under the condition that the degree of vacuum was maintained at 3×10^{-6} torr and then annealed at 600°C in an argon atmosphere.

The oxide removal performance test was carried out in an experimental apparatus consisting of a decontamination foam generator and a foam filling column. After the simulated specimens coated with nickel ferrite were placed in the foam filling column followed by filling with the decontamination foam through the foam generator. As the drainage is continuously generated from the liquid film of the filled foams, the volume of the solution discharged to the lower end of the foam filling column is increased. Therefore, the solution accumulated at the lower end of the filling column at intervals of 20 minutes is recirculated to the foam solution make-up tank. A new decontamination foam prepared via a foam generator was fed to the bottom of the foam filling column. As a result, the dry foam at the top of the filling column is pushed out and filled with new foam. This is called cyclic foam filling process. The oxide removal performance was improved by keeping the physicochemical properties of the decontamination foam substantially constant by

applying cyclic foam filling process.

The oxide removal performance of the oxide coated specimens was evaluated by measuring weight loss before and after decontamination.

3. Results and Discussion

For the removal of nickel ferrite film coated on the stainless steel specimen at 500 nm thickness using acidic decontamination foam, the oxide film was completely dissolved within 2 hours by strong acidic decontamination foam, AF-3 mixed with 2 M nitric acid and 0.5 M hydrofluoric acid. On the other hand, only *ca.* 3% of the oxide film was dissolved during the same time period by strong acidic decontamination foam, AF-1 containing only 2 M nitric acid.

Under the milder conditions of acidic and reductive decontamination foam, the nickel ferrite film hardly dissolved in the reductive decontamination foam, RF-1, containing only HyBRID reagent. On the contrary, the oxide film completely dissolved within 3 hours not only in the acidic decontamination foam, AF-2, containing 0.5 M HF with pH 3 adjusted by sulfuric acid but also in the reductive decontamination foam, RF-3, composed of a mixture of 0.5 M HF and HyBRID reagent as shown in Fig.1.

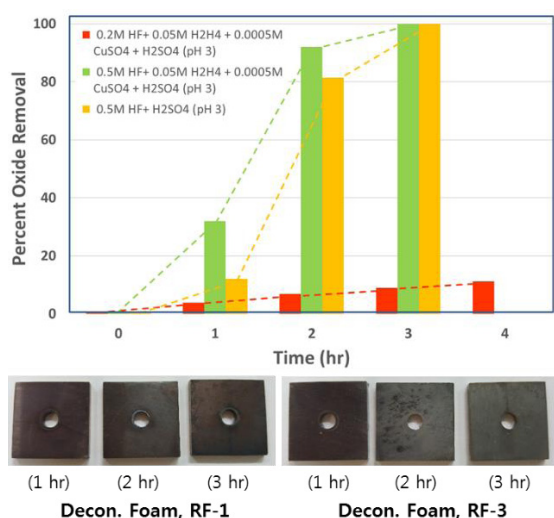


Fig. 1. Comparison of the Removal Performance of Nickel Ferrite Coating Specimens in the Mild Acidic and the Reductive Decontamination Foams.

The difference between the decontamination foams AF-2 and RF-3 lies in the presence or absence of HyBRID reagent. The reductive decontamination foam RF-3, which contains HyBRID reagent, has a much higher initial dissolution rate of oxide film than

the acidic decontamination foam, AF-2.

4. Conclusion

In the dissolution removal of the nickel ferrite oxide film by the decontamination foams, the performances of the mild acidic decontamination foam and the reducing decontamination foam were confirmed. Through this, it was confirmed that it is possible to secure the easiness of decontamination by replacing the existing strong acidic decontamination foam, and at the same time, it is also beneficial from the viewpoint of secondary waste treatment.

ACKNOWLEDGEMENT

This work was supported by the Nuclear R&D Program (2017M2A8A5015144) funded by Ministry of Science, ICT & Future Planning.

REFERENCES

- [1] C. Dame, C. Fritz, O. Pitois, and S. Faure, "Relations between physicochemical properties and instability of decontamination foams", *Colloids Surf., A*, 263, 210-218 (2005).
- [2] A.H. Love, C.G. Bailey, M.L. Hanna, S. Hok, A.K. Vu, D.J. Reutter, and E. Raber, "Efficacy of liquid and foam decontamination technologies for chemical warfare agents on indoor surfaces", *J. Hazard. Mater.*, 196, 115-122 (2011).
- [3] I.H. Yoon, C.H. Jung, S.B. Yoon, S.Y. Park, J.K. Moon, and W.K. Choi, "Effect of silica nanoparticles on the stability of decontamination foam and their application for oxide dissolution of corroded specimens", *Ann. Nucl. Energy*, 73, 168-174 (2014).
- [4] S. B. Kim, H. J. Won, J. K. Moon, and W. K. Choi, "Magnetite Dissolution Using Hydrazine-Acid Solution for Chemical Decontamination," *Trans. Am. Nucl. Soc.*, 115, 47 (2016).

Comparison of Point Cloud Segmentation Methods for Calibration of 3D Environment Scanning System

Sungmoon Joo*, Jonghwan Lee, Ikjune Kim, and Dongjun Hyun

Korea Atomic Energy Research Institute, 111, Daedeok-daero 989beon-gil, Yuseong-gu, Daejeon, Republic of Korea

*smjoo@kaeri.re.kr

1. Introduction

Robotic technologies have been applied to address unique needs in decommissioning of nuclear facilities. Recently, for example, an integrated robotic dismantling system has been proposed, where precise three-dimensional (3D) as-built information is required [1]. An accurate environment mapping system plays a key role in these robotic decommissioning systems, because planning for the safe and controlled decommissioning of highly contaminated nuclear facilities requires that engineers and managers fully understand the 3D work space in which personnel and equipment will operate [2].

Extrinsic calibration is a process of identifying extrinsic parameters of a 3D measurement system, and it is a critical process in order to get precise measurements. Authors proposed a practical extrinsic calibration method that uses a simple geometric object (i.e. sphere) as a target [3]. Fig. 1 shows the test setup using a 3D scanner attached to a robot manipulator.



Fig. 1. Test Setup for Extrinsic Calibration.

Identifying the target object from the point clouds measured by a scanner is a well-studied yet challenging task. It is a two-step process. First step is segmentation that is a process of classifying the point cloud into multiple homogeneous groups. Then we compare each segmentation with reference models to find out the closest match. This study compares two segmentation methods: conventional filtering approach and a deep learning approach, and discuss pros and cons.

2. Extrinsic Calibration System

The extrinsic calibration is to identify the transformation from the tool flange frame to the sensor frame, i.e.,

$${}^{Tool\ Flange}_{Sensor}T = {}^{Tool\ Flange}_{Scanner}T {}^{Scanner}_{Sensor}T$$

The coordinate frames are described in Fig. 2. The transformation from the (reference) world coordinate frame to the tool flange frame, ${}^{World}_{Tool\ Flange}T$, can be identified through a separate kinematic calibration process, and is assumed to be known. The position of a target object (i.e., the center of the sphere), ${}^{World}P$, is also known.

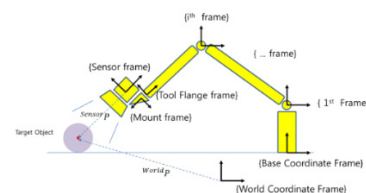


Fig. 2. Coordinate Frames for Extrinsic Calibration.

Extrinsic parameters are identified through the following steps:

Step 1. Identify points that belong to the surface of the target sphere

Step 2. Identify the geometric parameters of the points from Step 1, such as the radius and center position in the sensor coordinate frame, ${}^{Sensor}P$

Step 3. Solve the following for ${}^{Tool\ Flange}_{Sensor}T$ [6]

$${}^{Tool\ Flange}_{Sensor}T \cdot {}^{Sensor}P = [{}^{World}_{Tool\ Flange}T]^{-1} {}^{World}P$$

3. Point Cloud Segmentation Methods

Point cloud is a set of data points in some coordinate system. In a 3D coordinate system, these points are usually defined by X,Y, and Z coordinates, and often are intended to represent the external surface of an object. Fig. 3 shows a photo of the target on a table and the point cloud measured by a 3D scanner.

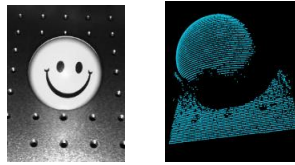


Fig. 3. Sphere Target on Table: Photo vs Point Cloud.

3.1 Classical Filtering Approach using PCL

If we know what to expect (e.g. sphere on table), we can efficiently segment our data. In Point Cloud Library (PCL), several extensions of randomized geometry modelling algorithm, called RANSAC, exist such as MSAC, MLESAC, or PROSAC. We can model several types of geometric shapes using PCL including plane, cone, cylinder, sphere, line and circle. In the sphere on table scenario for the extrinsic calibration, we can (i)create a SAC model to detect a plane, (ii)create a RANSAC algorithm, then (iii)compute the best model. Finally, we can retrieve the best set of inliers that represent the table.

Once we have a plane table model, we can find objects standing on the plane, i.e. sphere target, by computing the convex hull of the planar points and extruding this outline along the plane normal. Fig. 4 shows the segmentation results. The point cloud in Fig. 3 is segmented into two groups: table and sphere.



Fig. 4. Segmentation Result using PCL.

3.2 Deep Learning Approach

An alternative and more general method for point cloud segmentation is to use a deep learning network. The baseline network chosen in this study is PointNet [4]. PointNet directly consumes point clouds and provides a unified architecture for applications ranging from object classification, part segmentation, to scene semantic parsing. Fig.5 shows the architecture of PointNet [4].

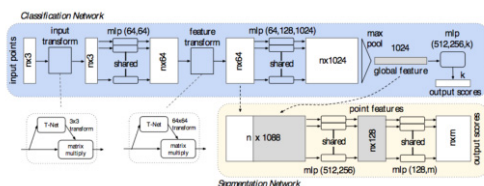


Fig. 5. PointNet Architecture [4].

Using PointNet, we can segment the point cloud

data into two groups. The result is similar to the PCL approach described in the previous section.

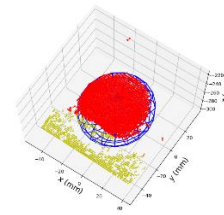


Fig. 6. Segmentation Result using PointNet.

4. Conclusion

This study applies two different approaches to segment point cloud. The segmentation results are similar, and both of them can be used for calibration introduced in [3]. The filtering approach using PCL can be applied to the cases when we know what to expect exactly. On the other hand, the deep learning approach is more general in the sense that, once we train the network using a model database, the deep neural network can segment a point cloud into groups even in the case we don't know the objects in the captured scene a priori. This implies that it is more flexible in the choice of target shape for calibration.

ACKNOWLEDGEMENT

This work was supported by the nuclear research and development program (2017M2A8A5015146) through the national research foundation of Korea funded by the Ministry of Science and ICT.

REFERENCES

- [1] I. Kim, B. Choi, D. Hyun, J. Moon, J. Lee, K. Jeong, S. Kang, "Integration of the Unit Modules of the Nuclear Facility Dismantling Simulation System", Proc. of the KRS 2017 Spring Conference, pp. 297-298, May 24-26, 2017, Busan.
- [2] S. Joo, J. Lee, I. Kim, D. Hyun, S. Kang, "Preliminary Study on Environment Mapping for Nuclear Reactor Dismantling", Poster Presentation at the KRS 2017 Autumn Conference, Oct. 18-20, 2018, Changwon, Korea.
- [3] S. Joo, D. Hyun, I. Kim, J. Lee, "Extrinsic Calibration of Robotic Laser Scanning System using Spherical Target", to be presented at 2018 ICCAS, Oct. 17 ~ 20, 2018, PyeongChang, Korea.
- [4] C. R. Qi, H. Su, K. Mo, L.J. Guibas, "PointNet: Deep Learning on Point Sets for 3D Classification and Segmentation", CVPR 2017, arXiv: 1612.00593.

Risk Assessment on Hazards for Safety of Nuclear Power Plant Decommissioning

HaeWoong Kim^{a),*}, KyuHo Chang^{a)}, KwangSoo Park^{a)}, HeeDong Sohn^{a)}, and ChangJe Park^{b)}

^{a)} Doosan Heavy Industries & Construction, 22, Doosan Volvo-ro, Seongsan-gu, Changwon-si,
Gyeongsangnam-do, Republic of Korea

^{b)} Sejong University, 209, Neungdong-ro, Gwangjin-gu, Seoul, Republic of Korea,

*haewoong.kim@doosan.com

1. Introduction

All facilities using radioactive materials should be proved to be safe over their lifetime, so safety assessment should be carried out in decommissioning plan and performing work according to national laws and internationally agreed recommendations.

Probabilistic risk assessment methods are applied in the design and operation of nuclear facilities. However, this is an approach that can be used when a certain amount of analytical data is accumulated, and thus is not suitable for applications such as disassembly processes.

Decomposing process risk assessment is basically using methods such as judging the level of risk by experience because of the lack of reliable empirical data. For this reason, the nuclear facility sector has traditionally relied on data from previous researchers or on engineering judgment based on expert experience.

In this study, we analyze several safety evaluation techniques and try to find a way to supplement risk assessment on hazards for safety related modules in the currently developing Decommissioning process simulation system.

2. Safety Assessment for Decommissioning

2.1 Safety assessment methodology

Nuclear facility decommissioning requires the

dismantling of equipment and structures. Radiological or non-radiological hazards occur during nuclear facility decommissioning activities. The safety assessment methodology of nuclear facility decommissioning plan is applied to identify the potential radiological or non-radiological hazards and risks. Safety assessments are required to support the decommissioning plan and, therefore, need to be incorporated into the decommissioning plan or be contained in supporting documents. For larger projects consisting of a number of phases, it is usual practice for the detailed safety assessments to be separated from, but complementary to, the decommissioning plan. The decommissioning plan for such projects may, however, contain an overall or preliminary safety assessment.

2.2 Radiological characterization

In cases where activation is significant, calculation methods for its assessment may be necessary. Methods for estimating neutron induced activity in a reactor core, its components and its surrounding structures involve the use of computer codes. For large power reactors, a full range of calculations may be needed, whereas for actual calculation of activation, simplified, regional and separate models would be used, with the results confirmed by sampling and local measurements, and by comparison with similar reactors.

We used MCNP6.1 modeling, which is a three -

dimensional Monte Carlo code, to evaluate the distribution of neutron species in the Kori unit 1 reactor. Monte Carlo calculations were used to obtain the distribution of neutron fluxes within and outside of the core, and the neutron flux distribution was calculated using the ORIGENS code. Nuclear internal structure, reactor pressure vessel, outer concrete area, etc.

Radiological and non-radiological working environments are defined first, and processes and scenarios are selected according to radiative assessment and air dose assessment, but it could be difficult to put workers into containment building without protective measures.

After the results of the radiological characterization have been obtained, the safety assessment can be planned. To first identify the hazards and then to perform a screening assessment in order to identify the relevant scenarios and to omit those with low consequences. Existing analyses, for example, from the operational phase, may be of help, and should be reviewed in this process.

2.3 Graded Approach

A graded approach can be used in all of the phases of the planning and implementation of the radiological characterization of a facility in order to ensure adequate characterization without performing unnecessary work.

The decommissioning technology can classify equipment and structures to be disassembled into concrete and metal by materials, and classify them according to each applied technology. This is because the main equipment used in nuclear power plant is metal, buildings are mainly made of concrete, and their material properties are different.

Therefore, considering different materials as well

as different shapes, the dismantling technology applied is very different.

And, depending on the level of contamination, workers may be exposed to radiation in contaminated equipment and structure dismantling work. In addition, worker exposure can also occur in preparation and waste treatment operations.

Owing to the complexity and variety of the activities during the decommissioning process, a graded approach is applied to the evaluation of safety during decommissioning, with technical resources being allocated in proportion to the risks presented by the planned decommissioning activities.

3. Conclusion

Decommissioning process simulation system is able to select the optimal dismantling process by quantitatively comparing the dismantling process with the decommissioning cost and the work safety. It can be used effectively as a dismantling engineering tool after completion of technology development.

ACKNOWLEDGEMENT

This work was supported by the National Research Foundation of Korea (NRF) granted financial resource from the Ministry of Science and ICT, Republic of Korea (NRF-2017M2A8A5041777).

REFERENCES

- [1] IAEA, "Safety Assessment for Decommissioning", Safety Report Series No.77, (2013).

Experimental Research on Decontamination of Co Containing Metal by Induction Melt

Beom-Kyu Kim, Hwa-Jeong Han, Jun-Hyeok Lee, Jae-Hong Yim, and Byung-Gi Park*

Soonchunhyang University, 22, Soonchunhyang-ro 22, Asan-si, ChungCheongnam-do, Republic of Korea

*qu@sch.ac.kr

1. Introduction

The dismantling of a nuclear power plant is the final finishing process for safely disposing and disposing of a nuclear power plant whose operating life has expired, it is imperative that the dismantling technology is uniquely established and internationally competitive. During a decommissioning of nuclear plants and facilities, large quantities of slightly contaminated steel wastes are generated. Radioactive metal wastes generated during nuclear dismantling process are primary targets for reduce volume and can be recycled if the radioactive contamination degree is reduced through the melting process.[1-2] Most of the radioactive contained in the metal contains Co-60, Co-58. In this study, we conducted an experimental study on the decontamination of radioactive metal waste using induction heating method for Cobalt, which is expected to be a major pollutant species, in the case of metal melt decontamination related to steam generator disassembly during disassembly process. Melting decontamination is accomplished by combining radioactive nuclides with oxygen or other elements to form a safer form of the compound when the metal contaminated with the radionuclide is melted. Therefore, in this melting experiment, the radionuclides in the contaminated metal are combined with oxygen in the air or the oxygen element in the slag to form the nuclide oxides, and the oxides of the radionuclides formed are in contact with the slag, it is moved to the slag phase by the difference or the like and is decontaminated.

2. Experimental

Since the actual radioactive element is not safe, the experiment is performed by replacing the simulated material. The simulated radioactive elements were Co_3O_4 , 1.0 g (Alfa Aesar, 99.7%), and the decontamination flux was purchased from Sigma Aldrich as CaO , SiO_2 , Fe_2O_3 and Al_2O_3 . The composition of the flux medium is CaO (40%) - SiO_2 (30%) - Fe_2O_3 (20%) - Al_2O_3 (10%) / 100 g. The molten metal was carbon steel (2 kg). Experiments were carried out in the induction chamber in Figure 1. The melting time was 6 hours, frequency was 15 kHz, the maximum applied power was 7.5 kVA and the temperature was carried out at about 1800°C as the melting temperature of the carbon steel. In the experimental procedure, a carbon steel metal and a nuclide (cobalt) are added to a magnesia crucible and melted to make a simulated specimen. Flux was then added as a medium for decontamination according to the composition. Then Samples were aliquoted and sampled over time. The concentration of cobalt in the metal was measured by ICP and compared with time. In addition, we confirmed the distribution behavior of slag and ingot through SEM-EDS.

3. Result and Discussion

In this experiment, the ingot was sampled acquired according to time and the process is shown in Fig. 1 (a). It is the process of being sucked into the sampling tube through the pressure. In Fig. 1 (b), the

sampled metal specimens were divided into 5 pieces, upper, middle and lower parts to perform ICP.

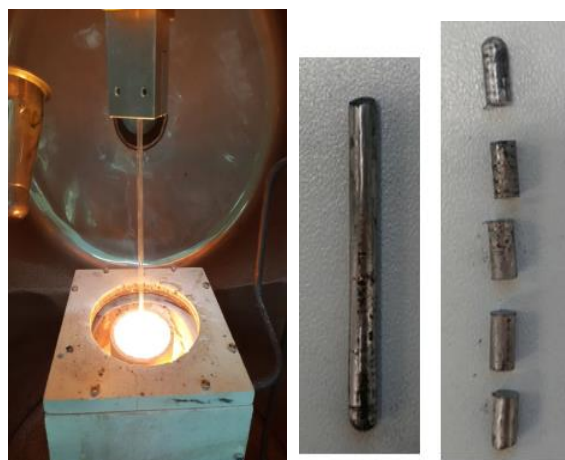


Fig.1. (a) Sampling process in the crucible inside the chamber (b) the sampled metal specimen.



Fig. 2. The final solid metal and slag at room temperature.

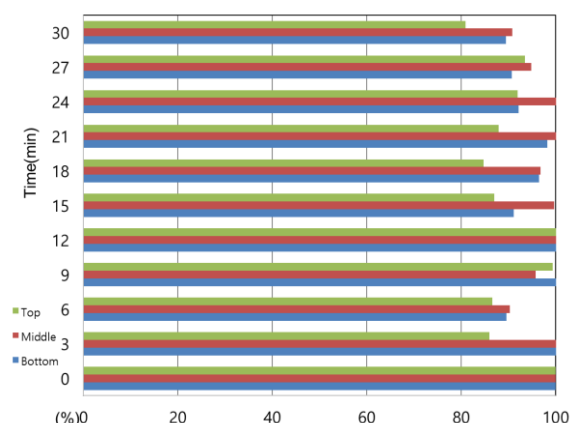


Fig. 3. Percentage (%) of late concentration/initial concentration over time as measured by ICP.

Figure 2 shows the ingot after melting. The change

in metal mass before and after melting was changed from 2.0 kg before melting to 1.45 kg after melting. It can be seen that the metal-oxidized metal oxide has migrated to the slag. It was confirmed that the slag and the ingot were clearly separated. Fig. 3 shows the results of ICP analysis of the metal phase. It was confirmed that Co contained about 80% finally.

4. Conclusion

As a result of the experiment, the removal rate of Co was about 10 ~ 15%. The ionic bond of cobalt is easier to react with the slag during melting than the metal bond. The first step in melt decontamination is to form oxides of radionuclides. However, since cobalt is smaller than oxygen and affinity than metals formed in Flux such as Si, Ca, Al, and Fe, oxygen is difficult to form cobalt oxide by bonding with metal elements having high affinity first. Cobalt is assumed to be stabilized in the metal phase

ACKNOWLEDGEMENT

This work was financially supported by Korea Hydro & Nuclear Power Co. Ltd. (Project No. L16S132000).

REFERENCES

- [1]. V. Adams, W. Murphie and M. Gresalfi, Proceeding of conference in Sagewaste, 1, 115 (2000).
- [2]. K. L. A. Hopkinson, M. T. Bishop, Cross, J. Harrison and F. Selgas, Recycling and reuse of radioactive material in the controlled nuclear sector, Nuclear safety and the environment, European Commission, EUR 18041 EN (1998).

Major Concerns of the Dismantling Project Schedule Development of Nuclear Power Plant

Jun Hee Lee* and Myung Duck Yang

Korea Electric Power Corporation E&C, 269, Hyeoksin-ro, Gimcheon-si, Gyeongsangbuk-do, Republic of Korea

*lee516@kepeco-enc.com

1. Introduction

The Kori Unit 1, which has been permanently shut-down in June 2017, is the first nuclear power plant (NPP) dismantling project in Korea.

Unlike NPP construction projects with multiple performances, Kori Unit 1 dismantling project has some anticipation of hardship due to unprecedented.

Therefore different ways are needed from those of construction project in developing the schedule.

Hence this paper proposes methods for generation of activity and the estimation of the working period, which are major concerns of the dismantling project schedule development.

2. Main Discussion

The activity generation and the appropriate period calculation for the nuclear power plant dismantling should be preferentially performed to plan the whole project period. And to this, the following tasks are proposed step-by-step.

2.1 Evaluation of amount of dismantling work

In order to establish a dismantling schedule of nuclear power plant, a precise assessment for radiation source term and waste generation amount is required.

However, Kori unit 1 project has insufficient information available regarding dismantling project which includes drawings and other materials for estimating the amount of waste

Accordingly, the quantity survey for calculating the proper working period of the dismantling project has been analyzed based on the report issued for the Kori unit 1; the method and outcome of the radioactive sources terms and waste volume [1] etc.

The unit to calculate the amount of waste for estimating the working period per activity has referred UCF(Unit Cost Factors) of DeCAT[2] and AIFF/NESP-036[3].

2.2 Area dividing for dismantling work

When the decontamination/dismantling works are

carried out in many areas on the same floor of a building, frequent interfaces are anticipated among those areas.

In order to perform the work efficiently, it is considered whether the area division is applied to the same floor of a building, which has a multiple working areas. The related drawings, decontamination/ dismantling method and securing the moving space of equipment & and waste should be taken into accounts for the area division.

The object buildings of Kori Unit 1 for dismantling are Main Auxiliary, Intermediate and Turbine Building. Example of Turbine building area division is shown on the figure 1 as below.

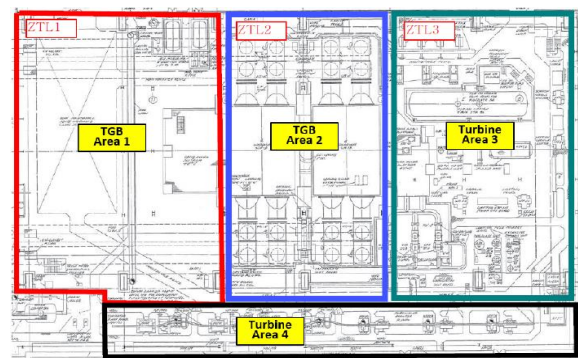


Fig. 1. Turbine building area division.

2.3 Evaluation work period based on integrated UCF

The dismantling period of each UCF has been calculated based on the amount of work per UCF in Kori unit 1.

The existing UCF concept has difficulties in schedule control because detailed tasks are individually divided into about 150 UCFs.

Integrated UCF concept has been applied to improve those issues in which similar UCFs are combined together.

Table 1. Generation of Integrated UCF

Integrated UCF	UCF	Integrated UCF	UCF
P&V	Piping/Valve etc	WCUT	Conc, Wire Cut etc
EQ	Equipment(Pump, Tank, Heat, Exchanger etc)	RVI	RVI etc

ELEC	Electrical(Cable, Tray, Conduit etc)	SG	Steam Generator
CRANE	RCB, TB, Other Crane etc)	PRESS	Pressurizer etc
HV	HVAC(Duct, HVAC Equip etc)	RCP	RCP etc
DISM	Decontamination/Dismantling(Building, Structure etc)	T&GEN	Turbine, Generator etc
SCAB	Scabbling etc	COND	Condenser etc

The working time of integrated UCF is the basis of each activity duration.

2.4 Estimate work period with added work difficulty Factor

The dismantling work requires additional working duration as well as the integrated UCF depending on the Work Difficulty Factor (WDF)[3].

○ Type and content of WDF

The five types of WDF will be based for additional working duration as below.

- ✓ Accessibility or Height Factor : To consider work difficulty in the need to work such as scaffolding, ladders, piping and confined spaces
- ✓ Respirator Factor : Related to protect the works from airborne contamination by using canister filter mask, etc.
- ✓ Radiation/ALARA Factor : To implement the administrative control and requirement to work in radiation area
- ✓ Protective Clothing Factor : The use of protective clothing, the associated procedural “suit-up”, controlled disposal of the clothing and the required exit frisking.
- ✓ Work Break Factor : The paid non-productive time, necessitated by agreement with labor for scheduled work breaks and predetermined intervals.

2.5 Dismantling activity generation for dismantling schedule and proper logic development

To generate an activity for the schedule analysis using P6 schedule software, the following concept has been applied

Schedule activity has been generated by PBS and integrated UCF.

Table 2. Generation method of Dismantling Activity

PBS(Area Group)	Integrated UCF	Remarks
321 Main Auxiliary Building EL-34'-0''(LEVEL 1)	P&V, EQ, ELEC etc	1(PBS) to N(Integrated UCF)

○ Major review points that need to be reflected in development of the project schedule

- ✓ Milestone, Key dates for licensing and Project policy
- ✓ Construction Logic based on construction method, considering construction sequences including decontamination and dismantling
- ✓ Identification of the activities to be performed in parallel to reduce the time

3. Conclusion

This paper introduces a method for schedule development of NPP dismantling project; integrated UCF, area division on the bases of work quantity, concept of activity generation, work period calculation methodologies, and major review points.

By applying this approach, it is expected to improve the schedule reliability of the first dismantling NPP project of at Kori unit 1 in Korea.

REFERENCES

- [1] KEPCO E&C, Evaluation of Decommissioning Source Terms and Wastes for the Pressurized Water Nuclear Power Plant and Heavy Nuclear Power Plant, Final Report, 2016.
- [2] RSCS, KEPCO E&C, Decommissioning Cost Analysis for the Korean pressurized Water Nuclear Power Plant, Final Report, 2009.
- [3] TLG Services, Inc., Guidelines for Producing Commercial Nuclear (AIFF/NESP-036), 1986.

Radioactive Contaminated Soil Segregation System for Waste Volume Minimization

Jae-Mun Han*, Sang-Chul Lee and Min-Jung Kim

HYUNDAI E&C, 17-6, Mabuk-ro 240beon-gil, Giheung-gu, Yongin-si, Republic of Korea

*jmhan@hdec.co.kr

1. Introduction

The permanent stop of Kori-1 is decided on June, 2017. The decommissioning of the nuclear power plant will proceed to the D&D design, decontamination, demolition, waste disposal and site restoration. Site restoration is a process of removing the contaminated soil and returning the site to a green field before the installation of a nuclear power plant. The removed radioactive contamination soil is disposed of as radioactive waste, and a high amount of site restoration costs is generated from disposal of waste. Therefore, the site restoration cost can be minimized by minimizing the radioactive waste generated at site restoration [1]. This study will demonstrate the measurement and segregation system that can minimize the generation of radioactive waste through the process of active separation of real-time radioactive contamination. The segregation are consist of two steps as particle size separation and radio activity level separation. By the new segregation system, the amount of radioactive waste can be decreased to 80%.

2. Methods of soil separation system

The radioactivity measurement of the soil is necessary to confirm whether the activity of soil is lower than the regulation criteria. The second separation is performed by the result of the measurement. In this study, the hydride segregation process using the separations by the particle size and

the activation level of soil is suggested. Fig 1 presents the process of the suggested segregation for the radioactive soil in NPP remediation site. By this hybrid segregation process, the amount of radioactive waste can be decreased to more than 80%.

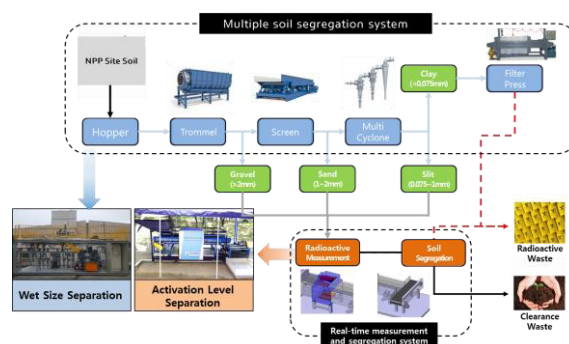


Fig. 1. Process of the hybrid segregation using the separation by the particle size and activation.

2.1 Particle size separation system

The particle size separation system is the first part of the radioactive soil segregation system. The efficiency of the particle size separation is increased using the multi-step equipment such as vibrating screens and cyclone. Fig. 2 presents the process of particle size separation. The separation efficiency of the system is better than 85%.

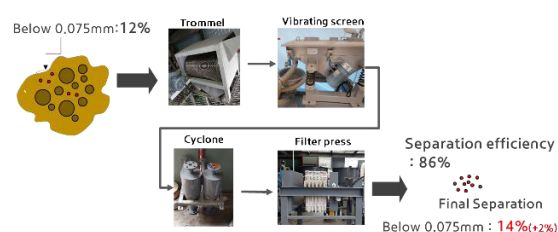


Fig. 2. Process of the particle size separation.

Fig. 3 shows the particle size separation system. The system emits the separated soil by particle to the activation level separation system using the automated conveyor system.



Fig. 3. Particle size separation system.

2.2 Soil measurement and segregation system

This is accomplished by passing the soil on a conveyor belt under an array of sensitive and rapidly reacting, radiation detectors that measure radionuclide concentrations. The contaminated soil above the desired cleanup limits is automatically diverted into a separate waste stream. As shown in fig. 4, contaminants are removed by soil measurement and segregation system. Thus, it can significantly reduce the overall amount of contaminated soil requiring disposition as radioactive waste. Fig. 5 presents the process algorithm of the activation level separation system.



Fig. 4. Real-time measurement and segregation system.

Typical radionuclides that can be measured by soil

measurement and segregation system including Cs-137 and Co-60. The main factors for measurement on this system depend on the ambient radiation background, conveyor belt speed, thickness of the soil layer on the conveyor, and contaminant gamma ray energy and abundance [2].

3. Conclusion

In this study, the radioactive soil segregation system is developed using the difference of the particle size and the radioactivity level of contaminated soil. By this system, the amount of radioactive waste will be decreased to almost 80%.

REFERENCES

- [1] IAEA, "Remediation of Sites with Mixed Contamination of Radioactive and Other Hazardous Substances", Technical Reports Series no. 442 (2006).
- [2] Alejandro U. Lopez, and Jeffrey W. Lively, "Application of soil Segregation Technology: Reducing Uncertainty and Increasing Efficiency at an NRC test reactor Decommissioning site", WM2011 Conference (2011).

Dismantling Procedure on the Decommissioning Cost for the Research Reactor

Hee-Seoung Park*, Yun-Jeong Hong, and Jeong-Guk Kim

Korea Atomic Energy Research Institute, 111, Daedeok-daero 989beon-gil, Yuseong-gu, Daejeon, Republic of Korea

*parkhs@kaeri.re.kr

1. Introduction

The DECOMMIS system was developed for systematic management of data generated at the dismantling site and for efficient operation of the dismantling project. The DES system consist of 5 unit systems such as the DEFACS system that can calculate the amount of dismantled waste, the DEWOCS system that elicits worker productivity factors, the DEEMOS system that can evaluate the costs of dismantling, and DEPES process.

This paper can manage data generated during the dismantling of KRR2 (Korean research reactor, TRIGA Mark-III) and calculate the amount of dismantled waste, derive worker productivity factors, and utilize these factors to assess the costs of dismantling and evaluate the decommissioning process in advance.

2. Decommissioning System Engineering

The decommissioning engineering system consists of five unit systems. Figure 1 illustrates the relationship between the decommissioning engineering system and the decommissioning project.

3. Activated concrete of the pool at the KRR2

3.1 Decommissioning cost on the dismantling procedure

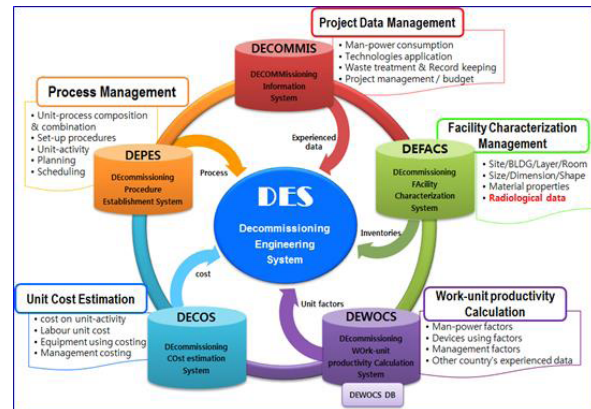


Fig. 1. Relationship diagram between unit systems.

Data entered in connection with the removal of activated concrete from the KRR-2 to the DEFACS which manages facility characteristics is shown in Table 1.

Table 1. The activated concrete structure input screen

Code Management	Facility Management	Productivity Calculation	Cost Evaluation	Prediction of Process
<input checked="" type="checkbox"/> Input WBS				<input checked="" type="checkbox"/> Input contamination
KRR-W>KRR-2>Remove an activated concrete>Dismantling an activated concrete				
Facility	KRR-W	Width(m)	17.7	
Building	KRR-2	Length(m)	9.9	
Layer/Area	Remove activated c	Height(m)	7.6	
Room		Diameter		
Equipment		Thickness(m)	0.01	
Capacity		Depth		
Amount		Specific gravity	2.7	
Building/Facility	<input checked="" type="checkbox"/> Buliding	Area(m ²)	15.96	
Contamination	<input checked="" type="checkbox"/> Contamination	Volume(m ³)	136.68	
Non-contamination	<input type="checkbox"/> Non-C			
Type	Cube	Weight(kg)	369.034	
Mateirals	Co-Concrete	Facility code		
Weighting factor		WBS code	K2-15.1	

The system has been programmed to enter detailed information about the structures to be dismantled in order to assess the amount of dismantled waste such as specifications and specific gravity, area, volume, weight, and contamination, form and material.

Worker productivity factors are evaluation factors that determine how much time an operator has spent in decontamination and dismantling the target structures (units, area, volume, and weight).

The equipment cost used for removal of an activated concrete during removal of concrete in the KRR 2 is calculated by multiplying the equipment cost associated with the equipment loss database with the corresponding equipment, equipment productivity factors and weights as basic data.

The costs incurred for each discipline are that 61,489,828 won was incurred for decommissioning operations, 13,724,189 won for radiation/radioactivity management and 8,069,112 won for quality control.

3.2 Results and Consideration

The reason why it is necessary to distinguish between the parts of activated and the non-activated prior to dismantling of KRR2 is not only that it can reasonably establish the dismantling process, but also it can reduce the exposure of workers and assess the costs of dismantling. Dismantling procedures were performed by considering that the buried piping is part of the radioactivity, and the remainder becomes the non-radiation part. We had a good lessons learned from the case study as below;

To prevent the contamination from spreading, the verification of the containment facility inside and outside was necessary during decommissioning of the activated structure, and also, for non-active parts, for the decommissioning in the environment wrapped

with temporary coating or temporary vinyl, it is necessary to prepare a contamination prevention plan.

One of the important issues during the decommissioning is to always consider the possibility of contamination spreading by decommissioning of the non-active parts using contaminated equipment.

There is a big difference in the decommissioning cost of the non-active part according to how to decide the active part and non-active zone. As a conclusion, in the process of assessing the decommissioning cost, as a result of decommissioning the non-active part first, the exposure reduction and contamination spread prevention effect can be obtained.

4. Conclusion

Using data generated from dismantling research reactors and conversion facilities, the dismantling engineering integration system was developed that can evaluate and predict significant factors such as the reduction of dismantling facilities and prediction of unit work productivity factors, cost of dismantling, and calculation of dismantling processes.

In addition, through the development of an integrated dismantling engineering system, other nuclear facilities and systems were developed to secure characteristics of dismantling unit, factors of dismantling unit productivity, quantity of dismantling waste, and field data of conversion facilities.

The calculated decommissioning productivity values can be used as a basis for inferring the plant's decommissioning productivity values, and since the plant has been programmed to provide the cost assessment results for dismantling operations by applying the actual government labor cost per dismantling operation.

6분과

방사선환경 및 안전 (Oral)



History of the Environmental Radioactivity Survey in Korea

Ju-Yong Yun

Korea Institute of Nuclear Safety, 62, Gwahak-ro, Yuseong-gu, Daejeon, Republic of Korea

k153yjy@kins.re.kr

1. Introduction

Space, including Earth, is filled with radiation. In any place, under any circumstances, the amount of radiation is extremely low, but it cannot be completely eliminated. Human beings are in a radiation environment because radiation exists in the entire environment that human beings are in contact with. I would like to describe the history of the environmental radioactivity survey in Korea.

2. Environmental Radioactivity Survey

2.1 Propose

The main propose of the environmental radioactivity survey are protecting the public health and preserving of environment from any radiological accident.

2.2 History

Environmental radioactivity survey was mainly aimed at assessing the impact of radioactive fallout caused by ground nuclear experiments in the 1950s and 1960s.

In the 1970s and 1980s, the survey was carried out to check whether nuclear facilities such as nuclear power plants had an environmental impact.

And in the 1990s there was a Russian dumping of radioactive material in the East Sea. Also, in the 2000s, it was necessary to monitor the radiation terrorism with the 9.11 terror. The targets of environmental radioactivity survey have been changed according to the times, such as the monitoring and detection of radioactivity leakage due to the nuclear activities of neighboring countries such as North Korea's underground nuclear tests.

In particular, the Fukushima nuclear power plants accident in Japan in March 2011 was an opportunity for the public to experience the importance of

environmental radiation monitoring.

2.3 Monitoring system

Environmental radiation monitoring system in Korea can be divided into the monitoring of the environmental radiation of the whole country and the environmental radiation monitoring around the nuclear facilities.

The Korean Institute of Nuclear Safety (KINS) has been conducting the environmental radioactivity monitoring for the entire country under the leadership of the government.

The main purpose of environmental radiation monitoring in the vicinity of nuclear facilities is to investigate the current concentrations and the long-term accumulation trends of radionuclides released from the nuclear facilities.

The environmental radioactivity monitoring was independently conducted by regulation body and its monitoring results are implemented to evaluate the environmental radioactivity monitoring results of licensees.

The normal environmental radiation/radioactivity level monitoring and emergency purpose environmental radiation/radioactivity monitoring on varying kinds of environmental samples, collected by the KINS (central radioactivity monitoring station) and the 15 regional radioactivity monitoring stations, are conducted based on the Article 105 (Monitoring of Nationwide Radiation Environment) of the Nuclear Safety Act.

Gross beta and gamma radioactivity concentration in the airborne dust, fallout, precipitation and tap water were periodically carried out at 15 Regional Radioactivity Monitoring Stations. Gamma-ray emitting radionuclides in airborne dust, fallout and precipitation collected at the Central Radioactivity Monitoring Station were also periodically analyzed.

The radiation monitoring station monitors the fluctuation of the environmental radiation level in real time. At this time, Integrated Environmental

Radiation Monitoring Network (IERNet) monitors ambient gamma dose rates by real-timely for a total of 170 sites, including 15 regional radioactivity monitoring stations and 155 radiation monitoring posts.

The monitoring data of the ambient gamma dose rate measured in these areas are collected and managed by the KINS in real time. The monitoring results are published to the public through the internet web page (<http://iernet.kins.re.kr>). The KINS also developed a real-time environment radioactivity information app (eRAD@NOW) using a mobile app to provide information to the public on anytime, anywhere.

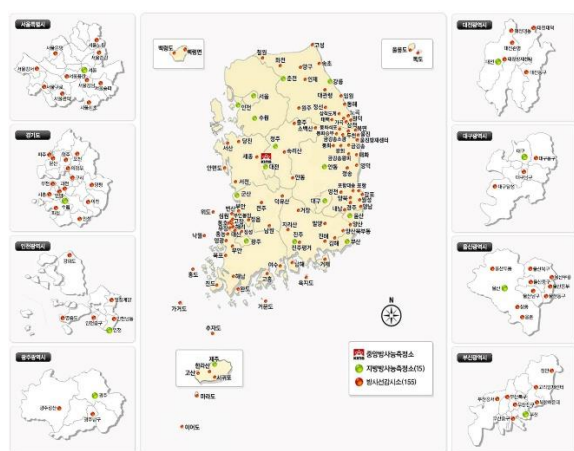


Fig. 1. Locations of radiation monitoring posts.

On the other hand, the marine environmental radioactivity survey around the Korean peninsula began with the announcement of the white paper on the Russian government's radioactive waste disposal at the East Sea in 1993, and KINS started to monitor the radioactivity of the seawaters around Korean peninsula in 1995.

The concentrations of ^{137}Cs , ^3H , ^{90}Sr , and $^{239+240}\text{Pu}$, and $^{240}\text{Pu}/^{239}\text{Pu}$ isotopic ratio were analyzed and assessed in the seawater samples, marine organism samples, and sediment samples, which were collected by help of the National Fisheries Research and Development Institute.

In order to monitor environmental radioactivity for the surface seawater, the seawater samples have been collected biannually at the fixed 21 stations off coast of Korea since 1994. The concentration of radionuclides and isotopic ratio between radionuclides in surface seawater were assessed using surveyed data cumulated from 1994.

The seawater in the specific layer and sediments were collected, respectively, at 6 stations and 16 stations once a year in order to obtain the concentrations and isotopic ratio of artificial radionuclides. The environmental radioactivity in marine organisms (fish, shellfish and seaweed) were determined biannually.

In Korea, the operator of facility shall conduct the survey of radiological environment and the evaluation of the impact of radiation on environment and file a report thereon to the Nuclear Safety and Security Commission (NSSC) in pursuance of Article 104 (1) of the Nuclear Safety Act.

Independently, when the NSSC deems it necessary to confirm the results of the survey and the evaluation of the operator of facility, he may conduct radiological environmental monitoring programs pursuant to the Article 104 (2) of the same act.

The KINS carries out the above radiological environmental monitoring around facilities every year in terms of implementation of the Article 104 (2) authorized by the NSCC in accordance with the Article 111(Delegation of Authority) of the same act.

3. Conclusion

As a part of environmental monitoring activities, the results of the environmental radioactivity analysis conducted by each institution are published in the form of reports on the internet site. And the government plans to database all the environmental radiation data of Korea and will provide it to the general public.

REFERENCES

- [1] Ministry of Science & Technology, Korea Institute of Nuclear Safety, "40 years of Environmental Radioactivity Monitoring" (2005).
- [2] Korea Institute of Nuclear Safety, "Environmental Radioactivity Survey in Korea", KINS/ER-028, vol.49 (2017).
- [3] Korea Institute of Nuclear Safety, "Marine Environmental Radioactivity Survey", KINS/ER-092, vol.13 (2017).
- [4] Korea Institute of Nuclear Safety, "The Annual Report on the Environmental Radiological Surveillance and Assessment around the Nuclear Facilities", KINS/AR-140, vol.28 (2017).

Experiences With the Ground Based and Mobile Gamma-Ray Spectrometry in Contaminated Areas of the Fukushima Prefecture

Young-Yong Ji^{1)*}, Mee Jang¹⁾, Taehyung Lim²⁾, Kun Ho Chung¹⁾, Mun Ja Kang¹⁾, and Wanno Lee¹⁾

¹⁾ Korea Atomic Energy Research Institute, 111, Daedeok-daero 989beon-gil, Yuseong-gu, Daejeon, Republic of Korea

²⁾ SI Detection Co., Ltd., 441, Expo-ro, Yuseong-gu, Daejeon, Republic of Korea

*yyji@kaeri.re.kr

1. Introduction

According to the lesson learned from nuclear accidents in Fukushima Daiichi nuclear power plant (FDNPP), the response technology against the accident should be systematically prepared to produce the quick and reliable information to appropriately support the decision making by the accident aspect, such as the early, intermediate, and recovery phase. This technology includes the assessment of the radioactivity distribution in the environment owing to the release from the accident. In JAEA (Japan Atomic Energy Agency), the mapping project [1-3] around Fukushima prefecture has been conducting to obtain the information on contaminated conditions, that is, contaminated ranges, radionuclides and their depth profiles and concentrations in the ground, and their temporal variations.

Diverse survey platforms, which mean backpack, carborne, and airborne survey, are generally applied to assess the dose rate and radioactivity from a series of large-scale environmental radiation monitoring. In addition, a ground-based gamma-ray spectrometry at 1 m above the ground should be accompanied with the mobile survey, because it can be particularly useful as reference values of mobile gamma-ray spectrometry. In KAERI (Korea Atomic Energy Research Institute), the studies on comprehensive environmental radiation survey (ERS) have been conducting for the purpose of systematically integrating diverse survey methods and their results.

The purpose of this study is to apply the method developed in KAERI to the ERS to around FDNPP in cooperation with JAEA. The joint experiments were then conducted in several contaminated areas of the Fukushima prefecture and the results were evaluated by comparing the data of JAEA. The dose rate and

radioactivity of radiocesium deposited in the ground were assessed using the ground based and mobile gamma-ray spectrometry equipped with LaBr₃(Ce) scintillation detectors.

2. Method and Results

2.1 Survey methods

Fig. 1 shows the survey sites around FDNPP. As a reference site, in situ gamma-ray spectrometry at 1 m above the ground was first conducted in Sendai city, which is located to about north 100 km distance from the FDNPP. Then, the mobile survey was performed using a backpack based on a LaBr₃(Ce) around the same site in which the ground based survey was done. With the same method, the ground based and mobile survey was conducted in two contaminated sites, which were about north 6 km and north-west 60 km distance from the FDNPP.



Fig. 1. The sites for the environmental radiation survey around the FDNPP.

2.2 Ground based gamma-ray spectrometry

Fig. 2 show the result of the ground based gamma-

ray spectrometry using a $\text{LaBr}_3(\text{Ce})$ detector, which was performed at 1 m above the ground using a tripod during about 1600 sec. The intrinsic background of used $\text{LaBr}_3(\text{Ce})$ detector was successfully subtracted and then three peaks contributing radiocesium, as shown in Table 1, analyzed to calculate the dose rate and radioactivity of ^{134}Cs and ^{137}Cs .

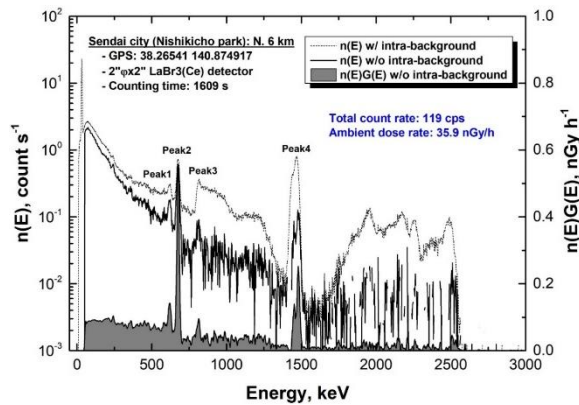


Fig. 2. The energy spectra for count rate and dose rate measured in Sendai city.

Table 4. The peak information in measured energy spectrum

Peak	Peak information
1	^{134}Cs (605 keV, 97.6%), ^{214}Bi (609 keV, 46.4%)
2	^{137}Cs (662 keV, 85.0%)
3	^{134}Cs (796 keV, 85.5%), ^{134}C (802 keV, 8.69%)
4	^{40}K (1461 keV, 10.6%)

2.3 Mobile gamma-ray spectrometry

The backpack and carborne survey based on a $\text{LaBr}_3(\text{Ce})$ detector were performed in contaminated areas around the FDNPP, after the ground based gamma-ray spectrometry. Fig. 3 shows the mapping result of ambient dose rate using the backpack survey at the site of about north 6 km from the FDNPP. The averaged ambient dose rate was 68.1 ± 13.7 nGy/h in the survey site.

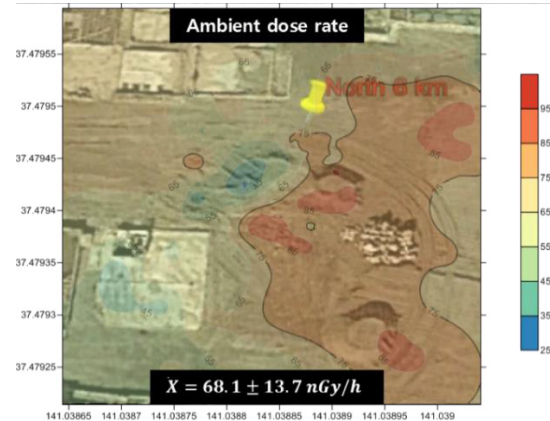


Fig. 3. The mapping results of ambient dose rate using the backpack survey.

3. Conclusion

The diverse survey methods were developed to calculate the ambient dose rate as well as individual dose rate of detected gamma nuclide and its radioactivity in the contaminated area. Therefore, it is very important to conduct the feasibility of developed survey technology in the real contaminated site. From the joint experiment with JAEA, the KAERI's method was successfully performed and applied to the environmental radiation survey around the FDNPP.

ACKNOWLEDGMENTS

This work was performed under the auspices of the Ministry of Science and ICT of Korea, NRF contract No. NRF-2017M2A8A4015256.

REFERENCES

- [1] S. Mikami et al., "The air dose rate around the Fukushima Dai-ichi Nuclear Power Plant: its spatial characteristics and temporal changes until December 2012", J. Environ. Radioact. 139: 250-259 (2012).
- [2] S. Mikami et al., "In situ gamma spectrometry intercomparison in Fukushima, Japan", Jpn. J. Health Phys. 50(3): 182-188 (2015).
- [3] S. Tsuda et al., "Characteristics and verification of a car-borne survey system for dose rate in air: KURAMA-II", J. Environ. Radioact. 139: 260-265 (2015).

Gaseous Tritium Measurement Using Plastic Scintillator

Jun Woo Bae* and Hee Reyoung Kim

Ulsan National Institute of Science and Technology, 50, UNIST-gil, Eonyang-eup, Ulju-gun, Ulsan, Republic of Korea

*skypia12@unist.ac.kr

1. Introduction

Tritium is one of concerning radioactive nuclide during operating or decommissioning of nuclear power plant. Tritium is difficult to detect because it only emits beta ray with very low energy (~ 18.6 keV). In general, radioactivity of tritium is analyzed using liquid scintillation counter (LSC) [1]. Tritium detection using LSC has merit of high accuracy, but it generates organic waste which is harmful to the environment. Therefore, analysis of huge amount of sample using LSC is not preferred. For this reason, studies to measure the tritium using vaporization or gasification have been conducted for routine monitoring of tritium [2–3]. Detection efficiency of the beta ray emitted from the tritium in liquid state is extremely low due to self-absorption. So that, detection of gasified tritium has a merit of increase of detection efficiency without using liquid scintillation cocktail.

In this study, two types of gaseous tritium detector based on the plastic scintillator were designed. The detectors were designed suitable for the continuous and waste-less detection of gaseous tritium. Estimation of detection efficiency was carried out for those detectors.

2. Materials and Methods

2.1 Design of detectors

Two types of detector design were proposed: one was pellet-filling type and the other one was reflector type. All scintillators were polystyrene based plastic scintillator with maximum emitted wavelength of 415 nm. For pellet-filling type, 200 of small cylindrical plastic scintillators (5 mm (H) \times 5 mm (Φ)) were filled in a detection chamber (20 mm (H) \times 50 mm (Φ)). Two circular plastic scintillators (1 mm (H) \times 50 mm (Φ)) were used to seal the detection

chamber. For reflector type, there was no pellet scintillator in the chamber. Otherwise, Teflon tape was coated inside the detection chamber to increase light collection efficiency.

The detection chamber was same to the both type. The detection chamber was fabricated by processing 60 mm \times 60 mm acrylic bulk. There were holes for two facing sides with diameter of 51 mm to fix the photomultiplier tubes (PMTs).

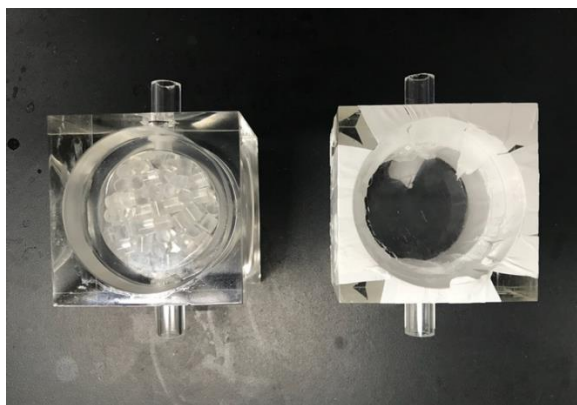


Fig. 1. The pellet-filling type detector (left) and the reflector type detector (right).

2.2 Light detecting apparatus

The light detecting apparatus was used to detect the light produced by interaction between beta ray and the scintillator. The apparatus consisted PMT and sockets, and nuclear instrument modules(NIMs) for coincidence measurement of the signals from two PMTs. The photomultiplier tubes were optically coupled with the plastic scintillators which were attached to the detection chamber.

2.3 Hydrogen gas preparation

The detection efficiency of each detector was estimated by using self-produced tritiated hydrogen gas through electrolysis. 10-stack of proton-exchange membrane electrolysis cell was used and 7A of

current was applied to the electrolysis cell. The tritium concentration of the produced gas was quantified using a fractionation factor [4]. The tritium concentrations of self-produced hydrogen gas were 1,600 and 1,020 kBq/m³, respectively. Fig. 2 shows the conceptual diagram of the experimental process.

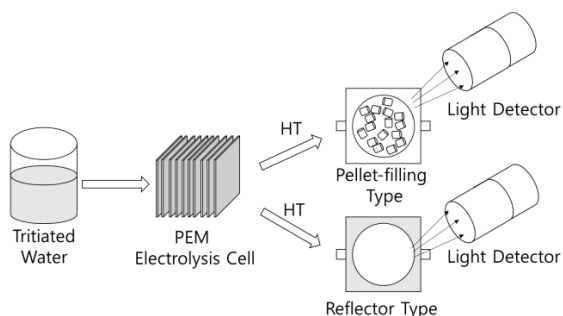


Fig. 2. Conceptual diagram of the experimental process.

3. Results

The detection efficiency of each detector was estimated using the self-produced tritiated hydrogen gas. Net counting rates for pellet-filling and reflector type detector were 0.56 and 1.7 cps, respectively. The tritium activity in the chamber was calculated taking into account the volume reduction of the detection chamber by the pellets. Detection efficiencies for the detectors were 1.78 and 4.25%, respectively. The reflector type showed 2.4 times higher detection efficiency than the pellet-filling type.

Table 1. Detection efficiency estimation according to the type of detector

Detector	Pellet-filling	Reflector
Net Counting Rate (cps)	0.56	1.7
Tritium Concentration (kBq/m ³)	1,600	1,020
Volume of the Chamber (m ³)	1.96×10^{-5}	3.93×10^{-5}
Tritium Activity in the Chamber (Bq)	31.4	40.1
Detection Efficiency (%)	1.78	4.25

4. Conclusion

Two designs for the gaseous tritium measurement using plastic scintillator were proposed. One was

designed to increase the area of the interaction with tritium, and the other was designed to increase the light collection efficiency. It was confirmed that the light intensity after the interaction with the tritium was very low, so that it was effective to increase the light collection efficiency. For future works, detector designs to increase both light collection efficiency and interaction area with tritium will be considered. Also, increasing the size of the detection chamber without loss of detection efficiency will be further studied to allow more tritium into the chamber and lower the detection limit.

ACKNOWLEDGEMENT

This work was supported by the Industrial Technology Innovation Program (Real-Time Underwater Tritium Monitoring Technology by Electrolysis) through the Korea Institute of Energy Technology Evaluation and Planning under Grant 2016520101340.

REFERENCES

- [1] S. Yoon, W.H. Ha, and S.S. Lee, "Tritium analysis of urine samples from the general Korean public.", *Applied Radiation and Isotopes*, 81, 276–278 (2013).
- [2] E. Furuta, Y. Kato, and S. Fujisawa, "Measurement of tritium with plastic scintillators in large vials of a low background liquid scintillation counter: an organic waste-less method", *Journal of Radioanalytical Nuclear Chemistry*, 314, 701–708 (2017).
- [3] A.M. SOREEFAN and T. A. DEVOL, "Proportional Counting of Tritium Gas Generated by Polymer Electrolyte Membrane (PEM) Electrolysis", *Journal of Radioanalytical Nuclear Chemistry*, 282, 517 (2009).
- [4] J.W. Bae, U. Lee, and H.R. Kim, "Development of continuous inflow tritium measurement in water technology using electrolysis and a plastic scintillator", *Journal of Radioanalytical and Nuclear Chemistry*, 314(2), 689–694 (2017).

Review of Radiological Criteria for License Termination in Korea

Jung Hwan Jang¹⁾, Ki Hoon Kim¹⁾, Sang Jin Kim¹⁾, Cheol Kyu Choi²⁾, and Kwang Pyo Kim^{1)*}

¹⁾ Kyunghee University, 1732, Deokyoung-daero, Giheung-gu, Yongin-si, Gyeonggi-do, Republic of Korea

²⁾ Korea Institute of Nuclear Safety, 62, Gwahak-ro, Yuseong-gu, Daejeon, Republic of Korea

*kpkim@khu.ac.kr

1. Introduction

Korean government decided permanent shutdown of Kori #1, the first commercial nuclear power plant (NPP) in Korea. The Nuclear Safety Act defines ‘decommissioning’ as all activities for the purpose of excluding from the application of the Nuclear Safety Act by permanently shutdown of a facility that has been licensed or designated, dismantling the facility and site, or removing radioactive contamination [1]. In order to release the site, it is necessary to establish radiological criteria for license termination after decontamination and dismantling.

In 2016, radiological criteria for license termination was enacted from Nuclear Safety and Security Commission Notice 2016-33. This is to organize the safety regulation system in preparation for the decommissioning of nuclear facilities, such as permanent shutdown of Kori #1. However, there is a lack of technical review about radiological criteria for license termination.

The objective of this study was to review the radiological criteria for license termination in Korea. Radiological criteria and rationales in foreign country and international organization were reviewed.

2. Radiological criteria for license termination

Table 1 shows domestic and overseas radiological criteria for license termination. Radiological criteria are generally classified as unrestricted use and restricted use of a site.

Table 1. Summary of domestic and overseas radiological criteria for license termination

Nation	Type	Dose constraint
Korea [2]	Unrestricted use of a site	The effective dose for a member of a critical group that considering all relevant exposure pathways due to residual radioactivity should not exceed 0.1 mSv/y

	Dose is expected to exceed 0.1 mSv in a year	Restricted use is allowed if the dose for a member of a critical group does not exceed 0.1 mSv/y
	Restricted condition is to fail when reuse in the second criteria	Demonstrate that the dose for a member of a critical group does not exceed 1 mSv/y
US [3]	Radiological criteria for unrestricted use	Background radiation results in a TEDE to an average member of the critical group that does not exceed 25 mrem/y(0.25 mSv/y)
	If the institutional controls were no longer in effect	100 mrem /y(1 mSv/y) 500 mrem/y (5 mSv/y)
IAEA [4]	Unrestricted use of a site	Optimization of protection that the effective dose to a member of a critical group is kept below the dose constraint of 0.01 mSv/y ~ 0.3 mSv/y.
	Restricted use of a site	0.3 mSv/y (if the restrictions were to fail in the future the effective dose should not exceed 1 mSv/y)
ICRP [5]	Dose constraint for public exposure and for prolonged exposure	No more than about 0.3 mSv/y and should be less than 1 mSv/y

2.1 Korea

Radiological criteria for license termination in Korea are specified in Nuclear Safety and Security Commission Notice 2016-33. Domestic criteria were established by reviewing criteria for international organization and countries with decommissioning experiences such as the United States.

2.2 US

U.S. Nuclear Regulatory Commission analyzed the

impacts and costs associated with obtaining various dose levels for release considerations of the sites. As a result, the following trends can be seen. (1) For unrestricted use, no definitive conclusion can be made on a basis which would distinguish between acceptable alternative residual radioactivity levels in the range of 15-25 mrem/y. (2) For soil, level less than 25 mrem/y generally result in a cost-benefit ratio not considered reasonably justifiable under NRC's regulatory framework. NCRP No.116 also recommended that no single source or set of sources under one's control should result in an individual being exposed to more than 25 mrem/y.

2.3 IAEA

Figure 1 shows dose constraint for the release of sites from IAEA. According to IAEA WS-G-5.1, it is reasonable and appropriate to have different dose constraints for the release of sites than for the clearance of material from regulatory control. The clearance of material may take place frequently over the lifetime of a practice, as well as at the termination stage. The cleared material may enter into trade with a broad range of potential uses and should comply with clearance criteria, which are of the order of 0.01 mSv in a year. The dose criteria for the release of site from regulatory control can be higher than those for the clearance of material, because site remains in place and hence the degree of certainty about the potential uses of the site is higher than the degree of certainty associated with the uses of material after its release from regulatory control. Therefore it is reasonable to allow a larger fraction of the individual dose limit for the release of sites.

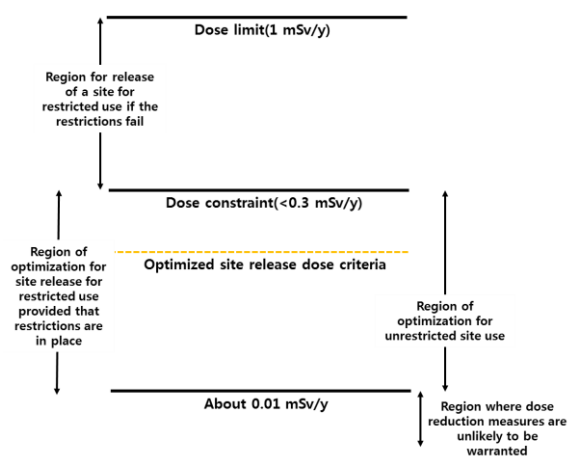


Fig. 1. Constrained optimization and regions of effective dose for members in the release of sites.

2.4 ICRP

ICRP 77 was the first publication proposing a numerical value for the public dose constraint. It is described that the dose constraint should be less than 1 mSv and that a value of no more than about 0.3 mSv would be appropriate. Dose constraint level should be established on a case-by-case basis, 'with consideration of the maximum annual dose that would be acceptable from a new source at a single location, taking into account exposures from other sources subject to control and equity considerations'. The value of 0.3 mSv/y implicitly means to allow for exposures to multiple sources.

3. Conclusion

In this study, we reviewed the radiological criteria and rationales in US, IAEA and ICRP. Domestic criteria were established by reviewing international organization and criteria for countries with decommissioning experiences such as the United States. Based on this information, it will contribute to improve the regulatory system in accordance with the site restoration.

ACKNOWLEDGEMENT

This work was supported by the Nuclear Safety Research Program through the Korea Foundation Of Nuclear Safety(KoFONS) using the financial resource granted by the Nuclear Safety and Security Commission(NSSC) of the Republic of Korea. (No. 1805016).

REFERENCES

- [1] Nuclear Safety Act, Act No.12666 (2018).
- [2] NSSC, Criteria for Reuse of Site and Remaining Buildings after Completion of Decommissioning of Nuclear Facilities, Notice 2016-33 (2016).
- [3] 10 CFR Part 20 Subpart E, Radiological Criteria for License Termination, 20.1401, 20.1402, 20.1403, 20.1404 (2017).
- [4] IAEA, Release of Sites from Regulatory Control on Termination of Practices, WS-G-5.1 (2006).
- [5] ICRP, Protection of the Public in Situations of Prolonged Radiation Exposure, ICRP 82 (1999).

Geometric Effects of YAlO₃:Ce Scintillator to Autonomous Radiation Monitoring Performance in the Marine Environment

Chanki Lee* and Hee Reyoung Kim

Ulsan National Institute of Science and Technology, 50, UNIST-gil, Eonyang-eup, Ulju-gun, Ulsan, Republic of Korea

*lck1992@unist.ac.kr

1. Introduction

Scintillation detector has wide-range application to in-situ environmental radiation monitoring thanks to its advantages such as rapid analysis, low sensitivity to temperature change, and so on. However, there have been limited attempts [1] to measure marine environmental radiation in the depth up to few kilometers on site, while YAlO₃:Ce is seen to be suitable material having chemical and mechanical stability. Also, an improved radiation detection system can be developed if combined with autonomous underwater vehicles, which provide ability to survey wide-range area. In this paper, therefore, we suggest a new marine radiation monitoring system based on a YAlO₃:Ce scintillation detector and autonomous underwater vehicle. Especially, geometric effects of the scintillator to hydrodynamic performance and detection efficiency are analyzed computationally.

2. Experimental methods

2.1 Description of detection system

Among various autonomous underwater vehicles, autonomous underwater glider having body length and diameter of 150 cm and 20 cm, respectively, was assumed. The forward section of the glider was supposed to be replaced with YAlO₃:Ce scintillator of semispherical and conical geometry with specific thickness (Fig. 1). The surface area (S) of both shapes was set to be same.

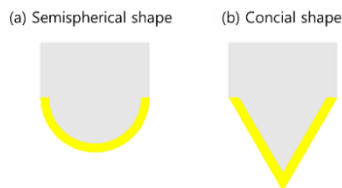


Fig. 1. Assumed geometry of YAlO₃:Ce scintillator adopted to an autonomous underwater glider.

2.2 Hydrodynamic performance calculation

Stress and drag coefficient on the scintillator were calculated to optimize thickness and analyze shape effect, respectively. Submerging seawater depth of the detection system was set as 2 km, and minimum thickness ($t_{semisphere}$ and t_{cone}) to resist relevant hydrostatic pressure (p) is calculated as Equations 1 and 2 with safety margin (f) of 3.

$$t_{semisphere} = \frac{p \cdot d \cdot f}{4\sigma_{max}} \quad (1)$$

$$t_{cone} = \frac{p \cdot d \cdot f}{2\sigma_{max} \cos(0.5\theta)}, \quad (2)$$

where d is body diameter, σ_{max} is flexural stress, and θ is cone angle.

In order to calculate drag coefficient, velocity of seawater flow (v) was assumed to be 0.3, 0.6, 0.9, 1.2, and 1.5 m/s through $\Phi 2 \times 10$ meters open enclosure. Drag force (F_d) calculated by using ANSYS code was converted to the drag coefficient (c_d) by Equation 3, where ρ is density of water.

$$c_d = \frac{2 \cdot F_d}{\rho \cdot v^2 \cdot S'} \quad (3)$$

2.3 Detection efficiency calculation

After determining the minimum thickness required to resist high pressure of surrounding seawater, detection efficiency was calculated by F8 tally of MCNP6 code. Maximum thickness was set as 2.5 cm [2]. Detection efficiency (ϵ) was converted to volumetric efficiency (ϵ_v), defined as Equation 4, where effective surrounding volume (v_{eff}) of radioactive sources was calculated from effective range (R_γ) experiencing 99.7% attenuation (Equation 5, where μ is attenuation coefficient).

$$\epsilon_v = \epsilon \cdot v_{eff}, \quad (4)$$

$$R_\gamma = -\frac{\ln 0.003}{\mu \cdot \rho} \quad (5)$$

3. Results and discussion

Minimum thickness required for semispherical and conical shape is 1.1 cm and 2.4 cm, respectively. Calculated drag coefficient of each shape is represented in Fig. 2, which is in the range around 0.1. Conical shape has lower drag coefficient because of its relatively sharp and streamlined geometry toward seawater flow.

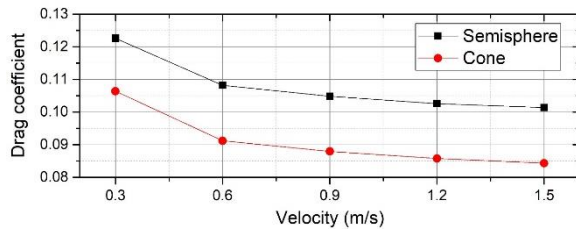


Fig. 2. Drag coefficient of semispherical and conical shape for different flow velocity.

Volumetric efficiency according to $\text{YAlO}_3\text{:Ce}$ thickness in case of semispherical shape is described in Fig. 3. As energy increases, the efficiency difference among different thickness becomes significantly larger, while the efficiency of 2.5 cm thickness reduces smaller than 50% at 2.0 MeV.

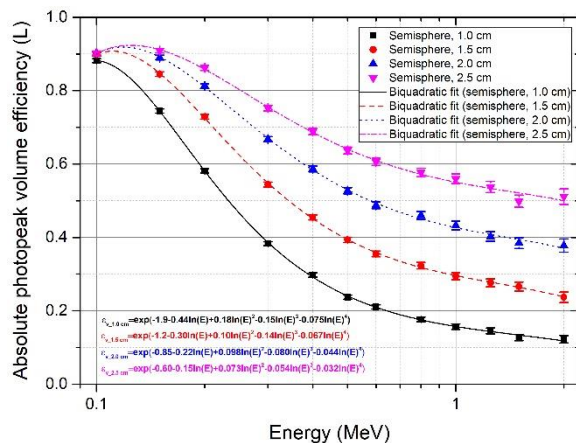


Fig. 3. Volumetric efficiency for different thickness of semispherical $\text{YAlO}_3\text{:Ce}$ scintillator.

Difference of volumetric efficiency with 2.5 cm thickness between semispherical and conical shape is shown in Fig. 4. Both shapes have similar tendency, where the difference of efficiency values are within 10 % throughout the entire range of 0.1-2.0 MeV. They have much higher efficiency (> 0.3 L) than general $\Phi 3 \times 3$ inches NaI scintillator.

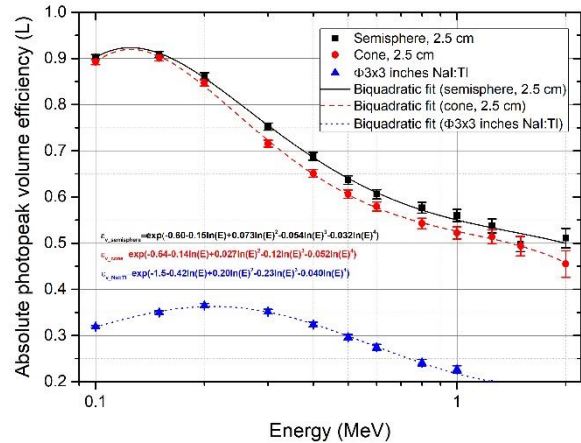


Fig. 4. Volumetric efficiency for different shapes of $\text{YAlO}_3\text{:Ce}$ scintillator.

4. Conclusion

In order to suggest and optimize a new autonomous radiation monitoring system, geometric effects of $\text{YAlO}_3\text{:Ce}$ scintillator were computationally analyzed. If proper thickness is provided, conical shape is beneficial to minimize drag force about 20% less than that of semispherical one. In contrast, semispherical shape is advantageous having detection efficiency higher than about 10% than conical one. For further optimization, the other streamlined shape (e.g., Myring shape) should be analyzed.

ACKNOWLEDGEMENT

This work was supported by the Ulsan City Support Project Research Fund (1.180026.01) of UNIST (Ulsan National Institute of Science & Technology).

REFERENCES

- [1] C. Tsabaris et al., An autonomous in situ detection system for radioactivity measurements in the marine environment, *Applied Radiation and Isotopes*, 66, 1419-1426 (2008).
- [2] J.D. Stachiw, Glass or Ceramic Spherical-Shell Window Assembly for 20,000-PSI Operational Pressure, Naval Undersea Center (1974).

Experimental Characterization on Accuracy of Multi-Detector Boron Meter

Si Hyeong Sung^{a)*}, Jin Bok Cho^{b)}, and Hee Reyoung Kim^{a)}

^{a)} Ulsan National Institute of Science and Technology, 50, UNIST-gil, Eonyang-eup, Ulju-gun, Ulsan, Republic of Korea

^{b)} USERS Incorporated Company, 65, Techno3-ro, Yuseong-gu, Daejeon, Republic of Korea

*shlove912@unist.ac.kr

1. Introduction

Accurate measurement of the concentration of boric acid can improve the safe operating environment by preventing dilution accident of PWR. The boron meter, which is a boron concentration measurement technique, is capable of on-line measurement but has a high error (2%). Therefore, a study was conducted to solve the error by measuring the stable count regardless of the concentration using the selective detector measurement method. The previous MCNP simulation studies show that the accuracy of the multi detector boron meter is improved (0.4%) [1] and the accuracy improvement is 65% compared with the single detector boron meter through experiments which based on simulation [2]. The accuracy of the multi - detector boron meter was confirmed through previous studies and the system was constructed for the experiment in the actual cooling water circulation environment. In this paper, a study was conducted to measure and analyze the accuracy of 0 to 5000 ppm boric acid concentration measurement of a multi-detector boron meter in a real reactor environment through a coolant circulation system.

2. Method

Fig. 1 shows the design of a multi-detector boron meter. The fast neutrons emitted from the source (Eckert & Ziegler, N20 capsule, 1 Ci) inserted in the central. The internal detector uses four LND 20292 BF₃ detectors (11.3 cps/nv) and two LND 2528 ³He detectors (28 cps/nv).

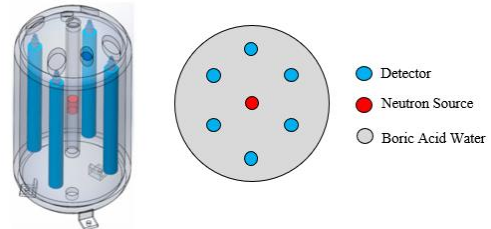


Fig. 1. Design of Boron Meter.

Fig. 2 shows the boron water circulation system including the boron meter.

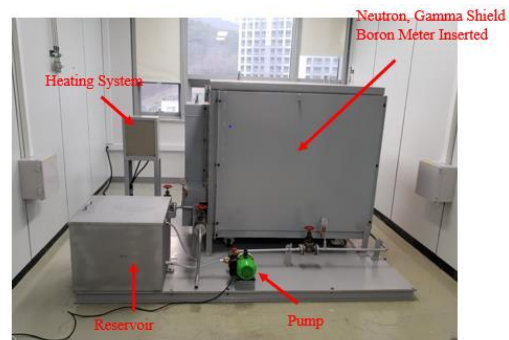


Fig. 2. Boric Acid Water Circulation System.

A circulation system creates a reactor coolant circulation environment (60 psig). A temperature of 49°C is set through the heating system, and 18 concentrations (0 ~ 5000 ppm) of boric acid are prepared and inserted into the circulation system. Based on the measured values, boron concentration conversion equation shown as Eq. (1) was produced.

$$P = \frac{1}{c_1 X^4 + c_2 X^3 + c_3 X^2 + c_4 X + c_5} \quad (1)$$

The coefficients C_{series} of the fitting function were obtained by using least square fitting, and the boron concentrations X were obtained from the curve with the known coefficients and the count rate P were measurement values. The accuracy of the fitting function was confirmed by a repeatability test of seven concentrations.

3. Result and discussion

The measured count rate and the fitting curve which obtained by 18 concentrations are shown in Fig. 3.

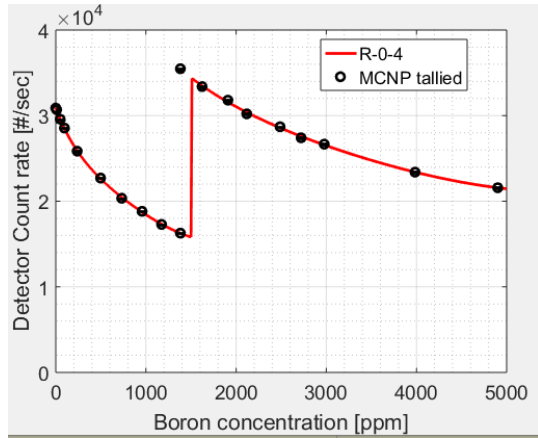


Fig. 3. Measure count rate and rational-0-4 fitting curve.

The accuracy of the boron concentration conversion equation was verified by comparing the boron concentration calculated by the fitting curve with the boron concentration value used in the actual experiments. A standard error of 6.964 ppm was observed in the range of less than 1500 ppm using the low sensitivity detector and a standard error percentage of 1.131% was observed in the range of 1500 ~ 5000 ppm. Therefore, it is possible to confirm the improved accuracy compared to the single-detector boron meter which generates 2% standard error percentage in 0 ~ 5000 ppm range.

Table 1 shows the comparisons and errors between manufactured concentration values and fitting curve calculation values.

Table 1. Experimental value and theoretical value

Boron concentration [ppm]	Rational-0-4 equation calculation [ppm]	Error [ppm]
98.212	105.075	6.863
488.865	490.270	1.405
933.040	944.806	11.766
1418.220	1338.500	-79.720
1418.220	1341.710	6.510
1903.190	1892.160	-11.030
2825.790	2887.570	61.780
3753.500	3777.110	23.610

The standard error of 19.91 ppm was observed in the range of less than 1500 ppm and standard error percentage of 1.76% was observed in the range of 1500 ~ 5000 ppm. which means that accuracy is 12% improved when the multi-detector boron meter method is introduced.

4. Conclusion

Accuracy analysis of multiple detector boron meter in actual coolant circulation environment was performed and the results were analyzed Compared to conventional single-detector boron meters, 43.45% improved accuracy is achieved. For the repeatability test, the re-measured count rate was used to evaluate the accuracy and the performance was improved by 12%. The introduction of a new concept of boron meter is expected to improve the stability of the nuclear power plant operation.

ACKNOWLEDGMENTS

This work was supported by the Nuclear Power Core Technology Development Program of the Korea Institute of Energy Technology Evaluation and Planning (KETEP) granted financial resource from the Ministry of Trade, Industry & Energy (No. 20151520100930).

REFERENCES

- [1] C. Kong, H. Lee, S.H. Kim, S. Lyou, D. Lee, "Accuracy Improvement of Boron Meter Adopting New Fitting Function and Multi-Detector, Nuclear Engineering and Technology, Volume 48, pp 1360-1367 (2016).
- [2] S.H. Sung, H.R. Kim, "Experimental characterization of the accuracy of multidetector boron meter for operational safety of reactors, Int J Energy Res. 2018;1-9 (2018).

Environmental Radioactivity Evaluation of Water Samples Around Nuclear Power Plant Near Ulsan

Ki Joon Kang*, Chanki Lee, and Hee Reyoung Kim

Ulsan National Institute of Science and Technology, 50, UNIST-gil, Eonyang-eup, Ulju-gun, Ulsan, Republic of Korea

*roffl1234@unist.ac.kr

1. Introduction

Recently, the public concern about nuclear safety has been elated because of Gyeongju earthquake. In this paper, the radioactivity of tritium, and gross β of samples from sea and river water around nuclear power plant near Ulsan in Korea are measured by using LSC (Liquid Scintillation Counter) and gas proportional counter. The results are analyzed in comparison with radioactivity from the site around other nuclear power plants for the public safety.

2. Material and Methods

2.1 Water Sampling

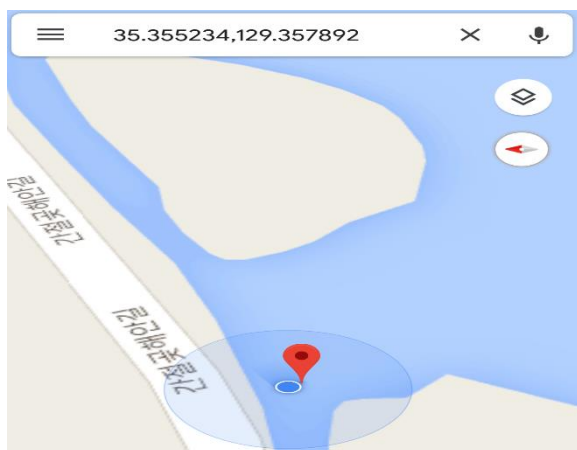


Fig. 1. GPS Data of Sampling Place (Gangeolgot).

Samples are taken in august. Seawater samples are taken from three sites (Gangeolgot, Bangerjin, Columnar Joint) in consideration of the distance from the nuclear power plant. The river water samples are taken from other three sites (Myeongchon bridge, Gaeun bridge, Samho bridge). The consideration of water sampling is TDS (Total Dissolved Solids). TDS is important indicator determine the quantity of gross β pretreatment.

2.2 The Pretreatment

In the case of tritium, samples are pretreated by heat exchange between inner tube and outer tube. By heating samples, water vapor containing HTO molecules is separated from impurities. And water vapor of inner tube is cooled by the cold water (20°C) pass outer tube and liquefied. Liquefied water is captured in vial. Up to be 20 mL of liquefied water, pretreatment process is proceeded. Before pretreated sample is detected by LSC, detection efficiency should be calibrated. Calibration method is referred in “H3 Analysis Guide in Solid Samples”, Korea Atomic Energy Research Institute [1]. The cocktails with diverse mixing ratio of tritium standard source and liquid scintillator are detected by LSC. And optimal mixing ratio should be found by calculating quenching efficiency. Quenching efficiency, E_c is calculated by equation (1).

$$E_c = \frac{\text{Net count rate of the standard (cpm)}}{\text{Activity of the standard (dpm)}} \times 100(\%) \quad (1)$$



Fig. 2. Tritium Pretreatment (Heat Exchange Cooler).

After calibration, pretreated samples are detected in LSC. In the case of and gross β , only river water samples are pretreated. Because there is much natural radionuclide like potassium, so artificial radioactivity detection results can be incorrect. According to TDS value, 10 mL or 250 mL of each river sample are

filled in evaporating dish. Preventing burn up, samples of evaporating dish are heated on heating plate during 30~40 minutes. After evaporation of water by heating plate, samples are dried in infrared ray drying machine. And then, dried samples for detection of gross β are measured by using gas proportional counter.

2.3 Radioactivity Analysis

As shown in equation (2), the radioactivity concentration, R is calculated using detection efficiency by calibration, count rate by detector (cpm), the volume of sample, V and detection time, t.

$$R \text{ (Bq/L)} = \frac{60 \times \text{Net count rate of the sample (cpm)}}{0.01 \times E_C \times V} \quad (2)$$

3. Results and Conclusion

The results by detection are compared to radioactivity survey results from other nuclear power plants. Tritium radioactivity concentration around other nuclear power plant is referred in “Environmental Radiation Monitoring Around the Nuclear Facilities”, Korea Institute of Nuclear Safety [3]. In case of tritium, the results are lower than the radioactivity concentration standard of drinking water, 5 Bq/L. These results can be evaluated as safety data. However, detail detection by more sampling and analysis are needed.

Table 1. Tritium Radioactivity Concentration around Nuclear Power Plant, 2016 (Unit: Bq/L)

Power Plant	KINS Survey Result Average (Min-Max)	KHNP Survey Result Average (Min-Max)
Kori	2.05 (0.09-2.43)	1.62 (0.99-24.4)
Wolsung	11.8 (0.28-113)	2.85 (1.08-33.5)
Hanbit	3.79 (0.34-13.1)	6.40 (1.81-60.9)
Hanul	0.412 (0.15-1.09)	1.39 (1.05-2.96)

In case of gross β , the results from river water is

similar with the results from Wolsung power plant. The results from Wolsung power plant is referred in “Environmental Radiation Monitoring Around the Nuclear Facilities”, Korea Institute of Nuclear Safety [3]. The difference between ‘Samho bridge’ and other two points is large. And, the results from other two points are also lower than gross β thresholds. Therefore, the results of gross β are evaluated as safe data.

Table 2. Gross β of Water around Wolsung Power Plant (Unit: Bq/L)

Sample	Radioactivity Concentration Average (Min-Max)
1 Drain	11.01 (6.52-14.5)
2 Drain	11.6 (8.23-12.5)
Bonggil	7.58 (5.77-12.9)

Table 3. Gross β Radioactivity Concentration of Water Samples (Unit: Bq/L), August

Water Type	Sampling Place	Gross β
River Water	Samho bridge	0.52
	Gaeun bridge	6.79
	Myeongchon bridge	9.40

ACKNOWLEDGEMENT

This work was supported by the Ulsan City Support Project Research Fund (1.180026.01) of UNIST (Ulsan National Institute of Science & Technology).

REFERENCES

- [1] Hee Reyoung Kim, “H3 Analysis Guide in Solid Samples”, Korea Atomic Energy Research Institute, March 31, 2007.
- [2] “The Annual Report on the Environmental Radiological Surveillance and Assessment around the Nuclear Facilities”, Korea Institute of Nuclear Safety, December, 2016.
- [3] “Environmental Radiation Monitoring Around the Nuclear Facilities”, Korea Institute of Nuclear Safety, March, 2017.

6분과

방사선환경 및 안전 (Poster)



Review of Emergency Alert System for Foreigner

Bongseok Kim*, Goanyup Lee, Jongsoo Kim, Hyun Ki Kim, Seungyeon Baek, Kanghyeon Lee, and Hae-Cho Lee
Korea Atomic Energy Research Institute, 111, Daedeok-daero 989beon-gil, Yuseong-gu, Daejeon, Republic of Korea

*kbs@kaeri.re.kr

1. Introduction

If an emergency situation occurs in KAERI, the emergency information will be broadcast only in Korean. However, foreigners who are work or research in KAERI is about 100. And they could not understand Korean well. What would happen to these people in real emergency situation without emergency broadcast for them? They could not get adequate information in adequate time. Which means that it can cause casualties.

The purpose of emergency preparedness is to save the lives. Thus, emergency information should be broadcast in adequate language for everyone.

2. Case study

2.1 Tsunami warning in Japan

In Japan, when a tsunami occurs, tsunami warning is broadcast on TV. Tsunami warning initially appears as subtitle in Japanese with a map. After subtitle, the full screen alarm starts with specific information of tsunami in Japanese. After then, tsunami warning broadcast in other languages, which are English, Korean, Chinese and Portuguese.



Fig. 1. Tsunami warning screen.

2.2 Multilingual App in Japan

Docomo, which is mobile service provider in Japan, develops prototype multilingual app for disaster warning. This app notify information of disaster in English, Chinese, Korean, Spanish and Portuguese.

The disaster warning service, which is called 'Area Mail', distributed disaster warnings issued by the Japan Meteorological Agency, and also local disaster and evacuation information issued by national and regional public institution. However, these disaster information is provided only in Japanese.

The new app provide disaster information from 'Area Mail' in the preset language. Thus, people who don't understand Japanese could receive the disaster information in time.



Fig. 2. Example of information in multilingual app.

2.3 Phone interpreters in Japan

Japan will host the Olympics in 2020. Thus, Japanese government plan to develop a new helping

foreigners who need emergency assistance. Currently, there is language barrier between tourists and fire department in Japan. The new support system, which is planned to develop, could mediate phone conversation between tourists and fire department.



Fig. 3. Example of phone interpreters.

2.4 Fire Alarm of Hotel and Airport

In general, there is many foreigner in hotels and airport. If an emergency situation occurs in these places, the alarm should be broadcast in multiple languages. The most hotels and airports have multilingual emergency broadcast systems. It could be helpful for foreigners.

2.5 Multilingual disaster alert app in Korea



Fig. 4. Emergency Ready app screen.

Korea hosted the PyeongChang Olympics in 2018. Thus, Korean government launched ‘Emergency Ready’ app. The real-time disaster information such as storms and earthquakes, could be sent in English and Chinese through this app. This app bolster emergency support for foreigners.

3. Application in KAERI

In KAERI, emergency alarm broadcast through a speaker which is installed in all buildings in KAERI. All foreigners in KAERI could understand English. Therefore, if emergency alarm broadcast in English, emergency information could reach out all foreigners in KAERI. Thus, the emergency alarm system is added to English broadcast which follows Korean broadcasting.

4. Conclusion

The adequate emergency information spread is essential to save the lives. Thus, emergency information should be understandable for everyone regardless of the language used by receiver. Therefore, Emergency alarm system should be developed in multiple languages.

REFERENCES

- [1] Nuclear emergency preparedness team, KAERI, “EPIP-2.2 Emergency Warning, Instruction and Call of Emergency Worker” (2017).
- [2] “Japan bolstering emergency support system for foreigners”. Nikkei Asian Review, Mar 02, 2017.
- [3] “Docomo develops prototype multilingual App for disaster warning”. NTT Docomo, Mar 10, 2015.
- [4] Kim Min-joo. “Korea developing multilingual disaster alert system for foreigners”. The Korea Herald, Nov 20, 2017.

Safety Evaluation of a NORM Site Restoration in Korea

Z.H. Woo^{1)*}, Y.J. Kim¹⁾, B.U. Chang¹⁾, N.M. Hassan²⁾, and J.H. Jang¹⁾

¹⁾ Korea Institute of Nuclear Safety, 62, Gwahak-ro, Yuseong-gu, Daejeon, Republic of Korea

²⁾ Zagazig University, Shaibet an Nakareyah, Markaz El-Zakazik, Egypt

* k698wzh@kins.re.kr

1. Introduction

There are several types of industries generating naturally occurring radioactive material (NORM) residues in Korea. Of these, the manufacture of titanium dioxide (TiO₂) pigments belongs to the specific industry sectors given in IAEA SRS No.49, identified as being the most likely to require regulatory consideration. In 2016, one facility stopped the operation and completed decommissioning including site clean-up. To estimate the safety of restoration site, Korea Institute of Nuclear Safety (KINS) performed a car-borne radiation survey using NaI(Tl) detector and *in-situ* HPGe spectrometry. Based on the *in-situ* measurement results, the equivalent activity concentration distribution levels of ²³⁸U, ²³²Th, and ⁴⁰K before and after the restoration were evaluated.

2. NORM Residue Site

2.1 TiO₂ Pigment Manufacture

Titanium minerals contain basically radionuclides of natural origin in the ²³²Th and ²³⁸U decay series. The radionuclide activity concentrations are known to be moderately elevated in compared to common rocks and soil. During processing, these radionuclides may become mobilized and migrate to dusts, scales and other process residues, leading to

the possibility of radionuclide activity concentrations higher than those in the raw materials. In particular, Ra may be concentrated in the scales.

2.2 Site Description

The closed facility is an area of 72,727 m², which had been operated for 47 years using a sulphate process route.

3. Materials and Methods

3.1 Radiation Measurement Equipment

All radiological surveys were performed using two survey cars equipped with the following.

- Large volume NaI(Tl) scintillation detector (4" x 4" x 16", SAINT-GOBAIN)
- Multi-Channel Analyzer (MCA, ORTEC)
- High pressure ionization chamber (HPIC, GE)
- GPS terminal
- LTE wireless communication system
- Operating software (RadSearch Co.)

3.2 Car-borne Survey and Evaluation Method

While a vehicle is moving at low speeds (< 10 km/h), gamma spectra, gamma dose rates and GPS signals are being continuously collected with the NAI

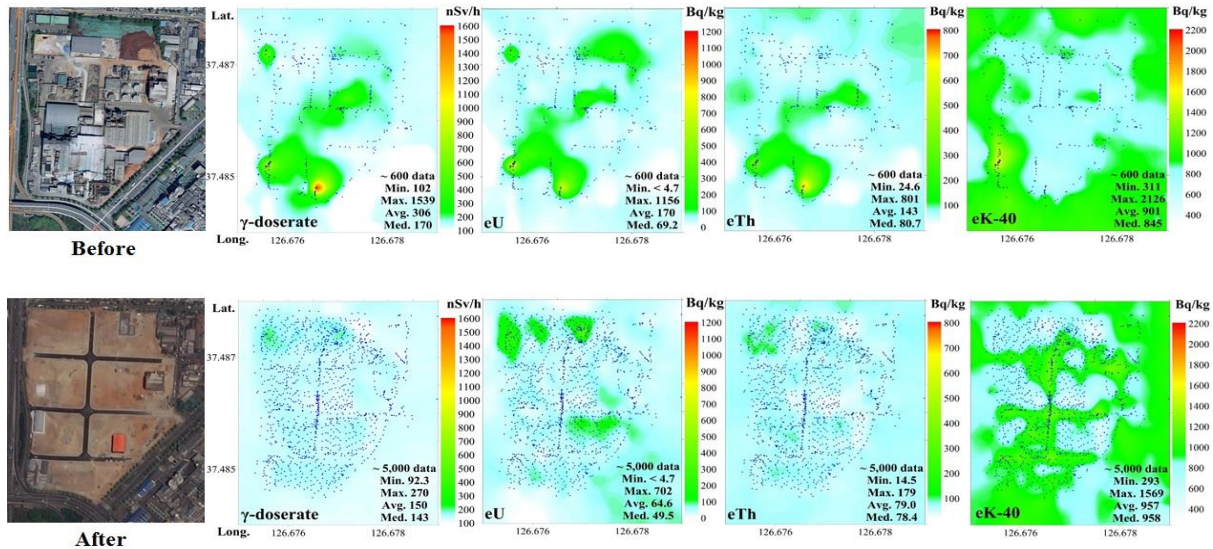


Fig. 1. The comparison of the distribution of the gamma dose rate and activity concentration before/after D&D γ -dose rate by HPIC and eU, eTh and eK-40 activity by NaI(Tl).

(Tl) detector, HPIC and GPS terminal, respectively.

The correlation equations between the cps and the activity concentration (Bq/kg) in surface soil for each nuclide were obtained based on the activity concentration calculated from the *in-situ* HPGe measurement. Finally, the distribution maps for each nuclide were contoured as using the Bq/kg unit with the mapping program, Surfer 13 (Golden Software LLC., USA).

4. Results

The equivalent concentration of ^{238}U during the decommissioning and dismantling (D&D) was 4.7 ~ 1,156 Bq/kg, which was reduced to 4.7 ~ 702 Bq/kg after the restoration. In the case of ^{232}Th , the activity was 24.6 ~ 801 Bq/kg during D&D, but it was maximum 179 Bq/kg after the restoration. Additionally, the average for the gamma dose rate by HPIC was 145 nSv/h. The before and after distribution comparison of the gamma dose rate and activity concentration is represented in contour maps shown in Fig. 1.

5. Conclusion

A first case for the decommissioning of NORM facility was happened in Korea. As a result of safety evaluation of the site restoration, the restoration site has no more influence on the environment.

REFERENCES

- [1] IAEA, Accessing the need for radiation protection measures in work involving minerals and raw materials, SRS No.49, 2006, Vienna.
- [2] McNulty, G.S., Production of titanium dioxide, Proceedings of the 50th international symposium on NORM, 2007, Seville.

A Practical Measure to Deal With Linear Power Signal Saturation of a WRFC

Sanghoon Bae*, I.K. Hwang, W.M.Park, G.Y.Park, and C.H.Kim

Korea Atomic Energy Research Institute, 111, Daedeok-daero 989beon-gil, Yuseong-gu, Daejeon, Republic of Korea

*shbae@kaeri.re.kr

1. Introduction

The sensitivity of a fission chamber in the neutron measurement system (NMS) is considered a key factor during a commissioning. Because the wide range fission chamber (WRFC) sensitivity influences the linearity and power coverage during a power ascension test and it indicates how much the design requirement is met. However, if this sensitivity of WRFC is severely deviated from what it should be due to a certain reason, the aftermath of this impact must be exactly analyzed and an appropriate countermeasure should be prepared. In particular, taking account for the importance of nuclear test the reactor power measuring capacity should be fully negotiated with a core team. The delicate issue about its sensitivity compensation, herein is intensively introduced.

2. Nuclear Test and Signal Saturation of WRFC

2.1 Nuclear pretest scheme for Safety NMS

Nuclear test are involved in the type test sequence for safety NMS which generally proceeds according to the specified manual. Before the nuclear test, every process is almost identical to other safety systems. The Nuclear pretest was performed with a WRFC which is used as a detector of NMS. The test specimen is usually prepared for conventional test with being connected via the field cables to the signal processing unit.

The WRFC is mounted and electrically isolated in a dedicated movable standpipe in the test reactor pool as shown in Fig. 1 with the detector axis parallel to the standpipe axis. The same vertical position to the reactor core for all measurements is maintained during the test. The WRFC is placed in the reactor pool at two different locations, referred to position 1 (low neutron flux, far from the reactor core, SE-Pool1) and position 2 (high neutron flux, close to the reactor core, NE-Pool2), to achieve the required neutron fluxes. This scheme is employed to always operate the reactor at power levels above 2.5E-3 %FP to be able to stabilize desired reactor operation at the chosen power level and to improve the accuracy of power measurement by the reference instrumentation.

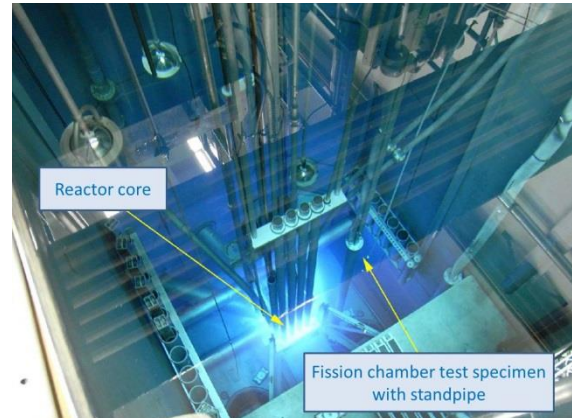


Fig. 1. Nuclear Pretest Setup of NMS channel.

2.2 WRFC linear power signal saturation

The discrepancy was found on the DC sensitivity of WRFC which occurs between the produced ones and its associated datasheet. As a result, the practical range of current NMS is limited to a maximum of 5E+9 nv (instead of the design value of 1.5E+10 nv) at the detector position. In general, the DC sensitivity of a WRFC is determined by amount of uranium coating, geometry of the electrode system, gas filling including gas mixture and density, and applied high voltage. During the design phase, the DC sensitivity of a new WRFC can only be estimated which is based on precedent data with same detector specification.

However, if a detector manufacturer does not receive correct information on the actual sensitivity of the WRFC as it was qualified by a different company, in this case, the detector's sensitivity had to be assumed the predefined specification. This non-conformance resulted from wrong gas mixture (95% N and 5% He) being filled into the test specimen, which was alleged due to temporary malfunction at the filling station. For this reason the increased DC sensitivity was not detected in time to apply corrective actions (regarding to the detector housing dimension). But the detectors shipped are filled with the correct gas and at the correct pressure as specified in the final design documents. The impact due to this sensitivity deviation can be categorized as elicited in the Table 1. The pulse range has no impact, on the contrary, the Campbell and DC current signal range has partiall been influcled because of saturation effect which results from the WRFC malfunction not fulfilling the full power measurement.

Table 1. Impact on WRFC sensitivity deviation

NMS channel	Signal	Impact on processing	Impact on analogue output
log power	Pulse count	No impact.	No impact.
signal processing unit	Campbell (MSV)	It is because the pulse count is used only up to end of the overlapping region of $2E+05$ cps. Partially influenced. For the power above a neutron flux of $5E+9$ nv where the Campbell (MSV) measurement will show some saturation effects.	Partially influenced.
Linear power signal processing unit	DC current	Partially influenced The DC current measurement is limited by the input range of the NA 31.31 to 2 mA.	Partially influenced.

Fig. 2, for example, shows data obtained during the second reactor test. The WRFC test specimen was operated with the NMS electronics. The system response is linear up to neutron flux of $5E+9$ nv. But the saturation due to the high DC sensitivity of the detector begins occurring above $5E+9$ nv. The analysis is still to be considered as preliminary as the neutron flux is estimated using not calibrated power levels. The neutron flux of $5E+9$ nv is a conservative value for the definition of the 150% full power, taking into account the slight variations of the DC sensitivity.

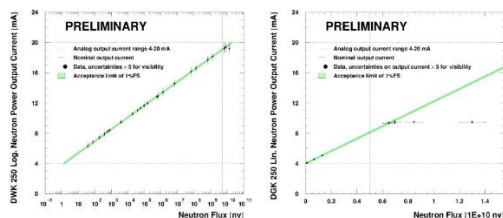


Fig. 2. First Test Result of NMS with curve fitting.

3. Field Test Result for WRFC and Modification for Curve Fitting

The previous nuclear test verified the current performance of WRFC may compromise the required specification with regard to neutron flux and power measurement. The re-evaluation results showcased that the DC sensitivity for the linear power signal for NMS outputs deviated from the specification by a factor 2 to 3, which DC current signal is used for linear power signal. The circuit modification was decided to compensate the some portion of deviation which is aimed at the extension of the DC current output, from 2 mA to 3 mA as feasible as it can.

This modification allows desired full measurement to be unsaturated before the maximum DC current. The signal conditioning modules modification in the

NMS constitutes as followings; High voltage module and DC current input module. Then these components were tested in the field with the relevant procedure. The nominal output current of the high voltage module was increased from 2mA to 3mA, which requires the replacement of concerned components on the modules.

At the same time, the WRFCs were recommended to be relocated by traversing their housing toward the reactor core in order to fit DC current. If the detectors were relocated inwards, the neutron flux at the new position could be formulated around $2E+10$ nv which can be interpreted to fulfill the requirement. This approach was effective in combination with the circuit modification. Fig. 3 showcases the neutron flux distribution at the initial core of 5 MW after the detector relocation.

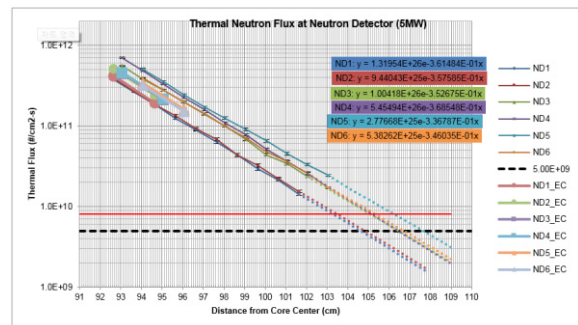


Fig. 3. Thermal neutron flux distribution at WRFC at 5 MW for initial core.

4. Conclusions

Thus far, the issue on the nuclear test result and signal saturation of WRFC has been introduced with several field experiences. This practical approach was suggested based on the test data. The nuclear test finally ended up the circuit modification and retesting, however it implies this case should be dealt with precarious attention factoring in the severity of the linear power signal.

REFERENCES

- [1] F. K. Glenn, Radiation Detection and Measurement, 4th Edition, John Wiley & Sons, 2010.
- [2] S.S. Kapoor, V.S. Ramamurthy, Nuclear Radiation Detectors. New Age International, (1986) 34.
- [3] N. Tsoulfanidis, S. Landsberger, Measurement and Detection of Radiation, 3rd Edition, CRC press, 2009, pp.375-377, 2011.
- [4] C.G. Clayton, Nuclear Geophysics: Selected Papers on Applications of Nuclear Techniques in Mineral Exploration, Mining and Process Control, (1983), 261-263.

The Long-Term Simulation of ^{137}Cs in the North Atlantic Ocean Using the Lagrangian Particle Model

Byung-Il Min*, Kihyun Park, Sora Kim, Byung-Mo Yang, Jiyeon Kim, and Kyung-Suk Suh

Korea Atomic Energy Research Institute, 111, Daedeok-daero 989beon-gil, Yuseong-gu, Daejeon, Republic of Korea

*bimin@kaeri.re.kr

1. Introduction

A number of researches on ^{137}Cs distributions in the Atlantic Ocean environment, release from nuclear fuel reprocessing at Sellafield (UK), have been published. The ocean dispersion models have been simulated the radionuclide concentration in the European Shelf and Atlantic oceans [1-2]. The purpose of this work is to improve a Lagrangian dispersion model for long-term numerical experiments for more than 50 years. The oceanic dispersion model used in this work was LORAS (Lagrangian Oceanic Radiological Assessment System) has been developed in Korea Atomic Energy Research Institute since 2011 [3].

2. Model Description

2.1 Marine dispersion model

A stochastic method is used to estimate the dispersion of non-conservative radionuclides and provide concentration in water, suspended matter and bottom sediments. The differential equations which describe transfers between the three phases are expressed the following.

$$\frac{\partial C_w}{\partial t} = -k_{1m}C_w - k_{1s}C_w, \frac{\partial C_s}{\partial t} = -k_2C_s, \frac{\partial C_b}{\partial t} = -k_2PC_b \quad (1)$$

Where C_w , C_s and C_b are radionuclide concentrations in seawater, suspend mater and bottom sediments respectively. K_{1m} is the kinetic coefficient describing radionuclide transfer from water to suspended matter, K_{1s} describes the transfer

from water to bottom sediments and K_2 is the kinetic transfer coefficient which describes radionuclide release from suspended matter or bottom sediments to water. P is a correction factor which takes into account that some of the sediment particle surface may be hidden by other particles.

Radionuclide concentrations in seawater, suspended mater and seabed sediments are calculated in the domain of interest by counting the number of particles as follows.

$$C_w = \frac{I.N_w}{\Delta x \Delta y \Delta z}, C_s = \frac{I.N_s}{m \Delta x \Delta y \Delta z}, C_b = \frac{I.N_b}{\Delta x \Delta y H \rho_b} \quad (2)$$

Here $I=Q/NP$, where Q is the source term and NP is the number of particles used in the simulation $\Delta x \Delta y \Delta z$ is the volume of the each cell, m is suspended matter concentration, H is the mixing depth in the bottom sediment and ρ is sediment bulk density finally N_w , N_s and N_b are the number of particles in each phase.

2.2 Source Term

Annual ^{137}Cs releases from Sellafield and La Hague nuclear fuel reprocessing plants, presented in Fig. 1, are introduced from 1952 to 2009, which is the simulation period. These releases define the number of Bq corresponding to each released particle. It is considered that radionuclides are released in a dissolved form. Sellafield releases peaked in 1975, when 5200 TBq were released. In the case of La Hague releases, they started in 1966 and peaked in 1971, with 243 TBq. Later they were reduced by about two orders of magnitude (Fig. 1). Releases from both plants have been simulated by a total

number of 6×10^7 particles. The calculation time was a total of 5 days using a 160 cpu core. Atmospheric fallout and deposition from nuclear weapon tests and Chernobyl accident in 1986 are not included, since the deposition from Chernobyl accounts for a 10% (4) of the total cesium inventory in ocean.

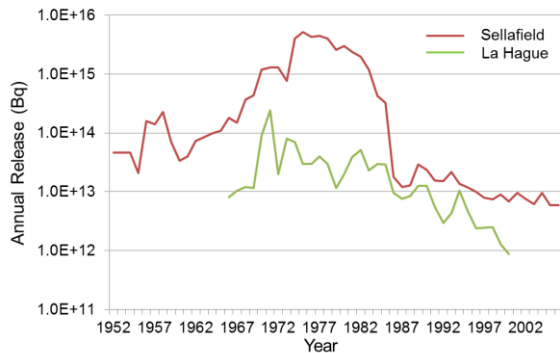


Fig. 1. Annual ^{137}Cs release from Sellafield and La Hague reprocessing plants.

3. Numerical Results

Fig. 2 shows the concentration of ^{137}Cs in the North Atlantic Ocean in seawater 50 years after the start of the 1952 calculations. The ^{137}Cs leaked from Sellafield spread mainly in the southwest of England. In the previous study ([4]), there was a very low concentration, but some of the northeastern propagation pattern passed through the northern coast of England, but this trend did not appear in this study. The main reason is due to the characteristics of the applied ocean circulation model. In this study, the effect of tide is not taken into consideration, so there are some differences.

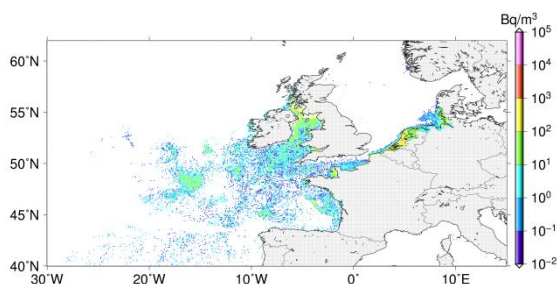


Fig. 2. Simulation results of ^{137}Cs concentration in ocean surface layer at the end of 2002.

The ^{137}Cs concentration of the English Channel

located in the south of England is mainly influenced by runoff in the La Hague reprocessing plant. According to observational data [5], the concentration of this region was approximately 10 to 20 Bq/m^3 , and the calculation results of this study showed similar 10 to 50 Bq/m^3 . Concentrations tend to be overestimated when a large number of Lagrangian particles are located in areas with small volumes in the coast.

Future studies will use more particles and more detailed comparisons with observed data to improve some overestimated results.

ACKNOWLEDGEMENT

This work was supported by the National Research Foundation of Korea (NRF) and funded by the Korea government (MSIP) (MSIP: NRF-2017M2A8A4015253, NRF-2015M2A2B2034282).

REFERENCES

- [1] D. Prandle, "A modelling study of the mixing of ^{137}Cs in the seas of the European Continental Shelf Philos", *Trans. R. Soc. Lond. A*, 310, 407-436 (1984).
- [2] M. Villa, et al., "The behaviour of ^{129}I released from nuclear fuel reprocessing factories in the North Atlantic Ocean and transport to the Arctic assessed from numerical modelling", *Mar. Pollut. Bull.*, 90, 15-24 (2015).
- [3] B.I. Min, et al., "Marine dispersion assessment of ^{137}Cs released from the Fukushima nuclear accident", *Mar. Pollut. Bull.*, 72(1), 22-33(2013).
- [4] P.P. Povinec, et al., "Temporal and spatial trends in the distribution of ^{137}Cs in surface waters of Northern European Seas a record of 40 years of investigations Deep Sea Res. Part II", 50 2785-2801 (2003).
- [5] J. Herrmann, et al., "The distribution of artificial radionuclides in the English Channel southern North Sea, Skagerrak and Kattegat 1990–1993", *J. Mar. Syst.*, 6, 427-456 (1995).

Field Experiment for Evaluation of Long-term Behavior of Radiocesium Deposited on Land

Byung-Il Min*, Kihyun Park, Sora Kim, Byung-Mo Yang, Jiyeon Kim, and Kyung-Suk Suh

Korea Atomic Energy Research Institute, 111, Daedeok-daero 989beon-gil, Yuseong-gu, Daejeon, Republic of Korea

*bimin@kaeri.re.kr

1. Introduction

Following the accident at the Fukushima Dai-ichi Nuclear Power Plant in March 2011, radionuclide, including radiocesium, were deposited over eastern parts of Japan. In land, most of the fallout was initially trapped by the tree canopy, some of which was then washed out by rainfall and gradually migrated into ground surfaces by throughfall and stemflow. Once radiocesium reaches the ground surface and infiltrates into the soil, especially finer soil particles such as clay and silt, the rainfall-runoff process plays an important role in its redistribution [1]. In this study, field monitoring was conducted to estimate radiocesium runoff from forest area and to simulate soil and radiocesium erosion and transport.

2. Field Experiment

The key issue in field experiments to understand soil erosion process due to rainfall is which instruments are used to measure soil splash and erosion. In literature review, most of equipment in this research is not commercially available and researchers manufacture themselves what is needed for their scientific purposes [2]. In this study, we have designed a research instrument based on the assumption that radiocesium is very strongly bound to the soil particles for long-term estimation. As shown in the figure, the equipment consists of a part that insulates about 10 cm from the surface of the soil

and isolates it from the surrounding soil particles, and a tank part which collects when the inside soil is eroded by the rain. Rainfall is observed by rainfall gauges every 10 minutes. As a result, it is possible to analyze the relationship between rainfall intensity, soil particle size and weight. Two experimental equipment were built, one is on the mountain near the Korea Atomic Energy Research Institute and the other is installed on the mountain near Daejong Stream in Gyeongju. In this study, we analyzed the results of observations at KAERI.



Fig. 1. Observation equipment schematic and photograph of installed equipment in KAERI.

3. Results and Discussion

Six eroded soil samples were collected from June to August 2017. The collected soil samples were analyzed for soil particle size distribution by image analysis technique.

Table 1. Observation data of rain and soil

No	D ₁₀	D ₆₀	C _u	Rainfall (mm)
28 June	0.0497	0.2192	4.41	14.00

3 July	0.0462	0.2471	5.35	54.20
7 July	0.0444	0.2934	6.61	75.20
17 July	0.0488	0.2574	5.27	27.30
25 July	0.0490	0.2238	4.57	9.90
1 August	0.0483	0.2348	4.86	75.20

D_{10} is termed as the effective particle size it means that 10 percent of the particles are finer. Similarly, D_{60} means diameter of the soil particles for which 60 percent of the particles are finer and 40 percent of the particles are coarser than D_{60} . The uniformity coefficient C_u is defined as the ratio of D_{60} by D_{10} [3]. As shown in the table 1, the uniformity coefficient is large, relatively large amount of coarser soil are contained in the soil samples.

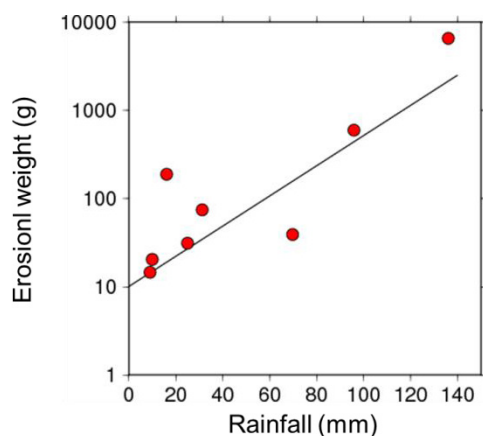


Fig. 2. Relationship between rainfall and uniformity coefficient.

Rainfall erosion is a complex process and, in reality, no absolute measure of rainfall erosivity exists. Various parameters (eg. rainfall kinetic energy) and combinations of parameters (eg. product of storm rainfall energy and the maximum 30-minute intensity) are used as indices of rainfall erosivity and, as a consequence, soil erodibility is nothing more than an empirical coefficient in the relationship between an index of rainfall and soil loss. The general form of equation used by U.S. Department of Agriculture is

following

$$e_s = C_f \exp(-c_h h) r^2 \quad (1)$$

in which C_f is a constant related to soil and surface properties, c_h represents the damping effectiveness of surface water. The parameter r is rainfall intensity; h is water layer thickness on land. The function $\exp()$ is 1.0 prior to runoff and its minimum is 0 for very deep flow. In general, the parameter C_f is known to have a value between 20 to 500 [4], in this study, the C_f of evaluation using Eq.1 was 198.3.

Future studies, we will also present a numerical model using this analysis and a river transport model for long-term evaluation.

ACKNOWLEDGEMENT

This work was supported by the National Research Foundation of Korea (NRF) and funded by the Korea government (MSIP) (MSIP: NRF-2017M2A8A4015253, NRF-2015M2A2B2034282).

REFERENCES

- [1] International Atomic Energy Agency, "Handbook of parameter values for the prediction of radionuclide transfer in terrestrial and freshwater environments", Technical Report Series No. 472 (2010).
- [2] M. Fernández-Raga, et al., "Splash erosion: a review with unanswered questions", Earth-Science Reviews, 171, 463–477 (2017).
- [3] A. Verruijt, "Soil Mechanics", Delft University of Technology, 315 (2001).
- [4] L. D. Meyer, et al., "Mathematical simulation of the process of soil erosion by water", Transactions of the American Society of Agricultural Engineers, 12(6), 754-762 (1969).

The Quantitative Analysis of Uranium and Thorium in Soil Using HPGe Gamma-Ray Spectrometry

Kwang Heon Park* and Hyoung Gyu Park

Kyunghee University, 1732, Deokyoung-daero, Giheung-gu, Yongin-si, Gyeonggi-do, Republic of Korea

*kpark@khu.ac.kr

1. Introduction

Alpha spectrometry and ICP-MS (Inductively Coupled Plasma Mass Spectrometry) have been widely used to determine the radio-activities of ^{238}U and ^{232}Th . Even though these methods are useful to assess low level radioisotopes, several pretreatment are required to know the amounts of nuclides in the soil [1].

HPGe gamma-ray spectrometry needs simple preparation to determine the quantitative analysis of uranium and thorium by measuring their decay products in the soil [2]. According to the decay schemes of ^{238}U and ^{232}Th , the daughter nuclides are ^{214}Pb , ^{214}Bi , and ^{228}Ac . They should be measured using gamma-ray spectrometry to use secular equilibrium [1,2].

The purpose of this study is to perform the quantitative analysis of the concentration of ^{238}U and ^{232}Th in the soil using HPGe gamma-ray detector.

2. Materials & Method

The experiment was carried out using a coaxial p-type HPGe detector (ORTEC, GEM20P4-70). The relative efficiency is 20%. The resolution and the Peak-to-Compton ratio are 1.8 keV and 52:1 at 1.33 MeV, respectively. The software to collect and analyze the gamma-ray spectra is Gamma Vision.

2.1 Calibration

The energy and efficiency calibration were conducted using 1 L marinelli beaker standard source. The type of standard source is agar from KRISS. 10 types of nuclides, ^{241}Am , ^{109}Cd , ^{57}Co , and etc., are included in the standard source.

An empty marinelli beaker was also measured for 24 hours to consider the peaked background correction [3].

2.2 Sample preparation

The soil sample was collected from the specific site located near Kyunghee University. After the miscellaneous substances like pebbles and branches were sifted out, the sample was dried in the drying oven at 150°C for 50 hours. Following the dryness, the sample was sieved with fine sieve to reduce the void. The dried sample was sealed in 1 L marinelli beaker [4]. The processes for sample preparation are shown in Fig. 1.

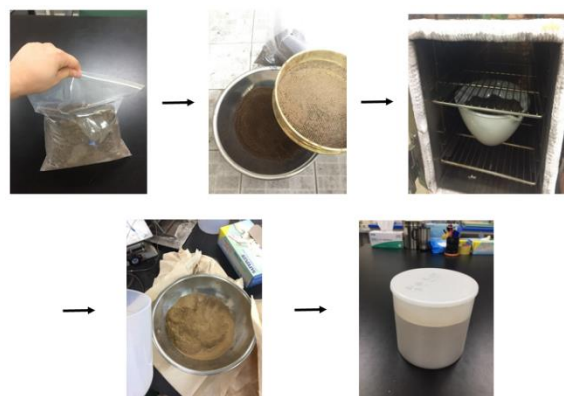


Fig. 1. The processes of sample preparation for gamma-ray detection.

2.3 Decay schemes

The decay schemes of ^{238}U and ^{232}Th are illustrated in Fig. 2. The sample was stored during 20 days to reach the secular equilibrium. In order to know the activity of ^{238}U , the activities of ^{214}Pb (351 keV) and ^{214}Bi (1120 keV, 1764 keV) were measured. The activity of ^{228}Ac (968 keV) was also measured to know the activity of ^{232}Th [4].

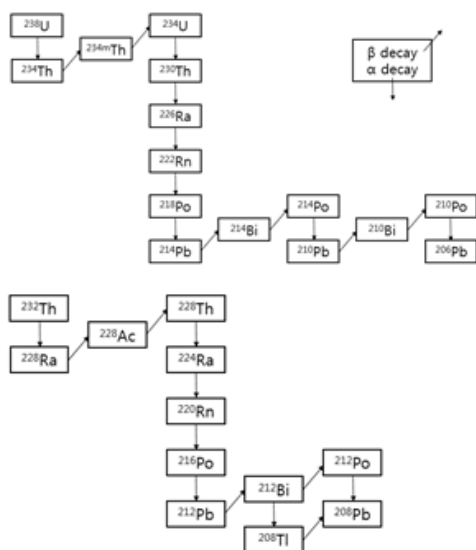


Fig. 2. The decay schemes of uranium and thorium.

3. Results

The sample was measured for 24 hours and the counts were acquired with Gamma Vision. The sample was also detected several times at same condition to know the average and standard deviation. The specific activities of ^{238}U , ^{232}Th and ^{40}K , which is commonly detected at 1460 keV, were calculated using the Absolute Method [4].

$$A = \frac{CPS_{net}}{\varepsilon \cdot I \cdot m} \text{ (Bq/kg)} \quad (1)$$

where CPS_{net} is the net count rates of nuclides, ε is the efficiency of energy, I is the photon yield or emission probabilities, and m is the mass of sample in kg.

Table 1 indicates the specific activities of ^{238}U and ^{232}Th using Eq. (1).

Table 1. The values of specific activities at each of the energies

	Energy (keV)	Activity (Bq / kg)
^{238}U	351	23.61 ± 0.90
	1120	26.83 ± 1.34
	1764	29.17 ± 0.12
^{232}Th	968	63.89 ± 1.16
^{40}K	1460	854.92 ± 18.27

4. Conclusion

The experiment was carried out to know the activities of ^{238}U and ^{232}Th using Absolute Method.

There are several advantages to use HPGe detector instead of alpha spectrometry. The sample for gamma-ray spectrometry doesn't need complicated pretreatment processes comparing with the alpha spectrometry, which makes lots of waste.

However, it is required to compare the quantitative analysis of uranium and thorium using alpha spectrometry with our results. Because the natural soil used for our experiment had low level radioactivity and uncertainty.

ACKNOWLEDGEMENT

This work was supported by the National Research Foundation of Korea (NRF) funded by the Ministry of Science and ICT (The grant number: NRF-2018M2B2B1065635).

REFERENCES

- [1] W.N. Lee, H.R. Kim, J.H. Chung, Y.H. Cho, M.J. Kang, C.W. Lee, and G.S. Choi "Uranium Activity Analysis of Soil Sample Using HPGe Gamma Spectrometer", Journal of Radiation Protection, 35(3), 105-110 (2010).
- [2] C.A. Papachristodoulou, P.A. Assimakopoulos, N.E. Patronis, and K.G. Ioannides "Use of HPGe γ -ray spectrometry to assess the isotope composition of uranium in soils", Journal of Environmental Radioactivity, 64, 195-203 (2003).
- [3] I.H. Saleh and A.A. Abdel-Halim "Determination of depleted uranium using a high-resolution gamma-ray spectrometer and its applications in soil and sediments", Journal of Taibah University for Science, 10, 205-211 (2016).
- [4] D.M.M. Olivares, E.S. Koch, M.V.M. Guevara, and F.G. Velasco "Determination of uranium and thorium using gamma spectrometry: a pilot study", Journal of Physics: Conf. Series, 975, 012035 (2018).

Radiation Measurement by Compensation Method Using Optic Fiber Scintillator With Passive Fiber Cable

Jongsoo Kim*, Sung-Ho Lee, and Hae-Cho Lee

Korea Atomic Energy Research Institute, 111, Daedeok-daero 989beon-gil, Yuseong-gu, Daejeon, Republic of Korea

*jskim4@kaeri.re.kr

1. Introduction

The optical fiber scintillator(OFS) of Ce^{+3} (cerium) activator detects radiation by converting the radiation energy into visible light. In the case of gamma rays, photoelectrons are generated by the interaction with glass materials (photoelectric effect, calculation effect, electron pair generation) in OFS, and this photoelectron loses energy and generates light. The neutrons detect charged particles from the (n, α) nuclear reaction of ^6Li and neutrons in OFS.

If a system for transmitting light from an OFS through a passive fiber cable(PFC) is developed, it is not necessary to attach electronic equipment for signal detection in a high radiation zone, thus preventing equipment damage due to radiation exposure. However, since PFC also generates light due to interaction with radiation, a method of detecting only the OFS signal is necessary.

2. Radiation detection by Subtraction

Method

2.1 Hardware Configuration

Although it is possible to consider how optical filters can be used to block light emitted from PFCs, this method is known to have a removal rate of about 87%. Therefore, we want to develop a subtraction system that completely removes the influence of PFC

and uses only the signal detected by OFS. As shown in Fig. 1, the system installs a PFC2 to compensate for the signals of PFC1, and the signals from these are configured to be compensated by a computer program. If the values of these two signals are the same under the same radiation dose conditions, only the signal generated by the OFS will be measured by the compensation method.

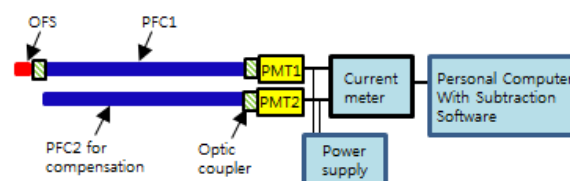


Fig. 1. Radiation Measurement System by Compensation.

2.2 Compensation Experiments

To investigate the radiation sensitivity from PFC, two PFCs of the same length without OFS were irradiated from 100 rad/h to 4,000rad/h of Co-60. As shown in Figure 2, these PFCs showed almost the same sensitivity. The software program for this sensitivity was almost subtracted and showed 0.5% difference at over 3,000 rad/h. These results suggest that the compensation method sufficiently removes the influence of PFC signals on measured values.

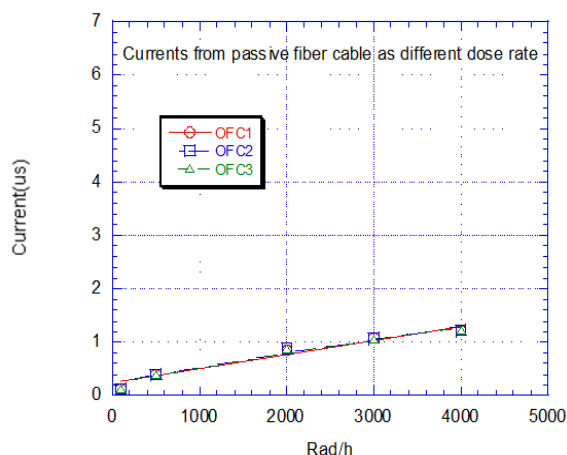


Fig. 2. Radiation Response of PFC.

The OFS for neutron measurement used in the experiment is 0.1 mm and 1 mm in diameter, respectively, and the length is 10 cm. the OFS for gamma ray measurement is also 0.1 mm and 1 mm in diameter and 10 cm in length. The PFC is 1 mm in diameter and 15 m in length. These OFSs are shown in Fig. 3 as a result of subtracting the radiation dose from 100 rad/h to 4000 rad/h. The 0.1 mm diameter OFS was measured at almost the same value and the 1 mm OFS was larger than the OFS for gamma and OFS for neutron.

Therefore, in the case of measuring neutrons in areas with high gamma - ray intensity such as spent nuclear fuel, it is found through this experiment that a system development or a method for selecting neutron signals is necessary. The measured values for dose changes showed excellent linearity within 5% for all four OFSs. Therefore, the compensation method can be used for the measurement of high radiation.

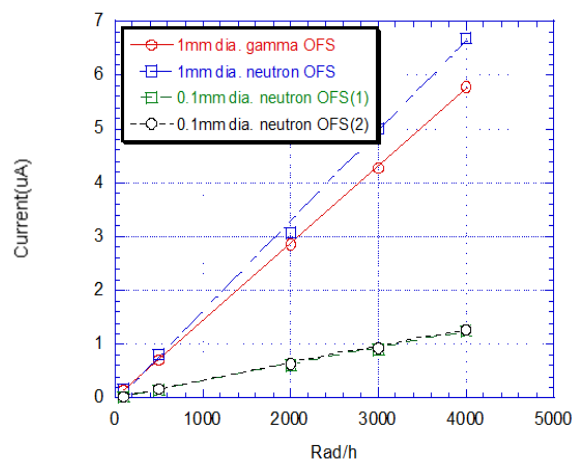


Fig. 3. Measured Linearity by Subtraction.

3. Conclusion

In this paper, a study was made using PFC as a transmission medium of light when using OFS for radiation measurement. The compensation method showed that 99% or more of the effects of PFC were eliminated, and linearity for 4 different OFSs was excellent within 5%. Therefore, the OFS can be used for measurement of high-radiation at a very small point, because it can utilize various detection sensing areas by simple manufacturing and does not need electronic equipment for transmitting OFS signals.

REFERENCES

- [1] KAERI, "National Nuclear Material Account and Control Technology Development", KAERI/RR-2212, 2002.
- [2] G.F. Koll, "Radiation Detection and Measurement", 2nd Edition, John Wiley & Sons, Inc., 1989.

A Consideration of Emergency Action Level Initiation Condition for Research Reactor HANARO

Hae-Cho Lee*, Jongsoo Kim, GY Lee, JS Kim, HK kim, BS Kim, GH Lee, and SY Baek
Korea Atomic Energy Research Institute, 111, Daedeok-daero 989beon-gil, Yuseong-gu, Daejeon, Republic of Korea
*hcleee@kaeri.re.kr

1. Introduction

Because reactors are used for different purposes and their safety characteristics are designed differently, it is difficult to apply emergency publicity standards for certain accidents such as power generation reactors. However, applying the safety characteristics inherent to the research reactor in accordance with the emergency notification standard proposed by the IAEA, the technical basis of the emergency notification standard can be standardized to some extent. Therefore, in this study, based on the emergency level (EAL) proposed by the IAEA, the applicability of the research reactor HANARO was investigated.

2. Emergency Action Level

2.1 IAEA Emergency Action Level

The IAEA threat class II research reactor emergency standards are classified into core safety function disturbance and fission product barrier damage for safety system accidents. In addition to raising the radiation level due to these accidents, Incidents of fire, natural disasters, fuel handling, and spent fuel storage are described. This study investigated the applicability of the Emergency Report Standard for Emergency Causes and Radiation Levels of HANARO to the IAEA Emergency Announcement Criteria.

2.2 Application of Emergency Action Level

IAEA emergency situations can be classified into

three categories: critical safety system failures, fission product barrier losses, and radiation dose escalation. Table 1, Table 2 and Table 3 show the HANARO applicability results for the start conditions of each IAEA EAL. The results are based on Hanaro SAR and the Emergency Plan.

Table 1. Key Safety System Obstacles

IAEA initiation conditions	Applicability analysis for HANARO
Failure to stop nuclear reaction	Not applicable under Hanaro SAR
Inadequate core cooling	-The beam tube rupture is applied as a limitation accident of HANARO -Cooling channel blockage accident is applied.
AC or DC power loss	Not applicable under HANARO SAR
Includes system equipment Safety system Loss or worsening control	Not applicable under HANARO SAR

Table 2. Loss of fission product barrier

IAEA initiation conditions	Applicability analysis for HANARO
Significant damage risk of core or irradiated fuel	Applicability analysis for HANARO
High concentration radioactivity in water tank or reactor building	This starting condition applies because of the possibility of a small leakage of radioactive material from the fuel during output operation due to manufacturing defects or other causes.

Damage to reactor	The release of large quantities of radioactive material from the containment of reactor buildings can not be expected from research reactors. No accident cases. Not applicable.
-------------------	--

Table 3. Increase of Radiation Level

IAEA initiation conditions	Applicability analysis for HANARO
Exhaust emission above the limit	Environmental releases are important in terms of on-site and off-site protection measures. Applied the chimney monitor indicator to HANARO
High radiation level of control room etc.	Control room is applicable. Since the control room is important for maintaining the reactor control function, the loss of the operator's ability due to the increase in the radiation level in the control room is applied.
High radiation levels in areas requiring frequent access for safety system maintenance or control	Nuclear (Emergency) Emergency Plan is unilateral. It does not take into consideration that all workers in other areas except the control room are evacuated or introduced immediately.
High radiation levels in non-core areas (eg., laboratories)	Not considered under the nuclear emergency plan.
Raising the radiation level of the reactor building	Since it is necessary to take into consideration on-site and out-of-site protection measures due to provisional hazards and surface release due to the increase of radiation levels of nuclear reactors after emergency ventilation system shutdown.
Unplanned increase in reactor radiation levels	This is applicable because there may be an increase in the radiation level due to unforeseen unplanned incidents in core fuel.
High radiation dose rate at or above site boundaries	Actual standards for inhabitant protection measures on site, and the actual measured radiation dose rates at site boundaries are applied.

The results of the applicability analysis as one can be summarized as shown in Table 4 for the

emergency start conditions.

Table 4. Summary of EAL Initiation Conditions for HANARO

Incident classification	HANARO Application Emergency release criteria Starting condition
Core Safety System	○ Beam tube breakage accident (loss of coolant accident)
	○ Cooling channel cut-off accident (loss of coolant flow rate)
Fission product barrier	○ Fuel defect accidents
Increase in radiation level	○ Emissions above the limit
	○ Jay's loss of residence
	○ Increase of radiation level in Reactor building
	○ Unplanned increase in reactor radiation levels
	○ High radiation dose rate at the site boundary

3. Conclusion

It is important to establish the ability to timely recognize the emergency classification according to the severity of the accident in order to respond promptly to the radiation emergency preparedness and emergency response of nuclear facilities. This function is only possible if emergency guidelines have been prepared in advance for nuclear safety facilities. Therefore, based on the results of this study, specific and quantitative emergency standards are required depending on the severity of the accident.

REFERENCES

- [1] IAEA, "Generic Procedures for Response to a Nuclear or Radiological Emergency at Research Reactors", EPR-RESEARCH REACTOR, Sep. 2011.

Shielding Capability Simulation for Neutron and Gamma Rays Using Metal Hydride Materials

Jeong-Kwon Kwak, Muth Boravy, Chang-Je Park, and Sun-Jae Kim*
Sejong University, 209, Neungdong-ro, Gwangjin-gu, Seoul, Republic of Korea
*sjkim1@sejong.ac.kr

1. Introduction

From the Chernobyl nuclear accident to the recent Fukushima nuclear accident, the problems related to radiation exposure occurred. The exposed radioactive materials pollute environment and cause serious damage when irradiated to electronic devices and human body. [1] Gamma rays are strong enough to penetrate a few centimeters of lead panel, making it thicker to shield. Neutron radiation should be shielded by providing high density concrete with a mixture of boron, cadmium and so on. There are problems such as human toxicity, environmental pollution caused by disposal, high manufacturing cost. [2] We should develop a new shielding material that complements the disadvantages of neutron and gamma ray shielding materials that have been used in the past. Our research have conducted to apply metal hydride as a shielding material because the heavy metal compounds with a lot of hydrogen contents seem the possibility of simultaneous shielding of neutron and gamma rays.

2. Experiment

In our study, we conducted computer simulation using MCNP6(Monte Carlo Neutron and Photon code6). The analytical model is a spherical model with a radius of 10 cm as shown in Fig. 1, and is designed to tally the flux from the outside with a

dotted source of 10 Mev. Our researches on light metal hydride (B, Li, etc.) and high performance shielding materials (B, Be, Fe, Li, W, etc.) addition was carried out.

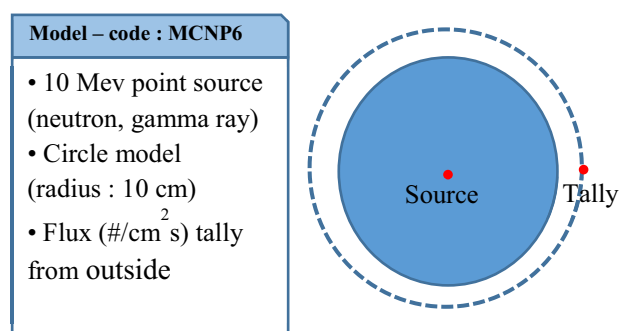


Fig. 1. MCNP6-based shielding capability analysis model design.

3. Results

In table 1, simulation results show that the metal hydride materials such as LiAlH_4 , LiNH_2 , and LiBH_4 have a low density compared to the conventional shielding material, and have excellent neutron shielding ability, and the gamma ray shielding ability is also good. Mg_2FeH_6 showed 176% shielding ability against gamma rays, and LiBH_4 showed 422% neutron shielding ability compared to concrete.

Table 1. Evaluation of shielding ability for lightweight materials using MCNP6 code

No	Material	Density (g/cc)	Gamma flux	Neutron flux
1	Concrete	2.4	1.11E-03	7.95E-04

2	Lead	11.3	4.61E-05	1.30E-03
3	LiBH ₄	0.666	8.67E-04	6.79E-04
4	Mg ₂ FeH ₆	2.74	1.08E-03	7.44E-04
5	MgH ₂	1.45	1.07E-03	8.68E-04
6	B ₄ C	2.52	1.07E-03	8.26E-04
7	TiH ₂	3.76	1.02E-03	6.77E-04
8	LiH	0.78	9.76E-04	8.36E-04
9	NaBH ₄	1.074	9.69E-04	7.06E-04
10	LiAlH ₄	0.917	9.64E-04	7.94E-04
11	LiNH ₂	1.178	9.47E-04	6.94E-04
12	CaH ₂	1.7	1.17E-03	7.67E-04
13	BeH ₂	0.65	8.63E-04	1.06E-03
14	Iron	7.9	4.52E-04	9.41E-04
15	Tungsten	19.2	3.62E-06	1.54E-03

Based on the high-performance shielding materials such as B, Ta, W, Gd, and others, computer simulation of the composition of hydrogen compounds that do not exist at present is performed as shown in Table 2. The results show that the hydrides such as WBH₄, LiWH₄, and WFeH₆ have a similar density to the conventional shielding materials and have excellent gamma ray and neutron shielding ability.

Table 2. Evaluation of shielding ability against new non-existent composition using MCNP6 code (density estimation)

No	Material	Density (g/cc)	Gamma flux	Neutron flux
1	PbBH ₄	9.2	4.67E-04	4.79E-04
2	CeBH ₄	5.8	4.60E-04	5.83E-04
3	NdBH ₄	5.9	4.28E-04	5.85E-04
4	GdBH ₄	6.6	3.36E-04	5.55E-04
5	TaBH ₄	11.8	5.28E-05	2.54E-04
6	WBH ₄	13.0	3.45E-05	2.16E-04
7	LiWH ₄	14.7	1.60E-04	1.89E-04
8	WFeH ₆	15.1	2.01E-05	5.06E-05
9	PbB ₄ C	6.53	8.29E-04	1.01E-03

4. Conclusion

To overcome the disadvantages of conventional radiation shielding materials, new light metal hydride materials were searched through Monte Carlo

simulation. As a result, metal hydride materials such as LiAlH₄, LiNH₂, and LiBH₄ exhibited excellent neutron shielding ability while maintaining low density characteristics compared to the conventional shielding materials. Also, simulations were carried out on the composition of metal hydrides that do not exist at present. The results show that hydrides such as WBH₄, LiWH₄, and WFeH₆ have a similar density to the existing shielding materials, but have excellent neutron and gamma ray shielding ability.

ACKNOWLEDGEMENT

This research was carried out through the development of radiation technology supported by the Korea Research Foundation of the Ministry of Science and Technology. (2017M2A2A4A01071249)

REFERENCES

- [1] Dubrova, Y. E., Nesterov, V. N., Krouchinsky, N. G., Ostapenko, V. A., Neumann, R., Neil, D. L., & Jeffreys, A. J. (1996). Human minisatellite mutation rate after the Chernobyl accident. *Nature*, 380(6576), 683.
- [2] Singh, K. J., Kaur, S., & Kaundal, R. S. (2014). Comparative study of gamma ray shielding and some properties of PbO–SiO₂–Al₂O₃ and Bi₂O₃–SiO₂–Al₂O₃ glass systems. *Radiation Physics and Chemistry*, 96, 153-157.

Derivation of Preliminary Derived Concentration Guideline Level (DCGL) by Containment Building Reuse Scenario for Kori Unit 1 Using RESRAD-BUILD

SangJune Park*, Jihyang Byon, and Seokyoung Ahn

Pusan National University, 2, Busandaehak-ro 63beon-gil, Geumjeong-gu, Busan, Republic of Korea

*xelidake2@pusan.ac.kr

1. Introduction

In South Korea, the Kori Unit 1, the first South Korean commercial nuclear power plant, came into commercial operation in 1978 and continued to operate until 2007, when its operation was extended for 10 more years. Finally, it was shut down in June 2017 without the second extended operation.

This study provides a method of calculating a Kori Unit 1 preliminary site-specific DCGLs, by using RESRAD-BUILD code, for radionuclides on the surface of buildings which will be expected to still stand after decommissioning. Additionally, this study provides a method for calculating the exposure dose to receptors such that it satisfied the site release criteria.

2. RESRAD-BUILD code description

The RESRAD-BUILD code is an exposure path analysis code for assessing the potential exposure dose of an individual or worker in a building contaminated with residual radioactive material. In the RESRAD-BUILD code, radioactive particulates in the air, aerosol indoor radon decay products, and tritium water vapor, including external exposure to penetration radiation, due to the air submersion of the radioactive material and radioactive particulates that have accumulated at the source, are considered. Additionally, consideration is given to the intake and ingestion pathways of materials emitted from the source and to materials that have accumulated on the building surface.

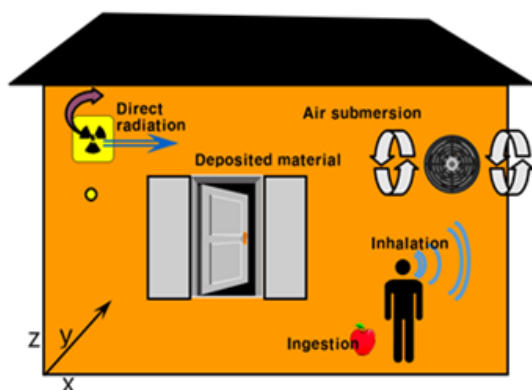


Fig. 1. Exposure pathway considered in RESRAD-BUILD [1].

3. Containment building worker scenario input values

For parameters related with the dose/risk, input values are set to the latest data in ICRP 60, the exposure duration was set to 179 days, and the indoor fraction was set to 0.351 [1, 2]. It is reported that the decommissioning process will begin in June 2022, and that the release of the site will begin in 2031 [3]. As a result, the worker dose evaluation time was set after 13 years (2030, when the decommissioning will be completed). The containment building was assumed to be consist of a single large room. The deposition velocity and resuspension rate were treated as probabilistic parameter. Tritium was set to zero for the deposition velocity.

For the Kori Unit 1 containment building, a cylindrical shape, height measured from the ground level to the containment building concrete height, and volume including the external reinforced concrete annulus, was taken into account. The calculated concrete volume inside the containment building was 62,287 m³, based on a diameter of 35.48 m and a height of 63 m.

The floor and ceiling area was set to 988.18 m² for cylinder type. In the Kori Unit 1 containment building, the supply and exhaust fans were operated one by one and the building exchange rate was 0.68 h⁻¹, due to the flow rate per unit being 25,000 CFM. The area of the floor and ceiling was 988.18 m², and the length of one side was 31.44 m for rectangle type. To make the cross-sectional area of the containment building's cylindrical side equal to the width of the cuboid, the height of the cuboid was considered as 55.83 m.

By assuming that the concrete of the Kori Unit 1 containment building was a source, the worker was located 1 m from the wall of the building.

Under this scenario, the lead density was assumed as 11.36 g/cm³ and the worker was assumed to wear a lead shielding suit (0.3 cm thickness). The direct ingestion rate was set to 0.052 for the volume source, 8.94×10^{-8} for the ceiling and floor in the area source, and 7.97×10^{-8} for the side.

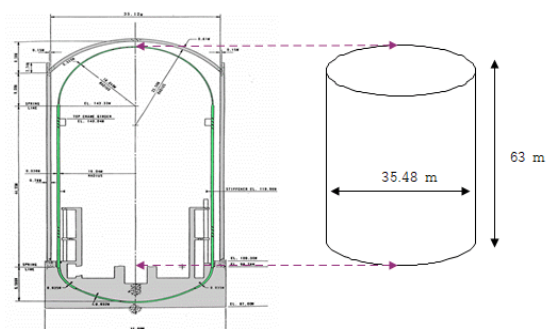


Fig. 2. Determination of building value for Kori Unit 1 Containment Building.

The radionuclides for calculating DCGL were selected from the radionuclides detected both at the Zion NPP and Rancho Seco NPP, which was selected as a reference NPP. Table 1 shows the radionuclides used in this study.

Table 1. Radionuclides detected in Rancho Seco and Zion NPP buildings [4, 5]

Radionuclide			
^3H	^{90}Sr	^{137}Cs	^{239}Pu
^{14}C	^{94}Nb	^{152}Eu	^{240}Pu
^{55}Fe	^{99}Tc	^{154}Eu	^{241}Pu
^{59}Ni	$^{108\text{m}}\text{Ag}$	^{155}Eu	^{241}Am
^{60}Co	^{125}Sb	^{237}Np	^{244}Cm
^{63}Ni	^{134}Cs	^{238}Pu	

4. DCGL calculation

In this scenario, DCGL was calculated using the volume source. The reinforced concrete density used in the containment building was calculated as 2.4 g/cm^3 , and the source thickness was 15 cm. DCGL results are shown below.

Table 2. DCGL in Containment building worker scenario (dpm/100 cm^2)

Radionuclide	2030y 0.1 mSv/yr	Radionuclide	2030y 0.1 mSv/yr
^3H	1.70×10^8	^{137}Cs	2.18×10^3
^{14}C	8.13×10^5	^{152}Eu	1.49×10^3
^{55}Fe	7.84×10^7	^{154}Eu	1.87×10^3
^{59}Ni	8.06×10^6	^{155}Eu	6.77×10^6
^{60}Co	1.65×10^3	^{237}Np	3.67×10^2
^{63}Ni	3.22×10^6	^{238}Pu	5.79×10^2
^{90}Sr	1.45×10^4	^{239}Pu	4.70×10^2
^{94}Nb	5.55×10^2	^{240}Pu	4.73×10^2
^{99}Tc	1.16×10^6	^{241}Pu	1.80×10^4
$^{108\text{m}}\text{Ag}$	6.72×10^2	^{241}Am	4.67×10^2
^{125}Sb	7.27×10^4	^{244}Cm	1.35×10^3
^{134}Cs	4.62×10^4		

5. Conclusion

In this study, DCGL is derived through the probabilistic analysis of the RESRAD-BUILD code. Deterministic and probabilistic parameters that reflect the characteristics of Kori Unit 1 are applied then sensitivity analysis are performed for the containment building worker scenario. Through this process, we derived the Kori Unit 1 preliminary DCGL.

The location of the receptor was calculated at 1 m from the containment building wall and the Kori Unit 1 source area was 1.13 times larger than that of Rancho Seco. Also Site release criteria of South Korea is lower than Rancho Seco. According to different parameter values, the results dose obtained in the case of the Kori Unit 1 were more conservative. Applying more site-specific parameters of Kori Unit 1 will deduce more site-specific DCGL.

ACKNOWLEDGEMENT

This work was supported by the National Research Foundation of Korea grant funded by the Korea government (No. NRF-2018M2B2B1065637); and was supported by the National Research Foundation of Korea grant funded by the Korea government (No. NRF-2018M2B2B1065637).

REFERENCES

- [1] C. Yu, D.J. LePoire, J.J. Cheng, E. Gnanapragasam, S. Kamboj, J. Arnish, B.M. Biwer, A.J. Zielen, W.A. Williams, A. Wallo III, H.T. Peterson, Jr, "User's Manual for RESRAD-BUILD Version3", Argonne National Laboratory (2003).
- [2] Sacramento Municipal Utility District, "Rancho Seco License Termination Plan Chapter 6" (2006).
- [3] Ministry of Trade, Industry and Energy, "Conference for Permanent shut down of Kori Unit 1" (2017).
- [4] ZionSolutions, TSD14-019, "Radionuclides of Concern for Soil and Basement Fill Model Source Terms" (2014).
- [5] Sacramento Municipal Utility District, DTBD-05-007, "Rancho Seco Nuclear Generating Station Decommissioning Technical Basis Document, Containment Buildings DCGLs" (2006).

Derivation of Surface Soil Area Factor for Kori-1 NPP by Using RESRAD-ONSITE

Ji Hyang Byon, Sang June Park, and Seokyoung Ahn*

Pusan National University, 2, Busandaehak-ro 63beon-gil, Geumjeong-gu, Busan, Republic of Korea

*sahn@pusan.ac.kr

1. Introduction

Currently, decommissioning procedure and related preparations for Kori Unit 1 are being prepared based on MARSSIM, U.S. standard decommissioning procedure guidance manual. MARSSIM recommends derivation of DCGLs to establish safety assessment methods for site de-regulation in preliminary survey and final status survey. DCGLs are derived differently from DCGL_w, which is calculated by applying the uniformly distributed residual radioactivity over a wide area, and DCGL_{EMC}, which is applied when there is elevated residual radioactivity in small areas. In this study, a suite of potential radionuclides of Kori Unit 1 was selected in the same way as the preceding DCGL_w derivation, and area factor for DCGL_{EMC} of surface soil exposure was derived by referring to the decommissioning technical documents of U.S. nuclear power plants.

2. Potential Radionuclides of Concern

A suite of potential radionuclides of Kori Unit 1 was selected by combining the methodologies of Rancho Seco and Zion NPPs. Table 1 lists the theoretical potential radionuclides.

Table 1. Theoretical Radionuclides of Concern

NPP	Rancho Seco (PWR, Babcocks&Wilcox)	Zion 1,2 (PWR, Westinghouse)
Document	NUREG/CR-3474 [1]	
Common	^{108m} Ag	³⁹ Ar
	⁴¹ Ca	³⁶ Cl
	¹³⁷ Cs	¹⁵² Eu
	^{178m} Hf	³ H
	^{166m} Ho	⁸⁵ Kr
	^{121m} Sn	⁹⁴ Nb
	²⁰⁵ Pb	¹⁴⁵ Pm
	¹⁴⁶ Sm	¹⁵¹ Sm
	⁹⁹ Tc	²³³ U
	^{93m} Nb	¹³⁵ Cs
Difference		²⁴⁰ Pu
Document	NUREG/CR-4289 [2]	
Common	²³⁸ Pu	²⁴¹ Am
	¹²⁵ Sb	²³⁷ Np
Difference	²⁴⁰ Pu	²⁴³ Am
Document	NUREG/CR-0130, Vol. 1 [3]	WINCO-1191 [4]
Difference		¹⁴⁷ Pm
ORIGEN code		19 samples [5]
¹⁴⁷ Pm		²⁴¹ Pu
²⁴³ Am		²⁴³ Cm
NCRP Report No.58 [6]		²⁴³ Cm
²³⁴ U		²³⁵ U
²³⁶ U		²³⁸ U

Referring NUREG/CR-3474, NUREG/CR-4289, NUREG/ CR-0130, vol. 1, WINCO-1191, radionuclides with a half-life of more than 2 years were initially selected. Remaining radionuclides were supplemented with reference to the results of the ORIGEN code execution and NCRP Report No. 58 in Rancho Seco NPP and Zion NPP added radionuclides through 19 sample analyzes, including waste stream analysis actually collected at the site. As a result, theoretical radionuclides of concern for Rancho Seco

and Zion NPP were 54 and 47, respectively.

However, in order to select the site-specific radionuclides, a process of summarizing the nuclides of Table 1 is necessary. In the case of Rancho Seco NPP, site-specific suite of radionuclides was established by using the results of the NUREG/CR-3474 radioactive fraction and ORIGEN code results, radionuclides with less than 0.1% concentration of total radioactivity were excluded and added via 10 CFR Part 61 waste stream analysis [7]. Zion NPP excluded radionuclides with an active concentration of less than 0.0001 (0.01%) compared to the active concentration calculated from the sum of ⁶⁰Co and ⁶³Ni, the main radionuclides identified in 19 representative samples. Although it does not appear in the documentation, ^{92m}Nb of Zion NPP has been excluded with a half-life of 10.13 days. In common, inert gases and naturally occurring radionuclides were also excluded. Finally, 26 site-specific radionuclides were determined for both NPPs. (Common radionuclides: ^{108m}Ag, ¹⁴C, ⁶⁰Co, ¹³⁴Cs, ¹³⁷Cs, ¹⁵²Eu, ¹⁵⁴Eu, ¹⁵⁵Eu, ⁵⁵Fe, ³H, ⁵⁹Nb, ⁵⁹Ni, ⁶³Ni, ²³⁸Pu, ²³⁹Pu, ²⁴⁰Pu, ²⁴¹Pu, ⁹⁰Sr, ⁹⁹Tc, ²⁴¹Am, ²⁴⁴Cm, ²³⁷Np, ¹²⁵Sb, ¹⁴⁷Pm, ; Radionuclides specific to Rancho Seco NPP: ²²Na, ²⁴²Pu, ; Radionuclides specific to Zion NPP: ²⁴³Am, ²⁴³Cm).

Rancho Seco NPP selected site-specific radionuclides for soil by positively detected radionuclides through pool cooler pad soil sample, which was the most contaminated during characterization, and found that the contribution dose was less than 10% through nuclide fraction (*n*/*f*). Radionuclides applied to soil for Zion NPP were selected which accounted for more than 99.5% of the total dose in the auxiliary building [8]. The concerned radionuclides selected for the two NPPs were the same, with the exception of ¹⁴C for Rancho Seco NPP. Since the characterization survey of Kori Unit 1 has just started, there is not enough information about radionuclides that can be directly applied to soil of the site. Referring to methodologies for selecting concerned radionuclides in soil of two U.S. NPPs cases, the remaining radionuclides were assumed to be same as Rancho Seco NPP. Concerned radionuclides of Kori Unit 1 were preliminarily selected as listed in Table 2.

Table 2. A preliminary suite of concerned radionuclides for soil at Kori Unit 1 reuse scenario

Radionuclides of concern	
Radionuclide	Half-life (years)
¹⁴ C	5.73×10 ³
⁶⁰ Co	5.27×10 ⁰
¹³⁴ Cs	2.06×10 ⁰
¹³⁷ Cs	3.02×10 ¹
⁹⁰ Sr	2.86×10 ¹
⁶³ Ni	1.00×10 ²

3. Area factor for DCGL_{EMC}

DCGL_w is the average concentration of a wide area calculated as a result of an average member of a critical group receiving a dose at the appropriate dose limit, assuming that the concentration of radionuclide is homogeneous. Given the potential for elevated residual radioactivity of small areas, an assessment should be performed to assess the likelihood of missing such areas during a scan outside of a fixed

measurement range. As shown in Fig. 1, $DCGL_{EMC}$ is a site release standard concentration applicable to the hot spot area, Class 1, which is applied to a region where there is locally elevated residual radioactivity to be measured. The use of elevated measurement comparisons (EMC) represents a conservative approach in that all measurements must be below the action level. The level of investigation for this comparison is called $DCGL_{EMC}$ [9].

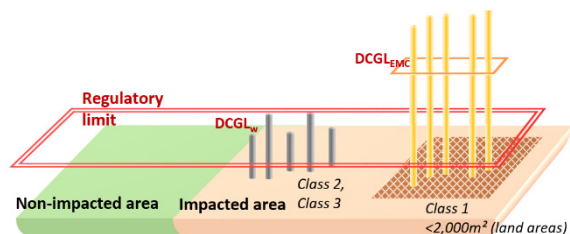


Fig. 1. Conceptual figure of area classification related to DCGLs.

In order to determine $DCGL_{EMC}$, modified $DCGL_w$ using an area factor that takes into account the difference in area and hence the dose change. Area factor is influenced by how the smaller area affects the dose to average member of critical group, for example, a smaller area may mean that the external dose is more limited because it is not reasonable to expect it to be exposed at the same time as when the individual is in a larger area. Area factor is derived by calculating Equation (1).

$$AF_i = DSR_{base} / DSR_i \quad (1)$$

Where AF_i is area factor of EMC area i , DSR_{base} is the Dose to Source Ratio (DSR) of the baseline area, and DSR_i is DSR of the EMC area i . DSRs were calculated through RESRAD-ONSITE probabilistic analysis.

4. Results & Discussion

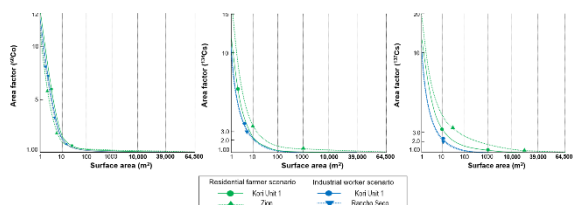


Fig. 2. Surface soil area factors for gamma emitters.

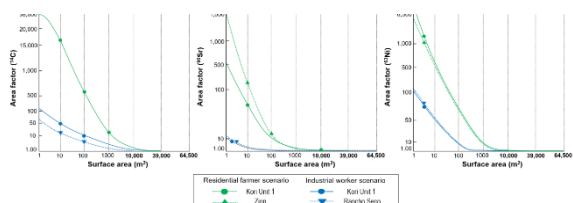


Fig. 3. Surface soil area factors for beta emitters.

Fig. 2 and Fig. 3 show gamma emitters and beta emitters in order to confirm the trend of area factor according to scenarios rather than direct comparison. Baseline areas for each Rancho seço, Kori Unit 1, Zion NPP were specified by 10,000 m², 39,000 m², 64,500 m² [7, 10]. Of the gamma emitters, ⁶⁰Co had a maximum difference of about 8% based on 1 m², regardless of scenarios. As area factors were derived with the same values as Zion NPP in same residential farmer scenario, there was also no effect of increasing exposure pathways. Similarly, for ¹³⁴Cs and ¹³⁷Cs, there

was little difference in area factors applying industrial worker scenario. The difference between area factors of Zion NPP in the same residential farmer scenario was greater than the difference between the area factors of residential farmer scenario and industrial worker scenario. In the case of beta emitters, differences in area factors by scenario were much larger than gamma emitters. ⁹⁰Sr showed the greatest difference in area factor from Zion NPP in the same residential farmer scenario, while ⁶³Ni showed maximum difference according to the scenario. Area factors in both gamma and beta emitters were derived to a value higher than industrial worker scenario when residential farmer scenario was applied.

5. Conclusion

Preliminary area factors for class 1 soil surface were derived in consideration of the presence of elevated residual radioactivity in impact area for further FSS of Kori Unit 1. Classification of impact area via area factors is essential during the decommissioning process, and the level of survey effort is determined by the classified area. Survey designs will be developed that provide coverage by selecting appropriate instrumentation and techniques through a combination of scans, instrument measurements, and sampling. It is expected that appropriate sensitivity of scanning technique and additional sampling points could be adjusted through the area factors and applied to elevated residual radioactivity evaluation during the FSS.

ACKNOWLEDGEMENT

This work was supported by the Nuclear Safety Research Program through the Korea Foundation Of Nuclear Safety (KoFONS) using the financial resource granted by the Nuclear Safety and Security Commission (NSSC) of the Republic of Korea (No.1305009); and was supported by the National Research Foundation of Korea (NRF) grant funded by the Korea government (No. NRF-2018M2B2B1065637).

REFERENCES

- [1] NRC, NUREG/CR-3474, "Long-Lived Activation Products in Reactor Materials", 1984.
- [2] NRC, NUREG/CR-4289, "Residual Radionuclide Contamination Within and Around Commercial Nuclear Power Plants", 1986.
- [3] NRC, NUREG/CR-0130, Vol. 1, "Technology, Safety, and Costs of Decommissioning a Reference Pressurized Water Reactor Power Station", 1986.
- [4] Westinghouse Idaho Nuclear Company Inc., WINCO-1191, "Radionuclides in United States Commercial Nuclear Power Reactors", 1994.
- [5] Zion Solutions Inc., TSD 14-019, "Radionuclides of Concern for Soil and Basement Fill Model Source Terms", 2014.
- [6] National Council on Radiation Protection and Measurement, NCRP Report No. 58, "A Handbook of Radioactivity Measurements Procedures", 1984.
- [7] NRC, "Rancho Seco License Termination Plan", 2014.
- [8] Zion Solutions Inc., TSD 14-019, "Radionuclides of Concern for Soil and Basement Fill Model Source Terms", 2014.
- [9] NRC, EPA, DOD, DOE, "Multi-Agency Radiation Survey and Site Investigation Manual (MARSSIM)", 2000.
- [10] Zion Solutions Inc., TSD 14-011, "Soil Area Factors", 2014.

A Study on Calculation Program Verification Test Method to Reflect the Latest Standard of Sample Transfer Rate

Ju-Young Yoon* and Cheon-Woo Kim

Korea Hydro & Nuclear Power Co., Ltd. Central Research Institute, 70, 1312-gil, Yuseong-daero,
Yuseong-gu, Daejeon, Republic of Korea

*august63@khnp.co.kr

1. Introduction

Radiation monitors of gaseous effluents from nuclear power plants shall meet the design requirements of a sample transport efficiency of at least 50% when applying the ANSI-HPS N13.1 technical standard. In order to enable the design of the sample transport line with the calculation program and the verified correction values without the sample transfer verification test, the method of substituting the transport line verification test method need. During development, test method for the Deposition code(2001), a calculation program, were studied.

2. Test Method

2.1 Test Condition

The sample transfer rate varies depending on the temperature, pressure, flowrate, nozzle specifications, particle dispersion, and other factors. According to design requirements, the test was carried out under the following conditions at 25 °C and 1 atm.

2.1.1 There should be no inward facing step that minimizes the length of the horizontal tube and the number of bends, and reduces the tube diameter by more than 1% at the tube connection.

2.1.2 There should be no burrs or crimping at the end of the transport line.

2.1.3 The curvature ratio of the bend shall not be less 3.0 and not more than 15% flattening.

(flattening = reduced axis/angular midpoint axis)

2.1.4 Criteria for particle sample loss: 50% or more of sample permeability for 10 μm particles

2.1.5 Materials used: To give stainless steel to the nuclear industry

2.1.6 The internal surface smoothness of the

transfer line is allowed to be a tube having a ε/d_i of about 5×10^{-5} or less.

(ε =surface roughness, d_i =inside diameter of tube)

2.2 Intuition transport rate test

To apply the test requirements, cut the length of the transfer line from 1m to 12m to verify the sample transport rate in the horizontal tube.

In order to investigate the difference in the transport rate to the tube slope of the transfer line, the sample transfer test is performed by applying the conditions of the tube slope of 30°, 45°, 60°, and 90°. To determine whether there is a difference in the sample transport rate between the up-stream and the down-stream, the transport rate performance test is performed by applying the condition of each tube.

2.3 Curve transport rate test

In ANSI N13.1 (1999), the bending radius is defined as above 3DR, but the sample transfer rate is verified conservatively by applying 5DR.

Deposition 2001a has the same transport rate even under different conditions of tilting of the bend or different direction of suction and discharge. The effect of the transport rate is verified by applying the inclination condition of five curves.

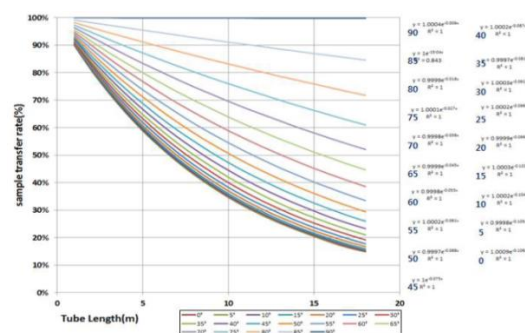


Fig. 1. Calculation results of tube transfer rate.

3. Test Result

The sample transport rate performance test of the transfer tube was performed by measuring five sets of U/S (up-stream) and D/S (down-stream) 10 times each using a particle counter and taking valid data out of the results.

This test was conducted by installing particle generator, particle counter, suction pump, flow regulator, transport line, etc.



Fig. 2. Installation of test equipment.

The sample transport rate was measured by 4m length tube with a diameter of 1-1/2" under the condition of 2cfm flowrate. The results of the verification and the sample transport rate of the sample transport rate calculation program were similar. The results of the test are as follows.

Table 1. Test results of tube transfer rate

	U/S	D/S		T/R
AVG	92,963	60,012	Verification Test	64.55%
STD	1,076	2,127		
COV	1.1%	3.5%	Deposition 2001a	65.50%
T/R	64.55%			

SET	#1		#2		#3		#4		#5	
POINT	U/S	D/S	U/S	D/S	U/S	D/S	U/S	D/S	U/S	D/S
1	90,069	63,526	93,570	61,441	93,607	61,195	93,492	56,062	93,925	62,137
2	91,742	60,790	92,883	57,713	91,902	60,015	91,615	59,899	93,856	59,503
3	91,844	61,729	94,064	60,296	91,425	59,367	92,789	60,080	94,157	63,986
4	94,574	62,690	92,184	54,468	93,155	60,354	93,044	56,932	93,687	60,598
5	93,816	63,107	92,470	57,249	92,799	57,172	93,407	59,677	95,617	64,425
6	93,352	63,356	91,617	60,356	94,208	62,578	92,776	57,353	92,537	62,332
7	92,576	62,259	92,798	57,571	91,627	60,135	93,700	59,759	93,145	59,484
8	93,420	59,521	90,725	58,748	92,102	61,740	94,584	60,409	92,706	57,551
9	93,187	58,852	93,288	58,853	92,170	59,088	91,744	59,884	93,662	59,573
10	93,656	59,739	91,603	57,732	93,391	58,685	93,350	58,913	94,548	61,740
AVG	92,824	61,557	92,520	58,443	92,639	60,033	93,050	58,897	93,784	61,133
STD	1,303	1,722	1,015	1,982	931	1,570	888	1,538	898	2,179
COV	1.4%	2.8%	1.1%	3.4%	1.0%	2.6%	1.0%	2.6%	1.0%	3.6%
T/R	66.3%		63.2%		64.8%		63.3%		65.2%	

4. Conclusion

If the radiation monitoring system has to be applied to the latest technical standards requirements in accordance with the revision of the technical standards, it is necessary to apply the calculation program and the proven calibration values without the sample transfer verification test. And we have studied the test method for verifying the calculation program.

The preliminary test was performed before the full-scale test, and the test result was similar to the sample transfer efficiency of the calculation program.

In the future, we will develop a methodology for the substitution of the transport line test based on the results of the demonstration test with various locations and bending tests.

REFERENCES

- [1] ANSI/HPS N13.1-1999, "Sampling and Monitoring Releases of Airborne Radioactive Substances from the Stacks and Ducts of Nuclear Facilities", American National Standards Institute and the Health Physics Society.
- [2] 40 CFR 60, Appendix A, Method 1. "Method 1—Sample and Velocity Traverses for Stationary Sources." Code of Federal Regulations, U.S. Environmental Protection Agency.

Analysis of Occupational Radiation Exposure in Nuclear Power Plant in Korea

Gang Woo Ryu¹⁾, Woo Jin Kim¹⁾, Byeong Soo Kim²⁾, and Kwang Pyo Kim^{1),*}

¹⁾ Kyunghee University, 1732, Deokyoungdae-ro, Giheung-gu, Yongin-si, Gyeonggi-do, Republic of Korea

²⁾ Korea Institute of Nuclear Safety, 62, Gwahak-ro, Yuseong-gu, Daejeon, Republic of Korea

*kpkim@khu.ac.kr

1. Introduction

The number of radiation workers in radiation and nuclear industries is increasing every year. In Korea, there are the largest number of radiation workers in nuclear power plants. Radiation workers in nuclear power plants are exposed by various factors such as waste management during the operation of nuclear power plants.

Radiation exposure data in nuclear power plants are collected and managed monthly. The radiation exposure dose in nuclear power plants is necessary to manage the radiation workers.

In this study, radiation and nuclear industries were classified by industry and we analyzed the number of radiation workers, collective dose, and average dose in 2017. In order to analyze the radiation exposure in nuclear power plant, we analyzed the collective dose and average dose for the last 10 years (2008-2017).

2. Materials and Methods

Radiation exposure data is collected from Korea Information System on Occupational Exposure (KISOE). Radiation and nuclear industries were classified into 10 types. To analyze the radiation exposure dose to radiation workers, use a SAS program that is suitable for the analysis of big data. As of 2017, the number of radiation workers, collective dose, and average dose of radiation and nuclear industries were analyzed. To analyze in detail detailed, we analyzed the collective dose and average dose of nuclear power plants for the last 10 years (2008-2017).

3. Results

Fig. 1 shows the number of radiation workers in each industry in 2017. As of 2017, the total number of

radiation workers in Korea was about 42,000. Nuclear power plants accounted for the highest percentage of the total number of radiation workers, about 33%. Non-destructive test institutions, medical institutions and general industries were 14%, 13.1%, 12.8% each.

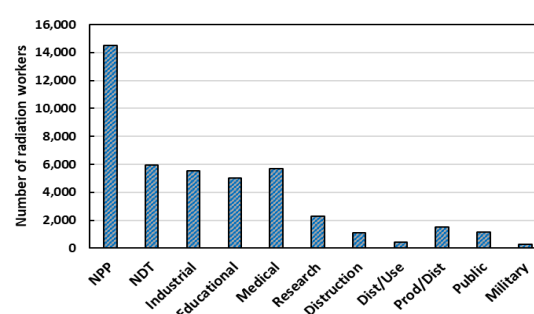


Fig. 1. The number of radiation workers with institution classification.

Fig. 2 shows the collective dose and average dose for each industry in 2017. As of 2017, the collective dose of all industries was about 17,000 man·mSv and the average dose was about 0.4 mSv. The collective dose was about 7,300 man·mSv in nuclear power plant, accounting for 42% of the total. Non-destructive test institutions and medical institutions were 36%, 14% each. The average dose of non-destructive institutions was the highest, followed by nuclear power plants and medical institutions.

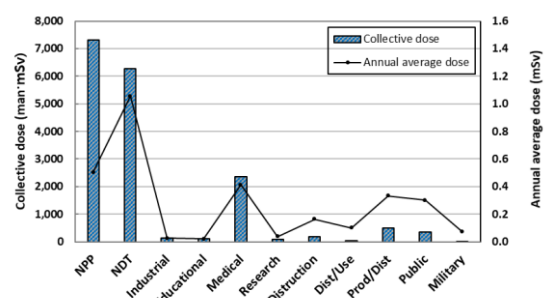


Fig. 2. Collective dose and annual average dose with institution classification.

Fig. 3 shows the trend of the collective dose and average dose for the last 10 years (2008-2017). In 2017, the collective dose and average dose of nuclear power plants have decreased by about 30% compared with last year. Over the last 10 years, collective dose and average dose have generally decreased, reaching their lowest in 2017.

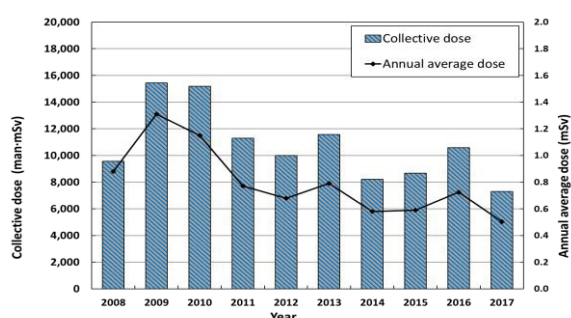


Fig. 3. Collective dose and annual average dose for a decade in NPP.

Fig. 4 shows the number of radiation workers in nuclear power plants by dose range over the last 10 years (2008-2017). In 2017, the number of workers included in the dose range of 1 mSv or less accounted for more than 85% of the total workers. Over the last 10 years, the number of workers in the dose range of 1 mSv or less occupied the largest portion. The number of workers included in the 1-15 mSv dose range was the lowest in 2017 over the last 10 years.

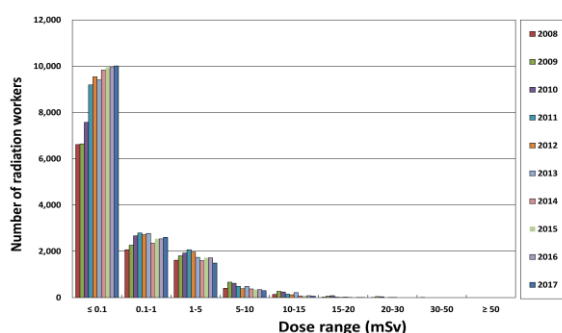


Fig. 4. Collective dose and annual average dose for a decade in NPP.

4. Conclusion

In this study, the number of radiation workers, collective dose, and average dose of radiation and nuclear industries were analyzed based on radiation

exposure data. To analyze in detail, we analyzed the collective dose, average dose, and number of workers in nuclear power plants by dose range. As a result, it accounted for 33% of the total number of workers in nuclear power plants in 2017. The collective dose was 42% of the total collective dose. Over the last 10 years, collective dose and average dose in nuclear power plants have generally decreased, reaching the lowest in 2017.

The data analyzed through this study can be used as basic data for radiation dose management and radiation safety management of radiation workers in nuclear power plants. It will contribute to the reduction of radiation dose of radiation workers.

ACKNOWLEDGEMENT

This study was supported by (Development of base data for analysis of occupational radiation exposure in 2017) the Korea Institute of Nuclear Safety.

REFERENCES

- [1] DOE, DOE 2016 Occupational Radiation Exposure, Department of Energy (2017).
- [2] NRC, Occupational Radiation Exposure at Commercial Nuclear Power Reactors and other Facilities 2016, NUREG-0713 (2016).

Evaluation of Ambient Dose Equivalent of Silicon Carbide by Neutron Irradiation

Ki-Man Lee* and Byong-Gun Park

Korea Atomic Energy Research Institute, 111, Daedeok-daero 989beon-gil, Yuseong-gu, Daejeon, Republic of Korea

*lkm@kaeri.re.kr

1. Introduction

Neutron transmutation doping (NTD) of semiconductors is an important method for applications that require high dopant homogeneity [1]. Silicon carbide (SiC) single crystal has been a substrate material for high power and high frequency electronic devices. When the SiC is irradiated by neutrons, Si, C and impurities become radioactive nuclides. Radiations emitted from these radioactive nuclides constantly damage to the SiC and operators until they have been completely decayed. In this study, the time variation of ambient dose equivalent $H^*(10)$ of radionuclides in the irradiated SiC is calculated in terms of safety.

2. Methods and Results

2.1 Monte Carlo simulation

A Monte Carlo particle transport simulation code PHITS (Particle and Heavy Ion Transport code System) version 3.02 was used for calculating the ambient dose equivalent of radionuclides in SiC. The DCHAIN program linked to PHITS was used to calculate the time variation of ambient dose equivalent during irradiation and cooling. Neutrons in NTD1 irradiation hole of HANARO research reactor were considered as a source term. Neutrons were assumed to be uniformly distributed on the surface of a vertical channel with a radius of 10.125 cm as the NTD1 irradiation hole. A sample for neutron irradiation was modeled as 5-inch cylindrical single crystal SiC with a volume of $3.8 \times 10^3 \text{ cm}^3$.

Aluminum, boron, iron and titanium that are major impurities in the SiC wafer were considered [2]. Concentration of each impurity was conservatively assumed as 10 ppm. For the t-dchain tally, the current of neutron beam was set corresponding to the neutron flux of $4.33 \times 10^{13} \text{ n/cm}^2 \cdot \text{sec}$ in SiC. Neutron irradiation time was set to 24 hours, and the ambient dose equivalent of each nuclide was calculated by the hour during irradiation. The total ambient dose equivalent was calculated until 10 days later after irradiation. And the ambient dose equivalent of main radionuclides was calculated for 1 days after irradiation.

2.2 Results of simulation

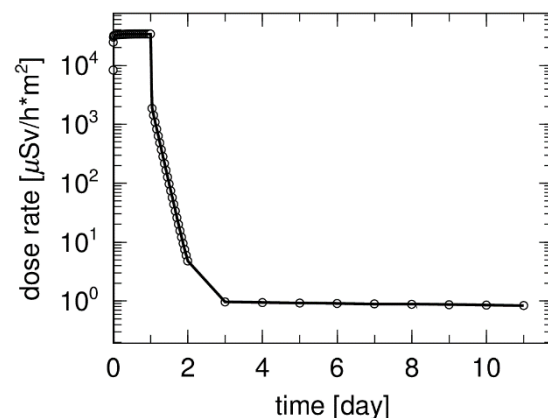


Fig. 1. Time variation of the total ambient dose equivalent of SiC during and after neutron irradiation of 1 day (plotted by ANGEL 4.50).

The time variation of the total ambient dose equivalent of SiC during and after neutron irradiation of 1 day is showed in fig. 1. Total ambient dose equivalent increases until the end of neutron irradiation, and it continues to decrease sharply for 2 days.

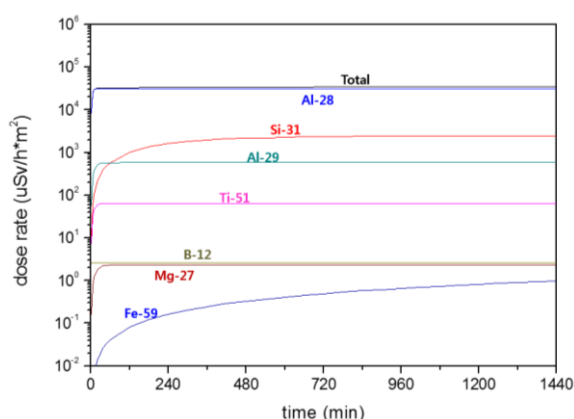


Fig. 2. Time variation of ambient dose equivalent of radionuclides in SiC during neutron irradiation of 1 day.

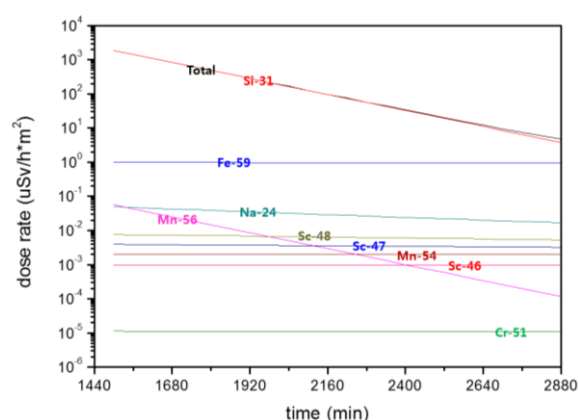


Fig. 3. Time variation of ambient dose equivalent of radionuclides in SiC after neutron irradiation of 1 day.

The time variations of ambient dose equivalent of neutron induced radionuclides in SiC during and after neutron irradiation are showed in fig. 2 and fig. 3, respectively. During the neutron irradiation, ^{28}Al produced by activation of impurity element ^{27}Al is a main contributor to ambient dose equivalent because of its short half-life. After the neutron irradiation, the radionuclides with short half-life are early decayed and ^{31}Si becomes the main contributor. Among the radionuclides produced by activation of impurity elements, ^{59}Fe represents the highest dose rate.

3. Conclusion

Total ambient dose equivalent of SiC is sufficiently decreased in 2 days because the main

radionuclides ^{28}Al and ^{31}Si have short half-life in minutes or hours. The main radionuclides which contribute to dose rate are also evaluated to control the unintended effect and study the radiation damage to SiC by NTD. These results will be used as the basis for future study.

ACKNOWLEDGEMENT

This work was supported by the National Research Foundation of Korea (NRF) Grant funded by the Korea government (MSIP) (NRF-2017M2A2A6A05018527).

REFERENCES

- [1] IAEA, "Neutron Transmutation Doping of Silicon at Research Reactors", Report IAEA-TECDOC series, 1681, (2012).
- [2] D. G. Shin, H. R. Son, S. Heo, B. S. Kim, J. E. Han, K. S. Min and D. H. Lee, "Impurity Behavior of High Purity SiC Powder During SiC Crystal growth", Material Science Forum, 778, 22-25 (2014).

Development of a Concept of Dynamic Integrated Safety Analysis for Accident Predictions

Seok-Jun Seo^{1),*}, Jong Yol Park²⁾, and Seung Nam Yu¹⁾

¹⁾ Korea Atomic Energy Research Institute, 111, Daedeok-daero 989beon-gil, Yuseong-gu, Daejeon, Republic of Korea

²⁾ RIA Institute Inc., 9, Nongdae-ro 2benon-gil, Yuseong-gu, Daejeon, Republic of Korea

*sjseo@kaeri.re.kr

1. Introduction

In nuclear related facilities, safety is one of the most significant issues for reliability and sustainability of the facility operations. In case of a fuel cycle facility, U.S. Nuclear Regulatory Commission (NRC) requests to conduct integrated safety analysis (ISA) for protecting public, facility workers, and the environment. The ISA has been conducted to examine potential hazards with relatively higher likelihood of occurrence and to prevent and mitigate accidents by designating items relied on for safety (IROFS), finally meeting a performance requirements of 10 CFR 70.61 [1].

Although the ISA has several advantages for applying to relatively smaller-scale nuclear facilities containing various types of chemical process equipment [2], it gives a natural limitation that the values of likelihood of occurrence are determined and fixed by vague engineering judgments comparing with a probabilistic safety assessments (PSA). In case of PSA, currently, dynamic-PSA has been developing by considering system dynamics with Monte Carlo simulation and dynamic event tree [3].

In this study, a concept of dynamic ISA(D-ISA) is devised for an accident prediction by utilizing internet of things (IoT) technologies. Recently, there are also similar researches especially for fire prediction, red tide detection and prediction, and disaster safety platform technologies.

2. Methodology

This D-ISA concept is based on a risk index matrix of the ISA (see Table 1). After conducting ISA for a smaller-scale nuclear facility, specific sequences of design basis accidents are examined. Then, a consolidated IoT system with several IoT sensors such as temperature, pressure, electrical current, water level, wind speed, radiation, and so on is connected to a central big data server system for calculating real-time likelihood of occurrence and consequence of each DBAs.

Table 1. 3x3 Risk Index Matrix

		Likelihood of Occurrence		
		Highly Unlikely [1]	Unlikely [2]	Not Unlikely [3]
Consequence	High [3]	Acceptable 3	Not Acceptable 6	Not Acceptable 9
	Intermediate [2]	Acceptable 2	Acceptable 4	Not Acceptable 6
	Low [1]	Acceptable 1	Acceptable 2	Acceptable 3

ACKNOWLEDGEMENT

This work was supported by National Research Foundation of Korea (NRF).

REFERENCES

- [1] NUREG-1520, Standard Review Plan for Fuel Cycle Facilities License Applications, U.S. Nuclear Regulatory Commission(2015).
- [2] A Comparison of Integrated Safety Analysis and Probabilistic Risk Assessment, U.S. Nuclear Regulatory Commission, ML103330478 (2010).
- [3] H. Lee, T. Kim, G. Heo., Application of Dynamic Probabilistic Safety Assessment Approach for Accident Sequence Precursor Analysis: Case Study for Steam Generator Tube Rupture, Nuclear Engineering and Technology 49, 306-312 (2017).

Improved Facility Exhaust Stability Using Drive Synch System

Heeseok Kang*, Seonho Noh, Youngkuk Jang, Wonkyoung Lee, Daeyong Song, and Ilje Cho

Korea Atomic Energy Research Institute, 111, Daedeok-daero 989beon-gil, Yuseong-gu, Daejeon, Republic of Korea

*hskang1@kaeri.re.kr

1. Introduction

The Korea Atomic Energy Research Institute (KAERI) operates a Nuclear Cycle Experimental Research Facility, which is a testing facility capable of simulating all processes of nuclear material process testing on a laboratory scale for the purpose of peaceful use of nuclear materials. Argon gas for maintaining the atmosphere in the glove box and various types of toxic gases generated during the experiment should be discharged outside the facility. If the exhaust becomes unstable due to the abnormality of the exhaust system, there is a concern that the radioactive contaminants may spread out of the facility and become a social problem, which can cause serious health problems to workers in the facility. Therefore, Nuclear Cycle Experimental Research Facility center introduced a drive synch system to improve the operation stability of the exhaust system of the facility. After the drive synch system was installed, stability improvement of the exhaust system was compiled by comparing the stability of operation with existing facilities.

2. Drive Synch System

2.1 Overview of drive synch system

A drive sync systems are systems double(multiple) a drive in a critical facility that requires continuous operation, as shown in Figure 1. It synchronizes single AC motor control with a drive-load N: 1 configuration drive. Even if one of the drives fails, the remaining drives can be continuously operated,

so that replacement or repair during operation can be performed without stopping the drive facility in which the failure occurs. In addition, it is possible to perform normal operation continuously after repairing the fault of the equipment, and it is possible to prevent preventive maintenance and maintenance of the drive even during normal operation of the facility. Even momentary power failure has the advantage of being able to maintain normal operation without stopping for a few seconds, so that it is ready for some power failure. Therefore, the stability of such continuous operation is widely used in various industries such as steel, automobile, chemical, shipbuilding, marine, waterworks, sewage and sewage relay pumping stations. Nuclear Cycle Experimental Research Facility introduced this system to improve the operation stability of the exhaust system of the facility by taking advantage of the above mentioned drive synch system.



Fig. 1. Drives synch system configuration.

2.2 Improved operation stability after installation of drive synch system

Nuclear Cycle Experimental Research Center omic runs a total of six exhaust systems for the exhaust gas generated during the process test and the facility vent for ventilation. In the past, a single inverter was

connected to one exhaust system to control each exhaust system. However, in this system, the intermittent momentary power interruption in the researcher has been shut down whenever the plant is out of power, and sometimes the exhaust fan has been shut down due to an unknown electrical shock. In some cases, some of the exhaust fans were shut down unintentionally, causing some workers in the laboratory to experience discomfort. In order to improve the instability of the exhaust system, a drive synch system of C-1 type was installed as shown in Fig. 2 and Fig. 3. The three exhaust systems are grouped together and connected in parallel by two drive sync systems. In this facility, six exhaust systems are in operation, requiring four drive synch systems.

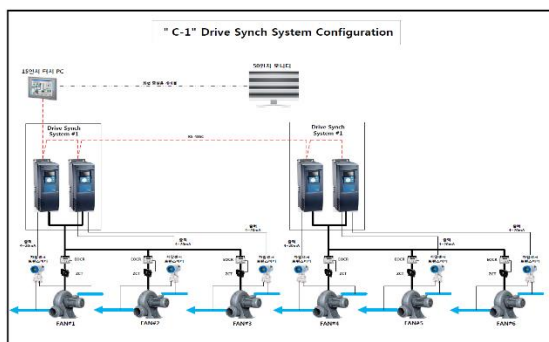


Fig. 2. C-1 drive synch system configuration.

The post-installation effect of the drive synch system has been proven by the operational stability of the exhaust system. There was no single shutdown of the exhaust system even during several instantaneous power failures and I have not experienced the shutdown of the exhaust system, No shutdowns had been experienced in some devices or no shutdowns that had been seen in the entire exhaust. Currently, two parallel inverters are connected to three



Fig. 3. Control panel of C-1 drive synch system.

exhaust systems, respectively, so that parallel operation is possible, and maintenance of power unit and control unit can be separated easily. In addition, it is possible to program in the form desired by the built-in PLC function. Even if one inverter failed, the inverter was repaired or replaced without stopping the exhaust system. After replacement of the failed inverter, the unit was returned without stopping the plant, and the exhaust system was ready for 100% operation. The operation stability of the exhaust system is improved compared with the previous system because it is designed not to stop the operation of the plant even in case of power failure in a moment that does not exceed 1 second.

3. Conclusions

The control of the existing exhaust system has a disadvantageous effect on ventilation in the laboratory and exhaust of the toxic gas generated during the experiment due to the stopping of the exhaust system when the inverter failure occurs due to the operation of operating one exhaust fan according to the inverter. System, it was possible to maintain a comfortable laboratory environment by completely solving the operation stop of the exhaust system due to the failure of the inverter, and it was possible to realize safer working environment by strengthening the monitoring of the operating condition of the exhaust system.

Study of the ECCS Water's pH Agent(TSP) Neutralizing Ability Performance Test

Ki-Bang Sung* and Kyunghee Lee

Korea Hydro & Nuclear Power Co., Ltd. Central Research Institute, 70, Yuseong-gu 1312beon-gil, Daejeon, Republic of Korea

*kind.sung@khnp.co.kr

1. Introduction

Tri Sodium Phosphate(TSP) relating to the OPR1000 and APR1400 Operating Technical Specification is stored in a rack on the floor inside the reactor building and dissolved in the recirculation tank during recirculation after LOCA, and sustained the pH 7 or more. This prevents sodium phosphate from volatilizing the iodine dissolved in the reactor coolant into the containment (CV) atmosphere and suppressing stress corrosion cracking (SCC) of an austenitic stainless steel in the reactor building material during the recycle phase. Technical review of the Operating Technical Specification and periodic inspection procedures of the OPR1000 nuclear power plant was conducted. Periodic inspection procedures were prepared according to the TSP limits and technical background of most operating technical specification. However, there are differences in some items, and the results of the review and discussion are described.

2. Background

2.1 OPR1000 NPP's ECCS Neutralizing Agent

In SRP 6.5.2, fission products (especially iodine) can be removed from the containment building atmosphere without pH adjustment of the containment tank water in the containment building sump tank. In recirculation mode, the Emergency Core Cooling System (ECCS) water from the cooling water to the containment building inside air, it is necessary to keep the pH of the containment sump coolant at above 7.0 before the recirculation mode is started because it is necessary to prevent iodine re-volatilization.

OPR1000's "ECCS Trisodium Phosphate Inspection Procedure" is designed and prepared to ensure that iodine dissolved in the reactor coolant does not recur after the reactor coolant loss event (LOCA). Procedures have been established to check the storage capacity of sodium and its ability to control pH.

1) Checking the storage status

Perform visual inspection of the structural deformation or corrosion state of the trisodium phosphate storage box and check the storage condition of the chemical(TSP).

To confirm that the minimum amount of TSP, TSP stored in the total trisodium phosphate storage tank is more than 23.5 m³, measure the height of each storage box, convert the volume into total volume, record it in the TSP test record .

Storage volume(V) : 1.193 (m) x 1.193 (m) x trisodium phosphate height (m)

2) TSP Sampling

Take approximately 50 g of dry TSP from each of the 4 TSP storage racks and place in the sample bottles

Open the outlet valve of the Boric Acid Makeup Pump in operation according to the 1st system sampling procedure and collect about 15.1 L in the pre-filled sample bottle.

3) Solubility test

Put 3.61 ~ 3.99 liters of the total volume in a suitable container.

Heat the entire reheating water to a temperature of 60.0 ~ 65.6 °C with a heating plate.

Measure the temperature and pH of the reconstituted whole water and record it on the trisodium phosphate test record.

20.4 to 21.4 g of solid trisodium phosphate is immersed in the central surface of the heated recharge water and immersed, and the time is recorded.

Record the time taken for the pH to be 7.0 or higher in the trisodium phosphate test record.

3. Discussion on the Plant's Procedures and Technical Specification

3.1 OPR1000 nuclear power plant

As a result of reviewing technical guidelines of OPR1000 nuclear power plant and periodical inspection procedures of power plant to implement them, periodic inspection procedures were written according to TSP limits and technical background of most operational technical manuals. However, there are differences in some items.

1) Check quantity of TSP storage box

In the operating technical manual, the representative samples were taken from one storage box and checked. However, in the procedure, samples are collected from four storage boxes according to the recommendation of the regulatory agency.

However, the storage amount of TSP is designed to be sufficiently conservative that the pH can be raised to 7 or more, and accordingly, it is proper to analyze one sample as it is stored accordingly.

If periodic inspections require the regulator inspectors to measure the pH of one or more storage compartments, it is advisable to ask for further confirmation. (For the regular inspection results of Hanul 5,6, 30 cases were satisfied with pH reaching time)

2) Stirring method for checking neutralization ability

The operating technical manual prohibits stirring because proper standards for the stirring method are not provided. However, in the general chemical experiment, stirring is carried out using a magnet rod or the like in order to minimize the measurement error in pH measurement or neutralization process. Therefore, for the safety of the power plant, it is necessary to accurately measure the neutralizing ability of the pH, which is the chemical ability of the TSP. This can prevent unnecessary measures due to unsatisfactory periodical inspection due to pH measurement error, thus lowering safety reliability of the power plant.

3) Measures when dissatisfied with TSP limit

In the Operating Technical Guideline, measures should be taken to restore the limit of the TSP, the pH dissolution time, and the failure of the pH reaching time. However, one of the regular inspection procedures is that if the pH is less than 7 within 25 minutes, the whole storage TSP should be replaced so that it can not be resolved by finding the cause. If you need to replace the TSP so that it can be recovered beyond the limit (volume)

4. Conclusions

In order to neutralize the pH of the boric acid solution, pH 4.2, in the emergency core cooling system of OPR1000 from acidic to neutral, the contents of periodic inspection of the TSP installed in the reactor building reviewed.

The results of review are as follows.

4.1 OPR1000 nuclear power plant

1) Quantity to be sampled by TSP storage rack

Since the representative samples were collected from one storage box in the operating technical manual, the representative samples were collected from one storage box, and periodical experiments were carried out. When necessary, or when the regulator inspectors measured the pH neutralization capacity of one or more storage boxes If so, it is advisable to carry out additional checks at this time.

2) Stirring method for checking neutralization ability

In general chemical experiments, stirring is carried out using a magnet rod or the like in order to minimize measurement errors in pH measurement or neutralization process. Therefore, for the safety of the power plant, it is necessary to accurately measure the neutralizing ability of pH, which is the chemical ability of TSP, and it is desirable to allow stirring.

3) Measures when dissatisfied with TSP limit

In the Operating Technical Guideline, measures should be taken to restore the limit of the TSP, the pH dissolution time, and the failure of the pH reaching time.

However, one of the regular inspection procedures is that if the pH is less than 7 within 25 minutes, the whole storage TSP should be replaced so that it can not be resolved by finding the cause. It is advisable to carry out TSP replacement if necessary, so that it can be recovered beyond the limit value (volume) after finding the cause in the manual.

REFERENCES

- [1] ShinKori 1,2 power station TSP inspection procedure.
- [2] SRP 6.5.
- [3] Plant's Technical Specification.

Estimation of X-ray Beam Qualities for Performance Test on Personal Dosimetry Systems

Hyeongjin Kim*, Yuho Won, Moonhyung Cho, and Jae-eun Lee

Korea Hydro & Nuclear Power Co., Ltd Central Research Institute, 70, Yuseong-daero 1312-beongil, Yuseong-gu, Daejeon, Korea

*kim.hj1222@khnp.co.kr

1. Introduction

Nuclear utilities should be taken performance test on personnel dosimetry systems to assure the quality of dosimetry performance. According to the Enforcement Regulations for the Nuclear Safety Act, test is carried out in the eight test categories of ionizing radiation, such as low and high energy photons, beta particles and neutrons. And several NIST beam codes are used as low energy photon in the test categories[1]. To provide the reference radiation field for the performance test regarding low energy photon categories, the X-ray generators have been installed in the laboratory of KHNP CRI. X-ray beam qualities are affected by tube voltage/current, collimator, filtrations and the objects in the facility. Therefore, in this work, to ensure that the beam codes made by KHNP-CRI are consistent with the regulations, beam qualities were estimated

2. Method

The X-ray beam qualities could be evaluated by the measurements of the 1st half value layer and the homogeneity coefficient, spectral measurement and a computer simulation. In this work, the measurements of 1st HVL and homogeneity coefficient were performed.

2.1 Characteristics of NIST Beam code

The characteristics of X-ray beam qualities are listed in Table 1. According to the reference, the specified half value layer and homogeneity coefficient should be duplicated to within 5% and

10%, respectively, if necessary by adjusting the tube potential [1].

Table 1. Characteristics of NIST photon beam techniques

No	added filter	Half-value Layer ¹⁾	Homogeneity Coefficient ²⁾	\bar{E} (keV)
M30	0.5 mm Al	0.36 mm Al	65 (Al)	20
M60	1.56 mm Al	1.68 mm Al	68 (Al)	34
M100	5 mm Al	0.2 mm Cu ³⁾	55 (Cu ³⁾)	51
M150	5 mm Al +0.25 mm Cu	0.67 mm Cu ³⁾	62 (Cu ³⁾)	70
H150	4 mm Al + 4 mm Cu +1.51 mm Sn	2.5 mm Cu ³⁾	95 (Cu ³⁾)	117

1) Half-value layer : The thickness of material that reduces the air kerma of a radiation beam by one half

2) Homogeneity coefficient: The ratio of the first and second half-value layers times 100

3) Values are equivalent to those of Al

2.2 Estimation of 1st HVL and Homogeneity coefficient

The X-ray generator, used in this experiment, consists of 160 kVp high voltage generator and tube with tungsten target material. The inherent filtration inside the tube is 0.8 mm Be, which has been validated in the preliminary study[2]. The X-ray generator was set as 2 mA, the tube voltage and added filter were controlled for each beam code given in the reference. A calibrated spherical ionization chamber (model A3, Exradine) was used to measure the output of the X-ray generator. The chamber was positioned in the center of the 18 cm × 25 cm field at a distance of 2 m from the source to obtain the desirable beam size considering the

amount of dosimeter tested. Measurements were repeated by adjusting the filter thickness until approached the expected 1st HVL and 2nd HVL. 1st HVL and 2nd HVL were calculated as a function of filter thickness and current measured by ion chamber. Finally, homogeneity coefficients for each beam qualities were determined.



Fig. 1. X-ray generator in KHNP CRI.

3. Results and Discussion

The results of comparison between X-ray beam qualities of KHNP and those of NIST are listed in Table 2. Except for M30 beam code, the relative difference of 1st HVL against NIST are ranged from -1.5% to 3.6% and those of homogeneity coefficients are ranged from -2.8% to 1.2%, which is satisfied with the acceptance criteria.

Table 2. Comparison between X-ray beam qualities of KHNP and those of NIST[1]

Beam code	Half-value Layer(KHNP)	Difference (%)	Homogeneity Coefficient (KHNP)	Difference (%)
M30	0.42 mm Al ¹⁾	17.0	-	-
M60	1.741 mm Al	3.6	68.8 (Al)	1.2
M100	0.197 mm Cu	-1.5	55.5 (Cu)	1.0
M150	0.666 mm Cu	-0.6	60.2 (Cu)	-2.8
H150	2.503 mm Cu	0.1	92.4 (Cu)	-2.7

In case of M30, beam qualities given in the

reference was defined at a distance of 0.5 m from the generator to the chamber. However, in this experiment conditions, the increase of the distance hardens X-ray spectrum which results in out of acceptance criteria of 1st HVL. To compensate for those hardening effect, added filter thickness was adjusted from 0.5 mm Al to 0.384 mm Al. As a result, the relative difference of 1st HVL against NIST is 0.2% and that of homogeneity coefficient is 0.5% as shown in Table 3.

Table 3. The results of corrected M30 beam qualities of KHNP

Beam code	Half-value Layer(KHNP)	Difference (%)	Homogeneity Coefficient (KHNP)	Difference (%)
M30	0.361 mm Al ¹⁾	0.2	64.3 (Al)	0.5

4. Conclusion

1st HVL and homogeneity coefficient for each beam qualities were determined. The results are within the acceptance criteria. The X-ray generator of KHNP CRI was proved that it could provide the reference radiation field. However, further study on estimation by other method such as MCNP simulation and comparison of measurement results are necessary to obtain comprehensive information on X-ray beam qualities.

REFERENCES

- [1] Ministry of Science, ICT and Future Planning, “Enforcement Regulations for the Nuclear Safety Act”(2016).
- [2] M.H. Cho, et al, “MCNP simulation of inherent filter in X-ray generator for performance test on personnel dosimetry system”, Proc. of the KARP 2017 Fall Conference, 8(27), Nov 22-24, 2017, Jeju.

Deduction of the Optimal Operation Mode of Purifier System

*Youngkuk Jang, Seonho Noh, Hui-seok Kang, and Ilje Cho

Korea Atomic Energy Research Institute, 111, Daedeok-daero 989beon-gil, Yuseong-gu, Daejeon, Republic of Korea

*jangyk@kaeri.re.kr

1. Introduction

Korea Atomic Energy Research Institute(KAERI) has a Pyro-processing Integrated Inactive Demonstration facility(PRIDE) for the development of pyro-technology. In essence, the PRIDE enable integrated pyro-systems testing at engineering scales using depleted uranium or surrogates for depleted nuclear fuels.

The PRIDE must maintain an inactive (argon) atmosphere due to the characteristics of processes that take place in it, such as electrochemical reduction, electrochemical refining, and electrochemical smelting. In concentrating impurities at the facility, oxygen and moisture must be lower than 100 ppm. This paper describes the optimal operation mode using the purifier system among the methods for managing the atmosphere of argon cell of the PRIDE facilities

2. Main

2.1 Consist of Ar cell

The PRIDE of the Korea Atomic Energy Research Institute maintains the atmosphere of the Ar cell with the largest scale (L40*W4.8*H6.4) in Korea at below 100 ppm. The argon cell of PRIDE consist of a argon cell, a purifier system, a circulation and discharged system as shown in Figure 1 below.

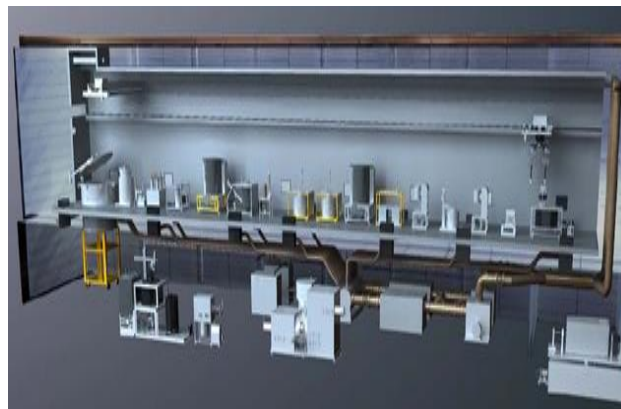


Fig. 3. Schematic of Ar cell.

2.2 Optimal operation mode of the purifier system

2.2.1 The air intake rate of the argon cell shall not be less than 0.02%/day of the argon cell.

2.2.2 The design basis concentration of the argon cell's oxygen and moisture is 50 ppm and kept lower than 100 ppm

2.2.3 If the concentration of moisture and oxygen is more than 1000 ppm, reduce the concentration of the contamination to 200 ppm or less by purging through argon gas for the efficiency of the purifier, and then operate and manage it below 100 ppm

2.2.4 If the argon cell is contaminated by more than 1000 ppm, it will take approximately two to three days to reduce the flow rate of 200CMH to less than 200 ppm. (24hours purging can shorten time)

2.2.5 The argon compressor discharge pressure value is 5 to 6 kg/cm² when two purifiers are operated simultaneously and 3 to 3.5 kg/cm² when one purifier is operated.

3. Conclusion

3.1 Design criteria for Argon cells.

$$0.02V\%/day = 0.02 \times 0.01 \times 1200 \text{ m}^3 = 0.24 \text{ m}^3/day$$

3.2 Argon cell leakage rate

Using the leak Volume equation, calculate the argon cell leakage rate.

$$\begin{aligned} C_1 &= 200,000ppm, C_2 = 12ppm \\ V_1 &= \text{leakage volume}, V_2 = \text{Ar Cell Volume}(1200m^3) \\ 200,000ppm \times V_1 &= 12ppm \times 1200m^3 \\ V_1 &= 0.072m^3/day \end{aligned}$$

Argon cell leakage rate running 24 hours the moisture analyzer is satisfied, and oxygen, argon manages less than 100 ppm a cell's pollution.

3.3 conclusion

The secretive performance of Argon cells currently operated by the Korea Atomic Energy Research Institute is 30 percent higher than the design basis, and the standard procedure for managing the contamination of argon cells by obtaining the optimal operation mode of argon cell.

REFERENCES

- [1] ANL-7959 Hot Fuel Examination Facility/North Facility Safety Report, February 1975, Argonne National Laboratory pp.42-53.
- [2] The EBR-II Fuel Cycle Story, Charles E. Stevenson, American Nuclear Society pp.16-25.

A Study of ^{222}Rn Concentration in Jeju Spring Water (Yongcheonsoo)

Chung-Hun Han^{1),*} and Seong-Pil Ryu²⁾

¹⁾ Jeju National University, 102, Jejudaehak-ro, Jeju-si, Jeju-do, Republic of Korea

²⁾ Jeju Special Self-Governing Provincial Council, 13, Munyeon-ro, Jeju-si, Jeju-do, Republic of Korea

*tang007@jejunu.ac.kr

1. Introduction

Yongcheonsoo is the spring water that flows through the ground after the precipitation and flows naturally through the cracks and open gaps in the ground layer. These spring water is distributed over 900 from Mt. Halla to the coast in Jeju Island. Yongcheonsoo has been used not only as a drinking water source but also as a living and agricultural water source until the 1980s when waterworks were not available. Environmental radiation studies of characterization of these spring water are not enough.

Radon originates from the radioactive decay of naturally occurring uranium and thorium deposits. The radon can be found, in trace amounts, in almost all soils and rocks. Being a gas, radon can escape from mineral surfaces and dissolve in ground water, which can carry it away from its point of origin. Typical groundwater sources average between 200 and 600 pCi/L of radon [1].

Since radon occurs naturally in soil and rocks, it is virtually omnipresent on earth. It accounts for more than 50% of the total dose from all sources of ionizing radiation absorbed by the population [2].

In this paper, we present the first measurement of radon concentrations in spring water (Yongcheonsoo) in Jeju Island.

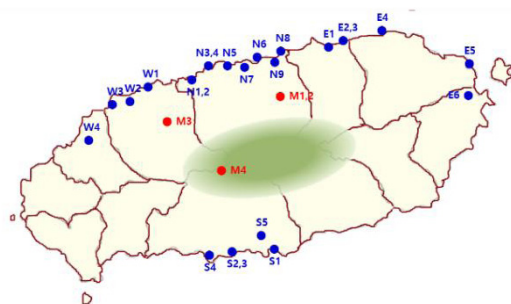


Fig. 1. Sampling sites of spring water.

2. Materials and methods

2.1 Sampling locations

Spring water (Yongcheonsoo) 28 samples were

collected from 9 Northern (JN), 6 East (JE), 4 West (JW), 5 South (JS), and 4 Mountain (JM) of Jeju in April to May 2018 (Fig. 1). We have sampled them from 1 to 6 p.m.

2.2 Sample Analysis

The measurements were carried out on samples by using RAD H₂O of RAD7 (DurrIDGE Co.). The decomposition products ^{218}Po and ^{214}Po of ^{222}Rn are in ionic state and adsorbed to other materials easily. Therefore, the instrument was purged for about 10 minutes before the sample was measured, and then the moisture in the chamber was dropped to 6% or less. When samples were taken, spring water was poured for more than 5 minutes, and bubbles were collected so as not to generate as much as possible. Measurements were taken within 30 minutes after sampling. The sample measurement vessel was sampled at a predetermined capacity (250 mL) in the "wat250" mode, and then measured 4 times for 5 minutes.

3. Results and discussion

We have measured, using the RAD H₂O of RAD7, ^{222}Rn concentrations in spring water (Yongcheonsoo) in Jeju Island.

The concentration of radon was found to be 17.60–558.00 pCi/L (mean 152.33 pCi/L, median value 131.50 pCi/L (Table 1). The radon content of S3 ("Seogaleummul" Yongcheonsoo) was the highest at 558.00 pCi/L. The spring water of the lowest radon concentration was M3 ("ongseongmul" Yongcheonsoo) at 17.60 pCi/L.

The radon content of Jeju Yongcheonsoo was 32 times lower than the average concentration (4,946 pCi/L) of radon in the global groundwater by NCRP report. There was no spring water exceeding the range of 4,000 pCi/L proposed by the US Environmental Protection Agency (EPA). But the three spring waters of S3 (558.00 pCi/L), N6 (333.00 pCi/L) and N7 (300.00 pCi/L) were higher than Maximum Contamination Level (MCL) by the USEPA. However, it was much lower than the radon

standard or recommended value for drinking water of the world.

Table 1. ^{222}Rn concentrations in spring water (Yongcheonsoo) in Jeju Island

Sample	Low (pCi/L)	High (pCi/L)	Mean (pCi/L)	
JN	N1	121±51.7	140±55.0	131 ±7.99
	N2	106±49.2	133±54.0	119 ±12.00
	N3	131±53.5	211±65.8	160 ±36.50
	N4	159±58.1	207±65.2	186 ±20.00
	N5	169±60.1	218±67.1	201 ±22.00
	N6	284±75.8	320±79.4	300 ±15.80
	N7	273±74.5	383±86.6	333 ±50.20
	N8	137±54.7	176±60.8	161 ±16.90
	N9	109±49.9	188±62.5	147 ±32.00
	Mean			193.11 ±74.76
JE	E1	43.1±35.0	90.5±46.4	65.8 ±20.00
	E2	27.1±29.6	46.4±35.6	37.6 ±8.59
	E3	66.5±41.0	94.5±47.2	82.6 ±11.80
	E4	42.7±34.7	81.6±44.2	58.2 ±17.60
	E5	19.3±26.7	34.8±32.2	26.1 ±6.60
	E6	31.3±31.3	70.8±42.2	48 ±17.20
	Mean			53.05 ±20.26
JW	W1	62.2±39.8	97.1±47.4	85.4 ±16.50
	W2	162±59.2	243±70.6	208 ±33.70
	W3	69.6±41.4	89.4±45.8	77.6 ±8.51
	W4	119±52.0	158±58.6	132 ±18.00
	Mean			125.75 ±59.86
JS	S1	194±63.9	259±72.6	234 ±28.80
	S2	258±71.8	318±79.0	280 ±26.70
	S3	488±96.7	614±108	558 ±52.10
	S4	236±69.2	261±72.6	249 ±10.50
	S5	191±63.7	272±74.5	235 ±41.60
	Mean			311.2 ±139.21
JM	M1	34.8±32.2	54.1±37.7	41.6 ±9.13
	M2	27.1±29.6	50.5±36.9	36.8 ±9.84
	M3	15.7±25.3	19.6±27.0	17.6 ±2.24
	M4	47.2±36.3	63.0±40.3	54 ±6.71
	Mean			37.5 ±15.12
Total Mean			152.33 ±120.43	

The radon concentrations in Jeju Island were in the order of South (311.20 pCi/L) > North (193.11 pCi/L) > Western (125.75 pCi/L) > East (53.05 pCi/L) > Mountain (37.50 pCi/L).

Overall, the higher the altitude, the lower the concentration of radon. It shows that radon has some relation with altitude. Spring water located in high altitude areas show water quality close to that of rainfall. This phenomenon is due to the fact that the circulation rate of groundwater is very fast and water-rock reaction is hardly occurred in the stratum, so radon is less dissolved in rock.

4. Conclusions

We have measured, using the RAD H₂O of RAD7, ^{222}Rn concentrations in spring water (Yongcheonsoo) 28 samples in Jeju Island. The mean concentration of radon was 152.33 pCi/L. The radon content of S3 was the highest at 558.00 pCi/L. The spring water of the lowest radon concentration was M3 at 17.60 pCi/L. The radon content of Jeju Yongcheonsoo was 32 times lower than the average concentration of radon in the global groundwater by NCRP report. There was no spring water exceeding the range of 4,000 pCi/L proposed by the US Environmental Protection Agency (EPA). But the three spring waters of S3, N6 and N7 were higher than Maximum Contamination Level (MCL) by the USEPA. However, it was much lower than the radon standard or recommended value for drinking water of the world. The radon concentrations in Jeju Island were in the order of South > North > Western > East > Mountain. Overall, the higher the altitude, the lower the concentration of radon. It shows that radon has some relation with altitude.

ACKNOWLEDGEMENT

This research was supported by Science Research Program through the Jeju Green Environment Center (JGEC, No. 18-18-02-15-36-03).

REFERENCES

- [1] Milvy, P. and Cothorn C.R., Scientific Background for the Development of Regulations for Radionuclides in Drinking Water, Chapter 1 in Cothorn and Rebers (1990).
- [2] United Nations Scientific Committee on the Effects of Atomic Radiation (UNSCEAR), Sources and Effects of Ionizing Radiation. United Nations, New York (1995).

7분과

방사화학 (Oral)



Research on High-level Waste at KIT-INE in the Context of Prolonged Interim Storage and the New Site-selection Process for a Deep Geological Repository in Germany

Volker Metz* and Horst Geckeis

Karlsruhe Institute of Technology, Hermann-von-Helmholtz-Platz 1, Eggenstein-Leopoldshafen, Germany

*volker.metz@kit.edu

1. Background

In the year 2011, the Federal Parliament of Germany decided, based on a broad societal consensus, to phase-out nuclear electricity production with the last German nuclear power plant to be shut down in 2022. According to projections for the nuclear power phase-out, about a total of 17,000 tons of spent nuclear fuel (SNF) and about 600 cubic metres of vitrified reprocessing waste will accumulate in Germany. A new site selection process for final disposal of the aforementioned high level waste (HLW) was started in 2013 by billing a site selection act which has been amended in 2017. A specific challenge of the German process being distinctly different to international approaches is the provided comparison of different disposal concepts in the different host rock types (rock salt, crystalline and argillaceous rock).

The site selection process shall be based on scientific criteria and transparent procedures with public participation. It will comprise three phases, where the number of eligible regions/sites will be successively reduced until a final decision for a site will be made. According to plans of the Federal Ministry for Environment, Nature Conservation and Nuclear Safety, a deep geological repository is planned to be operational already in the second half of this century. Due to expected delays in site selection, licensing and construction of a deep geological repository, one cannot exclude that

interim storage of HLW has to be extended for 100 or more years.

2. Scientific profile and mission of KIT-INE

At KIT-INE, the focus of research lies on fundamental aspects of radionuclide chemistry in aquatic systems, on applied studies related to radioactive waste forms (including SNF and HLW-glass) and radionuclide behavior in various repository barrier systems, on the development of tools contributing to a geochemistry based safety case and to a science-based site selection process. In collaboration with social science teams of a partner institute at KIT a more comprehensive view towards specific topics related to management of HLW and the site selection process is developed.

In the present communication we outline aspects of prolonged interim storage of spent nuclear fuel and the site-selection process for a deep geological repository for HLW in Germany, and we present selected research highlights of KIT-INE with respect to HLW behavior under conditions of extended dry storage and final disposal.

3. Research on high level waste behavior under repository conditions

At KIT-INE, investigations on the behavior of HLW under repository conditions focus on experimental determination, process understanding

and numerical modelling of radionuclide release and retention during corrosion of SNF, activated metallic components of nuclear fuel rods and HLW glass. Experiments with these irradiated materials are conducted in the shielded box-line of KIT-INE.

Amongst other international projects, SNF behavior in various repository systems has been investigated within KIT-INE coordinated European projects (e.g. the 7th FP project FIRST-Nuclides). In our experiments, both the Instant Release Fraction (IRF) of radionuclides and the relatively slow release of radionuclides from the SNF matrix were quantified. IRF of twelve different types of high burn-up SNF were experimentally determined within FIRST-Nuclides. KIT-INE compiled a database of all available information of the studied fuels, including their IRF, fuel fabrication data and irradiation histories. Our evaluation of the database showed a close correlation between IRF, fission gas release (FGR) and in-reactor operation parameters (in particular the linear heat generation rate).

In a unique approach, KIT-INE scientists determined both the Kr and Xe inventories in the plenum of an irradiated fuel rod segment and in leaching experiments with samples of the same SNF segment. Experimental results showed a relatively high FGR to I-129 release ratio, whereas the release ratio of the fission gases to Cs-137 was 1:1.

In experiments with irradiated Zircaloy and stainless steel, about 99% of the C-14 was found as gaseous or dissolved organic C-14 bearing compounds after release from the samples. These results are of high relevance for the role of C-14 in safety assessments for SNF repositories, because volatile and dissolved C-14 bearing organic species possess a high potential mobility through various geo-engineered and geological barriers.

For the first time ever, a real HLW glass sample

with a dose rate of 0.6 mSv/h (sampled from the Karlsruhe vitrification plant) was analyzed by means of XAS/XRF at the KIT synchrotron facility. Based on high quality XANES data, speciation of actinides (Am(III), Pu(IV), Np(V), U(VI)), Zr (Zr(IV)), Se (identified as selenite), and Tc (identified as pertechnetate) in the HLW glass was determined.

4. Research on spent nuclear fuel behavior under dry interim storage conditions

Experimental studies were initiated to examine possible mechanisms of cladding corrosion at the SNF / zircaloy interface and the potential relevance for the fuel pin integrity during extended interim storage conditions. Such scenarios have to be considered in view of the long interim storage times exceeding licensed periods of storage canisters by far according to the present plans for site selection in Germany.

In recent studies pellet-cladding-interactions and cladding corrosion by volatile fission products were studied using Zircaloy-4 specimens, which had been sampled from irradiated UO₂ and MOX fuel rod segments. Composition of agglomerates found at the inner surface of plenum sections and fuel-cladding interaction layers were analyzed by means of μ -XAS and μ -XRF at the KIT synchrotron facility, as well as by means of SEM-EDS and XPS. It was found that a significant amount of Cs had been volatilized during irradiation from subjacent fuel pellets and deposited at the Zircaloy of the fuel rod plenum, whereas in lower parts of the pellet pile Cs precipitated as Cs-halogenide at the pellet-cladding interface.

Research on Radiochemistry and Geochemistry at KIT-INE, Germany, in Support of the Nuclear Waste Disposal Safety Case

Marcus Altmaier* and Horst Geckeis

Karlsruhe Institute of Technology, Hermann-von-Helmholtz-Platz 1, Eggenstein-Leopoldshafen, Germany

*marcus.altmaier@kit.edu

1. Research profile of KIT-INE

The demand of a science based and transparent procedure to select a repository site providing safety over a time period of 1 million years represents an unique and fascinating challenge.

Research and development at the Institute for Nuclear Waste Disposal (INE) at the Karlsruhe Institute of Technology (KIT) are conducted as an integral part of the national provident research in the frame of the Helmholtz Association of German research centers (HGF) research program NUSAFE. INE develops and operates unique radiochemical and analytical infrastructures for the investigation of radionuclide materials. With about 100 employees KIT-INE is the largest institute inside the HGF, covering research for various aspects of nuclear waste disposal and nuclear waste management.

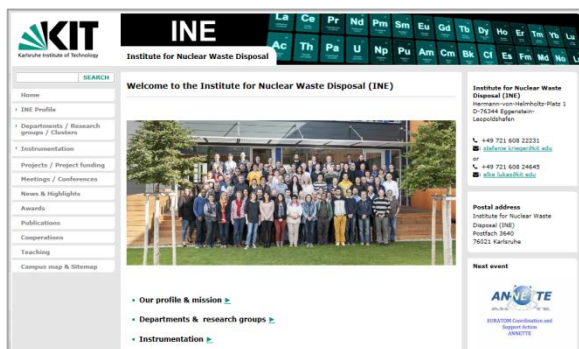


Fig. 1. The website www.ine.kit.edu, offers detailed information on KIT-INE, including the comprehensive Annual Reports issued by the institute.

2. Selected Research Highlights

2.1 Aquatic chemistry and thermodynamics

KIT-INE is providing comprehensive scientific information on key aspects controlling radionuclide behavior in solution, i.e. solubility phenomena, redox processes, complexation reactions with inorganic and organic ligands or ion-interaction processes. Recent work on fundamental actinide chemistry includes Pu(VI) solubility and speciation studies, with a strong focus on the chemical characteristics of solubility limiting solid phases. Similarities of Pu(VI) phases and related Np phases in NaCl and CaCl₂ media are given. In addition to the Th(IV) system studied at KIT-INE previously, new studies on mixed hydroxo-carbonate complexation have investigated tetravalent Uranium, Neptunium and Plutonium. A full set up data and thermodynamic descriptions are now available in the An(IV)-OH-CO₃ series, also extending to Tc(IV). A focus of recent R&D at KIT-INE is centered on actinide-organics complexation reactions. Complexation and solubility increase of Pu(III) and Pu(IV) due to interaction with isosaccharinic acid was extensively investigated. The topic actinide-organic-interactions will be further developed within a current research proposal coordinated by KIT-INE within a joint European research initiative. Research on aquatic radionuclide chemistry uses synergies with the INE operated EXAFS beamlines at KARA (formerly ANKA).

2.2 Radionuclide sorption

The interaction of radionuclides with relevant mineral surfaces is a key activity at KIT-INE followed over several decades. Studies are presently focused on coupled redox-surface reactions, the influence of organics on sorption, and assessing the influence of high ionic strength conditions on sorption processes. An example will be given on the sorption of europium in presence of gluconate or citrate onto clay minerals. As part of a German research consortium, KIT-INE will increase research activities in underground laboratories, investigating several aspects of radionuclide retention and transport at the Mont Terri site in Switzerland. Within the EC funded CEBAMA project (www.cebama.eu) coordinated by KIT-INE, research on processes at the interphases between cement-based-materials and other components is performed in view of predicting radionuclide mobility. An example on Beryllium sorption on cementitious materials investigated by KIT-INE will be given.

2.3 Radionuclide retention on Fe corrosion phases

The retention on radionuclides on Fe phases, forming in the near field of the waste due to canister corrosion processes, is a growing research field at KIT-INE. Work is performed on identifying relevant secondary Fe mineral phases forming under different chemical boundary conditions, and investigating radionuclide retention and incorporation on these solids. Work is combining wet chemistry experiment and advanced spectroscopy available at KIT-INE.

2.4 Coordination chemistry

Coordination chemistry is focusing on liquid-liquid extraction processing using N-Donor ligands, with the aim of deriving fundamental understanding of processes controlling the selectivity of these

ligands toward trivalent Actinides and Lanthanides. Classical extraction studies are combined with spectroscopy and modern quantum-chemical calculations at KIT-INE which promise an innovative predictive assessment of ligand properties in extraction studies. Fundamental studies are likewise performed in order to derive improved process understanding on the interaction of radionuclides with the human Transferrin protein and other related bio-molecules.

2.5 Thermodynamic Data and Databases

Selected estimation methods for thermodynamic data, which may allow to derive a workable thermodynamic database for aquatic systems at elevated temperature conditions ($< 100^{\circ}\text{C}$), are being developed within the ThermAc project coordinated by KIT-INE. Systematic estimation approaches are combined with experimental investigations of selected key systems, thus allowing for a critical assessment of the estimation approaches. Activities within the NEA-TDB are continuing at KIT-INE as a main contribution to this field, including researchers co-chairing the new Update Volume and a report on Pitzer modelling. The German THEREDA database project, where KIT-INE is responsible for actinide and radionuclide data, is likewise further developed.

3. Summary

Within this contribution, an overview of recent research performed in the radiochemistry division at KIT-INE is given. Examples are taken from R&D activities performed within the HGF NUSAFE programme, but also from studies performed within collaborations on the national and international level. It finally may contribute to increased interaction and exchange of KIT-INE with Korean research groups interested in nuclear waste disposal topics.

Institute of High Temperature Electrochemistry (IHTE), Ekaterinburg, Russia.

Current Status of Pyrochemical Research in IHTE

Alexei Potapov*, Kirill Karimov, Alexey Shishkin, Vladimir Shishkin, Alexander Dedyukhin, and Yury Zaykov
Institute of High Temperature Electrochemistry, Akademicheskaya Ulitsa, 20, Yekaterinburg, Sverdlovskaya oblast', Russia

*A.Potapov_50@mail.ru

1. Institute of High Temperature Electrochemistry

The Institute of High Temperature Electrochemistry of the Ural Branch of the Russian Academy of Sciences (IHTE UB RAS) was founded in January 1958 on the base of the Laboratory of Molten Salts Electrochemistry, a worthy part of the Ural electrochemistry research school tradition. Professor Smirnov M.V., Doctor of Science (Chemistry), honored Master of Science and Technology of RSFSR, was the founder and the first head of the Institute. In the following years the Institute was led by such distinguished people as Corresponding Member of the USSR Academy of Sciences Karpachev S.V., Academician Baraboshkin A.N, professor and Doctor of Science (Chemistry) Khokhlov V.A. Since 2006, the Institute was headed by Honored Scientist of the Russian Federation, Doctor of Chemical Sciences, Professor Yu.P. Zaykov. From 2017 to the present time the Director of the Institute is Doctor of Chemical Sciences M.V. Ananyev. Nowadays IHTE is the only institution in Russia that specializes in the field of high temperature physical chemistry and electrochemistry of molten salts and solid state electrolytes. During 60 years IHTE has been engaged in fundamental studies focused on creation, development and application of the following:

- theoretical and experimental foundations of modern physical chemistry and electrochemistry of molten salts and solid state electrolytes;
- principles of electrochemical processes for the

production and physical-chemical analysis of new materials for various applications in corrosive environment and high temperatures;

- scientific fundamentals of resource saving, human and environment friendly technologies for electrochemical processes used for the production, refining, and protection of metals and processing inorganic raw materials;

- principles for construction of high temperature molten and solid electrolyte devices which provide the most rational direct conversion of molecular energy into electric power.

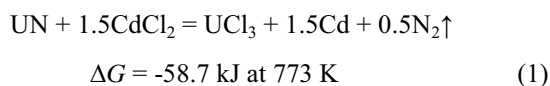
For several decades Institute performs research work in the field of physical chemistry and electrochemistry of molten salts for nuclear application.

Properties such as electrical conductivity, density, viscosity as far as structure of melts are studied. Halides of actinides, rare earth metals and other their compounds has been researched. Electrochemical processes and their mechanisms for liquid and solid electrodes has been investigated and modeled, interaction and behavior of different constructive materials in molten salt media were subjects of work aiming to development of fundamentals for the novel pyrochemical technologies of spent nuclear fuel recycling.

2. Progress in study of pyrochemical processing of spent nuclear fuel (SNF) in IHTE

2.1 "Soft chlorination" of nitride SNF

As a first step in the processing of nitride SNF it is proposed to dissolve it in the molten LiCl-KCl eutectic using CdCl₂ as a chlorinating agent:



The results of a typical experiment are shown in Figure 1.

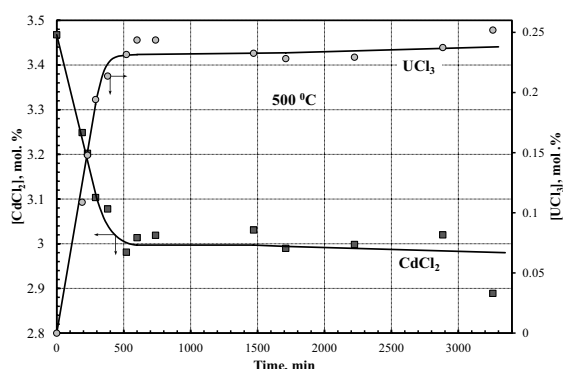


Fig. 1. The CdCl₂ and UCl₃ concentration time dependences according to chemical analysis.

Initial molar ratio CdCl₂ / UN = 4.42.

Based on experimental results and thermodynamic modeling, it was found:

- at 500°C, only ~30% of UN is converted to UCl₃. The remaining uranium passes into a black precipitate consisting of a mixture of UNCl, UN_{1.50}, UN_{1.51}, UN_{1.55}, UN_{1.59}, UN_{1.69}, UN_{1.73}, UN₂.
- at a temperature of 750°C and above, a 100% conversion of UN → UCl₃ is achieved;
- the reaction of UN + CdCl₂ proceeds by several parallel reactions and, at least, in two stages.

2.2 Electrolytic reduction of UO₂, rare earthes oxides and their mixtures

The electrolytic reduction of the UO₂ tablets of various porosities in the LiCl + (0.5-2.0)wt.% Li₂O

melt at 650°C was studied. The process was monitored by measuring the cathodic potential, with a brief disconnection of the electrolysis current. A complete reduction of UO₂ was observed after passing 165-180% of electricity from the theoretically required amount. Various materials were used as the anode: platinum, graphite, oxide ceramics. The best results were obtained using ceramic non-consumable anodes.

The metallization of the model nuclear fuel UO₂ + La₂O₃, CeO₂, Nd₂O₃ (5-17wt.% in total) was studied. It is found that UO₂ is also completely reduced to metallic uranium, while rare earth metal oxides remain unchanged. Only CeO₂ is reduced to Ce₂O₃.

Individual rare-earth oxides also did not reduced in wide ranges of Li₂O concentrations and cathodic potential.

These results give us a probable way of dividing the fission products. In the electrolytic reduction, alkali and alkali-earth metals will dissolve in the melt, uranium and plutonium will be reduced to the metals, and the lanthanides will remain in the oxide forms. These conditions are favorable for further separation.

2.3 Other research areas

In addition to the above-described works, IHTE performed in a wide range of research aimed at creating a pyrochemical technology for reprocessing spent nuclear fuel. These, for example:

- development of non-consumable anodes;
- thermodynamic modeling of all possible processes;
- physicochemical properties of working media et all.

ATR-FTIR Spectroscopic Investigation on the Interaction of U(IV) Nanoparticles With Organic Molecules

Hyejin Cho* and Wansik Cha

Korea Atomic Energy Research Institute, 111, Daedeok-daero 989beon-gil, Yuseong-gu, Daejeon, Republic of Korea

*hcho921@kaeri.re.kr

1. Introduction

In deep groundwater systems, tetravalent uranium (U(IV)) is a dominant redox form of uranium because of the anaerobic condition [1]. Natural organic complexing agents present at contaminated sites may not only affect the mobility of uranium, but also its microbial transformation and reductive precipitation. It is thus very important to understand the behaviors of U(IV) interacting with organic molecules in order to assess the geological migration of actinide species in the groundwater environment.

2. Results and Discussions

In this study, we developed a hydrothermally-induced U(IV) nanoparticle preparation method using acidic U(IV) aqueous solutions (pH ~2) to investigate the complexation of phosphoester on the surfaces of U(IV) nanoparticles (U(IV)_{NPs})

employing surface-enhanced infrared absorption (SEIRA). SEIRA is a near-field phenomenon where IR absorption of molecules adsorbed on or in the vicinity of small metal-/metal oxide-clusters is enhanced by a factor of 10 to 1000 due to the electromagnetic fields produced by the surface plasmon of clusters [2]. Herein, we report that U(IV)_{NPs} induces SEIRA for *p*-nitrophenyl phosphate (NPP). As demonstrated in Figure 1, the overall IR absorption of 5 mM NPP is enhanced in the presence of 1 mM U(IV)_{NPs}. The strong band (indicated by '*' in Figure 1) at 1350 cm⁻¹ has been assigned as a symmetric NO₂ stretching vibrational mode in previous SEIRA studies and is used to examine the molecular orientation of the ligand adsorbed on noble metal-based and metal oxide-based nanoparticle systems [3]. Overall, such SEIRA effects indicate that the crystalline primary particles of U(IV)_{NPs} possessing UO₂-like semiconductor

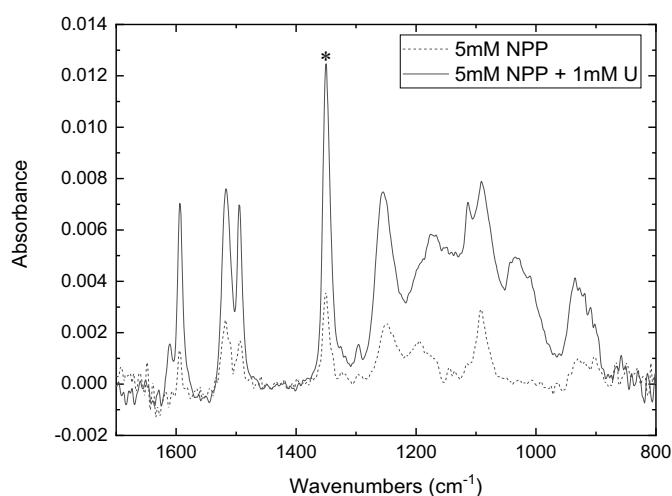


Fig. 1. ATR-FTIR spectra of reaction mixture exhibiting SEIRA effects at pH 5.2; dashed line: 5 mM NPP without U(IV)_{NPs}; solid lines: addition of 1 mM U(IV)_{NPs} to 5 mM NPP.

properties can effectively create polarized local electromagnetic fields interacting with the oscillating dipoles of the adsorbed molecules. Notably, the synthesized $\text{U(IV)}_{\text{NPs}}$ display unique colloidal properties, as measured by dynamic light scattering (DLS, Fig. 2) and transmission electron microscopy (TEM): (i) highly positive zeta-potential values (+35 - +40 mV), which is a strong indicator of the presence of partially hydrolyzed surface structures such as $\equiv\text{U}(\text{OH})^+$ on the crystalline primary particles; (ii) high surface areas originating from the rough cluster morphology composed of primary particles. We believe that the inter-particle Coulombic repulsion

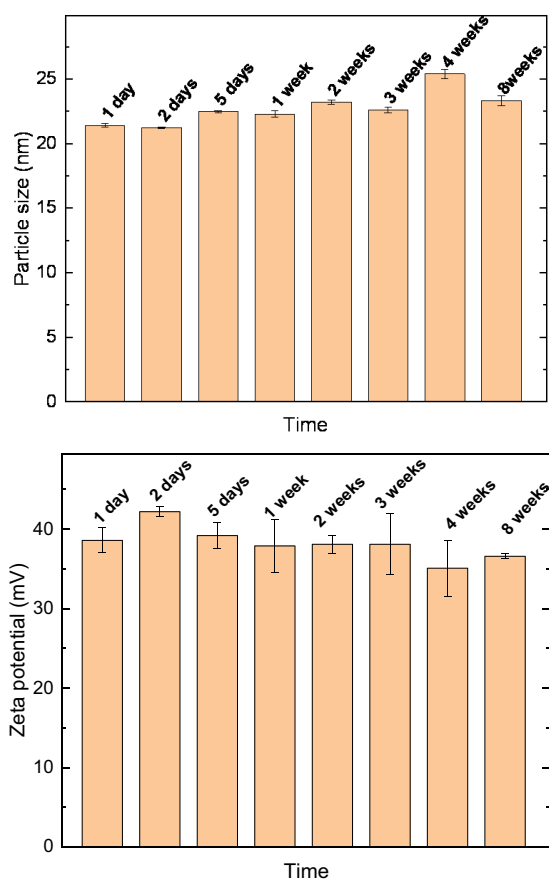


Fig. 2. Size and zeta potential measurements of 1- mM $\text{U(IV)}_{\text{NPs}}$ over time by DLS. The data were collected using the average values of three measurements. The measured size of the particles was 23 ± 6 nm and the same size was constantly observed for up to 8 weeks.

resulting from the surface charges is a critical

interfacial determinant of the colloidal stability of $\text{U(IV)}_{\text{NPs}}$ and gives rise to reproducible particle/cluster sizes. These properties are the major factors facilitating the surface adsorption of NPP anions on $\text{U(IV)}_{\text{NPs}}$.

3. Conclusion

We conclude that the SEIRA effects of the NPP- $\text{U(IV)}_{\text{NPs}}$ system provide strong evidence for the inner-sphere surface complex formation of NPP on $\text{U(IV)}_{\text{NPs}}$, and more specifically, its molecular orientation perpendicular to the surface in a bidentate fashion for surface coordination. The SEIRA of a variety of nitrophenyl derivative ligands such as carboxylates, oxalate, and sulfates with $\text{U(IV)}_{\text{NPs}}$ also will be discussed.

ACKNOWLEDGEMENT

This study is supported by the Nuclear Research and Development program of the National Research Foundation of Korea (Grant code: 2017M2A8A 5014 719).

REFERENCES

- [1] J. -I. Kim, "Significance of actinide chemistry for the long-term safety of waste disposal", *Nuclear Engineering and Technology*, 38(6), 459-482 (2006).
- [2] P. R. Griffiths, "Surface-enhanced infrared absorption spectroscopy: principles and applications" *Spectroscopic Properties of Inorganic and Organometallic Compounds*, 44, 95-122 (2013).
- [3] M. Osawa and M. Ikeda, "Surface-enhanced infrared absorption of *p*-nitrobenzoic acid deposited on silver island films: contributions of electromagnetics and chemical mechanisms", *The Journal of Physical Chemistry*, 95(24), 9914-9919 (1991).

Synthesis of Functionalized Mesoporous Carbon for Uranium Sorption in Acidic Conditions

Hyeseung Kim, Yongheum Jo, and Jong-Il Yun*

Korea Advanced Institute of Science and Technology, 291, Daehak-ro, Yuseong-gu, Daejeon, Republic of Korea

*jiyun@kaist.ac.kr

1. Introduction

Since the Kori nuclear power plant in Korea was shut down permanently, researchers have focused on the development of decommissioning and decontamination technology of nuclear power plant. Various radionuclides generated from nuclear power plants are mainly removed by conventional filters or resins. However, a large amount of secondary radioactive wastes is generated. Recently, in order to reduce secondary radioactive wastes, radionuclide separation technology conjugating solid phase extraction has been intensively developed.

In this work, the ordered mesoporous carbon of CMK-3 was used as an adsorbent for uranium extraction from liquid phase since it has very good thermal, chemical and mechanical strength [1]. CMK-3 has been successfully functionalized with phenyl phosphate. Studies on the U(VI) sorption behavior on CMK-3 and CMK-3-AP-PO₄ will be performed as the next step.

2. Methods

2.1 Adsorbent preparation

The ordered mesoporous carbon of CMK-3 was synthesized using the ordered mesoporous silica of SBA-15 as the hard template and sucrose as the carbon source [2,3]. CMK-3 was functionalized with amino phenol through diazotization method. The resulting material of CMK-3-AP was phosphorylated using phosphoric acid for obtaining CMK-3-AP-PO₄.

2.2 Characterization of CMK-3

Small angle X-ray diffraction patterns were recorded using Cu-K_α radiation. The N₂ adsorption-desorption isotherms at 77 K were operated to identify the surface area and pore structure of the materials. The specific surface area was measured by the Brunauer-Emmett-Teller (BET) method, and the total pore volume was obtained using Brunauer-Joyner-Halenda (BJH) method. The surface topography was analyzed by transmission electron microscopy (TEM). Fourier transform-infrared spectra (FTIR) were obtained to identify phenyl phosphate on the surface of CMK-3.

2.3 Sorption experiments

Batch U(VI) sorption experiments were carried out as function of pH. 10 mg of sorbent was suspended in 50 mL solution containing 10⁻⁴ M U(VI) with different pHs. The ionic strength and pH was adjusted by using 0.1 M NaClO₄ and 0.1 M HClO₄/NaOH, respectively. Separating the sorbent from solution was conducted with 220 nm PES membrane filters. The concentration of U(VI) in the filtrate was determined by inductively coupled plasma optical emission spectrometer (ICP-OES). The sorption capacity (q_e , mg/g) and the distribution coefficient (K_d) were calculated as follows.

$$q_e = \frac{(C_0 - C_e)}{m} \times V \quad (100) \quad (1)$$

$$K_d = \frac{(C_0 - C_e)}{C_e} \times \frac{V}{m} \quad (2)$$

where C_0 and C_e (mg/L) is the initial and equilibrium U(VI) concentration, respectively. V is the volume of the solution (L) and m is the mass of sorbent (mg).

3. Results

Fig. 1 shows the SAXRD patterns of CMK-3 and CMK-3-AP-PO₄. The three peaks are assigned to (100), (110) and (200) planes associated with $p6mm$ hexagonal symmetry [2]. The result indicates that the ordered structure of CMK-3 was preserved.

From the N₂ adsorption-desorption isotherms at 77 K, it was found that CMK-3 exhibits large surface area (1495 m²/g) and pore volume (1.26 cm³/g). After functionalization with phenyl phosphate, the surface area and the pore volume decreased to 1011 m²/g and 0.73 cm³/g. It is attributed to loading of functional groups onto the surface of CMK-3.

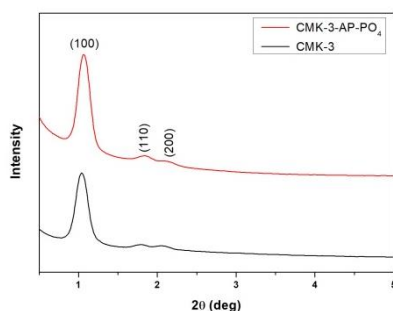


Fig. 1. SAXRD patterns of CMK-3 and CMK-3-AP-PO₄.

TEM images shown in Fig. 2 demonstrated that the pore structure remains retained even after functionalization. The FTIR analysis was conducted to identify the functional group, as presented in Fig. 3. The peaks at 1178 and 1507 cm⁻¹ appeared in CMK-3 and CMK-3-AP-PO₄, which are assigned to the C-O and C=C stretching vibrations of aromatic ring, respectively. The peak at 1076 cm⁻¹ in CMK-3-AP-PO₄ is attributed to phosphate group.

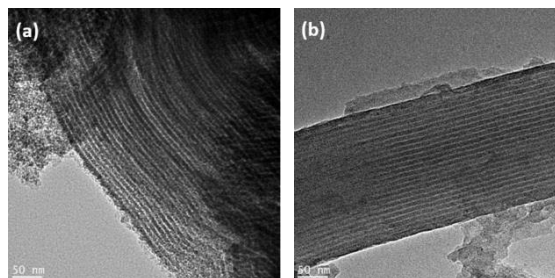


Fig. 2. TEM images of (a) CMK-3 (b) CMK-3-AP-PO₄.

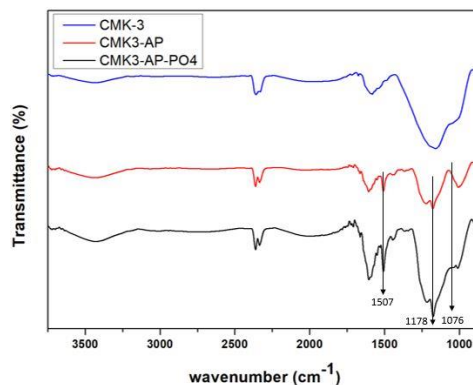


Fig. 3. FTIR spectra of CMK-3, CMK-3-AP and CMK-3-AP-PO₄.

ACKNOWLEDGEMENT

This work was supported by a grant from the Nuclear R&D Program of the National Research Foundation of Korea funded by the Korean Ministry of Science and ICT (Grant codes: 2017M2A8A5014801).

REFERENCES

- [1] J.-S. Lee, S.H. Joo and R. Ryoo, Journal of American Chemical Society, 124(7), 1156-1157 (2002).
- [2] S. Jun, S.-H. Joo, R. Ryoo, M. Kruk, M. Jaroniec, Z. Liu, T. Ohsuna and O. Terasiki, Journal of American Chemical Society, 122(43), 10712-10713 (2000).
- [3] D. Zhao, J. Feng, Q. Huo, N. Melosh, G. H. Fredrickson, B. F. Chmelka, G. D. Stucky, Science, 279 (5350), 548-552 (1998).

Electrochemical Properties of Uranium and UxBi_y IMC in the LiCl-KCl Eutectic

Beom-Kyu Kim¹⁾, Byung-Gi Park^{1)*}, Sang-Eun Bae²⁾, and Tae-Hong Park²⁾

¹⁾ Soonchunhyang University, 22, Soonchunhyang-ro, Asan-si, Chungcheongnam-do, Republic of Korea

²⁾ Korea Atomic Energy Research Institute, 111, Daedeok-daero 989beon-gil, Yuseong-gu, Daejeon, Republic of Korea

*qu@sch.ac.kr

1. Introduction

Uranium is the major element in most nuclear fuel cycles, thus the assessment of accurate thermochemical data for this element in molten salts is of high importance. In recent years, various studies have been conducted to develop a behavior of lanthanide and transition metal to form the intermetallic compound(IMC), and to reduce lanthanide and other metals. Many studies have been conducted on the electrochemical reaction and behavior of U^{4+}/U^{3+} , U^{3+}/U in molten chloride salts by Cyclic voltammetry, square wave voltammetry and various voltammetry [1-4]. If Liquid Bismuth is used as a liquid metal electrode in an electrolytic reduction-electrolytic and refining process, Bismuth is likely to be present with the ionic state in the electrolyte. In this case, we need to study the behavior of mixed bismuth and uranium ions in the LiCl-KCl electrolyte. Therefore, the electrochemical reaction of cerium present in the LiCl-KCl molten salt was confirmed by using electrochemical method, and the characteristics study of the existence of Bi ion was carried out.

2. Experimental

Experiments were carried out in a glove box under an argon atmosphere in which oxygen and moisture were kept at 1 ppm or less. And were performed to experiment at an elevated temperature using an electric furnace at the bottom of the glove box. LiCl-KCl and BiCl₃ were all purchased from Sigma Aldrich.

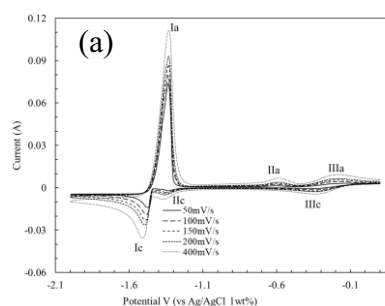
Electrochemical measurements were performed in Quartz Cell. Working Electrode (WE) were Tungsten wire (1 mm diameter) and glassy carbon (GC) were used Counter Electrode (CE). The Pyrex guide tube was used to prevent contact between electrodes.

The reference electrode was consisted of an one-end closed Pyrex tube, in which LiCl-KCl eutectic salt containing 1wt% AgCl was placed and a silver wire (Alfa-Aesar, 99%, OD: 1 mm) was immersed in the salt. The Electrochemical measurements were performed using a Gamry Reference 3000. Temperature of the salt was measured with Chromel-Alumel thermocouple.

3. Result and Discussion

Figure 1 shows the cyclic voltammogram of UCl₃ in the molten salt LiCl-KCl. The applied potential was reduced from 0 V (vs Ag / AgCl 1wt%) to -2 V and oxide 0 V again. Typically, two oxidation / reduction peaks (Ia/Ic, IIIa/IIIc) were produced. The oxidation/ reduction peak potentials of U^{4+}/U^{3+} and U^{3+}/U were confirmed to be the same as those of most of the researchers, and IIa/IIc generated between them was caused by deposition after adsorption on working electrode.

Figure 2 shows CV results measured with BiCl₃ (0.5wt%) added. As a result of CV, an oxidation / reduction peak of Bi was generated near 0.2 V, and a Li₃Bi oxidation/reduction peak was generated near -1.8 V. [5] And the dislocation of Bi-U's intermetallic compound was observed between U and Bi (A to E). Both of the Bi and U intermetallic compounds evaluated by KALPHAD show three reactions. [6]



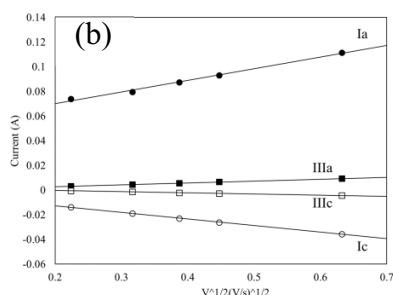


Fig. 1. (a) Cyclic voltammogram obtained for UCl_3 in LiCl-KCl melt, Scan rate: 0.05, 0.1, 0.15, 0.2, 0.4 V/s. (b) Dependence of Redox peaks current on square root of scan rate. working electrode: W wire, concentration of UCl_3 : 1.00wt%, temperature: 773 K.

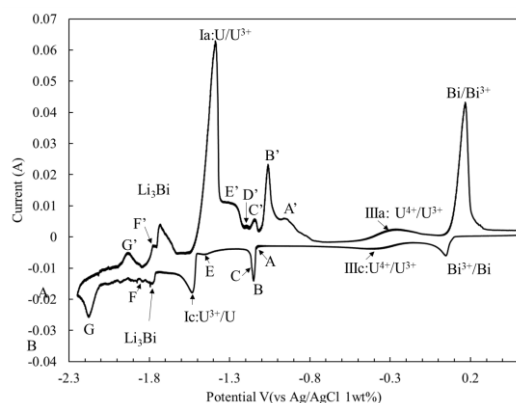
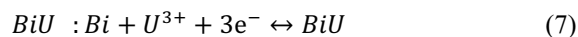
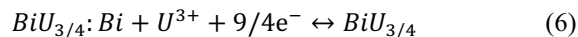
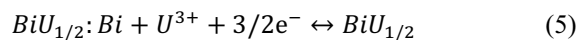
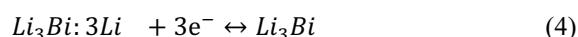


Fig. 2. Cyclic voltammogram obtained for LiCl-KCl with UCl_3 (1wt%) and BiCl_3 (0.5wt%) melt using the tungsten electrode at 773 K, scan rate: 0.1 V/s.



4. Conclusion

We conducted electrochemical measurements to explore the intermetallic compounds of U and U-Bi. Electrochemical test results confirmed the formation potential of UxBi_y intermetallic compounds.

ACKNOWLEDGEMENT

This work was financially supported by the National

Research Foundation of Korea(NRF) grate funded by the Ministry of Science, ICT and Future Planning, Republic of Korea. (NRF-2016M2B2B1945263).

REFERENCES

- [1] B. Prabhakara Reddy, S. Vandarkuzhali, T. Subramanian, P. Venkatesh "Electrochemical studies on the redox mechanism of uranium chloride in molten LiCl-KCl eutectic", *Electrochimica Acta* 49, 2471–2478 (2004).
- [2] Patrick Masset, David Bottomley, Rudy Konings, Rikard Malmbeck, Alcides Rodrigues, Jérôme Serp, and Jean-Paul Glatz, "Electrochemistry of Uranium in Molten LiCl-KCl Eutectic", *Journal of The Electrochemical Society*, 152(6) A1109-A1115 (2005).
- [3] Robert O.Hoover, et al., "Electrochemical studies and analysis of 1–10 wt% UCl_3 concentrations in molten LiCl-KCl eutectic", *Journal of Nuclear Materials*, Volume 452, 389-396(2014).
- [4] Dalsung Yoon and Supathorn Phongikaroon, "Electrochemical and Thermodynamic Properties of UCl_3 in LiCl-KCl Eutectic Salt System and LiCl-KCl-GdCl_3 System", *Journal of The Electrochemical Society*, 164 (9) E217-E225 (2017).
- [5] Pavlyuk, Volodymyr, Sozanskyi, Martyn, Dmytriv, Grygoriy, Indris, Sylvio, Ehrenberg, Helmut, "Amendment of the Li-Bi Phase Diagram Crystal and Electronic Structure of LiBi ", *Journal of Phase Equilibria & Diffusion.*, 36 (6) p544-553 (2015).
- [6] Jian Wang, Kun Wang, Chunhua Ma, Leidong Xie, "Critical evaluation and thermodynamic optimization of the (U + Bi), (U + Si) and (U + Sn) binary systems", *J. Chem. Thermodynamics*, 92, 158–167(2016).

Raman Spectroscopic Study of Eu(II) and Yb(II) in Molten LiCl-KCl Eutectic

Seung Park and Jong-Il Yun*

Korea Advanced Institute of Science and Technology, 291, Daehak-ro, Yuseong-gu, Daejeon, Republic of Korea

*jiyun@kaist.ac.kr

1. Introduction

Molten salts have been widely studied for a broad application since they typically provide superior properties, such as good electrical conductivity, high energy density, excellent radiation resistance, nonflammability, etc. The efficiency of molten salts in diverse applications depends on the solvation of metal ions in molten salts, *i.e.* the local structure of liquid [1]. In molten alkali chloride melts, some of lanthanide elements (Sm, Eu, Tm, and Yb) can be present in the divalent state, while other lanthanides mostly exist in the trivalent state.

In this work, the Raman study of EuCl_2 -LiCl-KCl and YbCl_2 -LiCl-KCl system were performed to gain the structural information of divalent lanthanide ions in molten LiCl-KCl.

2. Experimental

2.1 Sample preparation

EuCl_3 , EuCl_2 and YbCl_3 (99.99% purity) were purchased from Sigma-Aldrich. Yb(II) was prepared by the electrochemical reduction of Yb(III) using a potentiostat (Bio-Logic Science Instruments, SP240). Tungsten was used as a working electrode and a counter electrode, and the detailed electrochemical system has been described in [2]. All experimental procedures including sample handling were conducted in a glove box under argon atmosphere (H_2O , $\text{O}_2 < 1$ ppm)

2.2 Raman spectroscopic system for molten salt

An in-situ Raman spectroscopic system for molten salt built in our laboratory uses a 532 nm light of the DPSS laser (CNI Optoelectronics Technology, MLL-U-532) with a maximum power of 400 mW as excitation source. The laser beam was focused into the inside of sample through an optical furnace window. The back-scattered Raman signal was measured with an intensified CCD (Andor Technology, iStar) coupled with a Czerny-Turner spectrometer (Andor Technology, shamrock sr-303i).

3. Results and Discussions

3.1 Raman spectra of Eu(III) and Eu(II)

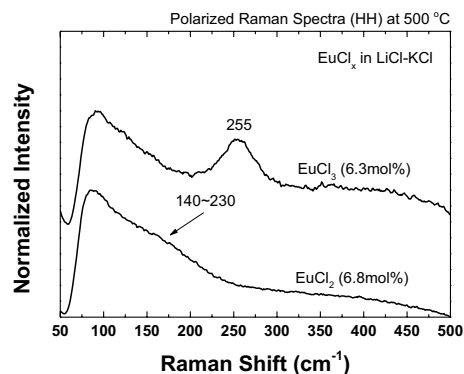


Fig. 1. Raman spectra of EuCl_3 and EuCl_2 in LiCl-KCl eutectic salt at 500°C.

The trivalent lanthanide ions in alkali chloride melts are known to be present as LnCl_6^{3-} with the octahedral coordination environment [3]. Fig. 1 shows the Raman spectra of Eu(II) and Eu(III) in a linear polarized mode of HH. EuCl_3 (6.3mol%) in LiCl-KCl eutectic salts has the $\nu_1(\text{A}_{1g})$ peak of the

octahedral symmetry (O_h) at 255 cm^{-1} . On the other hand, EuCl_2 (6.8mol%) in the same chloride eutectic revealed a relatively broad peak in the range of 140 to 230 cm^{-1} , as shown in Fig. 1.

3.2 Raman spectra of Yb(III) and Yb(II)

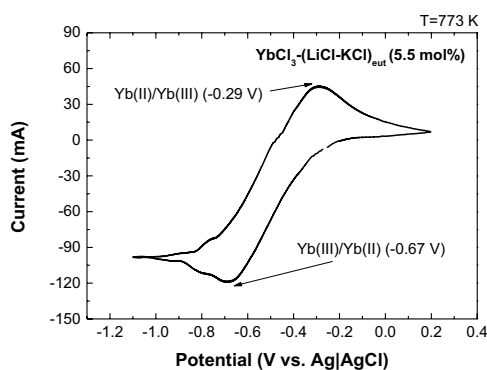


Fig. 2. Cyclic voltammogram of YbCl_3 in LiCl-KCl molten salt at 5.5mol% and 773 K.

YbCl_3 (5.5mol%) in LiCl-KCl eutectic salts showed the $\nu_1(A_{1g})$ peak at 262 cm^{-1} . The reduction and oxidation peaks were found from the cyclic voltammogram of $\text{YbCl}_3\text{-LiCl-KCl}$ consistently (Fig. 2), as reported by Smolenski et al. [4]. The polarized Raman spectrum of Yb(II) was measured in the course of chronoamperometry at the reduction potential of -0.67 V (vs. 1wt.% Ag|AgCl).

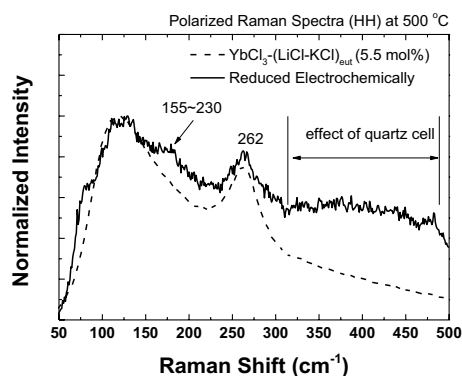


Fig. 3. Raman Spectra of YbCl_3 before and after electrochemical reduction.

Fig. 3 shows Raman spectra of electrochemically reduced $\text{YbCl}_3\text{-LiCl-KCl}$ sample. The total applied electric charge of 154 C in the present work induces a reduction of initially prepared Yb(III) by 44%, so that the $\nu_1(A_{1g})$ peak of YbCl_6^{3-} could be observed as well. The reduced Yb(II) has a weak but broad Raman band between 155 and 230 cm^{-1} , similar to Eu(II) . It implies that Ln(II) has different coordination environment in LiCl-KCl system, compared to Ln(III) .

4. Conclusions

The vibrational modes of EuCl_3 and YbCl_3 are associated with the octahedral local structure of LnCl_6^{3-} . The Raman bands of EuCl_2 and YbCl_2 show a change in their molecular structure, which should be further identified using computational chemistry.

ACKNOWLEDGEMENT

This work was supported by the National Research Foundation of Korea (NRF) grant funded by the Korea government (No. 2017M2A8A5014801).

REFERENCES

- [1] A.-L. Rollet and M. Salanne, "Studies of the local structures of molten metal halides," *Ann. Reports Sect. "C" (Physical Chem.)*, 107, 88, (2011).
- [2] K. H. Lim *et al.*, "Study on Exchange Current Density and Transfer Coefficient of Uranium in LiCl-KCl Molten Salt," *J. Electrochem. Soc.*, 162 (14), E334–E337, (2015).
- [3] G. D. Zissi *et al.*, "Vibrational modes and structure of the $\text{LaCl}_3\text{-CsCl}$ melts," *Vib. Spectrosc.*, 40 (1), 110–117, (2006).
- [4] V. Smolenski *et al.*, "Electrochemistry of ytterbium (III) in molten alkali metal chlorides," *Electrochim. Acta*, 54 (2), 382–387, (2008).

7분과

방사화학 (Poster)



Electrolytic Reduction of Uranium and Rare Earth Oxides in LiCl-Li₂O Molten Salt

Alexei Shishkin¹⁾, Vladimir Shishkin¹⁾, Albert Mullabaev¹⁾, Vadim Kovrov¹⁾, Alexander Dedukhin¹⁾, Anna Kholkina, ¹⁾ Vladimir Tsvetov¹⁾, Sang-Eun Bae²⁾, and Yury Zaykov¹⁾,*

¹⁾ Institute of High Temperature Electrochemistry, Ekaterinburg, Russia

²⁾ Korea Atomic Energy Research Institute, 111, Daedeok-daero 989beon-gil, Yuseong-gu, Daejeon, Republic of Korea

*A.Potapov_50@mail.ru

The electrolytic reduction of tablets of uranium oxides, rare earths oxides and their mixtures has been studied in LiCl melt with additives 0-2.0 wt.% Li₂O at temperature 650 °C. Electrolysis was carried out in galvanostatic mode with a step change of current. The cathode potential was measured with a short-time current cutoff for monitoring the process. Platinum, graphite and ceramic anodes were used in the experiments. The process duration was determined by the amount of electricity passed, that was varied from 130 to 230% of the theoretically necessary one for oxides reduction.

The reference electrode was Bi-Li(~ 60 at.%) alloy behind the porous MgO diaphragm. During the experiments its potential was controlled against the potential of lithium discharged on the Mo electrode. The anode was inside the MgO tube without a bottom. The anode gases evolved were removed from the cell by a constant argon flow. The experiments made in a glove box with a controlled atmosphere, H₂O < 1 ppm, O₂(initial) < 5 ppm.

Electrolytic reduction of the UO₂ tablets was performed at cathode potential of 20-50 mV more positive than the lithium potential.

Practically complete UO₂ reduction to metallic uranium at Li₂O concentration ~ 1 wt.% was achieved. The amount of electricity passed was 160-200% of the theoretical one.

In the experiments with electrolytic reduction of UO₂ tablets containing 5-17 wt.% rare-earth oxides it

was found that UO₂ is also completely reduced, according to preliminary data, whereas rare-earth oxides were not reduced at all. Only CeO₂ was reduced to Ce₂O₃. The cathode potential was equal to the lithium discharge potential only during the last third of the experiment.

To confirm the results several attempts were made to metallize tablets of individual and mixed rare-earth oxides that do not contain uranium dioxide. The initial Li₂O content was varied from 0 to 1.0 wt.%. Electrolysis was carried out at cathode potentials equal to the lithium discharge potential. The amount of electricity passed was from 160 to 200% of the theoretical one. The samples after the reduction were investigated with different independent analyses. The total content of oxygen was also determined. Rare earth oxides were confirmed not to be reduced in the experiments. CeO₂ was reduced to Ce₂O₃.

Conclusion

The experimental results obtained allow making encouraging conclusions on the possibility of the fission products separation from the target product for the the pyrochemical technology of spent nuclear fuel recycle. At electrolysis the alkali or alkali - earth metals are will in the LiCl melt. Rare-earth metals will stay in the U-Pu phase as an oxide form that creates favorable conditions for further separation.

Distillation of Lithium Chloride From the Metallization Products of Uranium Dioxide

Alexander Salyulev, Alexey Shishkin, Alexei Potapov*, Vladimir Shishkin, and Yury Zaykov

Institute of High Temperature Electrochemistry, Ekaterinburg, Russia

*A.Potapov_50@mail.ru

To separate uranium from lanthanides in oxide spent nuclear fuel (SNF), a method of oxides metallization with metallic lithium is proposed. This process is carried out in a medium of molten LiCl. As a result, the metallized product captures 10-36wt.% of the electrolyte which should be removed.

The aim of this work is to find the optimal regimes for distilling the trapped electrolyte from the metallization products.

Samples for distillation were powders or tablets (4–40% porosity) of UO_2 or $\text{UO}_2 + 5\text{-}15\text{wt}\% \text{La}_2\text{O}_3$, CeO_2 , Nd_2O_3 after electrolytic reduction with lithium in molten $\text{LiCl-Li}_2\text{O}$ (0.8-1.5wt% Li_2O) mixture.

Metallized powders or tablets were placed in nickel or molybdenum containers. Distillation was carried out in quartz tubes under continuous evacuation ($P = 1.2\text{--}2.5 \text{ mPa}$) for 1-3 hours. The temperature was 700-900°C. The Li, U, La, Ce, and Nd content in metallized products and in vapor condensates was determined with an atomic emission spectrometry using an Optima 4300DV ICP-OES spectrometer before and after distillation.

It was found that the main component of the vapor condensates is LiCl. Lithium oxide, together with LiCl, is practically not co-evaporated. This conclusion agrees with the data [1]. The content of rare-earth elements and uranium in condensates is also negligible.

As an example, the results of several experiments are shown in Table 1. In accordance with our experimental results, the optimum temperature range is 780-850°C. As the temperature decreases, a share of the evaporated LiCl goes down. At a higher temperature, an undesired back reaction of metallic

uranium oxidation to UO_2 by residual lithium oxide occurs:

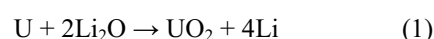


Table 1. The results of elemental analysis of metallized uranium dioxide pellets (4% porosity) after distillation of electrolyte from them

$t, ^\circ\text{C}$	703	780	841	841
Time, h	1	2	2.2	2.2
Li, mg	3.76	0.132	0.055	0.093
U, mg	249	633	473	463
Li, wt. %	1.49	0.021	0.012	0.020
LiCl in condensates, mg	5.1	10.5	6.6	6.7
LiCl in condensates, wt%	57.7	98.8	99.2	98.6

Thus, it is shown that 98.8-99.9% of the captured LiCl is removed from the metallized product under optimal conditions. The residual content of lithium in the metallized product (mainly in the form of Li_2O) does not exceed a few hundredths of a percent.

REFERENCES

- [1] H.W.Kang, E.-Y. Choi, S.-W. Kim, S.-S. Hong, M.K. Jeon, S.-K. Lee, S.-C. Oh, W. Park, and J.-M. Hur, "Distillation characteristics of $\text{LiCl-Li}_2\text{O}$ electrolyte for UO_2 electrolytic reduction process", *Journal of Radioanalytical and Nuclear Chemistry*, 310, 1165–1171 (2016).

Electrical Conductance of Molten (LiCl-KCl)_{eut} With Components of Spent Nuclear Fuel

Alexander Salyulev, Alexei Potapov*, Vladimir Shishkin, and Yury Zaykov

Institute of High Temperature Electrochemistry, Ekaterinburg, Russia

*A.Potapov_50@mail.ru

Pyrochemistry is one of the most innovative approaches for spent nitride nuclear fuel reprocessing. The first stage of SNF reprocessing is its dissolution in the LiCl-KCl eutectic. As a result, complex multicomponent solutions are formed, the properties of which have not yet been adequately studied.

The aim of this work is to develop a model for the electrical conductivity of complex melts based on LiCl-KCl eutectic, containing the SNF components. This communication is a continuation of our work [1].

To achieve this goal, we measured the electrical conductivity of a number of quasi binary melts (LiCl-KCl)_{eut.}, containing CeCl₃, NdCl₃, UCl₃, as well as CsCl and CdCl₂, and some of 3-4 component (LiCl-KCl)_{eut.} - CeCl₃ - NdCl₃ - UCl₃ mixtures.

In the work a capillary quartz cell with platinum electrodes and the AC-bridge method at the input frequency of 10-75 kHz were used. The measurements over the entire concentration and in wide temperature (up to 800-950°C) ranges were carried out. The lowest temperature was 5-10 degrees below the liquidus of all compositions in order to fix the temperature of crystallization onset.

The electrical conductivity of all melts increases with temperature and decreases as the concentration of trichlorides increases. The specific electrical conductivity (κ , S/cm) of molten mixture of LiCl-KCl eutectic with CeCl₃ (890-1122 K, 50.8 mol.% CeCl₃) is exemplified below:

$$\kappa = -3.7858 + 6.8563 \cdot 10^{-3} \cdot T - 1.7911 \cdot 10^{-6} \cdot T^2 \quad (1)$$

For the mixtures under study the density was

estimated and the molar conductivity was calculated. In all molten (LiCl-KCl)_{eut.} - LnCl₃ mixtures studied the significant negative deviations (up to -70% in maximum) of molar conductivity from additive values were observed over the whole concentration range, indicating a strong complexation in the systems. The results obtained are analyzed in terms of coexistence and mutual competition of complexes, which are formed by Li⁺ and Cd²⁺, Ce³⁺, Nd³⁺, U³⁺ cations.

The data obtained are necessary for the proper organization of the respective production processes.

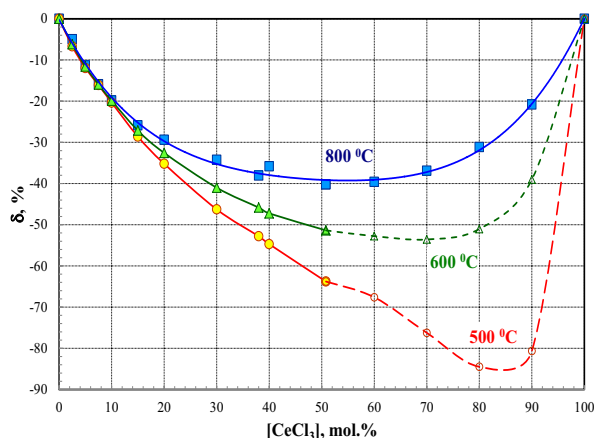


Fig. 1. Molar conductivity relative deviations from the additivity in the molten (LiCl-KCl)_{eut.} + CeCl₃ system.

Extrapolated values are shown in phantom.

REFERENCES

- [1] A. Salyulev, A. Potapov, V. Khokhlov, and V. Shishkin, "The electrical conductivity of model melts based on LiCl-KCl, used for the processing of spent nuclear fuel", *Electrochimica Acta*, 257, 510-515 (2017).

Influence of Metal-doping on the Surface Structure and Electrochemical Reactivity of Uranium Dioxide

Jeongmook Lee^{a)*}, Jandee Kim^a, Young-Sang Youn^{a)}, Seohyun Park^{a)b)}, Jeong-mi Park^{a)b)}, Jong-Yun Kim^{a)c)} and Sang Ho Lim^{a)c)}

^{a)} Korea Atomic Energy Research Institute, 111, Daedeok-daero 989beon-gil, Yuseong-gu, Daejeon, Republic of Korea

^{b)} Chungnam National University, 99, Daehak-ro, Yuseong-gu, Daejeon, Republic of Korea

^{c)} University of Science & Technology, 217, Gajeong-ro, Yuseong-gu, Daejeon, Republic of Korea

*leejm@kaeri.re.kr

1. Introduction

Spent nuclear fuels (SNFs) have totally different microstructure from initial fresh UO_2 fuel due to the formation of fission products, transuranium elements, and activation products with many different phases during irradiation [1-3]. Additionally, the physical and chemical properties of UO_2 lattice were also changed. In particular, some actinide and lanthanide elements can form a solid solution with UO_2 lattice and make non-stoichiometry depending on their oxidation state and specific conditions. These alterations of UO_2 lattice could strongly be related to chemical reactivity such as corrosion and oxidation of UO_2 [4-5]. Thus, it is critical to characterize the physical and chemical properties of SNFs affected by specific elements doping. Much information from those characterizations should be useful to plan the final disposal or interim storage of SNFs.

Herein, the influence of metal-doping on the surface structure of UO_2 has been investigated by X-ray diffraction (XRD), scanning electron microscopy (SEM), and Raman spectroscopy. Various simulate fuels (Nd^{3+} -, Gd^{3+} -, Zr^{4+} -, Th^{4+} -doped UO_2) were used. Their electrochemical properties were also investigated.

2. Experimental sections

UO_2 and Nd_2O_3 (or Gd_2O_3 , ZrO_2 , ThO_2) powders for $\text{U}_{1-y}\text{Nd}_y\text{O}_2$ (or $\text{U}_{1-y}\text{Gd}_y\text{O}_2$, $\text{U}_{1-y}\text{Zr}_y\text{O}_2$, $\text{U}_{1-y}\text{Th}_y\text{O}_2$) with various y components were mixed and pelletized. The sample pellets were sintered in the tube furnace at 1700°C for 18 h with hydrogen atmosphere. XRD data was collected by Bruker D8 Advance using $\text{CuK}\alpha$ line source (beam current 40 mA at 40 kV). The lattice parameters of the samples were calculated from XRD spectra with refinement process. The surface morphologies of sample pellets were obtained by SEM. Raman spectra were measured using ANDOR Shamrock SR500i spectrometer with 632.8 nm He-Ne laser and analyzed by peak deconvolution method.

3. Results

The lattice parameters for $(\text{U},\text{Nd})\text{O}_2$, $(\text{U},\text{Gd})\text{O}_2$, $(\text{U},\text{Zr})\text{O}_2$, and $(\text{U},\text{Th})\text{O}_2$ linearly varied as the doping level increased. These linear variations represented that sample pellets were formed as a solid solution.

The grain size observed in SEM images for $(\text{U},\text{Gd})\text{O}_2$, $(\text{U},\text{Nd})\text{O}_2$, and $(\text{U},\text{Zr})\text{O}_2$ decreased with increasing doping level. However, there was less change of the grain size with various Th doing levels in $(\text{U},\text{Th})\text{O}_2$.

Raman spectra of $\text{U}_{0.9}\text{Th}_{0.1}\text{O}_2$ and UO_2 showed same feature as shown in Fig. 1. However, there were

defect structures related to oxygen vacancy in Raman spectra of $\text{U}_{0.9}\text{Gd}_{0.1}\text{O}_{2-x}$ and $\text{U}_{0.9}\text{Nd}_{0.1}\text{O}_{2-x}$ at $500 \sim 650 \text{ cm}^{-1}$. Trivalent elements replacing U^{4+} could make oxygen vacancy that distorts UO_2 fluorite lattice. For $\text{U}_{0.9}\text{Zr}_{0.1}\text{O}_2$, there was no defect structure related to oxygen vacancy. But distinct peak at $\sim 598 \text{ cm}^{-1}$ was observed. This peak would be assigned as a formation of ZrO_8 -type complex in UO_2 lattice.

Electrochemical experiments showed that this surface structure would be strongly related to chemical reactivity.

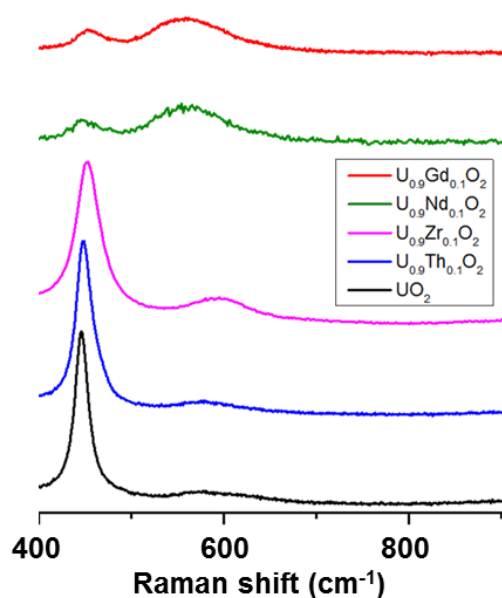


Fig. 1. Raman spectra of UO_2 , $\text{U}_{0.9}\text{Th}_{0.1}\text{O}_2$, $\text{U}_{0.9}\text{Zr}_{0.1}\text{O}_2$, $\text{U}_{0.9}\text{Nd}_{0.1}\text{O}_2$, and $\text{U}_{0.9}\text{Gd}_{0.1}\text{O}_2$ from bottom to top.

4. Conclusion

Summarizing results, trivalent doping elements, Gd^{3+} and Nd^{3+} , form the oxygen vacancy and the smaller grain size in UO_2 surface structure. Tetravalent dopant, Th^{4+} , has small influence on UO_2 surface structure. However, other tetravalent dopant, Zr^{4+} , shows large influence on UO_2 surface structure. Electrochemical properties depends on the doping

element.

ACKNOWLEDGEMENT

This work was supported by the National Research Foundation of Korea (NRF) grant funded by the Korean government (MSIT) (2017M2A8A5014754)

REFERENCES

- [1] H. Kleykamp, The chemical state of the fission products in oxide fuels, *Journal of Nuclear Materials*, 131, 221-246 (1985).
- [2] R. J. M. Konings, T. Wiss, and O. Beneš, Predicting material release during a nuclear reactor accident, *Nature Materials*, 14, 247-252, (2015).
- [3] R. C. Ewing, Long-term storage of spent nuclear fuel, *Nature Materials*, 14, 252-257 (2015).
- [4] M. Razdan and D. W. Shoesmith, Influence of Trivalent-Dopants on the Structural and Electrochemical Properties of Uranium Dioxide (UO_2), *Journal of the Electrochemical Society*, 161, H105-H113 (2013).
- [5] J. Kim, J. Lee, Y.-S. Youn, N. Liu, J.-G. Kim, Y.-K. Ha, S.-E. Bae, D. W. Shoesmith, and J.-Y. Kim, The Combined Influence of Gadolinium Doping and Non-stoichiometry on the Structural and Electrochemical Properties of Uranium Dioxide, *Electrochimica Acta*, 247, 942-948 (2017).

Formation of Calcium Uranyl Carbonate Species at Variable Temperatures

Yongheum Jo¹⁾, Hee-Kyung Kim²⁾, and Jong-Il Yun^{1)*}

¹⁾ Korea Advanced Institute of Science and Technology, 291, Daehak-ro, Yuseong-gu, Daejeon, Republic of Korea

²⁾ Korea Atomic Energy Research Institute, 111, Daedeok-daero 989beon-gil, Yuseong-gu, Daejeon, Republic of Korea

*jiyun@kaist.ac.kr

1. Introduction

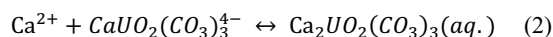
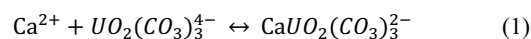
Due to geothermal gradient (typically + 3°C/100 m) and decay heat from radioactive waste, the temperature of repository system for high-level radioactive waste is likely to be elevated. However, thermodynamic data for elevated temperature effect are still scarce. Even though calcium uranyl carbonate species, $\text{CaUO}_2(\text{CO}_3)_3^{2-}$ and $\text{Ca}_2\text{UO}_2(\text{CO}_3)_3(\text{aq.})$, have been regarded as the most dominant species in groundwater and seawater, the influence of temperature on the formation of $\text{Ca-UO}_2\text{-CO}_3$ has not been reported yet. In this work, thermodynamic data (formation constants at variable temperatures and reaction enthalpy) of $\text{Ca-UO}_2\text{-CO}_3$ species were determined by time-resolved laser fluorescence spectroscopy (TRLFS), UV/Vis absorption spectrophotometry, potentiometry using a Ca^{2+} -ion selective electrode, and calorimetry. In addition, the estimation to predict the temperature-dependent formation constants was modeled.

2. Experimental Methods

2.1 Sample preparation

Determination of formation constants at variable temperatures (10 – 85°C) was carried out by three different analytical methods, and the chemical condition of samples was set to be adjusted to the sensitivity of each method. Using TRLFS, the

experiment was conducted at a micromolar level of uranium concentration due to its high sensitivity. On the other hand, UV/Vis absorption spectrophotometry and potentiometry analysis were performed at millimolar U(VI) concentration. Initially, all uranium samples were set to form $\text{UO}_2(\text{CO}_3)_3^{4-}$ abundantly by adding sufficient carbonate ions, and then the quantitative spectrophotometric or potentiometric change with increasing calcium concentration was observed. As the Ca^{2+} ion concentration increases, a sequential complexation of calcium ions and $\text{UO}_2(\text{CO}_3)_3^{4-}$ may occur (equation 1 and 2).



2.2 Determination of formation constants of $\text{Ca-UO}_2\text{-CO}_3$ at variable temperatures

A laser wavelength of 266 nm from Nd:YAG pulse laser was utilized for TRLFS analysis. Time-resolved emissions from U(VI) samples were recorded with Czerny-Turner spectrometry with ICCD camera. An enhanced fluorescence in terms of intensity and lifetime with increasing $[\text{Ca}^{2+}]$ gives quantitative information on the formation of $\text{Ca-UO}_2\text{-CO}_3$.

Due to a large difference in molar absorptivity, absorption spectra were collected in the wavelength 220 – 400 nm and 360 – 500 nm with 1 cm cuvette

and 100 cm liquid waveguide capillary cell, respectively. The observed spectrophotometric data were processed with the software, HypSpec2014 [1,2].

Moreover, Ca^{2+} selective electrode was used to the potentiometric titration. The measured potential corresponds to the concentration of free Ca^{2+} , as shown in equation (3).

$$E = E_0 + S \cdot \log[\text{Ca}^{2+}] \quad (3)$$

(where E_0 is the standard potential of electrode in mV and S is the slope of the electrode response.)

Prior to potentiometric titration with uranium samples, a calibration titration was performed to obtain E_0 and S in equation 3. In order to avoid an interference of carbonate ion, argon-purged 0.1 m NaCl solution was utilized for the calibration. The potentiometric data were analyzed by Hyperquad2013 [1,2].

All experiments were conducted at various temperatures of 10, 25, 40, 55, 70, and 85°C using a water-jacketed cell by circulating the temperature-controlled water.

2.3 Calorimetry

Reaction enthalpies corresponding to equation 1 and 2 were measured with isothermal titration calorimeter and nano-calorimeter at 25°C. The measured heat flow was corrected by the subtraction of heat flow of titrant dilution and side reactions during titration. The reaction enthalpies were determined by U(VI) speciation using the formation constants obtained in this work and by least-squares regression.

3. Results and Discussion

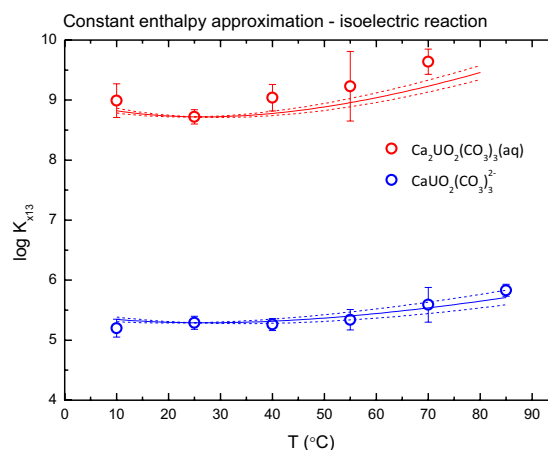


Fig. 1. Formation constants of calcium uranyl carbonate species (derived from TRLFS, UV/Vis absorption spectrophotometry, potentiometry) and estimation model for variable temperatures.

Figure 1 illustrates the formation constants of $\text{Ca-UO}_2\text{-CO}_3$ at various temperatures. Constant reaction enthalpy model in isoelectric reaction provided a successful prediction of the formation constants at variable temperatures.

ACKNOWLEDGEMENT

This work was supported by a grant from the Nuclear R&D Program of the National Research Foundation of Korea funded by the Korean Ministry of Science and ICT (Grant codes: 2016M2B2B1945252).

REFERENCES

- [1] P. Gans, A. Sabatini, A. Vacca, *Talanta*, 43, 1739 (1996).
- [2] L. Alderighi, P. Gans, A. Ienco, D. Peters, A. Sabatini, A. Vacca, *Coord. Chem. Rev.*, 184, 311 (1999).

The Comparison of Selective Zirconium Removal Between TBP Extraction and POM Complexation

Kyungwon Suh*, Jaeseok Lee, and Jong-Yun Kim

Korea Atomic Energy Research Institute, 111, Daedeok-daero 989beon-gil, Yuseong-gu, Daejeon, Republic of Korea

*kyungwon0707@kaeri.re.kr

1. Introduction

Zirconium is one of the significant elements in nuclear materials because of its excellent corrosion resistance, sufficient mechanical properties and low neutron absorption coefficient. For a nuclear application, boron and cadmium in zirconium and its alloy should be present less than 0.5 ppm [1] because of their high neutron absorption cross-section. So it is important to quantify the amount of boron and cadmium in zirconium and its alloys.

ICP-OES (Induced Couple Plasma-Optical Emission Spectroscopy) is routinely used to quantify the amount of metal. However, zirconium is a line rich element, which makes difficult to determine trace elements like boron and cadmium in zirconium and its alloys due to the interference between trace element and zirconium in solution. [2] Therefore, boron and cadmium should be selectively separated from zirconium containing sample solution.

Among several conventional methods for removal of Zr, TBP extraction is a well-established method for zirconium extraction because zirconium has a higher distribution coefficient in nitric acid medium than that of boron and cadmium.

POM (polyoxometalate) is pure inorganic compound which is composed of transition metal like W, Mo, Nb, and Ta and heteroatom such as B, P, and Se. There are two categories of POM: plenary POM and lacunary POM. A plenary POM has no defective sites, while a lacunary POM has defective sites by losing metal-oxide from a plenary POM through the modification of synthetic condition. These lacunary

POMs could be used as inorganic ligands, so zirconium could be selective removed from the sample solution containing boron and cadmium.

Herein, we present that the complexation with POM shows a better method for zirconium separation by comparison between TBP extraction and POM complexation.

2. Experimental Section

2.1 General Information

All reagents were used without further purification and purchased from commercial source as follows: TBP (Sigma-Aldrich), boron and cadmium (AccuStandards), $\text{ZrOCl}_2 \cdot 8\text{H}_2\text{O}$ (SHOWA Chemical Co.), $\text{H}_3\text{PW}_{12}\text{O}_{40}$ (Kanto chemical Co.). The amount of each metal was determined using Thermo iCAP 7400 coupled with Teledyne Cetac ASX-560.

2.2 TBP extraction

For TBP extraction in 1:1 (V/V) HNO_3 , two kinds of sample solutions were prepared: one contained zirconium only, the other included zirconium, boron, and cadmium. The next experiment procedure was as follows: Dry the sample solution by evaporation. Dissolve the dried sample using 1:1 HNO_3 . Mix TBP and HNO_3 by 1:1 volumetric ratio. Separate the HNO_3 from the mixture using a separation funnel.

2.3 POM complexation

As mentioned earlier, a lacunary POM could be ligands for zirconium complexation. So, a lacunary POM was prepared by adding sodium carbonate to dissolved $\text{H}_3\text{PW}_{12}\text{O}_{40}$ in deionized water. As with TBP extraction, two kinds of sample solutions were prepared. And then, zirconium solution made from $\text{ZrOCl}_2 \cdot 8\text{H}_2\text{O}$ was added to each sample solution. To determine the amount of each metal in solution, the suspensions were centrifuged.

3. Results

3.1 Single component case

In TBP extraction, the recovery of Zr in nitric acid was about 7%, meaning most Zr was transferred to TBP. Although the recovery of Zr in POM complexation was dependent on the amount of $\text{H}_3\text{PW}_{12}\text{O}_{40}$, 400 mg $\text{H}_3\text{PW}_{12}\text{O}_{40}$ gave the lowest recovery of Zr in POM complexation, which value (~9%) was similar to that of TBP extraction.

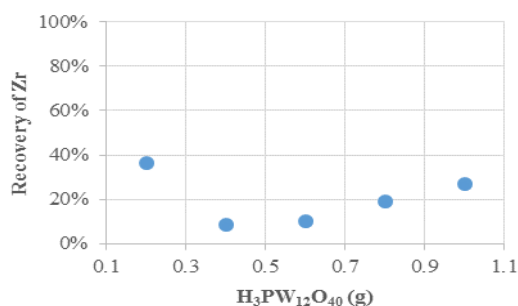


Fig. 1. Recovery of Zr vs the amount of $\text{H}_3\text{PW}_{12}\text{O}_{40}$.

3.2 Ternary component case

In the case of ternary component Zr-B-Cd, the recovery of each metal was summarized in Table 1. POM complexation gave better selective separation of Zr than TBP extraction, although the recovery of each metal was dependent on the volume of sodium carbonate in POM complexation.

Table 1. The recovery of each metal in Zr-B-Cd

Na ₂ CO ₃ (1 M, mL)	Recovery		
	Zr	B	Cd
0.0	0.08	0.96 ± 0.02	1.04 ± 0.01
0.5	0.02	0.97 ± 0.01	1.00 ± 0.01
1.0	0.18 ± 0.01	0.88 ± 0.01	0.46 ± 0.05
2.0	0.84 ± 0.07	0.73 ± 0.04	0.35 ± 0.09
TBP	0.13 ± 0.01	0.83 ± 0.05	0.81 ± 0.04

4. Conclusions

We present that the complexation between POM and oxophilic Zr(IV) provides the better removal than conventional method through the comparison of Zr removal between TBP extraction and Zr-POM complexes.

REFERENCES

- [1] ASTM B349, "Standard specification for zirconium sponge and other forms of virgin metal for nuclear application"; ASTM B350, "Standard specification for zirconium and zirconium alloy ingots for nuclear application"; ASTM B352, "Standard specification for zirconium and zirconium alloy sheet, strip, and plate for nuclear application"; ASTM B353, "Standard specification for wrought zirconium and zirconium alloy seamless and welded tubes for nuclear service".
- [2] R. M. Li, Z. S. Li, Y. F. Xin, Appl. Sci. Technol. 2001, 9, 52; Michiko Banno, Eiichi Tamiya, Yuzuru Takamura, Anal. Chim. Acta. 2009 634 153.

Laser-Based Spectroscopic Studies of Actinide Complexes: Uranium

Euo-Chang Jung*, Hye-Ryun Cho, Hee-Kyung Kim, Tae-Hyeong Kim, Hyejin Cho, and Wansik Cha
Korea Atomic Energy Research Institute, 111, Daedeok-daero 989beon-gil, Yuseong-gu, Daejeon, Republic of Korea
*ecjung@kaeri.re.kr

1. Introduction

In the last year, a new book titled “The Heaviest Metals: Science and Technology of the Actinides and Beyond” was designed by John Wiley & Sons to cover both the fundamentals and recent advances in the science and technology of the “heaviest metals,” i.e., the actinide and transactinide elements, starting with actinium, up to the current end of the periodic table [1]. This book will also be published online as part of the Encyclopedia of Inorganic & Bioinorganic Chemistry. We contribute one chapter entitled “Laser-Based Spectroscopic Studies of Actinide Complexes” and we would like to present description of the techniques and several representative application studies introduced in the chapter in a series of three poster presentations. Each poster presentation is specific to uranium, plutonium and americium.

The chemical speciation of actinide complexes is considered to be a key concept for the safe management of spent nuclear fuels in the back-end of a nuclear fuel cycle. Methodological approaches for chemical speciation have been reported in detail in several studies [2, 3]. However, it appears that most nuclear and chemical engineers who work in nuclear industries are not familiar with laser-based spectroscopic techniques. In this presentation, applications of the laser-based spectroscopic techniques to the chemical speciation of actinide complexes are introduced for those who are interested in the highly sensitive analytical techniques applicable in the nuclear industry.

In the Uranium part, the spectroscopic properties of hydroxo complexes of U(VI) in aqueous solutions are demonstrated as representative examples. The luminescence characteristics of U(VI) species are

measured by using time-resolved laser fluorescence spectroscopy (TRLFS). We demonstrate here that TRLFS is a sensitive and specific technique, enabling the speciation of trace amounts of natural uranium in groundwater without any sample pretreatment. As an application, a few μM of Ca-U(VI)-carbonate complex is identified as dissolved uranium species in groundwater.

2. Experimental Considerations

The U(VI) sample preparation procedure and the experimental setup of TRLFS are described in detail in the previous literatures [4, 5].

3. Results and Discussion

The U(VI)-hydroxo complexes are denoted as (1,0), (1,1), and (2,2) species and $(\text{UO}_2)_m(\text{OH})_n^{2m-n}$ is usually denoted as (m, n) for simplicity. It is well known that the (1,1) and (2,2) species show relatively different luminescence lifetimes compared to that of (1,0) species. However, a direct comparison of spectral shapes of (1,1) and (2,2) species is still of interest. Fig. 1 shows the luminescence spectra measured from solutions containing U concentrations of 100 μM at pH 4.26 and 10 μM at pH 4.79 in 0.1 M NaClO_4 . The spectral shapes of (1,1) and (2,2) species are directly compared in Fig. 1.

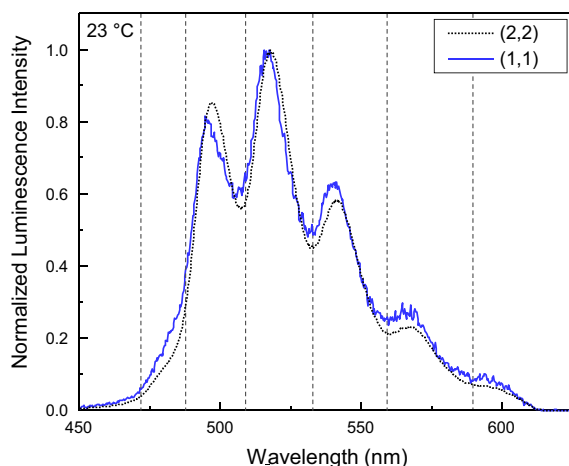


Fig. 1. Luminescence spectra of (2,2) and (1,1) species measured from solutions containing $100 \text{ } \mu\text{M}$ of uranium at pH 4.26 (dotted line) and $10 \text{ } \mu\text{M}$ of uranium at pH 4.79 (solid line). The dotted and solid lines are measured at $t_d = 20 \text{ s}$, $t_w = 50 \text{ s}$ and at $t_d = 120 \text{ s}$, $t_w = 50 \text{ s}$, respectively. The vertical lines represent the peak positions of UO_2^{2+} .

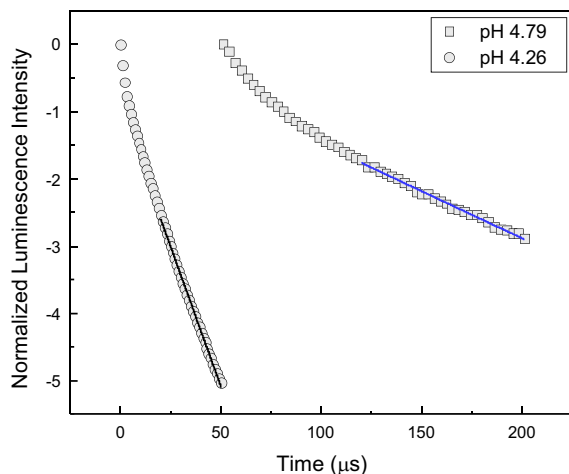


Fig. 2. The symbols represent the normalized luminescence intensity measured using the kinetic mode of ICCD. The solid lines represent fitting of the data to the linear regression. The luminescence lifetimes are $\tau = 12.0$ and $71.4 \text{ } \mu\text{s}$ at pH 4.26 and 4.79, respectively.

The symbols in Fig. 2 represent the normalized luminescence intensities in a natural logarithmic scale. For the solution at pH 4.26, the short- and long-lived species correspond to the (1,0) and (2,2) species, respectively. For the sample at pH 4.79, the short- and long-lived species correspond to the (2,2) and (1,1) species, respectively. The luminescence lifetimes of (2,2) and (1,1) species are determined to be 13.0 ± 2.0 and $57.4 \pm 11.7 \text{ } \mu\text{s}$, respectively.

4. Conclusion

The chemical speciation of actinides in aqueous solutions is important for the long-term isolation of high-level radioactive wastes. The laser-based spectroscopic technique, TRLFS is very useful for speciation studies of these elements in dilute concentrations. Speciation studies related to the identification of U(VI)-hydroxo and U(VI)-carbonate complexes in groundwater can be performed using TRLFS. The combined information on the luminescence spectrum with the luminescence lifetime, which depends on the nature of the ligands in aqueous solutions, makes the chemical speciation of U(VI) complexes at trace-level concentrations possible.

ACKNOWLEDGEMENT

This work was supported by a grant from the Nuclear Research and Development Program of the National Research Foundation of Korea funded by the Korean Ministry of Science and ICT (Grant code: 2017M2A8A5014719).

REFERENCES

- [1] E. C. Jung, H.-R. Cho, H.-K. Kim and W. Cha, in 'The Heavies Metals: Science and Technology of the Actinides and Beyond' eds. W. J. Evans and T. P. Hanusa, 2019 (ISBN: 978-1-119-30409-8).
- [2] A. M. Ure, and C. M. Davidson, in 'Chemical Speciation in the Environment', eds. A. M. Ure and C. M. Davidson, Blackwell Science Ltd, p. 1 (2007).
- [3] D. M. Templeton, F. Ariese, R. Cornelis, L.-G. Danielsson, H. Muntau, H. P. Van Leeuwen and R. Lobinski, Pure Appl. Chem., 72, 1453 (2000).
- [4] E. C. Jung, H.-R. Cho, M. H. Baik, H. Kim, W. Cha, Dalton Trans., 44, 18831-18838 (2015).
- [5] Euo Chang Jung, Min Hoon Baik, Hye-Ryun Cho, Hee-Kyung Kim, Wansik Cha, Journal of Nuclear Fuel Cycle and Waste Technology, 15(2), 101-116 (2017).

Laser-Based Spectroscopic Studies of Actinide Complexes: Plutonium

Hye-Ryun Cho*, Euo-Chang Jung, Hee-Kyung Kim, and Wansik Cha

Korea Atomic Energy Research Institute, 111, Daedeok-daero 989beon-gil, Yuseong-gu, Daejeon, Republic of Korea

*hrcho@kaeri.re.kr

1. Introduction

In the last year, a new book titled “The Heaviest Metals: Science and Technology of the Actinides and Beyond” was designed by John Wiley & Sons to cover both the fundamentals and recent advances in the science and technology of the “heaviest metals,” i.e., the actinide and transactinide elements, starting with actinium, up to the current end of the periodic table [1]. This book will also be published online as part of the Encyclopedia of Inorganic & Bioinorganic Chemistry. We contribute one chapter entitled “Laser-Based Spectroscopic Studies of Actinide Complexes” and we would like to present description of the techniques and several representative application studies introduced in the chapter in a series of three poster presentations. Each poster presentation is specific to uranium, plutonium and americium.

The chemical speciation of actinide complexes is considered to be a key concept for the safe management of spent nuclear fuels in the back-end of a nuclear fuel cycle. Methodological approaches for chemical speciation have been reported in detail in several studies [2, 3]. However, it appears that most nuclear and chemical engineers who work in nuclear industries are not familiar with laser-based spectroscopic techniques. In this presentation, applications of the laser-based spectroscopic techniques to the chemical speciation of actinide complexes are introduced for those who are interested in the highly sensitive analytical techniques applicable in the nuclear industry.

The spectroscopic properties of hydroxo complexes of Pu(VI) are demonstrated as representative examples. The absorption

characteristics of Pu(VI) species are measured by using laser-induced photoacoustic spectroscopy (LPAS) and spectrophotometry coupled with a liquid waveguide capillary cell(LWCC). We demonstrate here that LPAS and LWCC is a sensitive and specific technique, enabling the speciation of trace amounts of plutonium being different oxidation states. As a representative example, a few μM of Pu(VI)-OH complexes are identified and thermodynamic data of Pu(III)-OH are determined.

2. Experimentals

The Pu(VI) and Pu(III) samples preparation procedure and the experimental set-up of LPAS and spectrophotometry coupled with LWCC (LWCC-3100, WPI Inc.) were described in detail in the previous literatures [1, 4, 5].

3. Results and Discussion

Fig. 1 shows absorption spectra of plutonium samples (concentration of 0.05 mM) at different pH values from 5.9 to 6.8 measured by spectrophotometry coupled with LWCC (optical pathlength of 100 cm). The absorbance of Pu^{3+} ions decrease with the formation of Pu(III) hydroxo complexes as increase of pH. The formation constant of PuOH^{2+} species and solubility data of $\text{Pu}(\text{OH})_3$ (am) were reevaluated by chemical speciation using this sensitive absorption measurement system [5]. Spectrophotometry coupled with an LWCC in the visible wavelength region is considered as a comparable technique with LPAS especially for Pu(III-V), U(IV), U(VI) and Np(IV) species [1].

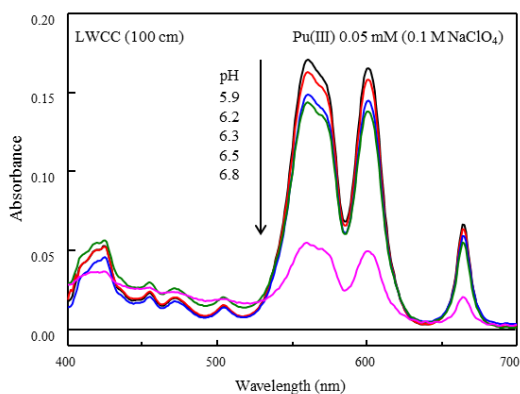


Fig. 1. Absorption spectra of Pu(III) measured by spectrophotometry coupled with LWCC (optical pathlength of 100 cm).

However, absorption spectrum in a near-IR wavelength region cannot be measured using LWCC. Thus, LPAS is a useful technique for the chemical speciation of aqueous actinide ions such as Pu(VI) and Np(V). Fig. 2 shows the LPAS spectra of plutonium samples (Pu concentration of 0.05 mM) at different pH values of 5.8, 8.0 and 10.4. Four peaks are observed at 830, 842, 850 and 861 nm. The peak at 830 nm represents the PuO_2^{2+} ions and the red-shifted peaks indicate the sequential formation of $\text{PuO}_2(\text{OH})^+$, $\text{PuO}_2(\text{OH})_2(\text{aq})$ and $\text{PuO}_2(\text{OH})_3^-$ species

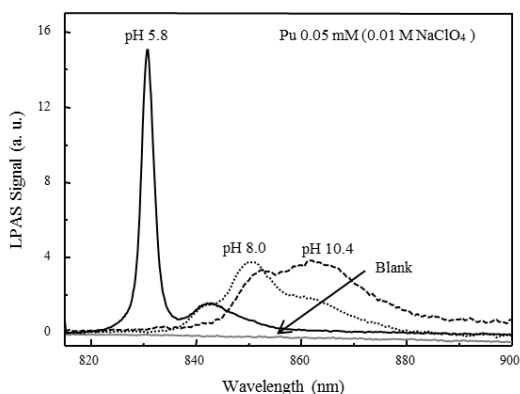


Fig. 2. Absorption spectra of Pu(VI)-OH complexes measured by LPAS.

4. Conclusion

The chemical speciation of actinides in aqueous solutions is important for the long-term isolation of

high-level radioactive wastes. The laser-based spectroscopic technique, LPAS and spectrophotometry coupled with LWCC are very useful for speciation studies of these elements in dilute concentrations. Speciation studies related to the identification of Pu(VI)- and Pu(III)-hydroxo complexes in groundwater can be performed using LPAS or spectrophotometry coupled with LWCC.

ACKNOWLEDGEMENT

This work was supported by a grant from the Nuclear Research and Development Program of the National Research Foundation of Korea funded by the Korean Ministry of Science and ICT (Grant code: 2017M2A8A5014719).

REFERENCES

- [1] E. C. Jung, H.-R. Cho, H.-K. Kim and W. Cha, in 'The Heaviest Metals: Science and Technology of the Actinides and Beyond' eds. W. J. Evans and T. P. Hanusa, 2019 (ISBN: 978-1-119-30409-8).
- [2] A. M. Ure, and C. M. Davidson, in 'Chemical Speciation in the Environment', eds. A. M. Ure and C. M. Davidson, Blackwell Science Ltd, 2007, p.1.
- [3] D. M. Templeton, F. Ariese, R. Cornelis, L.-G. Danielsson, H. Muntau, H. P. Van Leeuwen and R. Lobinski, *Pure Appl. Chem.*, 72, 1453 (2000).
- [4] H.-R. Cho, E. C. Jung, K. K. Park, W. H. Kim, K. Song and J.-I. Yun, *Radiochim. Acta*, 98, 765 (2010).
- [5] H.-R. Cho, Y.-S. Youn, E. C. Jung and W. Cha, *Dalton Trans.* 45, 19449 (2016).

Laser-Based Spectroscopic Studies of Actinide Complexes: Americium

Hee-Kyung Kim*, Hye-Ryun Cho, Eui-Chang Jung, and Wansik Cha

Korea Atomic Energy Research Institute, 111, Daedeok-daero 989beon-gil, Yuseong-gu, Daejeon, Republic of Korea

*hkim11@kaeri.re.kr

1. Introduction

In the last year, a new book titled “The Heaviest Metals: Science and Technology of the Actinides and Beyond” was designed by John Wiley & Sons to cover both the fundamentals and recent advances in the science and technology of the “heaviest metals,” i.e., the actinide and transactinide elements, starting with actinium, up to the current end of the periodic table [1]. This book will also be published online as part of the Encyclopedia of Inorganic & Bioinorganic Chemistry. We contribute one chapter entitled “Laser-Based Spectroscopic Studies of Actinide Complexes” and we would like to present description of the techniques and several representative application studies introduced in the chapter in a series of three poster presentations. Each poster presentation is specific to uranium, plutonium and americium.

The chemical speciation of actinide complexes is considered to be a key concept for the safe management of spent nuclear fuels in the back-end of a nuclear fuel cycle. Methodological approaches for chemical speciation have been reported in detail in several studies [2, 3]. However, it appears that most nuclear and chemical engineers who work in nuclear industries are not familiar with laser-based spectroscopic techniques. In this presentation, applications of the laser-based spectroscopic techniques to the chemical speciation of actinide complexes are introduced for those who are interested in the highly sensitive analytical techniques applicable in the nuclear industry.

In the americium part, spectroscopic properties of dicarboxylate complexes of Am(III) are investigated by using UV-Vis absorption spectroscopy coupled with a liquid waveguide capillary cell (LWCC) and

time-resolved laser fluorescence spectroscopy (TRLFS). We demonstrate here that UV-Vis-LWCC and TRLFS are sensitive and specific techniques, enabling the speciation of Am(III)-organic ligand complexes.

2. Experimentals

Am³⁺ and dicarboxylate solutions (sodium oxalate (Ox), sodium malonate (Mal), sodium succinate (Suc), Sigma-aldrich) were prepared in 0.1 M NaClO₄ and pH were adjusted to be in the range of pH 6 - 6.3. Am(III)-dicarboxylate samples were prepared by adding concentrated dicarboxylate solutions (10-400 mM) into the Am³⁺ solutions (1-10 μ M). UV-Vis absorption spectra were measured by using Cary3 (Varian) coupled with a LWCC (WPI) with a path length of 100 cm. Luminescence spectra were collected by TRLFS equipped with a nanosecond pulsed laser (OPO, Vibrant B, OPOTEK Inc.) as an excitation source (503 nm, 3.5 mJ). Detailed experimental setups can be found elsewhere [4, 5]. All the measurements were carried out at 25-26 °C.

3. Results and Discussion

Am³⁺ exhibits relatively strong absorption properties with an absorption peak at 503 nm ($\epsilon = 424 \pm 8 \text{ cm}^2\text{M}^{-1}$) in comparisons to other actinide ions (Fig. 1 (a), black). Am³⁺ is also luminescent with a maximum luminescence peak at 689 nm ($^5\text{D}_1 \rightarrow ^7\text{F}_1$), although the luminescence is very weak with a short lifetime of 23 ns (Fig. 1 (b) and (c), black). Additions of dicarboxylates (Ox, Mal, Suc) into the

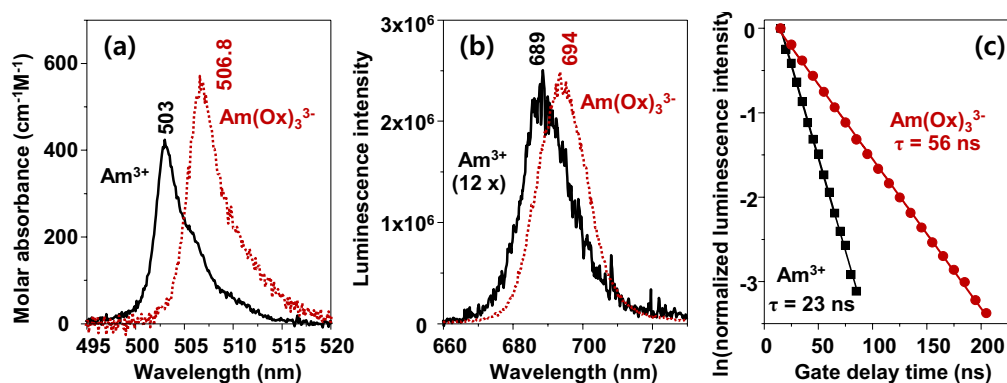


Fig. 1. Spectroscopic speciation of $\text{Am}(\text{Ox})_3^{3-}$ complexes by using (a) UV-Vis absorption spectra and (b) luminescence spectra. (c) Luminescence lifetime measurements by TRLFS. The sample is $8.35 \mu\text{M Am}^{3+}$ in 0.1 M NaClO_4 , $\text{pH} \sim 6$.

Am^{3+} samples induced gradual shifts of the absorption and luminescence spectra towards the longer wavelength directions as a function of the dicarboxylate concentrations. Representative spectral changes induced by the presence of 50 mM Ox are shown in Fig. 1 (red dots). Luminescence intensities and lifetimes are also gradually increased as increasing the ligand concentrations. Deconvolution of the absorbance spectra suggest that $\text{Am}(\text{Ox})_n^{3-3n}$ ($n = 1 - 3$) species are formed with increasing the higher complexes distributions as increasing the Ox concentration. $\text{Am}(\text{Ox})_3^{3-}$ complex becomes the major species in the presence of 50 mM Ox . Mal and Suc were also examined for the systematic investigation of the $\text{Am}(\text{III})$ interactions with dicarboxylates. Detailed spectral speciations including deconvolution results will be presented. Formation constants and probable molecular structures of the complexes will also be discussed in the presentation.

4. Conclusion

Absorption and luminescence property changes upon $\text{Am}(\text{III})$ -dicarboxylate complexations are investigated by using UV-Vis-LWCC and TRLFS. The observed distinct spectral changes and deconvolution of them using a calculation program enable speciation of the complexes. We demonstrate here that UV-Vis-LWCC and TRLFS are powerful in the study of $\text{Am}(\text{III})$ -organic ligand complexations. These techniques can be applied further to the study

of chemical speciation of $\text{Am}(\text{III})$ interacting with organic matters in groundwater system.

ACKNOWLEDGEMENT

This work was supported by a grant from the Nuclear Research and Development Program of the National Research Foundation of Korea funded by the Korean Ministry of Science and ICT (Grant code: 2017M2A8A5014719).

REFERENCES

- [1] E. C. Jung, H.-R. Cho, H.-K. Kim and W. Cha, in 'The Heaviest Metals: Science and Technology of the Actinides and Beyond' eds. W. J. Evans and T. P. Hanusa, 2019 (ISBN: 978-1-119-30409-8).
- [2] A. M. Ure, and C. M. Davidson, in 'Chemical Speciation in the Environment', eds. A. M. Ure and C. M. Davidson, Blackwell Science Ltd, 2007, p.1.
- [3] D. M. Templeton, F. Ariese, R. Cornelis, L.-G. Danielsson, H. Muntau, H. P. Van Leeuwen and R. Lobinski, *Pure Appl. Chem.*, 72, 1453 (2000).
- [4] H. -R. Cho, E. C. Jung, K. K. Park, W. H. Kim, K. Song and J. -I. Yun, *Radiochim. Acta*, 98, 765 (2010).
- [5] H. -K. Kim, S. Choi, E. C. Jung, H.-R. Cho, J.-I. Yun, W. Cha, *J. Lumin.*, 202, 469 (2018).

Study on Chemical Variation of Interface Between Gd-doped UO_2 and Zr Through Annealing With Various Temperatures

Jeongmi Park^{1,2)}, Young-Sang Youn¹⁾, Jeongmook Lee¹⁾, Jandee Kim¹⁾, Seohyeon Park^{1),2)},
Choong Kyun Rhee²⁾, and Sang Ho Lim^{1,3),*}

¹⁾ Korea Atomic Energy Research Institute, 111, Daedeok-daero 989beon-gil, Yuseong-gu,
Daejeon, Republic of Korea

²⁾ Chungnam National University, 99, Daehak-ro, Yuseong-gu, Daejeon, Republic of Korea

³⁾ University of Science and Technology, 217, Gajeong-ro, Yuseong-gu, Daejeon, Republic of Korea

*slim@kaeri.re.kr

1. Introduction

The interaction between UO_2 and Zr has been studied to comprehend the interfacial reaction between the nuclear fuel and the cladding [1-3]. Especially, their interaction at high temperature has been considered in order to understand the situation for the loss-of-coolant accident (LOCA). Various fission products generated from the irradiation of the UO_2 fuel and could affect the physical and chemical properties of UO_2 and Zr. Therefore, the influence of temperature and fission product on the interfacial reaction between UO_2 and Zr should be important.

Among the various fission product, Gd has often been chosen as a dopant in simulated spent nuclear fuel and easily forms solid solutions with UO_2 [4-6]. It is also important element which is used as a burnable absorber. In this study, we selected Gd as a representative fission product.

Herein, we demonstrate the chemical variations at the interface between Gd-doped UO_2 and Zr before and after annealing at various temperatures using X-ray diffraction (XRD), scanning electron microscopy (SEM), and Raman spectroscopy.

2. Experimental

UO_2 and Gd_2O_3 powders were mixed to fabricate Gd-doped UO_2 ($\text{U}_{1-y}\text{Gd}_y\text{O}_2$) pellets with various compositions (0, 2, 6, and 10mol% Gd). Mixed powders were compacted into a pellet form (6.35 mm diameter). Compacted pellets were sintered in an alumina tube at 1700°C for 18 hours under H_2 atmosphere. Disc type Zr sample having a diameter of 6.35 mm was produced by cutting a Zr rod (Sigma Aldrich Korea Ltd). The Gd-doped UO_2 pellet was placed on a Zr sample so that they physically contacted each other. Annealing was performed for 10 minutes after reaching intended temperatures of 300, 700, and 1200°C in HTK-2000N chamber (Maintain pressure below 5×10^{-6} torr) respectively. After annealing, the interfacial surfaces of the Gd-doped UO_2 pellet and a Zr sample were analyzed. The SEM experiments were fulfilled using a JEOL JSM-6610LV with an Oxford Instruments EDS. Raman spectroscopy was performed using ANDOR Shamrock SR500i Raman spectrometer (He-Ne laser with a wavelength of 632.8 nm). XRD data were measured by Bruker-AXS D8 Advance system (Cu K_α radiation) in the 2θ range of 20 to 120° with a scanning step of 0.02° for 0.1 s. The lattice parameter was calculated using the Bruker TOPAS program.

3. Results

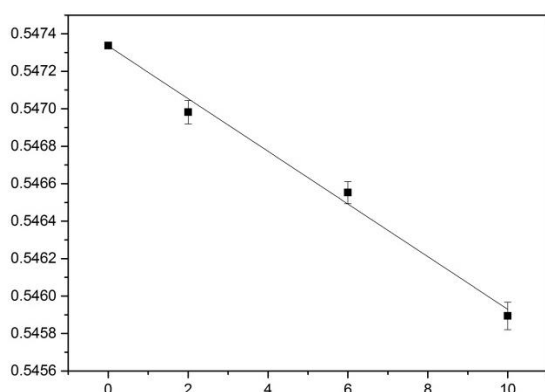


Fig. 1. The calculated lattice parameter of $U_{1-y}Gd_yO_2$ ($y = 0, 2, 6$, and 10) at Room temperature.

The calculated lattice parameters of the Gd-doped UO_2 at room temperature are shown in Fig.1. As the Gd concentration in the sample increased, the lattice parameter decreased. The similar features are observed at 300, 700, and 1200°C. There is no significant change in XRD data of Zr samples before and after annealing.

The Raman spectra of Gd-doped UO_2 after annealing at various temperatures show similar results each other. There are two main peaks at 445cm^{-1} and 1150cm^{-1} . Those peaks are the fingerprint of the UO_2 fluorite structure. The intensities of peaks at 445 and 1150cm^{-1} decreased with increasing Gd doping level. However, it is hard to find significant difference in Raman spectra between before and after annealing. It is expected that Gd doping could inhibit the reaction between UO_2 and Zr or the temperature may not be high enough to cause an interfacial reaction.

4. Conclusions

We simulated the interfacial reaction between Gd-doped UO_2 and Zr at various temperatures. The interface was analyzed using XRD and Raman

analysis, but no specific changes were observed before and after annealing. Gd doping could lower the reactivity of the surface of UO_2 . The higher temperature may be required to occur the interfacial reaction between Gd-doped UO_2 and Zr. We will discuss the effect of Gd doping on the interfacial reaction in detail.

ACKNOWLEDGEMENT

This research was supported by the National Research Foundation of Korea (NRF) grant funded by the Korean government (MSIP) (No. 2017M2A8A5014754)

REFERENCES

- [1] M. Miyake, M. Katsura, S. Yamanaka, "A study of the reaction between UO_2 and Zr", J. Nucl. Mater. 154, 123-127(1988).
- [2] P. Hofmann, "Current knowledge on core degradation phenomena, a review", J. Nucl. Mater. 270, 194-211(1988).
- [3] Y.-S. Youn, J.-G. Kim, S.D. Park, Y.-K. Ha, "Temperature-dependent variations of the interface between UO_2 and Zr", Bull. Korean Chem. Soc. 36, 2068-2072(2015).
- [4] T.K. Campbell, E.R. Gilbert, G.D. White, G.F. Piepel, B.J. Wrona, "Oxidation Behavior of Nonirradiated UO_2 ", Nucl. Technol. 85, 160-171(1989).
- [5] L.E. Thomas, R.E. Einziger, H.C. Buchanan, "Effect of fission products on air-oxidation of LWR spent fuel", J. Nucl. Mater. 201, 310-319(1993).
- [6] G.-S. You, K.-S. Kim, D.-K. Min, S.-G. Ro, "Oxidation kinetic changes of UO_2 by additive addition and irradiation", J. Nucl. Mater. 277, 325-332(2000).

The Influence of Neodymium Doping and Non-stoichiometry on the Structural and Electrochemical Properties of Uranium Dioxide

Seohyeon Park^{1),2)}, Jandee Kim¹⁾, Jeongmook Lee¹⁾, Jeong-mi Park^{1),2)}, Young-Sang Youn¹⁾,
Choong Kyun Rhee²⁾, and Sang Ho Lim^{1),3),*}

¹⁾ Korea Atomic Energy Research Institute, 111, Daedeok-daero 989beon-gil, Yuseong-gu,
Daejeon, Republic of Korea

²⁾ Chungnam National University, 99, Daehak-ro, Yuseong-gu, Daejeon, Republic of Korea

³⁾ University of Science and Technology, 217, Gajeong-ro, Yuseong-gu, Daejeon, Republic of Korea

*slim@kaeri.re.kr

1. Introduction

The deep geological disposal method has been internationally considered as final disposal of spent nuclear fuels (SNFs) [1]. However, this method has risks such as the exposure of SNFs to ground water due to container failure or unpredictable natural disasters. The geologic disposal condition could be significantly changed for long-term disposal period, hundreds of thousands of years and could affect the physical and chemical properties of SNFs. Thus, it is necessary to characterize SNFs under various conditions to evaluate the safety of disposal strategy.

SNFs include various fission products and have partially non-stoichiometry. Those are strongly related to the structure and reactivity of SNFs [2-4].

In this study, the influence of Nd doping and non-stoichiometry on the structural and electrochemical properties of UO_2 has been investigated to understand the behavior of SNFs in deep geologic repositories.

The pellets were sintered in a linear tube furnace with H_2 atmosphere at 1700°C for 18 h to form UO_{2-x} or $\text{U}_{1-y}\text{Nd}_y\text{O}_{2-x}$. And then sintered pellets were oxidized with CO/CO_2 mixed gas at 1500°C for 12 h to form UO_{2+x} or $\text{U}_{1-y}\text{Nd}_y\text{O}_{2+x}$. The surface morphologies of prepared pellets were observed by scanning electron microscopy (SEM). To obtain the lattice parameter of prepared pellets, X-ray diffraction (XRD) was conducted under Bruker AXS D8 Advance using $\text{Cu K}\alpha$ line source filtered with a Ni foil at room temperature. Raman spectroscopy was conducted with ANDOR Shamrock SR500i spectrometer with a wavelength of 632.8 nm from He-Ne laser. All electrodes were polished with 3000 grid sand paper and then the oxide layer on the surface was removed through a cleaning process at a potential of -1.5 V for 5 minutes prior to an electrochemical experiment. Electrochemical experiments were carried out with cyclic voltammetry (CHI-600D, USA) with 0.01 M carbonate ion in 0.1 M NaClO_4 aqueous solution.

2. Experimental

The UO_2 and/or Nd_2O_3 (weighed as 0, 2, 6, and 10mol% Nd) powders were mixed and pelletized.

3. Results

The grain structures of $\text{U}_{1-y}\text{Nd}_y\text{O}_{2\pm x}$ greatly vary depending on the Nd-doping level as shown in Fig 1.

In case of the hypo-stoichiometric $U_{1-y}Nd_yO_{2-x}$, the domain size sharply decreases as the Nd doping level increases. On the other hand, hyper-stoichiometric pellets produced through CO/CO₂ oxidation have larger domain sizes.

The lattice parameters of $U_{1-y}Nd_yO_{2-x}$ pellets linearly decreased with doping levels. However, the lattice parameters for $U_{1-y}Nd_yO_{2+x}$ pellets do not show a linear change but have much lower value than those of $U_{1-y}Nd_yO_{2-x}$ pellets.

Raman spectra of $U_{1-y}Nd_yO_{2-x}$ pellets have defect structures related to oxygen deficiency (500 to 650 cm⁻¹). As the Nd doping level increased, the defect structure grew. Raman spectra of $U_{1-y}Nd_yO_{2+x}$ also have similar features.

In the cyclic voltammetry (CV) analysis of the $U_{1-y}Nd_yO_{2\pm x}$ electrodes, the surface oxidation are observed at about -0.2 to 0.2 V in a 0.01 M carbonate ion in 0.1 M NaClO₄ electrolyte. The surface oxidation of the hypo-stoichiometry pellets is characterized by the increasing Nd doping level. The surface oxidation of the hyper-stoichiometry pellets decreased as Nd doping level decreased.

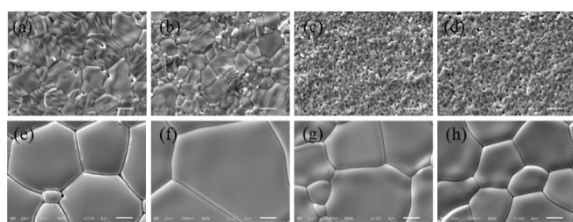


Fig. 1. SEM images for (a-d) $U_{1-y}Nd_yO_{2-x}$ surface (hypo-stoichiometric) and (e-h) $U_{1-y}Nd_yO_{2+x}$ (hyper-stoichiometric): (a, e) $y = 0$, (b, f) $y = 0.02$, (c, g) $y = 0.6$ and (d, h) $y = 0.10$.

4. Conclusions

The influence of Nd doping and non-stoichiometry on the physical and electrochemical properties of

UO₂ is investigated by SEM, XRD, Raman spectroscopy and electrochemical measurement. $U_{1-y}Nd_yO_{2-x}$ and $U_{1-y}Nd_yO_{2+x}$ have shown distinctive surface structure and electrochemical oxidation behaviors. Non-stoichiometry is more effective than Nd doping.

ACKNOWLEDGEMENT

This research was supported by the National Research Foundation of Korea (NRF) grant funded by the Korean government (MSIP) (No. 2017M2A8A5014754)

REFERENCES

- [1] P. Hofmann, C. Politis, "THE KINETICS OF THE URANIUM DIOXIDE-ZIRCALOY REACTIONS AT HIGH TEMPERATURES", J. Nucl. Mater. 87, 375-397(1979).
- [2] M. Miyake, M. Katsura, S. Yamanaka, "A STUDY OF THE REACTION BETWEEN UO₂ AND Zr", J. Nucl. Mater. 154, 123-127(1988).
- [3] H. KLEYKAMP, "The Chemical State of the Fission Products in Oxide Fuels", J. Nucl. Mater, 131, 221-246 (1985).
- [4] R.C. Ewing, "Long-term storage of spent nuclear fuel", Nat. Mater, 14, 252-257 (2015).

First-principles Computational Study on Nucleation and Growth Mechanisms of U on Mo(110) Surface Solvated in an Eutectic LiCl-KCl Molten Salt

Choah Kwon, Joonhee Kang, and Byungchan Han*

Yonsei University, 50, Yonsei-ro, Seodaemun-gu, Seoul, Republic of Korea

*kwonchoah@gmail.com

1. Introduction

In this paper, we extensively utilized first principles density functional theory (DFT) calculations and ab-initio molecular dynamic (AIMD) simulations to figure out underlying mechanisms of the initial stage of nucleation and growth behaviors of U on Mo(110) surface in a eutectic LiCl-KCl molten salt at $T = 773$ K. To rigorously investigate effect of the molten salt electrolyte we compared the results with those calculated under vacuum condition.

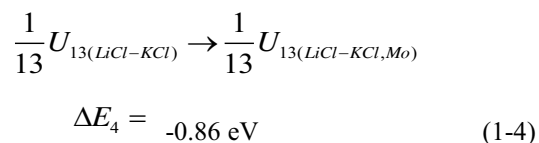
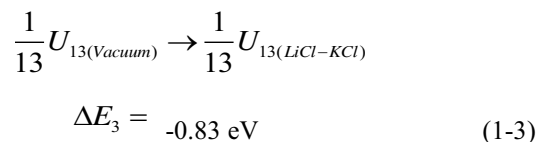
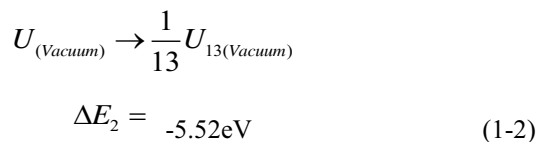
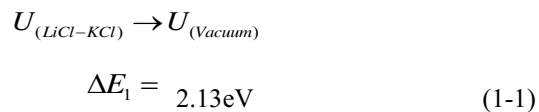
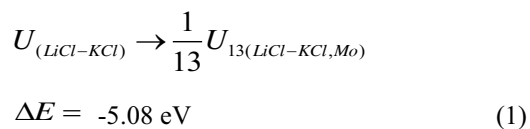
2. Model systems

Deposition of U on Mo occurs with bordering on three phases, which are LiCl-KCl molten salt, Mo(110) electrode and nucleus of U. LiCl-KCl molten salt were modeled based on density at 773 K based on experimental value. Mo electrode was constructed by stacking five layers of (110) plane. The last layers were fixed to simulate the bulk of Mo. Cuboctahedron shape of U nanocluster was assumed as nuclei of U while electrocrystalization occurs.

3. Results and Discussion

Thermoelectrochemical processes where U ions solvated in eutectic LiCl-KCl molten salt coalesce into a U nanocluster, followed by its adsorption on Mo(110) surface in LiCl-KCl eutectic molten salt.

Equation (1) describes the overall reaction for uranium atom to be adsorbed in form of U nanocluster in molten salt system, and the reaction can be separated into several steps, from equation (1-1) to equation (1-4).



U and U_{13} means an U atom and a U nanocluster, respectively. Round bracket means the state of U: $X_{(Vacuum)}$ means the X is in vacuum while $X_{(LiCl-KCl)}$ does the X is in eutectic LiCl-KCl molten salt, $X_{(LiCl-KCl, Mo)}$ indicate the X is adsorbed on Mo(110) surface in eutectic LiCl-KCl molten salt. ΔE is energy change of the reaction (1). ΔE_n is energy change for

the elementary reactions from (1-1) to (1-4). The equation (1-1) is the reversal reaction of a U solvation into eutectic LiCl-KCl molten salt from vacuum, and the energy change ΔE_1 equals to 2.13 eV implying the reaction is thermodynamically unfavorable. The second step, reaction (1-2) describes the formation of a U nanocluster from U gas in vacuum. It is exothermic reaction with -5.52 eV. Third reaction step of the equation (1-3) indicates that the solvation of U nanocluster from vacuum into the eutectic LiCl-KCl molten salt releases heat of -0.83 eV. The magnitude of ΔE_1 is bigger than $-\Delta E_3$. $-\Delta E_1$ represents the solvation energy of a U atom into eutectic LiCl-KCl molten salt while the ΔE_3 does for a U nanocluster. This makes sense since the chemical potential of U in the eutectic molten salt increases as U composition increases. Equation (1-4) represents adsorption of the U nanocluster on Mo(110) surface in the LiCl-KCl molten salt. It indicates that the U nanocluster is stable as much as -0.86 eV. Using these sequential steps the energy change (ΔE) for the reaction described at Equation (1) was calculated by summing ΔE_1 , ΔE_2 , ΔE_3 and ΔE_4 , which is equal to -5.08 eV. It means that the nucleation of U in LiCl-KCl molten salt favorably occurs and adsorption of U nanocluster on Mo(110) surface in eutectic LiCl-KCl molten salt is also a spontaneous reaction. These results support the instantaneous nucleation mechanism of U in eutectic LiCl-KCl molten salt.

4. Conclusion

Our results clearly unveiled surprisingly different mechanisms govern the nucleation and growth behaviors depending on the kinds of environmental conditions. Under vacuum U favored a uniform atomic layers electrodeposition on Mo(110) surface,

while strong chemical interaction between U nanocluster with Cl ions stabilized and tapered the U nanocluster into sharp tip like an atomic-scale dendrite. Our results fully based on ab-initio methods accurately captured the structural evolution as a function of time on atomic scale, which is invaluable for understanding fundamental principles on not only the electrorefining process for recycling spent nuclear fuels but also on other electrochemical reactions involving various electrolytes potentially leading to design of efficient electrochemical systems.

REFERENCES

- [1] Kwon, Choah, Joonhee Kang, and Byungchan Han. "First- principles based computational study on nucleation and growth mechanisms of U on Mo (110) surface solvated in an eutectic LiCl-KCl molten salt." *International Journal of Energy Research* 40.10 (2016): 1381-1388.

Determination of Sr and Zr Using Microextraction Chromatography

Jihye Kim*, Jong-yun Kim, and Taehong Park

Korea Atomic Energy Research Institute, 111, Daedeok-daero 989beon-gil, Yuseong-gu, Daejeon, Republic of Korea

*jihyekim21@kaeri.re.kr

1. Introduction

A microextraction chromatography system with a column containing Eichrom Sr Resin™ was used for separation of Sr and Zr. The mixture of Sr and Zr was injected into the column. Zirconium was passed through the column using 3 M HNO₃, otherwise, strontium was retained on the column with the same matrix. Then the strontium was eluted with 1% acetic acid with 270 microliters of the elution volume. Total flow rate was about 100 µL/min. The recoveries were 91.0% ± 0.7% and 96.1% ± 0.9% for Sr and Zr, respectively.

2. Materials and methods

2.1 Instrument

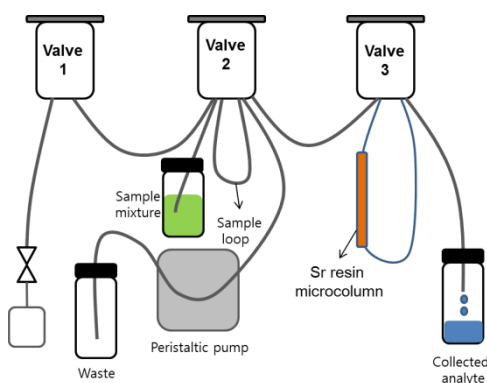


Fig. 1. Setup of microextraction chromatography.

2.2 Analytical procedure

2.2.1 Conditioning of Sr-resin.

- 1 cycle (1 cycle: 270 µL) of deionized water into the injection valve
- 1 cycle of 3 M HNO₃ into the injection valve
- 2 cycles of deionized water into the injection valve

2.2.2 Sample loading (Sr and Zr mixture in 3 M HNO₃).

- 1 cycle of sample is injected into the sample loop at a flow rate of 100 µL/min.

2.2.3 Collection of Zr. Zirconium from sample matrix (3M HNO₃) was passed through the column and collected at the collection vial.

2.2.4 Elution of Sr. The Sr was retained on the column from sample matrix (3M HNO₃). 270 µL of 1% acetic acid was into the sample loop and passed through the column at a flow rate of 100 µL/min.

3. Results and discussion

3.1 Effect of successive elution

The efficiency of successive elution on column from sample matrix was demonstrated the recovery (%) versus the number *n* of successive elution in Figure 2. The measured recovery in the residual Sr on the column decreased significantly during the first elution, clearly showing that the Sr was efficiently removed with 1% acetic acid.

3.2 Recovery

The calculated recoveries of MEC were $91.0\% \pm 0.7\%$ and $96.1\% \pm 0.9\%$ for Sr and Zr, respectively.

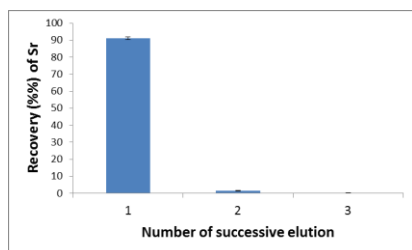


Fig. 2A. Effect of successive elution of Sr,

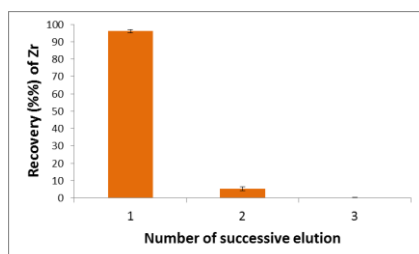


Fig. 2B. Effect of successive elution of Zr.

4. Conclusions

The microextraction chromatography was applied to separate the Sr and Zr mixture using Sr resin. The recoveries of sample were obtained 91% and 96% for Sr and Zr, respectively. Our method used the hundred microliter scaled sample volume, washing and elution solvent volume resulted in reducing the radionuclide waste significantly compared to traditional extraction chromatography.

REFERENCES

- [1] J. L. Steeb, et. al. "Application of mass spectrometric isotope dilution methodology for ^{90}Sr age-dating with measurements by thermal-ionization and inductively coupled-plasma mass spectrometry" J. Anal. At. Spectrom. 28, 1493-

1507 (2013).

- [2] J. L. Steeb et. al., "Microseparations of cesium and barium in glass" J. Radioanal. Nucl. Chem. 292, 757-762 (2012).

Direct Formation of Lanthanide Trichloride From Lanthanide Oxide

Sang-Eun Bae^{1),2),*}, Dong-Chul Choi¹⁾, and Tae-Hong Park^{1),2)}

¹⁾Korea Atomic Energy Research Institute, 111, Daedeok-daero 989beon-gil, Yuseong-gu, Daejeon, Republic of Korea

²⁾University of Science and Technology, 217, Gajeong-ro, Yuseong-gu, Daejeon, Republic of Korea

*sebae@kaeri.re.kr

1. Introduction

In a pyrochemical process, uranium dioxide, actinide dioxide, and lanthanide oxide have been converted to their trichloride forms for their dissolutions and electrodepositions. However, we reported that the lanthanide oxides such as Nd_2O_3 , Gd_2O_3 , etc. are not fully reduced to their metallic form during an electro-reduction process so that the lanthanide elements may not be dissolved during an electro-refining process. In this work, in order to fully dissolve the lanthanide oxide into molten salt, we studied its direct dissolving method as the form of the lanthanide trichloride and report the results in the conference.

2. Experimental

All the experiments were carried out in a glove box under Ar where O_2 and H_2O level were maintained to be less than 1 ppm. Lithium chloride (LiCl)/potassium chloride (KCl) eutectic salts (anhydrous beads), and silver chloride (AgCl) were obtained from Sigma Aldrich. Neodymium oxide (Nd_2O_3) and gadolinium oxide (Gd_2O_3) were purchased from Alfa Aesar (purity $\geq 99.99\%$).

Electrochemical measurements were performed in a quartz tube (20 mm in outer diameter and 2 mm in wall thickness). W wire (Alfa Aesar, dia. 0.2 mm) and glassy carbon (Alfa Aesar, dia. 2 mm) electrodes were used as the working and counter electrodes,

respectively. The W wire electrode was mechanically polished with sand paper prior to use. The reference electrode was Ag wire immersed in 1 mol% AgCl-LiCl-KCl melt. The Electrochemical measurements were performed using a Gamry Reference 3000.

3. Results and Discussion

In order to test the conversion of the lanthanide oxide to the lanthanide trichloride in LiCl-KCl melt, we chose Nd_2O_3 and Gd_2O_3 as the representatives of lanthanide oxides. Fig. 1 shows a picture of Nd_2O_3 dissolved LiCl-KCl melt. We added Nd_2O_3 powder in transparent LiCl-KCl melt and shook the cell. The Nd_2O_3 were not dissolved and existed as a form of colloids. The white blue of the picture is typical color of the Nd_2O_3 colloids. In order to dissolve Nd_2O_3 and get rid of the oxygen from the oxide, here we introduced ammonium chloride (NH_4Cl) in the melt. We expected that NH_4Cl may supply HCl in the melt. The HCl is very acidic molecule so that it can absorb the oxygen anion of the lanthanide oxides. Because the NH_4Cl is very volatile, we also expected that residuals of NH_4Cl after the reactions can be easily removed as a gas. The mechanism of the reaction can be described as shown below.



The products of the reaction are all gas phases except for the NdCl_3 , which means that the by-

product of the reaction can be easily evaporated from the melt.

Fig. 1b and 1c show the pictures of LiCl-KCl melt containing Nd_2O_3 after NH_4Cl was added into the LiCl-KCl melt. As soon as the addition of the NH_4Cl , there was a vigorous formation of gas bubbles and then the bubbles gradually disappeared in 5 minutes. After the reaction was completed, the melt turned into transparent and clean sky blue color (Fig.1c).

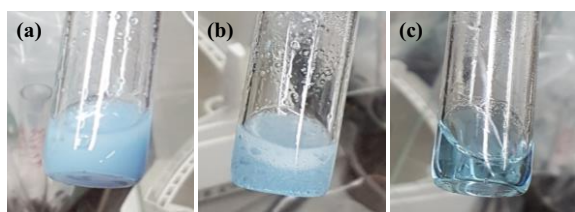


Fig. 1. Pictures of Nd_2O_3 dissolved LiCl-KCl melt at 450°C . (a) Before and (b, c) after the addition of NH_4Cl .

Fig. 2 shows a cyclic voltammogram obtained from a W wire immersed in LiCl-KCl melt containing Nd_2O_3 after addition of NH_4Cl . It is obvious that cathodic and anodic currents around -2.0 V occurred. The current can be attributed to the electrodeposition and dissolution of Nd in LiCl-KCl melt. This result indicates that the NdCl_3 were directly formed from Nd_2O_3 with addition of NH_4Cl in the LiCl-KCl melt.

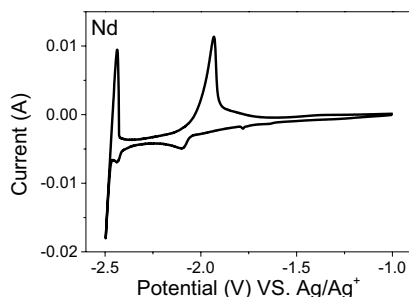


Fig. 2. A cyclic voltammogram obtained from a W wire immersed in LiCl-KCl melt containing Nd_2O_3 after addition of NH_4Cl .

4. Conclusion

In this work, we reported that lanthanide trichlorides can be directly formed from lanthanide oxide by the addition of NH_4Cl . The color of the transparent sky blue of the melt and CV results indicated that the NdCl_3 was successfully formed in the LiCl-KCl. In the conference, we report the results that are concerning the other lanthanide elements as well.

ACKNOWLEDGEMENT

This work was supported under the mid- and long-term nuclear research and development program through the National Research Foundation of Korea (NRF-2017M2A8A5014710) funded by the Korean Ministry of Science and ICT.

REFERENCES

- [1] T. Park, Y. Cho, B. Kang, J. Kim, K. Suh, J. Kim, S. Bae, J. Kim, J. J. Giglio, and M. M. Jones, "Constituent analysis of metal and metal oxide in reduced SIMFuel using bromine-ethyl acetate", *Journal of Radioanalytical and Nuclear Chemistry*, 316, 1253-1259 (2018).

Microfluidic Fabrication of Macroporous Polymer Particles for the Separation of Uranium in Aqueous Solution

Jai Il Park*, Kwang-eun Lee, Sang Ho Lim, and Jong Yun Kim

Korea Atomic Energy Research Institute, 111, Daedeok-daero 989beon-gil, Yuseong-gu, Daejeon, Republic of Korea

*jaipark@kaeri.re.kr

1. Introduction

Uranium is an important element for the production of nuclear energy. However, it also possesses high chemical and biological toxicity. Various nuclear-related activities have released excess amounts of uranium into environment. In this regard, the removal/separation of uranium is highly required. So far, many methods such as ion-exchange, solvent extraction and filtration and reverse osmosis have been developed to remove uranium from aqueous waste streams generated from nuclear activities. Among such methods, sorption has drawn much attention, thus has been extensively investigated due to its low cost, high sorption selectivity, capacity, and various choices for source materials. In particular, polymer-based porous adsorbents are advantageous due to their high surface area and highly interconnected macroporous structures that enable high transport rates [1]. Suspension, precipitation, dispersion and seeded emulsion polymerization, membrane emulsification and microfluidics (MFs) are the main techniques for the fabrication of such porous materials. Among those, MF approach makes it possible to precisely control particle sizes and morphologies.

In this study we present the MF preparation of poly (glycidylmethacrylate-co-ethyleneglycoldimethacrylate), P(GMA-co-EGDMA), polymer particle. Since 1980s, GMA and EGDMA have been widely used as monomers leading to macroporous beads with controlled porosity upon polymerization in the presence of inert diluents [2]. We further investigate the potential

utilization of such particle for the removal of uranium from aqueous solution by copolymerizing the monomers with phosphate-containing monomers.

2. Experimental

2.1 Reagents

Poly(vinyl alcohol) (PVA, Mw 31 000–50 000 g/mol), GMA, EGDMA, vinylphosphonic acid (VP), bis(2-(methacryloyloxy)ethyl)phosphate (BMEP) 1-undecanol, and 2-hydroxy-2-methylpropiophenone (HMPP) were purchased from Sigma-Aldrich, Korea, and used as received.

2.2 Methods

A simple MF co-flow device was fabricated using common laboratory tubing, glass capillary and needles. Two immiscible liquids were introduced into the device by two separate syringe pumps allowing independent control of flow rates. The organic contained a mixture of GMA, EGDMA, and VP (or BMEP) in different proportions with 4.5wt.% of HMPP as a photo-initiator. The aqueous continuous phase was made of 2wt.% PVA. To obtain polymer particles, monomer droplets generated from the MF device were exposed to UV light (Innocure 2000, UV output: 3 W/cm², 250–450 nm) for 5 min.

3. Results

Droplets with well-defined monodisperse

morphology are produced in the MF co-flow device. The resulting droplets are converted into micron-sized beads with macroporous surface morphologies upon UV polymerization (Figure 1a, b). Using a mixture of acrylate monomers with an inert diluent as a dispersed phase, the porosity of the particle surface is generated through phase separation between the growing polymer chains and inert diluent (Figure 1c). Both surface and inside of the bead consist of a network of interconnected polymer particles (Figure 1d). The co-polymerization of the functional polymers with a mixture of GMA-EGDMA was indirectly monitored by an energy-dispersive X-ray spectrometer (Figure 1d, inset).

The removal of uranium from aqueous solution was evaluated by adding 0.01 g of the synthesized beads into 10 $\mu\text{g/mL}$ of uranium with different molarity of nitric acid. The efficiency increases as the acidity of the solution decreases (Figure 2) possibly due to the competition of H^+ ion and uranyl ion towards the functional group of the bead. We determined the maximum capacity of the beads reached 32.4 mg-U/g.

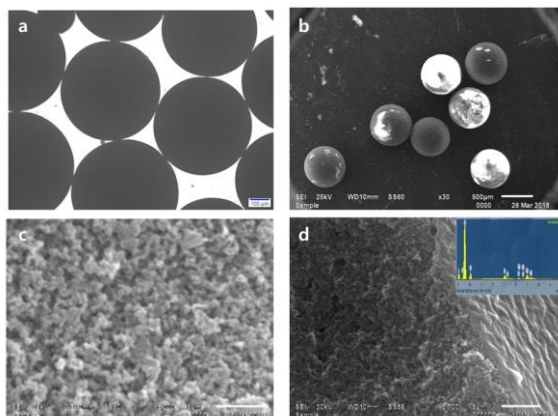


Fig. 1. MF preparation of phosphate-bearing P(GMA-EGDMA) macroporous particles. a) optical microscope image, b-d) SEM images of the P(GMA-EGDMA-BMEP) particles, particle surface, and internal morphology, respectively.

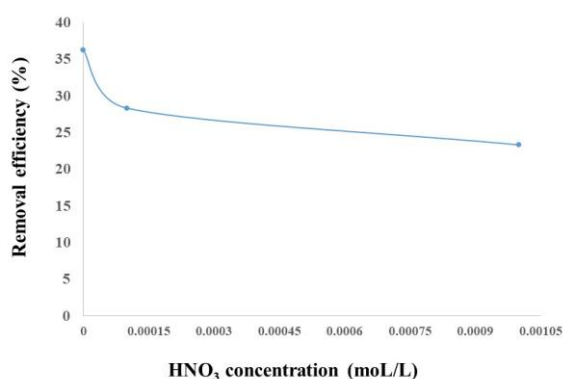


Fig. 2. Uranium removal efficient as a function of HNO_3 concentration.

4. Conclusion

We synthesized phosphate-bearing macroporous polymer particles using a MF method. We characterized the beads using different techniques and showed the beads possessed uranium sorption capacity to some extents. Current research is only preliminary, thus further studies will be carried out in near future.

ACKNOWLEDGEMENT

This work was supported by the Ministry of Science and ICT of South Korea.

REFERENCES

- [1] G. Bayramoglu, M. Y. Arica, "Polyethylenimine and Tris(2-aminoethyl)amine modified P(GA-EGMA) Microbeads for Sorption of Uranium Ions: equilibrium, kinetic and thermodynamic studies", J Radioanal Nucl Chem, 312, 293-303 (2017).
- [2] J. I. Park, A. Saffari, S. Kumar, A. Gunther, and E. Kumacheva, "Microfluidic Synthesis of Polymer and Inorganic Particulate Materials", 40, 415-443(2010).

Determination of Uranium, Molybdenum and Aluminum of U-Mo Alloy by Isotope Dilution Mass Spectrometry and Inductively Coupled Plasma Atomic Emission Spectrometry

Jung Suk Kim*, Byungman Kang, Yang-Soon Park, Kyungwon Suh, and Yeong Keong Ha
Korea Atomic Energy Research Institute, 111, Daedeok-daero 989beon-gil, Yuseong-gu, Daejeon, Republic of Korea
*njskim1@kaeri.re.kr

1. Introduction

The quality assurance of the uranium compound in nuclear industry is very important because that is useful for a reactor work as well as for the effective utilization of a nuclear fuel. Several analytical approaches have been applied to the determination of component elements of uranium compound. Thermal ionization mass spectrometry (TIMS) is quite useful for analyzing very small amounts of uranium compound, due to its high accuracy and precision for isotopic measurement. Uranium and molybdenum in uranium alloy can be measured using isotope dilution mass spectrometric techniques (IDMS), and can be also determined with a detection limit of 0.1-0.2 $\mu\text{g/mL}$ by inductively coupled plasma atomic emission spectrometry (ICP-AES) [1,2].

The aim of the present work is to determine simultaneously the contents of U, Mo and Al, and the their isotopic compositions for U and Mo in a U-Mo alloy sample manufactured at KAERI using the TI-IDMS and ICP-AES techniques, to determine the respective validity of the methods

2. Experiments

2.1 Chemicals

The Certified ^{233}U (99.470atom%) and ^{96}Mo (95.78atom%) spikes were obtained from Oak Ridge National Laboratory (ORNL). These spike solutions were prepared by dissolving their oxides in 8 M HNO_3 -0.01 M HF. The concentrations of the spike solutions were prepared by calibrating them with a standard solution. Uranium, molybdenum, aluminum and silicon standard solutions were obtained from AccuTrace and Spex Industries Inc.

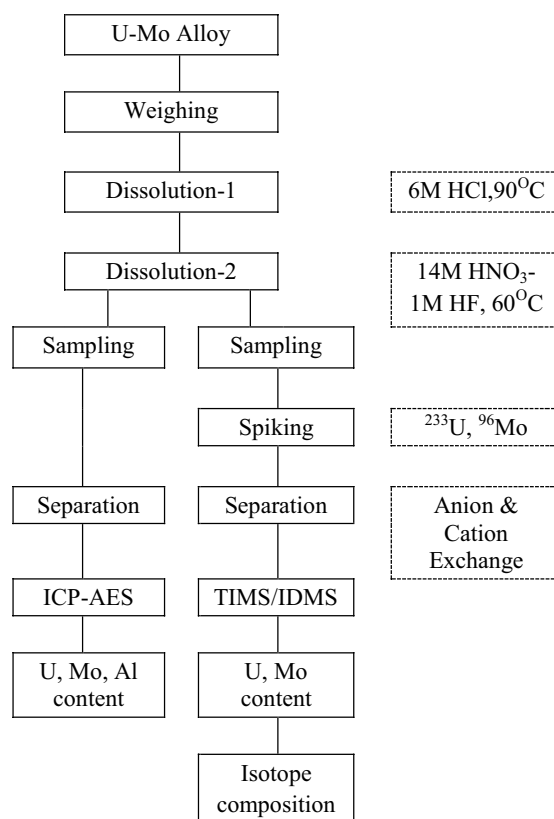


Fig. 1. Analytical processes for the determination of U, Mo and Al in the U-Mo alloy sample.

2.2 Sample preparation, separation and isotopic measurement

The U-Mo alloy consists of an aluminum matrix dispersion of uranium 7wt.% molybdenum (U-7Mo) metallic alloy. The matrix contains a little of silicon and the cladding material of the U-Mo alloy consists of aluminum alloy. The dissolution procedure of the U-Mo alloy sample was composed of two-steps for sequential dissolution of the cladding material and the alloy with 6 M HCl and 14 M HNO_3 -1M HF mixture [2]. Chemical separations for IDMS and ICP-AES were carried out by the separation procedures using two sequential anion and cation exchange resins. The basic processes in the analytical laboratory for the

determination of U, Mo and Al are shown in Figure 1. Chemical separation for IDMS was carried out for both the unspiked and the spiked sample solutions in the same experimental conditions. The isotopic compositions of U and Mo in the unspiked and spiked samples were determined using a thermal ionization mass spectrometer (Finnigan TRITON).

2.3 Determination of U and Mo by IDMS

The concentrations of U and Mo in the sample solution were determined by the IDMS according to Eq. (1):

$$C_n = C_a \cdot G_a / G_n \cdot M_n / M_a \cdot (R_a - R_m) / (R_m - R_n) \cdot \frac{(\sum nR_i)}{(\sum aR_i)} \quad (1)$$

Where,

C_n : concentration of Mo in sample soln. ($\mu\text{g-Mo/mL}$)

C_a : concentration of Mo in spike soln. ($\mu\text{g-Mo/mL}$)

G_n : volume of sample soln. taken (mL)

G_a : volume of spike soln. taken (mL)

M_n : mean atomic weight of Mo in sample

M_a : mean atomic weight of Mo in spike

R_a : ratio of two basic isotopes in spike ($^{96}\text{Mo}/^{98}\text{Mo}$)

R_m : ratio of two basic isotopes in mixture ($^{96}\text{Mo}/^{98}\text{Mo}$)

R_n : ratio of two basic isotopes in sample ($^{96}\text{Mo}/^{98}\text{Mo}$)

$\sum nR_i$: sum of ratios of total isotopes for basis isotope in sample

$\sum aR_i$: sum of ratios of total isotopes for basis isotope in spike

3. Results & Discussion

3.1 Isotopic compositions of U and Mo

Table 1 shows the isotopic compositions of U and Mo in the U-Mo alloy sample measured by the TIMS.

Table 1. Isotopic compositions of U and Mo separated from the U-Mo alloy

Element	Isotope	Atom%
U	U-234	0.0010±0.0002
	U-235	0.223±0.002
	U-238	99.78±0.04
	Mo-92	14.67±0.22

Mo	Mo-94	9.22±0.01
	Mo-95	15.95±0.02
	Mo-96	16.82±0.03
	Mo-97	9.56±0.02
	Mo-98	24.16±0.04
	Mo-100	9.62±0.02

3.2 Total quantities of U and Mo by IDMS

Table 2 shows the contents of U and Mo in a U-Mo alloy sample determined by the IDMS.

Table 2. Determination of U and Mo in the U-Mo alloy by IDMS

Element	g /g-sample
U	0.529±0.011
Mo	0.0406±0.0008

3.3 Determination of U, Mo and Al by ICP-AES

The analytical results of U and Mo in the U-Mo alloy sample determined by the ICP-AES compared with those by the IDMS, and those estimated from the manufacturing history.

4. Conclusion

The contents of U, Mo and their isotopes in the U-Mo alloy can be determined simultaneously by the isotope dilution mass spectrometric method using ^{233}U and ^{96}Mo as spikes. The contents of U, Mo and Al in the U-Mo alloy can be determined simultaneously by the inductively coupled plasma atomic emission spectrometry. A comparison between independently determined values provides a check on the validity of the results

REFERENCES

- [1] P. W. J. M. Boumans, "Inductively Coupled Plasma Emission Spectroscopy", Chemical Analysis: Volume 90, John Wiley & Sons, Inc. (1987).
- [2] J. S. Kim et al., "Dissolution and Simultaneous Determination of U, Mo and their Isotopes of U-Mo Alloy Nuclear Fuel", Korean Radioactive Waste Society AUTUMN 2014, 155-156 (2014).

Characterization of Neutron Irradiated Materials Using ESR Spectroscopic Method

Young Hwan Cho*

Korea Atomic Energy Research Institute, 111, Daedeok-daero 989beon-gil, Yuseong-gu, Daejeon, Republic of Korea

*yhcho@kaeri.re.kr

1. Introduction

Neutron irradiation produces a stable defect center to a lattice of various solid materials [1]. Electron Spin Resonance (ESR) spectroscopy is a convenient and powerful tool for quantifying this defect center rapidly and nondestructively. Silicon carbide, SiC, is a candidate semiconductor material to be used under intense irradiation environment such as nuclear reactor and space. Alanine is also a candidate radiation dosimeter material useful for multi-purpose dosimetry. Several metal oxide single crystals host defect centers by irradiation applicable for new optoelectronic materials development. Here, for these materials, the post neutron irradiation properties are studied using ESR spectroscopy

2. Experimental

2.1 Materials

Silicon carbide, SiC, alanine, and metal oxide materials are purchased having high purity, 99.99%. Neutron irradiation experiments are carried out at HANARO Research Reactor.

2.2 ESR Measurements

The ESR spectroscopy was used to measure the concentration of defect center of the neutron irradiated samples. All ESR measurements were

made at X-band (9.6 GHz) and room temperature on a Bruker EMX spectrometer.

3. Results

Figure 1 shows the esr spectra of neutron irradiated SiC with varying neutron fluence. It shows the relative paramagnetic defect center concentration dependent on neutron irradiation.

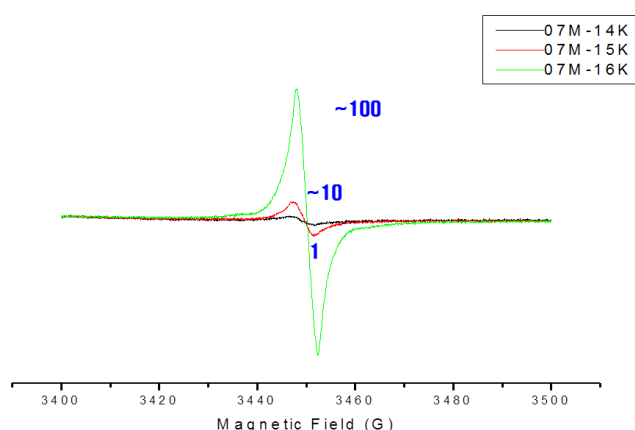
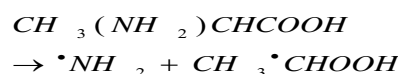


Fig. 1. ESR spectra of neutron irradiated SiC with varying neutron fluence 1:10:100 ratio.

Figure 2 shows the ESR spectra of neutron irradiated alanine. The concentration of the paramagnetic defect is also proportional to the neutron fluence. The irradiation effect on alanine molecules can be explained by following reaction.



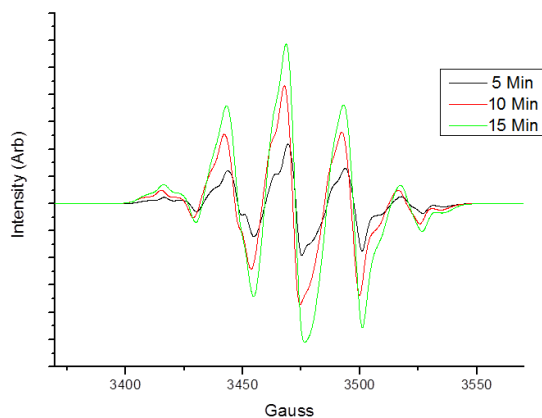


Fig. 2. ESR spectra of neutron irradiated alanine with varying neutron fluence.

4. Discussions

Neutron irradiation produces various types of stable defect center within solid lattice of a material of interest for nuclear applications. Electron Spin Resonance (ESR) spectroscopy is a convenient tool for quantifying this defect center rapidly and nondestructively. Alanine can be used for neutron dosimeter material that can be used for retrospective, emergency dosimeter method. Neutron irradiation can produce useful paramagnetic defect center that can alter the opto-electromagnetic properties of metal oxide materials. For this purpose, ESR can be used to quantify the concentration as well as investigating the structure of the defect center.

5. Conclusion

Neutron irradiation produces a stable defect center to certain materials useful for nuclear applications. Electron Spin Resonance (ESR) spectroscopy is a convenient tool for quantifying this defect center rapidly and nondestructively.

REFERENCES

- [1] V. Bratus, et al. Semiconductor Physics, Quantum Electronics & Optoelectronics, 2015. V. 18, N 4.P. 403-409 (2015).

Preliminary Calculation of CRUD Source-term With Modified Corrosion Product Transport Model for PWR Primary Circuit

Hwa Jeong Han, Beom Kyu Kim, and Byung Gi Park*

Soonchunhyang University, 22, Soonchunhyang-ro, Sinchang-myeon, Asan-si, Chungcheongnam-do, Republic of Korea

*byunggi@sch.ac.kr

1. Introduction

Corrosion products are released from the surface of materials of the primary coolant circuit, which contacts with the coolant. These corrosion products become mixed with primary coolant due to a continuous interaction of turbulent flow with the corroded surfaces of primary coolant circuits. Corrosion products deposited on the out-of-core surface in PWR primary coolant systems, is a major source of CIPS (Crud Induced Power Shift) or CILC (Crud Induced Localized Corrosion) [1,2]. Modelling and numerical estimation of crud and corrosion product can be used to estimate the mechanism of the boron hideout during plant operation.

2. Methodology

2.1 CRUD source-term calculation

In this study, the governing equation of the reference study [3] was used for the calculation of CRUD source-term. The governing equation was calculated the molar conservation of either iron(Fe) or nickel(Ni) in coolant around the primary circuit.

$$\frac{dx_i}{dt} = \frac{\dot{m}}{\rho_{f,i} V_i} (x_{i-1} - x_i) - \frac{A_i J_i}{V_i C_i} \quad (1)$$

In order to conduct the calculation of CRUD source-term, the variables contributing to CRUD source-term clarified. The molar flux, J_i is the molar flux of iron or nickel from the bulk coolant to the

surface of the section.

$$J_i = C_{bulk} [x_{bulk} u + k_m (x_{bulk} - x_{surf})] \quad (2)$$

This equation is obtained by summing the flux equations for the component metal ions in solution. The total molar concentration in the bulk and the mole fractions of iron or nickel in the bulk and at the surface are used to calculate the molar flux.

2.2 PWR primary circuit thermodynamics

One of the important parameters contributing to CRUD source-term is the thermodynamic problem for solution species and solid phase iron and nickel compounds in the primary circuit of a PWR. In this study, we used the method of decoupling the Fe, Ni problem and the Li-B-H₂ problem. First, solve for the Li-B-H₂ mole fractions in the bulk coolant and secondly, determine the Fe and Ni mole fractions for the precipitation of solids at the surface. A numerical method which like the quasi-newton method is used to obtain mole fractions. These processes are applied to each section of the primary coolant circuit.

2.3 Corrosion release and deposition

The release of iron or nickel due to corrosion at the surface is described by the release flux [3]. The release flux is expressed by the following equation,

$$J_{release} = \frac{am_{corroded}}{At_{corroded}} \quad (3)$$

Therefore, the unit mass of metal corroded, the molecular weight and the weight fraction of atom in the alloy are required to calculate the variables on the release flux.

Precipitation of iron or nickel compounds at the surface of a section is described by the precipitation flux [3]. The precipitation flux is expressed by the following equation,

$$\frac{dM_{precipitation}}{dt} = J_{precipitation} \quad (4)$$

Which if any of the solid phase compounds are precipitated is determined by a logical sequence of test using appropriate values for the surface mole fractions of iron and nickel. The surface mole fractions of iron and nickel, the precipitation of solid phase species are required to calculate the variables on the precipitation flux. A numerical method which like the van Wijngaarden-Dekker-Brent method is used to obtain the surface mole fractions.

3. Results and Conclusion

The model was run for a complete PWR cycle in the absence of boiling on the core section. Table 1 lists the iron and nickel mass balance during the cycle. The distribution of corrosion products around the primary coolant circuit is shown in Figure 1. This shows almost all the Ni are deposited in the Steam generator, on the other hand, the Fe has mainly deposited in the core.

The result obtained with the model was the prediction of soluble iron concentrations in the coolant of a PWR in good agreement with the reference study. However, predicted nickel concentrations appeared to be low as like a consequence of reference study. This result is thought to be the inclusion of particulate in the measured value for nickel, therefore, this model will need to contain an analysis model of particulate deposition.

Table 1. Iron and nickel mass balance(without boiling)

	Metal (g)	Metal (mol)
Steel corroded	10000	179.1
Inconel corroded	20000	340.8
Fe released	3630	65.0
Ni released	12739	217.0

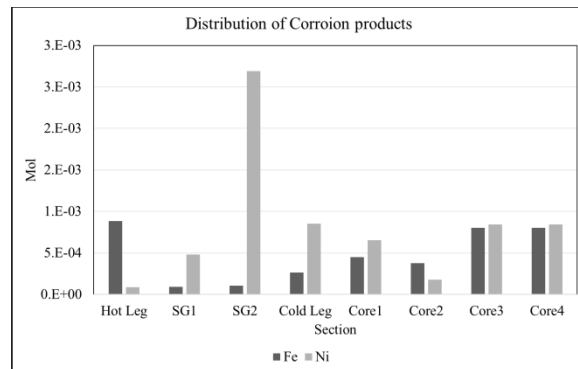


Fig. 1. Distribution of Corrosion products (without boiling).

ACKNOWLEDGEMENT

This work was financially supported by Korea Hydro & Nuclear Power Co. Ltd. (Project No. L17S019000).

REFERENCES

- [1] Lee CB, "Modeling of corrosion product transport in PWR primary coolant.", PhD Thesis, Nuclear Engineering Department, MIT, Massachusetts (1990).
- [2] Frattini, P. L., et al. "Axial offset anomaly: coupling PWR primary chemistry with core design." *Nuclear Energy* 40.2: 123-35 (2001).
- [3] EPRI, "Corrosion Product Transport Model for PWR Primary Circuit Applications.", EPRI, Palo Alto, 1015023 (2007).

Improved Analytic Crackling Core Model for the Description of UO₂ Sphere and Pellet Oxidation

Ju-Ho Lee*, Jae-Won Lee, and Yung-Zun Cho

Korea Atomic Energy Research Institute, 111, Daedeok-daero 989beon-gil, Yuseong-gu, Daejeon, Republic of Korea

*jhlee835@kaeri.re.kr

1. Introduction

The oxidation behavior of UO₂ to U₃O₈ is especially characterized by sigmoid behavior and mainly modeled by nuclear-growth model. Crackling core Model(CCM) proposed by Park and Levenspiel was found to exhibit sigmoid behavior [1] and applied to the modeling of UO₂ oxidation [2]. However, the close description of the experimental data was not achieved. In this study, for the improved description of UO₂ oxidation, we propose an analytic CCM accounting for area expansion effect and evaluate the applicability of the model toward the description of UO₂ sphere and pellet oxidation.

2. Model development

In CCM, the overall conversion is obtained from individual grain conversion by integration

$$1 - X(t) = \frac{\int_0^R [1 - X_g(r, t)] r^2 dr}{\int_0^R r^2 dr} = \frac{3}{R^3} \int_0^R [1 - X_g(r, t)] r^2 dr \quad (1)$$

where $X(t)$ is overall conversion at give t time and R denotes the initial radius of UO₂ sphere or pellet. $X_g(r, t)$ refers to the conversion of grain at position r . In this study, UO₂ particle and grain are assumed to follow Shrinking Core Model(SCM) considering reaction rate as rate limiting step. Then the radius of UO₂ particle is related to the following equation

$$-\frac{d}{dt} \left(\frac{4}{3} \pi r^3 \rho_B \right) = 4 \pi r^2 k_c C_A \quad (2)$$

where ρ_B refers to the density of solid and k_c to reaction constant. C_A indicates the concentration of gaseous species A in bulk phase. The time required for complete reduction of r to zero, τ_c , is defined by

$$\tau_c = \frac{\rho_B R}{k_c C_A} \quad (3)$$

Then the radius r is related to time by

$$\frac{r}{R} = Y = 1 - \frac{t_c}{\tau_c} \quad (4)$$

where t_c denotes the age of solid particle .

In original CCM, the non-porous surface of solid particle is considered to be transformed into porous surface through crackling of surface. This assumption implies that the reactive surface area becomes increased due to the newly formed porosity. In this study, the area expansion effect is included in eq (2) as follows

$$-\frac{d}{dt} \left(\frac{4}{3} \pi r^3 \rho_B \right) = \frac{4 \pi r^2 k_c C_A}{\left(1 - \beta \frac{t}{\tau_c^*} \right)^2} \quad (5)$$

where β is area expansion coefficient and τ_c^* is related to $\tau_c(1-\beta)$. Then the radius r is newly obtained.

$$Y = \frac{1 - \frac{t_c}{\tau_c^*}}{1 - \beta \frac{t_c}{\tau_c^*}} \quad (6)$$

As grain reaction follows SCM, the conversion of grain is related to t_g , grain age, and τ_g , the conversion time of grain

$$\frac{t_g(r)}{\tau_g} = 1 - \left[\frac{1 - X_g(r, t)}{1 - X_i} \right]^{1/3} \quad (7)$$

where X_i refers to the conversion of intermediate. If w is defined by $\tau_c/\tau = \tau_c/(\tau_c + \tau_g)$ and $t_g = t - t_c$, the overall conversion in three steps is determined.

Initiation step : $t/\tau_c^* < 1-w$

$$1 - X(t) = Y_c^3 + 3 \int_{Y_c}^1 [1 - X_g(Y, t)] Y^2 dY \quad (8)$$

Propagation step : $1-w < t/\tau_c^* < w$

$$1 - X(t) = Y_c^3 + 3 \int_{Y_c}^{Y_a} [1 - X_g(Y, t)] Y^2 dY \quad (9)$$

Termination step : $w < t/\tau_c^* < 1$

$$1 - X(t) = 3 \int_0^{Y_a} [1 - X_g(Y, t)] Y^2 dY \quad (10)$$

where Y_a and Y_c is defined by

$$Y_c = \frac{1 - \frac{t_c}{w\tau_c^*}}{1 - \beta \frac{t_c}{w\tau_c^*}} \quad Y_a = \frac{\frac{1}{w} \left(1 - \frac{t_c}{\tau_c^*} \right)}{1 - \beta - \frac{\beta}{w} \left(\frac{t_c}{\tau_c^*} - 1 \right)} \quad (11)$$

The unreacted conversion in eq (8)-(10) is formulated as follows-

$$1 - X_g(Y, t) = (1 - X_i) \left(1 - \frac{1}{1-w} \left(\frac{t}{\tau} - \left(\frac{1-Y}{1-\beta Y} \right) w \right) \right)^3 \quad (12)$$

X_i is assumed to 0.375 implying that UO_2 is oxidized to U_3O_8 through the conversion to intermediate U_4O_9 . As demonstrated in Fig. 1 and 2, the proposed model showed a good agreement with experimental conversion data of UO_2 sphere and pellet. The optimized parameters were $\tau_c^* = 683$, $w = 0.5$ and $\beta = 0.92$ for UO_2 sphere and $\tau_c^* = 383$, $w = 0.8$ and $\beta = 0.94$ for UO_2 pellet. The high value of β indicates that area expansion was significantly proceeded in the oxidation of both sphere and pellet.

3. Conclusions

In spite of its simplicity formulation, the improved CCM accounting for area expansion effect was found to closely describe the experimental behavior of UO_2 oxidation behavior. The overall performance of the model will be evaluated by correlating more experimental data.

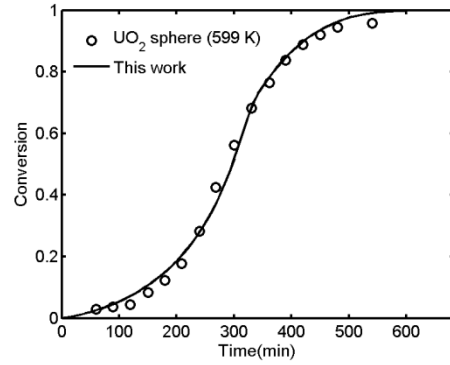


Fig. 1. Optimized conversion curves of UO_2 sphere in air atmosphere at 599 K.

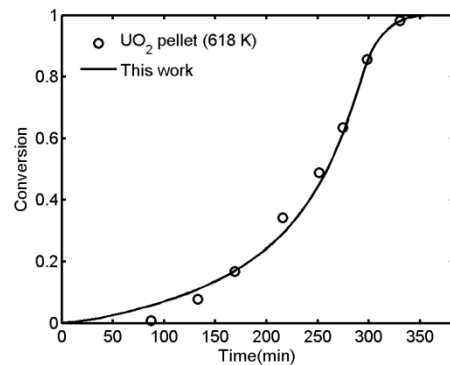


Fig. 2. Optimized conversion curves of UO_2 pellet in air atmosphere at 618 K.

ACKNOWLEDGEMENT

This work was supported by a grant (NRF-2017M2A8A5015075) from the Nuclear Research & Development Program of National Research Foundation (NRF) funded by the Ministry of Science ICT & Future Planning (MSIP), Republic of Korea.

REFERENCES

- [1] J.Y. Park and O. Levenspiel, "The Crackling Core Model for the reaction of solid particles", Chem. Eng. Sci., 30, 1207-1214 (1975).
- [2] J.H.Lee, S.C.Jeon, Y.H.Kim, S.J.Kang, K.Y.Lee, and G.I.Park "Modeling of Low-Temperature Voloxidation Processes based on Modified Shrinking Cylinder Model", Proc. of the KRS 2014 Spring Conference, 12(1), May 7-9, 2014, PyeongChang.

Measurement of Dew Point Temperature of Pyroprocess Automation Mock-up for Basic Design of Emergency Gas Supply System

Jonghui Han*, Byungsuk Park, and Seungnam Yu

Korea Atomic Energy Research Institute, 111, Daedeok-daero 989beon-gil, Yuseong-gu, Daejeon, Republic of Korea

*jhan@kaeri.re.kr

1. Introduction

An airtight dry room in Pyroprocess automation mock-up was constructed [1]. Currently, a drying system for the room is under construction. For this drying system design, the leak rate and dew point temperature (DP) of the dry room according to purge flow rate of compressed dry air was evaluated [2].

For preventing the equipment in the room from corrosion by salt, the humidity should be controlled at a low level ($DP < -40^{\circ}\text{C}$). However, the humidity of the dry room can be out of control during blackout, since no compressed air is supplied into the room, and the drying system does not operate at the same time. Hence, in this study, based on the observed moisture trend in the dry room during blackout, a gas supply system is considered as an emergency system.

2. Trend of Moisture Concentration

2.1 DP measurement system

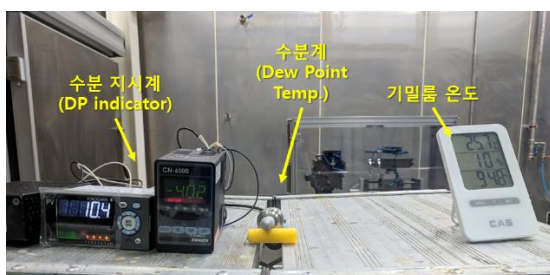


Fig. 1. Moisture measurement system.

As shown in Fig. 1, the moisture and room temperature in the dry room are measured by DP transmitter (DMT-143, VAISALA) and thermometer, respectively. It can be assumed that the measured values are the averaged values in the dry room.

2.2 Measurement of DP trend

The dew point temperature was observed twice in this paper. When no dry air is supplied and the drying system does not work, the DP is expected to be increased even under no pressure difference between the dry room and outer space. It is needed to investigate how DP changes during power outage. Hence, the DP variation was observed two times, one of which was blacked out.

In real blackout, the DP was changed from -36.3°C to -22.4°C for 49 hours, or from 122 ppm to 523 ppm when weight basis in air. Hence, the increase rate is about $0.29^{\circ}\text{C}/\text{hour}$ ($8.2\text{ ppm}/\text{hour}$).

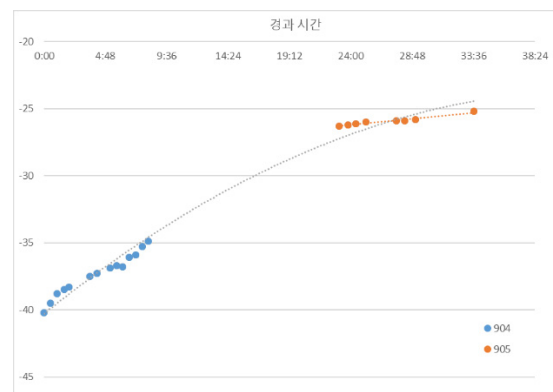


Fig. 2. DP trend in the first measurement.

In second measurement, the blackout was simulated to get detail tendency as time elapsed. Currently, the drying system is not prepared yet, so just the dry air supply was cut for 33 hours. Fig. 2 shows the change of DP, where DP was changed from -40.2°C to -25.2°C , or from 79 ppm to 390 ppm. The average change rate is about $0.49^{\circ}\text{C}/\text{hour}$ or $9.4\text{ ppm}/\text{hour}$. But the rate of the first 12 hours ($-0.54^{\circ}\text{C}/\text{hour}$) is larger than that of the last 12 hours (-0.09°C). It seems that the increase of moisture gets saturated as time elapsed.

The average rates of two cases are little different. This is because the rate depends on the ambient temperature and moisture level. If the level of estimated final moisture concentration based on this rate is not acceptable, a compensation or assistant system should be prepared to decrease the change rate of DP.

3. Basic Design of Gas Supply System

3.1 Basic Design of Emergency Gas Supply System

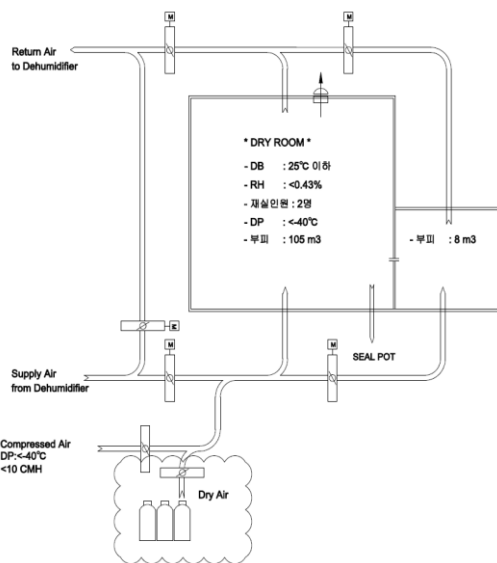


Fig. 3. P&ID of emergency gas supply system.

As shown in Fig. 3, the basic design of an emergency gas supply system will be tied with the supply line of compressed air which will be connected into the supply air duct of the drying system.

The emergency gas supply system is designed as gas cylinders which will supply dry air during power outage. To maintain the DP of the dry room, the flow rate should be 5 CMH at least [2]. Based on this result, the required amount of dry air is about 150 m^3 for 30 hours, but more experiments will perform to get more accurate capacity.

4. Conclusion

In this paper, to design an emergency gas supply system, the change of DP was observed. Based on these observations, detail design such as gas capacity will be continued.

REFERENCES

- [1] J. Han, et al., "Construction of Dry Room for Pyroprocessing Automation Verification Mock-up", Proc. of the KRS 2018 Spring Conference, May 30-June 27, 2018, Busan.
- [2] B. Park, et al., "Preliminary Evaluation of Process Equipment Test Mock-up for Construction of Drying System", Proc. of the KRS 2016 Spring Conference, 14(1), May 30-June 27, 2016, Mokpo.

Quality Assurance of Head-end Process of PYRO

Kweon Ho Kang, Yung Jun Cho, Seok-Min Hong, Jae Won Lee, Young Hwan Kim, Ju Ho Lee, Do Youn Lee, Young Soon Lee, and Joo Young Yoon

Korea Atomic Energy Research Institute, 111, Daedeok-daero 989beon-gil, Yuseong-gu, Daejeon, Republic of Korea

*nghkang@kaeri.re.kr

1. Introduction

In Research & Development (R & D), quality assurance is defined by all planned and systematic activities to obtain reproducible and reliable data with reduced uncertainty. Thus, the quality assurance in research activities is necessary to achieve reliability of experimental data. Especially, ensuring the stability of spent fuel is important because a PYRO process deals with highly radioactive materials inside the spent fuel. Therefore application of the R&D quality assurance is necessary and important to ascertain the reliability of the data in PYRO process from lab-scale research and development step.

In this study, the quality assurance requirements for nuclear facility application were reviewed for the head-end process of PYRO, and project quality assurance plan was established. The quality assurance was applied to input process into the hot-cell using mock-up facility.

2. Project Quality Assurance Plan

There are four important factors in quality assurance in field of R&D activities; quality assurance of experimental methods, quality assurance of equipments, quality assurance of materials, and quality assurance of experimental testers. To meet these factors, 18 items of the quality assurance general requirements for nuclear facility application

are listed up. [1] To apply quality assurance to R&D activities, it is necessary to review these 18 items and to select the items if necessary. Then the researchers have to fill in the project quality assurance plan and check the selected items. Fig. 1 shows the form of project quality assurance plan and the 18 items of quality assurance requirements. [2]

PYRO-PYRO-QA-01 (Rev. 0)		Project Quality Assurance Plan	
1. 조직	<input checked="" type="checkbox"/> 네트웍 조직 체계서 작성 및 검토	2. 품질보증조직	<input checked="" type="checkbox"/> 품질보증조직의 구성 및 역할
3. 품질보증조직	<input checked="" type="checkbox"/> 품질보증조직의 구성 및 역할	4. 품질보증조직	<input checked="" type="checkbox"/> 품질보증조직의 구성 및 역할
5. 품질보증조직	<input checked="" type="checkbox"/> 품질보증조직의 구성 및 역할	6. 품질보증조직	<input checked="" type="checkbox"/> 품질보증조직의 구성 및 역할
7. 품질보증조직	<input checked="" type="checkbox"/> 품질보증조직의 구성 및 역할	8. 품질보증조직	<input checked="" type="checkbox"/> 품질보증조직의 구성 및 역할
9. 품질보증조직	<input checked="" type="checkbox"/> 품질보증조직의 구성 및 역할	10. 품질보증조직	<input checked="" type="checkbox"/> 품질보증조직의 구성 및 역할
11. 품질보증조직	<input checked="" type="checkbox"/> 품질보증조직의 구성 및 역할	12. 품질보증조직	<input checked="" type="checkbox"/> 품질보증조직의 구성 및 역할
13. 품질보증조직	<input checked="" type="checkbox"/> 품질보증조직의 구성 및 역할	14. 품질보증조직	<input checked="" type="checkbox"/> 품질보증조직의 구성 및 역할
15. 품질보증조직	<input checked="" type="checkbox"/> 품질보증조직의 구성 및 역할	16. 품질보증조직	<input checked="" type="checkbox"/> 품질보증조직의 구성 및 역할
17. 품질보증조직	<input checked="" type="checkbox"/> 품질보증조직의 구성 및 역할	18. 품질보증조직	<input checked="" type="checkbox"/> 품질보증조직의 구성 및 역할

Fig. 1. Form of Project Quality Assurance Plan.

3. Apply Quality Assurance to the Head-end Process

We applied quality assurance to input process of equipment into the hot-cell of head-end process project. We reviewed 18 items and selected several items to perform in head-end process project: 1. Organization, 2. Quality Assurance Program 5. Instructions, Procedures, and Drawings, 11. Test Control, 12. Control of Measuring and Test Equipment, 16. Corrective Action, 17. Quality Assurance Records, 18. Audits. We established project quality assurance plan and checked the items


selected to execute. Fig. 1 also shows the established project quality assurance plan and selected items to execute. [3] We also established the operating procedures and test checklists as shown in Fig 2 and 3 respectively. [4]

파이어로봇 컨테이너형 기술개발 과제			
제출번호	제출일자(연월일)	제출분류	제출번호
			0

개 정 예 령					
제출번호	날 자	제출분류(제출구분)	제출번호, 날 자	제출분류	제출일자
	2024.03.20	안 제		제출 번호	

복합 인력 OPDF 운영형식 개발 내 집합식형 열차서

구분	주요내용	공 일	기 일	분 일
제출번호	복합인력운영형식개발연구개발		제출번호	
제출분류	복합인력운영형식개발연구개발연구개발		제출분류	
제출번호	복합인력운영형식개발연구개발연구개발		제출번호	
제출분류	복합인력운영형식개발연구개발연구개발		제출분류	
제출번호	복합인력운영형식개발연구개발연구개발		제출번호	
제출분류	복합인력운영형식개발연구개발연구개발		제출분류	
제출번호	복합인력운영형식개발연구개발연구개발		제출번호	
제출분류	복합인력운영형식개발연구개발연구개발		제출분류	



한국과학기술연구원

KARI

Korea Research Institute of Science and Technology

개정은 한국과학기술연구원 홈페이지(www.kari.ac.kr)를 통해 가능하며, KARI 홈페이지(www.kari.ac.kr)에 등록된 연구 과제에 대해서만 개정이 가능합니다.

Fig. 2. Operating Procedure on the input process of compactor into the DFDF using mock-up facility.

제 1 차 시험 (2024. 11. 24. 토요일)		제 2 차 시험 (2024. 11. 25. 일)	제 3 차 시험 (2024. 11. 26. 화요일)	제 4 차 시험 (2024. 11. 27. 수요일)
시험장명 (Test Checklist)			시험장명 (Test Checklist)	
시험장명 : 제 1 차 시험 (2024. 11. 24. 토요일)			시험장명 : 제 2 차 시험 (2024. 11. 25. 일)	
시험장명 : 제 3 차 시험 (2024. 11. 26. 화요일)			시험장명 : 제 4 차 시험 (2024. 11. 27. 수요일)	
시험장명 : 제 5 차 시험 (2024. 11. 28. 목요일)			시험장명 : 제 6 차 시험 (2024. 11. 29. 금요일)	
1	제 1 차 시험 (2024. 11. 24. 토요일)	제 2 차 시험 (2024. 11. 25. 일)	제 3 차 시험 (2024. 11. 26. 화요일)	제 4 차 시험 (2024. 11. 27. 수요일)
2	제 5 차 시험 (2024. 11. 28. 목요일)	제 6 차 시험 (2024. 11. 29. 금요일)	제 7 차 시험 (2024. 12. 1. 일)	제 8 차 시험 (2024. 12. 2. 월)
3	제 9 차 시험 (2024. 12. 3. 수요일)	제 10 차 시험 (2024. 12. 4. 목요일)	제 11 차 시험 (2024. 12. 5. 금요일)	제 12 차 시험 (2024. 12. 6. 토요일)
4	제 13 차 시험 (2024. 12. 7. 월요일)	제 14 차 시험 (2024. 12. 8. 화요일)	제 15 차 시험 (2024. 12. 9. 수요일)	제 16 차 시험 (2024. 12. 10. 목요일)
5	제 17 차 시험 (2024. 12. 11. 일요일)	제 18 차 시험 (2024. 12. 12. 월요일)	제 19 차 시험 (2024. 12. 13. 화요일)	제 20 차 시험 (2024. 12. 14. 수요일)
6	제 21 차 시험 (2024. 12. 18. 일요일)	제 22 차 시험 (2024. 12. 19. 월요일)	제 23 차 시험 (2024. 12. 20. 화요일)	제 24 차 시험 (2024. 12. 21. 수요일)
7	제 25 차 시험 (2024. 12. 25. 일요일)	제 26 차 시험 (2024. 12. 26. 월요일)	제 27 차 시험 (2024. 12. 27. 화요일)	제 28 차 시험 (2024. 12. 28. 수요일)
8	제 29 차 시험 (2024. 12. 31. 토요일)	제 30 차 시험 (2025. 1. 1. 일)	제 31 차 시험 (2025. 1. 2. 월)	제 32 차 시험 (2025. 1. 3. 화)
9	제 33 차 시험 (2025. 1. 6. 월요일)	제 34 차 시험 (2025. 1. 7. 화요일)	제 35 차 시험 (2025. 1. 8. 수요일)	제 36 차 시험 (2025. 1. 9. 목요일)
10	제 37 차 시험 (2025. 1. 13. 월요일)	제 38 차 시험 (2025. 1. 14. 화요일)	제 39 차 시험 (2025. 1. 15. 수요일)	제 40 차 시험 (2025. 1. 16. 목요일)
11	제 41 차 시험 (2025. 1. 20. 월요일)	제 42 차 시험 (2025. 1. 21. 화요일)	제 43 차 시험 (2025. 1. 22. 수요일)	제 44 차 시험 (2025. 1. 23. 목요일)
12	제 45 차 시험 (2025. 1. 27. 일요일)	제 46 차 시험 (2025. 1. 28. 월요일)	제 47 차 시험 (2025. 1. 29. 화요일)	제 48 차 시험 (2025. 1. 30. 수요일)
13	제 49 차 시험 (2025. 2. 3. 월요일)	제 50 차 시험 (2025. 2. 4. 화요일)	제 51 차 시험 (2025. 2. 5. 수요일)	제 52 차 시험 (2025. 2. 6. 목요일)
14	제 53 차 시험 (2025. 2. 10. 월요일)	제 54 차 시험 (2025. 2. 11. 화요일)	제 55 차 시험 (2025. 2. 12. 수요일)	제 56 차 시험 (2025. 2. 13. 목요일)
15	제 57 차 시험 (2025. 2. 17. 일요일)	제 58 차 시험 (2025. 2. 18. 월요일)	제 59 차 시험 (2025. 2. 19. 화요일)	제 60 차 시험 (2025. 2. 20. 수요일)
16	제 61 차 시험 (2025. 2. 24. 일요일)	제 62 차 시험 (2025. 2. 25. 월요일)	제 63 차 시험 (2025. 2. 26. 화요일)	제 64 차 시험 (2025. 2. 27. 수요일)
17	제 65 차 시험 (2025. 3. 3. 월요일)	제 66 차 시험 (2025. 3. 4. 화요일)	제 67 차 시험 (2025. 3. 5. 수요일)	제 68 차 시험 (2025. 3. 6. 목요일)
18	제 69 차 시험 (2025. 3. 10. 월요일)	제 70 차 시험 (2025. 3. 11. 화요일)	제 71 차 시험 (2025. 3. 12. 수요일)	제 72 차 시험 (2025. 3. 13. 목요일)
19	제 73 차 시험 (2025. 3. 17. 일요일)	제 74 차 시험 (2025. 3. 18. 월요일)	제 75 차 시험 (2025. 3. 19. 화요일)	제 76 차 시험 (2025. 3. 20. 수요일)
20	제 77 차 시험 (2025. 3. 24. 일요일)	제 78 차 시험 (2025. 3. 25. 월요일)	제 79 차 시험 (2025. 3. 26. 화요일)	제 80 차 시험 (2025. 3. 27. 수요일)
21	제 81 차 시험 (2025. 3. 31. 토요일)	제 82 차 시험 (2025. 4. 1. 일)	제 83 차 시험 (2025. 4. 2. 월)	제 84 차 시험 (2025. 4. 3. 화)
22	제 85 차 시험 (2025. 4. 7. 월요일)	제 86 차 시험 (2025. 4. 8. 화요일)	제 87 차 시험 (2025. 4. 9. 수요일)	제 88 차 시험 (2025. 4. 10. 목요일)
23	제 89 차 시험 (2025. 4. 14. 월요일)	제 90 차 시험 (2025. 4. 15. 화요일)	제 91 차 시험 (2025. 4. 16. 수요일)	제 92 차 시험 (2025. 4. 17. 목요일)
24	제 93 차 시험 (2025. 4. 21. 일요일)	제 94 차 시험 (2025. 4. 22. 월요일)	제 95 차 시험 (2025. 4. 23. 화요일)	제 96 차 시험 (2025. 4. 24. 수요일)
25	제 97 차 시험 (2025. 4. 28. 일요일)	제 98 차 시험 (2025. 4. 29. 월요일)	제 99 차 시험 (2025. 4. 30. 화요일)	제 100 차 시험 (2025. 5. 1. 수요일)
26	제 101 차 시험 (2025. 5. 5. 월요일)	제 102 차 시험 (2025. 5. 6. 화요일)	제 103 차 시험 (2025. 5. 7. 수요일)	제 104 차 시험 (2025. 5. 8. 목요일)
27	제 105 차 시험 (2025. 5. 12. 월요일)	제 106 차 시험 (2025. 5. 13. 화요일)	제 107 차 시험 (2025. 5. 14. 수요일)	제 108 차 시험 (2025. 5. 15. 목요일)
28	제 109 차 시험 (2025. 5. 19. 일요일)	제 110 차 시험 (2025. 5. 20. 월요일)	제 111 차 시험 (2025. 5. 21. 화요일)	제 112 차 시험 (2025. 5. 22. 수요일)
29	제 113 차 시험 (2025. 5. 26. 일요일)	제 114 차 시험 (2025. 5. 27. 월요일)	제 115 차 시험 (2025. 5. 28. 화요일)	제 116 차 시험 (2025. 5. 29. 수요일)
30	제 117 차 시험 (2025. 6. 2. 월요일)	제 118 차 시험 (2025. 6. 3. 화요일)	제 119 차 시험 (2025. 6. 4. 수요일)	제 120 차 시험 (2025. 6. 5. 목요일)
31	제 121 차 시험 (2025. 6. 9. 월요일)	제 122 차 시험 (2025. 6. 10. 화요일)	제 123 차 시험 (2025. 6. 11. 수요일)	제 124 차 시험 (2025. 6. 12. 목요일)
32	제 125 차 시험 (2025. 6. 16. 일요일)	제 126 차 시험 (2025. 6. 17. 월요일)	제 127 차 시험 (2025. 6. 18. 화요일)	제 128 차 시험 (2025. 6. 19. 수요일)
33	제 129 차 시험 (2025. 6. 23. 일요일)	제 130 차 시험 (2025. 6. 24. 월요일)	제 131 차 시험 (2025. 6. 25. 화요일)	제 132 차 시험 (2025. 6. 26. 수요일)
34	제 133 차 시험 (2025. 6. 30. 토요일)	제 134 차 시험 (2025. 7. 1. 일)	제 135 차 시험 (2025. 7. 2. 월)	제 136 차 시험 (2025. 7. 3. 화)
35	제 137 차 시험 (2025. 7. 7. 월요일)	제 138 차 시험 (2025. 7. 8. 화요일)	제 139 차 시험 (2025. 7. 9. 수요일)	제 140 차 시험 (2025. 7. 10. 목요일)
36	제 141 차 시험 (2025. 7. 14. 월요일)	제 142 차 시험 (2025. 7. 15. 화요일)	제 143 차 시험 (2025. 7. 16. 수요일)	제 144 차 시험 (2025. 7. 17. 목요일)
37	제 145 차 시험 (2025. 7. 21. 일요일)	제 146 차 시험 (2025. 7. 22. 월요일)	제 147 차 시험 (2025. 7. 23. 화요일)	제 148 차 시험 (2025. 7. 24. 수요일)
38	제 149 차 시험 (2025. 7. 28. 일요일)	제 150 차 시험 (2025. 7. 29. 월요일)	제 151 차 시험 (2025. 7. 30. 화요일)	제 152 차 시험 (2025. 7. 31. 수요일)
39	제 153 차 시험 (2025. 8. 4. 월요일)	제 154 차 시험 (2025. 8. 5. 화요일)	제 155 차 시험 (2025. 8. 6. 수요일)	제 156 차 시험 (2025. 8. 7. 목요일)
40	제 157 차 시험 (2025. 8. 11. 일요일)	제 158 차 시험 (2025. 8. 12. 월요일)	제 159 차 시험 (2025. 8. 13. 화요일)	제 160 차 시험 (2025. 8. 14. 수요일)
41	제 161 차 시험 (2025. 8. 18. 일요일)	제 162 차 시험 (2025. 8. 19. 월요일)	제 163 차 시험 (2025. 8. 20. 화요일)	제 164 차 시험 (2025. 8. 21. 수요일)
42	제 165 차 시험 (2025. 8. 25. 일요일)	제 166 차 시험 (2025. 8. 26. 월요일)	제 167 차 시험 (2025. 8. 27. 화요일)	제 168 차 시험 (2025. 8. 28. 수요일)
43	제 169 차 시험 (2025. 8. 31. 토요일)	제 170 차 시험 (2025. 9. 1. 일)	제 171 차 시험 (2025. 9. 2. 월)	제 172 차 시험 (2025. 9. 3. 화)
44	제 173 차 시험 (2025. 9. 8. 월요일)	제 174 차 시험 (2025. 9. 9. 화요일)	제 175 차 시험 (2025. 9. 10. 수요일)	제 176 차 시험 (2025. 9. 11. 목요일)
45	제 177 차 시험 (2025. 9. 15. 일요일)	제 178 차 시험 (2025. 9. 16. 월요일)	제 179 차 시험 (2025. 9. 17. 화요일)	제 180 차 시험 (2025. 9. 18. 수요일)
46	제 181 차 시험 (2025. 9. 22. 일요일)	제 182 차 시험 (2025. 9. 23. 월요일)	제 183 차 시험 (2025. 9. 24. 화요일)	제 184 차 시험 (2025. 9. 25. 수요일)
47	제 185 차 시험 (2025. 9. 29. 토요일)	제 186 차 시험 (2025. 9. 30. 일)	제 187 차 시험 (2025. 10. 1. 월)	제 188 차 시험 (2025. 10. 2. 화)
48	제 191 차 시험 (2025. 10. 6. 월요일)	제 192 차 시험 (2025. 10. 7. 화요일)	제 193 차 시험 (2025. 10. 8. 수요일)	제 194 차 시험 (2025. 10. 9. 목요일)
49	제 195 차 시험 (2025. 10. 13. 일요일)	제 196 차 시험 (2025. 10. 14. 월요일)	제 197 차 시험 (2025. 10. 15. 화요일)	제 198 차 시험 (2025. 10. 16. 수요일)
50	제 199 차 시험 (2025. 10. 20. 일요일)	제 200 차 시험 (2025. 10. 21. 월요일)	제 201 차 시험 (2025. 10. 22. 화요일)	제 202 차 시험 (2025. 10. 23. 수요일)
51	제 203 차 시험 (2025. 10. 27. 토요일)	제 204 차 시험 (2025. 10. 28. 일)	제 205 차 시험 (2025. 10. 29. 월)	제 206 차 시험 (2025. 10. 30. 화)
52	제 209 차 시험 (2025. 11. 3. 월요일)	제 210 차 시험 (2025. 11. 4. 화요일)	제 211 차 시험 (2025. 11. 5. 수요일)	제 212 차 시험 (2025. 11. 6. 목요일)
53	제 213 차 시험 (2025. 11. 10. 일요일)	제 214 차 시험 (2025. 11. 11. 월요일)	제 215 차 시험 (2025. 11. 12. 화요일)	제 216 차 시험 (2025. 11. 13. 수요일)
54	제 217 차 시험 (2025. 11. 17. 일요일)	제 218 차 시험 (2025. 11. 18. 월요일)	제 219 차 시험 (2025. 11. 19. 화요일)	제 220 차 시험 (2025. 11. 20. 수요일)
55	제 221 차 시험 (2025. 11. 24. 일요일)	제 222 차 시험 (2025. 11. 25. 월요일)	제 223 차 시험 (2025. 11. 26. 화요일)	제 224 차 시험 (2025. 11. 27. 수요일)
56	제 225 차 시험 (2025. 11. 30. 목요일)	제 226 차 시험 (2025. 12. 1. 금요일)	제 227 차 시험 (2025. 12. 2. 토요일)	제 228 차 시험 (2025. 12. 3. 일)
57	제 231 차 시험 (2025. 12. 7. 토요일)	제 232 차 시험 (2025. 12. 8. 일)	제 233 차 시험 (2025. 12. 9. 월)	제 234 차 시험 (2025. 12. 10. 화)
58	제 237 차 시험 (2025. 12. 14. 토요일)	제 238 차 시험 (2025. 12. 15. 일)	제 239 차 시험 (2025. 12. 16. 월)	제 240 차 시험 (2025. 12. 17. 화)
59	제 241 차 시험 (2025. 12. 21. 토요일)	제 242 차 시험 (2025. 12. 22. 일)	제 243 차 시험 (2025. 12. 23. 월)	제 244 차 시험 (2025. 12. 24. 화)
60	제 245 차 시험 (2025. 12. 28. 토요일)	제 246 차 시험 (2025. 12. 29. 일)	제 247 차 시험 (2025. 12. 30. 월)	제 248 차 시험 (2025. 12. 31. 화)
61	제 251 차 시험 (2026. 1. 4. 토요일)	제 252 차 시험 (2026. 1. 5. 일)	제 253 차 시험 (2026. 1. 6. 월)	제 254 차 시험 (2026. 1. 7. 화)
62	제 257 차 시험 (2026. 1. 11. 토요일)	제 258 차 시험 (2026. 1. 12. 일)	제 259 차 시험 (2026. 1. 13. 월)	제 260 차 시험 (2026. 1. 14. 화)
63	제 261 차 시험 (2026. 1. 18. 토요일)	제 262 차 시험 (2026. 1. 19. 일)	제 263 차 시험 (2026. 1. 20. 월)	제 264 차 시험 (2026. 1. 21. 화)
64	제 265 차 시험 (2026. 1. 25. 토요일)	제 266 차 시험 (2026. 1. 26. 일)	제 267 차 시험 (2026. 1. 27. 월)	제 268 차 시험 (2026. 1. 28. 화)
65	제 269 차 시험 (2026. 2. 1. 토요일)	제 270 차 시험 (2026. 2. 2. 일)	제 271 차 시험 (2026. 2. 3. 월)	제 272 차 시험 (2026. 2. 4. 화)
66	제 273 차 시험 (2026. 2. 8. 토요일)	제 274 차 시험 (2026. 2. 9. 일)	제 275 차 시험 (2026. 2. 10. 월)	제 276 차 시험 (2026. 2. 11. 화)
67	제 277 차 시험 (2026. 2. 15. 토요일)	제 278 차 시험 (2026. 2. 16. 일)	제 279 차 시험 (2026. 2. 17. 월)	제 280 차 시험 (2026. 2. 18. 화)
68	제 281 차 시험 (2026. 2. 22. 토요일)	제 282 차 시험 (2026. 2. 23. 일)	제 283 차 시험 (2026. 2. 24. 월)	제 284 차 시험 (2026. 2. 25. 화)
69	제 285 차 시험 (2026. 2. 29. 토요일)	제 286 차 시험 (2026. 3. 1. 일)	제 287 차 시험 (2026. 3. 2. 월)	제 288 차 시험 (2026. 3. 3. 화)
70	제 291 차 시험 (2026. 3. 8. 토요일)	제 292 차 시험 (2026. 3. 9. 일)	제 293 차 시험 (2026. 3. 10. 월)	제 294 차 시험 (2026. 3. 11. 화)
71	제 297 차 시험 (2026. 3. 15. 토요일)	제 298 차 시험 (2026. 3. 16. 일)	제 299 차 시험 (2026. 3. 17. 월)	제 300 차 시험 (2026. 3. 18. 화)
72	제 301 차 시험 (2026. 3. 22. 토요일)	제 302 차 시험 (2026. 3. 23. 일)	제 303 차 시험 (2026. 3. 24. 월)	제 304 차 시험 (2026. 3. 25. 화)
73	제 305 차 시험 (2026. 3. 29. 토요일)	제 306 차 시험 (2026. 3. 30. 일)	제 307 차 시험 (2026. 3. 31. 월)	제 308 차 시험 (2026. 4. 1. 화)
74	제 309 차 시험 (2026. 4. 5. 토요일)	제 310 차 시험 (2026. 4. 6. 일)	제 311 차 시험 (2026. 4. 7. 월)	제 312 차 시험 (2026. 4. 8. 화)
75	제 313 차 시험 (2026. 4. 12. 토요일)	제 314 차 시험 (2026. 4. 13. 일)	제 315 차 시험 (2026. 4. 14. 월)	제 316 차 시험 (2026. 4. 15. 화)
76	제 317 차 시험 (2026. 4. 19. 토요일)	제 318 차 시험 (2026. 4. 20. 일)	제 319 차 시험 (2026. 4. 21. 월)	제 320 차 시험 (2026. 4. 22. 화)
77	제 321 차 시험 (2026. 4. 26. 토요일)	제 322 차 시험 (2026. 4. 27. 일)	제 323 차 시험 (2026. 4. 28. 월)	제 324 차 시험 (2026. 4. 29. 화)
78	제 325 차 시험 (2026. 5. 3. 토요일)	제 326 차 시험 (2026. 5. 4. 일)	제 327 차 시험 (2026. 5. 5. 월)	제 328 차 시험 (2026. 5. 6. 화)
79	제 329 차 시험 (2026. 5. 10. 토요일)	제 330 차 시험 (2026. 5. 11. 일)	제 331 차 시험 (2026. 5. 12. 월)	제 332 차 시험 (2026. 5. 13. 화)
80	제 333 차 시험 (2026. 5. 17. 토요일)	제 334 차 시험 (2026. 5. 18. 일)	제 335 차 시험 (2026. 5. 19. 월)	제 336 차 시험 (2026. 5. 20. 화)
81	제 337 차 시험 (2026. 5. 24. 토요일)	제 338 차 시험 (2026. 5. 25. 일)	제 339 차 시험 (2026. 5. 26. 월)	제 340 차 시험 (2026. 5. 27. 화)
82	제 341 차 시험 (2026. 5. 31. 토요일)	제 342 차 시험 (2026. 6. 1. 일)	제 343 차 시험 (2026. 6. 2. 월)	제 344 차 시험 (2026. 6. 3. 화)
83	제 345 차 시험 (2026. 6. 7. 토요일)	제 346 차 시험 (2026. 6. 8. 일)	제 347 차 시험 (2026. 6. 9. 월)	제 348 차 시험 (2026. 6. 10. 화)
84	제 349 차 시험 (2026. 6. 14. 토요일)	제 350 차 시험 (2026. 6. 15. 일)	제 351 차 시험 (2026. 6. 16. 월)	제 352 차 시험 (2026. 6. 17. 화)
85	제 353 차 시험 (2026. 6. 21. 토요일)	제 354 차 시험 (2026. 6. 22. 일)	제 355 차 시험 (2026. 6. 23. 월)	제 356 차 시험 (2026. 6. 24. 화)
86	제 357 차 시험 (2026. 6. 28. 토요일)	제 358 차 시험 (2026. 6. 29. 일)	제 359 차 시험 (2026. 6. 30. 월)	제 360 차 시험 (2026. 7. 1. 화)
87	제 361 차 시험 (2026. 7. 5. 토요일)	제 362 차 시험 (2026. 7. 6. 일)	제 363 차 시험 (2026. 7. 7. 월)	제 364 차 시험 (2026. 7. 8. 화)
88	제 365 차 시험 (2026. 7. 12. 토요일)	제 366 차 시험 (2026. 7. 13. 일)	제 367 차 시험 (2026. 7. 14. 월)	제 368 차 시험 (2026. 7. 15. 화)
89	제 369 차 시험 (2026. 7. 19. 토요일)	제 370 차 시험 (2026. 7. 20. 일)	제 371 차 시험 (2026. 7. 21. 월)	제 372 차 시험 (2026. 7. 22. 화)
90	제 373 차 시험 (2026. 7. 26. 토요일)	제 374 차 시험 (2026. 7. 27. 일)	제 375 차 시험 (2026. 7. 28. 월)	제 376 차 시험 (2026. 7. 29. 화)
91	제 377 차 시험 (2026. 7. 31. 토요일)	제 378 차 시험 (2026. 8. 1. 일)	제 379 차 시험 (2026. 8. 2. 월)	제 380 차 시험 (2026. 8. 3. 화)
92	제 381 차 시험 (2026. 8. 8. 토요일)	제 382 차 시험 (2026. 8. 9. 일)	제 383 차 시험 (2026. 8. 10. 월)	제 384 차 시험 (2026. 8. 11. 화)
93	제 385 차 시험 (2026. 8. 15. 토요일)	제 386 차 시험 (2026. 8. 16. 일)	제 387 차 시험 (2026. 8. 17. 월)	제 388 차 시험 (2026. 8. 18. 화)
94	제 389 차 시험 (2026. 8. 22. 토요일)	제 390 차 시험 (2026. 8. 23. 일)	제 391 차 시험 (2026. 8. 24. 월)	제 392 차 시험 (2026. 8. 25. 화)
95	제 393 차 시험 (2026. 8. 29. 토요일)	제 394 차 시험 (2026. 8. 30. 일)	제 395 차 시험 (2026. 8. 31. 월)	제 396 차 시험 (2026. 9. 1. 화)
96	제 397 차 시험 (2026. 9. 5. 토요일)	제 398 차 시험 (2026. 9. 6. 일)	제 399 차 시험 (2026. 9. 7. 월)	제 400 차 시험 (2026. 9. 8. 화)
97	제 401 차 시험 (2026. 9. 12. 토요일)	제 402 차 시험 (2026. 9. 13. 일)	제 403 차 시험 (2026. 9. 14. 월)	제 404 차 시험 (2026. 9. 15. 화)
98	제 405 차 시험 (2026. 9. 19. 토요일)	제 406 차 시험 (2026. 9. 20. 일)	제 407 차 시험 (2026. 9. 21. 월)	제 408 차 시험 (2026. 9. 22. 화)
99	제 409 차 시험 (2026. 9. 26. 토요일)	제 410 차 시험 (2026. 9. 27. 일)	제 411 차 시험 (2026. 9. 28. 월)	제 412 차 시험 (2026. 9. 29. 화)
100	제 413 차 시험 (2026. 10. 3. 토요일)	제 414 차 시험 (2026. 10. 4. 일)	제 415 차 시험 (2026. 10. 5. 월)	제 416 차 시험 (2026. 10. 6. 화)
101	제 417 차 시험 (2026. 10. 10. 토요일)	제 418 차 시험 (2026. 10. 11. 일)	제 419 차 시험 (2026. 10. 12. 월)	제 420 차 시험 (2026. 10. 13. 화)
102	제 421 차 시험 (2026. 10. 17. 토요일)	제 422 차 시험 (2026. 10. 18. 일)	제 423 차 시험 (2026. 10. 19. 월)	제 424 차 시험 (2026. 10. 20. 화)
103</				

Fig. 3. Test Checklist.

4. Conclusion

To apply quality assurance to R&D activities, we reviewed the 18 items of quality assurance requirements and selected the items needed. Then we filled in the project quality assurance plan and checked the selected items. We also established the corresponding operating procedures and test checklists. These quality assurance activities for PYRO process are expected to increase the reliability of safe management of spent fuel.

ACKNOWLEDGEMENT

This work was supported by the Korea Institute of Energy Technology Evaluation and Planning (KETEP) granted financial resource from the Ministry of Trade.

REFERENCES

- [1] Korea Electric Association, “Quality Assurance-Nuclear Quality Assurance” KEPIC-QAP, (2012).
- [2] Korea Atomic Energy Research Institute, “Quality Assurance Manual for Nuclear R&D” RDQAM-100 (2015).
- [3] Kweon Ho Kang, Jae Eon Jeon, Chan Kook Park, Yong Jun Cho, “Project Quality Assurance Plan” PQAP-PYRO-01 (Rev. 2) (2017).
- [4] J.W. Lee, D.Y. Lee, J.H. Yang, Y.S. Lee, K.H. Kang, Y.J. Cho, “Operating Procedure of Input Test of Compactor into the DFDF Hot-cell Using Mock-up”, PYRO-PRE-TP-01 (2016).

Abstracts of Proceedings of the
Korean Radioactive Waste Society AUTUMN 2018

www.krs.or.kr

KOREAN RADIOACTIVE WASTE SOCIETY



사단 한국방사성폐기물학회
법인 Korean Radioactive Waste Society